COASTAL ENGINEERING

PROCEEDINGS OF SEVENTH CONFERENCE

ON

COASTAL ENGINEERING

THE HAGUE, NETHERLANDS

AUGUST 1960

Edited by
J. W. JOHNSON
Professor of Hydraulic Engineering

UNIVERSITY OF CALIFORNIA
BERKELEY

VOLUME 1

PUBLISHED BY
COUNCIL ON WAVE RESEARCH
THE ENGINEERING FOUNDATION

1961

Lithographed in the United States of America
The National Press, Palo Alto, California

ACKNOWLEDGMENTS

This conference was sponsored jointly by the Council on Wave Research, Berkeley, California, and the Rijkswaterstaat, of the Netherlands Dean Morrough P O'Brien is Chairman of the Council on Wave Research and Mr. A. G Maris is Director-General of the Rijkswaterstaat. Mr. J B Schijf, Chief Engineer-Director of the Rijkswaterstaat, acted as secretary of the conference. Appreciation is expressed to the Rijkswaterstaat for photographs supplied to illustrate the cover and the section title pages of this publication.

CONTENTS

VOLUME 1

CONTENTS

PART 2
BEACH AND SHORELINE PROCESSES

CONTENTS

CONTENTS

CONTENTS

CONTENTS

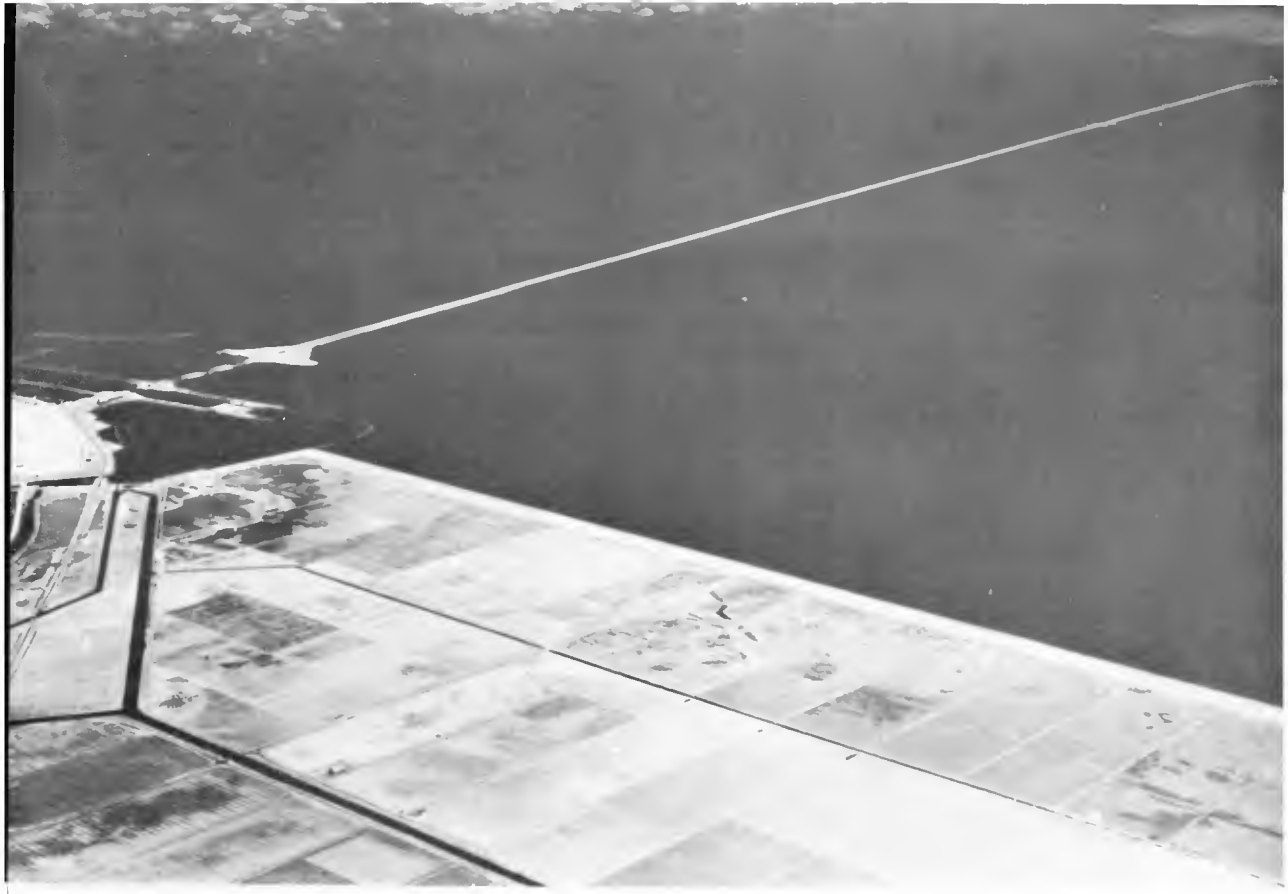

Zuider Zee Dam

Part 1

WAVE THEORY AND MEASUREMENTS

Zuider Zee Dam

CHAPTER 1

WIND WAVES AND SWELL

R. L. Wiegel
Associate Professor of Civil Engineering
University of California
Berkeley, California

Winds blowing over the water surface generate waves. In general the higher the wind velocity, the larger the fetch over which it blows, and the longer it blows the higher and longer will be the average waves. Waves still under the action of the winds that created them are called wind waves, or a sea. They are forced waves rather than free waves. They are variable in their direction of advance (Arthur, 1949). They are irregular in the direction of propagation. The flow is rotational due to the shear stress of the wind on the water surface and it is quite turbulent as observations of dye in the water indicates. After the waves leave the generating area their characteristics become somewhat different, principally they are smoother, losing the rough appearance due to the disappearance of the multitude of smaller waves on top of the bigger ones and the whitecaps and spray. When running free of the storm the waves are known as swell. In Fig. 1 are shown some photographs taken in the laboratory of waves still rising under the action of wind and this same wave system after it has left the windy section of the wind-wave tunnel. It can be seen that the freely running swell has a smoother appearance than the waves in the windy section. The motion of the swell is nearly irrotational and non-turbulent, unless the swell runs into other regions where the water is in turbulent motion. Turbulence is a property of the fluid rather than of the wave motion. After the waves have travelled a distance from the generating area they have lost some energy due to air resistance, internal friction, and by large scale turbulent scattering if they run into other storm areas, and the rest of the energy has become spread over a larger area due to the dispersive and angular spreading characteristics of water gravity waves. All of these mechanisms lead to a decrease in energy density. Thus, the waves become lower in height. In addition, due to their dispersive characteristic the component wave periods tend to segregate in such a way that the longest waves lead the main body of waves and the shortest waves form the tail of the main body of waves. Finally, the swell may travel through areas where winds are present, adding new wind waves to old swell, and perhaps directly increasing or decreasing the size of the old swell.

1. Wave Characteristics

An observer stationed high above the area in which wind waves

pass from the fetch into an area of calm (called the decay area) would notice that the waves in both regions vary in heights, lengths, and breadths. If he were to follow a particular wave crest he would notice that it would gradually disappear; he would also notice new crests form.

An observer watching the crests leaving the fetch and measuring the time intervals between the successive crests as well as the heights would have a true picture of the surface waves at a particular point without having a true picture of the phenomenon. This is because the surface phenomenon is a result of other complex phenomena. Because there is a spectrum of lengths (or periods) and heights present there must be some sort of a group phenomenon; that is, there are no permanent wave forms. Instead, wave crests and troughs gradually appear and disappear. The longer wave components of the group, traveling with greater speeds than the shorter wave components, gradually move ahead, with the shortest wave components dropping behind. Hence, a spreading of the wave system occurs.

In order to understand what happens in an actual case, where the generating areas vary in size, the winds vary in speed and direction and exist for different lengths of time, it is necessary first to consider the simplified case of a stationary storm of constant dimensions with winds that immediately spring up to a constant speed and remain at that speed for a short time, long enough to generate a considerable number of waves and then die down immediately. In addition, the decay distance must be long enough for complete segregation of wave components to take place. Shortly after the wind starts blowing over the entire generating area the waves will be short, but probably close to maximum steepness ($H/L = 1/7$ in deep water). At some distance downwind from the start of the fetch the waves will gradually grow in height and length as time increases. The maximum wave dimensions at this point will be obtained when all of the waves generated upwind of this point have reached it, this time depending upon the group velocity of the waves. When this has occurred a quasi-steady state condition has been reached.

An observer traveling along with the wave system in the decay area would notice that the long wave components would gradually move in front of the system and short wave components would drop to the rear of the system. The longer the wave system has traveled the greater would be this segregation. If the group were to travel many thousands of miles, and were there no other disturbances, this segregation and stretching of the system would become complete. An observer at a fixed distance from the storm would notice a steady decrease in wave period with increasing time.

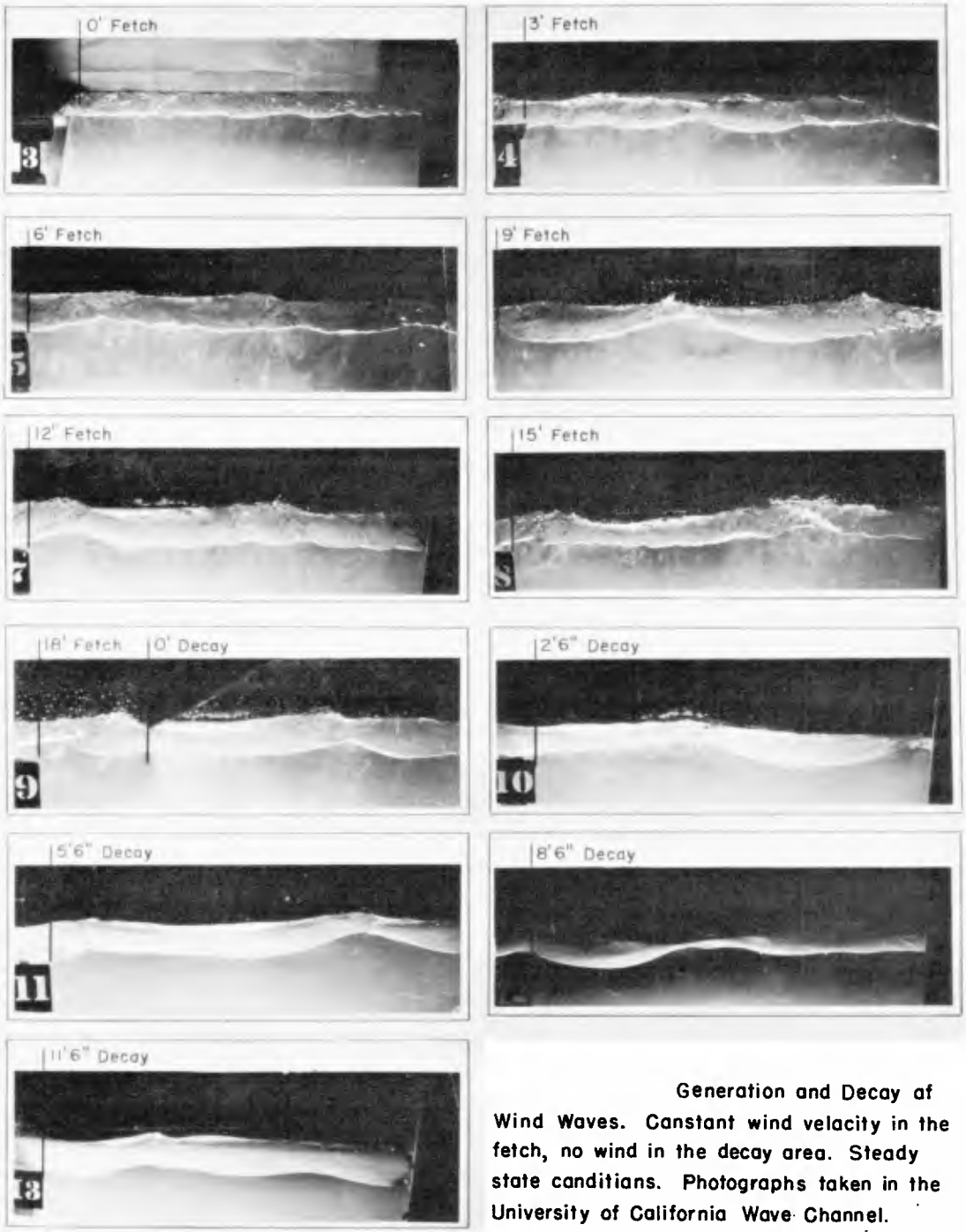

Generation and Decay of Wind Waves. Constant wind velocity in the fetch, no wind in the decay area. Steady state conditions. Photographs taken in the University of California Wave Channel.

Fig. 1

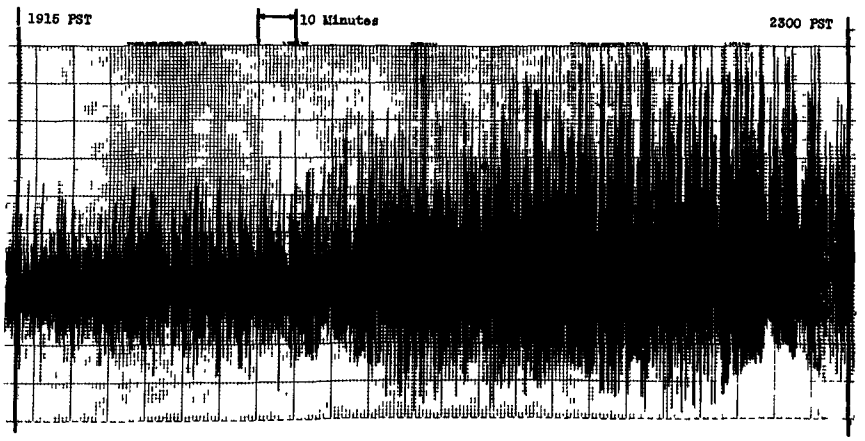

Notes: Averages of periods (T) and significant breaker heights ($(H_{1/3})_B$) are for fifteen minute interval on each side of indicating lines.

1915 PST. T = 12.0 seconds, $(H_{1/3})_B$ = 4.0 feet.
2300 PST. T = 10.3 seconds, $(H_{1/3})_B$ = 8.0 feet.

Fig. 2. Mark V, No. 1A, record for 1915 to 2300 PST, 18 October, 1949, Camp Pendleton, Oceanside, California.

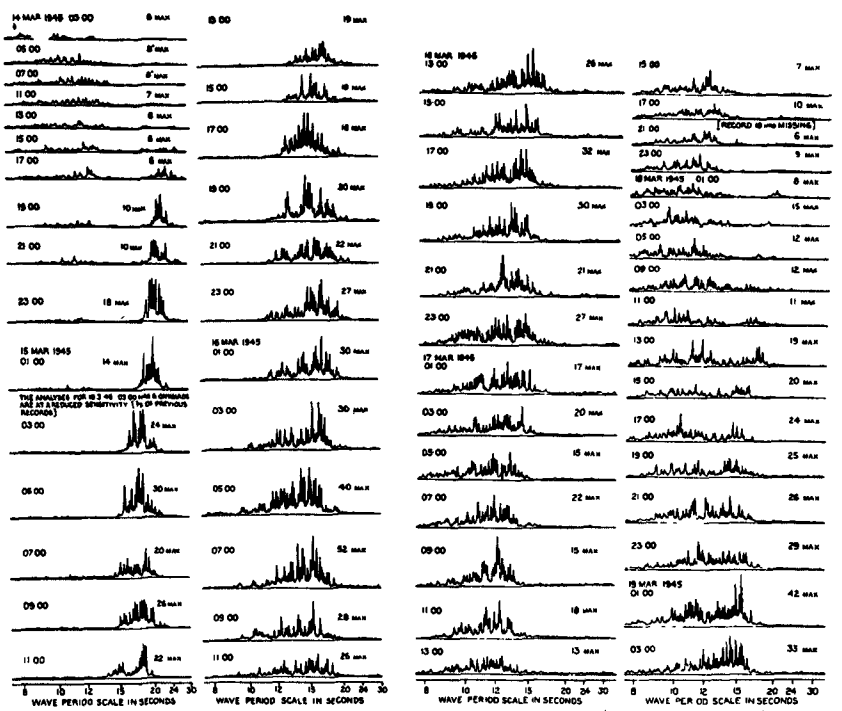

(after Barber and Ursell, 1948)

Fig. 3. Wave spectra at Pendeen, 16 to 18 March, 1945.

Actually, the duration of the storm and the relatively short decay distances (even several thousands of miles) are such that complete segregation never takes place. In local storms almost no segregation takes place and the lengths and periods are relatively short, even if the winds were great, the fetch long and the duration long; stretching of wave system does not occur so that the energy density is high. As the decay distance increases the segregation increases and so the long waves, often called "forerunners of storms", reach the coast before the main body of waves. For a particular storm the longer the decay distance the greater is the time between these forerunners and the main body of waves (high energy density).

The normal case is more complicated. For example, suppose the storm lasts for two days and that it takes only one day for the medium length wave component to reach the section of coast under consideration. The longer waves are being continually generated as are all the shorter wave periods. Thus, even as the first of the shortest waves are arriving at the coast the longer waves which were being formed after the shorter waves have left the generating area, overtake the shorter waves and arrive at the same time.

It can be seen then that a section of coast a considerable distance from a storm will be subject to long, low waves first with the mean "period" of the waves (with the "period" being defined as the time necessary for two successive crests to pass a fixed point) decreasing with time but with the period spectrum width about the mean value increasing. The wave "heights" (with the "height" being defined as the vertical distance between a trough and the following crest) will be increasing because the greatest energy density is concentrated in the waves with medium periods. An example of such a "wave front" reaching the coast can be seen in Fig. 2. As the last of the waves reach the coast an abrupt decrease in wave period and height will be observed. The average period of even these short waves, at the coast, will always be longer than the period observed at the end of the fetch because of the spreading phenomenon and because the smallest waves will have been either captured by the large waves or dissipated.

The actual phenomenon is more complex than has been described because the winds gradually rise to a maximum speed, then decrease again, always fluctuating, with the wind field varying in size and the storm moving.

As an example, consider the wave spectra at Pendeen, England, during 14 to 15 March 1945, which has been presented in Fig. 3 (Barber and Ursell, 1948). The wave record at Pendeen, the bottom pressure type, was analyzed by a frequency analyzer so that the component period spectra was obtained. It can be seen that the forerunners

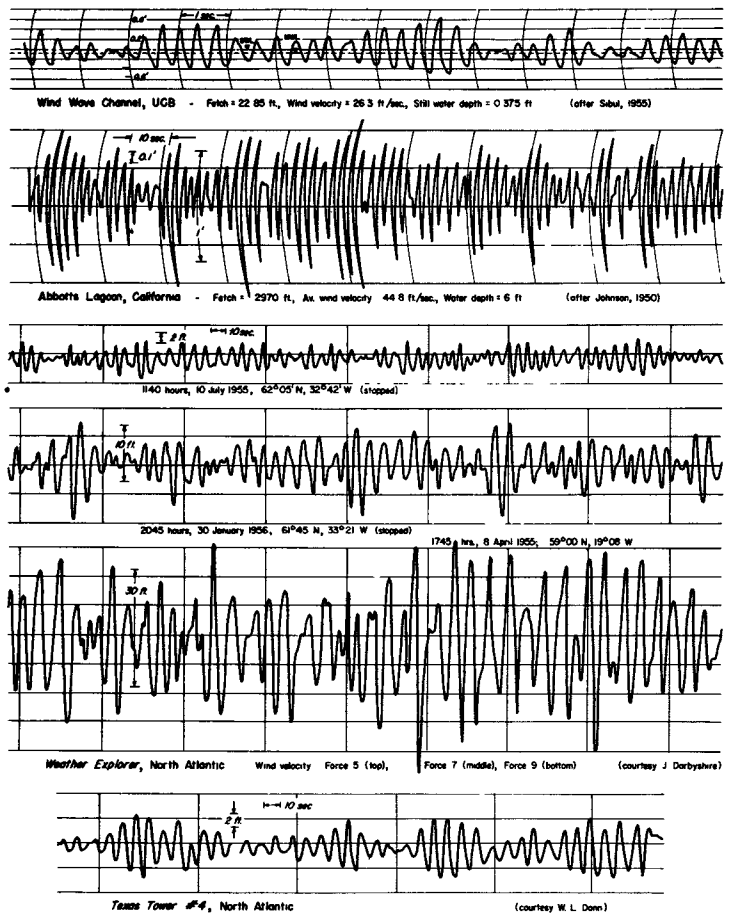

Fig. 4. Sample records of waves unaffected by refraction.

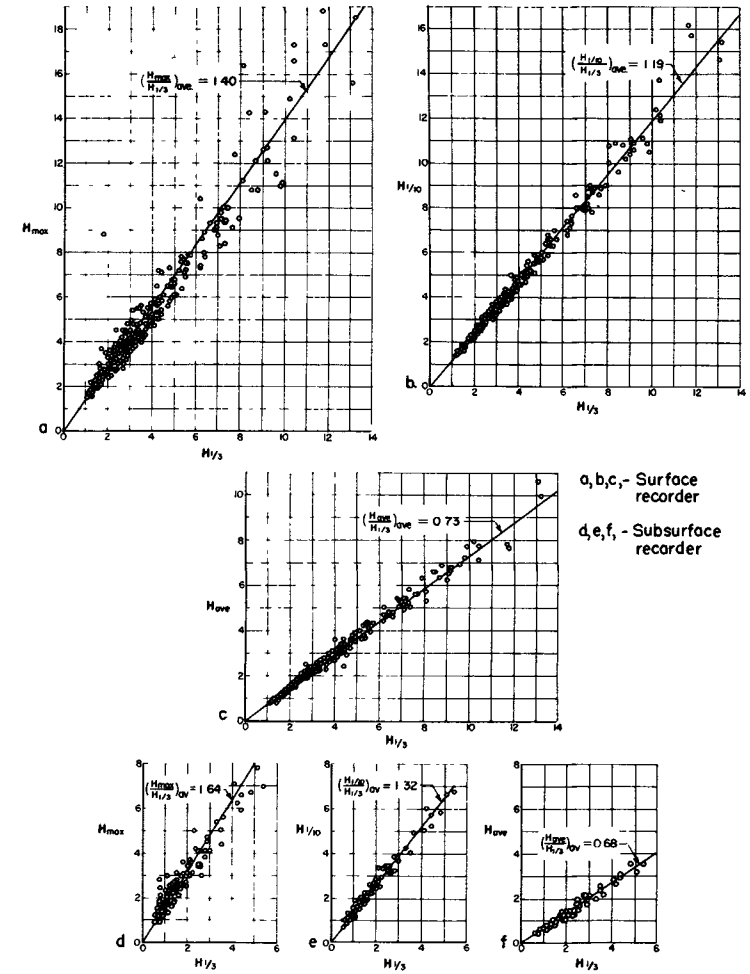

Fig. 5. Wave height relationships (after Wiegel and Kukk, 1957)

of a new wave system first appeared at 1300 on 14 March 1945. The mean of the periods gradually decreased while at the same time the width of the spectra increased.

In the literature on ocean waves the terms gaussian and random are often used when referring to the heights and periods of wind waves and swell. These terms must be used with caution as they oversimplify the true nature of waves and they are not descriptive to the layman of the many groups of nearly periodic waves that exist. That these groups exist can be seen in Fig. 4 in which records of waves in the generating area are presented for laboratory, lakes and ocean conditions. The statistical techniques used in obtaining the information that will be presented in the following sections neglect the time sequence of the phenomena. Thus, one entire class of information is often thrown away in the analysis of waves. From an engineering standpoint it is the groups of several periodic waves, which are almost always the highest waves in a wave system, that are the most effective in causing structural damage. Donn and McGuinness (1959) report that the waves they measured in a relatively open ocean area occurred in striking sinusoidal groups in contrast to the far more irregular patterns observed in the shallow water off coasts in the area.

One of the main problems connected with describing waves is that of defining what we will call a wave. Should every small bump be considered a wave? For some purposes, such as scattering of radar or the reflection and scattering of light, the answer should be yes. For many purposes the answer should be no. One concept that is useful in this respect is to neglect the very small waves and to measure the highest one third of the remaining waves, the average of the highest one third being called the significant or characteristic wave height. This concept was developed during studies of landing craft operations in the surf in World War II. It was found that the wave height estimated by observers corresponded to the average of the highest 20 to 40 percent of the waves (Scripps Institution of Oceanography, 1944). Originally, the term significant wave was attached to the average of these observations, the highest 30 percent of the waves, but has evolved to become the average of the highest 33-1/3 percent (designated as H_S or $H_{1/3}$).

It can be seen in Fig. 4 the higher waves often occur in groups which are nearly periodic. The average period of these high groups in a record was termed the significant period (designated at T_S or $T_{H_{1/3}}$).

In order for the concept of significant wave height and period to be of more value studies were made of the distribution of wave heights and periods about their mean values (Ehring, 1940; Seiwell, 1948; Wiegel, 1949, Rudnick, 1951; Munk and Arthur, 1951; Darbyshire, 1952;

TABLE I. MEASURED STATISTICAL RATIOS FOR OCEAN WAVES

Location and Type Wave Recorder	Statistical Ratios							Remarks
	$\frac{H_{max}}{H_{1/10}}$	$\frac{H_{max}}{H_{1/3}}$	$\frac{H_{max}}{H_{mean}}$	$\frac{H_{1/10}}{H_{1/3}}$	$\frac{H_{1/10}}{H_{mean}}$	$\frac{H_{1/3}}{H_{mean}}$	$\frac{H_{3/10}}{H_{mean}}$	
1a. Davenport, Calif. surface rec'dr		1.40	1.90	1.19	1.61	1.37		11 mos., 12-20 min. interval every 12 hrs water depth 46' MLLW (WIEGEL & KUKK, '57)
1b. Davenport, Calif. bottom-pressure recorder		1.64	2.64	1.32	2.09	1.48		5 mos., 12-20 min. interval every 12 nre., water depth 46' MLLW (WIEGEL & KUKK, 1957)
2. N. Atlantic Ocean NIO ship-borne recorder			2.40			1.60		138 records, 26-144 waves per record (mean of 69 waves) every 3 hrs. (DARLINGTON, 1954)
3. Pt.Arguello, Calif. bottom-pressure recorder	1.42	1.85		1.30				3 mos., 20 min. every 8 nrs.; figures refer to daily ave. & max., recorder in 75' of water MLLW (WIEGEL, 1949)
4. Pt. Sur, Calif. bottom-pressure recorder	1.46	1.85		1.27				14 mos., 20 min. interval every 8 hrs.; figures refer to daily ave. & max.; recorder in 68' of water MLLW (WIEGEL, 1949)
5. Hecata Head, Ore. bottom-pressure recorder	1.47	1.91		1.30				14 mos., 20 min. interval every 8 hrs.; figures refer to daily ave. & max.; recorder in 50' of water MLLW (WIEGEL, 1949)
6. Cuttyhunk, Mass. bottom-pressure recorder						1.57		10 mos., 20 min. interval every 6 hrs., wave recorder in 75' of water (SHINELL, 1948)
7. Bermuda bottom-pressure recorder						1.57		4 mos., 20 min. interval every 2 hrs., recorder in 120' of water (SHINELL, 1948)
8. Cape Cod, Mass.							1.56	1 record, 14 waves; 1 record, 28 waves, waves only 2-3 sec. period (GIBSON, 1944)
9. LaJolla, Calif. bottom-pressure recorder		1.63				1.49		46 waves (MUNK & ARTHUR, 1951)
10. North Sea pressure recorder hanging on cable below float						1.85		688 waves (every bump counted as a wave); wind waves (EHRING, 1940)
		1.5				(1.58)		517 waves (neglecting all waves less than 14.8 cm high in above sample (HARNEY, SAUR & ROBINSON, 1949)
11. Pacific Coast, U.S.A. & Guam, M.I., bottom-pressure recorder						1.63		25 records, 20 min. interval (PUTZ, 1952)
12. Greymouth, N. Z. bottom pressure recorder				1.24	1.94	1.58		109 records, 17 min. interval, every 2 hrs. (WATTERS, 1953)
13. Hachijo I. Japan (surface ?)			2.0			1.5		11 records, 10 min. interval, various locations (YOSHIDA, KAJIURA & HIDAKA, 1953)
14. Long Branch, N.J. BEB surface recorder		1.29	1.93			1.50		1 record of 102 waves (PIERSON, NEUMANN & JAMES, 1955)
15. Bermuda, NIO ship-borne recorder				1.24		1.61		6 records, 12-18 min. interval (FARMER, 1956)
16. Oceanside, Calif. bottom-pressure recorder				1.25				1 mo., 20 min. interval every 8 hrs. (WIEGEL & KUKK, 1957)

Putz, 1952; Pierson and Marks, 1952; Watters, 1953; Yoshida, Kajuira, and Hidaka, 1953; and Darlington, 1954). These papers advanced the concept of the "statistical nature" of ocean waves. Many of the data were summarized by Longuet-Higgins (1952) in his paper on the statistical distribution of heights of ocean waves.

Almost all of the data were obtained from bottom pressure-type recorders, with their inherent practical and theoretical limitations (Folsom, 1949; Pierson and Marks, 1952; Fuchs, 1955; Gerhardt, Jehn and Katz, 1955; Neuman, 1955). Similar studies were made with both surface recorders and bottom pressure recorders by Wiegel and Kukk (1957), the results of which are shown in Fig. 5. It was found that the statistical ratios obtained by measuring the waves at the surface differed from the ratios obtained from the sub-surface pressure recorders (Table 1). It is believed that the difference, and the sign of the difference, can be explained by the method of analyzing the records of the sub-surface pressure recorders combined with the fact that the sub-surface dynamic pressures decrease more rapidly with depth for the lower period waves than for the longer period waves. Of particular importance is the fact that the surface measurements in the ocean of wind waves and swell of Wiegel and Kukk (1957) resulted in nearly the same ratios as those of the surface measurements by Sibul (1955) of wind-waves generated in a wind-wave tunnel. Although many of the measurements of Sibul were for waves in relatively shallow water the author states that no observable shallow water effect was noticed in the wave height ratios. It should be noted that the wave height ratios obtained by Wiegel and Kukk were for swell with wind waves often superimposed, while the ratios obtained by Sibul were only for wind waves. It appears then that the wave height distribution about a mean value is about the same for swell as for wind waves.

Several investigators were able to fit existing mathematical curves to the empirical wave height data, curves of the "random distribution" type (Putz, 1952; Longuet-Higgins, 1952; and Walters, 1953). The work of Longuet-Higgins is in most general use (it predicts nearly the same values as do the curves of Putz). It allows the prediction of the most probable maximum wave height for a given number of waves, providing the mean wave height (or some other measure of wave height) is known. These values are presented in Table 2. In this table N is the number of consecutive waves considered and $\mu(a_{max})$ is the most probable maximum wave amplitude (half the wave height) that will occur in N consecutive waves if the sample has a root mean square wave height of $2\bar{a}$. In order to find the most probable maximum wave to expect in N waves if the significant height is known, rather than the root mean square wave height, it is only necessary to divide the value $\mu(a_{max})$ by 1.416 (Table 3). For example, if N = 500 waves, from

Table 2

Value of $E(a_{max})/\bar{a}$ and $\mu(a_{max})/\bar{a}$ for different values of N, for a narrow spectrum (after Longuet-Higgins, 1952)

N	$(\log N)^{\frac{1}{2}}$	$E(a_{max})/\bar{a}$ exact expression	$E(a_{max})/\bar{a}$ asymptotic expression	$\mu(a_{max})/\bar{a}$
1	0.000	0.886		0.707
2	0.833	1.146		1.030
5	1.269	1.462		1.366
10	1.517	1.676	1.708	1.583
20	1.731	1.870	1.898	1.778
50	1.978	--	2.124	2.010
100	2.146	--	2.280	2.172
200	2.302	--	2.426	2.323
500	2.493	--	2.609	2.509
1,000	2.628	--	2.738	2.642
2,000	2.757	--	2.862	2.769
5,000	2.918	--	3.017	2.929
10,000	3.035	--	3.130	3.044
20,000	3.147	--	3.239	3.155
50,000	3.289	--	3.377	3.296
100,000	3.393	--	3.478	3.400

Table 2, $\mu(a_{max})/\bar{a} = 2.509$, from Table 3 $a^{(0.333)}/\bar{a} = 1.416$, and the most probable maximum wave height/significant wave height = 2.509/1.416 = 1.77. If the significant wave was 10.0 ft. then the most probable maximum wave height would have been 17.7 ft.

The entire spectrum of wave heights can be obtained by use of Table 3.

Table 3

Representative values of $a^{(p)}/\bar{a}$ in the case of a narrow wave spectrum (after Longuet-Higgins, 1952).

p	$a^{(p)}/\bar{a}$	p	$a^{(p)}/\bar{a}$
0.01	2.359	0.4	1.347
0.05	1.986	0.5	1.256
0.1	1.800	0.6	1.176
0.2	1.591	0.7	1.102
0.25	1.517	0.8	1.031
0.3	1.454	0.9	0.961
0.3333	1.416	1.0	0.886

In Table 3 p = 0.1 refers to the average of the highest one tenth of the waves, p = 0.333 refers to the average of the highest one third of the waves p = 1.0 refers to the mean of all of the waves, etc. The ratio $H_{1/10}/H_{1/3}$ can be obtained from Table 3 as 1.800/1.416 = 1.28; and the ratio $H_{1/3}/H_{mean}$ as 1.416/0.886 = 1.60. It is evident from a comparison of these values with those shown in Table 1 that the wave height distribution function of Longuet-Higgins is of practical importance.

The wave height distribution function of Longuet-Higgins is for the case of a narrow wave spectrum. For a wide spectrum the work of Cartwright and Longuet-Higgins (1956; also, Williams and Cartwright, should be considered.

Another important set of statistical data deals with the wave period (or frequency) spectrum. Putz (1952) made measurements of twenty-five wave records (bottom pressure type), each record of approximately twenty-minute duration. He found the relationship between the significant wave period to the mean wave period shown in Fig. 6. The complete period distribution function of Putz is shown in Fig. 7. As an example of its use, suppose the significant period was 11.5 sec., then from Fig. 6 it would be found that the mean wave period would be 11.0 sec. From Fig. 7 it would be found that 99.5 percent of the wave periods would be less than 18 seconds and that only 0.5 percent would be less than 4.5 sec. Of more importance in the consideration of waves in the generating area is the work of Darbyshire (1959), the data on wave frequency distribution being given in Fig. 14.

Darlington (1954) has made a similar study of wave records obtained with the NIO shipborne wave recorder (Tucker, 1956) in the North Atlantic. Most of the recordings reported were made with the ship stopped. As can be seen in Table 1 his results on wave height distribution agree well with those of Putz, and the data extended the results to a mean wave height up to 28 ft. with a maximum wave height of 42 ft. The results of the relationship between the period of the highest one third of the waves and the mean period are shown in Fig. 6. The results are not the same as those obtained by Putz, but are not too different. Part of the difference must be due to the fact that Putz's records were obtained from a bottom pressure recorder. In addition, Darlington's measurements were made in storm areas (with background swell in many cases), while Putz's measurements were mostly of swell. It is interesting to note that both results show that for lower period waves T_m should be greater than $T_{H_{1/3}}$. Darlington found that by interpolating the best fit straight line that $T_m > T_{H_{1/3}}$ for $T_m < 6$ sec, while Putz found that $T_m > T_{H_{1/3}}$ for $T_m < 9$ sec. No actual measurements of this condition were made however, Both of these findings are in conflict with Sibul's (1955) measurements of short period waves generated in a wind-wave tunnel, Fig. 8. It would appear then that the relationship

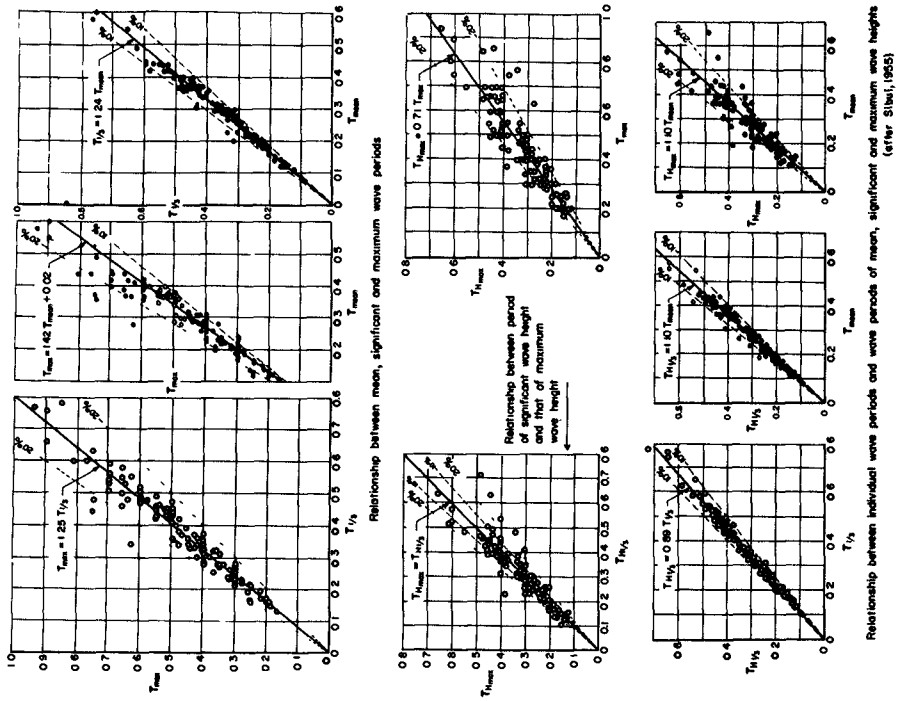

Fig. 8

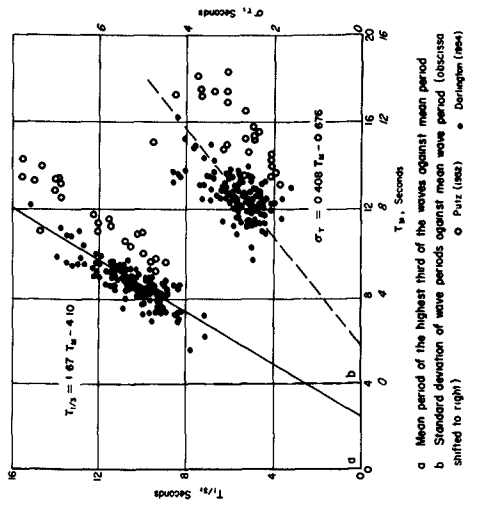

Fig. 6

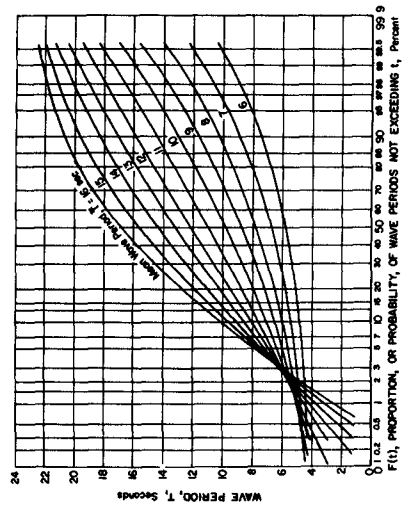

Fig. 7. Prediction curves for wave period distributions for various mean periods (after Putz, 1952).

between $T_{H1/3}$ and T_m is a non-linear one. Part of the difference may be that both Putz's and Darlington's wave measurements are either wholly or partially dependent upon the prediction of surface waves from sub-surface pressure measurements with some inherent difficulties in measuring the true mean and significant wave periods.

What is the relationship between the heights and periods of the wind waves? In Fig. 9 are shown the relationship between T_{mean} (the length of the wave record divided by the number of waves in the record) and $H_{1/3}$. These two parameters were chosen as they were the most generally available ones. The data shown are for wind waves rather than swell, although there may be some swell present in the records of Bretschneider (1954) and Darlington (1954). A line was drawn through the wind-wave tunnel data of Sibul (1955), neglecting the smallest waves as these probably were affected considerably by surface tension. This line was extended through several cycles on the log-log paper. This line is expressed by

$$H_{1/3} = 0.45\ T_{mean}^2 \tag{1}$$

If we assume that for non-periodic waves $L = gT^2/2\pi$

$$\frac{H_{1/3}}{(L_{mean\ o})} = \frac{1}{11.4} \tag{2}$$

If we assume that the relationship derived by Pierson, Neumann and James (1955) for a gaussian sea surface is correct, that is the apparent wave length L* is about 2/3 the value of a period wave, then

$$\frac{H}{(L^*_{mean\ o})} = \frac{1}{11.4} \times \frac{3}{2} = \frac{1}{7.6} \tag{3}$$

which is very close to the theoretical maximum wave steepness, and nearly identical to the maximum steepness of mechanically generated waves. This appears to be the physical reason for the limit of the maximum wave heights; for a given mean wave period this is the maximum that can exist without breaking.

The California Research Corporation (1960) has measured waves from several oil platforms in the Gulf of Mexico using a step resistance gage that is essentially self-calibrating in that as each electrode is shorted by the sea water passing over it a "step" occurs on the record. The data shown in Fig. 9 are for four hurricanes in the Gulf of Mexico, with the measurements being made in water 30 feet deep. Each point shown was obtained from a sample of between 100 and 200 waves. The

fact that the water was not deep should be considered as the maximum wave steepness in transitional water is not as great as it is in deep water On the other hand, some of the data were for essentially deep water waves, and these data show the same trend with respect to the dashed line as do transitional waves.

The extension of the line through Sibul's data does not go through all of the data taken in the field. Many of the field data were obtained with instruments either entirely or partially dependent upon subsurface pressure measurements. It is known that these pressure measurements projected to surface values by use of the first order theory relationship between wave height and sub-surface pressures, when using an average pressure factor associated with a mean period, underpredicts the surface wave by an average of about 25 percent (Folsom, 1959; Gerhardt, John and Katz, 1955). This same technique utilizes a subjective method of determining the number of waves in a record which when combined with rapid attenuation with distance below the water surface of the short period wave components, results in a mean wave period that is longer than would be the case in analyzing a surface wave record. The field data, then, should be shifted in the manner indicated by the arrows in Fig. 9. The data of Darlington (1954) and Darbyshire (1959) should probably be rotated in the manner shown in the figure as the recorder used in obtaining the data is very insensitive to waves with periods less than about 6 sec (Marks, 1955; Marks, 1956; Williams and Cartwright, 1957). In addition, the NIO shipborne recorder utilized a vertical acceleration sensing device, the output of which must be integrated twice to give a reference for the pressure cells. The reliability of the results of such a technique are not yet fully understood. This would tend to make them conform to the other data.

The data shown in Fig. 9 due to Sibul (1955), Johnson (1950) and the California Research Corporation (1960) are for only wind waves while these of Bretschneider (1954) and Darlington (1954) probably include swell as well as wind waves. Studies made of data largely of swell do not show this trend, as can be seen in Fig. 10 (Putz, 1951).

Is there any clear relationship between the heights and periods of individual waves? For wind waves generated in the laboratory the answer is a qualified yes. The results for this case can be seen in Fig. 11 (Johnson and Rice, 1952). In general, the longer the wave the higher the wave. For swell, or a mixture of swell and wind waves the joint frequency distributions are shown in Fig. 12 (Putz, 1951, 1952). There is no evidence of a relationship between these quantities although there is a tendency for highest wave heights to occur with near average periods.

Ocean waves can be considered to be the combination of a series

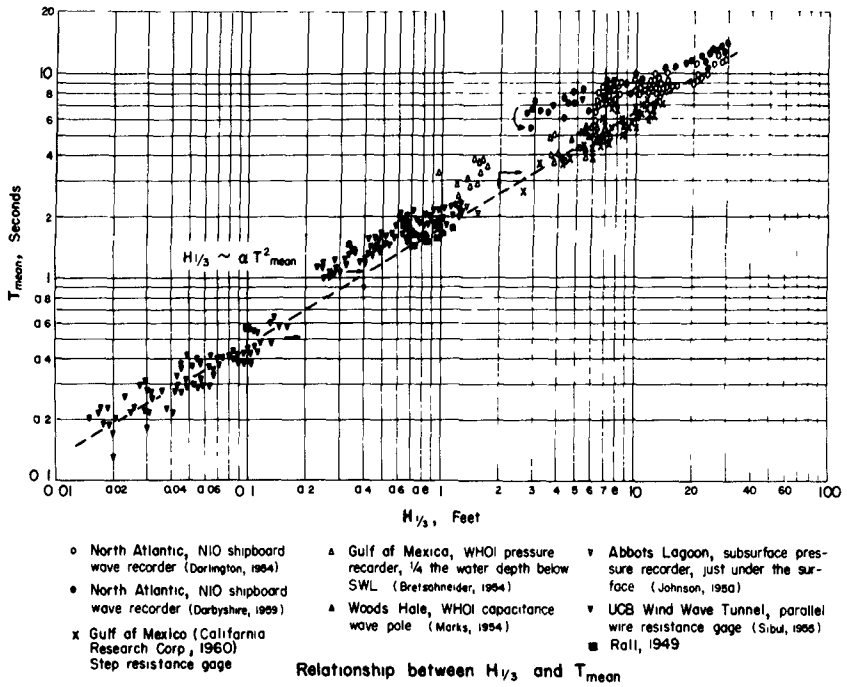

Relationship between $H_{1/3}$ and T_{mean}

Fig. 9

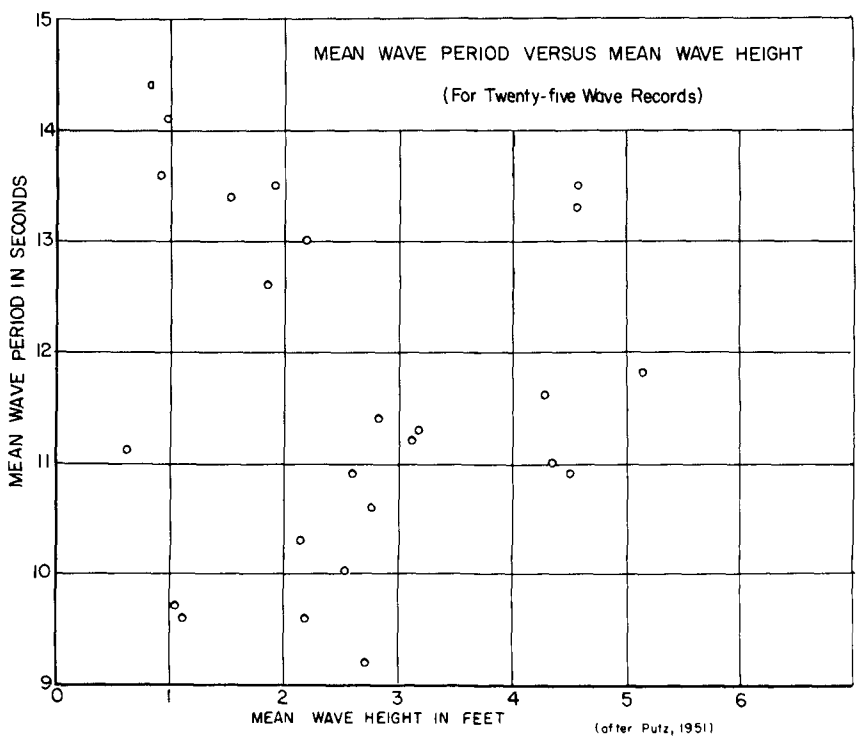

Fig. 10

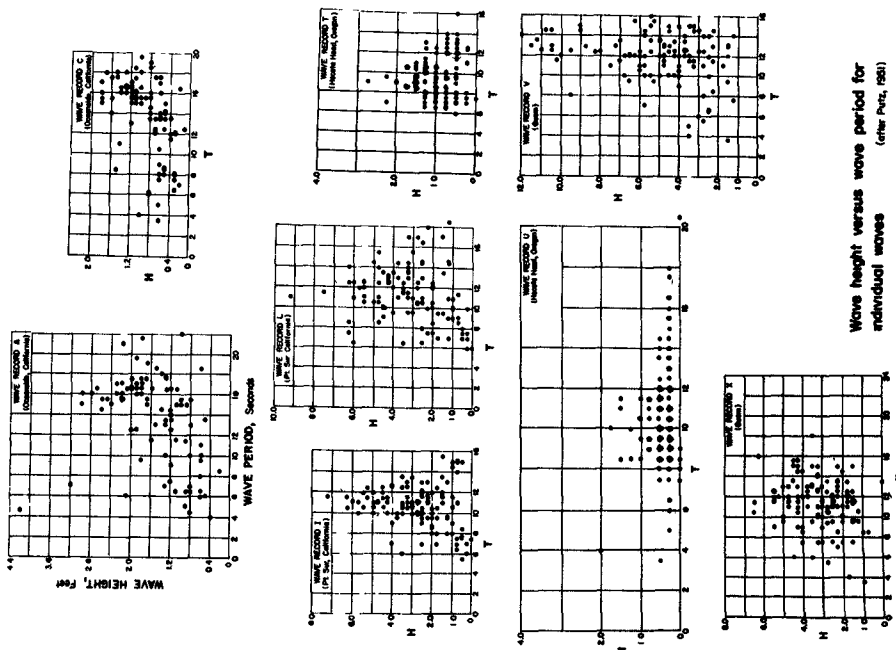

Fig. 12

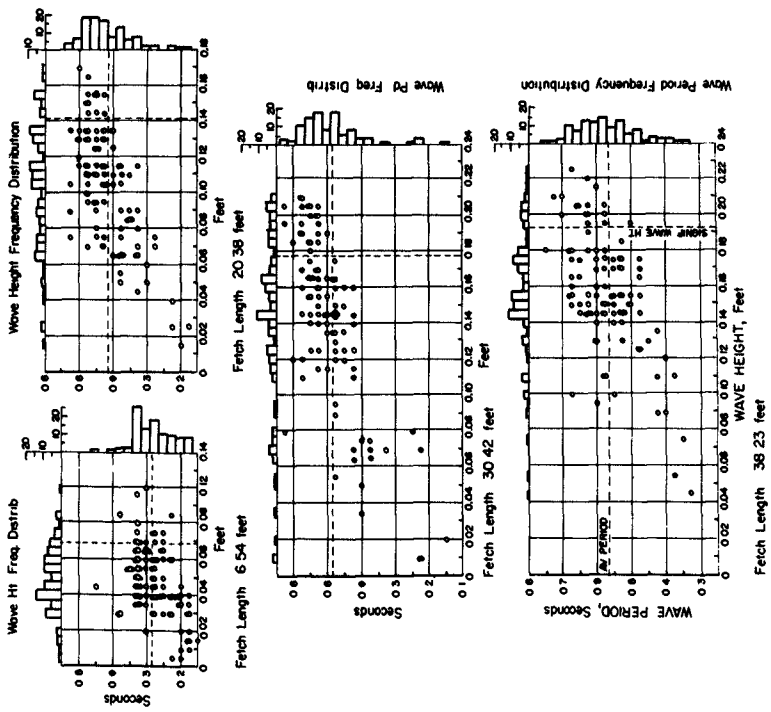

Joint frequency distribution of wave period and wave height
(U = 42 7 ft/sec)
(after Johnson and Rice, 1962)

Fig. 11

of components of different periods, or frequencies, with a certain amount of power being transmitted by each component. In describing waves using this concept the term wave spectrum is used. The "spectrum" describes in some manner the distribution of the energy density present in a wave system with respect to the wave period, or frequency. An example of one type of wave spectrum is shown in Fig. 3.

Darbyshire (1959) has obtained the wave spectra for recorded waves of a large number of storms in the North Atlantic using the NIO shipborne wave recorder. The records were analyzed first to obtain values of $T_{H1/3}$, $H_{1/3}$, etc., using a wave recorder calibration curve based upon the wave component percent associated with f_o. Then the records were analyzed by an approximate Fourier method to obtain certain information on the wave spectra, namely, the square of the wave height components, H_f, within each frequency interval $\Delta f = 0.007$ sec.$^{-1}$. f_o was defined as the frequency of the class having the largest value of H_f^2 on the spectrum. The heights H_f were corrected using a calibration curve based upon the component period associated with each frequency f. The wave period associated with this, T_{fo}, was found to be closely related to the significant wave period ($T_{fo} = 1.14\ T_{H1/3}$) as is shown in Fig. 13. It appears from this, and from the relationships shown by Putz and Sibul, that the choice of the significant wave to describe waves was a good one.

Darbyshire (1959) has found a consistent relationship between H_f^2/H^2 and $f - f_o$ (Fig. 14), where H is defined as the height of a hypothetical single sine wave train which has the same energy density as the actual wave system. The close relationship between this hypothetical wave and other surface wave characteristics can be seen in Fig. 15, where $H_{max} = 2.40$ H and $H = 0.604\ H_{1/3}$ with very little scatter of the data.

The scatter of data of H_f^2/H^2 vs $f - f_o$ is considerable when compared with the scatter of data for $H_{1/3}$ vs H_m, $T_{H1/3}$ vs T_m. For example, if H were 10 ft., H_f could be between 41 and 56 ft. at its maximum.

As pointed out by Darbyshire this empirically determined spectrum is inconsistent with the previous spectrum of Darbyshire (1952; 1955), the spectrum of Neumann (1953) and the spectrum of Roll and Fisher (1956).

Burling (1955) computed the spectra associated with various fetches and meteorological conditions on a reservoir (fetches from 1200 to 4000 feet and wind speeds from about 15 to 25 ft/sec. The results are shown in Fig. 16a, where ω is the circular wave frequency component ($2\pi/T$) and

$$\Phi(\omega) = \frac{1}{2\pi}\int_{-\infty}^{\infty} \xi(X, t+\tau)\, \xi(X, t+\tau)^{-i\omega\tau} d\tau \qquad (4)$$

Eq. 4 is given in the form of Phillips (1958b) where $\xi(x,t)$ is the surface displacement at fixed point, and τ is a time displacement. $\Phi(\omega)$ has the dimensions of ft^2 - sec, (or cm^2 - sec) and the area under the curve $\Phi(\omega)$ versus ω is related to the energy per unit area being transmitted by the wave system. It is important to note that Burling's data seem to lie along a single curve for circular frequencies greater than about 6 radians/sec (wave periods smaller than about 1 sec). The curve in this region has been developed theoretically by Phillips (1958b).

$$\Phi(\omega) \approx \alpha\, g^2\, \omega^{-5} = \text{constant}/\omega^5 \qquad (5)$$

The solid curves in Fig. 16 are $\Phi(\omega) = 7.4 \times 10^{-3}\, g^2\, \omega^{-5}$, in cgs units. In Fig. 16b the results of Project SWOP (Chase, et al, 1957) are shown compared with Eq. 5 (Phillips, 1958c). This extends the relationship shown in Fig. 16a to ocean conditions, and it appears that the "fully developed sea" extends only to wave components down to $\omega \approx 2$; i.e., wave period components up to about 3 seconds. The physical significance of this limiting curve is that a wave of a given frequency can increase in energy only up to a certain limit ($H/L = 1/7$ in deep water for a uniform periodic wave). Hence, if the fetch and duration are long enough $\Phi(\omega)$ must have a unique value which depends only upon the frequency.

Some of the differences between the spectra of different investigators have been explained by Pierson (1959a) based upon a random nonlinear model of waves (Tick, 1958). An additional spectrum plus a discussion of the above cited spectra have been presented by Bretschneider (1959).

Directional spectrum have been measured by Chase et al (1957), but their results are difficult to interpret. Phillips (1958c) and Cox (1958) offer conflicting interpretations of the results. The major difficulty, aside from experimental errors is that the measurements were made of ocean waves, and it is not possible to be sure of the level of wave action with respect to the local winds.

Wave are short-crested: that is, they have a dimension in the horizontal direction normal to the direction of wave advance. This dimension has been termed the crest length of a wave. There are very few measurements of this wave dimension. The average ratio of crest length to wave length (L'/L) of some waves measured on aerial photographs was from 2 to 3. Johnson (1948) made some measurements on waves in a lake and found (L'/L) = 3. Yampol'ski (1955) found that the distribution curves for wave lengths and crest lengths were nearly

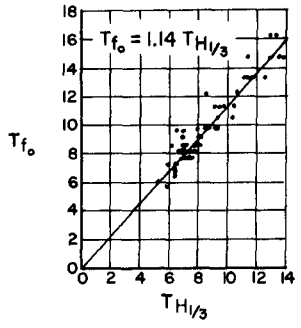

Relationship between T_{f_o} and $T_{H_{1/3}}$

(after Darbyshire, 1959)

Fig. 13

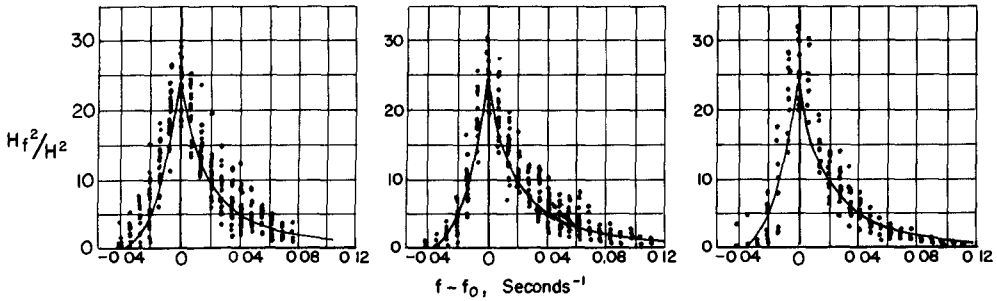

Relationship between $H_f{}^2/H^2$ and $f - f_o$

Fig. 14

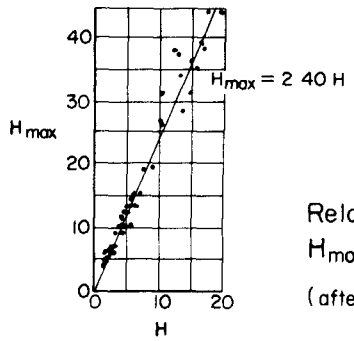

Relationship between H_{mox} and H

(after Darbyshire, 1959)

Fig. 15

identical in appearance, the measurements being made from aerial photographs of the sea surface.

A three-dimensional laboratory study was made by Ralls and Wiegel (1956) of wind-generated waves in which the crest length was measured as shown in Fig. 17 (notice surface tension waves also in this figure). The results of measurements of crest lengths and wave lengths are shown in Fig. 18. In deep water the ratio is approximately 3.

2. Relationships among Wave Dimensions, Winds, and Fetches

The relationships among the wave dimensions, wind speeds and direction, atmospheric stability, fetch length, and wind and fetch variability are not well established. It is not surprising, considering the extreme difficulty in obtaining reliable measurements in the open ocean combined with the near impossibility of obtaining sea conditions consisting of only wind waves, with no swell present. To these difficulties must be added the problems of determining the wind fetches and durations. Because of this the data obtained will be presented, but ideas from studying data obtained in the laboratory and in lakes will be used to interpret the ocean data.

First, let us consider waves from the standpoint of wave spectra. The data of Burling (1955) has already been covered. The remaining data will pertain to ocean waves.

In deep water the average power, averaged over a complete cycle, transmitted per unit area of surface is proportional to the square of the wave height and inversely proportional to the wave period. The energy per unit area, the energy density, is proportional to the square of the wave height. Darbyshire (1952; 1955) used the equation

$$E_T = \frac{1}{8} \rho g \sum_{T-\frac{1}{2}}^{T+\frac{1}{2}} h_n^2 = \frac{1}{8} \rho g H_T^2$$

where E_T is the energy per unit area of horizontal sea surface in a wave-period interval from $T-\frac{1}{2}$ to $T+\frac{1}{2}$, and H_T is defined as the equivalent wave height for waves of period between $T-\frac{1}{2}$ and $T+\frac{1}{2}$ (that is, in a one-second interval) as obtained by a Fourier analysis and taking the square root of the sum of the squares of the peaks within each one-second interval of wave period. The results, plotted in terms of H_T/T versus T/U, where U is the gradient wind speed, are shown in Fig. 19. The solid line curve shown in the figures is the gaussian function that Darbyshire states expresses the relationship between H_T/T and T/U. It is evident that the scatter is extreme, and that the relationship between the

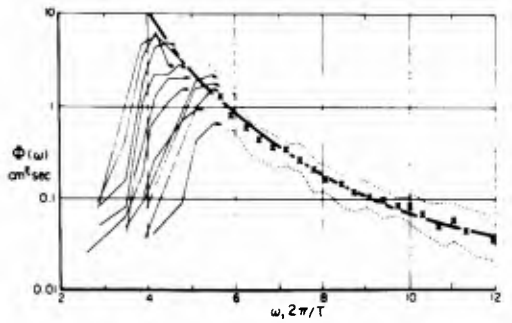

Spectra of wind-generated waves measured by Burling (1955). The cluster of lines on the left are representative of the spectra at low frequencies for which equilibrium has not been attained. On the right the curves merge over the equilibrium range, and the dotted lines indicate the extreme measured values of $\Phi(\omega)$ at each frequency ω. The x's represent the mean observed value at each ω, and the heavy line the relation $\Phi(\omega) = \alpha g^2 \omega^{-5}$ with $\alpha = 7.4 \times 10^{-3}$. (after Phillips, 1958b)

(a)

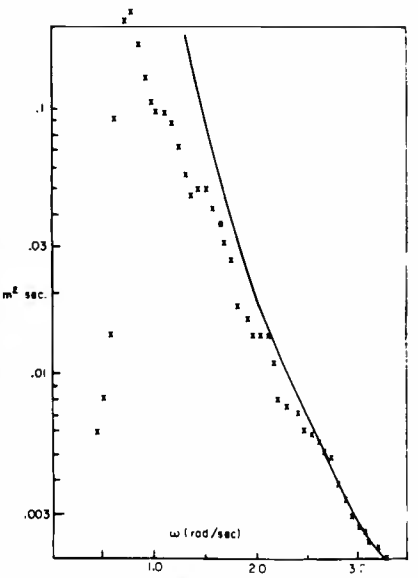

The frequency spectrum $\phi(\omega)$ from the S-W OP wave pole data. The solid curve represents the equilibrium range spectrum $\phi(\omega) \sim 7.4 \times 10^{-3} g^2 \omega^{-5}$. (after Phillips, 1958c)

(b)

Fig. 16

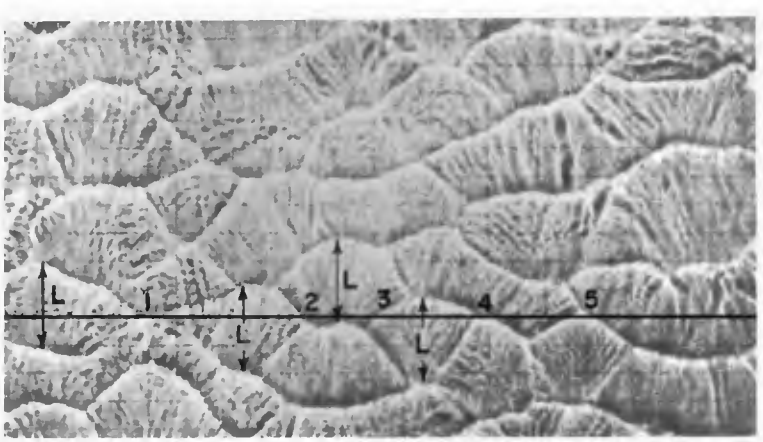

Fig. 17. Distribution method of measuring crest lengths (after Ralls and Wiegel, 1956).

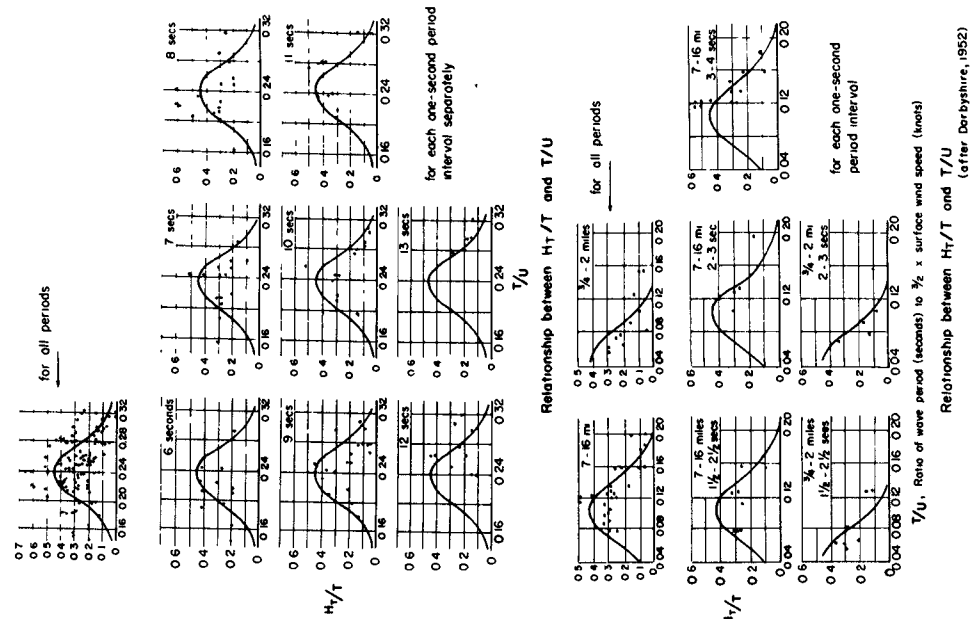
for all periods
6 seconds
7 secs
8 secs
9 secs
10 secs
11 secs
12 secs
13 secs
for each one-second period interval separately
Relationship between H_T/T and T/U
for all periods
7 - 16 m
7 - 16 miles
7 - 16 mi
3 - 4 secs
2 - 3 secs
¾ - 2 miles
1¼ - 2½ secs
for each one-second period interval
T/U, Ratio of wave period (seconds) to ½ x surface wind speed (knots)
Relationship between H_T/T and T/U
(after Darbyshire, 1952)

Fig. 19

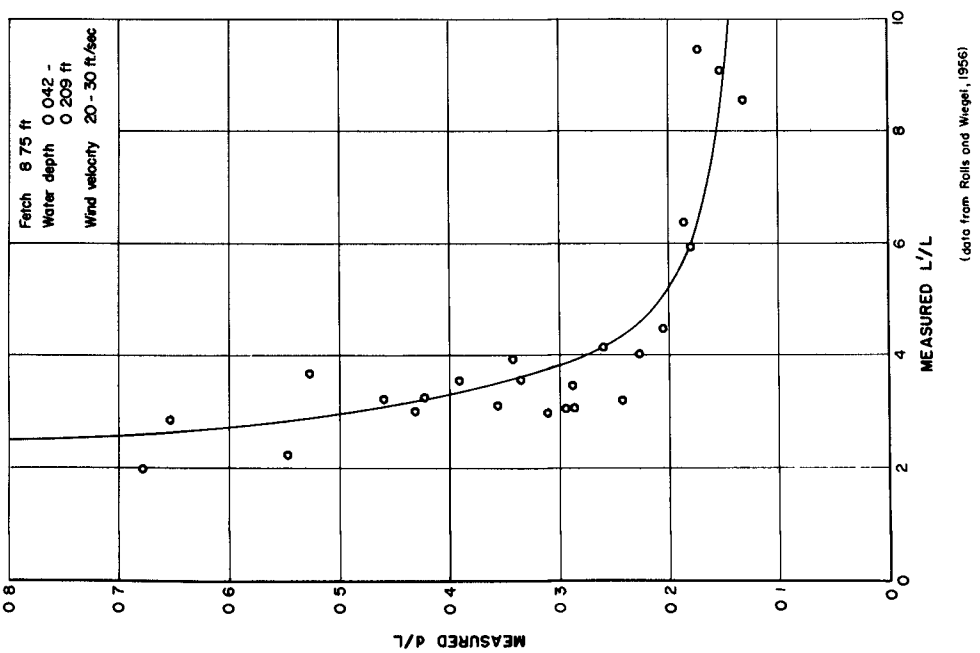
Fetch 8 75 ft
Water depth 0 042 - 0 209 ft
Wind velocity 20 - 30 ft/sec
MEASURED d/L
MEASURED L'/L
(data from Rolls and Wiegel, 1956)

Fig. 18

data and the curves practically non-existent. Darbyshire has found a much more reliable spectrum, leaving out the relationship of the spectrum to the wind (Fig. 14).

Other data for which a spectrum equation has been developed are shown in Fig. 20 (Neumann, 1953). The relationships among wave height, wave period and wind speed, as given by Neumann, is stated to be an exponential curve, and that this curve forms the upper envelope of the data in Fig. 20. The values of H and T used in this figure refer to the height and period of surface waves, many of them visual observations from a ship. They do not refer to data obtained by a Fourier analysis or similar method. This upper envelope is considered by Neumann to represent the "fully arisen sea," where the term refers to the case where no more energy can be added to the wave system regardless of the length of time the wind blows or the length of the fetch (Pierson, Neumann and James, 1955). This means that the waves, at all frequencies, are dissipating energy and radiating it from the storm area at the same rate that wind is transferring wave energy to the sea surface. It is doubtful that this condition exists in the open ocean for all frequencies although it does exist for the higher frequency components (Fig. 16). It is, in fact, contradicted by the tendency for wave steepness to decrease with increasing values of T/U.

Some actual measurements of ocean wave spectra have been made by Ijima (1957), but these are for cases so complicated that it is difficult to compare anything but their gross characteristics with the simple expressions of wave spectra (Fig. 21). The spectrum for a relatively simple case is shown in Fig. 16b (Chase, et al, 1957).

It is difficult to obtain certain data for wind waves in the ocean, such as the wave height and period as a function of wind speed for a constant fetch, the wave height and period as a function of fetch for a constant wind speed. In fact it is difficult even to obtain data for either a constant wind speed or fetch, or for even a stationary storm. It is possible to obtain these data in the laboratory or in relatively small lakes or reservoirs. These data are presented in Figs. 22 and 23, together with some ocean data where the fetches were not constant, nor were the fetch limits even stated. The wind velocities were often measured at different elevations above the water surface. However, the elevation where the winds are measured, as long as it is fairly close to the surface, should not affect the power relationship between H and U and T and U, although it will affect the constant of proportionality. That this is true can be seen from a study of the wind-speed data of Thornthwaite and Kaser (1943) for winds at 1/2 and at 15 ft. above the ground, the data of Deacon (1949) for winds at 1/2 and 4 inches above the ground, and the data of Deacon, Sheppard and Webb (1956) for winds at 6.4 and 13 meters above the sea surface. These data show that the winds are linearly related (Fig. 24), the

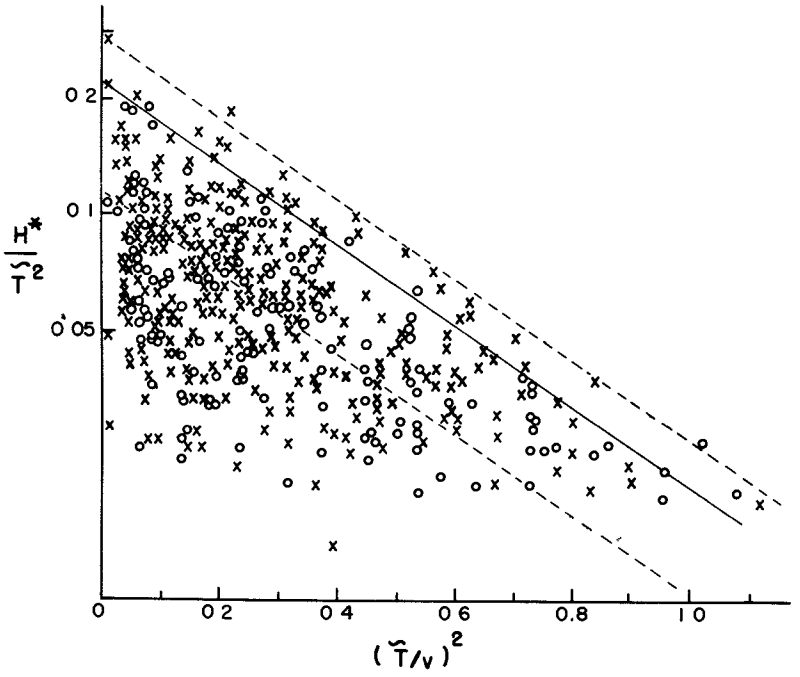

Ratio of the wave heights to the square of the apparent wave periods plotted against the square of the ratio of the apparent wave period to the wind velocity

(after Neumonn, 1953)

Fig. 20

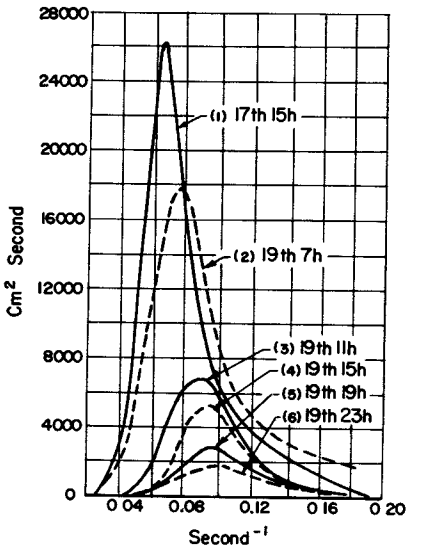

Time changes of wave energy spectrum in the decrease of swell of a typhoon

(after Ijima, 1957)

Fig. 21

slope of the line on the log-log plot being unity.

There is scatter in the data. Some data were taken for neutral stability winds (all of Sibul's laboratory data, for example), some of the data for unstable winds and some of the data for stable winds. A good deal of the scatter is probably due to the different wind types. That this is so has been shown by Roll (1952), Burling (1955) and Brown (1955). The data of Brown are presented in Fig. 25. It can be seen that for a given wind speed the wave heights are higher for both stable and unstable winds for neutral winds (essentially $T_s - T_a = 0$, where T_s is the temperature of the sea surface and T_a is the air temperature). Examples of the three types of wind profiles over the ocean are shown in Fig. 26.

Figures 22 and 23 show that in the laboratory $T_{1/3} \propto U^{0.8}$ and $H_{1/3} \propto U^{1.1}$, approximately (Stanton, Marshall and Houghton, 1932; Hamada, Mitsuyasu, and Hase, 1953; Flinsch, 1946; Sibul, 1955, Ralls and Wiegel, 1956). Studies in a lagoon and in a reservoir show that $T_{mean} \propto U^{0.5}$, $T_{1/3} \propto U^{0.4}$ to $U^{0.5}$ and $H_{1/3} \propto U^{1.1}$ to $U^{1.4}$ (Johnson, 1950; Burling, 1955). Studies in a lake show that $T \propto U^{0.35}$ and $H_{max} \propto U^{1.2}$ to $U^{1.5}$ (Darbyshire, 1956). Most of the data available for ocean waves do not include information even as to the range of fetches for which the measurements were made. The relationships among T, H, and U are for a variety of fetches. The ocean data show $T \propto U^{0.3}$ to $U^{0.4}$ and $H \propto U^{0.5}$ to $U^{1.1}$ (Brown, 1953; Roll, 1953).

The relationships between wave period and fetch and wave height and fetch are not as clear as the relationships among H, T. and U. The laboratory data for constant wind velocities show approximately that $T_{1/3} \propto F^{0.3}$ to $F^{0.5}$, $T' \propto F^{0.5}$, and $H_{1/3} \propto F^{0.5}$ (Hamada, Mitsuyasu and Hase, 1953; Sibul, 1955; Ralls and Wiegel, 1956). The reservoir measurements, for constant wind velocity (Burling, 1955) show $T_{1/3} \propto F^{0.25}$ and $H_{1/3} \propto F^{0.4}$ (Darbyshire, 1956) measurements on a lough give $T/T_{infinity} \propto F^{0.3}$ and $H_{max}/H_{infinity} \propto F^{0.3}$, for varying wind speeds, where $T_{infinity}$ and $H_{infinity}$ refer to values of T and H for infinite fetches. It is interesting to note that Stevenson (1886) found the wave height to be proportional to the square root of the fetch. Because the wave height is proportional to $F^{0.3}$ to $F^{0.5}$ an increase in fetch from 400 nautical miles, say, to 600 nautical miles would cause an increase in wave height of from 12-1/2 to 22-1/2 percent which might not be noticed in the scatter of the data.

The physical reason for the increase in height and period with wind velocity and fetch is clear considering the way wave records are analyzed. Waves in deep water can have a maximum steepness (H/L) of 1/7. Thus at the end of a short fetch enough energy has been trasnferred from the wind to the water to make only the shortest waves of any significant height. As the fetch is increased more energy can only be added to the

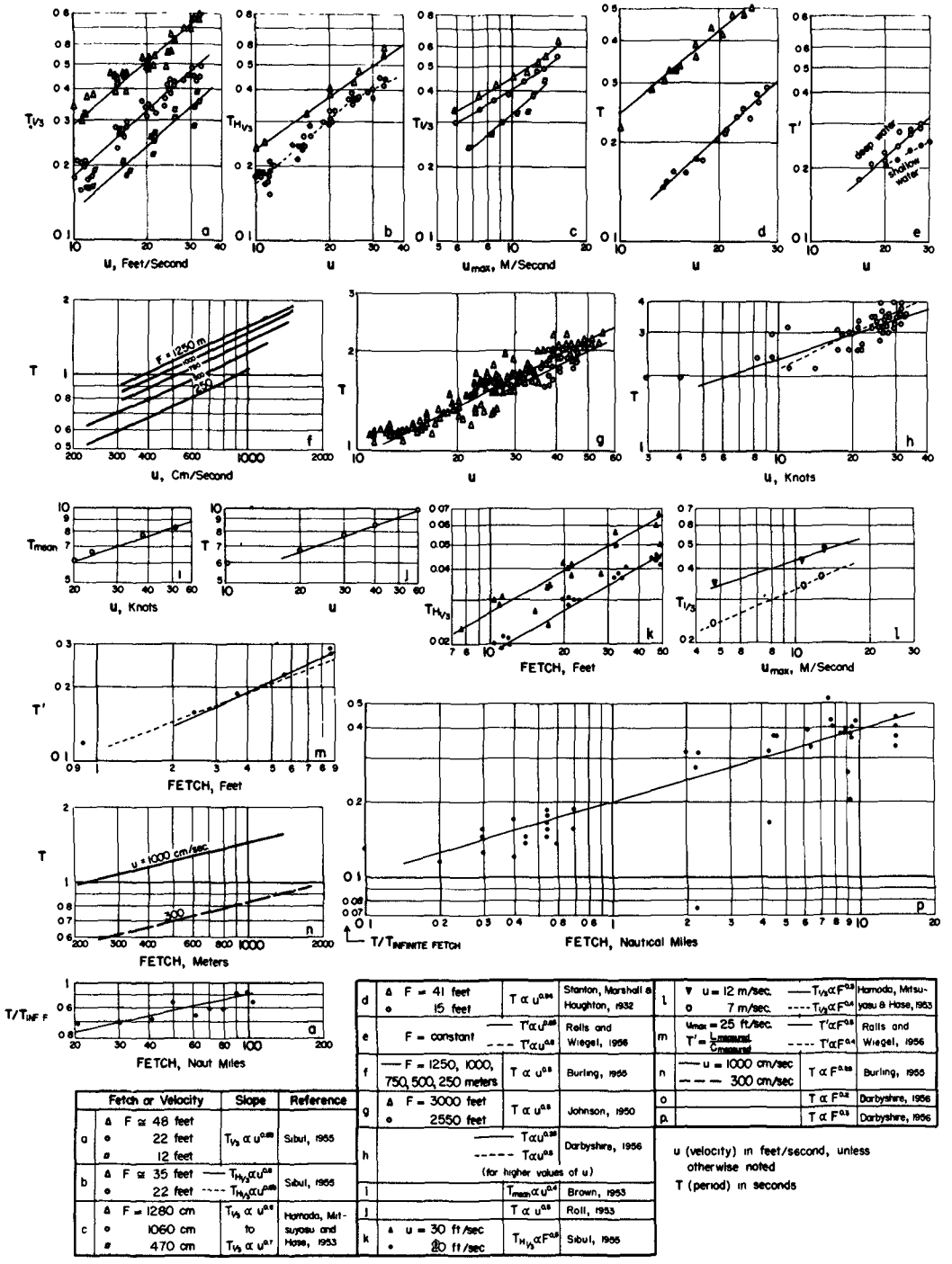

	Fetch or Velocity	Slope	Reference
a	Δ F ≅ 48 feet o 22 feet ▫ 12 feet	$T_{1/3} \propto u^{0.88}$	Sibul, 1955
b	Δ F ≅ 35 feet — $T_{H_{1/3}} \propto u^{0.8}$ o 22 feet ---- $T_{H_{1/3}} \propto u^{0.88}$		Sibul, 1955
c	Δ F = 1280 cm o 1060 cm ▫ 470 cm	$T_{1/3} \propto u^{0.6}$ to $T_{1/3} \propto u^{0.7}$	Hamada, Mitsuyasu and Hasa, 1953
d	Δ F = 41 feet o 15 feet	$T \propto u^{0.96}$	Stanton, Marshall & Houghton, 1932
e	F = constant — $T' \propto u^{0.88}$ --- $T' \propto u^{0.8}$		Rolls and Wiegel, 1956
f	— F = 1250, 1000, 750, 500, 250 meters	$T \propto u^{0.8}$	Burling, 1955
g	Δ F = 3000 feet o 2550 feet	$T \propto u^{0.8}$	Johnson, 1950
h	— $T \propto u^{0.88}$ ----- $T \propto u^{0.8}$ (for higher values of u)		Darbyshire, 1956
i		$T_{mean} \propto u^{0.4}$	Brown, 1953
j		$T \propto u^{0.8}$	Roll, 1953
k	Δ u = 30 ft/sec o 20 ft/sec	$T_{H_{1/3}} \propto F^{0.8}$	Sibul, 1955
l	▽ u = 12 m/sec. — $T_{1/3} \propto F^{0.3}$ o 7 m/sec. ---- $T_{1/3} \propto F^{0.4}$		Hamada, Mitsuyasu & Hasa, 1953
m	u_{max} = 25 ft/sec. — $T' \propto F^{0.3}$ $T' = \frac{L_{measured}}{C_{measured}}$ ---- $T' \propto F^{0.4}$		Rolls and Wiegel, 1956
n	—— u = 1000 cm/sec — — — 300 cm/sec	$T \propto F^{0.88}$	Burling, 1955
o		$T \propto F^{0.2}$	Darbyshire, 1956
p		$T \propto F^{0.3}$	Darbyshire, 1956

u (velocity) in feet/second, unless otherwise noted

T (period) in seconds

Fig. 22. Wave period as a function of fetch and wind speed.

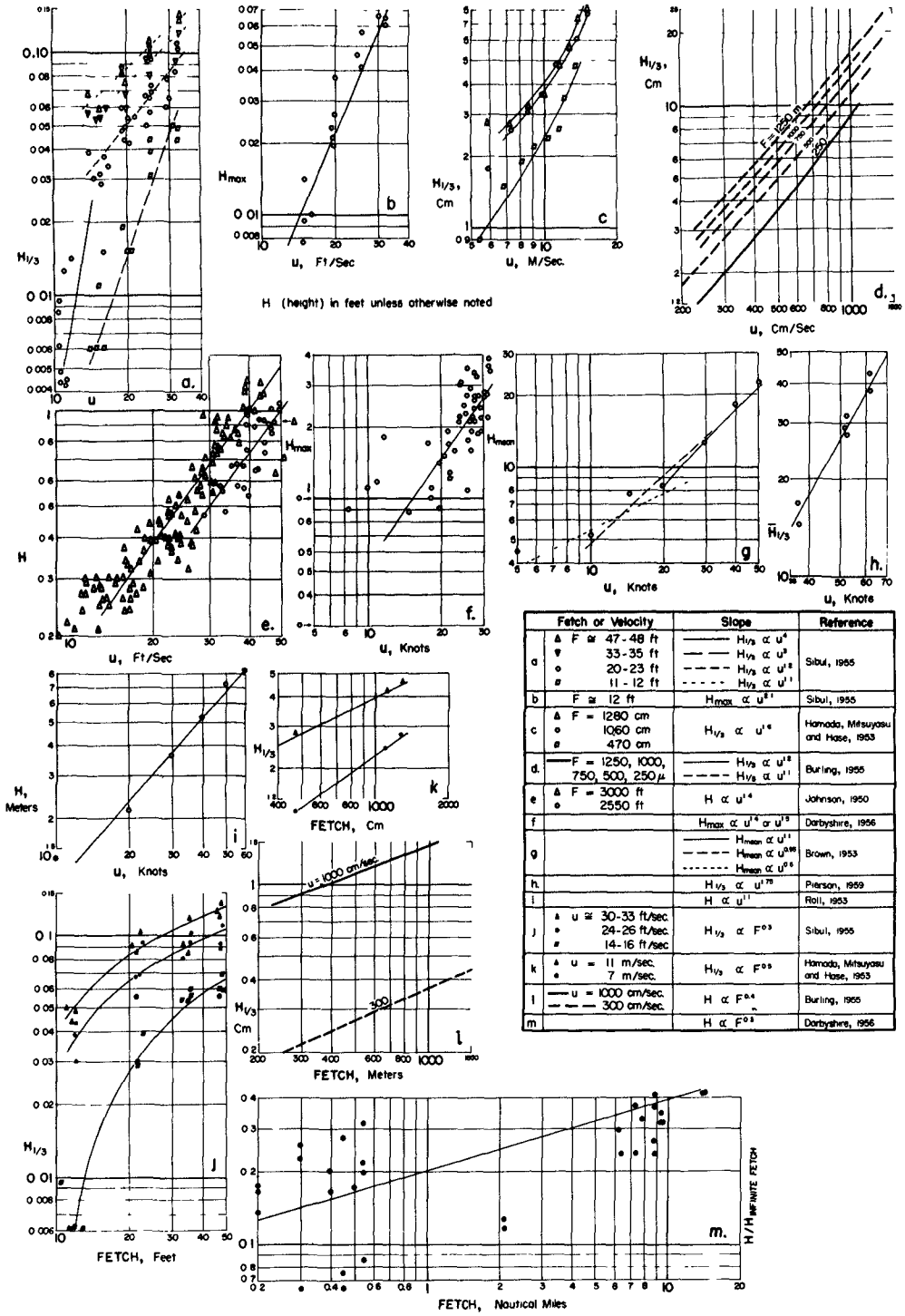

	Fetch or Velocity	Slope	Reference
a	Δ F ≅ 47-48 ft ▼ 33-35 ft ○ 20-23 ft # 11-12 ft	$H_{1/3} \propto u^4$ $H_{1/3} \propto u^3$ $H_{1/3} \propto u^{1.8}$ $H_{1/3} \propto u^{1.1}$	Sibul, 1955
b	F ≅ 12 ft	$H_{max} \propto u^{2.1}$	Sibul, 1955
c	Δ F = 1280 cm ○ 1060 cm # 470 cm	$H_{1/3} \propto u^{1.6}$	Hamada, Mitsuyasu and Hase, 1953
d	F = 1250, 1000, 750, 500, 250 μ	$H_{1/3} \propto u^{1.8}$ $H_{1/3} \propto u^{1.1}$	Burling, 1955
e	Δ F = 3000 ft ○ 2550 ft	$H \propto u^{1.4}$	Johnson, 1950
f		$H_{max} \propto u^{1.6}$ or $u^{1.5}$	Darbyshire, 1956
g		$H_{mean} \propto u^{1.1}$ $H_{mean} \propto u^{0.98}$ $H_{mean} \propto u^{0.6}$	Brown, 1953
h		$H_{1/3} \propto u^{1.78}$	Pierson, 1959
i		$H \propto u^{1.1}$	Roll, 1953
j	Δ u ≅ 30-33 ft/sec ○ 24-26 ft/sec # 14-16 ft/sec	$H_{1/3} \propto F^{0.3}$	Sibul, 1955
k	Δ u = 11 m/sec. ○ 7 m/sec.	$H_{1/3} \propto F^{0.5}$	Hamada, Mitsuyasu and Hase, 1953
l	—— u = 1000 cm/sec. – – – 300 cm/sec.	$H \propto F^{0.4}$ $H \propto F^{0.3}$	Burling, 1955
m		$H \propto F^{0.3}$	Darbyshire, 1956

Fig. 23. Wave height as a function of fetch and wind speed.

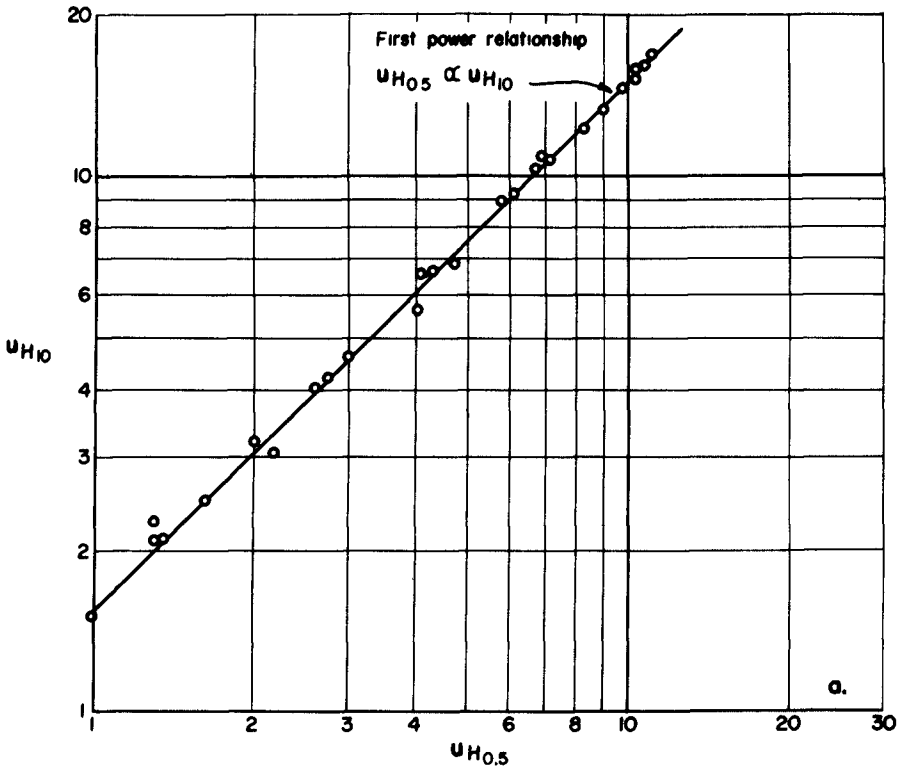

Winds over land (data from Thornthwaite and Kaser, 1943)

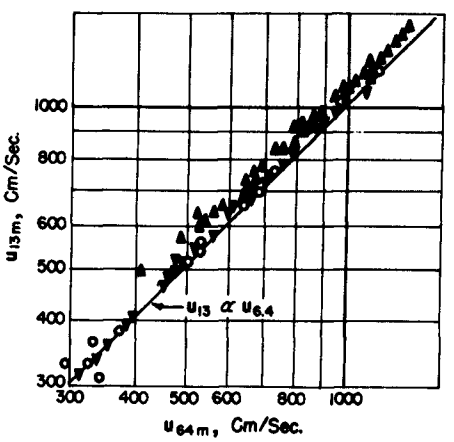

Winds over the sea

▼ $T_a - T_s < -1°F$ ▲ $T_a - T_s > +1°F$
o $T_a - T_s$ from $-1°F$ to $+1°F$

(data from Deacon, Sheppard and Webb, 1956)

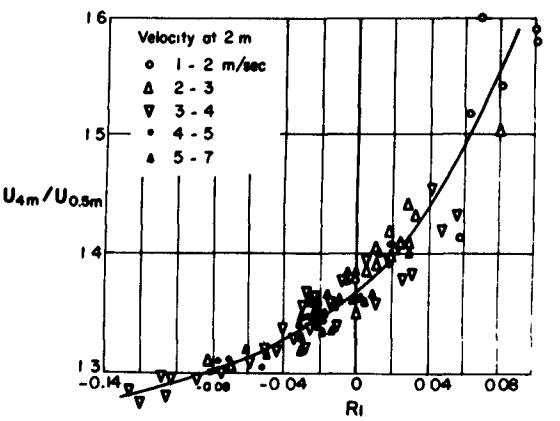

4:0.5 m wind ratio related to Richardson number; short grass surface

(after Deacon, 1949)

Fig. 24

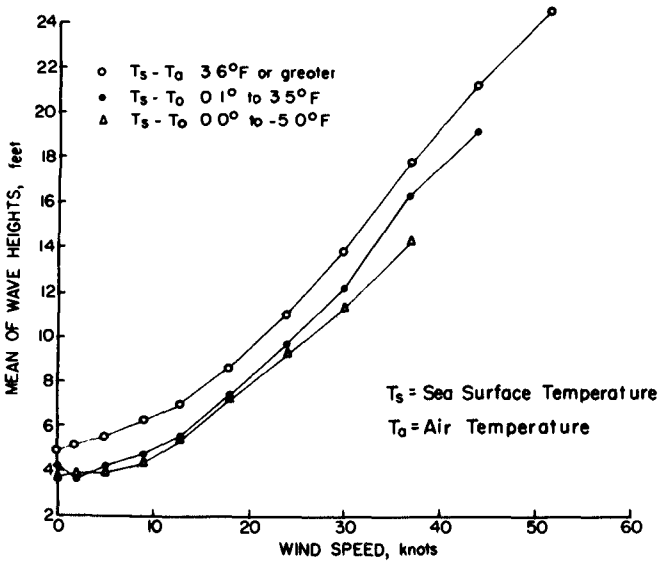

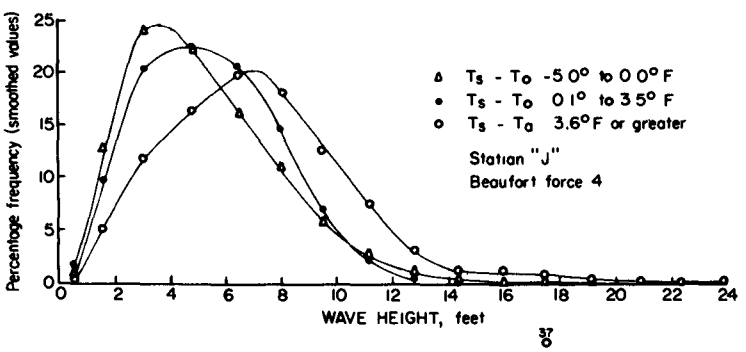

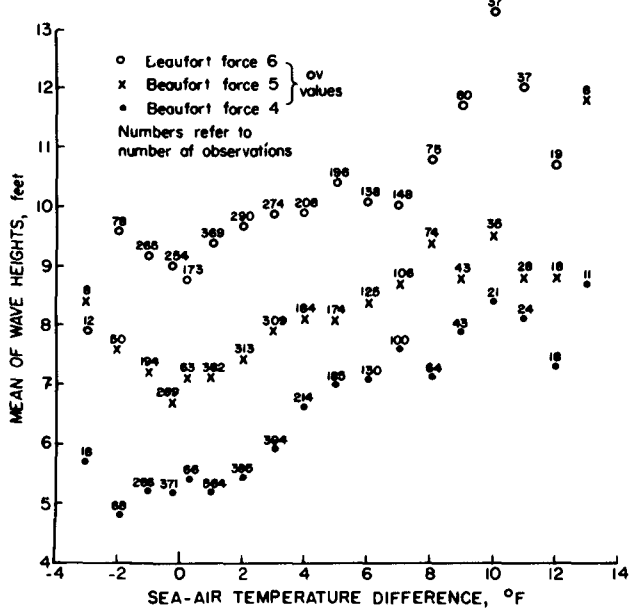

(after Brown, 1953)

Fig. 25

longer waves as the short ones have reached their maximum steepness; the longer waves then dominate the wave system as far as the eye is concerned.

If the wave height and wave period depend upon wind velocity, fetch, duration of wind, air temperature and sea surface temperature, then by dimensional analysis

$$\frac{gT}{U} = f_1\left(\frac{gF}{U}, \frac{gt}{U}, \frac{T_a}{T_s}\right) \tag{7a}$$

$$\frac{gH}{U^2} = f_2\left(\frac{gF}{U^2}, \frac{gt}{U}, \frac{T_a}{T_s}\right) \tag{7b}$$

The functions f_1 and f_2 cannot be determined by dimensional analysis; they must be determined either empirically or theoretically. Effectively then, after quasi-steady-state conditions are reached (gt/U large), the wave height and period depend upon the stability of the wind blowing over the water surface and a Froude number based upon the linear dimension of the storm, as long as the waves are in "deep water." The wave height and period should depend critically upon the turbulence of the air flow, and a logical criteria for this would be a modified Froude number based upon the mean horizontal length of the eddies in the air, such a criteria would be useful in studying coupled wave effects. A more complete analysis would show that in deep water the wave height and period would also depend upon Reynolds number (damping), Webers number (surface tension effects), Richardson number rather than simply T_a/T_s, the ratio of fetch length to fetch width, and a boundary roughness parameter H/L (which of course would be a function of the wind speed, etc., again). The air-sea boundary process is one of fluid flow and thus the dimensionless numbers controlling all other fluid flow processes should be the ones used in describing it, neglecting the ones which obviously are not important in this such as Mach number and the cavitation number. In Fig. 27 are shown the empirical relationships between gT/U and gF/U^2 and gF/U^2 with the effect of T_a/T_s being lost in the scatter of data. The empirical relation ship between gT/U and gt/U and gH/U^2 and gt/U are shown in Fig. 28. In some references curves have been drawn through the data in such a manner that they leveled off in the region of gt/U and gF/U^2 greater than about 10^5. This is because the lines are drawn through the averages of all of the data. A close inspection of the data show that this leveling off did not occur for any of the individual sets of measurements, with the exception of Darbyshire's (1959) data for $gH_{1/3}/U^2$. The best curves through

these individual sets of measurements giving approximately $gT/2\pi U \propto (gF/U^2)^{0.3}$ to $(gF/U^2)^{0.4}$, or $T \propto U^{0.2}$ to $U^{0.4}$, $T \propto F^{0.3}$ to $F^{0.4}$, and $gH/U^2 \propto (gF/U^2)^{0.25}$ to $(gF/U^2)^{0.35}$ or $H \propto U^{1.3}$ to $U^{1.5}$, $H \propto F^{0.25}$ to $F^{0.35}$. These data seem to indicate that the "fully developed sea" does not occur in the open ocean for winds of any importance. Fig. 28 can be treated in a similar manner. Here, $gT/2\pi U \propto (gt/U^{0.3}$, or $T \propto U^{0.7}$, $T \propto t^{0.3}$, and $gH/U^2 \propto (gt/U)^{0.4}$ to $(gt/U)^{0.5}$, or $H \propto U^{1.5}$ to $U^{1.6}$, $H \propto t^{0.4}$ to $t^{0.5}$.

It is clear that these data are in conflict with the original empirical spectrum of Neumann, where $H \propto U^{2.5}$ (Neumann and Pierson, 1957). In order for $H \propto U^{2.5}$ the curve relating gH/U^2 and gF/U^2 would have to have a negative slope, which would also mean that $H \propto F^{-0.25}$ which is in obvious conflict with the physical situation. However, the original spectrum is apparently in the process of being modified to include recent findings (Pierson, 1959b).

There is evidently still a pressing need for a large number of reliable measurements of waves in the open oceans.

The data shown in Fig. 27 are for the case described by Sverdrup and Munk (1947) as "fetch-limited", the other condition being "duration-limited",(Fig. 28). Phillips (1957; 1958) developed a mathematical model that predicted that the mean square wave height is proportional to the square root of time for the duration limited case and to the square root of fetch for the fetch limited case. What is meant by these two terms? Consider an infinite fetch, with the wind suddenly starting with a given velocity and then remaining at this velocity. At any point in the fetch the significant wave height and period will increase with time. The significant waves moving past this point will have travelled a distance equal to the product of the group velocity of the significant waves and the length of time the wind has been blowing. Power will have been added to the wave system by the wind during the entire time. Now real fetches are finite, so eventually the significant waves reaching a given point will be associated with the component wave periods that originated at the beginning of the fetch. The time for this to occur will be the distance divided by the group velocity (Sverdrup and Munk, 1947; Phillips, 1958a). After this duration has been reached the waves are said to be fetch-limited.

It is possible for a third case to exist, the fully developed sea. This case would require a storm duration and fetch both long enough that energy is being dissipated and radiated at the same rate that it is being transferred from the wind to the water in the form of waves.

Some measurements in the laboratory of Sibul (1955) show the

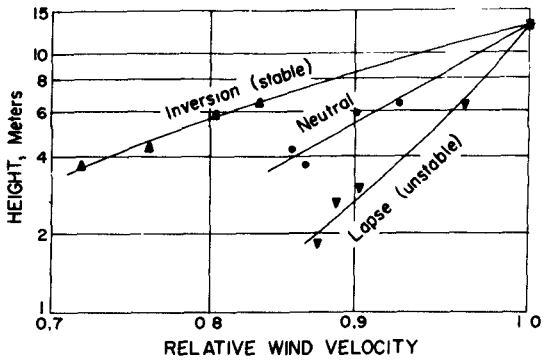

Sample wind profiles

▼ R_i (13 4) = −0 07 • R_i (13 4) = 0 01
▲ R_i (13 4) = 0 18

(after Deacon, Sheppard and Webb, 1956)

Fig. 26

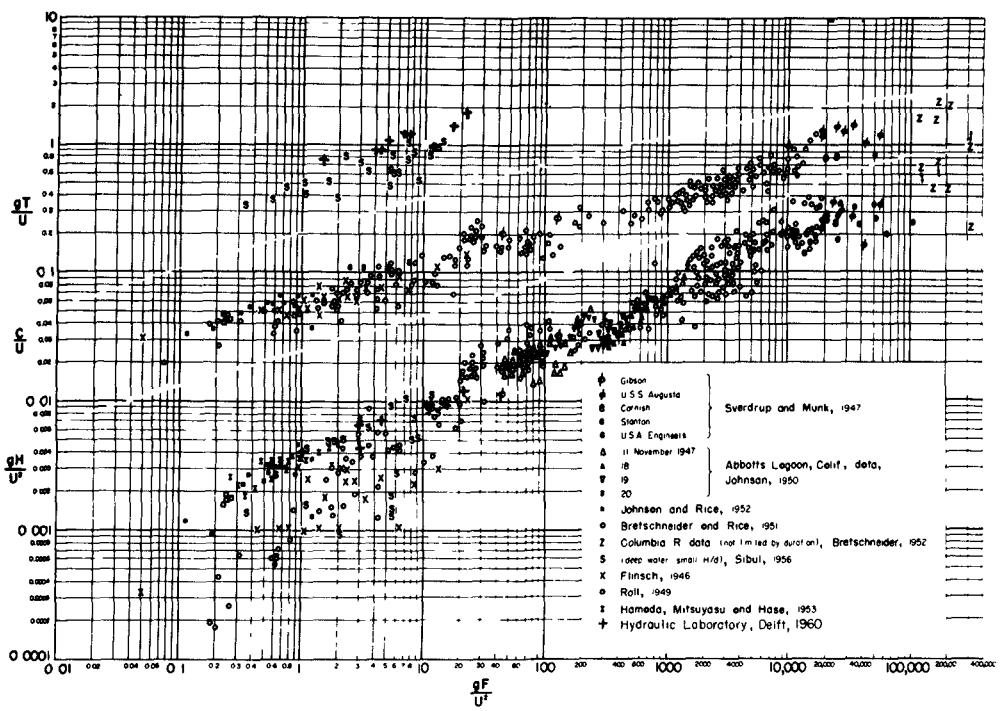

Fig. 27. Relationship among fetch, wind velocity and wave height, period and velocity.

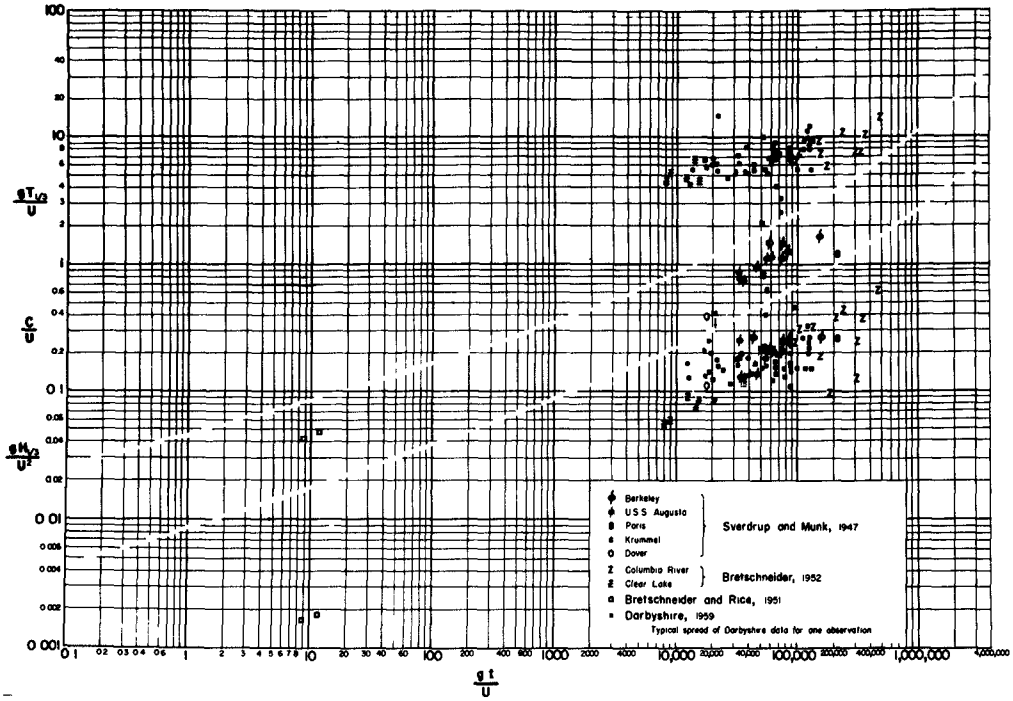

Fig. 28. Relationship among duration wind velocity and wave height, period and velocity.

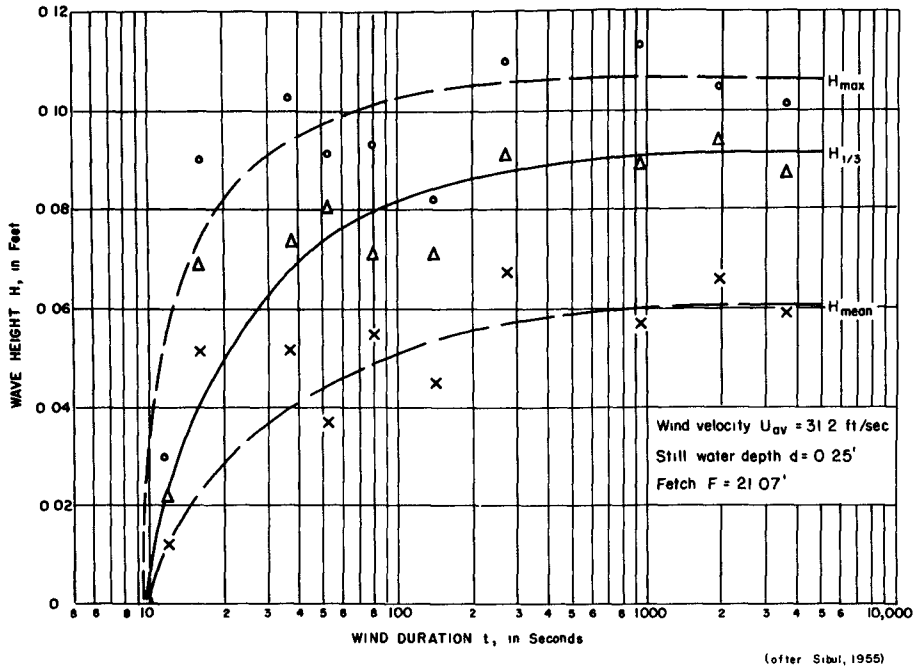

Fig. 29. Wave height as a function of wind duration.

effect of duration-limited and fetch-limited conditions on the wave height as can be seen in Fig. 29.

In Fig. 27 are shown the data for C/U vs gF/U^2. There are a considerable number of measurements that show C/U in excess of unity. This is not surprising, nor is it a paradox. The flow of air over water is a boundary layer phenomenon and the phase speeds of the waves should be related to the free stream wind speed (the geostrophic wind speed) which is in considerable excess of the wind speed at anemometer height, which is the wind speed given for the ocean data of Figs. 27 and 28.

REFERENCES

Arthur, Robert S., Variability in direction of wave travel, Annals of the New York Academy of Sciences, Vol. 51, Art. 3, pp 511-522, May 1949.

Barber, N. F. and F. Ursell, The generation and propagation of ocean waves and swell; I: Wave periods and velocities, Trans. Roy. Soc (London), Ser. A, Vol. 240, No. 824, pp 527-560, Feb. 1948.

Bretschneider, C. L., The generation and decay of wind waves in deep water, Trans. Amer. Geophys. Union, Vol. 33, No. 3, pp 381-389, June 1952.

Bretschneider, Charles L., Field investigation of wave energy loss of shallow water ocean waves, U. S. Army, Corps of Engineers, Beach Erosion Board, Tech. Memo. No. 46, 40 pp, Sept. 1954.

Bretschneider, C. L. and E. K. Rice, The generation and decay of wind waves in a sixty-foot channel, Univ. of Calif., Inst. of Eng. Res., Tech. Rept. 3-327, 16 pp, July 1951 (unpublished).

Bretschneider, C. L., Wave variability and wave spectra for wind-generated gravity waves, U. S. Army, Corps of Engineers, Beach Erosion Board, Tech. Memo. No. 118, 192 pp, Aug. 1959.

Brown, P. R., Wave data for the Eastern North Atlantic, The Marine Observer, Vol. 23, No. 160, pp 94-98, April 1953.

Burling, R. W., Surface waves on enclosed bodies of water, Proc. 5th Conf. on Coastal Engineering, Council on Wave Research, The Engineering Foundation, pp 1-10, 1955.

Burling, R. W., Wind generation of waves on water, Ph.D. Dissertation, Imperial College, University of London, 1955.

California Research Corporation, Table of significant wave heights and mean periods for four hurricanes in the Gulf of Mexico in 30 feet of water, private correspondence, 1 p, May 1960.

Cartwright, D. E. and M. S. Longuet-Higgins, The statistical distribution of the maxima of a random function, Proc. Roy. Soc. (London), Ser. A, Vol. 230, pp 212-232, 1956.

Chase, Joseph, et al, The directional spectrum of a wind generated sea as determined from data obtained by the Stereo Wave Observation Project, New York Univ., College of Engineering, Research Division, Contract Nonr-285(03), 267 pp, July 1957.

Cox, Charles S., Comments on Dr. Phillip's paper, Jour. Marine Research, Vol. 16, No. 3, pp 241-245, Oct. 1958.

Darbyshire, J., The generation of waves by wind, Proc. Roy. Soc., Series A 215, pp 299-328, 1952.

Darbyshire, J., An investigation of storm waves in the North Atlantic Ocean, Proc. Roy. Soc. (London), Ser. A, Vol. 230, pp 560-569, 1955.

Darbyshire, J., The distribution of wave heights, a statistical method based upon observations, The Dock & Harbour Authority, Vol. 37, No. 427, pp 31-32, May 1956.

Darbyshire, J., Attenuation of swell in the North Atlantic Ocean, Quart. Jour. Roy. Met. Soc., Vol. 83, No. 357, pp 351-359, July 1957.

Darbyshire, J., A further investigation of wind generated waves, Deutschen Hydrographischen Zeitschrift, Vol. 12, No. 1, pp 1-13, 1959.

Darlington, C. R., The distribution of wave heights and periods in ocean waves, Quart. Jour. Roy. Met. Soc., Vol. 80, pp 619-626, 1954.

Deacon, E. L., Vertical diffusion in the lowest layers of the atmosphere, Quarterly Journal of the Royal Meteorological Society, Vol. 75, No. 323, pp 89-103, Jan. 1949.

Deacon, E. L., P. A. Sheppard and E. K. Webb, Wind profiles over the sea and the drag at the sea surface, Australian Jour. of Physics, Vol. 9, No. 4, pp 511-541, Dec. 1956.

Donn, William L., and William T. McGuinness, Some results of the IGY island observatory program in the Atlantic, National Academy of Sciences IGY Bull., No. 22, pp 9 - 12, April 1959.

Ehring, H., Kennzeichnung des gemessener Seegans auf Grund der Haufigkeitsveteilung von Wellenhohe, Wellenlange und Steilheit, Techn. Ber., 4, pp 152-155, 1940; translation by Scripps Inst. Oceanogr. Rep. 54, Contract NObs 2490, 1944.

Farmer, H. G., Some recent observations of sea surface elevation and slope, Woods Hole Oceanogr. Inst. Ref. 56-37, 67 pp, June 1956 (unpublished manuscript).

Flinsch, H. V. N., An experimental investigation of wind-generated surface waves, Ph.D. Thesis, Univ. of Minn., June 1946 (unpublished).

Folsom, R. G., Measurement of ocean waves, Trans. Amer. Geophys. Union, Vol. 30, 691-699, 1949.

Fuchs, R. A., On the theory of irregular waves, Proc. First Conf. on Ships and Waves, Council on Wave Research and the Soc. Nav. Arch. and Mar. Engineers, pp 1 - 10, 1955.

Gerhardt, J. R., K. H. Jehn, and I. Katz, A comparison of step-pressure, and continuous-wire-gage wave recordings in the Golden Gate Channel, Trans. Amer. Geophys. Union, Vol. 36, pp 235-250, 1955.

Gibson, George E., Investigation of the calming of waves by means of oil films, Woods Hole Oceanogr. Inst., 20 April 1944 (unpublished)

Hamada, Tokuichi, Hisashi Mitsuyasu, and Maoki Hase, An experimental study of wind effect upon water surface, Report of Transportation Technical Research Institute (Tokyo), 22 pp, June 1953.

Harney, L. A., J. F. T. Saur, Jr. and A. R. Robinson, A statistical study of wave conditions at four open-sea localities in the North Pacific Ocean, N.A.C.A. Tech. Note 1493, Washington, D. C., 28 pp, 1949.

Hydraulics Laboratory, Delft, Golfaanval haringvlietsluizen. Deel II, Systematisch onderzoek golfaangroei en dynamische golfbelasting,

Code 32.79, M 399-II, 61 pp, March 1960.

Ijima, Takeshi, The properties of ocean waves on the Pacific Coast and the Japan Sea Coast of Japan, Transportation Technical Research Institute, Tokyo, Report No. 25, 87 pp, June 1957.

Johnson, J. W., The characteristics of wind waves on lakes and protected bays, Trans. Amer. Geophys. Union, Vol. 29, No. 5, pp 671-681, Oct. 1948.

Johnson, J. W., Relationship between wind and waves, Abbots Lagoon, California, Trans. Amer. Geophys. Union, Vol. 29, No. 3, pp 671-681, June 1950.

Johnson, J. W., and E. K. Rice, A laboratory investigation of wind-generated waves, Trans. Amer. Geophys. Union, Vol. 33, No. 6, pp 845-854, December 1952.

Longuet-Higgins, M. S., On the statistical distribution of the heights of sea waves, J. Mar. Res., Vol. 11, No. 13, pp 245-266, Dec. 1952.

Marks, Wilbur, Analysis of the performance of the NIO Ship-borne wave recorder installed in the R. V. Atlantis, Woods Hole Ocean. Inst., Ref. No. 55-64, 27 pp, November 1955 (unpublished manuscript).

Marks, Wilbur, Woods Hole Oceanographic Institution participation in the stereo-wave observation program, October 1954, Woods Hole Ocean. Inst., Ref. No. 56-44, 51 pp, July 1956 (unpublished manuscript).

Munk, W. H. and R. S. Arthur, Forecasting ocean waves, Compendium of Meteorology, Amer. Met. Soc., pp 1082-1089, 1951.

Neumann, Gerhard, Uber die komplexe natur des seeganges, Deutsche Hydrographische Zeitschrift, Vol. 5, No. 2/3, pp 95-110, 1952.

Neumann, Gerhard, On wind generated ocean waves with special reference to the problem of wave forecasting, New York University, College of Engineering, Department of Meteorology, Contract Nonr-285(05), May 1952 (unpublished).

Neumann, Gerhard, On ocean wave spectra and a new method of forecasting wind-generated sea, U. S. Army, Corps of Engineers, Beach Erosion Board, Tech. Memo. No. 43, 42 pp, Dec. 1953.

Neumann, Gerhard, On wind-generated wave motion at subsurface

levels, Trans. Amer. Geophys. Union, Vol. 36, No. 6, pp 985-992, Dec. 1955.

Neumann, Gerhard and Willard Pierson, Jr., A detailed comparison of theoretical wave spectra and wave forecasting methods, Deutschen Hydrographischen Zeitschrift, Band 10, Heft 3, pp 73-92, and Band 10, Heft 4, pp 134-146, 1957.

Phillips, O. M., On the generation of waves by turbulent winds, Jour. of Fluid Mechanics, Vol. 2, Part 5, pp 417-445, July 1957.

Phillips, O. M., Wave generation by turbulent wind over a finite fetch, Proc. Third U. S. National Congress of Applied Mechanics, ASME, pp 785-789, June 1958(a).

Phillips, O. M., The equilibrium range in the spectrum of wind-generated waves, Jour. of Fluid Mechanics, Vol. 4, Part 4, pp 426-434, Aug. 1958(b).

Phillips, O. M., On some properties of the spectrum of wind-generated ocean waves, Jour. Marine Research, Vol. 16, No. 3, pp 231-240, Oct. 1958(c).

Pierson, Willard J., Jr., A note on the growth of the spectrum of wind-generated gravity waves as determined by non-linear considerations, New York Univ., College of Engineering, Research Division, Contract Nonr-285(03), 11 pp, Feb. 1959(a) (unpublished).

Pierson, Willard J., Jr., A study of wave forecasting methods and the height of a fully developed sea on the basis of some wave records obtained by the O. W. S. Weather Explorer during a storm at sea, New York Univ., College of Engineering, Research Div., Contract Nonr-285(03), 33 pp, June 1959 (b) (unpublished).

Pierson, Willard J., Jr. and Wilbur Marks, The power spectrum analysis of ocean-wave records, Trans. Amer. Geophys. Union, 33, pp 834-844, 1952.

Pierson, Willard J., Jr., Gerhard Neumann, and Richard W. James, Practical methods for observing and forecasting ocean waves, U. S. Navy Hydrographic Office, Pub. 603, 284 pp, 1955.

Putz, R. R., Joint variation of wave height and wave period for ocean swel Univ. of Calif., Inst. of Eng. Res., Tech. Rept. 3-328, 18 pp, Oct. 1951 (unpublished).

Putz, R. R., Statistical distributions for ocean waves, Trans. Amer. Geophys. Union, Vol. No. 33, No. 5, pp 685-692, Oct. 1952.

Ralls, G. C., Jr. and R. L. Wiegel, A laboratory study of short-crested wind waves, U. S. Army, Corps of Engineers, Beach Erosion Board, Tech. Memo. No. 81, 28 pp, June 1956.

Roll, Hans Ulrich, Uber die ausbreitung der meereswellen unter der wirkung des windes (auf grund von messungen im wattenmeer), Deutsche Hydrographische Zeitschrift, Band 2, Heft 6, 1949.

Roll, Hans Ulrich, Uber groszenumterschiede der meereswellen bei warm-und kaltluft, Deutsche Hydrographische Zeitschrift, Vol. 5, No. 213, pp 111-114, 1952.

Roll, H. U., Height, length and steepness of seawaves in the North Atlantic and dimensions of seawaves as functions of wind force, Special Publication No. 1 of the Office of Sea-Weather Service, 1953, Translation by Manley St. Denis, Tech. Res. Bull. No. 1-19, The Society of Naval Architects and Marine Engineers, 98 pp, Dec. 1958.

Roll, H. U. and G. Fischer, Eine kritische bemerkung zum Neumann-spektrom des seeganges; Deutschen Hydrographischen Zeitschrift, Vol. 9, No. 1, pp 9, 1956.

Rudnick, P., Correlograms for Pacific Ocean waves, Prof. Second Berkeley Symposium on Mathematical Statistics and Probability, Univ. Calif. Pres, pp 627-638, 1951.

Scripps Institution of Oceanography, Proposed uniform procedure for observing waves and interpreting instrument records, Wave Project Report No. 26, 1944.

Seiwell, H. R., Results of research on surface waves of the western North Atlantic, Paper Phys. Oceanogr. Met., Vol. 10, No. 4, 56 pp, 1948.

Sibul, Oswald, Laboratory study of the generation of wind waves in shallow water, U. S. Army, Corps of Engineers, Beach Erosion Board, Tech. Memo. No. 72, 35 pp, March 1955.

Stanton, T., D. Marshall and R. Houghton, The growth of waves on water due to action of the wind, Proc. Roy. Soc., Ser. A, Vol. 137, pp 283-293, 1932.

Stevenson, Thomas, Generation of waves, Ch. 3, "The Design and

Construction of Harbours", 3rd Ed., A. & C. Black, Edinburgh, pp 26-40, 1886.

Sverdrup, H. V. and W. Munk, Wind, sea and swell. Theory of relatio for forecasting, U. S. Navy Hydrographic Office Pub. No. 601, 4 pp, 1947.

Thornthwaite, C. W. and Paul Kaser, Wind-gradient observations, Tra Amer. Geophys. Union, Part I, pp 166-182, Oct. 1943.

Tick, Leo J., A non-linear random model of gravity waves, New York University, College of Engineering, Research Division, Scientific Paper No. 11, 11 pp, Oct. 1958 (unpublished).

Tucker, M. J., A ship-borne wave recorder, Proc. First Conf. Coasta Eng. Inst., Council on Wave Research, The Engineering Foundation, pp 112-118, 1956.

Watters, Jessie K. A., Distribution of height in ocean waves, New Zealand J. Sci. Tech., B, Vol. 34, 408-422, 1953.

Wiegel, R. L., An analysis of data from wave recorders on the Pacific Coast of the United States, Trans. Amer. Geophys. Union, Vol. 3 pp 700-704, 1949.

Wiegel, R. L. and J. Kukk, Wave measurements along the California co Trans. Amer. Geophys. Union, Vol. 33, No. 5, pp 667-674, Oct. 1957.

Williams, A. J. and D. E. Cartwright, A note on the spectra of wind waves, Trans. Amer. Geophys. Union, Vol. 38, No. 6, pp 864-86 Dec. 1957.

Yampol'ski, A. D., On a certain characteristic of three dimensional wave motion, Priroda, Vol. 5, pp 80-81, 1955.

Yoshida, K., K. Kajiura, and K. Hidaka, Preliminary report of the observation of ocean waves at Hachijo Island, Rec. Oceanogr. Works Japan, ser. 1, pp 81-87, March 1953.

CHAPTER 2

THE QUALITY OF TABULATED DECK LOG SWELL OBSERVATIONS

Marvin D. Burkhart and Clifford H. Cline
Division of Oceanography
U. S. Navy Hydrographic Office, Washington 25, D. C.

INTRODUCTION

To determine the areas of data deficiencies, the totals of sea and swell observations were summarized by unit Marsden squares for the world. An interesting result of this summary was a comparison of the totals of sea and swell observations. The totals of swell observations averaged two-thirds those of sea observations. Although this ratio was fairly representative of the ocean basins, considerable variation occurred in semi-enclosed seas where swell observations averaged only one-tenth those of sea observations. A few ocean basin locations had totals of swell observations that approached those of sea observations, but no Marsden square had more swell observations than sea observations. Strangely enough, swell tabulations, in areas where the ratio of swell to sea observations were smallest (semi-enclosed basins), appeared least reliable although it was suspected at the time that this was probably due to smallness of the sample. Subsequent additions of card decks have neither changed these ratios appreciably nor the suspect reliability.

Thus, due to the relative sparseness of observations in some areas and the inexplainable ratios of swell to sea observations in others, the quality of observations contained in IBM listings have for some time been questioned.

DEFINING THE PROBLEM

An investigation of log sheets and listed observations from marine-punched card decks show that many observers never seem to make swell observations. Hundreds of sea observations will be noted in the log sheets, but the adjoining swell columns are left blank. It is probable that these sea observations are actually wave observations and include both sea and swell. A small number of swell observations may be recorded with no associated sea observations. In some instances cards contain neither a sea nor a swell observation. In many log sheets, the same code figures are recorded in both the sea and swell columns. Here the observer may have made an observation of waves and, being unable to distinguish between sea and swell, may have recorded the same code figure in each column.

By the time these sea and swell observations are included in IBM listings, little can be done to counteract these misrepresentations. Even if corrections were attempted on the original log sheets, it would be necessary to second guess the observer, something which is seldom reliable. Nevertheless, some systematic approximation is desirable to increase the reliability of such data.

THE BASIS FOR AN APPROXIMATE SOLUTION

No solution to the problem of identical data is apparent because some of these observations may be valid and others may be associated with some type of swell incorrectly coded. It can only be hoped that these errors represent a small portion of the total observations.

The cards containing neither sea nor swell observations can be eliminated immediately because they constitute no observation of the sea surface.

Sea observations are included on most marine punched cards. Nevertheless, in Marsden square 116, February, 264 out of 3,235 cards recorded a swell observation without a sea observation. More than half of these "missing" sea observations were associated with winds of Beaufort force 3 or less; therefore, it might be assumed that the sea surface was relatively smooth on these occasions. In any event this represents less than 9 percent of the total chances to observe the sea. Other Marsden squares exhibit similar ratios of "missing" sea observations, and this loss of observations probably will not materially affect the sea tabulations.

Swell, however, is considerably different. Of the Marsden squares checked the totals of swell observations were always less than those of sea observations. For example, in Marsden square 116, February, there were 2,871 sea observations and 701 swell observations. In Marsden square 149, August, there were 4,805 sea observations and 2,135 swell observations while in Marsden square 214, January, there were 981 sea observations and only 81 swell observations. At first glance this reflects what should be expected in the open ocean — a sea of some kind usually present, and a discernable swell present only part of the time. However, if no swell were present, or if swell were present but completely masked by the sea, the observer should have recorded "no swell" in the swell column; consequently, his log sheets would have shown as many swell observations as sea observations. For example, if 1,000 observations of the sea surface were made by an observer, and he observed and recorded swell only 100 times, the swell rose would be based only on these 100 observations and would not show observations of "no swell". A rose based on data of this type implies that there is always swell present and its various heights occur 100 percent of the time. Actually 1,000 observations were made, of which 900 indicated "no swell". Thus a rose made from data of this type implies that 90 percent of the time no swell occurs and the various observed swell heights occur only 10 percent of the time. In practice it can not be said with certainty that there was no swell the 900 times the swell column was left blank. The blank column only implies that the observer either saw no swell or was not sufficiently impressed by what he saw and did not complete the observation. It is also possible that the observations in the sea column are really wave observations, embodying both sea and swell.

THE QUALITY OF TABULATED DECK LOG SWELL OBSERVATIONS

Two points might explain why observers sometimes fail to record swell: 1) With winds of Beaufort force 7 or higher, 10 foot significant waves can be generated over a fetch of only 40 miles. With such winds it is difficult or impossible for an observer to distinguish any swell. Also a fully developed sea from Beaufort force 7 winds would have sea waves with heights as high as and periods as long as any swell present. 2) With winds of Beaufort force 3 or less, a fully developed sea rises to less than 2 feet. Any observer, seemingly, could detect a swell of 1 or more foot (swell code 1 and above) when seas are low and periods are less than 6 seconds (average periods of 3 seconds). When the winds are of Beaufort force 3 or less and nothing is recorded in the swell column, presumably no swell occurred.

Such arguments might also apply to the "missing" swell observations associated with Beaufort force 4, 5, and 6 winds. If the observation was taken during the onset of such winds, the seas would still have been very low and the swell present could have been seen easily; however, seas may have been nearly fully developed and high enough to obscure any swell.

The above reasons obviously cannot be valid for all the "missing" swell observations; nevertheless, when the observer fails to record swell, he implies "no swell" whatever the actual conditions might have been at the time of observation. Seemingly, all the "missing" swell observations should be considered as "no swell" if a true distribution of observations, as seen by the observers, is to be presented. To test this idea observations from a number of Marsden squares were listed by month. Examples of these listings are shown in Table I.

Table I

SUMMARY OF LISTINGS OF OBSERVATIONS FROM TWO MARSDEN SQUARES

	Marsden square 149 - August	Marsden square 116 - February
Total number of cards	6,051	3,182
Total sea observations	4,805	2,871
Total swell observations	2,135	701
No swell	216	95
Confused swell	112	23
Swell 1 to 12 feet	1,711	492
Swell greater than 12 feet	96	91
Total occurrences of sea and swell on same card	1,186	437
Total chances to observe sea surface	5,754	3,135
Total "missing" swell observations (assumed "no swell")	3,619	2,434

Percentage frequencies of the various swell height categories were computed based on the actual total of swell observations and the total number of chances to observe the sea surface. Examples of these results are presented in Table II.

Table II

PERCENT FREQUENCY OF SWELL IN VARIOUS HEIGHT CATEGORIES BASED ON UNMODIFIED AND MODIFIED DATA

Marsden square 149 - August

	Based on 2,135 actual swell observations	Based on 5,754 chances to observe the sea surface
No swell	10.1	66.6
Confused swell	5.3	2.0
Swell 1 to 12 feet	80.1	29.7
Swell > 12 feet	4.5	1.7
	100.0	100.0

Marsden square 116 - February

	Based on 701 actual swell observations	Based on 3,135 chances to observe the sea surface
No swell	13.5	80.7
Confused swell	3.3	0.7
Swell 1 to 12 feet	70.2	15.7
Swell > 12 feet	13.0	2.9
	100.0	100.0

Table II indicates quite clearly that the inclusion of the large number of "no swell" observations radically increases the percent of time without swell, thereby decreasing the percentage of time with other swell conditions. In many studies the percentages of swell observations greater than 12 feet, within a defined area, are contoured and then spoken of as the "percent of time swell is greater than 12 feet". Actually the contours are of the percent of swell observations that record swell greater than 12 feet and are not at all representative of the percent of time. However if the observations of swell greater than 12 feet were related to the total number of chances to observe the sea surface, they would then be representative of the percent of time.

Except for listings covering a limited number of widely separated Marsden squares, the actual number of chances to observe the sea surface is unavailable in the data tabulations at the Hydrograph Office. Sea and swell have been summarized separately, and the only totals available are those for sea observations and those for swell observations. The true number of chances is some number that lies between the number of sea observations and the number of sea observations plus the number of swell observations. In the few Marsden squares checked, about one-half of the swell observations was taken at the same time as a sea observation. This would indicate that the total number of chances would be the number of sea observations plus one-half of the total number of swell observations. However, the

squares checked do not constitute a large sample, and in view of the available data it is suggested that the total number of sea observations be used to determine a corrected value. In Table III the present method is compared with the three suggested methods of modification.

Table III

COMPARISON OF DERIVED PERCENTAGES OF SWELL HEIGHTS FOR MARSDEN SQUARE 149 - AUGUST

1st row: Present method — using only the swell cards as the total number of chances to observe swell.

2nd row: Using the number of sea observations as the total number of chances.

3rd row: The true number of chances, i.e., the number of cards with a sea and/or a swell observation.

4th row: Number of sea observations plus 1/2 the number of swell observations.

Row	No swell < 1 foot	Low and medium swell 1 to 12 feet	High swell > 12 feet	Confused swell
1	10.1	80.1	4.5	5.3
2	60.1	35.6	2.0	2.3
3	66.6	29.7	1.7	2.0
4	67.4	29.1	1.6	1.9

MODIFICATION OF ISOLINE PRESENTATIONS

Figures 1 through 6 were prepared to illustrate the comparison between the present method and the method of modification using the number of sea state observations as the total number of observations. On these figures isolines of the frequency of occurrence of swell greater than 12 feet are presented for a representative month of each season. The isolines are based on tabulations by 2-degree quadrangles for the entire North Atlantic Ocean and its adjacent seas. These tabulations are based upon the entire volume of punch-card observations available at National Weather Records Center, Ashville, N. C. and the U. S. Navy Hydrographic Office as of 1958. Certain portions of the area, in particular north of 50°N. and west of 50°W., parts of the Baltic and its adjacent gulfs, and the entire water area north of Iceland except for the shipping lane along the Norwegian coast, contain little data. Therefore, the analysis of these sections merits a lesser degree of confidence than elsewhere in the area. The analysis in certain remote sections is based upon as few as 20 chances to observe the sea surface per 2-degree quadrangle or as many as 8,000 per 2-degree quadrangle along the most frequently traveled routes. In general 200 to 400 chances to observe the sea surface per 2-degree quadrangle occur over the major portion of the area from 20°N. to 60°N.

Figure 1, the winter chart, is based only upon original totals of actual swell observations and shows an axis of maximum frequency of high swell along each of the major storm tacks in the North Atlantic. Throughout a large portion of the central North Atlantic, frequencies of high swell reach and exceed 40 percent. A comparison with frequencies of seas equal to and exceeding 12 feet in height for the same area and based upon the same card decks reveals that no frequency reaches 40 percent. Although this excess of swell is possible (because swell has many origins), it appears unlikely along the major storm tracks where low wind speeds are rare and where seas are almost always predominant.

Perhaps even more significant are the high frequencies of swell greater than 12 feet in the Mediterranean and especially in the Baltic. In the Baltic, for example, swells greater than 12 feet, since they must originate from local seas, should never exceed the frequencies of seas of the same height or higher. This figure shows frequencies as high as 40 percent for high swell in the Baltic while sea charts, based upon the same data sources, show only 5 to 10 percent frequencies for seas equal to or greater than 12 feet in the same area.

The swell frequencies used in Figure 1 have been modified in Figure 2 by using the total of the sea state observation as the number of chances to observe swell. The 40 percent maximum frequencies of high swell in the central North Atlantic have now been reduced to two small cells west of Ireland. Similar reductions occur almost everywhere in the North Atlantic and Mediterranean. In the Baltic, meanwhile, in view of the small ratio of swell to sea frequencies of high swell are now in the 1 to 5 percent range and well within that realm of occurrence allowed by the 5 to 10 percent frequencies of seas equal to or greater than 12 feet.

In the summer chart (Figure 4, original swell data) the storm tracks have been forced northward by the expanded North Atlantic high pressure cell. Two significant features of this map are the maximum of high swell south and east of Greenland and the ever present maximum in the Baltic. In the same month, Figure 5, based upon modified swell data, indicates a great reduction in the Greenland high swell maximum and complete destruction of the Baltic maximum.

Modified data for spring and autumn (May and November) are included to complete the series in Figures 3 and 6 respectively. These figures have undergone similar reductions in data and result in patterns that show better agreement to the climatology. Figure 6 although the result of considerable modification, is indicative of rough autumn conditions in the North Atlantic and appears to overemphasize frequencies of high swell. Although this points out the incompleteness of the approach, it is much better than the original method. Data based upon the total number of chances to observe the sea surface would probably be more representative of actual conditic

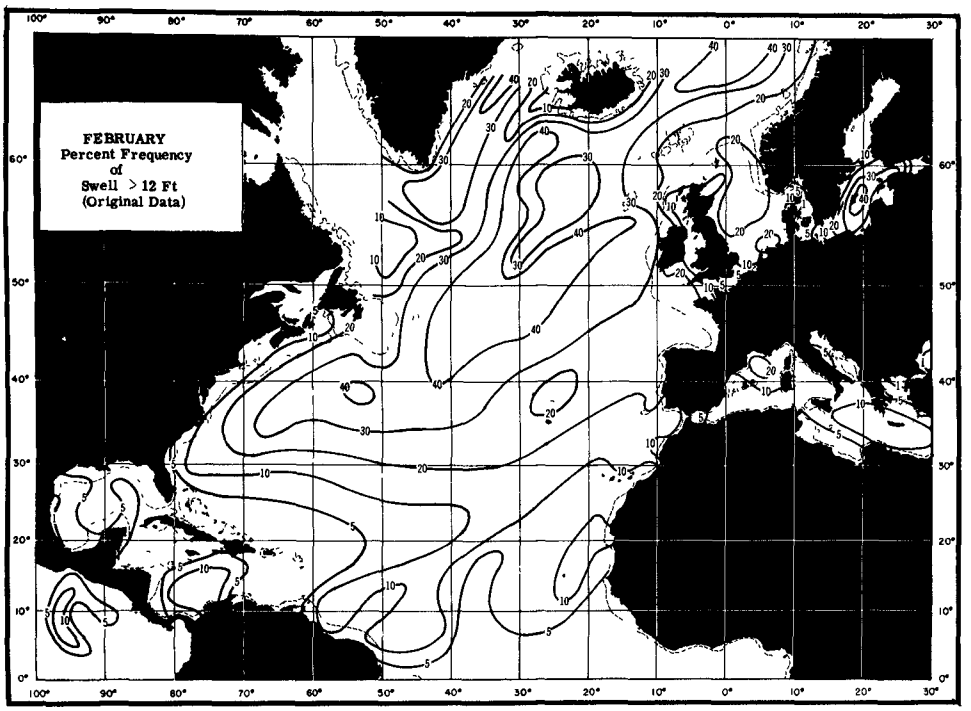

Fig. 1. Swell > 12 feet, February (Original Data)

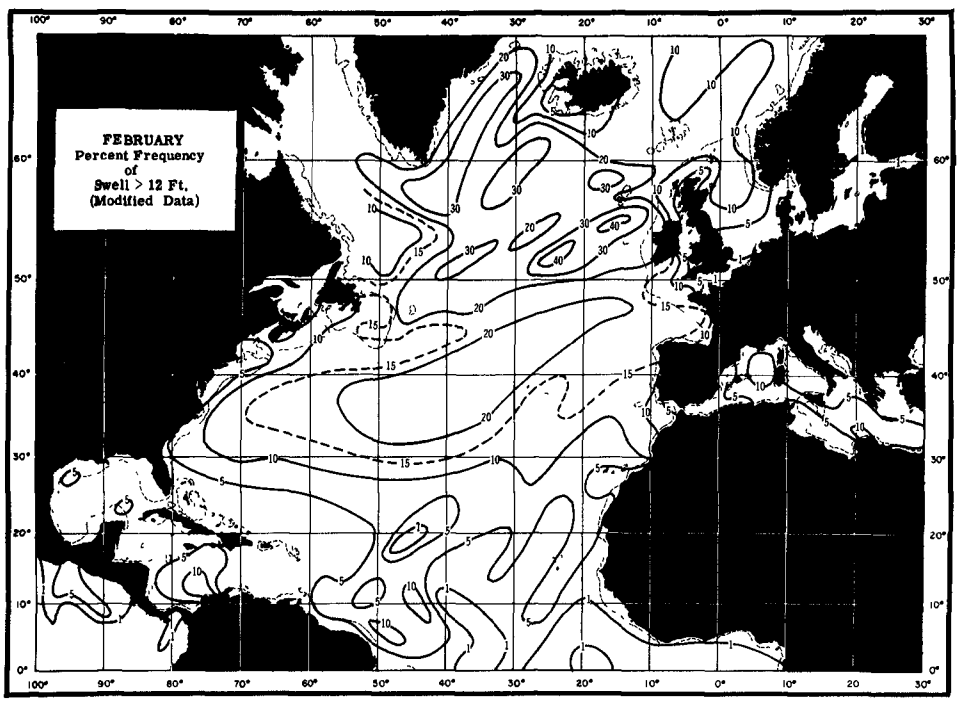

Fig. 2. Swell > 12 feet, February (Modified Data)

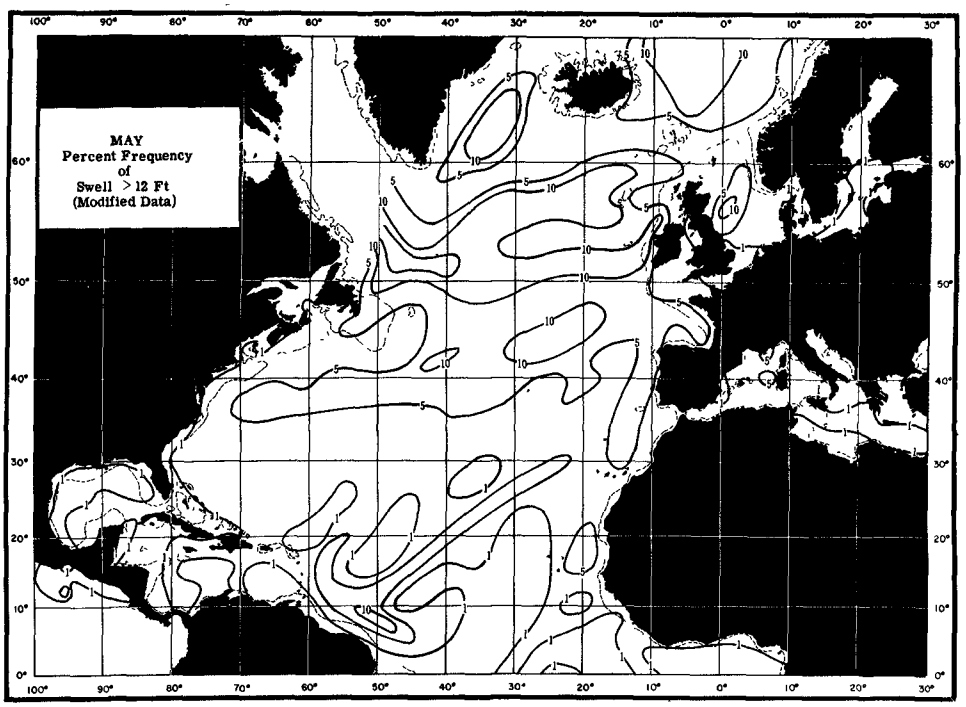

Fig. 3. Swell > 12 feet, May (Modified Data)

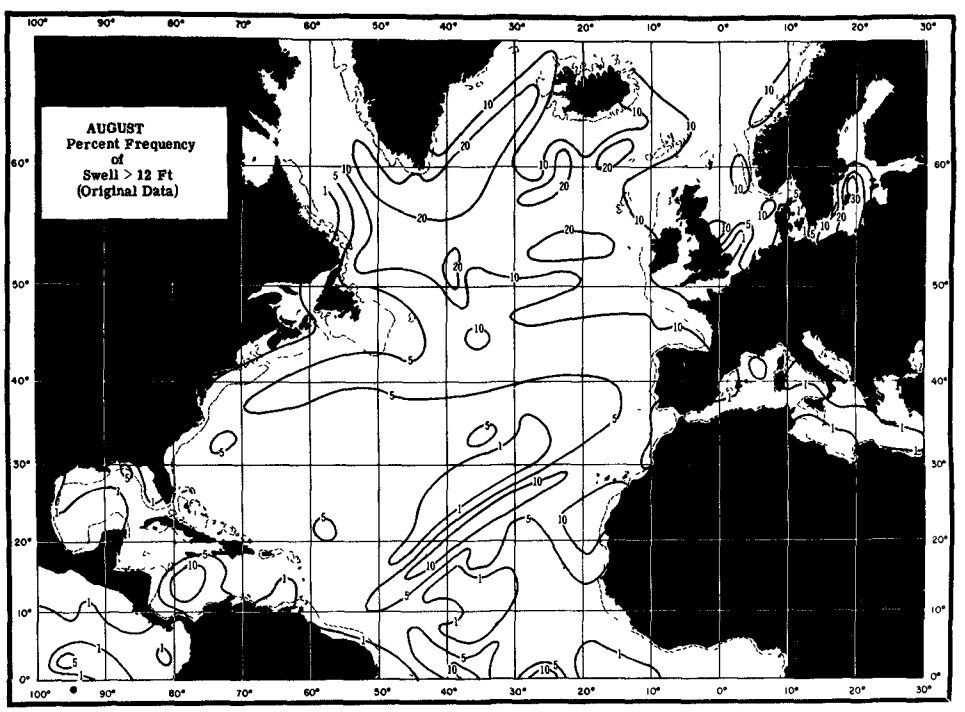

Fig. 4. Swell > 12 feet, August (Original Data)

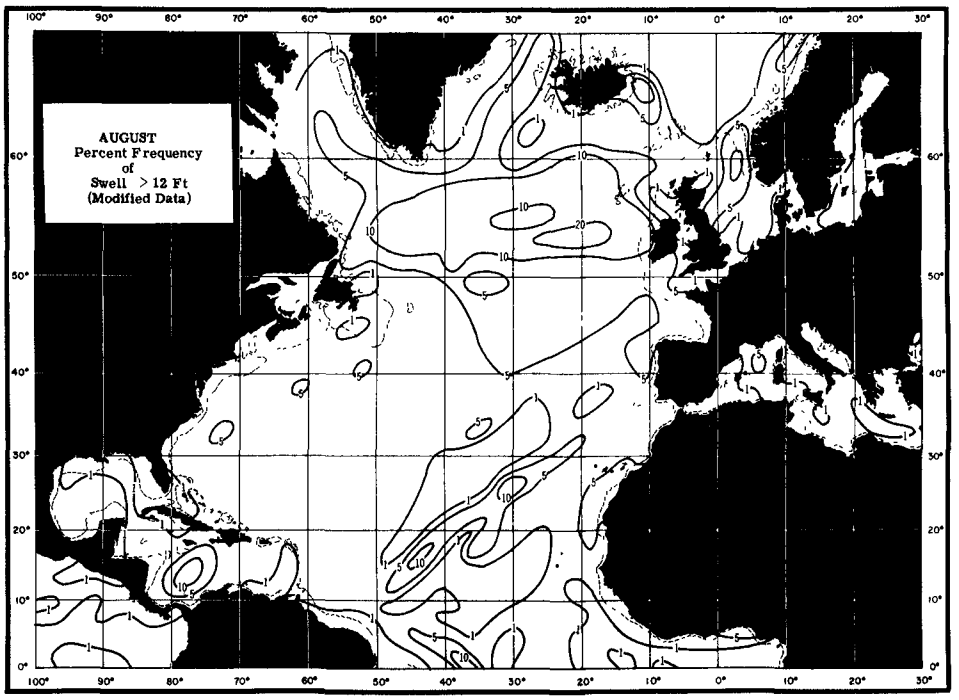

Fig. 5. Swell > 12 feet, August (Modified Data)

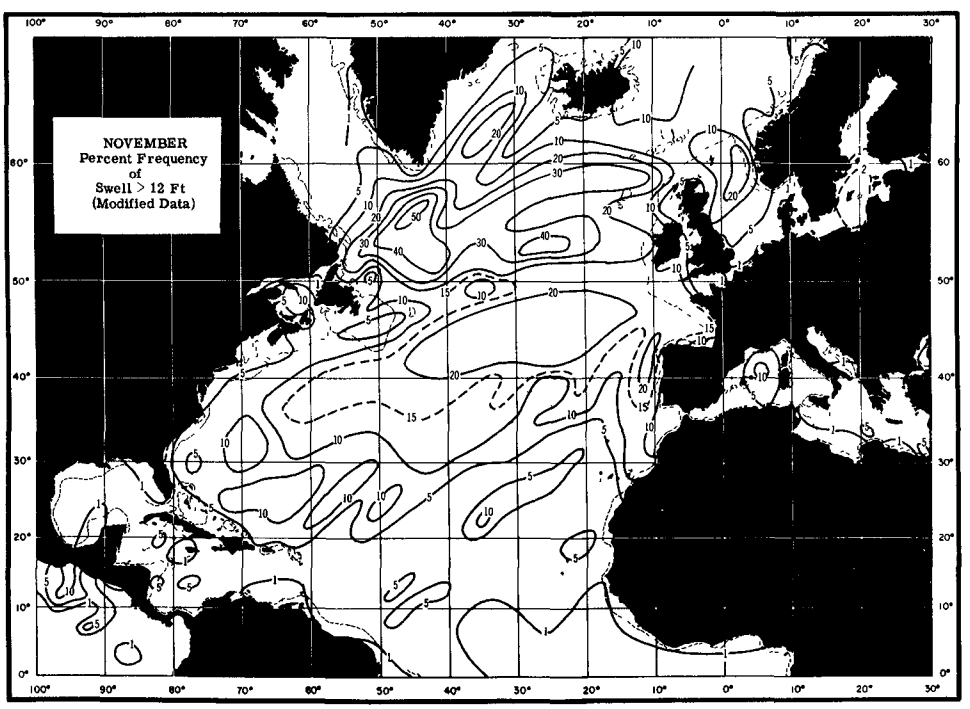

Fig. 6. Swell > 12 feet, November (Modified Data)

As a further check of this modification method, an attempt was made to locate swell data that were not included in the analysis of the charts and were taken by trained observers. NWRC, Ashville, provided microfilm records of weather ship observations covering the period 1940 through 1948. From these records only two months of observations were extracted (February and August), and only three locations had as much as three years of record in approximately the same location (Figure 7). In view of the limited number of years of record at any location, the data were totaled and averaged as a single sample for each season, comparing observed data, actual chart data, and modified chart data. The results are shown in Table IV.

Table IV

COMPARISON OF PERCENTAGE FREQUENCIES OF HIGH SWELL FROM SHIP WEATHER STATION OBSERVATIONS WITH ACTUAL AND MODIFIED MARINE DECK OBSERVATIONS

		February		
		Swell greater than 12 feet (percent)		
Ship station	Years of record*	Ship station data	Actual marine deck data	Modified marine deck data
A	3(46,47,48)	21	25	23
C	3(46,47,48)	8	40	30
1	3(42,43,44)	26	39	21
1,E	2(45,46)	18	30	20
C	1(45)	11	13	9
E	1(45)	22	25	25
B	1(46)	18	19	14
F	1(46)	4	33	22
B	1(45)	24	41	21
1	1(41)	42	33	17
1	1(40)	54	33	23
	Average	21	32	22

		August		
		Swell greater than 12 feet (percent)		
Ship station	Years of record*	Ship station data	Actual marine deck data	Modified marine deck data
A	3(46,47,48)	4	22	7
C	3(46,47,48)	2	13	13
1	2(42,43)	4	4	4
1,E	2(44,45)	0	4	3
B,F	2(44,45)	3	7	4
C,B	2(44,45)	2	18	12
1	2(40,41)	6	5	4
C	1(45)	3	10	8
	Average	3	11	7

*Data are grouped by approximate position.

This table shows large sample variations that are to be expecte in such short periods of record. The weighted averages for the two seasons present a much better comparison — here the averages are co siderably closer to those of the modified swell data than to those o

the original swell data. In general the modified swell averages show frequencies of high swell greater than those of the weather ships.

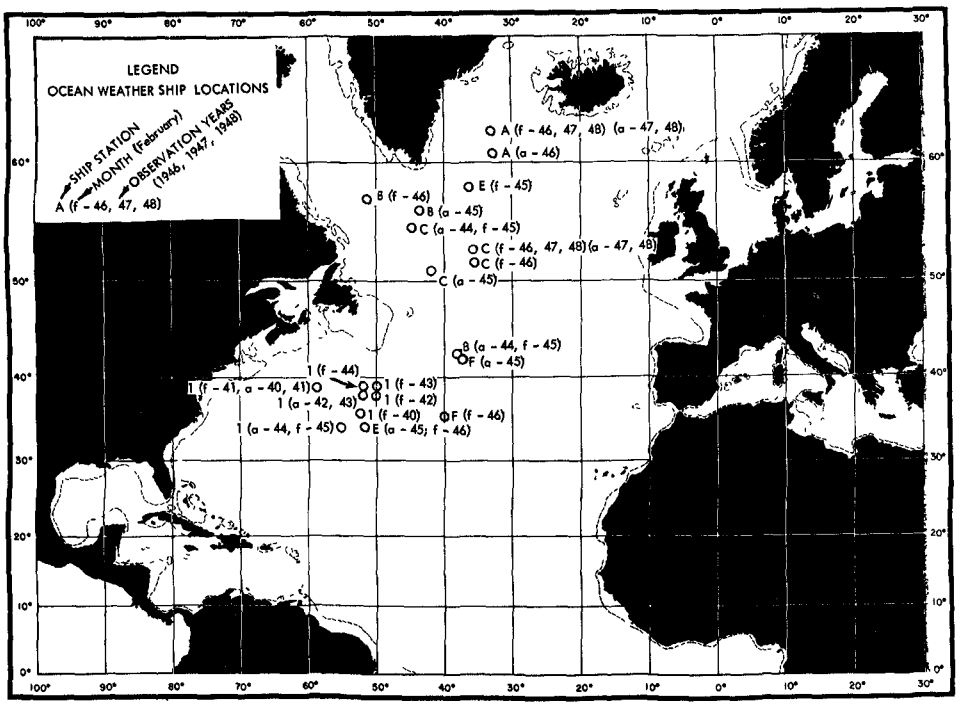

Fig. 7. Ocean weather ship locations, February and August

MODIFICATION OF SWELL ROSE CHARTS AND DATA

Some type of correction should be extended to the rose since it is still one of the most complete pictorial methods used on charts today. A complete modification based upon the total number of observation chances would often result in a significant reduction in the lengths of the arms of the swell rose, thereby providing a pattern which may be more difficult to interpret than the original rose. Besides, most data are already in a tabulated form, and without the addition of new data, a retabulation by machine would be difficult to justify. Hand tabulation of the entire rose is too time consuming and expensive. However, a simplified form of hand tabulation is a solution that involves only the computation of a factor based upon the ratio of total swell observations to total sea observations by unit rose area. This factor, included with each swell rose graphic, would provide the planner with a more complete means of interpreting ocean swell.

CONCLUSIONS AND RECOMMENDATIONS

The modification of swell data, utilizing the total number of sea observations as the number of chances to observe swell, does not provide an exact picture of ocean swell distribution. Nevertheless, all evidence indicates that this modification provides an interpretation of swell distribution which is logical and reasonably similar t the actual swell distribution.

The total number of observation chances, i.e., cards with a sea and/or a swell observation, requires further study and comparison with results obtained using totals of sea observations.

Individual decks should be studied and compared to determine th sources of biased data and the possible modification by deck.

Some thought should be given to an analysis based on a simultaneous summary of both sea and swell data.

REFERENCES

U. S. Coast Guard. Deck logs from Coast Guard vessels. Unpublished.

U. S. Navy, Bureau of Naval Personnel. Deck logs from naval vessels. Unpublished.

U. S. Navy Hydrographic Office. Listings of observations from specific Marsden squares ir the North Atlantic Ocean and adjoining seas. Listed from H 1-9 Current Report Form deck and from 192 (Hamburg, Deutsche Seewarte). Unpublished.

U. S. Navy Hydrographic Office. Sea and swell data for Marsden squares 001-009, 036-046, 073-082, 109-118, 141-152, 176-187, 214-223, 250-252. Tabulated by the U. S. Navy Hydrographic Office from H 1-9 Current Report Form deck, and from summary cards furnished by the U. S. Weather Bureau from the following decks: 110 (WBAN 11, U. S. Navy Marine 1945-1951); 115 (U. S. Merchant Marine, 1938-1948); 116 (U. S. Merchant Marine, 1949-1955); 192 (Hamburg, Deutsche Seewarte); 193 (Nederlands, Meteorologisch Institut); 194 (Great Britain, Meteorological Office); 195 (U. S. Navy Ships' Logs Observations); 196 (Hamburg, Deutsche Seewarte, 1949-1953); 197 (Denmark, Meteorologiske Institut); and 281 (U. S. Navy MAR Synoptic). Unpublished.

U. S. Weather Bureau, National Weather Records Center. Microfilm records of ocean weather station observations (1940-1949). Unpublished.

U. S. Navy Hydrographic Office, Division of Oceanography, Sea and Swell Unit (1960). Sea Conditions - North Atlantic Ocean. IOM No. 11-60, April 1960. Unpublished manuscript.

CHAPTER 3

WAVE RECORDING ON THE IJSSELMEER

P.W. Roest
Engineer, Zuiderzee Works
The Hague Netherlands

SUMMARY

The preliminary results of waverecording on the IJsselmeer are presented in this paper. The measurements have been carried out with a floating waverecorder (accelerometer on raft).

Wave heights and periods, windvelocity, fetch, depth, temperature of water and of the atmosphere and the siltcontent of the water have been determined.

The results have been compared with the diagrams of Thijsse and Bretschneider. The distribution of the wave heights is mentioned.

INTRODUCTION

The dimensions of the dikes in the IJsselmeer are mainly determined by wave-attack.

The dimensions of the waves as a result of the design gale are calculated with the diagram of the Hydraulics Laboratory at Delft (ref. 1). This diagram is based on data of Sverdrup for deep water and principally on laboratory studies for shallow water.

For a long time there has been a need of wave recordings on the lake in order to verify the calculated wave heights. A problem is the impossibility of maintaining a permanent recording station on the lake due to ice-drift in wintertime. Otherwise the IJsselmeer lends itself admirably to wave-research, because there are vast regions with only small variations in waterdepth. Another advantage is that frequently more or less stationary conditions will occur under the influence of winds of constant force and direction.

When Dr. Dorrestein of the Royal Dutch Meteorological Institute introduced his new floating waverecorder, it was possible to take observations in every place of the lake. Soon it appeared that this recorder has many advantages.

The equipment consists of an accelerometer mounted on a little raft of one meter each way, that follows the movement of the water surface. The signal of the accelerometer is transmitted by an electric cable to the ship, where it is double integrated and then recorded (ref. 3).

During the last winter several observations have been carried out with an instrument of this type. As a result of initial troubles with the electronic equipment the number of observations during gale-conditions has been limited.

The usual duration of each recording is about 15 minutes. The average period of the waves lies between three and a half and five

seconds, so each diagram consists of 180 to 250 waves.

Wave height is measured as the difference in height between a trough and the next crest. The average period is determined by dividing the total recording time by half the number of zero-crossings.

OBSERVATIONS ON THE IJSSELMEER

In order to simplify the interpretation, observations were taken in places, where the fetch is measured over an area of nearly constant depth.

On fig. 1 - a map of the lake - the different places and their fetches are shown. In the southern part of the lake the depth is up to 4 meters; the northern part is somewhat deeper.

The velocity of the wind was measured on board a ship, three meters above sea-level. Besides the recordings of the meteorological station at Lelystad were available. There the wind is measured at 10 meters above sea-level. The temperature of the atmosphere and of the water and the silt-content of the water were also measured.

The appendix gives a summary of the results.

It appears that all distributioncurves of waveheights have the same shape and that they agree very well with the Raleigh distribution, just like deep water waves. Fig. 2 shows the cummulative distribution of the wave heights of several recordings. The scale has been chosen in such a way that Raleigh distributions become straight lines.

The distributions may have been slightly affected due to drifting of the raft.

The significant wave heights have been compared with the diagrams for shallow water waves of Thijsse and Bretschneider. It appears that almost all strong wind observations give smaller heights than those calculated with these diagrams, but that the only observation under gale conditions is comparable with the calculated one.

Fig. 3 shows the Delft diagram in which the observed wave heights have been plotted. As known the diagram is dimensionless. The height (H), fetch (F) and depth (D) are divided by twice the velocity head of the wind.

The dots are the calculated points from fetch, depth and windvelocity. The circles are giving the observed heights on the same dimensionless scale.

To use this diagram the observed windvelocity ought to be converted into the velocity W_0 on a level proportional to the square of the windvelocity. This means, that with small windvelocities the observation height must be reduced to a lower level than with high velocities.

On fig. 4 the observed wave heights have been plotted against the water depth. Only observations with a long fetch have been plotted. The solid line agrees with the Delft diagram. It appears,

Fig. 1. The IJsselmeer.

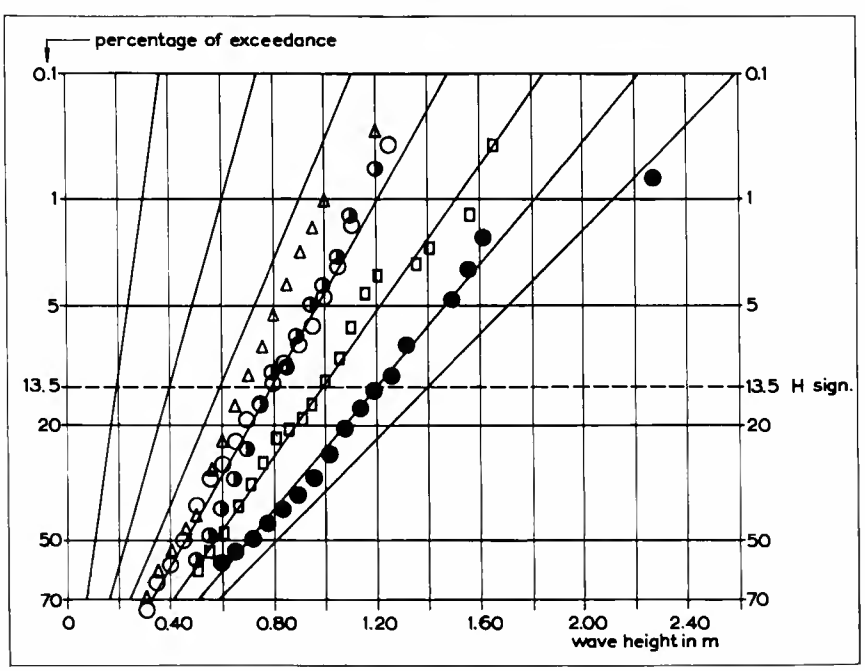

Fig. 2. Cumulative distribution of wave heights of 5 recordings.

that the observed values are systematically lower than this line.

Besides the results have been compared with a diagram of Bretschneider (ref. 2). This diagram gives smaller waves as the Delft diagram in the region of long fetch and shallow water. This leads in this region to a somewhat better agreement with the observations on the IJsselmeer.

DISCUSSION OF THE RESULTS

There is not yet a good explanation for the difference between the measured waveheights and the ones determined from the mentioned diagrams, based on observations elsewhere.

Some explanations have been considered.

The waverecorder. - In the first place there may be errors of the waverecorder e.g. due to the tilting of the raft (ref. 3). This has been examinated by comparing the floating recorder with a step-resistance recorder as well as with a recorder measuring with a float. Both recorders are suspended on poles off the coast in the Northsea.

Simultaneous recordings of both meters with the floating recorder have been carried out. The waves could not be compared individually. Only the statistical similarity of the recordings has been examinated.

The differences of the significant waveheights computed from simultaneous recordings of the stepresistance and the floating recorder were less than 10%. A comparison with the second type recorder gave exactly the same distributions of the waveheights.

For the present it may be concluded from these comparisons that the results of the floating recorder do not deviate appreciable from other known methods of observation.

The temperature. - Secondly there is the influence of the temperature. Most observations have been made while the temperature of the atmosphere was somewhat higher than that of the water. The observations under different conditions indicate a small influence of the difference of temperature between water and air.

The siltcontent. - A single remark on the influence of the silt content of the water may be made. The top layer of the bottom of the southern part of the lake consists mainly of clay. During a long stormy period the silt content of the water may increase to about 1 gram per liter. Boatmen familiar with the lake state a reduction of the waveheight when the siltcontent of the water increases and as a result of this, navigation seems to be easier according as a windy period lasts longer. The wave recordings did, however, not show any clear influence of the siltcontent on the height of the waves.

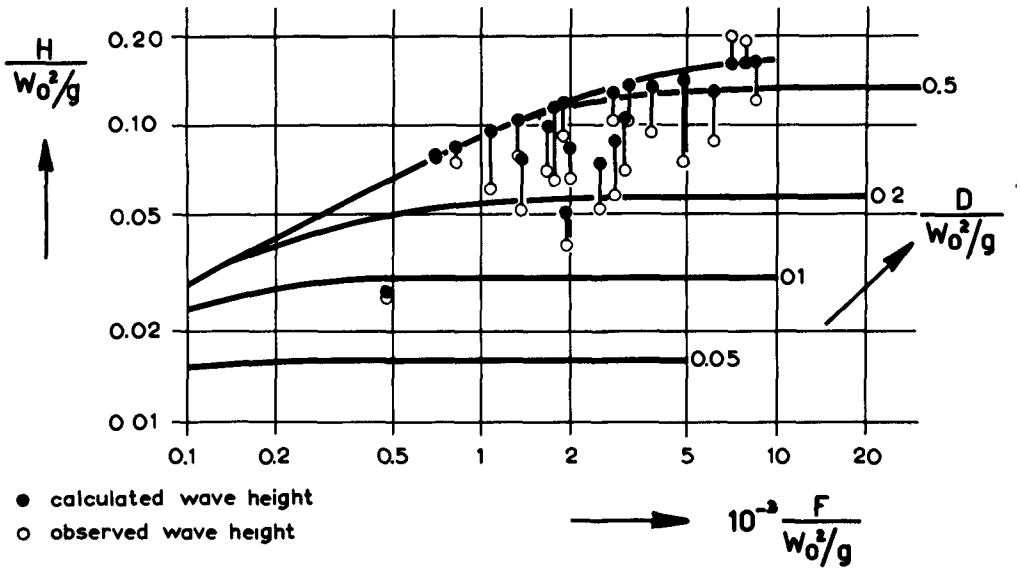

Fig. 3. Measured and calculated wave heights plotted in the Delft diagram.

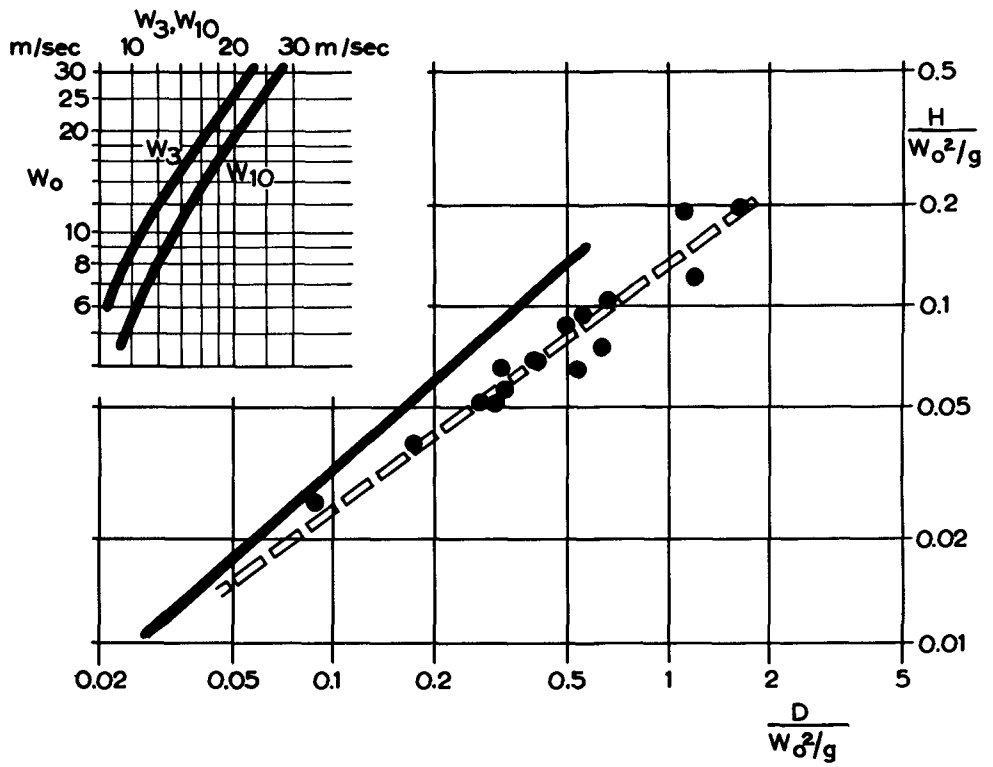

Fig. 4. Measured wave heights (shallow water and long fetch).

All things considered, it does not appear that the results are affected by local circumstances. The dashed line in fig. 4 may have a more general significance. Further wave observations will have to prove this.

REFERENCES

1. Thijsse, J.Th. "Dimensions of wind-generated waves". Assembly I.U.G.G. Oslo,1948. International association of scientifical hydrology.

2. Bretschneider, C.L. "Revisions in wave forecasting, deep and shallow water". Proceedings of sixth conference on Coastal Engineering, 1957.

3. Dorrestein, R. "A wave recorder for use on a ship in the open sea". Proceedings symposium. On the behaviour of ships in a seaway. Wageningen, 1957.

APPENDIX

Summary of the results

Date	D	F	W_3	W_{10}	t_w	t_a	Silt	Hsign	H_{50}	Period
	m	10^3m	m/sec	m/sec	°C	°C	$\frac{mg}{liter}$	m	m	sec
6- 1-'58	3,50	9	-	11	2,6	4	-	0,43	0,26	3,4
6- 1-'58	4,30	32	-	12	2,6	8	-	0,46	0,28	3,5
7- 1-'58	4,10	22	-	21.5	3,3	5	1033	1,21	0,71	5,0
29-10-'59	4,35	54	11	12	9,9	11	64	0,77	0,45	3,6
9-11-'59	3,15	20	12	11	6,1	5	250	0,65	0,42	3,4
9-11-'59	3,95	35	13	11	6,6	5	163	0,69	0,39	3,5
4- 3-'60	4,05	19	9	12	5,8	7	248	0,64	0,38	3,5
4- 3-'60	4,60	32	8	11	4,7	7	50	0,45	0,28	3,2
7- 3-'60	4,35	7	11	12	3,5	1	297	0,64	0,38	3,5
8- 3-'60	4,20	14	11	11	3,1	-2	242	0,51	0,30	3,8
9- 3-'60	4,20	12	11	12	2,7	3	398	0,68	0,43	3,8
9- 3-'60	3,65	17	9	10	2,7	6	196	0,66	0,39	3,4
11- 4-'60	4,20	19	12	14	9,3	9	284	0,70	0,46	3,8
11- 4-'60	5,70	12	11	14	8,4	9	109	0,66	0,40	3,8
12- 4-'60	4,15	18	8	9	9,4	10	185	0,50	0,28	3,0
12- 4-'60	5,90	5	11	10	9,2	11	96	0,58	0,36	3,2
13- 4-'60	4,35	29	11	11	9,3	10	245	0,73	0,44	3,8
13- 4-'60	3,95	45	16	13	9,3	12	372	0,89	0,58	4,2
14- 4-'60	4,15	17	11	13	9,3	10	294	0,70	0,44	3,6
14- 4-'60	3,75	34	12	14	9,3	10	181	0,71	0,43	3,7
6- 7-'60	4,35	30	-	10.5	15,3	15	160	0,72	0,46	3,8
18- 7-'60	4,30	21	10	12	17,1	18	125	0,76	0,49	3,6
18- 7-'60	4,55	35	12	12.5	18,2	19	159	0,79	0,53	3,8

Explanation

W_3 Windvelocity at 3 m ebova sealeval (place of observation)

W_{10} Windvelocity at 10 m above sealevel (Lelystad)

t_w temperature of the water

t_a temperature of tha atmosphere

Heign significant wave height

H_{50} height exceaded by 50% of the waves

Chapter 4

THE USE OF RADAR IN HYDRODYNAMIC SURVEYING

H.M. Oudshoorn

Engineer, Hydraulic Division of the
Delta Works, Rijkswaterstaat, The Hague.

INTRODUCTION

During several kinds of surveys at sea or in the wide estuaries in the South West of the Netherlands the location of moving objects presents a problem. When studying the various systems of radio location it appeared that radar, an instrument which gives a birds eye view of a fairly extensive area, could be a useful aid in solving this problem. Especially when it was shown that with the newly developed short-wave radar sets wave crests were clearly visible on the radar screen, it was considered worth while to carry out some tests to see whether radar would really be useful for surveying purposes. In 1958 the Rijkswaterstaat hired an 8 mm radar set for a trial period. The tests were carried out at the mouth of the entrance channel to the Rotterdam harbour, the Rotterdam Waterway.
During these tests it became evident that radar could solve several problems and that valuable information about wave patterns could be gathered with this instrument. The set was bought and then used to determine

1. flow patterns
2. wave patterns
3. the behaviour of ships in fairways.

In paragraphs 2 and 3 some basic principles of radar are discussed in order to establish the special requirements the radar equipment must satisfy for this particular purpose. [1]
In paragraphs 4-7 the methods of observation and the results obtained for the purposes mentioned above are discussed and some practical examples given.

GENERAL PRINCIPLES OF RADAR

A radio transmitter, operating on a very short wavelength radiates frequent and regular pulses of energy. These pulses travel out into space like a train of short radio waves of a certain length. By means of a suitable aerial system the transmitted energy is focussed to form a narrow pencil or beam.
When the wave train hits an object a certain amount of the radio energy is reflected, generally in many different directions. Only a very small amount of energy travels back to the point of transmission in exactly the opposite direction. Here the returning energy is received by an aerial and amplified in the radar receiver unit.

The time that has elapsed between the moment of transmission of a certain pulse and the receipt of its echo is a measure of the distance between the transmitter and the reflecting object, using the known speed of the propagation of radio waves, which is about 300,000 km/sec.

The aerial system that focusses the transmitted energy is rotated mechanically at a constant speed of about 20 revolutions per minute, consequently, the transmitted beam of energy "scans" the horizon. For this reason the aerial system if often called the scanner.

The distance and the azimuth of the object appears on a cathode-ray tube.

The cathode of the tube radiates a stream of electrons which is focussed to a beam with spot-size diameter at the inner surface of the tube.

By gradually increasing the current supplied to the deflection coils this beam is deflected radially from the centre of the tube to the edge, starting at the moment of transmission of a pulse. The radial line followed by the beam at the surface of the tube is called the time base.

According to the range scale selected by setting the range switch the time base current rises at a rate appropriate to the speed at which the beam should travel from the centre to the edge. If, for instance, the radius of the tube has to represent a target range of 10 kilometers, the electron beam has to reach the edge of the tube in the period that the pulse radiated by the radar transmitter makes the trip to the target and back of 20 km, i.e. 67 microseconds.

The inner surface of the tube is coated with a substance that becomes fluorescent when it is hit by a sufficiently strong beam of electrons. The beam following the time base, is not strong enough to make the trace visible. The reception of an echo by the radar receiver unit, however, results in an extremely short momentary increase in the intensity of the beam of electrons, sufficient to make the coating fluorescent. The afterglow of the coating causes the spot to remain visible for some time. The distance of the brillant spot from the centre, measured along the time base is proportional to the distance between the transmitter and the reflecting object.

The time base appearing on the screen as a radial line is rotated with the scanner by means of a servo system, which synchronizes the rotation of the scanner with the rotation of the deflection coils of the cathode ray tube. By this arrangement the difference in azimuth of the various targets in the field is shown on the screen and the location of the objects is visible on the screen in their correct relative positions.

THE USE OF RADAR IN HYDRODYNAMIC SURVEYING

CHOICE OF EQUIPMENT

Resolving power. If it is desired to use radar for surveying purposes the apparatus used must be capable of working very accurately indeed.
One of the most important points to watch when choosing radar equipment is its resolving power. [2]
The resolving power of radar can be divided up into two categories, viz., radial and tangential. Radial resolving power is determined by the duration of the pulses transmitted.
Two targets situated at a radial distance ΔR can only be distinguished when the difference in the time taken by a pulse to reach and return from both targets is longer than the pulse-length τ. If c is the propagation speed of radio waves the resolving power is $\Delta R = \frac{c\tau}{2}$
A short pulse-length is required to obtain high resolving power. For technical reasons the pulse-length cannot be shortened indefinitely. However, the shorter the wavelength is the shorter the pulse-length can be made.
For a radar set with a wavelength of 3 cm the minimum pulse-length is about 0.1 μ sec giving a resolving power of 15 m. When a wavelength of 8 mm is applied the pulse-length is about 0.05 μsec giving ΔR = 7.5 m.
For a wavelength of 4 mm the min. pulse-length is about 0.01 μsec and ΔR = 1.5 m.
Tangential resolving power is determined by the width of the horizontal beam of the energy radiated.
For longer ranges the width of the beam θ is proportional to $\frac{\lambda}{D}$ when λ = wavelength and D = width of the scanner. Good tangential resolving power can be obtained by using a short wavelength or a large scanner. For a 1.5 metre scanner we find the following data for θ and the resolving power $R\theta$ for a distance R = 1000 m for various wavelengths.

λ = 3 cm	$\theta = 1.2^{o}$	$R\theta$ = 21 m
λ = 8 mm	$\theta = 0.4^{o}$	$R\theta$ = 7 m
λ = 4 mm	$\theta = 0.2^{o}$	$R\theta$ = 3.5 m

A short wavelength must be used to obtain a high tangential resolving power to avoid making the scanner awkwardly large.
It will be evident that the resolving power of the cathode ray tube of the display unit will have to match the resolving power of the radar set itself. The spot diameter of the electron beam on the radar screen is about 0.3 mm. The max. screen diameter of radar sets is mostly 30 cm, giving for a max. range of 3,000 m a scale of 1:20,000. Then the diameter of the spot on the screen represents a circle of 6 m in the field.
This implies that the resolving capacity of the tube and the max. scale which can be applied during the survey in view of the accuracy desired determines the max. range at which the radar can be used. In most cases this max. possible range does not exceed 5 km.

Radio-wave propagation. During the propagation of radio-waves through the earth's atmosphere the transmitted energy attenuates. The ratio of this attenuation depends largely on the wavelength. Oxygen gives an attenuation which has sharp peaks at 5 mm and 3 mm wavelength. The presence of water in the atmosphere gives an additional attenuation which depends again on the form in which the water appears. An increase in the amount of water in the atmosphere causes greater attenuation. [2]
Fig.1 shows the attenuation for wavelengths under 32 mm for oxygen and water in various forms in the atmosphere.
From this graph may be concluded that the wavelengths of 5 and 2-3 mm is unsatisfactory for radar in any case. Of the very short wavelengths 8 mm and 4 mm are the most satisfactory for this purpose, but these wavelength will only be useful for radar sets for special short-range purposes.

Response of targets. A natural target is very seldom an ideal reflector and usually only a very small amount of the energy striking it is reflected, while an even smaller amount will be reflected in exactly the opposite direction.
The reflection properties of a target depend on the size, shape orientation and material of the object. Metal or water have better reflecting proporties than wood or sand. It has been observed that a wet wooden pole reflects much better than the same pole dried by the sun. Size and shape however, are the main factors. Given a certain shape and material and a given inclination of the surface with respect to the radar waves, the amount of energy reflected will increase roughly proportionally to the size. Sizes larger than the cross section of the radiated beam of course do not contribute to the echo strength.
If the transmitted energy is E_t, the energy hitting the target per unit of area will be $\frac{\gamma E_t}{4 \pi R^2}$
γ is a factor expressing the degree of focussing.
A target with a reflecting capacity σ reflects a quantity of energy unit of area near the receiver of

$$\frac{\sigma}{4\pi R^2} \cdot \frac{\gamma E_t}{4\pi R^2}$$

If the receiver aerial has a cross-sectional area of F_R the energy received will be

$$E_R = \alpha \frac{\gamma E_t \sigma F_R}{16 \pi^2 R^4}$$

α is the atmospheric attenuation discussed in 2.1. As mentioned in 2.1 the narrowness of the beam of energy transmitted increases as the wavelength decreases. So γ depends on λ and the energy received will increase, too as the wavelength decreases.
This R^{-4} relation only holds good up to a certain distance from the radar mounting. This area is called the near zone. Outside this range an R^{-8} relation obtains. This division into two zones has been shown to be due to an interference phenomenon caused by reflection from the surface of the water. In the far zone the target is wholly below the lowest lobe of the interference pattern, so that the illumination of the target is less than the free space value, and becomes progressively less as the target moves

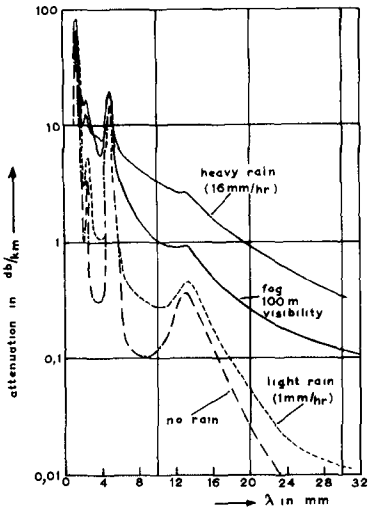

Fig. 1. Atmospheric attenuation of radar waves.

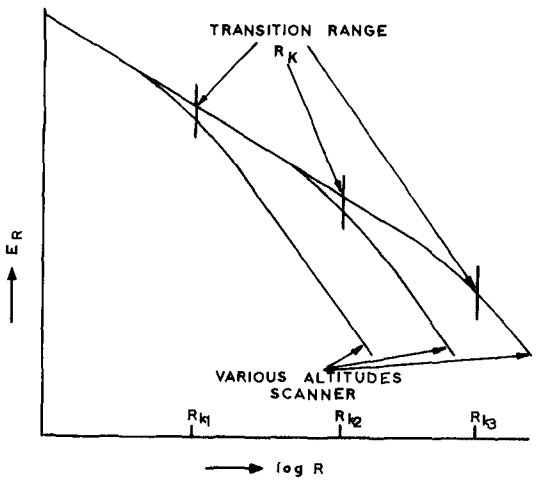

Fig. 2. Position of the transition range of various altitudes of the scanner.

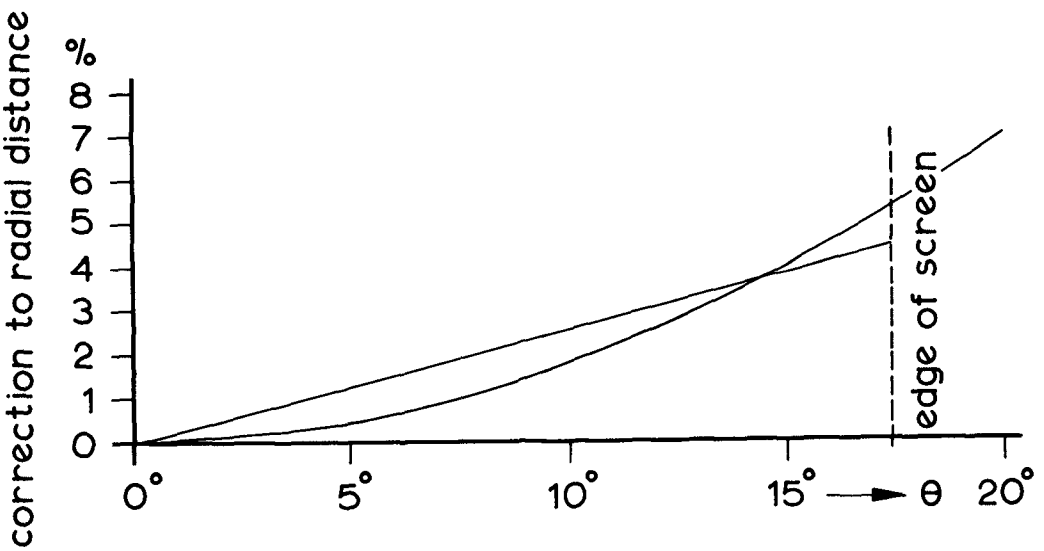

Fig. 3. Correction curve for radar photographs.

out of range. [3]
The location of the transition zone between the near and the far zone is expressed approximately by the formula

$$R_K = 2\pi \frac{h_1 h_2}{\lambda}$$

in which R_K = range of the transition zone
h_1 = height of the scanner above sea level
h_2 = height of the target above sea level
λ = wave length.

From this formula it appears that the range of the transition zone increases in proportion as the wavelength decreases. In the following table some values for R_K are given for various wavelengths, scanner heights and target heights [2]

λ	R_K $h_1 = 5$ m $h_2 = 1$ m	R_K $h_1 = 5$ m $h_2 = 5$ m	R_K $h_1 = 10$ m $h_2 = 1$ m	R_K $h_1 = 10$ m $h_2 = 5$ m
32 mm	1 km	5 km	2 km	10 km
8 mm	4 km	20 km	8 km	40 km
4 mm	8 km	40 km	16 km	80 km

The response of wave crests is of special importance to the use of radar in hydrodynamic surveying.
It has been shown that a swell itself does not reflect radar waves, but that the small wind-generated facets which overlie the main large-scale wave pattern are due to the reflecting properties of the waves.
The phenomenon of sea return, what is known as "sea clutter", has been studied for several purposes, but mainly with the aim of suppressing it in the receiver unit, because it tends to obscure the echos of ships.
Out of the many publications on the subject attention is drawn to [3].
It will be evident that only facets of a suitable size and orientation will reflect in the desired direction.
The distribution of these facets has been studied statistically and it has been shown that scattering is concentrated in the vicinity of wave crests. Ideal reflection is from perpendicular facets facing the radar equipment. They have also been shown statistically to be most frequent near the wave tops, especially to windward, where the crests of the waves tend to be steepest.
When the angle of incidence of the radar waves is small the wave crests screen the troughs and only the wave crests facing the radar equipment are irradiated by the radar waves. If radar views an area-extensive target like a choppy sea the azimuthal extent of the surface illuminated is equal to $R\theta$. So here instead of the R^{-4} relation for a target of limited dimensions discussed above an R^{-3} law holds for the intensity of the energy received in the near zone. Outside the transition zone for sea-clutter an R^{-7} law holds instead of the R^{-8} relation for targets of limited size. It will be evident that outside the transition zone the naturally weak response from wave crests will soon cease to be

detectable on the radar screen. Therefore a radar set with a short wavelength, giving a big range for the transition zone is required for wave research. The values of the energy received on a given wavelength from the sea surface, for different altitudes of scanner and under the same sea conditions should give a group of curves as shown in fig.2. Here the transition zone is only a function of the height of the scanner.
For this reason the scanner should be placed as high as possible, consistent with local conditions.

Conclusions.

1. A short wave-length radar set is suitable for getting high resolving power both radially and tangentailly.
2. The use of short wavelengths implies that these sets can only be used for short-range work because of the relatively strong attenuation of radio energy in the earth's atmosphere. However, as radar is only practicable in hydrodynamic surveying for relatively short ranges (about 5 km max.) short-wave sets are satisfactory.
3. The energy received from the target is stronger for short wavelengths, owing to the better focussing of the energy transmitted.
4. The range outside which targets reflect rapidly decreasing amounts of energy increases as wavelengths shorten.
5. A short-wave radar set is required for wave-research.

All the above-mentioned conclusions point to the desirability of using short-wave radar for hydrodynamic surveying.
As mentioned under 3.2 of the very short wavelengths the 4 and 8 mm waves show a relative minimum attenuation and are therefore most suitable.
Since 4 mm radar sets are not yet being manufactured commercially an 8 mm radar set is being considered. A Decca 8 mm radar set is being used for surveying purposes in the Deltaworks.
Specifications:

aerial system	
reflectors	Double 6 ft "cheese" (one transmitting one receiving)
horizontal beam	of the order of 23'
vertical beam	of the order of 14°
pulse characteristics	
pulse length	0.05 μsec
recurrence frequency	4000 per sec
display	
screen diameter	30 cm
scales	0.5, 1, 3 and 10 nautical miles

Most navigational radar sets work on a wavelength of 3 cm. The use of these sets for surveying purposes is only justified when the objects are of the same size as or bigger than objects lying within the resolving power of the equipment, e.g., ships. For

the determination of the courses of ships a good 3 cm radar specially adjusted for short-range use like river-radar sets are satisfactory.
A set working on a shorter wavelength is required for the determination of wave patterns and flow lines.

RECORDING OF DATA AND ACCURACY THEREOF

The moving objects which have to be located appear on the radar screen and their continuously changing positions relative to objects known to be stationary, such as the shore line is observed.

In most cases the situation at a particular moment must be retained at regular intervals. This can be done in several ways, viz.,

1. by measurement on the radar screen direct
2. photographically.

A fluorescent circle of any desired radius can be made to appear on the screen by means of an electronic device (the variable range marker) built into the 8 mm radar set mentioned before. The radius selected can be read off a scale direct. The distance an object is from the radar set can be determined instantly by making the circle pass through the image of the object.

The azimuthal location of the object can be determined by means of a rotatable cursor fitted on the top of the screen. The scale factor of the variable range marker and its zero correction can be determined by checking the variable range marker against some suitable landmarks the coordinates of which are known.

If these constants are applied to the scale readings reasonable accuracy of location can be obtained.

If a maximum range of 3000 m is used for the radar picture the standard error of range measurement is of the order of 15 m, which includes an error of about 5 m caused by backlash in the gearing of the mechanical part of the device. The standard error in the measurement of the azimuthal location of the object is of the order of 0.3°.

This method of location however takes much time and is therefore not suitable when numerous objects have to be located. Then it is better to take photographs of the picture on the radar screen. This method has the advantage that the situation at a given moment can be recorded, thus facilitating subsequent examination. A standard 6 x 6 cm^2 camera is used for photographing the 30 cm tube of the 8 mm radar.

In order to avoid geometrical distortion as far as possible care should be taken that the camera axis is in line with the axis of the cathode ray tube. The camera should be rigidly attached to the radar set.

A radial distance on the curved surface of the cathode ray tube appears on the photograph as a straight line. That is the main problem connected with the geometrical interpretation of radar photographs. The degree of distortion depends on the radius of curvature of the cathode ray tube, on the radial distance of the image from the centre of the tube and on the distance between

the camera and the tube.
In our case the camera is 48 cm from the tube, which has a radius of curvature of 40 cm. Fig.3 shows the magnitude of the distortion for this case in expressed as a percentage of the radial distance as a function of the angle θ between the axis of the camera and the line joining the centre of the objective to the echo of an object on the radar screen. From this figure it can be seen that the correction which has to be applied to the radial distance shown on the photographs increases progressively up to 5.5%. However, this percentage can be reduced considerably by applying a correction increasing proportionally to θ , which in fact merely means attaching another scale to the photograph.
Fig.3 shows a max. correction of about 0.9% when this is applied. This means that if the max. range is fixed at 3000 m the correction at 1500 m is about 15 m; at 2200 m the correction is negligible, beyond this range the correction increases sharply up to 27 m at the edge of the screen. In most cases this degree of accuracy is satisfactory.

If greater accuracy is desired the actual corrections must be applied but this is very laborious when numerous locations have to be determined.

If the approximation of the correction curve to a straight line is acceptable it is a simple matter to deduce the information required from the photographs.

Then the negatives can be projected direct on to a chart bearing the desired scale.
Standard photographic enlarging apparatus can be used for this surpose. Care should be taken that enough landmarks can be distinguished on the negatives equally distributed through out the range. Their echos are used to place the projected image correctly on the chart.
All the data can then be filled in on the chart. When dealing with moving targets like floating buoys the successive negatives should all be projected on to the same chart, thus indicating the flow lines direct.

CURRENT MEASUREMENTS

The way in which currents are measured depends largely on the purpose for which they are intended. In the complicated estuaries in the south-west of the Netherlands it is often necessary to determine the total flow as a function of time in various gullies and over adjoining sandbanks. Here simultaneous measurements are required, because measurements carried out on different days are not easy to compare because of the variations in the tides, in the discharges of rivers, in the wind, in the density differences, etc.

Current velocity is determined at numerous points on lines running at right-angles to the gullies. This indicates the flow in the gullies and over the sandbanks. The flow across each of these lines can be ascertained by measuring the velocity and direction of the current at fairly short time intervals at a sufficient number of spots and at several depths at each of these

spots. This method calls for a large number of vessels, instruments and operators, especially in extensive areas.
By this method information can be obtained about the flow distribution in a cross-section at any moment and about the variation in time of the total flow through a cross-section of an estuary. In many cases however, detailed information is also desired about the patterns of the flow lines, so that they can be compared with the results obtained from model tests and used for the study of erosion problems. These data cannot be derived from simultaneous measurements. Floats are used to determine the flow pattern. Especially in wide estuaries, like those in the southwest of the Netherlands, the main difficulty is how to locate the floats.
They can be located as follows:

1. Terrestrially, with the aid of sextants from a survey launch, following the floats.
2. With the aid of a radio location system, e.g., the Decca system, on a following launch.
3. Photogrammetrically.
4. By radar.

The number of floats usable in the first two methods is limited because there are limits to the number of operations that can be carried out on board a launch. When the velocity of the current is fairly high readings must be taken every few minutes and the number of floats which can be handled by one launch is limited. to two or three . This means that for wide areas to be covered with numerous floats the first two methods can be rejected. Therefore, they are only used for incidental detailed surveys of small areas.

The use of the third method employing airial photography requires that the aircraft return to the same point at regular intervals to photograph the area concerned. This means that as a rule not more than two points can be taken from which the whole area must be seen, unless more than one aircraft is used. This means that the aircraft must fly at a fairly high altitude if the area is at all extensive. This in turn calls for very good visibility and clear recognisability of the floats. If readings must be taken continuously throughout a tidal cycle two planes will be required as a rule and thus the use of this method will be still further restricted when the days are short.

The last method of location, with the aid of radar, has the advantage that with two launches numerous floats can be tended. One boat drops the floats and the other picks them up again, so work on board is reduced to a minimum. This method is also independent of daylight and visibility. Only very heavy rain and a rough sea can reduce the visibility of the floats on the radar screen but under such conditions operations at sea are also impossible.

The floats have to be provided with radar reflectors to make them visible on the radar screen.

Radar reflectors consist of prisms and pyramids similar in shape to those used in optics. They look like the corner of a box

so they are called corner-reflectors. For use on buoys the corner reflector has to be designed in such a way that its wind resistance is as low as possible. A Swedish invention the spiral reflector has been chosen for this purpose. It consists of a folded sheet metal strip twisted into a spiral with transversely welded plates to produce a large number of horizontally directed corner reflectors (fig.4). [4]

The spiral reflectors used here are 9 cm in diameter and are 47 cm high.
Comparative tests on stagnant water have shown that the wind catch of these reflectors is less than or does not exceed the wind catch of other traditional markers on buoys such as flags or the foam-rubber plates used for making them clearly visible from the air.
Finally, an example of current measurement will be discussed, one which was carried out in the Haringvliet during the construction of the building pit for the big sluices. It was evident that such an obstacle, occupying about one third of the cross-sectional area of the estuary would lead to an important change in the flow pattern and that these changes in turn would cause considerable erosion in the neighbourhood of the pit. For this reason an extensive survey was carried out to determine the changes in the flow pattern. Along four lines perpendicular to the main gullies simultaneous measurements were carried out at various stages in the construction of the pit.

The changes in the velocity-distribution in the cross sections could be derived from these measurements and an overall picture of the flow lines in the entire estuary could also be worked out from them.

Fig.5 shows the cross-sections along the axis of the pit before and some months after its construction, together with the corresponding current diagrams. The overall picture of the flow-patterns of the maximum flood and ebb currents before and after the construction pit was built are shown in figs. 6 a/d.
These patterns, however, do not give enough information about the flow pattern in the immediate vicinity of the pit, which is 1400 m long.

In order to establish this flow pattern additional float measurements with 8 mm radar have been carried out.

Fig.7 shows the results of a reading taken during construction at the instants of max. ebb en flood currents. The position of the Decca 8 mm radar set is marked. The radar apparatus was working on a max. range scale of 3000 m so that the scale of the image on the radar screen was 1 : 20.000. Two boats which had continous radio contact with the radar post were used to handle the floats. Every 2 or 3 minutes the location of the floats was recorded by photographing the radar screen.

WAVE MEASUREMENTS

Information with regard to the waves can be obtained by making use of weather maps or wind data measured direct. Wind fields over a certain sea area can be determined with the help

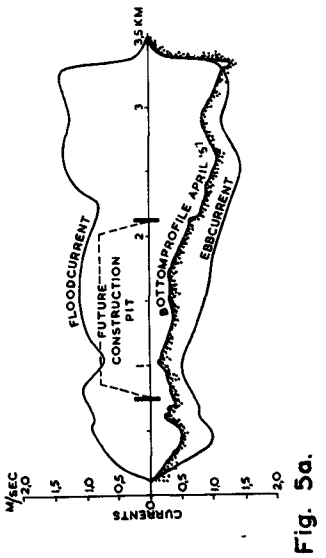

Fig. 5a.

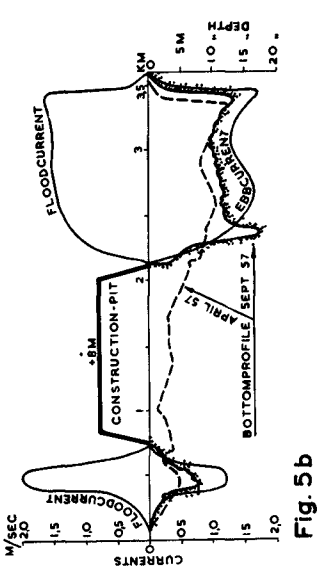

Fig. 5b

Fig. 5. (a) Currents and cross-section in axis of pit before its construction. (b) Currents and cross-section in axis of pit after its construction.

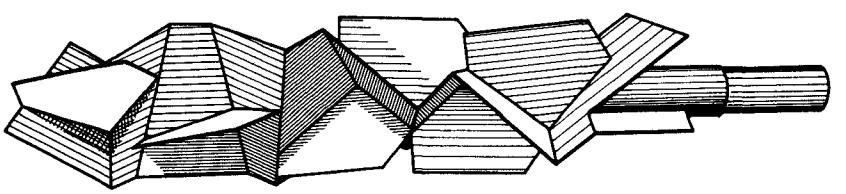

Fig. 4. Spiral radar reflector.

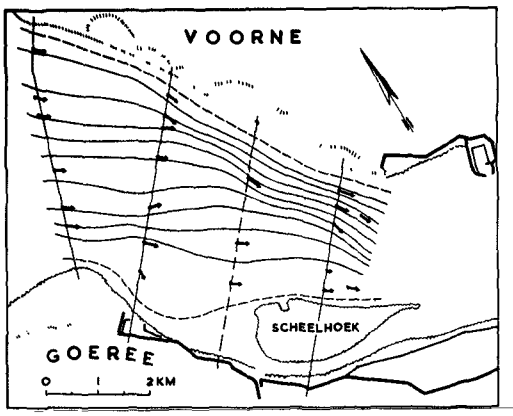

Fig. 6a

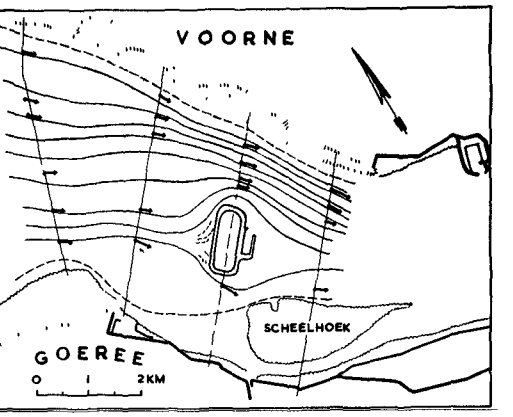

Fig. 6b.

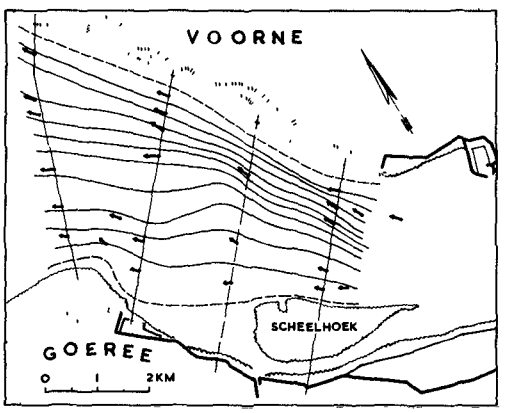

Fig. 6c.

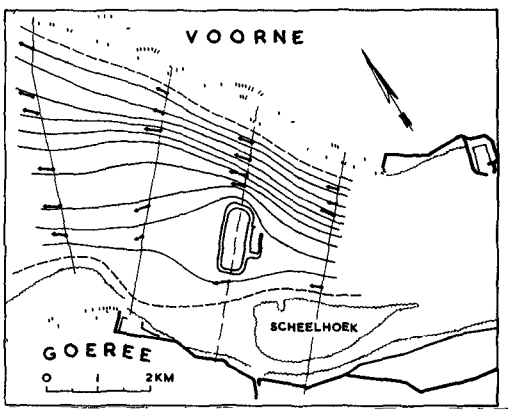

Fig. 6d.

Fig. 6

(a) Flood current in Haringvliet without construction pit.
(b) Flood current in Haringvliet with construction pit.
(c) Ebb current in Haringvliet without construction pit.
(d) Ebb current in Haringvliet with construction pit.

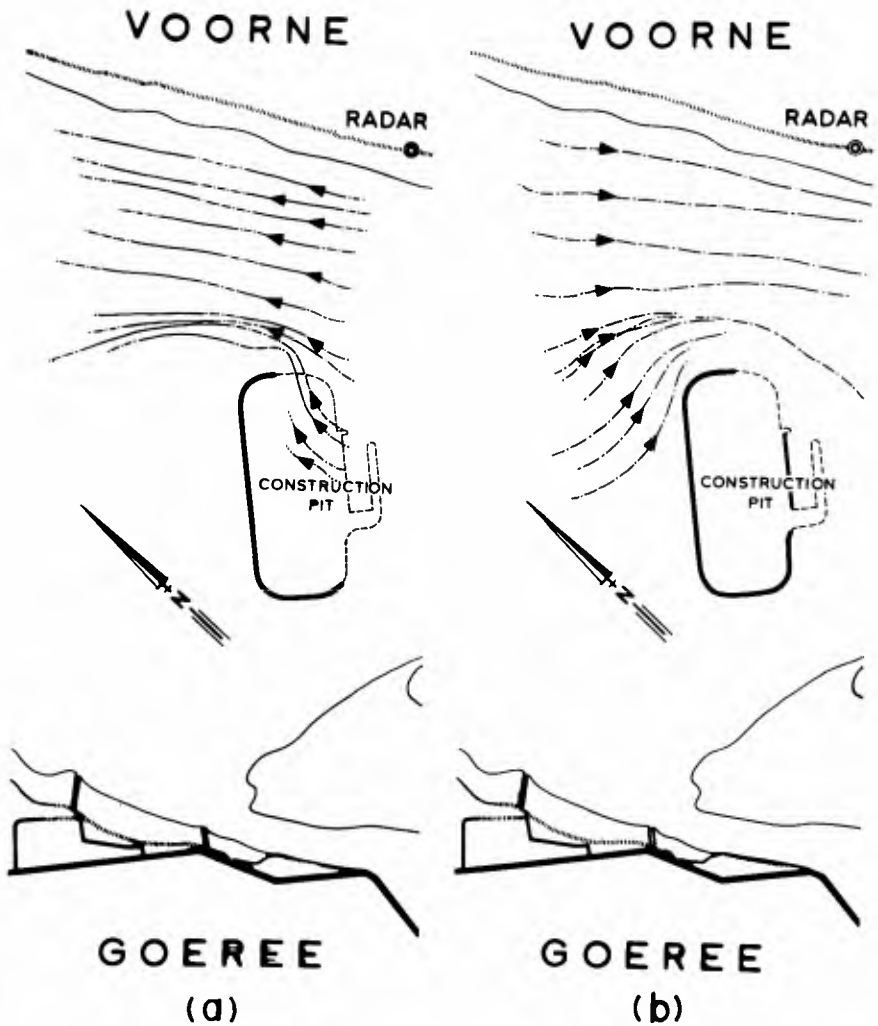

Fig. 7. (a) Ebb flow pattern determined with radar. (b) Flood flow pattern determined with radar.

Fig. 8. Radar picture of wave pattern Veerse Gat.

Fig. 9. Radar picture of wave pattern Haringvliet.

of weather maps and the wave motion at a certain place and moment can be determined roughly in the case of a deep sea by means of the relevant well-known formulae or graphs. Similar calculations can also be applied in the case of more shallow waters, but many difficulties are met with when such factors as diffraction, refraction, bottom friction, breaking, currents, etc., play an important part. Many such like problems also arise in the case of the coastal waters and the complicated estuaries in the south-west and here this method is generally impracticable. Then it is necessary to collect all the wave characteristics such as height, period and pattern locally by direct measurement and compare these data with the meteorological conditions.

The measurement of the height and period of waves only as a function of time at certain fixed points can be done visually or with the help of various kinds of instruments developed in recent years. Measuring poles equipped with wave recorders have been at placed at various spots in the Delta area. Determination of the direction of propagation of waves, or more generally the wave pattern, is a more complicated matter.

Visual observation of wave direction is usually unsatisfactory. Only a limited area can be seen from the shore or ship generally. Often it is very difficult to distinguish between waves coming from different directions, especially when the observer is low down. Moreover, short waves generated by local winds often hide the more important ground swell arriving from distant storms so that the observer will often only report the direction of local wind-waves and not that of a swell.

One of the oldest ways of measuring wave direction is the photogrammetrical method. This and the radar method, which will be discussed later, are the only means so far known by which the wave pattern in the coastal region and in the estuaries in the south-west could be studied systematically.

For extensive areas the photogrammetrical method can only be used when the photographs are taken from an aircraft. In the Delta project this method is used to study the deformation of waves during their propagation as they move from the relatively deep sea in towards the shore.
Stereographic aerial photographs are taken from two aircrafts flying at a speed of about 540 km.p.h and an altitude of 5000 ft. The shutter mechanisms of the cameras are synchronised electronically. This method has the advantage that wide areas can be covered in a relatively short period. On the other hand, however, this method can only be used when weather conditions are favourable. They are not often so when gales are blowing. The altitude of the clouds and unfavourable illumination of the sea surface are the main limiting factors. This disadvantage becomes apparent when the wave pattern has to be determined under various tidal conditions and for different wind directions. For this purpose numerous flights have to be made, which is in most cases almost impossible and very expensive. The only alternative is radar. This method is almost independent of weather conditions and observations can be made at night as well as in

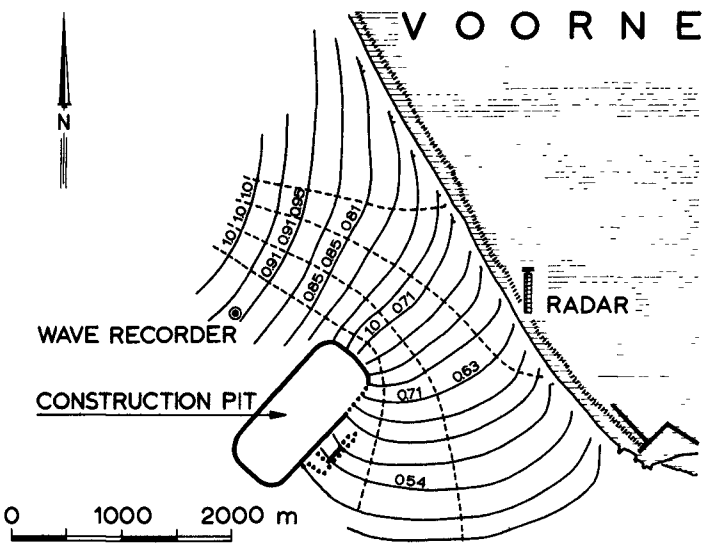

Fig. 10. Schematisation of wave pattern Haringvliet.

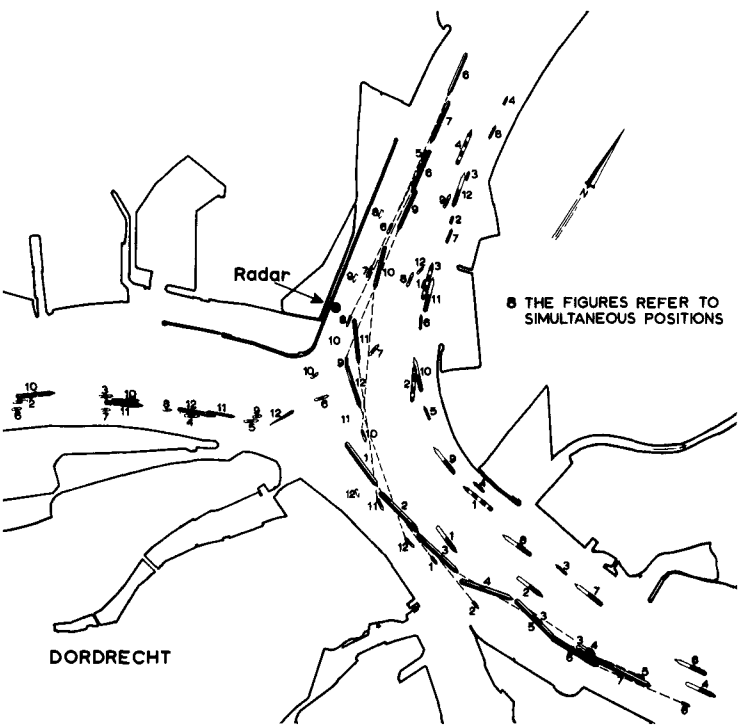

Fig. 11. Ship tracks at Dordrecht junction.

day-light. Readings can be taken continuously throughout a storm and under all tidal conditions.

For this purpose the 8 mm radar set is used with its scanner located about 12 m above sea level. This enables the wave pattern to be determined up to about 3 km from the radar set. Fig.8 shows a radar picture of the wave pattern at Veersche Gat in the south-west. In this picture the wave pattern is visible 2500 mtrs away. Radar photographs obviate the necessity of making refraction computations which can be very laborious for complicated estuaries. Fig.9 shows a radar picture of the wave pattern at the Haringvliet estuary in the vicinity of the building pit. A simplified wave pattern can be obtained direct from this photograph. Fig.10 shows this simplified pattern on which the orthogonals have been drawn, together with the calculated reduction in the wave height.

A skilled man is needed for this work, one who is familiar with the method of making refraction computations, especially when several wave patterns are superimposed.

DETERMINING THE BEHAVIOUR OF SHIPS IN FAIRWAYS

The changes in tidal movement at several shipping-route junctions due to the construction of the Deltaworks will give rise to some problems. Hydraulic reduced-scale models of these junctions are being constructed in which the future flow-pattern and the consequences of the changes for navigation will be investigated.

In these models the movements of ships are imitated by self-propelled scale models of several types. The model is tested by observing the behaviour of these ships under the present flow-conditions. For this purpose the tracks of actual ships have to be determined in reality.

In view of the high speed of the ships they have to be located at intervals of about 45 sec. This rules out the use of aerial photographs; this method is also very expensive because of the numerous flights which have to be made to get enough material. Shipping is very dense at various junctions from 6 to 10 ships approaching the junction simultaneously. This makes it impossible to determine the positions of the ships in the fairway from the shore with theodolites.

This is where radar comes in. Fig.11 shows the result of a radar shipping measurement carried out in the vicinity of Dordrecht.

A 3 cm Decca 214 river radar was used. This type of radar is specially designed for short-range work, and it is sufficiently accurate when one considers the size of the vessels.

The photographs of the radar screen were taken at intervals of 45 sec. The radar picture extended to 2000 mtrs.

The results of this and numerous other measurements carried out under various conditions were a great help in evaluating the model results.

REFERENCES

[1] The use of radar at sea, published by the British Institute of Navigation; Hollis and Carter, London 1952

[2] R.J. Heyboer Millimeter radar."De Ingenieur". Jrg.79 nr.14 (Dutch text)

[3] M. Katzin On the Mechanisms of Radar Sea Clutter. Proceedings of the I.R.E., January 1957

[4] B. Holm
E. Palmgen Reflecteurs de Radar - Quelqùes Nouvelles conceptions
International Conference on Lighthouses and other aids to Navigation, Scheveningen 1955.

CHAPTER 5

AN INSTRUMENTATION SYSTEM FOR WAVE MEASUREMENTS, RECORDING AND ANALYSIS

by

H. G. Farmer and D. D. Ketchum

Woods Hole Oceanographic Institution
Woods Hole, Massachusetts

ABSTRACT

For the instrumentation system to be described, it was required that the system detect the sea surface accurately, be flexible in dynamic range, be able to detect and record at least six wave records simultaneously, be able to record the data at a station remote from the detectors, and be able to convert the data from analogue to digital form for analysis by electronic computers. Two types of wave measurements were required, the wave elevation and the wave slope. Resistance wire detectors were used and the theory of their operation is presented. The data acquisition and reduction system utilize recently developed telemetry techniques. Raw data storage is on magnetic tape using an inexpensive tape recorder and the digital data storage utilizes punched paper tape. The resistance wires have proven most satisfactory for small and large waves. The data acquisition and reduction system is sufficiently general that it should have application to other type investigations.

INTRODUCTION

The instrumentation system to be described in this paper was developed for use with several research projects concerned with wind generated waves. It was developed at the Woods Hole Oceanographic Institution (WHOI) and has been in operation for the last year. These investigations required that the wave elevation be measured at several discrete points, these several channels of data to be recorded simultaneously as a function of time. A closely allied experiment required measurement of the instantaneous slope of the sea surface referred to two horizontal axes aligned parallel and perpendicular to the wind direction. To accomplish these aims it was necessary to develop a suitable measuring instrument, and because of the expected large quantity of data and extensive calculations to be done, an efficient and practical means for recording and data reduction was needed. It was assumed at the outset that nearly all of the calculations would be carried out on an electronic digital computer.

It was planned that a large number of the wave observations would be taken from a tower situated in Buzzards Bay, a line of sight distance of two miles from the Oceanographic Institution in Woods Hole.

*Contribution No. 1131 from the Woods Hole Oceanographic Institution.

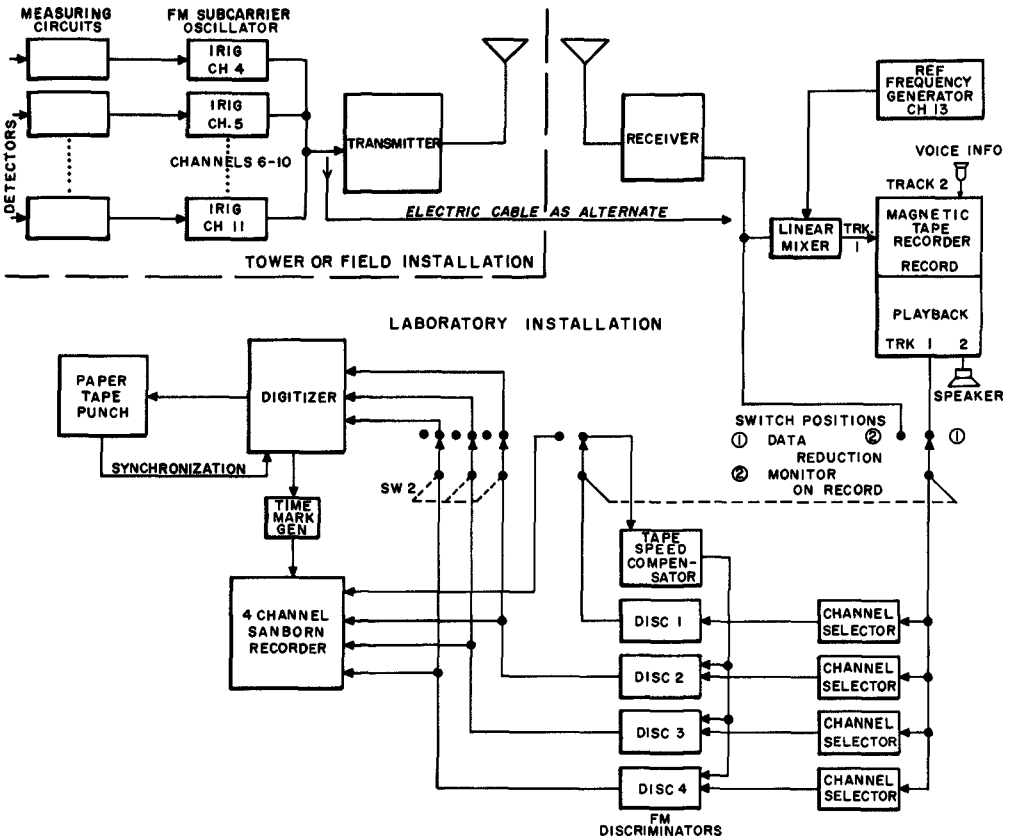

Fig. 1. WHOI multi-channel data acquisition and reduction system.

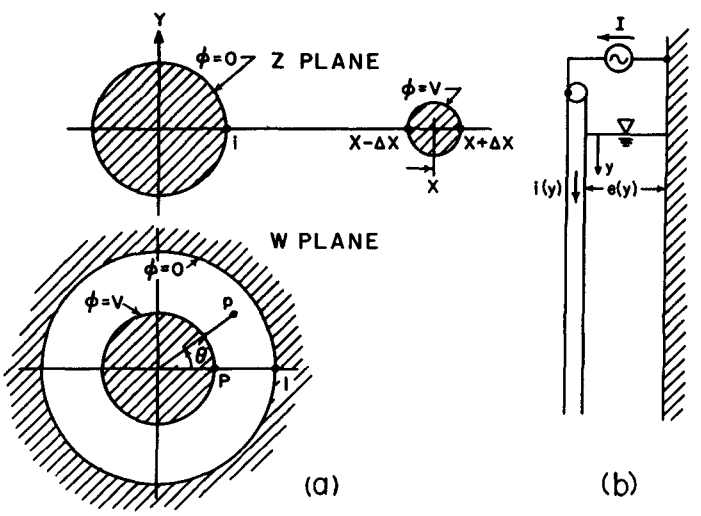

Fig. 2. (a) Geometry of wire and ground conductor and their transformation, (b) Schematic diagram of single wire transmission line and parallel ground plane, constant current source.

Because of the physical conditions at the tower, only the necessary measuring circuits would be placed there and the several data channels, a total of eight, would be telemetered by radio to the laboratory, where they could be monitored and recorded. Furthermore, it was anticipated that observations would be made from other installations, and therefore the measuring and monitoring equipment should be kept portable.

An accurate measurement of the sea surface elevation immediately precluded any use of the well known pressure type wave recorder. Other techniques considered included the step-resistor type, Caldwell (1948), capacitance wire type, Tucker and Charnock (1955) and Whittenbury (1956) and the resistance wire type, Gerhardt, Jehn and Katz (1955). To take the difference in elevation of the sea surface between two points spaced close together, say approximately 6 inches, was considered adequate for the slope determination. This would require an accurate measure of the elevation at each point, and consequently the detectors must cause an absolute minimum disturbance to the water surface. It was hoped to make such measurements on waves up to six feet in height. For just the elevation observations, waves considerably higher than this were to be measured. The step-resistor gage was discarded as not having sufficient resolution, and the capacitance gage, although it was briefly investigated, was discarded as not being sufficiently reliable. The resistance wire gage had also been reported by Caldwell (1948), but was not rated favorably as a general purpose, durable, service instrument. The work of Gerhardt, Jehn, and Katz (1955), and also Clayton, Ivey and Teegardin (1954), suggested that this type of instrument, if properly designed and used, would be most satisfactory. A detailed analysis of this method of measurement was made for both the elevation and slope observations. An account of this analysis is given in a later section of this paper.

The complete multi-channel data acquisition and reduction system is illustrated in Fig. 1. In its most recent usage, the eight channels of data comprised six wave records, wind velocity and direction. With the provision of suitable measuring circuits there is no limit to the type of data that can be handled, except for the upper limit of the frequency content of the information. The system can easily accommodate up to twelve data channels, and, by eliminating the voice information, twenty-four data channels can be recorded. Data with frequencies up to 110 cps can be faithfully recorded. A maximum frequency limit of about 10 cps is imposed if the data is to be converted from analogue to digital form using the WHOI electronic digitizer. A 1% accuracy for the overall system was a desirable requirement. Rather than specify this, however, each component was selected for a 1% accuracy, or as close to this as practicable, so that the complete system might well be expected to have an accuracy of 3%. Data would be recorded for time intervals up to one half an hour. This system will also be discussed in detail. The Inter-Range Instrumentation Group (IRIG) Standards used in the system are briefly described in the text.

Finally, a brief description will be given of the field installation, a few practical considerations concerned with it and several examples of the type data collected.

Aside from the contribution this paper may make to the rather specialized subject of wave measurements, it is hoped that the telemetering and recording system will be of general interest since it is flexible enough to lend itself to a number of other uses without major modification. Although the techniques and most of the components involved are familiar to, and indeed were evolved largely be engineers in the missile industry, the authors are of the opinion that the subject is still sufficiently novel to oceanographers to warrant giving a description.

THE RESISTANCE WIRE WAVE MEASURING SYSTEM

The successful use of resistance wires for the measurement of waves requires careful design of the measuring circuits and a knowledge of the electrical behavior of the wires in the water. The wave height sensing devices consist of vertically supported stainless steel wires partly immersed in sea water. A constant current at audio frequency (4 kc/s) flowing in each wire and returning through the water path causes a voltage drop across the exposed portion of the wire proportional to the length of wire exposed. The voltage at the wire terminal after suitable amplification and detection is converted to a proper signal for telemetering to the laboratory for recording.

For the two types of measurements to be made, i.e., surface elevation and surface slope, the principal factors to be considered in the design are as follows:

a) The current and voltage distribution along the wire as a function of depth below the water surface;

b) The degree to which the generator feeding the wires must approximate an ideal current source;

c) The effect on the slope measuring circuits of the finite input impedance of the differential amplifiers;

d) The resolution of the wire in terms of the smallest measurable increment of the height of the surface.

In actual conditions of usage the resistance wire may be supported from quite different types of towers. At Woods Hole the wires were simply hung outboard of a light steel frame tower which served as the return path for the electrical current exciting the wire. This comprises

a most complicated geometry to analyze in detail. Thus an analysis of (a) may best be performed by idealizing the geometry of the complete wire system. If the wire is considered to be supported parallel to a large vertical cylindrical conductor, partially immersed in a body of water of infinite extent, then it is possible to treat the immersed portion of the system as a transmission line with series resistance per unit length determined by the type of wire and shunt conductance per unit length determined by the geometry, the conductivity of the water and the polarization impedance at the wire-water interface.

In the following analysis, for the type of operation of the wire contemplated, it is found that for proper linearity of the voltage output with a constant current input it is necessary to maintain a certain minimum length of wire beneath the water surface at all times. For use in sea water with practical wire diameter and assumed geometry, the requirement for this minimum length of submerged wire may be easily met. This particular mode of operation of the wires proves impractical for use in fresh water. However, it is shown that a constant voltage system using a wire of very high conductivity should prove satisfactory. Further, for either the constant voltage or constant current system, it is shown that so long as certain minimum requirements are met, the exact current and voltage distribution along the subsurface portion of the wire are unimportant.

Since the specific resistance of the wire is known or can readily be measured, determination of the properties of the "transmission line" depends upon a knowledge of the shunt admittance existing between the wire and the ground plane. This admittance has two components in series: the polarization admittance arising from the electrochemical reaction at the surface of the wire electrode, and the admittance of the electrolyte, dependent upon the configuration of the electrodes and the physical properties of the water. Each of these admittances is complex, having a component of capacitive susceptance as well as conductance. However, it is well known to those familiar with the technique of sea water conductivity measurements that at frequencies above about 1 kc/s the effect of the capacitance becomes small enough to neglect, and the polarization admittance is essentially constant at a fixed frequency. It is for this reason that the 4 kc/s frequency was selected for the wire excitation. Therefore, although the polarization admittance accounts for a substantial part of the total effect, it can be regarded as a constant, which, since it is in series with the electrolyte admittance, reduces the total admittance to a value below that of the electrolyte admittance alone. In the case of the electrolyte admittance it is also true that the capacitance between the wire and the ground plane is small enough to be neglected at the operating frequency. Hence it only remains to calculate the real part of the electrolyte admittance, which will hereafter be simply termed the shunt conductance.

THE WIRE-GROUND CONDUCTOR FIELD PROBLEM

The determination of the shunt conductance requires the solution of the field problem associated with the configuration shown in Fig. 1a, where a wire of radius Δx is maintained at a potential V with respect to a parallel conductor of unit radius. If it is assumed that the immersed part of the system extends to infinite depth, then because of symmetry the solution for the potential may be found in two dimensions. Application of the following transformation, Churchill (1948), results in a coaxial configuration whose potential can easily be found:

$$w = \frac{z - a}{az - 1} \tag{1}$$

where

$$a = \frac{1 + (x + \Delta x)(x - \Delta x) + \sqrt{[(x+\Delta x)^2-1][(x-\Delta x)^2-1]}}{2x} \tag{2}$$

and the transformed radius is

$$P = \frac{(x + \Delta x)(x - \Delta x) - 1 - \sqrt{[(x+\Delta x)^2-1][(x-\Delta x)^2-1]}}{2x} \tag{3}$$

$$x - \Delta x < a < x + \Delta x \qquad 0 < P < 1 \quad \text{when } x - \Delta x < 1$$

The potential ϕ of the transformed system is

$$\phi = \frac{V}{\ln P} \ln p \tag{4}$$

and the total current per unit length flowing from the wire to the large conductor may be found as follows:

$$\vec{E} = \text{GRAD}\phi = -\frac{\partial \phi}{\partial p} \tag{5}$$

$$i = -\sigma \int_0^{2\pi} \vec{E}\, p\, d\theta = -\frac{2\pi\sigma V}{\ln P} \tag{6}$$

where σ = the conductivity of the water

$\vec{E}$ = the electric field vector

The shunt conductance per unit length is then

$$g = \frac{i}{V} = -\frac{2\pi\sigma}{\ln P} \tag{7}$$

In the practical case being considered the wire diameter is very small compared with the radius of the ground conductor, making the accurate computation of P tedious. The expression for P, eq. (3), may be simplified by replacing the square root term by the first two terms of its binominal expansion and neglecting the term in Δx to the fourth power. This approximation, eq. (8), is therefore valid for values of $\Delta x << x$.

$$P = \Delta x \left(\frac{1}{x^2-1} \right) \tag{8}$$

Rescaling the dimensions of the Z plane to the actual physical dimensions

$$P = \frac{k}{K} \left(\frac{1}{D^2/K^2-1} \right) \tag{9}$$

and from eq. (7) the shunt conductance becomes

$$g = \frac{2 \pi \sigma}{\ln \frac{K}{k} \left(\frac{D^2}{K^2} -1 \right)} \tag{10}$$

where D = Distance between centers

K = Ground conductor radius

k = Wire radius

RESISTANCE WIRE ANALYSIS, CONSTANT CURRENT SOURCE

With the value of the shunt conductance established, the wire and ground conductor may now be regarded as a single wire transmission line parallel to a perfectly conducting ground plane (Fig. 2b). This last assumption is valid since the actual ground conductor is a pipe whose series resistance, because of its relatively great diameter, is negligible compared to the series resistance of the wire. If the original assumption of infinite immersed depth is for the moment maintained, the classic transmission line equations may be written, without, however, the complication of accounting for the reactive components, since the frequency of the wire current will be low enough to neglect series inductance, and the leakage, or shunt conductance, is so high in sea water that the effect of shunt capacitance will be negligible.

The general solution for the voltage with respect to the ground plane and the current in the wire as functions of distance along the

wire are found by well-known methods, Guillemin, (1935), to be

$$e(y) = A\, e^{\sqrt{\rho g}\, y} + B\, e^{-\sqrt{\rho g}\, y} \tag{11}$$

$$i(y) = \sqrt{g/\rho}\ \left[-A\, e^{\sqrt{\rho g}\, y} + B\, e^{-\sqrt{\rho g}\, y} \right], \tag{12}$$

where ρ is the resistance per unit length of the wire,

and y is distance measured from water surface.

The constants are evaluated by applying the end conditions:

$$i(0) = I, \quad i(\infty) = 0 \tag{13}$$

where I = the current in the wire above the water surface.

The voltage and current along the wire are seen to be simple exponential functions of depth.

$$i = I\, e^{-\sqrt{\rho g}\, y} \tag{14}$$

$$e = I \sqrt{\rho/g}\ e^{-\sqrt{\rho g}\, y} \tag{15}$$

Of interest is the depth at which the current decays to a negligible value. If this critical depth y_c is defined as the depth at which the current in the wire is reduced to 1% of I, then

$$y_c = \frac{4.60}{\sqrt{\rho g}} \tag{16}$$

It therefore follows that so long as the wire is immersed at least to its critical depth, it will behave as though immersed to infinite depth, and the voltage drop from the wire to ground at the water surface will remain constant as the level of the water changes with respect to the wire. It is this fact that permits us to regard the instantaneous level of the water surface as the position of a short circuit to ground, since the constant voltage drop simply represents a constant zero shift which can be calibrated out.

Substituting the formula for the shunt conductance into eq. (16) and expressing ρ in terms of the wire radius shows how the critical depth depends upon the wire radius with all other parameters held constant. The result of this manipulation is

$$y_c = \frac{4.60\, k}{\sqrt{2\, \sigma\, \rho'}} \sqrt{\ln \left[\frac{K}{k} \left(\frac{D^2}{K^2} - 1 \right) \right]} \tag{17}$$

where ρ' is the resistivity of the metal used for the wire. The critical depth is found to be very nearly linear with respect to the wire radius as is seen in Fig. 3. This is a plot of eq. (17) for the case of stainless steel wire spaced 10 inches on centers from a pipe of one inch radius in sea water of conductivity 0.127 mhos per inch.

When the wire is immersed to a depth λ which is less than the critical depth, the behavior of current and voltage along the wire as a function of depth can be found by noting that the end conditions now become

$$i\ (0) = I,\ i\ (\lambda) = 0 \tag{18}$$

Thus:

$$i\ (y) = I\ \frac{\sinh \sqrt{\rho g}\ (\lambda - y)}{\sinh \sqrt{\rho g}\ \lambda} \tag{19}$$

$$e\ (y) = I \sqrt{\rho / g}\ \frac{\cosh \sqrt{\rho g}\ (\lambda - y)}{\sinh \sqrt{\rho g}\ \lambda} \tag{20}$$

Under these conditions the voltage at the water surface and the voltage at the end become respectively

$$e\ (0) = I \sqrt{\rho / g}\ \coth \sqrt{\rho g}\ \lambda \tag{21}$$

$$e\ (L) = I \sqrt{\rho / g}\ \operatorname{csch} \sqrt{\rho g}\ \lambda \tag{22}$$

The voltage at the surface was measured experimentally in a tank of sea water, using .015" stainless steel wire spaced 5.5 inches on centers from a 3/4" diameter stainless steel pipe. The curve from this experimental data was found to be similar in shape to eq. (22) but displaced from it. This discrepancy is expected to be due principally to the effect of the unknown but nonetheless real polarization admittance. For the manner in which the resistance wires were to be used an estimate of this polarization admittance was not required. However, an experiment of this sort could provide such an estimate.

In situations where it may be impractical to employ a wire of sufficient length to reach critical depth, terminating the wire in its characteristic impedance, $\sqrt{\rho / g}$, should, in theory, simulate an infinite length of wire below the surface. In this manner e (0) could be held constant for short lengths of wire.

In order for the voltage drop across the exposed portion of the wire to be proportional to the exposed length, the current I must be constant and independent of the position of the water surface. Indeed,

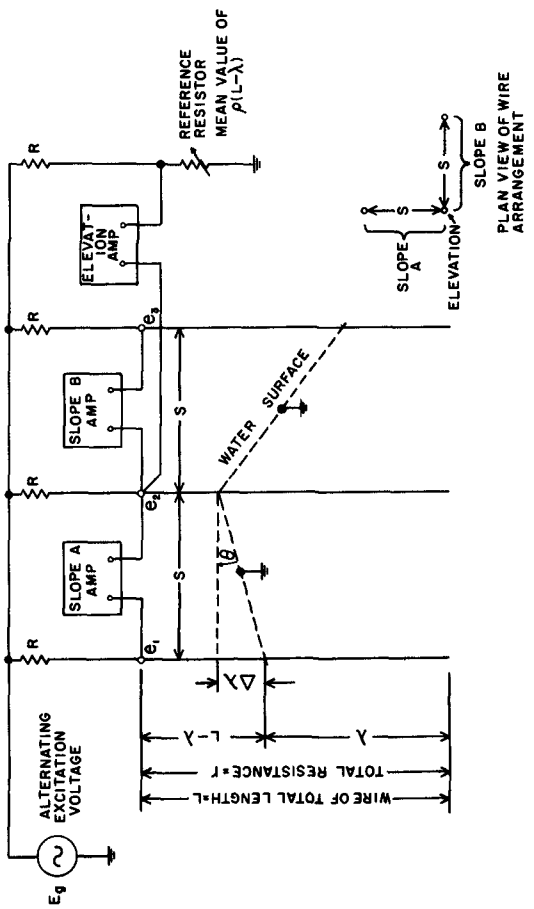

Fig. 4. Schematic diagram of measuring circuits and wire detectors.

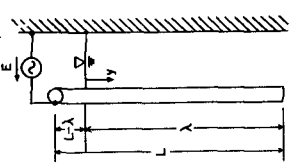

Fig. 5. Schematic diagram of single wire transmission line and parallel ground plane, constant voltage source.

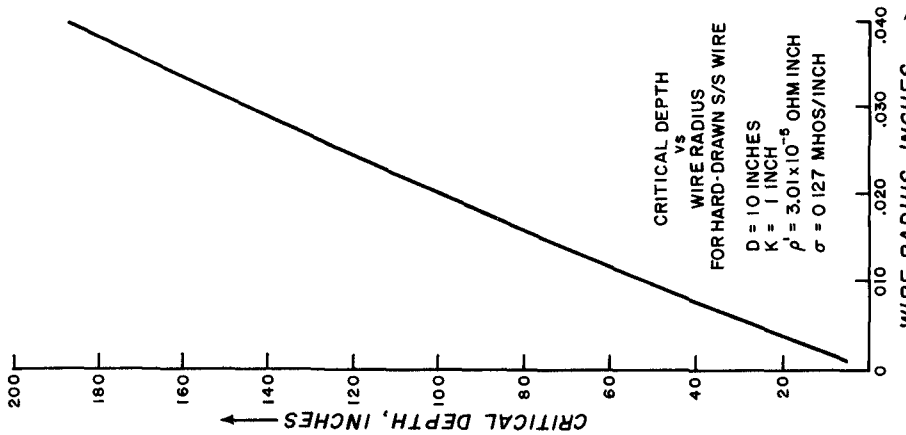

Fig. 3. Critical wire depth vs. wire radius, eq. 17.

the preceding analysis is based upon this assumption. The accuracy of the device is therefore dependent, among other things, upon two factors: namely, the degree to which the wire excitation source approximates a current source, and the degree to which the input impedance of the amplifiers associated with the wire approximates an open circuit.

The diagram in Fig. 4 shows how the equal current sources are approximated. Current regulation with respect to load variations is achieved by making the resistors R large compared to the sensing wire resistance r. The voltage source E_g is electronically regulated for stability. A simple calculation shows the ratio of series resistance to wire resistance required for a given percentage linearity of the output voltage appearing between one of the terminals and the water.

Assuming for the moment that the inputs of the amplifiers are open circuits, and for simplicity that the water surface is a short circuit, we will consider one individual wire. It is desired that the relation between the wire output voltage and the water height be linear within specified limits over the total range of interest. The output voltage is given by

$$e_2(\lambda) = \frac{E_g \, r/L \, (L - \lambda)}{r/L \, (L - \lambda) + R} \tag{23}$$

The elevation sensitivity $d e_2/d\lambda$ must remain between specified limits to insure the desired linearity. (24)

Thus for 1% linearity,

$$\left.\frac{d e_2}{d\lambda}\right|_L - \left.\frac{d e_2}{d\lambda}\right|_0 = \frac{1}{100} \left.\frac{d e_2}{d\lambda}\right|_0 \tag{25}$$

Solution of (25) for R yields

$$R = 200\, r \tag{26}$$

In the case of a slope determination the difference between the voltages at the terminals of two parallel wires whose spacing is known is measured by means of a differential amplifier. Analysis of the effect of the ratio R/r on the accuracy of this measurement shows that the voltage representing the slope is not nearly so sensitive to change in the elevation of the water surface as the elevation linearity. If we consider a pair of wires and assign the symbols e_1 and e_2 to the voltages at the terminals of the two wires, see Fig. 4, with respect to

the water surface (considered as ground), then the slope of the water surface in the direction of a line connecting the two wires is proportional to e_{12} , the difference between e_1 and e_2 . We must investigate how this difference varies for a constant slope over the length λ . Sufficient information for this purpose is given by comparing the expressions for the slope voltage at maximum and minimum elevation. Thus,

$$e_{12} = e_1 (\lambda) - e_2 (\lambda + \Delta\lambda) \tag{27}$$

and eq. (23) may be used for e_1 and e_2 .

By taking the difference of e_{12} determined at $\lambda = L - \Delta\lambda$ and $\lambda = 0$, assuming $r \Delta\lambda << R L$, and allowing a maximum slope voltage variation of 1% over the range L, the following value of the resistance R is obtained

$$R = 1.58 r \tag{28}$$

Thus the requirement of eq. (26) more than fulfills the requirement for slope voltage accuracy over the length of the resistance wires.

The preceding discussion has been based on the assumption that the input impedance of the differential amplifiers is infinite. Although this is far from the actual case, it may be shown that if these impedances can be made high compared to the wire resistance, the above assumption is valid. Since the highest value of wire resistance contemplated in this design is about 20 ohms, it was possible to obtain an adequately high input impedance to the differential amplifiers which are of transistor design.

In the preceding analyses, the derived relations define the parameter of the sensing circuit and establish criteria for the sensitivity of the amplifier detector units and the output level of the stabilized voltage source. The maximum exposed wire resistance was chosen as nominally 20 ohms, which corresponds to about 10 feet of .015" diameter stainless steel wire. Thus, in providing the constant current source for the wire excitation, the series resistors R must be at least 4000 ohms according to eq. (26). Precision resistors with an accuracy $\pm$ .05% were used to insure that the currents flowing in each wire were identical.

RESISTANCE WIRE ANALYSIS, CONSTANT VOLTAGE SOURCE

An extension of the foregoing analysis shows how a wire may be used to measure waves in fresh water, where the conductivity is several orders of magnitude less than that of sea water. In this case a wire of very low specific resistance is driven with a voltage source E, as shown in

Fig. 5. Below the fresh water surface $y \geq 0$ equations 11 and 12 hold, and for $y \leq 0$:

$$e(y) = E - \rho (L - \lambda + y) i_0 \tag{29}$$

$$i(y) = i_0 = i(0) \tag{30}$$

Applying the end conditions

$$e(0) = A + B = E - \rho (L - \lambda) i_0 \tag{31}$$

$$i(\lambda) = 0 = -A e^{\sqrt{\rho g}\,\lambda} + B e^{-\sqrt{\rho g}\,\lambda} \tag{32}$$

and solving for i_0, we find the current in the exposed portion of the wire to be

$$i_0 = \frac{(1 - e^{-2\sqrt{\rho g}\,\lambda})\sqrt{g/\rho}\,E}{e^{-2\sqrt{\rho g}\,\lambda} + 1 + (1 - e^{-2\sqrt{\rho g}\,\lambda})\sqrt{\rho g}\,(L - \lambda)} \tag{33}$$

So long as $2\sqrt{\rho g}\,\lambda << 1$, equation (33) reduces to the approximation

$$i_0 = g E \lambda \tag{34}$$

showing that the current from the voltage source is directly proportional to the length of the immersed portion of the wire. For the range of conductivity encountered in most tap water it appears that the above criterion can be met by using copper wire of moderate diameter in lengths up to 10 feet. Calculation of the shunt capacitance of a typical system indicates that at low to medium audio frequencies the shunt susceptance is very small compared to the shunt conductance in fresh water. Hence as in the sea water system the analysis is valid without consideration of the reactive components.

VERIFICATION, MEASUREMENT RESOLUTION AND ADDITIONAL COMMENTS

It was found experimentally that the mean resolution of the current-driven wave measuring wire was limited to the order of 0.2 inch for a 12 foot length of wire. This result was demonstrated by an experiment where a pair of parallel wires was lowered and raised in a deep tank of sea water over a distance of 12 feet and maintained perpendicular to the calm surface. The output voltage from a single wire was measured for elevation. The output voltage from the differential amplifier fed from the two wire terminals, instead of remaining at zero, was observed to vary about its zero value in an erratic fashion. With a wire spacing of 6 inches the standard deviation from the mean value corresponded to 0.17 inch which was equivalent to a slope of 1.6°. Since careful attention had been devoted to the design of the differential amplifier, this effect could not be attributed to faulty common mode rejection or imperfect balance in the

electronic circuits. The elevation measurements over the full range of immersion indicated the predicted linearity, but the difference measurements provided a measure of the resolution available.

The only plausible explanation for this "noise" appeared to be small random variations in the polarization admittance caused by surface contamination of the wire. Thus it was at least logical to assume that a thin but non-uniform layer of grease or contaminate could result in the admittance varying randomly with depth along the wire. Since the polarization admittance is a component of the shunt conductance, g, variations in the former would cause variations in e (0), upon whose constancy with surface height the system depends for its linearity. This thesis was partially supported by the fact that degreasing agents applied to the wires immediately prior to immersion caused changes in the effect, without, however, eliminating it.

In any case, since it would not be possible to maintain uncontaminated wires in field operation, a full-scale range of the order of two feet seems to be the practical limit where accuracy of one per cent of full scale is desired in an elevation wire, while the spacing of slope wires cannot be less than about six inches for angular accuracy of better than about 2^{o}.

In the equipment as it was actually built the signals from each of the elevation wires as well as the signals from the pairs of slope wires were amplified with differential amplifiers and detected with phase sensitive detectors. By adjustment of the various gain settings, the final output voltage was standardized to a 0-5 volt range for entry into the telemetering equipment. Differential amplifiers were used in the elevation circuits so that it would be possible to subtract from the wave wire signal another signal equivalent approximately to the mean length of unimmersed wire, refer to Fig. 4. This reference resistor is variable so that a proper adjustment may be made whatever the state of the tide. The total "swing" of the differential amplifier output is then primarily due to just the wave signal. The amplifier sensitivity is adjusted so that its full scale excursion in both directions is caused by the highest expected waves. The variable reference resistor may take the form of another wave wire which is supported in a tide tube. This tube would be designed so that the reference wire senses only tidal variation.

The design of the differential amplifier, particularly those for the slope measurements, required great care to be taken to insure high common mode rejection. The common mode rejection ratio of the amplifiers is determined by measuring the differential gain, the ratio of output voltage to the difference between the two input voltages. The two input voltages are made equal by tying the two input terminals together and the ratio of the output voltage to the common input voltage, or common mode gain, is measured. The common mode rejection ratio obtained was in the order of 10,000.

The 4 kc/s outputs of the differential amplifiers are detected in phase sensitive detectors, the magnitude of whose D.C. output is proportional to the amplified difference voltage applied. The polarity of each phase detector output is dependent upon the phase of the input compared to that of the fixed reference phase of the wire drive supply. Since the difference voltage undergoes a phase reversal at the point where the voltage difference input to the amplifier becomes zero, the sense of the instantaneous water level is preserved.

WHOI MULTI CHANNEL DATA ACQUISITION AND REDUCTION SYSTEM

The complete system in its present operational form is illustrated in Fig. 1. Two main divisions of the equipment have been made, the field installation and the laboratory installation. The means for telemetering the information between these two stations may be either by radio or electrical cable with each method requiring its own special terminal equipment. All of the data received at the laboratory in its full analogue form is recorded on magnetic tape, which serves as the raw data storage. Upon playback the data may be monitored, edited, digitized, or otherwise operated upon without altering the original data recording. Since the analysis was to be carried out on an electronic digital computer it was necessary to provide an analogue-to-digital converter and a means of storage, punched paper tape, for the digital information.

Besides the accuracy requirement of 1% for each component it was considered important to keep the system as adaptable as possible to a wide variety of applications and problems. As always it was necessary to keep the overall cost at a minimum.

The design of the telemetering apparatus was fortunately much simplified by the fact that the art of FM/FM telemetry has reached the advanced state where standard components are available from commercial manufacturers. Standard subcarrier frequencies, channel spacings and bandwidths, designed to permit optimum use of the available spectrum consistent with the requirements of bandwidth and signal-to-noise ratio have for some years been promulgated by the Inter-Range Instrumentation Group (IRIG) and are widely accepted by the industry. Nichols and Rauch (1957) give a comprehensive introduction to the theory and practice in the field of radio telemetry. When analogue information is to be transmitted any distance by radio, it is well known that frequency modulation best preserves the information against distortion by extraneous noise. Similarly, for magnetic tape recording as well as for radio transmission when the information data frequencies extend down to zero it is necessary to utilize frequency modulation (FM) to preserve this information. To

obtain a number of data channels for transmission over a single radio frequency carrier or for recording on a single track magnetic tape recorder, the range of frequencies extending from about .4 kc to 70 kc has been divided up into a number of bands each of which is assigned a center frequency. See Table I. The information signal is then used to frequency modulate this center frequency, the maximum deviation for each band being $\pm$ 7 1/2% of its center frequency. From the table it will be seen that the maximum intelligence frequency depends on the subcarrier band selected. The WHOI system utilizes the IRIG data channels 4 through 11 but can accommodate channels 1 through 12.

A most satisfactory means for recording these several channels of data is on magnetic tape. It is significant to note that an expensive instrumentation recorder is not required. A relatively inexpensive, portable, hi-fidelity, dual track tape recorder has proven adequate for the job. One track is used for data recording, and voice information is put on the second track. In this manner the data may be documented with whatever additional information is needed while it is being recorded. Because of slight irregularities in the motion of the tape on both record and playback, occurring in all tape recorders, FM recorded data may be very seriously distorted. This difficulty can be virtually eliminated, however, by recording along with the data a stable reference or control frequency. Upon playback the variations in this frequency are used to correct the data restoring it to its original form well within the accuracy limits of the overall system. This correction process is referred to as tape speed compensation.

The field installation comprises the detectors, measuring circuits, FM subcarrier oscillators and, if required, a radio transmitter. The FM subcarrier oscillators are voltage controlled, a 0 to 5 volt swing at the input causing the output frequency to range from its lower to its upper limit. In order effectively to utilize the accuracy available in this telemetering and recording system, the sensitivity of the measuring circuits should be so adjusted that full scale of the information corresponds to the full 0-5 volt range of the subcarrier oscillator. Generally this can be easily done. The outputs of the oscillators are then linearly mixed and the combined signal is fed to the FM transmitter. It is by virtue of the information frequency modulating the subcarriers, and the several subcarriers frequency modulating the radio frequency carrier that the system is referred to as FM/FM telemetry. In those field installations where electrical power is primarily supplied by batteries, it is desirable to use as much transistorized circuitry as possible in order to prolong battery life and reduce the number of batteries required. Transistorized subcarrier oscillators are commercially available and are extremely rugged and highly dependable. The measuring circuits designed and built at WHOI for the wave observations were also transistorized.

TABLE I

IRIG STANDARD SUBCARRIER BANDS

Channel	Center Frequency (cps)	Deviation (cps)	Lower Limit (cps)	Upper Limit (cps)	Maximum Intelligence Frequency (Modulation Index 5) (cps)
		± 7 1/2% Deviation Channels			
1	400	± 30	370	430	6.0
2	560	42	518	602	8.4
3	730	55	675	785	11
4	960	72	888	1,032	14
5	1.3 kc/s	98	1,202	1,398	20
6	1.7	128	1,572	1,828	25
7	2.3	173	2,127	2,473	35
8	3.0	225	2,775	3,225	45
9	3.9	293	3,607	4,193	59
10	5.4	405	4,995	5,805	81
11	7.35	551	6,799	7,901	110
12	10.5	788	9,712	11,288	160
13	14.5	1,088	13,412	15,588	220
14	22.0	1,650	20,350	23,650	330
15	30.0	2,250	27,750	32,250	450
16	40.0	3,000	37,000	43,000	600
17	52.5	3,940	48,560	56,440	790
18	70.0	5,250	64,750	75,250	1,050

In choosing the means for telemetering the information from the field to the laboratory installation several factors must be considered. Among these are the total number of data channels, the channel center frequencies, the range of transmission, whether or not line of sight communication exists, etc. Generally if a large number of data channels are required and IRIG channel 7 or greater is used, the total band width of these data channels will require for radio transmission a VHF (say 230 mc) carrier with frequency modulation. This VHF-FM radio link will provide high quality telemetry, but the line of sight transmission may introduce a range limitation. With fewer data channels, IRIG 1 thru 6, the total band width of the several channels will permit use of an HF (2-6 mc) carrier but with amplitude modulation. In this case, the range of transmission will be greatly increased but there may also be some sacrifice in quality.

Electrical cables may also be used for the telemetering link. In this case the subcarrier signals are fed directly to the cable. Here again the band width and frequencies of the transmitted signals will dictate the selection of the cable. Generally if the band width is large and the higher frequency data channels are used a coaxial cable will be required.

At the laboratory the output of the FM receiver is linearly mixed with the reference frequency, 14.5 kc/s the center frequency of IRIG channel 13, and recorded with the magnetic tape recorder. At the same time, with switch 1 in position 2 any four of the data channels may be selected, using the appropriate channel selectors, sharp cut off band pass filters, discriminated and recorded on the four channel Sanborn recorder. This ability to monitor the data while it is being recorded is considered an important function of the system.

In the data reduction phase, one, two or three data channels may be arbitrarily chosen using the channel selectors. The fourth discriminator is used in conjunction with the tape speed compensator. The graphic recorder and the digitizer are both fed directly from the discriminator outputs, which are faithful reproductions of the original data.

The paper tape punch is driven by a 3600 rpm synchronous motor and contact closures operated by the motor provide timing signals and synchronization to the digitizer. The digitizer accepts a maximum of three data channels and digitizes them sequentially. Each channel is switched in, a sample is taken, converted to a seven level binary number and punched out on the paper tape, all in 1/60 second. The same sequence of events follows for the next two channels, a total of 1/20 of a second being required for the complete operation on all three

channels. Following this sequence the paper tape is advanced with no punch, thus providing a space, i.e., a fourth channel with zero punch, to separate this data group from the next data group to be punched. Preselected sample rates of 15, 10, 5, 3, 2, 1 per second are provided. A time mark generator controlled by the digitizer provides a tick mark on the graphic record at each time a group is sampled.

A seven level binary code was selected for the digital format for two reasons. First, the seven level binary code provides for any number from 0 to 127 thus permitting a digitizing accuracy of better than 1%. The second reason is that with the straight binary code the Teletype tape punch can punch any number up to 127 in a single operation, thus permitting a rapid digitizing rate and also the optimum packing density of information on the paper tape. The relatively fast operation approximates simultaneous digitization of the three data channels if their signals do not vary rapidly. This scanning rate was a specific requirement in setting forth the specifications for the digitizer and tape punch. In any event the time difference between adjacent channels is 1/60 second plus or minus approximately 3/4 millisecond on the average.

There is one disadvantage to the use of the seven level binary code which should be clearly emphasized. No electronic computer known to the authors or their associates uses this particular code for normal entry of data. However, data entry has been easily accomplished in two cases using available paper tape readers. The IBM 46 tape-to-card punch has been used to transfer the data to IBM cards. This IBM 46 has been more effectively used, however, as a tape reader for direct entry of the data into an IBM 650 computer. A tape reader has also been provided for entry of the data directly into the Autonetics Recomp II computer. In both of these computers, through programming, the data is then put into proper format for subsequent calculation. Mr. R. G. Stevens of the WHOI has done all the work pertaining to the entry of the punched paper tape data into these two computers.

The digitizer was specially built because of its particular operating characteristics. The only other piece of equipment which required any special attention in its selection was the tape recorder. Because of the recording of FM signals, in selecting the tape recorder it was necessary to specify that the intermodulation distortion be kept as low as practicable. This was satisfied with the installation of a higher quality recording-reproducing head than normally supplied. However, in so doing, the frequency response of the recorder was reduced to 15 kc/s at 15 inches/second. It is for this reason that the total number of data channels that could be recorded on each track of the tape was limited to the first twelve, the thirteenth channel being required for tape speed compensation. The recorder has three standard operating speeds, 15, 7 1/2 and 3 3/4 inches/second, and with a small modification 1 7/8 inches/second. At this lowest tape speed using standard 1.5 mil magnetic

Fig. 6. WHOI tower situated in Buzzards Bay, Mass., water depth 42 feet. 0.015 inch diameter SS wire detectors hang from coaxial cables supported off left edge of tower.

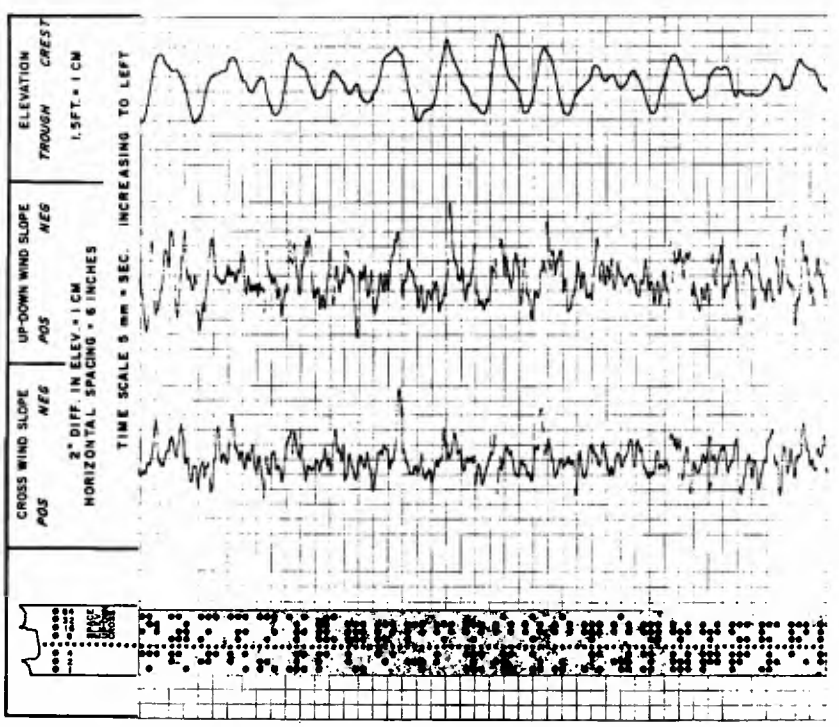

Fig. 7. Sample data obtained with resistance wire detectors. The heave lines are at 5 mm spacing. Bottom figure is sample of punched paper tape digitized at 10 groups per second. Tape is unrelated to data above.

tape, recordings of eight hours in duration can be made using the first five data channels. By in large, the intelligence frequencies present in oceanographic data are very low. For the wave studies carried out at WHOI it was necessary, however, to be able to record faithfully frequencies up to 10 cps. As is apparent in Table I, the system can record intelligence frequencies up to 110 cps. Thus, with faster digitizing equipment, the system may have a much wider range of application in other types of research. For the WHOI or similar type system further applications more directly related to the field of oceanography have been discussed briefly in Ref. 10.

In this section the intent has been to describe the data acquisition and reduction system through a rather general description, but of sufficient detail that its operating characteristics are clearly understood. Several practical features of the system have been emphasized because of their versatile and practical aspects. Finally, it is believed that the system presents a unified and logical concept in data handling.

THE FIELD INSTALLATION AND RECENT OBSERVATIONS

An extensive program of wave observations has been carried out using the equipment described in the preceding sections. A tower was placed in Buzzards Bay in water 42 feet deep and at a location 2 miles line of sight distance from the laboratory in Woods Hole. The tower, which is of light steel frame construction and 60 feet in height, was originally designed as a wind mill structure. The bottom of each leg is fitted with a large box shaped foot to provide a bearing surface. The lower sections of the tower were reinforced so as to support an additional 6 ton weight to "anchor" the tower to the bottom. A large cast concrete and scrap iron anchor had been previously placed at the proper site. The tower is placed over the anchor and attached to it with an hydraulic cylinder. By pumping oil into the cylinder the tower is anchored to the bottom with a predetermined part of the anchor weight. This manner of installation has proven most satisfactory and the tower has withstood winds in excess of 60 knots and waves up to 6 feet in height. The tower is disconnected from its anchor, picked up and carried to shore and stored during the winter months when heavy icing conditions may prevail. A detailed description of this facility is given by Carver, (1958), and an illustration of the tower is given in Fig. 6.

The wave wires are electrically connected to the input of the measuring circuits with a relatively inexpensive coaxial cable, RG-58AU. Equal lengths of coaxial cable were used for each wave wire detector. The simplest, most expedient and satisfactory means for holding the resistance wire in place was to hang each wire by means of a clamp on the coaxial cable with a small lead ball of about 3 pounds weight tied

on the end of the wire. The submerged length of wire was about 20 feet so that the small lead ball was not subjected to any appreciable fluid velocities resulting from the wave field. The estimated critical length of the 0.015 inch stainless steel wire was about 3.5 to 4 feet. At no time were the wires observed to move because of wave motion or wind.

Referring to Fig. 6 there may be seen the wooden box in the shape of a dog house which encloses all the necessary electronics for obtaining the wave and wind data and telemetering it to the laboratory. Mounted on masts above the tower are the anemometer and wind direction indicator and the 230 mc tuned ground plane antenna. At the laboratory a corner reflector and antenna were mounted above the roof from which sufficient signal strength was obtained for reliable operation. The accumulator and oil tank for the hydraulic anchoring system are also visible.

On another occasion these same type resistance wires were used from a much larger tower installation. Approximately 40 foot lengths of 0.015 inch resistance wire were used and approximately 25 to 30 feet of this was below water level. Satisfactory wave records were obtained in winds in excess of 40 knots and waves 20 to 25 feet in height. The wires were observed to be in some motion dependent upon the size waves encountered. The maximum horizontal motion of the wire was about 1 foot for the highest and longest waves observed.

A sample record of elevation, up-down wind slope and crosswind slope is shown in Fig. 7. The wind speed at the time of recording was 16 knots, having been this speed for the previous hour and before that time the wind had been blowing at about 10 knots. For the up-down wind slope record the negative sign refers to the slope found, on the average, on the side of the wave facing the direction in which it is propagating. The same rule holds for the crosswind slopes if the wave were traveling from left to right when looking into the wind. To obtain the actual slope it is necessary to divide the indicated differences in elevation by the wire spacing which was 6 inches.

At the bottom of Fig. 7 there is reproduced a sample of the punched paper tape for a record similar to that above it. The four channels, crosswind slope, up-down wind slope, elevation and space are indicated in the figure. The group punching rate was 10 times/second.

ACKNOWLEDGMENTS

The developments reported in this paper were made possible through a grant to the Woods Hole Oceanographic Institution from the National Science Foundation of the National Academy of Sciences and in part through a contract with the U. S. Navy Office of Naval Research.

REFERENCES

1. Caldwell, J. M. (1948). An ocean wave measuring instrument: Tech. Memo. No. 6, U. S. Army Corps of Engineers, Washington, D. C.

2. Carver, C. E. Jr. (1958). The WHOI wave tower research facility: Ref. No. 58-51, Woods Hole Oceanographic Institution, Woods Hole, Mass. (Unpublished manuscript)

3. Churchill, R. V. (1948). Introduction to complex variables and applications: McGraw-Hill Book Co., New York

4. Clayton, L., Ivey, H. D. and Teegardin, H. H. (1954). Preliminary study for the development of a sea state meter: Tech. Report No. 6 Engineering Experiment Station Proj. No. 157-96, Georgia Inst. of Tech.

5. Gerhardt, J. R., Jehn, K. H. and Katz, D. (1955). A comparison of step-, pressure- and continuous wire-gage wave recordings in the Golden Gate Channel: Trans. Amer. Geophys. Union Vol. 36, No. 2

6. Guillemin, E. A. (1935). Communication networks: John Wiley and Sons, Inc., New York, Vol. II

7. Nichols, M. H. and Rauch, L. L. (1957). Radio telemetry: John Wiley and Sons, Inc., New York

8. Tucker, M. J. and Charnock, H. (1955). A capacitance-wire recorder for small waves: Proc. 5th Conf. Coastal Eng. Council Wave Res. Univ. of Calif. Berkeley

9. Whittenbury, C. G. (1956). A capacitance probe for recording water waves: Report No. R-84, Control Systems Lab. Univ. of Ill. Urbana, Ill.

10. Proceedings of the conference on automatic data handling for oceanographic observations (1959) Ref. No. 60-10, Woods Hole Oceanographic Institution, Woods Hole, Mass. (Unpublished manuscript)

Chapter 6

SPLASHNIK–THE TAYLOR MODEL BASIN DISPOSABLE WAVE BUOY

WILBUR MARKS*
Head, Ship Hydrodynamics Division
Davidson Laboratory
Stevens Institute of Technology, Hoboken, N. J.

and

ROBERT G. TUCKERMAN
Electronic Engineer, David Taylor Model Basin
Department of the Navy, Washington, D. C.

INTRODUCTION

In connection with full scale ship trials, it is often necessary to have a description of the state of the sea which may be used as a scale against which to measure ship performance. Visual observations of waves have proven to be unreliable in the past and are, in any event, not sufficiently detailed to be adequately descriptive, for many problems. Hindcasting** the state of the sea depends on wind information (speed, duration, area of sea covered, and rate of growth and/or decay) obtained from six hourly weather maps. The wind data is used in conjunction with certain empirical-theoretical formulations to produce an energy spectrum of waves at the place and time of interest. The energy spectrum is a good descriptive tool, because it gives information on the energy content of the wave frequencies present and provides an estimate of the height distribution of the waves as well as certain other statistical quantities. However, hindcasting the wave spectrum is unsatisfactory for two reasons: 1) estimation of the wind field from sparse observations spaced six hours apart is highly subjective, and 2) no specific energy spectrum formulation has as yet been verified.

There is still another method for description of the seaway. If the waves at a fixed point can be measured for a sufficient length of time, then this sample record can be converted into a wave (energy) spectrum that will adequately characterize the state of the sea.

There are many systems that will measure waves, but the requirement that wave measurements complement simultaneous ship motions measurements, in all states of sea, eliminates most of the known instruments. In particular, it is required that the waves be observed at a fixed point for a period of hours, while the ship conducts certain maneuvers which may remove it several miles from the point of observation. This means that the wave measurement system must be physically divorced from the

---

*Physicist, David Taylor Model Basin during the period when this investigation was made.

**Hindcasting is the prediction of an event after it has occurred but has not been observed.

ship*. Furthermore, many tests will be made in heavy seas so that it will not be practical to seek out the instrument and recover it. As a consequence of the conditions imposed by the particular problem stated here, the wave measuring system must be able to:

1. Telemeter information to the ship for at least 7 hours at a distance of at least 8 nautical miles,

2. Be launched from the deck of a ship in waves perhaps 25 feet high, and

3. Be inexpensively constructed ($125.00 - $150.00) so as to be expendable.

Since investigation revealed that no known instrument had embodied in it all three of these features, it was decided to design and build an appropriate system, at the David Taylor Model Basin. After some consideration of the imposed conditions, it was decided that a small floating buoy (SPLASHNIK) which measures apparent vertical acceleration and telemeters the information back to the ship could be designed to fulfill the requirements.

The intent of this paper is to describe the SPLASHNIK system, the data reduction method, some experimental verification of the method, and some proposed improvements. It should be noted that this technique of wave measurement (recording of vertical acceleration) is not new. In fact, one instrument described by Dorrestein (1957) is somewhat similar to the SPLASHNIK and has been in operation for several years. Other institutions are also known to be experimenting with accelerometer wave buoys. However, several basic design differences make the SPLASHNIK especially useful as a tool in the study of ship behavior. A drawing of the SPLASHNIK appears in Figure 1.

OPERATING PRINCIPLES

The general operation of the complete system of sending and recording is shown in Figure 2. An accelerometer consisting of a mass and a flexible arm is attached to the base of the float unit. Part of the mass is an eddy current damper attached near the outer end of the accelerometer arm. As the float moves up and down on the waves, the displacement of the mass in reference to the base causes a radio transmitter to change frequency. The change in frequency is proportional to the acceleration being experienced by the buoy. The output of the transmitter is fed to an antenna mounted on the wave height buoy float. The signal transmitted from the wave height buoy is received at the ship with a wide band receiver which converts the frequency changes of the transmitter into a varying d-c voltage. The varying d-c voltage is proportional to the acceleration being sensed by the accelerometer. The received signal contains high frequency components, which are caused by the very short

*The wave measurement system may be integral with the ship if measurements are made at zero forward speed.

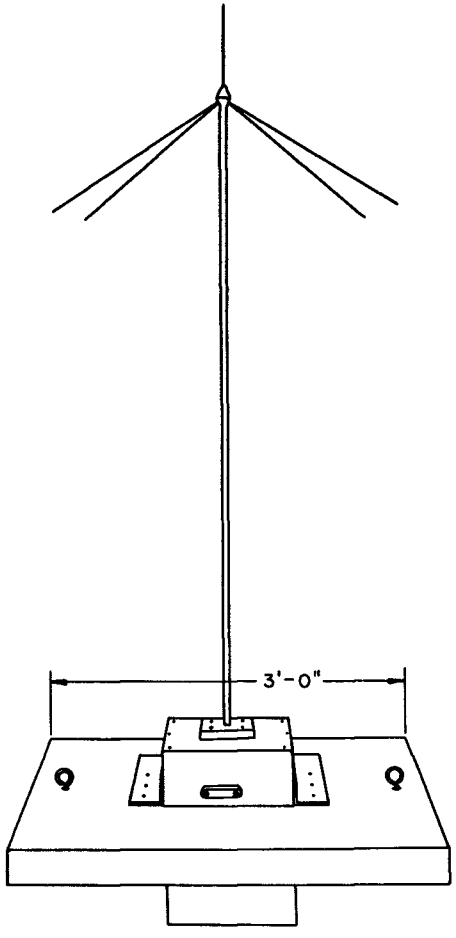

Fig. 1. The SPLASHNIK.

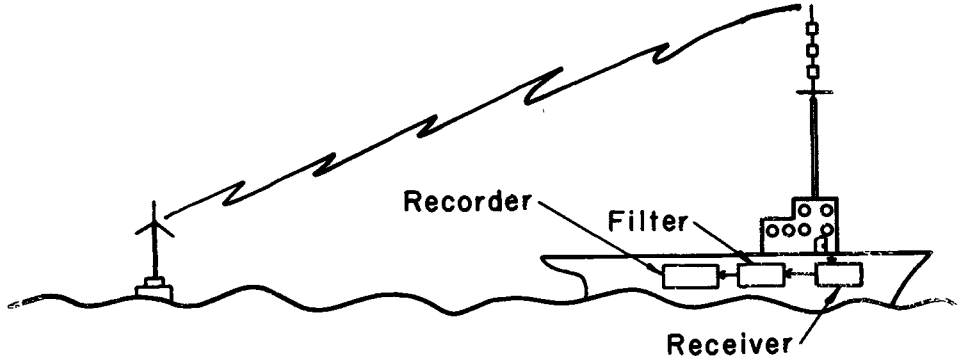

Fig. 2. Wave buoy sensing and recording system.

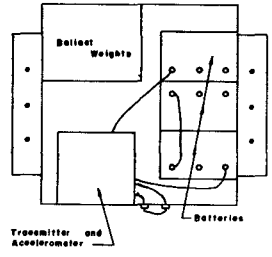

Fig. 3. Layout (top view) of SPLASHNIK instrument box.

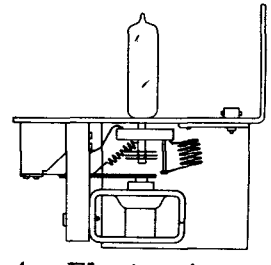

Fig. 4. Electronic system of SPLASHNIK. Transmitter unit appears in upper portion; accelerometer and damper in lower portion.

waves (which contribute little to the ship motions being studied), as well as by mechanical noise of the transmitter unit. These signals are of such a magnitude that if they were allowed to appear on the recording, they would completely mask the desired signal. That is, the gain of the recording system would have to be set so low that the desired signal (associated with frequencies below 1/3 cps) would be too small to read accurately. For this reason, the output of the receiver is applied to a low-pass filter which removes the undesirable high frequencies but allows the desired information to pass through unaltered, except for some phase distortion which is not considered significant for the intended application. The output of the filter is then recorded by whatever means are available, i.e., tape recorder, direct writing recorder, etc.

Calibration of the system is accomplished by establishing a zero reference with the wave height buoy level and then tilting the buoy through 60°. The tilt will produce a frequency change in the transmitter which represents the 1/2-g change which the accelerometer senses due to the 60° tilt. When the signal is received, the receiver will produce a steady d-c voltage output proportional to the transmitter change in frequency and therefore proportional to acceleration. This d-c voltage and the zero obtained when the buoy is level are recorded. The difference between the zero and the voltage produced due to the 60° tilt is the calibration for 1/2-g and all records from that particular wave height buoy may be referred to this calibration.

DETAILED DESCRIPTION OF COMPONENTS

BUOY ASSEMBLY

The buoy assembly of the SPLASHNIK is composed of a buoyancy unit (float), an equipment box and an antenna. The buoyancy unit is made of styrofoam covered with fiberglass cloth impregnated with epoxy resin to give it strength. The float is 3 feet by 3 feet by 3 inches with a 1 foot by 1 foot hole through the center (see Figure 1). The equipment box is mounted through the hole and held fast to the float by sheet aluminum angles. Two eye-bolts are mounted through the float to be used when it is necessary to lower the assembly over the side of a ship into the water.

The equipment box is made of plywood and is coated inside and out with epoxy resin to assure its watertightness for the period of operation. The top of the box is held in place with machine screws and has a rubber gasket between it and the lip of the box to make a watertight closure. The antenna mast is mounted through the top of the box. A ground plane antenna, cut to operating frequency, is mounted on the top of the mast with its feed line running down through the mast into the box. The transmitter unit is attached to one side of the box and the batteries that provide its power are located in the bottom of the box (Figure 3). A bar switch is located on the outside of the box and is used to turn on the equipment.

ACCELEROMETER

The accelerometer is composed of a beryllium copper cantilever arm mounted on a pedestal. The pedestal is attached to the transmitter unit chassis (Figure 4). An aluminum cup is mounted on the lever arm near its free end. When the accelerometer arm moves, the aluminum cup moves in a magnetic field created by a magnet from a dynamic speaker. The motion creates eddy currents in the aluminum cup, which are proportional to the relative velocities of the arm and the base, thereby providing a damping force.

TRANSMITTER

The SPLASHNIK transmitter appears at the top in Figure 4. The transmitter uses a single tube which operates as a self-controlled oscillator on approximately 69 megacycles. The tube also operates as a frequency doubler and amplifier with an output at 138 megacycles. The lever arm of the accelerometer forms one plate of a variable capacitor which is in the oscillator frequency determining circuit. When the accelerometer arm moves, it changes the value of this capacitance which results in a frequency change of the oscillator. The change in frequency due to the movement of the accelerometer arm is very nearly proportional to the acceleration that the accelerometer senses. The capacitance change is adjusted so that a 1/2-g acceleration results in a frequency change of approximately 50 kcs. The output of the transmitter is fed through a coaxial cable to the ground plane antenna. It should be noted that the transmitter was designed with low cost in mind and because of its simplicity, the frequency of its output drifts with temperature and other change This effect will be noticeable in operation and will require the user to occasionally re-tune the receiver during operation.

BATTERY PACK

The battery pack used to power the transmitter is composed of six 45-volt dry batteries that furnish plate and screen voltage for the tube and one 3-volt battery for the tube filament. The batteries are wedged into the bottom of the instrument box and are held in place by wooden braces to prevent them from shifting in a rough sea. The batteries are of sufficient capacity to operate the transmitter for a period of more than eight hours.

RECEIVING ANTENNA

The receiving antenna is of the stacked coaxial type with a ground plane and has a gain of 6 db over a simple dipole. This antenna was used as it provides uniform reception from all directions and has a low angle of radiation. Also, temporary installation aboard ship is quite simple. It should always be installed as high as practical above the water, and clear of obstructions in all directions, to provide the greatest line-of-sight path from the transmitting antenna. The antenna is specifically cut to operate on the frequency of the transmitter (138 megacycles, in this case).

RECEIVER

The receiver is tunable from 55 to 260 megacycles and was chosen for its excellent sensitivity, stability and low noise figure which permits the system to receive signals from the buoy over the greatest possible range. The receiver also has a type of discriminator which produces a d-c output voltage that is quite linear for input frequency change. It has been modified to bring the output of the discriminator out to the back panel.

LOW-PASS FILTER

The output from the wave height buoy contains acceleration information caused by the high frequency short waves which contribute little energy to the wave spectrum in the frequency range of interest. This information will in fact mask the desired lower frequency accelerations of the important gravity wave range. To eliminate the undesired information, an electronic low-pass filter is used. The output of the receiver is fed into the low-pass filter which has adjustable cut-offs at a number of frequencies (Figure 5). This filter eliminates the higher frequency signals while passing the desired signals. The filter was specifically designed to drive the record amplifiers of an FM tape recoroer. However, it may be used with direct writing recorders as well. The filter system was developed at the Taylor Model Basin (Frillman, 1959 and Campbell, 1959).

RECORDING

The data received from the wave height buoy system can be recorded on any one of several types of recorder. It is usually recorded on a magnetic tape using FM electronics because this permits the information to be played directly into the Taylor Model Basin spectrum analyzer. The data could also be recorded on a strip chart recorder using the proper driving amplifiers. This would allow immediate access to the raw data.

SOME REMARKS ON THE ACCELERATION RECORD

The output of the SPLASHNIK is recorded as a filtered variable d-c voltage proportional to the acceleration experienced by the system. Several aspects of the SPLASHNIK output must be discussed before one can safely proceed to computation of the end product, the wave height spectrum.

The low-pass filter has already been mentioned. High frequency wave information above 1 cps cannot be recorded accurately because it is distorted by the frequency response of the 3 foot float. In addition, wave frequencies above 0.5 cps are usually of little concern to ship motion studies but do contribute rather large accelerations. If the sensitivity of a recording channel is adjusted to accept the highest signal, then the contributions in the important lower frequency range will be considerably smaller and may even be hardly discernible. Elimination of the higher frequency content serves to emphasize the important wave components. The adjustable frequency cut-off in the low pass filter provides a choice for elimination of undesired information.

Dorrestein (1957) points out that an error in the acceleration signal results from the tilt of the raft on the side of a wave. He concludes that the error is small, but being proportional to the square of the slope of the raft, it has a d-c component which must be removed befor double integration. The SPLASHNIK is, of course, subject to the same er Even if the accelerometer were satisfactorily stabilized, the low quality electronics (designed to keep cost down) still produces a d-c drift in t acceleration record. However, our method of analysis requires computatic of the acceleration spectrum and algebraic operation on this function to obtain the wave spectrum. Consequently, double integration is not necessary and the need for a high pass filter is eliminated. The result of this is an acceleration spectrum showing energy out to zero frequency, which is known not to exist. A "human filter" is applied at this stage by arbitrarily cutting off the acceleration spectrum where it approaches zero and at the frequency below which wave energy is known not to be present. This will be discussed further in the next section.

The error due to tilt of the accelerometer, mentioned by Dorrestein (1957), has been examined theoretically by Tucker (1959). Computations were made of the magnitude of the errors introduced into wave measurement by using an accelerometer shich sets itself in the "apparent vertical" , that is, perpendicular to the local water surface, instead of being stabilized to measure the true vertical acceleration. This applies directly to the SPLASHNIK. Tucker found that the spectrum of the error signal rises steeply at low frequencies but does not seriously affect the main wave components. Figure 6, from Tucker's paper shows several error spectra superposed on hypothetical wave spectra for three sea states. From these graphs, the following computations were made by Tucker:

Sea State	5	7	9
Error in spectral density at frequency of maximum energy	0.9 %	1.3 %	2.8 %
Error in r.m.s. wave height with high pass filter	3.9 %	1.6 %	1.1 %

The errors are seen to be relatively small, about 4 % in r.m.s. wave height in a state 5 sea and decreasing for higher sea states.

CALCULATION OF THE WAVE SPECTRUM

The SPLASHNIK will measure the apparent vertical acceleration of the environmental water particles such that a particular record may be represented by an integral of the form

$$a(t) = \int_0^\infty \cos\left[\omega t + \epsilon(\omega)\right] \sqrt{a(\omega)\, d\omega} \qquad (1)$$

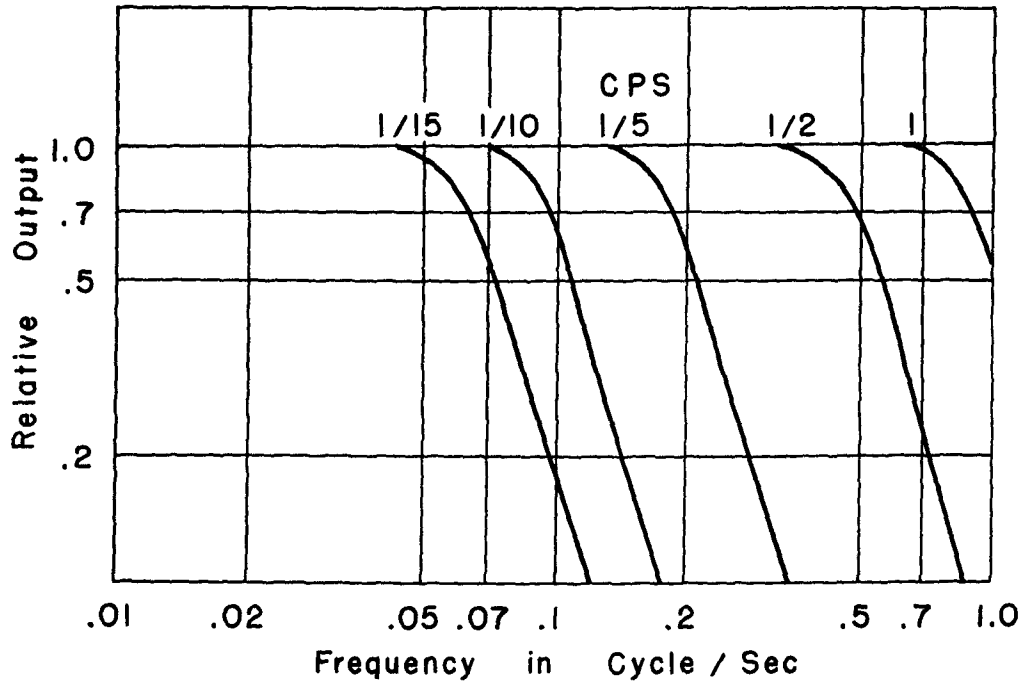

Fig. 5. Typical frequency response curves for DTMB low pass filter type 137-1A.

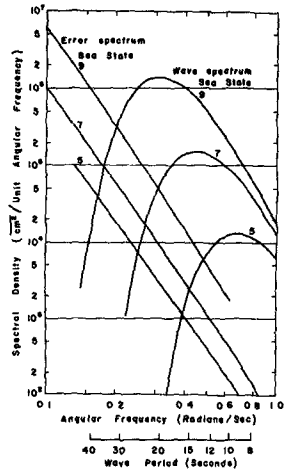

Fig. 6. Wave spectra computed from Neumann's formula for an equilibrium wave system, and the spectra of the errors introduced by measuring the wave using a buoy containing an unstabilized accelerometer . . . (from Tucker, 1959).

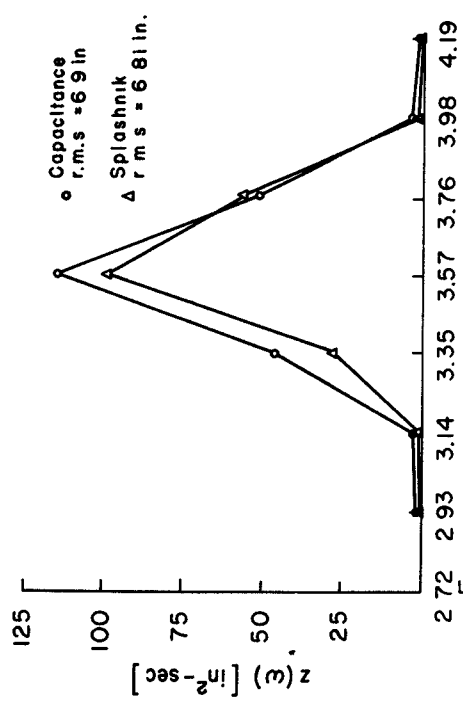

Fig. 7. Comparison of wave spectra measured in irregular long-crested waves in the TMB deep basin.

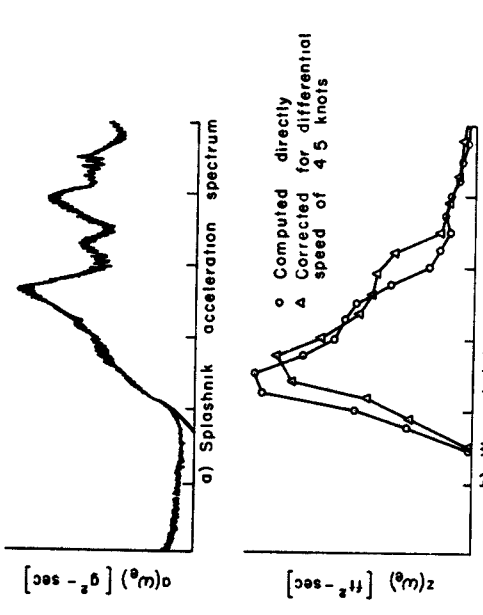

Fig. 8. Comparison of wave height spectra computed from records obtained by the SPLASHNIK and by a shipborne wave recorder -- Case I.

That is, it is supposed that the instantaneous apparent vertical acceleration [a(t)] is given by an infinite sum of sinusoids of all frequencies (ω) combined in random phase (ϵ). The amplitude of each sinusoid is assigned by the acceleration spectrum ordinate [a(ω)]. The integral in Equation (1) is not an ordinary integral in the Riemann sense; it cannot be formally integrated. It represents a mathematical abstraction which responds to the basic rules of the calculus and that will suffice for this discussion.

Using the form of Equation (1), a record of vertical displacement [z(t)] may be represented by

$$z(t) = \int_0^\infty \cos\left[\omega t + \epsilon(\omega)\right] \sqrt{z(\omega)\, d\omega} \qquad (2)$$

If Equation (2) is twice differentiated with respect to time, the result is

$$\frac{d^2z}{dt^2} = \int_0^\infty -\omega^2 \cos\left[\omega t + \epsilon(\omega)\right] \sqrt{z(\omega)\, d\omega} \qquad (3)$$

Equations (1) and (3) may now be equated to each other, the result being

$$z(\omega) = \frac{1}{\omega^4}\, a(\omega) \qquad (4)$$

Equation (4) states that the energy spectrum of the waves [z(ω)], may be derived from the energy spectrum of acceleration by an algebraic operation.

The errors that exist in a(ω) due to improper measurement of the true vertical acceleration are communicated to z(ω). In addition, there are errors in a(ω) due to the finite length of record and to the analysis technique. Failure to measure true vertical acceleration, plus drift in the electronics, results in an acceleration spectrum [a(ω)] which shows finite energy at $\omega = 0$ (Figure 8a) which by Equation (4) would propagate to z(ω) by indicating infinite energy at $\omega = 0$. This is overcome by arbitrarily cutting off a(ω) at a low frequency where the spectral density appears to go to zero. The chance of cutting off a low frequency band of swell which might actually be present cannot be ignored, nor can much be done about it since it is inherent in the system to propagate large errors at low frequencies.

Aside from the protective measures taken to prevent erroneous information from appearing at $\omega = 0$, and assuring maximum measurement accuracy with the low pass filter, there is little that can be done to establish confidence in the estimated spectrum of the wave except to compare results obtained from the SPLASHNIK with those obtained by a "reliable standard."

Accordingly, a series of experiments was made in which the output

of the SPLASHNIK was converted into a wave spectrum by Equation (4) and this spectrum was compared with the wave spectrum resulting from measurements made by other transducers (at the same time and physically close by which are considered to be fairly reliable standards. The philosophy of this approach is simply that good agreement in spectral shape and area will produce good agreement in prediction of the statistical characterist of the waves. Such a result would obviate the necessity for further inve tigation of errors in the SPLASHNIK measurement system. On the other han poor agreement would certainly indicate that further study of the system is required.

EXPERIMENTAL VERIFICATION

Initial tests were made in the TMB deep basin where irregular long-crested waves were generated with spectral peaks appropriate to wave lengths of 15 and 20 feet respectively. The waves were measured directly by a fixed capacitance probe and by the SPLASHNIK. The SPLASHNIK acceleration spectra were transformed according to Equation (4) and superimposed on the wave spectra measured by the capacitance probe. The results are shown in Figure 7. Although the individual spectral densities differ somewhat, the areas are almost identical as evidenced by the r.m.s. values The spectral peaks are well identified in both cases.

The model tank tests were quite successful but they were made in long-crested waves of relatively high frequency. It was necessary to test under actual sea conditions, in order to establish any real confidence in the system.

Preliminary tests in Chesapeake Bay, indicated that the SPLASHNIK had a life in excess of 8 hours and a range of about 11 miles over flat water. Since transmission of the signal is on a line-of-sight basis, one expects trouble in high seas as separation of SPLASHNIK and ship increases.

In a recent full scale trial, the SPLASHNIK system was tested in conjunction with a shipborne wave recorder (Tucker, 1955) in moderate states of sea (4-5). Several buoys were used in this experiment with varying degrees of success. One SPLASHNIK turned over which was quite unexpected. A few SPLASHNIKS ceased transmitting after 5 or 10 minutes because their batteries were shaken loose. (Batteries are now firmly secured). Several, however, transmitted successfully for periods ranging from half an hour to in excess of three hours. It is believed that lengthening the transmitting antenna by one foot and the SPLASHNIK float by one foot on each side will increase chances of successful transmission and reception of the signal.

Several simultaneous wave recordings were made with SPLASHNIKS and the shipborne wave recorder. Two of these events, each 20 minutes long, have been selected for analysis. Case I is depicted in Figure 8. The acceleration spectrum is computed on the Taylor Model Basin analog

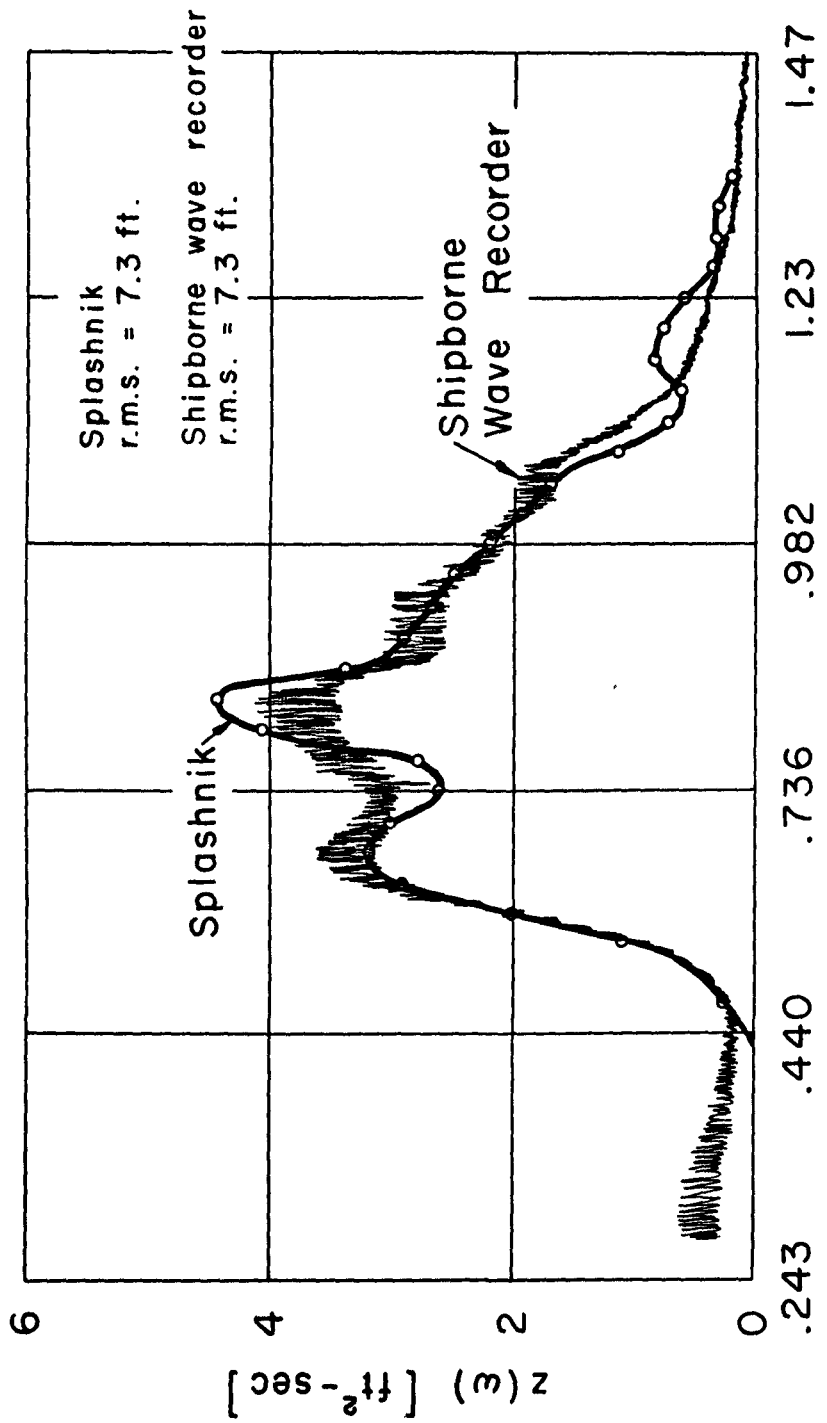

Fig. 9. Comparison of wave height spectra computed from records obtained by the SPLASHNIK and by a shipborne wave recorder -- Case II.

spectrum analyzer (Marks and Strausser, 1960). As expected, energy appears at the low frequencies where it is known not to exist. The arbitrary cut-off is made at $\omega = 0.342$ and then the wave spectrum is computed by Equation (4) (Figure 8b). In order to compare the SPLASHNIK with the shipborne wave recorder, it must be recalled that the ship was advancing into the waves at about 3.5 knots (to maintain heading) while the SPLASHNIK drifted in the opposite direction at about 1 knot; this Doppler effect must be taken into account. Since only a comparison of wave spectra is desired, in this case, it is only necessary to impose the same experimental conditions on the two systems. This was accomplished by a frequency transformation on the SPLASHNIK wave spectrum for a speed of 4.5 knots into the waves. The transformation is given by

$$\omega_e = \omega + \omega^2 \frac{v}{g} \cos \chi \tag{5}$$

where the Jacobian

$$J = \frac{\partial \omega}{\partial \omega_e} \tag{6}$$

is incorporated to conserve the energy in the transformed spectrum.

The transformation of the spectrum given by Equations (5) and (6) results in an estimate of the spectrum which would have been measured if the SPLASHNIK had traveled into the waves($\chi = 0$) at a speed (v) of 4.5 knots. Of course, the drift of the SPLASHNIK is a guess and the transforma tion assumes that the waves were all traveling in one direction; nevertheless at low speeds, the estimate should be fairly reliable. Figure 8b shows the computed and transformed SPLASHNIK wave spectra and Figure 8c shows the shipborne wave recorder spectrum superimposed on the transformed SPLASHNIK spectrum. The SPLASHNIK peak is somewhat lower than the SBWR peak and is located at a slightly higher frequency but shows more energy at higher frequencies than the shipborne wave recorder. In any case, the two spectra have the same general form and the r.m.s. wave heights as shown in Figure 8c are fairly close. A second case (Figure 9), shows even better agreement in spectral shape and a remarkable agreement in r.m.s. wave height.

It has been noted that the SPLASHNIK drifts. It is, of course, desirable to measure the waves at a fixed point and consequently a transformation is suggested to account for the drift. In view of Figure 8b, it may be inferred that a drift of 1 knot will neither change the shape of the spectrum materially nor will it shift the frequency of maximum energy very much. However, a drift of several knots could make a significant difference and this problem should be looked into.

In view of this evidence, there is some basis for confidence in the SPLASHNIK as a wave measuring device. It is, however, desirable to secure further verification under better controlled experimental conditions. To this end, the U. S. Navy Hydrographic Office is conducting an independent investigation of the SPLASHNIK, with a probe fixed to a platform in the open ocean as a standard.

PROPOSED IMPROVEMENTS

Plans are being made to replace some of the electronics of the SPLASHNIK with parts of better quality so that it may be used as a more accurate research tool. This will probably necessitate cost changes that may remove the "improved" SPLASHNIK from the category of "disposable item".

It is intended to replace the present transmitting system with a conventional type FM telemetering transmitter which is capable of carrying several channels of sea state information by FM subcarriers. The transducers will be a precision accelerometer and a vertical gyro which measures the tilt of the raft (equivalent to measuring roll and pitch on a ship). The vertical gyro will be used to correct for the tilt of the SPLASHNIK, by eliminating the horizontal and gravitational components in the apparent vertical acceleration measurement. The final recording will be a true vertical acceleration. All such information would be received, demodulated and recorded on tape. The anticipated accuracy of such a system (exclusive of the tape recorder) is expected to be within 1% of full scale signal.

The SPLASHNIK will be further out-fitted with a fin that orients the system with the wind. Wind direction will be recorded aboard ship and together with information from the gyro on the resultant tilt direction, the dominant wave direction can be estimated. It is believed that the directional wave spectrum may be resolved from the data of vertical acceleration and "tilt".

REFERENCES

Dorrestein, R. (1957). A Wave Recorder for Use on a Ship in the Open Sea: Proceedings Symposium on the Behavior of Ships in a Seaway, Wageningen, Holland, pp. 408-417.

Trillman, F.E. (1959). The DTMB Type 337-1A Electronic Low Pass Filter Instruction Manual: Taylor Model Basin Report 1337.

Campbell, W.S. (1959). On the Design of a Resistance Capacitance Filter for Use at Very Low Frequencies: Taylor Model Basin Report 1307.

Tucker, N.J. (1959). The Accuracy of Wave Measurements Made with Vertical Accelerometers: Deep Sea Research, Vol. 5, pp. 185-192.

Tucker, M.J. (1955). A Shipborne Wave Recorder: Proceedings of First Conference on Coastal Engineering Instruments, Berkeley, California.

Marks, Wilbur and Strausser, P.E. (1960). SEADAC -- The Taylor Model Basin Seakeeping Data Analysis Center: Taylor Model Basin Report 1353.

CHAPTER 7

WAVE HEIGHT MEASURING EQUIPMENT

E. H. Boiten
Instituut T.N.O. Voor
Werktuigkundige Constructies
Delft, Holland

The equipment was designed to obtain data from sea waves. It was developed by the Organization for Applied Scientific Research at Delft in coordination with the Royal Dutch Navy. The intention of the measurements with the wave height measuring equipment was to establish a correlation between the sea motion and the movements of a ship, which is steaming in that sea. So wave measurements and measurements of the ship movements were always carried out simultaneously. To have the movement of the ship free from the position of the wave meter, a telemetering system was chosen to transmit the data from the wave meter. The receiving and recording instruments are placed on board the ship.

The first measurement was made in December 1958. At that moment, the wave meter consisted of a buoy assembly in which was mounted a transmitter coupled with an accelerometer. The accelerometer measured the accelerations of the wave meter in a direction perpendicular to the water surface. The carrier of the transmitter was direct frequency modulated by the signal of the accelerometer.

After this measurement it became desirable to gather more data from the sea waves. For that reason the instrumentation of the wave meter was extended with a gyro, which measures the slope of the waves. The slope is determined by the angles of the water surface with respect to the horizontal plane in two directions perpendicular to each other. The angle signals frequency-modulate two subcarriers, which in their turn amplitude-modulated the transmitter carrier.

With this more complicated equipment a measurement was made in November 1959. In this paper a description is given of the instrumentation of the wave meter and the receiving and recording equipment as it is at the present with a slightly changed modulating system. As the data from the wave meter could be used to study only the wave motion apart from the ship, it seems reasonable to present this paper at this conference.

WAVE HEIGHT MEASURING EQUIPMENT

CONSTRUCTION OF WAVE METER

The floating element of the wave meter is a 9 ft x 6 ft aluminum raft. The housing of the accelerometer-transmitter and its batteries are suspended in the raft by means of a steel frame (Fig. 1). On the transmitter housing a removable mast is mounted with a length of about 16 feet. On top of the mast is the antenna. To put the center of gravity as low as possible and to obtain sufficient damping, the buoy was provided with a steel base plate of about 200 pounds. The natural frequency of the completed buoy showed to be about 0.5 c.p.s. The damping was nearly critical. On the base plate the other instruments are mounted in four watertight boxes. Figure 2 shows the unit on board a ship.

INSTRUMENTATION OF WAVE METER

General scheme of instrumentation. The complete block diagram of the wave meter instrumentation is given in Figure 3. The accelerometer is of the capacitive type. The capacity is connected into the tuned circuit of an oscillator, generating a frequency of about 80 Mc/s. A change of capacitance due to an acceleration changes the oscillator frequency, the frequency change being proportion to the acceleration. The transmitter consists of the oscillator as mentioned, followed by a doubler stage and a power stage. It is evident, that the transmitter is f.m. modulated by the accelerometer.

The angles of the wave meter-raft with the horizontal plane are measured by the gyro in two perpendicular directions: the roll angle and the pitch angle. The output voltages of the gyro, which are proportional to these angles modulate the frequency of two subcarrier oscillators. The subcarriers are added, amplified and fed into a ferrite modulator, connected into the oscillator tuned circuit of the transmitter. In this way, the oscillator of the transmitter is also f.m. modulated by the subcarriers. So the system is a mixed f.m. and f.m. - f.m. system. Power is obtained from accumulators. In the following sections more details about different building blocks of the wave meter instrumentation are given.

The accelerometer. The construction of the accelerometer is given in Figure 4. A mass is fixed in a casing by means of two membranes. The space between the mass and the casing is filled with oil. In this way a mass-spring system is obtained, which is nearly critically damped. The mass carries the grounded plate of a condenser. The isolated plate can be screwed up or down to adjust the plate distance and therewith the capacitance of the condenser.

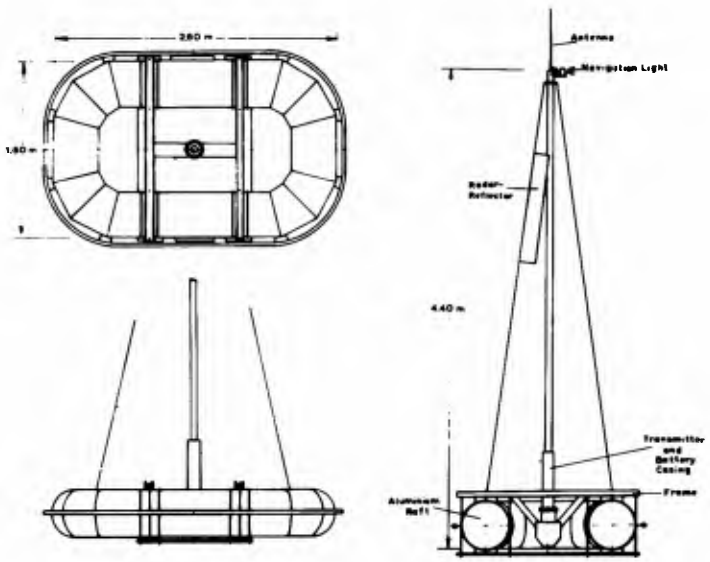

Fig. 1. Construction of the buoy-assembly.

Fig. 2. Wave metér prior to launching.

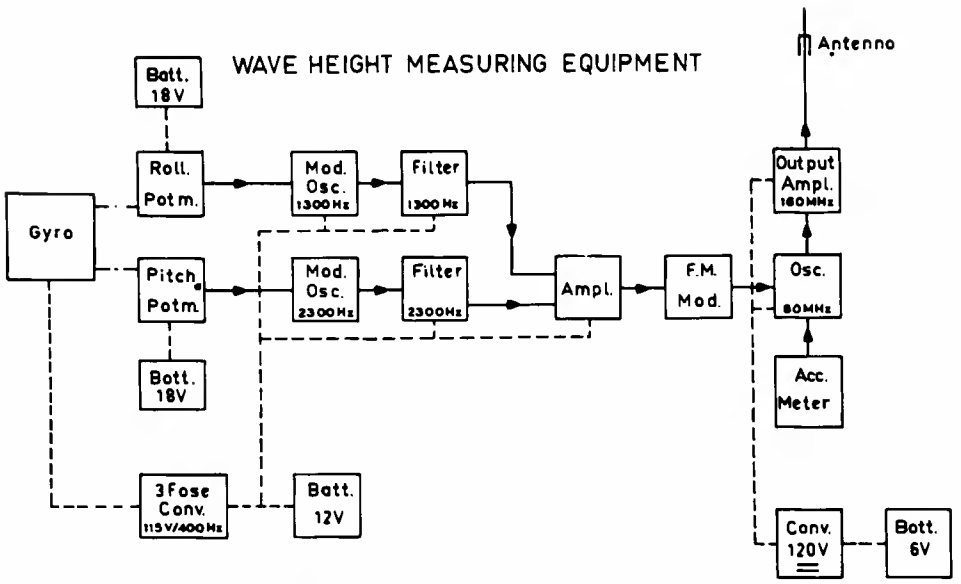

Fig. 3. Block diagram of wave meter instrumentation.

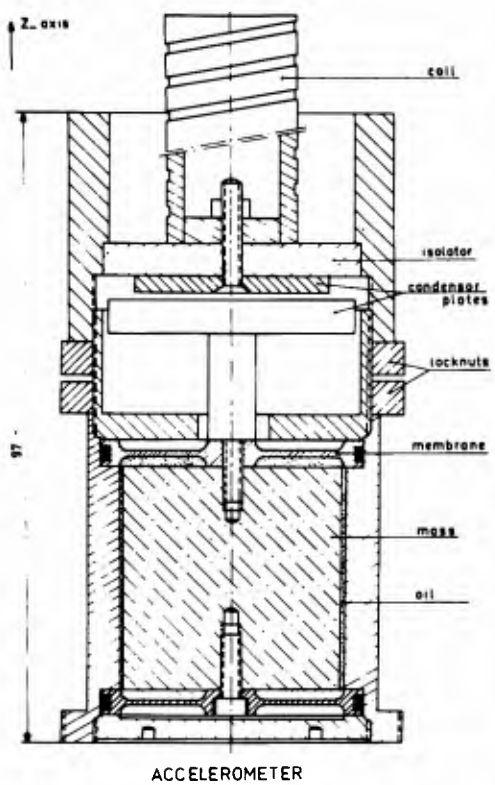

Fig. 4. Construction of the accelerometer.

Fig. 5. Transmitter on top of accelerometer.

The resonant frequency of the mass-spring system is about 150 c/s Since the frequency spectrum of the accelerations to be measured is below 15 c/s, no differences between static and dynamic deflections are to be expected. The static deflection (in the 1 g gravitational field) is 10 μm.

The transmitter. The transmitter consists of two stages: an oscillator/doubler stage, and a power stage. The oscillator circuit is of the Colpitt type, oscillating in the screen-grid circuit of an E 180 F tube at about 80 Mc/s. The frequency of the circuit is modulated by the varying capacitance of the accelerometer, and by the varying self inductance of a ferrite modulator, to which the subcarrier voltages, containing the gyro angle information are supplied. The anode circuit of the E 180 F tube is tuned to twice the oscillator frequency and is coupled to the power stage, which contains a double tetrode tube QQE 02/5 operating in push-pull connection. The anode circuit of the QQE 02/5 delivers power to a vertical dipole antenna.

Frequency shift and acceleration are related as shown in the formula

$$\frac{\Delta f}{f} = - K \cdot \frac{m}{c.d_{st}} \cdot (a + g) \qquad (1)$$

in which:

Δf = frequency shift

f = central frequency

K = dimensionless constant, depending on circuit constants

m = accelerometer mass

c = spring constant of accelerometer membranes

d_{st} = statical displacement constant of accelerometer

a = acceleration to be measured

g = acceleration of gravitational field

D.C. power for the transmitter is obtained from a transistor DC-DC converter, fed by Ni-Cd accumulators. These accumulators were chosen because of their flat load characteristic. Figure 5 shows the transmitter with the accelerometer.

Specifications of the transmitter are:

Central frequency	157.75 Mc/s
Adjustment range of frequency	500 Kc/s
Stability:	
Frequency drift (2 hrs after switching on)	4.10^{-5}/hour
Frequency fluctuations	10^{-5}
Frequency change for 10% heater voltage variation	-10^{-4}
Frequency change for 10% anode voltage variation	$+2.10^{-4}$
Sensitivity (freq. shift/acceleration)	ca. 450 Kc/s per g
Power in antenna	ca. 2 W

The angle transducers. Since the wave height is to be derived from the vertical acceleration by double integration, there will be an error, when the accelerometer axis is not vertical. This error can be calculated, when the angle between the accelerometer axis and the true vertical direction is known.* For these reasons a gyro is included in the instrumentation. The gyro measures the angles of the wave meter raft with the horizontal plane in two perpendicular directions (roll angle and pitch angle). The angle of the accelerometer axis with the true vertical direction can then be computed from the formula

$$\cos^2\gamma + \sin^2\delta_r + \sin^2\delta_p = 1 \qquad (2)$$

in which

γ = angle between accelerometer axis and true vertical direction
δ_r = roll angle
δ_p = pitch angle

The gyro-axis is erected and kept vertical by two erection-motors, controlled by mercury switches. Since the erection-motors act very slowly, the reference for the gyro-axis is the direction of the total acceleration, averaged over several minutes.

In the wave meter the gyro is subjected to accelerations of constantly changing directions. However, the average is the true vertical direction, so when the erection motors act slowly enough the gyro axis direction will be very close to the vertical direction and

*There is some evidence that this error is not significant. It is however of importance to ascertain this. Besides this, it is desirable to know the wave slope, from which information may be obtained on the incidence of power on e.g. a ship's hull.

can be used as a reference for the true vertical direction. Roll and pitch angles are measured by potentiometers, coupled to the roll axis and pitch axis of the gyro gimbals and connected to constant voltage Ni-Cd batteries. The 115 V 400 c/s power for the gyro-motor is obtained from a three phase transistor DC-AC converter. Figure 6 shows the gyro-unit.

Specifications of gyro-unit:

Type: Sperry Horizon Gyro Unit, type B.		
Accuracy of vertical direction:		1.5 degree
Erection velocity:	ca.	5 degree/min.
Sensitivity:	ca.	0.1 V/degree

The subcarrier oscillators. The voltages of the roll and pitch potentiometers modulate the frequencies of two multivibrator-type subcarrier oscillators with central frequencies of 1300 and 2300 c/s, respectively, in such a way, that the frequency deviations of the subcarriers are proportional to roll and pitch angle.

The subcarrier oscillators are followed by filter amplifiers to suppress all harmonics. In both oscillators and filter amplifiers use is made of transistors. The circuits are mounted on etched circuit cards.

Specifications of subcarrier oscillators:

Central frequency f_o	1300/2300 c/s
Max. frequency deviation Δf_{max}	$\pm$ 0.1 f_o
Stability freq. drift/Δf_{max}	1%
Input voltage for max. deviation	1.2 V
Linearity (freq./input voltage, deviation from straight line)	< 5%
Temperature drift ($\Delta f/\Delta f_{max}$)	<1% per °C
Amplifier output current	max. 4 mA

Instrument assembly. A general picture of the instruments as mounted in the raft is given in Figure 7. All instruments and accumulators are packed in water-tight boxes. The transmitter is mounted in the mast foot on which the flanged mast is bolted. In the mast provisions are made for access to the transmitter for adjustment purposes. All electric connections from instruments and accumulators are made through a central switching box with removable watertight lid. Through this switching box accumulators can be loaded. Apart from this, the

Fig. 6. Gyro unit.

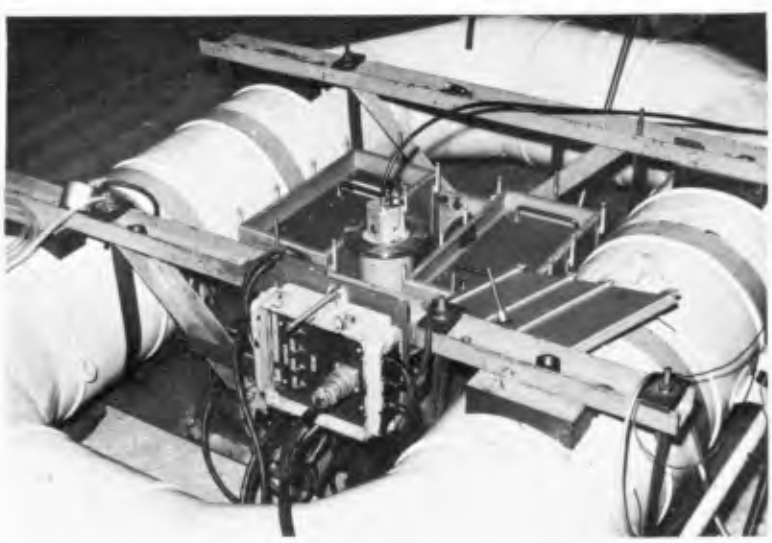

Fig. 7. Instrument assembly of wave meter.

gyro battery can be loaded with the gyro unit working. The reason for this is, that transportation hazards are minimum, when the gyro rotor is spinning, so that on transportation the gyro unit is always switched on.

RECEIVING AND RECORDING INSTRUMENTS

General scheme of receiving and recording system. A block diagram of the complete receiving and recording system is given in Figure 8. The receiver is a special sensitive broadband f.m. receiver of good linearity. It can be switched to the receiving antenna, or to the calibration oscillator. This calibration oscillator generates signals of the same kind as the wave meter transmitter, i.e. a carrier with a central frequency of 157.75 Mc/s, f.m. modulated by two subcarriers, with frequencies of 1300 c/s and 2300 c/s, respectively.

A calibration switch, which is incorporated in the calibration oscillator circuit shifts the frequencies of carrier and subcarriers over an amount, corresponding to frequency deviations of the wave meter transmitter for known values of acceleration and roll and pitch angles. At the start and at the end of a recording period the receiver is switched to the calibration oscillator, and the calibration values are recorded. In this way the complete receiving and recording system can be kept under control, and errors can be eliminated or corrected.

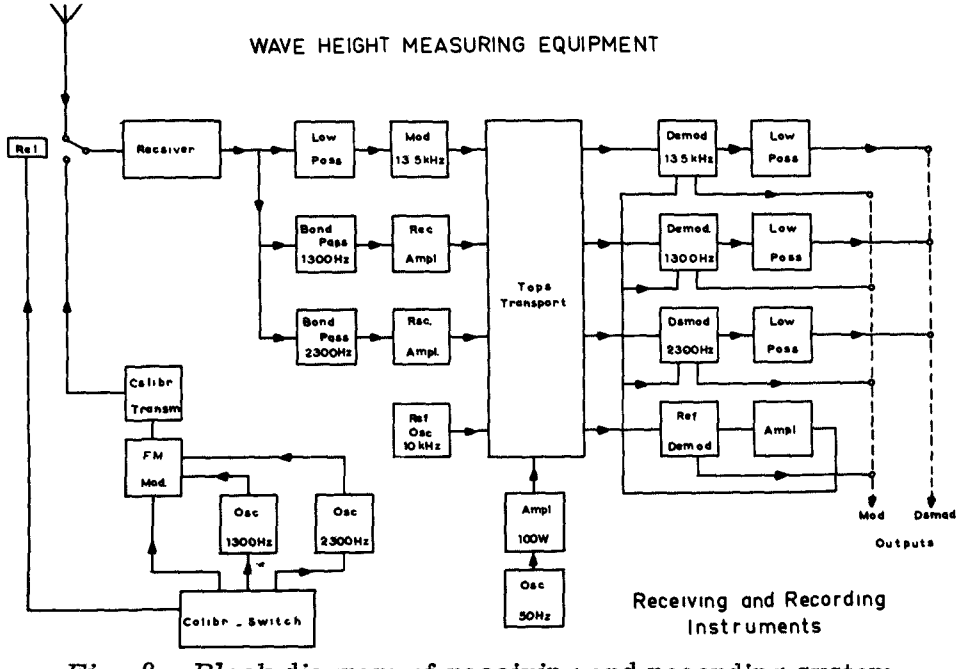

Fig. 8. Block diagram of receiving and recording system.

The receiver output consists of the accelerometer signal together with the two subcarriers, containing the information on roll and pitch angle. The three signals are separated by filters, and the accelerometer signal is f.m. modulated on a 13.5 kc/s subcarrier. Each of the three subcarriers is now recorded on a separate track of a 4 track magnetic tape recorder. On the fourth track a 10 kc/s reference signal of very accurate frequency is recorded. This reference signal is used for timing purposes on play back of the signal, and also for wow and flutter compensation.

The capstan motor of the tape recorder is driven from an amplifier, connected to a 50 c/s R.C. oscillator. The reason for this is, that in many cases main power of accurate 50 c/s frequency is not available.

The receiver. To obtain adequate sensntivity a superheterodyne receiver with double mixing is used. The first local oscillator is a crystal oscillator, whose frequency is multiplied by nine in a separate multiplier. The second local oscillator is an L.C. oscillator which has a ferrite modulator included. The i.f. stages, limiter discriminator are conventional. However, the discriminator output is fed back to the ferrite modulator of the second local oscillator. In this way three objectives are obtained:

a. good band width
b. good linearity
c. automatic frequency correction

The receiver has a balanced cathode follower output stage. A d.c. meter is connected over the output, indicating the frequency deviation. A second d.c. meter, connected to an a.m. detector, indicates signal strength.

Specifications:

Central frequency		157.75 Mc/s
Tuning range coarse		$\pm$ 1 Mc/s
fine		$\pm$ 300 kc/s
Band width	$\pm$ 150	- $\pm$ 300 kc/s
Stability (1 hour after switching on)		3.10^{-5}
Sensitivity on antenna input		5 μV
Linearity (max. deviation of straight line at max. freq. deviation)		4%
L.f. band width		0-7000 c/s

The calibration oscillator. The calibration oscillator is a replica of the wave meter transmitter, except for the power stage. The oscillator is frequency modulated by d.c. and by two subcarrier signals of 1300 c/s and 2300 c/s central frequency, respectively. The subcarrier signals are obtained from subcarrier oscillators, identical to those of the wave meter. These subcarrier-oscillators are also frequency modulated by d.c. signals. By means of a calibration switch a number of voltages can be switched to the ferrite modulator of the calibration-oscillator and both subcarrier oscillators. These voltages can be chosen as to represent exactly known values of acceleration and roll angle and pitch angle.

Specifications of the calibration oscillator are:

Carrier frequency	157.75 Mc/s
Roll angle carrier frequency	1300 c/s
Pitch angle carrier frequency	2300 c/s
Calibration switch positions:	
Acceleration $0_1 \pm 0.1$ g + 0.2 g $\pm$ 0.3 g m/sec^2	
Angles $0_1 \pm 5° \pm 10° \pm 15°$	

The magnetic tape recorder. The advantage of magnetic recording is, that the recorded data can be easily reproduced and processed afterward For this reason this method of registration was chosen. The tape recorder is a four track instrumentation type recorder with f.m. subcarrier system. One track is used for recording an accurate 10 kc frequency reference signal, which is used for wow and flutter compensation when analog signals are wanted on play back, and for timing purposes, when digital data processing is used. Since the data are available as f.m. modulated subcarriers, digital processing can be easily effected with electronic counters and gates.* The electronic part of the magnetic tape recorder is constructed as a rack with plug-in units.

Some specifications of the tape recorder are:

Reference frequency	10 kc/s + Hz
Reference frequency stability	10^{-5}
F.M. modulator stability	0.1%
F.M. demodulator stability	0.1%
Tape speeds	76 - 38 cm/se
Tape velocity fluctuations	<0.2%
Tape velocity drift	< 4%
Tape width	1/2 inc
Max. tape length	1000 m
Number of tracks	4

*F.M. modulated subcarrier output is obtained from the reading head amplifiers, analog output is bbtained from f.m. demodulator circuits.

WAVE HEIGHT MEASURING EQUIPMENT

SUMMARY

The system as described is the result of a number of improvisations, when measurements were a pressing necessity. It is now possible to indicate certain points, where improvements are needed.

1. The raft may be constructed much lighter, so that it could be more easily handled; besides a more logical assembly of the instrumentation is possible.

2. The acceleration signal may be f.m. modulated on a l.f. carrier. Although the stability of a l.f. carrier is not necessarily better than the stability of a h.f. carrier, much wider frequency deviations are possible, with as a result a better signal to drift ratio.

3. Since the hydrodynamic properties of the raft are not well known, the accelerations in two horizontal directions should preferably also be measured. The angle between accelerometer axis and true vertical direction could then be more accurately calculated.

4. Tape speed and subcarrier central frequencies are not optimally chosen. Improvements of these could result in lower tape use and longer measuring periods.

5. The resonant frequency of the accelerometer is higher than necessary for the low frequency content of wave motion. This results in loss of sensitivity, since with lower spring constants higher deflections of the accelerometer mass could be obtained.

CHAPTER 8

ETUDE THEORIQUE DE L'EXPLOITATION DES ENREGISTREMENTS DE HOULE

P. Caseau
Ingénieur des Ponts et Chaussées
en service détaché à Electricité de France.

INTRODUCTION

L'étude de la houle en un point, c'est-à-dire l'exploitation d'un enregistrement de houle, consiste à obtenir, à partir de cet enregistrement, le plus de renseignements possible sur le "spectre" de la houle.

Nous excluons le cas où la donnée $f(t)$ se présente sous la forme d'un tableau chiffré ou d'un courant électrique. Ces deux représentations ont en commun la propriété que l'addition de deux fonctions et l'opération $\frac{1}{T}\int_0^T f(t)^2 dt$ y sont faciles à réaliser. L'exploitation passera donc naturellement par la fonction de corrélation $\gamma(\tau) = \frac{1}{T}\int_0^T f(t) f(t+\tau)$ qui est très facile à obtenir

Au contraire, si l'enregistrement se présente sous forme de courbes sur film ou sur papier, aucune de ces deux opérations n'est facile à réaliser, ce qui enlève à $\gamma(\tau)$ beaucoup de son intérêt. Pour l'exploitation des enregistrements effectués par l'enregistreur autonome de Chatou, qui consistent en des courbes sur film de 35 mm, une méthode simplifiée est actuellement utilisée [5]. Cette méthode ne donne cependant pas tous les renseignements que l'on voudrait, et elle est moins rapide d'emploi qu'il ne serait nécessaire pour permettre le dépouillement des très nombreux enregistrements effectués avec les divers appareils en service. En modifiant un peu la méthode, M. Kowalski, de l'Instytut Morski, à Gdansk, en Pologne, a pu la mécaniser et la rendre plus pratique, sans cependant augmenter le nombre des renseignements obtenus. En s'inspirant du procédé utilisé par M. Kowalski, M. Valembois a imaginé le procédé que nous étudions ici.

Ce procédé consiste à faire défiler le film devant un appareil qui compte au moyen de cellules photoélectriques, le nombre de points d'intersection de la courbe $y = f(t)$ avec les droites $y = Cte$, pour diverses valeurs de la constante. M. Larras a proposé, au lieu de compter des nombres de points d'intersection, de totaliser des intervalles horizontaux (fig. 1).

L'étude mathématique de ces procédés conduit naturellement à considérer les "distributions" associées à $f(t)$, à voir leurs relations avec le spectre, et à sélectionner celles qui sont le plus faciles à obtenir et qui donnent le plus de renseignements sur celui-ci.

Après avoir passé en revue les hypothèses mathématiques et les résultats nécessaires au calcul, nous aborderons donc l'étude de ces distributions, et nous indiquerons quelques-unes de celles que l'on peut utiliser.

ETUDE THEORIQUE DE L'EXPLOITATION DES ENREGISTREMENTS DE HOULE

NOTATIONS

$\gamma(\tau) = \left[\eta(t)\,\eta(t+\tau)\right]$	$\sigma_{pq} = \sqrt[p-q]{\frac{m_p}{m_q}} \qquad p>q$
$\Gamma(n,p,\tau) = \left[\eta^{(n)}(t)\,\eta^{(p)}(t+\tau)\right]$	$\sigma_n = \sqrt{\frac{m_{2n}}{m_{2n-2}}}$
$\gamma(\tau) = \int_{-\infty}^{+\infty} e^{i\sigma\tau}\, dE(\sigma)$	$\Delta_{pq} = m_{2p}m_{2q} - m_{p+q}^2$
$dE(\sigma) = \frac{1}{2} A(\sigma)\, d\sigma$	$\epsilon_{pq}^2 = \frac{\Delta_{pq}}{m_{2p}\, m_{2q}}$
$m_n = \int_0^{\infty} A(\sigma)\, \sigma^n\, d\sigma$	$N_p = \frac{1}{\pi}\sqrt{\frac{m_{2p+2}}{m_{2p}}} = \frac{1}{\pi}\,\sigma_{2p+2}$

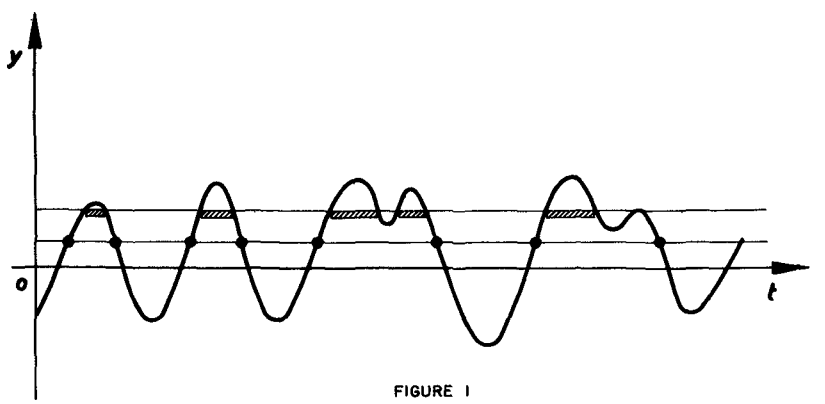

FIGURE 1

PROPRIETES GENERALES DES FONCTIONS REPRESENTANT LA HOULE

Cette partie concerne les propriétés des fonctions $\eta(t)$ représentant la houle ou plus exactement les enregistrements de houle.

La théorie de ces fonctions a été faite (Rice [4] et Longuet-Higgins [3]) en se basant sur les propriétés des fonctions aléatoires. L'inconvénient de ce point de vue est d'une part qu'il nécessite le recours à des théorèmes ergodiques, pour que les opérations et moyennes dans l'espace des probabilités coïncident avec les opérations réellement effectuées sur $\eta(t)$, et que d'autre part, alors que $F'(t)$ admet une décomposition spectrale, son "épreuve" $\eta(t)$ n'en admet en général pas.

Notre but au contraire a été de bâtir la théorie des opérations que nous faisons sur $f(t)$ au moyen d'hypothèses sur $f(t)$ seulement. Nous nous sommes servis pour cela de certains résultats de M. Bass sur les fonctions pseudo-aléatoires [1]. S'il est question de distribution de probabilité, c'est un raccourci de langage, car nous ne supposons pas un instant que $f(t)$ est une épreuve d'une fonction aléatoire.

On pourrait sans doute aller plus loin dans cette voie et renoncer à étudier $f(t)$, mais seulement $f(t)(0<t<T)$ fonction tronquée. Les opérations faites auraient toujours un sens. Les formules algébriques resteraient aussi simples vue la précision finalement demandée aux résultats (voir dernier paragraphe). Mais ce serait, en fait, masquer le problème. Si, en effet, lorsque T varie, les résultats changent beaucoup, alors l'échantillon n'est pas représentatif. Ainsi, nos hypothèses (lorsque $T\to\infty$, telle fonction a une limite) signifient, non pas que l'infini intervient réellement, mais que la valeur effective de T a peu d'importance. On pourra appliquer cette remarque à l'étude d'une tempête représentant un état non stationnaire de la mer. (Ces notions restent évidemment à préciser, une considération intéressante serait de voir à partir de quelle valeur τ_0, $\gamma(\tau)$ est pratiquement nulle. On pourrait alors relier T à τ_0). On aurait ainsi complètement "localisé" l'étude de $f(t)$.

Nous considèrerons les opérateurs suivants, définissant des moyennes :

$$M_T(f) = \frac{1}{T}\int_0^T f(t)\,dt \qquad M(f) = \lim_{T\to\infty} M_T(f)$$

Et nous poserons, pour deux fonctions quelconques f et g, mais telles que l'expression ait un sens :

$$[f,g] = M(fg)$$

Soit alors une fonction $f(t)$ sur laquelle nous ferons l'hypothèse (H_1) suivante :

1. $f(t)$ est indéfiniment dérivable,
2. $0=M(f^{(n)})$ quel que soit n,
3. $f^{(n)}(t)$ est bornée quel que soit n.

LA FONCTION DE CORRELATION - DEFINITION.

Nous définissons $\gamma[T,\tau] = M_T(f\,f(t+\tau))$. On voit facilement d'après (H_1) que $\gamma(T,\tau)$ existe et est continue et dérivable indéfiniment.

Appliquant le théorème de Bochner [1], on démontre alors qu'il existe une fonction monotone $E(T,\sigma)$ à variation totale bornée et telle que

$$\gamma(T,\tau) = \int_{-\infty}^{+\infty} e^{i\sigma\tau}\,dE(T,\sigma)$$

Et l'on a la formule d'inversion :

$$E(T,b) - E(T,a) = \lim_{U\to\infty} \frac{1}{2\pi}\int_{-U}^{U} \frac{e^{iUa} - e^{iUb}}{iU}\,\gamma(T,U)\,dU$$

pour toutes les valeurs a, b où $E(T,\sigma)$ est continue.

Nous ferons alors l'hypothèse nouvelle (H_2).
$\gamma(T;\tau) \to \gamma(\tau)$ pour $T \to \infty$ et $\gamma(\tau)$ est continue pour $\tau = 0$

On sait alors (grâce à des théorèmes dus en particulier à P. Lévy [2] et [1] que :

1. La convergence est uniforme dans tout segment $(-\tau, +\tau)$, donc $\gamma(\tau)$ est continue partout.
2. $E(T,\sigma) \xrightarrow{c} E(\sigma)$ le sens de la "convergence complète" [2] étant :
- $E(T,\sigma) \longrightarrow E(\sigma)$ quand $T \to \infty$, quel que soit σ,
- $\int g\, dE(T,\sigma) \to \int g\, dE(\sigma)$ quelle que soit la fonction g continue et bornée.

PROPRIETES ALGEBRIQUES DE $\gamma(\tau)$

Nous généraliserons d'abord (H_2) en (H_2')*.

$\Gamma(m,p,\tau) = \left[f^{(m)}(t), f^{p}(t+\tau)\right]$ existe et est continue en τ.

a. Nous pourrons alors démontrer les relations algébriques suivantes, par dérivation sous le $\int$, intégration par parties et passage à la limite.

$$\Gamma(n,p,\tau) = \Gamma(p,n,-\tau) = (-1)^n \gamma^{(n+p)}(\tau) = (-1)^p \gamma^{(n+p)}(-\tau)$$

d'où en particulier :

$$\Gamma(m,p,\tau) = (-1)^h \Gamma(m+h, p-h, \tau)$$

b. D'autre part, le même raisonnement qu'au I°, mais appliqué à f' nous montre que :

$$\gamma'' = \left[f, f''(t+\tau)\right] = -\left[f', f'(t+\tau)\right] = \int e^{i\sigma\tau}\, dB(\sigma)$$

En intégrant de 0 à τ et en utilisant le fait que $\gamma'(0) = 0$, on montre que γ' admet une représentation analogue. En intégrant à nouveau et en utilisant la formule d'inversion, on démontre que la formule :

$$\gamma = \int_{-\infty}^{+\infty} e^{i\sigma\tau}\, dE(\sigma)$$ est dérivable indéfiniment sous le signe $\int$.

Ainsi $\gamma^{(n)}(\tau) = \int_{-\infty}^{+\infty} (i\sigma)^n e^{i\sigma\tau}\, dE(\sigma) = (i)^n \int_{-\infty}^{+\infty} \sigma^n e^{i\sigma\tau}\, dE(\sigma)$

---

* Pour les propriétés "d'existence", il est plus simple d'étudier la fonction entre 0 et T, ce qui supprime tout problème de passage à la limite. Au contraire, on verra que les propriétés algébriques sont plus simples en faisant $T = \infty$.

Donc :

$$\Gamma(m,p,\tau) = (-1)^m (i)^{m+p} \int \sigma^{m+p} e^{i\sigma\tau} dE(\sigma)$$
$$\Gamma(m\ m,\tau) = \int \sigma^{2m} e^{i\sigma\tau} dE(\sigma)$$
$$\Gamma(m-h, m+h, \tau) = (-1)^h \int \sigma^{2m} e^{i\sigma\tau}\, dE(\sigma)$$

En particulier, pour $\tau=0$ on trouve :

$$\Gamma(m,p,0) = \left[f^{(m)}, f^{(m+p)}\right] = 0 \text{ si } m+p \text{ est impair,}$$
$$= (-1)^{\frac{m-p}{2}} \int \sigma^{m+p} e^{i\sigma\tau} dE(\sigma) \quad \text{si } m+p \text{ est pair}$$

Ceci nous permet de calculer la matrice des covariances de n'importe quelle suite de fonction : $f^{(n)}(t)$, $f^{(n_1)}(t+\tau_1), f^{n_2}(t+\tau_2) \ldots . f^{n_k}(t+\tau_k)$

Ces calculs sont développés en annexe.

LES DISTRIBUTIONS DE PROBABILITES.

Définition et existence - Soit $F(T,y) = \frac{1}{T} m\, E_T(f \leq y)$ mesure de l'ensemble des $t < T$ où $f(t) \leq y$. C'est une fonction de distribution croissante, à variation bornée par 1 et qui est familière aussi bien aux ingénieurs qu'aux mathématiciens. En hydrologie, on la nomme courbe des débits classés. Mais son utilisation la plus importante est celle de Lebesgue dans la théorie de l'intégrale.

Nous savons que si G est une fonction continue :

$$M_T\{G(f)\} = \int G(y)\, dF(T,y)$$

En particulier $\int y^2\, dF(T,y) = M_T(f^2)$. (On voit que la distribution possède des moments de tous les ordres).

Notons aussi que si $f \to g$, uniformément sur $(0,T)$:

$$F(T, f \leq y) \to F(T, g \leq y)$$

d'après les propriétés de la mesure sur un segment de longueur finie.
Nous ferons alors l'hypothèse :

$$F_T \xrightarrow{c} F \quad \text{quand} \quad T \to \infty$$

On voit donc que F définit une mesure sur des ensembles de l'axe des t liés à f et invariants par translation (c'est-à-dire invariants si on remplace $f(t)$ par $f(t+\tau)$.

On peut, en généralisant, considérer la fonction de distribution à plusieurs variables $F(T, y_0, y_1, y_2 \ldots y_n) = m\, E_T(f(t) \leq y_0, f(t+\tau_1) \leq y_1, \ldots f(t+\tau_n \leq y_n)$ t
Et sa limite $F(y_0, y_1 \ldots y_n)$.

ETUDE THEORIQUE DE L'EXPLOITATION DES ENREGISTREMENTS DE HOULE

Indépendance - Soient deux fonctions f et g et soient

$$F(T, y_0 y_1 \cdots y_n) = \frac{1}{T} m\, E_T\{f(t) \leq y_0, \ldots, f(t+\tau_n) \leq y_n)\}$$

$$G(T, z_0 z_1 \cdots z_n) = \frac{1}{T} m\, E_T\{g(t) \leq z_0, \ldots, g(t+\tau_n) \leq z_n)\}$$

$$\psi(T, y_0 y_1 \cdots y_n, z_0 \cdots z_n) = \frac{1}{T} m(\text{l'intersection des deux ensembles précédents})$$

Si, quelle que soit la suite $(\tau_1, \ldots \tau_n, u_1, \ldots u_n)$: $(\psi - FG) \to 0$ lorsque $T \to \infty$ uniformément par rapport à $(y_0 y_1 \cdots y_n, z_0, z_1 \cdots z_n)$ nous dirons que les deux fonctions sont indépendantes.

Comme sur le segment $(0, T)$ f et g sont dérivables, à dérivées continues uniformément, on peut trouver τ tel que :

$$\max\{f'(t) - [f(t+\tau) - f(t)]\} \leq \epsilon$$

$$\max\{g'(t) - [g(t+\tau) - g(t)]\} \leq \epsilon$$

donc, d'après la remarque du paragraphe précédent, f' et g' sont indépendantes si f et g sont indépendantes, de même pour $f^{(n)}$ et $g^{(n)}$.

Exemple : il est facile de démontrer que $e^{i\lambda t}$ et $e^{i\lambda' t}$ sont indépendantes si (condition nécessaire et suffisante) λ et λ' sont incommensurables.

- Si f est indépendant de g et si $M(f)$ et $M(g) = 0$, on a :

$$[f, g] = 0 \qquad [f(t), g(t+\tau)] = 0$$

$$[f+g, f+g] = [f, f] + [g\, g]$$

$$[f+g, f(t+\tau) + g(t+\tau)] = [f, f(t+\tau)] + [g, g(t+\tau)]$$

Ainsi, la fonction de corrélation Γ (ainsi que le spectre E) de la somme $f+g$ est la somme des fonctions de corrélations (ou des spectres) de f et de g.

Application - Soit alors une suite de fonctions indépendantes f_0 f_1 f_n que nous supposons uniformément bornées.

Soit $g_n = \sum_0^n f_k$ et soit :

F_n la fonction de distribution associée à f_n
G_n la fonction de distribution associée à g_n

D'après le paragraphe précédent, on en déduit :

$$G_1 = \int F_0\, dF_1 = \int F_1\, dF_0 = F_0 * F_1$$

Par récurrence :

$$\boxed{G_n = F_0 * F_1' * F_2 * \cdots * F_n}$$

Posons : $\sigma_k^2 = \int y^2\, dF_k = [f_k, f_k]$

$$S_n^2 = \sum_1^n \sigma_k^2 = \int y^2\, dG_n$$

On sait alors, comme conséquence du théorème de Liapounoff, que $\frac{q_n}{\sigma_n}$ a pour loi $G_n\left(\frac{x}{\sigma_n}\right)$ et que cette loi tend vers une loi de Gauss de moyenne et d'écart quadratique 1.

Nous supposerons donc, hypothèse (H_4), que la fonction f que nous considérons est constituée par une somme de fonctions indépendantes et uniformément bornées, en nombre suffisant pour que le théorème précédent s'applique.

Notons que, vue la précision recherchée, ce nombre n'a pas besoin d'être très grand et qu'on peut par exemple reconstituer une houle avec un petit nombre de composantes incommensurables.

En généralisant, on trouve que la fonction de distribution $F(y_0 y_1 \cdots y_n)$ associée à : $\left[f^{(p)}(t), f^{(p_1)}(t+\tau_1), f^{(p_n)}(t+\tau_n)\right]$ est une loi de Gauss caractérisée par la matrice des covariances :

$$a_{hk} = \left[f^{(p_h)}(t+\tau_h), f^{(p_k)}(t+\tau_k)\right] = \Gamma\left[p_h, p_k, \tau_k - \tau_h\right]$$

F est donc une distribution "continue" à laquelle on peut associer une densité $p = \frac{dF}{dv}$ et nous aurons :

$$p(y_0 y_1 \cdots y_n) = \frac{1}{(2\pi)^{\frac{n}{2}} \sqrt{\|a_{nk}\|}} \exp\left\{-\frac{1}{2} b_{nk} y_n y_k\right\}$$

$\|a_{nk}\|$ déterminant de la matrice a_{nk},
b_{nk} matrice inverse de a_{nk}.

On trouvera en annexe l'expression détaillée de cette loi.

PROPRIETES DES MOMENTS DE $E(\sigma)$.

Considérons la fonction de distribution $E(\sigma)$. Comme elle est symétrique, nous nous limiterons à $\sigma \geq 0$.

On sait que $y(n) = \log(m_n)$ est convexe, c'est-à-dire que si p, h, k sont trois nombres positifs :

$$\frac{y(p) - y(p-h)}{h} \leq \frac{y(p+k) - y(p-h)}{h+k} \leq \frac{y(p+k) - y(p)}{k}$$

et

$$y(p) \leq \frac{h\, y(p+k) + k\, y(p-h)}{h+k}$$

Soit alors $\sigma_{pq} = \sqrt[p-q]{\frac{m_p}{m_q}}$, on en déduit :

$$\sigma_{p\,p-h} \leq \sigma_{p+k,\,p-h} \leq \sigma_{p+k,\,p}$$

et

$$(m_p)^{h+k} \leq (m_{p+k})^h \cdot (m_{p-h})^k$$

Ces inégalités de convexité sont fréquemment utilisées.

ETUDE THEORIQUE DE L'EXPLOITATION DES ENREGISTREMENTS DE HOULE

Faisons alors l'hypothèse $[H_5]$ que $E(\sigma)$ est "à support compact" c'est-à-dire qu'il existe deux nombres σ_{min} et σ_{max} tels que :

$\sigma \leq \sigma_{min} \Rightarrow E(\sigma) = 0 \qquad \sigma \geq \sigma_{min} \quad E(\sigma) > 0$

$\sigma \leq \sigma_{max} \Rightarrow E(\sigma) \leq E_0 \qquad \sigma \geq \sigma_{max} \quad E(\sigma) = E_0$

On sait alors [3], [2], que :

$$\sigma_{min} \leq \sigma_{pq} \leq \sigma_{max}$$

$$\sigma_{pq} \to \sigma_{max} \quad \text{pour} \quad p \neq q \to +\infty$$

$$\sigma_{pq} \to \sigma_{min} \quad " \quad p \neq q \to -\infty$$

En particulier, si nous posons $\sigma_n = \sqrt{\frac{m_{2n}}{m_{2n-2}}}$, la suite σ_n est monotone et a pour limites σ_{min} et σ_{max}.

APPLICATION.

La considération des quantités σ_{pq} va nous permettre d'évaluer les valeurs moyennes des dérivées de f, nous avons en effet :

$$\| f^{(n)} \| = \sqrt{m_{2n}} = [\sigma_{2n\,0}]^n \| f_0 \|$$

$$\| f^{(n)} \| = \sigma_n \| f_{n-1} \|$$

Ceci va nous permettre d'évaluer le "reste" de certaines formules algébriques obtenues au paragraphe "Propriétés algébriques de $\gamma(\tau)$".

Soit par exemple :

$$\frac{1}{T}\int_0^T f^{(n+1)}(t)\, f^{(n-1)}(t+\tau)\,dt = -\frac{1}{T}\int_0^T f^{(n)}(t)\, f^{(n)}(t+\tau)\,dt + \frac{1}{T}\left[f^{(n)}(t)\, f^{(n-1)}(t+\tau) \right]_0^T$$

lorsque $T \to \infty$, nous obtenons la formule connue :

$$\left[f^{(n+1)}(t), f^{(n-1)}(t+\tau) \right] = -\left[f^{(n)}(t)\, f^{(n)}(t+\tau) \right]$$

Si nous écrivons :

$$\frac{1}{T}\int_0^T f^{(n+1)}(t)\, f^{(n-1)}(t+\tau)\,dt = -\frac{1}{T}\int_0^T f^{(n)}(t)\, f^{(n)}(t+\tau)\,dt$$

nous commettons une erreur qui, en valeur relative, est de l'ordre de grandeur de :

$$\Delta \simeq \frac{\frac{1}{T} f^{(n)}(t)\, f^{n-1}(t+\tau)}{\left[f^{(n)}(t)\, f^{(n)}(t) \right]}$$

$$\Delta \sim \frac{1}{T} \frac{\| f^{n-1} \|}{\| f_n \|} \cdot \frac{f^{(n)}(t)}{\| f_n \|} \cdot \frac{f^{n-1}(t+\tau)}{\| f_{n-1} \|} = \frac{1}{T\sigma_n} \cdot \frac{f^{(n)}(t)}{\| f_n \|} \cdot \frac{f^{(n-1)}(t+\tau)}{\| f_{n-1} \|}$$

Le produit des deux derniers termes est en général inférieur à 10.

On a donc : $\Delta < 1/100$ si $T\sigma_n > 1000$ et $T > \frac{1000}{\sigma_n}$

Comme $\sigma_n < \sigma_1$ et que $\frac{1}{2\pi\sigma_1}$ mesure une période apparente de la houle, on trouve $T > \frac{1000}{2\pi} T_1$, ce qui est en général réalisé assez largement.

RELATIONS ENTRE LE SPECTRE ET LES DISTRIBUTIONS ASSOCIEES A $\eta(t)$

Cette partie sera orientée vers les relations entre le spectre et les distributions associées à η . Le spectre lui-même sera caractérisé par la suite de ses moments $m_0, m_2 m_4 \quad m_{2n}$. Les trois premiers moments ont d'ailleurs une importance spéciale à la fois parce que l'on pense souvent que le spectre général des houles de vent ne dépend que de trois paramètres, et aussi parce que un certain nombre de phénomènes ne dépendent que de ces trois moments.

Cela étant, on peut se proposer deux buts :
a) D'abord, il est évident que certaines distributions (les hauteurs par exemple) sont intéressantes en soi. Il faut donc, connaissant le spectre, les obtenir.

b) Mais l'opération inverse peut être plus importante. Certaines distributions sont faciles à obtenir en pratique. Elles permettront donc de calculer certains éléments du spectre (voir Introduction).

La plupart des propriétés qui apparaissent ont déjà été étudiées par Longuet-Higgins [3]. Nous avons conservé une assez grande généralité. En effet, si la plupart des appareils donnent un enregistrement de $\eta(t)$, il ne faut pas oublier qu'ils pourraient aussi fournir η' ou η'' au prix de modifications assez faibles.

DISTRIBUTION DE $\eta(t)$ ET DE SES DERIVEES.

Rappelons les résultats de la première partie. La distribution de probabilité associée à la suite $\eta^{(p)}(t)$, $\eta^{(p_1)}(t+\tau_1)$, $\eta^{(p_n)}(t+\tau_n)$ suite dont la matrice des covariances est :

$$a_{hk} = \Gamma[p_h, p_k, \tau_k - \tau_h)$$

est $$p(y_0, y_1 \quad y_n) = \frac{1}{(2\pi)^{n/2}\sqrt{\|a_{nk}\|}} \exp\left\{-\frac{1}{2} b_{nk} y_n y_k\right\}$$

a) Nous allons appliquer ceci à η et η', on trouve :

pour η, $$p_0(x) = \frac{1}{\sqrt{2\pi}\sqrt{m_0}} \exp\left(-\frac{1}{2}\frac{x^2}{m_0}\right)$$

pour η', $$p_1(x) = \frac{1}{\sqrt{2\pi}\sqrt{m_2}} \exp\left(-\frac{1}{2}\frac{x^2}{m_2}\right)$$

Ces distributions sont faciles à obtenir, mais on voit qu'elles donnent très peu de renseignements sur le spectre. Seulement un moment pour chacune d'entre elles.

b) Distribution associée au couple $\eta(t)$, $\eta(t+\tau)$

$$p\left(\eta = y, \eta(t+\tau) = z\right) = \frac{1}{2\pi\sqrt{m_0^2 - \gamma(\tau)^2}} \exp\left\{\frac{-\frac{1}{2}(m_0 y^2 - 2\gamma yz + m_0 z^2)}{m_0^2 - \gamma^2}\right\}$$

Comme cette distribution contient deux variables, elle est moins facile à obtenir que les précédentes et les résultats seront moins précis. On peut tourner la difficulté en étudiant les fonctions $\Phi_1(t) = \inf[f, f(t+\tau)]$ $\Phi_2(t) = \sup[f, f(t+\tau)]$ dont les distributions sont :

$$F_1(u) = \int_{-\infty}^{u}\int_{-\infty}^{u} p(y,z)\,dy\,dz$$

$$1 - F_2(u) = \int_{u}^{\infty}\int_{u}^{\infty} p(y,z)\,dy\,dz$$

Les distributions F_1 et F_2 sont expérimentalement aussi simples à obtenir que les fonctions p_1 et p_2 précédentes. Elles dépendent des paramètres m_0 et $\gamma(\tau)$ et permettent donc d'obtenir ces deux nombres. Nous n'insistons pas cependant car la méthode est très lourde.

DISTRIBUTION DES POINTS SINGULIERS ASSOCIES A $f(t)$ OU A SES DERIVEES.

Nous allons étudier les points définis par l'équation du type $f^{(p)}(t+\tau) = a$ (τ et a fixés). Ces points constituent sur l'axe des t une "population" (un sous-espace) sur lequel on peut définir et étudier une probabilité.

Posons $N_T(f=a)$ nombre de points sur $(0,T)$ où $f=a$ divisé par T
$N(f=a)$ limite quand $T \to \infty$ de $N_T(f=a)$

Soit alors une fonction Φ quelconque. Nous considèrerons de même :

$$N_T\{f=a \quad \Phi \in (y, y+dy)\}$$

$$N\{f=a \quad \Phi \in (y, y+dy)\}$$

Et nous aurons la "probabilité" définie sur la suite $f=a$

$$\varpi\{\Phi \in (y, y+dy)\} = \frac{N(f=a,\ \Phi \in (y, y+dy))}{N(f=a)}$$

Ces définitions, (calquées sur la définition de la probabilité conditionnelle) sont parfaitement cohérentes et analogues à celles de la première partie (mais on opère sur une suite discrète et non sur des intervalles). De plus, il existe un lien entre les N_T et les F_T déjà définis. On a en effet :

$$N_T(f=a) = \int_{-\infty}^{+\infty} p_T(f=a\ f'=x)\,|x|\,dx = 2\int_{0}^{\infty} p_T(f=a\ f'=x)\,x\,dx$$

si la loi est symétrique en f'

$$N_T(f=a, \Phi=y) = \int_{-\infty}^{+\infty} p_T(f=a\ f'=x\ \Phi=y)\,|x|\,dx = 2\int_{0}^{\infty} p_T(f=a\ f'=x\ \Phi=y)\,x\,dx$$

(N_T désigne ici une densité en y)

Et à la limite :

$$N(f=a) = \int_{-\infty}^{+\infty} p(f=a\ f'=x)\,|x|\,dx$$

$$N(f=a\ \Phi=y) = \int_{-\infty}^{+\infty} p[f=a, f'=x, \Phi=y]\,|x|\,dx \quad (N \text{ densité en } y)$$

Les démonstrations sont reportées en annexe. Les N_T ou les N sont d'autre part plus faciles à obtenir par comptage que les p .

Nous allons appliquer ceci à quelques points particuliers.

Intersection avec des horizontales –

$$N(f=a) = 2\int_0^\infty \exp\left(-\frac{a^2}{2m_0} - \frac{x^2}{m_2}\right) x\,dx = N_0 \exp\left(\frac{-a^2}{2m_0}\right)$$

$$N_0 = \frac{1}{\pi}\sqrt{\frac{m_2}{m_0}} = \frac{1}{\pi}\sqrt{\sigma_2}$$

En généralisant immédiatement on obtient :

$$N\left(f^{(p)}=a\right) = N_p \exp\left(\frac{-a^2}{2m_{2p}}\right). \qquad N_p = \frac{1}{\pi}\sqrt{\frac{m_{2p+2}}{m_{2p}}} = \frac{1}{\pi}\sqrt{\sigma_{2p}}$$

Distribution de f quand $f'=0$; maximas et minimas –

La matrice des corrélations de $f f' f''$ est $\begin{vmatrix} m_0 & 0 & -m_2 \\ 0 & m_2 & 0 \\ -m_2 & 0 & m_4 \end{vmatrix}$

La matrice inverse $\frac{1}{\Delta m_2}\begin{vmatrix} m_2 m_4 & 0 & m_2^2 \\ 0 & \Delta & 0 \\ m_2^2 & 0 & m_2 m_0 \end{vmatrix}$

en posant $\Delta = m_0 m_4 - m_2^2$

D'où $p^*\left\{f=x_1, f'=0, f''=x_3\right\} = \frac{1}{2\pi^{3/2}\sqrt{\Delta m_2}} \exp\left\{-\frac{1}{2}\frac{m_4 x_1^2 + 2m_2 x_1 x_3 + m_0 x_3^2}{\Delta}\right\}$

et $N\left\{f=x_1\ f'=0\ f''<0\right\} = \int_0^\infty p\ x_3\,dx_3$

Les calculs ont été faits par Longuet-Higgins. On pose $\begin{cases} \eta = \frac{x_1}{\sqrt{m_0}} \\ \epsilon^2 = \frac{\Delta}{m_0 m_4} \end{cases}$

Et on obtient : $N = N_1 \tfrac{1}{2}\, p(\eta)$

$$p(\eta) = \frac{1}{(2\pi)^{1/2}}\left[\epsilon \exp\left(-\tfrac{1}{2}\eta^2/\epsilon^2\right) + (1-\epsilon^2)^{1/2}\,\eta \exp\left(-\tfrac{1}{2}\eta^2\right)\right] \int_{-\infty}^{\eta(1-\epsilon^2)^{1/2}/\epsilon} \exp\left(-\tfrac{1}{2}x^2\right) dx$$

Généralisation. Distribution de f quand $f^{(2p-1)}=0$ –

Posant $\Delta_{02p} = m_0 m_{4p} - m_{2p}^2$

$$\epsilon_{02p}^2 = \Delta_{02p} / m_0 m_{4p}$$

$$\eta = x_1/\sqrt{m_0}$$

On a $p\left\{f=x_1\ f^{(2p-1)}=0\ f^{2p}=x_3\right\} = \frac{1}{2\pi^{3/2}\sqrt{\Delta_{02p}\, m_{4p-2}}} \exp\left[-\frac{1}{2}\frac{m_{4p}x_1^2 + 2m_{2p}x_1x_3 + m_0 x_3^2}{\Delta_{02p}}\right]$

D'où $N = N_{2p-1}\ \tfrac{1}{2}\ p^*(\eta)$

$$p^*(\eta) = \frac{1}{(2\pi)^{1/2}}\left[\epsilon_{02p} \exp\left(\tfrac{1}{2}\eta^2/\epsilon_{02p}^2\right) + (1-\epsilon_{02p}^2)^{1/2}\,\eta \exp\left(-\tfrac{1}{2}\eta^2\right)\right] \int_{-\infty}^{\eta(1-\epsilon_{02p}^2)^{1/2}/\epsilon_{02p}} \exp\left(-\tfrac{1}{2}x^2\right) dx$$

$p^*(\eta)$ et $p(\eta)$ sont donc identiques en remplaçant ϵ par ϵ_{02p}.

ETUDE THEORIQUE DE L'EXPLOITATION DES ENREGISTREMENTS DE HOULE

Distribution de ξ quand $\xi''=0$. Points d'inflexion. - Le calcul est analogue au précédent, mais la matrice s'écrit :

$$\begin{vmatrix} m_0 & -m_2 & 0 \\ -m_2 & m_4 & 0 \\ 0 & 0 & m_6 \end{vmatrix}$$

D'où $N(\xi=x_1,\ \xi''=0) = \dfrac{2}{2\pi^{3/2}\sqrt{\Delta m_6}} \int_0^\infty \exp\left\{-\frac{1}{2}\left(\frac{m_4}{\Delta}x^2 + \frac{m_6}{\Delta}y^2\right)\right\} dy$

$$N(\xi=x_1,\ \xi''=0) = N_2 \sqrt{\frac{m_4}{2\pi\Delta}}\ \exp\left[-\frac{1}{2}\frac{m_4}{\Delta}x_1^2\right]$$

Généralisation. Distribution de ξ quand $\xi^{(2p)}=0$

On obtient de la même façon :

$$N\left[\xi=x_1,\ \xi^{(2p)}=0\right] = N_{2p}\ \sqrt{\frac{m_{4p}}{2\pi\,\Delta_{02p}}}\ \exp\left[-\frac{1}{2}\frac{m_{4p}}{\Delta_{02p}}x_1^2\right].$$

Les distributions sont donc cette fois des distributions de Gauss.

On peut généraliser encore en remplaçant ξ par $\xi^{(k)}$, il suffit d'ajouter $2k$ aux moments considérés. On voit ainsi qu'on a obtenu la distribution générale de $\xi^{(p)}$ quand $\xi^{(p+q)}=0$

Intersections entre $\xi(t)$ et $\xi(t+\tau)$ - Nous ne dirons rien de la distribution ξ quand $\xi(t+\tau)=0$, qui est facile à obtenir mais sans intérêt. Par contre, une autre fréquence est plus intéressante, c'est celle des points où $\xi(t) = \xi(t+\tau)$

Posons : $z = \xi(t+\tau) - \xi(t)$ $\qquad N(z=0) = \sqrt{\dfrac{[z',z']}{[z,z]}}$

$$[z',z'] = 2\,m_2 - \gamma^{(2)}(\tau) \qquad [z,z] = m_0 - \gamma(\tau)$$

D'où $N\left[\xi=\xi(t+\tau)\right] = \dfrac{1}{\pi}\sqrt{\dfrac{[z',z']}{[z,z]}_{(2)}} = \dfrac{1}{\pi}\sqrt{\dfrac{m_2-\gamma^{(2)}(\tau)}{m_0-\gamma(\tau)}}$

Quand τ devient assez grand $\gamma^{(2)}(\tau)$ et $\gamma(\tau) \to 0$ donc $N(\tau) \to N_0$

Quand $\tau \to 0$, nous avons $\gamma^{(2)}(\tau) = m_2 - m_4\dfrac{\tau^2}{2} + \ldots$

$\gamma(\tau) = m_0 - m_2\dfrac{\tau^2}{2} + \ldots$

Donc $N(\tau) \to N_1$

MOYENNES ASSOCIEES AUX POINTS SINGULIERS PRECEDENTS.

On est très vite limité par la difficulté qu'il y a à calculer effectivement ces moyennes. Il semble que seules les amplitudes (différence entre maximas et minimas) peuvent donner lieu à des moyennes faciles à obtenir.

Notons ainsi la moyenne des amplitudes (Longuet-Higgins) :

$$M_1 = 2\sqrt{m_0}\,(\tfrac{1}{2}\pi)^{1/2}\,(1-\epsilon^2)^{1/2}$$

Et, de même, la moyenne des amplitudes de ξ'

$$M_2 = 2\sqrt{m_1}\,(\tfrac{1}{2}\pi)^{1/2}\,(1-\epsilon_{13}^2)^{1/2}$$

CONCLUSION

Ainsi, pour obtenir les trois premiers moments, nous avons vu quelques

méthodes simples :

1. Le comptage de $N_0(\zeta = 0)$ et de $N_1(\zeta' = 0)$ qui donne m_2/m_0 et m_4/m_2

2. Le comptage des fréquences $N(\zeta = a)$ qui donne m_2/m_0 et m_0

3. La moyenne des amplitudes qui donne une relation entre m_0 et ϵ. Il suffit donc d'associer 1. et 3. ou 1. et 2. C'est cette méthode qui a effectivement été retenue à Chatou. Il va de soi que la mise au point d'appareils de comptage différents pourrait conduire à utiliser des distributions différentes parmi celles qui ont été étudiées.

PROBLEMES PRATIQUES LIES A L'ENREGISTREMENT DES HOULES

Cette fin d'étude est consacrée à deux problèmes pratiques liés à l'exploitation des enregistrements de houle.

Un des types d'appareil utilisé (capteurs de pression) enregistre non pas la fonction $\zeta(t)$ mais une fonction $\Phi(t)$ qui lui est liée (pression sur le fond au lieu de dénivellation en surface). On peut admettre que l'on passe du spectre de ζ à celui de Φ au moyen d'un facteur correctif $K(\sigma)$ connu. Il nous faut donc étudier les problèmes posés par cette correction.

L'autre problème est celui de la présence de "fonctions parasites" ou d'erreurs quelconques : le déplacement du niveau moyen, la présence de phénomènes d'agitation non liés à la houle en sont des exemples. Certains de ces phénomènes sont connus et on peut essayer d'évaluer leur influence et d'en tenir compte. De façon plus générale, il faut évaluer la marge d'incertitude sur les résultats obtenus.

RESTITUTION.

Si le spectre est continu, ce qui est le cas général (et le cas discontinu ne nécessiterait que de faibles modifications), on peut poser :

$dE(\sigma) = \frac{1}{2} A(\sigma) d\sigma$. La présence du facteur $\frac{1}{2}$ permet de ne considérer que l'intervalle $[0 \leq \sigma \leq \infty]$ et d'avoir :

$$m_n = \int_0^\infty \sigma^n A(\sigma) d\sigma$$

Le problème est donc de trouver le spectre $A^*(\sigma)$ en surface connaissant $A(\sigma)$. Il est résolu par la formule :

$$A^*(\sigma) = K(\sigma) \times A(\sigma)$$

$$K(\sigma) = \mathrm{Ch}.\left(\frac{2\pi d}{L}\right)$$ facteur correctif.

En fait, nous ne pouvons nous contenter de la formule précédente, car nous ne connaissons pas directement $A(\sigma)$. Notons que si $\Theta(u)$ est la transformée de Fourrier de $K(\sigma)$

$$\Theta(u) = \int_{-\infty}^{+\infty} e^{i\sigma u} K(\sigma) d\sigma$$

on a : $\gamma^*(\tau) = \gamma * \Theta = \int_{-\infty}^{+\infty} \gamma(t-u)\, \Theta(u) du$

Mais nous désirons résoudre le problème par des procédés algébriques n'impliquant qu'une connaissance partielle de $A(\sigma)$. Nous sommes donc amenés à chercher la suite $m_0^*, m_2^*, \ldots m_{2n}^*$ connaissant $m_0, m_1, \ldots m_{2n}$. Et, conformément à ce que nous avons vu dans la deuxième partie, nous nous intéressons surtout aux trois premiers moments.

Considérons une expression approchée de $K(\sigma)$ au moyen d'un polynome. D'après (H_5) il suffit de réaliser l'approximation sur le segment $(\sigma_{min}, \sigma_{max})$. Ce problème est toujours possible et nous pouvons poser :

$$K(\sigma) \simeq a_0 + a_2\sigma^2 + \ldots + a_{2p}\sigma^{2p}$$

Nous aurons alors :

$$m_0^* = a_0 m_0 + a_2 m_2 + \ldots + a_{2p} m_{2p}$$
$$m_2^* = a_0 m_2 + a_2 m_4 + \ldots + a_{2p} m_{2p+2}$$
$$m_{2n}^* = a_0 m_{2n} + a_2 m_{2n+2} + a_{2p} m_{2p+2n}$$

On voit que la connaissance de n moments en surface implique celles de $(n+p)$ moments au fond. Nous nous limiterons à $2p = 4$, ce qui est cohérent avec les hypothèses déjà faites.

Nous aurons alors :

$$m_{2n}^* = a_0 m_{2n} + a_2 m_{2n+2} + a_4 m_{2n+4}$$
$$= \left[a_0 m_{2n} + a_2 m_{2n+2} + a_4 \frac{m_{2n+2}^2}{m_{2n}}\right] + a_4 m_{2n+4}\left[1 - \frac{m_{2n+2}^2}{m_{2n}\, m_{2n+4}}\right]$$
$$= m_{2n} K\left(\frac{m_{2n+2}}{m_{2n}}\right)$$

$$\boxed{m_{2n}^* = m_{2n} K(\sigma_{2n+2})\left[1 + \frac{a_4}{K(\sigma_{2n+2})} \epsilon_{n,n+2}^2 \sigma_{2n+4}^2 \sigma_{2n+2}^2\right.}$$

C'est de cette formule que nous allons nous servir. Retranscrivons-la pour $n = 0$, 1 et 2. On trouve :

$$\boxed{\begin{aligned} m_0^* &= m_0 K(\sigma_2)\left\{1 + \frac{a_4}{K(\sigma_2)} \epsilon_4^2 \sigma_4^2 \sigma_2^2\right. \\ m_2^* &= m_2 K(\sigma_4)\left\{1 + \frac{a_4}{K(\sigma_4)} \epsilon_6^2 \sigma_6^2 \sigma_4^2\right. \\ m_4^* &= m_4 K(\sigma_6)\left\{1 + \frac{a_4}{K(\sigma_6)} \epsilon_8^2 \sigma_8^2 . \sigma_6^2\right. \end{aligned}}$$

On voit qu'il subsiste un certain nombre d'inconnues : $\epsilon_6^2, \epsilon_8^2$ et σ_8^2, σ_6^2. Mais nous pouvons remarquer que le terme où ils interviennent est un terme "complémentaire" et que nous pourrons faire des hypothèses sur ϵ_6^2 et ϵ_8^2 sans prendre beaucoup de risques d'erreur.

Nous savons déjà deux choses :

a) la suite σ_{2n}^2 est croissante,

b) la suite ϵ_{2n}^2 est décroissante et tend vers 0.

Nous supposerons donc que σ_{2m}^2 est une suite arithmétique.

Nous aurons alors :

$$\sigma_2^2 = \sigma_2^2 \qquad \epsilon_4^2 = \frac{h^2}{\sigma_2^2 + h^2}$$

$$\sigma_4 = \sigma_2^2 + h^2$$

$$\sigma_{2m}^2 = \sigma_2^2 + (n-1)h^2 \qquad \epsilon_{2m}^2 = \frac{h^2}{\sigma^2 + (n-1)h^2}$$

Posons alors $\lambda_{2m}\,\sigma_2^4 = \epsilon_{2m}^2\,\sigma_{2m}^2\,\sigma_{2m-2}^2$

Nous aurons facilement : $\lambda_{2m} = \frac{h^2}{\sigma_2^2}\left[1 + (n-2)\frac{h^2}{\sigma_2^2}\right]$

D'où

$$m^*_{2m} = m_{2m}\,K(\sigma_{2m+2})\left[1 + \frac{a_4\,\sigma_2^2}{K(\sigma_{2m+2})}\,\frac{h^2}{\sigma_2^2}\left[1 + n\frac{h^2}{\sigma_2^2}\right]\right]$$

Ce que nous retranscrivons pour les trois premiers moments, appelant ϵ_4, ϵ et remplaçant h^2/σ_2^2 par sa valeur :

$$m_0^* = m_0\,K(\sigma_2)\left[1 + \frac{a_4\,\sigma_2^2}{K(\sigma_2)}\cdot\frac{\epsilon^2}{1-\epsilon^2}\right]$$

$$m_2^* = m_2\,K(\sigma_4)\left[1 + \frac{a_4\,\sigma_2^2}{K(\sigma_4)}\,\frac{\epsilon^2}{(1-\epsilon^2)^2}\right]$$

$$m_4^* = m_4\,K(\sigma_6)\left[1 + \frac{a_4\,\sigma_2^2}{K(\sigma_6)}\,\frac{\epsilon^2}{(1-\epsilon^2)^2}(1+\epsilon^2)\right]$$

Remarque - Etude de $K(\sigma)$ - Les formules précédentes ne sont valables q si les termes "correctifs" méritent effectivement ce nom, c'est-à-dire sont suffisamment petits. Comme l'on a :

$$K = \mathrm{ch}\left(\frac{2\pi d}{L}\right) = K\left\{\frac{d}{2\pi g}\sigma^2\right\}$$ nous aurons des inégalités portant

$\frac{d}{2\pi g}\sigma_{max}^2$ et $\frac{d}{2\pi g}\sigma_{moy}^2$. On aura à vérifier deux conditions :

a) $\frac{a_4\,\sigma_2}{K(\sigma_2)}\cdot\frac{\epsilon^2(1+\epsilon^2)}{(1+\epsilon^2)^2}$ dé l'ordre de ϵ^2 (termes correctifs faibles).

Cela nous donne :

$$\boxed{T_{moy} \geqslant \sqrt{4d}} \qquad T_{moy} = 2\pi/\sigma_2$$

b) σ_{max} doit être tel que l'approximation parabolique soit encore valable. Nous admettons que ceci est réalisé si $d/L_{o\,max} \leq \frac{1}{2}$, ce qui conduit à :

ETUDE THEORIQUE DE L'EXPLOITATION DES ENREGISTREMENTS DE HOULE

$$\frac{2\pi}{\sigma_{max}} = T_{min} \geqslant \sqrt{\frac{4}{3}d}$$

On voit ainsi les limitations de l'appareil suivant les valeurs de d . Pratiquement, la zone intéressante est $d<10m$.

PROBLEMES LIES A L'INCERTITUDE DES RESULTATS.

Supposons qu'à la fonction f étudiée se superpose une fonction Δf parasite due à n'importe quelle cause (déplacement du niveau moyen, réactions de l'appareil, etc..). Nous allons voir que l'on peut passer des résultats relatifs à $f+\Delta f$ à ceux de f à condition du moins de connaître Δf . De plus, si Δf est suffisamment faible, l'erreur introduite est négligeable.

Une première difficulté provient du fait que, tandis que f représente la houle et satisfait donc aux hypothèses (H_1 à H_5), Δf ne représente rien et n'a aucune raison de satisfaire à ces hypothèses.

Mais en fait, ce n'est pas à Δf que nous nous intéressons, mais à Δf de 0 à T . Nous pouvons donc remplacer Δf par une fonction périodique de période T (qui satisfait à la plupart des hypothèses, mis à part celles conduisant à la loi de Gauss). Les résultats expérimentaux seront les mêmes car les opérations faites concernent toutes le segment$(0,T)$.

Enfin, comme $f(t)$ n'a aucune périodicité en T , nous pouvons supposer que f et Δf sont indépendantes. Nous supposerons aussi que Δf est à moyenne nulle car s'il n'en était pas ainsi, nous ferions une translation de Δf sur l'axe des ordonnées. La fonction Δf ainsi définie a des fonctions de distributions faciles à calculer et identiques à celles obtenues sur $(0,T)$. Cela va nous donner les fonctions de distributions de $f+\Delta f$.

Etude directe des fonctions de distribution –

Soit $p(y)$ la densité associée à f
$\varpi(y)$ " " Δf
$q(y)$ " " $f+\Delta f$

L'application des théorèmes sur les fonctions indépendantes nous donne :

$$q(y) = p * \varpi = \int_{-\infty}^{+\infty} p(y-v)\,\varpi(v)\,dv$$

Cette formule résout le problème, mais nous allons, comme $\varpi(v)$ est petit, utiliser un développement en série :

$$p(y-v) = p(y) - v\,p'(y) + \frac{v^2}{2!}\,p''(y) + \cdots + (-1)^n \frac{p^{(n)}(y)}{n!}\,v^n + \cdots$$

Nous aurons donc :

$$q(y) = p(y) + \frac{\mu_2}{2}\,p''(y) + \cdots + (-1)^n \frac{\mu_n}{n!}\,p^{(n)}(y) + \cdots$$

Avec $\mu_m = \int_{-\infty}^{+\infty} v^n \varpi(v)\,dv = M_T\left[\Delta f^n\right]$ et $\mu_1 = 0$

Si Δf est bornée par A on a $M_T[\Delta f^n] < A^n$, d'où une convergence assurée de la série précédente et une évaluation de la différence entre p et q. En particulier, si A est très petit $q(y) \simeq p(y)$

Généralisation – Le calcul précédent se généralise aux distributions à plusieurs dimensions. Ce calcul est fait en annexe. On peut donc, en intégrant, obtenir aussi les distributions des maxima et minima.

Autre méthode – Une méthode différente est de considérer directement le spectre de la fonction (périodique) Δf. Ce spectre est facile à obtenir et en particulier, on peut trouver la suite des moments $\Delta m_0, \Delta m_1 \cdots \Delta m_n$

Or, on a vu dans la première partie que, aussi bien le spectre que les moments ou la fonction de corrélation $\gamma(\tau)$ s'ajoutent. On aura donc $E + \Delta E$, $\gamma + \Delta\gamma$ et $m_{2n} + \Delta m_{2n}$. En particulier les fréquences d'intersections seront :

$$N_0 = \frac{1}{\pi}\sqrt{\frac{m_{2n} + \Delta m_{2n}}{m_0 + \Delta m_0}} \qquad N_1 = \frac{1}{\pi}\sqrt{\frac{m_4 + \Delta m_4}{m_2 + \Delta m_2}}$$

REFERENCES BIBLIOGRAPHIQUES.

1. Bass, J. (1959). Suites uniformément denses, Moyennes trigonométriques, Fonctions pseudo-aléatoires – Bull. Soc. Math. France – 87, pp. 1 à 64.

2. Loève, M. (1956). Probability Theory – Van Nostrand – New-York.

3. Cartwright, D.E. et Longuet-Higgins, M.S. (1956). Statistical distribution of the maxima of a raudom variable – Proc. of the Roy. Soc. London – Series A, Vol. 237, pp. 212-232.

4. Rice, S.O. (1944). Bell Syst. Tech. J. 23, 282.
(1945). Bell Syst. Tech. J. 24, 46.

5. Valembois, J., Germain, J. et Jaffry, P. (1956). Connaissance de la houle naturelle : le point de vue de l'ingénieur – Compte-rendu des 4ème Journées de l'Hydraulique – pp. 95-99.

ETUDE THEORIQUE DE L'EXPLOITATION DES ENREGISTREMENTS DE HOULE

ANNEXE A LA PREMIERE PARTIE.

Nous allons calculer quelques-unes des matrices de corrélations le plus fréquemment rencontrées. Toutes ces matrices s'exprimeront au moyen de la fonction $\gamma(\tau)$ et de ses dérivées. Comme $\gamma^{(2n)}(0) = (-1)^n m_{2n}$ nous avons aussi fait intervenir les moments $m_0\ m_2\ m_n$.

a. Suite $[f(t)\ ,\ f'(t)\ f''(t)\ ..\ f^{(2n)}(t)]$ n pair.

La matrice s'écrit :

$$\begin{vmatrix} m_0 & 0 & -m_2 & 0 & \cdot & (-1)^{\frac{n}{2}} m_n \\ 0 & m_2 & 0 & -m_4 & \cdots & 0 \\ -m_2 & 0 & m_4 & 0 & \cdots & (-1)^{\frac{n}{2}+1} m_{n+2} \\ 0 & -m_4 & 0 & m_6 & \cdots & 0 \\ \cdots & \cdots & \cdots & \cdots & \cdots & \cdots \\ (-1)^{\frac{n}{2}} m_n & (-1)^{\frac{n}{2}+1} m_{n+2} & \cdots & \cdots & \cdot & m_{2n} \end{vmatrix}$$

b. Suite $[f(t), f^{(1)}(t+\tau_1)\ f^{(2)}(t+\tau_2+\tau_1), f^{(3)}(t+\tau_1+\tau_2+\tau_3)$

La matrice s'écrit :

$$\begin{vmatrix} m_0 & \gamma'(\tau_1) & \gamma''(\tau_1+\tau_2) & \gamma'''(\tau_1+\tau_2+\tau_3) \\ \gamma'(\tau_1) & m_2 & \gamma^{(3)}(\tau_2) & \gamma^{(4)}(\tau_2+\tau_3) \\ \gamma''(\tau_1+\tau_2) & \gamma^{(3)}(\tau_2) & m_4 & \gamma^{(5)}(\tau_3) \\ \gamma'''(\tau_1+\tau_2+\tau_3) & \gamma^{(4)}(\tau_2+\tau_3) & \gamma^{(5)}(\tau_3) & m_6 \end{vmatrix}$$

c. Notons que, lorsque la distribution est continue et symétrique, nous avons, en posant $dE(\sigma) = \frac{1}{2} A(\sigma)$

$$\gamma(\tau) = \int_0^\infty A(\sigma) \cos(\sigma\tau) d\sigma \qquad \gamma(0) = \int_0^\infty A(\sigma)\, d\sigma = m_0$$

$$\gamma'(\tau) = -\int_0^\infty A(\sigma)\, \sigma\, \sin(\sigma\tau)\, d\sigma \qquad \gamma'(0) = 0$$

et, plus généralement :

$$\gamma^{(2m)}(\tau) = (-1)^m \int_0^\infty \cos(\sigma\tau)\, \sigma^{2m} A(\sigma)\, d\sigma \qquad \gamma^{(2m)}(0) = (-1)^m m_{2m}$$

$$\gamma^{2m+1}(\tau) = (-1)^{m+1} \int_0^\infty \sin(\sigma\tau)\, \sigma^{2m+1} A(\sigma)\, d\sigma \qquad \gamma^{(2m+1)}(0) = 0$$

Ces formules sont utiles parce qu'elles font intervenir uniquement des variables réelles. Elles montrent que la connaissance de $\gamma(\tau)$ et de toutes ses dérivées (ou de $A(\sigma)$) permet de calculer facilement les matrices de corrélations précédentes.

ANNEXE A LA DEUXIEME PARTIE.

a. Supposons que $f'(t)$ soit une constante (La fonction $f(t)$ serait alors composée de segments de droites reliés par des sauts).

N_T étant le nombre (déjà défini) des intersections avec la droite $f = a$ et da, dx deux variables reliées par $da = |f'|\, dx$

Nous avons :

$$\sum_{N_T} dx = N_T\, dx = p_T(f=a)\, da \quad \text{soit} \quad N_T = p(f=a)\, |f'|$$

De même, si nous définissons :

N_T = nombre de points où $\{f=a \text{ et } \phi \in (y, y+dy)\}$ nous avons

$$\sum_{N_T} dx = N_T dx = p_T\{f=a \text{ et } \phi \in (y, y+dy)\}\,|f'|$$

Soit $N_T = p_T\{f=a \text{ et } \phi \in (y, y+dy)\}\,|f'|$

définissant une densité $N_T^* = \frac{N_T}{dy}$ on a. $N_T^* = p(f=a, \phi=y)\,|f'|$

b. Si nous revenons au cas général où $f'(t)$ est variable, on voit qu'il suffit de considérer les probabilités composées :

$$p_T\{f=a, f'=x\} \qquad \text{et} \qquad p_T\{f=a, f'=x, \phi=y\}$$

et que les formules précédentes se généralisent en :

$$N_T = \int_{-\infty}^{+\infty} p_T(f=a\ f'=x)\,|x|\,dx$$

$$N_T^* = \int_{-\infty}^{+\infty} p_T(f=a\ f'=x\ \phi=y)\,|x|\,dx$$

qui sont bien les formules données dans le texte.

ANNEXE A LA TROISIEME PARTIE.

La généralisation des formules données dans le texte au cas de distributions plus générales à n variables ne présente aucune difficulté théorique et n'est qu'un exercice de calcul.

Soit un espace à dimensions. Nous introduirons les notations suivantes:

$X(x_1 x_2 \ldots x_n)$ et $Y(y_1, y_2, \ldots y_n)$ vecteurs de l'espace,

$(dX) = dx_1 dx_2 \ldots dx_n$ élément de volume,

$X \gg Y$ est équivalent à $x_1 \geq y_1,\ x_2 \geq y_2 \ldots x_n \geq y_n$

Cette relation d'ordre jouit de la propriété fondamentale suivante :

$$X \gg Y \quad \text{et} \quad X' \gg Y' \qquad \text{entraîne} \qquad X+X' \gg Y+Y'$$

Dans un tel espace, la notion de distribution de probabilité est très facile à définir. On peut définir soit la densité $p(X_0)$

$$p(X_0)(dX) = pr\left[X_0 \ll X \ll X_0+dX\right]$$

soit la distribution F

$$F(X_0) = p_r[X \ll X_0] = \int_{X \ll X_0} p(X)(dX)$$

Et l'on a $dF(X) = p(X)(dX)$ Si la distribution est continue.

Soient alors une variable X de fonction de distribution F et p ,
et une variable Y de fonction de distribution F' et p'.

Si elles sont indépendantes on a :

$$p_r[X_0 \ll X \ll X_0+dX \text{ et } Y_0 \ll Y \ll Y_0+dY] = p(X_0)\ p'(Y_0)\ (dX)(dY)$$

D'où il est facile de voir que, si G , q sont les fonctions de distribution de la somme $X+Y$, on a :

ETUDE THEORIQUE DE L'EXPLOITATION DES ENREGISTREMENTS DE HOULE

$$G(x_0) = \int F(x_0 - x)\, dF'(x) = \int F'(x_0 - x)\, dF(x)$$

$$q(x_0) = \int p(x_0 - x)\, dF'(x) = \int p(x_0 - x)\, p'(x)(dx)$$

Soit, en abrégé

$$\boxed{q = p * p'}$$

Nous sommes donc arrivés à la même formule que dans le cas de deux variables.

Si X désigne la variable associée à $f(t), f^{(p)}(t+\tau_p), f^{(q)}(t+\tau_q) \ldots f^{(n)}(t+\tau_n)$

Y $\Delta f(t), \Delta f^{(p)}(t+\tau_p), \Delta f^{(q)}(t+\tau_q) \ldots \Delta f^{(n)}(t+\tau_n)$

La formule précédente résout complètement le problème posé : trouver la distribution de probabilité associée à $(f + \Delta f)$ et à ses dérivées.

Bien entendu, on peut faire un développement en série de p, la formule précédente s'écrira alors :

$$q(x_0) = p(x_0) + \frac{1}{2} \frac{\partial^{(2)} p}{\partial x_i \partial x_j} \mu_{ij} + \ldots + \frac{(-1)^n}{n!} \frac{\partial^n p}{\partial x_{i_1} \ldots \partial x_{i_n}} \mu_{i_1 \ldots i_n} + \ldots$$

Avec :

$$\mu_{i_1 i_2 \ldots i_n} = \int x_{i_1} x_{i_2} \ldots x_{i_n}\, p'(x)(dx)$$

CHAPTER 9
A THEORY FOR WAVES OF FINITE HEIGHT

Charles L. Bretschneider *

ABSTRACT

A theory for waves of finite height, presented in this paper, is an exact theory, to any order for which it is extended. The theory is represented by a summation harmonic series, each term of which is in an unexpanded form. The terms of the series when expanded result in an approximation of the exact theory, and this approximation is identical to Stokes' wave theory extended to the same order. The theory represents irrotational - divergenceless flow. The procedure is to select the form of equations for the coordinates of the particles in anticipation of later operations to be performed in the evaluation of the coefficients of the series. The horizontal and vertical components of these coordinates are given respectively by the following:

$$kx = k(x-\xi) + \sum_{1}^{M} (kA_0)^N \frac{\cosh Nk(\ell + z - \eta)}{\sinh Nk\ell} \operatorname{Sin} Nk(x - Ct - \xi)$$

and

$$kz = k(z-\eta) + \sum_{1}^{M} (kA_0)^N \frac{\sinh Nk(\ell + z - \eta)}{\sinh Nk\ell} \cos Nk(x - Ct - \xi)$$

where

x and z are the coordinates; $k = 2\pi/L$, wave number; $A_0 = H/2$, half wave height; $C = L/T$, wave celerity and t is time.** ℓ is a parameter related to the undisturbed mean water depth, d. The constant term $kz_0 = k(\ell - d)$; ξ and η are the horizontal and vertical displacements of the water particles from their respective position of no motion. $a_N = a_1, a_2, a_3$, etc., coefficients of the series as N = 1, 2, 3, etc. to $N = M$. From the above equations it is possible to deduce the expressions for velocity potential and stream function. The horizontal and vertical components of particle velocity are obtained by differentiating ξ and η with respect to time. Along the free surface $z - \eta = 0$ and $z = \eta_s$ and all expressions reduce to simple forms, which in turn saves considerable work in the evaluation of the coefficients. The coefficients are evaluated by use of Bernoulli's equation. The final form of the solution is given by two sets of equations. One set of equations (same as above) is used to compute the particle position and the second set (the first time derivatives of the above) is used to compute the components of particle velocity at the particle position. That is, the particles and velocities are referenced to the lines of the stream function and the velocity potential. Expanding the two sets of equations, by approximation methods, results in one set of equation for computing particle velocity and no equations are required for the particle position. The unexpanded form requiring two sets of equations,

*Hydraulic Engineer, Beach Erosion Board, U. S. Army Corps of Engineers

** See Appendix for Symbols, p 182

being an exact solution, is more accurate theoretically, than the Stokes or the expanded form to the same order. Coefficients have been formulated for all terms of the order one to five for both the unexpanded and the expanded form of the theory, and are presented in tabular form as functions of d/L, as consecutive equations.

INTRODUCTION

Since 1847 when Stokes first presented his classical work on the theory of oscillatory waves, a number of authors have contributed to this fascinating subject. The reference list, which may not necessarily be complete, is given at the end of this paper. Except for the fact that the various developments given in these references entail certain difficulties and in some cases minor errors, no further discussions will be made thereof.

There is much to be discussed in the present paper and the usual formality of elementaries will be minimized. The inertia of the air and the atmospheric pressure along the wave surface can be neglected; i.e. these quantities are zero with respect to themselves, and the pressure within the fluid is assumed equal in all directions. There is to be no flow across the boundaries, the sea bed being rigid, flat, and impermeable, and the fluid is inviscid. The waves are long crests and x , z , t represent the two dimensional coordinates with respect to time. x is the horizontal direction measured from the crest, positive in the direction of wave propogation. z is the vertical coordinate measured negative below and positive above the undisturbed water elevation. The undisturbed water elevation is the mean water depth, and is that level the water seeks when all wave motion is absent. Finally the flow is irrotational, and since divergenceless, is Laplacian.

The equations by which the motion is described are as follows:

$$p = g\rho z - \rho \frac{\partial \phi}{\partial t} - \frac{1}{2} \rho \left\{ \left(\frac{\partial \phi}{\partial x} \right)^2 + \left(\frac{\partial \phi}{\partial z} \right)^2 \right\}$$

$$\frac{\partial^2 \phi}{\partial x^2} + \frac{\partial^2 \phi}{\partial z^2} = 0$$

$$\frac{\partial \phi}{\partial z} = 0 \quad \text{at} \quad z = -d$$

$$\frac{\partial p}{\partial t} + \frac{\partial \phi}{\partial x} \frac{\partial p}{\partial x} + \frac{\partial \phi}{\partial z} \frac{\partial p}{\partial z} = 0 \text{ , when } p = 0$$

Where ϕ is the velocity potential, g acceleration of gravity; ρ density of fluid; and p the pressure.

The first equation is the usual equation of hydrodynamics, the second specifies irrotational flow, the third specifies no flow across the sea bed, and the fourth specifies no flow across the free wave surface.

Coordinates

The coordinates of the particles of water can be represented by a set of equations around which a theory can be developed. If the equations are selected in anticipation of later operations to be performed, then one might be able to minimize the work envolved. In the presence of wave motion the horizontal and vertical displacements (ξ,η) of the water particles from the position of rest or the position of no motion can be represented respectively as follows:

$$k\xi = \sum_{1}^{M} a_N (kA_0)^N \frac{\cosh Nk(\ell + z - \eta)}{\sinh Nk\ell} \sin Nk(x - Ct - \xi) \qquad (1)$$

$$k\eta = \sum_{1}^{M} a_N (kA_0)^N \frac{\sinh Nk(\ell + z - \eta)}{\sinh Nk\ell} \cos Nk(x - Ct - \xi) \qquad (2)$$

(See Figure 1)

It then follows that the x, z coordinates of the particles are obtained from:

$$kx = k(x - \xi) + \sum_{1}^{M} a_N (kA_0)^N \frac{\cosh Nk(\ell + z - \eta)}{\sinh Nk\ell} \sin Nk(x - \xi) \qquad (3)$$

and

$$kz = k(z - \eta) + \sum_{1}^{M} a_N (kA_0)^N \frac{\sinh Nk(\ell + z - \eta)}{\sinh Nk\ell} \cos Nk(x - \xi) \qquad (4)$$

In the above equations

$2A_0 = H$, the wave height, vertical distance between crest and trough

$k = 2\pi/L$, the wave number

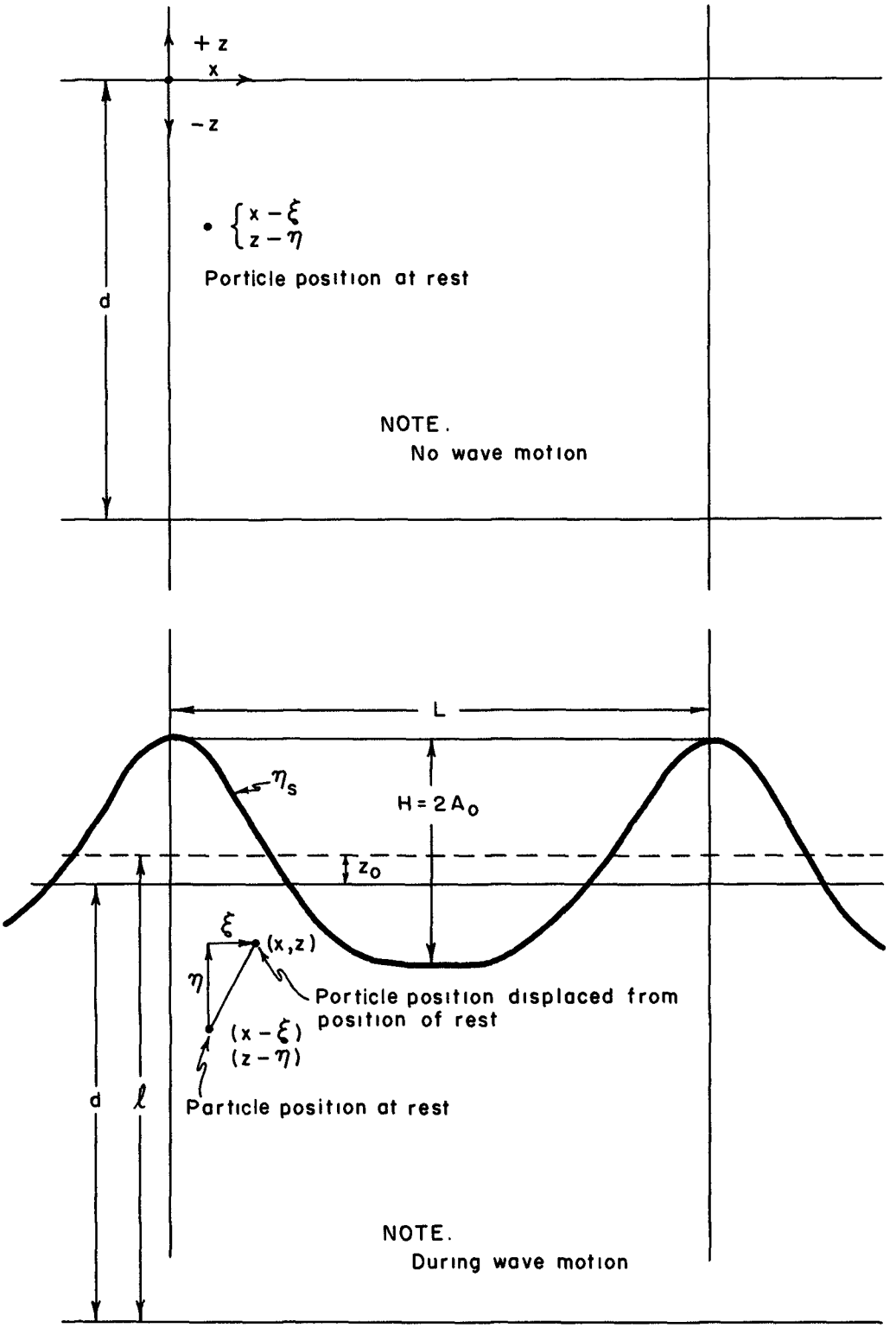

FIGURE I. SYSTEM OF COORDINATES

ℓ is a parameter related to the undisturbed water depth.

$z_o = \ell - d$ is a constant to be determined

x,z, are horizontal and vertical coordinates of the particle

ξ , η are the horizontal and vertical displacements of the particle from its initial undisturbed position of rest.

C = L/T is the wave celerity
L is the wave length
T is the wave period

$a_N = a_1, a_2, a_3, \ldots\ldots a_M$ (Mth order), consecutive coefficients of the series
N = 1, 2, 3, ... M (Mth order) corresponding to each of the above coefficients.

The parameter ℓ is related to the depth d according to

$$d = \frac{1}{L} \int_0^L \left(d + \eta_s \right) dx = \ell - z_o \tag{5}$$

where η_s is the surface elevation with respect to the undisturbed water elevation, and $kz_o = k(\ell - d)$. (See Figure 1)

The coefficients a_N, with the corresponding subscripts represent a convenient means for keeping track of the various terms of each order; i.e., a_1, is the first order term, a_2 and a_1^2 are the second order, a_3, a_1^3 and a_1 (a_2) are the third order terms, etc.

One of the conveniences of the system of coordinates used in the above equations is that the free surface conditions are obtained by setting $z - \eta = 0$, whence

$$k\eta_s = \sum_1^M a_N \left(kA_o \right)^N \cos Nk \left(x - \xi_s \right) - kz_o \tag{6}$$

where the constant kz_o is required as shown later

$$kx_s = k(x_s - \xi_s) + \sum_1^M a_N \left(kA_o \right)^N \frac{1}{\tanh Nk\ell} \sin Nk \left(x_s - \xi_s \right) \tag{7}$$

Horizontal and Vertical Components of Particle Velocity

The horizontal and vertical components of particle velocity may be obtained respectively from:

$$\frac{u}{C} = -\frac{1}{C}\frac{\partial \xi}{\partial t} = \frac{\partial \xi}{\partial x} = \frac{\partial \eta}{\partial z} \tag{8}$$

and

$$\frac{w}{C} = \frac{1}{C}\frac{\partial \eta}{\partial t} = \frac{\partial \xi}{\partial z} = -\frac{\partial \eta}{\partial x} \tag{9}$$

whence

$$\frac{u}{C} = (1-\frac{u}{C})\sum Na_N(kA_0)^N \frac{\cosh Nk(\ell+z-\eta)}{\sinh Nk\ell} \cos Nk(x-Ct-\xi) + \frac{w}{C}\sum Na_N(kA_0)^N \frac{\sinh Nk(\ell+z-\eta)}{\sinh Nk\ell} \sin Nk(x-Ct-\xi) \tag{10}$$

and

$$\frac{w}{C} = (1-\frac{u}{C})\sum Na_N(kA_0)^N \frac{\sinh Nk(\ell+z-\eta)}{\sinh Nk\ell} \sin Nk(x-Ct-\xi) - \frac{w}{C}\sum Na_N(kA_0)^N \frac{\cosh Nk(\ell+z-\eta)}{\sinh Nk\ell} \cos Nk(x-Ct-\xi) \tag{11}$$

The horizontal and vertical components of particle velocity are also given by:

$$\frac{u}{C} = -\frac{1}{C}\frac{\partial \phi}{\partial x} = -\frac{1}{C}\frac{\partial \psi}{\partial z} \tag{12}$$

and

$$\frac{w}{C} = -\frac{1}{C}\frac{\partial \phi}{\partial z} = +\frac{1}{C}\frac{\partial \psi}{\partial x} \tag{13}$$

Where ϕ and ψ are the velocity potential and the stream function respectively. It is seen from Equations 10 and 11 together with Equations 12 and 13 that the velocity potential and stream function except for arbitrary constants will have the following forms:

$$-\frac{k\phi}{C} = \sum_1^M a_N(kA_0)^N \frac{\cosh Nk(\ell+z+\psi/C)}{\sinh Nk\ell} \sin Nk(x-Ct+\phi/C) \tag{14}$$

$$-\frac{k\psi}{C} = \sum_1^M a_N(kA_0)^N \frac{\sinh Nk(\ell+z+\psi/C)}{\sinh Nk\ell} \cos Nk(x-Ct+\phi/C) \tag{15}$$

Proof of Irrotational Flow

Equations 10 and 11 represent irrotational flow irrespective of the actual values of the coefficients. That is:

$$\nabla^2 \phi = \frac{\partial u}{\partial x} + \frac{\partial w}{\partial z} = 0 \qquad (16)$$

Performing the above operation, it is found that

$$\frac{\partial u}{\partial x} + \frac{\partial w}{\partial z} = -\left(\frac{\partial u}{\partial x} + \frac{\partial w}{\partial z}\right) \sum N a_N (kA_o)^N \frac{\cosh Nk(\ell + z - \eta)}{\sinh Nk\ell} \cos Nk(x - Ct - \xi)$$
$$+\left(\frac{\partial w}{\partial x} - \frac{\partial u}{\partial z}\right) \sum N a_N (kA_o)^N \frac{\sinh Nk(\ell + z - \eta)}{\sinh Nk\ell} \sin Nk(x - Ct - \xi) \qquad (17)$$

The above does not yet prove that $\nabla^2 \phi = 0$ until the following is evaluated

$$\frac{\partial w}{\partial x} - \frac{\partial u}{\partial z} = -\left(\frac{\partial w}{\partial x} - \frac{\partial u}{\partial z}\right) \sum N a_N (kA_o)^N \frac{\cosh Nk(\ell + z - \eta)}{\sinh Nk\ell} \cos Nk(x - Ct - \xi)$$
$$-\left(\frac{\partial u}{\partial x} + \frac{\partial w}{\partial z}\right) \sum N a_N (kA_o)^N \frac{\sinh Nk(\ell + z - \eta)}{\sinh Nk\ell} \sin Nk(x - Ct - \xi) \qquad (18)$$

For the summation terms of equations 17 and 18 to exist, the only possible solution of the simultaneous equations 17 and 18 is

$$\frac{\partial u}{\partial x} + \frac{\partial w}{\partial z} = 0 \quad \text{and} \quad \frac{\partial w}{\partial x} - \frac{\partial u}{\partial z} = 0$$

therefore $\nabla^2 \phi = 0$

The above proof is more easily verified by performing the above operation on the equations given in the next section (Table I, for example).

Power Series Equations for Particle Velocity

In the development following it will be convenient to use

$$k(x - Ct - \xi) = \theta' \qquad (19)$$

and

$$U = \sum N a_N (kA_o)^N \frac{\cosh Nk(\ell + z - \eta)}{\sinh Nk\ell} \cos N\theta' \qquad (20)$$

and

$$W = \sum N a_N (kA_o)^N \frac{\sinh Nk(\ell + z - \eta)}{\sinh Nk\ell} \sin N\theta' \qquad (21)$$

whence

$$\frac{u}{C} = \left(1 - \frac{u}{C}\right) U + \frac{w}{C} W \tag{22}$$

and

$$\frac{w}{C} = \left(1 - \frac{u}{C}\right) W - \frac{w}{C} U \tag{23}$$

The simultaneous solution of Equations 22 and 23 can be made by the process of resubstitution to as high an order as required where the Mth order will include all terms of U^p, W^q, and $U^r W^s$, where p = 0 to M, q = 0 to M, and r + s = 1 to M.

The process of resubstitutions leads to the following terms:

TABLE 1

M	u/C	w/C
1	U	W
2	$-U^2 + W^2$	$-2WU$
3	$U^3 - 3UW^2$	$-W^3 + 3WU^2$
4	$-U^4 + 6U^2W^2 - W^4$	$4W^3U - 4WU^3$
5	$U^5 - 10U^3W^2 + 5UW^4$	$W^5 - 10W^3U^2 + 5WU^4$
6	$-6U^6 + 15U^4W^2 - 15U^2W^4 + W^6$	$-6UW^5 + 20W^3U^3 - 6WU^5$
7	$U^7 - 21U^5W^2 + 35U^3W^4 - 7UW^6$	$-W^7 + 21W^5U^2 - 35W^3U^4 + 7WU^6$

It will be seen that a general expression can be written for u/C, having the following power series equation:

$$\frac{u}{C} = \left[K_{r,s} \right]_u U^r W^s \tag{24}$$

where

$$\left[K_{r,s} \right]_u = -1 (-1)^r (-1)^{\frac{s}{2}} \frac{(r+s)!}{r!\, s!} \tag{25}$$

for $\left\{ \begin{matrix} r = 0,1,2,3,4 \\ s = 0,2,4,6,8 \end{matrix} \right\}$ except for $\left\{ \begin{matrix} r = 0 \\ s = 0 \end{matrix} \quad K_{0,0} = 0 \right\}$

and $M = r + s$

For example, consider the 8th order ($M = 8$), in addition to those terms for $M = 1$ through $M = 7$, there will be the 8th order term for the following combinations of $r,s = (8,0)$; $(6,2)$; $(4,4)$; $(2,6)$; and $(0,8)$, whence from equation 24 the 8th order terms for u/C are

$$- U^8 + 28U^6W^2 - 70U^4W^4 + 28U^2W^6 - W^8$$

Similarily for the term w/C the power series equation:

$$\frac{w}{C} = \left[K_{r,s} \right]_w U^r W^s \tag{26}$$

where

$$\left[K_{r,s} \right]_w = (-1)^r (-1)^{\frac{s-1}{2}} \frac{(r+s)!}{r!\, s!} \tag{27}$$

for

$$\left\{ \begin{matrix} r = 0,1,2,3,4 \\ s = 1,3,5,7 \end{matrix} \right\} \quad M = r + s$$

For example, the 8th order term will have the following combinations of $r,s = (7,1)$; $(5,3)$; $(3,5)$; and $(1,7)$, whence from equation 27 the 8th order terms for w/C are

$$- 8U^7W + 56U^5W^3 - 56U^3W^5 + 8UW^7$$

Thus equations 25 and 27 can be used to obtain all terms from the first order to the Mth order respectively for u/C and w/C

Bernoulli's Equation

The problem of wave motion can be reduced to one of steady state by superimposing a steady current on the wave motion equal to the wave celerity but of opposite direction. This operation, known as the Rayleigh principle, leads to Bernoulli's equation applicable along the free surface, where it is assumed that everywhere along the free surface the pressure is constant or is zero with respect to atmospheric pressure, whence

$$(u_s - C)^2 + w_s^2 + 2g\eta_s = \text{constant}, \tag{28}$$

where the subscript s refers to the conditions at the free surface, Equation 28 can be written as follows:

$$\left(\frac{u_s}{C} - 1 \right)^2 + \left(\frac{w_s}{C} \right)^2 + \frac{2g\eta_s}{C^2} = K = \text{constant} \tag{29}$$

or solving for $k\eta_s$

$$k\eta_s = \frac{kC^2}{g}\left\{\frac{u_s}{C} - \frac{1}{2}\left[\left(\frac{u_s}{C}\right)^2 + \left(\frac{w_s}{C}\right)^2\right] + \frac{k-1}{2}\right\} \qquad (30)$$

It will be convenient to define the Bernoulli term as

$$B_s = \frac{u_s}{C} - \frac{1}{2}\left[\left(\frac{u_s}{C}\right)^2 + \left(\frac{w_s}{C}\right)^2\right] \qquad (31)$$

Along the free surface equations 20 and 21, $z - \eta = 0$, whence

$$U_s = \sum N a_N (kA_o)^N X_N \cos N\theta' \qquad (32)$$

and

$$W_s = \sum N a_N (kA_o)^N \sin N\theta' \qquad (33)$$

where $X_N = \frac{1}{\tanh Nk\ell}$

From Table 1, one may obtain the Bernoulli term B_s which leads to the following terms:

TABLE II

Order (M)	$B_s = \frac{u_s}{C} - \frac{1}{2}\left[\left(\frac{u_s}{C}\right)^2 + \left(\frac{w_s}{C}\right)^2\right]$
1	U_s
2	$-3/2\ U_s^2 + \frac{1}{2} W_s^2$
3	$2U_s^3 - 2U_s W_s^2$
4	$-5/2\ U_s^4 + 5U_s^2 W_s^2 - \frac{1}{2} W_s^4$
5	$3U_s^5 - 10U_s^3 W_s^2 + 3U_s W_s^4$
6	$-7/2\ U_s^6 + 35/2\ U_s^4 W_s^2 - 21/2 U_s^2 W_s^4 + \frac{1}{2} W_s^6$
7	$4U_s^7 - 28U_s^5 W_s^2 + 28U_s^2 W_s^5 - 4U_s W_s^6$

It will be seen that a general expression can be written for B_s, having the following power series equation:

$$B_s = \left[K_{r,s}\right]_{B_s} U_s^{\,r} W_s^{\,s} \tag{34}$$

where

$$\left[K_{r,s}\right]_{B_s} = -1(-1)^r (-1)^{\frac{s}{2}} \frac{(r+s+1)!}{2(r+1)!s!} \tag{35}$$

for $\begin{Bmatrix} r = 0, 1, 2, 3, 4, 5 \ldots\ldots \\ s = 0, 2, 4, 6, 8\ldots\ldots\ldots \end{Bmatrix}$ except for $\begin{Bmatrix} r = 0 \\ s = 0 \end{Bmatrix}$; $K_{0,0} = 0\Big\}$

For example, the 8th order terms will have the following combinationsof (r,s) = (8,0); (6,2); (4,4); (2,6); and (0,8); whence from Equation 35 the 8th order terms for B_s are:

$$-9/2\ U_s^{8} + 42\, U_s^{6} W_s^{2} - 63\, U_s^{4} W_s^{4} + 18\, U_s^{2} W_s^{6} - \frac{1}{2} W_s^{8}$$

Thus Equation 35 can be used to obtain the Bernoulli term B_s to as high an order as required. The term B_s will have an expanded form as follows:

$$\begin{aligned} B_s = {} & \left[B_{11} + B_{13}(kA_0)^2 + B_{15}(kA_0)^4 + B_{17}(kA_0)^6 + \cdots\right] kA_0 \cos\theta' \\ & + \left[B_{22} + B_{24}(kA_0)^2 + B_{26}(kA_0)^4 + \cdots\right] (kA_0)^2 \cos 2\theta' \\ & + \left[B_{33} + B_{35}(kA_0)^2 + B_{37}(kA_0)^4 + \cdots\right] (kA_0)^3 \cos 3\theta' \\ & + \left[B_{44} + B_{46}(kA_0)^2 + \cdots\right] (kA_0)^4 \cos 4\theta' \\ & + \left[B_{55} + B_{57}(kA_0)^2\right] (kA_0)^5 \cos 5\theta' \\ & + \left[B_{JJ} + B_{JJ+2}(kA_0)^2 + \cdots\right] (kA_0)^J \cos J\theta' \\ & + B_M (kA_0)^M \cos M\theta' + R \end{aligned} \tag{36}$$

In the above, the first subscript refers to the terms corresponding with identical $(kA_0)^J \cos J\theta'$, J being the general term. The second subscript refers to the order. For example, B_{15} is the fifth order term for $\cos\theta'$, and B_{55} is the fifth order term for $\cos 5\theta'$ R is a constant and represents the sum of the remainder terms for which no $\cos N\theta'$ exists.

Procedure for the Evaluation of Coefficients

The coefficients a_1, a_2, a_3..... a_M must be evaluated such that the surface boundary conditions are satisfied. The surface profile elevation with respect to the undisturbed water level is given by Equation 6.

The surface boundary conditions are satisfied when Equation 6 is made identical to Equation 30. To whatever order is required Equation 30 is a means by which the solution is obtained. Incidentally, such a solution is similar to a least squares solution in statistical theory.

It will be convenient to use an expanded form of Equation 30 as follows:

$$k\eta_s = \sum a_N (kA_0)^N \cos N\theta \,, \text{ where}$$

$$\begin{aligned}
a_1 &= \left[A_{11} + A_{13}(kA_0)^2 + A_{15}(kA_0)^4 + A_{17}(kA_0)^6 + \cdots\right] \\
a_2 &= \left[A_{22} + A_{24}(kA_0)^2 + A_{26}(kA_0)^4 + \cdots\right] \\
a_3 &= \left[A_{33} + A_{35}(kA_0)^2 + A_{37}(kA_0)^4 + \cdots\right] \\
a_4 &= \left[A_{44} + A_{46}(kA_0)^2 + \cdots\right] \\
a_5 &= \left[A_{55} + A_{57}(kA_0)^2 + \cdots\right] + \cdots - kz_0
\end{aligned} \tag{37}$$

The wave height $H = 2A_0$ is obtained from the difference between η_s at $\theta = 0$ and η_s at $\theta = \pi$, and since A_{11} will always be equal to unity as long as $H = 2A_0$, whence from equation 37,

$$0 = (A_{13} + A_{33})(kA_0)^2 + (A_{15} + A_{35} + A_{55})(kA_0)^4 + (A_{17} + A_{37} + A_{57} + A_{77})(kA_0)^6 \tag{38}$$

Equating to zero terms of $(kA_0)^N$, one obtains the following:

$$\begin{aligned}
A_{13} &= -A_{33} \\
A_{15} &= -(A_{35} + A_{55}) \\
A_{17} &= -(A_{37} + A_{57} + A_{77}) \\
&\text{etc.}
\end{aligned} \tag{39}$$

The wave celerity can be expressed as follows:

$$\frac{kC^2}{g} = F_1 + F_3(kA_0)^2 + F_5(kA_0)^4 + F_7(kA_0)^6 + \cdots\cdots \tag{40}$$

Using Bernoulli's Equation 30, together with Equations 37, 39, and 40 and equating like terms of $\cos N\theta$ one obtains the following set of equations:

$$
\begin{aligned}
&\left[A_{11} + A_{13}(kA_0)^2 + A_{15}(kA_0)^4 + \quad\right] - \\
&\left[F_1 + F_3(kA_0)^2 + F_5(kA_0)^4 + \cdot\right]\left[B_{11} + B_{13}(kA_0)^2 + B_{15}(kA_0)^4 + \cdot\cdot\right] = 0 \\
&\left[A_{22} + A_{24}(kA_0)^2 + \quad\right] - \left[F_1 + F_3(kA_0)^2 + \quad\right]\left[B_{22} + B_{24}(kA_0)^2 + \cdot\cdot\cdot\right] = 0 \\
&\left[A_{33} + A_{35}(kA_0)^2 + \quad\right] - \left[F_1 + F_3(kA_0)^2 + \cdot\cdot\right]\left[B_{33} + B_{35}(kA_0)^2 + \cdot\right] = 0 \\
&\left[A_{44} + \quad\right] - \left[F_1 + \cdot\cdot\right]\left[B_{44} + \cdot\quad\right] = 0 \\
&\text{etc and } -kz_0 = \left[F_1 + F_3(kA_0)^2 + F_5(kA_0)^4 + \cdot\quad\right]\left[\frac{K-1}{2} + R\right]
\end{aligned}
\tag{41}
$$

The procedure is to expand each of the individual equations and then equate to zero like terms of $(KA_0)^N$. It will be convenient to present the higher order terms of the A's and the F 's in terms including the B's terms and the lower order term of A's and F's. Using Equations 41 (and also those of Equation 39) the results are summarized in Table III.

TABLE III

Term	Source	Order
$A_{11} = 1$	$H = 2A_0$	1
$F_1 = 1/B_{11}$	Eq 41	1 and 2
$A_{22} = F_1 B_{22}$	Eq 41	2
$A_{33} = F_1 B_{33}$	Eq 41	3
$A_{13} = -A_{33}$	Eq 39	3
$F_3 = A_{13}F_1 - B_{13}F_1^2$	Eq 41	3 and 4
$A_{44} = F_1 B_{44}$	Eq 41	4
$A_{24} = F_1 B_{24} + F_3 B_{22}$	Eq 41	4
$A_{55} = F_1 B_{55}$	Eq 41	5
$A_{35} = F_1 B_{35} + F_3 B_{33}$	Eq 41	5
$A_{15} = -A_{35} - A_{55}$	Eq 39	5
$F_5 = A_{15}F_1 - F_1^2 B_{15} - F_1 F_3 B_{13}$	Eq 41	5 and 6
$A_{66} = F_1 B_{66}$	Eq 41	6
$A_{46} = F_1 B_{46} + F_3 B_{44}$	Eq 41	6
$A_{26} = F_1 B_{26} + F_3 B_{24} + F_5 B_{22}$	Eq 41	6

The above scheme can be carried to as high an order as required, merely by writing down the additional terms. For example, the seventh order terms are obtained from Equation 41 as follows:

$$A_{77} = F_1 B_{77}$$

$$A_{57} = F_1 B_{57} + F_3 B_{55}$$

$$A_{37} = F_1 B_{37} + F_3 B_{35} + F_5 B_{33}$$

$$A_{17} = F_1 B_{17} + F_3 B_{15} + F_5 B_{13} + F_7 B_{11}$$

or F_7 from the last equation using $B_{11} = 1/F_1$ is as follows:

$$F_7 = F_1 A_{17} - F_1^2 B_{17} - F_1 F_3 B_{15} - F_1 F_5 B_{13}$$

Similarily the eighthorder terms can be written down directly as follows:

$$A_{88} = F_1 B_{88}$$

$$A_{68} = F_1 B_{68} + F_3 B_{66}$$

$$A_{48} = F_1 B_{48} + F_3 B_{46} + F_5 B_{44}$$

$$A_{28} = F_1 B_{28} + F_3 B_{26} + F_5 B_{24} + F_7 + F_7 B_{22}$$

Thus all expressions presented (Tables I, II, and III) can be carried to as high an order as required, with no difficulty whatsoever. These relations are convenient working parameters for the actual solution to a particular order.

Example: Fifth Order Solution

In order to continue the solution to any particular order, it is necessary to express the B_S - terms in terms of a_N, using Equations 32 and 33 and equations 34 and 35 (Table II). It will be seen from Table II that there will be cross product terms involving $\mathrm{Cos}N\theta'$ and $\mathrm{Sin}\ N\theta'$, and it will be necessary to replace these cross product terms using trigonometric identities. For example, the fifth order solution will require the terms of U_S, U_S^2, U_S^3, $U_S W_S^2$, etc. be determined. Using trigonometric identities these terms including all orders from one to five are as follows:

$$U_s = a_1 X_1 (kA_a) \cos\theta' + 2a_2 X_2 (kA_a)^2 \cos 2\theta' + 3a_3 X_3 (kA_a)^3 \cos 3\theta'$$
$$+ 4a_4 X_4 (kA_a)^4 \cos 4\theta' + 5a_5 X_5 (kA_0)^5 \cos 5\theta'$$

$$U_s^2 = \frac{1}{2} a_1^2 X_1^2 (kA_a)^2 + 2a_2^2 X_2^2 (kA_a)^4$$
$$+ \left[2a_1 X_1 a_2 X_2 (kA_a)^2 + 6a_2 X_2 a_3 X_3 (kA_a)^4\right] (kA_a) \cos\theta'$$
$$+ \left[\frac{1}{2} a_1^2 X_1^2 + 3a_1 X_1 a_3 X_3 (kA_a)^2\right] (kA_0)^2 \cos 2\theta'$$
$$+ \left[2a_1 X_1 a_2 X_2 + 4a_1 X_1 a_4 X_4 (kA_0)^2\right] (kA_a)^3 \cos 3\theta'$$
$$+ \left[2a_2^2 X_2^2 + 3a_1 X_1 a_3 X_3\right] (kA_a)^4 \cos 4\theta'$$
$$+ \left[4a_1 X_1 a_4 X_4 + 6a_2 X_2 a_3 X_3\right] (kA_a)^5 \cos 5\theta'$$

$$U_s^3 = \frac{3}{2} a_1^2 X_1^2 a_2 X_2 (kA_a)^4$$
$$+ \left[\frac{3}{4} a_1^3 X_1^3 (kA_0)^2 + (6a_1 X_1 a_2^2 X_2^2 + \frac{9}{4} a_1^2 X_1^2 a_3 X_3)(kA_0)^4\right] (kA_a) \cos($$
$$+ \left[3a_1^2 X_1^2 a_2 X_2 (kA_a)^2\right] (kA_a)^2 \cos 2\theta'$$
$$+ \left[\frac{1}{4} a_1^3 X_1^3 + (\frac{9}{2} a_1^2 X_1^2 a_3 X_3 + 3a_1 X_1 a_2^2 X_2^2)(kA_a)^2\right] (kA_a)^3 \cos 3\theta'$$
$$+ \left[\frac{3}{2} a_1^2 X_1^2 a_2 X_2\right] (kA_a)^4 \cos 4\theta'$$
$$+ \left[3a_1 X_1 a_2^2 X_2^2 + \frac{9}{4} a_1^2 X_1^2 a_3 X_3\right] (kA_a)^5 \cos 5\theta'$$

$$U_s^4 = \frac{3}{8} a_1^4 X_1^4 (kA_a)^4 + \left[4a_1^3 X_1^3 a_2 X_2 (kA_a)^4\right] kA_a \cos\theta'$$
$$+ \frac{1}{2} a_1^4 X_1^4 (kA_a)^4 \cos 2\theta'$$
$$+ 3a_1^3 X_1^3 a_2 X_2 (kA_a)^5 \cos 3\theta'$$
$$+ \frac{1}{8} a_1^4 X_1^4 (kA_a)^4 \cos 4\theta' + a_1^3 X_1^3 a_2 X_2 (kA_a)^5 \cos 5\theta'$$

$$U_s^5 = \frac{5}{8} a_1^5 X_1^5 (kA_a)^5 \cos\theta' + \frac{5}{16} a_1^5 X_1^5 (kA_0)^5 \cos 3\theta' + \frac{1}{16} a_1^5 X_1^5 (kA_0)^5 \cos 5\theta$$

$$W_s^2 = \tfrac{1}{2} o_1^2 (kA_0)^2 + 2 a_2^2 (kA_0)^4$$
$$+\left[2 o_1 o_2 (kA_0)^2 + 6 o_2 o_3 (kA_0)^4 \right] (kA_0) \cos\theta'$$
$$+\left[3 a_1 a_3 (kA_0)^2 - \tfrac{1}{2} a_1^2 \right] (kA_0)^2 \cos 2\theta'$$
$$+\left[4 a_1 a_4 (kA_0)^2 - 2 a_1 a_2 \right] (kA_0)^3 \cos 3\theta'$$
$$-\left[2 a_2^2 + 3 a_1 a_3 \right] (kA_0)^4 \cos 4\theta'$$
$$-\left[4 a_1 a_4 + 6 a_2 a_3 \right] (kA_0)^5 \cos 5\theta'$$

$$W_s^4 = \tfrac{3}{8} a_1^4 (kA_0)^4 + 2 a_1^3 a_2 (kA_0)^5 \cos\theta'$$
$$- \tfrac{1}{2} a_1^4 (kA_0)^4 \cos 2\theta' - 3 a_1^3 o_2 (kA_0)^5 \cos 3\theta'$$
$$+ \tfrac{1}{8} a_1^4 (kA_0)^4 \cos 4\theta' + a_1^3 a_2 (kA_0)^5 \cos 5\theta'$$

$$U_s W_s^2 = a_1^2 X_1 a_2 (kA_0)^4 - \tfrac{1}{2} o_1^2 a_2 X_2 (kA_0)^4$$
$$\left[\tfrac{1}{4} a_1^3 X_1 (kA_0)^2 + (2 a_1 X_1 o_2^2 + \tfrac{3}{2} o_1^2 X_1 a_3 - \tfrac{3}{4} a_1^2 a_3 X_3)(kA_0)^4 \right] (kA_0) \cos\theta'$$
$$+\left[o_1^2 a_2 X_2 (kA_0)^2 \right] (kA_0)^2 \cos 2\theta'$$
$$+\left[(\tfrac{3}{2} a_1^2 a_3 X_3 + 2 a_1 o_2^2 X_2 - a_1 X_1 a_2^2)(kA_0)^2 - \tfrac{1}{4} a_1^3 X_1 \right] (kA_0)^3 \cos 3\theta'$$
$$-\left[a_1^2 X_1 o_2 + \tfrac{1}{2} a_1^2 a_2 X_2 \right] (kA_0)^4 \cos 4\theta'$$
$$-\left[a_1 X_1 a_2^2 + \tfrac{3}{2} a_1^2 X_1 a_3 + 2 o_1 a_2^2 X_2 + \tfrac{3}{4} a_1^2 a_3 X_3 \right] (kA_0)^5 \cos 5\theta'$$

$$U_s^2 W_s^2 = \tfrac{1}{8} a_1^4 X_1^2 (kA_0)^4$$
$$+\left[a_1^3 X_1^2 a_2 (kA_0)^4 \right] (kA_0) \cos\theta'$$
$$-\left[(\tfrac{1}{2} o_1^3 X_1^2 o_2 - \tfrac{1}{2} o_1^3 X_1 a_2 X_2)(kA_0)^2 \right] (kA_0)^3 \cos 3\theta'$$
$$-\left[\tfrac{1}{8} a_1^4 X_1^2 \right] (kA_0)^4 \cos 4\theta'$$

$$-\left[\frac{1}{2}\,a_1^3 X_1^2 a_2 + \frac{1}{2}\,a_1^3 X_1\, a_2 X_2\right](kA_a)^5 \cos 5\theta'$$

$$U_s^3 W_s^2 = \left[\frac{1}{8}\,a_1^5 X_1^3 (kA_a)^4\right] kA_a \cos\theta'$$

$$-\left[\frac{1}{16}\,a_1^5 X_1^5 (kA_0)^2\right](kA_a)^3 \cos 3\theta'$$

$$-\left[\frac{1}{16}\,a_1^5 X_1^5\right](kA_0)^5 \cos 5\theta'$$

$$U_s W_s^4 = \left[\frac{1}{8}\,a_1^5 X_1 (kA_0)^4\right](kA_a) \cos\theta'$$

$$-\left[\frac{3}{16}\,a_1^5 X_1 (kA_a)^2\right](kA_a)^3 \cos 3\theta'$$

$$+\left[\frac{1}{16}\,a_1^5 X_1\right](kA_a)^5 \cos 5\theta'$$

Using the above expressions, together with Table II, it will be convenient to summarize the results in Table IV

TABLE IV — Terms of B_s to Fifth Order

R – Terms	$(kA_0)\cos\theta'$	$(kA_0)^2\cos 2\theta'$	$(kA_0)^3\cos 3\theta'$	$(kA_0)^4\cos 4\theta'$	$(kA_0)^5\cos 5\theta'$
$(kA_0)^2\cos 0$	$a_1 X_1$	$2a_2 X_2$	$3a_3 X_3$	$4a_4 X_4$	$5a_5 X_5$
$-3/4\ a_1^2 X_1^2$		$-3/4\ a_1^2 X_1^2$	$-3a_1 X_1 a_2 X_2$	$3a_2^2 X_2^2$	$6a_1 X_1 a_4 X_4$
$1/4\ a_1^2$	$(kA_0)^3\cos\theta'$	$-1/4\ a_1^2$	$-a_1\ a_2$	$-9/2 a_1 X_1 a_3 X_3$	$-9 a_2 X_2 a_3 X_3$
	$-3a_1 X_1 a_2 X_2$		$1/2\ a_1^3 X_1^3$	$-a_2^2$	$-2 a_1 a_4$
	$a_1\ a_2$		$1/2\ a_1^3 X_1$	$-3/2 a_1 a_3$	$-3 a_2 a_3$
	$3/2\ a_1^3 X_1^3$			$3a_1^2 X_1^2 a_2 X_2$	$6a_1 X_1 a_2^2 X_2^2$
	$-1/2\ a_1^3 X_1$			$2a_1^2 X_1 a_2$	$9/2\ a_1^2 X_1^2 a_3 X_3$
				$a_1^2 a_2 X_2$	$2a_1 X_1 a_2^2$
$(kA_0)^4$	$(kA_0)^5\cos\theta'$	$(kA_0)^4\cos 2\theta'$	$(kA_0)^5\cos 3\theta'$	$-5/16\ a_1^4 X_1^4$	$3a_1^2 X_1 a_3$
$-3\ a_2^2 X_2^2$	$-9a_2 X_2 a_3 X_3$	$-9/2 a_1 X_1 a_3 X_3$	$-6a_1 X_1 a_4 X_4$	$-5/8\ a_1^4 X_1^2$	$4a_1 a_2^2 X_2$
a_2^2	$3a_2 a_3$	$3/2\ a_1 a_3$	$2a_1 a_4$	$-1/16\ a_1^4$	$3/2\ a_1^2 a_3 X_3$
$3a_1^2 X_1^2 a_2 X_2$	$12a_1 X_1 a_2^2 X_2^2$	$6a_1^2 X_1^2 a_2 X_2$	$9a_1^2 X_1^2 a_3 X_3$		$-5/2\ a_1^3 X_1^3 a_2 X$
$-2\ a_1^2 X_1 a_2$	$9/2\ a_1^2 X_1^2 a_3 X_3$	$-2\ a_1^2 a_2 X_2$	$6a_1 X_1 a_2^2 X_2^2$		$-5/2\ a_1^3 X_1^2 a_2$
$a_1^2 a_2 X_2$	$-4a_1 X_1 a_2^2$	$-5/4\ a_1^4 X_1^4$	$-3a_1^2 a_3 X_3$		$-5/2\ a_1^3 X_1 a_2 X$
$-15/16\ a_1^4 X_1^4$	$-3a_1^2 X_1 a_3$	$1/4\ a_1^4$	$-4a_1 a_2^2 X_2$		$-1/2\ a_1^3 a_2$
$5/8\ a_1^4 X_1^2$	$3/2\ a_1^2 a_3 X_3$		$2a_1 X_1 a_2^2$		$3/16\ a_1^5 X_1^5$
$-3/16\ a_1^4$	$-10\ a_1^3 X_1^3 a_2 X_2$		$-15/2 a_1^3 X_1^3 a_2 X_2$		$5/8\ a_1^5 X_1^3$
	$5\ a_1^3 X_1^2 a_2$		$-5/2\ a_1^3 X_1^2 a_2$		$3/16\ a_1^5 X_1$
	$-a_1^3 a_2$		$5/2\ a_1^3 X_1 a_2 X_2$		
	$15/8\ a_1^5 X_1^5$		$3/2\ a_1^3 a_2$		
	$-5/4\ a_1^5 X_1^3$		$15/16\ a_1^5 X_1^5$		
	$3/8\ a_1^5 X_1$		$5/8\ a_1^5 X_1^3$		
			$-9/16\ a_1^5 X_1$		

Remembering the forms for a_N (Equation 34) it will be seen that certain a terms upon substitution will be transferred down the table from $(kA_0)^N$ to $(kA_0)^{N+2}$, $(kA_0)^{N+4}$, etc. The substitution and the proper tranfers result in the B_s terms and are conveniently summarized in Table V.

TABLE V – B_s – Terms to Fifth Order

$\left(\frac{-kz_0}{F_1+F_3(kA_0)^2}\right)=$	$B_{11}=$	$B_{22}=$	$B_{33}=$	$B_{44}=$	$B_{55}=$
$\frac{K-1}{2}$	X_1	$2A_{22}X_2$	$3A_{33}X_3$	$4A_{44}X_4$	$5A_{55}X_5$
+		$-3/4\ X_1^2$	$-3X_1A_{22}X_2$	$-3A_{22}^2X_2^2$	$-6X_1A_{44}X$
$(kA_0)^2$	$B_{13}=$	$-1/4$	$-A_{22}$	$-9/2X_1A_{33}X_3$	$-9A_{22}X_2A_3$
$-3/4\ X_1^2$	$X_1\ A_{13}$		$1/2\ X_1^3$	$-A_{22}^2$	$-2\ A_{44}$
	$-3X_1A_{22}X_2$		$1/2\ X_1$	$-3/2\ A_{33}$	$-3A_{22}A_3$
$1/4$	A_{22}			$3X_1^2A_{22}X_2$	$6X_1A_{22}^2X_2$
	$3/2\ X_1^3$			$2X_1\ A_{22}$	$9/2\ X_1^2A_{33}$
	$-1/2\ X_1$			$A_{22}X_2$	$2X_1\ A_{22}^2$
				$-5/16\ X_1^4$	$3X_1\ A_{33}$
+	$B_{15}=$	$B_{24}=$	$B_{35}=$	$-5/8\ X_1^2$	$4A_{22}^2X_2$
	$X_1\ A_{15}$	$2A_{24}X_2$	$3A_{35}X_3$	$-1/16$	$3/2\ A_{33}X_3$
$(kA_0)^4$	$-3X_1X_2A_{13}A_{22}$	$-3/2\ A_{13}X_1^2$	$-3X_1X_2A_{13}A_{22}$		$-5/2\ X_1^3A_{22}$
$-3/2\ X_1^2A_{13}$	$-3X_1X_2A_{24}$	$-1/2\ A_{13}$	$-3X_1X_2A_{24}$		$-5/2\ X_1^2A_2$
$1/2\ A_{13}$	$A_{13}A_{22}$	$-9/2\ X_1A_{33}X_3$	$-A_{13}A_{22}$		$-5/2\ X_1A_{22}$
$-3A_{22}^2X_2^2$	A_{24}	$3/2\ A_{33}$	$-A_{24}$		$-1/2\ A_{22}$
A_{22}^2	$9/2\ X_1^3A_{13}$	$6X_1^2A_{22}X_2$	$3/2\ A_{13}X_1^3$		$3/16\ X_1^5$
$3X_1^2A_{22}X_2$	$-3/2\ X_1\ A_{13}$	$-2\ A_{22}X_2$	$3/2\ A_{13}X_1$		$5/8\ X_1^3$
$-2\ X_1\ A_{22}$	$-9A_{22}X_2A_{33}X_3$	$-5/4\ X_1^4$	$-6X_1A_{44}X_4$		$3/16\ X_1$
$A_{22}\ X_2$	$3\ A_{22}A_{33}$	$1/4$	$2\ A_{44}$		
$-15/16\ X_1^4$	$12X_1A_{22}^2X_2^2$		$9X_1^2A_{33}X_3$		
$5/8\ X_1^2$	$9/2\ X_1^2A_{33}X_3$		$6X_1\ A_{22}^2X_2^2$		
$-3/16$	$-4X_1\ A_{22}^2$		$-3A_{33}X_3$		
	$-3X_1\ A_{33}$		$-4A_{22}^2X_2$		
	$3/2\ A_{33}X_3$		$2X_1\ A_{22}^2$		
	$-10X_1^3A_{22}X_2$		$-15/2\ X_1^3A_{22}X_2$		
	$5\ X_1^2A_{22}$		$-5/2\ X_1^2A_{22}$		
	$-\ A_{22}$		$5/2\ X_1\ A_{22}X_2$		
	$15/8\ X_1^5$		$3/2\ A_{22}$		
	$-5/4\ X_1^3$		$15/16\ X_1^5$		
	$3/8\ X_1$		$5/8\ X_1^3$		
			$-9/16\ X_1$		

Now from Table V, using the relations of Tables III, one obtains immediately the following fifth order solution.

TABLE VI

$$A_{11} = 1$$

$$F_1 = 1/X_1 = \tanh k\ell$$

$$A_{22} = \frac{F_1}{2F_1X_2 - 1}\left\{\frac{3X_1^2 + 1}{4}\right\}$$

$$A_{33} = \frac{F_1}{3F_1X_3 - 1}\left\{A_{22}(3X_1X_2 + 1) - \frac{X_1}{2}(1 + X_1^2)\right\}$$

$$A_{13} = -A_{33}$$

$$F_3 = F_1A_{13} - F_1^2\left[A_{13}X_1 - A_{22}(3X_1X_2 - 1) + \frac{3X_1^3 - X_1}{2}\right]$$

$$A_{44} = \frac{F_1}{4F_1X_4 - 1}\left\{A_{22}^2(3X_2^2 + 1) + \frac{3}{2}A_{33}(3X_1X_3 + 1) - A_{22}(3X_1^2X_2 + 2X_1 + X_2) + \frac{5X_1^4 + 10X_1^2 + 1}{16}\right\}$$

$$A_{24} = \frac{F_1}{2F_1X_2 - 1}\left\{\frac{A_{13}}{2}(3X_1^2 + 1) + \frac{3}{2}A_{33}(3X_1X_3 - 1) - 2A_{22}X_2(3X_1^2 - 1) + \frac{1}{4}(5X_1^4 - 1) - \frac{F_3}{4F_1}(8A_{22}X_3 - 3X_1^2 - 1)\right\}$$

$$A_{55} = \frac{F_1}{5F_1X_5 - 1}\left\{2A_{44}(3X_1X_4 + 1) + 3A_{22}A_{33}(1 + 3X_2X_3) - 2A_{22}^2(3X_1X_2^2 + X_1 + 2X_2) - \frac{3}{2}A_{33}(3X_1^2X_3 + 2X_1 + X_3) + \frac{1}{2}A_{22}(5X_1^3X_2 + 5X_1^2 + 5X_1X_2 + 1) - \frac{X_1}{16}(3X_1^4 + 10X_1^2 + 3)\right\}$$

$$A_{35} = \frac{F_1}{3F_1X_3 - 1}\left\{A_{13}A_{22}(3X_1X_2 + 1) + A_{24}(3X_1X_2 + 1) - \frac{3}{2}A_{13}X_1(1 + X_1^2) + 2A_{44}(3X_1X_4 - 1) - 3A_{33}X_3(3X_1^2 - 1) - 2A_{22}^2(3X_1X_2^2 - 2X_2 + X_1) + \frac{A_{22}}{2}(15X_1^3X_2 + 5X_1^2 - 5X_1X_2 - 3) - \frac{1}{16}(15X_1^5 + 10X_1^3 - 9X_1) - \frac{F_3}{2F_1}(6A_{33}X_3 - 6A_{22}X_1X_2 - 2A_{22} + X_1 + X_1^3)\right\}$$

TABLE VI con't

$$A_{15} = -A_{35} - A_{55}$$

$$F_5 = \Big\{ F_1 A_{15} - F_1^2 \Big[X_1 A_{15} - A_{13} A_{22}(3X_1 X_2 - 1) - A_{24}(3X_1 X_2 - 1) + \frac{3}{2} A_{13} X_1 (3X_1^2 - 1) - 3A_{22}A_{33}(3X_2 X_3 - 1) + 4A_{22}^2 X_1 (3X_2^2 - 1) + \frac{3}{2} A_{33}(3X_1^2 X_3 - 2X_1 + X_3) - A_{22}(10X_1^3 X_2 - 5X_1^2 + 1) + \frac{1}{8}(15X_1^5 - 10X_1^3 + 3) - F_1 F_3 \Big[A_{13} X_1 - A_{22}(3X_1 X_2 - 1) + \frac{X_1}{2}(3X_1^2 - 1) \Big] \Big] \Big\}$$

The constant in Bernoullis' equation is obtained from the first column of Table V, as follows:

$$K = \Big\{ 1 + (kA_0)^2 \frac{3X_1^2 - 1}{2} + (kA_0)^4 \Big[A_{13}(3X_1^2 - 1) + 2A_{22}^2 (3X_2^2 - 1) - 2A_{22}(3X_1^2 X_2 - 2X_1 + X_2) + \frac{1}{8}(15X_1^4 - 10X_1^2 + 3) \Big] - \frac{2kz_0}{F_1} \Big[1 - \frac{F_3}{F_1} (kA_0)^2 \Big] \Big\}$$

The above presentation of consecutive equations are in a convenient form for computing the A- terms and the F- terms for any selected value of $k\ell$, either by the long hand method or by use of a high speed computer. For example, consider $k\ell = 2\pi$ (deep water), then one obtains $\tanh k\ell = 1$; in fact, for $k\ell = 2\pi$, $\tanh Nk\ell = 1$, whence $X_1 = X_2 = X_3 = X_4 = X_5 = 1$. It will follow in turn:

$A_{11} = 1$, $F_1 = 1$, $A_{22} = 1$, $A_{33} = \frac{3}{2}$, $A_{13} = -\frac{3}{2}$, $F_3 = 1$, $A_{44} = \frac{8}{3}$

$A_{24} = -\frac{5}{2}$, $A_{55} = \frac{125}{24}$, $A_{35} = -\frac{31}{6}$, $A_{15} = -\frac{1}{24}$ and $F_5 = \frac{1}{2}$, and the constant in Bernoullis' equation becomes

$$K = 1 + (kA_0)^2 - 6(kA_0)^4 - 2kz_0 \Big[1 - (kA_0)^2 \Big]$$

The Undisturbed Mean Water Depth

The undisturbed mean water depth is obtained by use of Equations 5, 6, and 7, in which $\cos Nk(X - \xi_s)$ and $\sin Nk(X - \xi_s)$ are represented by sums of two products each respectively as follows:

$$\cos Nk(X - \xi_s) = \cos Nk\xi_s \cos Nkx + \sin Nk\xi_s \sin Nkx \qquad (42)$$

and

$$\sin Nk(X - \xi_s) = \cos Nk\xi_s \sin Nkx - \sin Nk\xi_s \cos Nkx \qquad (43)$$

Now cos $Nk\xi_s$ and sin $Nk\xi_s$ can be expanded by series to as high an order as required. For example, the fifth order expansion for equations 6 and 7 are as follows:

$$
\begin{aligned}
k\eta_s = a_1 &\left[1 - \frac{1}{2}(k\xi_s)^2 + \frac{1}{24}(k\xi_s)^4\right] kA_0 \cos kx \\
&+ a_1\left[k\xi_s - \frac{1}{6}(k\xi_s)^3\right] kA_0 \sin kx \\
&+ a_2\left[1 - 2(k\xi_s)^2\right](kA_0)^2 \cos 2kx \\
&+ a_2\left[2k\xi_s - \frac{4}{3}(k\xi_s)^3\right](kA_0)^2 \sin 2kx \\
&+ a_3\left[1 - \frac{9}{2}(k\xi_s)^2\right](kA_0)^3 \cos 3kx \\
&+ a_3\left[3k\xi_s\right](kA_0)^3 \sin 3kx \\
&+ a_4(kA_0)^4 \cos 4kx \\
&+ a_4\left[4k\xi_s\right](kA_0)^4 \sin 4kx \\
&+ a_5(kA_0)^5 \cos 5kx - kz_0
\end{aligned}
\tag{44}
$$

$$
\begin{aligned}
k\xi_s = a_1 X_1 &\left[1 - \frac{1}{2}(k\xi_s)^2 + \frac{1}{24}(k\xi_s)^4\right](kA_0) \sin kx \\
&- a_1 X_1\left[k\xi_s - \frac{1}{6}(k\xi_s)^3\right](kA_0) \cos kx \\
&+ a_2 X_2\left[1 - 2(k\xi_s)^2\right](kA_0)^2 \sin 2kx \\
&- a_2 X_2\left[2k\xi_s - \frac{4}{3}(k\xi_s)^3\right](kA_0)^2 \cos 2kx \\
&+ a_3 X_3\left[1 - \frac{9}{2}(k\xi_s)^2\right](kA_0)^3 \sin 3kx \\
&- a_3 X_3\left[3k\xi_s\right](kA_0)^3 \cos 3kx \\
&+ a_4 X_4(kA_0)^4 \sin 4kx \\
&- a_4 X_4\left[4k\xi_s\right](kA_0)^4 \cos 4kx \\
&+ a_5 X_5(kA_0)^5 \sin 5kx
\end{aligned}
\tag{45}
$$

In the above equations $X_N = \dfrac{1}{\tanh Nk\ell}$

The procedure for solution is first to eliminate $k\xi_s$ from the right hand side of Equation 45. This is done by the process of resubstitution: the first order is obtained as $k\xi_s = a_1 X_1 kA_o \sin kx$ and is substituted into equation 45 to obtain the second order, which in turn is again substituted into equation 45 to obtain the third order, etc. until the desired order is obtained. The resulting expression is then substituted into equation 44 to eliminate $k\xi_s$ from the right hand side, obtaining an expression for $k\eta_s$ independent of $k\xi_s$. Finally, this equation for $k\eta_s$ is substituted into equation 5 and the integration results is an expression for d/L as a function of ℓ/L. It will be convenient to write equation 5 as:

$$kz_o = k(\ell - d) = \frac{1}{L}\int_0^L k\eta_s \, dx \tag{46}$$

It was found to the fourth order (also fifth order) that:

$$kz_o = \frac{1}{2} a_1^2 X_1 (kA_o)^2 + a_2^2 X_2 (kA_o)^4 \tag{47}$$

Where all other terms vanished by integration. Based on equation 47, the sixth order term was predicted to be $3/2\, a_3^2 X_3 (kA_o)^4$, and was then verified by the detailed process of resubstitution and integration. Based on the above findings one can suppose the following power series equation:

$$kz_o = \frac{1}{2} \sum_1^M N a_N^2 X_N (kA_o)^{2N} \tag{48}$$

where $N = 1, 2, 3, \ldots M$, order $M = 2N$

For example, the eighth order term is found by setting $N = 4$, which results in

$$2\, a_4^2 X_4 (kA_o)^8$$

Since the depth is the known parameter it is desirable to obtain ℓ as a function of d, whence

$$k\ell = k(d + z_o) \tag{49}$$

Where $X_N = \frac{1}{\tanh Nk\ell}$ and letting $Y_N = \frac{1}{\tanh Nkd}$ by substituting $k(d + z_o)$ for $k\ell$ and using hyperbolic identities (sum of two products) one obtains

$$X_N = \frac{Y_N + \tanh Nkz_o}{1 + Y_N \tanh Nkz_o} \tag{50}$$

Equation 50 can be expanded to as high an order as required according to the following:

$$X_N = \left[Y_N + \tanh Nkz_o \right]\left[1 - (Y_N \tanh Nkz_o + (Y_N \tanh Nkz_o)^2 - \cdots \right] \tag{51}$$

$$\tanh Nkz_o = Nkz_o - \frac{1}{3}(Nkz_o)^3 + \frac{2}{15}(Nkz_o)^5 - \frac{17}{630}(Nkz_o)^7 + \cdots \Big] \quad (52)$$

Equations 51 and 52 are then used together with equation 47, and by the process of resubstitution kz_o is eliminated from the right hand side, and one obtains a relation of kz_o as a function of kd. For example to the sixth (also seventh order):

$$kz_o = \frac{1}{2} a_1^2 Y_1 (kA_o)^2 + \left[a_2^2 Y_2 - \frac{1}{4} a_1^4 Y_1 (Y_1^2 - 1) \right] (kA_o)^4 \quad (53)$$

$$+ \left[\frac{3}{2} a_3^2 Y_3 - a_1^2 a_2^2 \frac{Y_2 (Y_1^2 - 1) + 2Y_1 (Y_2^2 - 1)}{2} + a_1^6 Y_1 (Y_1^2 - 1) \frac{Y_1^2 - 2}{8} \right] (kA_o)^6$$

Returning now to the fifth order solution, and from Table IV

$$a_1 = 1 + A_{13} (kA_o)^2 + A_{15} (kA_o)^4$$

$$a_2 = A_{22} + A_{24} (kA_o)^2 , \quad \text{whence}$$

$$kz_o = \frac{1}{2} Y_1 (kA_o)^2 + \left[A_{22}^2 Y_2 - \frac{1}{4} Y_1 (Y_1^2 - 1) + A_{13} Y_1 \right] (kA_o)^4 \quad (54)$$

For the terms A_{22} and A_{13} above for the fifth order $\tanh k\ell = \tanh kd$, and using A_{22} and A_{13} as obtained before one obtains for equation 54

$$kz_o = K_2 (kA_o)^2 + K_4 (kA_o)^4 \quad \text{where} \quad (55)$$

$$K_2 = \frac{1}{2} Y_1$$

$$K_4 = \frac{Y_1}{64} (17 - 19 Y_1^2 - 21 Y_1^4 - 9 Y_1^6)$$

Accelerations

The horizontal and vertical components for the accelerations of the fluid particles are obtained respectively from the following expressions:

$$\frac{du}{dt} = \frac{\partial u}{\partial t} + \frac{1}{2} \left[\frac{\partial u^2}{\partial x} + \frac{\partial w^2}{\partial x} \right] \quad (56)$$

$$\frac{dw}{dt} = \frac{\partial w}{\partial t} + \frac{1}{2} \left[\frac{\partial u^2}{\partial z} + \frac{\partial w^2}{\partial z} \right] \quad (57)$$

The differential quantities on the right side of the above equations can be obtained by use of equations 24 and 26 together with equations 20 and 21, whence

$$\frac{\partial u}{\partial t} = C \left[K_{r,s} \right]_u \left[r\, U^{r-1} W^s \frac{\partial U}{\partial t} + s\, U^r W^{s-1} \frac{\partial W}{\partial t} \right] \tag{58}$$

$$\frac{\partial w}{\partial t} = C \left[K_{r,s} \right]_w \left[r\, U^{r-1} W^s \frac{\partial U}{\partial t} + s\, U^r W^{s-1} \frac{\partial W}{\partial t} \right] \tag{59}$$

$$\frac{1}{2} \frac{\partial u^2}{\partial x} = C^2 \left[K_{r,s} \right]_u U^r W^s \left[r\, U^{r-1} W^s \frac{\partial U}{\partial x} + s\, U^r W^{s-1} \frac{\partial W}{\partial x} \right] \tag{60}$$

$$\frac{1}{2} \frac{\partial w^2}{\partial x} = C^2 \left[K_{r,s} \right]_w U^r W^s \left[r\, U^{r-1} W^s \frac{\partial U}{\partial x} + s\, U^r W^{s-1} \frac{\partial W}{\partial x} \right] \tag{61}$$

$$\frac{1}{2} \frac{\partial u^2}{\partial z} = C^2 \left[K_{r,s} \right]_u U^r W^s \left[r\, U^{r-1} W^s \frac{\partial U}{\partial z} + s\, U^r W^{s-1} \frac{\partial W}{\partial z} \right] \tag{62}$$

$$\frac{1}{2} \frac{\partial w^2}{\partial z} = C^2 \left[K_{r,s} \right]_w U^r W^s \left[r\, U^{r-1} W^s \frac{\partial U}{\partial z} + s\, U^r W^{s-1} \frac{\partial W}{\partial z} \right] \tag{63}$$

In the above $\left[K_{r,s} \right]_u$ and $\left[K_{r,s} \right]_w$ are given respectively by equations 25 and 27.

Now $\frac{\partial U}{\partial t}$ and $\frac{\partial W}{\partial t}$ can be obtained from equations 20 and 21 respectively as follows:

$$\frac{\partial U}{\partial t} = \left(1 - \frac{u}{C}\right) kC \sum N^2 a_N (kA_0)^N \frac{\cosh Nk(\ell + z - \eta)}{\sinh Nk\ell} \sin N\theta' \tag{64}$$

$$- \left(\frac{w}{C}\right) kC \sum N^2 a_N (kA_0)^N \frac{\sinh Nk(\ell + z - \eta)}{\sinh Nk\ell} \cos N\theta'$$

$$\frac{\partial W}{\partial t} = \left(1 - \frac{u}{C}\right) kC \sum N^2 a_N (kA_0)^N \frac{\sinh Nk(\ell + z - \eta)}{\sinh Nk\ell} \cos N\theta' \tag{65}$$

$$- \left(\frac{w}{C}\right) kC \sum N^2 a_N (kA_0)^N \frac{\cosh Nk(\ell + z - \eta)}{\sinh Nk\ell} \sin N\theta'$$

In addition, one obtains the following:

$$\frac{\partial U}{\partial x} = -\frac{1}{C}\frac{\partial U}{\partial t} \tag{66}$$

$$\frac{\partial W}{\partial x} = -\frac{1}{C}\frac{\partial W}{\partial t} \tag{67}$$

$$\frac{\partial U}{\partial z} = \frac{\partial W}{\partial x} = -\frac{1}{C}\frac{\partial W}{\partial t} \tag{68}$$

$$\frac{\partial W}{\partial z} = -\frac{\partial U}{\partial x} = \frac{1}{C}\frac{\partial U}{\partial t} \tag{69}$$

Procedure for Computation

The first operation to be performed is the evaluation of the coefficients a_N, for example, the fifth order solution as outlined in Table V. This is done by selecting H, ℓ, and L, and perform computations to obtain the required a_N coefficients, water depth d and wave period T. These evaluations are then used to obtain expressions for the surface profile and the velocity potential.

The next step is to select $k(x - \xi)$ and $k(z - \eta)$, coordinates of the undisturbed particle positions, and from equations 3 and 4 compute kx and kz the coordinates of the particles. The surface profile is given for $z - \eta = 0$.

The next step is to compute U, W, $\frac{\partial U}{\partial t}$, $\frac{\partial W}{\partial t}$, $\frac{\partial U}{\partial x}$, $\frac{\partial W}{\partial x}$, $\partial U/\partial z$, and $\partial W/\partial z$, respectively by use of equations 20, 21, 64, 65, 66, 67, 68, and 69.

The horizontal and vertical components of u, w, $\frac{du}{dt}$ and $\frac{dw}{dt}$ are then obtained respectively using equations (24, 25), (26, 27), (56, 58, 60, 61) and (57, 59, 62, 63).

Transformation of equations to the form of Stokes'

The previous development resulted in equations in an unexpanded form. These equations can be expanded, using suitable approximations, and it will be shown that the expanded forms are identical to those obtained as outlined in Stokes' solution. The procedure is to expand the following identities.

$$\cosh Nk\,(\ell + z - \eta) = \cosh Nk\,(d + z)\cosh Nk\,(z_0 - \eta) + \sinh Nk\,(d + z)\sinh Nk\,(z_0 - \eta)$$

$$\sinh Nk\,(\ell + z - \eta) = \sinh Nk\,(d + z)\cosh Nk\,(z_0 - \eta) + \cosh Nk\,(d + z)\sinh Nk\,(z_0 - \eta)$$

$$\sinh Nk\,\ell = \sinh Nkd\,\cosh Nkz_0 + \cosh Nkd\,\sinh Nkz_0$$

$$\cos Nk\,(x - \xi) = \cos Nkx\,\cos Nk\xi + \sin Nkx\,\sin Nk\xi$$

$$\sin Nk\,(x - \xi) = \sin Nkx\,\sin Nk\xi - \cos Nkx\,\sin Nk\xi$$

In the above equations the expressions involving $k\xi$ and $k\eta$ are expanded by series to as high an order as required, and by the process of resubstitution expressions are obtained for $k\xi$, $k\eta$, u/C w/C in the expanded form.

For example, consider the second order solution involving the expansion of equations 6 and 7.

$$k\eta_s = o_1\, kA_0\left[\cos kx + k\xi_s \sin kx\right] + a_2\,(kA_0)^2 \cos 2kx - kz_0 \qquad (70)$$

$$k\xi_s = o_1\, X_1\,(kA_0)\left[\sin kx - k\xi_s \cos kx\right] + a_2 X_2\,(kA_0)^2 \sin 2kx \qquad (71)$$

For the second order it will be seen from equation 54 $kz_o = \frac{1}{2} Y_1\,(kA_0)^2$ and from equation 50 that $X_1 = Y_1$ and $X_2 = Y_2$. For the third order $X_2 = Y_2$ $X_3 = Y_3$, but

$$X_1 = Y_1\left[1 + (kA_o)^2\,\frac{Y_1^2 - 1}{2}\right]$$

The first order solution of equation 71 is $k\xi_s = a_1 X_1 (kA_o) \sin kX$, and is substituted into equations 70 and 71 to obtain the second order equations.

$$k\xi_s = o_1\, X_1\, kA_0 \sin kx + (a_2 X_2 - \tfrac{1}{2} o_1^2 X_1^2)(kA_0)^2 \sin 2kx \qquad (72)$$

$$k\eta_s = o_1\,(kA_0)\cos kx + (o_2 - \tfrac{1}{2} a_1^2 X_1)(kA_0)^2 \cos 2kx \qquad (73)$$

Using $a_2 = A_{22}$ and $a_1 = A_{11} = 1$ as given before, equation 73 for the surface profile becomes:

$$\eta_s / A_0 = \cos kx + \frac{3 - \tanh^2 kd}{4\tanh^3 kd}\,(kA_0)\cos 2kx \qquad (74)$$

Which is identical to Stokes' solution

Consider now the second order solution for particle velocity for which from Table I

$$\frac{u}{C} = U - U^2 + W^2 \tag{75}$$

$$\frac{w}{C} = W - 2WU \tag{76}$$

To the second order the expanded forms of U and W (equations 20 and 21) become:

$$U = \frac{a_1 kA_0}{\sinh kd}\left[\cosh k(d+z)\cos k(x-Ct) + k\xi \cosh k(d+z)\sin k(x-Ct) - k\eta \sinh k(d+z)\cos k(x-Ct)\right] + 2a_2(kA_0)^2 \frac{\cosh 2k(d+z)}{\sinh 2kd}\cos 2k(x-Ct) \tag{77}$$

and

$$W = \frac{a_1 kA_0}{\sinh kd}\left[\sinh k(d+z)\sin k(x-Ct) - k\xi \sinh k(d+z)\cos k(x-Ct) - k\eta \cosh k(d+z)\sin k(x-Ct)\right] + 2a_2(kA_0)^2 \frac{\sinh 2k(d+z)}{\sinh 2kd}\sin 2k(x-Ct) \tag{78}$$

The first order solution for $k\xi$ and $k\eta$ for substitution in the above are obtained from equations 1 and 2, respectively as follows:

$$k\xi = a_1 (kA_0) \frac{\cosh k(d+z)}{\sinh kd}\sin kx \tag{79}$$

$$k\eta = a_1 (kA_0) \frac{\sinh k(d+z)}{\sinh kd}\cos kx \tag{80}$$

Substituting equations 79 and 80 into equations 77 and 78 one obtains the following:

$$U = o_1 kA_0 \frac{\cosh k(d+z)}{\sinh kd} \cosh x + 2o_2 (kAo)^2 \frac{\cosh 2k(d+z)}{\sinh 2kd} \cos 2k(x-Ct)$$

$$+ o_1^2 (kA_0)^2 \frac{1-\cosh 2k(d+z) \cos 2k(x-Ct)}{2 \sinh^2 kd}$$

and

(8

$$W = a_1 (kA_0) \frac{\sinh k(d+z)}{\sinh kd} \sin k(x-Ct) + 2a_2 (kA_0)^2 \frac{\sinh 2k(d+z)}{\sinh 2kd} \sin 2k(x-$$

$$- a_1^2 (kA_0)^2 \frac{\sinh 2k(d+z)}{2 \sinh^2 kd} \sin 2k(x-Ct)$$

Substituting equations 81 and 82 into equations 75 and 76, one obtains:

$$\frac{u}{C} = o_1 kA_0 \frac{\cosh k(d+z)}{\sinh kd} \cos k(x-Ct) \qquad (83)$$

$$+ \left[\frac{2a_2}{\sinh 2kd} - \frac{o_1^2}{\sinh^2 kd} \right] (kA_0)^2 \cosh 2k(d+z) \cos 2k(x-Ct)$$

$$\frac{w}{C} = o_1 kA_0 \frac{\sinh k(d+z)}{\sinh kd} \sin k(x-Ct) \qquad (84)$$

$$+ \left[\frac{2a_2}{\sinh 2kd} - \frac{a_1^2}{\sinh^2 kd} \right] (kA_0)^2 \sinh 2k(d+z) \sin 2k(x-Ct)$$

Using $a_2 = A_{22}$ and $a_1 = A_{11} = 1$, as given before, equations 83 and 84 become:

(85)

$$\frac{u}{C} = (kA_0) \frac{\cosh k(d+z)}{\sinh kd} \cos k(x-Ct) + \frac{3}{4} (kA_0)^2 \frac{\cosh 2k(d+z)}{\sinh^4 kd} \cos 2k(x-Ct)$$

(86)

$$\frac{w}{C} = (kA_0) \frac{\sinh k(d+z)}{\sinh kd} \sin k(x-Ct) + \frac{3}{4} (kA_0)^2 \frac{\sinh 2k(d+z)}{\sinh^4 kd} \sin 2k(x-Ct)$$

In general Stokes' equations can be written as follows:

$$-\frac{k\phi}{C} = \sum_1^M a_N' (kA_0)^N \frac{\cosh Nk(d+z)}{\sinh Nkd} \sin Nk(x-Ct) \qquad (87)$$

$$\frac{u}{C} = \sum_1^M N o_N' (kA_0)^N \frac{\cosh Nk(d+z)}{\sinh Nkd} \cos Nk(x-Ct) \qquad (88)$$

$$\frac{w}{C} = \sum_{1}^{M} N a_N' (kA_0)^N \frac{\sinh Nk(d+z)}{\sinh Nkd} \sin Nk(x-Ct) \tag{89}$$

$$k\eta_s = \sum_{1}^{M} b_N (kA_0)^N \cos Nk(x\ Ct) \tag{90}$$

It will be convenient to write

$$\begin{aligned} a_1' &= 1 + a_{13}(kA_0)^2 + a_{15}(kA_0)^4 + \\ a_2' &= a_{22} + a_{24}(kA_0)^2 + \cdot \\ a_3' &= a_{33} + a_{35}(kA_0)^2 + \\ a_4' &= a_{44} + \cdots \end{aligned} \tag{91}$$

etc.

$$\begin{aligned} b_1 &= 1 + \beta_{13}(kA_0)^2 + \beta_{15}(kA_0)^4 + \\ b_2 &= \beta_{22} + \beta_{24}(kA_0)^2 + \cdots \\ b_3 &= \beta_{33} + \beta_{35}(kA_0)^2 + \\ b_4 &= \beta_{44} + \end{aligned} \tag{92}$$

etc

$$\frac{kC^2}{g} = \gamma_1 + \gamma_3 (kA_0)^2 + \gamma_5 (kA_0)^4 + \tag{93}$$

The procedure applied to the second order solution has been extended to the fifth order, using also the expanded relationship of tanh $Nk\ell$. The results of this expansion leads to the following relations for the coefficients:

TABLE VII

$$\gamma_1 = t = \tanh kd$$

$$a_{22} = \frac{3}{4} \frac{1-t^2}{t^3}$$

$$\beta_{22} = a_{22} + \frac{1}{2t} = \frac{3-t^2}{4t^3}$$

$$a_{33} = \frac{3+t^2}{8t^2} \left[\beta_{22} \frac{1-t^2}{2t} + a_{22} \frac{1-2t^2}{t} \right]$$

$$\beta_{33} = \alpha_{33} + \frac{1}{8} + \frac{1}{2}\,\frac{\beta_{22}}{t} + \frac{1}{2}\,\alpha_{22}\,\frac{1+t^2}{t}$$

$$\alpha_{13} = -\beta_{33} - \frac{6-t^2}{8t^4}$$

$$\beta_{13} = -\beta_{33}$$

$$\gamma_3 = \beta_{13} - \alpha_{13} + \frac{5}{8} - \frac{\beta_{22}\,t}{2} + \alpha_{22}\,\frac{1-t^2}{2t}$$

$$\alpha_{44} = \frac{1+t^2}{5+t^2}\left[\beta_{33}\,\frac{1-t^2}{2t^3} + \frac{1-t^2}{48t^3} + \alpha_{22}\,\frac{1-3t^2}{4t^2} + \alpha_{22}\,\beta_{22}\,\frac{1-3t^2}{2t^3} + 3\alpha_{33}\,\frac{1-3t^2-2t^4}{t^3(3+t^2)} + \alpha_{22}^2\,\frac{1-2t^2+t^4}{4t^3}\right]$$

$$\beta_{44} = \alpha_{44} + \frac{1}{4}\,\beta_{22} + \frac{1}{2}\,\frac{\beta_{33}}{t} + \frac{1}{48t} + \frac{\alpha_{22}}{2} + \alpha_{22}\,\beta_{22}\,\frac{1+t^2}{2t} + 3\alpha_{33}\,\frac{1+3t^2}{2t(3+t^2)}$$

$$\alpha_{24} = 2\alpha_{22}\,\alpha_{13} + \frac{47-29t^2}{96t^3} - \frac{3-5t^2}{4t^3}\,(\alpha_{13}+\beta_{33}) + \beta_{22}\,\frac{7+3t^2}{8t^2} + \beta_{33}\,\frac{1-t^2}{2t^3} + \alpha_{22}\,\frac{1+11t^2-6t^4}{8t^4} + 3\alpha_{33}\,\frac{1-t^4}{t^3(3+t^2)} + \alpha_{22}(\alpha_{13}+\beta_{33})\,\frac{1+t^2}{t^2} + \alpha_{22}\,\beta_{22}\,\frac{1+t^2}{2t} - \alpha_{22}^2\,\frac{1-t^4}{2t^3}$$

$$\beta_{24} = \alpha_{24} + 2\alpha_{13}\,(\beta_{22}-\alpha_{22}) - \frac{\alpha_{13}+\beta_{33}}{2t} + \frac{1}{2}\,\beta_{22} + \frac{1}{12t} + \frac{1}{2}\,\frac{\beta_{33}}{t} + \alpha_{22} + 3\alpha_{33}\,\frac{1+3t^2}{2t\,(3+t^2)}$$

$$\alpha_{55} = \frac{5+10t^2+t^4}{8t^2(5+3t^2)}\left[\beta_{22}\,\frac{1-t^2}{16t} + \beta_{44}\,\frac{1-t^2}{2t} + \alpha_{22}\,\beta_{22}\,\frac{1-5t^2}{4} + \alpha_{22}\,\beta_{33}\,\frac{1-3t^2}{2t} + \alpha_{22}\,\frac{7-15t^2}{48t} + 3\alpha_{33}\,\frac{1-4t^2}{3+t^2} + \frac{3}{2}\,\alpha_{33}\,\beta_{22}\,\frac{1-6t^2-3t^4}{t\,(3+t^2)} + \alpha_{44}\,\frac{1-4t^2-9t^4}{t\,(1+t^2)} + \frac{3}{2}\,\alpha_{22}\,\alpha_{33}\,\frac{1-2t^2+t^4}{t\,(3+t^2)}\right]$$

$$\beta_{55} = \alpha_{55} + \frac{1}{8}\,\beta_{22}^2 + \frac{1}{4}\,\beta_{33} + \frac{1}{384} + \frac{1}{2}\,\frac{\beta_{44}}{t} + \frac{1}{16}\,\frac{\beta_{22}}{t} + \alpha_{22}\,\beta_{22} + \alpha_{22}\,\beta_{33}\,\frac{1+t^2}{2t} + \alpha_{22}\,\frac{1+t^2}{12t} + \frac{9}{8}\,\alpha_{33} + \frac{3}{2}\,\alpha_{33}\,\beta_{22}\,\frac{1+3t^2}{t(3+t^2)} + \alpha_{44}\,\frac{1+6t^2+t^4}{2t\,(1+t^2)}$$

$$a_{35} = 3a_{33}a_{13} + \frac{3+t^2}{8t^2}\left[\frac{17}{192} + \frac{a_{13}+\beta_{33}}{8} + (\beta_{24}-2\beta_{22}\beta_{13})\frac{1-t^2}{2t}\right.$$
$$+ \frac{1}{4}\beta_{22}^2 t^2 + \beta_{33} + \beta_{44}\frac{1-t^2}{2t} + \beta_{22}\frac{11+t^2}{16t} + \beta_{22}\frac{a_{13}+\beta_{33}}{2}t$$
$$+ (a_{24}-2a_{22}a_{13})\frac{1-2t^2}{t} - a_{22}(a_{13}+\beta_{33})\frac{1-4t^2}{t} + a_{22}\beta_{22}\frac{7+5t^2}{4}$$
$$+ a_{22}\frac{19-11t^2}{16t} + \frac{3}{8}a_{33}\frac{35-39t^2}{3+t^2} + a_{44}\frac{1+12t^2+7t^4}{t(1+t^2)} + 3a_{33}(a_{13}+\beta_{33})\frac{1+3t^2}{3+t^2}$$
$$\left.+ \frac{3}{2}a_{33}\beta_{22}t\frac{1+3t^2}{3+t^2} - \frac{3}{2}a_{22}a_{33}\frac{1+2t^2-3t^4}{t(3+t^2)} + a_{22}^2\frac{1-6t^2+5t^4}{4t^2}\right]$$

$$\beta_{35} = a_{35} + 3a_{13}(\beta_{33}-a_{33}) - \frac{a_{13}+\beta_{33}}{4} + \frac{\beta_{24}-2\beta_{22}a_{13}}{2t} - \frac{a_{22}}{2}(a_{13}+\beta_{33})\frac{1+t^2}{t}$$
$$+ \frac{a_{24}-a_{22}a_{13}}{2}\frac{1+t^2}{t} + \frac{1}{2}\beta_{33} + \frac{1}{8}\beta_{22}^2 + \frac{5}{384} + \frac{1}{2}\frac{\beta_{44}}{t} + \frac{3}{16}\frac{\beta_{22}}{t}$$
$$+ a_{22}\beta_{22} + a_{22}\frac{1+t^2}{4t} + \frac{9}{4}a_{33} + a_{44}\frac{1+6t^2+t^4}{2t(1+t^2)}$$

$$a_{15} = -\left\{\beta_{35}+\beta_{55} - 3a_{13}(\beta_{33}+a_{13}) - \frac{3}{4}(a_{13}+\beta_{33}) + \frac{\beta_{24}-2\beta_{22}a_{13}}{2t}\right.$$
$$+ \frac{5}{192} + \frac{1}{4}\frac{\beta_{22}}{t} + \frac{1}{4}\beta_{22}^2 + \frac{1}{4}\beta_{33} + \frac{a_{24}-2a_{22}a_{13}}{2}\frac{1+t^2}{t}$$
$$- \frac{a_{22}(\beta_{33}+a_{13})}{2}\frac{1+t^2}{t} + 2a_{22}\beta_{22} + a_{22}\beta_{33}\frac{1+t^2}{2t}$$
$$\left.+ a_{22}\frac{1+t^2}{3t} + \frac{9}{8}a_{33} + \frac{3}{2}a_{33}\beta_{32}\frac{1+3t^2}{t(3+t^2)}\right\}$$

$$\beta_{15} = -\left[\beta_{35} + \beta_{55}\right]$$

$$\gamma_5 = 2a_{13}\gamma_3 - \frac{13}{8}(a_{13}+\beta_{33}) + (\beta_{24}-2\beta_{22}a_{13})\frac{1-t^2}{2t} + \frac{171}{192}$$
$$+ \frac{3}{8}\left(\frac{2-t^2}{t}\right)\beta_{22} + \frac{1}{4}\beta_{22}^2 t^2 + \frac{a_{24}-2a_{22}a_{13}}{t} - a_{22}(a_{13}+\beta_{33})\frac{1-2t^2}{t}$$
$$+ a_{22}\beta_{22}(2+t^2) + a_{22}\beta_{33}\frac{1-3t^2}{2t} + a_{22}\frac{65+81t^2}{24t} + a_{33}\frac{12+3t^2}{3+t^2}$$
$$+ 3a_{33}\beta_{22}\frac{1-6t^2-3t^4}{2t(3+t^2)} + \frac{1}{2}\beta_{22}(a_{13}+\beta_{33})t$$
$$+ 3a_{22}a_{33}\frac{1+10t^2+5t^4}{2t(3+t^2)} + a_{22}^2\frac{1+14t^2+17t^4}{4t^2}$$

Using kz_o as determined, etc.

$$K = 1 + (kA_0)^2 \frac{t^2-1}{2} + (kA_0)^4 \left[\frac{18 + 63t^2 - 72t^4 - 59t^6 + 26t^8 + 24t^{10}}{64t^8} \right] \quad (\text{}$$

The above coefficients may be solved conveniently in consecutive orde For example, for deep water t = tanh kd = 1, whence,

$$\gamma_1 = 1, \quad \alpha_{22} = 0, \quad \beta_{22} = \frac{1}{2}$$

$$\alpha_{33} = 0, \quad \beta_{33} = \frac{3}{8}, \quad \alpha_{13} = -1, \quad \beta_{13} = -\frac{3}{8}, \quad \gamma_3 = 1, \quad \alpha_{44} = 0, \quad \beta_{44} = \frac{1}{3}$$

$$\alpha_{24} = \frac{1}{2}, \quad \beta_{24} = \frac{1}{3}, \quad \alpha_{55} = 0, \quad \beta_{55} = \frac{125}{384}, \quad \alpha_{35} = \frac{1}{12}, \quad \beta_{35} = \frac{99}{128}$$

$$\alpha_{15} = -\frac{7}{16}, \quad \beta_{15} = -\frac{211}{192}, \quad \gamma_5 = \frac{1}{2}, \quad K = 1$$

Loss of Accuracy in the Expanded Form

When the exact solution of the wave problem to a particular Mth order is expanded to obtain the Stokes' solution to the same Mth order there will be a loss of accuracy. The greatest errors will be with the higher order terms. The first term will have minimum error. The reason for the errors arises from the fact that the coefficients a_N of the series (either the expanded or the unexpanded form) are evaluated on the basis of the unexpandec form. The above statement appears somewhat difficult to understand if one inadvertently considers Stokes' solution to be in an exact form to the Mth order. If this is the case, then Stokes' form must be expanded along the free surface (which results in the unexpanded form) prior to substitution into Bernoullis' equation. This operation results in an evaluation of the corresponding coefficients based on the unexpanded form, but are then applied incorrectly to the Stokes' or the expanded form.

For example the velocity potential component for the Mth or last term of the Mth order, for the unexpanded form and Stokes' form are respectively as follows:

$$-\frac{k\phi_M}{C} = a_M (kA_0)^M \frac{\cosh Mk(\ell + z - \eta)}{\sinh Mk\ell} \sin Mk(x - Ct - \xi) \qquad (95)$$

and

$$-\frac{k\phi_M}{C} = a_M' (kA_0)^M \frac{\cosh Mkd}{\sinh Mkd} \sin Mk(x - Ct) \qquad (96)$$

Along the free surface $z = \eta = \eta_s$ and the above equations become respectively:

$$-\frac{k\phi_{M_s}}{C} = a_M (kA_0)^M \frac{\cosh Mk\ell}{\sinh Mk\ell} \sin Mk(x - Ct - \xi_s) \qquad (97)$$

$$-\frac{k\phi_{M_s}}{C} = a_M' (kA_0)^M \frac{\cosh Mk(d + \eta_s)}{\sinh Mkd} \sin Mk(x - Ct) \qquad (98)$$

For evaluation of the coefficients of the Mth or last term, the expansion of cosh Mk $(d + \eta_s)$ will be cosh Mkd which is the same idea as $z = \eta = \eta_s = 0$. Any consideration of finite η_s for the Mth term of Stokes' Mth order results in M + 1, M + 2, etc. order terms, which are neglected by the mechanics of the solution.

It then follows that the error in the Mth term of Stokes' solution will be in proportion to:

$$\frac{\cosh Mk\,(d + z)}{\cosh Mk\,(d + z - \eta)}$$

Along the free surface the error will be

$$\frac{\cosh Mk\,(d + \eta_s)}{\cosh Mkd}$$

and along the sea bottom there will be no error since the above ratio reduces to unity.

If one considers the last term of the third order wave theory, M = 3, and for example, the wave H = 35 ft., T = 12 sec. and d = 85 ft., then one obtains L = 581 feet, η_c = 22.1 feet at the crest and η_o - H = - 12.9 feet at the trough and from the above ratio:

$$\frac{\cosh Mk\,(d + \eta_s)}{\cosh Mkd} = \frac{16.057}{7.869} = 2.04 \quad \text{at the crest}$$

and

$$\frac{5.225}{7.869} = 665 \quad \text{at the trough}$$

The deviations of the above ratio from unity reflects considerable error. For the unexpanded form the above ratio is always unity.

For the M-1 or next to the last term of the Mth order, the percent error will be less since the expansion of this term for Stokes' solution will be $\cosh\left[(M-1)\,k\,(d + \eta_s)\right] = \cosh\left[(M-1)\,kd\right] + (M - 1)\left[k\eta_s \sinh (m-1)\,kd\right]$

In view of the above considerations it appears that the use of Stokes' higher order solutions should be limited to low wave steepness, i.e. η_s small compared with d.

With the aid of electronic computors, the unexpanded form given in the present paper can be utilized easily for computing wave properties and thereby obtain greater accuracy theoretically than by utilizing Stokes' equations.

SUMMARY AND CONCLUSIONS

A theory for waves of finite height, presented in this paper is an exact theory, to any order for which it is extended. Two sets of equations are given in an unexpanded form, when upon expansion represents an approximation to the exact theory, and this approximation is identical to Stokes' theory extended to the same order. The waves are irrotational.

Consecutive order of equations are given which can be used, either by the long hand method of computation or by use of high speed computors for computing the wave properties. These equations have been worked out to the fifth order, both in the exact form and also the approximation or Stokes' form.

ACKNOWLEDGEMENTS

The author extends appreciation to the staff of the Beach Erosion Board for making available the time and personnel required in the preparation of this paper. In particular, Mr. George Simmons who helped to check the algebraic manipulations required to obtain the equations presented. Finally, appreciation is extended to Mr. John Chappelear of Shell Development Company who's encouragements persuaded the author to develop the concepts put forth.

REFERENCES

Airy, G. B. (1842) On tides and Waves:
Encyclopedia Metropolitana, London p. 289

Beach Erosion Board (1942) A summary of the theory of oscillatory waves:
Technical Report No. 2, Washington, D. C., 43 pp.

Borgman, L. E. and J. E. Chappelear (1958) The use of the Stokes-Struik Approximation for waves of finite height: Proc. VIth Conference on Coastal Engineering

Daily, J. W. and S. C. Stephan, Jr. (1951) Characteristics of the solitary wave: Proc. American Society of Civil Engineers , Vol. 77, No. 107

Daily, J. W. and S. C. Stephan, Jr. (1953) The solitary wave, Proc. third Conference on Coastal Engineering, Chapter 2, Council on Wave Research, The Engineering Foundation, pp. 13-30

Danel, Pierre (1952) On the limiting Clapotis, National Bureau of Standards Cir. No. 521, Gravity Waves, Chapter 6, pp. 35-45

De, S. C. (1955) Contr. to the theory of Stokes' Waves: Proc. Conf. Philadelphi Soc., Vol. 51, pp. 713-736

Gerstner, F. (1952) Theorie de Wellen, Abhandlungen der Koniglichen Bohmischen Gesellschaft der Wissenschafte, Prague 1802, translated from German to English by R. M. Kay, University of California Berkeley, Report Series No. 3, Issue 339.

Havelock, T. H. (1919) Periodic irrotational waves of finite height, Proc. Roy. Soc., London, Ser. A. Vol. 95, pp. 38-51

Hunt, J. N. (1953) A note on gravity waves of finite amplitude: Quart. Journal Mech. and Applied Math., Vol. VI, Pt. 3, pp. 336-343

Lamb, Horace (1945) Hydrodynamics, 6th Ed., Dover Pub., New York XV, 738 pp.

Levi-Civita, Tullio (1925) Determination rigoureuse des ondes permanentes d'anpleur finie; Math. Ann., Vol. 43, pp. 264-314

Mason, M. A. (1942) Surface wave theories, Proc. A.S.C.E. Vol.78 No. 120, 29 pp.

McCowan, T. (1891) On the solitary wave, The London, Edinburgh, and Dublin Philosophical Magazine and Journal of Science, Vol. 32, No. 5, pp.45

Miche, M. (1954) Undulatory movements of the sea in constant or decreasing depths, a translation from French to English, University of Calif., Berkeley, Tech. Report Ser. 3, Issue 363, 96 pp. (unpublished)

Munk, W. H. (1949) Solitary wave theory, Annals New York Academy of Sciences, Vol. 51, New York, pp. 376 -424

Schulejkin, W. W. (1956) Theorie der Meereswellen, Abh. des Seehydrophys Inst. der Ak. d. Wiss, der UdSSR, 9, S.115, translated from Russian to German by Dr. Erich Bruns (1960) Akademie-Verlag-Berlin.

Skjelbreia, Lars (1958) Gravity Waves Stokes' third order approximation Tables of Functions, Council on Wave Research, the Engineering Foundation, 337 pp.

Skjelbreia, Lars (1960) Fifth order Gravity Wave theory, presented at VIIth Conference on Coastal Engineering, The Hague, Holland

Suquet, F. and A. Wallet (1953) Basic Experimental Wave Research, Proc. Minnesota International Hydraulics Convention (IAHR, ASCE) pp. 173-191

Tanaka, Kiyoshi (1953) On sea waves: Tech. Report of Osaka University, No. 65

Wiegel, R. L., and J. W. Johnson (1951) Elements of Wave Theory, Proc. First Conf. Coastal Engineering, Council on Wave Research, The Engineering Foundation, pp.5-21

Wiegel, R. L. (1954) Gravity Waves Tables of Functions: Council on Wave Research, The Engineering Foundation, 30 pp.

APPENDIX

SYMBOLS

A_o = H/2, half wave height

a_N = a_1 a_2, a_3 etc. Coefficients of velocity potential series

B_s = B_{11}, B_{13}, etc. Terms for the Bernoulli Equation

C = L/T Wave celerity

d = Undisturbed mean water depth

F = F_1, F_3, F_5, etc. Higher order terms for wave celerity

g = Acceleration of gravity

H = Wave height, vertical distance between crest and trough

k = $2\pi/L$, Wave number

K = Constant for Bernoulli Equation

ℓ = Parameter related to mean water depth

L = Wave length, horizontal distance between two successive wave crests

M = Mth term of the Mth order

N = 1, 2, 3, 4, to M, Consecutive terms of the series

p = pressure

R = Remainder terms in expansion of equation for particle velocity

r = Exponent

s = Exponent

T = Wave period

t = time also used to denote t = tanh kd

u = horizontal component of particle velocity

u_s = u at the free surface

U = A form of notation used related to u for higher order terms

w = vertical component of particle velocity

w_s = w at the free surface

W = A form of notation used related to w for higher order terms

x = horizontal coordinate of particle

$X_N = X_1, X_2$, etc. = $1/\tanh Nk\ell$

$Y_N = Y_1, Y_2$, etc. = $1/\tanh Nkd$

z = Vertical coordinate of particle

$z_o = \ell - d$

η = Vertical displacement of particle from its undisturbed position of rest

$\eta_s = \eta$ for the free surface

ξ = Horizontal displacement of particle from its undisturbed position of rest

$\xi_s = \xi$ for the free surface

ρ = density

$\Theta = k(x - Ct)$

$\Theta^1 = k(x - Ct - \xi)$

∇^2 = Operator

∂ = Notation for partial differential

ϕ = Velocity potential

ψ = Stream function

CHAPTER 10

FIFTH ORDER GRAVITY WAVE THEORY

Lars Skjelbreia, Ph.D
Associate Director

James Hendrickson, Ph.D
Technical Staff

National Engineering Science Company
Pasadena, California

INTRODUCTION

In dealing with problems connected with gravity waves, scientists and engineers frequently find it necessary to make lengthy theoretical calculations involving such wave characteristics as wave height, wave length, period, and water depth. Several approximate theoretical expressions have been derived relating the above parameters. Airy, for instance, contributed a very valuable and complete theory for waves traveling over a horizontal bottom in any depth of water. Due to the simplicity of the Airy theory, it is frequently used by engineers. This theory, however, was developed for waves of very small heights and is inaccurate for waves of finite height. Stokes presented a similar solution for waves of finite height by use of trigonometric series. Using five terms in the series, this solution will extend the range covered by the Airy theory to waves of greater steepness. No attempt has been made in this paper to specify the range where the theory is applicable. The coefficients in these series are very complicated and for a numerical problem, the calculations become very tedious. Because of this difficulty, this theory would be very little used by engineers unless the value of the coefficient is presented in tabular form The purpose of this paper is to present the results of the fifth order theory and values of the various coefficients as a function of the parameter d/L.

The co-ordinate system and description of the wave to be considered in this paper is shown in Fig. 1.

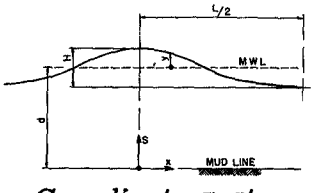

Coordinate system
Fig. 1

FIFTH ORDER GRAVITY WAVE THEORY

The waves to be considered in this analysis are oscillatory, non-viscous, water waves of constant depth and of infinite extent in a direction normal to their propagation. Hence, the particle velocities may be obtained from a potential function as follows:

$$u = \frac{\partial \phi}{\partial x} \quad , \quad v = \frac{\partial \phi}{\partial s} \tag{1.}$$

provided

$$\nabla^2 \phi = 0 \tag{2.}$$

and the necessary boundary conditions on ϕ are satisfied. The boundary condition at the mud line is that the normal velocity be zero.

$$\left.\frac{\partial \phi}{\partial s}\right|_{s=0} = 0 \tag{3.}$$

One of the free surface (S = d + y) boundary conditions arises from the fact that the water particles stay on the surface. The other free surface boundary condition is that the pressure is zero. These conditions may be written as follows:

$$\left.\begin{aligned} v &= u\frac{\partial y}{\partial x} + \frac{\partial y}{\partial t} \\ P &= 0 \end{aligned}\right\} \text{ at } S = d + y \tag{4.}$$

The relationship between the pressure and the particle velocities is expressed by the Bernoulli equation.

$$\frac{2P}{\rho} + (u^2 + v^2) + 2\frac{\partial \phi}{\partial t} = -2g(K + S - d) \tag{5.}$$

where

K = a constant.

Since we are dealing with an oscillatory wave of length L, the wave profile and the potential function may be expressed in terms of a phase angle

$$\theta = \frac{2\pi}{L}(x - \bar{C}t) = \beta(x - \bar{C}t) \qquad 6.$$

where

$\bar{C}$ = the wave celerity.

Thus, combining equations 1, 4, 5, and 6, the free surface boundary conditions may be written in the form

$$\frac{\partial y}{\partial x} = \frac{-v}{\bar{C} - u} \qquad 7.$$

and $$-2u\bar{C} + (u^2 + v^2) = -2g(K + y)$$

or $$(\bar{C} - u)^2 + v^2 = C^2 - 2g(K + y) \qquad 8.$$

where

$$u = \frac{\partial \phi}{\partial x}, \quad v = \frac{\partial \phi}{\partial y} \qquad \text{evaluated at } S = d + y.$$

The solution to the problem is obtained by finding a solution to equation 2 that satisfies equations 3, 7, and 8. The expression for the wave profile will come out of such a solution in the process of satisfying equations 7 and 8.

Other investigators have obtained solutions correct to the third order of approximation (Ref. 1). Also, solutions for the case $d \to \infty$ have been obtained to high orders of approximation (Ref. 2). We shall proceed by assuming a similar series form of solution for the profile and the velocity potential. The unknown constants appearing in these series will then be evaluated using an iterative procedure by substitution into equations 7 and 8.

The series form for ϕ, which satisfies equations 2, 3, and symmetry requirements, will be assumed as follows:

$$\frac{\beta\phi}{\bar{C}} = \frac{2\pi\phi}{L\bar{C}} = (\lambda A_{11} + \lambda^3 A_{13} + \lambda^5 A_{15}) \cosh \beta S \sin\theta + (\lambda^2 A_{22} + \lambda^4 A_{24}) \cosh 2\beta S \sin 2\theta + (\lambda^3 A_{33} + \lambda^5 A_{35}) \cosh 3\beta S \sin 3\theta + \lambda^4 A_{44} \cosh 4\beta S \sin 4\theta + \lambda^5 A_{55} \cosh 5\beta S \sin 5\theta \qquad 9.$$

The series form for the profile, y, which satisfies symmetry requirements, will be assumed to be

$$\beta y = \lambda \cos\theta + (\lambda^2 B_{22} + \lambda^4 B_{24}) \cos 2\theta + (\lambda^3 B_{33} + \lambda^5 B_{35}) \cos 3\theta + \lambda^4 B_{44} \cos 4\theta + \lambda^5 B_{55} \cos 5\theta \qquad 10.$$

Further, the following forms will be assumed for the constant K and the wave celerity $\bar{C}$.

$$\beta K = \lambda^2 C_3 + \lambda^4 C_4 \qquad 11.$$

$$\beta \bar{C}^2 = C_0^2 (1 + \lambda^2 C_1 + \lambda^4 C_2) \qquad 12.$$

Equations 9, 10, 11, and 12 may be substituted into equations 7 and 8 by performing the necessary expansions and retaining those terms of importance to and including the fifth order of approximations. The order of any term is represented by the power of the coefficient λ which modifies that term.

The method of expansion used in the present paper is to solve for the value of $\beta u / \bar{C}$ and $\beta v / \bar{C}$ from equations 7 and 8 and set these values equal to $\beta/c \; \partial\phi/\partial x$ and $\beta/c \; \partial\phi/\partial S$, respectively, at S = d + y. Such a procedure results in two equations involving the undetermined constants, powers of cos ϕ, and powers of the coefficient λ. These equations are grouped according to powers of λ and sub-grouped according to powers of cos ϕ. Since the equations must hold for any value of ϕ, terms in each equation involving the same order of approximation and the same power of cos ϕ are set equal, this results in twenty equations involving the twenty constants Aij, Bij, and Ci. The solution to these equations is listed below and numerical

values are given in tables I, II and III. The constants involve the ratio of water depth to wave length (d/L) as a parameter. For brevity in listing the coefficients the notation is made that $s = \sinh(2\pi d/L)$ and $c = \cosh(2\pi d/L)$.

$$C_o^2 = g(\tanh \beta d)$$

$$A_{11} = 1/s$$

$$A_{13} = \frac{-c^2(5c^2+1)}{8s^5}$$

$$A_{15} = \frac{-(1184c^{10}-1440c^8-1992c^6+2641c^4-249c^2+18)}{1536s^{11}}$$

$$A_{22} = \frac{3}{8s^4}$$

$$A_{24} = \frac{(192c^8-424c^6-312c^4+480c^2-17)}{768s^{10}}$$

$$A_{33} = \frac{(13-4c^2)}{64s^7}$$

$$A_{35} = \frac{(512c^{12}+4224c^{10}-6800c^8-12,808c^6+16,704c^4-3154c^2+107)}{4096s^{13}(6c^2-1)}$$

$$A_{44} = \frac{(80c^6-816c^4+1338c^2-197)}{1536s^{10}(6c^2-1)}$$

$$A_{55} = \frac{-(2880c^{10}-72.480c^8+324,000c^6-432,000c^4+163,470c^2-16,245)}{61,440s^{11}(6c^2-1)(8c^4-11c^2+3)}$$

$$B_{22} = \frac{(2c^2+1)c}{4s^3}$$

$$B_{24} = \frac{c(272c^8-504c^6-192c^4+322c^2+21)}{384s^9}$$

$$B_{33} = \frac{3(8c^6+1)}{64s^6}$$

$$B_{35} = \frac{(88,128c^{14}-208,224c^{12}+70,848c^{10}+54,000c^8-21,816c^6+6264c^4-54c^2-}{12.288s^{12}(6c^2-1)}$$

$$B_{44} = \frac{c(768c^{10}-448c^{8}-48c^{6}+48c^{4}+106c^{2}-21)}{384s^{9}(6c^{2}-1)}$$

$$B_{55} = \frac{(192,000c^{16}-262,720c^{14}+83,680c^{12}+20,160c^{10}-7280c^{8})}{12,288s^{10}(6c^{2}-1)(8c^{4}-11c^{2}+3)} +$$

$$+ \frac{(7160c^{6}-1800c^{4}-1050c^{2}+225)}{12,288s^{10}(6c^{2}-1)(8c^{4}-11c^{2}+3)}$$

$$C_1 = \frac{(8c^{4}-8c^{2}+9)}{8s^{4}}$$

$$C_2 = \frac{(3840c^{12}-4096c^{10}+2592c^{8}-1008c^{6}+5944c^{4}-1830c^{2}+147)}{512s^{10}(6c^{2}-1)}$$

$$C_3 = -\frac{1}{4sc}$$

$$C_4 = \frac{(12c^{8}+36c^{6}-162c^{4}+141c^{2}-27)}{192cs^{9}}$$

There still remains the problem of determining the coefficients β and λ. We will assume that the wave is described by the independent parameters H, d, L (crest to trought height, water depth and wave length respectively). It is easily seen that H is related to the profile expression y by the relation

$$H = y\big|_{\theta=0} - y\big|_{\theta=\pi} \qquad 13.$$

Thus, using equation 10 and rearranging

$$\frac{\pi H}{d} = \frac{1}{(d/L)}\left\{\lambda + \lambda^{3}B_{33} + \lambda^{5}(B_{35}+B_{55})\right\} \qquad 14.$$

Also, using equation 12 and the expression for $C_o^{\,2}$ it is easily shown that

$$\frac{d}{L_o} = \left(\frac{d}{L}\right)\tanh\beta d\left\{1 + \lambda^{2}C_1 + \lambda^{4}C_2\right\} \qquad 15.$$

where

$L_o = \frac{gT^{2}}{2\pi}$, T = wave period and g = acceleration due to gravity.

Since the parameters H, d and L are assumed to be known for the wave and since B_{33}, B_{35}, B_{55}, C_1 and C_2 are functions of only d/L, the simultaneous solution of equations 14 and 15 yield both the values of d/L and the coefficient λ. Knowing the value of d, the value of β is easily obtained and hence the wave may be completely described in all its properties.

Unfortunately, the solution of equations 14 and 15 is rather complex and tedious. It would be advantageous to perform a computer solution to equations 14 and 15 and list the results in the manner used by Skjelbreia (Ref. 1) in a similar analysis of the third-order approximation.

The results of the fifth order theory presented in this analysis will be compared with both the third-order approximation and the first-order Airy theory for the following wave.

Given:

water depth	d = 30 ft.
wave height	H = 18 2/3 ft.
wave period	T = 7.72 sec.

Determine:

1. Wave length and wave velocity.
2. Equation for wave profile and horizontal particle velocity.

After substituting the given values for d, H, and T into equations 14 and 15, the simultaneous solutions of these equations yield the correct values for d/L and λ. The following results are obtained

$d/L = 0.120$ $\lambda = 0.1885$

(Note for this example a digital computer was used to solve these simultaneous equations.)

From Tables I, II, and III the following coefficients are obtained.

Wave profile:

$B_{22} = 2.5024$, $B_{33} = 5.7317$ $B_{44} = 14.034$

$B_{24} = -3.7216$ $B_{35} = -4.8893$ $B_{55} = 37.200$

Potential function:

$A_{11} = 1.2085$ $A_{22} = 0.7998$ $A_{35} = -1.5042$

$A_{13} = -5.1153$ $A_{24} = -4.9710$ $A_{44} = 0.0587$

$A_{15} = -10.6530$ $A_{33} = 0.3683$ $A_{55} = -0.0750$

FIFTH ORDER GRAVITY WAVE THEORY

TABLE I

FIFTH ORDER GRAVITY WAVE COEFFICIENTS

d/L	B_{22}	B_{24}	B_{33}	B_{35}	B_{44}	B_{55}	A_{11}	d/L
.0500	2.5817 1	-1.0339 4	5.1727 2	-1.3425 5	9.5495 3	1.7157 5	3.1313	.0500
.0550	1.9661 1	-4.6442 3	3.0222 2	-1.1586 5	4.3146 3	6.0431 4	2.8369	.0550
.0600	1.5369 1	-2.2450 3	1.8619 2	-4.4307 4	2.1132 3	2.3733 4	2.5908	.0600
.0620	1.4016 1	-1.7082 3	1.5539 2	-3.0881 4	1.6200 3	1.6772 4	2.5032	.0620
.0640	1.2825 1	-1.3114 3	1.3057 2	-2.1782 4	1.2548 3	1.2018 4	2.4210	.0640
.0660	1.1771 1	-1.0151 3	1.1041 2	-1.5534 4	9.8140 2	8.7254 3	2.3437	.0660
.0680	1.0836 1	-7.9174 2	9.3932 1	-1.1193 4	7.7465 2	6.4136 3	2.2708	.0680
.0700	1.0004 1	-6.2195 2	8.0366 1	-8.1420 3	6.1678 2	4.7698 3	2.2020	.0700
.0720	9.2592	-4.9177 2	6.9131 1	-5.9747 3	4.9515 2	3.5868 3	2.1369	.0720
.0740	8.5916	-3.9120 2	5.9771 1	-4.4201 3	4.0062 2	2.7257 3	2.0752	.0740
.0760	7.9911	-3.1205 2	5.1931 1	-3.2965 3	3.2655 2	2.0921 3	2.0166	.0760
.0780	7.4494	-2.5164 2	4.5329 1	-2.4724 3	2.6807 2	1.6211 3	1.9610	.0780
.0800	6.9593	-2.0331 2	3.9741 1	-1.8670 3	2.2155 2	1.2675 3	1.9081	.0800
.0820	6.5149	-1.6497 2	3.4989 1	-1.4179 3	1.8429 2	9.9961 2	1.8576	.0820
.0840	6.1109	-1.3438 2	3.0930 1	-1.0823 3	1.5423 2	7.9483 2	1.8095	.0840
.0860	5.7427	-1.0986 2	2.7448 1	-8.2988 2	1.2984 2	6.3696 2	1.7636	.0860
.0880	5.4063	-9.0089 1	2.4447 1	-6.3879 2	1.0992 2	5.1428 2	1.7196	.0880
.0900	5.0985	-7.4092 1	2.1852 1	-4.9330 2	9.3566 1	4.1820 2	1.6775	.0900
.0920	4.8161	-6.1062 1	1.9599 1	-3.8193 2	8.0053 1	3.4741 2	1.6372	.0920
.0940	4.5566	-5.0429 1	1.7636 1	-2.9625 2	6.8832 1	2.8219 2	1.5986	.0940
.0960	4.3177	-4.1710 1	1.5920 1	-2.3003 2	5.9466 1	2.3403 2	1.5614	.0960
.0980	4.0973	-3.4534 1	1.4413 1	-1.7864 2	5.1609 1	1.9525 2	1.5256	.0980
.1000	3.8936	-2.8609 1	1.3088 1	-1.3860 2	4.4988 1	1.6384 2	1.4915	.1000
.1020	3.7052	-2.3700 1	1.1918 1	-1.0729 2	3.9382 1	1.3825 2	1.4584	.1020
.1040	3.5304	-1.9621 1	1.0881 1	-8.2743 1	3.4614 1	1.1728 2	1.4266	.1040
.1060	3.3682	-1.6222 1	9.9610	-6.3440 1	3.0543 1	9.9991 1	1.3959	.1060
.1080	3.2174	-1.3383 1	9.1415	-4.8229 1	2.7053 1	8.5673 1	1.3664	.1080
.1100	3.0770	-1.1005 1	8.4099	-3.6222 1	2.4048 1	7.3752 1	1.3378	.1100
.1120	2.9460	-9.0102	7.7550	-2.6732 1	2.1452 1	6.3779 1	1.3102	.1120
.1140	2.8238	-7.3328	7.1673	-1.9226 1	1.9201 1	5.5395 1	1.2835	.1140
.1160	2.7096	-5.9199	6.6388	-1.3288 1	1.7242 1	4.8316 1	1.2577	.1160
.1180	2.6026	-4.7282	6.1622	-8.5947	1.5532 1	4.2313 1	1.2327	.1180
.1200	2.5024	-3.7216	5.7317	-4.8893	1.4034 1	3.7200 1	1.2085	.1200
.1220	2.4084	-2.8704	5.3418	-1.9711	1.2717 1	3.2829 1	1.1850	.1220
.1240	2.3202	-2.1501	4.9881	3.1870 -1	1.1557 1	2.9076 1	1.1623	.1240
.1260	2.2372	-1.5402	4.6665	2.1065	1.0531 1	2.5843 1	1.1402	.1260
.1280	2.1591	-1.0235	4.3735	3.4927	9.6217	2.3047 1	1.1188	.1280
.1300	2.0855	-5.8591 -1	4.1061	4.5572	8.8134	2.0621 1	1.0980	.1300
.1320	2.0162	-2.1533 -1	3.8617	5.3640	8.0929	1.8508 1	1.0778	.1320
.1340	1.9507	9.8285 -2	3.6377	5.9645	7.4490	1.6663 1	1.0582	.1340
.1360	1.8889	3.6341 -1	3.4323	6.3998	6.8723	1.5046 1	1.0391	.1360
.1380	1.8304	5.8719 -1	3.2435	6.7080	6.3544	1.3624 1	1.0205	.1380
.1400	1.7751	7.7571 -1	3.0697	6.9009	5.8883	1.2371 1	1.0024	.1400
.1420	1.7228	9.3409 -1	2.9095	7.0150	5.4679	1.1263 1	9.8485 -1	.1420
.1440	1.6731	1.0667	2.7615	7.0626	5.0878	1.0281 1	9.6770 -1	.1440
.1460	1.6260	1.1772	2.6247	7.0579	4.7434	9.4080	9.5100 -1	.1460
.1480	1.5814	1.2689	2.4980	7.0122	4.4308	8.6300	9.3471 -1	.1480
.1500	1.5389	1.3443	2.3805	6.9346	4.1465	7.9349	9.1884 -1	.1500
.1520	1.4986	1.4059	2.2714	6.8327	3.8874	7.3124	9.0335 -1	.1520
.1540	1.4602	1.4555	2.1700	6.7124	3.6508	6.7536	8.8824 -1	.1540
.1560	1.4237	1.4950	2.0756	6.5787	3.4338	6.2508	8.7348 -1	.1560
.1580	1.3889	1.5257	1.9876	6.4353	3.2361	5.7974	8.5908 -1	.1580
.1600	1.3557	1.5489	1.9055	6.2855	3.0541	5.3878	8.4502 -1	.1600
.1620	1.3241	1.5657	1.8288	6.1317	2.8868	5.0168	8.3127 -1	.1620
.1640	1.2940	1.5770	1.7570	5.9761	2.7327	4.6802	8.1784 -1	.1640
.1660	1.2652	1.5836	1.6898	5.8201	2.5906	4.3743	8.0472 -1	.1660
.1680	1.2377	1.5863	1.6269	5.6650	2.4594	4.0956	7.9188 -1	.1680
.1700	1.2114	1.5855	1.5678	5.5118	2.3380	3.8413	7.7933 -1	.1700
.1720	1.1863	1.5819	1.5123	5.3614	2.2255	3.6089	7.6705 -1	.1720
.1740	1.1622	1.5758	1.4601	5.2141	2.1212	3.3961	7.5503 -1	.1740
.1760	1.1392	1.5677	1.4110	5.0706	2.0244	3.2009	7.4327 -1	.1760
.1780	1.1172	1.5579	1.3647	4.9310	1.9343	3.0215	7.3175 -1	.1780
.1800	1.0961	1.5467	1.3211	4.7957	1.8504	2.8565	7.2047 -1	.1800
.1820	1.0759	1.5343	1.2800	4.6647	1.7721	2.7044	7.0943 -1	1820
.1840	1.0565	1.5209	1.2411	4 5380	1 6991	2 5641	6 9861 -1	1840
.1860	1.0378	1.5068	1.2043	4 4158	1 6309	2 4344	6 8801 -1	1860
.1880	1.0200	1.4921	1.1696	4 2980	1 5671	2 3143	6 7762 -1	1880
.1900	1.0028	1.4769	1.1367	4 1846	1 5073	2 2031	6 6744 -1	1900
.1920	9.8635 -1	1.4614	1.1055	4 0754	1 4512	2 0998	6 5745 -1	1920
.1940	9.7052 -1	1.4456	1.0760	3 9704	1 3986	2 0038	6 4766 -1	1940
.1960	9.5531 -1	1.4296	1.0479	3 8694	1 3492	1 9145	6 3806 -1	1960
.1980	9.4067 -1	1.4136	1.0213	3 7725	1 3027	1 8314	6 2864 -1	1980
.2000	9.2660 -1	1.3976	9.9601 -1	3 6793	1 2590	1 7538	6 1939 -1	2000
.2100	8.6373 -1	1.3190	8.8675 -1	3 2665	1 0748	1 4353	5 7568 -1	2100
.2200	8.1146 -1	1.2457	8.0058 -1	2 9300	9 3521 -1	1 2033	5 3575 -1	2200
.2300	7.6769 -1	1.1794	7.3168 -1	2 6551	8 2747 -1	1 0304	4 9916 -1	2300
.2400	7.3081 -1	1.1204	6.7594 -1	2 4296	7 4294 -1	8 9887 -1	4 6553 -1	2400
.2500	6.9958 -1	1.0686	6.3038 -1	2 2436	6 7567 -1	7 9700 -1	4 3454 -1	2500
.2600	6.7299 -1	1.0231	5.9279 -1	2 0893	6 2148 -1	7 1686 -1	4 0591 -1	2600
.2700	6.5026 -1	9.8348 -1	5.6152 -1	1.9606	5.7733 -1	6.5294 -1	3.7942 -1	.2700
.2800	6.3076 -1	9.4892 -1	5.3534 -1	1.8527	5.4103 -1	6.0135 -1	3.5485 -1	.2800
.2900	6.1397 -1	9.1882 -1	5.1328 -1	1.7617	5.1093 -1	5.5927 -1	3.3204 -1	.2900
.3000	5.9948 -1	8.9259 -1	4.9458 -1	1.6846	4.8578 -1	5.2462 -1	3.1084 -1	.3000
.3100	5.8694 -1	8.6974 -1	4.7866 -1	1.6191	4.6464 -1	4.9585 -1	2.9110 -1	.3100
.3200	5.7607 -1	8.4981 -1	4.6505 -1	1.5631	4.4677 -1	4.7180 -1	2.7270 -1	.3200
.3300	5.6662 -1	8.3241 -1	4.5338 -1	1.5151	4.3157 -1	4.5156 -1	2.5554 -1	.3300
.3400	5.5839 -1	8.1721 -1	4.4332 -1	1.4738	4.1861 -1	4.3444 -1	2.3953 -1	.3400
.3500	5.5122 -1	8.0392 -1	4.3465 -1	1.4382	4.0749 -1	4.1988 -1	2.2456 -1	.3500
.3600	5.4495 -1	7.9230 -1	4.2714 -1	1.4075	3.9794 -1	4.0744 -1	2.1058 -1	.3600
.3700	5.3948 -1	7.8212 -1	4.2062 -1	1.3808	3.8970 -1	3.9678 -1	1.9750 -1	.3700
.3800	5.3469 -1	7.7320 -1	4.1495 -1	1.3577	3.8258 -1	3.8761 -1	1.8526 -1	.3800
.3900	5.3049 -1	7.6537 -1	4.1002 -1	1.3379	3.7640 -1	3.7970 -1	1.7380 -1	.3900
.4000	5.2681 -1	7.5851 -1	4.0572 -1	1.3200	3.7104 -1	3.7286 -1	1.6308 -1	.4000
.4200	5.2076 -1	7.4719 -1	3.9868 -1	1.2914	3.6231 -1	3.6178 -1	1.4361 -1	.4200
.4400	5.1608 -1	7.3846 -1	3.9329 -1	1.2694	3.5566 -1	3.5339 -1	1.2650 -1	.4400
.4600	5.1247 -1	7.3170 -1	3.8915 -1	1.2526	3.5057 -1	3.4699 -1	1.1147 -1	.4600
.4800	5.0968 -1	7.2647 -1	3.8596 -1	1.2397	3.4666 -1	3.4210 -1	9.8237 -2	.4800
.5000	5.0752 -1	7.2242 -1	3.8350 -1	1.2297	3.4366 -1	3.3835 -1	8.6590 -2	.5000
.5500	5.0400 -1	7.1583 -1	3.7951 -1	1.2136	3.3880 -1	3.3230 -1	6.3190 -2	.5500
.6000	5.0213 -1	7.1233 -1	3.7740 -1	1.2050	3.3624 -1	3.2912 -1	4.6133 -2	.6000

TABLE II

FIFTH ORDER GRAVITY WAVE COEFFICIENTS

d/L	A_{13}	A_{15}	A_{22}	A_{24}	A_{33}	A_{35}	A_{44}	d/L
.0500	-2.6997 2	-1.5812 4	3.6054 1	-1.7843 4	3.9630 2	-2.9907 5	4.1585 3	.0500
.0550	-1.7098 2	-4.4631 3	2.4290 1	-7.3634 3	1.9646 2	-9.0711 4	1.4905 3	.0550
.0600	-1.1307 2	-1.3365 3	1.6895 1	-3.2977 3	1.0288 2	-3.0495 4	5.7854 2	.0600
.0620	-9.6847 1	-8.3832 2	1.4724 1	-2.4389 5	8.0465 1	-2.0206 4	4.0341 2	.0620
.0640	-8.3406 1	-5.3159 2	1.2863 1	-1.8219 3	6.3359 1	-1.5557 4	2.8370 2	.0640
.0660	-7.2201 1	-5.4183 2	1.1514 1	-1.5738 3	5.0202 1	-9.2007 3	2.0121 2	.0660
.0680	-6.2804 1	-2.2396 2	9.9711	-1.0450 3	4.0009 1	-6.3113 5	1.4381 2	.0680
.0700	-5.4881 1	-1.5052 2	8.8160	-8.0134 2	3.2061 1	-4.4723 5	1.0351 2	.0700
.0720	-4.8166 1	-1.0462 2	7.8186	-6.1920 2	2.5823 1	-3.0568 5	7.4987 1	.0720
.0740	-4.2446 1	-7.5850 1	6.9541	-4.8188 2	2.0899 1	-2.1553 3	5.4651 1	.0740
.0760	-3.7551 1	-5.7724 1	6.2020	-3.7752 2	1.6989 1	-1.5316 3	4.0048 1	.0760
.0780	-3.3344 1	-4.6207 1	5.5455	-2.9761 2	1.3870 1	-1.0963 3	2.9499 1	.0780
.0800	-2.9713 1	-3.8784 1	4.9706	-2.3600 2	1.1368 1	-7.8988 2	2.1872 1	.0800
.0820	-2.6566 1	-3.3883 1	4.4655	-1.8817 2	9.3519	-5.7258 2	1.6212 1	.0820
.0840	-2.5828 1	-3.0526 1	4.0205	-1.5081 2	7.7205	-4.1736 2	1.2088 1	.0840
.0860	-2.1438 1	-2.8106 1	3.6274	-1.2145 2	6.3947	-3.0572 2	9.0432	.0860
.0880	-1.9344 1	-2.6249 1	3.2791	-9.8249 1	5.3130	-2.2494 2	6.7843	.0880
.0900	-1.7504 1	-2.4728 1	2.9698	-7.9818 1	4.4272	-1.6615 2	5.1019	.0900
.0920	-1.5881 1	-2.3408 1	2.6945	-6.5102 1	3.6991	-1.2313 2	3.8442	.0920
.0940	-1.4445 1	-2.2208 1	2.4488	-5.3296 1	3.0988	-9.1501 1	2.9009	.0940
.0960	-1.3177 1	-2.1063 1	2.2291	-4.3781 1	2.6022	-6.8140 1	2.1912	.0960
.0980	-1.2039 1	-2.0010 1	2.0323	-3.6080 1	2.1902	-5.0816 1	1.6459	.0980
.1000	-1.1029 1	-1.8977 1	1.8556	-2.9822 1	1.8473	-3.7922 1	1.2511	.1000
.1020	-1.0126 1	-1.7979 1	1.6966	-2.4718 1	1.5619	-2.8296 1	9.4455 -1	.1020
.1040	-9.3160	-1.7015 1	1.5533	-2.0538 1	1.3220	-2.1089 1	7.1197 -1	.1040
.1060	-8.5884	-1.6086 1	1.4240	-1.7104 1	1.1213	-1.5682 1	5.3532 -1	.1060
.1080	-7.9352	-1.5193 1	1.3070	-1.4274 1	9.5264 -1	-1.1617 1	4.0107 -1	.1080
.1100	-7.3417	-1.4339 1	1.2011	-1.1954 1	8.1056 -1	-8.5587	2.9901 -1	.1100
.1120	-6.8067	-1.3522 1	1.1050	-9.9941	6.9064 -1	-6.2556	2.2145 -1	.1120
.1140	-6.3218	-1.2746 1	1.0177	-8.3809	5.8921 -1	-4.5215	1.6256 -1	.1140
.1160	-5.8814	-1.2009 1	9.3824 -1	-7.0360	5.0126 -1	-3.2170	1.1792 -1	.1160
.1180	-5.4807	-1.1312 1	8.6567 -1	-5.9122	4.3051 -1	-2.2375	8.4167 -2	.1180
.1200	-5.1153	-1.0653 1	7.9986 -1	-4.9710	3.6828 -1	-1.5042	5.8724 -2	.1200
.1220	-4.7816	-1.0032 1	7.3954 -1	-4.1809	3.1545 -1	-9.4751 -1	3.9695 -2	.1220
.1240	-4.4764	-9.4475	6.8439 -1	-3.5165	2.7041 -1	-5.5265 -1	2.5601 -2	.1240
.1260	-4.1966	-8.8982	6.3389 -1	-2.9967	2.3191 -1	-2.5481 -1	1.6870 -2	.1260
.1280	-3.9398	-8.3826	5.8760 -1	-2.4843	1.9903 -1	-3.8641 -2	7.1619 -3	.1280
.1300	-3.7037	-7.8989	5.4512 -1	-2.0850	1.7087 -1	1.1586 -1	1.5986 -3	.1300
.1320	-3.4863	-7.4456	5.0610 -1	-1.7470	1.4673 -1	2.2379 -1	-2.3380 -3	.1320
.1340	-3.2858	-7.0210	4.7021 -1	-1.4605	1.2601 -1	2.9864 -1	-5.0474 -3	.1340
.1360	-3.1007	-6.6234	4.3718 -1	-1.2175	1.0822 -1	3.4322 -1	-6.8355 -3	.1360
.1380	-2.9295	-6.2512	4.0675 -1	-1.0111	9.2936 -2	3.7025 -1	-7.9370 -3	.1380
.1400	-2.7709	-5.9029	3.7869 -1	-8.3577 -1	7.9784 -2	3.8284 -1	-8.5317 -3	.1400
.1420	-2.6238	-5.5769	3.5278 -1	-6.8666 -1	6.8464 -2	3.8491 -1	-8.7567 -3	.1420
.1440	-2.4873	-5.2719	3.2885 -1	-5.5983 -1	5.8714 -2	3.7943 -1	-8.7166 -3	.1440
.1460	-2.3604	-4.9864	3.0672 -1	-4.5193 -1	5.0312 -2	3.6866 -1	-8.4908 -3	.1460
.1480	-2.2422	-4.7191	2.8625 -1	-3.6013 -1	4.3068 -2	3.5430 -1	-8.1392 -3	.1480
.1500	-2.1321	-4.4689	2.6729 -1	-2.8206 -1	3.6822 -2	3.5763 -1	-7.7068 -3	.1500
.1520	-2.0294	-4.2345	2.4972 -1	-2.1571 -1	3.1434 -2	3.1965 -1	-7.2270 -3	.1520
.1540	-1.9334	-4.0150	2.3342 -1	-1.5935 -1	2.6786 -2	3.0099 -1	-6.7245 -3	.1540
.1560	-1.8457	-3.8092	2.1830 -1	-1.1154 -1	2.2777 -2	2.8224 -1	-6.2172 -3	.1560
.1580	-1.7596	-3.6164	2.0425 -1	-7.1051 -2	1.9318 -2	2.6575 -1	-5.7178 -3	.1580
.1600	-1.6809	-3.4354	1.9120 -1	-3.6825 -2	1.6335 -2	2.4579 -1	-5.2352 -3	.1600
.1620	-1.6071	-3.2657	1.7906 -1	-7.9688 -3	1.3765 -2	2.2853 -1	-4.7752 -3	.1620
.1640	-1.5377	-3.1065	1.6777 -1	1.6285 -2	1.1547 -2	2.1209 -1	-4.3415 -3	.1640
.1660	-1.4726	-2.9566	1.5725 -1	5.6590 -2	9.6392 -3	1.9654 -1	-3.9360 -3	.1660
.1680	-1.4112	-2.8160	1.4746 -1	9.3507 -2	7.9972 -3	1.8191 -1	-3.5596 -3	.1680
.1700	-1.3535	-2.6838	1.3833 -1	1.2518 -1	6.5857 -5	1.6820 -1	-3.2122 -3	.1700
.1720	-1.2991	-2.5594	1.2981 -1	1.5035 -1	5.3737 -3	1.5541 -1	-2.8932 -3	.1720
.1740	-1.2477	-2.4425	1.2187 -1	1.7013 -1	4.5346 -3	1.4350 -1	-2.6015 -3	.1740
.1760	-1.1993	-2.3320	1.1445 -1	1.8557 -1	3.4451 -3	1.3244 -1	-2.3352 -3	.1760
.1780	-1.1535	-2.2281	1.0752 -1	1.9693 -1	2.6853 -3	1.2220 -1	-2.0933 -3	.1780
.1800	-1.1101	-2.1302	1.0104 -1	2.0455 -1	2.0576 -3	1.1272 -1	-1.8740 -3	.1800
.1820	-1.0691	-2.0378	9.4988 -2	2.0883 -1	1.4871 -3	1.0397 -1	-1.6757 -3	.1820
.1840	-1.0305	-1.9506	8.9325 -2	2.1017 -1	1.0206 -3	9.5867 -2	-1.4967 -3	.1640
.1860	-9.9345 -1	-1.8682	8.4025 -2	2.0892 -1	6.2681 -4	8.8436 -2	-1.3343 -3	.1660
.1880	-9.5848 -1	-1.7904	7.9064 -2	2.0541 -1	2.9583 -4	8.1570 -2	-1.1902 -3	.1880
.1900	-9.2530 -1	-1.7168	7.4416 -2	2.1545 -1	1.9110 -5	7.5247 -2	-1.0598 -3	.1900
.1920	-8.9378 -1	-1.6472	7.0062 -2	2.1528 -1	-2.1079 -4	6.9426 -2	-9.4284 -4	.1920
.1940	-8.6380 -1	-1.5814	6.5981 -2	2.1467 -1	-4.0053 -4	6.4069 -2	-8.5800 -4	.1940
.1960	-8.3527 -1	-1.5190	6.2154 -2	2.1370 -1	-5.5514 -4	5.9141 -2	-7.8416 -4	.1960
.1980	-8.0811 -1	-1.4598	5.8563 -2	2.1244 -1	-6.8010 -4	5.4606 -2	-6.6024 -4	.1980
.2000	-7.8225 -1	-1.4038	5.5194 -2	2.1092 -1	-7.7945 -4	5.0435 -2	-5.8526 -4	.2000
.2100	-6.6955 -1	-1.1634	4.1187 -2	2.0097 -1	-1.0051 -3	3.4077 -2	-3.1592 -4	.2100
.2200	-5.7940 -1	-9.7612 -1	3.0896 -2	8.9427 -2	-9.7708 -4	2.5256 -2	-1.6607 -4	.2200
.2300	-5.0624 -1	-8.2840 -1	2.3281 -2	7.8045 -2	-8.5102 -4	1.6046 -2	-8.4257 -5	.2300
.2400	-4.4608 -1	-7.1039 -1	1.7613 -2	6.7580 -2	-7.0020 -4	1.1197 -2	-4.0458 -5	.2400
.2500	-3.9605 -1	-6.1498 -1	1.3570 -2	5.8291 -2	-5.5693 -4	7.9020 -5	-1.7649 -5	.2500
.2600	-3.5392 -1	-5.3697 -1	1.0180 -2	5.0200 -2	-4.3339 -4	5.8585 -5	-6.2124 -6	.2600
.2700	-3.1815 -1	-4.7252 -1	7.7713 -5	4.3224 -2	-3.3225 -4	4.0667 -5	-8.1765 -7	.2700
.2800	-2.8744 -1	-4.1873 -1	5.9460 -5	3.7244 -2	-2.5202 -4	2.9654 -5	1.4553 -6	.2800
.2900	-2.6089 -1	-3.7341 -1	4.5584 -3	3.2128 -2	-1.8969 -4	2.1808 -5	2.1816 -6	.2900
.3000	-2.3775 -1	-3.3489 -1	3.5008 -5	2.7755 -2	-1.4194 -4	1.6200 -5	2.1927 -6	.3000
.3100	-2.1742 -1	-3.0187 -1	2.6927 -3	2.4014 -2	-1.0573 -4	1.2142 -3	1.9148 -6	.3100
.3200	-1.9945 -1	-2.7336 -1	2.0739 -3	2.0811 -2	-7.8487 -5	9.1765 -4	1.5562 -8	.3200
.3300	-1.8348 -1	-2.4855 -1	1.5992 -3	1.8064 -2	-5.8102 -5	6.9903 -4	1.2113 -6	.3300
.3400	-1.6919 -1	-2.2681 -1	1.2344 -5	1.5702 -2	-4.2917 -5	5.3645 -4	9.1628 -7	.3400
.3500	-1.5635 -1	-2.0765 -1	9.5567 -4	1.3669 -2	-3.1644 -5	4.1453 -4	8.7931 -7	.3500
.3600	-1.4476 -1	-1.9066 -1	7.3759 -4	1.1914 -2	-2.3298 -5	3.2239 -4	4.9624 -7	.3600
.3700	-1.3426 -1	-1.7551 -1	5.7056 -4	1.0398 -2	-1.7135 -5	2.5222 -4	3.5846 -7	.3700
.3800	-1.2469 -1	-1.6193 -1	4.4174 -4	9.0841 -3	-1.2586 -5	1.9841 -4	2.5668 -7	.3800
.3900	-1.1597 -1	-1.4971 -1	3.4219 -4	7.9445 -3	-9.2388 -6	1.5688 -4	1.8253 -7	.3900
.4000	-1.0797 -1	-1.3866 -1	2.6521 -4	6.9542 -3	-6.7768 -6	1.2461 -4	1.2908 -7	.4000
.4200	-9.3873 -2	-1.1950 -1	1.5949 -4	5.3412 -3	-3.6402 -6	7.9605 -5	6.3720 -8	.4200
.4400	-8.1874 -2	-1.0351 -1	9.6042 -5	4.1132 -3	-1.9520 -6	5.1976 -5	3.1059 -8	.4400
.4600	-7.1584 -2	-9.0008 -2	5.7892 -5	3.1744 -3	-1.0454 -6	3.3805 -5	1.5004 -8	.4600
.4800	-6.2708 -2	-7.8514 -2	3.4924 -5	2.4538 -5	-5.5939 -7	2.2366 -5	7.2013 -9	.4600
.5000	-5.5015 -2	-8.8655 -2	2.1081 -5	1.8994 -5	-2.9911 -7	1.4910 -5	3.4397 -9	.5000
.5500	-3.9842 -2	-4.9448 -2	5.9790 -6	1.0054 -3	-6.2404 -8	5.5409 -6	5.3497 -10	.5500
.6000	-2.6968 -2	-9.5848 -2	1.6985 -6	9.3408 -4	-1.2997 -8	2.1042 -6	8.2250 -11	.6000

FIFTH ORDER GRAVITY WAVE THEORY

TABLE III

FIFTH ORDER GRAVITY WAVE COEFFICIENTS

d/L	A_{55}	C_1	C_2	C_3	C_4	SINH($\frac{2\pi d}{L}$)	COSH($\frac{2\pi d}{L}$)	d/L
.0500	4.0709 4	1.1897 2	7.5369 5	-7.4973 -1	-3.5557 2	3.1935 -1	1.0498	.0500
.0550	1.0458 4	8.1917 1	9.9955 4	-6.6889 -1	-1.7030 2	3.3249 -1	1.0603	.0550
.0600	2.9402 3	5.8396 1	4.2948 4	-6.0425 -1	-8.5525 1	3.8598 -1	1.0719	.0600
.0620	1.8067 3	5.1438 1	3.1292 4	-5.8115 -1	-6.5353 1	3.9949 -1	1.0768	.0620
.0640	1.1213 3	4.5511 1	2.3054 4	-5.5941 -1	-5.0280 1	4.1305 -1	1.0819	.0640
.0660	7.0206 2	4.0436 1	1.7164 4	-5.3692 -1	-3.8826 1	4.2668 -1	1.0872	.0660
.0680	4.4301 2	3.6070 1	1.2906 4	-5.1945 -1	-3.0071 1	4.4037 -1	1.0927	.0680
.0700	2.8141 2	3.2297 1	9.7969 3	-5.0122 -1	-2.3941 1	4.5414 -1	1.0983	.0700
.0720	1.7975 2	2.9022 1	7.5036 3	-4.8384 -1	-1.8140 1	4.6796 -1	1.1041	.0720
.0740	1.1532 2	2.6169 1	5.7966 3	-4.6736 -1	-1.4105 1	4.8169 -1	1.1101	.0740
.0760	7.4212 1	2.3673 1	4.5147 3	-4.5167 -1	-1.0960 1	4.9588 -1	1.1162	.0760
.0780	4.7841 1	2.1482 1	3.5439 3	-4.3674 -1	-8.5003	5.0994 -1	1.1225	.0780
.0800	3.0845 1	1.9552 1	2.8028 3	-4.2251 -1	-6.5712	5.2409 -1	1.1290	.0800
.0820	1.9851 1	1.7847 1	2.2328 3	-4.0892 -1	-5.0542	5.3832 -1	1.1357	.0820
.0840	1.2724 1	1.6336 1	1.7911 3	-3.9594 -1	-3.8589	5.5265 -1	1.1425	.0840
.0860	8.0967	1.4992 1	1.4464 3	-3.8352 -1	-2.9157	5.6704 -1	1.1496	.0860
.0880	5.0942	1.3794 1	1.1756 3	-3.7163 -1	-2.1706	5.8153 -1	1.1568	.0880
.0900	3.1500	1.2724 1	9.6148 2	-3.6024 -1	-1.5820	5.9611 -1	1.1642	.0900
.0920	1.8963	1.1764 1	7.9112 2	-3.4931 -1	-1.1173	6.1079 -1	1.1718	.0920
.0940	1.0938	1.0902 1	6.5475 2	-3.3881 -1	-7.5073 -1	6.2536 -1	1.1795	.0940
.0960	5.8568 -1	1.0126 1	5.4497 2	-3.2873 -1	-4.6236 -1	6.4043 -1	1.1873	.0960
.0980	2.6930 -1	9.4249	4.5609 2	-3.1903 -1	-2.6362 -1	6.5541 -1	1.1936	.0980
.1000	7.7244 -2	8.7912	3.8374 2	-3.0970 -1	-1.5986 -2	6.7048 -1	1.2040	.1000
.1020	-3.4780 -2	8.2168	3.2454 2	-3.0071 -1	7.6924 -2	6.8567 -1	1.2128	.1020
.1040	-9.5826 -2	7.6952	2.7586 2	-2.9205 -1	1.8191 -1	7.0096 -1	1.2212	.1040
.1060	-1.2491 -1	7.2206	2.3562 2	-2.8370 -1	2.6153 -1	7.1636 -1	1.2301	.1060
.1080	-1.3443 -1	6.7880	2.0221 2	-2.7565 -1	3.2084 -1	7.3187 -1	1.2392	.1080
.1100	-1.3241 -1	6.3929	1.7435 2	-2.6788 -1	3.6396 -1	7.4750 -1	1.2485	.1100
.1120	-1.2398 -1	6.0315	1.5099 2	-2.6037 -1	3.9415 -1	7.6325 -1	1.2580	.1120
.1140	-1.1240 -1	5.7004	1.3134 2	-2.5312 -1	4.1406 -1	7.7912 -1	1.2677	.1140
.1160	-9.9660 -2	5.3965	1.1473 2	-2.4611 -1	4.2582 -1	7.9511 -1	1.2776	.1160
.1180	-8.6963 -2	5.1171	1.0069 2	-2.3933 -1	4.3114 -1	8.1123 -1	1.2677	.1180
.1200	-7.4980 -2	4.8600	8.8625 1	-2.3277 -1	4.3147 -1	8.2746 -1	1.2980	.1200
.1220	-6.4054 -2	4.6229	7.8354 1	-2.2642 -1	4.2776 -1	8.4385 -1	1.3085	.1220
.1240	-5.4324 -2	4.4041	6.9535 1	-2.2027 -1	4.2108 -1	8.6036 -1	1.3192	.1240
.1260	-4.5805 -2	4.2018	6.1936 1	-2.1432 -1	4.1211 -1	8.7701 -1	1.3301	.1260
.1280	-3.8433 -2	4.0146	5.5365 1	-2.0855 -1	4.0149 -1	8.9379 -1	1.3412	.1280
.1300	-3.2119 -2	3.8410	4.9663 1	-2.0296 -1	3.8951 -1	9.1072 -1	1.3526	.1300
.1320	-2.6750 -2	3.6800	4.4697 1	-1.9753 -1	3.7674 -1	9.2779 -1	1.3641	.1320
.1340	-2.2213 -2	3.5304	4.0360 1	-1.9228 -1	3.6341 -1	9.4500 -1	1.3759	.1340
.1360	-1.8396 -2	3.3913	3.6550 1	-1.8718 -1	3.4977 -1	9.6237 -1	1.3879	.1360
.1380	-1.5199 -2	3.2617	3.3217 1	-1.8223 -1	3.3601 -1	9.7989 -1	1.4001	.1380
.1400	-1.2529 -2	3.1410	3.0271 1	-1.7743 -1	3.2229 -1	9.9756 -1	1.4125	.1400
.1420	-1.0307 -2	3.0289	2.7665 1	-1.7276 -1	3.0871 -1	1.0134	1.4251	.1420
.1440	-8.4608 -3	2.9250	2.5354 1	-1.6824 -1	2.9537 -1	1.0334	1.4380	.1440
.1460	-6.9315 -3	2.8246	2.3299 1	-1.6384 -1	2.8235 -1	1.0515	1.4511	.1460
.1480	-5.6667 -3	2.7324	2.1466 1	-1.5957 -1	2.6968 -1	1.0699	1.4644	.1480
.1500	-4.6227 -3	2.6461	1.9828 1	-1.5542 -1	2.5741 -1	1.0883	1.4780	.1500
.1520	-3.7625 -3	2.5652	1.8359 1	-1.5139 -1	2.4557 -1	1.1070	1.4918	.1520
.1540	-5.0588 -3	2.4892	1.7039 1	-1.4747 -1	2.3416 -1	1.1258	1.5058	.1540
.1560	-2.4735 -3	2.4179	1.5850 1	-1.4366 -1	2.2320 -1	1.1448	1.5201	.1580
.1580	-1.9970 -3	2.3508	1.4777 1	-1.3995 -1	2.1268 -1	1.1640	1.5346	.1580
.1600	-1.6069 -3	2.2877	1.3806 1	-1.3635 -1	2.0262 -1	1.1834	1.5493	.1600
.1620	-1.2881 -3	2.2282	1.2924 1	-1.3285 -1	1.9299 -1	1.2030	1.5645	.1620
.1640	-1.0281 -3	2.1722	1.2124 1	-1.2944 -1	1.8380 -1	1.2227	1.5796	.1640
.1660	-8.1654 -4	2.1193	1.1395 1	-1.2613 -1	1.7503 -1	1.2427	1.5951	.1660
.1680	-6.4471 -4	2.0695	1.0729 1	-1.2290 -1	1.6667 -1	1.2628	1.6108	.1680
.1700	-5.0550 -4	2.0223	1.0121 1	-1.1976 -1	1.5871 -1	1.2832	1.6268	.1700
.1720	-3.9305 -4	1.9778	9.5639	-1.1671 -1	1.5113 -1	1.3057	1.6431	.1720
.1740	-3.0247 -4	1.9357	9.0525	-1.1374 -1	1.4591 -1	1.5245	1.6596	.1740
.1760	-2.2978 -4	1.8938	8.5824	-1.1085 -1	1.3705 -1	1.3454	1.6763	.1760
.1780	-1.7168 -4	1.8380	8.1494	-1.0803 -1	1.3052 -1	1.3686	1.6934	.1780
.1800	-1.2546 -4	1.8222	7.7500	-1.0529 -1	1.2432 -1	1.3880	1.7107	.1800
.1820	-8.8893 -5	1.7869	7.3610	-1.0262 -1	1.1843 -1	1.4096	1.7283	.1820
.1840	-6.0149 -5	1.7560	7.0394	-1.0002 -1	1.1283 -1	1.4314	1.7461	.1840
.1860	-3.7734 -5	1.7254	6.7229	-9.7493 -2	1.0751 -1	1.4555	1.7642	.1660
.1880	-2.0420 -5	1.6964	6.4291	-9.5030 -2	1.0246 -1	1.4798	1.7627	.1880
.1900	-7.2076 -6	1.6687	6.1561	-9.2631 -2	9.7637 -2	1.4983	1.8013	.1900
.1920	2.7225 -6	1.6424	5.9019	-9.0294 -2	9.3098 -2	1.5210	1.6203	.1920
.1940	1.0036 -5	1.6174	5.6650	-8.8018 -2	6.8766 -2	1.5440	1.8396	.1940
.1960	1.5275 -5	1.5936	5.4439	-6.5801 -2	8.4656 -2	1.5673	1.8591	.1960
.1980	1.8879 -5	1.5709	5.2374	-8.3642 -2	8.0749 -2	1.5907	1.8790	.1980
.2000	2.1204 -5	1.5492	5.0441	-8.1538 -2	7.7038 -2	1.6145	1.8991	.2000
.2100	2.1944 -5	1.4550	4.2434	-7.1804 -2	6.1082 -2	1.7371	2.0044	.2100
.2200	1.6255 -5	1.3797	3.6510	-6.3252 -2	4.8698 -2	1.8665	2.1175	.2200
.2300	1.0620 -5	1.3190	3.2024	-5.5734 -2	3.9048 -2	2.0033	2.2391	.2500
.2400	6.4895 -6	1.2696	2.8561	-4.9118 -2	3.1493 -2	2.1481	2.3694	.2400
.2500	3.7992 -6	1.2289	2.5840	-4.3295 -2	2.5545 -2	2.3015	2.5092	.2500
.2600	2.1545 -6	1.1953	2.3670	-3.8166 -2	2.0839 -2	2.4636	2.6588	.2600
.2700	1.1891 -6	1.1673	2.1919	-3.3648 -2	1.7094 -2	2.6556	2.8190	.2700
.2800	6.3915 -7	1.1436	2.0489	-2.9668 -2	1.4098 -2	2.8181	2.9902	.2800
.2900	3.3367 -7	1.1259	1.9511	-2.6159 -2	1.1887 -2	3.0116	3.1795	.2900
.5000	1.6799 -7	1.1071	1.8537	-2.5066 -2	9.7559 -5	5.2171	5.5689	.3000
.5100	8.0589 -8	1.0928	1.7515	-2.0540 -2	8.1491 -5	5.4355	5.5779	.5100
.3200	3.5471 -8	1.0806	1.6622	-1.7957 -2	6.8515 -5	5.6670	5.8009	.5200
.3500	1.3536 -6	1.0701	1.6238	-1.5817 -2	5.7647 -5	5.9132	6.0590	.5500
.3400	3.1093 -9	1.0611	1.5740	-1.3949 -2	4.9034 -5	6.1749	6.2930	.5400
.3500	-1.1659 -9	1.0535	1.5315	-1.2501 -2	4.1717 -3	6.4531	6.5640	.3500
.3600	-2.5496 -9	1.0466	1.4950	-1.0848 -2	3.5615 -3	6.7488	6.8529	.5600
.3700	-2.6985 -9	1.0407	1.4635	-9.9667 -5	3.0499 -3	7.0635	7.1611	.3700
.3800	-2.3355 -9	1.0356	1.4364	-8.4369 -3	2.6195 -3	7.3978	7.4896	.3800
.3900	-1.8455 -9	1.0312	1.4129	-7.4406 -3	2.2559 -3	7.7536	7.8399	.3900
.4000	-1.5835 -9	1.0274	1.3926	-6.5617 -3	1.9475 -3	8.1321	8.2131	.4000
.4200	-7.0894 -10	1.0211	1.3594	-5.1034 -3	1.4668 -3	8.9454	7.0349	.4200
.4400	-3.5793 -10	1.0165	1.5345	-3.9692 -3	1.1038 -3	7.9048	7.9678	.4400
.4600	-1.5439 -10	1.0126	1.3150	-3.0871 -3	8.3908 -4	8.9712	9.0268	.4600
.4800	-6.8651 -11	1.0098	1.3003	-2.4011 -3	6.4090 -4	1.0179 1	1.0226 1	.4800
.5000	-2.9969 -11	1.0076	1.2889	-1.8675 -3	4.9141 -4	1.1549 1	1.1592 1	.5000
.5500	-3.5928 -12	1.0040	1.2706	-9.9627 -4	2.5605 -4	1.5825 1	1.5867 1	.5500
.6000	-4.1440 -13	1.0021	1.2609	-5.3150 -4	1.3483 -4	2.1677 1	2.1700 1	.6000

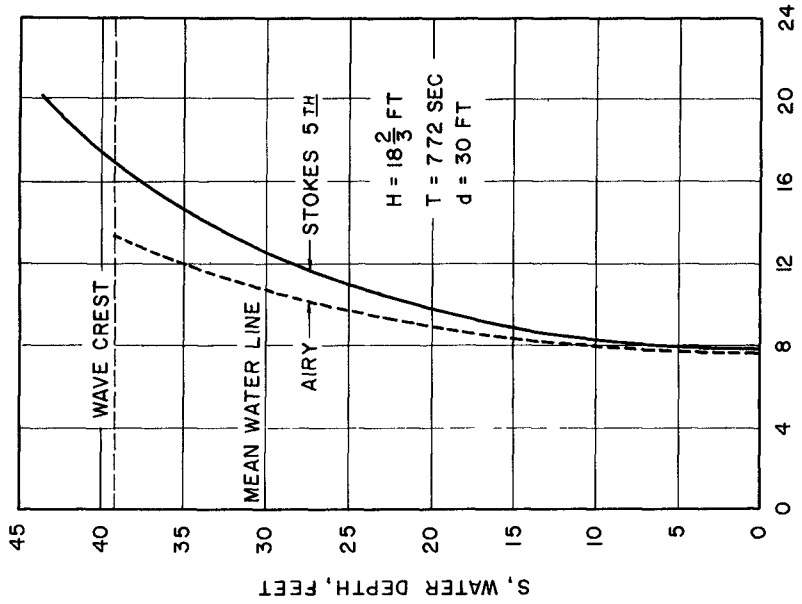

Fig. 3 - Horizontal velocity distribution on vertical section through crest

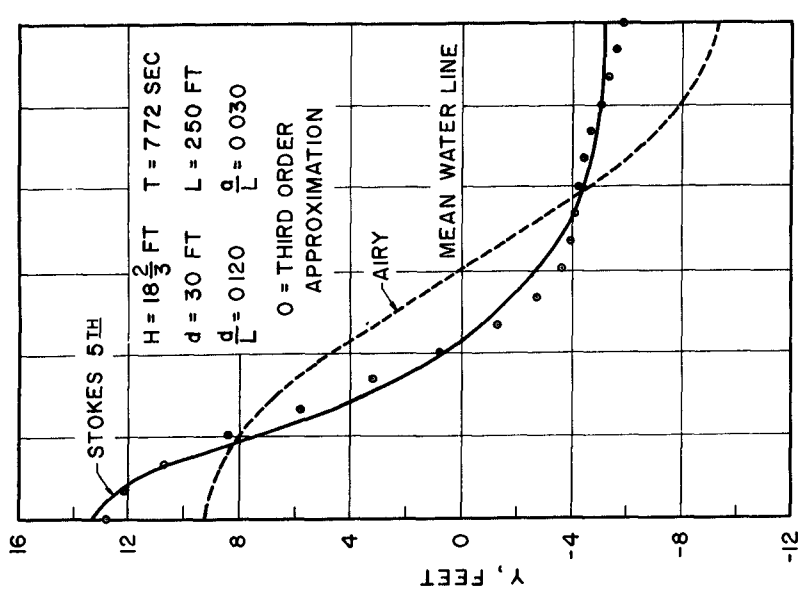

Fig. 2 - Wave profile

Other constants:

$C_1 = 4.8600 \quad C_3 = 0.2328 \quad \sinh \beta d = 0.8275$

$C_2 = 88.6250 \quad C_4 = 0.4314 \quad \cosh \beta d = 1.2980$

Substituting these constants into equations 12, 10, 9, and 1 the following results are obtained.

Wave velocity: $\overline{C} = 32.39$ ft/sec
Wave length: $L = \overline{C}T = 250$ ft.

Wave profile:

$$y = 7.50 \cos \Theta + 3.35 \cos 2\Theta + 1.48 \cos 3\Theta + 0.70 \cos 4\Theta + 0.35 \cos 5\Theta$$

Horizontal particle velocity:

$$u = 6.186 \cosh \beta s \cos \Theta + 1.434 \cosh 2\beta s \cos 2\Theta + 0.205 \cosh 3\beta s \cos 3\Theta + 0.021 \cosh 4\beta s \cos 4\Theta - 0.003 \cosh 5\beta s \cos 5\Theta$$

The wave profile is plotted in Fig. 2 together with profile obtained by the Airy theory-points obtained from the Third Order Approximation as also shown on the same graph.

The horizontal particle velocity distribution at the crest station ($\Theta = 0$) is plotted in Fig. 3 together with the velocity distribution obtained by the Airy theory.

NOMENCLATURE

$\overline{C}$	=	Wave celerity
Θ	=	$\beta (X - \overline{C}r)$ = phase angle
β	=	$2\pi / L$
L	=	Wave length
d	=	Mean water depth
H	=	Trough to crest wave height
T	=	Wave period = $L/\overline{C}$
P	=	Absolute pressure
X	=	Horizontal coordinate distance, measured from crest

t	=	Time
S	=	Vertical coordinate distance, measured positively upwards from mud line
y	=	Profile coordinate, measured positively upward from mean water line
ϕ	=	Velocity potential function
∇^2	=	Laplacian operator = $\partial^2/\partial x^2 + \partial^2/\partial y^2$
c	=	$\cosh \beta d$
s	=	$\sinh \beta d$
v	=	Vertical particle velocity
u	=	Horizontal particle velocity
λ	=	βa
a	=	A constant to be determined for each wave
Lo	=	$\frac{gT^2}{2\pi}$ = wave length for "deep-water" wave

REFERENCES

1. Skjelbreia, Lars, Gravity Waves Stokes' Third Order Approximation Tables of Functions, (June 11, 1958).

2. Wilton, J. R., On Deep Water Waves, Phil. Mag. S. 6 Vol. 27, No. 158, (Feb. 1914).

WADDEN AREA

PART 2

BEACH AND SHORELINE PROCESSES

WALCHEREN DIKE

Chapter 11

THEORETICAL FORMS OF SHORELINES

W. Grijm
Engineer Coastal Research Department
Rijkswaterstaat, The Hague, Netherlands.

INTRODUCTION.

In previous publications Pelnard-Considère, Bruun and Larras have derived theoretical shore formations. When doing so, it is necessary to idealize the conditions, such as a littoral transport by waves only, unvarying wave characteristics and a simple relation between the angle of wave approach and the littoral transport. Moreover various other simplifications have to be made in order to make it possible to handle the equations.

The question may arise whether results, obtained from such an idealized situation, have any value for practical cases, where the conditions are much more complex and variable. The answer is no when we expect to obtain a true and detailed picture of the development of any particular stretch of coast. Such theoretical exercises can be of real value, however, because they help us to understand why and how certain formations come into being and how they are influenced by certain physical processes. This is the case for instance with such formations as deltas, spits and tombolos.

We cannot say that we really know the function which determines the littoral transport. Up to now one of the simplifications in the mathematical treatment has been the restriction to stay within an area in which the values of α are so small that the transport may be assumed to increase in direct proportion to the increase of the value of α (α being defined as the angle between the wave direction and the direction of the normal on the coast in the point considered). However, experiments indicate that the littoral transport very likely reaches a maximum for a wave angle between 45° and 60°. Interesting phenomena are bound to occur when this maximum is approached.

With this in mind we have tried to introduce a transport function $T = A \sin 2\alpha$, having its maximum when $\alpha = 45^{\circ}$.

THE MATHEMATICAL TREATMENT.

Considering a stretch of shore of length ds (fig. 1), the quantity of deposited (or eroded) material must be equal to the difference between the quantity of transported material in A and in B. Expressed by mathematical terms, we have:

$$-D \frac{\partial y}{\partial t} \, dl \, dx = \frac{\partial T}{\partial x} \, dx \, dt$$

or

$$\frac{\partial T}{\partial x} + D \frac{\partial y}{\partial t} = 0 \qquad (1)$$

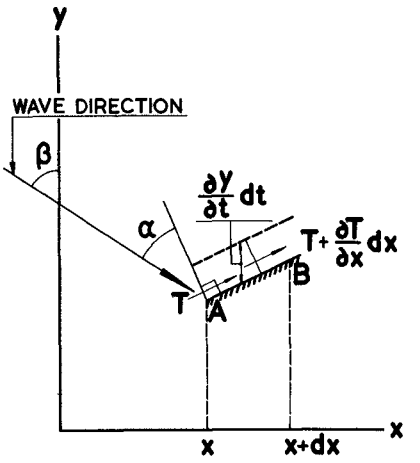

Fig. 1

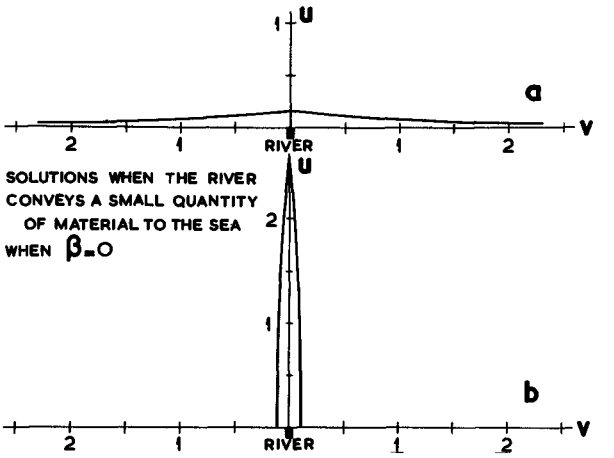

Fig. 2

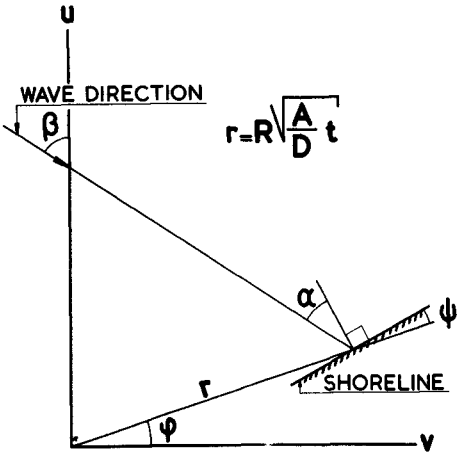

Fig. 3

in which:

T is the transport function
D is the waterdepth
t is the time
x and y are the coordinates

In fig. 1 the angle β defines the wave direction with respect to the system of coordinates and the angle α the value of T. Since we take T only depending on α, it is sufficient to differentiate T to one variable. Substituting $T = A \sin 2\alpha$, the equation (1) can be worked out as:

$$\frac{4A\cos 2\beta}{D} \cdot \frac{1 + 2\tan 2\beta \frac{\partial y}{\partial x} - \left(\frac{\partial y}{\partial x}\right)^2}{\left[1 + \left(\frac{\partial y}{\partial x}\right)^2\right]^2} \frac{\partial^2 y}{\partial x^2} = \frac{\partial y}{\partial t} \qquad (2)$$

In order to obtain a set of solutions suitable to our purpose, we shall confine ourselves to such coastlines as remain similar in shape whereas the scale of this shape is varying in the course of time. Hence we introduce new variables u and v, proportional to y and x respectively and we require that there exists a functional relation between u and v independant of the time t. An important property of this type of solutions derives from the fact that the transport along the coast depends on its direction only. Since the direction in a point of the coastline is independant of the scale, the transports at the end of a coastline segment remain constant, so that the volume behind this segment must increase proportional to t. Some of these solutions, therefore, are suitable more in particular to describe the development of a delta of a river which charges the shore with material at a constant rate. By the substitution:

$$y = u\sqrt{t} \qquad x = v\sqrt{t}$$

the differential equation (2) reduces in the requisite way to

$$\frac{4A\cos 2\beta}{D} \frac{1 + 2\tan 2\beta \frac{du}{dv} - \left(\frac{du}{dv}\right)^2}{\left[1 + \left(\frac{du}{dv}\right)^2\right]^2} \cdot \frac{d^2u}{dv^2} + v\frac{du}{dv} - u = 0 \qquad (3)$$

provided the depth is taken as a constant, which means that the seabed is horizontal.

This equation can be simplified somewhat further for a few special cases. First we consider the case in which $\tan 2\beta$ and $\frac{du}{dv}$ are very small in comparison with unity. The equation (3) then yields:

$$a\frac{d^2u}{dv^2} + v\frac{du}{dv} - u = 0$$

in which

$$a = \frac{4A\cos 2\beta}{D}$$

The solution of this equation is:

$$u = C_1 \left(e^{-\frac{v^2}{2a}} + \frac{v}{a} \int_{\infty}^{v} e^{-\frac{v^2}{2a}} dv \right)$$

when the shore at time t = 0 is a straight line. In a slightly differ form this solution has already been presented several times in previo publications.

Likewise we can consider a second case where tan 2β is very sma and $\frac{du}{dv}$ so large that we can now neglect the first and second terms o the numerator and the first term of the denominator of the fraction i (3). This equation turns now into:

$$-a \frac{\frac{d^2u}{dv^2}}{\left(\frac{du}{dv}\right)^2} + v \frac{du}{dv} - u = 0$$

of which the solution is:

$$v = C_1 \left(e^{\frac{u^2}{2a}} - \frac{u}{a} \int_{0}^{u} e^{\frac{u^2}{2a}} du \right)$$

also when the shore at time t = 0 is a straight line. Figure 2 shows t diagrammatical representation of these two special cases in which β do not differ much from zero while the quantity of material that the rive conveys to the sea is small in comparison with the transport of the coastal regime.

It can be shown that the numerator of the fraction in the equatio (3) becomes zero in the point where $\alpha = 45^\circ$. This means that in that point either $v\frac{du}{dv} - u$ must be zero or $\frac{d^2u}{dv^2}$ becomes infinite. The first solution corresponds to the trivial case of a straight line through th origin. The second solution means that the variation in the gradient o the tangent divided by the variation in v, is infinite. That indicates an abrupt change in the direction of the coastline at the point in question. From a physical point of view, however, we cannot have a sudden jump in the quantity of material transported. Hence, such a poi must be a cusp.

These results can be obtained from analytical considerations of equation (3). For more general solutions it is necessary to integrate this equation numerically. Then it is more convenient to use polar-coordinates instead of Cartesian coordinates and to introduce two parameters, viz. the angle α mentioned before and the angle ψ between the shoreline and the radius-vector (fig. 3). We obtain the following syste of two simultaneous equations

$$d\varphi = 2\cos 2\alpha \, d\alpha = \frac{1}{2} R^2 d\psi \qquad (4$$

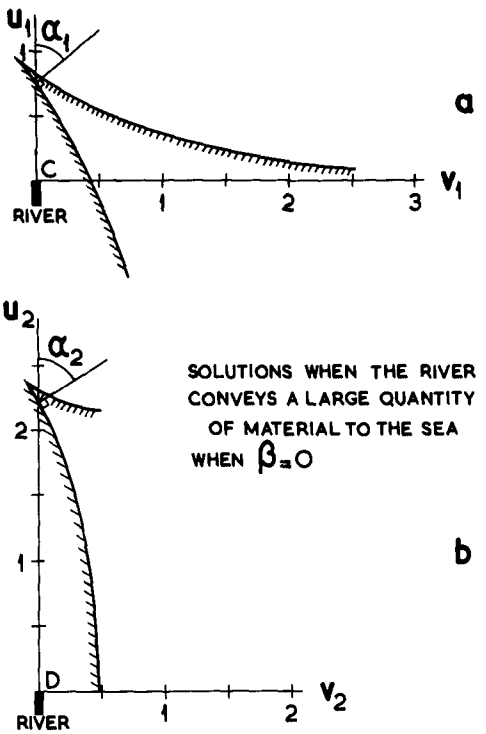
u_1
α_1
a
C
RIVER
1
2
3
v_1
u_2
α_2
SOLUTIONS WHEN THE RIVER CONVEYS A LARGE QUANTITY OF MATERIAL TO THE SEA WHEN $\beta=0$
b
2
1
D
RIVER
1
2
v_2

Fig. 4

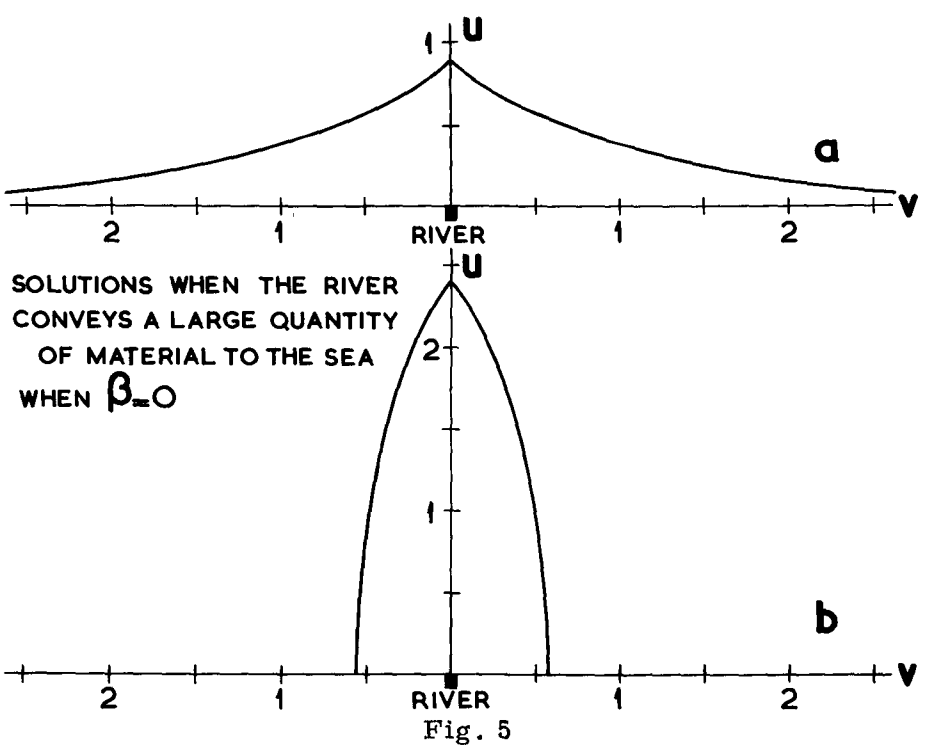
u
1
a
2
1
RIVER
1
2
v
SOLUTIONS WHEN THE RIVER CONVEYS A LARGE QUANTITY OF MATERIAL TO THE SEA WHEN $\beta=0$
u
2
1
b
2
1
RIVER
1
2
v

Fig. 5

$$\tan \Psi \, dR = R \, d\varphi \tag{5}$$

in which φ en Ψ are linked by

$$\alpha + \varphi + \Psi = \beta \tag{6}$$

The equation (4) determines the displacement of the shoreline and corresponds with equation (3). The equations (5) and (6) are geometrical conditions. Q is defined as $\frac{I}{A}$ for which we adopted the function sin 2α.
Solutions are being constructed by means of a computer. By this way of approach it will also be possible, if necessary, to adopt other functions for Q and to alter the assumption that the seabed is horizontal.

In the solutions two integration parameters appear. We intend to produce sets of curves for various values of these parameters. At the moment we write this paper, we are still engaged in pursuing this programme and we have to confine ourselves to show a few preliminary results. Two of the solutions obtained so far with β equal to zero, are shown in the figure 4a and 4b. The curves are solutions which obey the differential equations and each of them has a special value of one of the integration parameters. Mathematically the solutions are correct, but the question is whether physical conditions can be found corresponding to them. This can be done by locating the initial shoreline along the axis v_1 and v_2 and in C and D the mouth of a river conveying a quantity of material corresponding with the angles α_1 and α_2. In this figure 4 we recognize the solutions shown in figure 2. Now, however, the solutions are not restricted to the condition that the ratio between the quantity of material transported by the river to the sea and the quantity which the coastal regime is able to convey, is small. As a matter of fact figure 5 shows the solutions in which α_1 and α_2 are equal to 45°. The ratio mentioned before is then equal to 2.

The work is being continued and further publication of the result is intended.

I wish to thank Dr. Schönfeld of our Department for his aid in the mathematical treatment of the problem.

References.

Bruun, P.: Forms of equilibrium coasts with a littoral drift. Univ. California, Institute of Engineering Research, No. 347, Febr. '53.

Pelnard-Considère, R.: Essai de théorie de l'évolution de sables et de galets: IV Journées de l'Hydraulique, Question III, rapport 1, juin '56.

Larras, J.: Plages et côtes de sable: Collection du Laboratoire d'Hydraulique, Eyrolles '57.

CHAPTER 12

WAVE EFFECT ON THE COAST FORMATION AND EROSION

Walenty Jarocki
Professor, Construction Engineering
Institute, Warsaw

KINDS OF SEDIMENT MOVED BY WAVES

Sediment may be moved in consequence of the action of wind waves and of water currents. These two factors may act separately or together.

Sediment may be divided into 3 types: suspended load, bed load and detritus load. Depending on kind of movement of particles a bed load may be: rolled, slip, sprung and swollened.

In the near-shore or in the open zone for waves the bed load and detritus load moves mostly in consequence of the action of wind waves. In open zones for waves where the tidal flow and tidal fall are appearing, the bed and detritus load are moving inconsequence of the action of the wind waves and of water currents.

The wind waves usually are small and the velocity of water currents may be larger in the narrow and long straits. Therefore the water current is in these zones the principal factor which moves the suspended, bed and detritus loads.

The wind waves and water currents move the suspended, bed and detritus loads in the shallow external zones of the water area especially if the bottom is argillaceous.

VARIOUS DEPTH EFFECT ON THE SEDIMENT MOVEMENT

The waves may cause the sediment movement on the depth equal about 0,4 of the greatest possible length of wave. Intensity of waves action decreases when the depth of sea decreases. Therefore in the shallow parts of sea the waves cause a larger scoure of bottom and they raise a great quantity of sediment. If the sea has a great depth then the scoure of the bottom and the raising of sediment may be caused only by means of heavy waves.

The waves are moving a suspended load towards the wave propagation and in the opposite direction. Thus the suspended load are moving from a shallow parts of the sea to a deep parts in which the transport of suspended material is smaller. In these deep parts a suspended load may fall on the bottom. Thus the bottom erosion takes place in shallow parts of sea and the accumulation of sediment in deep parts.

INVESTIGATION OF THE ACTION OF WAVES ON THE SEDIMENT MOVEMENT.

Various authors explain differently the mechanism of action of waves on the sediment movement. Some authors consider that the waves are raising the soil fractions from the bottom and water currents transfer them along the seaboard. The other authors suppose that each wave shears some soil in the bottom in littoral zone of the waves and wind is oblique to the shoreline. Beach currents catch and transport the sediment particles along the seaboard.

These authors suppose when the wind is in the direction of seaboard /from sea/ then the bottom currents move in the opposite direction. These currents transport the ground particles in the direction of sea and thus the seaboard erosion arises. When the wind direction is opposite, the botto currents arise in the direction of seaboard and they cause the transportation of ground and the accumulation of seaboards

These reasons show that the action of waves would cause only the separation of ground particles and their ascending.

Our last investigations and observations of the sediment movement have led the conclusion that the waves may cause the raise of the sediment partciles and also their tran port . The character of this transport depends on the wave kind and on the height and length of waves.

General quantity of the lifted particles by means of waves increases as the power of waves or height and length of waves increases. If the power of waves decreases these particles fall.

The waves are able to transport the bed load and detritus load without cooperation of the water current in spite of horizontal or inclined bottom. Under the action of waves the sediment moves the oscillatory movement.

The waves move the bed load in the shallow exterior zones with the horizontal bottom only, towards the wave propagation. This material may be moved perpendicular the slope, according to the wave direction or in the opposite on

If the approaching wave creates the acute angle to the shoreline then the bed load moves near the seaboard.

The transport of the bed load and of detritus loa change if the water current and waves appear simultaneously. The water current acts generally on the detritus load becaus the water moves this material easier than the bed load which rolls on the bottom.

COAST FORMATION AND EROSION

The action of waves causes the movement of suspended load from zones with a great quantity of this material to zones with a smaller one.

The observations are showing that the bottom and the board slope of the shallow open zones consists usually of the coarse-grained particles because their raising is difficult. This phenomenon may be explained this way, the all light clayey close-grained particles were lifted up firstly and than they fell in deep zones.

The movement of waves is the main factor which causes the formation of the coast and bottom in littoral zones. The action of waves may cause the erosion of seaboard or may cause the accumulation of coast. The investigations showed that the short waves cause the erosion of seaboard and the long ones - the accumulations /fig. 1,2,3/.

The process of action of waves be divided into 3 stages. In the first stage, when the wave reaches the critical depth, the wave crest comes down, pierces the water mass and attaines the slope surface. The orbital velocities of the superficial particles of water are always larger then the near-bottom velocities. Therefore the superficial particles of water carry along the ground particles from the slope to the limit of the critical depth because they keep the rotary motion.

Thus the cylindrical hollow arises on the slope in this place, where the water strikes. The ground particles move down of the slope and underwater rampart raises about hollow.

In second stage the wave strikes against a water surface and it causes the two new waves which strike against a slope. The strokes of these waves are weaker than the strokes of the main first wave. In that way these two new waves produce two hollows and two ramparts on the slope. The size of these hollows and ramparts decreases as they approach to the water surface.

In the third stage the oscillatory motion of water particles turns into translatory motion and it cause the uprush.

At first the velocity of movement of the rampart and hollow down is considerable, later this velocity quick decreases and the rampart and hollow become stable.

The length of way from the place of the formation of underwater rampart to the lasting position may be taken

$$l_1 = 5/2h/$$

The water depth above rampart in the stage of stabilization

$$H_1 = 0,75/2h/$$

The depth above hollow

$$H_2 = 1,6/2h/$$

The depth above hollow is proportional to 2 h and inversely proportional to D and i

$$H_2 = f/\frac{2h}{Di}/$$

The distance between the top of the rampart and the centre of hollow

$$l_2 = 3/2h/$$

The average width of the erosion on the slope

$$l_3 = 6/2h/$$

where : 2h - length of wave
D - dimension the sediment partioles
i - wave steepness.

The process of the action of the long waves is other than the action of short ones. The intensity of the subsidence of wave crest is smaller and the second new wave do not formed. The larger quantity of water goes up slope and this water turns into the uprush.

When the slope consists of impervious ground then almost all water rolls up on the slope. This water carries a ground particles which were raised first from water zones where was the critical depth. When this water meets the main beachcomber then the velocity this water decreases. At that time the ground particles fall and create a rampart of the sediment on the slope.

When the slope consists of coarse-grained soil then the considerable quantity of water penetrates in the slope and the ground particles stay on the slope near the water level. This quantity of water, which rolls on slope, is not taken of the sediment.

Therefore the long waves forme the supermarine rampart independently of inclination of slope, if it consists of coarse-grained soil.

It is the opinion that the material for formation of rampart is forthcominged from sea. The investigations showed

Fig 1

Fig 2

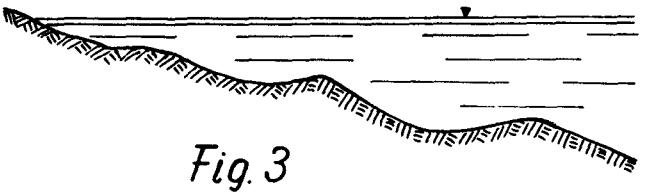

Fig. 3

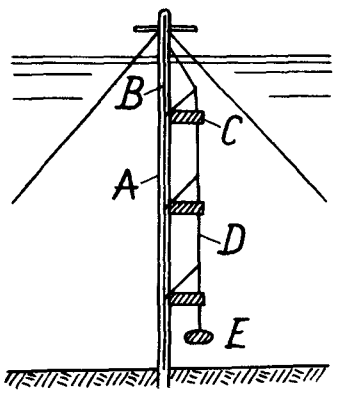

Fig. 4

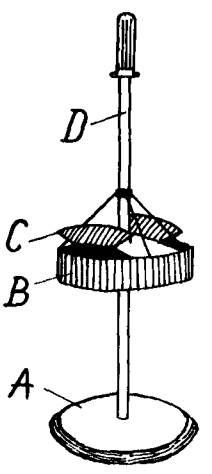

Fig. 5

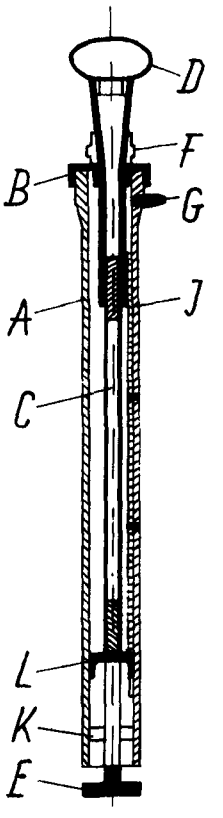

Fig. 6

Fig. 1. Action of short waves on the coast formation
Fig. 2. Action of long waves on the coast formation
Fig. 3. Cross - section of the coast after action of short waves
Fig. 4. Samoilow's device
Fig. 5. Bottom bathometer of Bozich-Guriew
Fig. 6. Water sound of Bozich

that this opinion is wrong.

At first the intensity of the board reforming is large and afterwards it decreases. The intensity depends on the board height.

INSTRUMENTS OF SEDIMENT MEASUREMENT

The transport of near-shore sediment was investigated by Samoilow's device, by bottom bathometer of Bozich-Guriew and by testing ditches and walls.

Samoilow's device /fig.4/ consists of following main parts: a/ a metallic tube A with longitudinal crenel, b/ a chain B which links are moved along the tube, c/ a set of metallic disches C with caps, fastened to the chain, d/ a wire rope D with the upper end over water-level and the lower one in water together with charge E. The disches may be opened, shuted or may be lifted along the tube.

The device plunges into water when there are no waves. The dishes are suspended along the submarine part of the tube. These dishes are filled with non-cohesive soil and they are opened in water. Systematic observations are made in time of the action of waves. When the waves are calmed down then the dishes shut and partly taken from water. The aim of this procedure is to state from which of these dishes the sand is removed. When the lower dish without ground will be taken out then the depth of plunge of this dish should be noted.

These measurements are performed with sand of various fractions. Thus the action of waves of various intensity on the movement of different particles of sediment is determined. By these measurements also the depth of the wave action of various intensity may be defined.

The bottom bathometer of Bozich-Guriew /fig.5/ consists of following main parts: a/ round metallic bedplate A with sharp borders; the thin layer of sand is pasted to the upper surface of the bedplate, b/ cylindrical cap B, which is fastened to the short tube with valves C, c/ compass which may be moved along the rod but may not be turned around, d/ the raising cap velocity regulator, e/ vertical metallic tube D, which is screwed up under bedplate of bathometer which serves to take the ground samples.

The construction this bathometer enables to load the bed sediment from all sides of the bathometer bedplate. This is important, because the diredtion of the sediment movement may be different as the direction of waves.

This bathometer serves to determine:

a/ the quantity of transported sediment in a time unit,
b/ main direction of the sediment movement,
c/ average velocity of the sediment movement,
d/ average thickness of the sediment layer.

The approximate measurements of sediment were performed in various places in bottom by testing ditches. The filling of these ditches depends on intensity of sediment movement.

Approximate quantities of sediment were determined also by means of testing walls, which were built perpendicularly to the principal direction of the sediment movement.

The measured profiles serve to compare the sediment transport in time of the action of waves of various intensity direction etc.

INSTRUMENTS OF SEDIMENT MEASUREMENT IN THE LABORATORY.

The various instruments were used in laboratory to the investigation of dynamics of suspended and ditritus sediment, to the observation of dynamics of separate particles of bed and detritus load, and to the examination of movement of near-bottom sediment.

Fixation of the dynamics of suspended and detritus load was performed by means of water sound of Bozich. This device enables the sampling of water with suspended and detritus particles in every time and in every place.

The quick sampling is necessary because the velocity of water fluctuation is large and the role of various phases of the wave action /e.g. crest and hollow/ must be fixed.

The time of sampling of water hesitates from 0, 015 to 0, 20 sec including the time of opening and of closing of sound. The device gives the possibility also of sampling of detritus load without the artificial raising of small particles which are on bottom.

The water sound /fig.6/ consists of following main parts: a/ cylindrical dish A with hermetic cap B, b/ vertical rod C with arm D above, and with buckler E below, c/ arrangement F to regulation of height opening of buckler, d/ tripod, e/ little pumping unit.

The cylindrical dish A has inside a guide rod I and guide ring K. The end of vertical rod C has the treading on which may move a piston L. This piston is connected with guide rod I, the piston L moves along the dish A if the rod C is turned.

The buckler E is fastened stationary to the rod C. This buckler is immovable, when the rod C is turned, but the piston L moves if the rod C is moved along the dish A.

The sampling of this sound consists of the following operations:

a/ putting of piston L, by revolution of arm D, in this position which allows to take the water samples of the necessary capacity,

b/ putting of regulator F in this position which insures the necessary opening device,

c/ closing of dish A from below by means of buckler E,

d/ decrease of air pressure 0,3 - 0,5 atmosphere,
e/ closing of tap G,
f/ putting of lower end of water sound in place of sampling,
g/ quick opening of device by means of arm D.

The water penetrates from below to the dish A, because the air pressure there small.

The dymamics of the separate particles of sediment was investigated by means of conventional large particles of soil and by means of floaters. As conventional particles were used: aniline drops, pea stones, small balls of plaster etc.

Intensity of the transference of bed load was examined by means of the survey of bottom profiles befor and after the investigation

REFERENCES

Bozich P.K./1948/. Wave observations and investigations.
Cebertowich R. /1958/. Model investigations of water buildings. Warsaw.
Gugniaiew J. E./1955/. Laboratory investigations of dinamics of sand slope formation. Moscow
Jarocki W. /1957/ Sediment movement in rivers. Gdynia.

CHAPTER 13

MOUVEMENTS DES MATERIAUX DE FOND SOUS L'ACTION DE LA HOULE

P. Lhermitte
Ingenieur des Ponts et Chaussees
Ministère des Travaux Publics - Paris

NOTATIONS ET SYMBOLES

a_f (1) : excursion théorique d'une partioule du fluide eain située près du fond.

a (1) : paramètre caractérietique de la houle $a = \frac{\pi}{L}$.

b : paramètre caractérietique de la houle $b = \frac{\pi}{T^2}$.

D : diamètre dee partioulee.

d : demi-distance entre axes des rides.

h : demi-amplitude de la houle.

L : demi-longueur d'onde de la houle.

p : preesion.

p^* : partie variable de la preseion.

T : demi-période la houle.

t : temps.

u : viteese horizontale.

u_M : viteeee maximum dans le fluide.

u_f : viteeee théorique maximum près du fond.

$u\delta_M$: viteeee théorique maximum à la frontière de la couche limite.

$u\delta$: viteeee à la frontière de la couche limite.

v : viteeee verticale.

w : viteeee de chute.

δ : épaiseeur de la couche limite.

$\bar{\delta}$: valeur réduite de δ. $\bar{\delta} = \sqrt{\frac{b}{\nu}}\,\delta$

δ_{th} : valeur théorique caractérietique de l'épaieseur de la couche limite.

$$\delta_{th} = \sqrt{\frac{\pi}{2}}\sqrt{\nu T}$$

ε : dimension de la rugoeité.

ν : coefficient de viscosité cinématique.

ν_r : viecoeité relative.

ρ : densité dee matériaux.

ρ_0 : densité du fluide.

S : demi-amplitude de la ride.

τ : force de frottement.

X : paramètre sans dimension :

$X_1 = \frac{b^{1/2} p^*}{\nu^{1/2} \rho g}$ (paramètre caractérietique de la etabilité de la couche limite et de la formation dee rides).

$X_2 = \sqrt{\frac{u_f}{(\nu b)^{\frac{1}{2}}}} \cdot \frac{\partial}{\partial x}\left(\frac{2p^*}{\rho g}\right)$ (paramètre caractérietique du mouvement en masse du sable).

(1) Il importe de bien noter que a_f a lee dimensions d'une longueur, alors que a a les dimensions de l'inverse d'une longueur.

INTRODUCTION

Nous exposerons dans cet article, les résultats d'expériences que nous avons obtenues, relativement aux mouvemen des matériaux de fond sous l'action des houles progressives, et nous tenterons de fournir des schémas d'explication des différen phénomènes observés.

Certains aspects des mouvements de matériaux sous l'action des houles, ne peuvent s'expliquer que par l'extension de certains phénomènes hydrauliques liés à la propagation des houles progressives : répartition des courants d'entraînement, effet de viscosité des fluides, développement de la couche-limit près du fond, etc ....

Nous nous bornerons d'ailleurs dans cette étude, à la description des mouvements de matériaux, qui dépendent directemer des caractéristiques hydrauliques du mouvement du fluide, et plus particulièrement des caractéristiques de la couche limite, mais nous ne nous attacherons pas à l'étude de l'influence des caractères géologiques ou sédimentologiques du matériau sur le comportement de ce dernier, l'étude détaillée de ces phénomènes sortant du cadre de cette étude.

Sans exposer de façon complète et rigoureuse les phénc mènes hydrauliques, il nous a semblé utile, pour la compréhensior du texte, d'indiquer sommairement certains aspects shhématiques de ces phénomènes. Les lecteurs désirant approfondir ces questions pourront se reporter aux ouvrages cités en bibliographie -(6) (7) pour les courants d'entrainement, (3) et (4) pour les phénomènes de couche limite.

a) Les courants d'entrainement.

Différents auteurs, et en particulier M. MICHE, dans un article paru aux Annales des Ponts et Chaussées en 1942, ont mont que les mouvements périodiques progressifs d'un fluide (houle) n'étaient définis par les conditions aux limites, qu'à un paramèt près : la distribution du rotationnel le long d'une verticale. Il en résulte donc qu'il existe une simple infinité de houles de caractéristiques données. Physiquement ces différentes houles se distinguent par la distribution des courants moyens d'entrainemen dans l'épaisseur de la lame d'eau.

En pratique, les houles naturelles, comme les houles de laboratoire, présentent en l'absence de phénomène perturbateur (action du vent, courant marin, etc...) une distribution caractéristique de ces courants d'entrainement, signalé en particulier p de Coligny et Longuet Heggins :

- en surface et près du fond le courant d'entrainement est dirigé dans le sens de propagation de la houle,

- au centre de la lame d'eau, le courant d'entrainement est dirigé dans le sens contraire de propagation de la houle.

Une houle théorique répondant à ces caractéristiques peut donc être déterminée par extension des résultats de M. MICHE, en introduisant une double distribution de rotationnel l'une traduisant l'influence des effets de surface, l'autre traduisant l'influence des effets de fond.

On obtient alors le résultat schématisé sur la figure ci-dessous :

DISTRIBUTION DES VITESSES D'ENTRAINEMENT DANS UN MOUVEMENT DE HOULE PERIODIQUE PROGRESSIVE

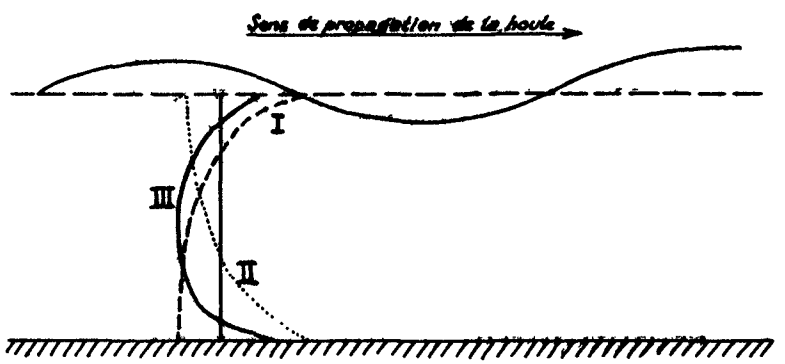

I) Courbe des vitesses d'entrainement dues à un rotationnel de surface.
II) Courbe des vitesses d'entrainement dues à un rotationnel de fond.
III) Courbe composée en accord avec les observations.

b) Influence de la viscosité - Couche-limite.

Du point de vue théorique, l'introduction de ces rotationnels traduit l'influence de la viscosité du fluide, influence particulièrement sensible près des interfaces supérieure et inférieure.

En fait, les manifestations de la viscosité près du fond - interface inférieure - sont particulièrement importantes, et donnent lieu à l'existence d'une "couche-limite", dont l'importance est fondamentale dans le mouvement du fluide. Nous avons étudié les différents aspects de la couche-limite : couche limite laminaire, couche limite turbulente, couche limite partiellement turbulente, ainsi que les conditions de stabilité et l'influence de la couche limite sur le mouvement du fluide supérieur (fluide sain).

Nous indiquerons rapidement certaines caractéristiques des couches limites des houles en fonds fixes, ces résultats permettent de mieux comprendre les interactions entre le fluide et les matériaux lors de l'étude des mouvements de matériaux de fond sous l'action de houles.

c) Couche limite laminaire.

Tant que l'amplitude des houles ne dépasse pas une certaine valeur critique, on observe des couches limites près du fond parfaitement laminaires. Il est aisé de mettre en évidence, dans ce domaine, la couche limite laminaire, par la méthode colorimétrique, car celle-ci est très nettement différentiable du fluide situé hors de son domaine par sa coloration intense et surtout par la vitesse moyenne d'entrainement qu'elle présente très supérieure à la vitesse d'entrainement du fluide sain à la frontière de la couche limite.

En effet, la particularité essentielle des couches limites laminaires consiste dans l'existence d'une vitesse d'entrainement moyen dans le sens de propagation de la houle correspondant à un débit de fluide relativement important dans la zone située près du fond. Cette particularité qui permet de mettre nettement en évidence la couche limite, au cours des expériences, ne peut s'expliquer par les théories classiques de la houle. Elle est étroitement liée à la manifestation des forces de viscosité dans la couche limite.

Lorsque l'on observe attentivement la couche limite d'houle cylindrique de laboratoire, on observe en plus de ce débit moyen une " respiration" de la couche limite correspondant à une variation d'épaisseur au cours du temps. Enfin, d'une façon très générale, au cours du mouvement retour des particules du fluide, on observe également un décollement caractéristiques de la couche limite.

d) Couche limite turbulente.

Lorsque l'amplitude de la houle est suffisamment élevé et lorsque la rugosité du fond est suffisamment forte, la couche

limite est instable et l'observation colorimétrique met en évidence une émission particulièrement active de turbulence près du fond. Il s'agit alors d'une couche limite turbulente dont les mouvements moyens d'entrainement sont beaucoup moins importants que ceux observés au cours de l'étude des couches limites laminaires et fortement aléatoires, pouvant d'ailleurs être dirigés, soit dans le sens de propagation de la houle, soit dans le sens contraire.

L'émission de turbulence provenant de l'instabilité du mouvement, par suite de l'action de la viscosité dans la zone où se développe la couche limite, se traduit par une contamination du fluide sain qui devient progressivement également turbulent sur une hauteur importante.

Nous avons étudié ces divers phénomènes et donné des valeurs pratiques de leur domaine d'existence.

e) Couche limite partiellement turbulente.

Avant d'observer une couche limite totalement turbulente, on peut observer des couches limites présentant des phases sporadiques d'instabilité (émission de bouffées turbulentes) tandis que le mouvement dans son ensemble comporte les caractéristiques d'une couche limite laminaire (mouvement moyen dans le sens de la propagation de la houle, décollement, hauteur variable au cours d'une période de mouvement). Il semble que ce phénomène ne constitue pas uniquement un phénomène de transition entre la couche limite laminaire et la couche limite turbulente mais qu'il dépend, non seulement des conditions de stabilité près du fond, mais également de l'influence du mouvement général du fluide sur la stabilité de la couche limite.

Nous abordons ici un caractère particulier des couches limites des mouvements à déplacement moyen négligeable pour lesquelles l'influence du mouvement du fluide sain semble aussi importante sur la couche limite que l'influence du fond. Dans le cas particulier des houles, de nombreux phénomènes exigent, pour pouvoir être compris, de ne pas perdre de vue que le mouvement orbitaire caractéristique de la houle qui correspond à un mouvement particulièrement stable par suite de la faible consommation d'énergie dans le fluide sain comporte une certaine "rigidité" qui impose son influence sur les mouvements de la couche limite d'une façon comparable à l'influence de la paroi.

f) Influence de la couche limite sur le mouvement du fluide sain.

Si le fluide sain exerce une influence importante sur le développement de la couche limite, réciproquement le mouvement de celui-ci ne peut pas être étudié séparément de celui de la couche limite. Nous avons déjà dit que dans le cas d'une couche limite totalement turbulente, l'existence de celle-ci entraînait une émission continue de turbulence dans la zone du mouvement du fluide sain,

c'est-à-dire dans la zone du mouvement où la viscosité du fluide ne constitue pas un facteur d'émission de turbulence, mais constitue au contraire, un facteur d'évolution de la turbulence.

o

o o

Jusqu'à présent nous avons admis - en particulier en ce qui concerne les phénomènes de couche limite - que les fonds étaient invariables (fonds fixes). Mais si les fonds sont constitué de matériaux mobiles les interactions entre le fluide et les matériaux de fond modifient sensiblement l'aspect de l'écoulement.

Réciproquement, l'action du fluide sur les matériaux constitutifs du fond, provoque dans certaines conditions, la mise en mouvement de ceux-ci. Les mouvements du fluide près du fond, et ceux des matériaux de fond, réagissent alors les uns sur les autres, et les phénomènes sédimentologiques et hydrauliques deviennent alors indissolublement liés.

Nous exposerons successivement les mouvement sous l'action de la houle des matériaux pulvérulents du type sable, c'est-à-dire formés d'un ensemble de grains ne présentant pas de cohésion entre eux, puis les mouvements de matériaux du type vase c'est-à-dire formant une phase fluide homogène possédant une certaine cohésion et distincte du fluide dans lequel se propage la houle.

A - MOUVEMENTS DES MATERIAUX PULVERULENTS

I - ETUDES RECENTES CONCERNANT LES MOUVEMENTS DE MATERIAUX SOUS L'ACTION DE LA HOULE.-

De nombreux ouvrages ont été publiés, qui traitent du mouvement et du transport des matériaux - et en particulier des sables - sous l'action de la houle. La majorité de ces études concerne essentiellement le transport littoral ou les transports provoqués par des courants (rip-currents, courants de fond, courants de masse); d'autres donnent des renseignements fragmentaires sur le profil d'équilibre des plages de sable sous l'action moyenne de la houle. L'ensemble de ces études représente une documentation extrêmement intéressante; mais rares sont les auteurs qui se sont préoccupés du mouvement des matériaux provoqués, en eau profonde ou moyennement profonde, par l'action d'une houle cylindrique sur le fond; quant à la corrélation existant entre les mouvements de matériaux et les phénomènes de couche limite, elle n'est qu'effleurée lorsqu'il en est question.

Trois études méritent toutefois une mention spéciale par le sujet qu"elles traitent et les résultats récents qu'elles apportent.

a) Etude de M. LARRAS sur l'effet de la houle et du clapotis sur les fonds de sable, présentée aux IVes Journées de l'Hydraulique, 1956 (2).

L'étude de M. LARRAS a essentiellement porté sur les limites inférieures d'érosion alternative des fonds de sable sous l'action d'un clapotis. Le critère adopté par M. LARRAS pour définir le seuil d'érosion des sables correspond, non aux mouvements des grains en surface, mais essentiellement à l'apparition d'une érosion périodique sur le fond, du type ride, pouvant d'ailleurs ne s'effectuer qu'au bout d'un temps relativement long. Les études de M. LARRAS ont, d'autre part, permis de déterminer les profondeurs maxima d'érosion sous l'influence d'un clapotis. Quelques essais ont également été réalisés, en ce qui concerne l'action des houles pures sur les fonds de sable. Nous nous servirons des résultats obtenus par cet auteur au cours de nos études.

b) Communication de MM. VINCENT et RUELLAN au Comité Technique de la S.H.F. en Juin 1957, intitulée Mouvement solides provoqués par la houle sur un fond horizontal (15).

Les essais effectués par MM. VINCENT et RUELLAN au Laboratoire hydraulique de la S.O.G.R.E.H.A. étaient, en certains points, comparables, dans leur but, à ceux que nous avons effectué au Laboratoire Central d'Hydraulique de France. Ils ont distingué trois formes de mouvements de sable : mouvement de grains en surface, formation des rides, mise en saltation. Ces auteurs se sont particulièrement attachés à déterminer, dans la mesure du possible, les débits qui pouvaient être provoqués par l'action de la houle sur des fonds de sable. Si, dans l'ensemble, leurs résultats d'expériences sont comparables aux nôtres, ces auteurs n'ont pas donné d'explication en ce qui concerne les processus fondamentaux de formation des rides; ils ont, d'autre part, attribué aux courar de masse, le transport des sables près du fond, alors que celui-ci doit être relié directement à la vitesse moyenne, qui se développe dans une couche limite laminaire, ou partiellement turbulente, phénomène qui constitue une loi générale indépendamment des conditions aux limites.

c) Etude de M. MADHAV MANOHAR(5) publiée dans le Beach Erosion Board, n° 75, 1955.

Cette étude est particulièrement intéressante car l'auteur se proposait d'étudier le mécanisme du mouvement des sédiment sur le fond, sous l'action des vagues, en les reliant directement aux phénomènes de couche limite. En fait, cette étude fut le prolo gement de celle effectuée par M. HUON Li (1) sur la stabilité de l couche limite du mouvement des vagues, au Laboratoire de Berkeley

(U.S.A.). Ce dernier avait effectué une étude purement hydraulique, et M. MADHAV MANOHAR a utilisé la même méthode pour étudier le mouvement des sédiments de fonds (sable) sous l'action de la houle. Rappelons que cette étude, dans le but de couvrir un domaine comprenant, en particulier, les houles réelles, avait consisté à faire osciller le fond du canal d'essais, dont la masse d'eau restait immobile; le matériau mobile, dépose sur le fond, oscillait avec celui-ci.

L'auteur reconnait lui-même que les résultats obtenus concernant les mouvements de matériau, sont sujets à de nombreuses réserves, par suite des effets de vagues stationnaires et courants secondaires, qui pouvaient être engendrés par la paroi. D'autre part, les réserves qui doivent être formulées, au sujet de l'étude hydraulique effectuée dans les mêmes conditions, sont à fortiori valables pour l'étude sédimentologique : la masse d'eau restant immobile, l'oscillation du fond est d'autant moins justifiable dans ce cas, qu'il s'ajoute une force d'inertie des grains non négligeable, et le mouvement ainsi représenté est périodique en fonction du temps, mais non point en fonction du parcours des molécules.

Malgré ces restrictions, les études de M. MADHAV MANOHAR sont particulièrement intéressantes, car elles font apparaître la possibilité de mouvements dont les processus sont tout à fait différents, suivant l'amplitude des mouvements envisagés sur le fond :

1. Mouvements isolés des grains;

2. Formation des rides;

3. Disparition des rides et mise en saltation des grains.

La partie de nos études, qui concernait les matériaux de faible densité, a mis en évidence les mêmes étapes, mais nous n'avons pu retrouver, avec les houles de laboratoires, la troisième étape "disparition des rides et mise en saltation", pour des matériaux de densité supérieure à 2.

Etant donné qu'il est certain qu'une telle mise en saltation s'effectue dans la nature pour les houles de tempêtes, il est particulièrement intéressant qu'au cours de ses essais M. MADHAV MANOHAR ait pu réaliser ce phénomène.

Ces résultats permettent en fait, d'extrapoler dans une large mesure les résultats de nos expériences.

D'autre part, M. MADHAV MANOHAR a constaté que l'apparition d'un mouvement totalement turbulent du fluide, au-dessus des matériaux, avait lieu lorsque les grains étaient mobiles, bien plus tard que lors des études de M. HUON Li, effectuées avec des rugosités fixes.

Ce résultat est à rapprocher des conclusions auxquelles nous avons abouti, au cours de cette étude, concernant la stabilité relativement grande de l'écoulement au-dessus des rides, et l'existence de couche limite à caractéristiques laminaires lors de la mise en suspension du matériau dans la masse.

II - OBSERVATIONS EFFECTUEES SUR LES MOUVEMENTS DE MATERIAUX PULVERULENTS.

1°) Condition de réalisation des essais.-

Les essais relatifs aux mouvements de matériaux ont été réalisés dans le grand canal vitré du Laboratoire Central d'Hydraulique de France.

a) Caractéristiques des matériaux utilisés.

Les études ont porté sur sept matériaux différents, dont les caractéristiques physiques figurent dans le tableau ci-dessous

Une étude complète a été faite pour les quatre premiers matériaux, différent soit par la densité, soit par la granulométr

MATERIAU UTILISE	DENSITE	DIAMETRE moyen	VITESSE chute moyenne
Bakélite	1,45	0,075 cm	3,6cm/s
	1,45	0,028 cm	1,4cm/s
Sable de Seine	2,60	0,075 cm	9 cm/s
	2,60	0,028 cm	3,9cm/s
Sable de Fontainebleau	2,60	0,018 cm	4,1cm/S
Soufre	1,88	0,075 cm	7,7cm/s
	"	0,028 cm	2,8cm/s

b)Caractéristiques des houles.

La houle reproduite dans le canal avait une longueur d'onde variant de 1 à 8m. Les expériences furent reprises pour trois hauteurs d'eau différentes: 30, 40 et 50 cm. La cambrure s'échelonnait de 0,25 à 6,6 %, la houle devenant ensuite rapidement irrégulière Quelques essais supplémentaires ont été réalisés avec 20 cm d'eau, pour des houles de 2 L = 4 m puis 2 L = 6 mètres, et des cambrures variant de 1 à 3,5 %.

c) Mode opératoire.

Le matériau était étendu sur une couche de 1
de long, 10 cm. de large et 2 cm. de hauteur. Avant chaque essai, la
surface de la couche ~~limite~~ était rendue parfaitement plane. Pour cha
essai, on laissait agir la houle pendant une demi-heure environ.

2°) Description des phénomènes observés.

Les différents mouvements de matériaux, qui
développement sous l'action d'un mouvement progressif périodique cyli
drique du fluide situé au-dessus du matériau, peuvent revêtir trois f
différentes :

- déplacement en surface d'un nombre limité de grains;

- formation de rides régulières, avec ou sans déplacement, et évoluti
de ces rides;

- mise en saltation d'une quantité importante de matériaux, avec dépl
ment en masse de celui-ci.

a) Mouvement en surface.

Du point de vue expérimental, il faut distin
le mouvement à la surface d'un fond rigide de quelques grains isolés
matériaux et le mouvement en surface d'un massif pulvérulent relative
homogène.

Les grains isolés de matériaux, à la surface
fond rigide (fond de ciment du canal expérimental), sont animés d'un
vement de va-et-vient, par roulement ou saltation sur le fond, et cec
pour des amplitudes de houles relativement faibles. Leur mouvement al
est, toutefois, plus important que leur mouvement retour, de sorte qu
sont animés d'un mouvement moyen, dans le sens de propagation de la h
comparable au mouvement moyen de la couche limite.

L'étude des conditions critiques de mise en m
vement des grains isolés, n'a pas semblé devoir conduire à des résultat
pratiques intéressants, par suite des facteurs très diversifiés inter
nant dans le processus (coefficient de forme, rugosité, stabilité du
mouvement, dimensions des grains, etc..)

Le mouvement de grains à la surface d'un massi
pulvérulent relativement homogène s'observe pour des houles de faible

amplitudes. Leur mouvement visualise, en quelque sorte, celui des particules du fluide près du fond: mouvement alternatif, avec résultante moyenne dans le sens de propagation de la houle. Ce mouvement en surface des grains cesse, en général, au bout d'un certain temps, soit par élimination de ces grains en dehors du massif pulvérulent, et l'on observe alors une progression de ces grains sur le fond rigide du canal, soit par suite de l'incorporation des grains dans le massif homogène, les grains s'enchevêtrant les uns dans les autres.

Pour certaines houles d'amplitude assez faible, on observe, en début d'expérience, un léger mouvement en surface, qui disparaît au bout d'un certain temps; les grains s'étant calés les uns contre les autres, il n'y a plus d'oscillations, même sur place.

Le mouvement en surface, pour le sable, c'est-à-dire pour un matériau pulvérulent de forte densité, n'est que rarement observé. En général, dès qu'il y a mouvement, des rides se forment.

Pour des caractéristiques de houles correspondant à la limite de la formation des rides, on peut toutefois observer des mouvements de grains s'apparentant à un mouvement en surface, mais intéressant une quantité plus importante de matériau. Ces mouvements, à l'opposé de ceux des grains isolés, semblent dépendre étroitement des perturbations apportées par le décollement de la couche limite permettant l'aspiration des grains à la couche de matériau.

b) Formation des rides.

Suivant un processus que nous analyserons ci-dessous dès que le mouvement en surface devient relativement important, on observe, à la surface du massif pulvérulent, la naissance de rides régulières.

L'existence de rides stables constitue en général, la preuve d'un équilibre dynamique, accompagné de formation de tourbillons émis à des intervalles de temps égaux à la période de la houle, et entraînant la mise en suspension d'une partie du matériau.

On observe des projections de matériau, qui entrainent la formation régulière des rides et la génération de rides nouvelles. Corrélativement, se développe une turbulence partielle de la couche limite, qui propage la formation des rides par la houl

Ces rides peuvent être animées de mouvements de tran lation moyens non négligeables, en général dirigés dans le sens de propagation de la houle.

Dans une zone de rupture de pente, on observe assez fréquemment le cheminement, dans le sens opposé à la propagation de la houle, des trains de rides. Il s'agit alors d'un processus relativement complexe lié à l'évolution de la couche limite, qui tend à rétablir la continuité du mouvement. En introduisant une source colorante au sein du massif pulvérulent, on observe, dans le cas du recul des rides, les phénomènes suivants :

- il se forme une trainée colorée se dirigeant dans le sens de propagation de la houle, sur une épaisseur de l'ordre de 2mm;

- au-dessus de cette zone marginale, située à la limite supérieure du massif pulvérulent, existe une zone, dont la résultante du mouvement moyen est dirigée en sens inverse, d'épaisseur moyenne de l'ordre de 5mm environ;

- une diffusion, plus prolongée du permanganate, met en évidence la composante du courant de masse du fluide dans le sens de propagation de la houle.

c) Mouvement en masse.

Une houle de forte amplitude agit en profondeur sur la couche de matériau, et met ainsi la couche en suspension sur une épaisseur importante. Le grain individualisé est alors entrainé rapidement dans le sens de propagation de la houle. Le processus s'explique par l'action, en profondeur, dans le massif pulvérulent du gradient de pression dû à la houle. Il semble, en effet, que la mise en suspension soit le résultat des différences de pression existant entre les faces horizontales opposées de chaque grain.

Dans le cas de bakélite, dont le diamètre moyen des grains est de 0,28mm ceux-ci se regroupent toujours pendant la phase retour du mouvement de la houle, en donnant l'impression de rides, même lorsqu'il y a mouvement de toute la couche. Avec ce matériau, pour certaines caractéristiques de houles, au début de l'expérience la couche est mise en suspension sur toute son épaisseur, puis, lorsque son épaisseur est réduite par la houle à 0,5cm environ, il se forme, sur les 0,5 cm de matériau restant, des rides régulières progressant lentement vers la plage d'amortissement, suivant le processus décrit précédemment.

Tant que la couche est assez épaisse pour qu'il y ait projection, elle s'étend à l'arrière, bien que l'ensemble ait un mouvement de translation vers la plage. Dès qu'il n'y a plus projection, tout le matériau remonte vers la Plage.

En haut de la pente, on a quelquefois observé la formation de rides à l'arrière de la couche et un départ en masse à l'avant, mais ce cas est exceptionnel.

Ces observations ne sont pas contradictoires, mais mettent en évidence les différences fondamentales du processus qui régit les divers phénomènes. La formation des rides est un phénomène de stabilisation de l'écoulement, par formation périodiqu de tourbillons, tandis que la mise en saltation dépend essentiellement du gradient de pression existant dans la couche de matériau pulvérulent.

III - FORMATION DES RIDES.

1) NAISSANCE ET PROCESSUS DE FORMATION DES RIDES (Schéma 1).

Pour que les caractéristiques de la houle envisagée soient compatibles avec l'existence de rides, il est nécessaire que le nombre de grains mis en mouvement à la surface du massif pulvérulent soit suffisamment important. Pendant la période au cour de laquelle naissent les rides, et qui correspond à un régime transtoire dans le cadre du développement de l'expérience, les grains sont arrachés au massif d'une façon analogue à celle produisant uniquement les mouvements en surface, c'est-à-dire suivant un processus aléatoire. Ces particules solides révèlent, néanmoins, très rapidement une tendance à se rassembler, pour former une barre perpendiculaire au sens de propagation des lames (configuration présentant la s tabilité maximum de l'écoulement).

La distribution, dans le sens longitudinal du canal, de ces barres de très faibles dimensions, est elle-même absolument aléatoire au début du mouvement.

La présence d'une telle barre accentue le décollement de la couche limite au droit de cet obstacle, pendant la période de décélération du mouvement retour, et favorise l'arrachement et la sustentation par aspiration des grains de surface, situés à l'amont de la barre. (schéma 1a)

La mise en saltation de ces grains facilite l'entrainement de ceux-ci au cours du trajet aller des particules fluides. Les grains du matériau pulvérulent ainsi entrainés se déversent par-dessus la barre initiale. Cette configuration provoque, très rapidement, le décollement de la couche limite, pendant la période de décélération du mouvement aller, et favorise alors l'arrachement des grains situés à l'aval de la barre.

En définitive, l'obstacle que constitue la barre initiale (amorce de rides) tend à intensifier les mouvements de grains, en facilitant leur arrachement et leur mise en saltation de part et d'autre de celui-ci. Les dimensions de cette barre augmentent en même temps que raidit son profil, sous le vent de la houle. Le décollement simple de la couche limite, qui se produit

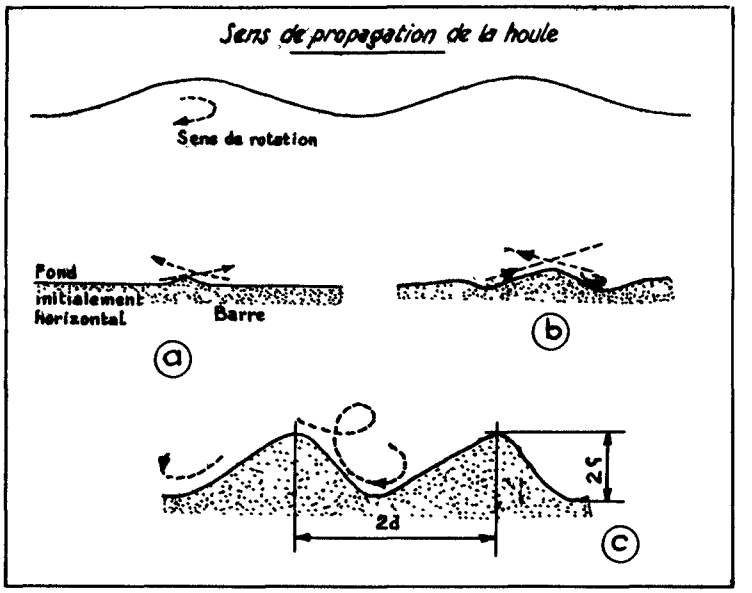

Schéma 1

à la fin du trajet aller, fait alors place à un tourbillon qui accentue, à son tour, le creusement au pied aval de la barre.

Jusqu'à l'apparition du tourbillon, phénomène qui doit se produire assez brutalement, lorsque les conditions de l'écoulement au voisinage de la barre le permettent, les particules issues des faces amont et aval de la barre, se déposent, en moyenne, dans des zones bien déterminées, à une distance qui dépe en premier lieu, des caractéristiques de la houle et des vitesses de chute des grains de matériau. Ces dépôts constituent de nouvel amorces de rides, au voisinage desquelles se développemt les mêmes phénomènes que ceux décrits plus haut.

Peu après l'apparition des tourbillons (un par rides) suivie d'une intensification des phénomènes de transfert de matériau, la couche présente un profil caractéristique en dents de scie, dont la face la plus raide correspond à la région sous le ve de la houle, la face la moins raide étant exposée au vent de la houle. (schéma 1_b)

La répartition dans le sens longitudinal du cana de ces ondulations dissymétriques, n'est toutefois pas définitive; en même temps que le profil des rides se creusent, leur répartitio varie jusqu'à être compatible avec l'établissement d'un équilibre dynamique.

Le processus, tel que nous l'avons décrit ci-dessus est particulièrement net avec les matériaux de faible densité, que nous avons utilisés. La formation de rides sur un lit de sable sous l'action de houles de laboratoire, est cependant plus long et moins caractéristique. Le processus est toutefois absolument comparable. Il se forme tout d'abord des zones privilégiées d'arrachement des matériaux de surface, formant des dépressions localisées. Celles-ci s'approfondissent progressivement et s'allongent jusqu'à ce que l'on observe nettement la formation du tourbillon caractéristique des rides. L'allongement du sillon générateur s'effectue en même temps que l'approfondissement de la partie centrale, ce qui explique la forme de croissant, à faible concavité tournée dans la direction de propagation de la houle, que l'on observe assez souvent.

2°) EQUILIBRE APPARENT DES RIDES.

Ainsi que nous l'avons vu, à une période relativement brève, au cours de laquelle la surface de la couche de matériaux initialement horizontale, se plisse pour présenter un profil en dents de scie, succède une période de pseudo-équilibre dynamique. Le fond continue à être le siège de transferts importants de grains cependant que le contour extérieur des rides semble présenter une stabilité définitive.

Lorsque cet état est atteint, l'ensemble des mouvements des particules du fluide et des particules solides se développe de la façon suivante :

α. Pendant le trajet aller du fluide sain, les forces de frottement développées dans la couche limite provoquent la remontée d'une certaine quantité de matériau le long de la face la moins raide de la ride qui vient se déverser par-dessus la crête de la ride sur la face/de celle-ci;
aval

β. Pendant la décélération du mouvement aller des particules du fluide sain au-dessus de la partie aval de la ride, il se forme un tourbillon qui constitue l'une des caractéristiques de l'évolution des phénomènes marginaux près du fond (il importe, pour bien situer le problème, de considérer que le deuxième phénomène se produit avec un certain retard dans le temps, par rapport au premier phénomène, par suite du déplacement dans l'espace. En effet, lorsque l'on parle de trajet aller ou retour, celui-ci dépend de la variable (bt - ax) . Les variations de pression consécutives à la formation du tourbillon, assure l'arrachement des particules solides du fond, et leur mise en suspension. De plus, le tourbillon reprend une partie du matériau déplacé en ;

γ. Ce tourbillon évolue et s'élève au-dessus du niveau de la ride entraînant une partie importante des grains de matériau mis en suspension;

δ. Pendant le trajet retour des particules du fluide sain, le tourbillon est entraîné, ainsi que les particules en suspension, vers l'arrière de la ride.

L'ensemble du mouvement s'effectue, en définitive, au cours d'une période égale à celle de la houle (2 T).

Le mouvement près du fond est alors devenu périodique dans le temps, et stationnaire dans l'espace (phénomène analogue aux ondes stationnaires du clapotis)(1)

3°) EVOLUTION DES RIDES.

Alors que le passage de chaque lame continue à soumettre les particules solides à un régime oscillatoire dissymétriqu une observation attentive du comportement des rides révèle que celles-ci sont l'objet d'une lente évolution.

On assiste d'abord à une régression et (ou) à une progression de certaines d'entre elles, jusqu'à obtention d'un état d'équilibre conforme aux rides régulièresde la nature. L'équilibre est atteint lorsque le tourbillon se reproduit avec des caractéristiques fixes, ce qui détermine l'amplitude des rides ($2\,\delta$) et lorsque la quantité de matériau qui est apportée à l'aval de la ride est égale à la quantité de matériau emportéepar suite de la mise en saltation sous l'action du tourbillon: ce qui détermine la distance entre rides ($2d$). (schéma 1_c)

La formation d'un tourbillon de sens opposé au tourbillon précédemment décrit, c'est-à-dire un tourbillon se formant lors de la décélération du mouvement retour des particules s'observe lorsque l'amplitude des rides devient relativement importante par rapport à la distance entre les rides. Son intensité est, en général inférieure à celle du tourbillon lié au mouvement de retour, mais il joue toutefois un rôle de stabilisateur vis à vis de la ride. En particulier, les mouvements deviennent plus symétriques, et la résultante du mouvement de la couche limite dans le sens de propagation de la houle devient négligeable.

En fait, la formation des rides correspond à une modification importante de la couche limite; d'une part les orbites des particules liées au fluide ne correspondent plus au mouvement de particules représenté valablement par les équations du fluide sain

---

(1) Cette remarque ne constitue pas qu'une image; elle explique, en fait, pourquoi la formation des rides, en présence d'un clapotis total ou partiel, est influencé par les distances entre ventres et noeuds .

qu'à une distance au-dessus de la ride au moins égale à trois ou quatre fois l'amplitude des rides, et d'autre part, le mouvement dans la zone marginale reste périodique en fonction du temps, mais n'est plus une fonction périodique de (bt - ax). En effet, il se forme, pour une suite de valeurs du temps discontinues, et à intervalles égaux (périodicité dans le temps) des tourbillons en certains lieux caractéristiques. Le schéma explicatif des phénomènes de couche limite devient, de ce fait, beaucoup plus complexe, et le schéma proposé dans le chapitre II n'est plus valable.

A la stabilité de forme des rides peut se superposer un mouvement d'entrainement moyen des particules solides, par suite de la prédominance soit du glissement des grains le long de la surface des rides dans le sens aller, soit du transport dans le sens retour par saltation des grains. Le sens du débit solide moyen peut donc être variable suivant les conditions hydrauliques.

Indiquons que nous avons observé la progression des derniers éléments constitutifs d'un train de rides, dans le sens opposé au sens de propagation de la houle, dans des zones correspondant à des discontinuités du fond (rupture de la pente). L'évolution de l'ensemble tend à rétablir la continuité de la pente du fond, et, par conséquent, de l'écoulement.

Si l'on augmente l'amplitude de la houle, on observe corrélativement une augmentation de l'amplitude des tourbillons, puis l'instabilité des rides alors formées; celles-ci disparaîssent et l'on observe une mise en saltation générale du matériau.

4°) STABILITE DE L'ECOULEMENT PRES DU FOND LIEE A L'EXISTENCE DES RIDES.

L'analyse des modes de formation des rides jusqu'à l'obtention de l'équilibre dynamique du fond, prouve que le phénomène de génération des rides constitue une réaction d'auto-défense du matériau, vis-à-vis de l'action de transport de la houle sur le fond, ou, ce qui revient au même, tend vers un équilibre correspondant à la consommation minimum d'énergie. En effet, les rides se forment lorsque le mouvement commence à être suffisamment important pour que la vitesse moyenne de la couche limite ne soit pas négligeable, ce qui correspondrait, une fois les matériaux mis en saltation lors du décollement de la couche limite, à un transport important au sein de cette couche limite. Mais la modification apportée à la couche limite, par la génération des tourbillons, enlève à celle-ci sa caractéristique de transfert uni-directionnel et rétabli l'équilibre entre les rides, soit que celles-ci deviennent stables par génération de deux tourbillons, soit qu'elles ne progressent plus que très lentement.

5°) LIMITE DE STABILITE DES RIDES.

Une augmentation progressive de l'amplitude de la houle s'accompagne corrélativement d'une augmentation de la dimensi des tourbillons et provoque, par la suite, l'instabilité des rides alors formées. Celles-ci disparaissent peu à peu, jusqu'à faire place à une mise en saltation générale du matériau.

La mise en saltation du matériau, sur une épaisseur relativement importante, entraîne, près du fond, un écoulement dont la forme générale se rapproche de l'écoulement d'une couche limite partiellement turbulente. En particulier, cette zone marginale possède une vitesse moyenne importante dans le sens de propagation de la houle. Il semble,même que les vitesses moyennes, qui ont été relevées dans ce cas, soient d'autant plus élevées que l'épaisseur de la zone intéressée est plus épaisse. Les mesures étaient toutefoi rendues difficiles par la rapidité du déplacement obtenu dans ce cas-là.

Il importe de noter que, très souvent,les caractéristiq considérées correspondent à une couche limite entièrement turbulent pour un fond infiniment rigide, alors que la présence de matériau conserve les caractéristiques laminaires de la couche limite, et semble introduire une modification des propriétés du milieu, comparable, du point de vue hydraulique, à une augmentation très appré ciable de la viscosité du fluide.

En fait, si nous augmentons encore l'amplitude du mouvement, nous obtenons un mouvement réellement turbulent, qui provoq la mise en saltation locale très intense, mais pour laquelle la résultante du transport moyen dans le sens de la houle est beaucoup plus faible.

6°) RELATION ENTRE LES CARACTERISTIQUES DES RIDES ET LES CARACTERIS TIQUES DE LA HOULE.-

Revenons en arrière, et considérons une houle dont les caractéristiques sont compatibles avec l'existence d'un train de rides stables.

Le processus de formation des rides, ci-dessus décrit, exige que la distance entre rides soit inférieure à l'excursion totale des molécules au-dessus des rides lorsque ces rides correspo dent à un équilibre, que ce soit un équilibre dynamique ou statique (avec ou sans déplacement des rides, dans le sens de propagation de la houle).

Ainsi que nous l'avons indiqué précédemment, la distanc entre rides est essentiellement déterminée par la capacité de trans port par le fluide des matériaux, préalablement mis en saltation, par le tourbillon qui se développe devant la face aval de la ride,

matériaux qui se déposent sur la crête de l'autre ride au cours du trajet de retour des molécules.

Etant donné qu'une partie du trajet de retour est nécessaire pour l'évolution du tourbillon, on peut écrire, en appelant r la distance nécessaire à l'évolution du tourbillon:

$$k\,d + r = a_f$$

k étant une fraction simple définissant le nombre de rides existant pour une longueur d'excursion.

En admettant que la longueur r nécessaire soit proportionnelle à l'amplitude 2 de la ride, on peut écrire l'équation ci-dessus sous la forme :

1) $$a_f = kd + \alpha S \quad (1)$$

α ne dépendant que des caractéristiques du matériau.

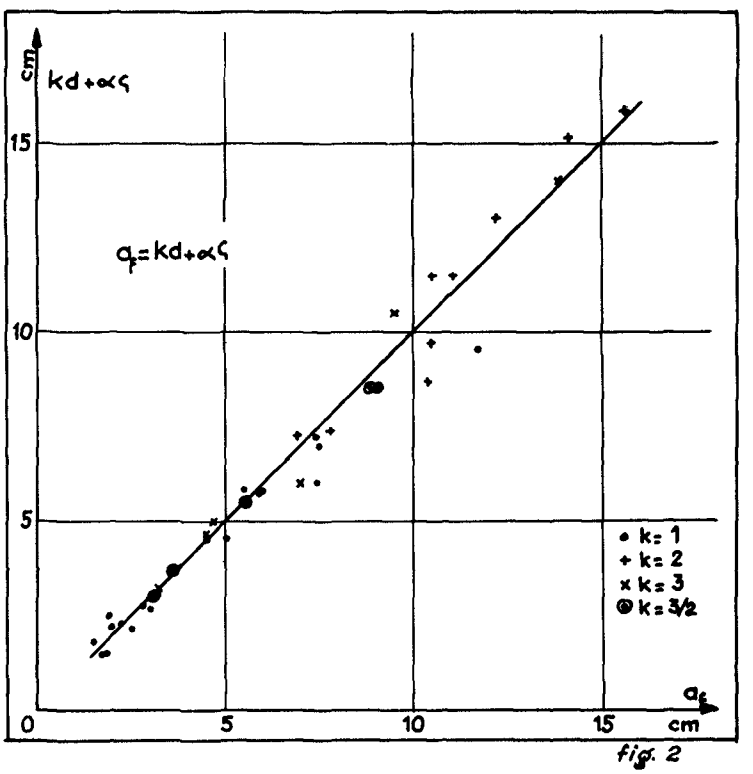

fig. 2

(1) Dans cette formule, le terme essentiel est k d, car d est en général 3 à 10 fois plus grand que S ; αS doit être considéré comme un terme correctif.

Nous avons tracé la courbe (2), qui justifie relativement bien ces considérations théoriques, en posant $\alpha = 1$ pour des grains de diamètre moyen égal à 0,28mm, et $\alpha = 2$ pour des grains de diamètre moyen égal à 0,75 mm.

Tous les essais représentés sur cette courbe ont été effectués en utilisant un matériau de faible densité: 1,45, la densité relative étant égale à 0,45. L'utilisation d'un matériau de faible densité a pour avantage de mieux mettre en évidence le processus hydraulique seul, les forces d'inertie pouvant alors être négligées, et la vitesse de chute des grains étant du même ordre de grandeur que la vitesse verticale des molécules du fluide

Pour ce matériau, nos expériences correspondaient à des valeurs de $k = 1, 2, 3$ et $3/2$, c'est-à-dire à la formation de une, deux, ou trois rides par longueur d'excursion, ou, dans certains cas, de trois rides pour deux longueurs d'excursions. Il résulte de ces considérations que les conditions de l'écoulement au-dessus des rides, conditions liées directement à la stabilité du tourbillon, constituent le facteur essentiel déterminant la longueur des rides. Les caractéristiques du matériau ont une influence plus directe sur les conditions limites de formation des ride et sur la durée nécessaire pour atteindre un système stable de rid ainsi que sur la profondeur des rides.

Rappelons d'ailleurs à ce propos, que M. LARRAS(15) avait trouvé, au cours de ses essais, le résultat inattendu suivan la limite d'érosion, de part et d'autre d'un obstacle, au bout d'u temps pratiquement infini, ne dépend, toutes choses égales par ailleurs, que la densité des matériaux remués, à l'exclusion pratiquement de leur diamètre moyen et de leur courbe granulométrique

Il y a là un résultat très intéressant et qui peut s'expliquer en considérant la formation des tourbillons, comme le phénomène essentiel de l'érosion. La profondeur limite d'érosion est celle à laquelle pour les caractéristiques données du mouvemen la turbulence engendrée par les tourbillons ainsi créés est suffisante pour soulever un matériau, de densité donnée. On conçoit que dans une certaine mesure la granulométrie du matériau n'influence pas la profondeur limite d'érosion (qui est toujours la même) mais influence directement le temps nécessaire pour obtenir cette profondeur limite.

IV - CRITERE DE FORMATION DES RIDES.

Ainsi que le fait remarquer M. l'Ingénieur en Chef des Ponts et Chaussées LARRAS, les mouvements de grains en surface ne correspondent pas à un phénomène caractéristique du mouvement, mais dépendent essentiellement de la compacité des grains à la

surface du fond. Il ne semble donc pas possible de donner une loi correspondant au début de l'entraînement en surface, sous l'action de la houle. Il faut toutefois noter que c'est là un processus qui peut effectivement exister et donner lieu à certains transports isolés, parfois non négligeables, en particulier lorsque les éléments déplacés sont de grandes dimensions (supérieurs à 5 cm).

Dans ses études, M. LARRAS a choisi comme critère, définissant le début de l'action érosive des houles et du clapotis, l'amorce de légères ondulations, du type rides, phénomène caractéristique des effets d'érosion des houles.

M. LARRAS a trouvé des résultats extrêmement précis, particulièrement intéressants, en ce qui concerne les mouvements stationnaires du type clapotis pur, et il semble que, dans ce cas, le début de formation des rides soit un phénomène fort bien défini, correspondant à des valeurs caractéristiques précises.

Les essais que nous avons effectués sur la houle ont donné des résultats relativement moins stables que les essais de M. LARRAS. En fait, d'après le processus ci-dessus expliqué de formation des rides, il semble que la ride puisse se produire en un endroit lorsque la mise en mouvement des grains en surface permet la formation d'une barre d'épaisseur suffisante pour provoquer, soit un décollement relativement important de la couche limite laminaire, assurant ainsi la mise en suspension d'une quantité de matériaux non négligeable au vent de la barre, soit la formation d'un micro-tourbillon amorçant l'érosion sous le vent de la barre.

On constate que ces phénomènes, de même que les phénomènes liés à l'émission de turbulence partielle, dépendent beaucoup de paramètres aléatoires divers : rugosité du fond, pente du fond, turbulence moyenne de la houle, stabilité initiale du mouvement .... Nous avons donc cherché essentiellement à déterminer un ordre de grandeur des paramètres caractéristiques de la formation de rides sous l'action de la houle. Dans l'exploitation de nos résultats, nous avons ajouté ceux provenant des essais effectués par M. LARRAS, qui possèdaient, entre autre, l'intérêt de concerner des caractéristiques de sédiments et de houles sensiblement différentes des nôtres.

RECHERCHE DE PARAMETRES CARACTERISTIQUES.

Les paramètres proposés par M. MADHAV MANOHAR ne nous ont pas permis de classer correctement nos résultats d'expérience. Nous avons donc recherché à mettre en évidence d'autres groupements de paramètres pour caractériser le début de formation des rides.

La formule proposée par M. LARRAS(1), qui s'écrit:

$$u_f - w = k \cdot \frac{(\rho - \rho_0)^{1/2}}{T^{1/2}}$$

semble particulièrement bien vérifiée dans le cas des clapotis (mouvements stationnaires) mais ne semble pas applicable à la formation de rides sous la houle progressive. Le domaine d'application de cette formule semble devoir être limité aux phénomènes d'érosion sous l'action de mouvements stationnaires périodiques cylindriques.

Dans l'étude des différents groupements de paramètres que nous avons effectués, nous avons cherché à déterminer les points différenciant le domaine de formation des rides et celui des mouvements en surface, en fonction d'un paramètre de la forme :

$$D^m \left[\frac{\rho - \rho_0}{\rho_0}\right]^n$$

Les meilleurs résultats ont été obtenus pour la valeur m = n et c'est, en particulier, ce choix qui nous a permis d'obtenir le meilleur regroupement de nos points avec ceux de M. LARRAS, dans un domaine légèrement plus étendu.

Physiquement, l'expression $kD\frac{(\rho-\rho_0)}{\rho_0}$ traduit le rapport des forces de gravité appliquées aux grains, à la force de tension exercée par le fluide sur celui-ci. En effet, la force de gravité peut s'écrire $k'D^3\left[\frac{\rho-\rho_0}{\rho_0}\right]$, et la force de tension peut s'écrire $k'D^2\vec{\gamma}$, en appelant $\vec{\gamma}$ le vecteur représentatif des forces de frottement, par unité de surface, exercée par le fluide sur le grain. Il semblerait donc que le début de formation des rides dépende essentiellement du rapport existant entre la force de tension exercée sur le grain par le fluide - ou la force d'aspiration exercée à la surface d'un grain lors de la dépression due au décollement de la couche limite laminaire - et les forces de gravité.

Nous avons porté sur le graphique 3, les différents points expérimentaux obtenus dans différentes conditions, en fonction des paramètres sans dimensions $D\frac{(\rho-\rho_0)}{\rho_0}\frac{b^{1/2}}{\nu^{1/2}}$ et X_1^2. Les différentes droites caractéristiques du phénomène correspondent à une équation de la forme :

(3) $$D\frac{(\rho-\rho_0)}{\rho_0}\frac{b^{1/2}}{\nu^{1/2}} = kX_1^2$$

---

(1) Pour déterminer les valeurs critiques d'apparition des rides.

ce qui correspondrait en appelant $\vec{Y}$ une valeur caractéristique de efforts de tension ou des pressions locales, à une relation de la forme :

$$\frac{\alpha}{g}\vec{Y} = k\frac{\nu^{1/2}}{b^{1/2}}X_1^2$$

L'expression (3) peut d'ailleurs s'écrire, en explicita la valeur de X_1:

(4) $$D\frac{(\rho-\rho_0)}{\rho_0} = \frac{\alpha}{g}\vec{Y} = k\frac{\nu^{1/2}}{b^{1/2}}\left(\frac{2p^*}{\rho g}\right)^2$$

formule dans laquelle p^* représente la partie variable de la pres sion exercée par la houle sur le fond.

L'ensemble des courbes caractéristiques du tableau 3, peut s'écrire :

$$D\frac{(\rho-\rho_0)}{\rho_0}\frac{b^{1/2}}{\nu^{1/2}} = kX_1^2$$

la valeur de k étant de 4.10^{-4} pour le fond horizontal.

La pente de 1 %, ainsi que nous l'avons vu, correspond un régime généralement plus stable que le fond horizontal; nous av obtenu des résultats correspondant à une valeur de k légèrement inférieure : $k = 1.10^{-4}$.

Sur les pentes de 2 % et 5 %, la valeur de k semble être légèrement supérieure au résultat obtenu avec la pente de 1 % ($k = 2.10^{-4}$). Signalons toutefois qu'il semble y avoir une plus grande dispersion, pour la pente de 5 %, des résultats provenant de l'augmentation de la probabilité d'émission de turbulence partielle qui dépend largement de la pente du fond, ainsi que nous l'avons vu précédemment.

Dans l'ensemble, les pentes suffisamment faibles constituent donc un facteur de stabilité, vis-à-vis de la formation des rides.

V - CRITERE DE DISPARITION DES RIDES ET D'APPARITI du MOUVEMENT en MASSE.

Dans nos conditions d'expérience, nous avons observé, ave les éléments de densité inférieure à 2, la disparition des rides e une mise en saltation des éléments à partir de certaines valeurs de l'amplitude de la houle.

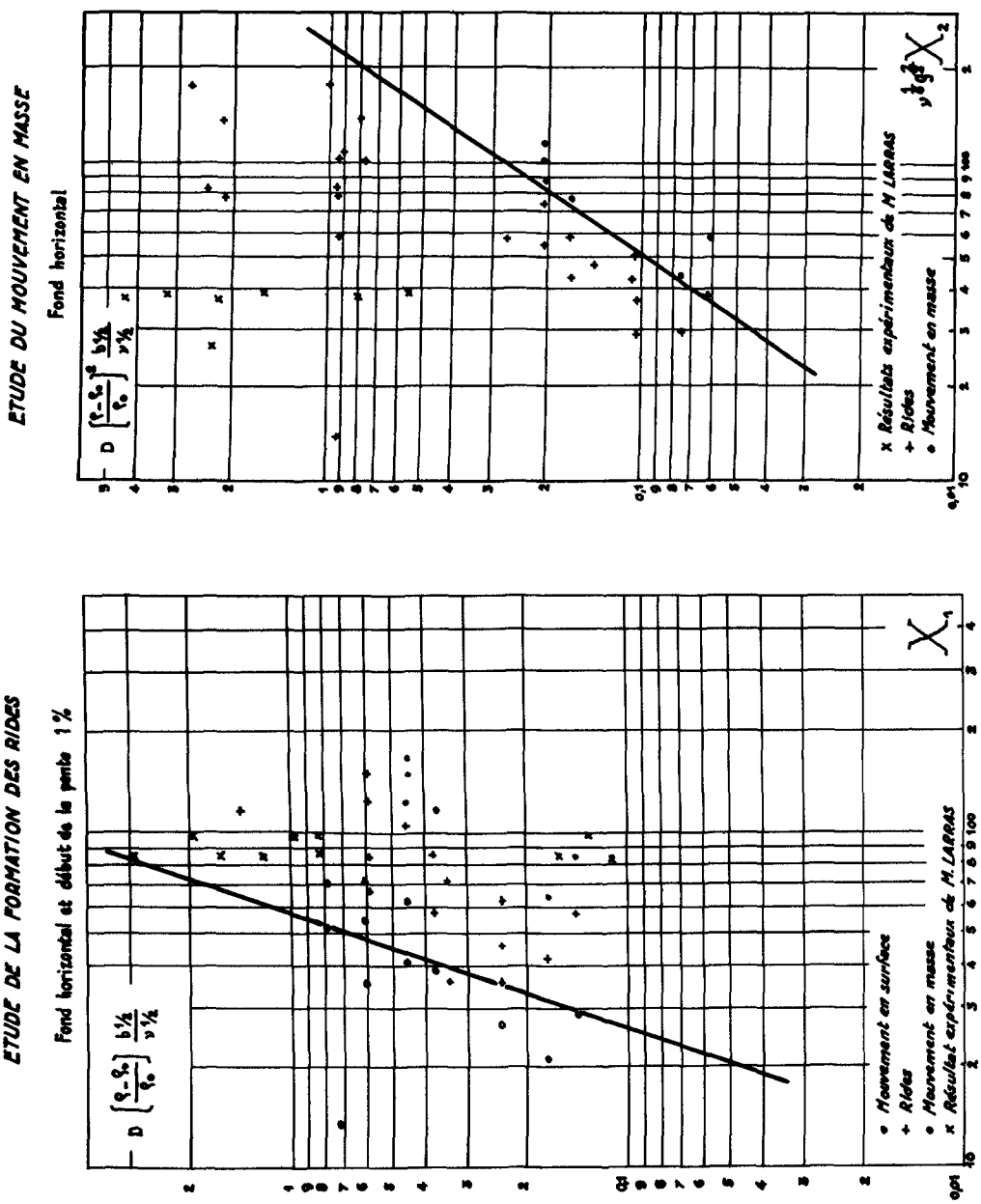

Graphique 4

Graphique 3

La zone marginale présentait les caractéristiques d'une couche limite partiellement turbulente et, en particulier, possédant une vitesse d'entraînement moyen, dirigée dans le sens de propagation de la houle, non négligeable.

L'épaisseur de la zone marginale était beaucoup plus importante que celle observée dans le cas d'un écoulement sur fond fixe, et pouvait atteindre plusieurs centimètres. Précisons qu général, les caractéristiques de houles nécessaires pour obtenir le mouvement en masse correspondaient souvent à des valeurs du paramètre X_1 déterminant une turbulence totale de la couche limite du mouvement sur fond stable.

Il semble donc que la mise en saltation d'une épaisseur importante de matériaux tende à développer une couche limite relativement plus stable à caractéristiques partiellement turbulen mais d'épaisseur beaucoup plus importante: autrement dit, la prése de particules solides mais mobiles aurait une influence comparable à celle d'une augmentation de viscosité.

Les expériences effectuées par d'autres auteurs qu ont mis en évidence l'existence de ces mouvements en saltation sur une grande épaisseur, en particulier dans le cas des clapotis, et résultats obtenus par M. MADHAV MANOHAR concernant la disparition rides de sable pour des oscillations du fond correspondant à des mouvements relatifs du fluide par rapport aux matériaux, comparabl à ceux engendrés par les houles de la nature, permettent d'étendre ce résultat au cas des sables pour des houles d'énergie supérieure celle des houles de laboratoire.

Rappelons que de tels mouvements sont d'ailleurs parfaitement visibles sur les plages près des zones de déferlement et, de plus, ils permettent seuls d'expliquer les destructions des digues à parois verticales, et, en particulier, la destruction de digue de Mustapha, à Alger, par la mise en suspension des matériau sur une hauteur importante.

Nous avons porté sur le graphique 4, les valeurs correspondant aux expériences au cours desquelles nous avons obser la disparition des rides et la mise en saltation du sédiment avec départ en masse. Il ne semble pas que les paramètres sans dimensio que nous avons adoptés pour déterminer les valeurs caractéristique de la formation des rides, puissent être aussi adoptés pour caract riser ce nouveau phénomène; en effet, les points représentatifs des résultats d'expérience relatifs à ce phénomène ne sont pas dis tincts des points représentant la formation de rides stables, si l conserve ces mêmes paramètres. Ceci n'est pas surprenant car le phénomène est totalement différent; la mise en saltation exige des caractéristiques de houles correspondant à un gradient de pression suffisant pour que la différence entre la pression en surface et l

pression à l'intérieur de la masse pulvérulente exerce sur les particules une force ascensionnelle suffisante.

Nous avons tout d'abord recherché, pour tenir compte des caractéristiques du grain, un paramètre de la forme $D^m\left(\frac{\rho-\rho_0}{\rho_0}\right)^n$ permettant de caractériser le phénomène; les meilleurs résultats ont été obtenus pour des valeurs de m et n définies par la relation $2m = n$, c'est-à-dire : $D\left(\frac{\rho-\rho_0}{\rho_0}\right)^2$

L'importance du facteur $\left(\frac{\rho-\rho_0}{\rho_0}\right)^2$, dans le groupement met en évidence l'influence prépondérante de la densité relative dans le phénomène de mise en saltation d'une masse importante de matériau. Ceci est à rapprocher du résultat trouvé par M. LARRA et que nous avons déjà cité, d'après lequel les profondeurs d'érosion limite sous l'influence de mouvements stationnaires ne dépendraient que de la densité et non pas des caractéristiques granulométriques du matériau.

Nous avons re-présenté, sur le graphique 4, les résultats d'expériences obtenus en fonction des paramètres sans dimensions :

$$D\left(\frac{\rho-\rho_0}{\rho_0}\right)^2 \frac{b^{1/2}}{\nu^{1/2}} \quad \text{et} \quad X_2$$

Les conditions d'observation de mouvements de masse, consécutifs à une mise en saltation générale du matériau, peuvent être définie comme correspondant à un domaine délimité par la droite caractéristique dont l'équation serait :

$$(5) \qquad D\left(\frac{\rho-\rho_0}{\rho_0}\right)^2 \frac{b^{1/2}}{\nu^{1/2}} = k X_2$$

Il est intéressant de remarquer que l'équation caractéristique de ce phénomène, proposée par M. MADHAV MANOHAR, est :

$$(6) \qquad D^{0,2}\left(\frac{\rho-\rho_0}{\rho_0}\right)^{0,4} \frac{g^{0,4}\nu^{0,2}}{u_f} = k$$

et que, dans cette équation, le groupement $D^{0,2}\left(\frac{\rho-\rho_0}{\rho_0}\right)^{0,4}$ est le même que dans notre équation. Par contre, les groupements des paramètres représentatifs de l'écoulement sont différents dans les deux formules.

On peut en conclure que les forces d'inertie, qui étaient prépondérantes dans les expériences de MADHAV MANOHAR, jouent un rôle essentiel dans le phénomène de mise en saltation générale du matériau. Par contre, les forces développées par l'oscillation du fond ne sont pas comparables à celles provoquées par l'existence d'un mouvement périodique réellement progressif.

L'équation (5) s'écrit, en explicitant X_2 :

$$D\left(\frac{\rho-\rho_0}{\rho_0}\right)^2 \frac{b^{1/2}}{\nu^{1/2}} = k \frac{u_f^{1/2}}{(b\nu)^{1/4}} \cdot \frac{\partial}{\partial x}\left(\frac{2p^*}{\rho g}\right)$$

D'autre part, il est intéressant de faire apparaître au lieu du diamètre des matériaux, les vitesses de chute w de ceux-ci, qui s'écrivent, pour les matériaux que nous avons utilisés :

$$w = k\, D^2 \left(\frac{\rho-\rho_0}{\rho_0}\right) \frac{g}{\nu}$$

L'équation s'écrit donc :

$$w^{1/2}\left(\frac{\rho-\rho_0}{\rho_0}\right)^{3/2} \frac{b^{1/2}}{g^{1/2}} = k' \frac{u_f^{1/2}}{(\nu b)^{1/4}} \cdot \frac{\partial}{\partial x}\left(\frac{2p^*}{\rho g}\right)$$

$$\frac{\partial}{\partial x}\left(\frac{2p^*}{\rho g}\right) = k''\left(\frac{w}{u_f}\right)^{1/2}\left(\frac{\rho-\rho_0}{T^{1/2}}\right)^{3/2} \frac{\nu^{1/4}}{g^{1/2}\rho_0^{3/2}}$$

Cette relation détermine la valeur critique du gradient de pression près du fond assurant la mise en saltation des grains, en fonction de deux paramètres sans dimensions :

- le rapport de la vitesse de chute des grains à la vitesse maximum près du fond;

- le rapport de la densité relative, à la racine carrée de la période du mouvement.

Il semble logique d'admettre que la valeur du gradient de pression constitue le facteur essentiel de la mise en saltation des matériaux sableux. En effet, par suite de la perméabilité des sables, les différences de pressions existant en surface se transmettent dans le massif pulvérulent, suivant une loi d'extinction exponentielle, et avec un certain déphasage dans le temps. L'instant où la pression est minimum en surface correspond, en conséquence, à une sous-pression importante susceptible d'expulser les grains avec une force vive non négligeable.

Influence de la pente.-

La pente du fond a pour effet de retarder sensiblement la mise en saltation de la masse du matériau. L'origine de ce phénomène peut être recherchée dans l'augmentation de l'influence des forces de gravité, par suite de l'existence d'une composante dirigée vers le bas.

Toutefois, ce-ci n'est sensible qu'à une certaine distance de l'extrémité amont de la pente, le début de la pente donnant lieu, pour les pentes de 2 % et 5 %, aux mêmes résultats que le fond horizontal.

Dans la formule $D\left(\frac{\rho-\rho_0}{\rho_0}\right)^2 \frac{b^{1/2}}{\nu^{1/2}} = kX_2$ les valeurs de k provenant de nos expériences sont :

- 100 pour le fond horizontal et de début de la pente,
- 70 pour la pente de 2 %,
- 50 pour la pente de 5 %.

VI - APERCU SUR LES LOIS GENERALES DU TRANSPORT SOLIDE SOUS L'ACTION DE LA HOULE.

Les résultats des études que nous avons exposées ci-dessus, permettent de définir les valeurs critiques des différent mouvements des matériaux pulvérulents tapissant le fond de la mer, sous l'action de la houle, dans les domaines de l'eau profonde ou assez profonde. Ces résultats ne permettent pas toutefois de formule des lois de débits qui sont, en fait, extrêmement variables en fonction d'autres paramètres que les seules conditions de propagation de la houle au voisinage du fond.

Mais il est possible, à partir de ces résultats, d'énoncer quelques considérations générales sur les débits solides.

a) Mouvements isolés de grains.

Les mouvements isolés de grains se produisent, ainsi que nous l'avons vu, pour des caractéristiques variables de la houle, qui dépendent dans une large mesure du coefficient de forme, de la position du grain sur le lit du fond, et des dimensions du gra par rapport à la rugosité moyenne du fond.

Les transports résultant des actions sur des grain isolés correspondent à des débits solides relativement faibles et ne présentent pas, en général, d'intérêt primordial. Toutefois, les

études effectuées permettent de chiffrer les profondeurs maxima à partir desquelles une houle donnée est susceptible de produire des érosions, pour un matériau donné.

En ce qui concerne les éléments relativement grossiers qui sont moins sujets que les sables aux mises en saltation et aux transports par les différents courants maritimes, ce procédé de détermination de la limite d'alimentation peut aussi donner des renseignements intéressants.

On pourra admettre en règle pratique, que les mouvements de grains isolés correspondent à des effets appréciables, dans certains cas particuliers, et doivent être pris en considération dans l'étude de l'équilibre des côtes, pour les gros galets, à partir de la limite correspondant à la formation des rides. En effet ces gros éléments ont beaucoup moins tendance que les sables à se former en rides, par suite de leurs dimensions mêmes; dans ce cas, la remontée des éléments isolés peut constituer un processus continu, non négligeable.

b) Transport des sables.

En ce qui concerne les sables, dès que le mouvement en surface tend à être relativement intense, la forme d'équilibre prise par le matériau du fond correspond à la formation de trains de rides relativement stables. Il n'y aura un transport non négligeable du sable que lorsque, sous l'action de la houle, le train de rides se déplacera suivant les processus analysés précédemment.

En fait, les transports appréciables de sable n'auront lieu que lorsque l'on aura atteint des amplitudes des houles correspondant à la mise en suspension d'une masse importante du matériau.

Il serait particulièrement intéressant de déterminer l'importance de ces transports et les débits auxquels on peut ainsi arriver, mais ces déterminations se heurtent à de nombreuses difficultés. En particulier, le débit résultant au droit d'une section, est lié, d'une part, au transport dans la couche limite, transport qui s'effectue toujours dans le sens de propagation de la houle et, d'autre part, aux transports des éléments mis en suspension sous l'action des courants de masse, dont le sens dépend du sens de ces courants de masse, ainsi que l'ont fait remarquer MM. VINCENT et RUELLAN (15).

En particulier, dans le cas des houles à fort courant d'entrainement en surface (zone du vent, approche de la zone de déferlement) l'influence du courant de retour se traduit par une action dans les zones voisines de la couche limite, dirigée dans le sens contraire à la propagation de la houle. Il peut donc y avoir là une cause de débit important dans le sens opposé à la propagatic

de la houle, auquel peuvent d'ailleurs s'ajouter, dans certaines zones, les transports dûs aux rip-currents.

En définitive, le débit à travers une section correspondrait à l'intégrale prise sur la hauteur de mise en saltation des grains, du produit de la turbidité locale par la valeur moyenne des courants de masse.

Une expérience intéressante permet d'avoir une idée des variations d'une telle intégrale pour le cas des houles de laboratoire. Si l'on étudie le déplacement de sphères sur un canal horizontal, sous l'action d'une houle d'amplitude donnée, on s'aperçoit que le sens du déplacement pour une même caractéristique de houle dépend essentiellement du diamètre de la sphère. Tant que l'épaisseur de la sphère croît, la vitesse de déplacement de la sphère décroît jusqu'à une valeur critique du diamètre correspondant à une vitesse nulle. Lorsque l'on étudie les mouvements de sphères de diamètres plus élevés, on s'aperçoit que les mouvements de celles-ci s'effectuent dans le sens contraire de la propagation de la houle.

Toutefois, il semble qu'en nature, avant que le transport dû au courant de masse annule totalement le transport provoqué par la progression de la couche limite laminaire partiellement turbulente sur le fond, l'on atteigne des valeurs pour lesquelles la couche limite au contact du fond est entièrement turbulente.

L'on a vu que, dans ce cas, il n'existait pas de l générale concernant la vitesse moyenne de la couche limite et que celle-ci, ainsi que la valeur des courants de masse, dépendaient, da une large mesure, des conditions aux limites de la zone envisagée.

On peut alors observer, dans ce cas, des débits variables suivant les conditions aux limites.

Rappelons d'autre part, que tous ces résultats ne sont valables que dans le domaine de l'eau profonde ou assez profond et cessent, en particulier, d'être valables près de la zone de déferlement. Le processus de transport devient alors totalement différent. L'écoulement dans cette zone est entièrement turbulent, et le débit résultant dépend essentiellement de la quantité des matériaux rejetés à la plage lors du déferlement de la lame (éléments qui proviennent de l'aspiration, par la houle, des matériaux mis en saltation à l'amont du déferlement) et de la quantité de matériaux entrainés lor du black-wash ou par les rip-currents dans le courant de masse à l'extérieur de la zone de déferlement.

Ce processus, bien que totalement différent, perm toutefois la continuité du transit littoral, sous l'action de la hou jusqu'à l'estran.

Sous l'action de ce transit littoral, les plages tendent, en fait, vers un état d'équilibre correspondant, ainsi que nous l'avons vu précédemment, à un profil à pente croissante à cour-

bure dirigée vers le haut, et qui constitue un profil de défense vis-à-vis de l'action de transfert des houles.

Ces considérations permettent, toutefois, d'expliquer en l'absence d'autres phénomènes, le résultat général, bien connu des hydrographes, suivant lequel les houles de tempête dégarnissen l'estran, alors que les houles d'amplitude moyenne le nourrissent.

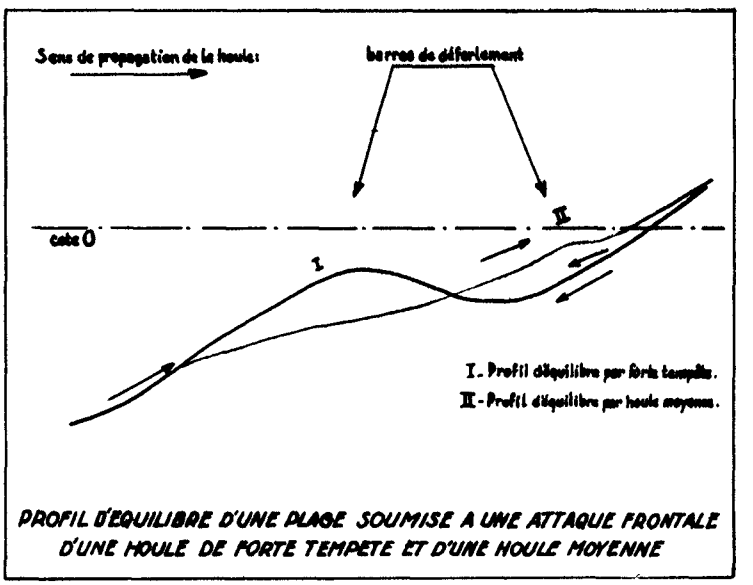

PROFIL D'EQUILIBRE D'UNE PLAGE SOUMISE A UNE ATTAQUE FRONTALE D'UNE HOULE DE FORTE TEMPETE ET D'UNE HOULE MOYENNE

Croquis 5

Sur le croquis 5 nous avons porté les profils d'équilibre par houles de forte tempête et houles de tempête moyenne. Une fort tempête détermine un profil d'équilibre dans lequel l'alimentatior de la barre située avant le déferlement est assurée par les matéri provenant de fonds relativement importants et, simultanément, par le sable ramené lors du black-wash depuis le haut estran vers le bourrelet de déferlement.

Cette forme de rivage devient instable dès qu'une houle d'amplitude inférieure, mais suffisante pour mettre en mouvement l matériaux jusqu'à une profondeur supérieure à celle du bourrelet de déferlement, transforme le profil I de la plage suivant le profil II. L'état d'équilibre correspond alors à une remontée du matériau provenant essentiellement du bourrelet de déferlement précédemment formé, vers la région de l'estran.

c) Applications pratiques. (10. 12. 8.)

Les quantités de matériaux participant à la remontée sous l'action des houles correspondent à des débits relativement faibles par rapport aux quantités transportées par les courants littoraux (8), les rip-currents, dans le transfert dit en "dents de scie"n sous l'action du black-wash et du déferlement, de l'undertow, et de la dispersion générale des sédiments vers le large(10) Toutefois, ilserait impossible d'expliquer le maintien de la majeure partie des plages, s'il n'existait pas une action continue ramenant une partie importante du matériau, qui risque d'être entraînée par les courants de masse, les rip-currents et les courants de fond, à partir des plages. Les études auxquelles nous avons procédé ont montré le rôle important des phénomènes de la couche limite dans ces remontées de matériaux et les processus suivant lesquels s'effectuent ces mouvements.

Il est, toutefois, des cas pratiques où le phénomène de remontée des matériaux s'effectue de façon relativement pure pour être évident par lui-même.

Citons, en particulier, quelques observations que nous avons effectuées sur les côtes méditerranéennes (mer sans marée dans laquelle oes mouvements sont en conséquence beaucoup plus visibles).

α. Remontée de galets sous l'action de la houle.

La plage de Carno (Hérault) avait complétement disparu par suite de la construction d'un mur vertical en bordure de plage destiné à soutenir le boulevard de bord de mer de cette station balnéaire. Toutefois, après la disparition de sables, il s'est formé une plage relativement importante de galets sous l'action des houles de forte tempête qui sévissent dans ces parages.

D'après les recherches qui ont été effectuées, ces galets ne pouvaient provenir que des fonds rocheux existant par profondeur de 7 à 8 m. au large de la côte.

Seule, la remontée des matériaux sous l'action de la houle permet d'expliquer cette arrivée de matériaux.

β. Exemple de remontée de sable à la plage.

Le Service des Ponts et Chaussées de l'Hérault a construit une série d' épis perpendiculaires à la mer sur la côte méditerranéenne à l'Est du port de Sète, pour protéger la route côtière attaquée par la mer au lieu-dit "la Peyrade". Par suite de la présence de ces épis, la plage s'est considérablement engraissée en sable fin et s'est avancée de plusieurs dizaines de mètres.

La plage, dans cette région, présente une courbure relativement constante et relativement faible, traduisant une plage en équilibre, sous l'action de la houle dominante, avec faible transport Est-Ouest. L'équilibre de cette plage, dans une zone de mer sans marée, ne peut s'expliquer qu'en faisant intervenir un apport frontal non négligeable, équilibré par l'action du faible transport littoral et le transport, vers le large, provoqué par les rip- current La construction de la route littorale a eu pour effet d'augmenter l'action du rip-current et du black-wash, ainsi que l'importance du transport littoral.

La réalisation d'épis, compartimentant la plage en divers tronçons bien définis, a diminué d'une façon importante le transport littoral et l'importance des rip-currents, ne laissant subsister que l'action de remontée du matériau depuis les fonds jusqu'à la plage. La ligne du rivage a alors avancé jusqu'à ce que l'action des rip-currents et des transports littoraux rétablissent l'équilibre du bilan de sable. Une des caractéristiques des engraissements de plage obtenus, en facilitant la remontée du matériau, et en supprimant les actions de dispersion, réside dans la parfaite symétrie de la ligne de plage de part et d'autre de l'épi.

γ. Exemple d'applications emprunté aux "études littorales" de A. RIVIERE (12).

Les "études littorales" de A. Rivière constituent la mise au point la plus récente publiée sur les mouvements de matériau pulvérulents (sable) aux abords d'un littoral. De nombreux phénomènes observés par les sédimentologues et exposés dans cette "étude" s'expliquent du point de vue hydraulique à la lumière des résultats que nous avons ci-dessus exposés. Nous en examinerons deux particulièrement importants.

La notion de dispersion des matériaux vers le large est essentiellement liée, semble-t-il, à l'existence d'une forte turbulence sur le fond provoquant l'entraînement vers le large sous l'action des divers courants. Parmi ces courants, les courants de masse près du fond dirigés dans le sens opposé à la propagation de la houle sont particulièrement importants lorsque la couche limite est turbulente car, ainsi que nous l'avons vu, il n'y a pas de composante de translation dans le sens de propagation de la houle. L'existence de ce courant de masse en profondeur particulièrement important, dans ce cas, a rendu nécessaire pour le sédimentologue, une notation particulière : c'est ce phénomène qui est désigné sous le vocable de : "undertow".

D'autre part, A. Rivière observe que "l'érosion provoquée par les vagues poussées par le vent cesse brusquement lorsqu'en fin de tempête celui-ci vient à diminuer de violence alors que la mer demeure encore très forte: il est même fréquent de voir des masses importantes de sédiment être ramenées à ce moment au rivage",

Ce phénomène s'explique si l'on admet que la houle de vent étant entièrement turbulente crée, au contact du fond, une couche limite turbulente sans mouvement moyen dirigé vers la côte, et donc l'action est essentiellement un entraînement de matériaux vers le large. Au contraire, dès que le vent cesse, la mer demeure très forte mais on se trouve alors en présence d'une houle partiellement établie dont l'action sur le fonds correspond à une mise en saltation du sable avec caractéristique de couche limite laminaire ou partiellement turbulente et transport important dans le sens de propagation de la houle, donc remontée des matériaux vers l'estran.

B - MOUVEMENTS DES VASES SOUS LA HOULE EN L'ABSENCE DE REMISE EN SUSPENSION

VII. DESCRIPTION DES ESSAIS.

1° Description sommaire des phénomènes observés.

En prolongement des études que nous avons effectuées, relativement aux propriétés de la couche limite des houles de laboratoire, sur un fond parfaitement rigide, nous avons étudié l'influence des houles sur des matériaux formant un fond déformable, et sur des sédiments à propriétés thixotropiques importantes, tels que les vases.

Cette étude portait essentiellement sur l'observation des phénomènes assimilables, par leurs propriétés, aux phénomènes de couche limite; l'action des houles qui déferlent ou celle des houles qui assurent la remise en suspension du matériau n'a donc pas été envisagée, le processus d'action étant fondamentalement différent. En effet, si l'action d'une houle assurant la remise en suspension d'un matériau vaseux est, en partie, comparable à celle du transport en masse, observé pour les sédiments sableux, ce phénomène est masqué par un phénomène essentiel du transport constitué par l'existence des courants de densité, phénomènes caractéristiques des transports de sédiments du type vase.

En nous limitant à l'action de la houle, avant que son amplitude soit suffisante pour assurer la remise en suspension du matériau, nous avons pu mettre en évidence un phénomène qui, à notre connaissance, n'a jamais été signalé et qui consiste en une translation lente, dans le sens de propagation de la houle, du fond de vase, et qui a pour résultat de provoquer une modification du profil des fonds de vase avec remontée du matériau vers l'estran, sans remise en suspension du matériau.

2° Condition de réalisation des essais - Généralités.

Le déplacement des vases sous la houle a été étudié en canal vitré au Laboratoire central d'Hydraulique de France:

La vase expérimentée était une vase marine de la région de la baie de l'Aiguillon, dont les caractéristiques avaient été préalablement étudiées (nature, composition granulométrique, vitesse de chute et de tassement, pour différentes concentrations, etc..) (1).

L'eau utilisée dans le canal àvait été préalablement traitée à l'aide d'une solution de chlorure de magnésium et de sodium, ce qui,lui conférait les mêmes actions floculantes que les eaux marines (concentration en chlorure de magnésium à 0,126 N, correspondant à la somme des concentrations en ions divalents de l'eau de mer).

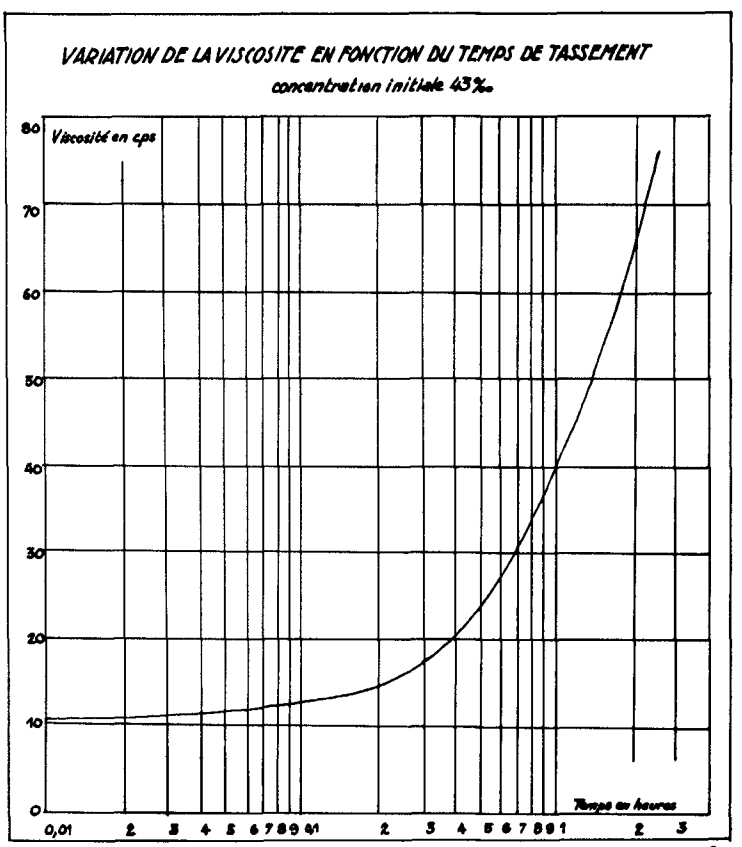

Graphique 6

(1) En ce qui concerne les méthodes d'analyse des matériaux argileux voir les ouvrages de M. le Professeur RIVIERE (9, 11).

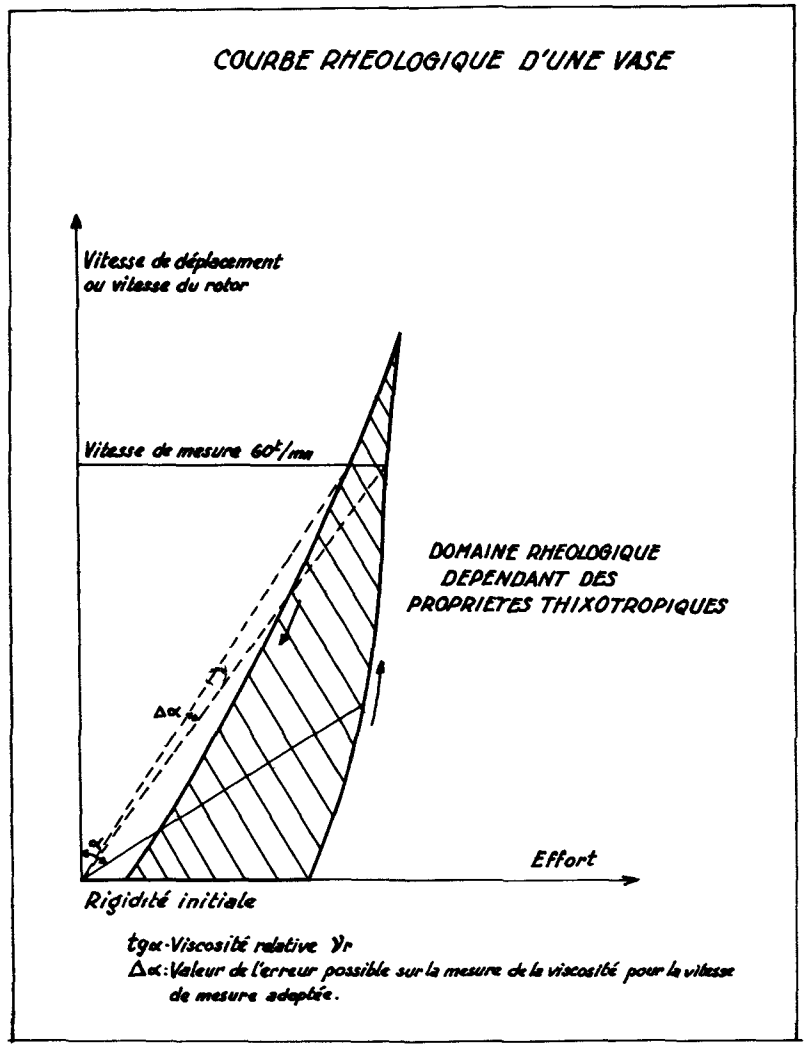
COURBE RHEOLOGIQUE D'UNE VASE
Vitesse de déplacement ou vitesse du rotor
Vitesse de mesure 60t/mn
DOMAINE RHEOLOGIQUE DEPENDANT DES PROPRIETES THIXOTROPIQUES
Effort
Rigidité initiale
tgα-Viscosité relative ηr
Δα:Valeur de l'erreur possible sur la mesure de la viscosité pour la vitesse de mesure adoptée.

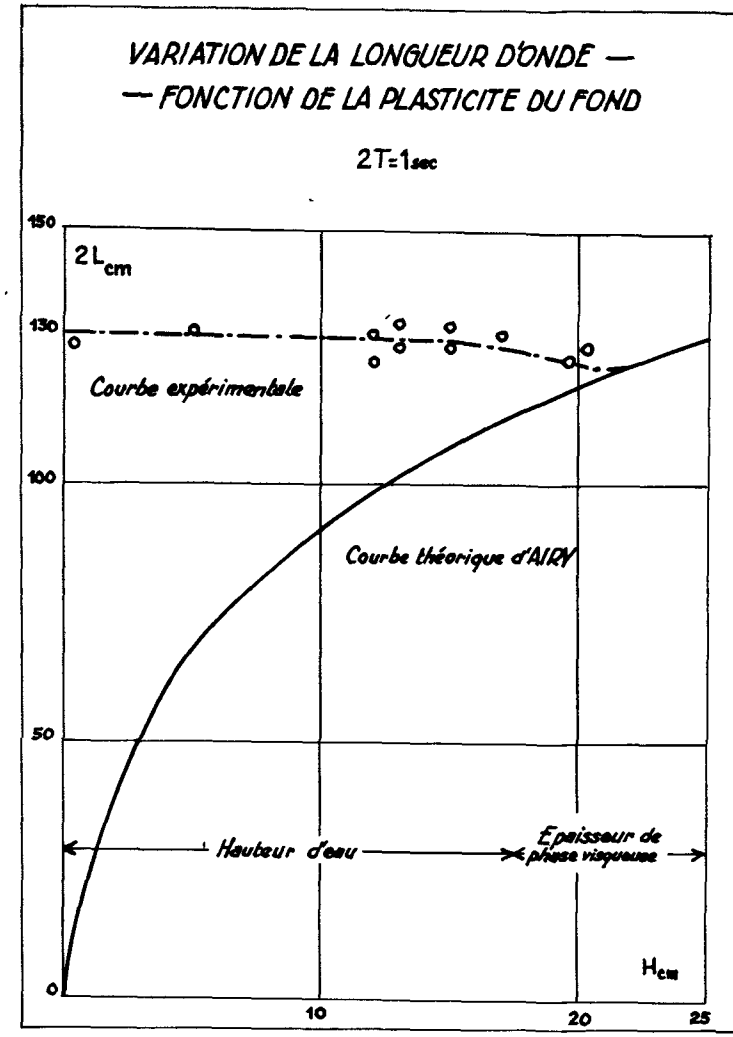
VARIATION DE LA LONGUEUR D'ONDE —
— FONCTION DE LA PLASTICITE DU FOND
2T=1sec
2Lcm
Courbe expérimentale
Courbe théorique d'AIRY
Hauteur d'eau
Epaisseur de phase visqueuse
Hcm
150
130
100
50
0
10
20
25

Graphique 8

Avant chaque expérience, la vase introduite dans l'eau du canal était soumise à un brassage mécanique intense afin d'obtenir un mélange initial homogène de concentration déterminée.

Les temps de dépôt et de tassement des vases ont été mesurés à partir du moment où l'on arrêtait ce brassage -temps t_0 - et les mesures effectuées pour différents temps de tassement t_1, t_2, t_3....t_n (graphique 6).

Au cours de ces essais, la viscosité de la vase était soigneusement enregistrée (1) à l'aide d'un viscosimètre Brookfield, dont le principe consiste à mesurer le couple résistant exercé sur un rotor tournant à une vitesse déterminée.

L'amplitude des trajectoires des particules, ainsi que leur déplacement, étaient mesurés en repérant des particules de matériaux à différentes profondeurs. Dans certains cas, des éléments très fins, colorés, d'une densité apparente voisine de celle de la vase (afcolène), étaient préalablement introduits dans la masse afin de faciliter le repérage des mouvements de vase.

Des prélèvements d'eau à différentes profondeurs permettaient de suivre avec précision la variation possible de la turbidité au-dessus du plan de séparation de l'eau et de la vase, au cas où une remise en suspension du matériau serait apparue.

Parallèlement à ces mesures, la variation du profil le long du canal était relevée, dans le but de suivre la variation de la profondeur due au tassement de la vase et de contrôler le déplacement sous la houle, de la masse de vase, et la modification de pente des dépôts en résultant.

---

(1) La mesure de la viscosité de la vase demande quelques précisons. En effet, la vase naturelle, qui constituait le matériau expérimental, possède des propriétés rhéologiques et thixotropiques très particulières, qui peuvent enlever toute signification aux mesures si celles ci ne sont pas effectuées dans certaines conditions.

Il importe tout d'abord, de préciser que toutes les mesures sont des mesures de viscosité relative, rapport de l'effort effectué par la vitesse de rotation. Etant donné que la vase possède une rigidité initiale non négligeable, cette valeur ne présente une signification que pour des vitesses élevées de rotation du rotor.

D'autre part, la vase douée de propriétés thixotropiques, ne donne de résultats cohérents que dans des conditions bien définies. Les mesures effectuées, l'ont été à une vitesse de 60t/mn, pour laquelle les variations dues aux propriétés thixotropiques sont négligeables. De plus, elles concernent la phase vaseuse ayant atteint sous l'action de la houle un état rhéologique stable (voir graphique 7).

VIII - RESULTATS DES ESSAIS.

1°) Propagation de la houle sur les fonds de vase.

La propagation d'un mouvement cylindrique monochromatique, sur un fond de vase, engendre un certain nombre de phénomèn qui la différencient notablement de la propagation d'une houle classique, que ce soit sur fond infiniment rigide, ou sur fond mobile constitué de sable ou de galets.

En laboratoire, les phénomènes illustrant les particularités de ces mouvements, sur fond de vase, peuvent être observés par des expériences de deux types :

- action d'une houle sur fond vaseux ayant subi un tassement plus ou moins prolongé,

- propagation d'une houle dans un domaine fluide de viscosité initialement homogène, subissant l'effet de tassement.

Cette description schématise les conditions naturelles moyennes, mais permet de suivre l'évolution des phénomènes en caus en fonction des caractéristiques du milieu dans lequel se propage le mouvement. Les conditions imposées par ces schémas représentent cependant - assez grossièrement, il est vrai - des milieux naturel qui correspondent respectivement aux deux états suivants :

- une période qui fait suite à un calme plat de longue durée et permet une consolidation des fonds vaseux;

- une période qui fait suite à une tempête exceptionnelle et provoque la mise en suspension du matériau vaseux dans toute la masse du fluide.

Le milieu naturel le plus fréquemment observé constitu donc un cas intermédiaire.

Notons, de plus, que la phase visqueuse, déposée dans canal d'essais, est limitée à une profondeur relativement faible, une chape rigide, au niveau de laquelle, dans la majorité des cas expérimentaux, le mouvement ondulatoire n'est pas négligeable; la vase des fonds naturels atteint, par contre, des profondeurs extr mement importantes.

1. Dans le cas d'un fond vaseux, ayant subi l'effet d'un tasser prolongé, l'existence d'une rigidité initiale (yeld value) a pour conséquence le fait qu'un mouvement progressif de très faible ampl tude s'identifie avec la propagation d'une houle sur fond rigide. longueur d'onde est alors donnée par la loi d'Airy, et les particu de fluide, au voisinage du fond, décrivent des ellipses infiniment aplaties; il se développe, entre autres, dans le fluide, une couch limite, dans des conditions qui ont été étudiées dans les chapitre précédents.

MOUVEMENTS DES MATERIAUX DE FOND SOUS L'ACTION DE LA HOULE

Dès que l'amplitude de la houle devient suffisante, on assiste à l'amorce d'un mouvement des particules de vase, à la surface du fond, qui présente un mouvement ondulatoire de plus en plus caractérisé et, corrélativement, une modification des trajectoires des particules d'eau situées près du fond : les ellipses infiniment aplaties de la théorie classique font place à des ellips dont la dimension du petit axe n'est plus négligeable.

Ce mouvement apparaît lorsque l'action des forces de pression, développées sur le fond de vase, est suffisante pour briser la rigidité initiale de la vase.(1) Dès que ce mouvement s'amorce, la rupture de la rigidité initiale se transmet en profondeur. Simultanément, les propriétés théologiques du milieu évoluent par suite des propriétés thixotropiques caractéristiques des vases. L'épaisseur de vase intéressée par le mouvement croît jusqu'à un état limite fonction des caractéristiques cinématiques du mouvement orbital à l'interface (variables pendant la période d'établissement du régime) et de celles de la vase elle-même (variables elles aussi); ces deux groupes de caractéristiques réagissent l'un sur l'autre, pour aboutir à l'état d'équilibre dynamique final.

On peut supposer, en première approximation, que les équations qui régissent le mouvement de l'eau claire - et, en particulier, celui de la surface libre - ont une forme identique à celles de la houle classique; mais il importe de noter que les conditions aux limites ne correspondent plus à un fond horizontal, mais à une ondulation périodique de l'interface, supposée bien définie. Cette ondulation peut être assimilée, en première approximation, au mouvement de la surface : $y_o = H$, définie par les molécules d'eau situées à la cote y_o au repos, relative à une houle se propageant par une profondeur H' supérieure à celle de l'eau claire H(2).

En conséquence, si cette hypothèse est exacte, la longueur d'onde d'une houle, pour une épaisseur d'eau claire donnée, variera suivant les caractéristiques du mouvement ondulatoire de l'interface, donc suivant la viscosité du milieu chargé de particule vaseuses.

---

(1) Les caractéristiques de la houle susceptible de rompre la rigidité initiale sont, a priori, fixées par les caractéristiques cinématiques du mouvement au contact du fond, et dépendent des propriétés de la vase et, en particulier, de son degré de tassement.

(2) L'expérience montre que l'interface est effectivement, dans la majorité des cas, animée d'un mouvement ondulatoire assimilable à celui d'une surface $y_o = C^{te}$; pour certaines houles particulièrement violentes, l'interface peut présenter néanmoins, une dissymétrie extrêmement prononcée, et des creux très élevés. Dans ce dernier cas, le mouvement de l'eau claire peut aussi être représenté par des équations d'une forme identique à celles de la houl classique, sauf, toutefois, au voisinage de l'interface.

On vérifie que, pour une période donnée du mouvement progressif, la longueur d'onde est comprise entre les longueurs d'onde des houles se propageant dans un milieu sans viscosité, par des profondeurs respectivement égales à l'épaisseur de la lame d'eau claire, et à l'épaisseur totale du milieu intéressé par le mouvement.

Il n'est pas dans notre intention de procéder à une description complète des expériences ayant porté sur les caractéristiques des mouvements progressifs sur fond de vase, ni d'en énumérer tous les résultats, car tel n'est pas le but de la présent étude. Nous nous contenterons de décrire, ci-après, une expérience typique, qui rassemble pratiquement tous les résultats susceptibles d'expliquer, par la suite, le comportement des fonds vaseux, à partir des phénomènes purement hydrauliques inhérents à la nature des mouvements progressifs.

2. L'expérience que nous allons décrire, a consisté à reproduire un mouvement progressif (houle établie de laboratoire) dans un milieu chargé de particules vaseuses, subissant les effets de tassement. La surface libre a été fixée à 25 cm. au-dessus d'une chape horizontale parfaitement rigide. L'eau était chargée d'une certaine quantité de vase, conférant au milieu fluide, après brassage, une viscosité homogène de l'ordre de 10 cps; ce milieu était excité par le "groupe générateur de houle" produisant des ondes progressives de 4,1 cm. de creux, avec une période égale à 1 seconde (voir graphique 8).

Au début de l'expérience, les longueurs d'ondes mesurées étaient sensiblement égales à celles que nous aurions obtenues pour 25 cm. d'eau claire; c'est-à-dire que, pour une viscosité de l'ordre de 10 cps, la longueur d'onde du mouvement est sensiblement la même que pour de l'eau pure. A la précisions des mesures près et dans ce cas limite - correspondant à une faible viscosité -, le mouvement en surface, c'est-à-dire en réalité, sur une épaisseur très faible, serait correctement rendu en écrivant les équations classiques de la houle pour une profondeur H' = 25 cm. Les équation ne pourraient rendre compte des mouvements au sein du fluide, car l'influence des termes de viscosité introduit un déphasage dans la propagation du mouvement en profondeur (1).

Au fur et à mesure que le tassement s'accentue, et qu corrélativement, la viscosité de la couche de vase croit, la longueur d'onde moyenne devient inférieure à celle de la longueur d'onde que permet de prévoir la courbe théorique d'Airy, appliquée pour la profondeur de 25 cm, mais supérieure à celle que permet de prévoir la courbe d'Airy pour la profondeur H existante d'eau clair

(1) Le déphasage apparaît d'une façon évidente pour la considératio des équations de NAVIER-STOKES. Son existence est cependant assez difficile à déceler avec les houles de laboratoire.

La courbe expérimentale (1) et la courbe d'Airy, susmentionnées, se confondent à partir d'un point qui correspond pratiquement, d'après nos expériences, à une hauteur qui ne laisse subsister qu'une épaisseur de vase égale à 2,5 cm, dont la valeur de la viscosité est relativement très élevée (2), (plusieurs milliers de cps au moins). On peut donc admettre qu'à partir de cette valeur, pour des houles de gradient de pression comparable à celui des houles de laboratoires, les fonds vaseux se comportent sensiblement comme un fond infiniment rigide en ce qui concerne la propagation du mouvement.

En ce qui concerne la propagation des houles en eau claire (de viscosité négligeable) relativement peu profonde, au-dessus d'une phase visqueuse, séparée de la phase fluide, de viscosité négligeable, par une interface bien définie, les observations effectuées au cours de cette expérience permettent de distinguer du point de vue purement hydraulique différents processus d'interaction entre les deux milieux.

Lorsque la viscosité du milieu chargé de particules de vase est inférieure à 10 cps environ, le mouvement est convenablement représenté par les équations classiques de la houle. La couche limite, qui se développe au contact d'un fond éventuel, est cependant plus épaisse (proportionnellement à $\sqrt{\nu}$), et les phénomènes propres à la couche limite engendrent des perte d'énergie par frottement sensiblement plus importantes que dans l'eau uniformément claire.

Lorsque la viscosité de la phase visqueuse augmente, tout en restant relativement faible, c'est-à-dire pratiquement inférieure à 100 cps environ, le mouvement se propage au-dessous de l'interface, et reste très analogue à celui de l'eau claire. Le milieu visqueux est, néanmoins, animé d'un mouvement qui ne peut être correctement représenté par les équations de NAVIER-STOKES simplifiées, dans lesquelles on néglige les effets de viscosité.

---

(1) On peut vérifier par des conditions d'ordre théorique que la courbe expérimentale passe par un minimum.

(2) Il semble qu'une détermination précise de la limite inférieur de la viscosité de la vase, au-dessus de laquelle le comportement du fond permet de l'assimiler à un fond rigide, doive révéler une variation de cette limite en fonction des caractéristiques de la houle. Il est, en particulier, évident que cette limite est très faible, pour une houle courte qui se situe dans le domaine de l'eau très profonde.

L'influence de la viscosité se traduit, en particulier, par un certain déphasage, qui varie avec la valeur de la viscosité et avec la profondeur au-dessous de l'interface.

Lorsque la viscosité de la phase visqueuse atteint et dépasse 100 cps, le mouvement dans la phase visqueuse devient relativement réduit, et l'on observe, dans le fluide situé au-dessus de l'interface, la naissance d'une couche limite. Autrement dit, alors que les pertes d'énergie par frottement se concentrent dans le milieu visqueux, lorsque celui-ci est doué d'une viscosité relativement faible, celles-ci se répartissent à la frontière de l'interface dès que la viscosité augmente. Le domaine marginal du fluide visqueux, intéressé par ces phénomènes décroît lorsque la viscosité augmente, tandis que le domaine marginal du fluide à viscosité négligeable croît. On observe donc, à nouveau, l'existence d'une couche limite dans le domaine de l'eau claire, dont l'importance augmente avec la viscosité de la phase visqueuse jusqu'à redevenir comparable à celle développée par un fond infiniment rigide, c'est-à-dire pratiquement à partir d'une valeur de la viscosité relative de l'ordre de 10.000 cps, pour des houles de gradient de pression au-dessus du fond, comparable à celui des houles de laboratoire expérimentées.

Nous pensons qu'il est inutile de s'étendre d'avantage sur les conditions de propagation des mouvements progressifs périodiques, dans les milieux comportant une partie d'eau claire et une partie, plus visqueuse, d'eau chargée de particules de vase. Rappelons, en effet, que les indications sommaires qui précèdent, n'avaient pour but que d'introduire l'étude des conséquences de la propagation du mouvement de la houle dans des milieux partiellement vaseux - lorsque la viscosité d'un tel milieu est comprise entre 10 et 100 cps; les phénomènes qui se développent, dans ces conditions constituent un processus naturel très particulier des déplacements de vase sous l'action des houles. Nous ne traitons, de plus, cette question qu'en tant qu'application de l'étude des phénomènes propres aux couches limites des houles.

2°) <u>Mouvements oscillatoires des particules de vase sous l'action d'une houle, à différentes profondeurs</u>.

Ainsi que nous l'avons exposé ci-dessus, la présence d'un mouvement progressif, périodique, dans la lame d'eau située au-dessus d'une vase de viscosité comprise entre 10 et 100cps développe dans celle-ci un mouvement périodique cylindrique qui ne répond plus aux équations classiques du fluide parfait, car il est indispensable de faire intervenir les termes de viscosité dans les équations de NAVIER-STOKES. Toutefois, les orbites décrites par les particules que l'on peut mettre en évidence par l'introduction de grains d'un matériau pulvérulent de même densité que la vase (afcolè sont sensiblement constituées par des ellipses dont les dimensions

du grand axe et du petit axe diminuent en fonction de la profondeur de la particule considérée dans la couche de vase (voir schéma 9).

Le graphique 10 donne les résultats des mesures des grands axes des orbites en fonction de la profondeur pour une houle particulière: H = 25 cm, 2 L = 1m.30, 2 T = 1 s, pour différentes valeurs de l'amplitude en surface 2 h, et pour différentes valeurs de la viscosité.

L'influence du terme de viscosité se traduit, près de l'interface, par une décroissance très rapide de l'amplitude du mouvement, alors qu'au contraire, dans un fluide non visqueux, l'amortissement du grand axe est extrêmement progressif (voir graphique 11). La profondeur, jusqu'à laquelle le phénomène est sensible, dépend de façon très directe de la viscosité de la vase, et de l'amplitude de la houle. Il s'agit là, nous le rappelons, d'un mouvement propre au fluide visqueux, qui ne peut généralement être considéré comme un mouvement de zone marginale.

Pratiquement, on peut admettre que l'amplitude des mouvements à faible distance de l'interface, n'est, dans la vase, qu'environ les 7/10 de l'amplitude des mouvements observés dans le fluide non visqueux au-dessus de l'interface, dès que la viscosité atteint des valeurs d'environ 40 cps.

Nous rappelons qu'il n'est pas possible de dégager des lois de ces mouvements sans faire intervenir les propriétés rhéologiques du milieu. En effet, la thixotropie de la vase, est telle que sa viscosité varie considérablement, lorsque l'on s'éloigne de l'interface, par suite de la mise en mouvement plus ou moins importante de la vase.

Le résultat essentiel de nos expériences concerne en fait le mouvement de translation moyen des particules de vase qui résulte des phénomènes de frottement près de l'interface, et que nous exposerons maintenant.

3°) Mouvements de translation des particules de vase dans le sens de propagation de la houle.

Le développement d'un mouvement laminaire, dans le fluide visqueux, sous l'action d'une houle cylindrique du fluide sain, situé au-dessus du milieu visqueux, se traduit par un mouvement de translation moyen des particules de vase dans le sens de propagation de la houle, d'une façon comparable aux phénomènes que nous avons étudiés et analysés, en ce qui concerne la couche limite des houles sur fond rigide.

Cette action se met particulièrement bien en évidence par son effet global, qui a pour résultat de faire évoluer un fond horizontal de vase dans un canal, vers un profil d'équilibre régulièrement croissant, de l'amont jusqu'à l'aval, avec accumulation

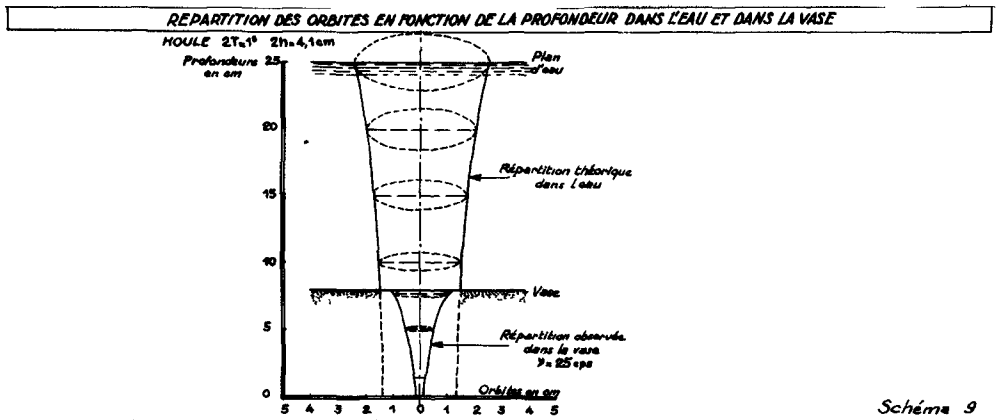

Schéma 9

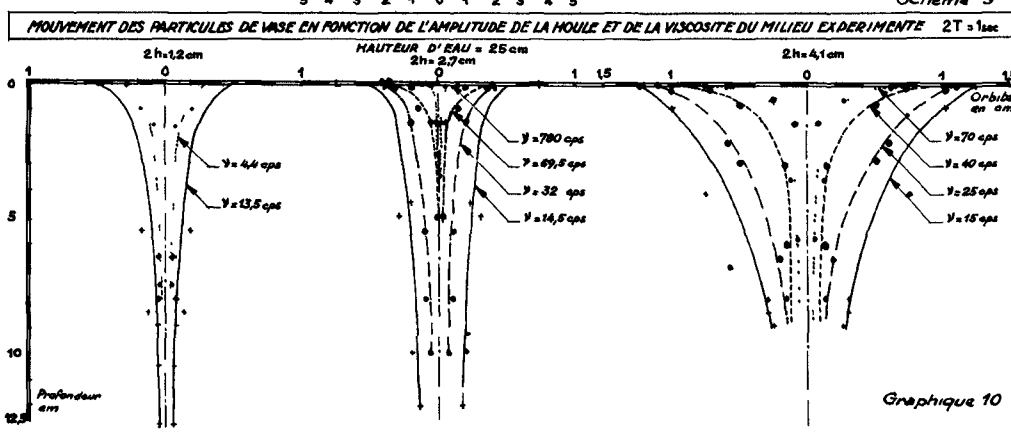

Graphique 10

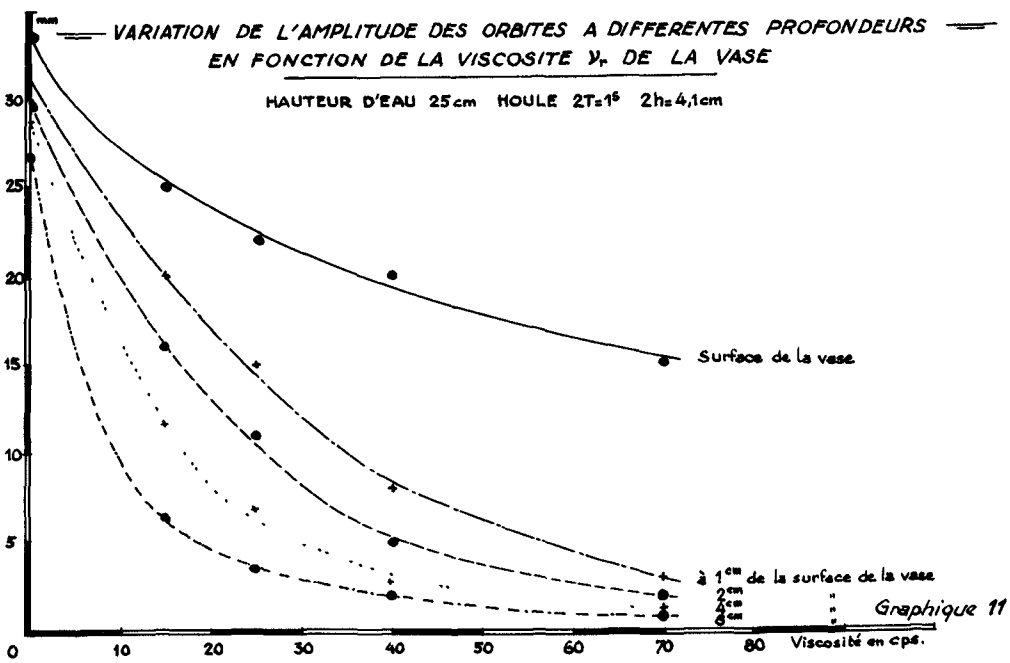

Graphique 11

dans la partie aval du canal, devant la limite aval de celui-ci, de matériaux provenant de la partie amont sans aucune remise en suspension de ce matériau.

Les études que nous avons effectuées avec des grains de même densité que la vase incorporés à celle-ci nous ont permis d'examiner les conditions qui influent sur les phénomènes de translation des particules de vase sous l'action de la houle.

Nous étudierons successivement :

- la répartition des vitesses de translation moyenne;
- l'influence de la viscosité sur les vitesses de translation;
- l'influence des caractéristiques de la houle;
- le débit solide des vases qui peut résulter de l'action de la houle dans une section type.

Le croquis 12 schématise la répartition des différents courants moyens existants, dans le fluide sain, pour lequel la viscosité est négligeable, et dans la vase sous-jacente pour laquelle les forces de viscosité jouent un rôle essentiel.

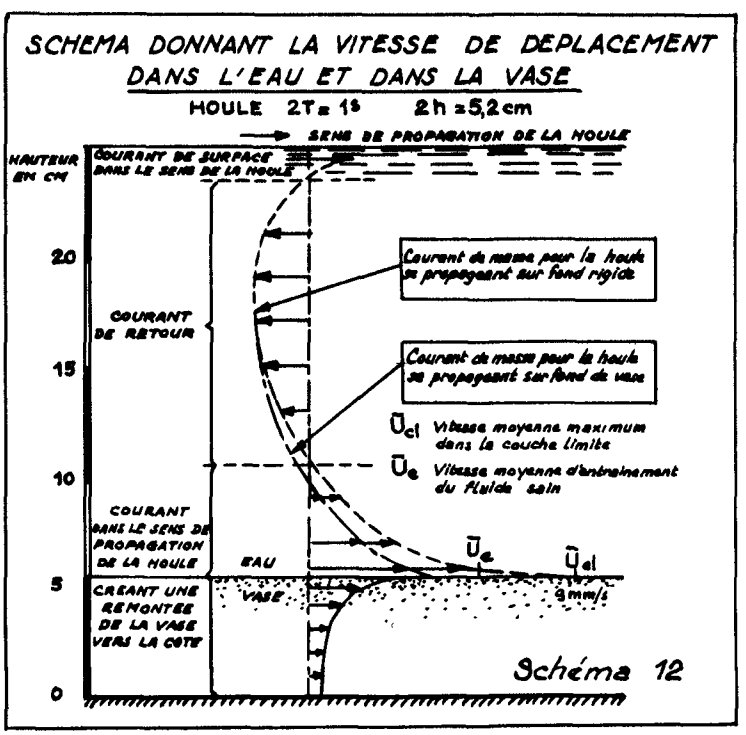

Le graphique 13 donne la répartition de la vitesse de déplacement de la vase, en dessous de l'interface de séparation des deux milieux pris comme zéro de référence. L'on constate, d'une part, une décroissance rapide des vitesses résultantes moyennes, en fonction de la viscosité, et, d'autre part, une atténuation brutale du mouvement près de la surface, dès que la valeur de la viscosité est importante. C'est, en effet, la zone ou le gradient des vitesses est très élevé, qui constitue pratiquement une zone marginale dans laquelle se développent les force de frottement. La variation du gradient des vitesses moyennes est peu sensible pour les viscosités de l'ordre de 10 à 30 cps, pourlesquelles on peut admettre que les phénomènes de frottement à l'interface sont négligeables. Le mouvement s'observe plus en profondeur et ne peut plus être assimilé aux mouvements de couche limite.

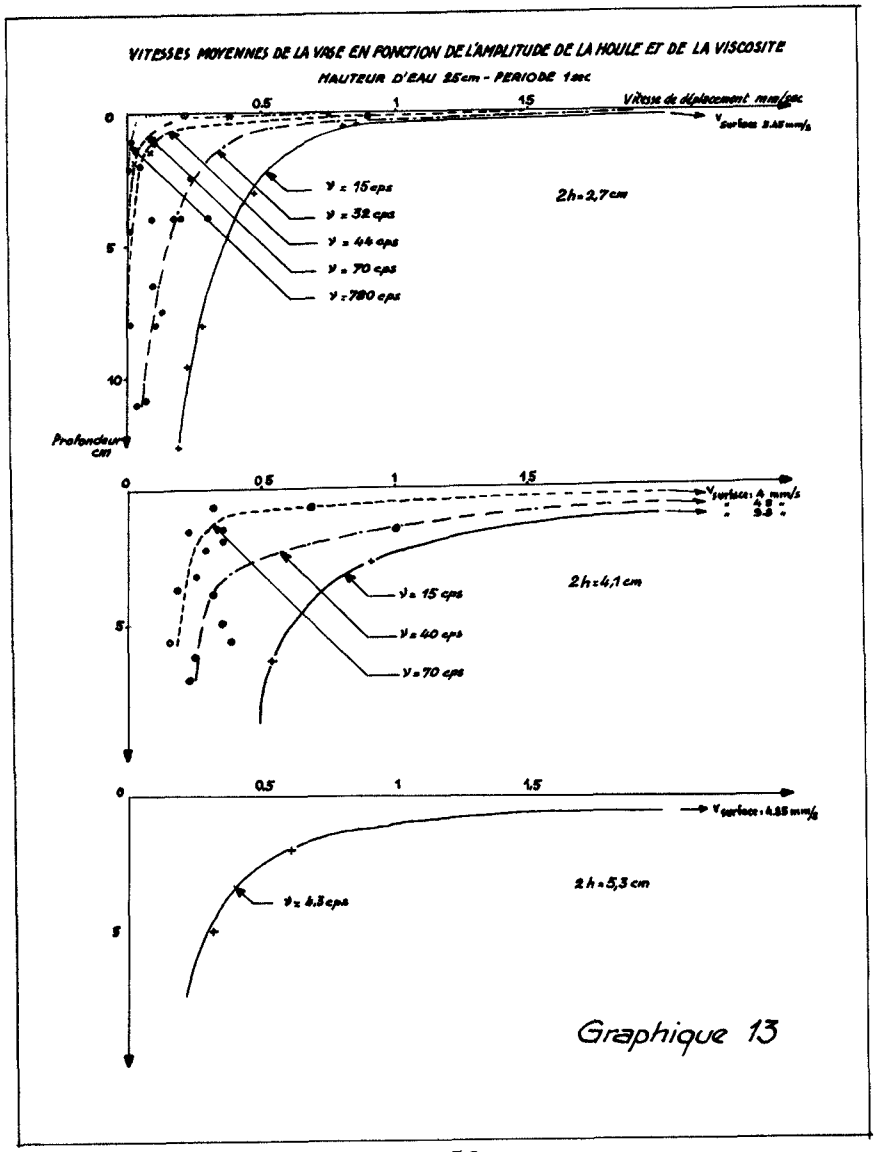

Graphique 13

Nous avons porté sur le graphique 14, la variation de la vitesse de déplacement à différentes profondeurs, en fonction de la viscosité de la vase pour une même houle. Ces courbes mettent en évidence l'influence essentielle de la viscosité sur les vitesses moyennes de déplacement, et l'interprétation de ces courbes permet de déduire une notion de débit solide possible en fonction de la viscosité.

Du point de vue théorique, il apparaît que l'influence de la viscosité, dans la propagation de mouvements progressifs cylindriques périodiques, se traduit par un mouvement moyen d'entraînement des particules dans le sens de propagation de la houle. La compensation de ce mouvement, qui permet de conserver une surface libre stable s'effectue dans la zone de viscosité minimum (la nappe d'eau claire dans le cas de nos expériences).

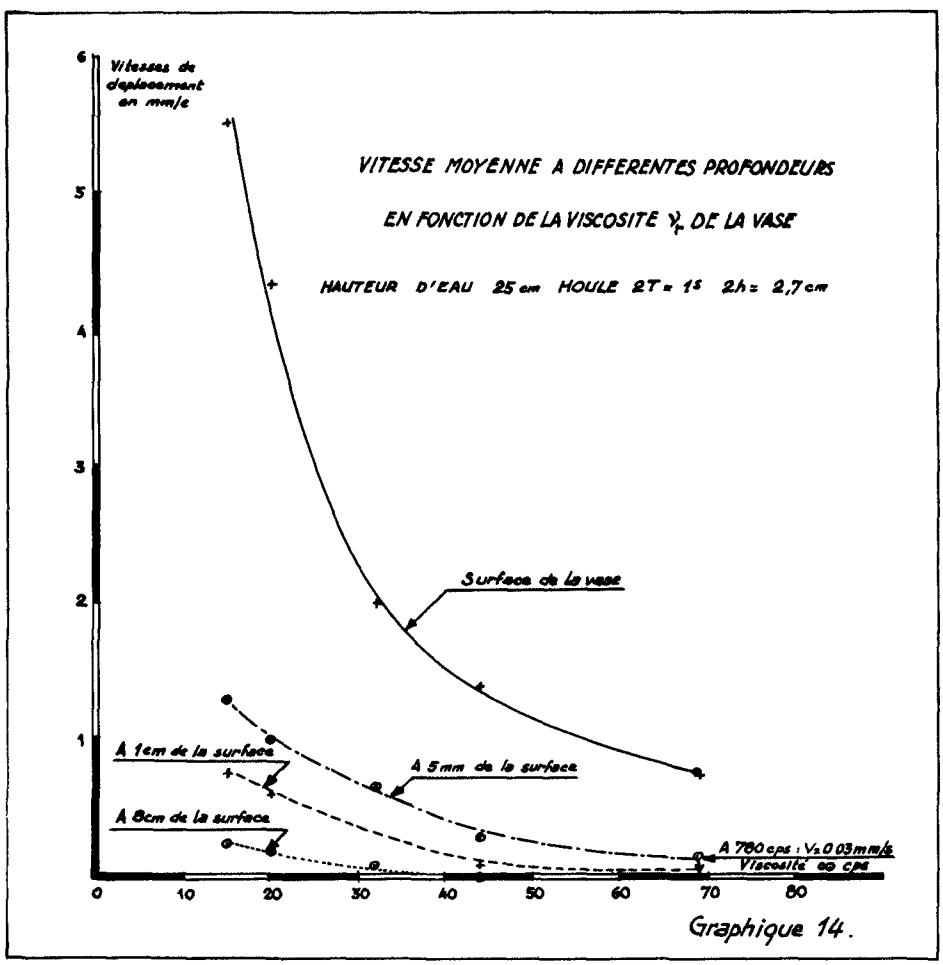

Graphique 14.

Dans le cas de propagation de ces mouvements dans un fluide peu visqueux (eau claire) sur un fond rigide, seules les zones de frottements marginaux (couche limite de fond et de surface) sont animées de ce mouvement de déplacement moyen dans le sens de propagation du mouvement.

Si le mouvement progresse dans une nappe d'eau, située au-dessus d'un milieu de viscosité supérieure, celui-ci s'anime dans un mouvement périodique, qui s'accompagne d'un déplacement dans le sens de propagation du mouvement.(1)

Ceci est valable, aussi bien dans le cas où le mouvement dans le milieu visqueux s'apparente à un mouvement de zone marginale à fort gradient de vitesse, où à un mouvement de masse sans zone privilégiée de dissipation d'énergie par frottement.

En pratique, ce résultat a pour conséquence d'entraîner une remontée vers la côte des matériaux du milieu visqueux jusqu'aux zones de turbulence élevée, qui assurent la remise en suspension du matériau (zone de déferlement essentiellement) Remarquons d'ailleurs que la propagation du mouvement sur fond déformable augmente la stabilité de l'interface et retarde l'apparition de turbulence de fond.

IX - APPLICATIONS PRATIQUES

Le phénomène de remontée de la vase sous l'action de la houle, que nous avons décrit ci-dessus, constitue une cause non négligeable d'alimentation des atterrissements de vase sur certains points des côtes; en particulier, les remontées de vases marines participent certainement, dans une mesure importante, à la formation des polders d'origine marine tels ceux de la Sèvre Niortaise, en France, ou ceux de la mer de Waden en Hollande.

Ce processus permet d'ailleurs de compléter l'explication de certains phénomènes, qui ont été souvent observés dans

---

(1) Une image physique du processus peut être donnée, si l'on considère que, bien que les particules du fluide parfait restent stables en valeur moyenne, l'énergie et, par conséquent, la pression sur le fond, progresse, au cours de l'évolution du mouvement progressif. L'action sur l'interface de ce mouvement est donc assimilable du point de vue pression, au passage d'un train de rouleaux successifs se déplaçant sans frottement. On pressent que le passage de ces rouleaux au-dessus d'un milieu visqueux entrainera le déplacement de celui-ci dans le sens général du mouvement.

les zones de poldérisation.(1)

Il suffit, en effet, que le gradient de pression soit de l'ordre de grandeur de la rigidité initiale (yeld value) des vases, pour que l'on observe une lente remontée du matériau. Or, la partie variable de la pression s'écrit :

$$\frac{p^*}{\rho g} = h \frac{ch\, a(H-y)}{ch\, aH} \cos(bt - ax)$$

d'où : $$\left(\frac{\partial p}{\partial x}\right)_{max.\ pour\ y=H} = \frac{ha}{ch\, aH}$$

Les houles les plus faibles, que nous avons expérimentées, et qui correspondaient déjà à des débits non négligeables de vase, possédaient les caractéristiques suivantes :

$$H = 25cm. \quad 2L = 1m.60$$

$$2T = 1\ s. \quad 2h = 2,7\ cm.$$

une houle océanique, correspondant à une période de 2 T = 12 s et une amplitude de 2 h = 4m, c'est-à-dire, une houle de tempête moyenne et non exceptionnelle, aura une influence comparable jusqu'à une profondeur H' telle que $\frac{\partial p}{\partial x}$ soit d'un ordre de grandeur comparable à la valeur de l'essai cité ci-dessus :

$$\frac{1}{\rho g}\frac{\partial p}{\partial x} = \frac{ha}{ch\, aH} = \frac{1,35\pi}{80\, Ch\frac{\pi 25}{80}} = 2,8\times10^{-2} = \frac{h'a'}{ch\, a'H'} = \frac{2h'\pi}{2L'ch\, a'H'} = \frac{400\pi}{2,2\times10^4 ch\, a'}$$

$$ch\, a'H' = \frac{4\pi}{2,8\times2,2} = 2,04\ ; \quad H' = 0,18\times220m \neq 40m.$$

Une houle de même période (2T = 12 s) et de 6 m d'amplitude aurait une action comparable pour :

$$ch\, a'H' = 3,06 \quad d'où \quad H' = 0,27\times220m \neq 60\ m.$$

On voit donc que les houles océaniques sont susceptibles de provoquer une remontée de la vase des fonds depuis des profondeurs pouvant atteindre plusieurs dizaines de mètres, et sans

(1) Cf. étude de M. VAN STRAATEN (13.14) et conférence prononcée par celui-ci, sur les faciès de la mer de Waden (Hollande) à la Sorbonne, le 11 Avril 1957.

doute même des profondeurs de l'ordre de 100 m, pour les grandes tempêtes océaniques.

Sous ces actions, il se produit une migration de la vase depuis les grands fonds vers la côte. En général, le matériau n'atteint pas la côte, car, dès que les fonds deviennent insuffisants, et , en particulier aux abords de la zone de déferlement, celui-ci est remis en suspension et entrainé vers le large, par suite de l'action des courants de masse (ripcurrents, ou courants de compensation), ou de l'action des courants de densité.

Le matériau remonte toutefois à la côte sous l'influence des courants de marée, ou de densité, si celle-ci est protégée de l'action brutale des lames -baie abritée, bassin des ports, etc...). Les bandes côtières abritées de la houle par une succession d'îles (îles Friesland en Hollande, île de Ré devant le Marais Poitevin, Noirmoutier, etc ..) constituent des plages particulièrement propices à l'atterrissement des matériaux vaseux, et permettent, en particulier, lorsque la houle est suffisamment atténuée par la diffraction, au processus de remontée de la vase, sous l'action de la houle, de se poursuivre jusqu'à l'estran. Ce phénomène permet d'expliquer certains envasements, et en particulier l'apport des vases dans les polders marins de la baie de l'Aiguillc

CONCLUSIONS

L'étude que nous avons entreprise, ne s'était donné que comme un but secondaire, la recherche des lois déterminan les mouvements des matériaux de fond sous l'action de la houle. Mai nous avons constaté au long du déroulement des études, que l'explic tion des mouvements du fluide près du fond, comportait un domaine d'application extrêmement fécond : celui du mouvement des matériaux de fond.

Nous pensons que la poursuite de telles études devrait permettre de mieux connaître ces phénomènes importants qui intéressent vivement l'ingénieur maritime, tant pour la protection des côtes, que pour le maintien des profondeurs.

Une conclusion que nous croyons devoir tirer de c études, concerne l'apport que les recherches en laboratoire permett d'obtenir dans l'étude de problèmes complexes et pour lesquels l'expérimentation en nature, est coûteuse et délicate. En particuli nous pensons que dans l'état actuel des connaissances des phénomène maritimes, l'étude systématique des phénomènes à échelle réduite do précéder toute campagne de mesures en natures, afin de mieux connaî le phénomène lui-même, les difficultés inhérentes à son observation à sa mesure, et de pouvoir dresser un tableau d'expérimentation en nature, rationnel et efficace.

.../...

- BIBLIOGRAPHIE -

(1) HUON LI - Stability of oscillatory laminar flow along a wall Beach Erosion Board, Technical memorandum n° 47, 1954.

(2) LARRAS - Effet de la houle et du clapotis sur les fonds de sable, IVèmes Journées de l'Hydraulique, Paris, 1956

(3) LHERMITTE P. - Etude de la couche limite dans le cas des mouvements progressifs périodiques, Comptes rendus de l'Académie des Sciences, 1957, p.2352 t. CCXLIV.

(4) LHERMITTE P. - Contribution à l'étude de la couche limite des houles progressives. Application aux mouvements de matériaux sous l'action de la houle . Paris 1958.

(5) MADHAV MANOHAR - Mécanique des sédiements de fond provoqués par l'action de la houle, Beach Erosion Board, Technical memorandum, n° 75, 1955.

(6) MICHE R. - Mouvements ondulatoires de la mer en profondeur croissante ou décroissante, Annales des Ponts et Chaussées, 1942.

(7) MICHE R. - Amortissement des houles dans le domaine de l'eau peu profonde, Houille Blanche, 1956, n° 5.

(8) PELNARD - Essai de théorie de l'évolution des formes de rivage en plages de sables et de galets, IVès Journées de l'Hydraulique, Paris, 1956.

(9) RIVIERE A. et MUNIER P. - Contribution à l'étude des argiles utilisées en céramique, Institut de Céramique française, 1948.

(10) RIVIERE A - Etudes littorales, Bulletin d'Information du C.O.E.C., Paris, Octobre 1957.

(11) RIVIERE A - Cours de sédimentologie professé en Sorbonne (1956-1957), non encore publié.

(12) A. de ROUVILLE - Le régime des côtes. Eléments hydrographiques des accès des ports, Imprimerie Nationale, 1942.

(13) VAN STRAATEN - Quelques particularités du relief sous-marin de la mer de Waden (Hollande), Sédimentation et quaternaire, France 1949.

(14) VAN STRAATEN - Environments of formation and facies of the Waden sea sediments, Tijdschrift vanhet Kon. Ned. Aardrijkskundig Genootschap, mai 1950.

(15) VINCENT et RUELLAN - Communication au Comité Technique de la S.H.F. en Juin 1957 : "Mouvements solides provoqués par la houle sur un fond horizontal"

CHAPTER 14

THE RELATIONSHIP BETWEEN WAVE ACTION AND BEACH PROFILE CHARACTERISTICS

P. H. Kemp
Department of Civil Engineering.
University College London, England.

ABSTRACT.

The rational design of coast protection works requires a knowledge of the behaviour of the beach under natural conditions. The understanding of the relationship between the waves acting on the beach and the characteristics of the beach profile produced, is thus a necessary preliminary to the analysis of the causes of beach erosion and the evaluation of the effect of projected remedial measures.

The present paper describes the results of a series of preliminary hydraulic model experiments carried out by the author prior to a model study of the behaviour of groynes in stabilising beaches. Most of the beach materials used represented coarse sand or shingle in nature.

The results demonstrate the fundamental importance of the "phase-difference" in terms of wave period between the break-point and the limit of uprush, in relation to flow conditions, cusp formation, and the change from "step" to "bar" type profiles.

Within the limits of the experiments an expression connecting the breaker height, beach profile length, and grain diameter is developed, and its implications examined in relation to beach slope, and to the previous "wave steepness" criterion for the change from step to bar type profiles.

Observations are included on the rate of recession of a shoreline due to the onset of more severe wave conditions.

INTRODUCTION.

BEACH CHANGES.

Changes in the coastline may be classified as:-

(1) Progressive changes resulting in prograding or recession of the shoreline over a long period of time.

(2) Short term variations which reflect the fluctuating nature of the forces acting on the beach.

An examination of both these aspects would require a study of the forces acting, the type, quantity, source and behaviour of the beach material, the submarine contours, and the regional geology.

THE RELATIONSHIP BETWEEN WAVE ACTION AND BEACH PROFILE CHARACTERISTICS

This paper relates to the mechanics of the short term variations in beach profile characteristics.

It is reasonable to suppose that if waves of given characteristics act on a beach composed of particles which are capable of being moved under the action of the wave forces, then the beach will take up a configuration or profile characteristic of the waves and of the beach material. This relationship was remarked upon by Cornish (1) who defined the final beach configuration due to a given set of wave conditions as the "equilibrium profile" or regimen of the beach. Fenneman (2) defined such a profile as "that which the water would impart if allowed to carry its work to completion". This equilibrium form is probably seldom attained in nature.

Whereas the hydraulic model is a valuable aid to the understanding of beach processes, the variability of wave conditions in nature, together with the lack of complete reaction by the beach, makes the problem of correlating model and prototype measurements correspondingly difficult.

BEACH STUDIES.

So far no generalised theory has resulted from the many observations which have been made both in the laboratory and in the field.

Beach profiles have however been broadly classified as one or other of two types. These types are generally associated with steep waves and with low waves. The two beach profile types have been variously defined as

(a) summer, ordinary, or berm type

(b) winter, storm, or bar type.

Typical profiles are shown in Figure 1. One basic difference between these profiles when well developed is the presence of a "step" in case (a), and a "bar" in case (b). Type (a) is frequently found on shingle beaches, and type (b) on sand beaches. The profiles will be referred to as step type and bar type.

Waters(3) carried out a series of experiments on beach profiles and concluded that the change from step to bar type profiles was a function of deep water wave steepness H_o/L_o. He found the critical value to lie between 0.02 and 0.03, the bar type existing for the higher values. Similar results have been found by other investigators. Field studies by Patrick and Wiegel (4) have not confirmed these model values of critical wave steepness, and much lower values have been quoted (5), (6).

Bagnold (7) has shown that for step type beaches, the beach crest height is proportional to the wave height. Experiments have also

shown that profiles produced during variations in tidal range and wave period do not differ appreciably from the profiles formed under constant conditions (8), (9).

PRESENT EXPERIMENTS.

APPARATUS.

The wave tank was a small three dimensional model with overall dimensions 15'0" x 9'0". The paddle was designed for translatory and rotary movement, and was driven by a constant speed motor, with fixed ratio reduction gears. The bed of the tank was concrete. The beach end was fitted with an adjustable bed plate to provide an inclined base for the beach material. The operational water depth was six inches.

Wave height and phase measurement were made by means of capacitance wire probes and long-after-glow oscilloscope. Details of breaking waves and run-up were obtained by cine photography.

BEACH MATERIAL.

For true similarity beach material should be moved by waves or currents at the corresponding depth, behave in a similar way in suspension, and be deposited in the correct relative position. In addition the rugosity and permeability of the material should correspond to the prototype values.

For the same specific gravity, fall velocity and permeability are similar functions of grain diameter. Absolute values depend on the coefficient of drag which in turn depends on the flow condition relative to the particle. This may be laminar, transitional or turbulent. If particles are scaled down they may be transferred from say turbulent prototype conditions to transitional or laminar flow conditions in the model. The general hydraulic environment of the particle is also important. Here distinction must be made between conditions seaward of the breakers, and those landward of the breakers. The flow conditions in the seaward zone are likely to be very different in prototype and model. In and shoreward of the breakers fully turbulent conditions exist in both model and prototype, and dynamical similarity is good.

It may be concluded that a beach material chosen to represent conditions shoreward of the breakers, may not show results which are representative in the offshore zone.

In the present instance the materials employed were chosen so that their fall velocities were outside the laminar range, with median diameters between 0.45 mm and 2.0 mm. Both quartz sand and pumice were used. The present paper relates only to the quartz sand experiments, except where otherwise stated.

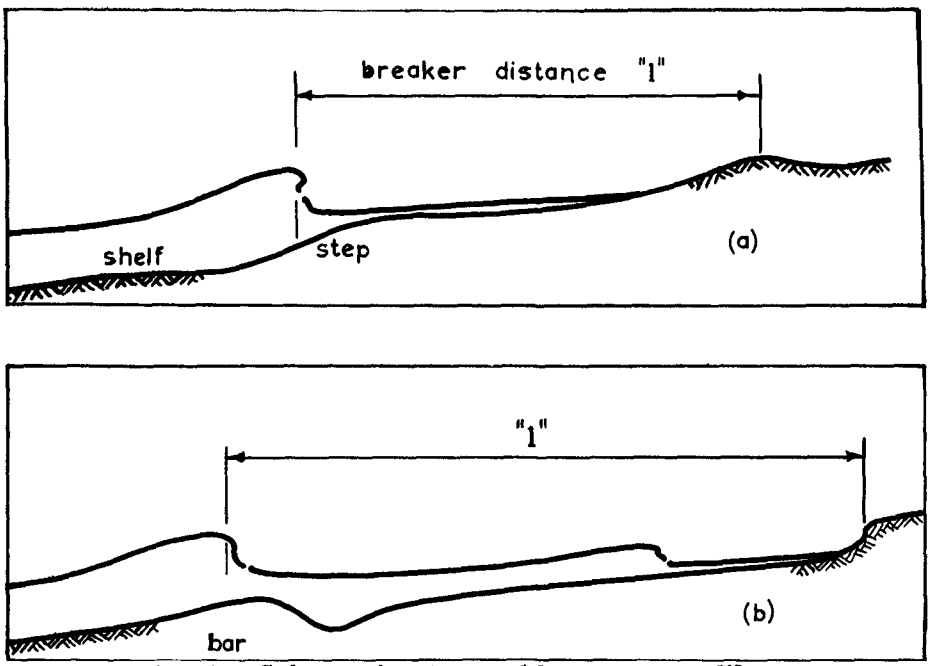

Fig. 1. Schematic step and bar type profiles.

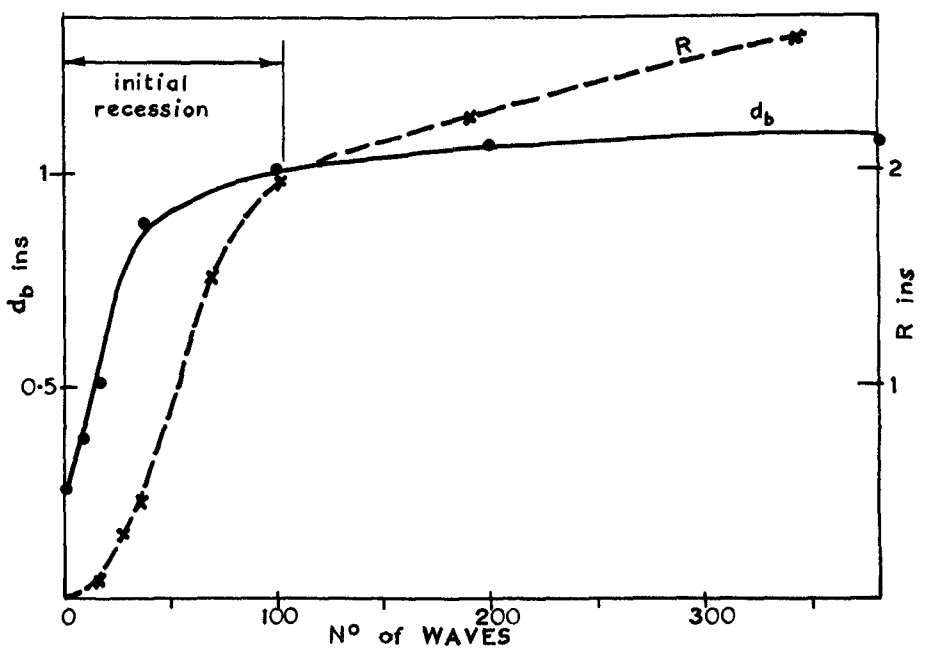

Fig. 2. Rate of shoreline recession R and increase in breaker depth d_b under severe wave attack.

EXPERIMENT : RATE OF BEACH ADJUSTMENT.

The rate at which a beach adjusts its profile to the onset of new and more severe wave conditions was first studied.

Having preformed the beach to a step profile using waves of period T = 0.55 secs, H_o = 0.48 inches, the beach was attacked by waves of period T = 0.42 secs, H_o = 1.17 inches. The beach material in this experiment was pumice, median dia 0.9 mm, specific gravity 2.0, and fall velocity 4.1 cm/sec. Beach profile measurements were made after the following numbers of waves:-

10, 20, 40, 70, 100, 200, 400, and thereafter at 4 minutes, 9 mins, 13 mins and 25 mins, measured from the beginning of wave attack.

The initial stages of beach adjustment are represented in Figure 2, where the rate of recession of the shoreline and the lowering of the beach step are plotted. The initial rate of recession is small until the original step has been destroyed.

Following this initial recession it was found that the rate of retreat of the shoreline was proportional to the logarithm of the time measured from the beginning of wave attack.

The most spectacular beach changes under storm conditions can therefore be observed in the early stages.

EXPERIMENT : PROFILE FORMATION, AND TRANSITION FROM STEP TO BAR PROFILE

General Description. With low waves a step profile is formed. The step is created by a vortex produced by the backwash. The water flowing down the beach in the backwash has a velocity distribution with a maximum in the upper layers and a minimum at the bed. On approaching the still water level the water is decelerated. The deceleration is usually accentuated by a rise in water level due to the proximity of the next wave crest. This deceleration results in the formation of a vortex with a horizontal axis, in which the upper layers rotate downwards towards the bed and thence in a shoreward direction. Figure 3. The high velocities associated with this motion produce a scour depression. Some of the scoured material goes into suspension. The heavier particles are moved landward by the component close to the bed.

As the crest of the next wave reaches the break-point the high velocity of the horizontal component of its orbital motion near the bed produces a reverse vortex at the edge of the scour depression. Figure 3. This deepens the scour hole. At the same time the orbital velocity "planes" the bed down in the area just seaward of the break-point, leaving a horizontal shelf. Some of this material is carried forward with the onwash to form the beach crest.

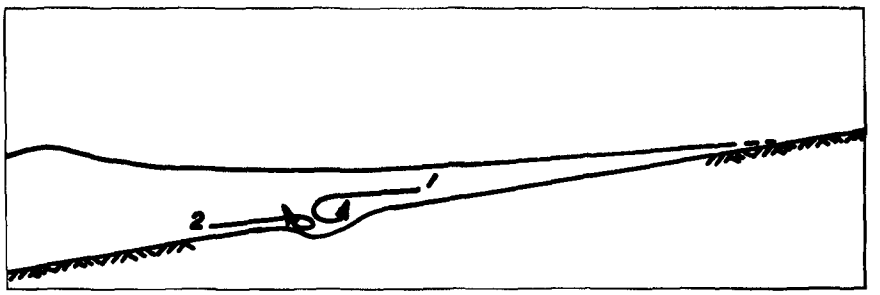

Fig. 3. Mechanism of step formation.

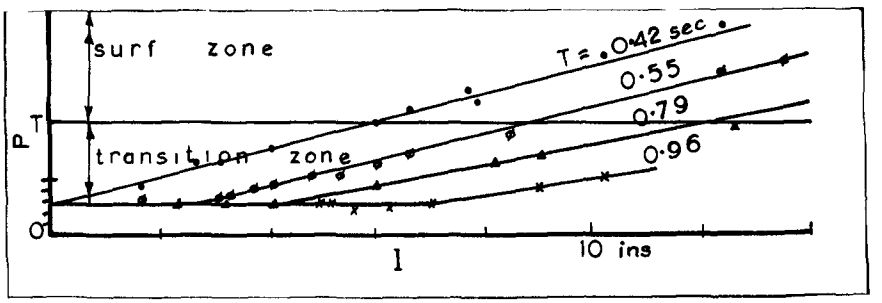

Fig. 4. Phase difference P versus breaker distance l.

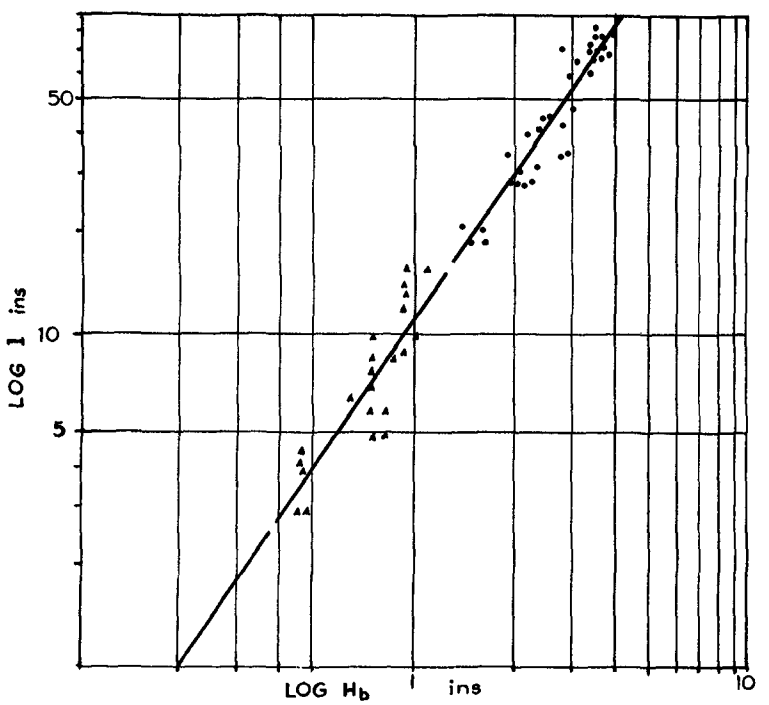

Fig. 5. Relationship between breaker distance and breaker height in the transition and surf conditions for several quartz sands.

With increase in wave height the step moves seaward and the crest moves landward, the crest height initially increasing. With successive wave height increments the crest first reaches a maximum height, then decreases, and is finally flattened by the highest waves. The step profile gradually elongates. Material from the foreshore moves seaward to the break-point. Here the fine material goes into suspension and moves seaward through the breakers. The coarsest material is trapped at the bed on the seaward face of the step, building it seaward.

During this transition from step to bar profile, a scour hole or plunge pocket may form landward of the break-point, due to the turbulence created by the breaking wave assisted by the interference of the seaward flowing current of the backwash in the lower layers.

The step profile gradually becomes indefinite and finally changes to a bar profile.

After the bar profile has fully formed the breakers become less violent, since the momentum effect of the backwash is reduced. This is explained by the character of the return flow referred to under the heading " The Surf Condition " below. The plunge pocket may partly fill in.

Detailed Examination. In these experiments each wave period was held constant while a series of runs was made using different wave heights, starting with low waves and increasing the wave height for each run. The following observations were made:-

(1) wave height
(2) distance from break-point to limit of uprush, referred to below as the "breaker distance"
(3) time for the wave to travel from the break-point to the limit of uprush
(4) type of flow in the zone shoreward of the breakers
(5) regularity of the shoreline in plan.

If the time of uprush mentioned in (3) above is expressed in terms of the wave period, then it can be described as the " phase-difference" between break-point and beach crest.

The phase-difference was found to be the dominant factor in the relationship between the waves and the beach profile, and resulted in the following classification of wave/beach conditions.

The Surge Condition. Figure 4 shows phase-difference plotted against breaker distance for varying periods and wave heights.

Increase in wave height produces an increase in the breaker distance. Figure 4 shows that initially the phase difference or time of uprush remains constant at a value of approximately 0.3 T, even though the breaker distance increases. The beach material in this instance was pumice 0.9 mm median diameter.

As the breaker distance is further increased a critical point is reached at which the phase-difference ceases to be constant. Thereafter the phase-difference increases with increase in wave height.

The behaviour of the wave and the beach profile in the initial zone of constant phase-difference resembles the behaviour of a simple pendulum. An increase in amplitude of the incident wave produces an increase in the velocity of the wave surge. The beach crest retreats and steepens but the time of the surge remains constant. This condition will be referred to as the " Surge Condition".

Flow conditions in the surge zone of behaviour are of the type noted by Bagnold (7) in which negligible mixing or interchange takes place between the water seaward of the break-point and the shoreline. The motion is characteristically oscillatory.

It was observed in the case of all wave periods, that beaches formed under surge conditions were well sculptured and perfectly regular along the line of the beach. There was no tendency for lateral circulation to take place.

The Transition Condition. With further increase in wave height a point is eventually reached at which the beach crest to breaker distance ratio no longer satisfies the surge condition. This is the critical point already referred to. The crest height ceases to increase and later begins to diminish. With the retreat of the beach crest and the seaward movement of the break-point, the time taken for the wave to reach the crest increases. The time available for back-wash before the next wave breaks is consequently reduced. As a result the backwash is not completed before the next wave plunges. This is the point of demarcation between the surge zone, with its stable oscillatory flow conditions, and the "transition zone" of behaviour characterised by unstable flow and lateral circulation.

The instability of the flow pattern under transition conditions inevitably results in local lateral circulations being set up which enable the lack coincidence between the completion of the backwash and the next plunge , to be replaced by a continuous and self - perpetuating pattern of flow between the break-point and the shore. This horizontal flow pattern is the origin of Beach Cusps.

Further observations on beach cusps were made which are outside the scope of the present paper. It will however be readily appreciated that if the waves are breaking obliquely to the shore, the littoral current forms an alternative or additional flow route for the backwash, and the development of cusps is retarded or eliminated according to the degree of phase-difference in relation to the obliquity of the breakers.

Transition conditions are characterised by some interchange between the water in the zone seaward of the breakers and the near-shore zone.

The Surf Condition. As the phase-difference increases, the partly oscillatory nature of the onwash and backwash with limited interchange of water through the breakers gradually gives way to continuous flow into and out of the breaker zone. Continuous flow conditions become fully developed when the phase-difference becomes equal to the wave period.

This is the point at which the bar type profile achieves full development.

The flow conditions for phase-differences greater than the wave period T will be calssified as the "surf condition".

The change from step to bar type profile is therefore a function of phase-difference. Hitherto the criterion has been that of critical wave steepness. However the variation in value quoted by different investigators is well known, and evidence that the value varies with beach slope (10) supports the phase-difference criterion.

Beach cusps disappear once surf conditions are established.

DOMINANT FACTORS RELATING BEACH AND WAVE CHARACTERISTICS.

This is in the nature of an interim report on the aspect of the investigation directed towards the determination of specific relationships enabling the results of model experiments to be applied to beaches in nature.

The model laws relating to gravity waves alone are well established. The difficulty arises in relation to the behaviour of the beach material under wave action.

One encouraging aspect of this problem is the observed fact that model beach profiles posess the general characteristics of their natural counterparts. A second point, already mentioned, is that the conditions for dynamical similarity are most likely to be found in the turbulent profile-forming zone between the break-point and the limit of the onwash.

It is clear that any scale relationship of this type must reconcile two generally acknowledged discrepancies between the model and nature, namely

(i) that the critical wave steepness values found in models for the change from step to bar type profiles are much higher than in nature

(ii) that model beach slopes are usually much steeper than in the prototype.

Choice of parameters. A number of investigators have made dimensional analyses of the problem. The number of variables included

has been large, and as a result a correspondingly large number of non-dimensional groups have been derived. By keeping the number of variables to a minimum experimental verification is facilitated. The minimum choice must include (i) a wave characteristic (ii) a beach characteristic (iii) a beach material characteristic.

(i)The wave characteristic was chosen after making a limited but detailed study of the breaking wave under surf conditions. This confirmed that at and subsequent to the break the wave velocity corresponds very closely to that given by the solitary wave theory. In addition these experiments indicated that the envelope of wave height between the break-point and the limit of the onwash, shows an approximately linear decrease with distance.

The wave height at the break-point was therefore selected as the wave characteristic. The wave height adequately describes the solitary wave, since the water depth at the break-point is directly proportional to the wave height. The effect of shoaling on the wave length, wave celerity and height of oscillatory waves is thus eliminated.

(ii)The beach profile characteristic normally chosen is the beach slope. However, the slope of a beach is different at different points between the offshore zone and the shoreline, and both the choice of reference position and the accurate measurement of the slope in a small model is not easy. On the other hand the engineer is primarily concerned with the determination of the landward limit of wave action under given conditions. In the present case therefore the variable chosen was the breaker distance. This in addition provided a link with the phase-difference experiments. Since the bed level at the break-point is related to the breaker height, an indirect measure of beach slope can be derived.

(iii) Both fall velocity and permeability are functions of grain diameter. Grain diameter is also a measure of roughness. To allow for the choice of materials posessing different specific gravities, both fall velocity and grain diameter were chosen as variables.

Using the following notation:-

H_b = breaker height
l = breaker distance (from break to limit of uprush)
w = fall velocity
D = grain diameter
g = force per unit mass due to gravity

and with constant fluid characteristics, dimensional analysis leads to :-

$$l = H_b \cdot \phi \left\{ \left(\frac{g^{\frac{1}{2}} H_b^{\frac{1}{2}}}{w} \right), \left(\frac{H_b}{D} \right) \right\} \quad \ldots\ldots\ldots (1)$$

$$\text{or} \quad l = H_b \quad \phi \left\{ \left(N_F \right)^{\frac{1}{2}}, \left(\frac{H_b}{D} \right) \right\} \quad \ldots\ldots\ldots (2)$$

where N_F is the Froude Number relating the wave and grain characteristics.

A series of preliminary experiments was undertaken to explore this relationship. Figure 5 shows a logarithmic plot of l v H_b for quartz sands ranging from 0.5 to 2.0 mm median diameter. The upper part of the curve consists of measurements computed from data published by Waters (3). The range of wave periods employed varied from 0.44 to 1.40 seconds. The effect of variation in grain diameter is not shown. The curve does not apply to the surge zone.

The curve indicates that for a constant specific gravity of grain of 2.64 and using coarse sands, the breaker distance l is proportional to $H_b\,(H_b)^n$ where n is approximately 0.5.

$$\text{i.e.} \quad l \propto H^{n+1}$$

Segregation of data based on grain diameter so far carried out indicates that l is in fact also a function of D, and that the relationship can be written

$$l = K.\, H_b \left(\frac{H_b}{D}\right)^n \qquad \ldots\ldots\ldots (3)$$

Although sufficient data are not yet available to enable final values of K and n to be established, the value of n seems to lie between o.45 and 0.65, and the approximate value of K is 24 when H_b is in feet units, and D is in m.m.

Provisionally therefore

$$l = 24\, H_b \left(\frac{H_b}{D}\right)^{0.5} \qquad \ldots\ldots\ldots (4)$$

The beach slope can be represented by the ratio $\frac{l}{H_b}$ since the breaker depth d_b is proportional to H_b. Thus if x is an horizontal coordinate, the cotangent of the beach slope becomes:-

$$x \propto \left(\frac{H_b}{D}\right)^n \qquad \ldots\ldots\ldots (5)$$

Hence for the same grain diameter and specific gravity in model and prototype, the beach gradient scale distortion is proportional to the n th power of the vertical scale in the model. This assumes that the waves are produced to the vertical scale. For example, with a vertical scale of 1/40, and n= 0.5, the model beach slope would have a distortion of 6.3 .

In the surge zone, $l \propto H^n$.

THE RELATIONSHIP BETWEEN WAVE ACTION AND BEACH PROFILE CHARACTERISTICS

APPLICATION TO THE CHANGE FROM STEP TO BAR TYPE PROFILES.

As already shown the change from step to bar type profiles depends on the phase-difference. This in turn is a function of wave period and wave height for a given grain diameter. The beach slope is similarly a function of wave height and grain diameter. It is possible therefore to relate the change from step to bar profile to these characteristics.

The phase-difference involves the time t for the wave to travel from the break-point to the limit of the onwash. Since the envelope of wave height decreases almost linearly with distance x from the break-point, then the wave height dimension h measured above the S.W.L. at any point distant x from the breakers is given by

$$h_x = h_b \left(1 - \frac{x}{l}\right) \qquad \ldots\ldots\ldots (6)$$

The celerity of the solitary wave is given by:-

$$C = \sqrt{g\,(d_b + h)} \qquad \ldots\ldots\ldots (7)$$

Since both d_b and h_b are proportional to H_b, then

$$C = \sqrt{k\,g\,H_b} \qquad \ldots\ldots\ldots (8)$$

Introducing equation (6)

$$C_x = \sqrt{k\,g\,H_b\left(1 - \frac{x}{l}\right)} \qquad \ldots\ldots\ldots (9)$$

The time for the wave to travel an elemental distance dx is $dt = \frac{dx}{C_x}$

whence $$t_x = \int_0^x \frac{dx}{C_x}$$

The total time t for the wave to travel from the break-point to the limit of the onwash is thus:-

$$t = \frac{-2\,l}{(k\,g\,H_b)^{\frac{1}{2}}}\left[\left(1 - \frac{x}{l}\right)^{\frac{1}{2}}\right]_0^1 \qquad ..(10)$$

$$\text{i.e. } t = \frac{2\,l}{(k\,g\,H_b)^{\frac{1}{2}}} \qquad \ldots\ldots\ldots (11)$$

Since the full change over from step to bar profile occurs when the time of uprush equals the wave period T, then for a given period the critical condition is given by :-

$$T = \frac{2\,l}{(k\,g\,H_b)^{\frac{1}{2}}} \qquad \ldots\ldots\ldots (12)$$

If the depth at which the wave breaks d_b is equal to $1.3\ H_b$, and the wave height asymmetry $h = 0.7\ H_b$ then

$$T = \frac{2\,l}{(2\,g\,H_b)^{0.5}} \qquad \ldots\ldots\ldots (13)$$

For a given grain diameter $l \propto (H_b)^{n+1}$

therefore $T \propto (H_b)^{n+0.5}$ $\qquad \ldots\ldots\ldots (14)$

If n is taken as 0.5, the critical breaker height then varies directly with the wave period

$$H_b \propto T \qquad \ldots\ldots\ldots (15)$$

$$\text{or} \quad H_b \propto (L_o)^{0.5} \qquad \ldots\ldots\ldots (16)$$

Comparison can now be made with the wave steepness criterion,

since $$\frac{H_b}{L_o} \propto \frac{(L_o)^{0.5}}{L_o} \propto \frac{1}{T} \qquad \ldots\ldots\ldots (17)$$

In other words, the critical value of wave steepness varies inversely with the wave period.

For example, with a given beach material with a critical wave steepness value H_b/L_o of say 0.032 for $T = 1$ second, the corresponding steepness value in nature for $T = 8$ seconds would be equal to 0.004.

By assigning specific values to K and n in equation (3) and to k in equation (12), calculated values of breaker distance, critical wave height, and beach slope can be easily derived.

DISCUSSION

The paper has attempted to present an integrated picture of the relationship between waves and beaches. Work is still proceeding, and where numerical values are given in the text, these must be regarded as provisional. It is never-the-less hoped that their presentation will lead to more specific evaluation.

In attempting to relate and apply the parameters to beaches of fine sand, it is possible that the immobility of such beaches under the action of small waves, may obscure the wave/beach profile relationship. In models, fine sand beaches not formed initially to the correct equilibrium slope, may be only partially adjusted by subsequent wave action. Similar beaches in nature may develop a profile characteristic of a dominant wave, with only significant movement in the breaker area. Similarly on shingle beaches, if the waves are

relatively small compared with the size of the beach material, the beach may behave as a permeable wave absorber.

For wave periods less than 2 seconds, Diephuis (11) has shown that the wave steepness becomes a differential factor in relation to the breaker depth. This could affect the breaker distance as computed from the breaker height. In the present experiments the exclusion of waves with high initial steepness and of short period from the results did not affect the wave/breaker distance relationship.

SUMMARY.

1. The turbulent conditions in and shoreward of the breakers in both model and prototype are conducive to dynamic similarity.

2. The rate of beach adjustment under more intense wave action is initially high, but decreases logarithmically with time.

3. The phase-difference or ratio between run-up time and wave period, is the dominant factor in determining the characteristic shape of the beach profile. The phase-difference criterion enables wave conditions to be classified as 'surge', 'transition', or 'surf', each with characteristic flow patterns.

4. The transition from step to bar type profile is fully achieved once surf conditions are established.

5. Beach cusps are initiated and developed by the three dimensional flow pattern which occurs when the phase-difference ratio is in the unstable transition zone. Cusps do not occur under surge or surf conditions.

6. The dominant factors for dimensional similarity in relation to beach profiles, are :-

(a) breaker height (H_b)
(b) breaker distance (l), i.e. the distance from the break-point to the limit of the onwash.
(c) the fall velocity of the grain (w), and the grain diameter (D).

7. For beach materials of a given specific gravity, the relationship between the beach profile dimensions and the wave characteristics is of the form below for transition and surf conditions

$$l = K H_b \left(\frac{H_b}{D}\right)^n$$

(For surge conditions $l \propto (H_b)^n$).

8. The cotangent of the beach slope is proportional to $(H_b/D)^n$. Model beach slope distortion is thus proportional to the n th power of the vertical scale.

9. The numerical value of the power n referred to in paragraphs 7 and 8 above, is of the order of 0.5 . The scatter of values so far obtained lies between 0.45 and 0.65.

10. The critical wave height at breaking for the transition from step to bar type profile is a function of the wave period T, viz

$$H_{b(crit)}^{n+0.5} \propto T$$

which for a value of n = 0.5 becomes $H_{b(crit)} \propto T$

11. Values of breaker distance, critical wave height, and beach slope, can be readily derived from the relationships developed above.

REFERENCES.

Kemp, P.H. The effect of groynes on beach formation and erosion. Ph.D Thesis. University of London. 1958.

1. Cornish Vaughan. On sea beaches and sandbanks. Geog. Jour. 11 1898, pp. 528-543, 628-651.

2. Fenneman, N.M. Development of the profile of equilibrium of the sub-aqueous shore terrace. Jour. Geol., 10, 1902, pp. 1 - 32.

3. Waters, C. H. Equilibrium slopes of sea beaches. Thesis. University of California, 1939.

4. Patrick D.A. & Wiegel R.L. Amphibian tractors in the surf. 1st Confce on Ships and Waves. 1955. Ch. 29.

5. Beach Erosion Board. Coast erosion and the development of beach profiles. Tech. Memo. 44, Corps of Engrs. U.S.A. 1954.

6. King, C.A.M. The relationship between wave incidence, wind direction and beach changes at Marsden Bay, Co. Durham. Inst. Brit. Geog. Trans. 1953. Pubn 19.

7. Bagnold, R.A. Beach formation by waves. Some model experiments in a wave tank. Jour.I.C.E., 15 , 1940 - 41. p. 38.

8. Beach Erosion Board. Laboratory study of effect of tidal action on wave-formed beach profiles. Tech. Memo. 52, Corps of Engrs U.S.A., 1954.

9. Beach Erosion Board. Laboratory study of the effect of varying wave periods on beach profiles. Tech. Memo 53, Corps of Engrs, U.S.A., 1954.

10. King, C.A.M. Beaches and Coasts. Arnold, London. 1959. p.184.

11. Diephuis, J.G.H.R. Scale effects involving the breaking of waves. Proc. 6th Confce Coastal Eng. 1957, p. 199.

CHAPTER 15

RESEARCH ON WAVE ACTION ON LAKE SHORES AND UNLINED SLOPES OF ARTIFICIAL EARTH STRUCTURES

A. A. Pichoughkin
Candidate of technical science
The All-Union Scientific Research
Institute of Hydrotechnics named for
B. E. Vedeneev

The construction of big modern hydro-electric plants makes it necessary to create large reservoirs, of which the surface area can be on the order of some hundreds or even thousands square kilometers. As for example, the surface area of the Kuibyshev reservoir is 5600 km^2 that one of the Sherbakov reservoir - 4500 km^2, of the Stalingrad reservoir - 3470 km^2, of Kahovka reservoir - 2155 km^2. The dimensions of reservoirs in plan being so considerable, the waves of 3-3,5m height can appear on the water surface. The shoreline of reservoirs created on U.S.S.R. plain rivers exceeds the length of 13000 km. The problem of the protection of the upstream slopes of artificial earth structures and natural shores against wave action is of extreme importance under these conditions.

From the very first days of the existence the reservoir shores are subject to a rather considerable reforming. The destructive force of the surface water waves is the principal factor for the determination of the volume of shore disintegration along the reservoir bottom contour. When combined with landslides, landslips and caving-in of macroporous soils, the surface water waves cause shore movement up to 250 m, measured horizontally, average year movement being 15-20 m (within th first 4-5 years).

Hundreds of settlements and industrial enterprises are often located on reservoir shores, which can turn out to be eroded and submerg consequently in some years. So when designing the hydro-electric proje it is necessary to determine the danger zone and to move all the settlements and enterprises out of it; otherwise some adequate measures for protection against submergence must be taken. These problems have assumed ever greater importance within the last few years.

The first knowledges of reservoir shore dynamics relates to thirties in the U.S.S.R. In 1935 the noted soviet hydro-geologist, academician F. P. Savarenski (1)* raised, for the first time, the questi

*See References

about the creating of the scientific basis for predicting the volume of the shore disintegration due to wave action for the reservoirs, projected on the Volga and Dnieper rivers at that time. He himself predicted the volume of shore disintegration for Iljinskaja power plant reservoir on the Lower Dnieper. His work was supplemented later by his disciples and followers: W. A. Shirjamov (2,3), B. W. Poljakov (4), E. G. Kachugin (5), who proposed some engineering methods of predicting the shore dynamics with a fair degree of accuracy. The above mentioned scientists having analysed the results of a great number of observations carried out on the Volga reservoirs: Ivankovskoje, Istrinskoje, Himkinskoje, Klaxminskoje and Uglichskoje proposed the design schemes for determining the stable profiles of underwater slopes. In the post-war period the scientific articles by B. A. Pyshkin (6), Gh. S. Solotarev (7), N. E. Kondratjev (8) and others were published. The results of systematical observations carried out on the reservoirs: Kahovskoje, Kuibyshevskoje, Gorkovskoje, Rybinskoje, Tsymljanskoje and others were analysed in those works.

Apart from storing and systematization of the quantitative data on final shapes and dimensions of underwater slope profiles the attempts are made to determine the effect of the shore-forming factors: the wave energy, the reservoir water level fluctuation, the lithology and the height of above-water shore zone, the initial under-water slope contour as well as the character of water surface undulation. The problem of interaction between the waves and the eroded reservoir bottom and natural laws of shore-forming processes, all as a function of the time, is presently under investigation.

All the problems above are to be solved. For this purpose it is necessary to obtain not only the prototype observational data but some model study data too. The latter should enable to determine the effect of each of shore-forming factors separately. That is why in the U.S.S.R. the most serious attention is given to the development of different methods of modeling of wave processes over inclined eroded bottoms and of movement of non-cohesive soils due to waves. Some achievements obtained have been already published (A. S. Ofitserov; 10). Published data indicate that by carrying out the laboratory tests properly it is possible to ensure the similarity of research on the model and on the prototype with a satisfactory approximation. The Soviet hydraulic engineers and scientists direct their efforts towards the construction of the earth dams and levees with gentle unlined slopes, having the contours similar to that of the old reservoir, lake or sea bottoms. The artificial shallow water parts of the reservoir are to favour the avoiding the expensive concrete and large stones to be used for earth structure slope protection. Some works in this field by B. A. Pyshkin (11), E. S. Tsaits (12), J. E. Gugnjaev (13) enable to build the 0.2 mm sand levee with unlined upstream

slope 1:20 on Kremenchug reservoir near Cherkassy. In 1958 on the Terek river (Sengeleevskoje) there was built the 7.5 m earth dam with the protective gravel-rubble prism 1:15 on the upstream slope (14).

As a result of the experimental research carried out by Hydraulic Laboratory of the All-Union Scientific Research Institute of Hydrc technics names for B. E. Vedeneev (VNIIG) in 1957-58 the empirical relations are obtained which determine the shapes and the dimensions of stable profiles of artificial earth structures and natural shores composed of non-cohesive soils and subject to the frontal wave action. The frontal wave approaching is often a design value, as:

(1) The earth dams are usually oriented perpendicularly to the river valley direction, so to the longest fetch direction.

(2) The levees are usually built on flat shores, this fact giving almost frontal wave approaching due to refraction in shallow water.

The report by engineer I. J. Popov on some model study data obtained at the Hydraulic Laboratory of VNIIG has been offered to the present Congress.

REFERENCES

1. F. P. Savarenski, To the problem of dammed river shore disintegration. "Hydrogeology and Engineering Geology" N1 (WIMS), Moscow, 1935.

2. W. A. Shirjamov, To the problem of reservoir shore disintegration. Transactions of the Institute of Geological Sciences of the U.S.S.R. Academy of Sciences, Issue 23, Engineering-Geological Series, N2, Moscow, 1940.

3. W. A. Shirjamov, To the methods of the reservoir shore study. Transactions of the Institute of Geological Sciences of the U.S.S.R Academy of Sciences, Issue 43, Engineering-Geological Series, N Moscow, 1940.

4. B. W. Poljakov, Hydrological analysis and designing. Leningrad 1946.

5. E. G. Kachugin, About the volume of dammed river disintegration. "Gidrotechnicheskoje stroitelstvo", N12, 1951.

6. B. A. Pyshkin, The reservoir shore disintegration dynamics. Edition of the Academy of Sciences of the Ukrainian S.S.R.

7. Gh. S. Solotarev, The reservoir shore disintegration research

carried out by the students of the geological faculty of the Moscow University in 1951.

8. N. E. Kondratjev, The wave design and the reservoir shore disintegration prediction. Hydrometeorological edition, Leningrad, 195

9. N. E. Kondratjev, Wave energy losses in shallow water. Transactions of the State Hydrological Institute, Issue 28, 1951.

10. A. S. Ofitserov, The problem of methods of laboratory research and lineal wave energy losses. Moscow, 1958.

11. B. A. Pyshkin, Designing of the profiles of the earth hydrotechnic structures with unlined upstream slopes composed of non-cohesive soils. Informational Letter N6, The Institute of Hydrology and Hydrotechnics of the Academy of Sciences of the Ukrainian S.S.R., Kiev, 1956.

12. E. S. Tsaits, Wave action on the slopes composed of noncohesive soils, Kiev, 1958.

13. J. E. Gugnjaev, Laboratory research of sand slope dynamics. Transactions of the Central Scientific Research Institute of Soil Mechanics and Foundations, Edition N25, 1955.

14. K. N. Sevastjanov, The usage of a wave damping slope for earth dams. Hydrotechnics and Reclamation, N11, 1959.

15. I. J. Popov, The basic planning and design of the earth structures with unlined, stable against wave action slopes. Collected annotations of scientific research on hydrotechnics, finished in 1958. Gosenergoisdat, M-L, 1959.

CHAPTER 16

EXPERIMENTAL RESEARCH IN FORMATION BY WAVES OF STABLE PROFILES OF UPSTREAM FACES OF EARTH DAMS AND RESERVOIR SHORES

I. J. Popov
Engineer, the All-Union Scientific
Research Institute of Hydrotechnics
named for B. E. Vedeneev
Leningrad, U.S.S.R.

INTRODUCTION

Within the last few years the Soviet hydraulic engineers have beer making continuous efforts to avoid use of concrete slabs and blocks and stone riprap as protective cover of upstream slopes of earth dams and reservoir shores against the disrupting effects of waves generated by the action of wind upon the water surface.

Their efforts have been aimed at finding the cheaper procedure. Of all the possible ways of slope and shore protection, an engineering measure, the idea of which consists in distributing the wave energy dissipation over a considerably large portion of a sufficiently gentle slope, should be given a special attention. This measure makes it possible to substantially relieve the protective cover and in some cases to leave the slope uncovered. The possibility of unlined slopes, stable enough agains wave action is proved out by the experience of reservoir operation. Shores and underwater slopes of artificial lakes composed of non-cohesiv soils are usually subject to considerable disintegration due to wave actio The process of disintegration which goes on rather fast at the initial stage of lake existance, slows down with the formation of a flat lake-side shallow, whereon dissipation of wave energy takes place. At a certain stage of development the underwater slope assumes such dimensions and outlines which enable it to dissipate the whole of the wave energy and practically to protect shores from further destruction. The profile of the slope at which it will permanently stand underwater is referred to as the "profile of equilibrium" or "dynamically stable profile". The term "equilibrium" in this case doesn't imply absolute immovability of the material acted on by waves, but stands for such a movable state at which particles of the soil are making oscillatory movements round some middle position without the resultant movement neither towards nor

off shore.

The problem, thus, is reduced to reproducing on the submerged slope of a dam during construction or on shores of a future reservoir the relief analagous to that of the bottoms of long-term reservoirs or artificial lakes (ponds) and seas.

Dimensions of waves, the direction in which the wave rides up the shore or structure, limits of reservoir water level fluctuations and size of soil particles are controlling factors determining outlines of the profile of equilibrium.

In 1957-58 the Hydraulic Laboratory of the All-Union Scientific Research Institute of Hydrotechnics named for B. E. Vedeneev initiated a test program on wave effect on the upstream slopes of earth dams and on reservoir shores.

The first series of tests have been carried out to study the influence of the two above-mentioned factors, that is: dimensions of waves (height and length) and size of particles of non-cohesive soil on the form of the profile of equilibrium.

The purpose of the test program was to set up the design relations by means of which it would be possible at given wave dimensions and grain-size distribution in an earth structure to determine the outlines and dimensions of the underwater slope which provide its stability without lining, the wave ride-up being frontal and the level of still water in a reservoir being constant.

The following notations are used in this paper

h = the height of the wave from trough to crest
λ = the length of the wave
d = the diameter of the soil grains
ν = the coefficient of kinematic viscosity of water
g = the acceleration of gravity

Symbols "m" and "p" indicate that the above values should be referred to model and prototype respectively.

α_l = the geometrical scale coefficient for values of linear dimensions

$$\left(\alpha_l = \frac{h_p}{h_m} = \frac{\lambda_p}{\lambda_m} = \frac{d_p}{d_m} \right)$$

I. INVESTIGATIONAL METHODS. TESTING PROCEDURE AND BRIEF DESCRIPTION OF EXPERIMENTAL SET-UPS

The stability of particles of non-cohesive soils on the slope subject to wave action is determined, apart from gravity, by the following principal forces:

1. Forces resulting from streamlining of soil particles by the liquid with variable in time, value and direction bottom velocities caused by wave action above the slope surface.

2. Variable in value and direction percolation forces normal to the surface of the slope acting on a particle out from the porous medium of the slope.

The shallow-water-wave-over-an-inclined bottom theory does not afford opportunities to set up the functional relationships permitting to determine by way of calculations the velocity and pressure fields in a bottom layer. In connection with this it should be noted that, at the time being, it seems impossible to obtain the equation of equilibrium of soil particles on the surface of pervious slope and to determine the gradients corresponding to the stable state of the latter. This largely explains for experimental way of studies.

The first and foremost problem arising from consideration of different testing procedures is the problem how the values obtained during tests should be adapted to prototype. If we were sure beforehand that the forces determining the stability of soils on the slope obey scaling-up according to the law of gravitational similarity (Froude's law) it would be enough to obtain in laboratory conditions the stable profiles of slopes for a number of wave height-to-grain diameter ratios $a_1 = \frac{h_1 m}{d_m}$, $a_2 = \frac{h_2 m}{d_m}$ etc. and using geometrical scale coefficient to adopt them to prototype for the same values of a_ℓ. It goes without saying that the grain diameter would be scaled-up in accordance with the geometrical scale coefficient of the model $(d_p = a_\ell \cdot d_m)$.

However, of all the forces acting on soil particles on the surface of the slope, only external wave pressure probably obeys Froude's law. Scaling-up of the bottom velocities by this law is strongly doubted, and as to seepage phenomena associated with reservoir roughness they can hardly obey, due to their nature, the law of gravitational scaling-up.

Taking into consideration the said above, a conclusion could be easily drawn that the geometrical scaling-up of grain-size and wave dimensions does not provide the same geometrical similarity of stable

profiles formed by waves (this is referred at least to those cases when model tests are carried out on a relatively small scale).

The absence of the theory of scaling-up the erosion and deposits of non-cohesive soils due to wave action necessitated that scale series of tests should be carried out in laboratory conditions, i.e. such tests when a phenomenon under investigation was reproduced on different geometrical scales.

Experimental research consisted of three testing series corresponding to three grain-sizes respectively: d_{60} = 2 mm[x] (1st series), d_{60} = 3.5 mm (2nd series) and d_{60} = 6.0 mm (3d series), the coefficients of non-uniformity being equal to $K = \frac{d_{60}}{d_{10}} = 1.2 \div 1.8$. 63 tests were made on sands of the above-mentioned grain-size, wave heights being from 5 to 40 cm and steepness $E = \frac{h}{\lambda} = \frac{1}{10}, \frac{1}{12}, \frac{1}{15}$ and $\frac{1}{20}$. The tests were carried out in two glass flumes: one 14 m long, 0.7m wide, and 1.3m deep, the other 30.5m long, 0.65m wide and 2.0m deep. Both flumes were provided with pusher-type wave generators.

II. THE RESULTS OF THE EXPERIMENTS

Numerous successive photographs of the profile of the slope in different stages of forming by waves, also measurements of bottom velocities by means of specially designed measuring calls make it possible to characterize the process in the following way.

Formation by waves of a stable profile is the continuous damping process of erosion of the upper part of the slope and of accumulation of the eroded material in the lower part. The stable slopes have peculiar curved outlines with four characteristic zones (Fig. 1, heavy line 1-2-3-4-5) being as follows:

1. Above-water zone limited from above by point 1, the uppermost point of wave ride-up on the slope, and from below, by point 2, the point of intersection of the profile of the slope with the still water level.

2. Below point 2 there is a comparatively flat underwater zone 2-3 elongated up to the bottom of the hollow.

3. Immediately after the hollow there is an underwater roller of which the uppermost point 4 may be assumed for the extreme right boundary of the third zone 3-4.

4. Finally there is the fourth zone ending with point 5 which is

x) d_{60} is the grain diameter; number 60 indicates that the content of finer grains in a sample is 60% by weight.

the lower limit of the stable slope formed by wave action. Below this point the profile of the slope is represented by a straight line inclined towards the horizon, the angle of inclination being that of the natural slope of soil in water.

The above outlines of the stable slope was characteristic for the whole test program with wave dimensions being as h_m = 5 to 40 cm and λ_m= 50 to 600 cm and grain-size of soils being as d_{60} = 2.0; 3.5 and 6.0 mm. Changes in wave dimensions and grain-size of soils leads only to changes in dimensions of the above-mentioned zones, of their slopes, etc., but does not lead to substantial difference in forms of slopes taken as a whole.

At the initial stage of the process of formation by waves of the stable profile erosion of the upper part of the slope is going on rather fast with point 1 and 2 moving continuously in the direction of the structu

The zone 2-3 in its upper part flattens. The lower limit of wave forming action - point 5 moves in the direction of the reservoir and slowly sinks below the still water level (SWL). As to the hollow and the underwater roller, these two elements of the profile formed at the very start of testing remain practically unchanged as far as their position and form are concerned.

Since the curved form of the profile of unlined slopes is not convenient both from the standpoint of calculations and mainly from the standpoint of construction works, we think it necessary to schematize this form, presenting the design scheme in the form of cut-off lines averaging the curved portions of the profile obtained in experiments. (Fig. 2, broken line ABCDE).

The relationship between dimensions of the stable profile on factors determining these dimensions may be written as

$$\mathcal{l} = f\ (d, h, \lambda, g, \nu) \qquad (1\text{-A})$$

where

$\mathcal{l}$ = certain linear characteristics of the profile (length, depth, etc.)

d = grain diameter of sand

h = wave height

EXPERIMENTAL RESEARCH IN FORMATION BY WAVES OF STABLE PROFILES OF UPSTREAM FACES OF EARTH DAMS AND RESERVOIR SHORES

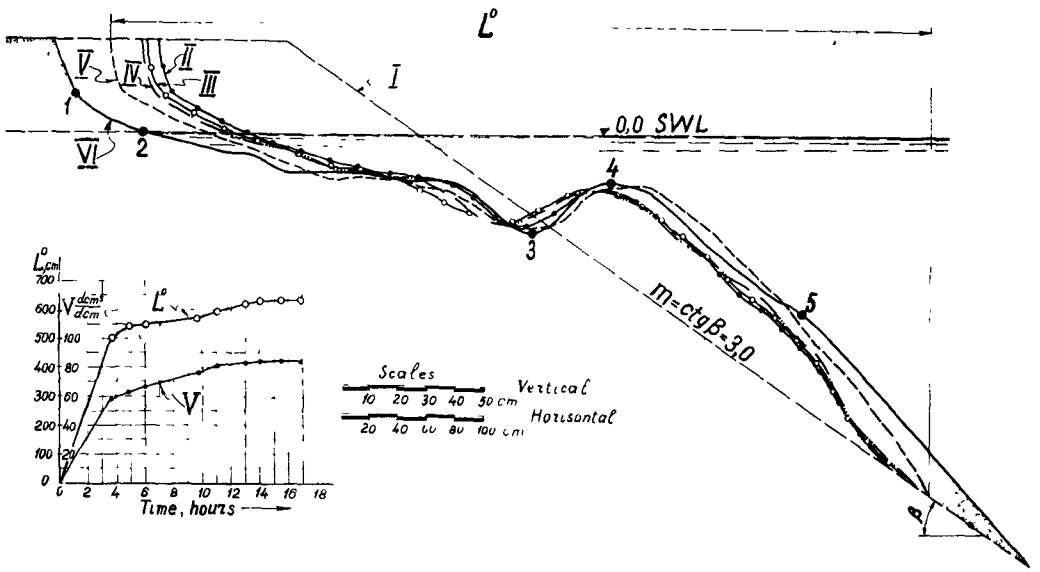

Fig. 1. Different stages of the process of formation by waves of a stable profile of the slope. Gravel with the grain diameter d_{60} = 6 mm. Wave parameters: h = 30 cm; λ = 450 cm; T = 1.73 sec.

I - original slope.
II - profile of the slope after 3.6 hours.
III - " " " " " 4.8 hours.
IV - " " " " " 6.0 hours.
V - " " " " " 9.6 hours.
VI - " " " " " 16.8 hours.

L^{o} - slope length, cm.
V - volume of erosion, dcm^3/dcm

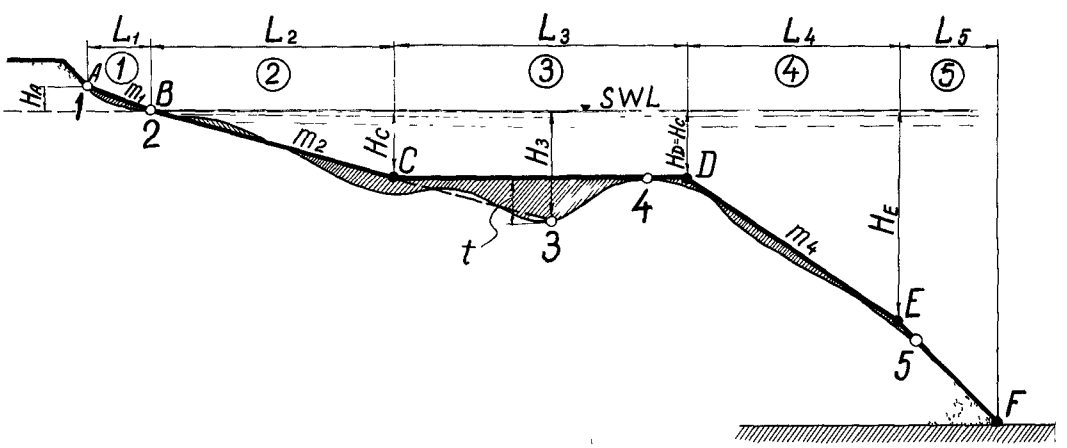

Fig. 2. Design scheme for construction of the profile of the stable unlined slope. Design values:

H_A; $M_1 = \frac{L_1}{H_A}$; $M_2 = \frac{L_2}{H_C}$; $H_C(H_D)$; L_3; $M_4 = \frac{L_4}{H_E - H_D}$; H_E

λ = wave length

g = acceleration of gravity

ν = coefficient of kinematic viscosity of water

Using methods of the theory of dimensions we have set up the following system of dimensionless parameters which determine the phenomenon under investigation and satisfy the requirements of the theory of similarity: $\frac{\ell}{h}, \frac{h}{d}, \frac{h}{\lambda}$ and $\frac{\sqrt{gd}\cdot d}{\nu}$ In connection with this equation (1-A) may be re-written in the following form:

$$\frac{\ell}{h} = \psi\left(\frac{h}{d}, \frac{h}{\lambda}, \frac{\sqrt{gd}\cdot d}{\nu}\right) \qquad \cdots \qquad (1\text{-B})$$

As a result of the analysis of the experimental data the following empiric relationships for the determination of the geometrical elements of the profile of equilibrium are obtained:

1. Relative height of the wave run-up on the slope at

$$10 < \frac{h}{d} \leq 100$$

$$\frac{H_A}{h} = 5.65\,\frac{d}{h} - 4.3\,\frac{h}{\lambda} + 0.58 \qquad (1)$$

and at $\frac{h}{d} > 100$

$$\frac{H_A}{h} = 0.63 - 4.3\,\frac{h}{\lambda} \qquad (2)$$

2. Coefficient of slope (cotangent of angle of inclination of the slope towards the horizon) M_1, elongation AB

$$\text{at } 200 < \frac{\sqrt{gd}\cdot d}{\nu} \leq 1200$$

$$m_1 = \left(2 - 5\cdot 10^{-4}\,\frac{\sqrt{gd}\cdot d}{\nu}\right)\left(\frac{h}{d}\right)^{1/4} \qquad \cdots \qquad (3)$$

and at $\frac{\sqrt{gd}\cdot d}{\nu} > 1200$

$$M_1 = 1{,}3\ \left(\frac{h}{d}\right)^{1/4} \quad \ldots \quad (4)$$

3. Coefficient of slope M_2, elongation BC.

$$M_2 = \left(2.9 - 10\ \frac{h}{\lambda}\right)\ \left(\frac{h}{d}\right)^{1/3} \quad \ldots \quad (5)$$

4. Deepening of the horizontal elongation CD below the water level.

$$H_C = H_D = 0.6h \quad \ldots \quad (6)$$

5. Relative length L_3, elongation CD.

$$\frac{L_3}{h} = \left(0{,}6 - 3\ \frac{h}{\lambda}\right)\ \left(\frac{h}{d}\right)^{1/3} \quad \ldots \quad (7)$$

6. Coefficient of slope M_4, elongation DE.

at $\frac{h}{d} > 40$

$$M_4 = \frac{460\cdot\nu}{\sqrt{gd}\cdot d} + 2{,}1 \quad \ldots \quad (8)$$

and at $\frac{h}{d} < 40$

$$M_4 = K\left(\frac{460\cdot\nu}{\sqrt{gd}\cdot d} + 2{,}1\right) \quad \ldots \quad (9)$$

where K should be assumed according to the following Table:

$\frac{h}{d}$	10	15	20	25	30	40
K	1.7	1.5	1.3	1.2	1.1	1.0

7. Relative depth above point E

$$\frac{H_E}{h} = \left[\frac{400 \cdot \nu}{\sqrt{gd} \cdot d} + 0.55 - \left(\frac{1800 \cdot \nu}{\sqrt{gd} \cdot d} + 2.3 \right) \frac{h}{\lambda} \right] \left(\frac{h}{d} \right)^n \qquad (10)$$

where

$$n = 0.27 - \frac{35.9 \cdot \nu}{\sqrt{gd} \cdot d}$$

In the above formulae for the design diameter of noncohesive soils was assumed the grain-size of which finer particles content is 60% of the material by weight.

When structures are being built of fine-grained sands it seems more economic to cover the upstream slope by the protective layer of coarse-grained materials according to the scheme, being as shown in Fig. 3. This will considerably reduce the volume of earth works. The following empiric formula is obtained to determine the thickness of the protective layer.

$$\delta = K \cdot 0.02 \left(\frac{h}{d} \right)^{2/3} \qquad (11)$$

where K is the safety factor which should be assumed as being equal to 2.0 at $\frac{h}{d} \leq 70$ and to 1.5 at $\frac{h}{d} > 70$.

The above formulae may be used in the design and construction of gentle slopes composed of soils with the grain diameter d= 2.0mm subject to wave action, the wave height being up to 1.5 m.

It is our opinion that the results of investigations obtained herein

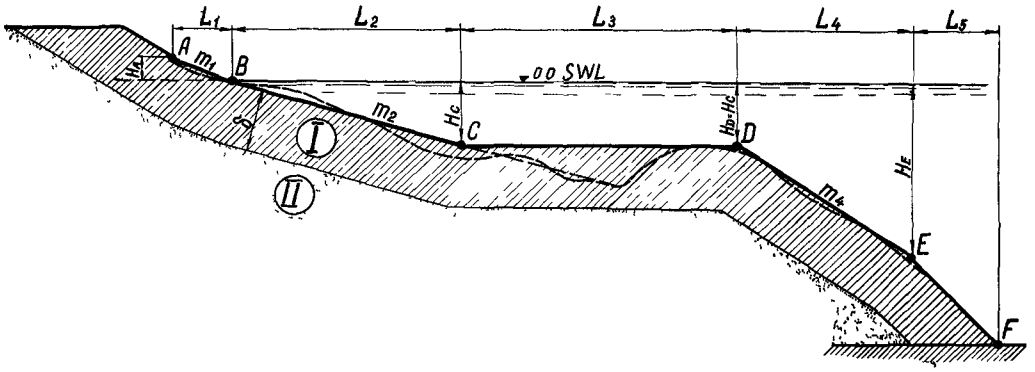

Fig. 3. Scheme of the slope of an earth structure with protective cover on it.

I - protective layer made of coarse sand or gravel.
II - hydraulically filled structure built of sand.

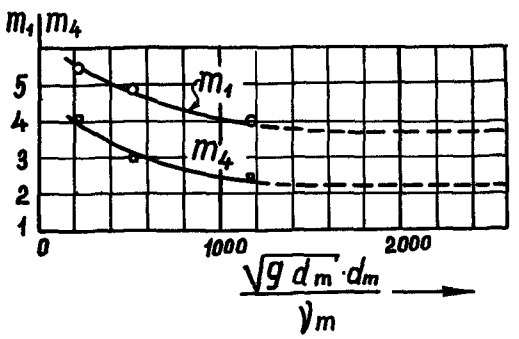

Fig. 4

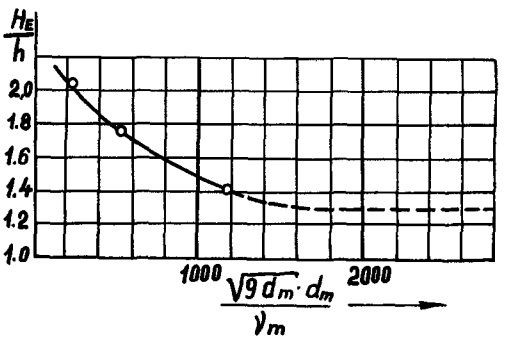

Fig. 5

Fig. 4 Variation of coefficients of slope M_1 and M_4 dependent on the value of $\frac{\sqrt{g \cdot d_m} \cdot d_m}{\nu_m}$

$\frac{h}{d} = 66.7$; $\nu = 0.0124 \frac{cm^2}{sec}$

Fig. 5 Relationship between relative depth (the lower limit of wave forming action) $\frac{H_E}{h}$ and the value of $\frac{\sqrt{g d_m} \cdot d_m}{\nu_m}$

$\frac{h}{d} = 66.7$; $\nu = 0.0124 \frac{cm^2}{sec}$

are of some interest from the point of view of predicting the volume of work made by waves on natural shores of newly built reservoirs.

III. SOME CONSIDERATIONS ON SCALING-UP EROSION AND DEPOSITION OF NON-COHESIVE SOILS DUE TO WAVE ACTION

The analysis of the results obtained from the point of view of scaling-up the elements of the profile, the geometrical scale of the model with geometrically scaled grain-size and wave dimensions being taken account for, made it possible to draw the following conclusions.

Elements of the stable profile according to the assumed design scheme (Fig. 2) may be divided into two groups being as follows:

1. The first group comprises values H_A, M_2, H_C, L_3 and δ determined by relations 1, 2, 4, 5, 6, 7 and 11 involving besides constant coefficients relative dimensionless values $\frac{h}{d}$ and $\frac{h}{\lambda}$. Thus in meeting requirements $\frac{h_m}{d_m} = \frac{h_p}{d_p}$ . . . (12) and $\frac{h_m}{\lambda_m} = \frac{h_p}{\lambda_p}$ . . . (13) and also in maintaining the boundary conditions the mentioned above values may be scaled-up to the prototype by way of multiplying the corresponding values obtained in the test by geometrical scale coefficient.

Such scaling-up is undoubtedly justifiable if sand with the grain diameter $d_m \geq 2.0$mm is used on the model as eroded material and the requirement $\frac{h}{d} \geq 20$ is met.

2. The second group comprises values M_1, M_4 and H_E for which as it may be seen from relations 3, 8, 9 and 10, geometrical similarity model and prototype might have been provided if an additional requirement

$$\frac{\sqrt{g d_m} \cdot d_m}{\nu_m} = \frac{\sqrt{g d_p} \cdot d_p}{\nu_p} \qquad (14)$$

besides conditions 12 and 13 was met.

If it was not, geometrical scaling-up of values M_1, M_4 and H_E is not guaranteed.

Moreover, at $\frac{\sqrt{g d_m} d_m}{\nu_m} \leq 1000$ it may lead to substantial error This circumstance is clearly illustrated by the diagrams shown in Figs. 4 and 5 [x]. These diagrams show the dependency of values M_1, M_4 and H_E

x) In Figs. 4 and 5 the curves shown by dotted lines have been plotted according to the corresponding empirical relations 3, 9 and 10.

on values of $\frac{\sqrt{gd_m} \cdot d_m}{\nu_m}$ for one particular case: $\frac{h}{\lambda} = 10$ and $\frac{h}{d} = 66.7$ (ratio between maximum wave height 40 cm and maximum grain-size $d_m = 6.0$mm i.e. $\frac{h_{m\,max}}{d_{m\,max}} = \frac{400}{6} = 66.7$). With $\frac{\sqrt{gd_m} d_m}{\nu_m} = \geq 1000$ i.e. with using sand of which the grain diameter $d_m = 5$ mm values M_1, M_4 and H_E can be practically scaled-up in accordance with geometrical scale of the model (the error being not more than 15% toward exaggeration).

It should be noted that supposition of possibility of scaling-up all elements of the profile is the basis of many investigational works associated with studying the disruptive effects of waves on shores and bottom reservoirs.

The preliminary results given in this paragraph show that such scaling is far from being always justifiable.

CHAPTER 17

ESSAI D'ANALYSE DES PHENOMENES INTERVENANT DANS LA FORMATION D'UN ESTUAIRE

M. Banal
Directeur-Adjoint des Etudes et Recherches
Electricité de France

INTRODUCTION

Les considérations qui vont être développées résultent des observations, des études, et des lectures que l'auteur a pu faire pendant qu'il était chargé du Service des accès au port de Rouen sur le fleuve Seine au nord-ouest de la France.

Il en résulte que d'une part elles ne valent que pour les estuaires possédant avec celui de la Seine les caractéristiques communes qui seront définies ci-dessous, mais d'autre part qu'on s'est efforcé d'en exclure ce qui est apparu comme trop particulier au cas de la Seine.

Les conditions auxquelles doit satisfaire un estuaire pour qu'on puisse lui appliquer les considérations qui suivent, sont :

- forte marée et faible débit fluvial,
- embouchure embarrassée de bancs découvrants constitués par du sable fin ou très fin (granulométrie voisine de 1/10 de mm).

MECANISME DE LA FORMATION DES BANCS ET DE L'EVOLUTION DES CHENAUX

La topographie d'un estuaire peut être examinée sous les trois aspects suivants :

- niveau moyen général des fonds,
- formation et évolution des chenaux et des bancs,
- largeurs et profondeurs des chenaux utilisables par la navigation.

NIVEAU MOYEN GENERAL DES FONDS.

Si l'on dispose de levés des fonds assez anciens, on constatera en général une remontée progressive des bancs traduisant une accumulation de sable dans l'estuaire.

Cet engraissement séculaire n'est pas un phénomène extraordinaire en soi, car le colmatage des baies paraît être au contraire une règle assez générale d'évolution des côtes, dès lors que les courants ou la houle trouvent des matériaux à mettre en suspension.

Dans le cas des estuaires, ce colmatage ne peut cependant être complet en raison du débit fluvial si faible soit-il.

ESSAI D'ANALYSE DES PHENOMENES INTERVENANT DANS LA FORMATION D'UN ESTUAIRE

Si l'aspect qualitatif de l'engraissement d'un estuaire n'a donc rien de surprenant, on ne peut prévoir au contraire le taux annuel d'engraissement et la cote d'établissement des dépôts.

Lieu des dépôts - Les matériaux accumulés dans un estuaire sont répartis dans des dépôts de trois sortes (fig. 1) :

- zones ayant atteint la cote des P.M. de vives-eaux moyennes et couvertes en général d'une écorce herbée,
- zones d'évolution des chenaux,
- zones de progression des bancs vers le large.

1°) Bancs herbés : Une extension rapide des bancs herbés est en général la conséquence de constructions d'ouvrages protégeant certains bancs de l'actior des courants. Toutefois, les bancs herbés peuvent progresser à partir de l'amont de l'estuaire et s'ils ne sont pas protégés par des digues être attaqués par les courants et disparaître après plusieurs années d'existence. Il faut cependant noter que la reprise des bancs dont le niveau atteint la cote de P.M. de V.E. qui ne peut se faire que par attaque du talus est toujours lente. Ces bancs sont donc relativement stables.

2°) Zone d'évolution des chenaux : C'est dans cette zone que s'observent les fluctuations rapides des chenaux. Si le niveau moyen de cette zone d'évolution des chenaux s'élève progressivement sous l'effet de l'engraissement séculaire, on peut dire qu'il est stable par rapport aux phénomènes se produisant pendant un petit nombre de marées.

Le flot provoque un déplacement de matériaux vers l'amont et le jusant effectue le transport contraire mais sans ramener les matériaux exactement là où ils ont été pris; le déplacement résiduel s'efface sur une période plus longue par suite de la fluctuation des chenaux pour ne laisser comme bilan final que l'engraissement séculaire.

3°) Zone de progression des bancs vers le large : Au large de la zone ci-dessus on observe des bancs (toujours immergés) dont la topographie ne se déforme que lentement.

Ces bancs se développent devant le débouché des chenaux de jusant et se rétractent ailleurs.

En moyenne, on observe une avancée progressive de ces bancs, conséquence de l'engraissement séculaire sauf pendant les périodes où des endiguements sont exécutés à l'amont.

Pendant ces périodes en effet, les bancs s'érodent de manière à fournir les matériaux qui s'accumulent derrière les digues.

Engraissement séculaire - Le taux annuel de l'engraissement de l'estuaire dépend grandement de la zone sur laquelle porte la comparaison.

Si l'on observe seulement la partie amont, l'engraissement est en général très faible sauf pour les années suivant des travaux d'endiguement, pour lesquels il devient considérable.

Si les cubatures comparatives portent sur tout l'ensemble de l'estuaire jusqu'au large (cote - 10 sous le niveau des BM par exemple), on constate au contraire un taux annuel d'engraissement assez peu variable d'une année à l'autre, qu'on a tendance à considérer comme une constante de la nature.

Avant d'admettre toutefois l'existence d'un taux permanent d'engraissement indépendant de l'action de l'homme, il faut se demander si son extension pendant 1000 ans ou davantage ne soulève pas des contradictions évidentes.

Usure des matériaux dans l'estuaire - Il était presque unanimement admis autrefois que le sable marin était formé par un broyage progressif, par l'agitation de la mer, à l'état de plus en plus fin, des produits de destruction de côtes.

On a plutôt tendance à considérer actuellement que la granulométrie des sables siliceux est celle des cristaux de silice du granit dont ils sont les produits de décomposition.

Par conséquent, aucun broyage des sables siliceux ne pourrait se produir dans l'estuaire et il y aurait une séparation complète entre le sable siliceux et la vase.

Il n'y aurait donc pas lieu de compter sur le broyage des matériaux pour combattre l'engraissement d'un estuaire comme on l'a cru autrefois, et on ne devait attribuer aucun avantage à ce point de vue à l'existence d'une grande surface de bancs mobiles.

FORMATION ET EVOLUTION DES CHENAUX ET DES BANCS - DISSYMETRIE DES ACTIONS DU FLOT ET DU JUSANT.

Le courant de flot se forme alors que le niveau a déjà sensiblement monté et atteint sa valeur maximum pour une cote assez voisine de la pleine-mer. Le jusant au contraire agit surtout au-dessous du niveau de la mi-marée (fig. 2).

L'action du flot consiste donc dans un décapage général de tout l'estuair se produisant de manière sensiblement égale sur les bancs et les chenaux, suivi d'un dépôt uniforme à l'étale de pleine mer.

Le jusant au contraire n'agit sur les bancs qu'au début et son action se concentre rapidement dans les thalwegs.

Il en résulte deux conséquences :

a) Les matériaux transportés par le jusant arrivent à la limite de l'estuaire par les chenaux et forment des barres d'embouchure aux débouchés de ces chenaux.

Au contraire, l'action de décapage du flot est uniforme sur la lisière aval des bancs.

Les fonds étant en moyenne en équilibre, il en résulte que des bancs se développent au débouché des chenaux et que des fosses se creusent ailleurs.

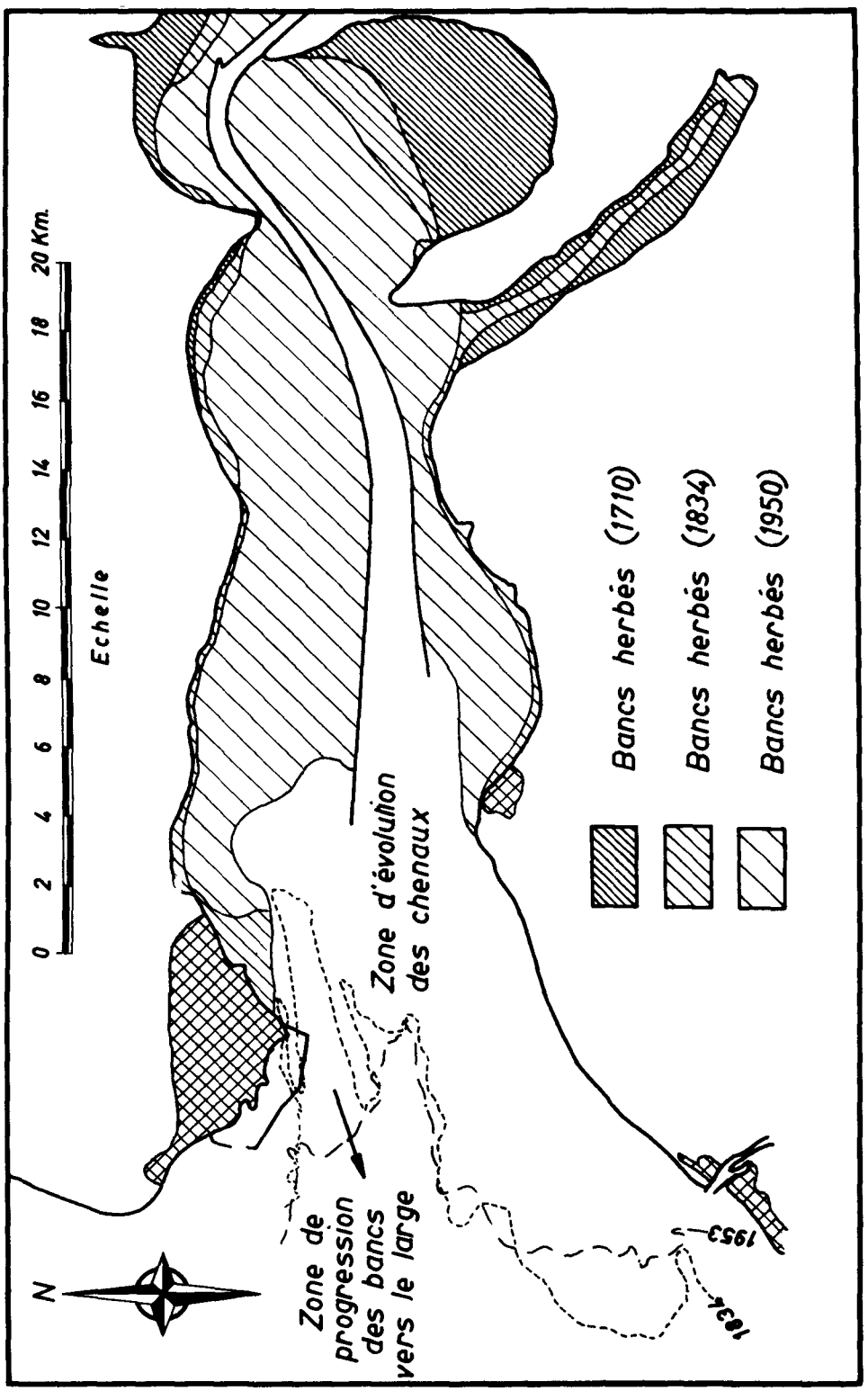

Fig. 1. Estuaire de la Seine: zones de dépôt.

L'équilibre de l'estuaire ne peut donc être obtenu que par les fluctuations des chenaux qui les font déboucher là où des fosses existaient précédemment.

Si cet effet d'auto-colmatage des chenaux est connu depuis très longtemps il ne semble pas que son importance ait toujours été complètement appréciée. Le cube des matériaux qui se déposent au débouché d'un chenal à partir du moment où il y a une concentration totale du débit de fin de jusant peut être considérable et hors de proportion avec le taux annuel moyen d'engraissement avec lequel il n'a a priori aucune relation.

Nous pensons que certaines fermetures brutales de chenaux imputées autrefois aux conditions atmosphériques n'étaient que le résultat du phénomène d'auto-colmatage.

b) Sauf à la lisière aval des bancs, le modelé des bancs et des chenaux résulte surtout de l'action du jusant.

Les évolutions des chenaux sont donc assez analogues à celles observées sur un fleuve non soumis à la marée et s'écoulant dans le sens du jusant.

On sait depuis Fargue que la disposition du lit d'un fleuve s'écoulant dans un terrain affouillable indéfini en l'absence de tout ouvrage d'endiguement est une suite de méandres.

Les évolutions d'un tel lit sont de deux sortes :

- Evolutions progressives (accroissement de l'amplitude des méandres ou déplacement vers l'aval),
- Evolutions brutales, formation des coupures (lorsque le débouché aval d'un chenal est colmaté).

Toutefois, l'existence ou la fréquence de certaines positions des méandres peuvent être influencées par les courants de flot dont la direction dépend notamment des courants au large et du tracé des berges de l'estuaire.

Il semble bien, par contre, que les tempêtes et les crues n'aient sur le modèlé des fonds de l'estuaire qu'une action réduite qu'il ne nous a pas été possible de constater d'une manière certaine.

RESUME DES TENDANCES ESSENTIELLES DE L'ESTUAIRE.

- Engraissement séculaire (formation des bancs herbés, engraissement du niveau général des bancs jusqu'à une certaine note moyenne, extension des bancs vers l'aval).

- Chenaux existant à un instant donné se déformant à la manière du lit d'un fleuve s'écoulant dans le sens du jusant.

- Remblaiement du débouché aval de tout chenal de jusant, le cube de matériaux déposés dépendant du décapage des bancs par le flot et non du taux d'engraissement séculaire de l'ensemble de l'estuaire.

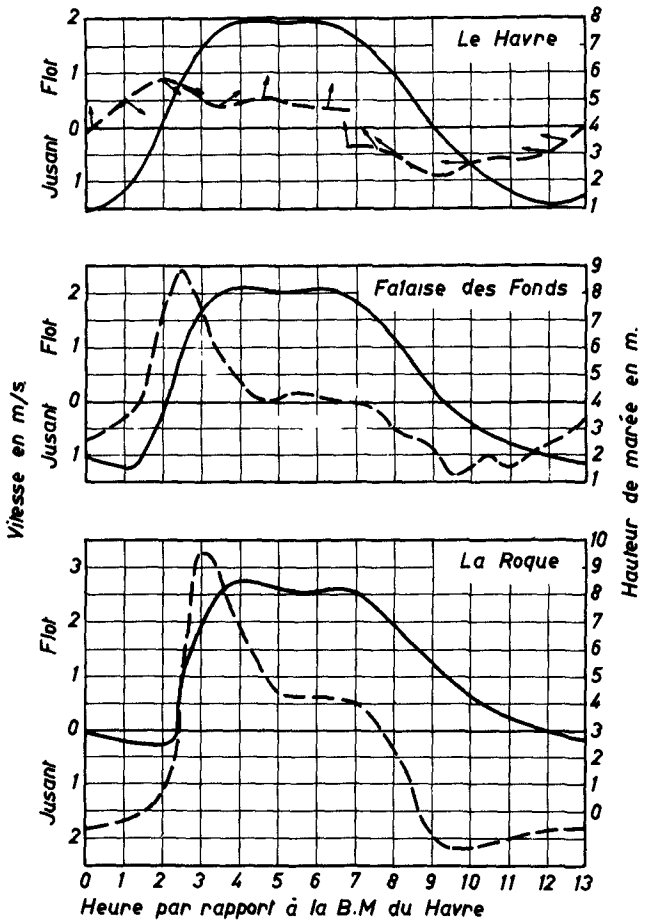

Fig. 2. Estuaire de la Seine: courbes marégraphiques et de vitesse de courant par coefficient 95 au Havre, à la Falaise des Fonds et à la Roque (Rive gauche).
(courbe de marée en trait plein ————————, courbe des vitesses en trait interrompu - - - - - - -).

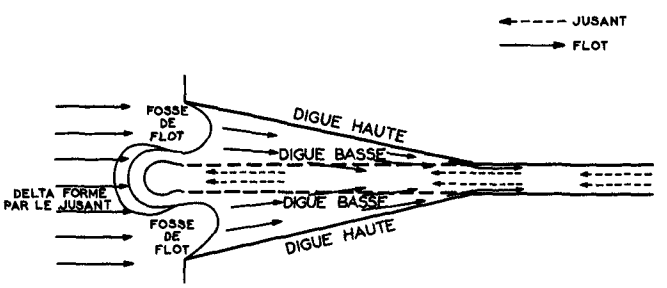

Fig. 3. Schéma des transports de matériaux dans un estuaire en entonnoir à endiguement de lit mineur.

- Echancrures des bancs à l'aval par le flot en dehors des débouchés des chenaux de jusant.

- Périodiquement, soit en raison du développement des méandres, soit en raison du colmatage à l'aval, formation d'un nouveau chenal par ouverture brutale d'une coupure.

HISTORIQUE DES EVOLUTIONS DE L'ESTUAIRE

Les règles élémentaires ci-dessus suffisent à peu près, dans une situatio donnée des ouvrages d'endiguement, à expliquer les évolutions à caractère sensiblement périodique constatées dans un estuaire sans qu'il soit nécessaire de faire intervenir les phénomènes aléatoires comme les tempêtes, les crues et encore moins le pur hasard.

Lorsque ces ouvrages sont modifiés, les évolutions se produisent dans de conditions différentes.

Mais on peut constater pendant et après la construction des nouveaux ouvrages une situation transitoire pendant laquelle l'estuaire présente un aspect "anormal".

Etant donnée la fréquence des interventions, un estuaire peut rarement être considéré comme évoluant librement, et les évolutions des fonds constituant des séquelles des travaux ont souvent masqué les lois réglant les mouvements des chenaux indiqués précédemment.

Il faut préciser également que les évolutions possibles du chenal dépendent de l'état d'engraissement de l'estuaire et des évolutions antérieures.

PROFONDEUR DES CHENAUX.
PRINCIPES DE L'AMELIORATION DE L'ESTUAIRE.

Nous étudierons simultanément les conditions qui fixent la profondeur des chenaux et les moyens de l'améliorer.

La profondeur d'un chenal utile à la navigation dépend de sa profondeur moyenne et de son modelé.

Un chenal de faible profondeur moyenne mais auquel une digue à forte courbure donne un profil en travers triangulaire peut être plus favorable à la navigation qu'un chenal de profondeur moyenne supérieure, mais à fond plat.

De même des mouilles très profondes sont sans intérêt si elles sont séparées par des seuils d'inflexion plus élevés.

Les principes d'aménagement indiqués par Fargue et Girardon doivent donc être appliqués au tracé des endiguements. Mais une profondeur satisfaisante du chenal de navigation sera d'autant plus facilement obtenue que la profondeur moyenne du chenal hydraulique et sa largeur seront plus grandes.

Si, d'autre part, on s'astreint à limiter le prolongement des digues vers l'aval, on se trouvera tôt ou tard dans l'obligation d'utiliser un chenal

libre pour lequel on ne pourra plus agir que sur les facteurs conditionnant la profondeur moyenne, à l'exclusion de tout effet d'ouvrage sur le courant de jusant.

Or, la profondeur moyenne est liée notamment à la "puissance hydraulique" du fleuve. Cette notion, à laquelle une importance exceptionnelle est attribuée depuis de très nombreuses années, mérite d'être examinée en détail.

SOLIDARITE ENTRE LES DIFFERENTES PARTIES D'UN FLEUVE A MAREE - LOI DE L'ELARGISSEMENT KILOMETRIQUE.

Nous citerons des extraits du mémoire célèbre de Mengin-Lecreulx sur la puissance hydraulique des fleuves à marée. (1).

"Les courants qui sont par eux-mêmes des agents de déblaiement, qui creusent et entretiennent des chenaux de navigation sont en même temps les agents de transport des matières qui les encombrent. Ils portent donc en eux-mêmes le mal et le remède, et le résultat utile dépend d'un certain équilibre dont la détermination constitue la difficulté du problème".

"D'autre part, en vertu du mouvement des eaux, toutes les parties d'un fleuve sont solidaires comme celles d'un organisme vivant, aucune d'elles ne peut être modifiée sans une répercussion plus ou moins forte sur toutes les autres, lors donc qu'on étudie une amélioration locale, il est essentiel de rechercher quelle sera, pour le tempérament du fleuve, la conséquence des mesures projetées".

"En vertu du même principe, lorsqu'on veut améliorer un fleuve, il importe de faire concorder entre elles, et autant que possible d'exécuter simultanément toutes les améliorations partielles, de manière que leurs effets se renforcent les uns les autres".

"Nous tiendrons pour acquis qu'on abordera les difficultés de l'embouchure dans des conditions d'autant plus favorables que le débit de marée sera plus considérable.(2) et que l'importance de ce débit doit être proportionnée à celle des difficultés à vaincre, soit qu'elles proviennent du débit solide d'amont, soit qu'elles proviennent du débit solide d'aval, c'est-à-dire des matières venant de la mer, qui se présentent à l'entrée du fleuve, y pénètrent avec le flot, en ressortent avec le jusant et dans cette lutte entre l'introduction et l'expulsion, donnent lieu à un état d'équilibre plus ou moins favorable à la navigation".

Mengin-Lecreulx se fixe donc comme but l'aménagement du fleuve dans la partie amont où il est endigué, en vue d'arriver au débit maximum considéré, a priori, comme la condition du succès pour l'aménagement de l'aval.

---

(1) 1880.

(2) Bien entendu, il ne faut prendre en considération que le débit concentré dans un chenal unique.

Il remarque que pour obtenir le débit maximum, il faut avoir les plus grandes largeurs possibles avec les profondeurs nécessaires à la fois à la transmission des marées et à la navigation et les plus faibles vitesses compatibles avec l'obtention des profondeurs.

Supposant connues, cette vitesse minimum et la profondeur à obtenir, Mengin-Lecreulx détermine une loi d'élargissement de l'amont vers l'aval qui est de la forme $(1+\lambda)^{x}$ (x abscisse en km, λ coefficient d'élargissement kilométrique).

Pour la vitesse de 0,8 m/s admise par Mengin-Lecreulx, il trouve $\lambda = 0{,}05$ environ, soit un élargissement de 50 % tous les 10 kilomètres.

L'idée qu'en fonds affouillables indéfinis seul un estuaire ayant une certaine loi d'élargissement de l'amont vers l'aval conserve la loi de profondeur désirée nous paraît incontestable, mais la formule donnée par Mengin-Lecreulx reste à démontrer et la loi d'élargissement devrait être fixée par des considérations expérimentales ou théoriques moins sommaires. Cette notion doit en outre être complétée sur différents points que nous allons examiner.

ENDIGUEMENT DU LIT MAJEUR.

La loi d'élargissement kilométrique est établie par Mengin-Lecreulx en considérant seulement le jusant.

Il se borne à donner sur le flot les indications suivantes :

"De plus, puisque le niveau moyen pendant le flot est plus élevé que pendant le jusant, tout accroissement de largeur dans les parties supérieures diminuera la vitesse du flot sans affecter au même degré celle du jusant, il y aura donc bénéfice.

"Il est ainsi très utile à ce point de vue aussi bien qu'à celui de l'augmentation du cube de marée qu'il y ait un lit majeur ou qu'au moins le lit soit plus large à la surface qu'au fond. M. Franzius a fait remarquer qu'au flot le niveau des eaux était convexe et que le lit central se déchargeait dans le lit majeur latéral tandis que pendant le jusant l'inverse se produisait, cette très intéressante observation conduit à la même conclusion".

Mengin-Lecreulx avait parfaitement compris que dans un estuaire comme celui de la Seine, le niveau d'équilibre des chenaux s'approfondissait si l'on réduisait la puissance de transport (et donc la vitesse) du flot par rapport à la puissance de transport du jusant.

Mais, il se trompe lorsqu'il pense pouvoir réduire le débit solide du flot en élargissant le lit majeur.

La vitesse instantanée du flot dans un profil en travers n'est pas conditionnée en effet par un débit déterminé à assurer, mais principalement par la loi locale de variation des hauteurs.

En élargissant le lit au-dessus du niveau de basse-mer, on accroît donc le débit instantané du flot sans réduire les vitesses et par conséquent on accroît le débit solide.

Cependant, si les digues du lit majeur sont peu convergentes et sensiblement parallèles aux digues du lit mineur, l'observation de Franzius permet de penser que l'élargissement du lit majeur peut avoir un effet favorable sur la profondeur d'équilibre du chenal.

Mais, si les digues du lit majeur sont très convergentes, un résultat tout à fait contraire est obtenu.

Au lieu de la réduction de la vitesse du flot escomptée par Mengin-Lecreulx, on constate un accroissement très rapide de ces vitesses vers l'amont.

Le cube accumulé à l'amont n'est que très faiblement accru par la surélévation de la cote de P.M. au fond du convergent, mais la durée du flot dans l'estuaire est par contre considérablement réduite.

Les graphiques des vitesses montrent l'extrême brièveté de la pointe de vitesse du flot et la dissymétrie existant dans l'intérieur de l'estuaire entre le flot et le jusant.

Or, cette dissymétrie est directement opposée au but cherché puisqu'un cube liquide donné peut entraîner une charge solide d'autant plus forte qu'il est débité pendant un temps plus court.

Dans plusieurs études anglaises, la dissymétrie du jusant et du flot est considérée comme un véritable critère d'aménagement d'un fleuve à marée qui est d'autant plus satisfaisant que la dissymétrie est plus faible.

Par ailleurs, bien loin de se décharger dans le lit majeur latéral, le lit central reçoit les produits de décapage des bancs de lit majeur comme il apparaît clairement sur la figure 3.

L'idée de compléter un endiguement du lit mineur par des digues hautes beaucoup plus largement évasées, nous paraît donc très fâcheuse.

OBSERVATIONS COMPLEMENTAIRES.

a) Pour une loi donnée de marée, la dissymétrie entre le flot et le jusant est d'autant plus accusée que les profondeurs sont plus faibles. Autrement dit, un estuaire tend à se dégrader d'autant plus rapidement qu'il part d'une situation naturelle plus mauvaise.

b) La dissymétrie naturelle de la marée au large est une condition défavorable qui est probablement une des causes du niveau naturellement élevé des bancs de certains estuaires.

c) Même s'ils ne sont pas limités par des digues très convergentes, les bancs du lit majeur peuvent constituer des dangers pour le chenal s'il n'est pas rectiligne.

Il n'est pas possible en effet de faire coïncider la direction du courant de flot avec le tracé des digues basses de lit mineur.

Le déversement dans le chenal des matériaux arrachés aux bancs par le flot sera une cause de perturbation dans le chenal.

Il semble donc bien que le maintien d'un très large lit majeur présente de graves inconvénients; il ne s'accommode notamment pas des inflexions. Franzius était partisan de laisser subsister de larges lits majeurs et de faire des endiguements rectilignes, la coïncidence de ces deux idées n'est peut-être pas fortuite.

APPLICATION DE LA LOI D'ELARGISSEMENT DE MENGIN-LECREULX - SIMILITUDE.

L'application pratique de la notion d'élargissement progressif vers l'aval paraît devoir être limitée en général à une mise en harmonie des différentes parties d'un fleuve comportant seulement l'exécution de retouches (élargissement ou rétrécissement de certaines parties d'endiguement, en considérant les autres comme acquises, dragages de fonds pas ou peu affouillables (1), etc...).

Compte tenu des incertitudes dans la détermination théorique de la loi d'élargissement, on la choisira en général d'après l'observation de la situation naturelle des fonds.

Le résultat obtenu sera certainement favorable aussi bien dans la partie endiguée qu'à son aval.

Cependant, bien des ingénieurs ayant étudié l'aménagement d'un estuaire ont fait observer qu'au lieu de l'étrangler à l'aval, comme on le fait souvent, il serait bien préférable de lui laisser son débouché naturel et de mettre l'endiguement amont en harmonie avec ce débouché.

Il paraît bien probable en effet que, toutes choses égales d'ailleurs, des estuaires géométriquement semblables en plan (2) présentent des profondeurs d'autant plus grandes qu'ils sont plus larges. Toutefois l'incertitude actuelle sur le résultat quantitatif d'une dilatation transversale d'un estuaire sur toute sa longueur a empêché jusqu'ici d'entreprendre les travaux considérables qu'elle nécessite (3).

---

(1) L'endiguement doit être conçu de manière que les fonds s'entretiennent naturellement et non pour obtenir l'enlèvement naturel de dépôts anciens qui peuvent être beaucoup moins mobiles que les dépôts se formant à chaque marée, bien que constitués par le même matériau.
(2) Pour pousser ce raisonnement par des considérations de similitude, on se heurte à deux difficultés du fait que le marnage et le débit fluvial ne sont pas modifiés.
(3) Cet élargissement doit être prolongé vers l'amont jusqu'à la limite de pénétration des sables de mer existant après la transformation (qui peut être très en amont de la position de cette limite avant la transformation).

ESSAI D'ANALYSE DES PHENOMENES INTERVENANT DANS LA FORMATION D'UN ESTUAIRE

REDUCTION DE L'AUTO-COLMATAGE.

La concentration des apports de jusant au débouché des chenaux constitue une difficulté supplémentaire à vaincre pour établir des profondeurs satisfaisantes au passage de la barre d'embouchure.

Il est entièrement conforme aux idées de Mengin-Lecreulx exposées précédemment que de penser qu'une réduction des apports solides du jusant provoquera un abaissement du niveau moyen du chenal.

Une réduction du débit de jusant dans le chenal pourra même être admissible si elle est la condition d'une réduction relativement plus importante du débit solide.

Enfin, l'efficacité des dragages sera d'autant plus grande que les apports solides du jusant seront plus faibles.

Les considérations qui précèdent, conduisent à ajouter aux principes d'aménagement déjà exposés la réduction des apports du jusant au débouché du chenal par l'un des artifices suivants :

a) Déviation d'une partie du jusant en dehors du chenal de navigation,

b) Si l'aménagement comporte un chenal unique de jusant, utilisation de l'effet de courbure d'une digue de soutien du chenal d'où résulte une répartition des dépôts sur un banc de convexité où ils sont repris par le flot.

c) Approfondissement local de la barre par un ouvrage agissant sur le flot.

d) Réduction de la turbidité du jusant en supprimant le balayage des bancs par le flot.

CONSEQUENCES DU PRINCIPE D'ACCROISSEMENT DE LA PUISSANCE HYDRAULIQUE SUR LA CONCEPTION DES TRAVAUX D'AMENAGEMENT.

Nous sommes convaincus que tout ce qui sera fait pour mettre en harmonie les unes avec les autres les différentes parties du chenal endigué aura certainement un effet très favorable sur les conditions de navigation dans ce chenal endigué et sur la profondeur du chenal libre à l'aval des digues.

Nous avons indiqué aussi qu'on pouvait escompter un résultat favorable de l'élargissement d'un estuaire sur toute sa longueur.

Nous ne pensons pas par contre que la considération de la puissance hydraulique puisse imposer une forme ou une autre pour l'endiguement de l'estuaire.

Si les tracés directs nous paraissent a priori préférables aux tracés sinueux, c'est parce qu'ils évitent des inflexions, mais mieux vaut certainement un tracé sinueux stable qu'un tracé direct de l'endiguement du lit majeur que le chenal ne suit pas.

Par contre, une sinuosité supplémentaire utile à la stabilité ne saurai réduire fâcheusement la puissance hydraulique.

L'aménagement de l'estuaire doit, en définitive, satisfaire aux conditions indiquées précédemment (stabilité et réduction de l'auto-colmatage) et si le souci d'accroître la puissance hydraulique doit faire poursuivre activement les rectifications locales des irrégularités de l'endiguement à l'amont, il ne doit pas faire abandonner un tracé d'endiguement donnant, par ailleurs, les meilleures conditions au débouché aval du chenal.

Nous avons indiqué, d'autre part, que tous les moyens ne sont pas bons pour accroître la puissance hydraulique et que les bancs de lit majeur notamment accroissaient relativement plus le cube des matériaux apportés par le flot que le débit du jusant susceptible de les remporter.

CHAPTER 18

ETUDE SUR MODELE DU TRANSPORT LITTORAL CONDITIONS DE SIMILITUDE

J. Valembois
Chef de la Division Recherches
Laboratoire National d'Hydraulique - Chatou
France

INTRODUCTION

L'objet de la présente note est d'étudier les conditions de similitude que l'on obtient, pour la représentation sur modèle du transport littoral, à partir de divers critères. Les résultats concernant les plages formées de sable fin, à l'exclusion des plages de galets et des zones où la vase existe en proportions importantes.

Le premier critère examiné est la reproduction du début d'entraînement des matériaux de fond sous l'action du mouvement oscillatoire de l'eau dû à la houle, la couche limite étant supposée laminaire dans la nature et sur le modèle.

Les résultats obtenus sont ensuite étendus à la représentation du début d'entraînement sous l'action du courant de transport de masse perpendiculaire à la plage, même lorsque cet écoulement est turbulent au voisinage du fond.

La représentation correcte du début d'entraînement conduit probablement à une bonne concordance entre le modèle et la nature pour la zone située bien au large du déferlement, mais il n'est pas du tout évident (et il serait même étonnant) qu'elle permette d'obtenir sur le modèle un transport littoral ressemblant au transport naturel dans les zones voisines du déferlement et près du rivage. En effet, les phénomènes hydrauliques sont tout à fait différents dans ces régions, où interviennent de façon prépondérante la turbulence créée par le déferlement, les courants de masse perpendiculaires et parallèles à la côte, et probablement la percolation dans la zone de l'estran, ainsi que l'action du vent sur la surface de l'eau.

Pour aller un peu plus loin, on a essayé de définir les conditions dans lesquelles le mouvement des matériaux en suspension est correctement représenté sur le modèle.

La connaissance incomplète que l'on a actuellement des lois du transport littoral ne permet pas de décider a priori si les critères retenus sont valables; cependant, on est arrivé dans divers Laboratoires, avec des modèles dont les échelles étaient voisines de celles auxquelles on aboutirait de cette façon, à représenter des transports littoraux assez semblables à ceux de la nature. On verra d'ailleurs que les conditions auxquelles on arrive laissent quelque liberté dans le choix des échelles. Cette liberté a probablement été utilisée dans le bon sens sur les modèles en question.

SIMILITUDE DU DEBUT D'ENTRAINEMENT. CAS DE LA COUCHE LIMITE LAMINAIRE.

Si l'on connaissait les lois du début d'entraînement dans la nature et sur modèle, on pourrait en déduire les conditions de similitude.

Comme on ne connaît pas les lois naturelles, il faut bien partir des lois établies sur modèle*, en admettant leur extrapolation à la nature.

RELATION DE SIMILITUDE DE GODDET.

Goddet [5] trouve, pour le début d'entraînement en modèle, la loi :

$$V_{max} = 27\,(\varepsilon\rho)^{2/3} D^{1/4} T^{3/8} \qquad (1)$$

(unités c.g.s.)

V_{max} est la vitesse maximum du mouvement oscillatoire de l'eau dû à la houle près du fond, immédiatement au-dessus de la couche limite,
ρ est la masse spécifique de l'eau,
ρ_s est la masse spécifique du sédiment,
$\varepsilon = (\rho_s - \rho)/\rho$ est la densité apparente du sédiment,
D est le diamètre des grains,
T est la période de la houle.

Il applique cette relation à un modèle où la houle est reproduite en similitude de Froude, l'échelle des longueurs d'ondes étant égale à l'échelle des hauteurs, dont l'échelle en plan peut être différente, et où l'échelle des creux de houle n'est pas forcément égale à l'échelle des hauteurs. Il en déduit une relation de similitude qui peut s'écrire sous la forme :

$$\xi^{5/4} = \mu^{2/3} \delta D_c^{-4} \qquad (2)$$

ξ est l'échelle des profondeurs = profondeur mod/profondeur nature,
μ est l'échelle des densités apparentes des matériaux de fond,
δ est l'échelle des diamètres D des matériaux de fond,
D_c est la distorsion des creux de houle par rapport aux profondeurs = échelle des creux $/\xi$.

La relation (2) n'est évidemment valable que pour autant que la relation (1) puisse être extrapolée à la nature, ce qui est vraisemblable tant que la couche limite y reste laminaire.

---

*Larras [1], Vincent [2], Madhav Manohar [3], Lhermitte [4], Goddet [5]

ETUDE SUR MODELE DU TRANSPORT LITTORAL
CONDITIONS DE SIMILITUDE

RELATION DE GODDET MODIFIEE.

Pour voir si la loi de début d'entraînement trouvée par Goddet a des chances d'être extrapolable, on peut essayer de la mettre sous une forme qui se rapproche de la forme adoptée par Shields [6] pour le début d'entraînement sous l'action d'un courant. Cette relation peut s'écrire :

$$\frac{\tau_0}{\varepsilon \rho g D} = f(R_*) \qquad (3)$$

τ_0 est la tension tangentielle exercée par l'eau sur le fond,
$R_* = u_* D/\nu$ est le nombre de Reynolds étoilé rapporté au grain,
ν étant la viscosité cinématique de l'eau et $u_* = \sqrt{\tau_0/\rho}$ la vitesse de frottement.

Nous introduirons ici un nombre sans dimension dont l'importance pour le transport solide semble considérable. C'est le rapport de $\tau_0/\varepsilon \rho g D$ à R_*^2. Il s'écrit :

$$G = \frac{\varepsilon g D^3}{\nu^2} \qquad (4)$$

Nous l'appellerons paramètre du grain. Il caractérise le comportement du grain dans le fluide.

La relation (3) de Shields peut s'écrire

$$G = f(R_*) \times R_*^2$$

ou, aussi bien,

$$G = f(R_*) \qquad (5)$$

La figure 1 montre la relation de Shields (canal) sous la forme (5), ou plutôt sous la forme $G = f(R_*^2)$.

On a porté sur le graphique les points expérimentaux de Goddet (houle). Pour cela, on a calculé la tension tangentielle maximum τ_0 au moyen de la théorie de la couche limite laminaire oscillatoire [7].

$$\tau_0 = \nu \rho V_{max} / \sqrt{\nu T}$$

On a alors :

$$R_*^2 = \frac{V_{max} D}{\nu} \times \frac{D}{\sqrt{\nu T}}$$

On voit que les points expérimentaux se groupent raisonnablement sur une droite pour R_*^2 compris entre 1 et 3×10^2. Si l'on admet comme équation de cette droite*

$$G = 10\, R_*^{8/3}$$

cela revient à :

$$V_{max} = 0{,}175\, g^{3/4} \varepsilon^{3/4} D^{1/4} T^{1/2} \qquad (6)$$

qui ressemble d'assez près (et ce n'est pas étonnant) à la loi (1) qu'admet Goddet.

La loi (6) donne comme condition de similitude :

$$\xi = \mu^3 \delta D_c^{-4} \qquad (7)$$

Nous ne nous étonnerons pas non plus que cette relation ressemble de fort près à la relation (2).

CONDITIONS D'APPLICATION DE CES RELATIONS.

Il semble bien que l'on puisse admettre l'une ou l'autre des relations de similitude, pourvu que les conditions suivantes soient remplies, aussi bien pour la nature que pour le modèle :

- la couche limite doit être laminaire,
- $G = \varepsilon g D^3 / \nu^2$ doit être inférieur à 2×10^4, ce qui correspond pour la nature à une dimension maximum des grains de sable de l'ordre du millimètre.
- $R_*^2 = V_{max} D^2 / \nu \sqrt{\nu T}$ doit être inférieur à 400. ($R_* < 20$).

Cette dernière relation, pour une houle de 10 secondes, conduit à une vitesse maximum admissible de l'ordre de 1 m/s pour des grains de 1 mm, et de 4 m/s pour des grains de 0,5 mm.

Afin de nous affranchir de ces limites, qui sont dues simplement aux limites des conditions expérimentales des essais sur lesquels nous nous sommes basés, nous allons essayer d'utiliser la liberté importante qui reste dans le choix des échelles. Cette liberté pourra aussi être mise à profit pour étendre le domaine d'application de la similitude envisagée.

---

* L'équation, choisie en toute bonne foi, se trouve éliminer ν de la relation (6). C'est pourquoi on ne trouve pas l'échelle des viscosités dans la relation de similitude (7).

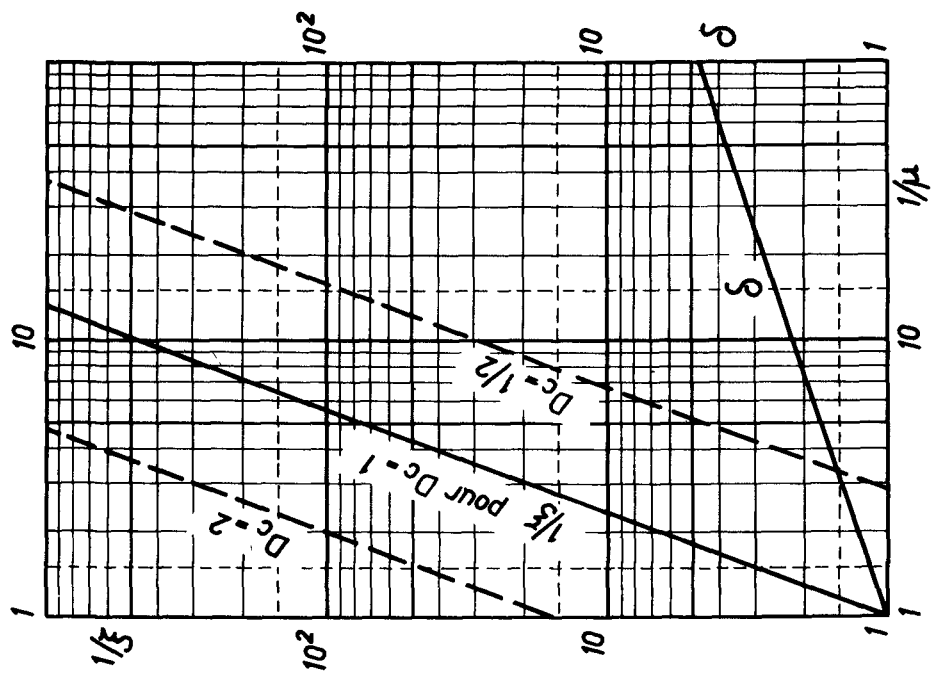

Fig. 2. Echelles des profondeurs d'eau (ξ) et des diamètres de grains (δ) en fonction de l'échelle des densités apparentes (μ). L'échelle des viscosités est supposée égale à 1.

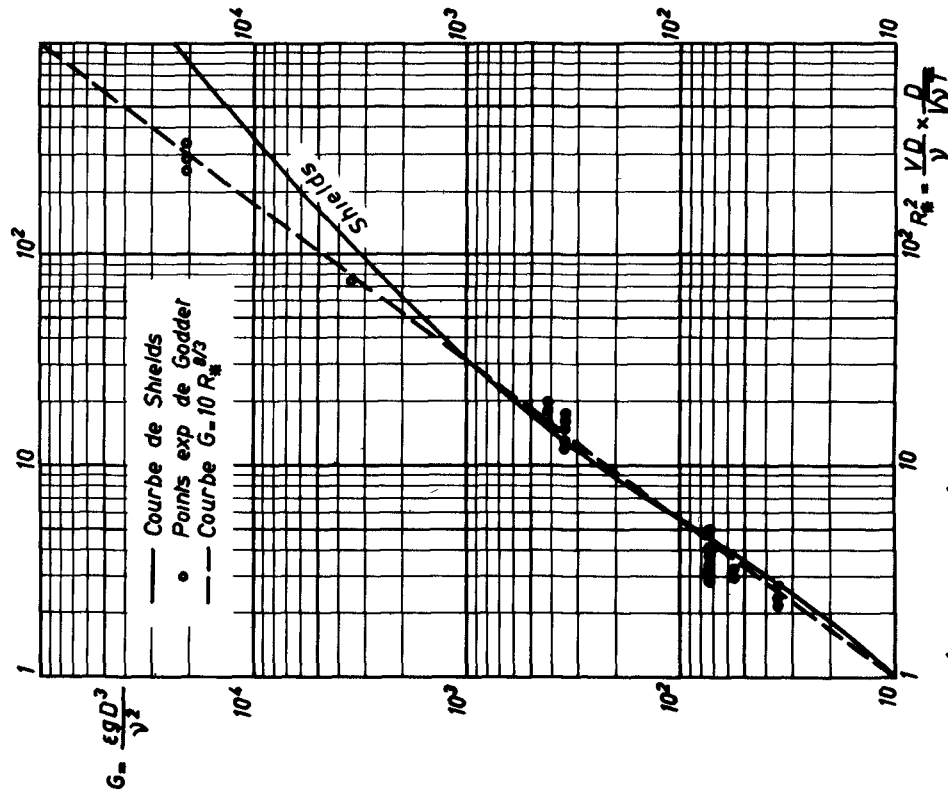

Fig. 1. Début d'entraînement: loi de Shields et résultats expérimentaux de Goddet, sous la forme $G = f(R_*^2)$.

RELATION DE SIMILITUDE PERMETTANT D'AVOIR SUR LE MODELE LA MEME VALEUR DE $G = \varepsilon g D^3/\nu^2$ QUE DANS LA NATURE

Les relations (2) et (7), qui caractérisent la similitude du début d'entraînement dans une couche limite laminaire oscillatoire, laissent une grande liberté dans le choix des échelles, puisque nous avons une seule relation obligée entre les échelles ξ, μ, δ, $\mathcal{D}_c$, φ et λ, cette dernière échelle étant l'échelle géométrique en plan, qui n'intervient pas dans les relations ci-dessus.

Il nous est donc possible d'essayer de faire intervenir d'autres critères

PROPRIETES DU PARAMETRE G

La conservation de la même valeur de $G = \varepsilon g D^3/\nu^2$ dans le modèle que dans la nature paraît être intéressante, car ce paramètre semble avoir des propriétés remarquables.

Si, par exemple, on écrit l'équation donnant la vitesse W de chute libre d'un grain de forme donnée en égalant le poids apparent et la poussée, on obtient la relation :

$$\boxed{G = f(R_w)} \qquad (8)$$

avec $R_w = WD/\nu$, nombre de Reynolds correspondant à la chute libre du grain

Donc, si l'on conserve G, on conserve R_w, c'est-à-dire que l'on se trouve dans le même régime d'écoulement autour du grain tombant en chute libre dans l'eau. On retrouve ici une propriété remarquable des lois de la chute d'un corps pesant dans un fluide : si deux corps de même forme (deux sphères par exemple) tombant dans le même fluide ont même poids apparent, leur R_w de chute est le même, c'est-à-dire que leur vitesse de chute est inversement proportionnelle à leur diamètre.

Si, d'autre part, on considère la façon dont les divers auteurs ont porté en graphique les lois de l'entraînement des matériaux de fond par l'eau (pour un courant unidirectionnel), on voit que le régime du matériau de fond (immobilité, début de charriage, rides, dunes, etc..) est caractérisé par la position du point représentatif du régime sur un graphique dont les coordonnées sont soit $\tau_0/\varepsilon\rho g D$ et R_*, soit u_*/W et R_*. Ces deux représentations s'équivalent, car on peut transformer le graphique $(\tau_0/\varepsilon\rho g D, R_*)$ en un graphique (G, R_*). La même opération peut être faite aussi bien sur le graphique $(u_*/W, R_*)$, puisque

$$u_*/W = R_*/R_w = R_*/f(G)$$

La correspondance entre les graphiques (G, R_*) et $(u_*/W, R_*)$ dépendra cependant de la forme des grains, puisque la relation $G = f(R_w)$ en dépend.

Mais, pratiquement, on peut dire que le régime du matériau de fond est caractérisé par les valeurs de G et de R_*.

ETUDE SUR MODELE DU TRANSPORT LITTORAL
CONDITIONS DE SIMILITUDE

Si l'on considère maintenant les diverses formules admises pour le débit transporté dans une rivière par charriage, on pourra remarquer que des formules aussi dissemblables que celles d'Einstein, de Meyer-Peter, de Frijlink (et sa forme simplifiée due à Bijker), se mettent toutes sous la forme :

$$T\,G^{-1/2} = f\left(R_*^2\,G^{-1}\right) \qquad (9)$$

$T = q_v / \nu$, est un nombre que nous appellerons paramètre de transport, dans lequel q_v est le débit en volume de matériau solide par unité de largeur du lit.

On voit que R_* et G caractérisent aussi le débit solide transporté par unité de largeur. Si ces lois sont valables, en conservant G et R_* sur un modèle, on y aurait le même débit solide en volume par unité de largeur que dans la nature*.

RELATION DE SIMILITUDE CONSERVANT G

La relation de similitude correspondant à l'égalité $G_{mod} = G_{nat}$ est la suivante :

$$\boxed{\delta = \mu^{-1/3}\,\varphi^{2/3}} \qquad (10)$$

Rappelons que :

$\delta = D_{mod} / D_{nat}$ est l'échelle des diamètres des matériaux,
μ est l'échelle des densités apparentes des matériaux,
φ est l'échelle des viscosités (on pourra souvent admettre que $\varphi = 1$).

RELATIONS DE SIMILITUDE CONSERVANT G ET R_*

Les relations de similitude (7) et (10) combinées donnent alors :

$$\boxed{\begin{aligned} \xi &= \mu^{8/3}\,D_c^{-4}\,\varphi^{2/3} \\ \delta &= \mu^{-1/3}\,\varphi^{2/3} \end{aligned}} \qquad (11)$$

Ces relations sont beaucoup plus restrictives que la relation (7) seule.

---

* Il faut noter que la relation (9) est incomplète, car les divers auteurs font intervenir aussi un coefficient tenant compte de la fraction de la force tractrice totale qui est utilisée pour le transport. Il faudrait évidemment en tenir compte dans une étude plus poussée.

Remarques -

a) La similitude définie par les relations (11) est plus générale qu'on ne pourrait le penser. En effet, elle résulte de la combinaison de la relation (7), établie à partir de l'équation $G = 10\, R_*^{8/3}$, et de la condition $G_{mod} = G_{na}$

On obtiendrait les mêmes relations à partir de la condition $G_{mod} = G_{nat}$ et d'une relation quelconque $G = f(R_*)$définissant le début d'entraînement. En effet, conserver G et une relation de la forme $G = f(R_*)$revient en fait à conserver G et R_*.

La similitude définie par les relations (11) consiste donc :
- à prendre le même paramètre de grain G sur le modèle que dans la nature,
- à prendre la même valeur de R_* sur le modèle que dans la nature, en admettant pour le calcul de τ_0 que la couche limite oscillatoire est laminaire. Si la condition de début d'entraînement est bien de la forme $G = f(R_*)$, on a automatiquement la similitude du début d'entraînement, avec les hypothèses restrictives indiquées ci-dessus.

b) L'échelle des densités apparentes conditionne l'échelle des diamètres de grains. Si l'on prend un matériau de densité plus faible que le sable, les grains seront plus gros sur le modèle que dans la nature. (Voir fig. 2). (Nous supposons ici la viscosité peu différente dans le modèle et dans la nature).

c) L'échelle des profondeurs est assez arbitraire, puisqu'il suffit de modifier un peu l'échelle des creux de houle pour la faire varier dans de larges limites. Pour une échelle des creux de houle égale à l'échelle des profondeurs, elle dépendrait uniquement de l'échelle des densités apparentes (fig. 2).

d) L'échelle en plan est absolument arbitraire.

On voit qu'il reste une grande liberté pour adapter le modèle à satisfaire à d'autres exigences.

DEBUT D'ENTRAINEMENT PAR LE COURANT GENERAL DE MASSE PERPENDICULAIRE A LA PLAGE

Longuet-Higgins [8] a calculé, pour une houle frontale, le courant de masse associé à la houle en supposant que l'écoulement reste laminaire. Ce courant porte à la côte au voisinage du fond.

Russel et Osorio [9] ont vérifié sur modèle que la formule de Longuet-Higgins donne de bons résultats pour le courant au voisinage du fond, même si l'écoulement devient turbulent. Longuet-Higgins a exposé les raisons de cette concordance dans le même article. Il calcule aussi la valeur moyenne de la tension tangentielle τ_0 sur le fond, qui, en régime purement oscillatoire est nulle, et il aboutit à une expression que nous écrirons sous la forme :

$$\tau_{0\,moyen} = \frac{\sqrt{\pi}}{2} \times \frac{\nu \rho V_m^2}{C \sqrt{\nu T}}$$

C étant la célérité de la houle.

Le $\mathcal{R}_*$ correspondant est donc donné par la relation :

$$\mathcal{R}_*^2 = \frac{\tau_0 D^2}{\rho \nu^2} = \frac{\sqrt{\pi}}{2} \times \frac{V_m D}{\nu} \times \frac{D}{\sqrt{\nu T}} \times \frac{V_m}{C} \qquad (12)$$

On voit que pour conserver la valeur de ce $\mathcal{R}_*$, il suffit, si l'on satisfait aux relations (11), de conserver sur le modèle la même valeur de V_m/C que dans la nature, car les relations (11) sont obtenues à partir de la conservation de $V_m D^2/\nu\sqrt{\nu T}$. Cette condition est réalisée si l'on a une échelle des creux égale à celle des profondeurs.

On restreint ainsi beaucoup le choix des échelles. L'échelle δ des diamètres de matériaux et l'échelle en hauteur ξ sont déterminées, dès qu'on a choisi μ, échelle des densités apparentes (fig. 2 avec $\mathcal{D}_c = 1$).

Cependant, si l'on s'écarte un peu de la condition de conservation de V_m/C, on change assez peu la valeur du $\mathcal{R}_*$ correspondant au courant de masse, mais on peut faire varier beaucoup l'échelle en hauteur, puisqu'elle varie comme $\mathcal{D}_c^{-4}$.

On peut remarquer que, si l'on partait de l'expression (12) pour $\mathcal{R}_*$, les relations de similitude correspondant à la conservation de G et $\mathcal{R}_*$ seraient les relations (11), où $\mathcal{D}_c^{-4}$ serait remplacé par $\mathcal{D}_c^{-3}$. La distorsion des creux de houle y est encore plus importante, ce qui se comprend, puisque la tension tangentielle introduite est proportionnelle au carré de ces creux.

REPRESENTATION DES TRANSPORTS EN SUSPENSION

Il faut, dans un modèle de plage, que le profil soit correctement représenté. Des essais en canal avec le matériau choisi et les houles du modèle indiquent le profil modèle correspondant au profil naturel, et déterminent la distorsion, donc l'échelle en plan à adopter.

Pour obtenir théoriquement cette distorsion, il faut trouver le phénomène déterminant dans la formation du profil. Or, le profil d'une plage dépend de nombreux phénomènes physiques, et particulièrement de la nature plus ou moins régulière de la houle incidente (une houle irrégulière érodant l'estran alors qu'une houle régulière le recharge), et aussi probablement [10] de la percolation près du rivage. Enfin, et surtout semble-t-il, le profil dépend de la façon dont les matériaux mis en suspension par le déferlement sont transportés par les courants de masse. L'influence du vent est aussi très sensible.

Il est cependant probable qu'une condition nécessaire, sinon suffisante, pour qu'un modèle de transport littoral soit représentatif, est que les chemins parcourus par les particules en suspension soient homologues aux parcours naturels. Pour simplifier, nous considèrerons le transport en suspension des matériaux sous l'action des courants de masse perpendiculaires à la plage, et nous écrirons la condition de similitude correspondante. Cette condition consiste à conserver dans le modèle la valeur naturelle du rapport suivant :

$$\frac{\text{vitesse de chute / profondeur d'eau}}{\text{vitesse du courant de masse / longueur perp. à la plage}}$$

Nous supposerons que nous avons déjà admis la conservation de R_* et de G.

L'échelle de la vitesse de chute W est, puisque l'on conserve $R_w = WD/$ en conservant G,

$$Ech\,(W) = \delta^{-1}\varphi$$

La vitesse du courant de masse au voisinage du fond est, d'après Longuet-Higgins,

$$U = 5\,V_m^2 / 4C$$

Son échelle est donc :

$$Ech\,(U) = \eta^2 \xi^{-3/2} = \xi^{1/2} D_c^2$$

(η est l'échelle des creux de houle).

Si on appelle λ l'échelle des longueurs perpendiculairement à la plage et $D_h = \xi/\lambda$ la distorsion géométrique correspondante, on obtient la relation de similitude suivante :

$$D_h = \delta^{-1} \xi^{-1/2} D_c^{-2} \varphi$$

Combinée avec les relations (11), cette relation devient :

$$\boxed{D_h = \mu^{-1}} \qquad (13)$$

Si, au lieu de la valeur de τ_* correspondant à la couche limite laminaire on avait utilisé la valeur correspondant au courant de masse pour écrire la conservation de R_*, on aurait :

$$D_h = \mu^{-1} D_c^2 \qquad (13\text{ bis})$$

Les valeurs données par la relation (13) sont du même ordre de grandeur que les valeurs obtenues par des essais en canal. Pour un matériau de densité absolue 1,4 par exemple, la distorsion à adopter est 4.

REFERENCES BIBLIOGRAPHIQUES.

1. Larras, J. (1956). Effets de la houle et du clapotis sur les fonds de sable – 4ème Journées de l'Hydraulique – Tome 2 – pp. 579-589.

2. Vincent, G.E. (1958). Contribution to the study of sediment transport on a horizontal bed due to wave action – 6th Conf. on Coastal Eng. pp. 326-355.

3. Madhav Manohar, (1955). Mechanics of Bottom sediment movement du to wave action – Beach Erosion Board rech. Mem. n° 75.

4. Lhermitte, P. (1958). Contribution à l'étude de la couche limite des houles progressives. Publ. n° 136 du C.O.E.C. – Paris – Imp. Nat.

5. Goddet, J. (1959). Etude du début d'entraînement des matériaux mobiles sous l'action de la houle – La Houille Blanche n° 2 – 1960.

6. Shields, A. (Voir par ex. Rouse : Engineering Hydraulics, p. 790).

7. Valembois, J. (1956). Quelques considérations sur la similitude dans les essais de houle sur modèle - 4ème Journées de l'Hydraulique - Tome 1 - pp. 252-256.

8. Longuet-Higgins, M.S. (1953). Mass Transport in Water Waves - Phil. Trans. Roy. Soc. London, Series A, n° 903, vol. 245, pp. 553-581.

9. Russel, R.C.H. and Osorio, J.D.C. (1958). An experimental investigation of drift profiles in a closed channel - 6th Conf. On Coastal Eng. pp. 171-193.

10. Silvester, R. (1959). Engineering aspects of Coastal Sediment Movement - Proc. A.S.C.E. Vol. 85 - WW3 - pp. 11-40.

Chapter 19

SCALE EFFECTS IN MODELS WITH LITTORAL SAND-DRIFT

R. Reinalda
Delft Hydraulics Laboratory.

INTRODUCTION

In the "De Voorst" Laboratory of the Hydraulics Laboratory, Delft, a model investigation has been carried out concerning the problems which present themselves around the Thyborøn Channel on the west coast of Denmark. This investigation was commissioned by the Danish Board of Maritime Works, who also supplied the necessary data and information. In this model a scale effect very clearly presented itself with regard to the littoral drift caused by waves, which led to phenomena in the model which deviated considerably from those in the prototype. As this scale effect is likely to occur in some degree in most of the models with littoral drift caused by waves, the publication of the phenomenon observed seems justified.

DESCRIPTION OF PROTOTYPE

The Jutland Peninsula, the mainland of Denmark, is divided into two by the Limfiord, which connects the Cattegat with the North Sea (figure 1). The western approach to the Limfiord is the Thyborøn Channel, which is actually a breach through the barrier separating the Limfiord from the North Sea, which occurred in 1862. In previous years this barrier had repeatedly been burst during heavy storms from the west, but in course of time the channels formed in this way sanded up again.

Ever since the existence of the Thyborøn Channel much sand has been introduced into the Limfiord, where an extensive sand-bank area was formed. This sand comes from the parts of the coast on either side of the entrance to the channel, each about 10 km in length. For the period from 1912 to 1943 about 0.77 million cubic metres of sand a year were calculated to be deposited in the Limfiord.

The recession of the coast-line during the first years after the development of the Thyborøn Channel was enormous, especially near the entrance to the channel. The first information about this dates from 1874, that is 12 years after the breach (figure 2). The average recession between 1874 and 1890 of the coast-line of 20 km was about 10 m a year.

In order to reduce coastal erosion, and to protect, for the benefit of navigation, the channel against sanding up many groynes were built along the coast, most of them between 1885 and 1905. The first groynes reached to only small depths, some no further than to about the low-water contour. The construction of the groynes was such that the position of their heads could not be maintained when the coast-line further receded.

2. After the building of the groynes the erosion of the bar and the scouring of the channel was too heavy. This was the result of the alteration of the scale for the littoral drift owing to the groynes. So the transport capacity of the current velocities in the channel and on the bar after the construction of the groynes was too great. This could be corrected in a simple way by reducing the current velocities to such an extent that the scale for the material movement in the channel and on the bar was again equal to that of the littoral drift.

CONCLUSION

The most important conclusion is that in small-scale models in which problems concerning littoral drift are studied, a considerable scale effect may occur in the transport distribution in a line perpendicular to the coast. At the same time it appears that this may result in phenomena in the model which greatly deviate from the prototype.

Now by visual observations the impression is created that in other coastal models in the Hydraulics Laboratory "De Voorst" where sand with d_m = 200 - 250 μ is used as transport material this scale effect occurs to a far lesser degree. From this it might be concluded that in similar models this sand is preferable to ground bakelite, which was used in the Thyborøn model. On the other hand, however, the critical velocity for the initial movement of the sand is higher than for ground bakelite. If an inlet is present, and sand is used, the current velocities in this inlet will often have to be exaggerated in order to obtain sufficient transport. In that case the condition $n_v = n_c = \sqrt{n_h}$ is no longer satisfied, which results in a deviating refraction pattern of the waves, and thus to an incorrect transport of solids. In future a transport material may have to be found which already starts moving at relatively low velocities, and for which the transport distribution by waves in a line perpendicular to the coast corresponds with the situation in nature. For this purpose, however, more data about the transport distribution in the prototype must be available than has been the case so far.

Experience has taught, however, that if the various factors which influence the littoral drift are taken into due account, and if, moreover, sufficient data are known of the changes in the bottom configuration during the past in the prototype, a very workable model can be designed (figure 5). If the model results are handled with caution, which in the majority of investigations is imperative in any case, a coastal model, too, will be an important aid in solving various problems.

that at the point of time mentioned the groynes reached to a depth of 8 cm on an average, so that the waves broke on the landward side of the line connecting the groyne heads. A further increase in the distance between the heads of the groynes and the coast-line only little influenced the littoral drift.

From the figures 3A and 3B a relation can be found between the points of time at which the recession of the coast-lines in prototype and model since 1874 were equal. This relation is shown in figure 4A, in which the years for the prototype on the horizontal axis are plotted against the hours for the model on the vertical axis. The relation over the period from 1874 to 1890 as well as after 1920, appears to be linear. Now the gradient is a measure for the time-scale of the coastal erosion, which is represented in figure 4B. For the period from 1874 to 1890 one year prototype corresponds with 1/2 hour model, after 1920 one year prototype corresponds with 2 hours model.

This change in the time-scale for the coastal erosion is caused by the fact that in the model the transport distribution in a line perpendicular to the coast deviates from that in the prototype. In the model relatively too much material migrates along the coast in the breaker zone. Consequently the groynes in the model exert a much greater influence on the littoral drift than in the prototype. In the prototype the ratio between the recession of the coast-line before 1890 and after 1920 is 4.5 : 1; in the model this ratio is 18 : 1.

The incorrect transport distribution in the model resulted in a number of phenomena which deviated from those in the prototype.

1. Before the groynes had been built the coast near the channel entrance in the model showed a tendency to accretion, in contrast with the prototype where at this place the coast eroded. In this area the wave motion near the coast was relatively slight, as the waves were breaking further seaward on the bar where, at the time, the depths were small. Hence the transport capacity of the waves was here less than at a greater distance from the channel entrance. Now in the prototype the reduced transport by the waves was compensated by higher current velocities near the channel entrance.

   As in the model the littoral drift was far more concentrated in the breaker zone the transport of solids close to the coast by the waves near the channel entrance was far more reduced than in the prototype. The current velocities, which were adjusted in such a way that the depths on the bar and in the channel were correctly represented, now appeared to be only partly capable of compensating the reduced transport capacity of the waves near the coast.

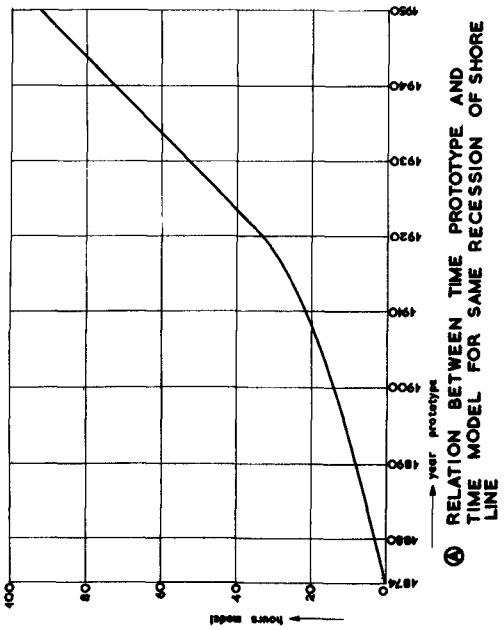

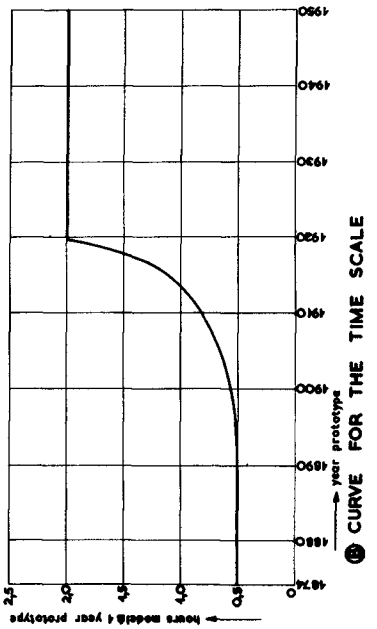

Fig. 4. Time scale for recession shore line.

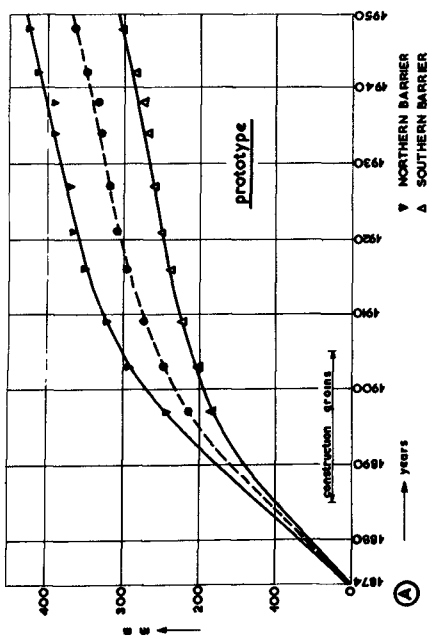

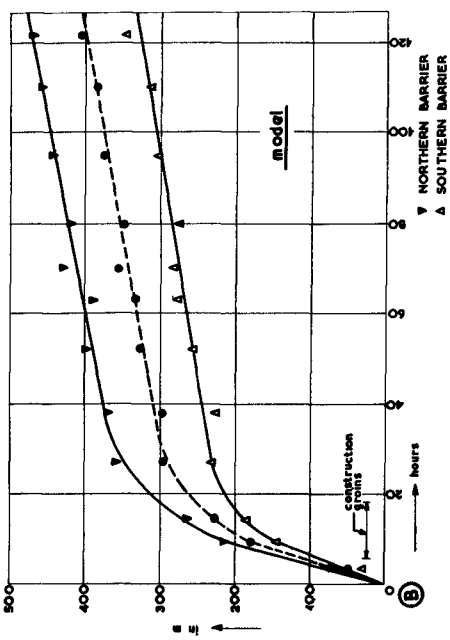

Fig. 3. Recession of the shore line.

SCALE EFFECTS IN MODELS WITH LITTORAL SAND-DRIFT

The boundary conditions to be adjusted with regard to the currents and waves were determined by reproducing the changes of the bottom topography in the prototype since 1874 in the model. For this purpose the wave motion and the littoral current were provisionally determined, so that the coastal erosion was simulated with reasonable accuracy. The current velocities and the tidal periods in the channel were adapted to this, the depths on the bar and in the channel corresponding with those in the prototype. Owing to the refraction of the waves caused by the tidal currents which occurred on the bar, the current velocities had to fulfil certain requirements. In order to obtain a correct representation of the refraction of the waves resulting from the sloping-up of the bottom the condition $n_c = \sqrt{n_h}$ must be applicable, and for a correct representation of the wave refraction caused by the currents $n_v = n_c$. Hence $n_v = \sqrt{n_h}$. In the model the wave period was T = 1.3 sec and the wave height H = 5 cm, which compared with prototype T = 8 sec, and H = 2 m.

For the judgment of the model results the following magnitudes for prototype and model have in the first place been compared:

a. The recession of the coast-line;
b. The erosion of the bar;
c. The scouring of the channel.

The recession of the coast-line since 1874 in prototype, both north and south of the channel has been represented in figure 3A. Between 1874 and 1890 the recession averaged 10 m a year. Owing to the presence of the groynes the annual recession between 1890 and 1920 became less. After 1920 the recession has been practically oonstant at 2.2 m a year. The reasons for this are the following:

a. Since 1920 the groynes reach, for most of the waves, beyond the breaker zone, and thus the greater part of the littoral drift has been checked. On the seaward side of the breaker zone the transport of solids per unit of width is little, and a further extension of the distance between the groyne heads and the coast-line has, after 1920, not much influence on the coastal erosion.
b. Moreover, the groynes in the prototype show some abrasion, so that the annual increase in the distance between the heads and the beach-line is even less than 2.2 m a year.

In the model a similar phenomenon was observable as in the prototype. After the building of the groynes, here, too, the coastal erosion became less, but much more so than in the prototype (figure 3B). It may be observed here that in the model the groynes were built at those points of time at which the position of the coast-line corresponded with that in the prototype. Most of them were built from 5,5 to 18 hours after the initial point of time. After operation of the model for 33 hours the position of the coast-line corresponded with that in the prototype in the year 1920. It is noteworthy that since that time the recession of the coast in the model had also a constant value. It appears

Hence the effect of the groynes on the coastal erosion was slight. By applying a heavier construction and by carrying out much maintenance work, the position of the groyne heads over the last dozens of years has been ensured with reasonable success. The recession of the coast-line has thus been reduced considerably and since 1920 it averages 2.2 m a year.

By the building of the groynes the sand transport to the channel entrance was greatly diminished. This resulted in serious erosion of the bar before the entrance to the channel and in scouring of the channel.

LAY-OUT OF THE MODEL

The model represents the Thyborøn Channel, a small part of the Limfiord and the stretches of coast on either side of the entrance to the channel, each 10 km in length. The horizontal scale of the model $n_L = 250$, the vertical scale $n_h = 40$. The distortion of the model has been chosen in such a way that the slopes of the coast in the model correspond with those in the prototype. Ground bakelite with $d_m = 1.8$ mm and a density $\varrho = 1350$ kg/m^3 was decided upon as transport material. The model is further fitted with a wave generator with a total length of 80 m. At sea in the model a north-going and a south-going current can be adjusted, combined with both an incoming and an outgoing current in the channel.

MODEL INVESTIGATION

Before the investigation on the measures proposed to improve the situation could be started, the transport of solids in the model had to be verified with that in the model. A further item of importance was the determination of the time-scale for the transport of solids.

According to the nature of the transport of solids three areas can be distinguished:

a. the coast, where the transport of solids is caused by the motion of the waves and the weak littoral current.
b. the bar and the channel entrance, where the waves and the strong tidal currents cause the transport of solids.
c. the channel, where the transport of solids is caused almost exclusively by the tidal currents.

There is a close connection between the phenomena which occur in these three areas. The rate of the coastal erosion for example, and consequently the movement of material to the channel entrance will influence the depths over the bar and in the channel. From this it follows directly that the currents and the waves in the model must be selected in such a way that the scale ratios for the transport of solids in the three areas mentioned must be equal so that there is one time-scale for the events.

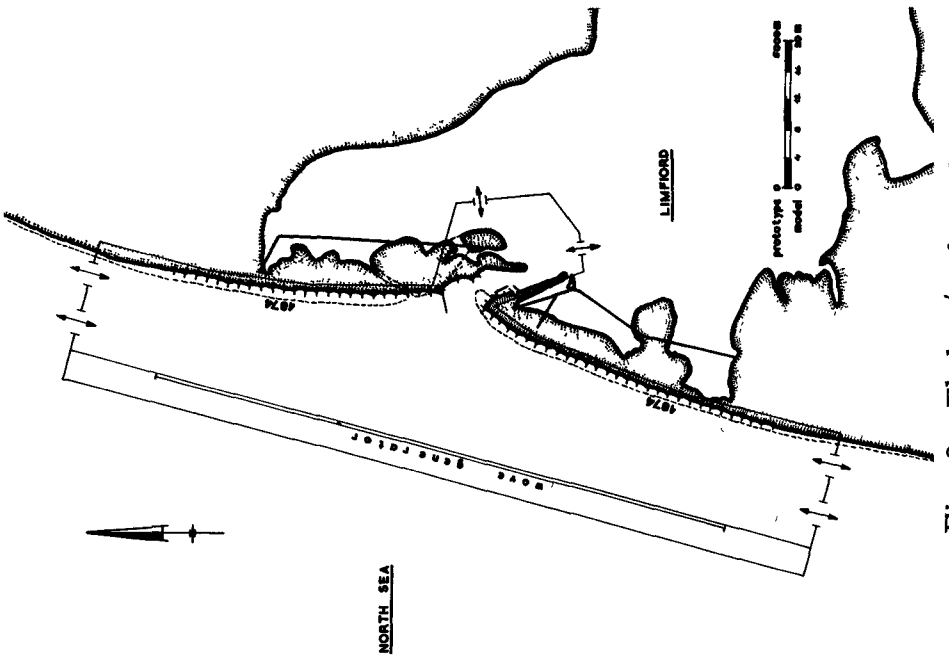

Fig. 2. Thyborøn channel.

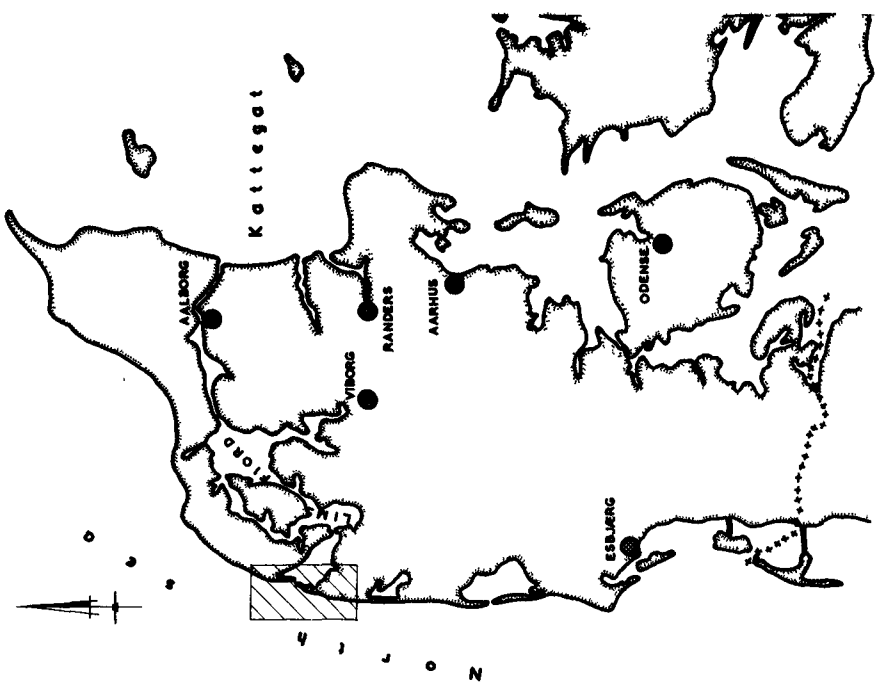

Fig. 1. Denmark.

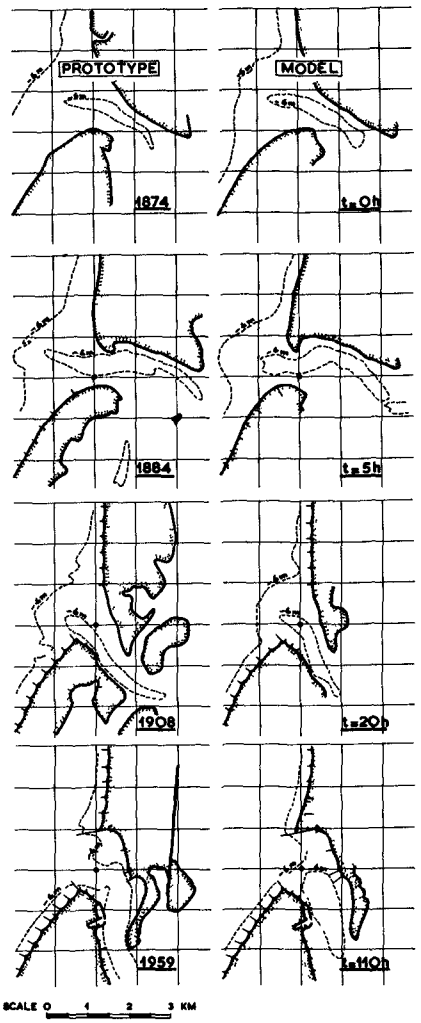

Fig. 5. Development Thyborøn channel.

ACKNOWLEDGMENTS

The author wishes to express his tanks to Mr A. Lehnfelt, Director of the Danish Board of Maritime Works for his permission to publish the above model results.

He also likes to express his most grateful thanks to Mr K. Otterstrøm, Civil Engineer of the Danish Board of Maritime Works for the valuable information which he has given concerning the development of the situation in the prototype. Without his help it would have been impossible to conduct this investigation satisfactorily.

He is further grateful for the assistance which he received from Ir E.W. Bijker, Head of the "De Voorst" Laboratory during the model investigation and the composition of this paper.

CHAPTER 20
LITTORAL TRANSPORT IN THE GREAT LAKES

Dr. L. Bajorunas
U. S. Lake Survey, Corps of Engineers

INTRODUCTION

The Great Lakes Superior, Michigan, Huron, Erie, and Ontario extend almost to the middle of the North American Continent. With their 95,000 square miles of water surface and their three navigable connections with the Atlantic Ocean and Gulf of Mexico, they affect the well-being of about 40 million people living within their vicinity in Canada and the United States. Possessing a shoreline of 6,600 miles, these waters have been called the fourth coast of the continent along with the Atlantic, Gulf, and Pacific coasts. This paper analyzes one of the many problems of the Great Lakes, the littoral transport problem.

Littoral transport has been defined as the movement of material along the shore in the littoral zone by waves and currents. The material thus transported is referred to as the littoral drift. The littoral drift originates from the beach material, being picked up by the water and transported along the shore and deposited in another location. Shore erosion, littoral transport, and deposition of drift are all factors in the littoral process.

A knowledge of the littoral process is important for many engineering projects including the construction and maintenance of shoreline harbors. The harbor breakwater extending from the shore into deep water forms a littoral barrier, and by stopping the transport action causes the deposition of drift on the updrift side. If the breakwater does not entirely stop the transport, or when the storage area on the updrift side is filled, the drift will bypass the breakwater and fill the dredged navigation channel causing frequent and expensive maintenance dredging. This problem is especially important in the small harbors on the Great Lakes planned every 25 to 30 miles as refuge for fishing and pleasure boats. These harbors have a rather small capacity for littoral drift, and the costs of maintenance dredging of so many entrance channels would be almost prohibitive.

In order to provide data required for the design and economic evaluation of the small refuge harbors on the Great Lakes, the United States Lake Survey, Corps of Engineers, conducted a study of the best method of estimating the rate of littoral transport along the shores of the Great Lakes. Although much of the data used in this paper was taken from the above study, the views and conclusions stated here do not necessarily reflect those of the Lake Survey.

LITTORAL TRANSPORT IN THE GREAT LAKES

DERIVATION OF TRANSPORT EQUATION

The present knowledge about littoral transport is briefly summarized by Savage, 1959, in the following way: "The mechanics of littoral transport are not precisely known, but it is generally agreed that the major portion of the littoral transport is caused by waves which approach the shore obliquely. Such waves have three main effects. First, before breaking, the waves create oscillatory currents along the bottom which tend to move material alongshore in suspension in the turbulent eddies generated by the interaction of the oscillatory currents and the sand surface of the bottom. Second, during breaking, these waves produce a current along the shore. Beach material placed into suspension by the turbulence of the breaking waves is carried alongshore in this current. Third, during and after breaking, these waves propel a mass of water up the foreshore. This mass of water has an alongshore velocity component, and therefore moves material slantwise up and down the foreshore; the net direction of material movement being alongshore in the direction of the alongshore energy component of the wave."

General agreement stops at the point where littoral transport is a function of waves in respect to their energy. No methods are generally accepted to bring the amount of drift into accord with the wave energy. Therefore a relationship is needed between transport and energy based on theoretical considerations and actual observations. For the purposes of harbor design, statistical data from long period observations are considered adequate to derive this relationship.

The material lying in the littoral zone must be stirred up before it is picked up and transported downdrift. The transport at a point along a straight shore is the summation of material picked up over a distance D updrift of the point.

$$Q = \int_0^D P \, dD \tag{1}$$

where,

- Q is the transport at a point.
- P is the pickup updrift of the point per unit length of shore.
- D is the distance updrift over which pickup is taking place.

The pickup is a function of the wave energy component perpendicular to the shore while the transport is a function of the component along the shore.

$$P_o = c \, E_o^n \cos \alpha_o \tag{2}$$

$$Q_o = a \, E_o^n \sin \alpha_o \tag{3}$$

where,

P_o is the potential pickup when transport is zero.
Q_o is the potential transport when pickup is zero.
c, a, n are constants.
E_o is the deepwater wave energy.
α_o is the angle between the wave crests and the shoreline.

Although the wave energy along a straight coastline is the same per unit length of shore, the portion of energy available for pickup of new material will be only what is left from the energy expended in picking up and transporting the material from updrift reaches. Therefore, the pickup at some distance is:

$$P = c\ (E_o^{\,n} - E^n)\ \cos\alpha_o \tag{4}$$

Substituting the energy from (3), the pickup becomes:

$$P = b\ \cot\alpha_o\ (Q_o - Q) \tag{5}$$

where $b = c/a$.

Substituting the pickup P from (5) in (1), the transport is:

$$Q = \int_o^D (Q_o - Q)\ b\ \cot\alpha_o\ dD \tag{6}$$

Integrating (6) and using (3) for Q_o, we derive the transport equation for a straight coastline:

$$Q = a\ E_o^{\,n}\ \sin\alpha_o\ \left[1 - e^{-\,b\,D\,\cot\alpha_o}\right] \tag{7}$$

When the coastline is not straight, it can be divided into several straight reaches, and the transport computed reach by reach. At the downdrift end of the first straight reach, the transport is obtained by equation (7), and at the end of each of the subsequent reaches by the equation:

$$Q_2 = Q_1 \left[e^{-\,b\,D_2\,\cot\alpha_{o2}}\right] + a\ E_o^{\,n}\ \sin\alpha_{o2}\ \left[1 - e^{-\,b\,D_2\,\cot\alpha_{o2}}\right]$$

where,

Q_1 is the transport at the end of the previous reach.
α_{o2} is the angle between the wave crest and the shoreline of the straight reach being considered, and
D_2 is the length of the latter reach.

LITTORAL TRANSPORT OBSERVATIONS

In deriving the constants a, b, and n in the transport equation (7), the observations were used on rate of littoral transport, deepwater wave energy, length and alignment of shore, available shore material, an the material in transport. Other elements affecting the transport, as

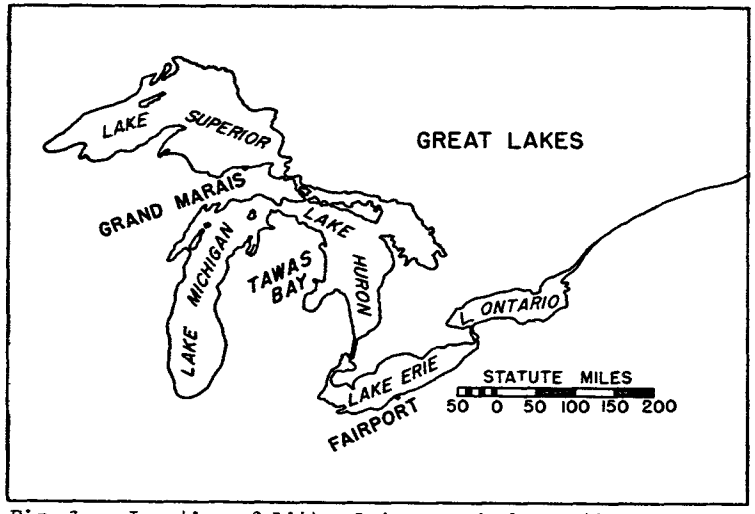

Fig. 1. Location of littoral transport observations.

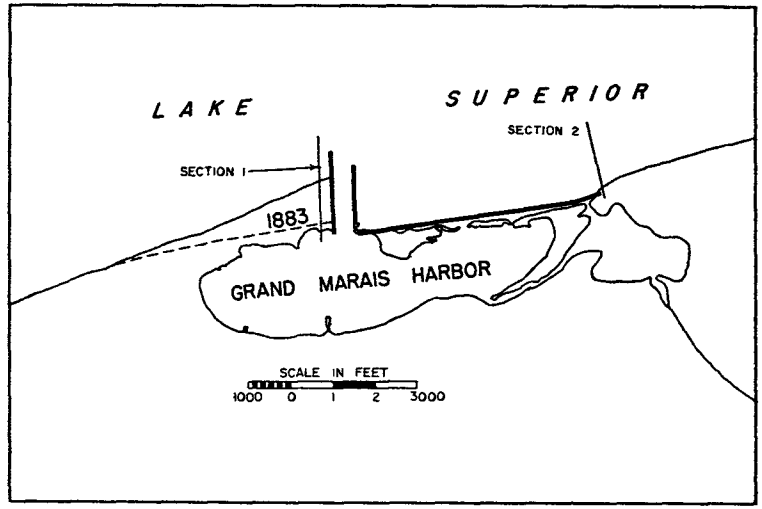

Fig. 2. Lake Superior shore at Grand Marais Harbor.

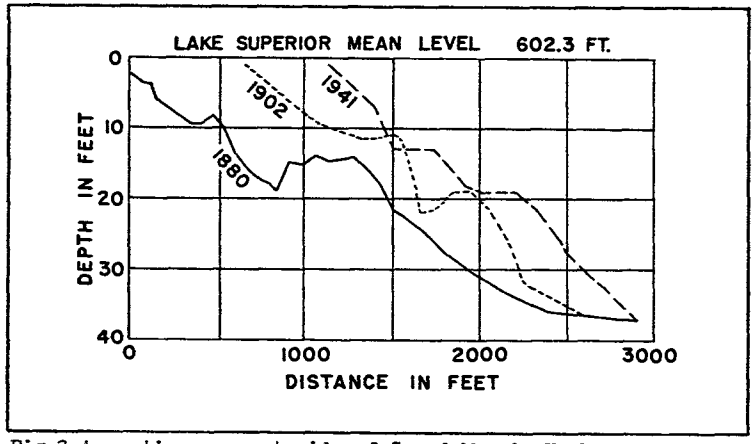

Fig.3.Accretion on west side of Grand Marais Harbor, Section 1.

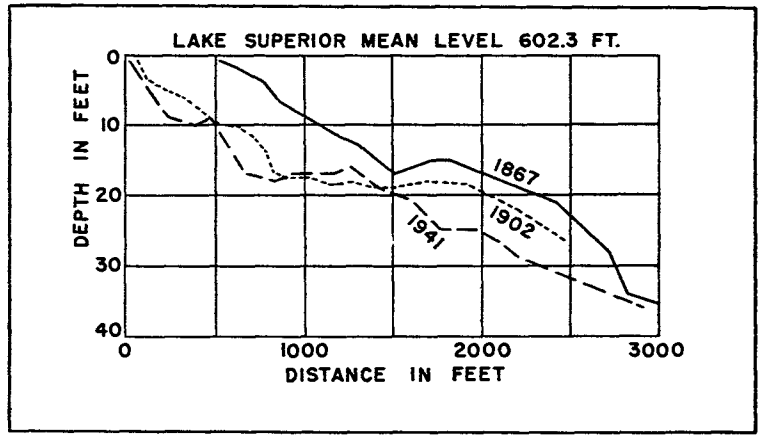

Fig.4. Erosion on east side of Grand Marais Harbor, Section 2.

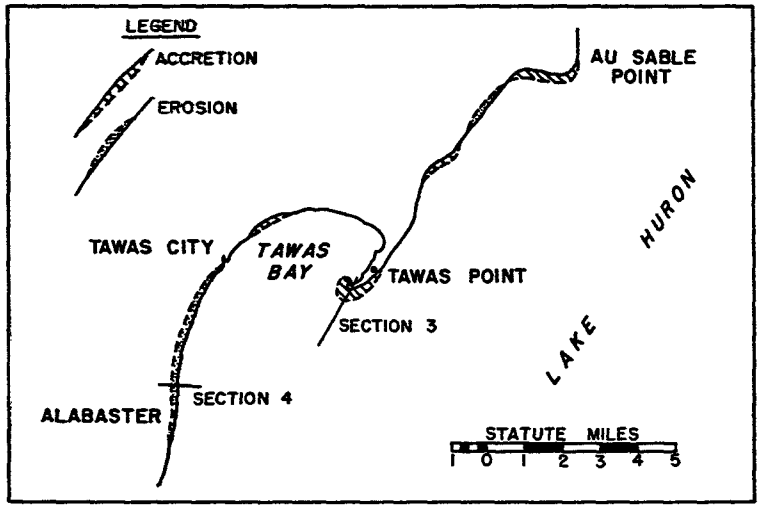

Fig. 5. Lake Huron shore at Tawas Bay.

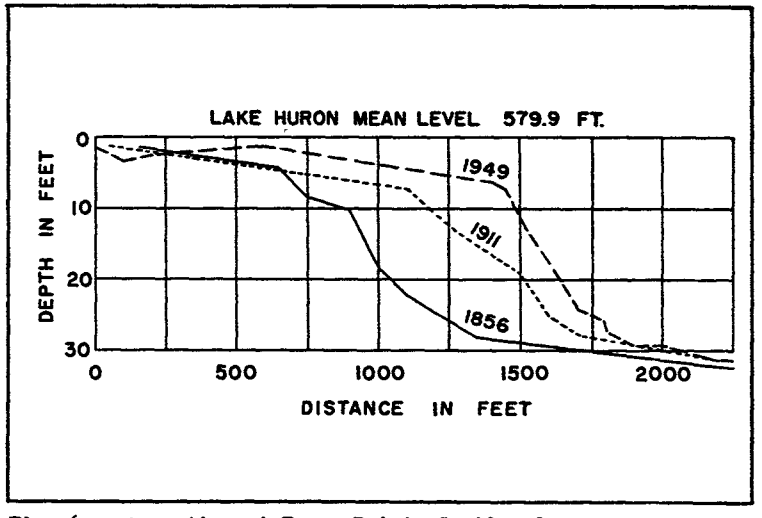

Fig. 6. Accretion at Tawas Point, Section 3.

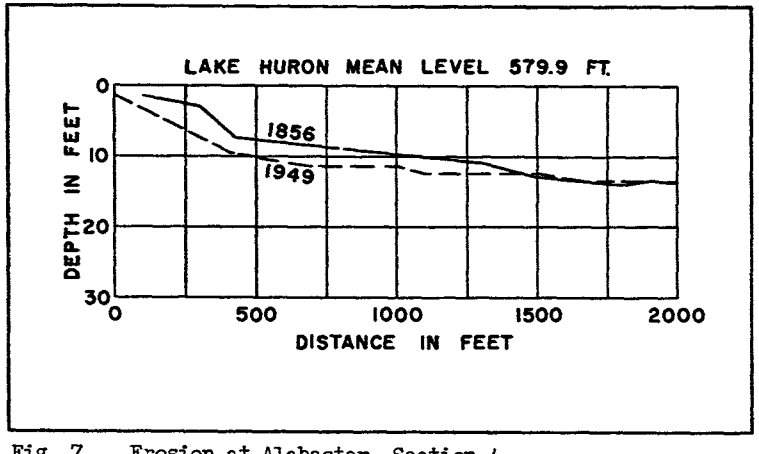

Fig. 7. Erosion at Alabaster, Section 4.

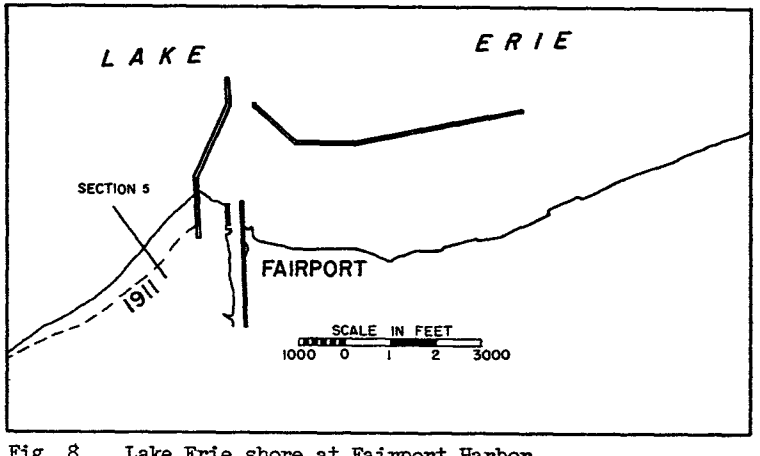

Fig. 8. Lake Erie shore at Fairport Harbor.

wave steepness, storm duration, wave refraction, lake level, and water temperature, were not considered in the interest of simplifying the problem. They are partly implicit in the statistical data used.

TRANSPORT RATE.

Remarkably accurate soundings of the offshore and beach areas of the Great Lakes were recorded by the Lake Survey during the last half of the 19th century. These early soundings when compared with more recent hydrographic surveys show the changes along the shore that have taken place over long periods of time. Because even small errors in the soundings or their location along areas of little change result in relatively large inaccuracies in computing the change in volume, the areas to be studied had to be carefully selected. The areas investigated for this study were located at natural or man-made barriers where the changes in volume were large. By catching the transport from one direction and excluding it from the opposite direction, the barriers also made it possible to correlate transport with the wave energy from one direction. Erosion from the relatively short face of the deposited drift is rather small and can be estimated without significant error. The location of the areas selected are shown in Figure 1, and the results of the detailed investigations are summarized below.

Grand Marais Harbor is located on the southern shore of Lake Superior, see Figure 2. The construction of the harbor was started in 1883 with two parallel breakwaters extending into the lake protecting a dredged navigation channel. Later the breakwaters were extended further into the lake and at the present time are about 2,000 feet long, extending into 20 feet of water. Many hydrographic surveys have been made of the areas on both sides of the harbor, however, most of these surveys did not fully cover the area involved. The soundings made in the vicinity of the harbor in 1880, 1902, and 1941 provided the best data for computing the changes in volume over long periods of time. Profiles from these soundings at Section 1 are shown in Figure 3. The accretion per year on the west side of the harbor was computed as 54,000 cubic yards over the 19-year period from 1883 to 1902, and 58,000 cubic yards over the 39-year period from 1902 to 1941. The average accretion was 57,000 cubic yards per year for the entire period of 58 years. The rate of erosion from the face of the deposits was estimated to be in the order of 2,000 cubic yards per year. Thus the average transport rate from the west becomes 59,000 cubic yards per year.

The soundings also indicate that a small amount of drift bypasses the west breakwater and is deposited at a depth of about 17 feet. On the east side of the harbor the soundings show a continuous erosion, Figure 4. A protective wall about 5,700 feet long was built along the shore to the east in the 1895-1898 period. The shore material on both sides of the harbor is fine sand, and the supply is unlimited. The deposited material west of the harbor is also fine sand.

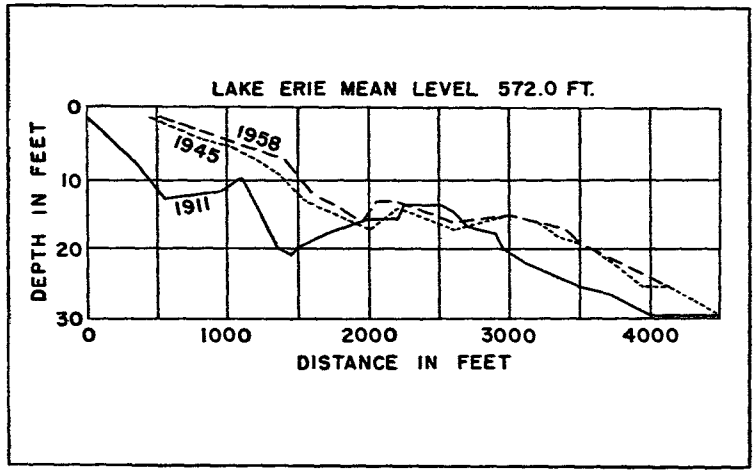

Fig. 9. Accretion on west side of Fairport Harbor, Section 5.

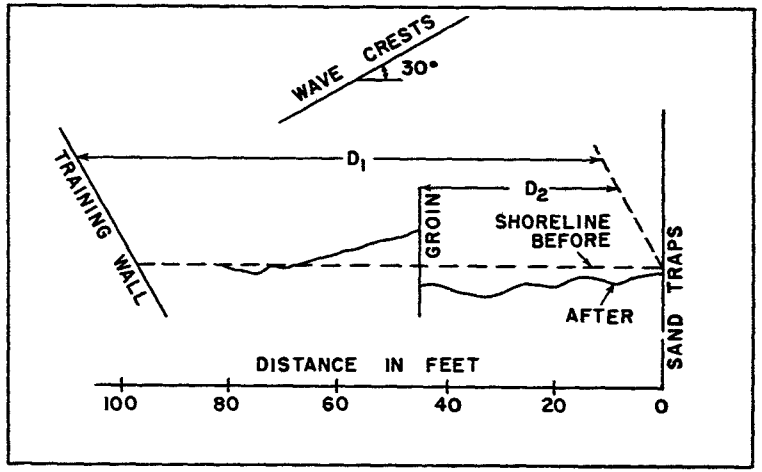

Fig. 10. Layout of model tests by Beach Erosion Board.

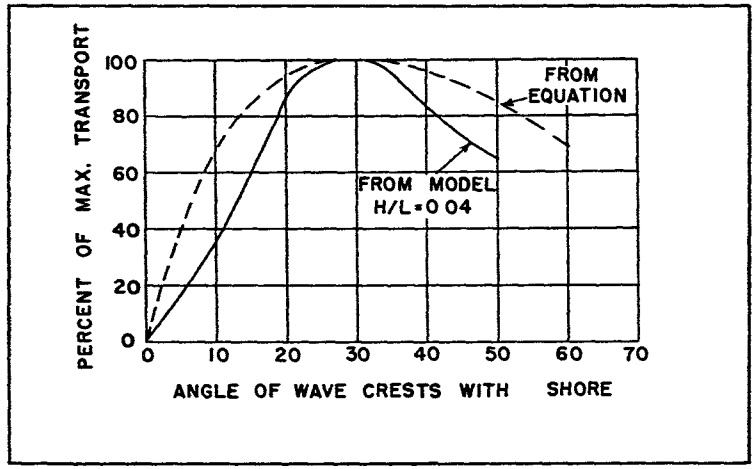

Fig. 11. Variation of transport with the angle of wave crests.

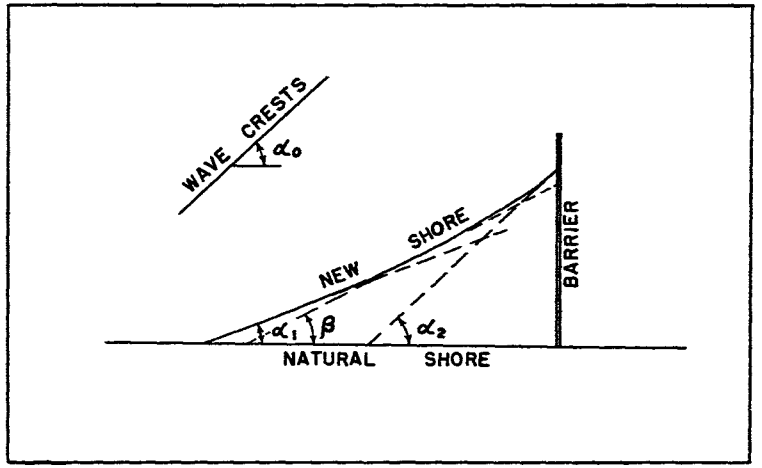

Fig. 12. Diagram of accretion in front of a barrier.

Au Sable Point is about 8 miles northeast of Tawas Point on the west shore of Lake Huron, see Figure 5. The coastline north of Tawas Point has a general northeasterly direction. At Au Sable Point the shore turns sharply to the east and then to the north forming a small bay south of the point. A part of the material being transported from the north is deposited just south of Au Sable Point while the rest of the drift is transported along the shore to be deposited at Tawas Point. Based on the soundings made in 1856 and 1949, the transport at Au Sable from the north was determined to be 121,000 cubic yards per year. The drift along this reach is sand, and the available beach material north of Au Sable Point is mainly sand with some rock outcrops.

Tawas Point is located on the westerly shore of Lake Huron at Tawas City, Michigan. The contour of the lake shore at this location is such that all the transport is trapped in the Tawas Bay. Most of the material transported along this shore comes from the north and is deposited at the end of Tawas Point. There is a small amount of transport from the south which is deposited at Tawas City.

The accretion at Tawas Point is composed of sand with a rather flat initial slope of 1 on 170. At a depth of about seven feet, the slope abruptly changes to about 1 on 25, and is more or less constant until the lake bottom is reached in about 30 feet of water. This changing slope is shown by the profiles in Figure 6. The soundings made in 1856 and 1911 indicate that the average accretion at Tawas Point was 67,000 cubic yards per year. The soundings in 1949 show an average accretion of 60,000 cubic yards per year for the period after 1911. The average for the 93-year period was 64,000 cubic yards per year. The accretion at Tawas City is in the order of 2,400 cubic yards per year.

Alabaster is a small town on the shore of Lake Huron about 5 miles south of Tawas City. The lake shore north of Alabaster shows evidence of considerable erosion over the years. It is here where the Lake Huron waves start to pick up new shore material after depositing the transport from the north at Tawas Point. The erosion at Section 4 near Alabaster is shown by the 1856 and 1949 profiles in Figure 7. Over the 93-year period, the erosion in the northerly mile of the reach shown in Figure 5 averaged 4,200 cubic yards per year while the average rate of erosion over the 5-mile reach was 25,000 cubic yards per year. These erosion values are not as accurate as the accretion values obtained because of the relatively large area affected with respect to the amount. The available beach material consists primarily of sand with rocks, clay and occasional gravel scattered throughout the reach.

Fairport Harbor is located near the middle of the southern shore of Lake Erie about 29 miles east of Cleveland. The breakwaters shown in the harbor layout, Figure 8, extend out from the shore into 20 feet of water. The dominant direction of transport in this area is from the west. In Figure 9 the profiles at Section 5 west of the harbor are based on soundings made in 1911, 1945, and 1958. These soundings indicate an accretion during the 1911-45 period of 124,000 cubic yards per year, and during the 1945-58 period

of 88,000 cubic yards per year. The large difference in accretion rates for the two periods may be due to shore construction west of the harbor, such as the water intake pier near the Chagrin River built in 1951, or to an increase in the transport passing the harbor. The erosion from the face of the deposits is estimated to be 6,000 cubic yards per year. On the east side of the harbor a serious erosion problem existed. In 1932 the east breakwater was extended 5,400 feet eastward parallel to the shore to protect the beach.

The Division of Shore Erosion, State of Ohio, made an extensive survey of the beach along the Lake Erie shore. In the reach from Cleveland to Fairport, samples were mostly sand ranging from fine to coarse with the sizes 0.2 to 0.4 mm predominant. The samples also included some clay, pebbles, and cobblestones. The material deposited on the west side of the harbor is very uniform and has a median size of 0.24 mm with a coefficient of sorting 1.1. This uniformity of size indicates that waves select the material being transported from the large assortment available on shore.

WAVE ENERGY.

Wave energy is the prime factor of littoral transport. The general circulatory currents and the currents resulting from water level disturbances do not significantly change the picture of the energy in the littoral zone of the Great Lakes. These currents might be a factor in some isolated restricted areas.

Wave energy for this study was computed by the generally accepted simplified equation for the energy of deepwater waves in fresh water:

$$E_o = 20\ H_o^2\ T\ t \qquad (9)$$

where,

E_o is the annual wave energy transmitted forward from deep water toward the shore in foot-pounds per foot of wave crest.
H_o is the deepwater wave height in feet.
T is the wave period in seconds.
t is the time, in seconds, during one year that waves are acting upon the shore from given direction.

Wave height and period.

The height and period of waves are the basic elements used to compute the wave energy. Primarily, these elements depend on the speed of the wind over the water, the fetch over which it blows, and its duration The graphical relationships between winds and waves prepared by Bretschneid and published by the Beach Erosion Board, 1954, were used to obtain the wav heights and periods for significant waves. A significant wave is the avera of the higher one-third of all the waves. The use of significant waves

results in a wave energy greater than actual. However, the ratio of the actual energy contained in a given wave train to that computed from the significant waves has been found by various authorities to be nearly constant, and in the order of 0.58. Therefore, the use of significant waves will indicate correctly the variation of the actual wave energy.

Wind speed. Wind statistics for land stations in the vicinity of the sites studied are available for seven to ten year periods. The data listed on IBM cards produced a tabulation of the duration of all winds from 16 different directions for speeds 0-12 mph and 13-24 mph, and of the individual wind speeds of 25 mph and higher. Wind speeds over large water areas are known to be significantly higher than those indicated at adjacent land stations. On Lake Superior some wind records are available for the small rocky island, Stannard Rock, 30 miles from the nearest shore. These records may be considered as those of the actual winds over Lake Superior. These overwater winds were found to be about 80 per cent faster than those recorded at the nearest land station. More detailed investigations of the relationship of overwater to overland winds in Lake Erie have been made by Hunt, 1958, using wind observations on commercial vessels equipped with anemometers and at the nearest land stations. The Lake Erie investigations showed the relationship depends upon the stability of the air masses of the overwater area and upon the heights of the anemometers above the land and water surfaces. Based on these findings, the wind speeds from the land stations were adjusted to speeds over the water at an 8 meter level before they were used in wave height and period computations.

Storm duration. From the data available, it was not possible to compute the duration for individual storms with wind speeds less than 25 mph. Therefore, it was assumed that these lesser storms lasted long enough to produce waves of ultimate height. The duration of the winds of 25 mph and over was studied in detail and the average values were used to determine the energy.

Fetches were determined from Lake Survey navigation charts for the sites where transport was studied.

Ice effect.

This factor must be considered in estimating the total time the waves act upon the shore. The presence of ice along the shore protects the beach from attack by the waves. The fresh water of the Great Lakes tends to freeze quite early in the winter season, with ice appearing first in the calm inlets and bays and later extending out from the shore into the lake. The ice-free part of the lake varies in size depending upon the severity of the winter, however, none of the Great Lakes has been known to completely freeze over. According to Zumberge and Wilson, 1954, the freezing progresses out from the shore in two steps, first forming an ice foot and then an ice cover. Once established the active ice foot, that borders the open lake, protects the shore from the impact of the breaking waves. However, since the ice often contains some sand, some shore erosion is probably still going on, but on a much smaller scale. Navigation season statistics show that ice and cold weather stops navigation

for an average period of 4.5 months on Lake Superior, 3.5 months on Lake Huron, and 3 months at the westerly end of Lake Erie. The period during which the shore receives the most protection from the ice is shorter than the closed navigation season. For this study the time during each year when no wave action occurs on the shore was considered to be 3 months for Lake Superior, 2.5 months for Lake Huron, and 2 months for Lake Erie. More precise determinations of the time of inactivity would require long observations in the field.

EXPONENT FOR ENERGY.

As indicated in equation (7), the transport varies as the deepwate wave energy with exponent n. Based on actual observations and on model tests this exponent was selected as being unity. Evaluation of the expone is possible when all the factors affecting transport are constant except the wave energy. Actual observations for one direction of wave approach are difficult to obtain and adjustment of several directions to one introduces some degree of error. The value of the exponent based on actual observations are listed by Caldwell, Watts, and Lee as follows:

Anaheim Bay, California	1.0
South Lake Worth Inlet, Florida	0.9
Fort Sheridan, Lake Michigan, Illinois	0.97

The data for California and Florida shows considerable scatter, but the accuracy should be within ten per cent. Fort Sheridan data for Lake Michigan is based on the energy of individual waves uncorrected for wave period variations, and the 0.97 value may be on the low side.

The data obtained by Sauvage and Vincent in France from model tes using a sand with 2.6 specific gravity, indicate a value of 1.1 for the energy exponent. Other model tests, as shown by Savage, 1959, indicate a lower value for the exponent, but the data have much more scatter.

GREAT LAKES TRANSPORT EQUATION

The constants in the equation (7) were determined by substituting the data developed above and solving the simultaneous equations. The resulting transport equation for a straight shore line in the Great Lakes is:

$$Q = 19\, E_o \sin \alpha_o \left[1 - e^{-0.023\, D \cot \alpha_o}\right] \qquad (10)$$

where

- Q is the average annual rate of littoral transport in cubic yards at the downdrift end of a straight reach due to waves from one direction.
- E_o is the annual deepwater wave energy from one direction i millions of foot-pounds per foot of wave crest.
- α_o is the angle between the shore line and the wave crests which are considered perpendicular to the wind directi
- D is the length of the shore in miles between the point of transport and the updrift barrier.
- 19 and 0.023 are the constants determined from the data.

Use of equation.

Equation (10) is designed to compute the annual rate of transport over a long period from long-period average wind data of winds from 16 directions. At the sites investigated the littoral drift is fine sand, and the beach material is mainly sand in unlimited supply. The effects of varying lake levels on the transport have been counterbalanced because of the long periods used. Adjustment of the constants would have to be made before equation (10) could be used under conditions other than those discussed above.

Another point to be considered when using the transport equation is that the shore length is limited by the duration of storms and by the speed the drift moves along the shore. When a storm begins and waves start hitting the lake shore, the transport is at first of uniform rate throughout the total length of a straight shore. As the storm continues the drift moves forward and the transport grows in size. However, there is always a point on an infinitely long shore up to which the transport is growing and from which in the downdrift direction the transport is of uniform rate. This distance from the barrier to the point of constant transport is termed the effective shore length. The effective shore length for the prevailing direction of storms in the Great Lakes may be over 50 miles, however, no observations are available to substantiate this figure.

TESTING THE EQUATION

The transport equation for the Great Lakes was compared with the available observations in nature or in model to assure that results are in good agreement with the observations.

Comparison with Actual Transport.

The observed transport rates are compared with the rates as computed by equation (10) in the table below.

Lake	Location	Period in Years	Shore Length in Miles	Annual Transport in 1000 Cubic Yards		
				Type	Actual	Computed
Superior	Grand Marais	58	6	accretion	59	60
Huron	Au Sable Point	93	34	accretion	121	123
Huron	Tawas Point	93	42	accretion	64	63
Huron	Alabaster	93	1	erosion	4.2	3.7
Huron	Alabaster	93	5	erosion	25	19
Erie	Fairport	34	21	accretion	130	115

Observations on most effective angle.

The littoral transport rate varies with the angle between the approaching wave crests and the shore. Waves having the same energy produce the highest transport when approaching the shore at a certain angle. This, most effective angle is generally believed to be constant all along the shore. Model tests by Shay and Johnson indicated that wave crests approaching at an angle of 43° produce the maximum transport. A later study by Johnson, 1955,

indicated a most effective angle of 30°. A widely adopted method of adjusting the wave energy per foot of wave crest to per foot of shore is that developed by the Los Angeles District, Corps of Engineers, where the factor of sin $2\alpha_o$ is used. This factor indicates that an angle of 45° produces the highest transport. Professor Munch-Petersen from his 40-year experience in research of littoral transport along the ocean coasts concluded that the transport is close to its maximum when the original wave (the deepwater wave) moves parallel to the shore (Svendsen, 1950.)

The transport equation derived for the Great Lakes indicates that the most effective angle is not constant but varies with the length of unobstructed shore. For various lengths of shore, the most effective angle were determined from the equation as follows:

Shore length, in miles	0.01	0.1	1	10	14	53	10
Most effective angle	4°	6°	13°	27°	30°	45°	5

The above relationship shows that along the shore just downdrift of a barrier, the most effective waves are those hitting the shore with their crests almost parallel to the shore. It is believed that such nearly direct waves and not the rip currents are the cause of the erosion at the downdrift side of a barrier. Going downdrift along the shore, the most effective angle increases until at a distance of about 14 miles it reaches 30°. This angle was also obtained in the model tests by Johnson and might be of help in determining the scale for that model. The most effective angle of 45° corresponds to a shoreline length of 53 miles. However, this distance was derived from the transport equation for the Great Lakes and cannot be transferred directly to ocean conditions. For a very long straight reach, the angle should be close to 90°, the angle observed by Munch-Petersen. Also in shorter reaches the maximum transport can be produced by waves moving parallel to shore when the downdrift portion of a convex beach is parallel to the direction of the wind.

Shore length and transport.

The Beach Erosion Board, Corps of Engineers, as reported by Savage, 1959, made model tests where the transport rates were compared for two different shore lengths with all other factors remaining unchanged. In the first series of tests the beach length was about 97 feet, and in the second series the same beach was divided into two reaches by a long, high groin as shown in Figure 10. The effective length of the beach downdrift of the groin was 34 feet. The rate of transport was measured at the end of the original long and subsequent short beaches. The average transport rates during the 50 hours of testing were 374 pounds per hour for the 97-foot beach, and 154 pounds per hour for the 34-foot beach.

It is not possible to compare the model transport rates directly with those observed in the Great Lakes because of the uncertainty of the model scale. However, both the model tests and the actual transport data from the Great Lakes show that the unobstructed shore length is an important factor affecting the quantity of transport. The tests in the model were made with an angle of 30° between the wave crests and the shore If this angle was the most effective angle for that model then, as shown

above, the corresponding long and short shore lengths in the Great Lakes would be in the order of 14 and 4.9 miles, respectively. The ratio between the computed transports for these long and short shore lengths in the Great Lakes is 2.41, and the ratio of the corresponding transports observed in the model is 2.43.

Wave-crest angle and transport.

As previously shown, at any point along the shore there is one wave direction which produces the maximum transport, and lesser amounts of transport are produced with the same energy from different wave directions. The variation of transport with changing wave angles was investigated in model tests by Johnson. The relationship between the angle of wave crests and per cent of maximum transport determined in the model and as computed for comparable conditions in the Great Lakes are shown in Figure 11. A wave steepness of 0.04 from model tests was selected for computing the transport. This wave steepness occurs during the larger storms on the Great Lakes. The transports observed in the model and computed by equation are in good agreement for wave angles around 30°, but deviate as the angle increases and decreases. One reason for the deviations probably is that the effective shore length of the model is not constant, but changes with the angle of the wave machines.

ACCRETION IN FRONT OF A BARRIER

When a barrier which would stop the littoral transport is planned, it is necessary to estimate the effects of the structure. Normally, an accretion of the drift will take place on the updrift side of the barrier, and an erosion of a larger or lesser extent will occur on the downdrift side. The accretion over a number of years is the sum of the annual transports less the erosion from the face of the deposits by waves from the downdrift direction. The erosion from the deposits is equal to the transport originating along the face of the deposits.

The accretion will occur within the triangle formed by the natural shore, the barrier, and the new shore as shown in Figure 12. Two sides of the triangle are known, but the new shoreline must be estimated. The concave shape of the new shoreline is more or less defined by two tangents. The angle between the new and natural shorelines, α_1, may be estimated by assuming that the transport would move along the tangent at this angle without depositing or picking up new material. Under these conditions, the transport would be equal to $19\ E_o \sin(\alpha_o - \alpha_1)$. Equating this transport to the actual transport at the point of intersection of the new and natural shorelines gives a relationship between α_1 and the updrift shore length as follows:

$$\sin(\alpha_o - \alpha_1) = (1 - e^{-0.023\ D \cot\alpha_o}) \sin\alpha_o \qquad (11)$$

Equation (11) shows that the angle between the new and natural shorelines will be small for long updrift shore length, and approaches the angle of the wave crests as the updrift shore length becomes very short.

The angle of the tangent at the barrier end of the new shore-line, α_2, is always less than the angle of the wave crests α_o. It would be equal to α_o if there were no energy losses in the movement of the drift.

The values of the angles of the new shore tangents discussed above were based on a consideration of some of the theoretical factors involved in the problem of accretion. These limits are considerably modified by other factors such as the increasing storage capacity due to the progressively deeper water out from the natural shore, and that some displacement of the material deposited with one wave direction takes place when the direction changes and also by wave reflections from the barrier. Therefore the angles of the new shore tangents derived above must be modified by observed data.

In most cases the angle between the mean new shore-line and the natural shore-line, angle β in Figure 12, can be estimated with sufficient accuracy by applying an experience factor to the mean of the wave-crest angles weighted to their transport. The equation to estimate the angle β is

$$\beta = k \frac{\alpha_{o1} Q_1 + \alpha_{o2} Q_2 + \alpha_{o3} Q_3 + \dots}{Q_1 + Q_2 + Q_3 + \dots} \qquad (12)$$

where

β is the mean angle the new shore makes with the natural shore.
k is the experience factor.
α_{oi} is the angle of wave crest for direction shown by second subscript.
Q_i is the transport corresponding to angle of wave crests for subscript direction.

The value of k obtained from observed data from Grand Marais and Fairport was found to be 0.33. The value of k determined from the Beach Erosion Board model tests illustrated in Figure 10 is 0.5 for waves approaching from a single direction at an angle of 30°.

PROBLEM OF EROSION

Although the problem of erosion is not the subject of this paper, some observations are being added for future studies. Because a barrier stops the littoral transport, the waves have a larger energy to pick up new material from the shore on the downdrift side of the barrier, and erosion of the shore takes place. Observations show that the volume eroded from the shore is usually much greater than the transport requiremer A portion of this eroded material is transported along the shore but a larger portion is used to change the profile of the beach. Observations a Grand Marais and Fairport indicate that a flattening of the profile occurs. The eroded material is transported some distance downdrift and deposited i the deeper places. Sooner or later the beach is changed so much that a ne equilibrium is established, and subsequent erosion is just enough to satis the needs of transport.

The profiles on the east side of Grand Marais Harbor (Fig. 4) show a large erosion between 1867 and 1902, but much smaller erosion during the 1902-1941 period. In the Alabaster reach in Lake Huron, where the erosion is not man-induced and the process has been going on for centuries, the profiles shown in Figure 7 indicate that the slope of the beach is already stable, and the amount of erosion is nearly equal to that needed for the littoral transport.

One must also consider the amount of drift from opposite directions being stopped on the downdrift side of a barrier. If the amount of that drift is significant, the expected erosion may not even take place, and deposition of drift material may occur on both sides of the barrier.

ACKNOWLEDGMENTS

Many of the data used in this paper were taken from a littoral transport study made by the United States Lake Survey, Corps of Engineers, United States Army. The author is greatly indebted to I. A. Hunt, Jr., Major, Corps of Engineers, at that time the District Engineer, who initiated and directed that study. His work on the relationship of overwater winds with overland winds and on wave energy created a firm basis for the present paper. The author gratefully acknowledges the help of two other Lake Survey engineers, Mr. J. A. Derecki who carried out the necessary calculations, and Mr. L. T. Schutze who edited the paper.

REFERENCES

Beach Erosion Board (1954). Shore protection, planning, and design: Technical Report No. 4.

Caldwell, J. M. (1956). Wave action and sand movement near Anaheim Bay, California: Beach Erosion Board, Technical Memorandum No. 68.

Hunt, I. A., Jr. (1958). Relationships between overwater wind and overland wind: Lake Erie: U. S. Lake Survey, Corps of Engineers, Detroit.

Johnson, J. W. (1953). Sand transport by littoral currents: Proceedings of the Fifth Hydraulics Conference.

Lee, C. E. (1954). Filling pattern of the Fort Sheridan Groin System: Proceedings of Fourth Conference on Coastal Engineering.

Savage, R. P. (1959). Laboratory study of the effect of groins on the rate of littoral transport: equipment development and initial tests: Beach Erosion Board, Technical Memorandum No. 114.

Svendsen, S. (1950). Munch-Petersen's littoral drift formula: Bulletin of the Beach Erosion Board, Vol. 4, No. 4.

Zumberge, J. H. and Wilson, J. T. (1954). Effect of ice on shore development: Proceedings of Fourth Conference on Coastal Engineering.

CHAPTER 21

SEDIMENT MOVEMENT AT INDIAN PORTS

Madhav Manohar
Professor & Head of Civil Engineering Department
Birla Institute of Technology
Ranchi - India

INTRODUCTION

India has a large coastline being bounded on three sides by water. On the west side, the coastline faces the Arabian Sea. Similarly the coastline on the east side is bounded by the Bay of Bengal. The Indian ocean separates the Arabian Sea and the Bay of Bengal at the southern-most end of the coastline (Fig. 1) Since the last 15 years, there have been proposals from time to time to establish new harbours or improve existing harbours or save vast lengths of coastal strips from erosion by wave action. In evaluating the merits and de-merits of the sites, a study of the coastal sediment movement is important since what may be beneficial to a harbour may be harmful for preservation of a coastal strip. Defective planning may cause the loss of the entire shoreline and or the complete blocking of the harbour areas. Improper use of protective structures such as seawalls, breakwaters, groins, jetties etc. will not only be unscientific and uneconomical but accelerate the changes along the shoreline rather than stop them.

The frequent or long-term changes in shoreline, beach, offshore zone, inshore zone, under ground bars, spits, lagoons, tombolas and similar characteristics of the coastline have significant meanings regarding the sediment motion at the coastline. With respect to sediment available for motion, the shore may be a source, a drain, overnourished, undernourished, sufficiently nourished (Per Bruun, 1955), or a physiographic unit (Mason, 1950). With each type, coastal works will be different for shoreline improvement and for harbour maintenance. Erosion and accretion by natural processes extend upto offshore zones while with man-made structures, erosion will always start in the inshore and foreshore zones of the shallow water area. This distinguishing feature in the changes of a shoreline will be a good and reliable preliminary check to determine the type of erosion. Having classified a shoreline according to its sediment nourishment and as a source or a drain, the type of coastal

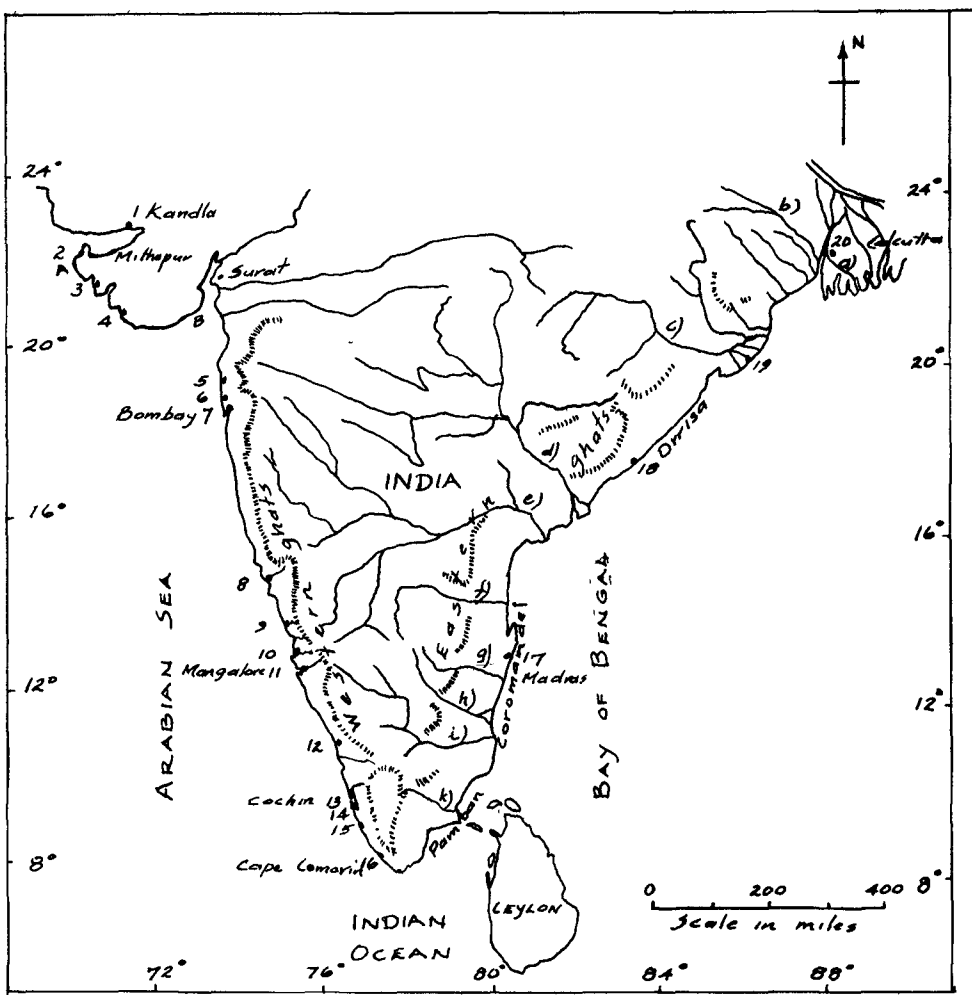

A) Coastal areas & ports:

1 Kandla
2 Mithapur
3. Porbundar
4 Veraval
5. Kelva
6 Versova
7 Bombay
8 Karwar
9 Bhaktal
10 Malpe
11 Mangalore
12. Calicut
13. Cochin
14. Chellanam
15. Alleppey
16 Ashtamudi
17. Madras
18. Vizagpatam
19 Paradip
20. Calcutta

B) Rivers:

a) Hoogly
b) Damoder
c) Mahanadi
d) Godavari
e) Kistna
f) Pennar
g) Palar
h) Ponniar
i) Cauvery
k) Vaigai

Fig. 1. Map of India with coastal areas considered.

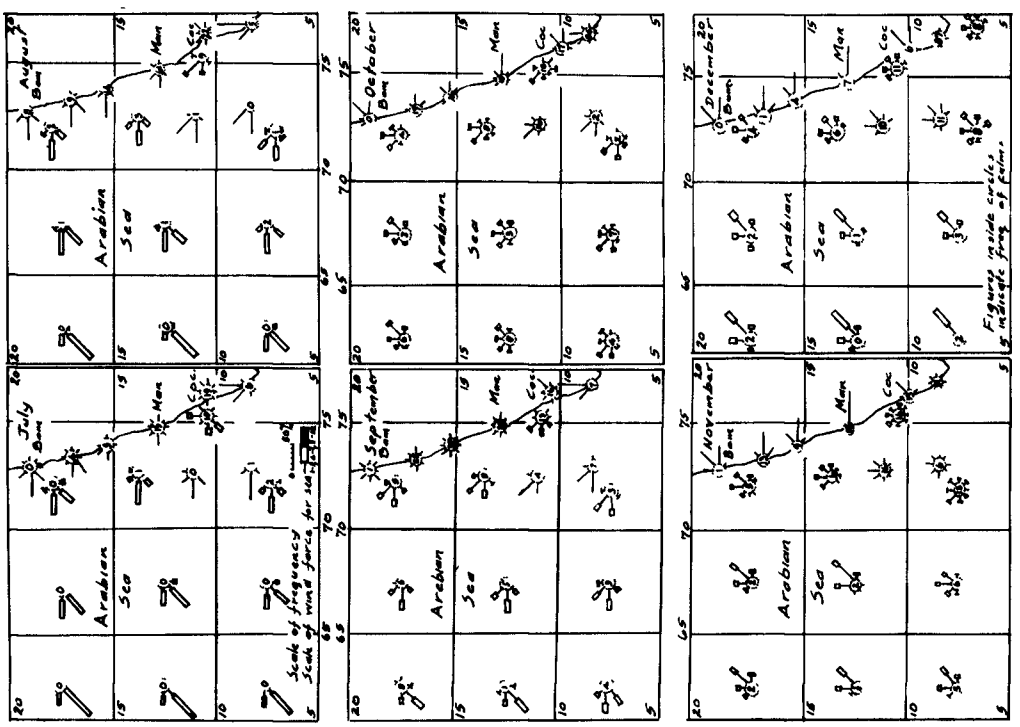

Fig. 2a. Wind roses for Arabian Sea - January to June

Fig. 2b. Wind roses for Arabian Sea - July to December

protection may be selected tentatively. The selected works may then be studied by model techniques. If the premilinary analysis was complete and accurate, the tentatively selected type of coastal work will be found to be most satisfactory thereby saving unnecessary waste of time and money from testing various types of works by model analysis. This method of analysis will be found to be extremely useful in many countries where investigations of the coastlines are far from adequate. Analysis of the changes at existing coastal structures along the coastline and the interpretations of the results as outlined above will be the most satisfactory method. The coastline of India may also be interpreted similarly in relation to erosion, accretion, and transportation of sediment from the data available from existing structures, harbours and coastal strips, and divided into arbitrary overnourished, sufficiently nourished and undernourished strips and classified as sources or drains as far as possible so that various suitable types of coastal protective structures may be suggested.

Indian coastline as a preliminary step may be divided into the West coast facing the Arabian Sea and the East coast facing the Bay of Bengal since the characteristic features of both the coastlines are entirely of different nature with respect to the wind forces, erosion, accretion, and littoral drift along them.

WIND SYSTEM

As described in an earlier article (Manohar, 1958), the whole year may, in general, divided into 4 seasons with respect to the wind system. They are:

1. N.E. monsoon season from December to March when the winds blow in a north-easterly direction.

2. S.W. monsoon season from June to September when the winds blow in a south-westerly direction.

3. Hot weather period in April and May just before the S.W. monsoons when N.E. winds are replaced by southerly winds.

4. Transition monsoon period in October and November when S.W. winds are replaced by northerly winds.

WIND SYSTEM ALONG WEST COAST

1. N.E. monsoon season - Figs 2a and 2b show the wind roses for the wind system on the west side. Though in the Arabian

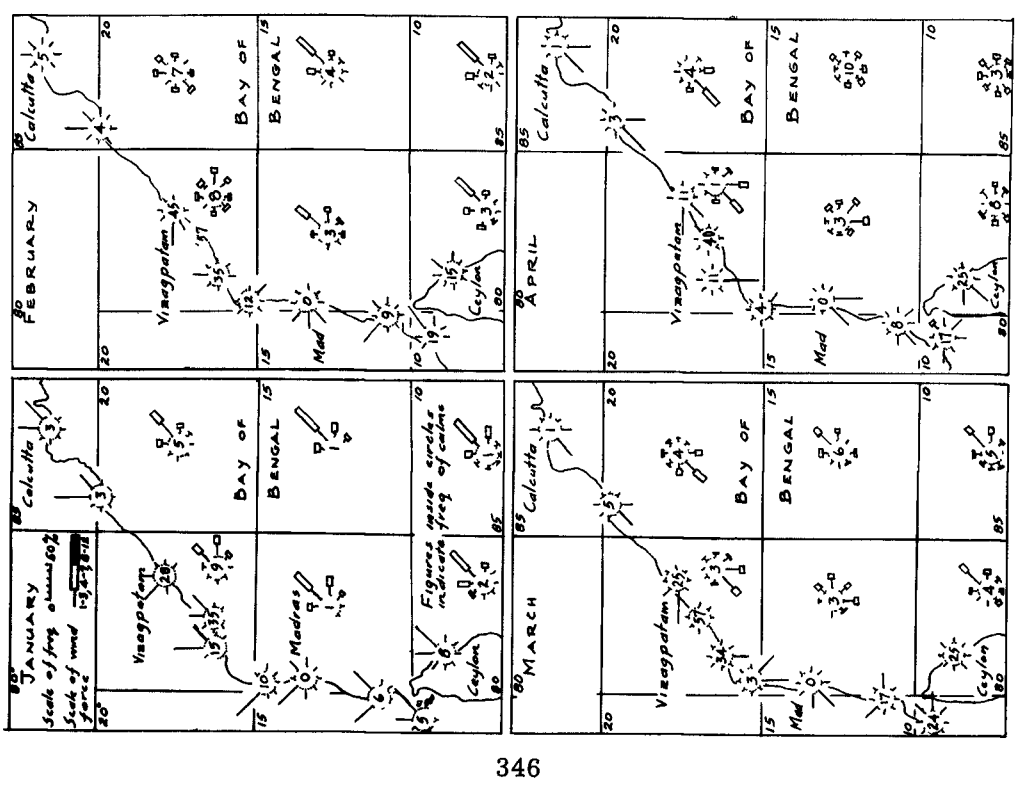

Fig. 3a. Wind roses for Bay of Bengal - Jan to Apr

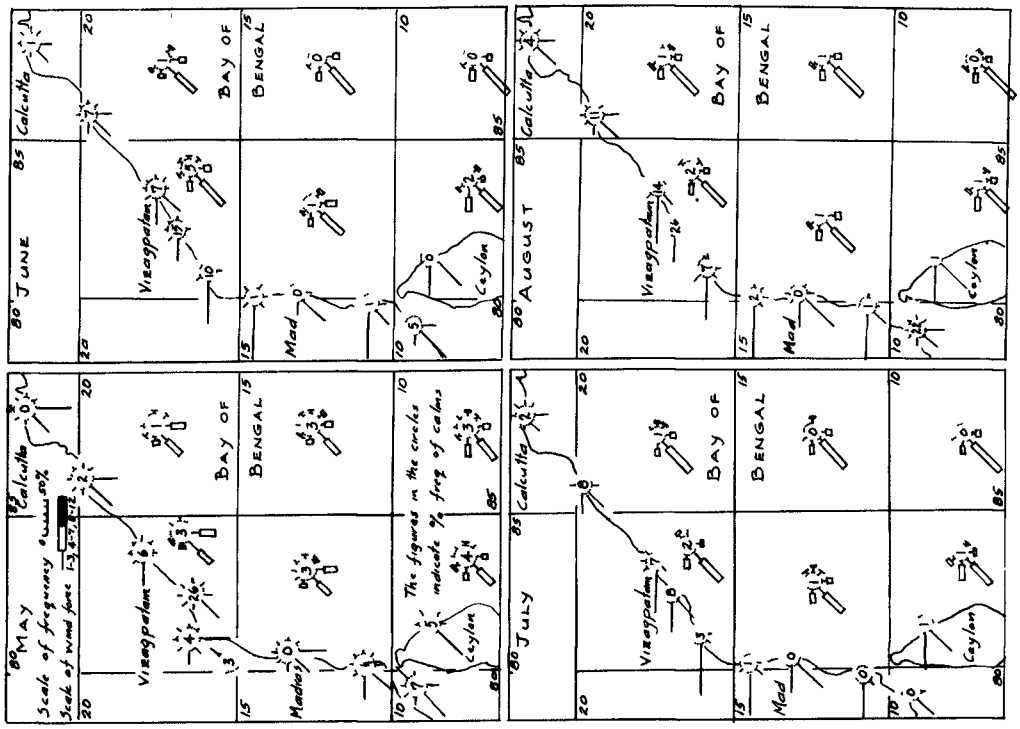

Fig. 3b. Wind roses for Bay of Bengal - May to

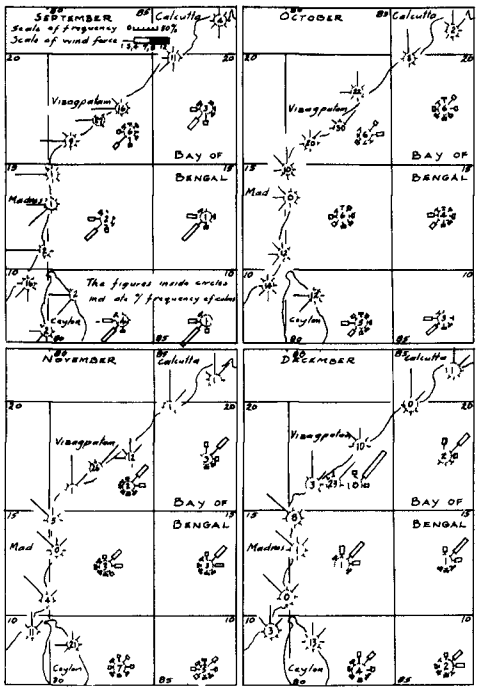

Fig. 3c. Wind roses for Bay of Bengal - September to December.

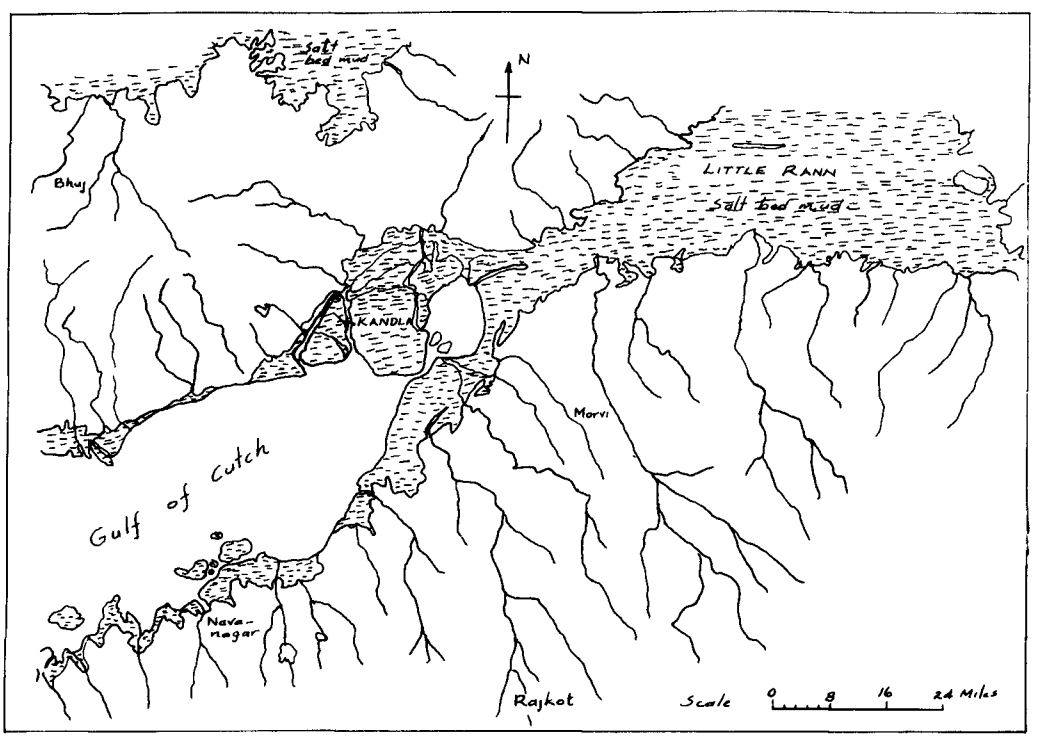

Fig. 4. Gulf of Cutch - Kandla port.

Sea, the wind direction is between N.N.E. and N.E. with force of 2 to 4 on the Beaufort scale, winds are lighter near the coast with N.E. or E. direction. The wind force gradually rises from north to south and is a maximum in January with an average force of 2 to 4 rising to 7 on frequent occasions. They progressively decrease in February and March and become northerly and north westerly along the coast.

During the hot weather period, the wind blows in the same direction as in March with force of 2 to 3.

2. S.W. monsoon season - The S.W. monsoon which is stronger in force and longer in duration starts in the third week of May in the lower part of the coast and over the whole area by the second week of June. Generally the direction of the wind is between south west and west with a wind force of 5 to 8 in the sea and west or north west along the coast with a force of 3 to 5. Winds are fairly constant in June, July and August. Gales of force 8 to 10 are encountered in the centre of the Arabian Sea with similar gales of slightly lesser intensity along the coast. In September, the wind force decreases to between 3 to 4 rising upto 7 occasionally but the winds are of the same general character as in previous months.

During the transition monsoon period, winds are of land origin blowing with a force of 2 to 4 in N. and N.E. direction

WIND SYSTEM ON THE EAST COAST

Wind roses (fig. 3a to 3c) show the direction and intensity of wind both in the sea and at the coastline. N.E. and S.W. monsoon winds over the Bay of Bengal and east coast of India vary in strength and direction at different parts of the coast. In the northern regions, the north-easterly and easterly winds of N.E. monsoons are fully established in the first week of December while they are in full swing in the southern part only in the third week of December. Similarly S.W. monsoons become regular in the southern part only at the end of April or beginning of May while in the north, they set in only in the middle of June.

1. N.E. monsoon season - In December and January, the average force of the wind is 4 while in the central region, a force of 6 is reached at times. On the Pamban coast (fig. 1) which is shielded by the island of Ceylon, the force is less and of the order of 2 to 3. On the Orissa coast, they are strongest in January while on the Coromandel coast, they are strongest in February, the direction being northerly to easterly. From th

beginning to the end of March, the winds gradually change beginning from the northern end to the southern end to a southerly to southerly-westerly direction.

In hot weather period, wind direction is variable with frequent occurrances of storms called "Nor'westers".

2. S.W. monsoon season - These continue consistantly from June to September with an average force of 5 though gale forces between 6 and 7 and storm forces between 8 and 9 are also experienced during this period. They are predominent over the central and western areas of the Bay of Bengal and their direction is south westerly.

In the post S.W. monsoon period in October, the direction of the wind is still south-westerly with an average force of 3 to 4 but there are many periods of calm weather, light winds and fair weather. In November, the N.E. winds start blowing with an average force of 2 to 4.

Therefore, on both coasts, the south and south-westerly winds are stronger and more durable and exist for almost 8 months a year generating an alongshore component from south to north. Similarly for the remaining 4 months the alongshore component travels from north to south because of north-easterly winds. Frequent storms of great intensity occur along both coastlines affecting the stability of the coastlines to a great extent.

WEST COAST

General topography - The west coast of India from latitude 23°N to the southern-most tip, namely, Cape Comorin has a coastline of about 2,000 miles. Along the coast upto latitude 21° N, and at 20 to 100 miles inland, a continuous chain of mountains rises upto an elevation of 8,000 feet. These mountains are known as the Western Ghats. The coastline is mostly sandy with the exception of a few rocky outcrops, a few marshy areas in the north and a few lagoons and a backwater in the south. Very few rivers discharge into the Arabian Sea. Even those which do so are small and since they start from the Western Ghats which is so near the coast, the sediment carried by them from land areas is comparatively little. Historical records show that the work of nature of millions of years had somewhat carved an equilibrium along this coast with only localised erosion and accretion at isolated coastal strips. As usual, because of the alongshore component, there was littoral drift getting its nourishment from rivers, lagoons and eroded areas. But unfortu-

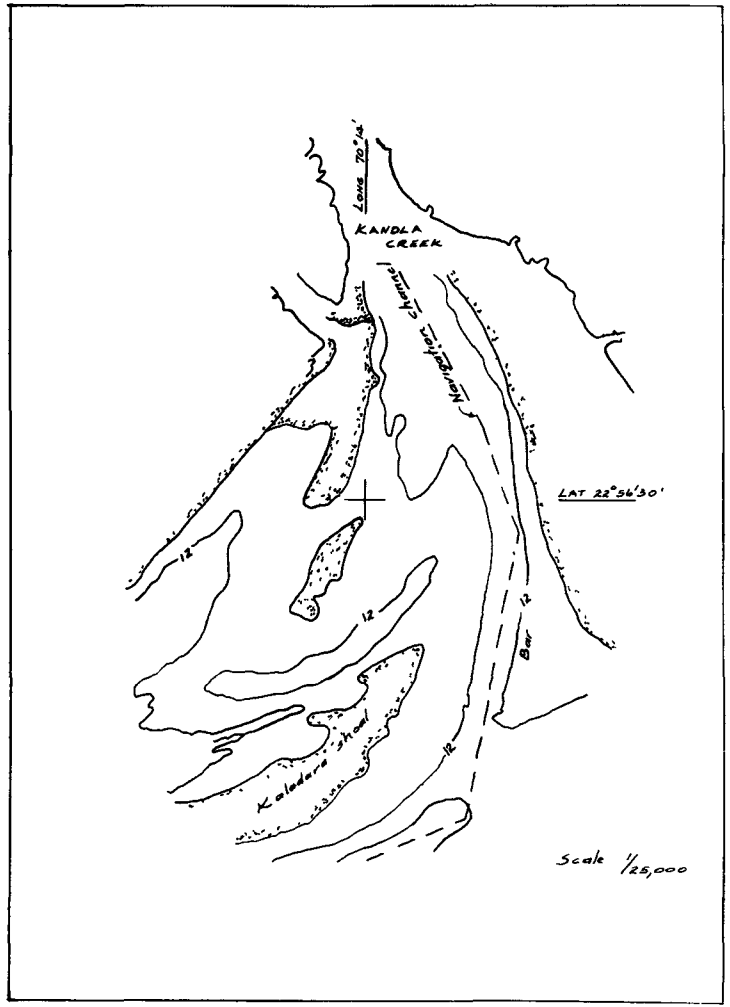

Fig. 5. Kandla port.

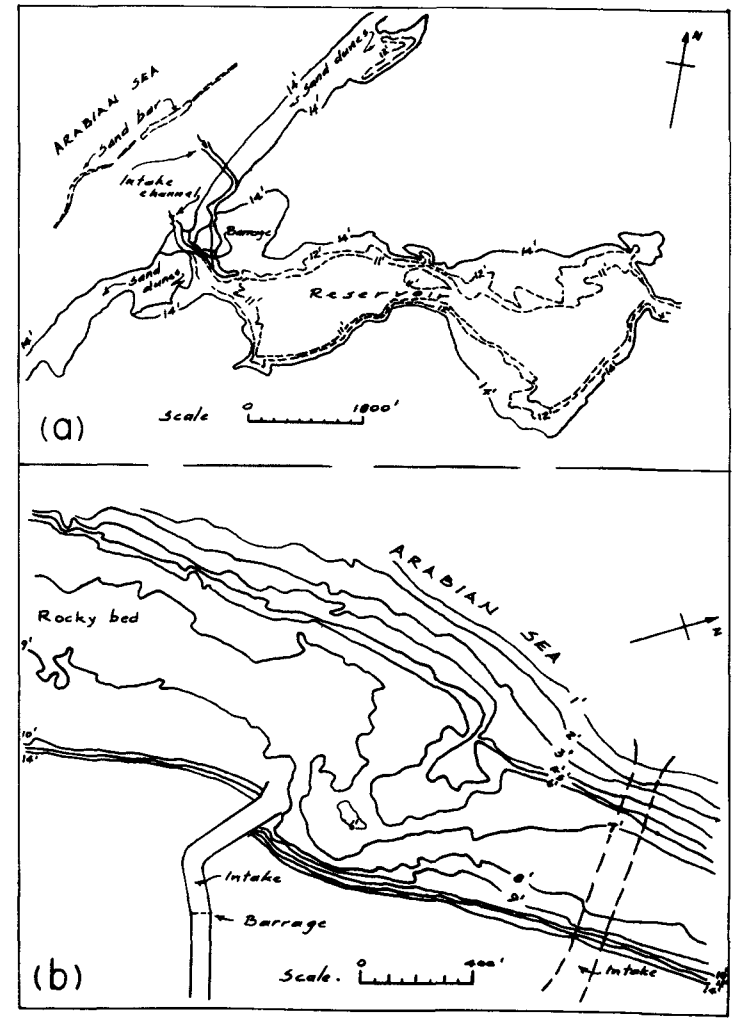

Fig. 6. (a) Mithapur intake channel (b) Foreshore

nately man-made installations such as construction of harbours, blocking of rivers discharging into the sea and natural disturbances such as silting of inlets, river mouths etc., have upset the material-energy balance resulting in large scale localised erosion along the entire west coast. Though natural disturbances are rather very slow in their occurrances, the one along the Kerala coast, namely, the blocking of the passage of the backwaters to the sea near Alleppey long ago seems to have upset the sediment supply along this coast with consequent disastrous erosion to which reference will be made later. To evaluate the methods necessary for the preservation or restoration of a shoreline or the maintenance of a harbour along this coastline, the coastline has to be interpreted on the basis of the behaviour of the existing coastal works and coastal strips which are in order from north to south as follows: (1) Kandla port, (2) Mithapur intake channel, (3) Porbunder port, (4) Veraval port, (5) Kelva, (6) Versova, (7) Bombay harbour, (8) Karwar, (9) Bhaktal port, (10) Malpe port, (11) Mangalore port, (12) Cochin harbour, (13) Chellanam coastal strip, and (14) Asthamudi port.

GULF OF KUTCH COASTLINE

Kandla port and vicinity - Kandla port is the northern-most port along the west coast and lies in the Gulf of Kutch at latitude 23° N and longitude 70° E. The shoreline along the Gulf of Kutch is low and marshy (fig. 4) and is inundated with salt bed mud in many places, the biggest marshy area being the Little Rann into which many streams and creeks discharge as much as 1,800,000 cfs during S.W. monsoon season. The tidal range in this area being high and as much as 23', the coastline along the Gulf of Kutch should be viewed as a tidal one. The tides as usual bring a large amount of sediment from the sea bottom and coupled with this, the sediment brought by rivers and streams are left along the coast resulting in marshy areas. With waves reaching the shore being comparatively small, sedimentation by tidal action causes large scale silting of the Gulf except where ebb tide follows certain channels of flow. Thus because of large ebb flow, there exists along the northern shore, a deep and wide creek called the Kandla creek at its eastern end (fig. 5). A depth of over 30' without dredging exists in this channel for about 6 miles in length ideally suited for anchorage and turning space for ships (C.W.P.R.S., 1952). This site is at present being developed into a port called the Kandla port. There are also many interconnected creeks which subsequently join the Kandla creek and the Little Gulf. The problem encountered in this region is the shifting of channels due to natural causes such

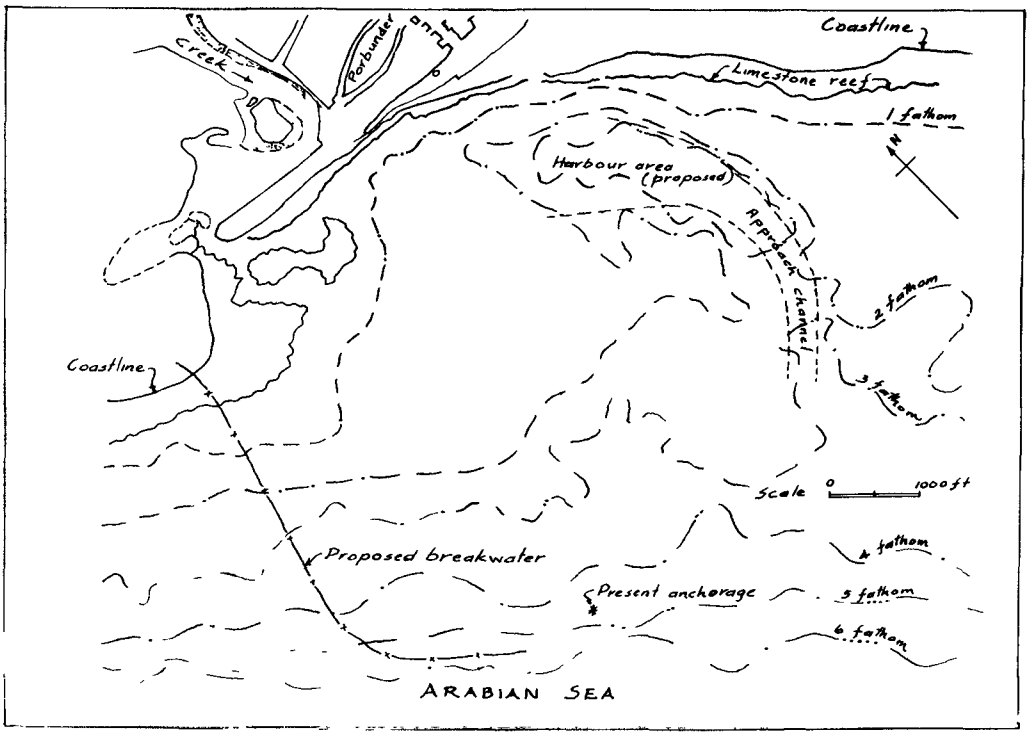

Fig. 7. Porbundar port.

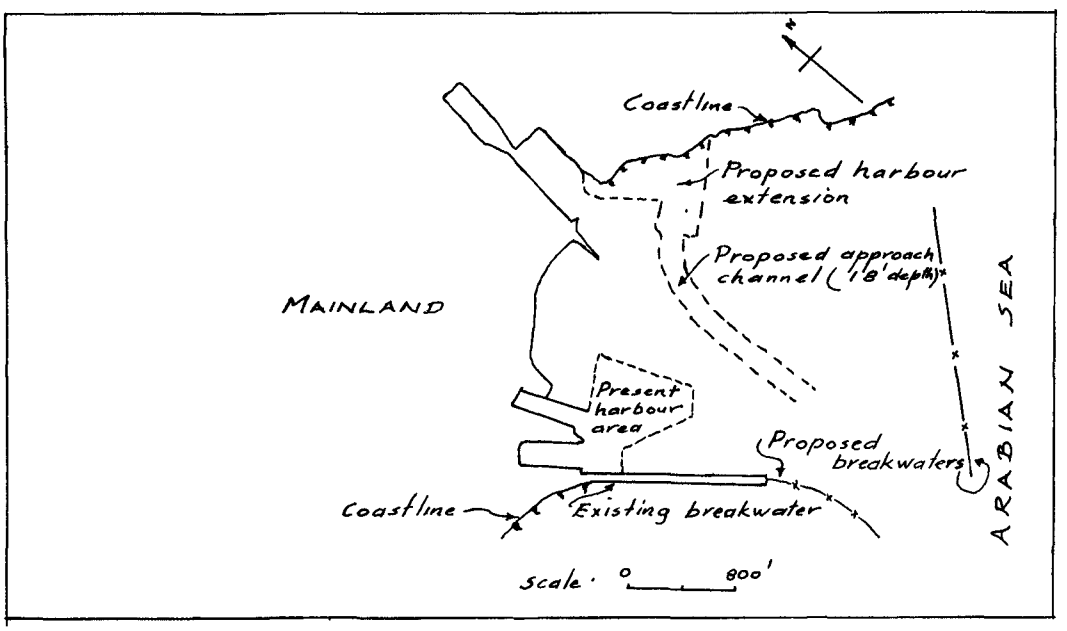

Fig. 8. Veraval port.

as deficiency of outflow and therefore the flushing velocity due to a weak monsoon season or the deficiency of ebb over tide or tide over ebb. The shifting of tidal channels may be rather a slow process or a sudden process but it has to be checked if the harbour is to be kept effective. If these changes are hastened due to human interference such as reducing the ebb flow by structures upstream, then the remedy will, obviously, be to restore the original conditions so that the scouring velocities of the ebb and tide are the same as they used to be. Dredging the silted portion will be the other remedy.

SAURASHTRA - KUTCH COASTLINE

1. Mithapur intake channel - Beyond the Gulf of Kutch and moving towards the south in the Saurashtra-Kutch region, an intake channel had been in existence since 1933 at Mithapur, 7 miles from Okha port (fig. 6a) (C.W.P.R.S., 1948). This intake channel was constructed to divert the sea water into two shallow water lakes existing inland from the shore. As soon as the intake channel was constructed, silting was noticed on both sides, the southern side accretion being far in excess of that on the northern side. The shoreline at the intake channel thus advanced every year and in order to prevent silting of the intake channel, it was extended towards the sea every year and walls were built on both sides normal to the shoreline. There was also considerable decrease of depth in the foreshore zones on both sides (fig. 6b).

2. Porbundar port - At Porbundar (fig. 7) which is situated a few miles south of Mithapur, at present an open roadstead exists and ships anchor about 1½ miles away from the shore (C.W.P.R.S., 1956). The present plans are to develop it into an all-weather port by providing an approach channel 26' deep and by providing a sufficiently long breakwater enclosing a basin for safe anchorage. Currents and tides are small and have no effect on coastal changes. Along this coast, the S.W. monsoon from April to October with waves reaching the coast from westerly direction is the strongest. Wave heights usually range from 6' to 15' with periods of 5 to 10 seconds. In June, frequent storms with waves as high as 20' are not uncommon. During the months from November to March, waves are relatively low in height varying from 3' to 6' with periods from 3 to 5 seconds. Thus littoral drift during the S.W. monsoon season is far greater than during the N.E. monsoon season. The rate of accretion measured at nearby existing structures as at Mithapur indicates the yearly littoral drift to be of the order of 7,000 tons from south to north, and 3,100 tons from north to south. This quantity is rather

very little to cause any difficulty in the maintenance of a harbour located in this area. The bed under the sea is exte sively rocky at comparatively shallow depths.

3. Veraval port - Veraval port (fig. 8) which is situated at about 70 miles south of Porbunder is at present a small fishing port having no protection from waves (C.W.P.R.S., 195 Though a small breakwater was built in 1931 to prevent waves of the S.W. monsoon entering the harbour from the south-west direction, it had been far too short to meet the requirements of an all-weather fishing port. In order to develop this port, an approach channel 150' wide and 18' deep has to be dredged and maintained and the existing breakwater extended further into the sea to give enough protection to the basin.

WEST COAST FROM SURAT TO MANGALORE

This coastline of about 670 miles has practically no river discharging into the sea except at the northern end and at Mangalore. Hence the littoral drift is very small except in the foreshore zones due to local erosion. Starting from the northern end, some information about the behaviour of the coastline and harbour works is available at (i) Kelva, 55 miles north of Bombay, (ii) Versova beach, a suburb north of Bombay, (iii) Bombay, (iv) Karwar, 350 miles south of Bomba; (v) Bhaktal, 415 miles south of Bombay, (vi) Malpe, 465 mile: south of Bombay, and (vii) Mangalore 500 miles south of Bomba; This coastline is exposed to a severe swell of S.W. monsoon and to a lesser extent to the waves induced by the north-westerly winds. Thus the littoral drift occurs from both directions, namely, from south to north and north to south, the former being greater in magnitude than the latter. Because of the absence of lagoons, tidal inlets, or big sediment carrying rivers and since the deep water areas are very near the coast, natural disturbances are few so that the coastline had been fairly stable except for localised changes. The localised changes have been mainly around river mouths due, chiefly, to the sediment load discharged into the sea travelling as littoral drift along the coast. Man-made structures, however, have disturbed the local equilibrium causing erosion and accretion.

1. Kelva - This is a fishing port (Joglekar, 1958) at the mouth of a creek 55 miles north of Bombay (fig. 1). The small amount of sediment brought by the creek resulted in the formation of low lying areas at its mouth. In the process of reclaiming the low lying marshy land, a salt water barrier and a bridge which constricted the waterway considerably were

constructed across the creek about 35 years ago resulting in the reduction of flushing velocities, tidal influx and sediment discharge into the sea. This, in turn, caused silting of the mouth of the creek, erosion of the downdrift side and the consequent change in the course of the creek to the sea (fig. 9). It may be noted that waves as high as 10' and tidal range as much as 14' occur in this area.

2. Versova - This is a suburban beach of Bombay situated north of the city (fig. 10). As at Kelva, waves as high as 10' with periods of 7 to 9 seconds reach the shore from S.S.W to W. direction during the S.W. monsoon period (Joglekar, 1958). With deep water zone very near the coast and the underwater slope as much as 1 in 40, high waves strike the coast eroding the coastline. Since 50 years, with Bombay city expanding to suburban areas, marshy areas at the Versova beach were being reclaimed by shutting off the creeks flowing into the sea and by filling those areas with sand removed from the beach. Though littoral drift by itself is very small along this coast, these reclamation processes caused depletion of the available littoral drift, and resulted in higher waves reaching the shore and eroding the coastline further. With tides as high as 14', there has been large scale erosion in this area.

3. Bombay - Bombay harbour (fig. 11) is one of best natural harbours in the world. Though waves as high as 10' with periods from 7 to 9 seconds reach the coast, the littoral drift as at Kelva and Versova is small. Coupled with this the tide is high at 20' so that the main entrance channel which is at present sufficiently deep to admit ships of drafts upto 30' has never been dredged upto the present time. However previous soundings indicate that silting occurs beyond that depth and that dredging will be necessary for maintaining any depth beyond.

4. Karwar - About 340 miles south of Bombay, there exists a bay called Karwar Bay with varying depths upto 25'. At the southern end of the bay, a rock outcrop named Karwar head extends into the sea giving protection to the bay from the S. W. monsoons. Protection from N.W. winds is partly afforded by a number of islands on the northern side. Rock is usually found at 32' to 58' below ground level. Clay and silt brought into the bay by river Kalinadi from the Western Ghats and by the tides from the sea are found above the rocky bottom. Littoral drift being very small and shoreline being very rocky, erosion and accretion of the shoreline area are negligible.

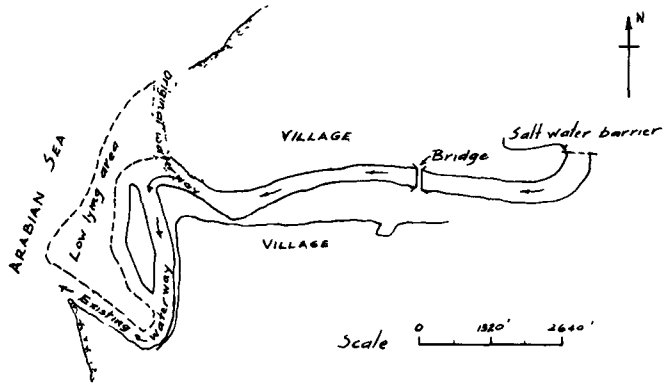

Fig. 9. Kelva and vicinity.

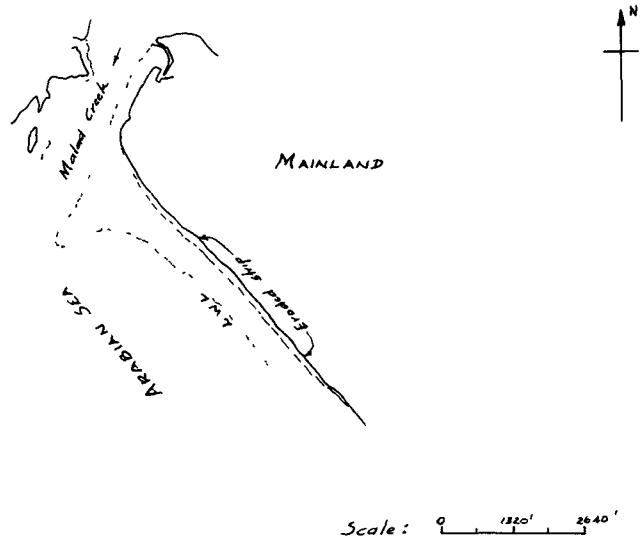

Fig. 10. Versova.

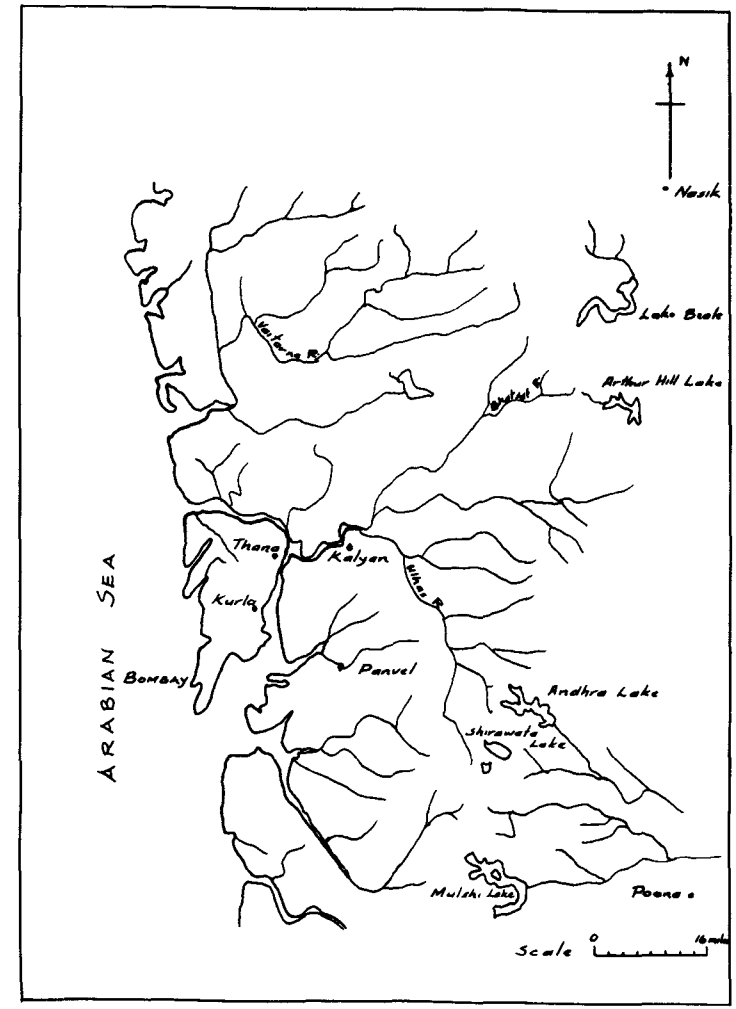

Fig. 11. Bombay harbour.

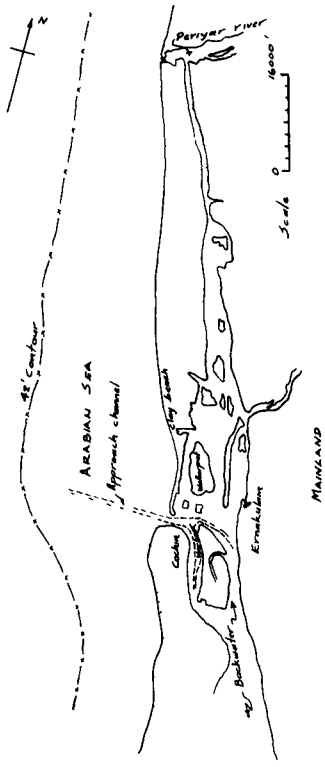

Fig. 13. Cochin and harbour vicinity.

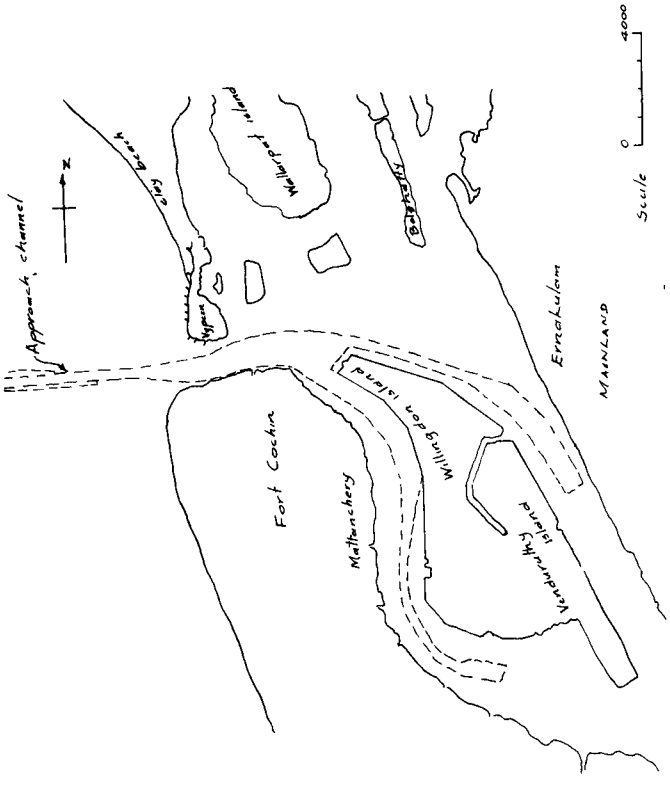

Fig. 14. Cochin harbour area.

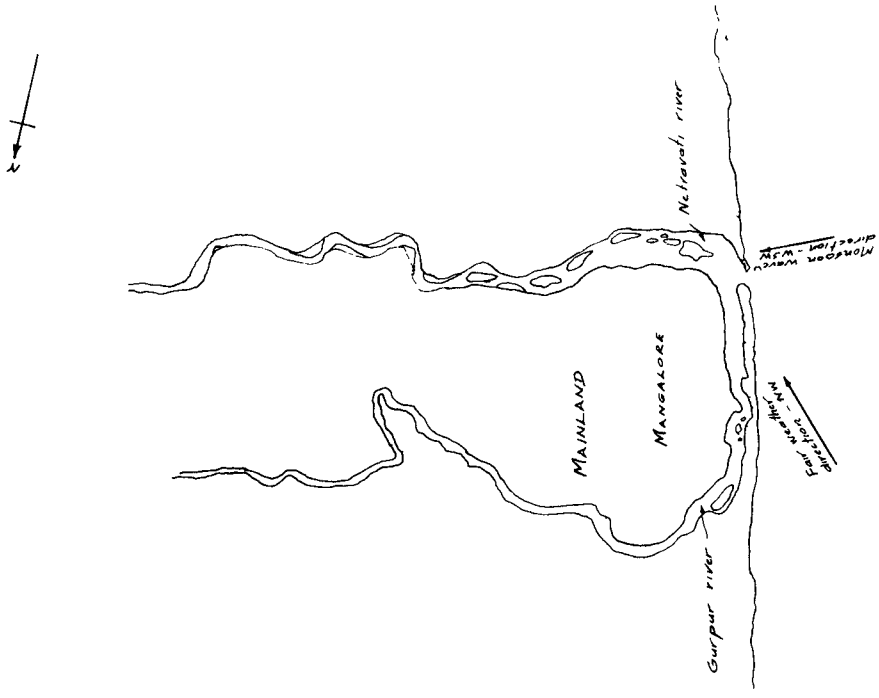

Fig. 12. Mangalore port.

5. Bhaktal - About 70 miles south of Karwar, there exists a small port where a river discharges into the sea. The river in question is Bhaktal river and it carries a large amount of sediment causing the formation of a large sand bar at its mouth. This area is subjected to a direct attack from the S.W. and N.E. monsoons with no natural protection of any kind existing in that area. The bottom is rocky and the 5 fathom line lies 3,000' from the shore. As in other cases, littoral drift is very small being fed mostly by the river sediment. The difficulty in providing an all-weather port at this place will be the construction of the breakwaters upto deep water areas on both north and south sides and to dig an approach channel through the rocky bottom.

6. Malpe - 50 miles further south from Bhaktal, a small river discharges into the sea in a northerly direction. About a mile from the shore, there exists a row of rock outcrops running parallel to the coast and offering protection to it from the monsoon waves. Rocky bottom exists 33' below sea level. Littoral drift is very small and erosion and accretion around the area are also very small. Since sediment carried by the river is not considerable, river mouth silting is also not considerable.

7. Mangalore - This is, at present, an open roadstead with vessels unloading about 2 miles away from the port (Manohar, 1958). Conditions are similar to those sites mentioned already except that they are of far greater magnitude. Two fairly large rivers, (fig. 12) Gurpur and Netravati having a maximum discharge of 60,000 cfs and 120,000 cfs respectively during the S.W. monsoon season and carrying a large quantity of coarse sediment flow into the sea through a tidal estuary at Mangalore. Part of the sediment settles in the estuary, another part forms a large sand bar at their common mouth in the sea and another part supplies material for the littoral drift. Two large sand spits separate the rivers from the sea so that the tidal estuary is protected from the waves. The depth over the sand usually varies from 7' to 9'. The sand bars and sand spits grow in size after the S.W. monsoons because of large river deposits and shrink during fair weather season apparently due to littoral drift and loss in deep sea areas. The net littoral drift is about 200,000 tons per year from south to north as estimated from erosion and accretion at a natural rock outcrop 3 miles south of the gut. However there is also considerable littoral drift from north to south during the N.E. monsoons. With a large sediment load from the Netravati river, the Netravati portion of the estuary is usually shallower than the Gurpur portion. A tide of 5' coupled with maxi-

mum wave conditions during the monsoons results in large sediment deposits in the estuary. During the ebb period, this sediment partly finds its way into the approach channel, and the sea providing littoral drift for localised accretion and erosion. Experiments indicate that the tidal influx is strong enough only to maintain a depth of 20' in the approach channel with some dredging and with the provision of a 1,000' long breakwater on either side of the channel. Since there is littoral drift from both sides along the coastline, coastline changes are few and to a small extent.

COASTLINE FROM MANGALORE TO CAPE COMORIN

Coastline from Mangalore to Cape Comorin is in many ways different from the coastline discussed above. The foreshore zone is covered with mud and silt. Several mud banks with their characteristic behaviour of sudden appearance and sudden disappearance exist at several places. The continental shelf has a gradual slope upto 100 fathoms and then there is a steep fall. Between Cochin and Cape Comorin, there exist several lagoons and a large sheltered area of backwater of 125 square miles extending as far as 40 miles south of Cochin with only one small outlet, 1,500' in width, open to the sea at Cochin. Mud banks have considerable calming effect on waves so that even the roughest waves are damped as they travel over them resulting in the stoppage of the littoral drift movement. The littoral drift as in other cases travels from south to north during the S.W. monsoon season and from north to south, during the N.E. monsoon season. Three mud banks have been known to appear between Mangalore and Cochin and two between Cochin and Cape Comorin. Because of their peculiar property of appearing at different places, these natural phenomena do not allow material-energy balance to exist so that erosion is considerable along this coastline. The following examples in order from north to south show the behaviour of the coastline under different situations.

1. Cochin harbour and adjoining areas - This harbour is located about 100 miles from the southern-most tip of India (Manohar, 1958). It is situated in the sheltered area of the backwater just behind the 1,500' wide outlet of the backwater to the sea (fig. 13). The southern end of the Western Ghats drains through many small rivers into this backwater bringing down silt and sand from its slopes. It is possible that the long peninsula between the backwater and the sea was formed as a result of the opposing forces of the waves and the discharging power of the rivers into the sea. At present, with only one opening of the backwater to the sea, namely, at Cochin,

most of the silt from the Ghats settles in the backwater itself though part of it finds its way out through the opening forming a bar at the entrance, causing siltation of the approach channel and supplying littoral drift material along the coast. Before the development of the harbour, an outer bar in the form of a horse-shoe with a depth of only 9' above, used to be formed just outside the entrance moving farther towards the sea during the monsoons and towards the peninsula during the fair weather season. However, two natural channels of depths 40' existed inside the backwater near the opening mainly due to the flushing power of the large quantity of water discharging into the sea during the ebb period. One may visualise the enormous quantity of water drained from the backwater from the fact that the backwater level is usually 3' to 4' higher than the sea level during the monsoon season. At present, with the approac channel maintained to a depth of 38', much of the littoral drift is arrested from forward movement at this point. As far as the harbour is concerned, maintenance by dredging for about 4 months a year is sufficient to keep a safe minimum depth of 32' at all times in the harbour.

As far as the neighbouring coastline was concerned, with the stoppage of the littoral drift movement by the deepening of the approach channel and with the net littoral drift occurring from south to north, there was considerable erosion on the northern side and accretion in the immediate neighbourhood in the south. There was also silting of the bottom on the south side and deepening of the bottom on the north side. The fact that there was littoral drift from north to south, was made use of to regain the lost coastline by providing a stone-faced bund in the lower part of the spit and a series of discontimuous stone groynes running nearly parallel to the shore and overlapping each other in an eschelon fashion for a distance of 2 miles (fig. 14). By making these groynes discontimuous, there had been less erosion at the outer toe and even silting was induced behind them. The result was that the shoreline was considerably restored to its original position.

It may be mentioned that S.W. monsoons are very strong along this coast with waves as high as 6' with a period of 10 seconds reaching the coast during a considerable part of this season. Frequently severe storms with waves as high as 13' also occur during this season. The net littoral drift is northwards at a comparatively small quantity of 42,000 tons per year, so that the littoral drift problem is not as great as the problem of silt brought into the backwaters from the Western Ghats.

2. Coastline, south of Cochin - Though there is considerable accretion on the south side of the approach channel of Cochin harbour causing the growth of the sandspit, a 20 mile strip of a shoreline southwards beyond 2 miles from the sand spit, and popularly called the Chellanam coastline (fig. 15) had been undergoing considerable erosion (C.W.P.R.S., 1955) threatening a break in the peninsula between the backwater area and the sea - an occurrence which would be a calamity endangering the entire disappearance of the peninsula separating the backwaters from the sea. Within the last 60 years, a coastal strip 20 miles in length and 1,300' in width had been completely lost to the sea as a result of the erosion. Seawalls were constructed along this stretch but most of them were destroyed after they experienced a few storms of the S.W. monsoons with waves as high as 13' striking the walls during the storms. During the fair weather season - November to March, with waves reaching the coast from west to north west, the southerly drift partly restored the eroded area but the net result however, was a loss by erosion of the coast. Since seawalls alone could not prevent erosion as experienced in this case, a mile length of seawall combined with groynes was constructed in the worst eroded section. These structures have since then, prevented erosion but because of very little littoral drift, only a few groins at the southern end were filled up. The erosion of the coastline has, however, been reduced and the groynes are slowly getting filled up. Measures are under way to protect the entire 20 mile strip with similar structures.

Beaches along the coast of Kerala are narrow with fairly steep (1 : 12) underwater slopes. During the S.W. monsoon season (June to September), the wave direction is between 10^{o} and 40^{o} south of west while during the fair weather period (October to May), it is usually in the north direction. Prior to the construction of protective structures, coastal strips as wide as 30' used to be eroded by storm waves within 48 hours. The net erosion per year used to be as much as 15' to 20' of the coastline.

3. Ashtamudi fishing port - Near Quilon, north of Trivandrum, there exists a lake called Ashtamudi Lake (C.W.P.R.S., 1956) with an outlet to the Arabian Sea (fig. 16). There are proposals, at present, to develop this lake into an all-weather fishing lake. At the entrance to the lake, there exists a bar with water to a depth of 3'. Waves break over the bar and during the monsoon season, these breakers assume large proportions making it difficult for any craft to pass through.

A number of shoals exist at the outlet between a channel in the south and one in the north. The northern channel has depth of 7' to 9' at all times while the southern one is shall and gets silted due to sand movement. Unlike in other parts of the west coast, this movement is not, most probably, due tc the S.W. monsoon waves since these waves reach the coast almos at right angles with no alongshore component in existance. These S.W. monsoon waves, however, which are sometimes, as hig as 10' probably bring sediment towards the shore from the sea bottom. The sediment thus brought by the waves along with th sediment discharged from the lake by the S.W. monsoons and by tides of 3' to 4' is moved alongshore from north to south by coastal currents of speeds upto 2 knots and from the south to north by less stronger currents. Obviously since there are r major rivers to supply the sediment for this drift, most of it is derived from the sea, by erosion of the coastline and from the lake.

Very near this lake and towards the south, there exists a rocky outcrop called Tangasseri Point projecting into the sea. Between the lake and this point, the coastline is rocky and the bottom is covered with sand (1 mm), mud and silt (0.25 mm The foreshore zone is flat and the waves break at a distance from the shoreline. Sediment analysis indicates that most of the coarse sediment between this Point and the lake must have been derived from coastal erosion and brought to this zone by diffraction of waves at this Point. The beach south of this Point is very steep causing waves to break at the shore and mo of the sediment in motion to disappear into deep sea areas. As such there seems to be very little sediment in motion beyon this point. On the other hand, the foreshore zone north of the lake is shallow containing silt (0.25 mm) and mud. Sedi ment analysis shows these to have their origin in the Lake and in the small streams discharging into the sea.

A feature of this coastline upto Cape Comorin is that there are many lagoons separated from the sea by small strips of land. In general, the outlets point towards the south ind cating sand drift in this region to be from north to south pro bably due to coastal currents.

WEST COAST-HARBOUR PRESERVATION

From the point of view of littoral drift, this coast is ideally suited for location of a harbour. With very few rive discharging into the sea, littoral drift is localised with onl local accretion and erosion. However with the rainfall heavy along the coast, rivers bring down a large quantity of sedimen

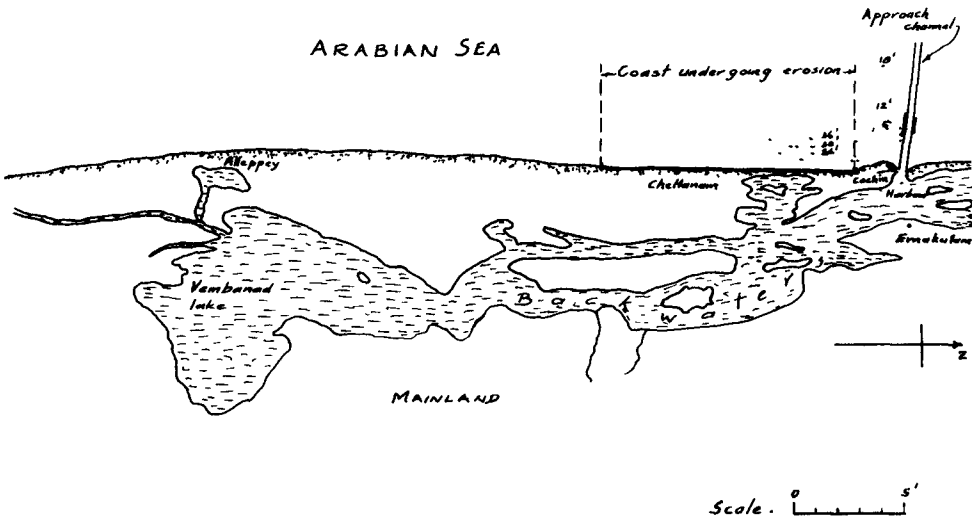

Fig. 15. Kerala coast near Chellanam.

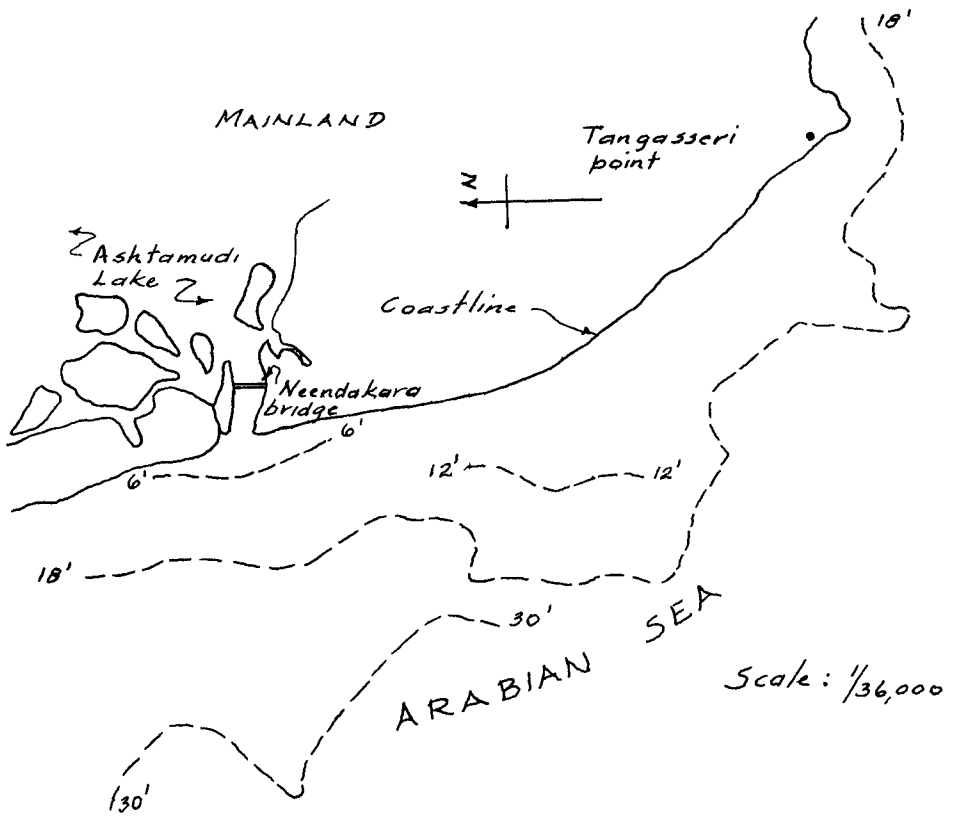

Fig. 16. Ashtamudi port.

which manifests itself in the form of sand bars, sand spits, shoals and littoral drift. In addition, with the severe and consistant S.W. monsoons for 4 months, heavy swells reach the coast making it difficult to do any effective dredging to keep the approach channel and the harbour basin from silting. In general, the foreshore zone is steep and thus the difficulty of extending the breakwaters to the sea as protective structures to the basin is a factor to be reckoned with. Considering the coastline from Kandla to Cape Comorin the following may be concluded.

(a) Coastline bordering Gulf of Kutch - With wave action and littoral drift small and tides high, the problem along this coastline is mainly a tidal one. With a large number of small streams discharging into the Gulf and with the coastlin consisting of low lying areas, there exist many flow channels to the Gulf which shift due to natural causes such as deficiency of outflow as a result of a weak monsoon, or deficiency of ebb over tide or tide over ebb. The shifting of tidal channels may be rather a slow process but it has to be checke if the harbour basin is to be kept effective. The only remedy will be to have regular depth soundings of the flow channels and prevent change of course of the channels by restoring the original ebb and tide discharges so as to have the same scouring velocities and resort to dredging if necessary.

(b) Saurashtra-Kutch Coastline - Beyond the Gulf of Kutch an towards the south on the west coast in the Saurashtra-Kutch region, the coastline between marks A and B in fig. 1 may be called a physiographic unit, that is, a coastal strip in whic the energy and the material available within the area and therefore erosion and accretion in the area are not dependent upon the adjacent areas. This area can, therefore, be treat as a separate unit by itself. From the behaviour of the coastline and harbour areas, the following may be interpreted Since the littoral drift is small of the order of 7,000 tons per year from south to north and 3,100 tons per year from north to south, maintenance of the harbour from this point of view will be easy. A little dredging during fair weather season will be sufficient. However, breakwaters have to be extended sufficiently into the sea for the littoral drift to be directed to deeper portions and to protect the harbour fro the severe swells of S.W. monsoons. Diffraction of waves an the resulting deposition of sediment in the lee of the breakwaters and ranging in the harbour have to be carefully analys in these regions. With very little littoral drift, the danger of erosion and accretion of the adjoining coastline is

slight except during storms. Seawalls to withstand the wave action and groins to trap the available sediment will be sufficient.

However for small intake channels such as at Mithapur, construction of long breakwaters will, not only, be expensive but is not warranted by the situation. In such cases, the high range of tide may be used beneficially and the original conditions especially the tidal velocities and discharges as they existed before the construction of coastal works should be restored. The coastline is bound to get shallow behind the breakwaters but if the tidal velocities especially those of the ebb are strong enough to flush the sediment deposits, no further remedial measures may be necessary.

An ideal example of accretion caused by man-made structures can be found at Mithapur. With coastal works, erosion and accretion will always start first in the inshore and foreshore zones, that is, in comparatively shallow water causing a gradual decrease in depths in the shallow water zones on the accretion side and gradual flattening of the beach profile. This is typically evident in fig. 6b.

(c) West coast from Surat to Mangalore - This coastline is directly in the zone of severe S.W. monsoon swell and to a lesser extent to the waves induced by the north-westerly winds. Thus the alongshore components occur from both south to north and north to south, though the former is stronger than the latter. The deep water areas are very near the coast and much of the material brought by the rivers go into those areas. Littoral drifts are localised and vary from 3,000 tons per year to a maximum of 200,000 tons per year at places where the sediment load carried by the rivers is great such as at Mangalore.

Harbours along this coastline can mostly be located at river mouths only because of the difficulty of construction of long breakwaters into deep sea areas near the coasts and because of the severe monsoon swells reaching the coast. However, river harbours of the type which can be constructed along this coast have the following disadvantages. Rivers bring a large amount of sediment which deposits partly at river mouths because of the tidal influx opposing the heavy swells at those places. Also the ebb tide takes part of it to the approach channel. Thus the harbour basin and the approach channel get silted and sand bars, sand spits and sandy shoals are formed. Usually along this coastline, the flushing power of the ebb is large enough only to maintain a maximum depth of 20' during the

monsoon season. Dredging of the approach channel will also difficult during the monsoon seasons due to high swells. Therefore for the maintenance of a harbour, river sediment should be arrested or disposed off before reaching the harbou basin. The proper remedy will be to build sand traps just above the harbour basin and to dispose off the trapped sedime to the sea by dredging during fair weather season. If the sediment is placed along the shoreline at proper places, the sediment thus placed will act as artificial nourishment for l toral drift. Because of high waves reaching the coast, sea walls and groins should be constructed at critical places of erosion to prevent erosion and restore the eroded strips resp tively.

Along this coast, Bombay is, however, an exception becau it is situated in a bay having a large tidal influx maintaini a depth of 30' in the approach channel without dredging and thus making it an ideal natural harbour.

(d) Coastline from Mangalore to Cape Comorin - Along this coastal strip, there exist many distinct features not found elsewhere and as described before. These are in the form of many lagoons, mud banks, and a large backwater separated from the sea by a peninsula. The direction and quantity of litto ral drift are almost the same as in the coastal strip above (northwards) except for the coastline below (southwards) from Ashtamudi Lake to Cape Comorin where the waves reach the coas almost at right angles leaving no alongshore component. How ever in this southern-most area, coastal currents are of sufficient magnitude for alongshore movement of the sediment. Except at Cochin where the flushing power of the ebb is great due to the large quantity of water discharged into the sea through the harbour entrance, it will not be possible to main tain a depth of more than 20' in the approach channel at any other place for reasons mentioned earlier. If however this depth is to be maintained, dredging for a few months of year : the fair weather season will be sufficient if a sand trap is built above the harbour basin to trap the sediment brought during the monsoon season.

COASTLINE PRESERVATION OF THE WEST COAST

Because of very little erosion along the coastline and that too localised to a great extent at places where the mate· rial-energy balance is disturbed by the construction of coas- tal works, the shoreline and foreshore zone considered as a whole seem to be in equilibrium. With very few rivers dis- charging into the sea and with no serious erosion or accretio

the littoral drift seems to be just sufficient to keep the shoreline in equilibrium moving in both directions, namely, from south to north and vice versa restoring the eroded parts of the previous season. However, erosion of considerable extent occurs during storms in isolated places and restoration of this area by littoral drift of the fair weather season is never complete because of insufficient littoral drift. Thus the erosion extends inwards gradually every year. In such cases, a seawall situated sufficiently inside the shore to prevent erosion and groins to trap the sediment in motion will be required. If littoral drift is insufficient to cause any accumulation of sediment at the groins, artificial nourishment in the form of the dredged sediment from the river mouths or harbour or accretion areas may be necessary if economically feasible and if this does not affect the nearby harbour areas to a harmful extent.

EAST COAST

General topography - The east coast of India which extends from Cape Comorin in the south to the mouth of Ganges in the north has a coastline of about 1,750 miles. The west coast of Gulf of Mannar shielded by the island of Ceylon extends from Cape Comorin to Pamban. From Pamban to about latitude 16° N, the coast is called the Coromandel coast. The remaining coastline is divided into Circars coast upto latitude 19° 23' N and the Orissa coast upto the River Hoogly. Numerous hills lie along the coast and unlike on the west coast, they are not continuous. For a considerable length, these hills are far inland from the coast and a broad strip of low lying land lies between them and the Bay of Bengal. Southwards of Madras, the width of the coastline is about 80 miles and in the north, it narrows to 30 miles. Most of the sediment carrying big rivers of the south and central India, such as Mahanadi, Godavari, Cauveri, and Kistna have their origin in the Western Ghats and flow into the Bay of Bengal in the east between the hills. North of Godavari river (lat. 16° 30' N), the Eastern Ghats are continuous and very near the sea. The coastline above Circars coast essentially consists of the wide deltas of Mahanadi and Hoogly rivers.

From the point of view of littoral drift, this coastline is at large variance from the west coast. Rivers discharge a large amount of sediment into the sea and this travels back and forth along the coast. As on the west coast, the littoral drift is from south to north during the S.W. monsoons and north to south during the N.E. monsoons. It has been estimated from existing installations that the net drift from south to north is of the order of 1 million tons per year. This large littoral

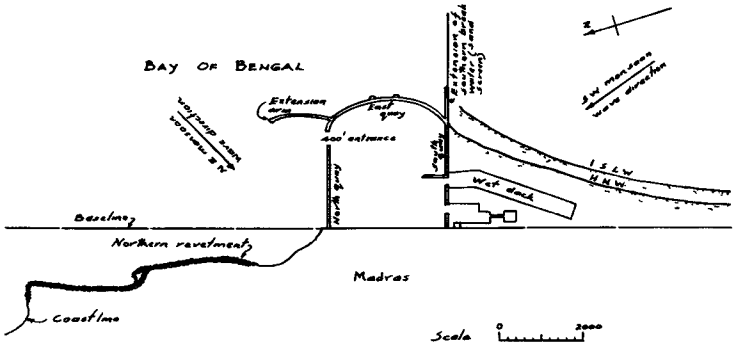

Fig. 17. Madras harbour.

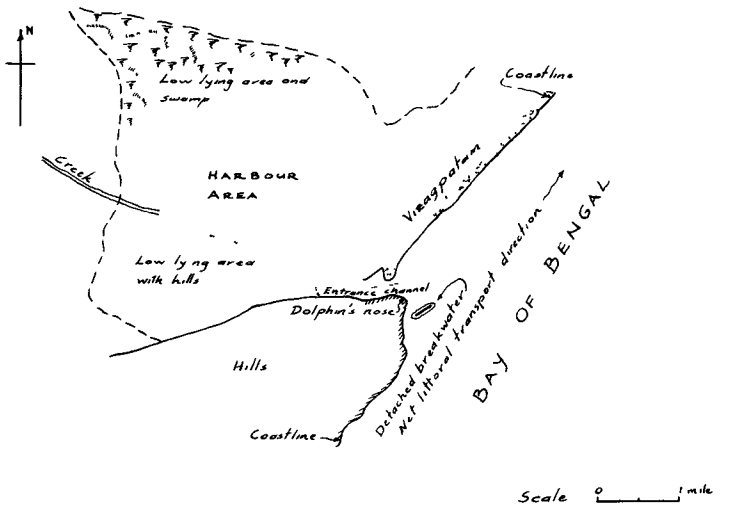

Fig. 18. Vizagpatam harbour.

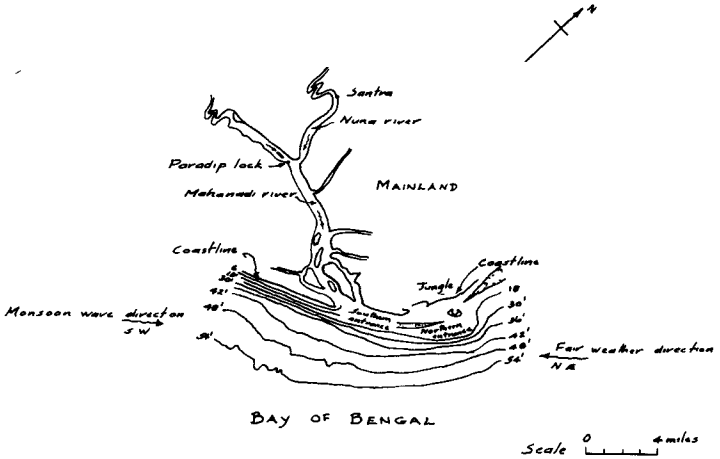

Fig. 19. Paradip port and vicinity.

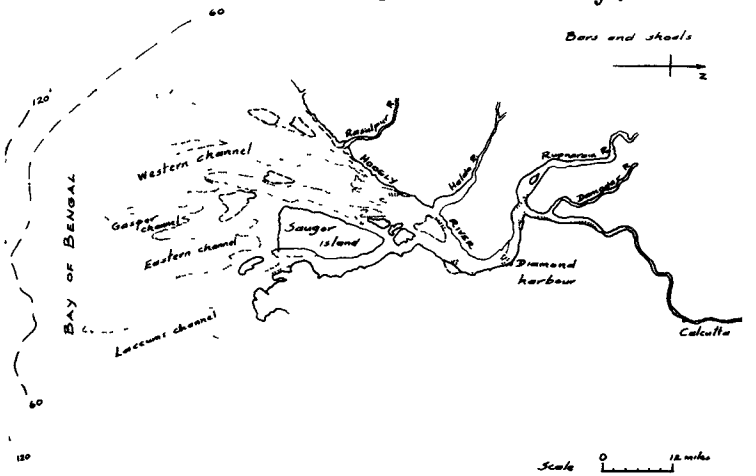

Fig. 20. Hoogly river and Calcutta port.

drift has resulted in flat foreshores for long distances on either side of the river outlets. Under natural conditions before the development of harbours and other coastal structures, there seem to have existed equilibrium conditions with this large quantity of sediment moving in comparatively shallow depths along the coastline balancing erosion and accretion. But with the construction of coastal works arresting the large littoral drift, there had been large scale accretion on the updrift side and large scale erosion on the downdrift side. The difficulty of restoring such a tremendous material-energy inbalance has been the bane of the east coast. The following descriptions of a few existing installations, the difficulties experienced and the methods used to overcome those difficulties will give a correct picture of the problem.

1. Madras - This is an artificial harbour situated in southern India along the east coast (fig. 17). This shoreline harbour is formed by the projection of two artificial breakwaters from the shoreline (Manohar, 1958). An extension of the southern breakwater northwards and called the sheltering arm protects the entrance on the northern side. A masonry arm of about 720 feet at the south-eastern corner of the southern breakwater prevents rapid silting of the foreshore zone on the south side with the sediment being deflected into deeper areas. Two rivers, one north of Madras, namely, Pennar and one south of Madras, namely, Cauvery contribute to most of the sediment to the coastline. Waves of the S.W. monsoons reach the shore at an angle of 30° and with the large scale northerly littoral drift the foreshore zone was advancing rapidly on the southern side till the construction of the sand screen. Because of silting, the original entrance on the east side was shifted to the present one on the northside. At present, with the foreshore zone flat on this side, the surf breaks at about 1,000' from the shore with waves as high as 14'. With the shallow coastal shelf very narrow and ocean depths comparatively close inshore, the danger of littoral drift silting the harbour entrance is no longer a problem with the provision of the sand screen (masonry arm) which serves two purposes, namely, deflection of a large amount of sand drift into deeper areas and allowing the removal of sediment by dredging from behind the screen. On the northern side where there had been considerable erosion, provision of stone revetments along the coastline and the sediment brought by the southerly drift during the N.E. monsoons have prevented further erosion. The trouble with this harbour, at present, is not from littoral drift but from 'ranging' which is sometimes, as high as 2'9".

2. Vizagpatam - This harbour is situated farther north of

Madras and unlike that harbour, the neighbouring coastline is bounded by hills in some places and rock outcrops in other places (fig. 18). It is a natural harbour at the mouth of a small river which flows into a bight and then into the Bay of Bengal (Ash & Rattenbury, 1935). The entrance channel is short and is situated between the high bluffs of Dolphin's nose in the south and Vizagpatam town with its small hills in the north. At times, the rainfall is intense so that the large quantity of silt brought by the river is deposited in the harbour basin. This slit, however, can easily be dredged and disposed off into the sea. As at Madras the worst troubl is from littoral drift estimated to be a million tons per year moving towards the north and about 20,000 to 300,000 tons per year moving towards the south. To keep the 300' wide approac channel in operation at all times and to a depth of 33', a detached breakwater in the form of two sunken ships and approximately 1,000 feet in length sunk in shallow water of 18' to 25' depths has been very effective in preventing sand from reaching the channel. The breakwater acts as a sand trap depositing sand in its lee from which it is dredged and disposed off to the northern side.

3. Paradip port - Halfway between Vizagpatam and Calcutta, on of the major rivers in India, namely, the Mahanadi river discharges into the Bay of Bengal. About 2 miles up the river, a port called Paradip port (fig. 19) is being developed to cater to traffic for areas between Vizagpatam and Calcutta.

River Mahanadi divides itself into a large number of tributaries just before reaching the sea. During the S.W. monsoon season when the discharge from the river is as much as 500,000 cfs, a large amount of silt and sand of the order of 28 million tons per year is discharged into the sea. Much of the sediment deposits at the mouth of the river or travels alongshore as littoral drift material with the result that a large triangular delta of 4,500 square miles is in existance at its mouth. During the fair weather season (October to Ma river discharge being very small and flood tide being comparatively large, some of the silt finds its way back into the river. At the southern entrance, however, a depth of 40' has always been maintained and it is at this place that a port is being developed (C.W.P.R.S., 1956). Between this basin and the sea, a sand bar is formed at a minimum depth of 11' below water moving towards the river during the fair weather season and shifting back to the sea during the S.W. monsoon season. Because of the large quantity of silt brought by the river, a long and narrow sand spit, 6 miles in length, always exists parallel to the coast. When it assumes a large size, a break

occurs for the river to flow into the sea and then it shifts its position from north to south and vice versa. This growth and movement of the sand spit with the consequent change of course of the river mouth is a recurring phenomenon, for, this area acts as a source for distribution of sediment to other areas. As in the case of Madras and Vizagpatam, the south-westerly winds with littoral drift from south to north exists for 8 months a year with the strongest drift occurring during the S.W. monsoon from June to September. Similarly there exists a drift from north to south during the other four months. S.W. monsoon waves are, sometimes, as high as 10' and with this intense wave action and large quantity of sediment available from the river, there is a net littoral drift of 1.5 million tons per year travelling from south to north. This drift along with the tides (maximum of 7') has been responsible for the various changes that occur in this area from time to time.

4. Calcutta - Calcutta port situated 120 miles up the river Hoogly from the sea (Bay of Bengal) is a typical river channel harbour (fig. 20). With the harbour far inland from the sea and with a large tidal influx, there are channels of sufficient depths at the river mouth which are not affected by the littoral drift. However, the large amount of sediment brought by the river from the upland reaches through its many tributaries, chiefly Rupnarain and Damodar moves back and forth in the river as a result of the large variation in the tides. The tidal range is as much as 17' near Calcutta and the effects of tides are felt upto Swarupganj, 84 miles north of Calcutta. Soundings indicate that the Hoogly estuary is deteriorating rapidly especially in the reaches above the Diamond harbour. Depths below Diamond harbour usually maintain themselves at 14' but depths above deteriorate to as low as 6' without dredging. It may be noted that but for the fact that only coarse sediment settles to the bottom, the river would have silted up long ago. It is also interesting to note that most of the sediment brought by the river settles in the river reaches themselves resulting in very little sediment discharge into the sea. Consequently about 70 to 80 million cubic yards of sand are dredged every year from the various bars to keep the navigational channels in operation. These bars are the worst from February to middle of May during the equinoxial perigree spring tides when there exists very little freshet discharge and a large influx discharge of the order of 50 to 60 million cfs creating many channels of flow through the bars. From middle of May to middle of July, these bars are prevented from further deterioration by the gradual increase in the freshet discharge. From middle of July to end of October, that is, during the S.W. monsoon season, the flood tide is held back by the large

freshet discharge which reaches a maximum of 210,000 cfs in the Hoogly and the bars improve so that in some places, depth are as much as 24'. However these freshet discharges create more flow channels and these being not the same as those form during the fair weather season and not being the same every year, result in the formation of a large number of bars, shoal and twisting channels in the river necessitating enormous continuous dredging to keep open the navigational channels. Ba and shoals deteriorate later during the post freshet period from November to January when the freshet discharge decreases and the flood tides predominate. In addition, Hoogly experiences variation in mean tide level from season to season resulting in change in velocity for the same range of tide and thus affecting the bar formation. Hoogly estuary shows another peculiarity in that there are rotary currents caused by the change in the direction of the flood and ebb tides in some places due to the peculiar regime of the estuary. Yet anothe peculiarity in the Hoogly river is the occurrence of the "hydraulic bore" with waves of 8' to 10' heights travelling very fast up the river and destroying the banks and neighbouring property in their path. All these affect the bar and channel formations and the depths in the river and therefore the harbour area, with the littoral drift along the coast havi very little to do with them.

EAST COAST-HARBOUR PRESERVATION

With the large amount of littoral drift of the order of 1 million tons travelling along the coast, construction of harbour works will result in rapid silting of the foreshore zones, approach channels and harbour basins as experienced at Madras. In addition, the difficulty of dredging such a large quantity of sediment under severe wave action of the S.W. monsoon season will also be a problem to be dealt with. If the harbour is an artificial one as at Madras with breakwaters extending from the shoreline to the sea, arrangements similar to those made at Madras for the disposal of the sediment deposit and for prevention of erosion may be made. A better arrangement would, probably, be to dispose off the accreted material to the erosion side, that is, the north side, to replenish the coastline. If the harbour is a natural one as at Vizagpatam, a similar arrangement in the form of a detached breakwater acting as a sand trap and disposal of the accreted material dredged from behind the same trap to the erosion side may be the best one if the foreshore depths are shallow. If the harbour is situated in a river delta as at Paradip it will be difficult to predict the type, position and nature of the coastal works because of the shifting nature of the flow

channels and sand bars and because of large littoral drift. In any case, for any harbour along this coastline, it will be difficult to state exactly the type of coastal works necessary unless rigorous model studies are conducted though the measures taken at Madras and Vizagpatam may be used as guides.

COASTAL PRESERVATION

From the point of view of coastal preservation under natural conditions, the methods to be adopted on the east coast are fairly straight forward because of the heavy littoral drift. A series of groynes spaced properly and with sloping top surface to allow the excess littoral drift to pass over them and seawall built sufficiently inside the beach to prevent the heavy waves from damaging the coastline will be more than sufficient. The groyne spaces will get rapidly filled restoring or extending the coastline. This coastline may be termed an overnourished coastline and the river mouths which are numerous, act as sources with sediment brought by the rivers acting as the littoral drift material. If, however, coastal works such as breakwaters, approach channels and other similar harbour works are built, consequences will be disastrous. The large material energy inbalance will be so large that large scale accretion on the updrift side (south side) and large scale erosion on the downdrift side (north side) will result. The best way to restore equilibrium along the shoreline will be by artificial nourishment from updrift to the downdrift side of the excess material available on the former side, if economically feasible.

REFERENCES

1. Ash, W.C. and Rattenbury, C.B. (1935-36) "Vizagpatam Harbour" Min. Proc. of Inst. of Civil Engineers, London, Vol. I, paper no. 5007, p. 235.

2. Central Water & Power Research Station (1948) "Annual Report - Technical", Ministry of Irrigation & Power, Government of India, p. 68.

3. Central Water & Power Research Station (1949) "Annual Report - Technical", Ministry of Irrigation & Power, Government of India, p. 352.

4. Central Water & Power Research Station (1952) "Annual Report - Technical", Ministry of Irrigation & Power, Government of India.

5. Central Water & Power Research Station (1955) "Annual Report - Technical", Ministry of Irrigation & Power, Government of India, p. 394.

6. Central Water & Power Research Station (1956) "Annual Report - Technical", Ministry of Irrigation & Power, Government of India, p. 364, p. 377, p. 390, p. 393.

7. Joglekar, D.V., Gole, C.V., & Apte, A.S. (1958) "Some Coastal Engineering Problems in India" Coastal Engineering, Council of Wave Research, Vol. VI, p. 510

8. Manohar, Madhav (1958) "Sediment Transport at South Indian Ports" Coastal Engineering, Council of Wave Research, Vol. VI, p. 359.

9. Mason, M.A. (1950) "Geology in Shore Control Problems" John Wiley & Sons Inc.

10. Per Bruun (1955) "Coastal Development & Coastal Protection" Florida Engineering & Industrial Experiment Station, University of Florida, Bulletin No. 76.

CHAPTER 22

SUR L'EVALUATION DE CERTAINES CARACTERISTIQUES DU TRANSPORT LITTORAL A LA BASE DES DONNEES METEOROLOGIQUES

Paweł Słomiańko
Professeur Agrégé à l'Institut Maritime. Gdańsk - Pologne.

Les transports littoraux de sables ou de graviers qui s'effectuent le long des côtes marines donnent lieu à un certain nombre de processus intéressants et importants, tant du point de vue scientifique que du point de vue des solutions pratiques. Ne citerais-je ici que les phénomènes de la formation de dépôts de sables, de l'ensablement des ports et des estuaires fluviaux, ainsi que de l'abrasion des côtes marines.

L'intensité et la direction du transport littoral en sont les traits caractéristiques essentiels. Les deux caractéristiques en quantité majeure et en premier lieu dépendent des courants de la houle agissant sur la zone côtière, ainsi que de la force et de la fréquence des vagues. Afin de pouvoir déterminer d'une manière exacte les caractéristiques précitées du transport littoral, on est tenu de poursuivre des études dont les méthodes, cependant, ne sont pas encore élaborées d'une manière définitive, quant aux études mêmes - - elles sont en général coûteuses et présentent des difficultés en cours d'essais.

Parmi lesdites études on peut citer la détermination du volume de l'apport de sable du côté au vent de l'obstacle transversal, ainsi que la méthode, assez récente d'ailleurs, d'usage de sable marqué à l'aide d'isotopes [4,7] , ou bien encore à l'aide de colorants luminophores [1,8] , Lesdites méthodes, cependant, comme il l'a été signalé plus haut, sont assez onéreuses dans leur application. Les nécessités pratiques imposent souvent des solutions, concernant la caractéristique générale des transports littoraux il se peut moins précises, mais plus promptes.

Les réponses satisfaisant lesdites exigences pratiques peuvent être obtenues le plus facilement au moyen du calcul de l'énergie totale des vagues attaquant la zone donnée de la côte de directions diverses. Il y a, toutefois, peu de pays qui puissent se louer de posséder un service hydrologique maritime tel qui soit à même de poursuivre des observations permanentes des éléments de la houle à l'exemple du Service météorologique qui poursuit des observations constantes de la force et de la direction des vents.

Donc, les tentatives faites jusqu'à ce temps dans le but d'établir une formule simple, caractérisant les forces charriant le transport solide, forment deux groupes essentiel et notamment*:

Le premier groupe comprend les formules basées sur les éléments mesurés de la houle; parmi ces formules, entre autre peut être classée la formule des ingénieurs américains [3] ;

$$Q = 0.5 \cdot k_1 \, w \cdot e \cdot \sin 2\alpha \qquad (1)$$

et la formule de Jdanov [14]

$$E_K = \frac{h \cdot L}{8\,T} \qquad (2)$$

Le deuxième groupe de formules, tout en partant du même principe, tente d'exprimer l'énergie de la houle par des fonction météorologiques, enregistrées depuis des années, sur presque toutes les côtes du monde civilisé.

A ce groupe appartient la formule de Munch-Petersen [9]

$$T_M = k \cdot v^2 \cdot \rho \cdot \sqrt{D} \cdot \sin\alpha \qquad (3)$$

modifiée par Knaps [6] , comme suit:

$$T_K = k \cdot v^3 \cdot \rho \cdot \sqrt{D} \cdot \beta \cdot \sin\alpha \cdot \cos\alpha \qquad (4)$$

Sur le Littoral Polonais nous nous servons précisément des formules du deuxième groupe, étant donné que les observations systématiques de la houle sont poursuivies en Pologne depuis peu et en certains endroits de la côte seulement, quant à l'application des sables à grains marqués on en est à peine aux tentatives d'application de ladite méthode, et cela à une petite échelle. Cependant, le transport littoral longitudina qualifié en Pologne de "flux du transport solide" s'effectue

*
Regardez le Tableau 1

sans doute sur toute la longueur des côtes polonaises. On comprend par cette définition de „flux du transport solide" un tel aspect de transport littoral, qui, étudié durant une période de 2 – 3 ans pour le moins, produise la résultante des charriages s'effectuant toujours dans la même direction. En raison des problèmes surgissant dans ce domaine l'auteur du présent rapport a soumis les deux formules précitées à une analyse plus minutieuse qui a donné lieu à de nouvelles modifications des expressions susmentionnées.

Sans porter préjudice au principe même, sur lequel sont basées les formules de Munch-Petersen et de Knaps, à voir de la formule initiale pour l'énergie de la houle sous la forme de:

$$E = \frac{1}{8} \cdot h^2 \cdot L \qquad (5)$$

où E – est l'énergie de la houle par unité de longueur de la crête de la vague,

h – la hauteur d'onde,

L – la longueur d'onde,

il est indiqué de tenir compte des circonstances suivantes:

1. Il existe un certain nombre de formules théoriques déterminant les éléments essentiels de la houle à l'aide de valeurs caractéristiques du plus important facteur météorologique – du vent. Dans les divers réservoirs d'eau on est tenu d'appliquer les formules qui accusent la plus grande conformité aux phénomènes pbservés en nature. Cependant les deux relations examinées, déterminat la force de transport (3) et (4) allèguent seulement les formules de Stevenson, élaborées d'ailleurs pour les côtes d'Angleterre [9] ; bien qu'elles introduisent en outre lè célérité du vent, dont la formule de Stevenson ne tient pas compte.

Il existe donc de ce fait deux méthodes d'évaluation des éléments de la houle: les constructeurs-hydrotechniciens, pour calculer les forces agissant sur les ouvrages hydrotechniques, se servent, dans le cas où ils ne disposent pas de mèsures en nature, de formules théoriques estimées comme les plus

propres pour la région donnée. En Pologne on admet la formule de Boergen pour déterminer la hauteur de la houle au large; quant à la détermination de la force d'entrainement du transport littoral on adoptait jusqu'à ce temps la formule de Munch-Petersen ou de Knaps qui renferme également les éléments de la houle, bien que sous une forme dissimulée et différemment interprétée. Il apparaît donc qu'il serait plûtôt logique d'introduire dans l'expression représentant la force de transport - la hauteur d'onde à titre d'élément de base et de calculer sa valeur à l'aide de la formule la plus conforme pour la région en question.

2. La capacité du transport solide est d'autant plus considerable que la largeur de la zone des profondeurs critiques - la zone dans laquelle se produit le deferlement des vagues - est plus grande. A des chutes plus ou moins régulières du fond, ladite largeur sera certainement et en premier lieu dépendante de la hauteur de la vague, donc elle lui sera proportionnelle, à voir la thèse de Munch-Petersen.

3. De plus, l'énergie de la houle, comme il s'ensuit de la formule (5), se trouve être directement proportionelle à la longueur de l'onde, ce dont la formule (3), ainsi que la formule (4) ne tiennent pas compte. De toute façon, ces deux éléments - la hauteur et la longueur de l'onde - sont étroitement liès. Par rapport aux conditions qu'offre la mer Baltiqu l'analyse des données allemandes ainsi que des observations polonaises en partie déjà publiées, démontre que ladite relation est analogue à la relation linéaire, ou pratiquement, elle peut être partagée en deux relations linéaires.

Ainsi par exemple, en raison des données rapportées par Roll [2] , on peut constater le fait que pour la Baltique occidentale il existe deux relations linéaires:

pour de petites ondes: $L = 14.9 \cdot h + 12.5$ (6)

pour des ondes plus considérables: $L = 48.6 \cdot h - 35.2$ (7)

Tableau 1

La signification des symboles appliqués

Q. — La quantité totale de material du transport littoral, qui passe un profile par an, sous l'influence de l'action des vagues d'une période et direction connue.

k, k_1. — les coefficients dependant de la pente de la plage, du diametre des grains et d'autres facteurs.

W — le travail total effectu par an par toutes les vagues d'une periode et direction connue.

e — le coefficient defini par le rapport des distances entre les orthogonales de vagues en eau profonde et dans la zone littorale.

α — en formule (1) l'angle entre les crêtes de vagues et la ligne de nivage dans la zone de déferlement de la houle

T. — le periode d'onde

$T_M; T_K, T_S$, la capacitéde transport des matériaux solides le long de la côte.

V. — l'intesitédes vents

p. — la frequence des vents en %

D. — l'extension de l'action des vents

β. — la coefficient, qui prende en consideration le periode d'existance de couverture du glace.

α. — en formule (3) l'angle formépar la ligne côtiere et la direction du vent.

α. en formules (4), (12), (13) l'angle formé par la normale a la ligne cotiere et la direction du vents ou du vagues.

Le graphique de Schumacher, élaboré de même pour la zone occidentale de la Baltique [2] , donne lieu à juger que lesdit rapports se posent respectivement comme il suit:

$$L = 26.7 \cdot h - 6.09 \tag{8}$$

et

$$L = 11.1 \cdot h + 22.5 \tag{9}$$

L'analyse des données polonaises pour l'estuiare de la Baie Poméranienne Swinoujście 13 donne lieu à la relation linéaire suivante:

$$L = 22.75 \cdot h + 3.64 \tag{10}$$

Les observations recueillies par l'auteur au cours des recherches poursuivies sur la flèche de Hel amènent également pour les houles de tempêtes à l'equation linéaire:

$$L = 50 \cdot h - 31.5 \tag{11}$$

A part les divergenoes obtenues, on peut affirmer cependant que, pratiquement, la longueur de l'onde peut être traitée comme grandeur proportionnelle à sa hauteur, au moins pour une vague influence peroeptible sur le transport littoral.

4. L'application des formules du type (3) et (4) récèle un danger, et notamment, on admet que la vague se produit seulement dans le cas où il fait du vent; de ce fait on ne tient pas compte de la houle. On peut obvier à cet incovénient en adoptant la proposition de Knaps [5] de tenir compte également de la houle apparaissant lors des vents de terre dans le cas, où la direction dê ces vents n'accuse pas de déviation-supérieure à 30° par rapport à la ligne côtière. Afin déterminer un coefficient convenable dérivant de l'admission précitée Knaps, comme on le sait, joint la courbe en fonction de $\sin\alpha \cdot \cos\alpha$ où α est l'angle formé par la normale à la ligne côtière et la direction du vent et la tangente à ladite courbe Fig.1.

Pour rendre les opérations uniformes il y a lieu également d'introduire une fonction trigonométrique qui remplirait les conditions suivantes: ayant $\alpha = 0^{\circ}$ et $\alpha = 120^{\circ}$, sa valeur s'exprimerait par zéro et le maximum aurait lieu à α raproché de 45°.

L'expression: formerait par exemple une fonction pareille.. $1{,}5\alpha \cdot \sin^2(\alpha + 60°)$

Les recherches effectuées durant les dernières années font preuve que le maximum de la force de transport apparait pour les directions de houles dont l'angle est supérieur à 45° et rapproché de 60° [11].

Dans ce cas ce serait l'expression: qui formerait la fonction propre. $\sin\alpha \cdot \sin(\alpha + 60°)\cos(\alpha - 60°)$

Les trois fonction trigonométriques sont rapportées par la Fig.1.

Tenant compte des considérations précitées la fonction de la force de transport des matériaux solides le long de la côte s'exprimera par l'expression suivante:

$$T_S = k \cdot h^4 \cdot p \quad \sin 1{,}5\alpha \cdot \sin^2(\alpha + 60°) \qquad (12)$$

ou bien

$$T_S = k \cdot h^4 \cdot p \left[\sin\alpha \cdot \sin(\alpha + 60°)\cos(\alpha - 60°)\right] \qquad (13)$$

Dans ce cas le coefficient k dépendrait non seulement de la granulométrie du matériel et de la pente du fond, mais aussi du coefficient de la proportionnalité de la longueur de l'onde à sa hauteur.

En ce qui concerne le problème des houles il serait utile de noter que l'analyse précise des vents et de la houle, réalisée pour la Baie Poméranienne, accuse une conformité très nette des roses de houle et de vents bien que pour les périodes mensuelles les roses de ce type dénotent de grandes différences. [13]. Il en résulterait qu'en analysant des cycles au moins annuels, les erreurs dues à la nonobservance des houles n'ont pas d'importance dans la pratique, au moins dans les conditions du littoral polonais. Le trait dominant des modifications apportées est certainement l'introduction d'une quatrième puissance de l'élément qui exerce une influence décisive sur le transport solide. Cette innovation met en relief, par rapport aux formules (3) et (4), le rôle des vents de tempête, donc le rôle de la houle également, éléments décisifs pour le transport littoral.

Afin de confirmer le bien-fondé de l'introduction d'une quatrième puissance, l'auteur présente les résultats de l'analyse des conditions existant sur les côtes polonaises.

Bien que les vents de directions occidentales soient prédominants sur le littoral polonais, on peut observer toutefois, le long des côtes de la pleine mer, au moins deux „flux de transport solide" - l'un dans la direction de l'est, donnant lieu, entre autres, à un constant allongement de la flèche de Hel, l'autre dans la direction de l'ouest, formant des dépôts de sables dans la Baie Poméranienne. L'endroit précis, où s'effectue le processus de bifurcation des deux „flux de transport solide" n'est pas connu. Sur la base des indices morphologiques on peut néanmoins supposer qu'il se trouve aux environs du port de Kołobrzeg. On observe que la zone se trouvant à l'est dudit port affectée par le transport littoral, est caractérisée du point de vue de sa morphologie par des apports de sables formant des dépôts du côté ouest des jetées portuaires et d'autres obstacles au travers. Il a été également constaté qu'il y avait tendance d'avancement des estuaires fluviaux, non-aménagés, dans la direction Est. Le processus d'érosion considérable des bords du côte Est des jétées et des groupes d'épis constitue également un indice caractéristique. L'accumulation des apports de sables des deux côtes des jétées portuaires de Kołobrzeg s'effectue d'une manière plus ou moins analogue; quant aux estuaires fluviaux situés à l'ouest du dit port, ils accusent, ou accusaient jusqu'au moment de leur aménagement en ouvrages réglant les conditions desdits estuaires, une tendance d'avancement dans la direction ouest. La comparaison toutefois des valeurs de la puissance de transport, calculées à l'appui de la formule Munch-Petersen et de celle de Knaps, pour différents endroits du littoral, indique que la bifurcation dont il a été question plus haut, n'a lieu, en dépit de toute attente, qu'aux environs de Dziwnów, c'est à dire, éloignée de 50 km environ, à l'ouest de Kołobrzeg. Quand à la capacité d'entraînement des sables, calculée selon la formule proposée par l'auteur, elle démontre que c'est précisément aux environs de Kołobrzeg que

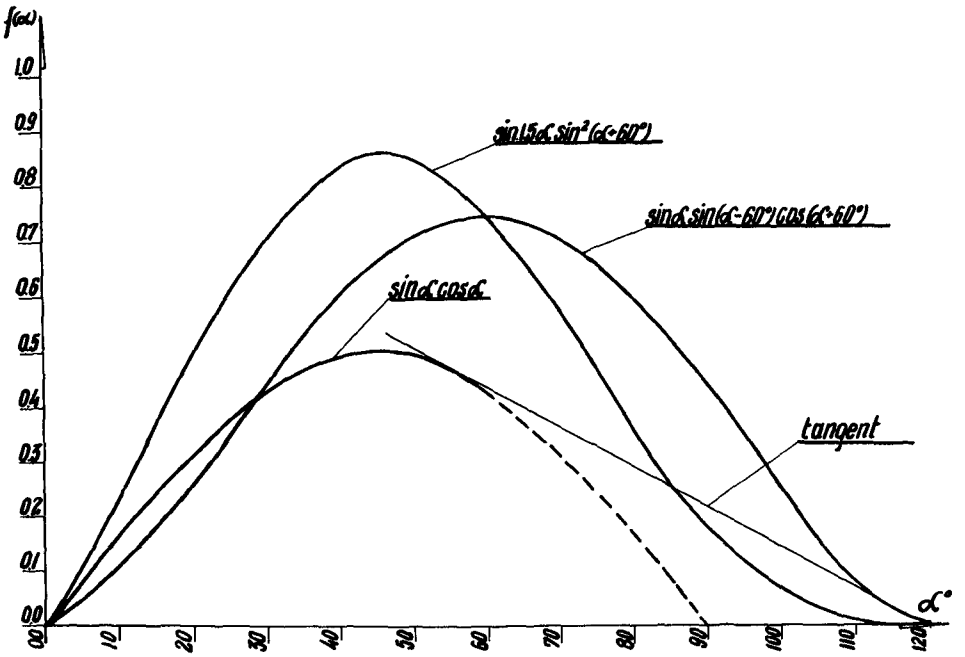
f(α)
1.0
0.9
0.8
0.7
0.6
0.5
0.4
0.3
0.2
0.1
0.0
sin1.5α sin²(α-60°)
sinα sin(α-60°) cos(α-60°)
sinα cosα
tangent
α°
0°
10
20
30
40
50
60
70
80
90
100
110
120

Fig. 1

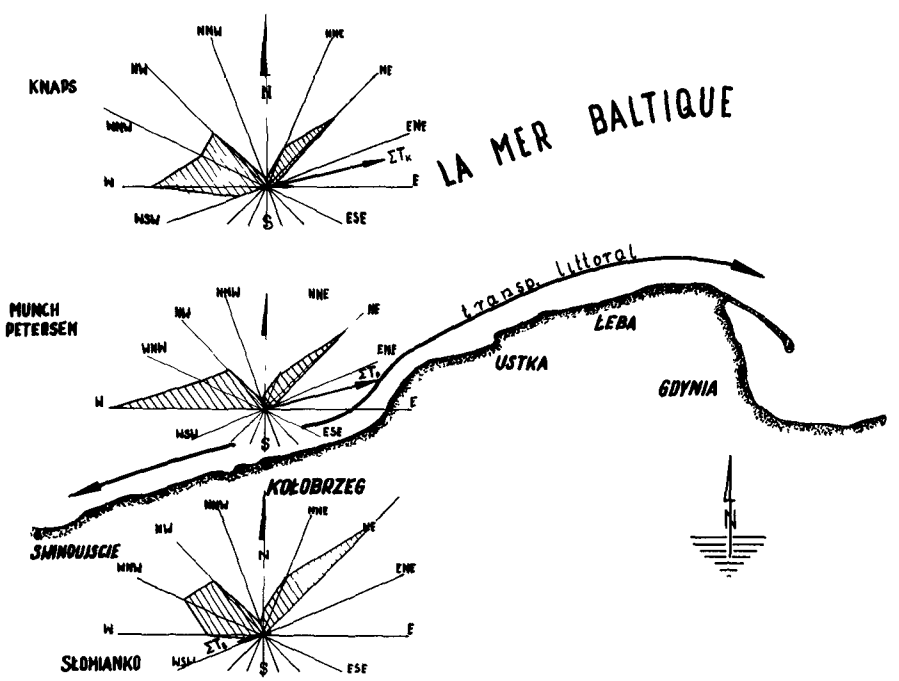
KNAPS
MUNCH PETERSEN
SWINOUJSCIE
SŁOWIANKO
KOŁOBRZEG
USTKA
LEBA
GDYNIA
transp. littoral
LA MER BALTIQUE
N
NNW
NNE
NW
NE
WNW
ENE
W
E
WSW
ESE
S

Fig. 2

„le flux de transport solide" change de direction en entraînant les sables vers l'ouest.

La Fig.2 raporte les roses énergétiques, représentant les forces de transport pour Kołobrzeg en la période 1947 - - 1955, calculées à l'appui des formules de Munch - Petersen, de Knaps et de l'auteur de ce rapport. Chaque direction comporte les valeurs totales en la période précitée, se rapportant à ladite direction. Les échelles des roses particulières ne peuvent être évidemment comparées. Les résultantes T_M, T_K, T_S sont représentées par de petites flèches parallèles à la ligne côtière. La valeur de la résultante Ts n'est pas grande, elle se monte à 3,7% à peine par rapport à la somme des valeurs obsolues des forces de transport /Ts/, mais ladite résultante est distinctement orientée dans un sens opposé à celui des résultantes calculées à l'appui des formules(3) et(4). Sa valeur minime fait preuve précisément que c'est dans cette zone que la bifurcation des „flux" doit avoir lieu, ce qui est en parfaite conformité des observations faites dans la nature.

Il en résulterait donc que cette simple détermination du problème du transport littoral longitudinal, proposée par Munch-Petersen, après y avoir apporté les modifications citées plus, se trouve être une méthode susceptible d'être appliquée à des buts pratiques, bien qu'elle ne tienne pas compte de phénomènes importants tels que la réfraction de l'onde et la naissance des courants de houle littoraux.

BIBLIOGRAPHIE

W.Ł.Bołdirov - L'usage des sables luminescents dans l'étude d'importants transports littoraux. - Académie des Sciences, URSS. Bulletin de la Commission Océanographique No.3, 1959.

E. Bruns - Handbuch der Wellen der Meere und Ozeane, Berlin 1955.

Per Bruun - Coast Stability - Copenhagen 1954.

J.Germain, G.Forest et P.Jaffry - Utilisation des traceurs radioactifs pour l'étude des mouvements de sédiments marins - Proceedings of sixth conference on coastal engineering, 1957.

W.Hartnack - Die Küste Hinterpommerns unter besonderer Berücksichtigung der Morphologie - 2 Beiheft zum 43-44 Jahrb. d. Pomm.Geogr.Ges., Greifswald, 1926.

R.J.Knaps - Prüfung der Formel von Prof.Munch-Petersen über Materialwanderung an der lettischen Küste. VI Hydrologische Konferenz der Baltischen Staaten, 1938.

O.Leontiev et B.Afanasiev - Essai de l'application des radioisotopes pour l'étude des transports littoraux. Académie des Sciences, URSS, Bulletin de la Commis. Océanograph. No.3, 1959.

W.S.Miedviediev et N.A.Aiboułatov - Utilisation des sables à grains marqués pour l'étude des transports littoraux. Informations de l'Académie des Sciences URSS, No 4, 1956.

Munch-Petersen - Materialwanderung längs Meerküsten ohne Ebbe und Flut - IV Hydrologische Konferenz der Baltischen Staaten, 1933.

W.J.Reid - Coastal Experiments with radioactive tracers - - Dock and Harbour Authority, Nr.453, 1958.

M.G.Sauvage de Saint Marc, M.G.Vincent - Transport littoral, formation de flèches et de tombols.
Proceed. of the 5-th Conference on Coastal Engin. 1955, Chapt.22.

P.Słomianko - Etude des côtes sur la flèche de Hel. Archives de l'Hydraulique, V. IV. cah.4, 1959.

Z.Szopowski - Analyse des roses de houle. Archives de l'Hydraulique, V. 5, cah.2, 1958.

A.M.Jdanov - Détermination de la résultante énergétique du régime de la houle sur une côte marine. Informations de l'Acad. d. Sciences, URSS, Série géographique et géophysique, V. 15, No.1, 1951.

CHAPTER 23
STABILITY OF COASTAL INLETS

P. Bruun and F. Gerritsen
Coastal Engineering Laboratory, University of Florida
Gainesville, Florida

ABSTRACT

This paper is a continuation of papers of earlier date (4) and (5) and is an abstract of (6). Pertinent factors involved in inlet stability are discussed briefly. Results of analysis of existing data are mentioned and a future research program is outlined.

PERTINENT FACTORS INVOLVED IN INLET STABILITY

In order to obtain a stable tidal inlet in alluvial material it appears to be an inevitable assumption that littoral drift material is being supplied continously to the inlet. Part of this material is deposited on the inlet bottom where the tidal currents will move it forward and back as a kind of "rolling carpet."

In order to obtain a relatively stable situation this carpet must not move back and forth too rapidly since it thus runs the risk of being lost at both ends (the ocean and the bay). Nor can it be allowed to move too irregularly, changing its velocity and travel time rapidly, since it may soon "get stuck" at one or at both ends in the form of excessive deposits. If -- because of insufficient littoral drift supply -- inadequate amount of material is available for building up this carpet the inlet will be constantly "shaved" and will gradually develop non-scouring open bay or perhaps estuary characteristics. Fig. 1 shows longitudinal sections through inlets of different length. In the first case the (unstable) channel is so short that the rolling carpet extends outside the inlet floor, which in turn causes material to be deposited on shoals in the sea and in the bay by the material-loaded ebb and flood-currents. In the second case the (also unstable) channel is so long that material is now deposited inside both ends of the inlet channel because it gradually became so long that currents were too slow to carry the material load out in the sea or in the bay for depositing. The third case demonstrates a stable "status quo" situation between inlet length, current velocities, and material load.

A rational approach to the material balance problem is given in (6).

To analyze the stability problem the cross-section area A of the inlet gorge is considered explicit as a function of various factors:

$$A = F\ (Q_m,\ \beta,\ \tau,\ B,\ \bar{c},\ W_a,\ M,\ Q_o,\ t) \qquad (1)$$

The factors Q_m (discharge) and β (form factor of cross-section) are interrelated, and shear stress τ, bottom composition B, and the littoral drift, M, to the inlet, also have a certain direct influence on β. Factors

τ, β, $\bar{c}$ (sediment concentration), W_a (wave action), and M are also interrelated. The friction factor not included in equation (1) enters the picture through τ. The fresh water discharge Q_o (head water from river or drainage canals) have a certain influence on flow distribution and thereby on τ and β. The time factor t represents "the time history" which is important because of the time lag between action of forces and the reaction of the elements acted upon by the forces.

The influence of the maximum flow, Q_m

Consider $A = F(Q_m\text{-----})$ when Q_m represents the maximum discharge per second through the inlet gorge. The relationship between A and Q_m can be expected to be fairly linear because if one inlet channel is stable with cross-sectional area A, and maximum flow Q_m joins with a neighbor channel which also has cross-section A and maximum flow Q_m, the result most likely will be a combined inlet with cross-sectional area of the order 2A and maximum discharge $2Q_m$. Changes in friction characteristics and other factors causing energy loss may distort this picture somewhat and the actual dimension of the inlet gorge and channel will depend upon the utilization of the cross-section for flow and the distribution and actual size of shear stresses as mentioned later in this paper.

The influence of the shape factor, β

Consider $A = F(Q_m, \beta, \text{-------})$. Studies of inlet gorges reveal a certain similitude between the cross-section of different gorges even though a considerable number of inlets are provided with gorges which do not have a simple cross-section. Some inlet channels have cross-sections split up in a "deep part" and a "shallow part". The "coefficient of utilization" for flow of these two parts are not equal. The shallow part carries comparatively little flow compared to its area while the opposite is the case with the deep part. The importance of the shape factor is thereby clear. Littoral drift, particularly with coarser material may often tend to develop steeper side slopes and therefore a more "economical" cross-section. Increased fresh water flow in certain periods may work similarly (16). With jetty-protected "improved inlets" there is usually only one channel with greater depth which means greater hydraulic radius and less loss of energy from banks, shoals and similar side effects. In other words conditions are better organized for flow; for this reason it can be expected that a comparatively smaller cross-sectional area is sufficient to carry a given amount of maximum flow.

The influence of the shear stress, τ

Consider $A = F(Q_m, \tau, \text{-----})$ in which τ is the force exerted by the flow on a unit area of the bottom. For a cross-section with horizontal bottom of unlimited width a linear relation between A and Q_m involving a certain shear stress (more simply but not accurate replaced by"average velocity") can be expected.

Assuming steady or slowly varying conditions we have $\tau = \rho g RS$ in which ρ = density of water, g = acceleration of gravity, R = hydraulic radius and S = slope of energy line.

By introducing $v = C\sqrt{RS}$ and $Q = Av$ we find:

$$Q_m = AC\sqrt{\frac{\tau_s}{\rho g}} \qquad (2)$$

whereby τ_s refers to spring tide conditions. τ_s is called the determining shear stress. For an alluvial bottom tidal inlet the requirement of stability is either that this shear stress stays below a certain value or is coordinated in such a way with water flow and material movement that the total transport of material away from one section equals the transport to this section from another section. According to equation (2)

$$\tau_s = \rho g \frac{Q_m^2}{A^2 C^2}$$

The problem of inlet stability is then reduced to the determination of the stability shear stress τ_s under a variety of boundary conditions.

In regard to the influence of channel friction reference is made to the authors (6), which in turn refers to comprehensive literature file on this subject. An increase in C is usually associated with an increase in τ_s.

As mentioned in the following paragraphs various other factors will influence τ_s. Coarse bottom material will usually result in a higher τ_s than fine material. Sediment load injected in the tidal inlet flow from rivers or from the longshore littoral drift will usually cause a higher τ_s; wave action will decrease τ_s. Increase of littoral drift will raise τ_s relatively; fresh water flow may also increase τ_s, particularly when it is concentrated in limited periods of time and causes "at a station changes" as observed in rivers (16).

The influence of soil condition of the inlet bottom, B

Consider $A = F(Q_m, B, \text{-----}, \tau_s)$ and $\tau_s = f(B, \text{------})$. A discussion on the influence of soil conditions is a discussion on the influence of soil conditions on the τ_s. Table 1 - see the following section and reference (6) - gives certain "limiting values" for the shear stress in canals and rivers with granular material considering clear water as well as sediment laden flow. The actual grain size does not seem to be very important within certain limits. Tidal inlets will because of supply of littoral drift material to the inlet and because of its origin almost always have alluvial material bottom and although the flow is continuously reversing it seems reasonable to expect a certain similarity between the behavior of rivers and tidal inlets.

The influence of suspended load, $\bar{c}$

Consider $A = F(Q_m, \bar{c}, \text{------}, \tau_s)$ and $\tau_s = f(\bar{c}, \text{-----})$. Sediment load may be derived from upstream sources or from the littoral drift. According to Table 1 sediment load increases the limiting shear stress. Increase is considerable for heavy load. It is reasonable to expect similar conditions at tidal inlets as we find at rivers. According to

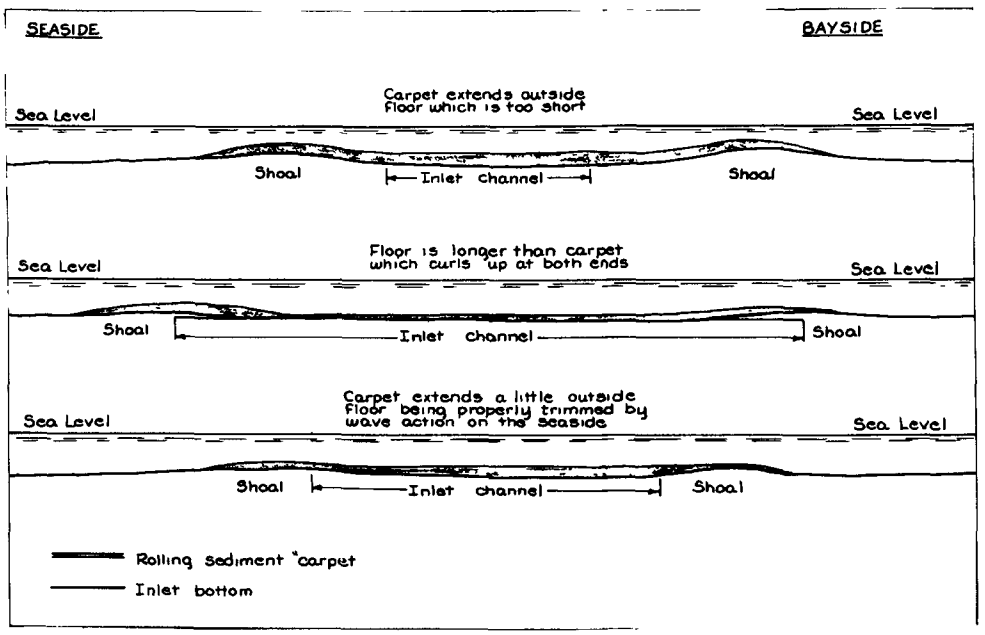

Fig. 1. Material transport in inlet channels as "Rolling Carpet".

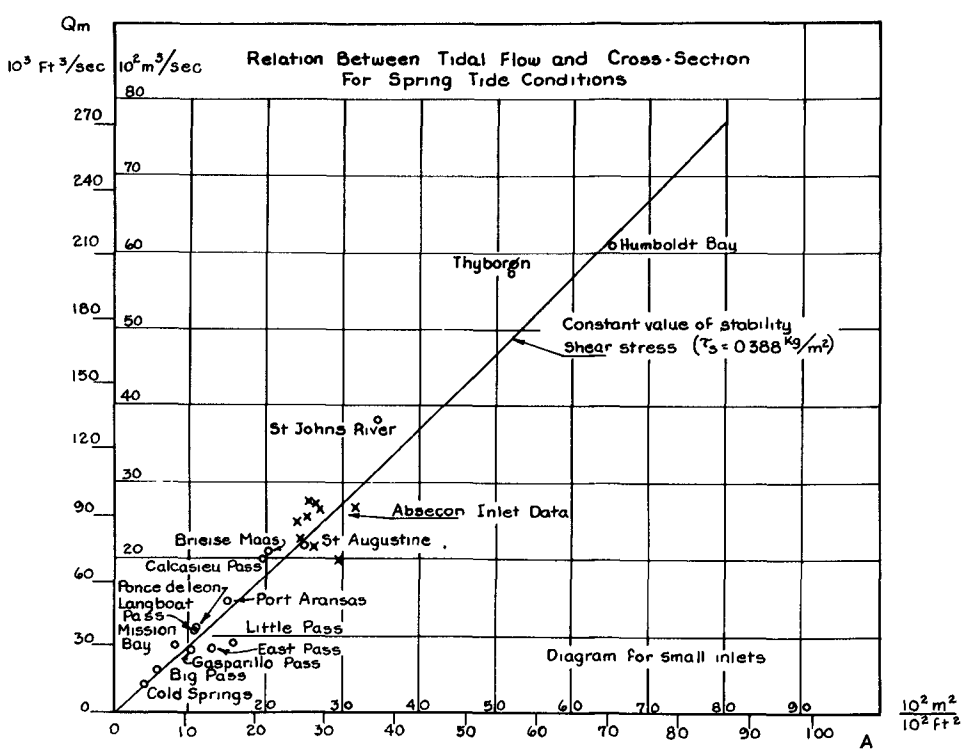

Fig. 2. Relation between maximum tidal flow and cross-section for small inlets at spring tide condition.

observations by Leopold and Maddock (16) the roughness of a channel decreases when suspended load increases. Vanoni (21) explains this effect as a result of decreased turbulence:

> "The increase in velocity or decrease in channel resistance, as suspended load is added to the flow can be explained by the effect of the sediment in reducing the turbulence. To keep the sediment from settling, work must be done on it. The energy for this work can be provided only by turbulence which is damped and reduced in intensity when it gives up energy. This means that the momentum transfer coefficient is also decreased thus allowing the velocity and velocity gradient to increase."

In regard to velocity distribution for silt laden flow the reader is referred to (8).

The influence of wave action, W_a

Consider $A = F\ (Q_m, W_a, \text{------}, \tau_s)$ and $\tau_s = f\ (W_a, \text{--------})$. The wave action makes the actual τ_s -values vary rapidly and increase material load and transport. At the present stage of our knowledge we have no specific knowledge of the influence of wave action under varying conditions including current activity. In the entrance area of an inlet flow will be more or less loaded with material stirred up by waves and currents This will decrease the τ_s in this area but may cause an increase of the τ_s further bayward because of the material load.

The influence of littoral drift, M

Consider $A = F\ (Q_m, M, \text{------}, \tau_s)$ and $\tau_s = f\ (M, \text{---------})$. The littoral drift may influence the development of inlets directly by deposits on the side slopes of the outer part of the inlet channel thereby influencing the shape factor and indirectly by the supply of suspended material to the flow as well as extra bed material for bed load transportation and; increased thickness of the "rolling carpet." (Fig. 1) This in turn may cause an increase of the τ_s.

The influence of river discharge, Q_o

Consider $A = F\ (Q_m, Q_o, \text{------})$. In the estuary type inlet a river discharges through the inlet and this will change the relation between A and Q_m which as a first approximation will now have to be replaced by $Q_t + Q_o$ where Q_t is the purely tidal flow. A consequence of the fresh water discharge may be that flood and ebb currents because of density differences differ greatly in regard to current distribution in the vertical plane as described in (19) and (20). The head water run-off may result in a higher value of C and in a higher τ_s. Siltation may result because of the density currents as mentioned in (12). The density problems at estuaries and their influence on siltation and flow are mentioned in a brief report published in "Hydraulic Research, 1958, by the

Hydraulic Research Station, Wallingford, England which distinguishes between two different types of estuaries; the"convective" type and the "salinity" type.

The time history of the inlet, t

Consider $A = F\ (Q_m,\ t,\ \text{--------})$. Detailed studies of inlet regimen have demonstrated that there is no single solution to the relative stability of a certain inlet but rather whole sets of solutions with different "degree of stability" depending upon how the various factors in equation (1) are put together and upon the "time history" and "age" of the inlet. The relative degree of stability

$$\text{Stab} = F\left(\frac{\Omega}{M},\ \frac{Q_m}{M},\ \tau_s\right)$$

mentioned later in this paper includes factors which all vary with time from the time the inlet was "born" and until it passed away because of various "diseases" or until it got a "heart attack" during one particular storm. This is elaborated further later in this paper referring to actual data.

RESULTS OF ANALYSES OF EXISTING DATA

Analyses of actual data demonstrated that the stability of the inlet gorge is usually better described by the ralation between A and Q_m than by A and Ω when Ω is the tidal prism. In his paper (17) O'Brien found the empirical relation

$$A = 1000\ \left(\frac{\Omega}{640}\right)^{0.85}$$

in which the tidal prism Ω (in acre feet) is taken between mean higher high water and mean lower low water, (both typical characteristics of the U. S. West Coast) and A is in sq. ft. at mean sea level. The analysis mentioned below also uses spring tide range whether tide is diurnal or semi-diurnal. For inlets having a pronounced daily inequality, the stronger ebb currents maximum was used.

RESULTS BASED ON SHEAR STRESS ANALYSIS FROM TIDAL INLETS

The solid lines on Figs. 2 and 3 represent the relationship:

$$A = \frac{Q_m}{C\sqrt{\frac{\tau_s}{\rho g}}}$$

with τ_s constant 0.388 kg/m^2 or 0.080 lb/ft^2 , τ_s being the average shear stress over the cross-section of the channel.

With respect to the value of Chezy's coefficient C, it is apparent that although C primarily depends on bottom material and bottom formation,

the existence of shoals, inlet curvature, bank protection works, etc., will also influence C, but to a smaller degree. However, increasing the size of the inlets tends to increase the value of C as a result of an increasing value R/k (hydraulic radius over roughness parameter). Where a wide variety of inlet sizes is involved, as depicted in Fig. 3, variation of C has been taken into consideration. C values were determined through use of the fundamental logarithmic expressions as well as empirical knowledge of inlet characteristics. By a diagrammatic plotting of computed values for C the relation between C and A can be approximated as follows:

$$C = 30 + 5 \log A \qquad (A \text{ in } m^2 \text{ and } C \text{ in } m^{1/2} \text{ sec}^{-1})$$

or

$$C = 45 + 9 \log A \qquad (A \text{ in } ft^2 \text{ and } C \text{ in } ft^{1/2} \text{ sec}^{-1})$$

The above empirical relation gives average values. In some of the Dutch tidal rivers values for C of 68-70 $m^{1/2}$ sec^{-1} had to be introduced to bring computed values on tides in agreement with observed conditions.

The slight curvature of the solid lines on Figs. 2 and 3 is caused by variation in C, τ_s being a constant. It can be seen that considerable individual deviation is caused by variations in average stability shear stress τ_s, as well as in C. For plottings above the average line, the cross-sectional area is amaller than according to the average conditions which means higher velocities and a consequent higher value of the stabil ity shear stress. Meanwhile it can be seen that for the inlets considere the deviations in $\sqrt{\tau_s}$ are usually within the 10 per cent limit.

As mentioned earlier, the following factors will influence the stability shear stress, and thus the Q_m/A ratio:

Shape factor	β	Wave action	W_a
Soil condition of bed	B	Littoral drift	M
Sediment concentration	$\bar{c}$	Fresh-water discharge	Q_o

Because each example includes certain observation and computation deviations, it is not deemed possible to explain all individual deviation: In some cases, however, a particular factor may be the main reason for the deviation. The shape factor β probably plays an important part in th actual value of the Q_m/A relation at Longboat Pass and Little Pass, Flori Gulf coast. At present Longboat Pass has a rather narrow and deep inlet and the whole cross-section is intensively used for the flow. Littoral-drift material, coming from both sides, is probably responsible for the steep slopes of the gorge which, in turn, cause a shear stress higher tha average.

Contrarily, Little Pass has a very irregular cross-section, parts of which, because of shoals, carry only a relatively small amount of flow. An uneconomical cross-section results in a lower τ_s than average.

The results of computation for the Absecon Inlet in Pennsylvania, based on detailed surveys by the U. S. Corps of Engineers, Philadelphia District, since 1880, are depicted by cross marks on Fig. 2. The shape

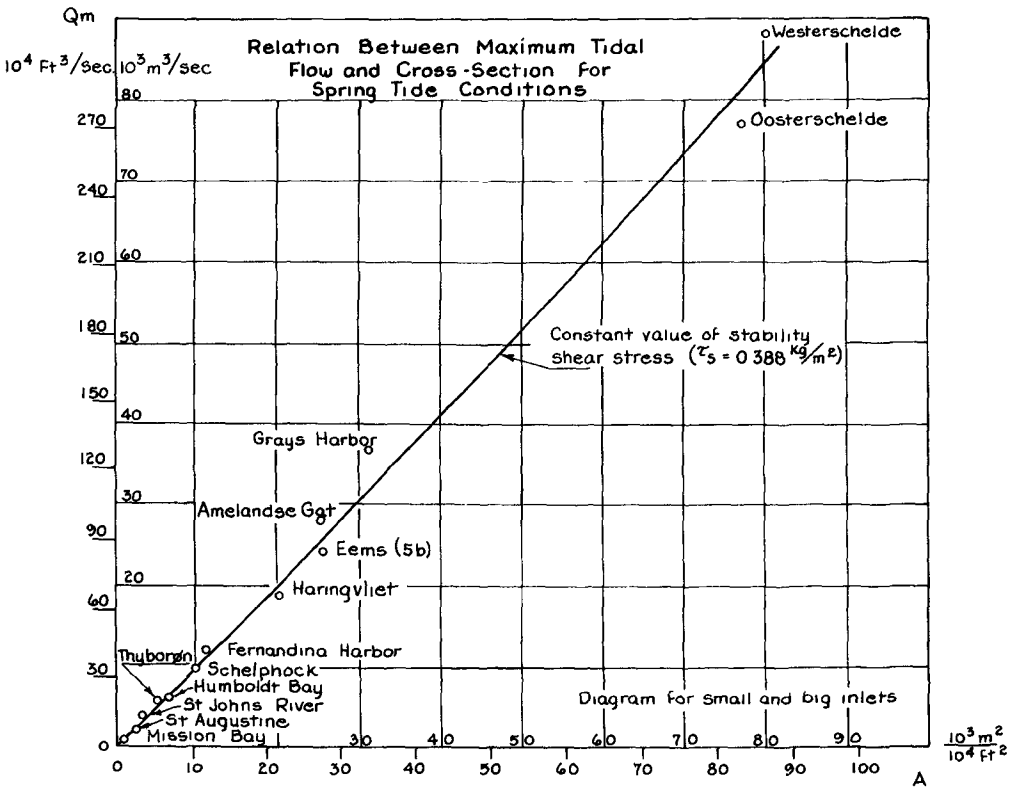

Fig. 3. Relation between maximum tidal flow and cross-section for small and big inlets at spring tide conditions.

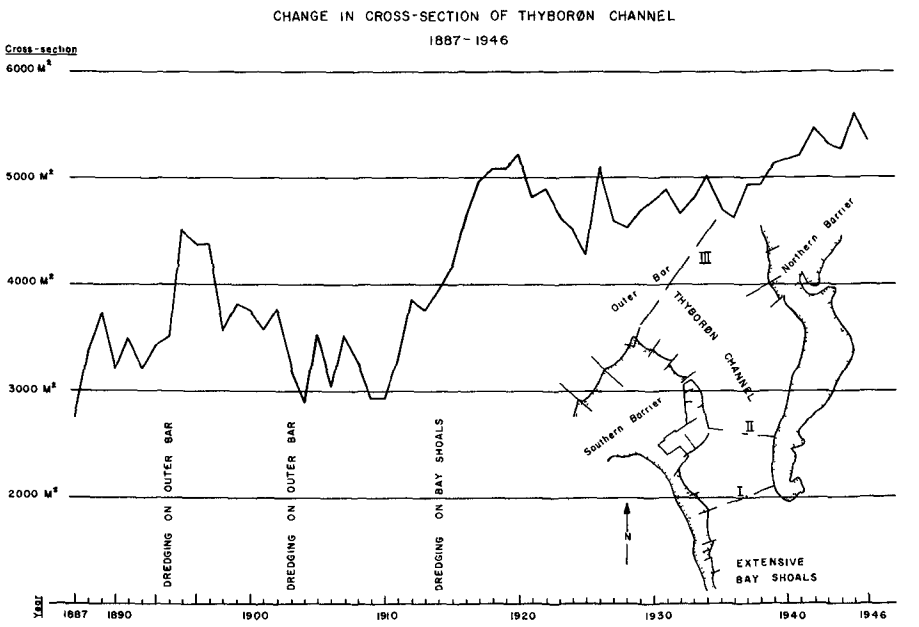

Fig. 4. Development of the gorge of Thyborøn Inlet on the Danish North Sea coast.

of the gorge is characterized by steep side slopes like Longboat Pass. This results in a higher τ_s which, for spring tide conditions seems to be approximately 0.63 kg/m^2 (0.129 lb/ft^2).

A few of the tidal inlets studied are located in areas with a diurnal tide as, e.g., on the west coast of Florida and the Texas coast. The following passes belong to this group: East Pass, Florida; Port Aransas, Texas; and Calcasieu Pass, Louisiana. For those inlets Q_m has been plotted in the same way as for other inlets with a predominantly semidiurnal tide. It can be seen that the data belonging to the three inlets mentioned are scattered around the average relationships. East Pass is at the lower side of the line and the other two at the upper side. Because of the difference in tidal cycle a slight difference in the behavior of those inlets is not surprising. The period during which high velocities occur is considerably longer, but the length of the slack water period, during which depositing of material takes place, is longer also.

In regard to the influence of bottom material or soil conditions, B, many inlets run through littoral drift barriers, which means that the bed material is sand. As can be seen from Table 1, there is little difference between the limiting shear stresses for sand of 0.1 to 0.5 mm, but it must be remembered that the grain size influences the development of the bed configuration which, in turn, affects Chezy's coefficient C and, thereby, the quantity of flow. Meanwhile, the τ_s value is influenced by sediment concentration as described below.

The possible influence of wave action W_a, sediment size and concentration of suspended material $\bar{c}$, and littoral-drift M on the results depicted in Figs. 2 and 3 can best be discussed as a unit.

Wave action increases bed-load transportation as well as suspended load concentration and transportation. Outside the area which is directly influenced by tidal currents to and from the inlet, the bed-load transportation caused by wave action will depend on the actual mass transport of water which is rather limited, but in tidal entrances wave action may considerably increase bed-load transport by tidal currents. In this way wave action tends to decrease the stability shear stress.

The influence of wave action on suspended load transportation will often be considerable, particularly when material from the littoral drift is carried to the inlet and its tidal currents. Generally speaking, the smaller the grains and/or the heavier the wave action, the more material will be suspended in the flow.

On the United States east coast, the south shore of Long Island and the coast between Sandy Hook and Barnegat Inlet, New Jersey, have heavy wave action and a high average grain size (0.4 - 0.5 mm), while Daytona Beach, Florida, has a more moderate wave action and smaller average grain size (0.2 mm). The Gulf coast in general has light to moderate wave action and an average grain size of less than 0.2 mm, while the Pacific coast has moderate to heavy wave action with an average grain size of 0.2 - 0.3 mm.

One could, therefore, expect to find a tendency to larger inlet entrance cross-sections on the Pacific -- and perhaps on the Gulf coast -- than on said part of the Atlantic coast, but the data available give no clear indications of this.

The maximum cross-section of inlets with considerable wave action is, usually found where the suspended load transportation is at its maximum, despite the fact that sediment load to some extent tends to increase the value of the stability shear stress. The decrease of τ_s caused by the wave action in the vicinity of the entrance, seems to be much more important.

The influence of wave action directly, as well as indirectly, on τ_s seems to be visible at some of the examples, as at Thyborøn Inlet on the Danish North Sea coast.

This inlet, cut by nature in 1862 and navigable a few years later, was continuously bothered by a big offshore bar with a controlling depth of only 10 ft. The bar was the result of heavy wave action and heavy littoral drift coming to the inlet entrance from both sides. About one million cu. yd. of sand material a year is transported into the inlet and deposited on extensive bay shoals. Fig. 4 shows the variation of the gorge of the inlet during the period 1887 to 1946. After 1892 important dredging operations were started on the outer bar and this factor is clearly reflected in the diagram as increasing cross-section. Since it became difficult to keep up with the extremely heavy littoral-drift deposits, a different strategy was adopted later. Dredging was transferred to the bay shoals channels and is now done there entirely. The result has been that the controlling depth on the outer bar increased to 15 feet and is now at least 20 feet. Construction in the early 1920's of a 3,000-foot-long jetty (recently repaired and extended on the northern barrier at the inlet) further improved this situation.

The inlet channel gradually adjusted itself to the actual flow and "τ_s" situation. Fig. 4 indicates that the gorge area is below average size; and, taking into account the approximately one million cu. yd. of sand material carried each year through this cross-section for depositing on the inlet shoals, it seems likely that the stability shear stress has increased because of the heavy material load and possibly the accompanying changes in friction factor. Since the gorge has very steep slopes, the shape factor, as compared to other inlets, may also have improved.

In comparing the gorge Cross-section I, Fig. 4, with Cross-sections II and III situated closer to the entrance, some interesting tabulations will be noted in Table 2. Compare Table 2, where τ_s under medium concentration of sediment transport is 0.45 kg/m^2 , and remarks on the Eems Estuary, Holland later in this paper (Fig. 6).

The variation of cross-sectional area of improved inlet channels is dealt with in Fig. 5 where, for a number of inlets with parallel jetties, the cross-section has been plotted along the length of the inlet channel in a dimensionless diagram.

The cross-sections (A) at different locations have been divided by the cross-section at the entrance (A_o) to obtain a dimensionless ratio, using the relative distance from the seaward end (x/L) as second parameter.

From Fig. 5 it can be seen that the entrance cross-sections generally are greater than the cross-sections in other parts of the channel. The presence of wave action apparently has decreased the stability shear stres τ_s for the tidal currents because the orbital velocities of the wave action along the bottom of the channel increase the actual shear stress values, resulting in greater cross-sections near the entrance of the channel.

The importance of variation of bottom friction and its relation to sediment transportation is further elaborated in (6) which also includes some information on the influence of freshwater flow which it for space limitations is not possible to include here.

Average stability shear stresses determined from studies of existing data are given in Table 4. Limiting values for stable channels were mentioned in Table 1.

In practically all tidal inlets the median size of material as mentioned earlier is between 0.1 and 0.5 mm. According to Table 1 there is only a minor variation in the limiting shear stress for this range of grain sizes. The same will probably hold true for the stability shear stress τ_s. Taking 0.2 mm as a diameter for comparison, the limiting values for the shear stress for canals in fine noncohesive materials seem to range between 0.052 lb/ft^2 for light load and 0.078 lb/ft^2 for heavy load of sediment. The average stability shear stress for tidal inlets seems to range between 0.072 and 0.103 lb/ft^2 .

Special conditions may raise the τ_s value considerably above average. Computations for the Absecon Inlet, gave a τ_s value of 0.63 kg/m^2 (0.129 lb/ft^2) for spring tide conditions. This figure is high but littoral drift is very heavy at Absecon Inlet--probably exceeding 500,000 cubic yards per year--and bed-load as well as suspended load transport through the inlet channel is high.

This is further elaborated in (6). The movable stability of inlets as compared to the absolute stability desired at certain canals are also dealt with in (6) with reference to Bretting's (2) and Lane's theories (15).

Estuaries are inlets with a river or waterway discharging through the inlet. In case the amount of head flow passing through the estuary is so small that its influence on the vertical distribution of flow velocity is only minor the tidal hydraulic aspects of the inlet stability can be handled as with normal tidal inlets in alluvial materials. An example of an estuary is the entrance to River Eems at the border between Holland and Germany. In 1952 an extensive program of investigation was

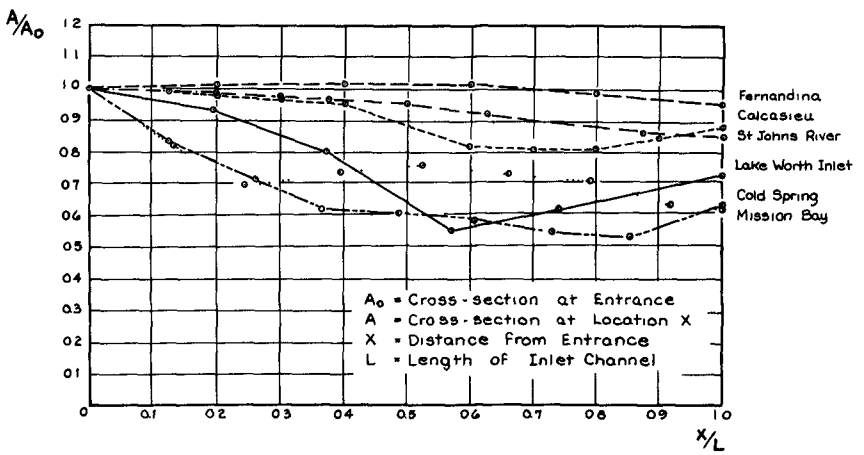

Fig. 5. Cross-sectional areas below M.L.W. for some jetty-improved inlets.

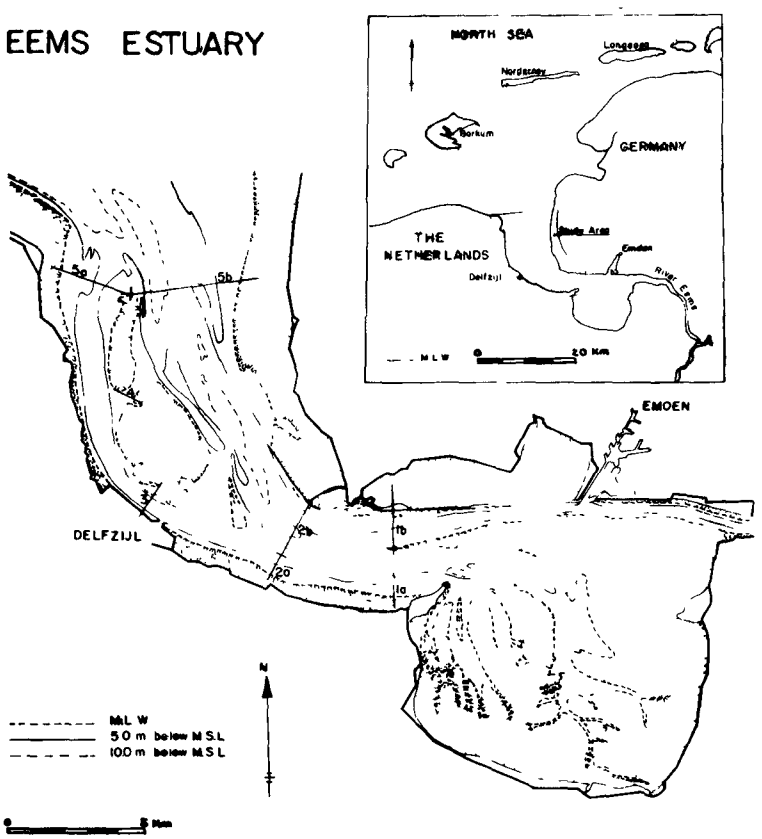

Fig. 6. The Eems Estuary, Holland.

undertaken by the Dutch "Rijkswaterstaat" to obtain information leading to the improvement of the estuary for navigation. Reference is made to (10).

The study included the following items:

a. Velocity measurements in the lines, indicated 1a, 1b,... through 5b in Fig. 6. Measurements were taken in every profile simultaneously in 5 to 8 locations. The vertical velocity distributions were determined by an Ott propeller-type current meter at 57 locations, which allowed rather precise determination of flow quantities and distribution of flow. Fig. 6 shows computed values for the maximum flood and ebb flow plotted against the profiles surveyed at the same time.

b. Measurements of sand and silt content. Samples were taken at the surface, about 1/2 ft. from the bottom and about 1/3 of the depth from the bottom. Silt and sand concentrations were highest in line number 1. The shallow tidal bay called "Dollart", east of line 1, with extended mud flats, is responsible for this. Measured values of maximum concentrations (volume-ratio) in line 1 near the bottom are:

Sand	7.6×10^{-4}
Silt	64.0×10^{-4}

In lines 2 through 5 the respective concentrations were much less. For sand and silt the maximum concentration near the bottom varied between 0.6×10^{-4} and 4.4×10^{-4} in volume ratios.

c. Bottom samples were taken at the velocity measurement point. Table 5 shows values for d_{50} (diameter for 50% finer).

The information obtained seemed to be useful for examination of the stability of different bottom profiles.

Fresh-water discharge probably will play only a negligible part in the stability conditions; only in line 1b and possibly, in 1a, may it have some influence. During the period of observations river discharge amounted to 2 million m^3 during a flood or ebb period, which is a very small quantity compared with the tidal prism which amounted to 83 million m^3 during ebb tide under average conditions in line 1b. For line 5b a tidal prism of about 300 million m^3 under average flood conditions has been determined.

Re a The solid line in Fig. 7 indicated the relationship:

$$A = \frac{Q_m}{C\sqrt{\frac{\tau'_s}{\rho g}}}$$

τ'_s is the stability shear stress referring to mean tide conditions. As in Figs. 2 and 3 a variable C value has been introduced according to: $C = 30 + 5 \log A$ (metric system). Fair agreement obtained between

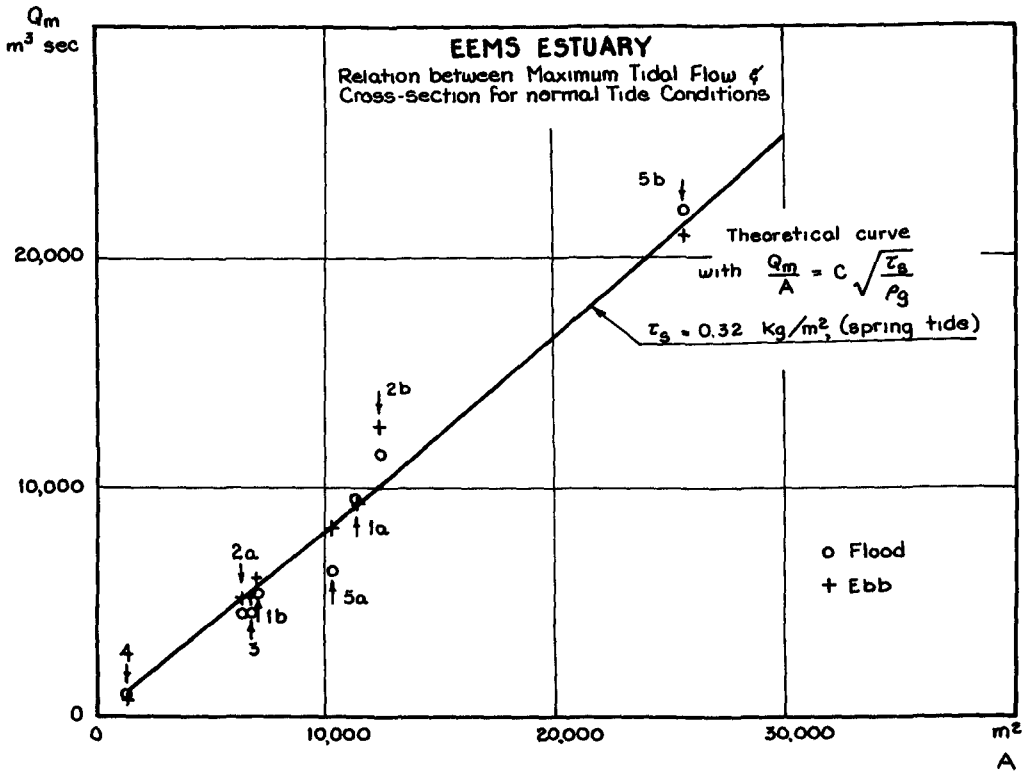

Fig. 7. Relation between maximum tidal flow and cross-section of Eems Estuary, Holland, for normal tide conditions.

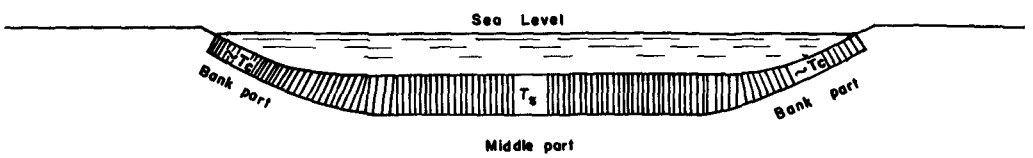

Fig. 8. Relative allowable shear stress for a tidal inlet cross-section.

observations and stability shear stress hypothesis is valid for mean range of tide conditions.

$$\tau'_s = 0.264 \text{ kg/m}^2 \quad \text{or} \quad 0.0534 \text{ lb/ft}^2$$

A constant value of τ'_s for this area seems reasonable because material load conditions are similar and the grain size of the material does not show much variation.

In order to compare the τ'_s value for the Eems with the τ_s values of Table 4 , the Eems value must be converted into spring tide conditions For this particular area of the North Sea coast, flow values during sprin; tide are about 10 per cent higher than during normal tide conditions. Because $\tau \sim v^2$, the value of τ_s for spring tide conditions will be $\tau_s = 0.264 \times (1.1)^2 \text{ kg/m}^2 = 0.320 \text{ kg/m}^2$ (or 0.0653 lb/ft²). Because of the sheltered location of this area (no or little wave action) this figure is considered close to a minimum value ror τ_s (ref. Table 4).

In comparing the individual experimental data with the average curve it is seen that most of the individual plottings coincide rather well with this curve. Meanwhile, the profiles No. 2b and 5a show some remarkable deviations. The following may be a possible explanation for those deviations:

It is known from the investigations that profile 2b has a relatively high sediment load. This means higher stability shear stress and comparatively smaller cross-section. A favorable shape factor may also lead to a higher value of τ_s.

In many profiles there is no significant difference between ebb flow and flood flow, but the situation is different in line 5a for which the maximum flood flow is considerably lower than the maximum ebb flow. Profile 5 a is a typical (so-called) "ebb-channel" in which the ebb currents dominate the flood currents. In this case the plotting for the maximum ebb flow fits the average curve; for the maximum flood it does not. This may lead to the conclusion that where either the ebb or the flood current dominates, the predominant current will determine the size of the cross-section profile with its characteristics of silt and material load.

Section 5.6 of reference (6) gives information on some very interesting comparisons by the suthors with some results of Leopold and Maddock's studies of the geometry of stream channels and some of its physiographic implications. The relationship V_m = constant $Q^{0.1}$ or A = factor x $Q^{0.9}$ is confirmed and compared to Bretting's theory which also has $A \sim Q^{0.9}$ (2)

THE RELATIVE STABILITY OF TIDAL INLETS

The problem of stability of an inlet can be considered in the "horizontal" as well as in the "vertical" plane. Horizontal (or location) stability is dealt with in (6). Speaking about the cross-sectional stability this problem can be said to include two kinds of stability:

the material transfer "stability" or "ability" and the cross-sectional stability described in this paper.

Material transfer stability is described by the authors in (5) and (6) which distinguishes between two different kinds of material transfer across inlets: bar-bypassing and tidal flow bypassing. If the predominant littoral drift (M_{mean}) is expressed in cubic units per year and the maximum tidal flow under spring tide conditions in the same cubic units per sec. (Q_{max}), by-passing may be described by the

$$\frac{M_{mean}}{Q_{max}} = r \quad \text{factor.}$$

Analysis demonstrated that:

with $r > 200 - 300$ we usually have bar by-passing

with $r < 10 - 20$ we usually have tidal flow by-passing

The mechanics of the by-passing and man-made influence on it is dealt with more detailed in (5) and (6).

In regard to the cross-sectional stability the relative "degree of stability" as mentioned earlier is tentatively expressed as follows:

$$\text{Stab} = F\left(\frac{\Omega}{M}, \frac{Q_m}{M}, \tau_s\right)$$

where the factors Ω, Q_m and τ_s are interrelated and depend on inlet and bay geometry, character of bottom soil, material load, and wave conditions. Of these factors, M may not vary much with long-range time, while Ω, Q_m and τ_s most likely will vary from the moment an inlet is "born" until it develops "full-size" and stabilizes itself before deterioration. This period may be a matter of decades or centuries and it therefore seems allowable to speak about a "number of stability solutions" which have varying degree of actual stability. It should also be remembered that the (spring tide) values of Ω and Q_m may fluctuate somewhat due to variation in tide characteristics.

Upward, the number of these stability possibilities is limited by a certain maximum tidal prism whereby for small bay areas the tidal range in the bay or lagoon equals the tidal range in the sea. The gorge cut in alluvial material will then assume its maximum size, while the actual value of τ_s will depend upon material, littoral drift and other factors as discussed earlier in this paper. Downward, the number of solutions is limited by a minimum cross-sectional area which is determined by certain minimum values of Ω/M and Q_m/M. Anyone who has worked with problems of "choking inlets" on littoral-drift coasts (5) knows that a newly opened or a natural break-through inlet is bound to close again rather soon unless the channel has attained a certain minimum cross-sectional area.

The value of τ_s may also be considered descriptive in the actual stability situation. Relatively higher values of τ_s may indicate good flushing action, and, thereby, better stability conditions. Contrarily,

lower values of τ_S may indicate less cleaning ability of the inlet flow and beginning or advancing deterioration of the inlet channel, perhaps associated with an uneconomical shape of cross-section (bad β- factor).

It is difficult to give specific values for the relative stability of inlets; to do so requires detailed knowledge about the time history of the inlet gorge, and such information is usually not fully available. Table 6 gives information concerning several tidal inlets for which we have some idea about the Ω/M and Q_m/M ratios from many years of deposits and dredging operations undertaken because of the importance of these inlets to navigation.

Considering first the Ω/M ratio the tidal prism Ω represents the total amount of flow passing through the inlet during one half tidal cycle. For the greater part of the time this flow is able to transport material and to clean the inlet of "surplus deposits".

In Table 6 the values of Ω/M are listed together with Q_m/M values and computed values of τ.

Keulegan's (14) expression:

$$\Omega = \frac{Q_m T}{C_2 \pi}$$

relates the tidal prism Ω to the coefficient C_2, the maximum discharge Q_m and the length of the tidal period T.

The value of C_2 generally deviates less than 20% from unity. The tidal period T may correspond to semidiurnal or diurnal tides.

For inlets with semidiurnal characteristics the yearly average value of M is used to compute the ratio Ω/M. For similarity reasons the factor for inlets with diurnal tide characteristics should then be computed as $\sim \Omega/2M$, because the length of the tidal period for diurnal tides is approximately twice as long as for semidiurnal tides. This has been considered by computing the Ω/M values in Table 6 and the comparisons made based on Ω/M values.

Consideration of the characteristics of the inlets listed reveals tha those having a ratio Ω/M in excess of 300 have a higher degree of stabilit Inlets with Ω/M ratios <100 seem to belong to that category which have a more predominant transfer of sand on (shallow) bars or shoals across the inlet entrance and less significant tidal currents; for this reason they may be rather unstable and are usually characterized by one or more narrow, frequently shifting channels with high velocity through shoals with shallow water as described in (5).

It is not possible to say where a transition ratio of Ω/M between stable and unstable inlet channels may lie because irregularity in quantit as well as in direction of the littoral drift will likely make it impossible to establish such fixed ratio. Some inlets still have a fair stabi-

lity for Ω/M ratios of 150 - 200, e.g., the Thyborøn Inlet, Denmark, which has to be dredged somewhat on its bay shoals. Compare Fig. 4 which shows the variation of the gorge of Thyborøn Inlet. Before 1910 the Ω/M ratio was < 100 and at that time dredging had to be carried out continuously on the outer bar. After 1910, when the Ω/M ratio was > 150, dredging on the outer bar became unnecessary; but as mentioned earlier some (minor) dredging operations had to be and are still being carried out in the bay channels and on the bay shoals where material carried through the inlet is deposited by the flood-currents.

In regard to the ratios Q_m/M mentioned in Table 6, the following can be said.

It is well known that only a certain (usually unknown) fraction ΔM of the longshore littoral drift M enters the inlet channel itself. The relation $\Delta M/M$ is not constant but assuming a certain similarity in inlet behavior we may expect that the relation M/Q_m (or Q_m/M) has an influence upon the stability shear stress values.

Table 6 suggests that Q_m/M ratios > 0.01 averagely present a more stable situation than ratios < 0.01.

The stability shear stress τ_s refers to the maximum tidal flow under spring tide conditions. If tide conditions were the same for all inlets considered an equal τ_s would result if all other conditions were equal. In this study inlets with quite different tide characteristics were used and this inevitably leads to local deviations in the stability shear stress.

Values for the stability shear stress were computed for various inlets according to the relation:

$$\tau_s = \rho g \frac{v_m^2}{C^2}$$

whereby v_m is the maximum value of the average current velocity during spring tide conditions, and C the Chezy coefficient.

Uncertainties in the values of v_m as well as C are introduced into the formula in the second power so that a very close determination of τ_s for most of the inlets studied was not possible. The effects of this are demonstrated in relatively strong variations of the τ_s values as indicated in Table 6. The large scale tendency of τ_s is indicated in Table 4.

Fortunately the lower limit of τ_s could be approached in the case of the estuary of the Eems as mentioned earlier in this paper.

The above should be remembered when considering some details on τ_s values included in Table 6, which is further developed in Tables 7 and 8, wherein Ft. Pierce Inlet (Florida), Averio and Figueira Da Foz Inlets (Portugal), and Gasparilla Pass (Florida), are omitted; Ft. Pierce Inlet because of some rock formation in the inlet channel; Averio Inlet

because its improvement by jetties was only completed in 1958 and experience is insufficient; Figueira Da Foz and Gasparilla Pass because they--as demonstrated by their τ_s values--- are in an unstable condition.

From Tables 7 and 8 it is apparent that large inlets, such as some of the big Dutch inlets and those like Grays Harbor, Washington, are characterized by an average τ_s value of about 0.46 kg/m^2 (0.094 lb/ft^2) with $\Omega/M \geq 600$ or $Q_{max}/M \geq 30 \cdot 10^{-3}$. Inlets with a more modest flow activity as compared to the littoral drift quantity, such as the minor Dutch inlets, Longboat Pass, Florida, and the diurnal type inlets on the Gulf of Mexico have τ_s values averaging about 0.50 kg/m (0.102 lb/ft) with $150 < \Omega/M < 600$ or $10 \cdot 10^{-3} < Q_{max}/M < 30 \cdot 10^{-3}$. The slight tendency towards increase may be explained in the way that littoral drift deposits are encroaching upon the inlet channel at these inlets partly improving its shape factor and partly increasing material movement both, in turn, increasing the τ_s.

Inlets with a still lower flow over littoral drift value, such as Big Pass and Ponce De Leon Inlet, Florida, and the now dredged Mission Bay, California, have an average τ_s value of about 0.51 kg/m^2 (0.104 lb/ft^2) with $\Omega/M \leq 150$ or $Q_m/M \leq 10 \cdot 10^{-3}$. There may be a tendency toward increased concentration of currents in the gorge caused by littoral drift deposits which the currents may have trouble keeping up with. Inlets within this group all have considerable bay and/or sea shoals.

Comparing the values of Tables 7 and 8 with the values of Table 1 it is also interesting to note that the most important difference apparently lies in the definition of "stability". While Russian standards indicate "critical" tractive forces in 0.2 - 0.5 mm material of about 0.15 kg/m^2 (0.03 lb/ft^2), Schoklitch, who recommends 0.39 kg/m^2 (0.08 lb/ft^2) for canals in fine sand, apparently counts on material movement and thereby on a unidirectional "rolling material carpet" (Fig. corresponding to the two-directional "rolling carpet" at littoral drift inlets. In the unidirectional canal flow there is no pouring in of materials from the sides, as with tidal inlets on littoral-drift shores, which may contribute to a "raise" of τ_s from about 0.39 kg/m^2 (0.08 lb/ft^2) in canals to about 0.50 kg/m^2 (0.103 lb/ft^2) at tidal inlets on littoral drift shores.

The τ_s values for tidal inlets mentioned above still refer to the maximum discharge Q_m during spring tide conditions which theoretically only occurs for a few seconds or minutes every half tidal cycle, but in practice may run for 2-3 hours. It is apparent, however, that it is the maximum velocity (and shear stress) which at tidal inlets determines the cross-sectional area which does not adjust itself to any lower value of τ_s, but leaves surplus cross-sectional area for lower velocities and quantities of flow. (Compare the Eems estuary) Because material movement almost stops at velocities lower than 1 ft/sec it would be of less

physical significance to relate the stability shear stress to an average stress over a tidal cycle.

Comparing this situation with the situation at rivers it can be said the difference lies in the time history. A river normally has ample time to adjust its cross-section to a given flow; inlets are "short of time" and tend to follow the most frequent "extremes" (peak tides).

DESIGN OF TIDAL INLETS ON A LITTORAL DRIFT SHORE

Experience has demonstrated that we are coping with a problem which involves many variables. These variables can be combined in different ways. Based on our present knowledge it is not possible to give a univalent answer to any particular problem.

However, under the assumption of noncomplex boundary conditions for a given "desirable cross-section" of simple geometrical shape, we can evaluate the size of the tidal flow necessary to keep this cross-section fairly stable, taking into consideration the actual situation of tides, bottom material, littoral material, suspended load, and different determining friction elements. If the required amount of flow is available, the desired combination of tides, bay, and inlet characteristics can be secured. Tidal hydraulics computations are necessary since they give the relationship between flow and inlet characteristics. Regime considerations determine which of the different possible combinations will produce the most "stable" condition.

Certain data are available for use in the "preliminary design". The design is usually based on average conditions, and nature does not always respect the "mean". Heavy storms may pour littoral-drift deposits in the inlet channel regardless of how ideal and well designed its cross-section and configuration are. Consequently, with little notice the inlet may be forced into a new situation where the tidal flow capacity will change because of the decrease in cross-sectional area. Luckily such littoral-drift deposits are almost never distributed equally over the inlet bottom but will usually accumulate at one side (often on the inside of the updrift jetty). The result may be a concentration of flow which tends to remove (shave off) the deposit. If bed-load material from the littoral drift is furnished to the shoal at a rate which makes the inlet currents unable to wash the deposit away, these deposits will have to be removed by dredging; otherwise, the inlet may close. Model experiments may indicate that such a situation can be taken care of partly or wholly by a design which gives the entrance an "intelligent shape" for cleaning of deposits. If the inlet is of considerable size and has the right configuration in the horizontal as well as the vertical plane, the condition may develop in which depositing occurring at any flood tide is washed away at any following ebb tide because the cross-section allows the inflow of enough water to provide ample flow for adequate cleaning. However, apart from special cases such as the lagoon harbor at Abidjan on the Gold (West) Coast of Africa, such a condition may not persist because the material removed by the ebb current might be so deposited in front of the inlet that the resistance against the inlet flow will gradually increase; and the

inlet, left to itself, may finally deteriorate.

The important factors which have to be considered for any inlet design are:

1. Size of the inlet gorge A, compared to the tidal prism Ω and maximum discharge Q_m

2. Geometrical shape of the inlet channel

3. Design shear stress

In order to secure a stable inlet a certain amount of tidal flow is necessary, which means Ω and Q_m of proper magnitudes as compared to the total littoral drift M at the inlet entrance. Q_m and Ω for a given inlet geometry can be determined by tidal hydraulics computations (7, 14). If a Ω/M ratio > 200 is not obtained the inlet probably will not develop the desired stability as explained earlier.

For the actual dimension of the inlet, requirements of navigation will establish the lower limits for the cross-sectional area. This limit may be satisfactory if it presents a reasonable Ω/M (and/or Q_m/M) ratio. If it does not, other problems than that of stability may be created simultaneously in the bay or lagoon, such as floods caused by too slow discharge of heavy rains, stagnancy, and problems of marine biology nature. The fish-killing "Red Tide" on the Florida lower Gulf coast has better opportunities for development in areas with insufficient exchange of water between the area and the open sea.

If, because of problems of stagnancy for example, it is necessary to increase Ω, no problems other than those of an economic character may exist. From the hydraulic standpoint the inlet's stability will be improved by increasing Ω. The situation is different if, because of danger of flooding from the sea, it becomes necessary to decrease Ω below the desirable value for obtaining a satisfactory Ω/M ratio for stability. In such case provision must be made to secure the highest possible utilization of the available Ω and to minimize or equalize M to avoid high peaks of drift deposits which cannot be absorbed by the available sand traps and flow quantities.

A higher utilization of Ω can be obtained by securing the best possible distribution of flow in the inlet, which means the most advantageous distribution of τ over the cross-section. Proper jetties and "canalization" of the inlet may secure the desired result. If the decrease in Ω (still considering a practical Ω/M ratio), cannot be obtained in this way, it is possible, to decrease M materially by "sand traps", possibly arranged as a bypassing sand plant permanently installed or by a continuous dredging arrangement. Ultimately it may be necessary to decrease the cross-sectional area of the gorge beyond the stable condition for loose sand bottom, thereby inviting erosion by high current velocities. In order to avoid such erosion it may be necessary to provide the bottom with a protection layer, which may be rock or specially built mattresses,

or nylon or plastic sheets loaded down or otherwise fastened to the bottom. Undesirable high-tide velocities can also be avoided by making the channel (very) long and/or providing it with friction arrangements. Often it is also necessary to protect the bottom of canals against currents caused by ships or ship screws. Velocities above 4 - 5 ft/sec are usually not desirable for reasons of navigation, and if maximum velocities are expected to exceed 5 - 6 ft/sec it may be necessary to take more radical measures, e.g., cutting off part of the tidal bay area if the configuration of the bay is such that it can be done without unreasonable expense. A cut-off dam, however, may raise a number of questions such as the establishment of sluices or other regulating works. The easiest thing, therefore, may be to build sluices in the inlet itself. This method offers various advantages such as better navigation conditions in the inlet inside the sluices, no necessity for bottom protection, no floods from the sea, and little or no sand deposit on bay shoals. Furthermore, such "closing" of an inlet may improve beach erosion conditions on the seashore (3). The disadvantages include an unstable inlet entrance subject to accretion, delays to navigation, and deposits on the seaside of the sluices which may cause difficult and costly dredging operations in improving navigation conditions and possibly the necessity for expensive longer jetties to protect the inlet from excessive littoral deposit. Economic analysis of the problem as a whole, however, may still justify such measures. The Netherlands presents a good example of such project at Ymuiden, the seaport of Amsterdam with the world's largest navigation locks.

An inlet channel should always be designed with a cross-section of simple geometrical nature, usually trapezoidal or rectangular, depending upon the structural character of the improvement itself. The question is how cross-sections should be designed when most stability is desired.

In practice one is usually faced with two situations--the construction of a new inlet, or the improvement of an existing one. Special requirements in regard to navigation necessitate certain dimensions and a certain shape and alignment of the navigation inlet. For navigation reasons, maximum peak current velocities as mentioned above should possibly be kept below 4 - 5 ft/sec; for stability reasons the shear stress at the bottom should be commensurable to the stability τ_s which depends upon the shape of the cross-section as well as on soil conditions, material load, wave action and possibly head flow.

A straight inlet channel is mostly to be preferred for reasons of navigation. Meanwhile, the entrance area may for reasons of littoral deposits have to be curved and it is moreover an experience that a curved (or slightly meandering) channel where the designer has a better chance of determining the flow pattern--instead of letting nature do it--is preferable.

Establishment of a proper design shear stress τ_s under the actual conditions corresponds to the establishment of rather the "ultimate strength" than the "allowable strength" in the field of solid mechanics in as much as we have to count on a material movement on the bottom of the inlet as a necessity in order to keep a certain cross-sectional area. The τ_s should not increase beyond this value.

The stability shear stress τ_s under the actual conditions of soil, material-load, wave action and possibly head flow, is mentioned. Values have been obtained which can be used as a guide for preliminary design. The composition of bottom material and the relative amount of littoral drift may be of considerable importance as in determining a proper τ_s. (Table 4) In inlets with only light littoral drift the smaller fractions of the bottom material may be carried away, leaving comparatively coarser particles behind. Compare the situation in canals and channels.

The finer particles will usually be deposited in bay shoals. In inlets with considerable littoral drift, bottom material under "calm weather conditions" may correspond to the material at similar depths on the seashore, while under or after more extreme current conditions the material may tend to be a little coarser because of selection by the currents. Badly sorted material on the seashore may eventually cause the inlet bottom to be composed of coarser material than the average on the seashore.

The tidal flow, released from its content of finer material on the bay shoals, will return to the sea in "purified condition" and may cause a higher shear stress at the bottom which will carry mainly finer particles seaward, away from the inlet channel. This means that the design shear stress for the inlet channel may often correspond to this ebb tide situation, which in turn may result in a slightly larger cross-section than that corresponding to flood flow.

Table 1 mentioned earlier, indicates the variation in τ_s because of grain size to be of limited importance. Supply of littoral drift to the entrance is apparently a more important factor because it brings suspended and bed material load into the tidal currents which may change friction characteristics of the flow as well as bottom roughness parameters. Heavy littoral drift is almost always connected with heavy wave action and the influence of the same amount of littoral drift on the inlet stability increases with relatively decreasing flow capacity of the inlet. In this connection it should always be remembered that it is the total quantity of material brought into the channel (from both sides) that counts, not the resultant predominant drift in one direction.

Based on the results of this study the average values shown in Table 4 for the stability shear stress seem to be useful as a first approach and guidance to the design.

As mentioned earlier in this paper, a shape factor depending upon the actual form of the cross-sectional area should always be considered in connection with a proper τ_s. In case of narrow and deep inlets the τ_s values above may be raised 10 to 20 per cent.

Summarizing the above mentioned proper practical approach to the design problem may be outlined as follows:

(a) A proper cross-section and the general channel alignment is determined by considering navigational requirement. The channel length is estimated by practical considerations.

(b) Preliminary computations of Q_m and Ω are then carried out based on a proper average τ_s value. Q_m/M and Ω/M ratios are considered as explained above.

(c) Isovels are then constructed, e.g., according to theories by Lane (15) or Olsen and Florey (18) for the entire cross-section including the bank part which amy be designed as nonerosive by trial and error using, e.g., Bretting's theory (2) as a guide.

In this connection careful consideration should be given to the difference between the "stability" shear stress τ_s to be used for the horizontal bottom part and the "critical" shear stress τ_c to be used for the bank part. (Fig. 8)

In regard to values of τ_c, see reference (15). Practical average τ_s values are listed in Table 4.

(d) After adjustments have been made for a "final cross-section", detailed tidal calculations including determination of actual Q_m, Ω, and τ values are carried out (7, 14). Those computations in combination with "regime-considerations" will tell at what length of the inlet channel a stable condition is obtained wherein the stability shear stress will be reached (but not exceeded) under the conditions given. The Ω/M and Q_m/M values are then checked again and if the channel length obtained in this way is too long, correction may be possible by decreasing the cross-sectional area of the inlet and/or by friction arrangements although this procedure may involve some adverse effects on navigation as well as on economy. If the calculated channel length is too short, the channel can be extended to a practical value by a corresponding increase of the cross-section. In some cases the length of the inlet channel will be given and the cross-section will then depend solely on boundary conditions such as tides in the ocean, bay geometry, and stability shear stress for the given material.

Every change in cross-section will require drawing of now isovels, corresponding adjustments according to given τ_s and τ_c values and, finally, repetition of tidal computations.

If the inlet cross-section is improved by man-made structures such as jetties, the design procedure of drawing isovels should also be followed. In some cases, and particularly when rubble mound (rugged) jetties are considered for the improvement of the inlet, some difficulties will be involved in determining the isovels in detail by theoretical methods. In such cases model experiments will be of great value. Meanwhile, it must be remembered that the determining shear stresses can be increased by proper channel bottom protection and friction arrangements. This can be investigated in detail by model experiments. Here the design cross-section should first be tested with fixed bottom in order

to compare the estimated discharge with the model flow; next, the tests should be run with proper bed material, e.g., perspex sand, baklite or gilsonite (siltation test). It can then be determined whether the flow will tend to create major irregularities in τ distributions, causing shoaling and/or erosion which require proper changes of its area and/or shape or protective measures on the bottom.

The contraction of inlet flow at the entrance as well as in the bay should also be taken into consideration. Reference is made to French's progress reports (9) dealing with the velocity distribution in tidal entrances. The part of the inlet cross-section outside the contraction zone is useless for flow and should not be included in the calculations. Through proper entrance design those deadpockets caused by the contraction can be partly or wholly eliminated.

In dealing with problems of fresh-water outflow and density currents special attention must be paid to the new conditions; depending upon the degree of changes in flow and velocity patterns, it should be determined whether a thorough model study based on detailed and accurate field surveys is essential to obtain a reliable picture of the flow conditions useful for design.

CONCLUSIONS

1. Investigations of existing data on tidal entrances in America, Denmark, Holland and Portugal have given considerable information of a general nature on the relationship between inlet characteristics.

While in earlier publications on this subject (4, 17) the tidal prism had been used to characterize flow conditions of the inlet, in this publication the maximum rate of flow per second during the tidal cycle Q_m has been used to describe the relation between flow and other inlet characteristics. Analysis demonstrated that Q_m is a better parameter than the tidal prism because the flow is directly related to the velocity and the latter to the bottom shear stress, τ, considering cross-sectional geometry.

2. The Ω/M ratio seems to be adequate for description of the actual "degree of stability". Investigations indicate that Ω/M ratios < 100 should be avoided and that ratios $\Omega/M > 200$ are preferable for inlets in sand material. The corresponding Q_m/M value should be >0.01 if possible.

3. The shape of the cross-section and the stability shear stress τ_s seem to be important factors for gorge stability considerations. Every new inlet to be dredged or any existing inlet to be improved by dredging or by jetties will probably be provided with a cross-section of simple geometrical shape, trapezoidal or rectangular. For this reason further studies, particularly those concerned with securing data useful for design, should be concentrated on the determination of τ_s which can be considered as a function of several variables. The most important

are: shape of cross-section, soil conditions of the bed, sediment load, wave action, littoral drift, and fresh-water discharge.

The suggestions for design of new inlets or improvement of existing inlets are based mainly on shear stress considerations. Shear stresses should be determined by drawing isovels for the flow. Use of the stability shear stress τ_s is recommended for the middle (horizontal) section of the channel and critical shear stress τ_c for the bank or slope part. Shear stress in the connecting part should increase from τ_c to τ_s.

Analysis of actual inlet data indicated an average value τ_s = 0.50 kg/m^2 = 0.103 lb/ft^2 . Values useful for preliminary inlet design are given in Table 4.

In comparing the "stability shear stress" with Lane's "limiting shear stress" (6, 15) it is found that the stability shear stress for tidal inlets as defined in this paper is higher than Lane's recommended values for the limiting shear stress in the design of stable channels.

4. In the future efforts should be concentrated on studies of the Ω/M and Q_{max}/M relationships to actual inlet stability under a great variety of conditions, studies of littoral drift and flow distribution in inlet channels and its relation to inlet geometry and studies of τ_s and its relation to the pertinent factors involved in inlet stability. Special hydraulic equipment as described in (6) and radioactive tracing technique may be of great value in securing such results.

REFERENCES

1. Bendegom, L. van, "Considerations About the Principle of Coastal Protection", Report, Rijkswaterstaat, Netherlands (Dutch text), 1949.

2. Bretting, A. E., "Stable Channels", Acta Polytechnics Scandinavia 245, Copenhagen, Denmark, 1958.

3. Bruun, Per, "Coast Stability", Danish Technical Press, 1954.

4. _____, and Gerritsen, F., "Stability of Coastal Inlets", Journal of the Waterways and Harbors Division, Proceedings, A. S. C. E., Paper 1644, 1958.

5. _____, "By-Passing of Sand by Natural Action at Coastal Inlets and Passes", Proceedings, A. S. C. E., Vol. 85, Journal, Waterways and Harbors Division, December 1959.

6. _____, "Stability of Coastal Inlets", North Holland Publishing Company, Amsterdam, 1960.

7. Dronkers, J. J., "Tidal Computations on Coastal Areas", Proceedings, A. S. C. E., Vol. 85, Journal, Waterways and Harbors Division, March, 1959.

8. Einstein, H. A., and Chien, H., "Effects of Heavy Sediment Concentration near the Bed on Velocity and Sediment Distribution", University of California, M. R. D. Sediment Series No. 8, 1955.

9. French, John L., "Second Progress Report on Tidal Flow in Entrances-- The Velocity Distribution in the Jet Issuing from a Channel int< an Ocean or Lagoon", Report N. B. S. No. 1141, 1951.

10. Gerritsen, F., "Motion of Water on the Eems", Report, Rijkswaterstaat (Dutch text) 1954.

11. Glover, E. G. and Florey, G. L., "Stable Channel Profiles", Hydraulic Laboratory Report No. Hyd-325, U. S. Dept. of the Interior, 1951.

12. Inglis, Sir Claude, and Allen, F. M., "The Regime of the Thames Estuary as Affected by Currents, Salinity and River Flow", Proceedings, I. C. E., Vol. 7, 1957, p. 827-878.

13. Johnson, J. W., "Sand Transport by Littoral Currents", Proceedings, Vth Hydraulic Conference, 1953.

14. Keulegan, Garbis H., "Third Progress Report on Tidal Flow in Entrances", N. B. S. Report No. 1147, 1951.

15. Lane, E. W., "Design of Stable Channels", Proceedings, A. S. C. E., Vol. 120, 1955.

16. Leopold, L. B., and Maddock, T. L., "The Hydraulic Geometry of Stream Channels and Some Physiographic Implications", Geological Survey Professional Paper 252, 1953.

17. O'Brien, M. P., "Estuary Tidal Prisms Related to Entrance Areas", Civil Engineering, May 1931.

18. Olsen, O. J., and Florey, Q. L., "Sedimentation Studies in open Channels, Boundary Shear and Velocity Distribution by the Membrane Analogy", Structural Laboratory Report No. SP-34, U. S. Dept. of the Interior, 1952.

19. Schultz, Edward A., and Simmons, Henry B., "Fresh Water-Salt Water Density Currents, A Major Cause of Siltation in Estuaries", XIXth International Navigation Congress, Section II, Comm. 3, 1957.

20. Stommel, Henry, "The Role of Density Currents in Estuaries", Proceedings, Minnesota International Hydraulics Convention, 1953.

21. Vanoni, V. A., and Nomicos, G. N., "Resistance Properties of Sediment Laden Streams", Proceedings, A. S. C. E., Vol. 85, No. Hy5, 1959

22. Wicker, C. F., and Rosenzweig, O., "Theories of Tidal Hydraulics", Corps of Engineers, U. S. Army, Evaluation of Present State of Knowledge of Factors Affecting Tidal Hydraulics and Related Phenomena, Committee on Tidal Hydraulics Report No. 1, 1950.

Table 1

LIMITING VALUES OF TRACTIVE FORCES, RIVER AND CANAL FLOW (*)
NONCOHESIVE MATERIAL
(lb/ft^2)

Median size of material, in millimeters	DESCRIPTION OF WATER		
	Clear water	Light load of fine sediment	Heavy load of fine sediment
0.1	0.025	0.050	0.075
0.2	0.026	0.052	0.078
0.5	0.030	0.055	0.083
1.0	0.040	0.060	0.090
2.0	0.060	0.080	0.110
5.0	0.140	0.165	0.185

(*) From: "Standards for Permissible Non-eroding Velocities", Bureau of the Methodology of the Hydro-Energo Plan, Moscow, 1936.

Table 2

CROSS-SECTIONAL AREAS OF THYBORØN CHANNEL

Situation	Cross-section		
	I	II	III
m^2	5,000	5,500	8,000
yd^2	6,000	6,600	9,600
Material load per year	1 million cu. yd.	1 million cu. yd	1 million cu. yd.
Wave action	Light to moderate	Moderate	Heavy
τ_s	ab. 0.5 kg/m^2	ab. 0.4 kg/m^2	ab. 0.2 kg/m^2

Table 3

RELATION BETWEEN LENGTH OF INLET CHANNEL AND CROSS-SECTIONAL AREA BELOW MLW FOR SOME JETTY-PROTECTED INLETS

Name of Inlet	Length L (ft)	Width (ft)	Cross-sect. Entrance A_o (ft^2)	Cross-sect. at end of channel A_L (ft^2)	$\frac{A_o}{W} = h$ (ft)	$\frac{W}{h}$	$\frac{A_L}{A_o}$
St. Johns River	4,000	1,600	62,000	52,500	38.7	41.3	0.847
Fernandina	2,500	3,900	124,500	118,800	31.9	12.2	0.954
Mission Bay before dredging	3,800	920	11,900	7,400	12.9	71.3	0.621
Cold Spring	4,100	850	21,000	13,250	24.7	34.4	0.630
Calcasieu Pass	5,000	1,000	11,750	10,300	11.75	8.5	0.876
Lake Worth	2,200	800	21,200	15,150	26.5	30.2	0.715

Table 4

STABILITY SHEAR STRESSES FOR TIDAL INLETS
BASED ON SPRING TIDE CONDITIONS

Condition	τ_s(kg/m²)	τ_s(lb/ft²)
Heavier littoral drift and sediment load	0.50	0.103
Medium conditions of littoral drift and sediment load	0.45	0.092
Lighter littoral drift and sediment load	0.35	0.072

Table 5

GRAIN SIZES OF BOTTOM MATERIAL IN EEMS ESTUARY, HOLLAND

Line	Range d_{50} (μ)	Average d_{50} (μ)
1a	80 - 365	134
1b	75 - 145	102
2a	60 - 130	86
2b	82 - 153	112
3	65 - 115	83
4	88 - 120	104
5a	79 - 97	86
5b	112 - 205	164

Table 6

FLOW AND LITTORAL DRIFT CHARACTERISTICS FOR SOME INLETS

Inlet (Kind of Improvement)	* Tidal Prism cu yd/half cycle	Q_{max} Maximum Discharge cu yd/sec	M** Predominant Littoral Drift cu yd/year	$\frac{\cdot}{M}$ or $\frac{\cdot}{2M}$	$\frac{Q_{max}}{M} \times 10^3$	τ_s lb/ft^2 (kg/m^2)
Amelandse Gat, Holland (Bank stabilization on north side)	600×10^6	36,600	1.0×10^6	~ 600	37	0.103 (0 50)
Aveiro, Portugal (Jetties)	150×10^6	9,000[1]	$0\ 75 \times 10^6$	~ 200	12	
Big Pass, Florida (None)	12×10^6	700	$< 0\ 1 \times 10^6$	120	7	0 115 (0 56)
Brielse Mass, Holland before closing (Closed)	40×10^6	2,700	$1\ 0 \times 10^6$	~ 40	3	0.086 (0 42)
Brouwershaven Gat, Holland (Will be closed)	430×10^6	30,000	1.0×10^6	~ 430	30	0 111 (0 54)
Calcasieu Pass, La. (diurnal) (Jetties and Dredging)	110×10^6	2,600	$0\ 1 \times 10^6$	~ 550[2]	26	0 090 (0 44)
East Pass, Florida (diurnal) (Dredging)	60×10^6	1,720	0.1×10^6	~ 300[2]	1	0 111 (0 54)
Eyerlandse Gat, Holland (None)	270×10^6	19,000	1.0×10^6	~ 270	19	0 119 (0 58)
Figueira Da Foz, Portugal (Dredging)	20×10^6	1,200	$0\ 5 \times 10^6$	~ 40	2	0 049 (0 24)
Fort Pierce Inlet, Florida (Jetties and Dredging)	80×10^6	3,700	$0\ 25 \times 10^6$	~ 320	15	0.22 3) (1 07)
Gasparilla Pass, Florida (None)	15×10^6	900	$< 0.1 \times 10^6$	> 150	9	0 051 (0 25)
Grays Harbor, Washington (Jetties and Dredging)	700×10^6	48,000	1.0×10^6	~ 700	48	0 105 (0 51)
Haringvliet, Holland (Being closed)	350×10^6	25,000	$1\ 0 \times 10^6$	~ 350	25	0 070 (0 34)
Inlet of Texel, Holland (Stabilization of south side)	1400×10^6	115,000	$1\ 0 \times 10^6$	~1400	115	0.094 (0.46)
Inlet of Vlie, Holland (None)	1400×10^6	110,000	1.0×10^6	~1400	110	0 090 (0.44)
Longboat Pass, Florida (None)	30×10^6	1,400	$< 0\ 1 \times 10^6$	> 300	14	0 115 (0.56)
Mission Bay, California before dredging (Jetties and Dredging)	15×10^6	1,100	0.1×10^6	~ 150	11	0 127 (0 62)
Oosterschelde, Holland (Will be closed)	1400×10^6	100,000	1.0×10^6	~1400	100	0.084 (0.41)
Oregon Inlet, N. Carolina (Occasional Dredging)	80×10^6	5,100	1.0×10^6	~ 80	5	0 092 (0.45)
Ponce De Leon Inlet, Florida (None)	20×10^6	1,500	0.5×10^6	~ 40	3	0.098 (0 48)
Port Aransas, Texas (diurnal) (Jetties and Dredging)	65×10^6	1,900	0.1×10^6	~ 325[2]	19	0.098 (0.48)
Thyborøn, Denmark (Minor Dredging)	140×10^6	7,500	0.9×10^6	~ 160	9	0.10 (0.49)
Westerschelde, Holland (Some Dredging)	1600×10^6	115,000	1.0×10^6	~1600	115	0 092 (0.45)

** Total amount of littoral drift interfering with the inlet may deviate from this value if drift direction is not too predominant and/or the inlet is not improved.

* Spring tide

1) Increasing

2) $\cdot/2M$

3) Rock gorge

Table 7

AVERAGE τ_s VALUES AS A FUNCTION OF DIFFERENT Ω/M VALUES

Ω/M	≥ 600	$150 < \frac{\Omega}{M} < 600$	≤ 150
τ_s kg/m^2	0.46	0.50	0.51
τ_s lb/ft^2	0.094	0.102	0.104

Table 8

AVERAGE τ_s VALUES AS A FUNCTION OF DIFFERENT Q_{max}/M VALUES

$\frac{Q_{max}}{M}$	$\geq 30 \cdot 10^{-3}$	$10 \cdot 10^{-3} < \frac{Q_{max}}{M} < 30 \cdot 10^{-3}$	$\leq 10 \cdot 10^{-3}$
τ_s kg/m^2	0.46	0.50	0.51
τ_s lb/ft^2	0.094	0.102	0.104

CHAPTER 24

THE USE OF FLUORESCENT TRACERS FOR THE MEASUREMENT OF LITTORAL DRIFT

by

R. C. H. Russell
Hydraulics Research Station, Wallingford, England.

ABSTRACT

The paper is concerned with experiments, carried out by the Hydraulics Research Station, in an attempt to measure littoral drift along natural beaches. A preliminary laboratory experiment is described in which the dilution method was used to measure unidirectional drift along a model shingle beach, and in which the measurement was found to be reasonably accurate. A modified dilution method is described for use on beaches where the direction of the drift reverses from time to time; and there is then a description of how this method was used to measure the littoral drift along three shingle beaches on the coast of England. In one case it was possible to measure the drift by alternative means and so obtain a check on the accuracy of the method. An Appendix describes how some of the tracer materials were made.

INTRODUCTION.

A considerable literature has grown up over the last 5 years relating to the detection of the movement of sediments by tracers. Many of the experiments, which have been carried out in a great variety of countries, have been purely of a tentative nature intended merely to study the feasibility of using a new technique. Although all the experiments have shown that the technique is indeed feasible, and have been successful in that they have shown the general direction in which material was moving, it has always been found difficult to interpret the result in quantitative terms. The second generation of experiments, which one might expect to be concerned with quantitative measurements of sediment discharge, have not yet begun to appear in print.

Tracers have already shown themselves to be most useful in those situations where there is the greatest uncertainty about the movement

of sediments; where experiments have been justified if they merely revealed a trend in a particular direction. There are beaches for example along which there is doubt concerning the direction of the predominant drift and where a tracer experiment which revealed the direction of movement might be justified. On many beaches, however, the direction of the predominant drift is already known and a tracer experiment would be pointless unless it revealed the actual quantity of material in movement. It is to the solution of this problem, of how to measure rates of littoral drift along beaches, that this paper makes a contribution.

The tracers used for the work have been fluoresoent ones. They have been developed during the past year or so from ideas and techniques described by Zenkovitch (1) and his colleagues (2) at the Institutes of Oceanology and Organic Chemistry of the U.S.S.R. Academy of Sciences. There are, however, differences between the work described in the Russian literature and the lines along which the work at the Hydraulics Research Station is developing.

Whereas the tracers described so far have been designed to have a short life, and have been used to study the movement of material under conditions which last unchanged for only hours or days, the tracers developed at the Hydraulics Research Station are designed to last for a year or more and so enable measurements to be made of the littoral drift occurring over a whole year. Another difference is that whereas the Russian experiments have been concerned with sand, those at the Hydraulics Research Station have been mainly with shingle beaches.

THE DILUTION METHOD IN UNIDIRECTIONAL FLOW.

The simplest possible quantitative measurement that could be made, using a tracer, would be the measurement of the sediment transported along a channel by steady unidirectional flow, in the case where the sediment was all of one size. The easiest method to employ - the so-called dilution method - involves the injection of tracer into the channel at a known steady rate for a long time, followed by sampling of the channel bed downstream of the injection point. Downstream of the injection point the material on the bed will contain tracer material mixed up with ordinary bed material in the ratio q/Q; where q is the rate (mass per time) at which tracer is injected, and Q is the rate (mass per time) at which sediment is transported past the injection point. Accordingly, the sediment transport rate can be calculated if the injection rate q and the concentration C of tracer in the sediment are known. Q is simply q/C.

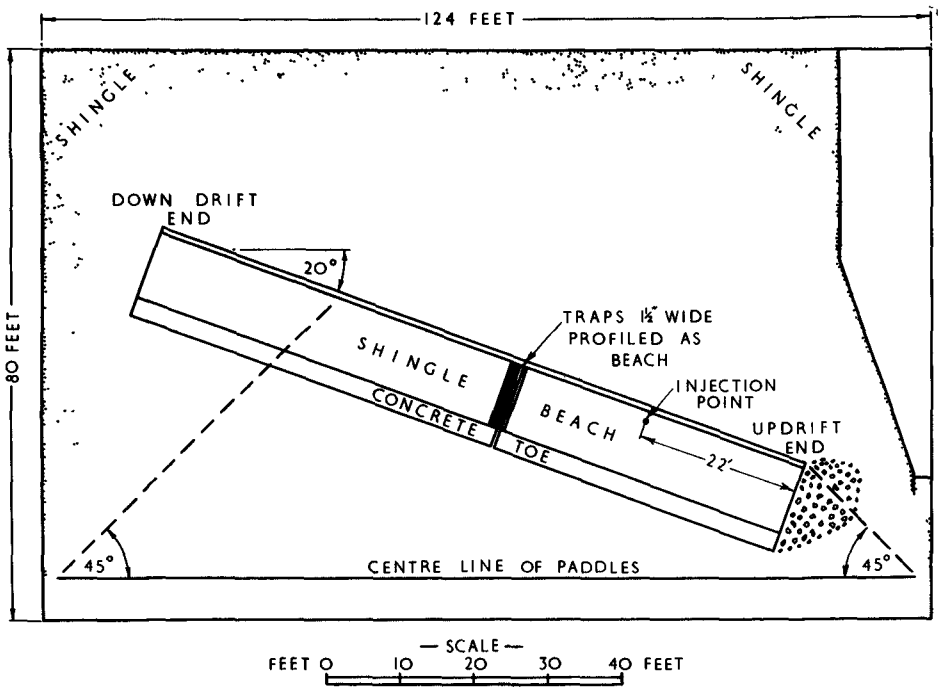

Fig. 1. Plan of the Model Shingle Beach.

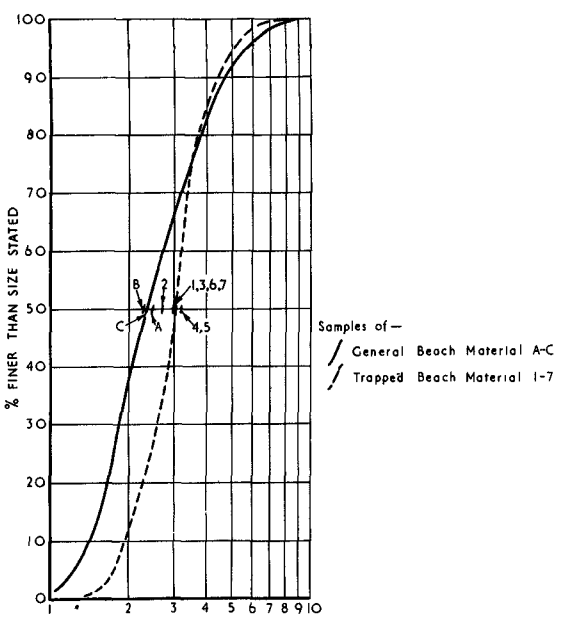

Fig. 2. Grading curves and values of d_{50} for shingle on the model beach, and for shingle caught in the traps of the model beach.

It is worth noting that the speed at which sediment travels does not enter into the calculation, nor does the width of the stream, nor the thickness of the sediment layer that is in motion.

A complexity would immediately be introduced into this imaginary experiment if the sediment were no longer all of one size. The complexity arises because the tracer material has to be typical of the material in transit i.e. it must have a particle size distribution typical of the material in transit; and the material in transit is likely to be different from the material lying on the bed. In this case it becomes necessary to trap and examine material in transit and to use the trapped material as a model for designing the correct tracer.

THE DILUTION METHOD APPLIED TO MEASUREMENT OF LITTORAL DRIFT ALONG A MODEL SHINGLE BEACH.

In order to find how accurate the method could be in favourable conditions, a model experiment was conducted, in which the littoral drift along a rather simplified shingle beach was measured by the dilution method and the result compared with the drift measured directly by catching it in traps. The beach was long and straight (as in Fig. 1) and consisted of fine stones described by the distribution curve shown in Fig. 2.

There are several differences between the conditions to which the model beach and a real beach would be subjected, many of them associated with the need to produce in the model a steady littoral drift. In this category was the ommission of any tides or reversing tidal currents from the model. The waves, furthermore, had an almost constant waveheight. There was indeed a small variation in waveheight of about 10% on either side of 2 inches, and a similar variation in the period, the cycle of which repeated every 4.7 minutes. The direction from which the waves came was held constant at 70° from the beach alignment.

The object of varying cyclically the characteristics of the waves was to cause periodic erosion and accretion of the beach and so to cause the surface shingle to mix with that in the lower layers. Had the beach been absolutely stable, the layer of shingle that was mixed with tracers might have been too thin, - only one stone thick for example - and then the method of measuring concentration, which involves counting visible tracer particles in situ, would have given false readings. All the simplifying conditions were designed to bring the processes of measuring the littoral drift by the dilution method almost to the simplicity found in the steady unidirectional case described above, but there is a major difference between the

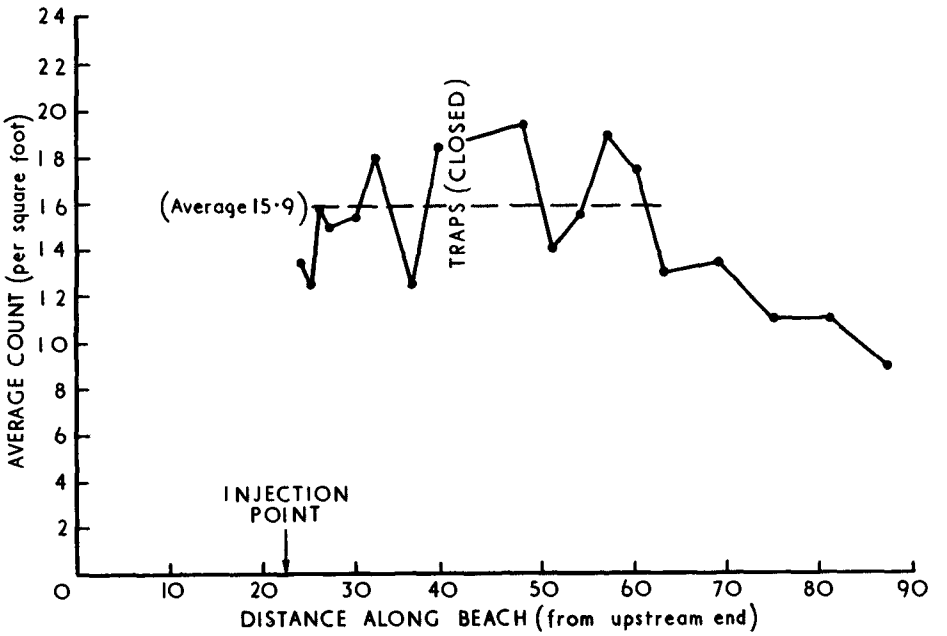

Fig. 3. Distribution of tracers, visible on the surface of the model beach.

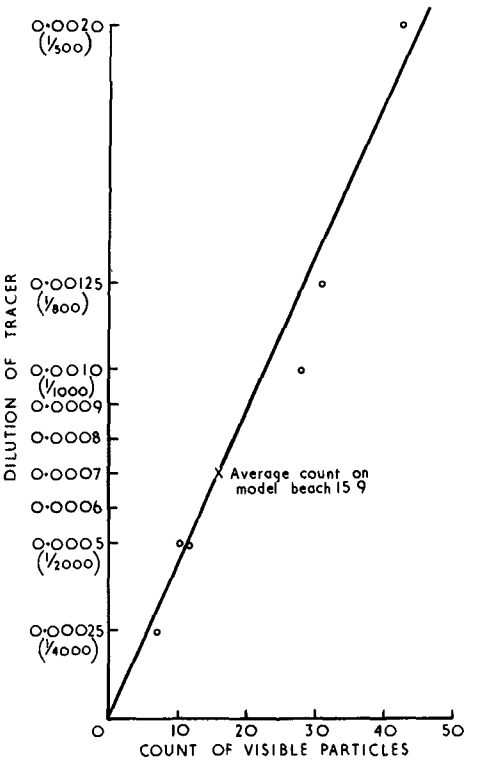

Fig. 4. Calibration test relating tracer particles visible per square foot to the proportion by weight of tracer in the in-situ beach material.

simplified shingle beach and unidirectional flow in a channel, to be found in the much greater sorting that takes place on a beach. On a beach the different grades of material are found on different contours, are subjected to different hydraulic forces, and are moved along at different speeds. In the model in question, for example, the finest material was found at the crest of the beach, while the coarsest particles stayed on the plunge-line.

The movement of different size fractions at different speeds along different contours should present no obstacle to the satisfactory working of the dilution technique provided:-

(i) The tracer material is typical of the material in transit.
(ii) That the tracer particles find their way to the contours that are appropriate to their size.

The first condition was satisfied in the simplified shingle beach experiment, by using as a tracer some material taken from traps in the beach and coating it by the process described in the Appendix.

It is inevitable, however, that if tracer is injected just casually on to the beach (as in this experiment it was), rather than placing the appropriate size fractions on appropriate contours that, for some distance along the beach, tracer particles will find themselves among particles of the wrong size and that their speed of travel will be different from that of beach particles of their size. Further along the beach the tracer can be expected to become properly sorted. Evidence that suggests this behaviour can be found in the results of the experiment.

Tracer was injected almost continuously at a point shown on Fig. 1 at a rate of 1/400 of a litre every three minutes. In the first experiment the tracer was injected for one hour, but a study of the beach revealed that the duration of the injection had not been long enough, in that there was not a sufficiently long length of beach along which the concentration of tracer was uniform. The figure required was the uniform concentration that would have been reached all along the beach, had the injection continued indefinitely; and this figure, in view of the scattered result was difficult to pick out.

Accordingly the experiment was repeated, this time with the injection continuing for two hours. The tracer was changed so as to avoid confusion between the two experiments, from Primuline which fluoresces blue to Eosine which fluoresces orange. The concentration of tracer at points along the beach is shown in Fig. 3, where the number of fluorescent particles visible per sq. ft of surface is plotted as a function of distance from the injection point. It can be seen that the concentration, expressed as counts per sq. ft., had not

reached its steady value at the down-drift end of the beach, but that it was roughly constant within 40ft of the injection point. It was assumed that the average count in this area - 15.9 per sq. ft - was the figure that would have been reached everywhere had the injection continued for a very long time.

Through the scatter of points on Fig. 4 one can possibly discern a lower figure for the counts close to the injection point than 20ft further from it. A likely explanation is that the tracers in this area had not yet been sorted and were not moving at a speed and along contours appropriate to their size.

In order to convert figures expressed as numbers of particles visible per sq. ft., into a concentration, one has the choice either of estimating the number of ordinary stones visible in a square foot from consideration of the particle size, or of carrying out calibration experiments. The latter course was in fact followed and the results are shown in Fig. 4. For making this experiment, tracers and stones were first mixed up in certain known concentrations, spread out in a layer at least 2" thick and examined for the number of visible tracer particles. Each mixing and counting was carried out three times, and the counts averaged. The best straight line through the averaged points has been drawn on Fig. 4. The steady concentration reached in the beach experiments can be found by referring to that corresponding in Fig. 4 to 15.9 counts per sq. ft. It is found to be .0007.

Therefore, the littoral drift can be calculated as

$$\frac{1}{.0007} \times \frac{1}{400} \times \frac{60}{3} \quad \text{litres per hour}$$

or 71.5 litres per hour.

The littoral drift was also obtained mechanically by trapping material, as it drifted along the beach, in two $1\frac{1}{2}$ inch wide slots, disposed as shown on Fig. 1. The measurement by traps and the measurement by tracer were carried out in different experiments but under conditions that were thought to be identical.

In three runs, which were each of 14.1 minutes duration; i.e. they each lasted for three whole wave period cycles, the trapped material amounted to 13.55, 13.13 and 13.99 litres, averaging at 13.56 litres. Accordingly the drift was

$$13.56 \times \frac{60}{14.1}$$

or 57.5 litres per hour.

The degree of agreement is encouraging. The lack of agreement, such as it is, is probably compounded of two main errors.

In the first place an error must be expected when using any method that involves the counting of randomly distributed particles. This error is shown in the Appendix to exceed 7% only once in every 10 similar experiments; and since the error in the result is about 20% there is likely to be another source of error.

The major error is probably due to the moving layer of shingle and tracer being undesirably thin. In the calibration test, by which the counts per square foot were related to concentration, some of the tracer particles that were visible were not on the surface but up to a particle diameter or so below the surface. One would, therefore, get the correct assessment of concentration on the beach only if the tracers were mixed down to a depth of one or two particle diameters. If only the surface layer was mixed one would underestimate the concentration by say 10% or 20%. Observations of the beach, when it was in movement, indicated that quite good mixing in depth was taking place on the upper beach but that on the lower beach where the waves broke, and to seaward, there was very little mixing in depth. Accordingly, there would have been an underestimate of the concentration and a corresponding overestimate of the calculated littoral drift. This is consistent with the results of the experiment.

A surprising feature of the results of the experiment was that the size of the material in transit was found, by analysis of the trapped material, to be coarser than the material of which the beach was composed. Typical size-distribution curves for the two materials are shown in Fig. 2 together with the values of d_{50} for a number of similar samples. This is in direct contrast to the behaviour of sediments in uni-directional flow. The explanation is that sorting moved the finest particles to the crest of the beach, where they were moved only by small hydraulic forces, and then only intermittently; while the larger particles stayed at the plunge-line and were subjected to the biggest hydraulic forces.

THE DILUTION METHOD. MOVEMENT OF MATERIAL IN TWO OPPOSITE DIRECTIONS.

In cases where the drift reverses from time to time owing to waves coming from different directions, tracer that is injected on a beach spreads out on both sides of the injection point, the greater part of it moving in the down-drift direction from the point of view of the bigger or more persistent waves. Under these more complicated conditions it has been found possible to obtain the littoral drift from the distribution of tracers, only when the drift is assumed to be much more consistent than it really is in nature. The most serious assumption that has to be made is that in each period between injections - in practice it is frequently one week - the littoral

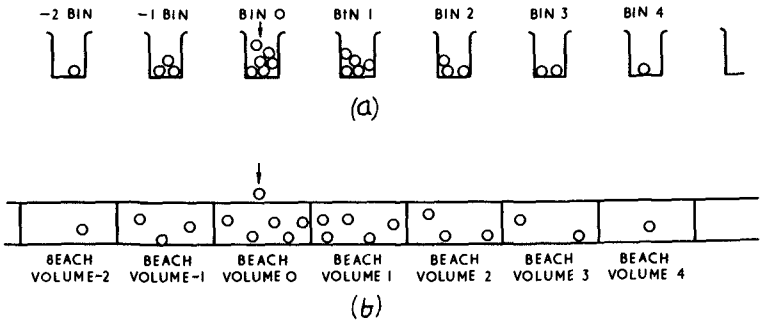

Fig. 5(a). An analogy to the spread of tracers through a beach: the spread of particles among bins. In each time interval the contents of each bin are completly shared with the bins on either side, and another quantity is injected into bin No. 0. (b) The bins are replaced by equal volumes of beach. The spread of tracer proceeds as in (a).

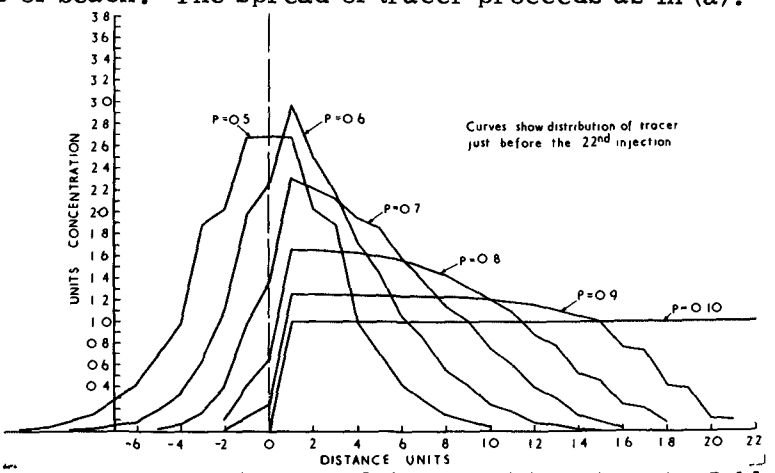

Fig. 6. The evaluation of the quantities given in Table II for various values of p and q.

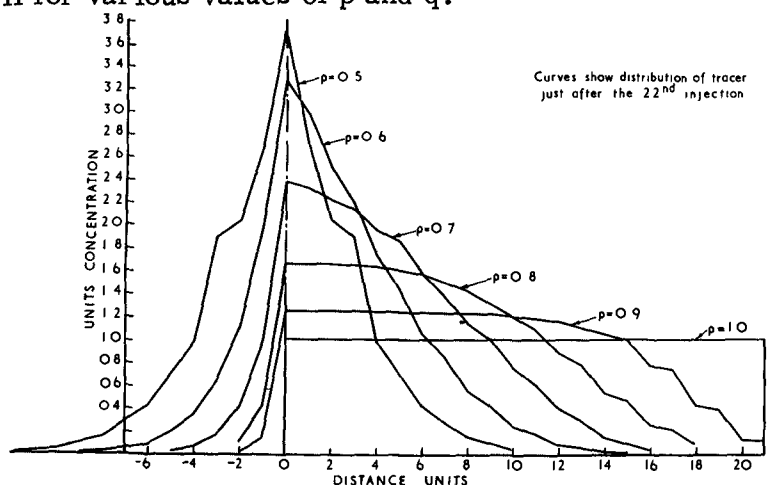

Fig. 7. The distribution of tracers just after the 22nd injection.

drift repeats itself precisely.

The mathematics that has been used to relate the movement of tracer to the littoral drift is exact when used to predict movement of quite different kinds and, for clarity, one of these other kinds of movement will be dealt with first.

An Analogy.

Suppose that there are a number of bins in a row (as shown in Fig. 5a the contents of which were continually being emptied into the bins on either side of them, while into the central bin Number '0' material is injected. In time the injected material would spread to all the other bins.

Let us assume that unit quantity of material is added to bin '0' in each interval of time.

In each interval of time let a proportion p of the contents of each bin be tipped to the right, and the remaining proportion q tipped to the left. $p + q = 1$.

The material then begins to spread through the bins, as shown in the following table. Each horizontal line shows the material contained in each bin after specified numbers of injections.

TABLE I

-2	-1	Bin '0'	Bin 1	Bin 2	Bin 3	Time
		1				After 1st Inject
	q	0	p			1st Exchange
	q	1	p			2nd Inject.
q^2	q	2pq	p	p^2		2nd Exchange
q^2	q	1+2pq	p	p^2		3rd Inject.
q^3 q^2	$q+3pq^2$	2pq	$p+3p^2q$	p^2	p^3	3rd Exchange
q^3 q^2	$q+3pq^2$	1+2pq	$p+3p^2q$	p^2	p^3	4th Inject.
q^3 q^2+4pq^3	$q+3pq^2$	$2pq+6p^2q^2$ etc.	$p+3p^2q$	p^2+4p^3q etc.	p^3 p^4	4th Exchange

After 21 time intervals, that is to say just before the 22nd injection, it can be shown that distribution of material in the different bins is that shown in Table II. In Fig. 6 is shown plotted the distribution curves for various values of p and q, namely:

$(p = 1, q = 0)$, $(p = .9, q = .1)$, $(p = .8, q = .2)$, $(p = .7, q = .3)$. $(p = .6, q = .4)$ and the symmetrical case where $p = q = .5$

It will be seen that the maxima occur at the bin next to the injectic point. If the distribution of material is examined directly after an injection but before the material has been exchanged, it will be found that the distribution is a maximum at the point of injection. For example, the distribution after the 22nd injection is that already given with one unit added to the quantity at the injection point. These distributions are shown in Fig. 7.

The problem of material distributing itself among the bins begins to show some similarity to the problem of tracers distributing themselves along a beach, if the injected material is looked upon as a tracer, and the bins are assumed already to contain equal volumes of beach material. The beach material moves from bin to bin without affecting the total volume of material in the bins. The addition of beach material to the bins does not affect the manner in which tracer spreads from bin to bin, and this remains predictable by the same mathematics.

In Fig. 5b the tins have been replaced by adjacent compartments of a beach. The size of the compartments is chosen so that the mass of material in each, M, is such that in one time-interval the drift to the right is pM and the drift to the left is qM, where $p + q = 1$. In each time-interval the whole contents of each compartment are completely re-distributed, partly to the right and partly to the left, as in the case of the bins. Then after 21 intervals of time, in which the moving mass M and the proportions p and q remained the same, tracer regularly injected into the central compartment would distribute itself, as in Table II.

If the standard time-interval were t weeks
The Littoral drift is at the rate $(p - q)\frac{M}{t}$

If the tracer is added to the beach at a rate $\frac{m}{t}$

After 21 t weeks the distribution of tracer along the beach is that shown in the table multiplied by m.
i.e. If the concentration in the table at a point x is N_x
the mass of tracer in compartment x is $m.N_x$
As the mass of ordinary beach material in the compartment is M
the concentration of tracer is $\frac{m N_x}{M}$

TABLE 2

Final Concentration after 21 Injections

x	
21	p^{21}
20	p^{20}
19	$p^{19}(1+21a)$
18	$p^{18}(1+20a)$
17	$p^{17}(1+19a+210a^2)$
16	$p^{16}(1+18a+190a^2)$
15	$p^{15}(1+17a+171a^2+1330a^3)$
14	$p^{14}(1+16a+153a^2+1140a^3)$
13	$p^{13}(1+15a+136a^2+969a^3+5985a^4)$
12	$p^{12}(1+14a+120a^2+816a^3+4845a^4)$
11	$p^{11}(1+13a+105a^2+680a^3+3876a^4+20349a^5)$
10	$p^{10}(1+12a+91a^2+560a^3+3060a^4+15504a^5)$
9	$p^9(1+11a+78a^2+455a^3+2380a^4+11628a^5+54264a^6)$
8	$p^8(1+10a+66a^2+364a^3+1820a^4+8568a^5+38760a^6)$
7	$p^7(1+9a+55a^2+286a^3+1365a^4+6188a^5+27132a^6+116280a^7)$
6	$p^6(1+8a+45a^2+220a^3+1001a^4+4368a^5+18564a^6+77520a^7)$
5	$p^5(1+7a+36a^2+165a^3+715a^4+3003a^5+12376a^6+59388a^7+203490a^8)$
4	$p^4(1+6a+28a^2+120a^3+495a^4+2002a^5+8008a^6+31824a^7+125970a^8)$
3	$p^3(1+5a+21a^2+84a^3+330a^4+1287a^5+5005a^6+19448a^7+75582a^8+293930a^9)$
2	$p^2(1+4a+15a^2+56a^3+210a^4+792a^5+3003a^6+11440a^7+43758a^8+167960a^9)$
1	$p(1+3a+10a^2+35a^3+126a^4+462a^5+1716a^6+6435a^7+24310a^8+92378a^9+352716a^{10})$
0	$0+2a+6a^2+20a^3+70a^4+252a^5+924a^6+3432a^7+12870a^8+48620a^9+184756a^{10})$
-1	q (same factor as for +1)
-2	q (" " " ")
-3	q (" " " ")
.	
.	
.	
.	
-19	$q^{19}(1+21a)$
-20	q^{20}
-21	q^{21}

NB $a = pq$

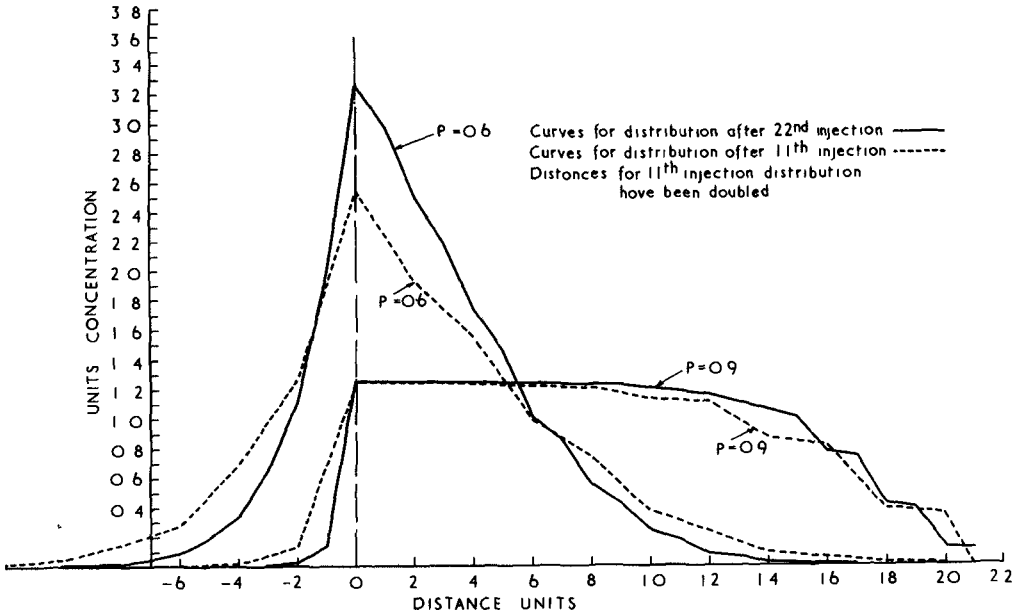

Fig. 8. A comparison between the distribution of tracer after 22 injections and that after 11 injections at the same mean rate.

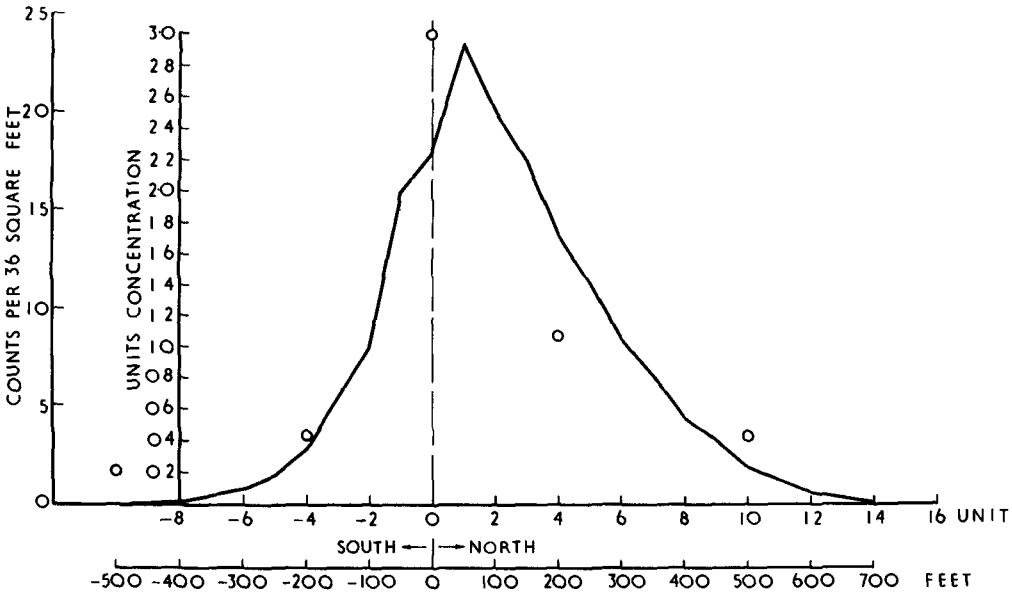

Fig. 9. The distribution of tracer at Deal after 22 days of injection at the rate of 1 cwt per day.

If the measured concentration at point x is C_x

The net rate of transport Q which is $(p - q)\frac{M}{t}$

Can be written $Q = \frac{(p - q)}{t} \times \frac{m N_x}{C_x}$ .....(1)

When the value of Q is required, the concentration C_x of tracer along the beach is measured and plotted as a function of distance along the beach. The curve so obtained is studied for its similarity to the various curves of Fig. 6 and the values of p and q that give the most similar theoretical curve are chosen.

If the experimentally found curve of $C_x : x$ is precisely similar to one of the curves in Fig. 6 then N_x/C_x has the same value at all distances from the injection point; and there is no doubt about the value of N_x/C_x to insert in equation (1). If on the other hand, the two curves are not precisely similar, judgement has to be used in order to select the most significant value of N_x/C_x . One could for example, use the maximum value of N_x/C_x that is found immediately down-drift of the injection point.

With p, q, N_x and C_x found and with m and t known from the rates of injection, the expression $\frac{p - q}{t} m \frac{N_x}{C_x}$ can be evaluated.

The computation of all the theoretical $N_x : x$ curves for large numbers of injections is a very lengthy process. Fortunately there is an indication that the number of injections is only of secondary importance in determining the $N_x : x$ curve and that the mean rate of injection is the important parameter. Curves of $N_x : x$ for a smaller number of injections, namely 11, are shown in Fig. 8 and compared with corresponding curves for 21 injections carried out at the same mean rate. The difference is seen to be small. The error introduced by assuming the tracer to be injected in 21 equal fractions when, in fact, a smaller amount was injected at shorter intervals but at the same mean rate, is probably small compared with the inevitable errors introduced by assuming that identical drift took place in each of the equal intervals of time.

Only at the origin has it been found possible to calculate the concentrations reached after injection has been continuing for an infinitely long time. The concentration N_o immediately after an injection can be shown to be $1/(p - q)$; while immediately before the next injection it is $1/(p - q)-1$.

MEASUREMENT OF LITTORAL DRIFT ALONG NATURAL SHINGLE BEACHES.

Measurements of littoral drift have been in progress since April 1959, when tracers were first dumped on the shingle beach at Deal on the coast of Kent. Measurements have since been made at Rye and Dungeness where the beaches are also shingle.

Shingle beaches were chosen for the experiments in order to avoid an added complication which is present when attempting to measure littoral drift along sandy beaches. The added complication is the unknown rate of loss of tracer from the beach. Continuous interchange of material between the beach and the sea-bed offshore, which persists without necessarily involving any changes in the beach profile, is responsible for the dispersion of the tracer offshore, and constitutes a serious difficulty. In order to use the modified dilution method, one either needs to know that there is no loss of tracer offshore or has to be able to measure the loss, and there is no obvious or easy way in which this measurement can be made.

In fact a preliminary experiment was carried out on the sandy beach at Dawlish in 1959, but it has not so far been followed up. 30 lb of fluorescent tracer sand was injected every day for 21 days, following which the beach was surveyed. The data obtained could be interpreted to reveal a figure for the littoral drift, using the modified dilution method, but we had no idea of how much tracer had been lost offshore nor of the exaggeration of the apparent littoral drift which this loss caused.

On the majority of shingle beaches, on the other hand, there is a sharp dividing line between shingle on the upper beach and the sand lower down, that is uncovered around the time of Low Water; and it is reasonable to assume that shingle-tracers, behaving like shingle itself, would be confined to the beach. In the experiments at Deal, Dungeness and Rye the general procedure was the same but with certain differences in detail.

The tracer that was initially dumped on the beach at Deal consisted of broken dense concrete, incorporating the fluorescent substance anthracene. After four months the tracer was changed to a concrete incorporating Rhodamine, manufactured as described in the Appendix. Later on the fluorescent substance was changed to a plastic manufactured by Messrs. Levy-West, and later still to a plastic incorporating Uvitex. These substances, in ultra-violet light, fluoresced green, red, yellow, and blue respectively and were easily distinguishable from one another. Similar changes were made in the tracers used at Rye.

The size of the particles of crushed concrete was matched as well as was possible to the stones lying on the beach but the size would have been matched to the material in transit, had the nature of this material been known. Even in the matching of the tracer to the material in situ, there was need to use subjective judgement; because the material in situ varied so much from place to place that

a sample of almost any size could be obtained by taking it from a selected contour.

Initially the tracer was dumped at the rate of 1 cwt. per day for 21 days; when a survey of the distribution of the tracer was carried out, and the rate of drift over the 21 days calculated. The tracer was then dumped at the same mean rate, but at 7 cwt. each week, and the distribution of tracer surveyed at various intervals. The distribution was always surveyed after 22 weeks and 52 weeks so that the drift during those periods could be calculated, but there were surveys at other periods as well.

The surveys were carried out at night using a portable ultra-violet lamp and generator. Posts were driven into the top of the beach-ridge at the injection point and at distances of 200 ft, 500 ft, 1000 ft, 2000 ft, and 3000 ft on either side of it. When a survey was carried out, the equipment was carried to each post in turn and the number of fluorescent pebbles visible in a given area at high-water, half-tide, and low-water was counted. The area in which pebbles were counted was initially 36 sq. ft, defined by a square Dexion frame, and later 100 square feet, defined by a lighter rod-and-string framework. It was found that a survey of one beach could be carried out by two people in two nights, though ideally three people were required to help carry the equipment.

The results of some of the experiments are presented below. There is the data for Deal after 21 daily injections - i.e. after 22 days - for Rye after 22 weeks, for Dungeness after 33 weeks, and for Rye again after 52 weeks.

The most interesting of the three sites from the experimental point of view is Rye, because there it has been found possible to measure the rate of drift of shingle by other means and compare the two figures. At Rye there is a dominant easterly drift and the shingle on the west beach is trapped by the Western Breakwater of the River Rother. For many years shingle has been removed; at one time for use as ballast, but more recently for beach nourishment elsewhere. The toe of the shingle beach is now well inshore of the seaward limit of the breakwater. Accordingly the drift past any point on the west beach can be equated to the amount of shingle, carried away by human agency, plus the accretion of beach between the point in question and the breakwater.

From a comparison between a survey carried out in June 1959 and another in June 1960 it was found that the beach had accreted by a total volume of 17,400 cubic yards. The Kent River Board inform us that the quantity of shingle removed from the beach during the same period was 32,000 cubic yards. Accordingly the drift past the injection point should have been

$$32{,}000 + 17{,}400 = 49{,}400 \text{ cubic yards.}$$
$$\text{or } 53{,}000 \text{ tons.}$$

which can be compared with a figure found below.

Deal after 22 days.

Data:-

Position ft	Counts per 36 sq ft
1000 south	0
500 south	1.8
200 south	3.5
0	24
200 north	8.6
500 north	3.5
1000 north	0

Calibration Test:-

$$\frac{\text{Concentration by weight}}{\text{Count per 36 sq ft}} = .00004$$

Best fit (p.q) curve is p = .6, q = .4 see Figure 9
Best length scale is 1 unit = 50 ft
Best concentration scale is 1 unit = 8 counts per 36 sq ft

$$\text{Drift} = (p - q).\frac{m}{t}.\frac{N_R}{C_R}$$

$$m/t = 1 \text{ cwt per day}$$

$$= \frac{1}{8 \times .00004}$$

$$\therefore \text{Drift} = \frac{(.6 - .4)\ 1}{8 \times .00004} \text{ cwt per day northwards}$$

$$= \frac{.2}{20 \times 8 \times .00004} \text{ tons per day northwards}$$

$$= 31 \text{ tons per day}$$

Rye after 22 weeks.

Data:-

Position ft	Counts per 100 sq ft
500 west	0
200 west	.6
0	4.5
200 east	25.6
500 east	16.1
1000 east	24.0
2000 east	10.0
3000 east	1.7

Calibration Test:-

$$\frac{\text{Concentration by weight}}{\text{Count per 100 sq ft}} = .000019$$

Best fit (p.q) curve is p = .9, q = .1 see Figure 10
Best length scale is 1 unit = 143 ft
Best concentration scale is 1 unit = 16.8 counts per 100 sq ft

$$\text{Drift} = (p - q).\frac{m}{t}.\frac{N_x}{C_x}$$

$$m/t = 7 \text{ cwt per week}$$

$$= \frac{1}{16.8 \times .000019}$$

$$\therefore \text{Drift} = \frac{(.9 - .1)\ 7}{16.8 \times .000019} \text{ cwt per week eastwards}$$

$$= \frac{.8 \times 7}{20 \times 16.8 \times .000019}$$

= 880 tons per week eastwards

Dungeness after 33 weeks.

Data:-	Position ft	Counts per 100 sq ft
	1000 west	0
	500 west	5
	200 west	4
	0	5
	200 east	3
	500 east	20
	1000 east	12
	2000 east	5
	3000 east	2

Calibration Test:-

$$\frac{\text{Concentration by weight}}{\text{Count per 100 sq ft}} = .000013$$

Best fit (p.q) curve is p = .8, q = .2 see Figure 11
Best length scale is 1 unit = 166 ft
Best concentration scale is 1 unit = 9.1 counts per 100 sq ft

$$\text{Drift} = (p - q).\frac{m}{t}.\frac{N_x}{C_x}$$

$$m/t = 7 \text{ cwt per week}$$

$$= \frac{1}{9.1 \times .000013}$$

$$\therefore \text{Drift} = \frac{(.8 - .2)\ 7}{9.1 \times .000013} \text{ cwt per week eastwards}$$

= 1,770 tons per week eastwards

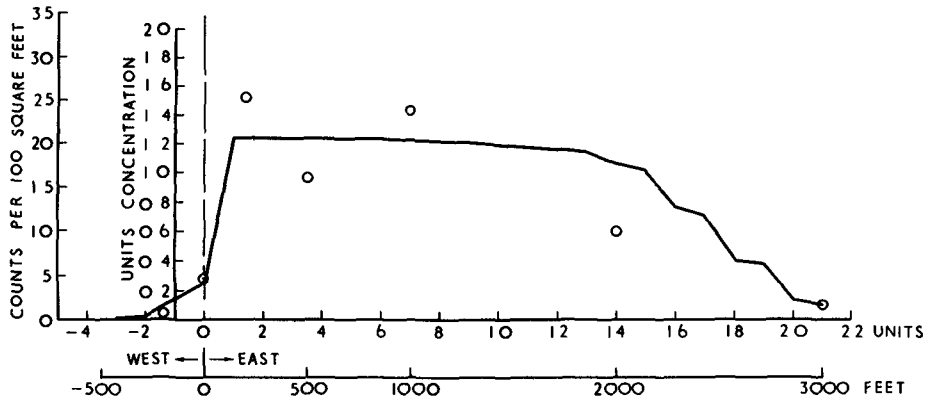

Fig. 10. The distribution of tracer at Rye after 22 weeks of injection at the rate of 7 cwt per week.

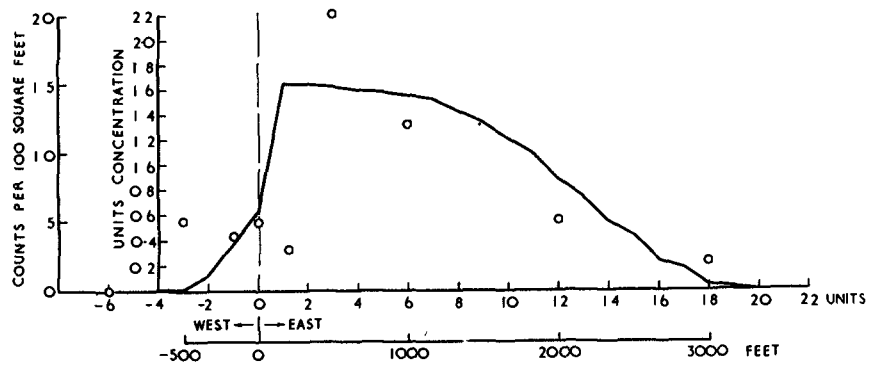

Fig. 11. The distribution of tracer at Dungeness after 33 weeks of injection at the rate of 7 cwt per week.

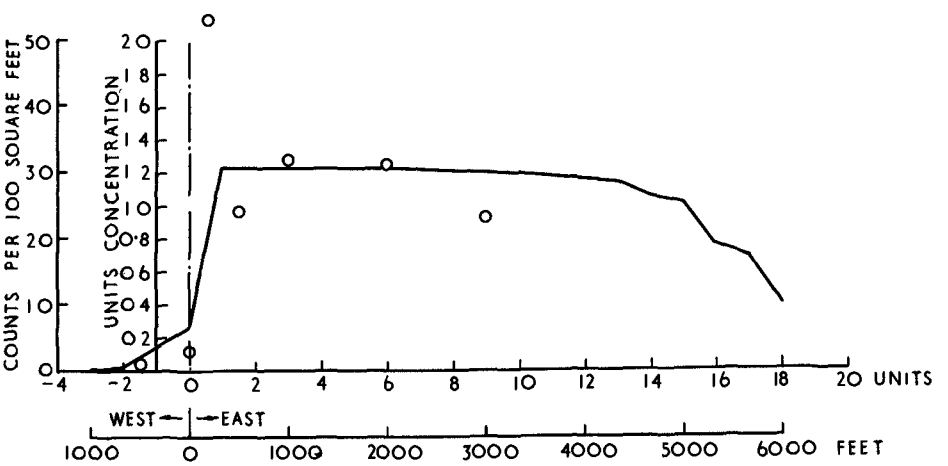

Fig. 12. The distribution of tracer at Rye after 52 weeks of injection at the rate of 7 cwt per week.

Rye after 52 weeks.

Data:-

Position ft	Counts per 100 sq ft
500 west	0
200 west	1
0	3
200 east	53
500 east	24
1000 east	32
2000 east	31
3000 east	23

Calibration Test:-

$$\frac{\text{Concentration by weight}}{\text{Count per 100 sq ft}} = .000019$$

Best fit (p.q) curve is p = .9, q = .1 see Figure 12
Best length scale is 1 unit = 333 ft
Best concentration scale is 1 unit = 24.8 counts per 100 sq ft

$$\text{Drift} = (p - q).\frac{m}{t}.\frac{N_x}{C_x}$$

$$m/t = 7 \text{ cwt per week}$$

$$= \frac{1}{24.8 \times .000019}$$

$$\therefore \text{Drift} = \frac{(.9 - .1)\ 7}{24.8 \times .000019} \text{ cwt per week eastwards}$$

= 590 tons per week eastwards
or 31,000 tons per year

Discussion

Although there is a check on the above results only in the case of 52 weeks' littoral drift at Rye, the other results are at least consistent. The smallest drift was found to be at Deal which is least exposed to big waves; and the biggest was at Dungeness which is most exposed and has the deepest water close inshore. The measure of agreement between drift at Rye calculated by cubature and that calculated from the distribution of tracers, 53,000 tons per year and 31,000 tons per year respectively, is fairly encouraging, considering the difficulties involved.

In view of the not very precise measurements of littoral drift that would be adequate for the design of sea-defences, the method can be said to be useful.

ACKNOWLEDGEMENTS

The work described in this Paper was carried out as part of the research programme of the Hydraulics Research Board and is published with the permission of the Director of Hydraulics Research.

The author wishes to acknowledge the contributions of other members of Hydraulics Research Station staff; of Mr. W. J. Reid who was in charge of the experiment on real beaches, of Mr. I. P. Jolliffe who carried out the field surveys, of Mr. D. E. Newman who developed both the tracers and the methods of manufacturing them, and of Mr. M. J. Abbott to whom are due the calculated quantities in the Table on page 4.

References.

V. P. Zenkovitch: Emploi des luminophores pour l'etude du mouvement des alluvions sablonneuses.
Bulletin. C.O.E.C. 10 (5) May 1958

S. L. Vendrov, B. F. Lytcheuko, V. V. Patrikeiev, K. M. Pekichev: Emploi des luminophores pour l'etude des mouvements d'alluvions le long des rives des barrages.
"Transport Fluvial" 4. 1957.

Appendix I

SAMPLING.

Initially the numbers of tracer pebbles visible in a 36 sq ft area were counted near the top of the beach, in the middle of the beach and at the lower limit of the shingle. Latterly the standard area was increased to 100 sq ft. The advantage of examining a larger area is that by counting larger numbers, when these numbers are subjected to random variations, one gets a proportionately more accurate result.

If n is the size of a sample i.e. the total nurber of stones visible in a given area.

And if P' is the probability that any pebble is a tracer,

P'n is the number of stones visible.

If P is the probability in the whole population of a pebble being a tracer,

Pn is the average number of visible tracers that would be determined by frequently repeated sampling.

If δ is the permitted error expressed as a fraction of P, i.e. δ is equal to $\frac{P - P'}{P}$ then it is known that, if the oonfidence level is to be .90, then

$$n \geqslant \frac{2.8}{P.\delta^2}$$

$$\delta \geqslant \sqrt{\frac{2.8}{n.P.}}$$

This indicates that the proportional errors that are likely to occur are inversely proportional to the square root of the numbers counted. It shows, for example, that if the average number of particles counted was 8, one in every ten counts would differ from the true mean by more $\frac{2.8}{8} \times 8$ or 4.7.

We can make use of this information to determine the likely errors introduced into the results of the model beach experiment by the counting of randomly distributed tracers.

The count of 15.9 particles per square foot was obtained by averaging the counts obtained in 3 square feet at 14 different sections along the beach.

$\therefore$ The total number of particles counted was 15.9 x 14 x 3 or 665

$\therefore$ At a confidence level of .9 $\sqrt{\frac{2.8}{665}}$

Interpreted, this means that if the experiments were repeated many times, one result in every ten would be in error by more than $\sqrt{\frac{2.8}{665}} \times 15.9$ or 1.04. This is about 7%.

Appendix II

PRODUCTION OF TRACERS

Concrete Tracer Pebbles.

The ideal tracer has not only to be fluorescent, it has also to be of the correct size, shape and density. It has to resist abrasion or, should there be some abrasion, it should nevertheless retain its fluorescent properties. The tracer pebbles used by H.R.S. have consisted mostly of a dense concrete, containing particles of fluorescent plastic in them. Size has been controlled by sieving, density and abrasive resistance by control of the cement-stone mix, but little attention has been paid to the shape. The pebbles produced by crushing and sieving appeared to be neither sharper, flatter or rounder than normal beach pebbles, and they were not further treated to alter their shape.

Most of the tracer pebbles used have incorporated the organic dye Rhodamine, but other dyes and phosphors have also been used and many others that have not been used have been tested and shown to be suitable. Suitable proportions of dye, plastic and concrete are given below, but other proportions can work equally well. The proportion of dye in the plastic can, in some cases, be varied through extraordinarily wide limits, as for example between .1% and .001% without appreciably effecting on the one hand the price and on the other hand the effectiveness of the tracer.

The plastic that is used is a proprietary brand of liquid urea resin known as Aerolite Resin C.B.U. combined with the hardening agent Acid Hardener G.B.Q, manufactured by C.I.B.A. (ARL) Ltd. of Duxford, Cambridgeshire.

The pebbles were prepared in the following way:-

(i) 37.5lbs Resin C.B.U. were poured into a concrete mixer.
(ii) .80lbs of Rhodamine B were dissolved in 3.75lbs of Acid Hardener G.B.Q. and added to the resin in the rotating mixer.
(iii) when mixed, the liquid was poured on to waxed sheets and allowed to set. It would set in slabs about $\frac{1}{4}$" - $\frac{3}{8}$" thick.
(iv) the plastic set in 2 or 3 days, depending on the ambient temperature and was then crushed and granulated. The biggest particles in the granulated material were approximately 3mm in diameter.
(v) concrete was made according to the following mix:-

13 parts cement.
26 parts quartz dolorite.
1 part granulated dyed plastic.

The wet concrete was spread out to set in slabs 3" thick.

(vi) the slabs were broken up in a jaw crusher and the required size fraction separated out by rotating soreens attached to the crusher. The rejected fraction - some 50% of the whole - was entirely fines. It was incorporated in subsequent batches of concrete as a filler.

Preparation of fine Fluorescent Shingle for the Beach Model.

The tracer material was made in four different colours, the dyes used were:-

Red - Rhodamine'B'
Blue - Primuline.
Orange - Eosine.
Yellow - Auramine.

One lb. of tracer of each colour was made. A solution of surface-coating Araldite 985-E was made up and separated into four beakers, each containing about ½ litre. Dye at 1% of the weight of the resin was added to each solution and well stirred. The stones were put in a dry beaker, and sufficient resin and solvent was poured over it to cover the surface. The resin was immediately decanted and the stones spread on thick wire gauze and allowed to stand for ½ hr. to permit of evaporation of excess solvent. The material was then stoved at 160°C for about 1½ hours and allowed to cool. Particles which had stuck together were separated by tumbling them in a cloth bag.

Surface coating Araldite 985-E is said to be 8/10ths as hard as glass as measured in Sward units and there was certainly no evidence in the beach model that any of the coating had been worn off the stones.

Sand Tracers.

Sand tracers have been produced by taking sand from the beach that has to be studied and coating each grain with a thin layer of fluorescent plastic. The process involves mixing sand up with a liquid fluorescent resin, allowing it to set into a cake, disintegrating the cake so that the individual particles are again separated, and then sieving to exclude particles of the wrong size.

The ingredients needed are:-

(i) Aerolite Resin C.B.U.
(ii) Acid Hardener G.B.Q.
(iii) Rhodamine or other suitable dye that will fluoresce in aqueous solutions.
(iv) Dry beach sand.

Preparation.

(The quantities given below are suitable for mixing in a concrete mixer of 5/3 cubic foot capacity).

(i) 37.5 lbs of resin CBU are poured into a concrete mixer.
(ii) 0.80 lbs of Rhodamine 'B' is dissolved in 3.75 lbs Acid Hardener GBQ, and added to the mixer while it is in motion.
(iii) 200 lbs of dry sand is added over a period of 3 or 4 minutes. When the coating appears to be complete, the machine is switched off and the mixture poured on to sheets of waxed + board. The mixture sets very rapidly in a warm atmosphere. It is important to spread the material quickly over the sheets with a trowel, so that it may be broken up conveniently when set. About $\frac{1}{2}$" is a suitable thickness for the layers. Breakage is facilitated by cutting lines with a trowel across the layers before they set.

Hardboard covered with Silicone Wax is very suitable. P.V.C. sheet +is also satisfactory.

It will be found that the surface of the drying mix will harden first. Setting is accelerated by turning the pieces over with a trowel and exposing the underside. At 80°F, complete hardening takes 2 - 3 days. The fumes given off after mixing are very strong and unpleasant, but we have been assured by the manufacturers of the resin, that they are in no way dangerous.

When the pieces of glued sand have set, they are broken up into pieces not bigger than $\frac{1}{2}$" x $1\frac{1}{2}$" x $1\frac{1}{2}$" in a jaw crusher, before granulating them to produce a material of the same particle size as the original sand. The fragments are granulated in a fixed-beater-cross machine, known by the trade name of Spruemaster, (supplied by Messrs. Christy and Norris Ltd., of Chelmsford, Essex) - in which the impact between the jaws shatters the lumps, and produces a finished product of the correct size. The machine has a screen in it with conical holes, which retain the large particles until they are reduced to the right size.

The material is sieved.

If only a few grammes of the sand are required, the above quantities can be reduced proportionately and the mixing can be carried out in a beaker. Crushing down the produot can be done with a hammer on a steel sheet. Most of the early samples were made by this method.

Other dyes can be substituted for Rhodamine 'B' if other colours are desired.

Dye	Colour	% of dye in resin	Supplied by
Titan Yellow	Pale blue	2%	The General Chemical & Pharmaceutical Co Sudbury.
Primuline	Blue	2%	
Auramine	Yellow	2%	
Rhodamine 'B' Extra 525%	Red	Not exceeding 1%	C. I. B. A. Clayt Bush House London W.2.
Rhodamine 6 A Extra	Red		
Kiton Rhodamine 3 R 250%	Red		
Kiton Rhodamine B 440%	Red		
Eosine YS 140%	Orange	1%	
Erythrosine BSB Special	Orange		
Kiton Yellow EFF	Yellow-Green		
Uvitex SWN Conc.	Bright-blue		
Kiton Yellow EFF + Kiton Blue A 190%	Green	1 - 2%	
Victoria Blue 150% + Auramine O 166%	Green	1 - 2%	

Most of the substances in the Table fluoresce only in solution. The exceptions are Uvitex and Kiton Yellow which are naturally fluorescent.

Nearly all the fluorescent pigments and hydro-carbons are subject to photolysis, i.e. their brilliance decays under the action of ultra-violet light. The substances mentioned above have been subjected to "weathering tests" and have been found the most satisfactory of all those that were tested. Fluorescein tends to decay in a few days, but might be useful for tests where the durability is not important, or

where a short life is an advantage.

Kiton Yellow, Rhodamine 'B' extra 525%, Uvitex SWN were all found to retain maximum brilliance when exposed to unfiltered UV tests equivalent to one year's natural weathering.

The above substances fluoresce strongly under U.V. emission in the region of 3660 A.U.

Choice of a colour.

It has been found that some beaches contain substances that have a natural fluorescence, and it is, therefore, advisable first to examine a beach at night using ultra-violet light. In one instance it was found that parts of a certain shell had a fluoresoence similar to that of Rhodamine B", but usually the numbers present are very small indeed. The use of a U.V. Lamp emitting shorter wavelengths (2537 AU) is neoessary if the fluorescence of most natural impurities in the samples is required to be omitted. The "Hanovia" Chromatolite lamp is particularly suitable for this purpose. If care is taken to ensure that the dye fluoresces with a different colour from that of any of the naturally occurring substances, detection of 1 fluorescent particles in 1×10^{6} is a simple matter.

CHAPTER 25

USE OF A RADIO-ACTIVE TRACER FOR THE MEASUREMENT OF SEDIMENT TRANSPORT IN THE NETHERLANDS

J.N. Svasek and H. Engel
Engineers, Hydraulic Division of the Delta-works, Rijkswaterstaat, The Hague.

INTRODUCTION

The "Rijkswaterstaat" has developed a method based on the use of radio-active tracers for the evaluation of sediment transport due to the combined action of waves and currents.

The results of preparatory studies and a laboratory test were published in a previous report by J.J. Arlman, P. Santema and J.N. Svasek [1].

The main principles of the method were

1. Detection by a sledge-mounted unit towed by a survey vessel and continuous registration on board of the radio-activity measured on the sea bottom.
2. Employment of low specific radio-activity of tracer material and a large quantity thereof.
3. Use of a long-life isotope and high radio-activity.
4. Measurement of the vertical distribution of radio-activity in core samples or if possible by discrimination.

In March 1958 the first lot of tracer material was placed on the sea bed. The tracer material consisted of the radio-active isotope Scandium^{46} emitting 2 curies incorporated in 100 kg "greensand". Scandium^{46} has a half-life of 84 days and emits strong gramma radiations with energies of 0.89 and 1.12 MeV.

Afterwards, in 1959, two series of measurements were taken near the entrance to the Rotterdam Waterway. Four droppings formed one series; they were generally carried out in the following manner: 50 kg greensand labeled with 2 Curies Scandium was dropped in 4 places at a safe distance from each other. 2 of the 8 portions consisted of smaller quantities of both radio-activity and green-sand.

In the following paragraphs the preparation, dropping and detection of the tracer, the working out of the registrations and the interpretation of the results of the 1959 measurements are discussed.

PREPARATION, DROPPING AND DETECTION

The scandium hydroxyde for one dropping (approx. 1.5 gr) is packed in a quartz tube and an aluminium can and irradiated in a reactor for about 4 weeks. On arrival at the place where the tracer is prepared the cans are taken out of their transport containers and stored temporarily.

The tracer material ("greensand") is an ionexchanger with a specific weight of 2.77 which approaches the specific weight of the sea-bed material (2.67) and is given sufficient hardness by

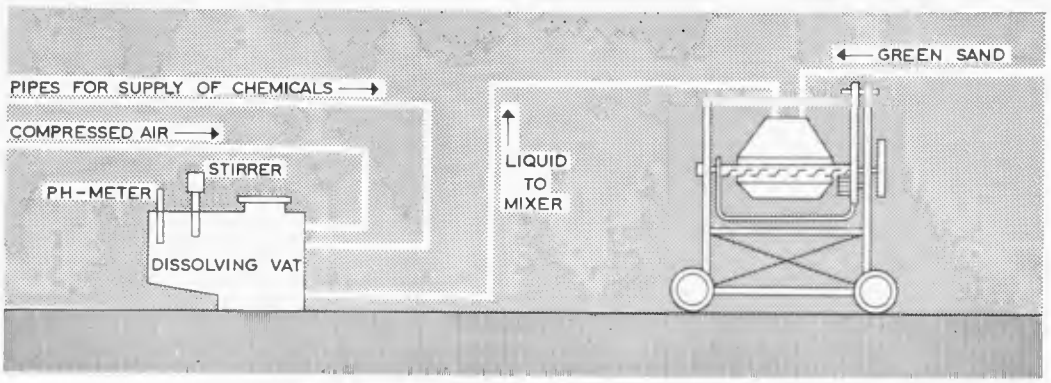

Fig. 1. Dissolving vat and mixer.

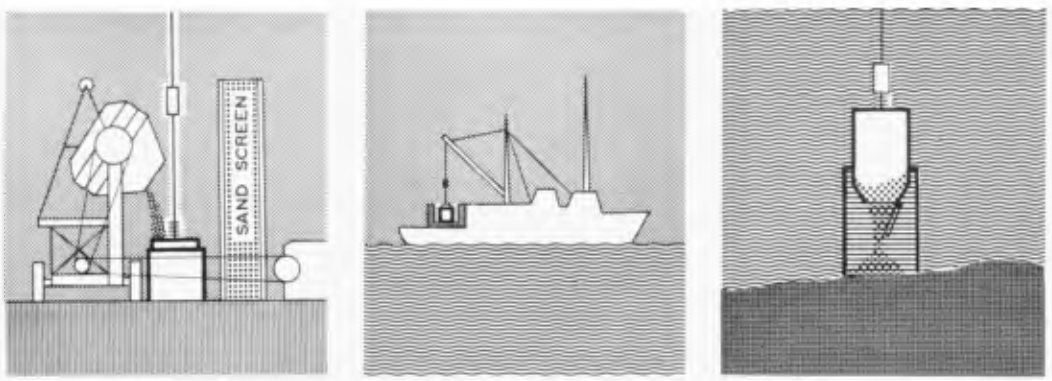

Fig. 2. Transport and injection of the tracer material.

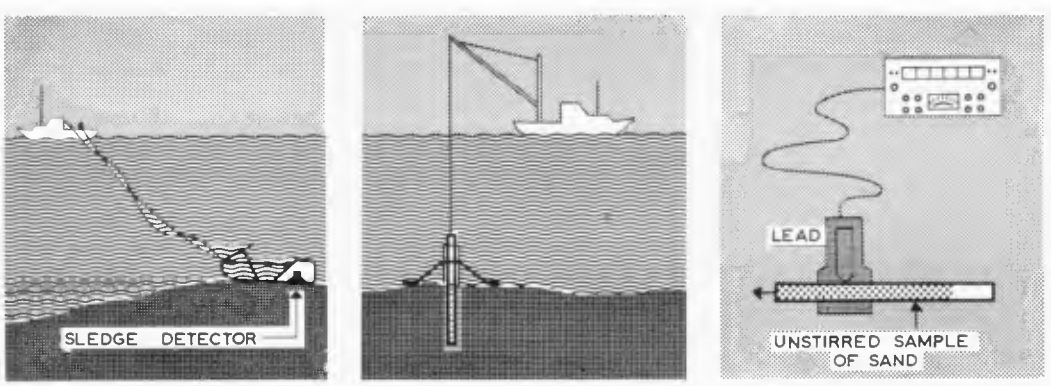

Fig. 3. Detection of tracer distribution.

roasting at 700° C.

For one dropping 50 kg of this material is mixed with a solution containing trivalent Scandium ions. The solution is made in a special vat were the aluminium can and the tube are broken open under concentrated nitric acid. After dissolving for a time the liquid is neutralised and aluminium chloride added. Finally the solution is pumped into the mixer and the vat rinsed with water. The labeling takes place in the mixer (fig.1).

The ion-exchanging capacity of the greensand is so great that without the addition of trivalent aluminium ions very irregular surface labeling takes place. With the surplus of aluminium ions in the solution more reasonable labeling throughout the mass is effected:

Distribution of radio-activity in the fractions of a sample of tracer material:

fraction	weight percentage	Calculated activity percentage		measured activity percentage in sample
		mass labeling	surface labeling	
300-420 μ	0.1	0.1	0.0	0.1
210-300 μ	2.9	2.9	1.3	2.8
150-210 μ	45.1	45.1	29.8	36.0
105-150 μ	21.5	21.5	20.0	21.6
75-105 μ	16.3	16.3	21.6	19.7
50- 75 μ	14.1	14.1	27.1	19.7

When the cans of radio-active scandium are stored and afterwards when they have to be placed in the dissolving vat handling is done by one man unsheilded at a distance of 2 mtrs, but only for a few seconds. The remaining work is done from behind a sand barrier where the radiation does not exceed the permitted level for 24 hours daily.
The maximum radiation received by one man in a week during the storing and preparing of 4 portions each containing 2 Curies of radio-activity was 75 mR, while 300 mR a week is permitted by law for 52 weeks per year.

From the mixer the tracer is poured into the injection device and placed on board the transport vessel. The injection device was modified several times during the experiments. In the perfected apparatus the tracer is lowered in a container that can be opened by means of a falling weight. After leaving the container the tracer material settles within a cylindrical screen. This screen is attached to the container in such a way that it stays on the bottom while the container follows the movement of the vessel (fig.2).

After the dropping operation the container is decontaminated with a strong jet of water and checked for radio-activity with a hand monitor.

The placing of the material on the sea bed can be carried out only when circumstances are favourable (no swell, wind waves not higher than 40 cm., current velocities below 40 cm/sec).

The movement of the radio-active material on the sea bed was followed chiefly by means of a sensitive scintillation detector mounted on a sledge (fig.3). The detector was protected against shocks by a foam rubber covering 18 mm thick.
Nevertheless, heavy shocks do show in the registration.

The 6-core cable between the scintillation detector and the registration instruments on board the towing survey launch proved to be very vulnerable. An experiment in which towing cable and electric cable were combined in one armoured cable was unsuccessful.

A stand-by detection unit was built because changing the six core cables took about a day and days suitable for working at sea are rare. This detection unit consisted of 24 Geiger-Müller tubes placed in a sledge similar to the one carrying the scintillation detector. The tubes are protected with foam-rubber and the power supply (15 batteries) for three months is built into the sledge. A one-core coaxial cable connects the detector with the instruments on board. Repairs to or change of cables can be carried out on board within half an hour.

The background detected by the scintillation detector increases as a result of the natural activity of the bottom sediment from 100 c.p.m at 5 cm above the bottom to 300 c.p.m on the bottom. Outside the tracer area we can also check whether the survey launch is not travelling too fast. This checking is not possible with a Geiger-Müller detector, however, because of its low sensitivity to the radio-activity of the bottom sediment. For good navigation it proved necessary to maintain a speed of about 1.2 m/sec.

The vertical distribution of the tracer in the sea bed was investigated in unstirred samples. The pneumatic sampling apparatus used during the first experiments proved to be too complicated for routine sampling. It was replaced by a simple mechanical device that produce about 6 samples a day with an average length of 0.80 m.
Supplementary samples were taken with a Van Veen Grab. Both kinds of sample were analysed in the laboratory. Due to absorption in the sample and the low rate of radio-activity available, relatively few of the samples showed a significant distribution pattern. No tracer material was found more than 10 cm below the sea bed (fig.4).
The maximum activity in a core sample 7 cm in diameter was 0.43 C, but most of them had less than 0.15 C.

A laboratory experiment was carried out to find out whether it is possible to get information concerning the depth of the tracer below the sea-bed by using a channel discriminator to measure the 2 emitted γ radiations (0.89 and 1.12 MeV) separately. [1] (page.38) This turned out to be impossible due to the fact that the 1.12 MeV γ's transfer part of their energy to the electrons of the absorber. The photon is deflected from its original course

USE OF A RADIO-ACTIVE TRACER FOR THE MEASUREMENT OF SEDIMENT TRANSPORT IN THE NETHERLANDS

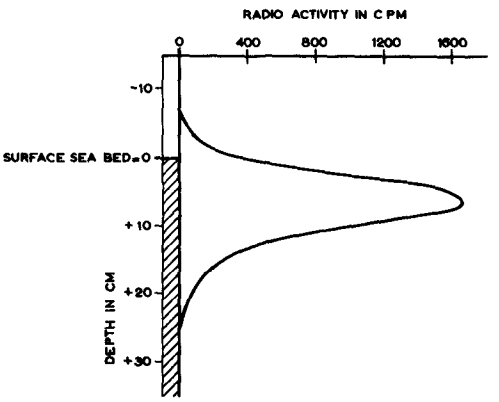

Fig. 4. Vertical distribution of tracer at one point.

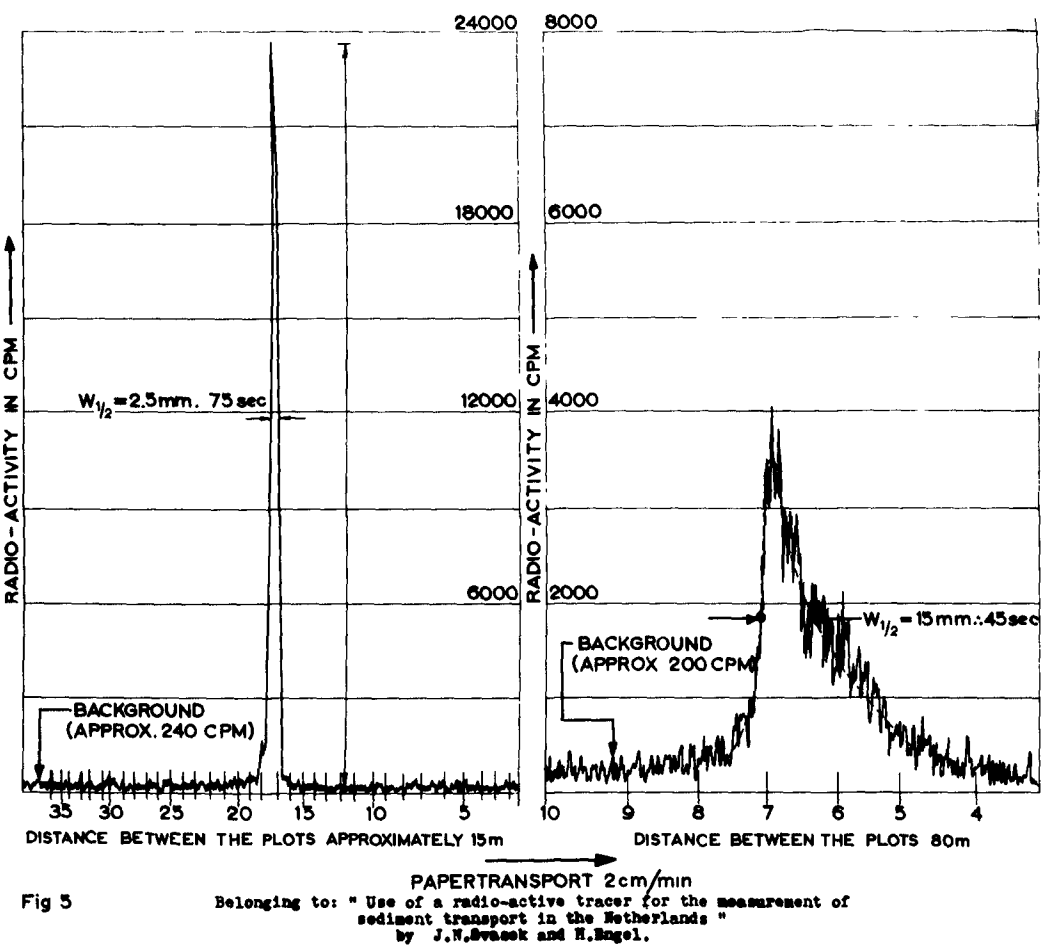

Fig. 5. Examples of registration of radio-activity of the sea-bed.

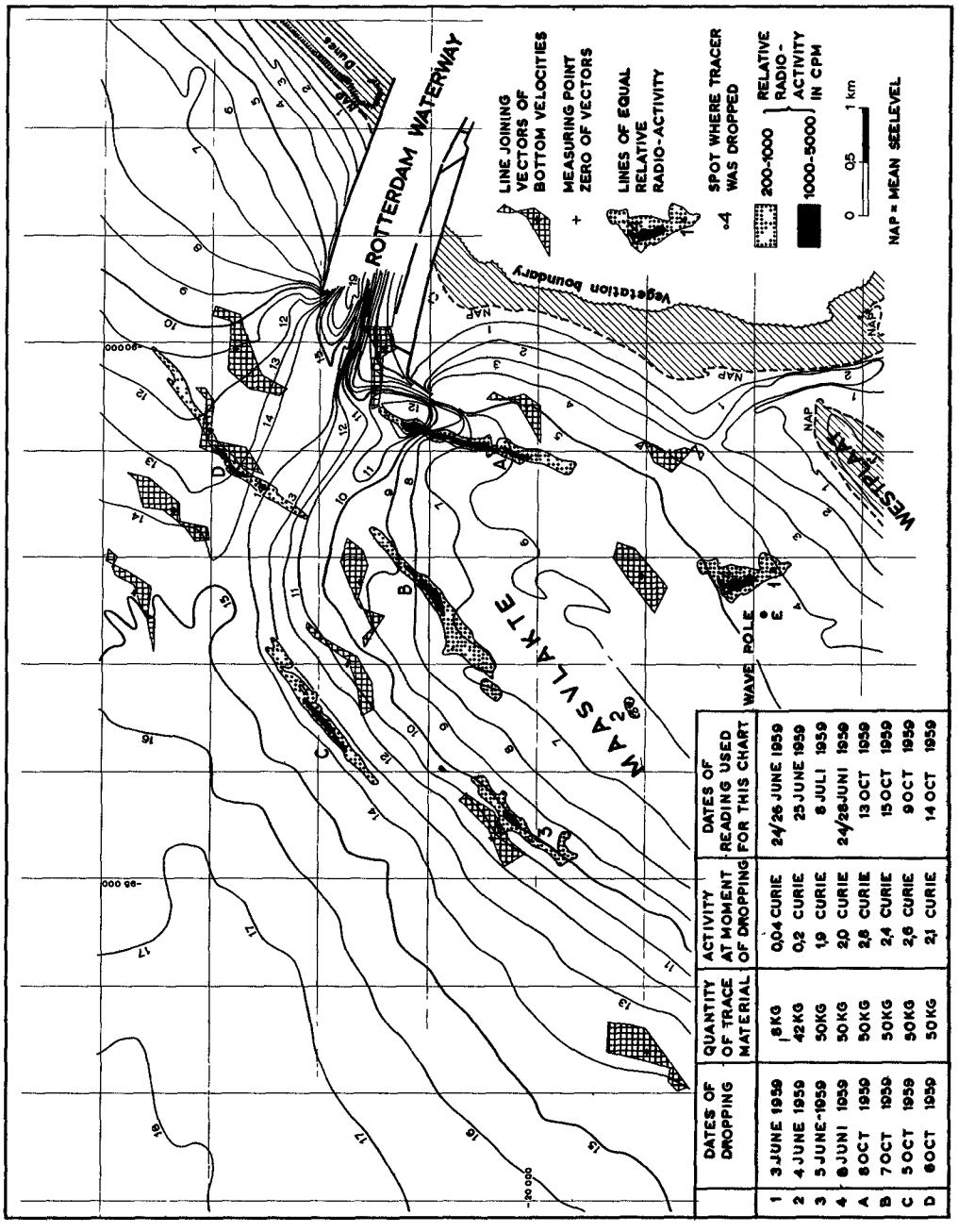

	DATES OF DROPPING	QUANTITY OF TRACE MATERIAL	ACTIVITY AT MOMENT OF DROPPING	DATES OF READING USED FOR THIS CHART
1	3 JUNE 1959	18 KG	0,04 CURIE	24/26 JUNE 1959
2	4 JUNE 1959	42 KG	0,2 CURIE	25 JUNE 1959
3	5 JUNE 1959	50 KG	1,9 CURIE	8 JULI 1959
4	8 JUNI 1959	50 KG	2,0 CURIE	24/28 JUNI 1959
A	8 OCT 1959	50 KG	2,8 CURIE	13 OCT 1959
B	7 OCT 1959	50 KG	2,4 CURIE	15 OCT 1959
C	5 OCT 1959	50 KG	2,6 CURIE	9 OCT 1959
D	6 OCT 1959	50 KG	2,1 CURIE	14 OCT 1959

Fig. 6. Synopsis of the 1959 measurements.

and degraded in energy so that the photo-peak of the 0.89 MeV γ's is not measurable (Compton effect).

The position of the survey launches during readings was fixed with the help of a Decca Survey System. The error in the area investigated seemed to be less than 10 m. Detection lines were chosen spaced 40 to 150 mtrs apart.

WORKING OUT THE REGISTRATIONS

Before dropping the tracer material the background of the area in which measurements were to be carried out was scanned with the sledge detector.

As a rule these measurements showed a background varying roughly between 200 and 300 c.p.m for the scintillation unit and between 130 and 200 c.p.m for the Geiger-Müller detection unit. The response factors of the detectors for a thin layer of radio-activity on the surface were $0.29.10^{-5}$ mC/m^2 per c.p.m and $0.54.10^{5}$ mC/m^2 per c.p.m respectively for Scandium^{46}. Consequently, the equivalent initial radio-activity of the sea bed was 0.58-0.87 μC/m^2 for the Scintillation unit and 0.70-1.08 μC/m^2 for the Geiger-Müller detection unit.

The total activity along a line is obtained by subtracting the background from the integration of the activity registered (fig.5) and multiplying it by the speed of the boat.

The maximum level of radio-activity remains below the real value because of the time constant T of the ratemeter. When the width of the radio-activity peak registered at half its height $W_{\frac{1}{2}}$ is more than 4 times the time constant the difference remains below 20%. In our experiments this width was nearly always more than 8 sec and T = 1 sec. so no corrections for the height of the peak were necessary.

INTERPRETATION OF THE RESULTS

In 1959 two series of simultaneous measurements were carried out for the purpose of investigating the main direction of the sand movement in the area around the entrance of the Rotterdam Waterway and the piers projected for the Europoort, the new harbour for supercargo vessels (fig.6).

In the first series various combinations of tracer quantity and radio-activity were placed on the Maasvlakte, a relatively shallow, faintly sloping area. It is generally supposed that the Maasvlakte is the main supplier of the sand that settles in front of and in the entrance to the Waterway. This sand, (about 800,000 m^3 a year) has to be dredged away continuously.

Figure 6 shows that only at points 3 and 4 the combination of tracer and radio-activity has been satisfactory. In both cases detection of tracer distribution proved to be possible 110 days after injection (fig.7). The limit of significance lay not more than some 600 mtrs from point 4 and 750 mtrs from point 3.

The influence of waves on sediment transport showed only at points 4 and 1. The tracer was at these points transported in two

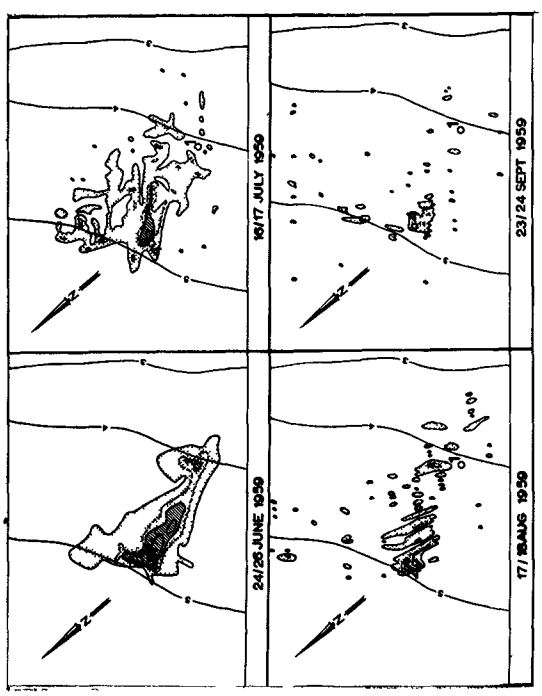

Fig. 7a

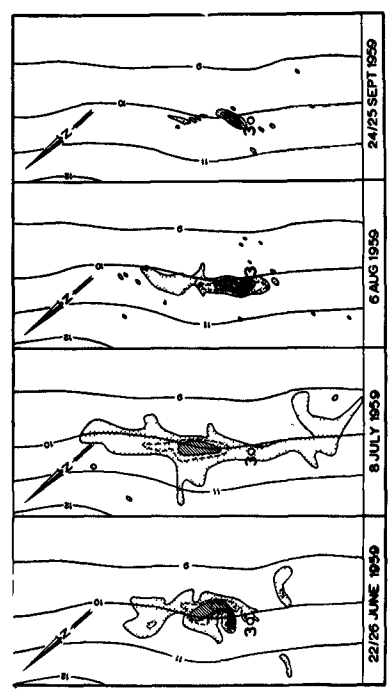

Fig. 7b

Fig. 7 Radio-activity readings taken in the same area at 4 [illegible]

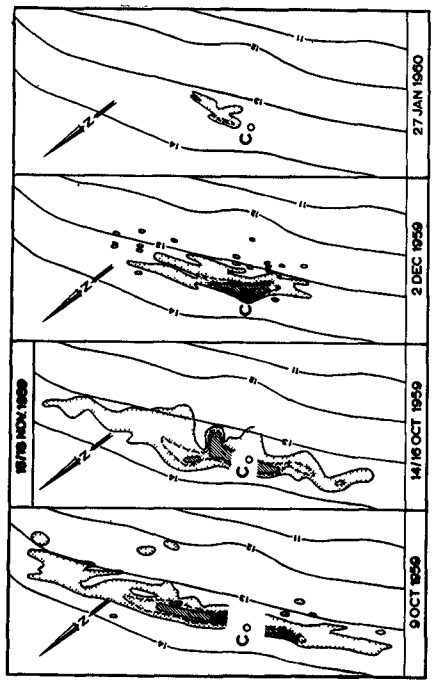

Fig. 7c

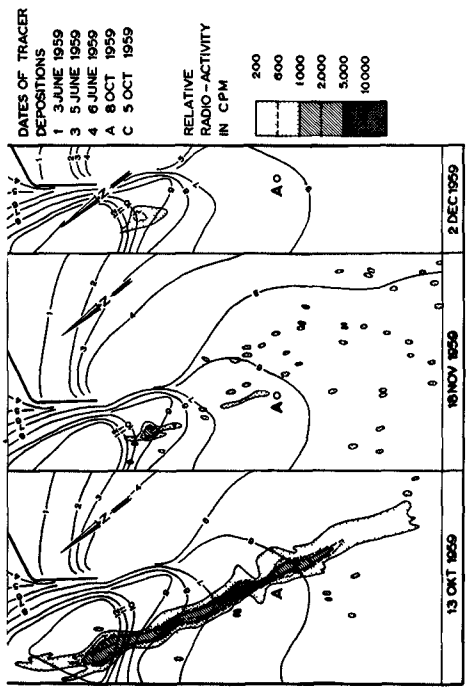

Fig. 7d

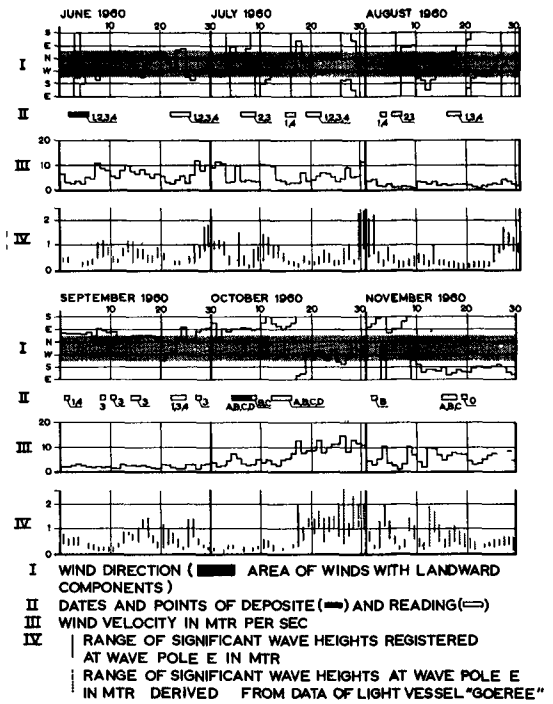

Fig. 8. Wind and wave data in the period in which readings were taken.

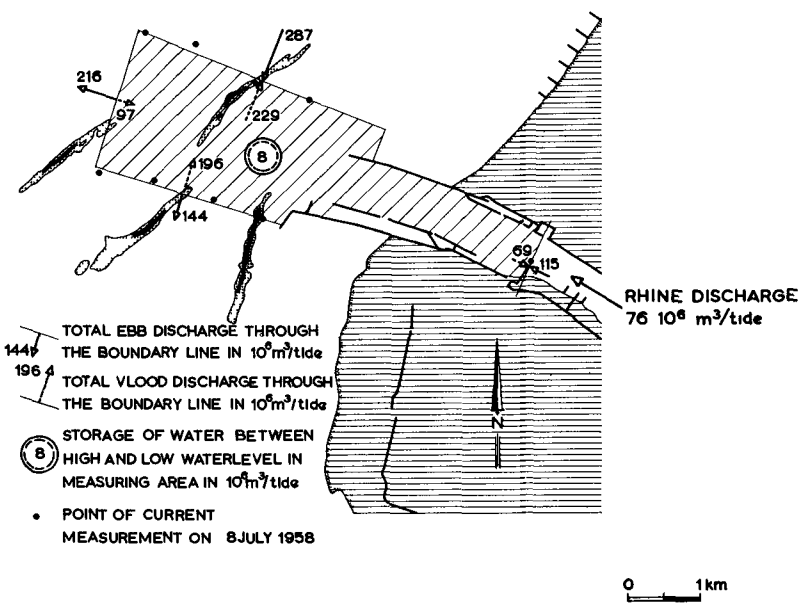

Fig. 9. Balance of current discharges at the entrance to the Rotterdam Waterway.

main directions, parallel to the contours by the current and in the direction of the Westplaat sandbank. During the period in which readings were taken the maximum significant wave height was 2 mtrs at the wave-pole E (fig.8).

In consequence of the results of the first series a second series of experiments was carried out in the same area (points A to D) with 50 kg tracer labeled with about 2 Curies Scandium^{46} per point.

A wave height of 2 mtrs at pole E was also registered in this period. The influence of these waves makes itself felt at point A and only above the contour of mean sea level minus 6 mtrs, while on the whole the waves are higher at point A than they are near pole. E.

The most important conclusion with regard to sand movement in the area is this, that the direction of transport in depths of over 6 mtrs is not influenced by the most common wave heights.

The current pattern in the vicinity of the entrance of the Rotterdam Waterway is rather complicated. The main tidal current parallel to the coast is strongly influenced by the currents passing in and out of the Rotterdam Waterway, which also discharges a large quantity of the fresh water of the river Rhine into the North Sea (fig.9). Nevertheless, the diffusion of the tracer is mainly parallel to the coast. Moreover, the shape of the lines joining points of equal radio-activity show but small diffusion perpendicular to the main transport direction. There was no significant prevalence of transport in either tidal direction.

The concentration of tracer material in the dip just beside the southern breakwater is remarkable (fig.7d). The frequent changes in depth of this dip (mostly about 2 mtrs in six months) lead to the hypothesis that the material dredged in the entrance to the Waterway comes mainly from the shallow areas beside it and that the deep places in front of the breakwaters serve as temporary storage accommodation.
Of course this hypothesis has to be checked very carefully by means of supplementary measurements near the breakwaters.

CONCLUSIONS

Measurements by tracer is still rather laborious but most technical problems concerning preparation, injection and detection have already been solved, so that the physical operations have become a matter of routine.

The results are most valuable compared with the results of soundings and current measurements. They give an impression of the direction of the bed-load transport and if more experiments are carried out simultaneously, an impression can also be obtained of the relative bed-load transport distribution in the area.

If similar tracer measurements are carried out in models and on the spot they may be of use for the interpretation of the results of the model studies.

REFERENCES

1. Progress report Rijkswaterstaat Juni 1957. Technical Memorandum no.105, March 1958, Beach Erosion Board.

CHAPTER 26

REJET DE MATERIAUX A LA MER PAR REFOULEMENT HYDRAULIQUE RISQUES DE POLLUTION DES PLAGES

Louis Greslou
Chef de Service à la Sogreah

Il peut paraitre intéressant lorsqu'une installation est implantée au bord de la mer de rejeter dans celle-ci les résidus de fabrication, qu'il s'agisse des cendres et suies d'une usine thermique, des stériles d'une mine, etc.

Divers procédés peuvent alors être utilisés et nous en énumèrerons rapidement quelques uns avant d'examiner plus en détail celui qui fait l'objet de la présente communication.

Le transport au large par chalands est une solution qui peut permettre le rejet du matériau à une grande distance dans une zone préalablement choisie pour éviter au maximum toute pollution éventuelle du rivage. Ce procédé suppose évidemment non seulement le matériel nautique nécessaire mais la proximité d'un port ou d'un abri naturel pour ces bateaux.

Le transport à une certaine distance du rivage par téléférique est une solution employée pour certains chargements de minerais. Mais l'installation que nécessite un tel dispositif risque d'entrainer des travaux trop onéreux pour l'évacuation de résidus de fabrication.

Dans le cas où la granulométrie du produit à rejeter est assez voisine de celle du matériau qui constitue les plages, ou évidemment si le rivage peut être pollué sans inconvénient majeur, le rejet peut être fait au voisinage de la laisse, la houle et les courants se chargeant d'entrainer au moins partiellement, le long du littoral ou vers le large, le stock ainsi réalisé à terre. Ce procédé, de beaucoup le plus simple et le plus économique, ne peut évidemment être employé qu'assez exceptionnellement.

Les solutions de rejet au large par chalands ou téléfériques étant donc en général beaucoup trop onéreuses, le déversement le long du rivage devant être souvent éliminé parce qu'inesthétique et même parfois dangereux, une solution consistant à refouler hydrauliquement le matériau à

*See English resume, p. 484

rejeter à une certaine distance du rivage peut alors paraitre séduisante.

Cette solution pose cependant un certain nombre de problèmes délicats, surtout lorsque la pente des fonds sous marins est douce et que le volume de matériaux à rejeter est important.

Dans cette communication nous exposerons les principaux résultats de deux etudes effectuées à la Sogreah, concernant le rejet par refoulement hydraulique de deux matériaux de granulométries très différentes.

En anticipant sur ce qui va suivre, un matériau rejeté au delà de la ligne de déferlement peut subir l'un des sorts suivants :

- soit demeurer sur place,
- soit être rejeté vers le rivage,
- soit être entrainé vers le large.

Un moyen particulièrement intéressant de réaliser cette dernière solution est de faire couler le matériau mêlé à l'eau sous la forme d'un "underflow" si la pente des fonds et la granulométrie le permettent.

Il est bien évident aussi que, suivant la granulométrie et les conditions hydrographiques et topographiques le matériau peut subir un tri : une partie peut demeurer sur place, une autre être entrainée au large, une autre enfin être rejetée vers le rivage.

On voit donc qu'avant d'aborder l'exposé proprement dit de nos résultats il peut être utile d'examiner les mécanismes élémentaires qui peuvent agir sur le matériau, et de façon plus précise l'action de la houle et des courants d'une part, le comportement d'un underflow d'autre part.

FACTEURS EN JEU

Les divers facteurs naturels susceptibles d'entrainer le matériau rejeté en mer sont essentiellement la houle et les courants.

La houle peut agir soit par la turbulence qu'elle provoque, soit par les courants qu'elle engendre.

REJET DE MATERIAUX A LA MER PAR REFOULEMENT HYDRAULIQUE RISQUES DE POLLUTION DES PLAGES

TURBULENCE PROVOQUEE PAR LA HOULE

Le mouvement orbitaire des particules d'eau tend à créer de la turbulence. Les dimensions des orbites sont bien connues et on déduit de la théorie de la houle irrotationnelle au 1er ordre l'expression de la vitesse orbitale maximum

$$V_o \max = \frac{2\pi a}{T} \quad \frac{1}{\operatorname{sh} \frac{2\pi h}{L}}$$

où $2a$ est l'amplitude (distance de crête à creux)
L est la longueur d'onde (distance entre 2 crêtes)
T est la période
h est la profondeur d'eau.

L'étude des conditions de début de mouvement des grains de matériaux constituant le fond révèle que la houle peut faire sentir son action même par des fonds de plusieurs dizaines de mètres. Une houle d'amplitude 6 m et de longueur d'onde 120 m doit être capable de mettre en mouvement un grain de sable de 0,3 mm par 60 m de fond. Mais s'il y a mise en mouvement, il n'y a pas forcément déplacement important. On peut même dire que l'intensité de ces déplacements est d'autant plus faible que l'on s'éloigne vers le large de la zone de déferlement.

COURANTS ENGENDRES PAR LA PROPAGATION DE LA HOULE A 2 DIMENSIONS

a) Pour une houle à deux dimensions, c'est à dire se propageant dans un canal, on constate que le mouvement orbitaire des particules s'accompagne, dans la masse fluide, d'un mouvement général. C'est ce qu'on appelle le "courant de transport de masse" ou "courant de masse".

Ce courant apparait d'ailleurs dans les équations de la houle en fluide parfait à partir du 2ème ordre et son existence dans la nature parait très vraisemblable pour une houle suffisamment régulière.

La distribution verticale des vitesses de ce courant de masse présente les caractéristiques suivantes :

- A proximité de la surface le courant porte en général dans le sens de propagation de la houle ; on a observé toutefois expérimentalement un courant portant en sens inverse pour les faibles valeurs du rapport h/L

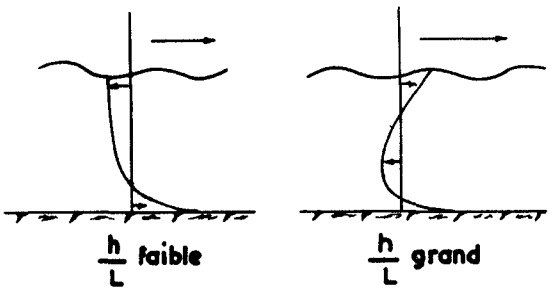

Fig. 1

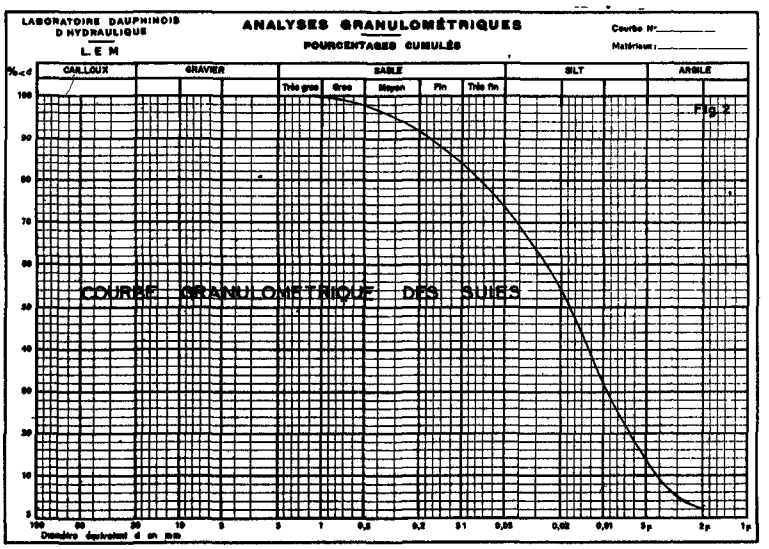

Fig. 2

SCHEMA DU CANAL A HOULE

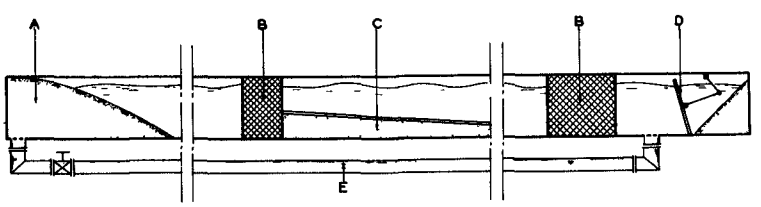

A Plage amortisseuse
B Filtre
C Chape en ciment
D Batteur à houle
E Conduite d'equilibrage

Fig. 3

- A proximité du fond, le courant porte toujours dans le sens de propagation ; il est particulièrement marqué dans une zone de faible épaisseur au voisinage immédiat du fond.

- Entre ces 2 zones le courant est de sens opposé : en canal fermé le débit sur une verticale étant nul, les débits dans les 2 sens sont égaux.

Nous avons indiqué sur la figure 1 de manière schématique deux répartitions types de ce courant observées en canal fermé.

b) Par ailleurs dans un liquide visqueux et dans un canal fermé du côté rivage, l'expérience montre qu'il existe sur le fond une couche limite dans laquelle se produit un courant dirigé dans le sens de la propagation de la houle progressive.

La valeur de ce courant est donnée par la théorie de Longuet-Higgins. Son intensité maximum est donnée par la formule :

$$U_{max} = \frac{1.376\,T}{L} V_{o}^{2}\,max$$

V_o max étant la valeur théorique maximum de la composante horizontale de la vitesse orbitale donnée précédemment (1er ordre, fluide parfait).

On voit donc que dans le cas schématique d'une houle à 2 dimensions atteignant un rivage, sans autre courant que ceux créés par la houle, le transport des matériaux peut se concevoir comme suit :

Le mouvement orbitaire des particules d'eau sur le fond et dans la masse tend à créer de la turbulence. Suivant le degré de turbulence ainsi crée et suivant la granulométrie et la densité du matériau, celui-ci pourra :

- soit rester immobile sur le fond,
- soit être mis en mouvement mais rester dans la couche limite du fond et donc avancer peu à peu vers le rivage,
- soit être mis en suspension et s'il est assez léger, monter dans la zone où existe un courant dirigé vers le large, une partie du matériau resté dans la couche limite ira donc vers le rivage comme décrit ci-dessus, une autre sera emportée vers le large,
- soit enfin être emporté encore plus haut par sa mise en suspension, jusque dans la zone où existe un courant de surface portant vers le rivage; outre les transports vers le rivage et vers le large décrits ci-dessus, s'ajoutera donc un transport vers le rivage au voisinage de la surface, de sorte que la mer entière dans toute sa masse

sera progressivement envahie par le matériau jusqu'à la ligne de déferlement.

Au déferlement se passent des phénomènes complexes de mise en suspension et de transport qui dépendent des caractéristiques de la houle, du mode de déferlement, de la nature du matériau, etc... Dans certains cas une partie au moins du matériau peut être rejetée sur le rivage et engraisser celui-ci.

COURANTS ENGENDRES PAR LA HOULE A 3 DIMENSIONS

Ce que nous venons d'exposer suppose que les mouvements dus à la houle sont à deux dimensions. En fait la houle se propage dans un milieu à trois dimensions et les résultats ci-dessus peuvent être profondément modifiés au moins en ce qui concerne les courants.

Les principaux courants engendrés par la houle du fait de cette 3ème dimension sont :

a) Le "longshore current" qui se produit lorsque la houle aborde obliquement un rivage constitué par un plan incliné. Il est en gros parallèle au rivage.

b) Le "ripcurrent" qui se produit sur un rivage à topographie irrégulière et qui résulte de l'accumulation de l'eau en un point du rivage. L'eau repart alors vers le large suivant un courant grossièrement perpendiculaire au rivage.

c) Le "courant d'Iribarren" qui se produit par exemple derrière un cap autour duquel diffracte la houle. Il se propage des zones de grande amplitude vers les zones de faible amplitude, par suite de l'accumulation de l'eau dans les premières. Il est en gros parallèle au rivage.

d) Le "beach drifting" mouvement des grains en dents de scie qui se produit dans le jet de rive quand la houle est oblique par rapport au rivage.

AUTRES COURANTS MARINS

D'autres courants que ceux dus à la houle peuvent également exister en mer. Ce sont en particulier :

a) les courants marins généraux,
b) les courants de marée,
c) les courants fluviaux si on se trouve à proximité d'une embouchure,

d) les courants dus au vent - Ces derniers sont généralement accompagnés par des vagues créées par ce même vent. Près d'un rivage avec un vent soufflant de la mer par exemple, on peut considérer que les vagues sont accompagnées d'un courant de surface relativement fort portant vers le rivage et d'un courant de retour en sens inverse au voisinage du fond.

e) les courants de densité - Ceux-ci peuvent être dus à des différences de température, de salinité ou de concentration en sédiments entre des couches d'eau voisines. Nous reviendrons plus loin sur le mécanisme de l'underflow, forme particuliere de ce courant de densité.

Si le mouvement orbitaire tend dans tous les cas à mettre le matériau en suspension et à le "livrer" en quelque sorte à l'action des courants ; l'existence des courants décrits dans les 2 paragraphes précédents peut modifier fondamentalement le processus de transport que nous avons esquissé plus haut sous l'action du courant de masse d'une houle à 2 dimensions.

Ce qui précède montre qu'avant de projeter une installation de rejet hydraulique il est nécessaire de mesurer de façon extrèmement soignée les conditions topographiques et hydrographiques locales (houles, courants, etc...)

L'UNDERFLOW

Les considérations qui précèdent conduiraient à penser que, dans le cas où le matériau a été disposé à des profondeurs telles qu'il puisse ensuite être remis en suspension par la houle, les courants de toutes sortes tendront à le répartir sur une zone très vaste de la mer, et en particulier sur les plages. S'il en était ainsi la solution de rejet en mer à une distance limitée du rivage serait insoluble.

Mais en réalité si le rejet hydraulique de matériau s'effectue dans certaines conditions de vitesse et de concentration on peut espérer obtenir l'écoulement du matériau vers le large par courant de densité sous forme d'underflow.

Parmi les très nombreux exemples de courant de densité, nous citerons celui du Rhône à son arrivee dans le lac Léman, car il se présente à l'état pur, les autres mouvements d'eau (vagues, seiches, courants généraux) ne jouant qu'un rôle négligeable.

Si l'on suit les eaux du Rhône en période de hautes eaux durant lesquelles le charriage de boue et sable fin glaciaire est relativement important, on voit d'abord ces eaux sales s'étaler à la surface du Lac, Puis après quelques centaines de mètres ces eaux plongent brusquement et verticalement vers le fond où un écoulement de fond (Underflow) s'établit.

A l'endroit où les eaux sales plongent, la ligne de séparation avec les eaux limpides du lac est très nette mais il y a de très forts tourbillons. Les eaux paraissent se livrer une violente bataille sans se mélanger, c'est pour cette raisons que le phénomène est appelé "bataillère" du mot français "bataille".

L'underflow ainsi formé s'écoule dans un chenal profond formé par le fleuve lui-même avec les alluvions qu'il transporte. Après 15 kilomètres environ ce chenal aboutit au fond du lac où les eaux sales se décantent suivant un plan horizontal de plusieurs kilomètres de côté.

Grâce à ce phénomène les eaux du lac Léman sont toujours parfaitement claires. Le même phénomène se produit sur le Rhin dans le lac de Constance.

Ce phénomène s'explique hydrauliquement de la manière suivante :

Lorsque un débit d'eau chargé de matériaux pénètre dans une masse d'eau claire il peut se produire à l'entrée et en surface une auréole colorée d'eau chargée où s'effectue un mélange. la masse d'eau chargée peut dans certaines conditions plonger dans l'eau claire et cheminer au fond.

Les facteurs qui déterminent la plongée sont en particulier le débit, la densité de l'eau chargée de sédiments donc la concentration. Dans le facteur débit intervient la vitesse de l'écoulement qui peut être plus ou moins grande du fait de la topographie des lieux.

La plongée est produite par l'ensemble des sédiments qui ont tendance à descendre et qui entraînent l'eau avec eux. Pour que la plongée s'effectue il faut que l'écoulement d'eau chargée parcourt une certaine longueur pour trouver une profondeur suffisante. Le vent peut faire varier la longueur de parcours.

Lorsque la plongée s'est effectuée un courant peut donc s'établir au fond de la masse d'eau claire; à cause de la turbulence de l'écoulement des sédiments suffisamment fins sont maintenus en suspension. A la partie supérieure du courant de densité existe un entraînement d'eau claire. Dans cette zone d' entraînement souvent appelée interface se produit un mélange. Lorsque le courant de densité est établi on rencontre sur une verticale à partir du bas, d'abord un écoulement très net dont la densité est supérieure à l'eau (mais si les sédiments en suspension sont très fins la densité dans la masse du courant varie peu), plus haut existe une zone où la densité décroît pour atteindre la densité de l'eau claire et au-dessus l'eau claire.

Les lois établies pour les courants de densité sont assez semblables aux lois régissant les courants à surface libre. Les principales caractéristiques des courants de densité sont établies en faisant intervenir les forces de pression, de pesanteur et de frottement du courant sur le fond et à l'interface. L'équation générale est la suivante :

$$U^2 = \frac{8}{k} \frac{\Delta\rho}{\rho + \Delta\rho} g \; Ri$$

U : vitesse de l'écoulement

ρ : masse spécifique de l'eau claire

$\rho + \Delta\rho$: masse spécifique du courant de densité

g : accélération de la pesanteur

i : pente du fond sur laquelle s'établit l'écoulement

R : rayon hydraulique de l'écoulement défini par le rapport de la section occupée par le courant au périmètre mouillé $R = \frac{lh}{l + 2h}$ avec

l = largeur de la section

h = profondeur de l'écoulement.

k : est un coefficient de frottement dépendant de la rugosité du fond et de l'interface.

La relation indiquée plus haut montre que les lois des courants de densité sont semblables à celles des écoulements à surface libre.

Cependant dans ces derniers la pesanteur intervient directement alors que pour les courants de densité la pesanteur est réduite d'une manière importante par le terme $\frac{\Delta \rho}{\rho + \Delta \rho}$. C'est pourquoi les courants de densité ont des vitesses d'écoulement assez faibles alors que les hauteurs sont assez importantes. Ceci explique que des courants même faibles dus à d'autres facteurs (houle, marée, etc...) puissent contrecarrer ce cheminement.

ETUDES PARTICULIERES EFFECTUEES A LA SOGREAH

Le problème du rejet en mer par refoulement hydraulique peut donc se ramener dans la plupart des cas à examiner :

1°- s'il est possible, compte tenu de la granulométrie du matériau à rejeter, d'obtenir une concentration du mélange d'eau et de matériau et une vitesse d'écoulement de ce mélange susceptibles de provoquer un underflow,

2°- si les facteurs océanographiques (pente des fonds, houle, courants, etc...) permettront à cet underflow de se propager suffisamment loin vers le large en entrainant avec lui la majeure partie du matériau.

Ce problème est malheureusement très complexe et les résultats obtenus dans des cas très différents ne peuvent donner des enseignements qui permettraient de résoudre tous les problèmes. Cependant les 2 études dont nous allons exposer maintenant les résultats et qui se rapportent à des matériaux de granulométries très différentes nous ont paru susceptibles de fournir des indications intéressantes sur la formation des dépots sous-marins.

Nous attirons d'autre part l'attention sur le fait qu'il est pratiquement impossible de réaliser une similitude correcte sur un modèle d'ensemble comme nous le verrons plus loin ; aussi est-on amené à étudier un certain nombre de cas schématiques dont les conclusions peuvent être utiles pour l'étude de cas plus complexes ; cette façon de procéder sera justifiée par la suite.

1ère ETUDE : REJET A LA MER DES SUIES D'UNE CENTRALE THERMIQUE

Exposé du problème

Le problème consistait à déterminer un procédé simple et économique pour évacuer 500.000 tonnes de suies chaque année avec un débit maximum de 2.000 tonnes par jour environ.

La granulométrie de ces suies était définie par la courbe ci-jointe (V. fig. 2), le diamètre moyen se situant vers 20 microns.

Le procédé habituellement utilisé pour se débarasser de la suie, quand la centrale est a proximité de la côte consiste à la déverser au large en utilisant des chalands. Cette méthode, d'ailleurs efficace, aurait entrainé, pour le projet considéré, des frais tant d'investissement que d'exploitation très importants et apparemment beaucoup plus élevés qu'un dispositif de pompage et de rejet, relativement près du rivage d'une mixture d'eau et de suie.

On pouvait espérer, la densité de la mixture étant supérieure à celle de l'eau, qu'un courant de densité se formerait au débouché de la conduite et qu'il s' écoulerait assez loin du rivage pour que la suie soit transportée au delà de la limite en deça de laquelle elle est indésirable. Sa présence soit sous forme d'un nuage en suspension large et épais, soit sous forme de dépots par faibles profondeurs pouvait polluer non seulement les plages balnéaires avoisinantes, mais aussi les emplacements fréquentés par les poissons.

Les problèmes posés à la Sogreah

Il a donc été demandé à notre Société de déterminer par une série d'essais :

- d'une part les chances de formation d'un underflow et les meilleures conditions pour l'etablissement de celui-ci, compte tenu de la granulométrie du matériau et de la pente des fonds,
- d'autre part l'effet sur cet underflow de la houle et des courants.

Les moyens employés

Comme nous l'avons signalé précédemment, il est impossible de realiser en similitude un modèle reproduisant l'ensemble des phénomènes à étudier.

En effet, si on réalise les écoulements et mouvements d'eau en similitude, il faut trouver alors un matériau qui, à l'échelle choisie, réagisse aussi en similitude à la mise en suspension et à la sédimentation. Ceci exigerait en particulier une similitude de turbulence et on sait que ceci est théoriquement impossible.

Pour tourner cette difficulté on peut essayer d'employer sur le modèle le même matériau que dans la nature et d'ajuster alors les facteurs hydrauliques pour qu'ils agissent sur lui de manière à peu près equivalente.

En ce qui concerne la houle, nous avons vu que celle-ci agit en particulier par le mouvement orbitaire des particules d'eau et par les courants de masse auxquels elle donne naissance.

Il est possible de trouver pour la houle modèle des valeurs de 2a, L et h telles que la vitesse orbitale sur le fond soit la même sur le modèle que dans la nature. Cette condition est réalisée, si h et L étant réduits dans le rapport λ , 2a est réduit dans le rapport $\sqrt{\lambda}$.

Cependant le mouvement orbitaire existe sur toute la hauteur et contribue à maintenir le matériau en suspension. Cette mise en suspension est fonction des vitesses des particules et de la distribution de ces vitesses. Du fait que l'amplitude des vagues et la profondeur sont plus petites sur le modèle que dans la nature, on ne peut obtenir la même répartition de vitesse, si on s'impose l'égalité des vitesses orbitales au fond. Par conséquent les effets du mouvement orbitaire de la houle dans toute la masse d'eau ne peuvent être reproduits en similitude si on emploie sur modèle le même matériau que dans la nature.

Quant aux courants de masse, ils sont trop mal connus pour définir leur similitude. Il est cependant admis que la vitesse du courant de masse au fond augmente pour une houle donnée quand la profondeur diminue et d'après Longuet Higgins, sa valeur maximum serait, comme nous l'avons vu précédemment, liée à celle de la vitesse orbitale maximum au fond par une relation de la forme

$$U_{max} = f\left(\frac{T}{L} V_{o\,max}^2\right)$$

Par conséquent, si la houle du modèle à la même vitesse orbitale au fond qu'une houle nature plus grande, les courants de masse près du fond ne seront pas les mêmes, Il est important cependant de noter que le courant induit va dans le même sens et agit dans une région où règne un degré de turbulence semblable (créé par les vitesses orbitales) : les mouvements seront donc proportionnels.

Ces considérations montrent qu'une étude sur modèle précise et quantitative des phénomènes est pratiquement impossible. On peut cependant utiliser les essais de Laboratoire:

- soit pour mieux connaitre le comportement des matériaux à certaines actions hydrauliques,
- soit pour fournir des images permettant une certaine analogie avec les images réelles et grâce auxquelles les Ingénieurs peuvent tenter des prévisions pour la réalité.

Les essais ont consisté dans le cas de cette étude :

a) à étudier d'abord à 2 dimensions dans un canal à houle le comportement du matériau nature soumis à la houle,

b) à chercher à caractériser sur un modèle plus vaste, l'action de la houle à 3 dimensions sur des écoulements de mixture suie et eau en fonction de la concentration de celle-ci.

c) à rechercher dans une installation spécialement aménagée pour l'étude des courants de densité, la concentration optimum à donner à cette mixture pour obtenir un underflow.

Description des essais

a) Essais en canal à houle

Nous avons utilisé un canal à houle de 70 m de long et 1 m,20 de large vitré sur 9 m de long et équipé d'un batteur plan articulé sur le fond (V. fig. 3). La période et l'amplitude de la houle étaient facilement réglables, la 1ère à l'aide du variateur de vitesse du groupe moteur d'entrainement du batteur, la 2ème par variation de l'excentricité du système bielle-manivelle d'attaque du volet. Un jeu de filtres placés devant le batteur purifiait les houles en supprimant les harmoniques et en empêchant les houles réfléchies de revenir jusqu'au batteur. Ces réflexions étant d'ailleurs réduites au minimum par d'autres filtres situés à l'autre extrémité du canal et en haut de la plage de manière à éviter les effets parasites sur la suie disposée dans le canal.

Après avoir aménagé dans le canal une plage en ciment de pente 5 % une bande de suie de 2 à 3 centimètres d'épaisseur et de 10 à 15 cm de largeur fut placée sur celle-ci, perpendiculairement à l'axe du canal à une profondeur de 60 cm.

Cette profondeur fut choisie aussi grande que possible afin que, pour une vitesse sur le fond donnée, la condition de répartition des vitesses dans la profondeur ne soit pas trop éloignée de la réalité.

On fit alors agir une houle de 1,35 sec de période dont l'amplitude fut montée progressivement de 40 mm à 160 mm.

Après avoir observé pour 75 mm la formation d'un léger nuage de suie, celui-ci s'épaissit pour des amplitudes plus fortes quelques grains commençaient à remonter la pente sur le fond et en suspension tandis qu'un underflow se formait et descendait lentement la pente. Les 2 mouvements inverses s'accentuaient pour 160 mm d'amplitude. Sur les fig. 4 et 4 bis, on a groupé quelques photographies montrant le phénomène et le front d'underflow.

Il convient de noter que tout près de la plage sur des fonds très faibles le matériau qui remonte se met en suspension et occupe toute la hauteur d'eau sur une certaine distance à partir du rivage. Lorsque la concentration de ce nuage augmente un underflow se forme, plonge et redescend vers le large sous l'eau claire. La vitesse de cet underflow très faible à cause de l'opposition des courants de houle, augmente considérablement dès que la houle s'arrête.

Ces essais permirent d'observer que les houles étaient capables :

- de remonter du matériau vers la plage malgré la pente des fonds,
- de permettre la formation d'underflow à partir d'un tas disposé en eau calme, un underflow se forme d'une part à l'aplomb du tas et d'autre part, par très faibles fonds, près du rivage quand la concentration du nuage devient suffisante.

Cet underflow subsiste et se propage malgré l'action turbulente de la houle qui tend à le désorganiser et le courant de masse vers le rivage, existant dans la couche limite, qui tend à le freiner.

On peut également déduire de ces essais par la théorie irrotationnelle au 1er ordre, en supposant que la vitesse orbitale sur le fond est en 1ère approximation la seule force agissant sur les grains, que pour le matériau considéré une houle de 10 sec de période et 1 m d'amplitude peut commencer à faire bouger les grains de suie considérés par une profondeur de 40 m environ et qu'une houle de même période et d'amplitude 3 m,50 peut avoir la même action pour une profondeur d'environ 75 m.

Fig. 4. Action de la houle sur un tas de suie.

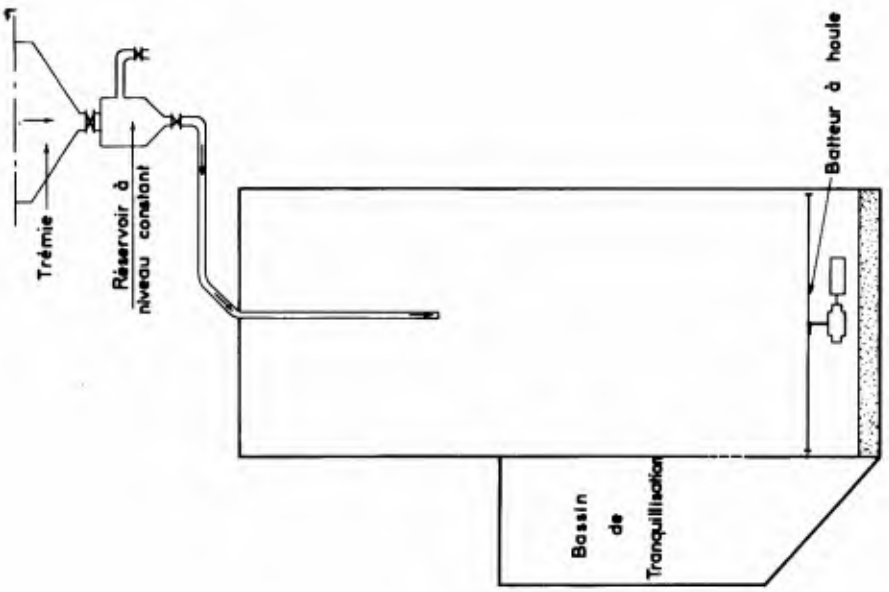

Fig. 5. Schema du bassin a houle.

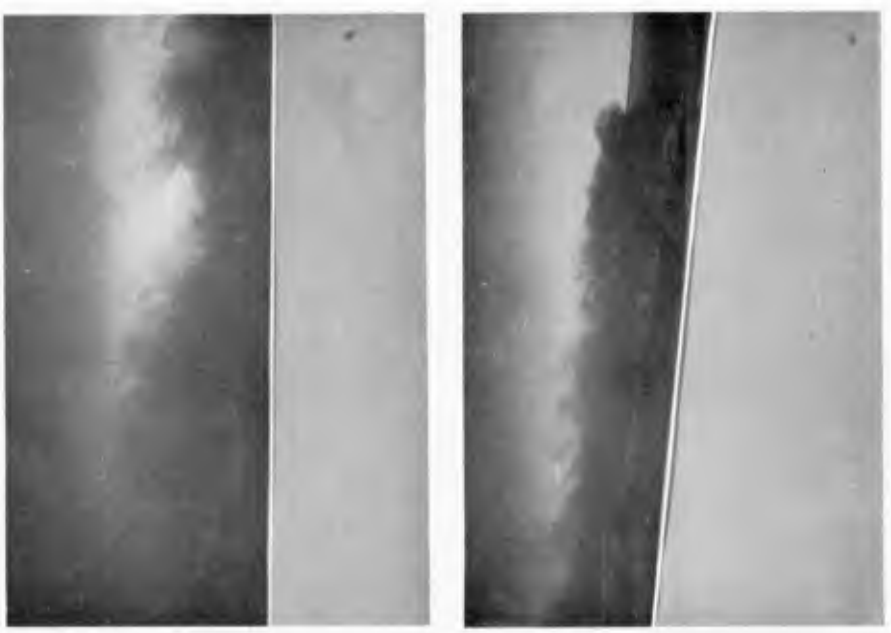

Fig. 4 bis. Action de la houle sur un tas de suie (underflow).

b) Essais dans un bassin de plus grandes dimensions

Ces essais ont été réalisés dans un bassin rectangulaire de 25 m de long par 10 m de large équipé d'un batteur à houle sur toute sa largeur. A l'autre extrémité du bassin était installée une cuve mélangeuse dans laquelle était préparée la mixture de suie à la concentration désirée. Celle-ci était envoyée ensuite après réglage du débit à la valeur désirée dans un tuyau flexible permettant de la rejeter dans le bassin à la distance voulue du rivage (V. fig. 5)

Dans le bassin avait été en effet reproduite une plage de pente uniforme en ciment de 1,3 % correspondant à la pente moyenne des fonds naturels dans la région considérée, avec distorsion de 2.

Les échelles adoptées ont été en effet le 1/200 en plan et le 1/100 en hauteur. Ces échelles avaient un caractère assez arbitraire, car le peu de temps dont on disposait pour effectuer cette étude n'avait pas permis au préalable d'effectuer des recherches systèmatiques pour définir les échelles et le matériau à utiliser, ni d'effectuer ensuite les essais sur un modèle encore beaucoup plus vaste et plus complexe pour s'affranchir complètement de tout effet de paroi susceptible de créer des courants parasites.

Les essais n'avaient donc pas la prétention de donner des résultats quantitatifs, mais seulement de fournir aux ingénieurs chargés du projet une image des phénomènes susceptibles de se produire au débouché de la conduite rejetant la mixture en mer.

L'échelle en plan de 1/200 a donc été choisie en fonction des dimensions de l'installation quant à l'echelle en hauteur nous l'avons prise égale à 1/100 afin d'avoir une profondeur d'eau suffisante sans modifier cependant de façon trop sensible la pente du fond par rapport à la réalité.

La houle de crêtes parallèles au rivage, engendrée par le batteur avait des caractéristiques telles que les essais soient matériellement réalisables et qu'une interprétation qualitative raisonnable soit possible. En effet respecter les vitesses sur le fond aurait nécessité de très fortes amplitudes, donc des houles extrèmement cambrées qui auraient donné une très mauvaise répartition des vitesses sur une verticale : mais respecter cette répartition de vitesses aurait conduit à adopter des houles très petites engendrant des vitesses au fond sans action sur le matériau. Nous avons donc choisi des caractéristiques moyennes entre celles qu' auraient données ces 2 conditions contratictoires.

Fig. 6. Forme du 1 er dépot sans houle.

REJET DE MATERIAUX A LA MER PAR REFOULEMENT HYDRAULIQUE RISQUES DE POLLUTION DES PLAGES

Les essais furent effectués d' bord sans houle avec différents débits et différentes concentrations de mixture, l'extrémité du tuyau se trouvant, sur le modèle, à une distance du rivage correspondant approximativement à 8 m,50 par une profondeur de 15 cm environ.

Un premier essai fut effectué en rejetant pendant 1 h.30 dans le bassin un débit de 0,15 l/s. d'un mélange de densité 1,03 (environ 60 gr. de suie par litre).

A l'extrémité du tuyau le jet s'élargit rapidement en éventail formant un dépot autour du débouché. Le mélange qui continue à arriver s'écoule par vagues successives sur les flancs du tas déjà constitué de façon analogue à un courant de densité mais en se répandant tout autour de l'orifice (V. fig. 6).

Le même essai repris en rejetant dans le bassin pendant 14 heures un débit 3 fois plus fort d'un mélange de densité plus faible 1,01 (soit 20 gr. par litre) donna des résultats très semblables. La différence essentielle résidait dans la force de l'écoulement qui maintenait le débouché dégagé, de sorte que le matériau avait moins tendance à remonter. Une remontée existait cependant encore en raison en particulier de la réflexion du jet sur le parement raide du dépot face au débouché. (V. fig. 7)

Ces 2 essais effectués sans houle pour des conditions de débit et de densité de mixture très différentes permirent de conclure qu'il n'y avait guère d'espoir d'obtenir un courant de densité limité en largeur.

Sur le dépot formé en eau calme lors du 2ème essai on fit alors agir une houle de 7mm d'amplitude, tout en continuant à introduire la mixture. On observa alors un certain arasement de l'ile formée par le dépot, un adoucissement de sa pente côté large et une recrudescence de l'écoulement de l'underflow vers le large. Ceci peut s'expliquer d'une part par le fait que la houle, favorisant la mise en suspension, augmente la concentration du mélange et alimente ainsi l'underflow, d'autre part parce qu'en arasant l'ile, la houle ouvre ainsi un chemin au jet et facilite sa propagation vers le large. Il n'en reste pas moins toutefois que, si la houle favorise le dépot de la suie au large, elle transporte également des grains vers le rivage. En prolongeant l'essai avec des houles de 14 mm puis de 30 mm d'amplitude on observe les mêmes phénomènes (V. fig. 8 et 8 bis).

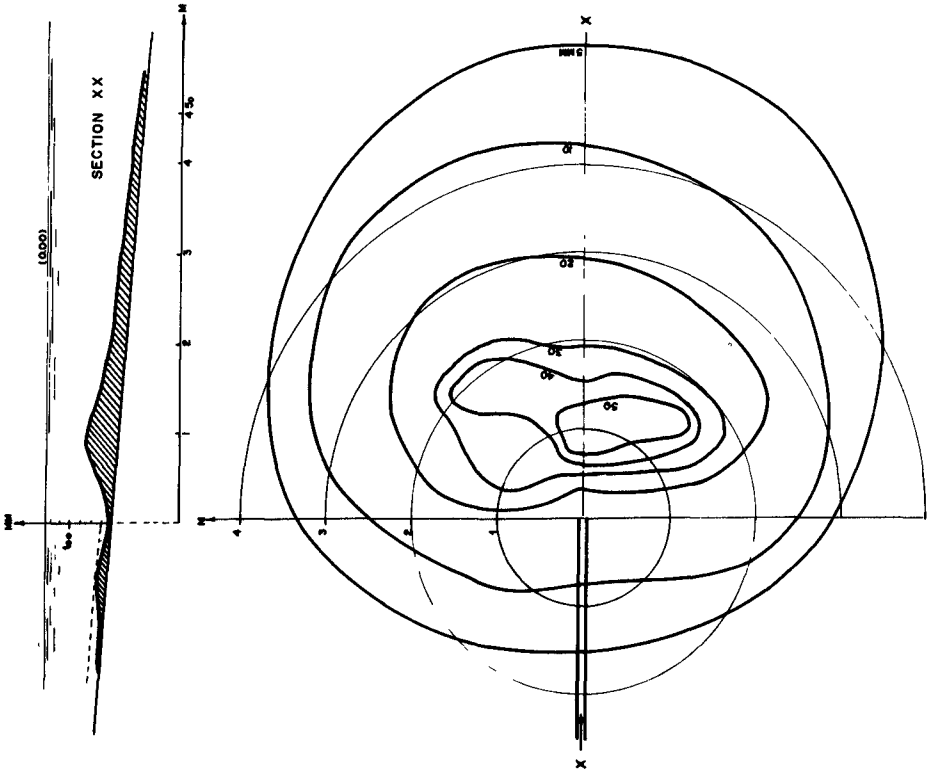

Fig. 8. Forme du 2 eme dépot avec houle.

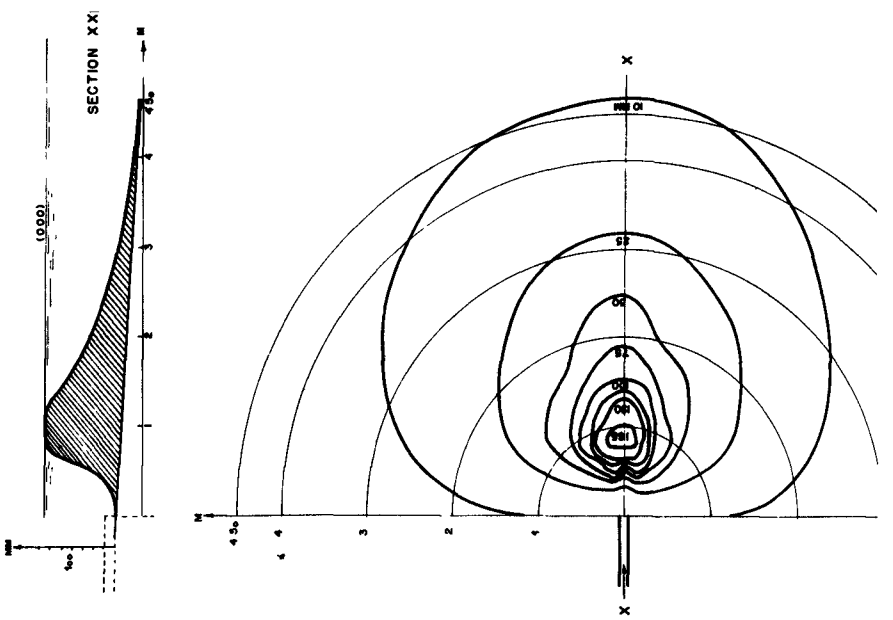

Fig. 7. Forme du 2 eme dépot sans houle.

Fig. 8 bis. Forme du 2 eme depot sans houle.

Il sembla alors utile d'effectuer un essai en faisant agir la houle des le début de l'introduction de la mixture. L'essai fut donc recommencé avec un débit de 0,45 l/sec de la mixture de densité 1,01 précédente et une houle de 1 sec de période et 30 mm d'amplitude et ceci pendant 10 h. de sorte que 400 Kg de suie furent introduits dans le bassin.

Quoique le processus de formation d'un tas en face du débouché ait été assez analogue, l'épaisseur de ce tas fut beaucoup plus faible, un courant de densité plus important se forma avec l'aide de la houle. Malgré cela la suie se déposa en une fine couche dans tout le bassin.

Une analyse granulométrique de plusieurs échantillons prélevés après chacun de ces essais dans le bassin à différentes distances du débouché du tuyau permit de vérifier un tri, les grains les plus fins étant les plus au large et en proportion plus importante quand la houle a agi.

c) Essais dans un canal spécialement aménagé pour les études d'underflow

Pour ne pas allonger outre mesure cet exposé, nous ne citerons que pour mémoire les essais effectués sur une installation spéciale de notre Laboratoire destinée à l'étude des courants de densité.

Le but de ces essais était de definir la concentration optimum permettant à l'écoulement d'entrainer le maximum de suie avec le dépot le plus faible. Il existe en effet simultanément deux tendances opposées. La première est de realiser un courant d'une densité assez élevée afin que les vitesses d'écoulement soient suffisantes pour entrainer les matériaux. Mais si les grains ne sont pas très fins, plus la densité est élevée, plus il faudra d'énergie à l'écoulement pour transporter le materiau. Par contre la deuxième tendance, consistant au contraire à réaliser un courant de densité assez faible, conduira à un écoulement à faible vitesse donc à des dépots.

Les essais effectués, quoique rapides et schématiques nous ont amenés à préconiser une concentration voisine de 20 à 30 gr/litre pour se trouver dans les conditions optima de formation d'un underflow.

d) Conclusions

Malgré la difficulté d'interprétation de ces essais il semble que l'on puisse en tirer les conclusions suivantes:

Si le matériau est rejeté à une certaine profondeur de 10 m par exemple, les grains les plus gros se déposeront à une certaine distance de l'extrémité du tuyau et l'accumulation qu'ils formeront sera rabotée par l'action directe des houles.

Sous l'action de ces vagues le matériau déposé remontera en partie vers le haut de la plage en formant un nuage en suspensions qui sera très sensible à l'action de courants parallèles au rivage ou de houles obliques qui contribueront à son étalement. Une partie du matériau pourra vraisemblablement se déposer sur la plage, mais une autre partie repartira vers le large car la masse en suspension aura tendance à plonger dès qu'elle aura atteint une concentration suffisante.

Par ailleurs à l'aval du tuyau la mixture après avoir perdu ses éléments les plus gros, s'écoulera vers le large sous forme de courant de densité. Cependant, étant donné la très faible pente des fonds dans le cas considéré, il se produira un étalement de cet écoulement, fonction aussi de la forme du dépot à proximité du tuyau ; ceci provoquera des dépots successifs de matériaux de plus en plus fins au fur et à mesure de sa propagation vers le large.

Autrement dit dans le cas précis qui a été étudié dans cette première étude, malgré la granulométrie assez fine du matériau rejeté, l'underflow qui se formera à la sortie de la conduite ne sera vraisemblablement capable de transporter vers le large que les matériaux les plus fins car, d'une part, étant donné l'hétérogénéité du matériau, il sera impossible d'éviter le dépot des grains les plus gros, d'autre part la faible pente des fonds et la présence du dépot précédent étaleront cet underflow, lui enlevant de ce fait une partie de son efficacité. L'action de la houle sur ces dépots pourra provoquer une remontée du matériau vers le rivage, mais une faible partie decelui-ci devrait seulement s'y déposer.

2ème ETUDE : REJET A LA MER DES STERILES D'UNE MINE D'AMIANTE

Exposé du problème

Il s'agissait cette fois d'évacuer par un procédé quelconque les 600.000 tonnes par an de stériles résultant de l'extraction de l'amiante d'une mine située à proximité de la mer.

La situation du gisement conduisait donc tout naturellement à envisager un rejet en mer.

Malheureusement le matériau à rejeter est beaucoup plus gros que celui étudié au cours de la précédente étude, son diamètre moyen étant de l'ordre de quelques mm. Il y avait donc tout lieu de penser qu'une solution par rejet hydraulique ne permettrait pas d'obtenir un underflow susceptible d'emporter le matériau vers le large. Les courants de densité ne se développent en effet qu'avec des matériaux dont la majorité des grains est nettement inférieure à 50 microns.

Les problèmes posés à la Sogreah

Il fut demandé à notre Société d'effectuer une étude critique, du point de vue hydraulique des divers procédés d'évacuation en mer, à savoir :

- transport vers le large par chalands
- refoulement hydraulique par conduite immergée
- rejet au rivage

afin d'apprécier leurs possibilités d'application.

Nous ne retiendrons dans cet exposé que la 2ème solution du refoulement hydraulique. La formation d'un underflow étant exclue, il restait cependant à examiner la possibilité de former des tas de stériles à une profondeur telle que l'action de la houle et des courants sur ces tas soit négligeable.

Les moyens employés

Les études comportèrent tout d'abord une campagne hydrographique très complète pour recueillir les données nécessaires à savoir :

- levé hydrographique au 1/2.500 de la zone intéressée,
- prélèvement de nombreux échantillons de fonds pour analyser la nature de ceux-ci,
- direction et intensité des courants marins,
- caractéristiques des houles,
- etc...

L'étude du transport hydraulique pour un débit solide de 100 tonnes/heures nécessitait la connaissance de l'écoulement des stériles à la sortie du tuyau en mer.

REJET DE MATERIAUX A LA MER PAR REFOULEMENT HYDRAULIQUE RISQUES DE POLLUTION DES PLAGES

Cet essai a été effectué avec un matériau analogue à celui de la réalité (V. fig. 9 sa courbe granulométrique) dans un canal vitré représentant la mer suivant une coupe verticale (la paroi vitrée). Devant la vitre arrivait une conduite d'amenée du matériau, qui était en réalité une 1/2 conduite plaquée contre la vitre pour permettre l'observation du phénomène en coupe. Une pompe à vitesse variable permettait des essais à différentes vitesses de transport. L'installation était complétée par un venturi pour mesurer les débits, donc les vitesses, et un manomètre pour suivre l'évolution de la pression nécessaire à assurer l'écoulement à la sortie de la conduite.

On put observer les phénomènes suivants :

Le jet de sortie transporte les matériaux à quelques dizaines de cm de l'extrémité de la conduite. Cette longueur varie avec la vitesse de transport. Les materiaux dont la granulométrie est étendue subissent une sorte de triage. Les gros grains s'arrêtent les premiers, les fins continuent un peu leur course. Les grains arrivant successivement se heurtent à ceux déjà déposés et le tri se continue.

Les gros grains sont stoppés, les fins sautent pardessus. D'où, dès le début, apparition d'une petite dune en face de l'orifice de sortie. Cette dune s'élève peu à peu et à mesure se développe un croissant (ou 1/2 croissant sur la maquette puisque le phénomène est reproduit en coupe).

Cette dune s'élève et se rapproche de l'orifice de la conduite. Elle présente une pente raide côté jet et une pente douce côté libre. La hauteur de la dune dépasse peu à peu la hauteur du tube et le jet s'infléchit vers le haut. Le croissant allonge ses bras et vient se refermer en arrière du jet.

Le phénomène se poursuit. L'extrémité de la conduite est prise dans un tas. Ce tas devient un cône tronqué dont le centre est un écoulement en forme de cheminée.

Les photos prises en cours d'essai et représentées sur la figure 10 montrent l'évolution du tas depuis le début jusqu'à la formation du cône.

Pour permettre une évolution plus rapide du phénomène, la vitesse de transport a été choisie basse : 1,20 m/s. La force du jet est affaiblie en proportion. On constate cependant que malgré la hauteur du cône et la quantité des gros grains accumulés dans la cheminée, l'écoulement reste libre. La pression nécessaire au maintien du débit ne s'accroît que faiblement avec la hauteur du cône.

En cas d'arrêt, tous les matériaux en mouvement dans la cheminée tombent et obstruent l'extrémité de la conduite. Le tas a alors l'aspect d'un volcan éteint (cône tronqué et incurvé à son sommet). C'est ce que montre la photo n° 5. La remise en route se fait aisément même à des vitesses de pompe très inférieures à celles de fonctionnement. La pression au démarrage par contre devient légèrement supérieure à celle au fonctionnement.

Ces observations permettent de conclure que :

a) Le rejet en extrémité de conduite forme un tas cônique dont la pente est la pente naturelle du matériau dans l'eau. Les caractéristiques du cône sont donc indépendantes :

- de la vitesse de transport
- de la position de l'extrémité du tube.

b) Seule la hauteur du cône, donc le volume de matériau rejeté, dépend de la force du jet.

c) La pression au redémarrage est supérieure à celle nécessaire au fonctionnement. C'est donc celle-ci qui, en définitive, déterminera la hauteur maximum admissible pour le fonctionnement de l'installation.

Il restait donc à déterminer les volumes maxima qui pourraient être rejetés ainsi en mer sous forme de cône en fonction du profil sous marin.

A cet endroit les pentes sous marines sont de l'ordre de 5 à 10 % jusqu'à une distance de 2 Km où elles atteignent 50 %. Mais ces pentes importantes ne prennent naissance qu'à une profondeur de 100 mètres. Leur intérêt est donc anéanti par l'impossibilité matérielle d'aller poser des conduites à de telles profondeurs.

Si on se limite alors au rejet par 40 m de fond la pente de ceux-ci ne permettra pas l'évacuation vers le large du matériau par glissement et on aura un cône analoque à celui observé sur modèle.

Pour éviter que les parties légères du matériau ne soient reprises par la houle il semble prudent de limiter la hauteur du cône à 25 m environ, on arrive donc ainsi à un cône de 65.000 m3. La quantité annuelle à rejeter étant de 400.000 m3, il faudrait donc réaliser 6 tas semblables c'est à dire déplacer 6 fois par an l'extrémité de la conduite d'une distance minimum de 100 mètres. Si on considère que les 50 derniers mètres de la conduite seront sous le talus, on voit de suite l'impossibilité de cette manoeuvre.

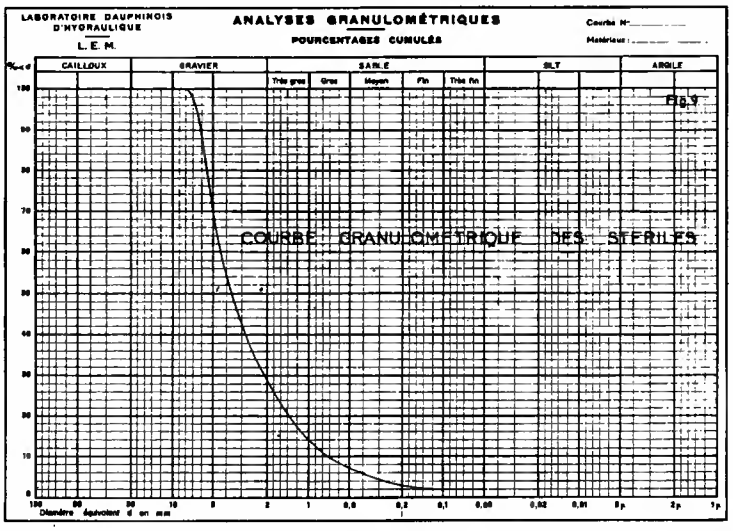

Fig. 9

TRANSPORT HYDRAULIQUE
DE STERILES D'AMIANTE

EXTREMITE DE LA CONDUITE


1


2


3


4


5

Fig. 10

Ces essais situent exactement le problème.

Le transport hydraulique est techniquement réalisable - dans le cas particulier le débit de 100 t/heure pourrait être refoulé sur 1 Km dans une conduite de 200 mm par 3 pompes en série donnant une puissance totale de l'ordre de 350 CV.-.

Le rejet en mer, même sous un tas important est possible, seul obstacle : le faible volume qui peut s'entasser naturellement à l'extrémité de la conduite.

Pour augmenter ce volume on peut jouer sur 2 facteurs : la hauteur du cône et le diamètre du cercle de base.

La hauteur du cône est liée à la profondeur à laquelle est installée l'extrémité de la conduite. On peut donc difficilement gagner sur ce facteur sans se heurter à des difficultés de pose de celle-ci.

Par contre le diamètre de base étant lié à la pente du talus naturel du matériau sous l'eau, on peut penser adoucir celle-ci en réduisant le diamètre des grains par broyage.

Nous avons repris les essais précédents en canal vitré en éliminant tous les grains supérieurs à 2 mm et en ajoutant 15 % de sable inférieur à 300 microns. Malgré la présence de ces éléments fins, la pente naturelle est restée la même. Un autre essai effectué uniquement avec du sable de 300 microns nous redonna encore la même pente de 50 % environ. Il faudrait donc arriver à un broyage à 50 microns pour trouver l'ébauche d'une solution. Le matériau ne serait plus alors qu'une fine poussière et ce serait une véritable boue qui s'écoulerait en mer suivant un processus analogue à celui examiné dans la précédente étude.

Dans le cas particulier ceci nécessiterait l'investissement de capitaux importants dans une installation de broyage.

CONCLUSION GENERALE

L'exposé précédent permet de se rendre compte de la complexité de tels problèmes;ceux-ci demandent a être étudiés dans chaque cas avec un soin tout particulier. On peut en effet difficilement dégager des lois générales, étant donné l'influence réciproque des différents facteurs en jeu.

Il semble toutefois qu'on puisse conclure des essais précédents et de l'expérience de notre Société en matière de courant de densité que :

Le rejet hydraulique d'un matériau dans la mer ne peut donner naissance à un courant de densité en eau calme que si le diamètre des grains est inférieur à 50 microns.

Malheureusement la turbulence due à la houle peut gêner l'écoulement de ce courant de densité et faciliter une mise en suspension d'une partie du matériau. Le nuage ainsi formé sera très sensible à l'action des courants de toutes sortes et il est impossible d'affirmer sans une étude hydrographique très complète que le matériau ne se déposera pas partiellement sur le rivage.

Dans le cas d'un matériau plus gros, on ne peut plus espérer obtenir en eau calme un underflow. La pente des fonds, si elle est assez raide, peut permettre des éboulements du tas. Quand à la houle et aux courants ils agiront sur celui-ci en l'écrêtant si son sommet atteint une profondeur suffisamment faible. Compte tenu du processus d'action de ces facteurs il n'est pas non plus impossible dans ce cas, si la distance au rivage de l'extrémité de la conduite n'est pas assez grande, qu'une partie du matériau puisse être également remontée jusqu'au rivage pendant les tempêtes.

L'étude de tels problèmes doit donc, comme nous l'avons dit, s'appuyer sur une campagne hydrographique assez complète, mais aussi peut bénéficier de l'aide du modèle réduit, même si la reproduction en similitude de ces phénomènes n'est pas possible. Des essais schématiques tels que ceux exposés dans la présente communication sont un guide précieux pour se faire une idée des phénomènes et en tirer des conclusions pratiques.

Bien entendu ces conclusions ne peuvent être déduites directement des résultats d'essais et doivent s'appuyer sur une synthèse des divers renseignements recueillis, basée elle-même sur la théorie et l'expérience de phénomènes analogues.

RESUME

Discharge of materials into the sea by pumping through a pipe and the risk of pollution of beaches

L. Greslou

For an industrial plant situated on the coast it may be a profitable proposition to discharge the waste products of the production process, such as ashes and soot from an electric power station,, wastes from a mine etc., into the sea.

It will generally be too expensive to convey these materials to the open sea by barges or overhead cableways, whilst discharge along the shore is often prohibitive because this would ruin the landscape or because the materials involve certain dangers. On the other hand, it may seem an adequate solution to discharge the materials by pumping them with water through a pipe line which deposits them at some distance off the coast.

However, this solution involves some serious problems, especially so in cases where the sea-bed has a slow gradient and where large volumes of wastes must be disposed of.

The author deals with the results of various theoretical and experi mental investigations carried out by the SOGREAH in relation with problems of this kind, with particular attentinn to the following points:

(a) The form such deposits assume at the end of the pipe.
(b) The possibility of the formation of a density current.
(c) Displacement of the deposits under the action of swell and the consequent risks of pollution of the beach by material taken back to the shore, etc.

These investigations have led to more exact knowledge of the difficulties which may arise from this method in connection with the grain size of the waste material, the topographic and hydrographic conditions, and with factors related with the running of an industrial plant.

PROCEEDINGS OF SEVENTH CONFERENCE

ON

COASTAL ENGINEERING

THE HAGUE, NETHERLANDS

AUGUST 1960

Edited by
J. W. JOHNSON
Professor of Hydraulic Engineering
UNIVERSITY OF CALIFORNIA
BERKELEY

VOLUME 2

PUBLISHED BY
COUNCIL ON WAVE RESEARCH
THE ENGINEERING FOUNDATION

1961

COUNCIL ON WAVE RESEARCH
Building 159
Richmond Field Station
University of California
Richmond, California

Lithographed in the United States of America
The National Press, Palo Alto, California

CONTENTS

VOLUME 1

CONTENTS

PART 2
BEACH AND SHORELINE PROCESSES

CONTENTS

VOLUME 2

PART 3

TIDES, TIDAL FLOW, AND STORM SURGES

CONTENTS

CONTENTS

CONTENTS

Veere-Gat Dam

Part 3

TIDES, TIDAL FLOW, AND STORM SURGES

Haringvliet Sluice

CHAPTER 27

DETERMINATION DES DENIVELLATIONS ET DES COURANTS DE MAREE

Par F. GOHIN - Ingénieur à SOGREAH - GRENOBLE

I - INTRODUCTION

I.1 HISTORIQUE

Les premiers résultats positifs obtenus dans la prévision des amplitudes de la marée dans les ports datent de plusieurs siècles ; depuis fort longtemps les courants de marée dans les mers côtières sont familiers aux navigateurs.

Rappelons simplement qu'encore de nos jours, la prévision des marnages (différence de niveau entre pleine et basse mer) et des phases (décalages de la pleine mer par rapport au passage de la lune au méridien) s'appuie sur l'analyse harmonique des enregistrements de maréographes. Cette analyse diffère de celle de FOURIER: les périodes des différentes composantes ne sont pas des sous-multiples entiers d'une même période élémentaire, mais ont des valeurs connues avec toute la précision désirée. La composante principale, dans nos régions européennes du moins, représente la marée qui serait dûe à une lune fictive tournant à distance constante de la terre et à vitesse constante dans le plan de l'équateur (marée dite M_2).

Depuis la fin du siècle dernier des recherches très nombreuses ont été faites parmi lesquelles il faut citer celles de POINCARE (méthode théorique de détermination des amplitudes et courants), HARRIS (tracé des lignes cotidales - c'est-à-dire équiphases - de la marée M_2), HANSEN (détermination des dénivellations et courants en Mer du Nord), DOODSON (détermination des lignes cotidales et équiamplitudes dans les mers bordant la GRANDE BRETAGNE).

I.2 DEFINITIONS et HYPOTHESES

Depuis la dernière guerre l'apparition des machines à calculer permet d'aborder le calcul des amplitudes et des courants (Vantroys). Il faut cependant bien saisir dès l'abord que tout calcul numérique pratique suppose le problème largement schématisé et simplifié.

Imaginons un observateur, disposant d'appareils parfaits et parfaitement appropriés, situé en un point géographiquement fixe - latitude φ, longitude G - de la mer. Cet observateur constatera que par rapport à lui l'eau se déplace verticalement et horizontalement ; nous admettrons que cet observateur est capable d'éliminer ceux de ces mouvements qui n'ont pas pour période la période de la marée semi-diurne lunaire - ou toute autre période de la force génératrice.

Nous noterons :

h : la profondeur de la mer en un point M (φ, G)

ζ : la dénivellation (variation du niveau de l'eau autour de la valeur moyenne h)

$\vec{V}$: le courant : vecteur vitesse de l'eau situé dans le plan local tangent en M à la terre.

Il est clair que ζ et $\vec{V}$ sont des fonctions du temps t et du point M ; pour préciser nous les noterons $\zeta_M(t)$ et $\vec{V}_M(t)$ - cf. figure 1.

Ces définitions étant posées, nous admettrons - sans en discuter le bien-fondé, les hypothèses simplificatrices suivantes :

a/ - la terre est sphérique, la pesanteur est constante,

b/ - les vitesses et accélérations verticales sont négligeables. De plus, de la surface au fond, en tous points d'une verticale, les vitesses horizontales sont identiques.

c/ -la force d'inertie spatiale - expression du type $\vec{V}\ \overrightarrow{\text{grad}\ V}$ est négligeable.

I.3 PRINCIPES DE L'ETUDE

Imaginons-nous provisoirement mis en face du problème suivant :

- déterminer les dénivellations et les courants de marée dûe à la composante M_2, dans l'Océan Indien.

Nous appellerons «domaine maritime» l'océan donné, et «solution $(\zeta, \vec{V})$ du problème posé» l'ensemble de toutes les fonctions $\zeta_M(t)$ et de tous les hodographes $V_M(t)$ de période T_{M_2}.

Dans les méthodes classiques on résoud le problème comme suit (cf. par exemple HANSEN) :

a/ - on introduit certaines hypothèses simplificatrices permettant de linéariser les équations.

b/ - on admet a priori que la solution stable est une fonction sinusoïdale du temps.

c/ - on ramène éventuellement le nombre d'inconnues pour chaque point M à deux - par exemple amplitude et phase de la dénivellation.

d/ - on résoud un système d' équations linéaires à 2ν inconnues (ν est le

nombre des points M).

La solution est obtenue sous la forme simple et claire suivante :

dénivellation $\zeta_M(t)$ = sinusoïde définie par { son amplitude ou «marnage» ; sa phase

courant $\vec{V}_M(t)$ = ellipse définie par { l'azimut du grand axe ; la longueur du grand axe ; l'excentricité ; le sens de parcours

ceci pour les ν points M .

Mais le temps de calcul est proportionnel à $(2\nu)^3$ au moins et devient prohibitif dès que ν dépasse quelques dizaines.

Pour éviter cet écueil majeur, nous avons été amenés à utiliser une méthode nouvelle particulièrement bien adaptée au calcul électronique.

Dans cette méthode, soulignons-le :

a/ - aucune hypothèse particulière n'est faite pour linéariser les équations - on sait que les frottements en particulier s'écartent de la loi linéaire.

b/ - aucune discrimination, du moins en principe, n'est faite entre les composantes de la marée : la force génératrice dûe à l'attraction des astres pouvant être prise en compte directement. Cependant nous nous sommes limités dans tout le travail présenté ici à l'étude de la seule composante M_2 afin d'aborder le problème posé et d'en présenter les solutions de la façon la plus claire possible.

La méthode employée consiste essentiellement à reproduire sur un véritable «modèle mathématique» - dont nous donnons ci-dessous la description - l'évolution du mouvement dans un océan à partir d'un état origine arbitraire - état de repos par exemple où toutes les dénivellations et tous les courants sont nuls.

Les équations dynamiques et de continuité permettent de suivre pas à pas l'évolution du phénomène sans qu'il soit besoin de résoudre un système d'équations simultané.

Ce procédé reproduit toute une phase transitoire qu'il faut laisser s'écouler avant d'obtenir le régime permanent définitif cherché, sous la forme pratique suivante :

$$\text{en } M_1 \quad \begin{cases} \zeta_{M_1}(t_0),\ \zeta_{M_1}(t_0+T),\ \text{---},\ \zeta_{M_1}(t_0+mT),\ \text{---}\ \zeta_{M_1}(t_0+\tau) = \zeta_{M_1}(t_0) \\ \vec{V}_{M_1}(t_0),\ \vec{V}_{M_1}(t_0+T),\ \text{---},\ \vec{V}_{M_1}(t_0+mT),\ \text{---}\ \vec{V}_{M_1}(t_0+\tau) = \vec{V}_{M_1}(t_0) \end{cases}$$

en M $\begin{cases} \text{-----}, \ \zeta_M(t_0+mT), \ \text{-----} \\ \text{-----}, \ \vec{V}_M(t_0+mT), \ \text{-----} \end{cases}$

en M_ν $\begin{cases} \zeta_{M_\nu}(t_0), \ \zeta_{M_\nu}(t_0+T), \ \text{---}, \ \zeta_{M_\nu}(t_0+mT), \ \text{---}, \ \zeta_{M_\nu}(t_0+\tau) = \zeta_{M_\nu}(t_0) \\ \vec{V}_{M_\nu}(t_0), \ \vec{V}_{M_\nu}(t_0+T), \ \text{---}, \ \vec{V}_{M_\nu}(t_0+mT), \ \text{---}, \ \vec{V}_{M_\nu}(t_0+\tau) = \vec{V}_{M_\nu}(t_0) \end{cases}$

c'est-à-dire en bref que pour les ν points du domaine nous obtiendrons la solution $\zeta_M(t)$, $V_M(t)$, à des instants séparés d'une durée fixe, que nous appellerons «pas de temps» et noterons T.

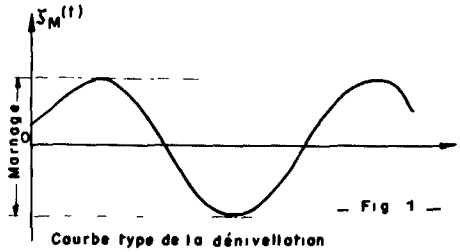

Courbe type de la dénivellation

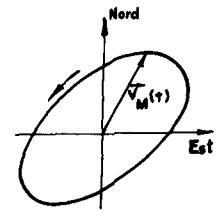

Hodographe type

— Fig 1 —

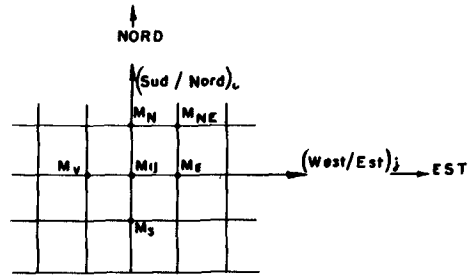

— Fig. 2 —

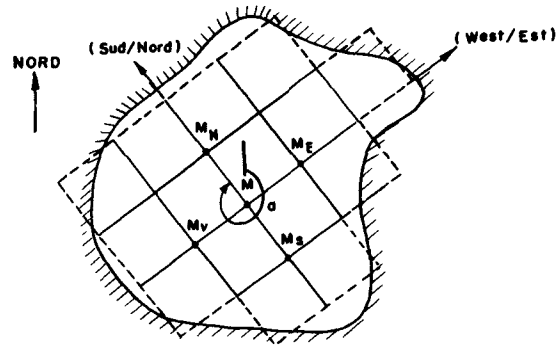

— Fig 3 —

II - BASES THEORIQUES

II.1 CANEVAS DES POINTS DE CALCUL

Nous appellerons «point de calcul» l'un quelconque des points M où nous recherchons la solution élémentaire $(\zeta, \vec{V})_M$ du problème posé.

Nous indiquerons ici brièvement comment s'effectue la mise en place sur la carte des points M .

Imaginons très provisoirement que la terre soit parfaitement plane, et le domaine sans frontière définie . nous tracerons alors sur la carte un double réseau de droites orthogonales équidistantes, (damier) orientées les unes vers le haut de la feuille (cf. figure 2), nous les appellerons (Sud/Nord) les autres vers la droite, nous les appellerons (Ouest/Est). L'intersection de la ligne $(Sud/Nord)_i$ et de la ligne $(Ouest/Est)_j$ détermine le point de calcul M_{ij}. Omettons l'indice de position pour noter M le point courant du canevas ; ce point est «entouré» de quatre points que nous noterons : au Nord : M_n, à l'Est : M_e, au Sud : M_s, à l'Ouest · M_w.

Le tracé de nos lignes est tel que, quel que soit M , $MM_n = MM_e = MM_s = MM_w = L$.

Nous appellerons «pas d'espace» cette longueur L . c'est une donnée fondamentale du canevas.

Prolongeons notre dessin en faisant apparaître le point M_{ne} : le polygone $MM_nM_{ne}M_e$ est un carré.

Nous appellerons «contour relatif à M» un polygone, formé par une ligne brisée constituée de segments tels que M_nM_{ne}, tel que M soit à l'intérieur ou sur ce contour.

Serrons de plus près et progressivement la réalité :

a/ - le domaine est limité - soit par des côtes, soit par des hauts fonds, soit arbitrairement par un segment joignant deux ports - · il est clair que les lignes de notre damier ne peuvent suivre de près la frontière du domaine : par endroits le damier sortira du domaine, par endroits au contraire la frontière sera extérieure au damier.

Tranformons, par une transformation conforme, le réseau de droites orthogonales en un réseau de coordonnées curvilignes orthogonales : dès lors, le pourtour extérieur du

réseau pourra serrer de très près la frontière.

b/ - la terre est sphérique :

La transformation conforme est valable pour la sphère : les coordonnées curvilignes sont des arcs de grands ou petits cercles. Notons que le pas d'espace est alors variable.

c/ - la côte est découpée, les fonds sont variables :

Nous modifierons le pas d'espace obtenu par la transformation conforme de telle sorte que le tracé des côtes soit suivi d'aussi près que possible. Nous nous efforcerons également de lier ce pas d'espace à la profondeur locale de l'Océan - Cf. ci-dessous paragraphe II.4.

Le réseau de coordonnées curvilignes obtenues forme un ensemble de carreaux. Nous continuerons à appeler (Sud/Nord) et (Ouest/Est) les lignes de coordonnées. Nous numéroterons ces lignes - par des nombres entiers - à partir d'une origine arbitraire : le point M - de coordonnées géographiques φ, G - a pour coordonnées «réseau» les nombres x et y . (Cf. Fig. 3)

La quasi totalité des points M est située à l'intérieur ou sur la frontière du domaine et le tracé répond aux conditions suivantes :

a/ - Les lignes des réseaux sont orthogonales.

b/ - Le canevas couvre par un nombre limité de petits carreaux curvilignes le domaine donné.

c/ - Le pas d'espace L varie lentement (ou pas) et régulièrement d'un point à un autre.

Notons M_v l'un quelconque des points de calcul entourant M (c'est-à-dire M_n ou M_e ou M_s ou M_w), nous poserons L = valeur moyenne des MM_v.

Nous appellerons profondeur moyenne locale h la valeur moyenne des sondes portées sur la carte dans un contour relatif à un point M donné.

En tout point M on repèrera ou l'on déterminera :

- La latitude ..... φ
- La longitude ..... G
- Le pas d'espace local L
- La profondeur ..... h
- L'angle a de la tangente orientée s/n par rapport au Nord vrai.

II.2 EQUATIONS DIFFERENTIELLES DU PROBLEME

Nous utiliserons les deux équations fondamentales suivantes :

- l'équation de continuité

- l'équation dynamique

L'écriture de ces équations est trop connue pour qu'il soit besoin de s'y arrêter longuement. Nous nous bornerons à préciser ici nos simplifications et nos notations.

a - Equation de continuité

Soit (C) un contour, relatif à M, d'aire s. En tout point à l'intérieur de (C) les dénivellations, au même instant t, ne sont pas exactement les mêmes - si petit que soit s -. Nous noterons $\overline{\zeta}$ la valeur moyenne de ces dénivellations à l'instant t, nous admettrons que $\overline{\zeta}$ est la dénivellation en un certain point M situé à l'intérieur de (C).

Soit N un point de (C) où nous connaissons : la dénivellation ζ_N, la profondeur h_N, la composante $V_{\perp N}$ de la vitesse sur la normale intérieure (cf figure 4).

L'équation de continuité s'écrit :

$$s \frac{\partial \overline{\zeta}}{\partial t} = \int_{(c)} (h_N + \zeta_N) \, V_{\perp N} \, dl$$

Nous poserons :

$$\Omega_\perp = \int_{(c)} h_N \, V_{\perp N} \, dl$$

Nous noterons enfin $\overline{h}$ la valeur moyenne des sondes portées sur la carte dans la zone limitée par (C).

Assimilant $\left(\frac{\zeta}{h}\right)_N$ à $\frac{\overline{\zeta}}{\overline{h}}$ nous écrirons l'équation de continuité sous la forme :

$$s \frac{\partial \overline{\zeta}}{\partial t} = \left(1 + \frac{\overline{\zeta}}{\overline{h}}\right) \Omega_\perp \qquad (1)$$

Précisons comment nous obtenons la vitesse $V_\perp$ implicitement contenue dans (1) :

1/ - *Cas général*

$V_\perp$ est inconnue. L'équation dynamique est alors utilisée pour le déterminer.

2/ - *Cas «batteur»*

Dansun modèle hydraulique la marée pourrait être engendrée par un batteur : la vitesse $u_\perp$ normale au plan du batteur serait une donnée.

Par analogie, nous appellerons «batteur» tout élément du contour où $V_\perp = u_\perp$ est donnée.

3/ - *Cas «absorbeur»*

Dans un modèle hydraulique il est d'usage courant d'utiliser des dispositifs propres à éliminer les mouvements parasites dûs aux réflexions sur les parois. Ces dispositifs absorbent une certaine fraction de l'énergie transportée par l'onde incidente.

Par analogie nous appellerons «absorbeur» tout élément du contour où une fraction de l'énergie est absorbée. Les absorbeurs que nous utiliserons seront définis par la relation :

$$V_{\perp_N} = - k \sqrt{\frac{g}{h_N}}\, \zeta_N$$

où k est un facteur constant arbitraire ou non - cette expression correspond bien à une absorption d'énergie.

b - Equation dynamique

Avec les simplifications indiquées (cf paragraphe 1.2), l'équation dynamique s'écrit :

$$\frac{\partial \vec{V}}{\partial t} = - g \vec{\text{grad}}\, \zeta - 2 \vec{\Omega} \wedge \vec{V} + \vec{F} - \vec{R}$$

où : $\vec{\Omega}$ est le vecteur instantané de rotation terrestre porté par la ligne des pôles.

$\vec{F}$ la «force génératrice de la marée»

$\vec{R}$ la force de frottement.

Tous les vecteurs considérés sont situés dans le plan horizon local et il est commode d'introduire l'écriture complexe (cf figure 5).

$$\frac{\partial V}{\partial t} = - g \,\text{grad}\, \zeta - j\omega V + F - R$$

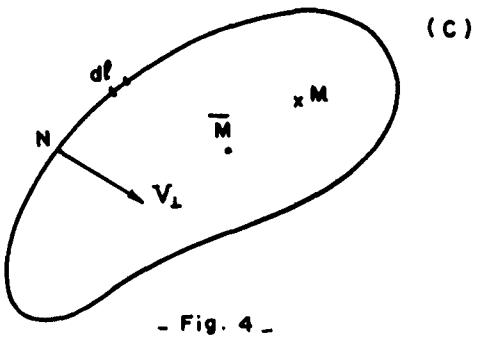

- Fig. 4 -

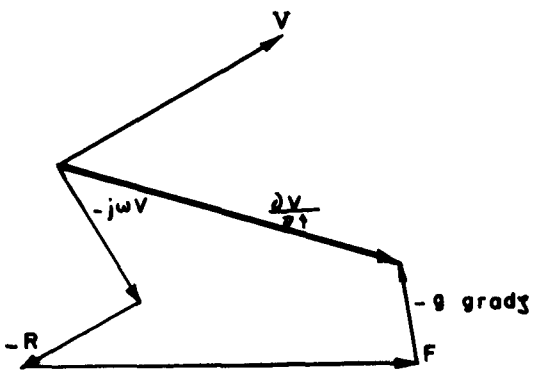

- Fig. 5 -

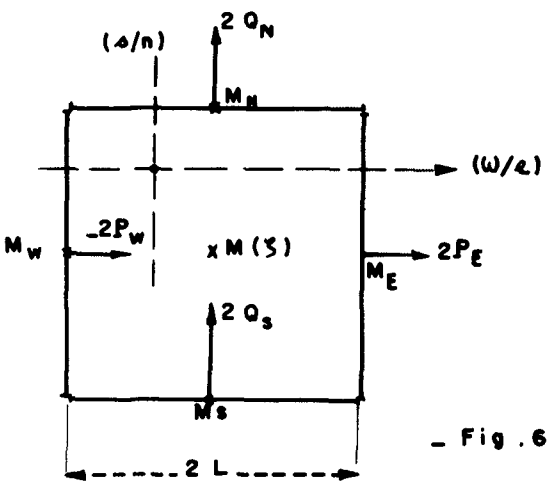

- Fig. 6 -

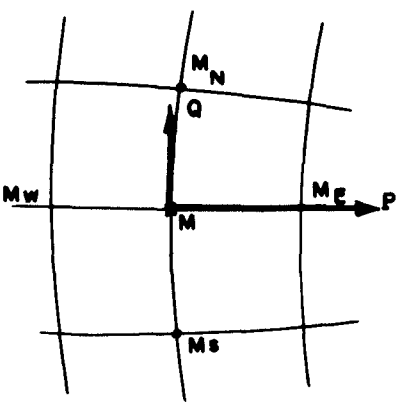

dans cette écriture V représente le vecteur $\vec{V}$, - jV représente le vecteur $-j\vec{V}$ déduit du vecteur $\vec{V}$ par une rotation de 90° dans le sens de la rose des vents.

Explicitons très succinctement les quatre quantités du deuxième membre :

1/ - De même que nous avons noté M_{ij} le point de calcul intersection de la ligne $(s/n)_j$ et de la ligne $(w/e)_j$, appelons x, y le point intersection des lignes fictives $(s/n)_x$ et $(w/e)_y$. Dans tout le domaine la dénivellation à un instant t, est une fonction $\zeta(x, y)$ où x et y sont des nombres purs :

$$\text{grad } \zeta = \left[\frac{\partial \zeta}{\partial x} + j \frac{\partial \zeta}{\partial y}\right] \frac{1}{2L}$$

2/ - Le vecteur instantané de rotation terrestre $\vec{\Omega}$ a pour intensité :

$$\Omega = \frac{2\pi}{24 \times 3600} \text{ sec}^{-1}$$

Sa composante sur la direction zénithale locale est :

$$\frac{\omega}{2} = \Omega \sin \varphi$$

3/ - Il est d'usage de décomposer la force génératrice de la marée en termes sinusoïdaux représentés par un indice k. Chaque composante - il faudrait dire plutôt chaque «marée indicielle» - est caractérisée par :

- sa période ..... τ_k
- son coefficient ... C_k

dont les valeurs sont déterminées par les lois de la mécanique céleste. En projetant la force correspondante sur les axes curvilignes locaux on obtient en utilisant des notations exponentielles usuelles :

$$F_k = X_k + jY_k = C_k\left[A_{xk}\, e^{i\left(\frac{2\pi t}{\tau_k} + \alpha_{xk}\right)} + jA_{yk}\, e^{i\left(\frac{2\pi t}{\tau_k} + \alpha_{yk}\right)}\right]$$

où C_k et τ_k sont des quantités tabulées (cf par exemple «Admiralty Manual of Tides»

où A_{xk}, α_{xk}, A_{yk}, α_{yk} sont des constantes pour un lieu donné et un groupe de composantes bien défini, constantes obtenues par un calcul simple de trigonométrie sphérique.

Dans ce qui suit nous ne considérerons qu'une composante M_2 correspondant rappelons-le à une lune fictive tournant à vitesse et distance constantes dans le plan de l'équateur. Pour alléger l'écriture nous omettrons l'indice k et poserons :

$$F = X + jY$$

4/ - Il est d'usage courant d'utiliser pour la force de frottement l'expression :

$$R = f\,[h + \zeta]^{-n}\,|V|\,V$$

où n est un exposant dépendant de la loi choisie

f est un coefficient dépendant de la loi choisie et de la nature du fond.

Nous introduisons le débit complexe $D = LhV$ et écrirons finalement l'équation dynamique sous la forme :

$$\frac{\partial D}{\partial t} = -\frac{gh}{2}\left[\frac{\partial \zeta}{\partial x} + j\,\frac{\partial \zeta}{\partial w}\right] - j\omega D + Lh\,(X + jY) - \frac{f\,|D|\,D}{Lh\,(h + \zeta)^n} \qquad (2)$$

II.3 EQUATIONS PRATIQUES DU PROBLEME

Rappelons que nous cherchons une solution $(\zeta, \vec{V})$ formée par l'ensemble des :

$$\zeta_M\,(t_o + mT),\ \vec{V}_M\,(t_o + mT)$$

pour $m = 0, 1, \ldots\ldots\ldots\ldots \frac{\tau}{T}$

$M = M_1, \ldots\ldots\ldots\ldots M_\nu$

Nous avons indiqué comment déterminer les points de calcul et souligné l'importance du «pas d'espace» local L , et du pas de temps T .

Les équations différentielles (1) et (2) doivent être mises sous forme de différences finies.

a - Equation de continuité

Le contour (C) est formé par une ligne brisée fermée, constituée par des élé-

ments de segments des réseaux (s/n), (w/e).

Le point de calcul M est :

à l'intérieur de (C) si M est à l'intérieur du champ de calcul,

sur le contour (C) si M est sur la frontière.

Le point $\overline{M}$ est par définition un point fictif à l'intérieur de (C) où la dénivellation est à chaque instant la dénivellation moyenne $\overline{\zeta}$ du domaine d'aire s limité par (C).

Nous calculerons $\overline{\zeta}$ à des instants multiples pairs, par exemple, de T par

$$s\,\frac{\overline{\zeta}_{2m+2} - \overline{\zeta}_{2m}}{2T} = \left[1 + \frac{\overline{\zeta}_{2m+2} + \overline{\zeta}_{2m}}{2h}\right] \Omega_{2m+1}$$

Pour passer de $\overline{\zeta}$ à la dénivellation cherchée ζ nous utilisons des formules de lissage que nous ne préciserons pas ici.

b - Equation dynamique

Nous poserons $LhV = D = P + jQ$ et calculerons le débit aux temps multiples impairs de T. Après quelques simplifications il vient :

$$\begin{aligned}\frac{(P+jQ)_{2m+1} - (P+jQ)_{2m-1}}{2T} = &- \frac{gh}{2}\,[\Delta_x\zeta + j\Delta_y\zeta]_{2m} \\ &+ \frac{\omega}{2}\,[(Q-jP)_{2m+1} + (Q-jP)_{2m-1}] \\ &+ Lh\,[X+Y]_{2m} \\ &- \frac{f\sqrt{P^2_{2m-1} + Q^2_{2m-1}}}{2Lh\,[h+\zeta_{2m}]^n}\,[(P+jQ)_{2m+1} + (P+jQ)_{2m-1}]\end{aligned} \qquad (2')$$

Nous n'expliciterons pas ici les expressions précises en différences finies des $\Delta_x\zeta$, $\Delta_y\zeta$, et ζ ; bornons-nous à indiquer que nous utilisons des formules de lissage.

En définitive partant du temps m = 0 et supposant par exemple que tous les $\zeta_M(0)$ et tous les $\overline{V}_M(0)$ (sauf naturellement les vitesses éventuellement données) sont ***nulles***, on applique la force astronomique et l'on calcule tous les V_{M_1} (m = 1), ... $\overline{V}_{M_v}$ (m = 1) par (2'). Puis par (1') tous les ζ_{M_1} (m = 2), ... ζ_{M_v} (m = 2), etc ...

à partir d'un certain temps on peut admettre que le régime stable est obtenu : la période suivante fournit alors la solution cherchée sous la forme :

$$(\zeta,\ \vec{V}) = \text{ensemble des } \zeta_M(m),\ \vec{V}_M(m)$$

II.4 CARACTERES DU MODELE MATHEMATIQUE

Nous entendons par «Modèle mathématique» l'ensemble des éléments nécessaires à l'étude c'est-à-dire :

1/ - Les données déduites du tracé du canevas, de la carte et des documents spécialisés.

2/ - Le programme de calcul, c'est-à-dire la séquence des ordres de calcul, permettant de résoudre le système des équations (1') et (2').

L'exploitation de ce modèle s'effectue à l'aide d'une machine à calculer.

a - Condition de stabilité du modèle

Seule en définitive la solution stable nous intéresse ; cette solution ne peut être obtenue qu'après extinction du régime transitoire. Pour que cette extinction ait lieu il faut qu'existe une certaine relation entre les pas de temps T et L .

soient (x le numéro d'ordre d'une des lignes (s/n)
(y le numero d'ordre d'une des lignes (w/e).

Prenons le système (1) + (2) sous la forme très simplifiée suivante :

$$s\ \frac{\partial \zeta}{\partial t} = 0_1$$

$$\frac{\partial D}{\partial t} = -\ gh\ \text{grad}\ \zeta - j\omega D$$

La solution stable, si elle existe, est de la forme :

$$\zeta = z\ e^{\alpha xL+\beta yL+\gamma mT}$$

$$D = LhV = P + jQ = (p+jq)\ e^{\alpha xL+\beta yL+\gamma mT}$$

où α, β, γ sont des nombres imaginaires purs.

Nous n'avons pas pris en compte la force astronomique et la force de frottement.

Pour fixer l'écriture considérons les schémas de la figure 6.

En différences finies notre système s'écrit :

$$(1'') : \quad \zeta_{\substack{x=o \\ y=o \\ m=2\mu+2}} - \zeta_{\substack{x=o \\ y=o \\ m=2\mu}} = \frac{T}{L^2}\left[P_{\substack{x=-1 \\ y=o \\ m=2\mu+1}} - P_{\substack{x=1 \\ y=o \\ m=2\mu+1}} + Q_{\substack{x=o \\ y=-1 \\ m=2\mu+1}} - Q_{\substack{x=o \\ y=1 \\ m=2\mu+1}}\right]$$

$$(2'') \quad \begin{cases} P_{\substack{x=o \\ y=o \\ m=2\mu+1}} - P_{\substack{x=o \\ y=o \\ m=2\mu-1}} = ghT\left[\zeta_{\substack{x=-1 \\ y=o \\ m=2\mu}} - \zeta_{\substack{x=1 \\ y=o \\ m=2\mu}}\right] + \omega T\left[Q_{\substack{x=o \\ y=o \\ m=2\mu+1}} + Q_{\substack{x=o \\ y=o \\ m=2\mu-1}}\right] \\ \\ Q_{\substack{x=o \\ y=o \\ m=2\mu+1}} - Q_{\substack{x=o \\ y=o \\ m=2\mu-1}} = ghT\left[\zeta_{\substack{x=o \\ y=-1 \\ m=2\mu}} - \zeta_{\substack{x=o \\ y=1 \\ m=2\mu}}\right] - \omega T\left[P_{\substack{x=o \\ y=o \\ m=2\mu+1}} + P_{\substack{x=o \\ y=o \\ m=2\mu-1}}\right] \end{cases}$$

Dans le système (1") + (2") portons la solution stable ; il vient après simplification :

$$p \frac{T}{L^2} \operatorname{sh} \alpha L + q \frac{T}{L^2} \operatorname{sh} \beta L + z \operatorname{sh} \gamma T = 0$$

$$p \operatorname{sh} \gamma T - q\, \omega T \operatorname{ch} \gamma T + z\, ghT \operatorname{sh} \alpha L = 0$$

$$p\, \omega T \operatorname{ch} \gamma T + q \operatorname{sh} \gamma T + z\, ghT \operatorname{sh} \beta L = 0$$

D'où la condition :

$$\begin{vmatrix} \frac{T}{L^2} \operatorname{sh} \alpha L & \frac{T}{L^2} \operatorname{sh} \beta L & \operatorname{sh} \gamma T \\ \operatorname{sh} \gamma T & -\omega T \operatorname{ch} \gamma T & ghT \operatorname{sh} \alpha L \\ \omega T \operatorname{ch} \gamma T & \operatorname{sh} \gamma T & ghT \operatorname{sh} \beta L \end{vmatrix} = 0$$

c'est-à-dire :

$$\operatorname{sh}^2 \gamma T + (\omega T)^2 \operatorname{ch}^2 \gamma T = \frac{ghT^2}{L^2}\left[\operatorname{sh}^2 \alpha L + \operatorname{sh}^2 \beta L\right]$$

en posant $\alpha = ia \quad \beta = ib \quad \gamma = ic$ il vient :

$$1 - [1 + (\omega T)^2] \cos^2 CT = \frac{ghT^2}{L^2} [\sin^2 aL + \sin^2 bL]$$

cette relation entraîne immédiatement :

$$\frac{ghT^2}{L^2}[\sin^2 aL + \sin^2 bL] \leq 1$$

Par conséquent, et dans le cas très simplifié où le système (1') + (2') se ramènerait au système (1") + (2") ; la condition de stabilité, - cette condition est en fait une condition nécessaire - a, b, c, réels, s'écrit :

$$T \leq \frac{L}{\sqrt{2gh}}$$

En pratique le système employé est (1') + (2') et non (1") + (2") ; d'autre part on utilise des formules de lissage ; finalement l'expression ci-dessus n'est qu'une indication.

On remarque que L et h sont variables d'un point de calcul à un autre, par conséquent seule la valeur minimum

$$\left(\frac{L}{\sqrt{h}}\right)_{mini} \quad \text{du rapport} \quad \frac{L}{\sqrt{h}}$$

est à considérer.

b - Temps de calcul

Soient : ν le nombre des points de calcul, $\overline{L^{-2}}$ la valeur moyenne du carré du step d'espace, Σ l'aire du champ de calcul.

On a approximativement : $\nu = \frac{\Sigma}{\overline{L^{-2}}}$

Soit : $\overline{\tau}$ le temps de calcul moyen d'un point-résolution du système (1') + (2'); à la durée nature 2T correspond le temps de calcul $\nu\overline{\tau}$, par conséquent le temps de calcul θ correspond à une période $\mathcal{T}$:

$$\theta = \nu\overline{\tau} \cdot \frac{\mathcal{T}}{2T} = \Sigma\, \mathcal{T}\, \frac{g}{2} \cdot \frac{\overline{\tau}}{\overline{L^{-2}}} \cdot \frac{1}{(Lh^{-1/2})_{mini}}$$

donc :

$$\theta \text{ est proportionnel à } \frac{\Sigma\, \zeta \bar{\tau} \sqrt{h_{maxi}}}{[\bar{L}^2]^{3/2}}$$

ou encore puisque la surface moyenne $\bar{s}$ est proportionnel à $\bar{L}^2$:

$$\frac{\theta}{\zeta} \text{ est proportionnel à } \Sigma \sqrt{h_{maxi}} \cdot \bar{\tau} \cdot \frac{1}{(\bar{s})^{3/2}}$$

dans cette expression on distinguera :

- Le facteur $\Sigma \sqrt{h_{maxi}}$: donnée du problème
- Le facteur $(\bar{s})^{3/2}$: dépendant du tracé du réseau
- Le facteur $\bar{\tau}$: dépendant de l'écriture du programme de calcul et de la machine utilisée.

Admettons par exemple que nous disposons d'un modèle mathématique établi pour l'Atlantique Nord et comportant en particulier 200 points environ. La célérité relative du calcul $\frac{\theta}{\zeta}$ est, disons de 1/25, la durée du régime transitoire est $\sim \zeta$.

Le temps de calcul total - régime transitoire + régime permanent - est :

$$\theta = \frac{1}{25} \times 10 \times 12{,}5 \simeq 5 \text{ heures}$$

Admettons que nous voulions étudier la marée semi-diurne sur le globe terrestre entier et utilisons un canevas ayant le même pas d'espace moyen. La surface Σ' est très approximativement 10 fois supérieure : le nombre de points ν' sera d'environ 2.000.

La durée du régime transitoire pourra être, disons de l'ordre de 50 ζ et par suite le temps de calcul sera d'environ :

$$\theta' = \frac{2.000}{200} \cdot \frac{50}{10} \cdot 5 = 250 \text{ heures}$$

Revenons alors aux méthodes de résolution classiques.- recherche directe de la solution d'un système d'équations simultanées.

Pour 200 points de calcul il y a 400 inconnues. La résolution d'un système de 400 équations à 400 inconnues exige par exemple 50 heures de calcul.

La résolution d'un système de 4000 équations à 4000 inconnues exige au moins :

$$\left(\frac{4000}{400}\right)^3 \times 50 = 50.000 \text{ heures}$$

La comparaison des deux valeurs :

50.000 heures : méthode classique

250 heures : méthode décrite ici

est parlante d'elle-même.

Sans même supposer que nous disposions d'une machine à calculer du tout dernier modèle, il est possible d'envisager par la méthode proposée d'obtenir les dénivellations et amplitudes de la marée M_2, et des autres composantes essentielles. C'est là une oeuvre de longue haleine certes .... mais c'est possible.

NB - Nous comptons effectivement effectuer ce calcul pour l'ensemble des mers du globe.

c - Comparaison d'un modèle mathématique et d'un modèle hydraulique

Il n'est pas possible dans le cadre limité de cet exposé d'établir une comparaison précise entre un modèle mathématique et un modèle hydraulique destinés à étudier le même problème. Une telle comparaison demanderait d'ailleurs à être très nuancée, car selon que l'on donne la priorité à tel ou tel point de vue les éléments à comparer diffèrent.

Bornons-nous à quelques indications :

1er point : Il est clair que plus un modèle hydraulique est à grande échelle, mieux le terrain sera représenté et plus le modèle sera fidèle. Un certain rapprochement peut etre fait entre l'échelle d'un modèle hydraulique et le pas d'espace d'un modèle mathématique : toutes choses égales d'ailleurs, la précision des résultats et le prix de réalisation de ces modèles croissent soit avec l'échelle, soit avec le nombre de points.

2ème point: Sur un modèle hydraulique la disposition des organes produisant (batteur) et contrôlant (absorbeurs, éléments rugueux) la marée doit être effectuée avec soin. De même sur un modèle mathématique le choix de l'emplacement des batteurs et des absorbeurs, le choix de loi précise de frottement doivent être étudiés soigneusement.

3ème point: Sur un modèle hydraulique, on ne peut modifier notablement certaines parties (batteur par exemple) sans dépense importante. Sur un modèle mathématique au contraire les modifications sont en général peu coûteuses.

4ème point: Lorsque l'on veut étudier des domaines de grandes dimensions (océans) le modèle hydraulique est nécessairement surclassé par le modèle mathématique : seul ce dernier peut tenir compte de la distribution des forces - force de Coriolis et force génératrice particulièrement - et de la topographie sphérique de la terre.

Pour des domaines de quelques centaines ou dizaines de kilomètres (mers littorales) les modèles physiques doivent être réalisés sur plaque tournante pour prendre en compte la force de Coriolis. Le coût de la réalisation est alors très élevé ; l'échelle, donc la fidèlité, est limitée.

Par contre pour des domaines de quelques kilomètres (baies) les études peuvent s'exécuter sur des modèles hydrauliques fixes qui sont alors vraisemblablement toujours supérieurs aux modèles mathématiques.

III - APPLICATIONS

Nous avons effectué, et nous poursuivons actuellement, différentes études de marée. Nous rendrons compte, ici partiellement de deux d'entre elles :

en premier lieu de l'étude de la reproduction sur modèle mathématique de la marée semi-diurne lunaire M_2 en Manche.

en second lieu du calcul des amplitudes-intensités et phases- de la marée semi-diurne lunaire en Atlantique Nord.

Dans l'un et l'autre cas nous avons utilisé une machine à calculer électronique IBM 650.

Nota - Nous comptons effectuer la determination des denivellations et des courants de maree à la surface du globe - par la methode preconisee - à l'aide d'une machine à calculer d'un modèle plus perfectionne.-

III.1 ETUDE DE LA MAREE SEMI-DIURNE LUNAIRE EN MANCHE

Ce modèle a été utilisé pour des études de la SEUM, qui a bien voulu nous permettre de divulguer certains des résultats obtenus pour leur compte.

L'on sait qu'en Manche la composante principale de la force génératrice de la marée est le terme dit " M_2 " de période 12 H. 24 mn. L'action de cette force sur la surface de La Manche est négligeable vis-à-vis de son action sur la surface de l'Atlantique.

Nota - En fait on a cherché à reproduire une marée ayant pour période 12 h.24 mn et pour amplitude l'amplitude de la marée de vive-eau moyenne.

III.1.1 Tracé du canevas

Les côtes bordant La Manche sont très découpées, les fonds sont très variables : le canevas des points de calcul doit être à mailles serrées, le rapport $L / \sqrt{gh}$ donc le pas de temps, sera faible et le temps relatif de calcul θ / τ important.

Pour établir le canevas des points de calcul, nous avons adopté pour base l'île de JERSEY : pour que cette île figure dans le modèle mathématique le pas d'espace local doit être de l'ordre de 10^4 mètres. Il atteint la moitié de cette valeur dans la région de St-MALO et le quadruple aux limites Ouest-et-Est.

Les profondeurs faibles du Golfe de St-MALO, nous ont conduit à adopter finalement pour le pas de temps la valeur :

$$T = 250 \text{ sec}$$

Dans ces conditions, le nombre des points de calcul est en gros de 200 et le rapport θ/ζ est de l'ordre de 1/6.

III.1.2 Forme des équations

a/ - La marée est engendrée par un «batteur» situé sur la ligne Ouessant/ Land's End : nous nous sommes donné les courants $u_\perp$, normaux à la ligne indiquée, d'après les indications contenues dans le document N° 426 A du Service Hydrographique de la Marine Française.

b/ - Nous avons admis qu'au Pas de Calais le courant était en phase avec la dénivellation. Les documents maritimes nous ont conduit à adopter :

$$k = - \frac{V_\perp}{\zeta \sqrt{g/h}} = 0,5$$

c/ - Nous avons admis comme loi de frottement :

$$|R| = 2,75.10^{-3} \frac{|V|^2}{h}$$

en nous basant sur l'expression utilisée par le Dr HANSEN en Mer du Nord.

d/ - Dans l'essai, dont il est ici rendu compte, nous avons admis que $\zeta/h << 1$: cette hypothèse exclue toute dissymétrie entre les dénivellations positives et négatives.

III.1.3 Résultats obtenus

Les résultats obtenus sont représentés sur les plans 1 et 2 joints.

Le plan N° 1 représente les amplitudes et phases calculées par le modèle. Il est à rapprocher du plan N° 1 bis représentant les amplitudes et cotidates établies par Mr. DOODSON . En fait la seule comparaison probante consiste à rapprocher les résultats obtenus par le calcul et les résultats mesurés. Le plan N° 1 ter condense cette comparaison.

Le plan N° 2 représente quelques ellipses de courant.

Nous sommes conduits à penser que des modifications de détail permettraient d'améliorer la concordance entre les résultats de calcul et les mesures. Parmi ces améliorations citons :

a/ - La prise en compte du terme correctif ζ/h - dans l'équation de continuité et dans l'expression de la force de frottement.

Marée semi_diurne lunaire

Résultats calculés

----V---- Cotidale *différence en heures entre les instants de la P.M. locale et de la PM à BREST*

___3___ Marnage en mètres

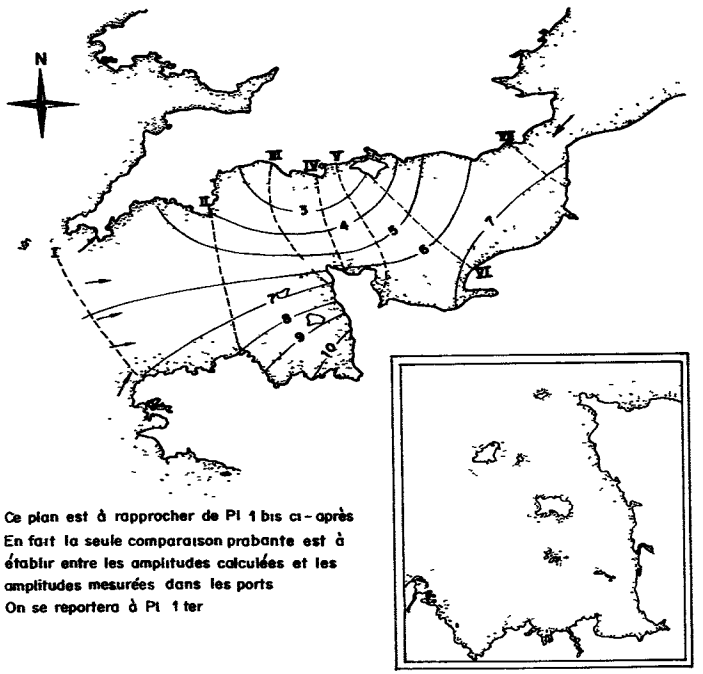

Ce plan est à rapprocher de Pl 1 bis ci-après
En fait la seule comparaison probante est à établir entre les amplitudes calculées et les amplitudes mesurées dans les ports
On se reportera à Pl 1 ter

Plate 1

Marée semi-diurne lunaire

Lignes cotidales selon Doodson et Corkon (1931)

___150___ Cotidale : *Différence entre l'heure de la PM et l'heure de passage de la lune au méridien de Greenwich*

___14___ Marnage en pieds de la Marée M_2

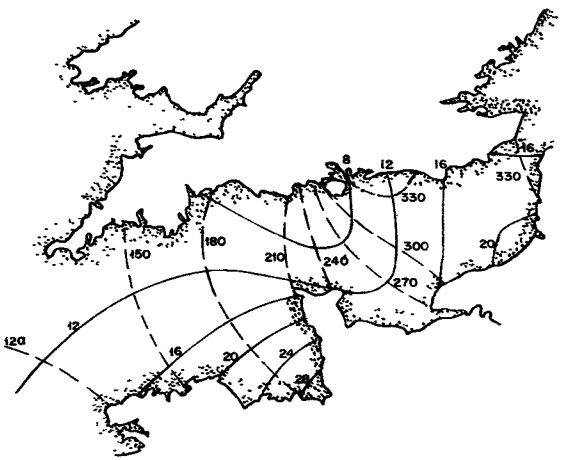

Plate 1 bis

Pl 1 ter

Marée semi-diurne lunaire

— Comparaison Marnages Modèle / Nature —
pour différents ports de la Manche

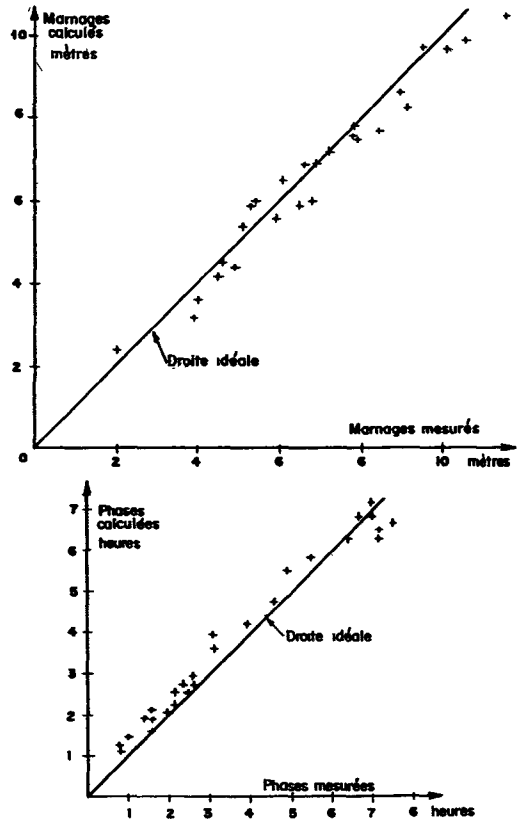

Plate 1 ter

Pl. 2

Marée semi-diurne lunaire

Résultats calculés

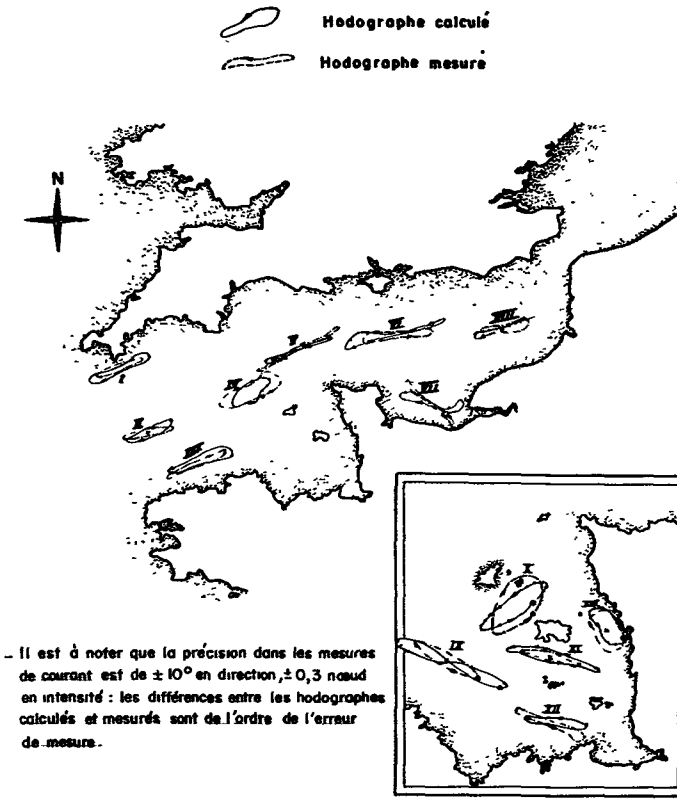

– Il est à noter que la précision dans les mesures de courant est de ± 10° en direction, ± 0,3 nœud en intensité : les différences entre les hodographes calculés et mesurés sont de l'ordre de l'erreur de mesure.

Plate 2

Marée semi-diurne lunaire

Réseau des points de calcul

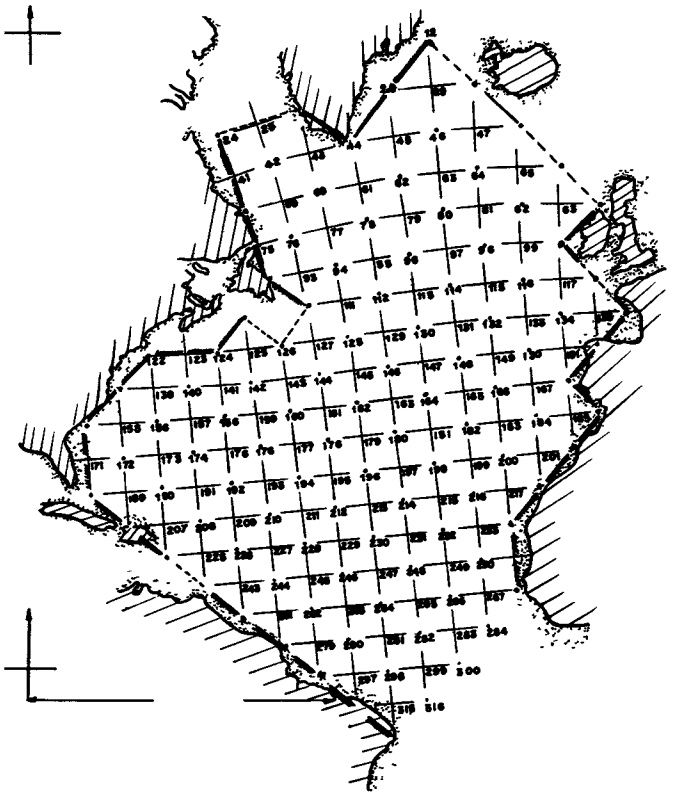

Plate 3

Marée semi-diurne lunaire

Résultats calculés et Amplitudes mesurées

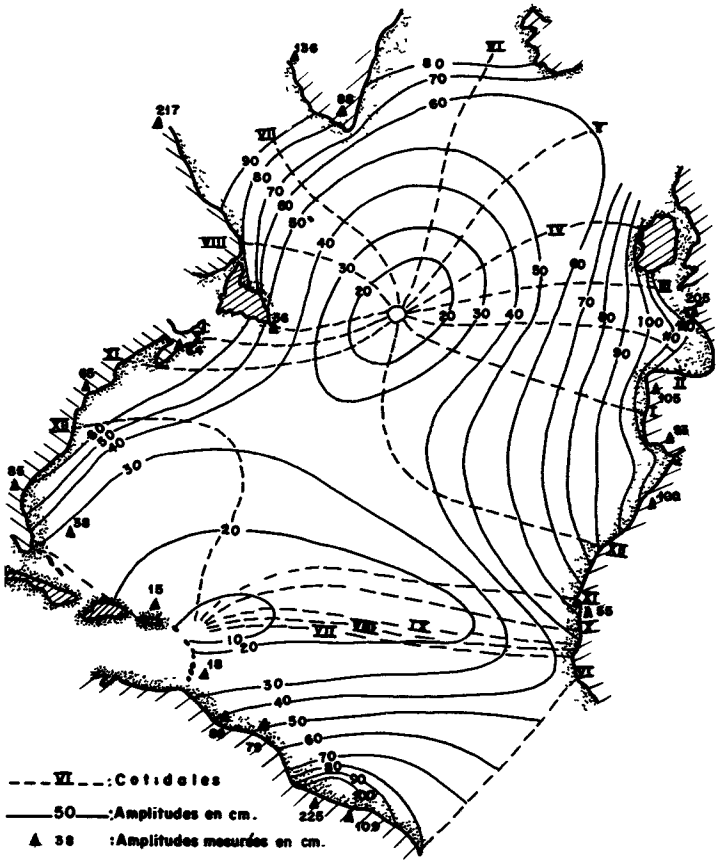

Plate 4

Marée semi-diurne lunaire

Comparaison des marnages mesurés et calculés pour différents ports de l'Atlantique Nord

× : Marnage mesuré dans le port indiqué

: Marnage calculé à la limite du plateau continental

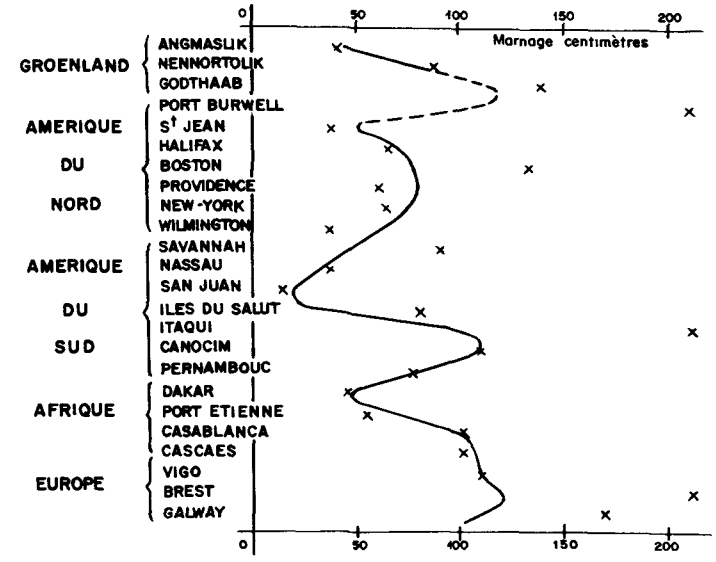

Plate 4 ter

Marée semi-diurne lunaire

— Cotidales selon HARRIS —

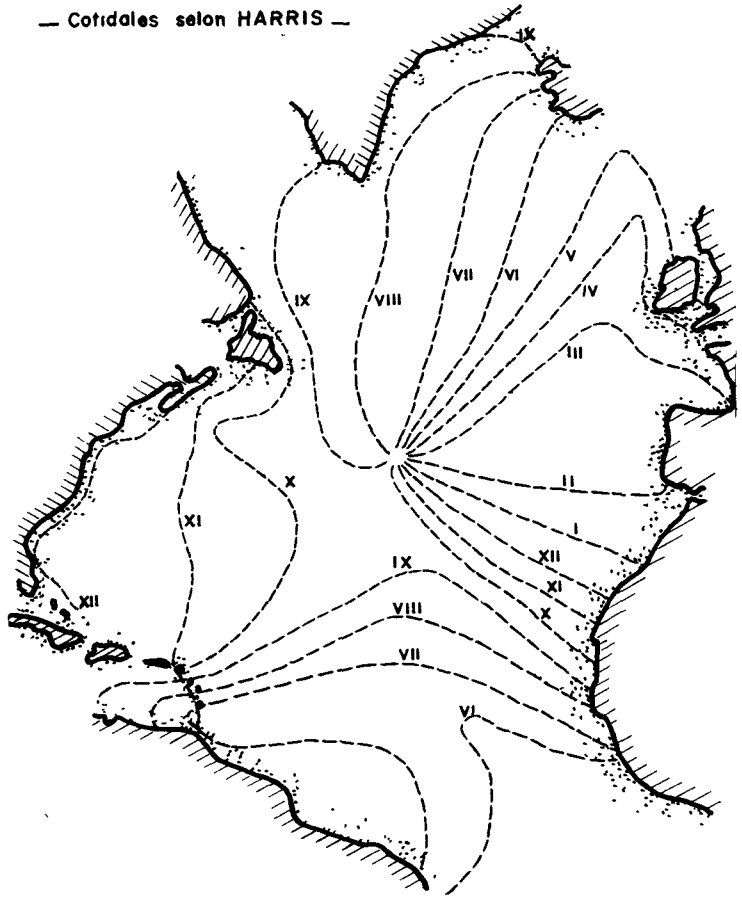

Plate 4 bis

b/ - La prise en compte de l'estuaire de la Seine.

En outre on pourrait envisager d'augmenter le nombre de points de calcul pour inclure expressément dans le modèle certains détails géographiques importants (îles de Wight, de Guernesey, etc ...).

III.2 ETUDE DE LA MAREE SEMI-DIURNE EN ATLANTIQUE NORD

Cette étude a été effectuée dans le cadre des recherches générales de la SOGREAH ; les résultats obtenus montrent que l'on peut espérer arriver à déterminer les lignes cotidales et équiamplitudes de toutes les composantes importantes de la marée réelle sur l'ensemble des océans.

III.2.1 Tracé du canevas

Le domaine considéré a été borné :

- au Nord par la ligne Angmassalik (Groenland) / Brest

- au Sud par la ligne Dakar / Pernambouc.

Nous nous sommes limités, à 200 points de calcul : la valeur moyenne $\bar{L}$ du pas d'espace est d'environ 450 kilomètres, et le pas de temps $T = 750$ sec.

III.2.2 Forme des équations

L'expérience nous a montré qu'il fallait, en raison de la valeur élevée du pas d'espace, améliorer les écritures aux différences finies des équations dénamique et de continuité : en particulier le point $\bar{M}$ de chaque contour (C) doit être précisé.

La marée est engendrée :

a/ - par un batteur situé sur la limite Sud : les mesures de courants faisant défau nous nous sommes donné les dénivellations le long de la ligne Dakar / Pernambouc.

b/ - par l'action de la force génératrice dans le domaine.

Les fonds étant de plusieurs kilomètres la force de frottement est négligeable : pour obtenir une solution stable nous avons introduit des absorbeurs sur certaines portions de la frontière du modèle -(limite Nord, détroit de Davis, Banc de Terre Neuve, Petites Antilles).

III.2.3 Résultats obtenus

Nous présentons ici :

a/ - Le tracé des points de calcul (plan N° 3). On remarquera en particulier :

1 - que le tracé est assez souple pour bien suivre le bord du plateau continental, sans qu'il soit nécessaire de courber exagérément les lignes du réseau.

2 - que, (la déformation des longueurs dûe à la projection mercator le masque), le pas d'espace est près de deux fois plus élevé au Sud - grands fonds du Sud Ouest de l'Atlantique Nord - qu'au Nord : ceci permet de conserver au rapport $L / \sqrt{2gh}$ une valeur sinon constante du moins comprise entre deux limites voisines.

b/ - Le tracé des cotidales et des courbes «équi-amplitudes» (plan N° 4).

Ce plan est à rapprocher du plan N° 4 bis représentant les cotidales établies par Harris. On remarquera que les cotidales calculées sont proches de celles de Harris au voisinage des côtes. Par contre on ne manquera pas de constater la différence du tracé au centre de l'Atlantique Nord. Nous estimons pour notre part que cette différence souligne la valeur du modèle mathématique.

Les courbes de Harris ne suffisent pas pour apprécier la validité du modèle. Afin de compléter la comparaison nous présentons sur le plan N° 4 ter un rapprochement entre les amplitudes mesurées et les amplitudes calculées dans certains ports. Cette comparaison peut sembler peu satisfaisante. En fait il faut bien saisir que :

1 - Le modèle est systématiquement limité au bord du plateau continental, et ne peut par suite représenter les amplitudes dans les ports situés sur un large plateau continental (Brest, Pasaquamody).

2 - La côte est schématisée et l'influence de détails - Floride par exemple - n'est pas sensible sur le modèle.

De toutes manières il est possible de prolonger le modèle sur le plateau continental par un canevas à mailles fines. On peut aussi étudier pour telle mer littorale, tel golfe, un nouveau modèle dont les conditions à la limite « haute mer » seraient données par le modèle de l' Atlantique Nord.

CONCLUSION

Les machines à calculer électroniques modernes permettent de réaliser et d'exploiter des modèles mathématiques adaptés à la détermination des dénivellations et des courants de marée dans un domaine maritime quelconque. Cette détermination s'effectue non pas brutalement - c'est-à-dire en recherchant directement les solutions sinusoïdales - mais en suivant de près la propagation des ondes - c'est-à-dire en serrant la réalité physique.

Pour un domaine restreint, où la force génératrice de la marée est négligeable, des modèles hydrauliques peuvent être réalisés, mais souvent le modèle mathématique constituera une approche efficace et sûre du projet définitif de modèle hydraulique. Il permettra en particulier de prévoir l'implantation des batteurs, des absorbeurs et évitera en grande partie les tâtonnements et les réglages. Après réalisation du modèle hydraulique, le modèle mathématique permettra de contrôler les résultats, de prévoir les modifications, bref guidera et assurera l'exploitation du premier.

Pour un domaine vaste où l'action locale de la force génératrice de la marée est prépondérante nous estimons que seul un modèle mathématique peut être conçu - ce modèle donnera, rappelons-le pour finir, non seulement les dénivellations - sur lesquelles HARRIS et DOODSON ont déjà donné des résultats d'importance majeure - mais aussi les courants.

CHAPTER 28

ESTUARINE CURRENTS AND TIDAL STREAMS

Roderick Agnew
Lecturer in Hydraulics, Civil Engineering Department
Imperial College of Science and Technology, London

INTRODUCTION

Fresh water spreading out from the mouth of a river as it enters a salt sea may preserve its identity for a considerable distance on the surface if wind-generated waves, longshore currents and tidal streams are capable of producing only weak mixing. Fig. 1 shows the three-dimensional shape of a fresh-water tongue overlying more dense salt water, derived by Takano (1954) on the assumption of constant eddy viscosity and constant density in the fresh water layer, below which the density increases according to an assumed law, making an asymptotic approach to the density of salt water. Takano's model is thus a water jet entraining salt from around and below it.

Salt or brackish water may penetrate along the deep channels of an estuary in the shape of a wedge complementary to the fresh water tongue, the salt wedge retreating seawards as heavy rainfall increases the river discharge, and advancing in dry weather intervals. Tidal streams cause a regular oscillation of both fresh and brack water in flood and ebb directions but the seasonal movements of the sloping boundary between fresh and salt water may still be important in low-lying delta regions. Strong tidal streams lead to intense mixing, when neither a fresh water tongue nor a salt wedge can be distinguished, but the isohalines (salinity contours) preserve the general wedge pattern - see Figs. 3 to 6.

In the upper reaches of an estuary it is possible to study the effect of the tidal motion by treating it as a simple harmonic perturbation of the uni-directional river flow. Even in the middle portion of the estuary where there is reversal of the horizontal motion, one may seek a "quasi steady" solution for the net effect (seaward movement of fresh water) while allowing for the increased turbulence due to the tidal action. At the seaward end of the estuary there is little deviation from the astronomical tidal rhythm, so the problem reduces to simple harmonic oscillations of salt water. Higher harmonics may be introduced as an extension of the simple solution. For a first approximation it is sufficient to consider flow in the longitudinal vertical plane, to assume that the pressure distribution is hydrostatic as in long wave theory, and even to neglect inertia terms when investigating net effects.

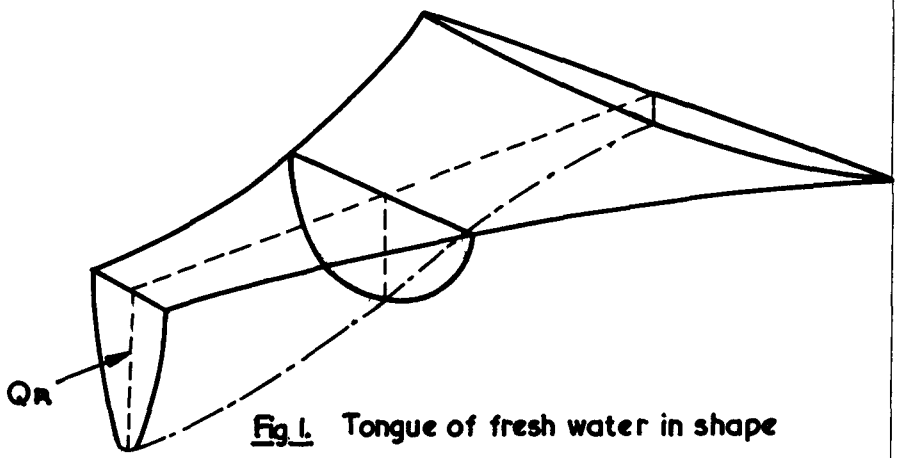

Fig 1. Tongue of fresh water in shape of hyperbolic paraboloid (after Takano).

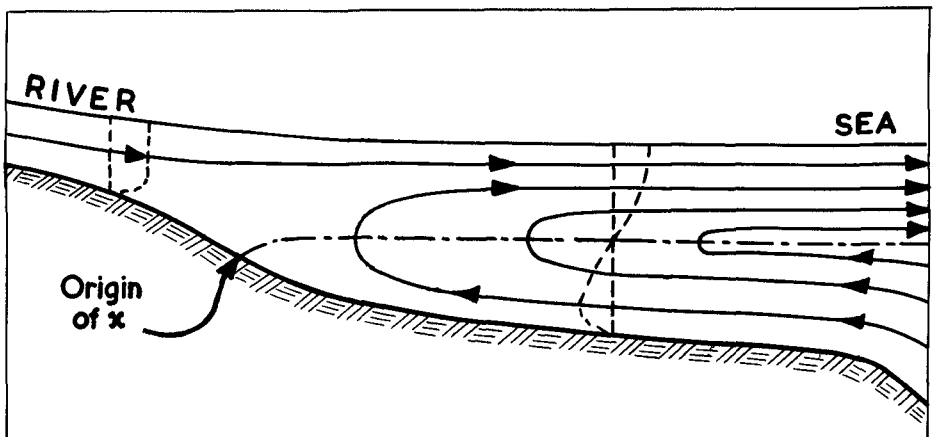

Fig. 2. Longitudinal section of estuary, to exaggerated vertical scale, showing the circulation pattern.

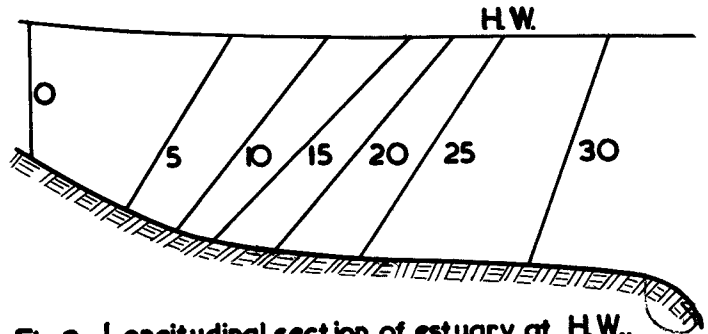

Fig 3. Longitudinal section of estuary at H.W., drawn to exaggerated vertical scale. (Salinities ‰)

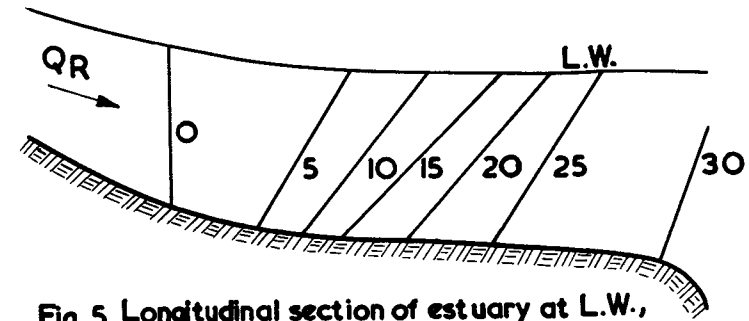

Fig. 5. Longitudinal section of estuary at L.W., drawn to exaggerated vertical scale. (Salinities ‰)

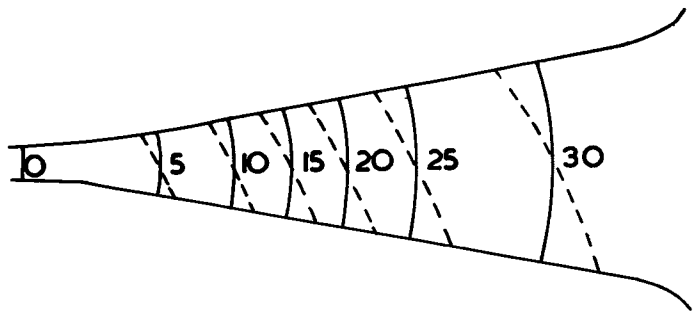

Fig 4. Plan of estuary at H.W. Full lines are isohalines in absense of earths rotation, dashed lines show salinity pattern in northern hemisphere.

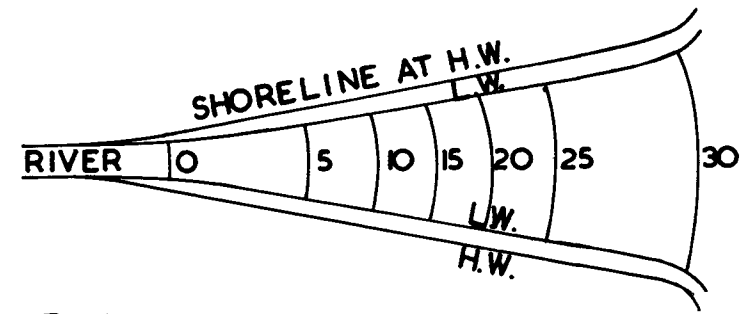

Fig 6. Plan of estuary at L.W. neglecting geostrophic effects.

DENSITY DISTRIBUTION

For engineering purposes we may regard the sea as an infinite reservoir of salt water, its edges being diluted by fresh river water and rain while the balance is maintained by evaporation from its surface to the atmosphere. We postulate a slow current of seawater landwards along the bed, its density being decreased by vertical diffusion and mixing, and a surface flow seawards of fresh water being gradually rendered brackish by salt rising from below. This circulation is illustrated in Fig. 2 by full-drawn streamlines, the broken lines being profiles of longitudinal velocity. The chain dotted line indicates the surface of zero net motion in the longitudinal direction, and is obviously a place where high shear stresses may be expected, even exceeding the bed shear stress. This is a valid picture even when tidal motion is superimposed, although then the surface of zero net motion must be defined by averaging over a tidal period; it has a real existence only near the instants of "slack water". O'Brien (1952) suggested that landward velocity near bed is approximately $C.\sqrt{H.D}$, where C = Chézy coefficient and $D = \frac{H}{2\rho}\cdot\frac{\partial \rho}{\partial x}$

In many estuaries it is observed that the average salinity over a cross-section, and hence the average density if temperature differences can be neglected, increases from river to sea in nearly linear fashion in the middle reaches (Fig. 7), the rate of increase being smaller near the river (x = 0) and the sea (x = L). This linear increase is related to the fact that the maximum velocity of the tidal stream $\bar{U}_o$ scarcely changes along the estuary* so the intensity of mixing shows little variation. The water and dissolved salt clearly oscillates a distance $X_o = \frac{\bar{U}_o}{\omega}$ which is usually a small fraction of the length L. For example, if $\bar{U}_o$ = 1.4 m/sec. or approximately 3 knots, and the angular velocity of the lunar semi-diurnal tidal stream is ω = 0.00014 rad/sec., then X_o = 10 km, whereas L $\approx$ 80 km for a typical estuary.

Fig. 7 shows the average density distributions at slack water after high water (change from flood to ebb), and slack water after low water (change from ebb to flood), on the assumption that

$$\bar{\rho} = \rho_0 + \Delta\rho \cdot \sin^2 \frac{\pi . x}{2 . L} \qquad (1)$$

---

* Indeed, Pillsbury (1939) inferred from the Delaware, and Otter and Day (1960) showed more rigorously with application to the Thames, that $\bar{U}_o$ is constant in a long estuary whose breadth increases exponentially with x.

where ρ_o = density of fresh water entering from river and $\Delta\rho$ = density difference between sea and fresh water. This density distribution fits the Thames data quoted by Inglis and Allen (1957), but other analytical curves such as the Gaussian integral and the hyperbolic tangent would also be suitable.

There is also an inorease of density from surface to bed, whioh is nearly linear in a well-mixed estuary, as indicated by the isohalines in Figs. 3 and 5. Unless there is a deep channel through tidal flats there is little variation of density in the transverse direction. The effect of the Earth's rotation is to tilt the isohalines (Fig. 4) much more than the water surfaoe. Assuming longitudinal translation of the isohalines without rotation, we now seek for a suitable law describing variation of the vertical density difference along the estuary.

Defining the salt concentration $c = \frac{\text{Mass of salt}}{\text{Mass of water}}$ at a point, the density is $\rho = (1+c).\rho_o$, and the vertioal flux or transfer of salt per unit area is $c\overline{\rho.w} = -\rho N_{Salt}.\frac{\partial c}{\partial z}$ where N_{Salt} is the vertical exchange coefficient for salt, or the eddy diffusion ooeffioient. The Reynolds shear stress, or vertical flux of momentum, is similarly $\tau = -\overline{\rho.uw} = \rho.N_{Momentum}.\frac{\partial U}{\partial z}$, and $N_{Momentum}$ is often called the eddy viscosity ooefficient. Here U and W are the time-mean velocities, u and w the velocity fluctuations, in the longitudinal and vertical directions respectively. Jacobsen's method of averaging over a tidal cycle then yields the equations

$$U.\frac{\partial c}{\partial x} = \frac{\partial}{\partial z}\left(N_{Salt}.\frac{\partial c}{\partial z}\right) \qquad (2)$$

$$\text{and } -g.\frac{\partial \rho}{\partial x} = \frac{\partial^2 \tau}{\partial z^2} = \frac{\partial^2}{\partial z^2}\left(\rho.N_{Momentum}.\frac{\partial U}{\partial z}\right) \qquad (3)$$

Extensive measurements have shown that the eddy coefficients are unequal, their ratio $\frac{N_{Momentum}}{N_{Salt}} = \gamma$ being a funotion of the local Richardson number $Ri = \frac{-g.\frac{\partial \rho}{\partial z}}{\rho.\left(\frac{\partial U}{\partial z}\right)^2}$ Thus Taylor (1931) showed that $\gamma = Ri$ if the work done by fluid turbulence is wholly devoted to mixing (i.e. increasing potential energy of variable density fluid), and $\gamma > Ri$ if some energy is dissipated by fluid visoosity.

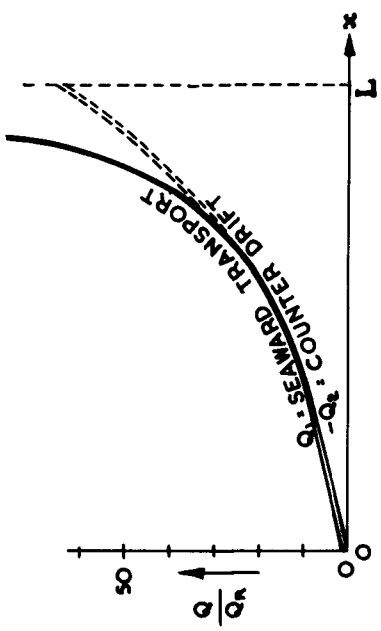

Fig 9. Quantities of water moving along estuary, independent of tidal streams.
[Full lines according to equation (8) must be adjusted at the seaward end, by snubbing.]

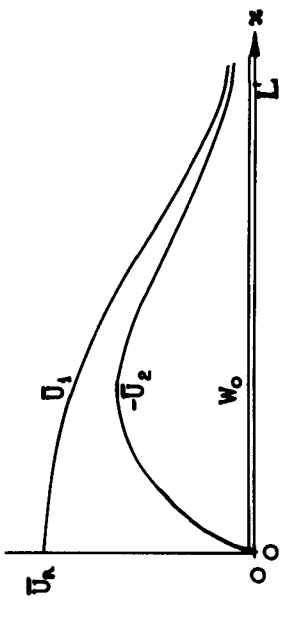

Fig 10. Typical variation of mean velocities above, below, and through the surface of zero net motion along the estuary.

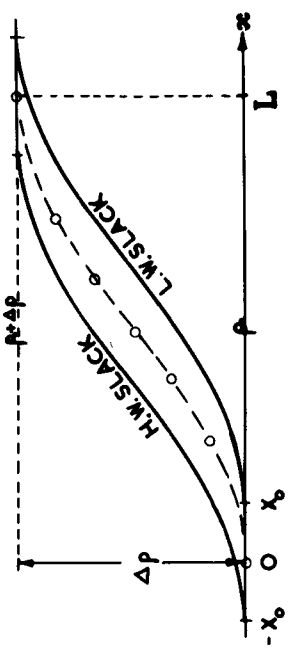

Fig 7 Mean density distribution along estuary, according to equation (1), showing effect of longitudinal oscillations with amplitude $x_0 = \frac{1}{8}L$

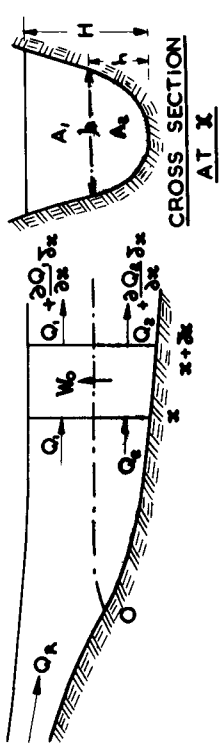

Fig 8. Definition sketch for continuity equations

With specified velocity and density distributions, Taylor showed that stable internal waves are possible when $Ri > 0.25$, but no waves can exist if $Ri < 0.25$. Other workers have derived different stability criteria.

Let us assume that the vertical distributions of $N_{Momentum}$ and N_{Salt} are similar, hence the ratio γ does not vary with z. Take $N_{Momentum} = K.U_*.z.(1-\frac{z}{H})$ as in a river, so $N_{Salt} = \frac{K}{\gamma}.U_*.z.(1-\frac{z}{H})$. The ratio γ has typical values 2 to 5 in a well-mixed estuary, and 20 to 50 in a stably stratified estuary with a salt wedge.

Now $\frac{\partial c}{\partial z} = \frac{\partial \rho}{\partial z} \approx -\frac{\delta\rho}{H}$ if the density difference between bed ($z = 0$) and surface ($z = H$) is $\delta\rho$, a function of x. Also $\frac{\partial c}{\partial x} = \frac{\partial \rho}{\partial x} \approx \frac{\partial \bar{\rho}}{\partial x} = \frac{\pi.\Delta\rho}{2.L}.\sin\frac{\pi x}{L}$ from (1). The advection term $U.\frac{\partial c}{\partial x}$ in (2) obviously changes sign in the vertical. To get an idea of its effect, assume zero net velocity at mid-depth and surface velocity U_H equal and opposite to velocity near the bed, thus $U = U_H(2\frac{z}{H}-1)$. Substitution in equation (2) gives:-

$$U_H\left(2\frac{z}{H}-1\right).\frac{\pi.\Delta\rho}{2.L}.\sin\frac{\pi x}{L} = \frac{\partial}{\partial z}\left[\frac{K.U_*}{\gamma}.\left(z-\frac{z^2}{H}\right).\left(-\frac{\delta\rho}{H}\right)\right]$$

$$= \frac{K.U_*}{\gamma.H}.\left(2.\frac{z}{H}-1\right).\delta\rho$$

whence

$$\delta\rho = \frac{\pi.\gamma.H}{2.K.L}.\frac{U_H}{U_*}.\Delta\rho.\sin\frac{\pi x}{L} \qquad (4)$$

Hence the vertical density difference is greatest in the middle reaches. It is zero at the river but not quite zero at the seaward end of the estuary, so that (4) is not reliable when $x \rightarrow L$.

If ρ_1 = mean density of water above surface of zero net motion and ρ_2 = mean density of water below surface of zero net motion, at section x, then the density difference between the two layers is $\rho_2 - \rho_1 \approx \frac{1}{2}.\delta\rho$.

Typical values of the longitudinal and vertical densities are

$$\frac{\Delta\rho}{\rho_0} \approx \frac{30}{1000} \text{ and } \frac{\delta\rho_{MAX.}}{\rho_0} \approx \frac{2}{1000} \text{ in a well-mixed estuary.}$$

MEAN VELOCITIES OF CIRCULATION

The equation of continuity for quasi-steady conditions states that the volume of water between two cross-sections is constant, neglecting precipitation, evaporation, and tidal motion. Referring to Fig. 8, let

Q_R = discharge of fresh water from river

$Q_1 = A_1.\bar{U}_1$ = flow above surface of zero net motion } at section x

$Q_2 = A_2.\bar{U}_2$ = " below " " " " " " }

Discharge and velocity are measured positive in the direction of x increasing, i.e. from river to sea. Let h = height above bed and b = breadth of surface of zero net motion, through which there is an upward velocity W_o meaned across the breadth, at section x.

Between 0 and x the continuity requirement gives

$$Q_1 + Q_2 = Q_R \qquad (5)$$

Considering the space between sections x and $(x + \delta x)$ above the surface of zero net motion in Fig. 8, the water entering per unit time is $Q_1 + W_o.b.\delta x$, and the water leaving per unit time is $Q_1 + \frac{\partial Q_1}{\partial x}.\delta x$, whence

$$\left.\begin{aligned} \frac{\partial Q_1}{\partial x} &= b.W_o \\ \text{Similarly,} \quad -\frac{\partial Q_2}{\partial x} &= b.W_o \end{aligned}\right\} \qquad (6)$$

Denoting salt concentrations by the same subscripts as densities, $c_o = 0$, $c_1 = \frac{\rho_1}{\rho_o} - 1$, $c_2 = \frac{\rho_2}{\rho_o} - 1$, there must be no change in the mass of salt in any part of the estuary, and by definition, the mass of salt is c.(Mass of water), $= \sum c.\rho.Q.\delta t$ = constant, therefore $\sum c.\rho.Q = 0$. More precisely, $\int_t^{t+T} c.\rho.Q.dt$ = constant. This is really a statement of Knudsen's hydrographic theorem.

Turning again to Fig. 8, we can draw up the salt balance between sections 0 and x. Application of the above theorem gives

$$c_o.\rho_o.Q_o + c_1.\rho_1.Q_1 + c_2.\rho_2.Q_2 = 0 .$$

Hence

$$0 + \left(\frac{\rho_1}{\rho_o} - 1\right).\rho_1.Q_1 + \left(\frac{\rho_2}{\rho_o} - 1\right).\rho_2.Q_2 = 0 .$$

On eliminating Q_2 by means of equation (5) and neglecting small quantities, we get

$$Q_1 \approx \frac{\rho_2 - \rho_0}{\rho_2 - \rho_1} \cdot Q_R$$

whence

$$Q_2 \approx -\frac{\rho_1 - \rho_0}{\rho_2 - \rho_1} \cdot Q_R \qquad (7)$$

This pair of equations implies an infinite discharge at $x = L$ if $(\rho_2 - \rho_1)$ is zero there, hence the restrictive clause after equation (4). Nevertheless it is instructive to use the density distributions (1) and (4) to calculate the variation of discharge with x. If we identify ρ_1 with the mean density $\bar{\rho}$, and take

$$\rho_2 - \rho_1 \approx \tfrac{1}{2} \cdot \delta\rho_{MAX.} \cdot \sin \frac{\pi x}{L} = \delta\rho_{MAX.} \sin \frac{\pi x}{2L} \cdot \cos \frac{\pi x}{2L} ,$$

substitution in equation (7) gives

$$\frac{Q_1}{Q_R} \approx 1 + \frac{\Delta\rho}{\delta\rho_{MAX.}} \cdot \tan \frac{\pi x}{2L}$$

and

$$-\frac{Q_2}{Q_R} \approx \frac{\Delta\rho}{\delta\rho_{MAX.}} \cdot \tan \frac{\pi x}{2L} \qquad (8)$$

Curves of discharge as a function of x are plotted in Figure 9 for the typical density ratio $\Delta\rho = 15.\delta\rho_{Max.}$ They show the enormous increase in the volume of water moving seawards, and the consequent counter drift, in a similar fashion to the curves deduced by Ketchum (1952) from a slightly different salinity distribution.

If the cross-sectional areas A_1 and A_2 (Fig. 8) were known, we could immediately calculate the mean velocities $\bar{U}_1$ and $\bar{U}_2$ as sketched in Fig. 10, but unfortunately we know only the sum $A_1 + A_2 = A$ as a geometrical function of x. The available facts are $A_1 = A_R$ and $A_2 = 0$ at $x = 0$, and $A_1 \approx A_2$ at $x = L$. The total depth H is known but the height h of the surface of zero net motion is determined by the bed roughness z_o and the intensity of mixing, which depends on the tidal streams. Both $\bar{U}_1$ and $\bar{U}_2$ are of order U_R.

If b is known, the mean velocity of upwelling (W_o) is readily determined from equation (6). It is of order $\frac{H}{L} \cdot \frac{\Delta\rho}{\delta\rho_{MAX.}} \cdot U_R \approx 0.001\ U_R$, say 1 mm/sec., which exceeds the maximum rate of rise and fall of the water surface due to normal tidal motion, but is an order of magnitude below the root mean square value of the vertical fluctuations w.

TURBULENCE MEASUREMENTS

Complete understanding of an estuary would need records of the variation of bed contours, water density, tide, shear stress, time-mean velocities U, V and W, and the velocity fluctuations u, v and w, over shoals and channels throughout several tidal cycles. Civil engineers take many observations in nature, and in hydraulic models, to deal with the problems of dredging away sand bars and stabilising the flood and ebb channels along the approaches to a port. Oceanographers, meteorologists, and coastal engineers have amassed considerable data on water density, sediment concentration, tidal levels and discharges, and the influence of fresh water flow, wind action, and atmospheric pressure irregularities on long term averages.

Increasing attention is now being paid to the rapid fluctuations of velocity and other elements in tidal streams, as a measure of fluid turbulence, but no investigator has yet measured simultaneously the velocity components in the three co-ordinate directions over the cross-section of a tidal channel. Several investigators have measured the longitudinal component (U+u) and a few the vertical fluctuation w at fixed positions.

Prior to, and in the first years of the Second World War, German oceanographers were obtaining velocity records from a paddlewheel current meter anchored on the sea bed. In Norway, about 1947, experiments on bottom friction were conducted by the University of Bergen, using sensitive cup or bucket type current meters attached to a tripod resting on the sea bed.

In the United Kingdom, about 1948, a team from Liverpool University made observations of U and u with Doodson pressure-operated current meters mounted in a stand or suspended from a boat in the Mersey, an example of a well-mixed estuary; here the R.M.S. value of u averaged 0.05 U to 0.10 U, without any clear trend in the vertical. Further observations, reported by Bowden and Fairbairn (1956) were carried out by the Liverpool team in the Irish Sea near the coast of Anglesey, using electromagnetic flow meters fixed to a tripod on the sea bed, to record u and w accurately, and U with less precision; the Reynolds stress - u.w. varied from 1 to 4 dyne/cm.^{2} near the strength of flood or ebb. The large amount of numerical data on turbulent velocities resulting from later experiments with the electro-magnetic flow meters off Anglesey is being analysed by the DEUCE computer. Measurements at the same site by Bowden et al. (1959) of the time-mean velocity U throughout the depth, at half-hourly intervals through the tidal cycle, using a Doodson meter suspended

from the research vessel and cup-wheel meters on a tripod for the velocities just above the bed, indicated a systematic departure from the logarithmic profile due to phase differences between the velocities at each measuring point. However, this effect of tidal inertia was negligible close to the bed, say for the bottom 2 m. in a total depth of 22 m., and here the logarithmic law

$$U = \frac{U_*}{\kappa} \cdot \ln \frac{z}{z_0}$$

was obeyed, with von Kármán's constant $\kappa = 0.4$ and the roughness height $z_0 = 0.16$ cm., corresponding to $k_s \approx 5$ cm. This equivalent sand roughness may be interpreted as due to ripples, for the bed consists of firm sand with small fragments of shell. The maximum value of bed shear stress $\tau_0 = \rho . U_*^2$ was about 8 dyne/cm^2. The eddy viscosity varied in space and time; it was somewhat higher at mid-depth than nearer the surface or bed, and tended to maximum values when the tidal stream was at a maximum, numerical values of $N_{Momentum}$ being of the order of 270 cm.^{2}/sec. near strength of flood, and 130 cm.^{2}/sec. near strength of ebb, when the depth-mean velocities were $\bar{U} = 45$ cm./sec., and $\bar{U} = 39$ cm./sec. respectively.

In the U.S.A., experiments by Lesser (1951) in which U was measured by four Ekman current meters suspended from a tripod in the lowest 2 m. of water 45 m. deep off the coast of California gave logarithmic velocity profiles with $z_0 = 0.1$ cm. over sand which was hydrodynamically rough, with maximum $\tau_0 = 5$ dyne/cm^2, and $z_0 = 0.02$ cm. over mud which behaved as a smooth boundary, with a maximum shear stress at the bed of only 0.2 dyne/cm^2. In 1952, workers at Woods Hole Oceanographic Institution measured U, u, and w (with less certainty) in the Kennebec estuary. Their turbulence meter was suspended from the research vessel, so observations near the water surface may have been distorted by its proximity. The R.M.S. values of u and w were of the same order, about $0.05_2 U$. High Reynolds stresses, of the order 10 to 30 dyne/cm^2, were associated with large velocity gradients $\frac{\partial U}{\partial z}$ in this stratified estuary, which has a well-marked salt wedge below the fast moving upper layer.

Turbulence measurements have been made for some years in the rivers and estuaries of the Netherlands. While working with the Rijkswaterstaat in 1958, the author was able to measure the longitudinal velocity simultaneously with temperature and salinity, using an instrument designed by the Technical Physics Department (T.N.O.) for the Rijkswaterstaat, which is being des-

cribed at the present Conference. Essentially this turbulence meter is a sensitive impeller, which responds rapidly to changes in water velocity, mounted on the streamlined body of an Ott current meter weighing 100 kg. It was suspended from a davit on the vessel "Christiaan Brunings" anchored at different positions in the Haringvliet. Observations were taken in one of two ways: either the instrument was steadily lowered to the bed, then winched to the surface, thus getting the vertical distribution over a short time interval, as in Fig. 11, or it was lowered in steps of 1 or 2 m. and held for 2 minutes at each depth, giving a record of velocity against time at each depth, from which the time-mean velocity U and the standard deviation $\sigma = (\overline{u^2})^{\frac{1}{2}}$ could be estimated.

Results of the latter method of observation are plotted in Fig. 12 for flood and Fig. 13 for ebb streams. It will be noted that while the curves of U(z) are markedly different due to the net seaward flow near the surface, the curves of $\sigma(z)$ are alike, with peak values of $\sigma \approx 0.1\ \overline{U}$ near the bed, similar to a river or other open channel with steady flow. The vertical fluctuations were not measured, so the Reynolds stresses could not be determined. However, if u and w are of the same order, we can estimate the mixing length ℓ from the formula

$$\ell \cdot \left| \frac{\partial U}{\partial z} \right| \approx \sigma$$

except where U(z) passes through a maximum. There is not sufficient information to deduce the vertical distribution of ℓ, but it seems to have a magnitude of order one tenth of the water depth. For purposes of calculation we will assume the mixing length distribution plotted in Fig. 14 is invariable throughout the tidal period. The curve in Fig. 14 has the equation

$$\left.\begin{aligned} \ell_1 &= \kappa . z . \sqrt{\frac{H-z}{H-h}} \quad \text{for} \quad H > z > h \\ \ell_2 &= \kappa . z \qquad\qquad\qquad \text{for} \quad h > z > 0 \end{aligned}\right\} \quad (9)$$

where von Kármán's constant $\kappa \approx 0.4$ and the figure is plotted for the case $h = 0.5\ H$.

EQUATIONS OF MOTION

z direction. Neglecting viscosity and the attractions of sun and moon, the vertical forces on a fluid element are due to hydrostatic pressure, gravity, and upwelling, the latter being very small. Application of Newton's

second law gives the vertical equation of motion:-

$$\frac{d}{dt}(\rho.W) + \frac{\partial p}{\partial z} + \rho.g = 0 \qquad (10)$$

An approximate solution, satisfying the boundary conditions $p = p_A$ and $W = 0$ at the free surface ($z = H$), but neglecting the vertical density gradient and variations of W with time, is

$$p = p_A + \rho.g.\left(H - z - \frac{W^2}{2g}\right) \qquad (11)$$

Hence the longitudinal pressure gradient, assuming constant atmospheric pressure, is

$$\frac{\partial p}{\partial x} \approx \rho.g.\frac{\partial H}{\partial x} + g.(H-z).\frac{\partial \rho}{\partial x} \qquad (12)$$

x direction. The longitudinal equation of motion, including friction but neglecting the tide-generating forces, is

$$\frac{d}{dt}(\rho.U) + \frac{\partial p}{\partial x} - \frac{\partial \tau}{\partial z} = 0 \qquad (13)$$

On expanding the first term, substituting equation (12) in the second term, and neglecting the variation of density with time, equation (13) may be re-arranged thus

$$\frac{\partial U}{\partial t} + U.\frac{\partial U}{\partial x} + \frac{g.(H-z) + U^2}{\rho}.\frac{\partial \rho}{\partial x} - \frac{1}{\rho}.\frac{\partial \tau}{\partial z} = -g.\frac{\partial H}{\partial x} \qquad (14)$$

If the bed of the estuary is horizontal, the term on the right hand side represents the gravity component parallel to the water surface. We will write $I = -\frac{\partial H}{\partial x}$ for the water surface slope, downwards from river to sea. This must equal the density-induced slope along the estuary, denoted by D, if all motion ceases; then equation (14) reduces to the simple form

$$\frac{H-z}{\rho}.\frac{\partial \rho}{\partial x} = D$$

, which can be integrated over the vertical, assuming $\frac{1}{\rho}.\frac{\partial \rho}{\partial x}$ = constant, to give $D = \frac{H}{2\rho}.\frac{\partial \rho}{\partial x}$ under zero flow conditions. Substituting D(x) and I(x,t) in equation (14) and changing the second term gives the working equation for this study:-

$$\frac{1}{g}.\frac{\partial U}{\partial t} + \frac{\partial}{\partial x}\left(\frac{U^2}{2g}\right) + 2D\left(1 - \frac{z}{H} + \frac{U^2}{gH}\right) - \frac{1}{\rho g}.\frac{\partial \tau}{\partial z} = I \qquad (15)$$

10^{-5} 10^{-6} 10^{-6} or 10^{-7} 10^{-5} 10^{-5}

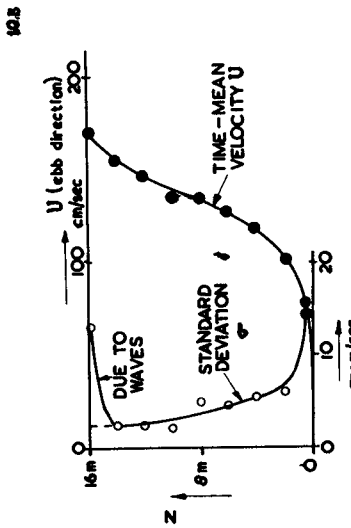

Fig. 13. Profiles of U and σ in ebb stream near building pit in Haringvliet, taken between 11·6 and 11·32 on 23rd July, 1958 (Water temp. 17·5°C., chlorinity increases linearly from 4·7 gm/l at surface to 5·3 gm/l at bed. False readings of turbulence near surface due to choppy sea.)

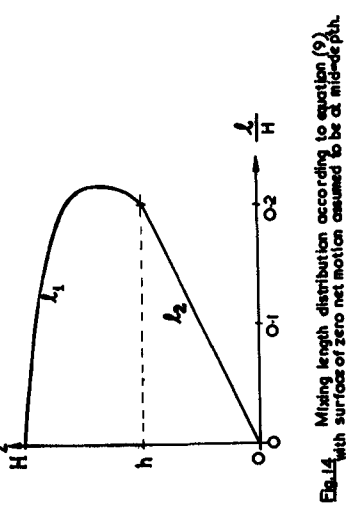

Fig. 14. Mixing length distribution according to equation (9), with surface of zero net motion assumed to be at mid-depth.

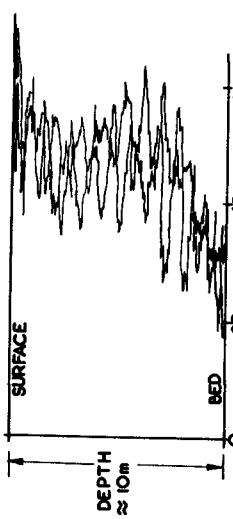

Fig. 11. Typical sounding showing velocity fluctuations, obtained with turbulence meter in the Haringvliet (Tracing from original record of pen on rotating drum)

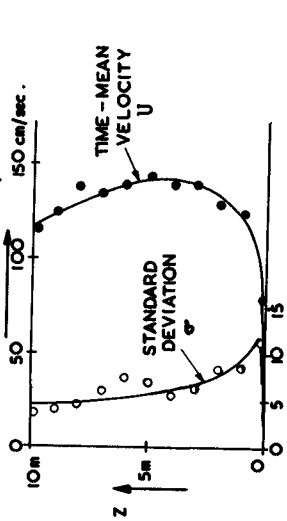

Fig. 12. Profiles of U and σ in flood stream near building pit in Haringvliet, taken between 17.38 and 18.02 on 22nd July, 1958 (Water temp. 18·1°C., chlorinity 5·0 gm/l, uniform through depth.)

The order of magnitude of each term in a typical estuary is quoted. The surface slope $I \approx D + I_0 . \cos \omega t$ is balanced by components due to inertia, kinetic head, density gradient, and friction. The case where $D = 0$ and the kinetic head is negligible has been solved. For laminar oscillations, Lamb (1932, p.622) gives the solution

$$U = \text{Real part of } i \cdot \frac{g I_0}{\omega} \cdot \left\{ \frac{\cosh (1+i) \cdot \frac{H-z}{\delta}}{\cosh (1+i) \cdot \frac{H}{\delta}} - 1 \right\} \cdot e^{i\omega t} \qquad (16)$$

where the boundary layer thickness is $\delta = \sqrt{\frac{2\nu}{\omega}}$, the most noteworthy feature being a phase advance near the bed. Longuet-Higgins (1953) has adapted this to find the mass transport under waves of finite amplitude, so correcting the frictionless theory of Stokes, and Abbott has applied this to a tidal estuary. For turbulent oscillations in water of constant depth, theoretical and experimental investigations by Schönfeld (1948), McDowell (1955) and the author show that the velocity distribution is qualitatively like that predicted by Lamb.

In order to study the effects of a density gradient along the estuary, we seek a quasi-steady solution, i.e. neglect the inertia term in (15) and assume the variation of kinetic head along the estuary is solely a density effect. As a first approximation take $\frac{\partial}{\partial x}\left(\frac{U^2}{2g}\right)$ to have a constant value $F_1 = \frac{\partial}{\partial x}\left(\frac{U_1^2}{2g}\right)$ above the surface of zero net motion, and another constant value $F_2 = \frac{\partial}{\partial x}\left(\frac{U_2^2}{2g}\right)$ below the surface of zero net motion, at any cross-section x. We will moreover assume that the Froude number $\frac{U^2}{g \cdot H}$ is small, so the remaining part of equation (15) is

$$F + 2D\left(1 - \frac{z}{H}\right) - \frac{1}{\rho g} \cdot \frac{\partial \tau}{\partial z} = I \qquad (17)$$

This is an ordinary differential equation which can be integrated for the vertical distribution of shear stress. Using subscripts 1 and 2 for the layers, the boundary conditions to be satisfied are $\tau_1 = 0$ at $z = H$, $\tau_1 = \tau_2$ at $z = h$, whence

$$\left.\begin{aligned} \frac{\tau_1}{\rho g H} &= I\left(1 - \frac{z}{H}\right) - D\left(1 - \frac{z}{H}\right)^2 - F_1 \cdot \left(1 - \frac{z}{H}\right) \\ \text{and} \quad \frac{\tau_2}{\rho g H} &= I\left(1 - \frac{z}{H}\right) - D\left(1 - \frac{z}{H}\right)^2 - \frac{F_1 \cdot (H-h) + F_2 (h-z)}{H} \end{aligned}\right\} \qquad (18)$$

At the bed, $\frac{\tau_2}{\rho g H} = I - D - F_1 + (F_1 - F_2) \cdot \frac{h}{H} = S$, say. Thus $\tau_0 = \rho \cdot g \cdot H \cdot S$ and we see that the direction of the net bed shear stress is very sensitive to the values of F_1, F_2, and h, for $I \approx D$ at slack water. Fig. 10 shows that F_1 and F_2 may be of opposite sign in the upper reach.

Writing $h = \alpha.H$, it will be shown that the fraction α is determined by F_1, F_2 and the roughness height z_o. In anticipation, we have plotted Fig. 15 for a cross-section where $\alpha = 0.5$, $F_1 = -3.6\ D$, $F_2 = +4.0\ D$, and $I = D.(1 + 10.\cos \omega t)$, at intervals of one lunar hour ($\omega t = 30^o$). As a second approximation, the discontinuity in the stress gradient $\frac{d\tau}{dz}$ at $z = h$ could be smoothed by making F variable in each layer, with $F_1 = F_2$ at $z = h$. Note the asymmetry in Fig. 15 despite the neglect of tidal inertia.

VELOCITY DISTRIBUTION IN DENSITY CURRENT

By definition, $\tau = \rho . l^2 . \left|\frac{dU}{dz}\right| . \frac{dU}{dz}$, except very close to the bed. Substitution in equation (18) with the mixing length distributions assumed in equation (9) gives the velocity gradient in each layer:-

$$\left.\begin{aligned} \frac{dU_1}{dz} &= \pm \frac{\sqrt{g.H.(1-\alpha).\left|R + D\frac{z}{H}\right|}}{K.z} \quad \text{for } H > z > h \\ \text{and } \frac{dU_2}{dz} &= \pm \frac{\sqrt{gH.\left|S - 2.P.\frac{z}{H} - D.\frac{z^2}{H^2}\right|}}{K.z} \quad \text{for } h > z > z_o \end{aligned}\right\} (19)$$

where $P = \frac{1}{2}I - D - \frac{1}{2}F_2$, $R = I - D - F_1$, and $S = I - D - (1-\alpha).F_1 - \alpha.F_2$, as above. Re-writing (19) with the dimensionless elevation $\eta = \frac{z}{H}$ gives

$$\left.\begin{aligned} \frac{K.U_1}{\sqrt{g.H}} &= \pm \sqrt{1-\alpha}.\int \frac{\sqrt{R + D.\eta}}{\eta}.d\eta + \text{const.} \quad \text{for } 1 > \eta > \alpha \\ \text{and } \frac{K.U_2}{\sqrt{g.H}} &= \pm \int \frac{\sqrt{\left|S - 2.P.\eta - D\eta^2\right|}}{\eta}.d\eta + \text{const.} \quad \text{for } \alpha > \eta > \frac{z_o}{H} \end{aligned}\right\} (20)$$

These are standard integrals but their solutions are too complicated for normal use. However, they may be simplified to yield the following approximations:-

$$\frac{K.U_1}{\sqrt{g.H}} \approx \sqrt{(1-\alpha)|R|}.\left\{\pm \ln \frac{z}{h} + \frac{D}{|R|}.\frac{z-h}{H}\right\} + \sqrt{|S|}.\left\{\pm \ln \frac{h}{z_o} - \frac{P}{|S|}.\frac{h-z_o}{H}\right\}$$

$$\text{and } \frac{K.U_2}{\sqrt{g.H}} \approx \sqrt{|S|}.\left\{\pm \ln \frac{z}{z_o} - \frac{P}{|S|}.\frac{z-z_o}{H}\right\} \quad (21)$$

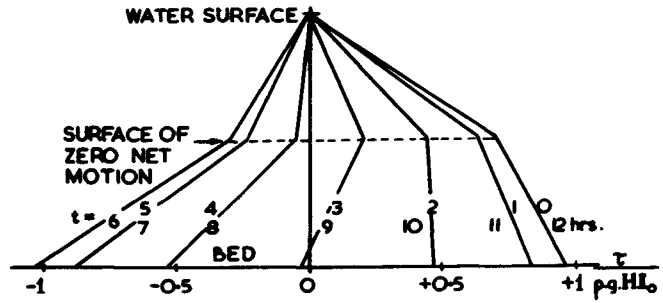

Fig. 15. Shear stress distribution in vertical, at hourly intervals through tidal cycle, neglecting inertia effects, according to equation 18.

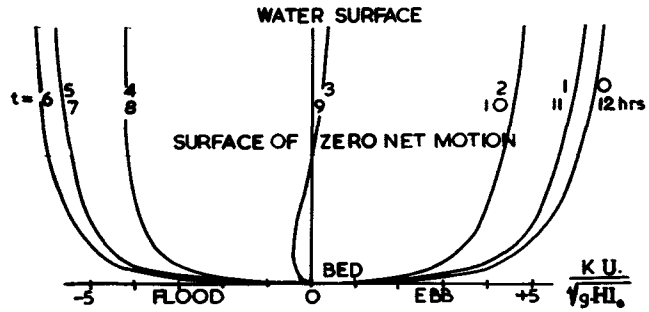

Fig 16. Velocity profiles at hourly intervals through tidal cycle, neglecting inertia effects, according to eqn. 21.

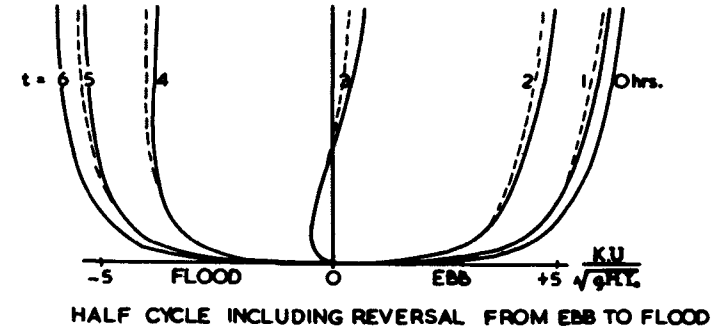

HALF CYCLE INCLUDING REVERSAL FROM EBB TO FLOOD

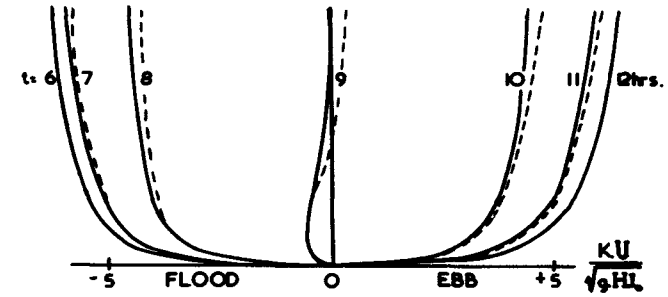

HALF CYCLE INCLUDING REVERSAL FROM FLOOD TO EBB

Fig. 17 VELOCITY PROFILES AT HOURLY INTERVALS THROUGH TIDAL CYCLE, SHOWING THE EFFECT OF INERTIA IN A TURBULENT TIDAL STREAM.

{Dashed lines indicate velocity due to density current alone, traced from Fig. 16, while full lines show velocities corrected according to eqn. 25.}

Take positive sign when R, $S>0$ (mainly ebb stream), and negative sign for R, $S<0$ (flood). The constants of integration were fixed by the boundary conditions of zero velocity near the bed ($U_2 = 0$ at $z = z_0$) and continuity of the velocity profiles at the surface of zero net motion ($U_1 = U_2$ at $z = h$), where the velocities are identically zero in the absence of tidal streams. This further condition produces the desired connection between α and z_0, for putting $U_2 = 0$ at $z = h = \alpha.H$ gives

$$\ln\left(\frac{\alpha.H}{z_0}\right) = \frac{P}{S}\cdot\left(\alpha - \frac{z_0}{H}\right) \approx \frac{\frac{1}{2}\cdot D + \frac{1}{2}\cdot F_2}{(1-\alpha)F_1 + \alpha.F_2}\cdot\alpha$$

writing $I = D$ and neglecting z_0 compared to h.

Hence $\ln\left(\frac{\alpha H}{z_0}\right) = \frac{\frac{1}{2}D + \frac{1}{2}F_2}{\frac{1}{2}F_1 - F_1 + F_2} = \mathcal{K}$, say, whence $\frac{z_0}{H} = \alpha.e^{-\mathcal{K}}$.

Since z_0 is small, we can write as a first approximation

$$\alpha \approx \frac{F_1}{F_1 - F_2}\cdot$$

The resulting velocity profiles are plotted in Fig. 16, taking the previous figures for the "constants", implying that the roughness elements are such that $\frac{z_0}{H} = 0.001$. Note the landward motion at slack water, due to the salinity current. The formulae (21) reduce to Prandtl's logarithmic velocity distribution

$U = \frac{(g.H.I)^{\frac{1}{2}}}{K}.\ln\frac{z}{z_0}$ near strength of flood and ebb,

unless the tidal streams are unusually weak.

Other formulae have been devised by meteorologists to link departures from the logarithmic wind profile with temperature inversion (stable) or lapse (unstable) conditions. Atmospheric stability is characterised by the Richardson number, being the ratio of buoyancy force to inertia force. These semi-empirical formulae may be classified as linear, of type $\frac{dU}{dz} = m.\frac{U_*}{K.z}$, or exponential, of type $\frac{dU}{dz} = \frac{U_*}{K.z^n}$, where m and n are equal to unity in neutral conditions, and in general are functions of Richardson number. · Thus Rossby and Montgomery (1935) suggested $m = (1 + \varepsilon.Ri)^{\frac{1}{2}}$ where ε = constant, and Deacon (1949) plotted his "profile index" n, showing a variation from about 0.8 for marked stability (Ri positive) to about 1.2 under unstable conditions (Ri negative). If m, n are not functions of z, integrate for the velocity profiles:-

$$U = \frac{m.U_*}{K} \cdot \ln\left(\frac{z}{m.z_0}\right) \qquad \text{or} \qquad U = \frac{U_*}{K} \cdot \frac{\left(\frac{z}{z_0}\right)^{1-n} - 1}{1-n}$$

$$\approx \frac{U_*}{K} \cdot \left\{ \ln \frac{z}{z_0} + \frac{1-n}{2} \cdot \left(\ln \frac{z}{z_0} \right)^2 \right\}$$

The first formula merely implies a change in von Karman's "constant", so that the velocity profile remains logarithmic, contradicting many observations in density currents. The second formula implies a deformation of the simple logarithmic profile, producing velocities concave to the (ln z) axis for unstable conditions (flood direction) and convex to the (ln z) axis for stable conditions (ebb direction for tidal current). The author's formula (21) causes a similar deformation of the logarithmic plot.

Recent work in the U.S.S.R., based on the idea of a layer of dynamic turbulence whose thickness d is defined in terms of the local Richardson number as follows $\frac{1}{d} = \left(\frac{\partial Ri}{\partial z}\right)_{z \to 0}$, indicates that the eddy viscosity coefficient for non-neutral conditions in the atmosphere is simply $N_{Momentum} = K \cdot U_* \cdot d \cdot Ri$, and that a good first approximation for the velocity distribution is then

$$U = \frac{U_*}{K} \cdot \left\{ \ln \frac{z}{z_0} + \beta \cdot \frac{z}{d} \right\} \quad \text{for } z \gg z_0 \qquad (22)$$

where the universal constants are $K \approx 0.4$ and $\beta \approx 0.6$, according to Monin and Obukhov (1954). This is precisely the author's equation (21), if β/d is identified with $\frac{-P}{|S| \cdot H}$ below the surface of zero net motion. It is interesting that $\frac{P}{S} \approx 0.5$ for large slopes, suggesting that d is of the same order as the water depth H.

EFFECTS OF THE NEGLECTED INERTIA TERM IN THE DYNAMIC EQUATION

The neglected term $\frac{1}{g} \cdot \frac{\partial U}{\partial t}$ distorts the velocity profiles, especially near slack water, but it has no net effect if the tidal range is small compared to the water depth. Let us seek an inertial correction for the conditions of constant depth and simple harmonic motion.

Omission of the first three terms in equation (15) leaves the equation of motion for uniform steady flow of a fluid with constant density:-

$$-\frac{1}{\rho.g}.\frac{\partial \tau}{\partial z} = I$$

This may be integrated twice, assuming that mixing length $\ell = \kappa . z . (1 - \frac{z}{H})^{\frac{1}{2}}$, to give the logarithmic velocity profile $U(z) = \frac{\sqrt{g.H.I}}{\kappa} . \ln \frac{z}{z_o}$. Hence the simplest approximation to the velocity distribution in a tidal stream, where surface slope $I \approx I_o . \cos \omega t$, is

$$U_1(z,t) = \frac{\sqrt{g.H.I_o}}{\kappa} . \ln \frac{z}{z_o} . \sqrt{\pm \cos \omega t}$$

$$\approx \sqrt{\frac{3\pi}{8}} . \frac{\sqrt{g.H.I_o}}{\kappa} . \ln \frac{z}{z_o} . \cos \omega t$$

The first term of the Fourier expansion has been taken, introducing the factor $(\frac{3\pi}{8})^{\frac{1}{2}} = 1.08$. Note that it is impossible to have simple harmonic motion of both surface slope and tidal stream when the flow is turbulent. Also it is impossible to have S.H.M. of both tide and stream, even in a rectangular channel, so to this extent all solutions in this paper must be regarded as approximate.

Retention of the first term in equation (15) gives

$$\frac{1}{g} . \frac{\partial U}{\partial t} - \frac{1}{\rho . g} . \frac{\partial \tau}{\partial z} = I$$

A trial solution is $U_2(z,t) = U_o . \cos(\omega t - \phi)$, where U_o and ϕ are functions of z. The velocity amplitude U_o is well approximated by a logarithmic expression, so take $U_o = \frac{(g.H.I_o)^{\frac{1}{2}}}{\kappa} . \ln \frac{z}{z_o}$. The phase lag ϕ will be assumed to be a linear function of z, although observations (e.g. Proudman, 1953, p.313, at Smith's Knoll) indicate that $\phi(z)$ is more nearly parabolic. If ϕ_o is the phase difference between velocities at surface and bed, we make the simple assumption that $\phi = \frac{z}{H} . \phi_o$, and we get the order of magnitude of ϕ_o from the value of ϕ_d = phase difference between mean velocity and bed shear stress or velocity gradient, as follows. Schönfeld (1948) applied the mixing length theory to compute the time difference t_d between $\bar{U}$ and τ_o. His result, for a rough bed, is $t_d = (\frac{3.2\ H}{f})^{\frac{1}{2}}$, where f = mean acceleration during reversal

of tidal stream. If the motion is simple harmonic, $f = \frac{\partial \bar{U}}{\partial t} = \omega . \bar{U}_o$, whence the phase difference is

$$\phi_d = \omega . t_d = \sqrt{\frac{3{\cdot}2\,\omega . H}{\bar{U}_o}} \text{ radians, or } \phi_d = 360 \sqrt{\frac{3{\cdot}2\,H}{2\pi T . \bar{U}_o}} \text{ degrees,}$$

since $\omega = \frac{2\pi}{T}$.

Just as Lamb's parameter $\frac{H}{\delta}$ governs the phase lags in laminar oscillations, it may be argued that a similar expression with δ defined by the eddy viscosity rather than the molecular viscosity will partly control the behaviour of turbulent fluid undergoing simple harmonic motion. By analogy with $\frac{H}{\delta} = \frac{H\sqrt{\omega}}{\sqrt{2\nu}}$, we find the dimensionless ratio $\frac{H.\sqrt{\omega}}{\sqrt{N_{MOMENTUM}}} \propto \frac{H.\sqrt{\omega}}{\sqrt{H.\bar{U}_o}} \propto \sqrt{\frac{H}{T.\bar{U}_o}}$ since eddy viscosity is proportional to U_*, which is proportional to $\bar{U}_o$, in fact $U_* = \frac{\sqrt{g}}{C} . \bar{U}$ if C = Chezy coefficient for steady flow, and we assume that tidal flow depends on the maximum value $\bar{U}_o$ of the mean velocity in a vertical. Seeing this unique combination of water depth H, tidal period T, and mean velocity amplitude $\bar{U}_o$, the author (1959) has defined the **LAMB** NUMBER as follows:-

$$\mathcal{L} = \sqrt{\frac{44714\ H}{T.\bar{U}_o}} \qquad (23)$$

The factor 44714 is included to facilitate calculations on natural tidal oscillations, where the lunar semi-diurnal period is 44714 sec., and to produce conveniently sized numbers. For example, the M_2 stream in a channel of depth 10 m. with maximum velocity 2 m./sec. has $\mathcal{L} = 2.24$. With this definition, Schönfeld's formula for the phase difference over a rough bed reduces to the simple expressions:-

$$\phi_d = 1.22\,\mathcal{L} \text{ degrees} \qquad (24)$$

Substitution in the above example gives $\phi_d = 2.7^\circ$. Hence the phase difference between surface and bed velocities (ϕ_o) is of the order of 3°.

The effect of the inertia term $\frac{1}{g} . \frac{\partial U}{\partial t}$ is to add a small velocity ΔU to the steady flow distribution.

Thus $\Delta U\,(z,t) = U_2 - U_1$

$$= U_o \cdot \left\{ \cos(\omega t - \phi) - \left(\frac{3\pi}{8}\right)^{\frac{1}{2}} \cdot \cos \omega t \right\}$$

$$\approx 2U_o \cdot \sin \frac{\phi}{2} \cdot \sin\left(\omega t - \frac{\phi}{2}\right), \text{ neglecting } \left[\left(\frac{3\pi}{8}\right)^{\frac{1}{2}} - 1\right]$$

$$\approx U_o \cdot \sin \phi \cdot \sin \omega t, \text{ if } \phi \text{ is small.}$$

Hence we must apply the inertial correction (25) to quasi-steady velocity profiles:-

$$\Delta U = U_o \cdot \sin \phi \cdot \sin \omega t \qquad (25)$$

This correction has been applied to the velocities in (21) to estimate the velocity distributions in the presence of both density and inertia effects, using the linear phase distribution $\phi = \frac{z}{H} \cdot \phi_o$ with $\phi_o = 3^o$, and the previously assumed values of slope components and roughness ratio, giving Nikuradse $k_s \approx 33$ cm. with H = 10 m., corresponding to a tidal channel with large sand ripples on the bed. Fig. 17 shows the resulting profiles. Although the velocity gradients near the bed, hence τ_o, are increased after reversal of the tidal stream, they are correspondingly decreased before reversal, and the maximum value of τ_o appears to be the same as that obtained when inertia is neglected, with this "slowly varied" flow; only at very short tidal periods, as in hydraulic models, is there a measurable increase in the maximum bed shear stress. However, the phase difference between velocity and water surface slope is by no means negligible, so linear superposition of the quasi-steady and inertial solutions of the dynamic equation cannot produce very reliable results. But here we are interested in the general behaviour of estuarine water, so further refinement in the correction ΔU will not be attempted.

Before leaving this subject, it should be emphasized that the phase differences inside the fluid, although small, may be important for the proper operation of tidal models with movable bed material, since grains set in motion relatively early in the tidal cycle may continue moving with the main stream even when the bed shear stress has fallen below the value required to initiate movement. For reproduction of inertia effects the Lamb number should be the same in model and prototype (unless the friction coefficient differs), calling for models without vertical exaggeration if the Froude scale law is followed.

EFFECTS OF FINITE TIDAL RANGE

If the tidal range is of the same order as the water depth, as occurs in many shallow estuaries, then the second term in equation (15) cannot be wholly attributed to the salinity circulation and it may change sign along an estuary due to changes in bottom topography (contractions and expansions) as well as the water surface profile varying in time and space. We must therefore apply a further correction to the velocity distributions at any cross-section.

Longuet-Higgins (1953) showed that at elevation $\delta = (\frac{2\nu}{\omega})^{\frac{1}{2}}$ above a smooth bed, there was a net velocity in the direction of wave propagation, equal to

$$\frac{5}{4} \cdot \frac{\omega^2 \cdot a^2}{c_o \cdot \sinh^2 \frac{\omega H}{c_o}} \approx \frac{5}{4} \cdot \left(\frac{a}{H}\right)^2 \cdot c_o$$

with "long" progressive waves, where a = amplitude, and c_o = celerity of wave. Experiments indicate that the net forward velocity over a rough bed is lower than this figure. The mass transport under a standing wave is smaller and distributed differently in the vertical. The case of a tidal estuary, which may be treated as a channel closed at one end and open to the sea at the other end, involves the combination of an incident wave whose amplitude decreases exponentially in the direction of propagation (from open to closed end), and a reflected wave whose amplitude decreases exponentially from the closed end to the sea. A general solution is very difficult, but the direction of net movement in a tidal estuary may be inferred from available data on the variation of tidal elevations and mean velocities along the estuary.

Abbott (1960) has suggested the criterion $\frac{d}{dx}(\overline{U}_o \cdot e^{\theta}) = 0$ for finding the positions along a tidal estuary where sediment collects, so explaining the Mud Reaches in the Thames estuary. Here $\overline{U}_o$ = maximum velocity of tidal stream, and θ = phase difference between tide and stream.

REFERENCES

Abbott, M.R. : Boundary Layer Effects in Estuaries, Journal of Marine Research, 1960.

Agnew, R. : Tidal streams in natural and artificial channels, Ph.D. thesis, Queen's University, Belfast, 1959.

Bowden, K.F. and Fairbairn, L.A. : Measurements of turbulent fluctuations and Reynolds stresses in a tidal current, pp. 422-438, Vol.A.237, Proc. Roy. Soc., 1956.

Bowden, K.F., Fairbairn, L.A. and Hughes, P. : The distribution of shearing stresses in a tidal current, pp. 288 - 305, Vol. 2, Geophysical Journal, 1959.

Deacon, E.L. : Vertical diffusion in the lowest layers of the atmosphere, pp. 89 - 103, Vol. 75, Q.J. Roy. Met. Soc., 1949.

Inglis, C.C. and Allen, F.H. : The regimen of the Thames estuary as affected by currents, salinities, and river flow, pp. 827 - 868, Vol. 7, Proc. I.C.E., 1957.

Ketchum, B.H. :Circulation in estuaries, pp. 65 - 76, Proc. 3rd Conf. Coast. Eng., 1952.

Lamb, H. : Hydrodynamics, C.U.P., 6th ed., 1932.

Lesser, R.M. : Some observations of the velocity profile near the sea floor, pp. 207 - 211, Vol. 32, Tr. A.G.U., 1951.

Longuet-Higgins, M.S. : Mass transport in water waves, pp. 535 - 581, Vol. A. 245, Phil. Trans. Roy. Soc., 1953.

McDowell, D.M. The vertical distribution of water velocities in tidal streams and in models of tidal regions, Paper A.1, Proc. I.A.H.R., The Hague, 1955.

Monin, A.S. and Obukhov, A.M. : Basic regularity in turbulent mixing in the surface layer of the atmosphere, U.S.S.R. Acad. Sci., Works of the Geophysical Institute, No. 24 (151) in Russian, 1954.

O'Brien, M.P. Salinity currents in estuaries, pp. 520 - 522, Vol. 33, Tr.A.G.U., 1952.

Otter, J.R.H. and Day, A.S. : Tidal flow computations, pp. 177 - 182, Vol. 209, "The Engineer", 29th January, 1960.

Pillsbury, G.B. : Tidal hydrualics, U.S. Army Corps of Engineers, revised ed., 1956.

Proudman, J. : Dynamical oceanography, Methuen, 1953.

Rossby, C.G. and Montgomery, R.B. : The layer of frictional influence in wind and ocean currents, Vol. 3, Papers in Physical Oceanography and Meteorology, Cambridge, Mass., 1935.

Schönfeld, J.C. : Resistance and inertia of the flow of liquids in a tube or open canal, pp. 169 - 197, Vol. A.1, Applied Sci. Res., 1948.

Takano, K. : On the salinity and the velocity distributions off the mouth of a river, pp. 60 - 67, Vol. 10, J. Oceanogr. Soc., Japan, 1954.

Taylor, G.I. : Internal waves and turbulence in a fluid of variable density, pp. 35 - 42, Vol. 76, Rapports et Procès-Verbaux des Réunions du Conseil Permanent International pour l'Exploration de la Mer, 1931.

NOTATION

A	area of cross-section
a	amplitude of long wave
b	breadth of surface of zero net motion
C	Chézy coefficient of friction
c	concentration of salt by weight
c_o	celerity of long wave, = $(g.H)^{\frac{1}{2}}$ in the absence of friction
D	slope component due to longitudinal density gradient, $= \frac{H}{2\rho}.\frac{\partial \rho}{\partial x}$
d	thickness of turbulent boundary layer in atmosphere
e	base of natural logarithms, = 2.718
F	slope component due to longitudinal velocity gradient, $= \frac{\partial}{\partial x}\left(\frac{U^2}{2g}\right)$
f	acceleration during reversal of tidal stream
g	acceleration due to gravity
H	water depth
h	elevation above bed of surface of zero net motion
I	surface slope, taken positive downwards to sea
i	imaginary number, defined by $i^2 = -1$
K	number defined in text
k_s	sand grain diameter in Nikuradse's experiments
$\mathcal{L}$	Lamb number
L	length of estuary
ℓ	mixing length
m,n	numbers defined in text
N	eddy coefficient
P	slope component defined in text
p	pressure
Q	discharge = volume per unit time

Ri	Richardson number
R,S	slope components defined in text
T	tidal period
t	time
U,u	time-mean and fluctuating velocities, respectively, in x-direction
V,v	time-mean and fluctuating velocities, respectively, in y-direction
W,w	time-mean and fluctuating velocities, respectively, in z-direction
X	fluid displacement in x-direction
x	longitudinal distance, positive from river to sea
y	transverse distance
z	vertical distance, positive upwards
z_o	roughness height
α	dimensionless elevation $\frac{h}{H}$ of surface of zero net motion
β	Obukhov's constant ≈ 0.6
γ	ratio of eddy coefficients of viscosity and diffusion
δ	thickness of laminar boundary layer in oscillating flow, $= (\frac{2\nu}{\omega})^{\frac{1}{2}}$
ε	"constant" introduced by Rossby and Montgomery
η	dimensionless elevation $\frac{z}{H}$ above bed
θ	phase difference between tide and tidal stream
κ	von Kármán's constant ≈ 0.4
ν	kinematic viscosity of fluid
ρ	density of fluid
σ	standard deviation of turbulent velocity u
τ	shear stress at elevation z
τ_o	shear stress at bed
ϕ	phase lag of velocity
ω	angular velocity of tidal stream $= \frac{2\pi}{T}$

CHAPTER 29

A STUDY OF DIFFUSION IN AN ESTUARY

W. E. Maloney and C. H. Cline
Division of Oceanography
U. S. Navy Hydrographic Office, Washington 25, D. C.

The problem of dispersion and flushing of contaminants from estuarine waters is of ever-increasing importance to engineers. To determine this reduction in concentration and removal of contaminants from estuarine water, several basic methods have been established. They are: (1) the classical tidal prism method, where the flushing is a function of the amount of water brought in and removed on each tide; (2) Ketchum's modified tidal prism method, where flushing is a function of tidal action and river discharge; and (3) a diffusion-advection method which may be based on a coefficient of eddy diffusivity. This third method, diffusion-advection, would seem to give the most realistic answer provided that confidence can be had in the coefficient of eddy diffusivity. This discussion will be confined to the third method. Furthermore, we will concern ourselves only with that portion of a contaminant that goes into solution and partakes of the motion of the water. Such factors as absorption onto particulate matter, settling out onto the bottom, and uptake of the contaminant by marine organisms will be neglected.

A convenient conservative property in an estuary from which a mean coefficient of diffusion may be computed is the distribution of river water. Stommel (1953) has described the finite difference form of the equation for the coefficient of eddy diffusivity as:

$$k = \frac{Q\ 2\ a\ (1 - f_n)}{S_n\ (f_{n-1} - f_{n+1})}$$

where k = Coefficient of eddy diffusivity
Q = River discharge
a = Distance between segments
f_n = Concentration of fresh water at segment n
f_{n-1} = Concentration of fresh water at segment $n-1$ (upstream)
f_{n+1} = Concentration of fresh water at segment $n+1$ (downstream
S_n = Cross sectional area at n.

This coefficient can then be used in a solution of the classical diffusion equation. Taylor (1954) derived the following equation as a solution for dispersion in turbulent flow with the conditions that the channel have uniform cross section, constant net velocity, and constant eddy diffusivity:

$$C = \frac{M}{2\ S\sqrt{\pi kt}} \qquad \exp\ \frac{-(X - Vt)^2}{4kt}\ ,$$

where C = Concentration of contaminant
S = Cross sectional area of channel
t = Time after introduction of contaminant
X = Distance from point of origin
V = Mean velocity of the stream
k = Coefficient of eddy diffusivity
M = Initial mass of contaminant.

Pritchard (1954) and Kent (1958) arrived at the same solution for estuaries having the same limiting conditions. The distribution with respect to X of the contaminant at fixed values of t is then symmetrical and Gaussian. Also the contaminant moves downstream with the mean speed of the stream flow. Experimental results have shown that the contaminant behaves as predicted by the equation. The important considerations of this equation are that it represents a one dimensional case in which at time t equal 0, the contaminant is considered to be uniformly distributed across the section S and subsequent diffusion takes place only in a direction normal to the section. A consequence of this is that for a normal point source release computations based on the equation will be too conservative for early time, that is, the equation will give concentrations which are too low for times less than a few tidal cycles. At some later time, probably after 2-3 tidal cycles, when the contaminant actually becomes uniformly distributed laterally, the results of the computation will be more nearly representative.

Assuming a mean value for the diffusion coefficient and a mean cross sectional area, a distribution of contaminant was computed along a longitudinal section of the James River Estuary (the embayment on which Norfolk and Newport News, Virginia are located), in the area shown in Figure 1. This computed distribution for 1, 2, 4, etc. tidal cycles after introduction is shown in Figure 2. The computed decrease of peak concentration as a function of time is shown in Figure 3.

In an effort to better determine the initial dispersion of a contaminant, a simple field test using sodium salt of fluorescein (uranine) was carried out in Hampton Roads during 5 and 6 August 1959. The results of this field test are reported here and comparisons made with the original computations.

TEST PROCEDURES

The general procedure consisted of releasing a quantity of dissolved fluorescein dye into the water and making longitudinal and/or transverse transits through the dye patch collecting water samples at 3 depths, 1 foot, 6 feet, and 15 feet. These water samples were examined on the boat for dye content using a Fisher Electrophotometer which has the capability of measuring fluorescein dye concentrations to about 1 part in 100 million. Fluorescein dye was used because it is commercially available in large quantities, is nontoxic and is relatively inexpensive. Although fluoreswill fade when exposed to sunlight, the rate of fading was not expected to appreciably affect the concentrations over a 6-hour period.

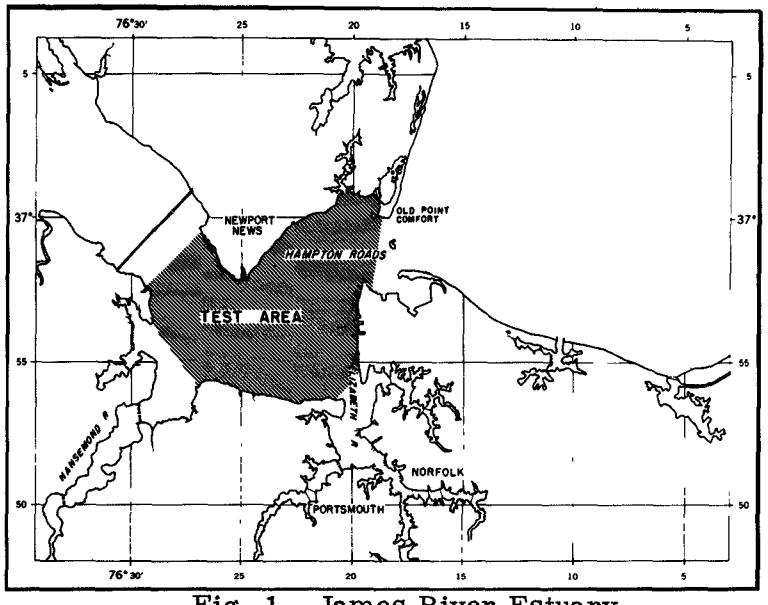

Fig. 1. James River Estuary.

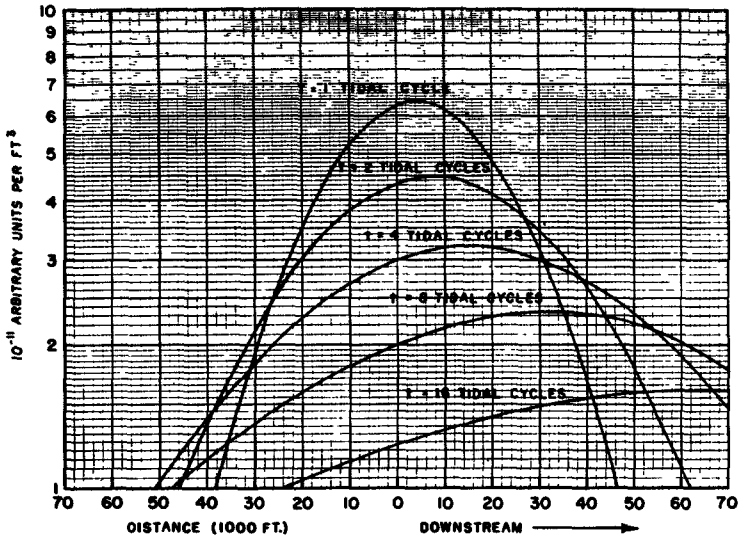

COMPUTED FROM FOLLOWING EQUATION

$$C = \frac{M}{2S\sqrt{\pi k t}} \exp\left[-\frac{(X-Vt)^2}{4kt}\right]$$

C = CONCENTRATION
S = CROSS SECTIONAL AREA
t = TIME AFTER INTRODUCTION OF CONTAMINANT
M = INITIAL MASS OF CONTAMINANT
X = DISTANCE FROM POINT OF INTRODUCTION
k = COEFFICIENT OF DIFFUSION
V = MEAN VELOCITY

$S = 28.8 \times 10^4 \text{ ft}^2$
$k = 1950 \times 10^4 \text{ ft}^2/\text{hr}$
M = 1 ARBITRARY UNIT
V = 323 ft/hr

Fig. 2. Space distribution of contaminant for James River.

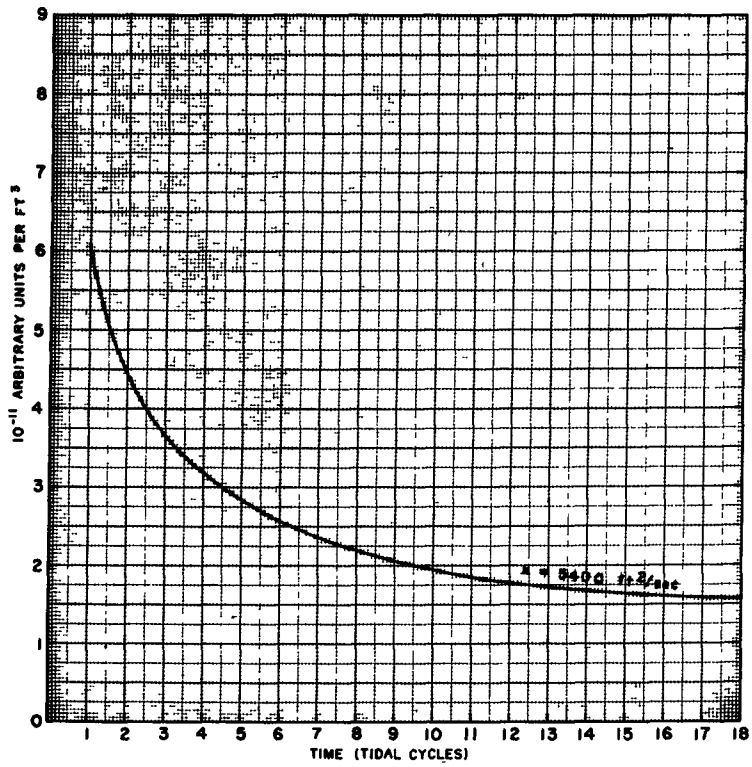

Fig. 3. Decrease of peak concentration with time.

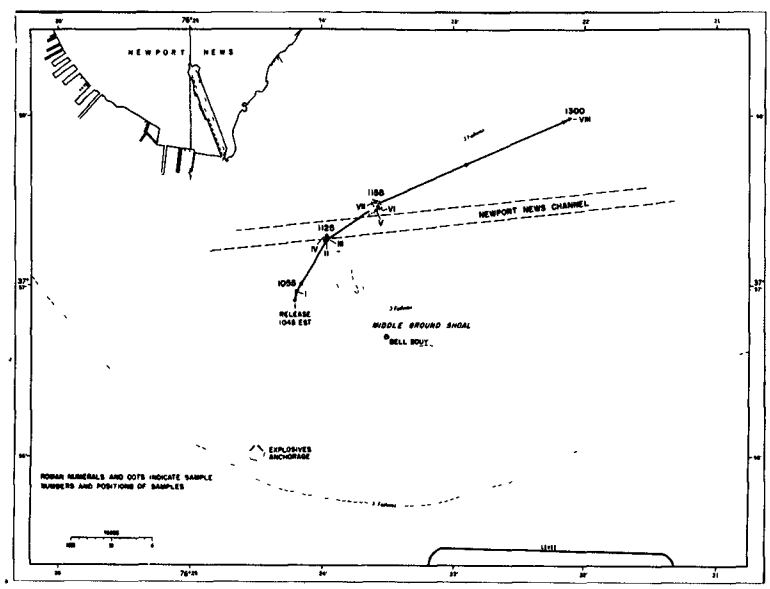

Fig. 4. Test location chart, 5 August.

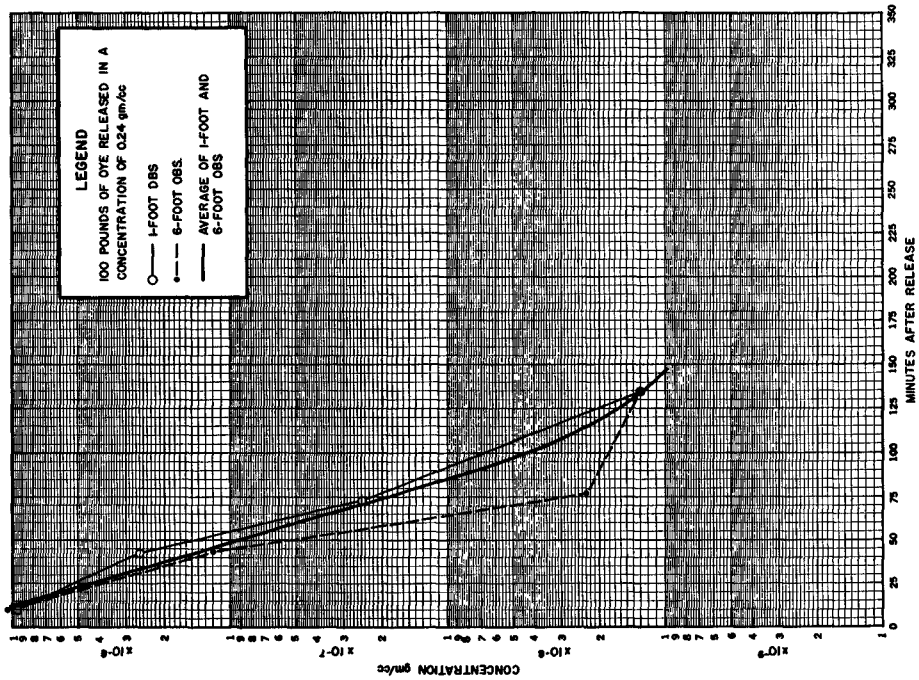

Fig. 6. Decrease of peak concentration with time - 5 August test.

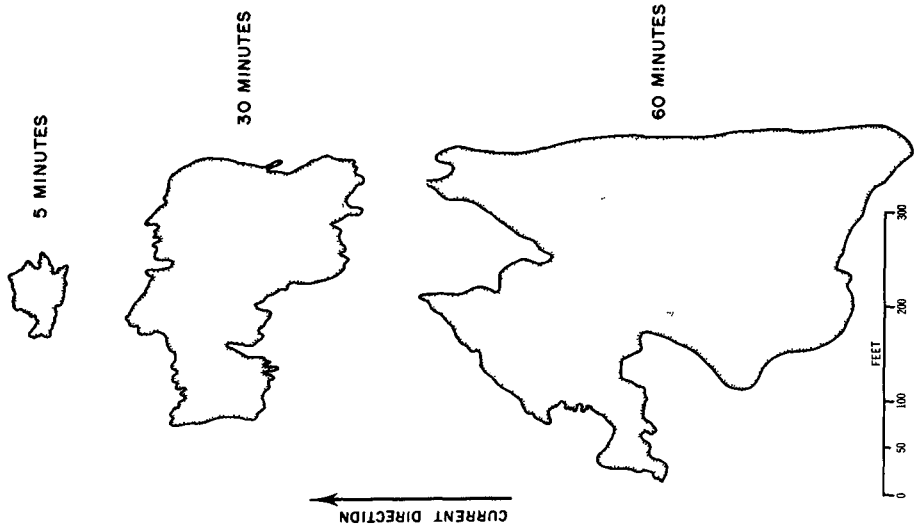

Fig. 5. Dye patch outlines at 5, 30, and 60 minutes after release, 5 August test.

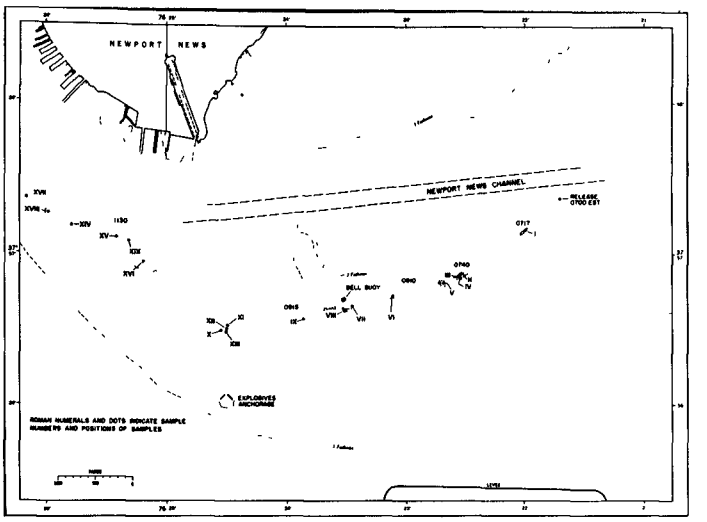

Fig. 7. Test location chart, 6 August.

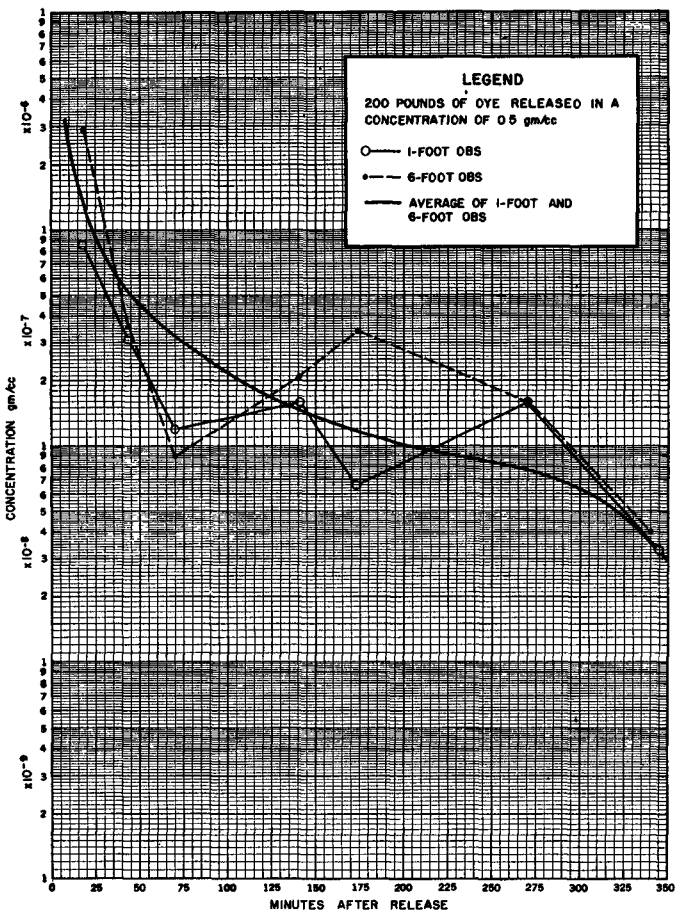

Fig. 8. Decrease of peak concentration with time - 6 August test.

The first test was held on 5 August 1959; the dye release point was at the west end of Middle Ground Shoal. The positions within the dye patch at which the samples were taken, the general outlines of the dye patch at each sampling time, and the direction of movement are shown in Figure 4. Winds were light; seas were less than 2 feet. At the time of release the water temperature was 77°F. and vertically isothermal. On this test, 100 pounds of fluorescein dye were used making an initial concentration of 0.3 gm/cc. At slack before ebb this solution was released beneath the surface at a depth of 6 feet by gravity feed through a 1½ inch hose. Release took only 1 to 2 minutes so that the dye was released essentially as a point source.

Aerial photographs of the dye patch were taken from a helicopter at 5, 30, 60, and 120 minutes after release. Figure 5 shows the outlines of dye patches at +5, +30, and +60 minutes drawn to the same scale and with the same orientation with respect to the current direction. The patch at +120 minutes was too diffused to attempt to determine an outline. A vertical temperature trace taken at this time showed a decrease in water temperature from 79.4°F. at the surface to 76.8°F. at 10 feet and was isothermal from there to the bottom at 20 feet.

The decrease of peak dye concentration with time is shown in Figure 6. The smooth curve is a mean of the 1- and 6-foot peak concentrations found at each sampling time. It shows a dilution factor of approximately 10^5 in 35 minutes and 10^6 in 70 minutes.

The 6 August tests were also conducted in the James River but with the dye release being near the east end of the Newport News Channel as shown in Figure 7. In contrast to the previous days test, these were conducted during the flood tide. During this test, winds and seas were light Surface water temperature was 76.9°F. and nearly vertically isothermal. The current was flooding at 1.1 knots in a direction 220°F. In an effort to increase the time duration of the tests, 200 pounds of dye were used on this day.

The current had begun to flood by the time the dye solution was released so that the dye patch at completion of release was a plume about 10 feet wide by 70 to 80-feet long. At +5 minutes the patch had lengthened to approximately 125 feet. Because of the rapid movement of the patch with the currents, some of the sample locations are not shown within the limits of the dye patch on Figure 7, which shows the general outline of the dye patch at each sampling time. The limits of the patch are drawn for the time of the first sample taken at each sampling time. By the time the boat arrived in position to sample the west end of the patch, the whole water mass had moved 300 to 400 yards. Similarly, when samples 11, 12, and 13 were taken, the patch had moved westward enough so that these samples were taken in about the longitudinal middle of the patch. The outline of the visible dye patch at +270 minutes was very vague, and only an estimated size is shown on Figure 7.

At slack before ebb, the dye patch had reached its greatest intrusion up river. At this time a definite tide rip was observed with a line of debris and seaweed in the clear water on the north and the dye water on the south. The rip line seemed to extend in a northeast-southwest direction. As the rip moved through the dye patch, several rather strong local concentrations were noted along the rip line. Elsewhere, dye color was not visible or only vaguely visible. After the rip passed, several runs were made across the river but no additional dye was visible. A vertical temperature trace taken at 1300 showed isothermal water conditions with a surface temperature 77.1°F.

The decrease of peak dye concentration with time is shown in Figure 8. The smooth curve is a mean of the 1- and 6-foot peak concentrations found at each sampling time. The general leveling off of the rate of change of peak concentrations after 1 to 2 hours was not apparent on the first test and is quite possibly a result of the sampling technique. However, the concentrations vary so much after 1 to 1½ hours that the mean curve could be drawn considerably different. The curve shows a dilution factor of 10^5 in about 10 minutes and 10^6 in about 40 minutes. The method of release and the faster current speeds probably account for the initial faster dilutions noted in this test than on the 5 August test.

DISCUSSION OF RESULTS

One of the original purposes of the tests was to determine a value for the coefficient of eddy diffusion to compare to that obtained from the salinity gradient. To do this, some estimate of the extent of vertical and horizontal dispersion was necessary. In the formula assumed for the decrease of peak concentration of any contaminant,

$$C = \frac{M}{2 S \sqrt{\pi k t}},$$

the cross sectional area through which the pollutant has spread should be known. Obviously, in the first few hours the contaminant will not extend completely and uniformly across the channel, nor completely from top to bottom as assumed in Figures 2 and 3. However, to use the same formula for the first few hours as well as for later times, some estimate of this cross sectional area should be made.

The method of sampling used in this test does not permit any precise indication of the vertical extent of mixing. However, mixing from top to bottom apparently took place rather rapidly. All releases took place at the surface or 6 feet, and within two hours or less, concentrations at 15 feet were as high as the 1- or 6-foot samples. The extent of horizontal dispersion, at least at the surface, can be readily determined from visual observations and aerial photographs. Using the 5 August test, because of the better aerial photographs, a measure of the vertical and surface lateral spreading with time was determined. From these two dimensions of the dye patch, the cross sectional area was determined as a function of time.

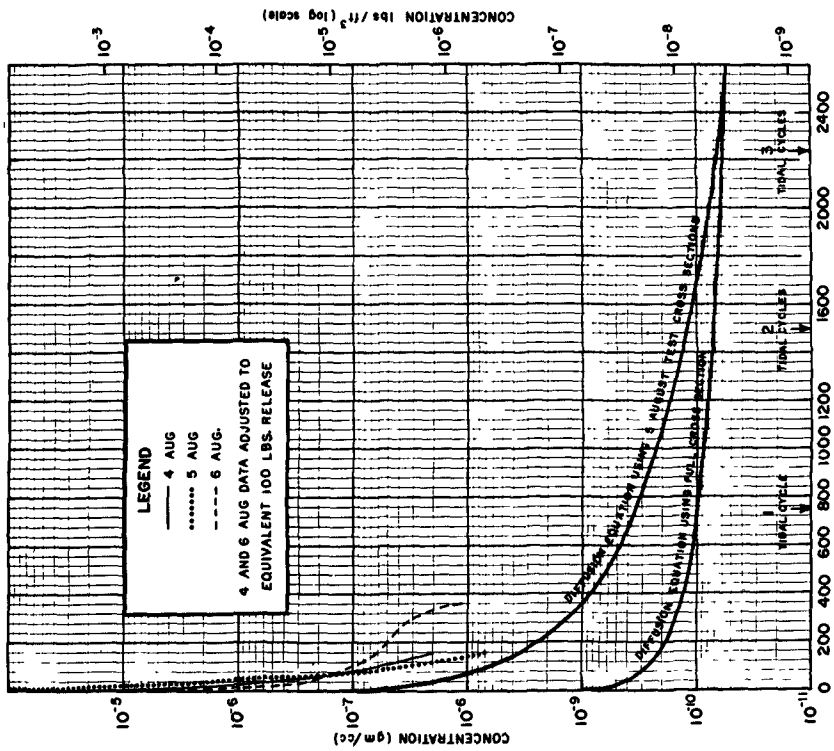

Fig. 10. Comparison of test and computed peak concentration curves.

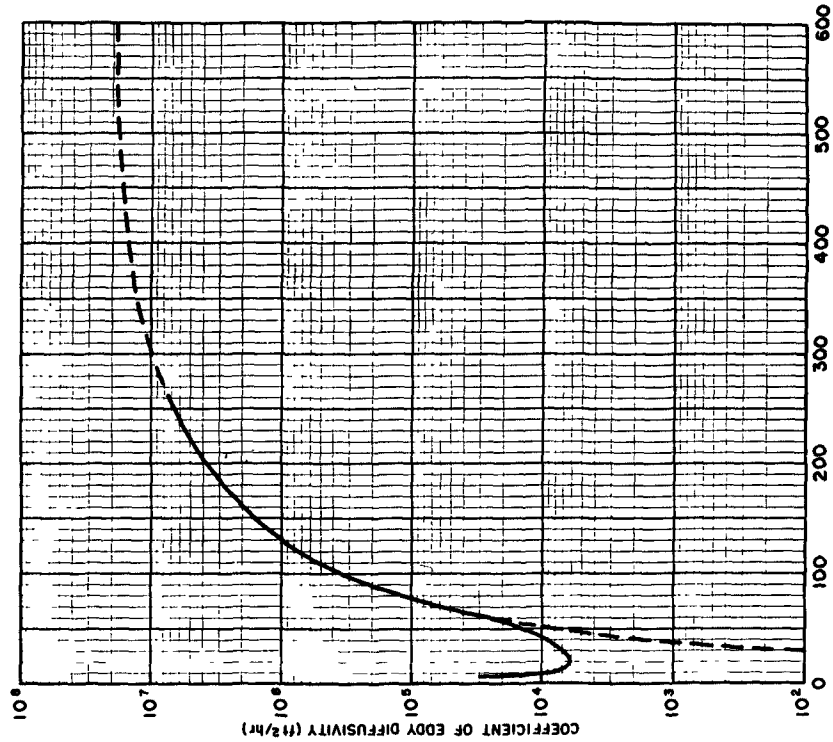

Fig. 9. Coefficient of eddy diffusivity with time - 5 August test.

Using these values of cross section, and the peak concentration values from Figure 6, the original formula for peak concentration was solved for k, the coefficient of eddy diffusion. These values of k, as a function of time, are shown in Figure 9.

This curve shows that the value of the coefficient was not a constant, at least for the first few tidal cycles. Instead k was an increasing function of t for small dispersion times, eventually approaching a constant for large dispersion times. In the case of the James River in the Hampton Roads area, k presumably should have approached 1950 X 10^4 ft^2/hr, the mean value derived from the salinity data.

A comparison of the peak concentration curves with time from the two tests to those that were computed from the diffusion equations are shown in Figure 10. In an attempt to make the test results compatible, the 6 August concentrations were reduced by one-half. This should closely approximate the results that would have been attained if 100 pounds of dye had been used on each day.

The different rates of dilution on each day must have been largely a result of the speed of the tidal currents. On the 5th the dye was injected at slack before ebb with the currents gradually increasing from near slack to more than 1 knot. On the other hand, on 6 August even though the dye was released very near slack before flood, the currents at the beginning of the test were more than 1 knot, increasing to almost 1.5 knots within one-half hour and gradually decreasing toward the slack before ebb some 5 hours later. The spreading of dye in a very long plume in the direction of the current probably was due not only to the method of release, but also to the higher current speeds with their greater longitudinal turbulent fluctuations.

The test concentration curves when compared with those computed from the original equation using the full cross section and assuming a 100 pound release, show concentrations as much as 3 to 4 orders of magnitude higher. When the test cross sections are used in the diffusion equation, this difference becomes about 1 to 2 orders of magnitude in the first hour with differences decreasing with increasing time. After perhaps 1 or 2 tidal cycles, when near the mean value of eddy diffusion is actually attained, this difference should disappear; in fact, Figure 10 indicates such a trend.

A rough check on the concentrations computed for any area can be made by determining the lowest limits of possible concentrations. That is: (1) any dissolved pollutant released will be diluted by the volume of water contained in one tidal prism (or volume delineated by one tidal excursion) within one tidal cycle, and (2) the pollutant will be diluted by all the water available within several days.

In the lower James River Estuary, an average tidal prism or volume of a tidal excursion is something more than 3 X 10^{14} cc. The entire volume of

water available for dilution is assumably that volume lying between Old Point Comfort and the James River Bridge, approximately 12 X 10^{14} cc.

Using these approximate volumes, it can be estimated that 45,400 grams (100 pounds) of contaminant would be diluted by 3 X 10^{14} cc. of water in about one tidal cycle. This gives a mean concentration of 1.5 X 10^{-10} gm/cc and approximates the peak value of 3.5 X 10^{-10} gm/cc indicated on Figure 10 for one tidal cycle. After several days, the 100 pounds should be diluted by 12 X 10^{14} cc of water; its mean concentration should be 3.8 X 10^{-11} gm/cc, which is very close to that estimated by the diffusion equation.

To summarize and to simplify using the results of the test and the theory on the release of other amounts of dissolved contaminants in this area, a set of emperical dilution factors have been computed. They were derived from the curves of Figure 10 and could be used to estimate the peak concentrations that would occur in the vicinity of Hampton Roads if a known mass of contaminant was introduced. These dilution factors are shown in Table 1 and, when multiplied by the amount of introduced contaminant, will give the peak concentration of the substance at the indicated time.

TABLE 1

DILUTION FACTORS FOR HAMPTON ROADS, VIRGINIA AREA.

Time after release t	Dilution Factor /cc	Dilution Factor /ft^3
10 min.	2.2 X 10^{-10}	6.3 X 10^{-6}
30 min.	7.1 X 10^{-11}	2.0 X 10^{-6}
60 min.	1.1 X 10^{-11}	3.0 X 10^{-7}
3 hours	1.3 X 10^{-13}	3.8 X 10^{-9}
6 hours	2.4 X 10^{-14}	8.5 X 10^{-10}
1 tidal cycle	7.7 X 10^{-15}	2.2 X 10^{-10}
2 tidal cycles	2.6 X 10^{-15}	7.5 X 10^{-11}
3 tidal cycles	1.5 X 10^{-15}	4.2 X 10^{-11}

1. The total amount of contaminant released multiplied by the appropriate dilution factor gives the concentration at that time.

2. Two dilution factors are given so that computations may be made either in terms of cubic centimeters or cubic feet.

3. The rapid leveling off of the dilution factors after about 1 tidal cycle assumes that none of the contaminant is advected out of the area.

REFERENCES

1. Kent, Richard Eugene. Turbulent diffusion in a sectionally homogeneous estuary. Chesapeake Bay Institute Technical Report XVI. Reference No. 58-1. The Johns Hopkins University. 86 p. April 1958.

2. Pritchard, D. W. A study of flushing in the Delaware model. Chesapeake Bay Institute Technical Report VII, Reference 54-4. The Johns Hopkins University. 143 p. April 1954.

3. Taylor, Sir Geoffry. The dispersion of matter in turbulent flow through a pipe. Proceedings of the Royal Society of London, Series A, v. 223, no. 1155, 20 May 1954. p. 446-468.

4. Stommel, Henry. Computation of pollution in a vertically mixed estuary. Sewage and Industrial Wastes, v. 25, no. 9, Sept. 1953. p. 1065-1071.

5. U. S. Navy Hydrographic Office. Division of Oceanography. Oceanographic Publications Branch. Flushing time and dispersion of contaminants in tidal waters with applications to the James River by C. H. Cline and L. J. Fisher. July 1959. 42 p.

CHAPTER 30

HURRICANE TIDE PREDICTION FOR NEW YORK BAY

Basil W. Wilson
Professor, Department of Oceanography and Meteorology
Texas A. & M. College, College Station, Texas

ABSTRACT

This paper is concerned with the solution of the problem of correlating, on a two-dimensional basis, the meteorological parameters of several off-shore storms with the known surge induced by them in New York Bay and with the application of the results to the prediction of likely effects in New York Bay from a design hurricane of given strength traversing a given path at a given speed. A purely theoretical approach would have been beyond practical possibility within the time available for this study; the method adopted therefore is empirical but with some degree of theoretical guidance. A recursion formula is evolved, using the method of finite differences for time increments of 1/3 hour, which relates tide elevation at the bay-mouth with two values of the elevation at 1/3 and 2/3 hour earlier and with values of wind-stress and pressure-gradient driving-force components (directed towards New York Bay from several remote two-dimensionally spaced offshore-stations on the continental shelf) at times earlier by the periods taken for free long gravity waves to travel from the stations to the bay-mouth. The formula includes a comulative forcing function term which allows for the geostrophic influence of the earth's rotation and also for an "edge-wave" effect northward along the eastern seaboard. Moreover it takes into account the observed tendencies of hurricane storm tides in New York Bay to develop resurgences at periods of 7 hours with decay rates of 50% amplitude decrease per cycle. The coefficients of the "forcing functions", determined by correlation, tend to represent the storm size and speed and also the dynamic augmentation of the forced wave. Predicted maximum storm tide heights are in fair agreement with crude empirical estimates based on central pressures within the hurricanes. Predictions, however, provide complete time-sequences of water level for periods up to 24 hours inclusive of the first resurgence after the main surge.

HURRICANE TIDE PREDICTION FOR NEW YORK BAY

1. INTRODUCTION

The two-dimensional problem of a non-radially symmetric tropical storm approaching an irregular coastline over water of shelving depth at variable speed is, theoretically, of formidable proportions and, so far as is known, has not yet been solved. The best hope for its eventual solution in special cases lies in the use of finite-difference procedures. Some notable advances have been made in this direction by such investigators as Hansen, Weylander, Kreiss [Reid 1957 (i)], Kivisild [1954], Reid [1957 (ii)], Platzman [1958], Fischer [1959] and others, and these lend hope that the difficulties of the problem may finally be overcome. The major difficulties concern the boundary conditions at the edge of the continental shelf, seaward of which the response of the sea surface to the storm driving forces may be quite unknown; here also the reflective properties of the continental slope may be difficult to determine.

To avoid these inherent problems and withal reach reasonable estimates (within a short time) of the potential menace of hurricane storm tides to New York Bay it was decided to use an empirical approach under the guidance of theory. The method here described differs rather considerably from other empirical methods devised for the North Sea area by Schalkwijk [1947], Corkan [1950], the Darbyshires [1956], Hansen [1957], Weenink and Groen [1958], and others. It departs also from the several empirical endeavours of American investigators who have previously studied surge effects along the United States east coast, notably Miller [1956], Zetler [1957], Kussman [1957], Donn [1958] and Tancreto [1958] as also Reid [1955], Conner, et al [1957], Hoover [1957], Dunn [1957], and Harris [1957, 1959]. Most of these empirical approaches are unsuited to transient, fast-moving circular storms in which inertial effects and influences of the earth's rotation are likely to be important.

In what follows an attempt is made to take due account of the speed of the storm, the direction of its approach, the two-dimensional topography of the continental shelf area which it would have to traverse, the size of the storm, its meteorological parameters (pressure and wind velocity) in a two dimensional sense, its geostrophic effect along-shore and its dynamic effect in producing inertial oscillations of the observed period, magnitude and evanescence.

2. TWO-DIMENSIONAL MOTION OF WATER UNDER IMPULSION FROM ATMOSPHERIC DRIVING FORCES

With reference to a rectangular co-ordinate system having its origin and xy-plane in the horizontal still water surface, the equations of motion and continuity of the water at any point (x, y) may be rendered in the form,

for motion in the x-direction,

$$\text{(i)}\quad \frac{\partial Q_x}{\partial t} - fQ_y + g(d+\eta)\frac{\partial \eta}{\partial x} = \frac{\tau_{sx} - \tau_{bx}}{\rho} - \frac{(d+\eta)}{\rho}\frac{\partial p_a}{\partial x}$$

for motion in the y direction,

$$\text{(ii)}\quad \frac{\partial Q_y}{\partial t} + fQ_x + g(d+\eta)\frac{\partial \eta}{\partial y} = \frac{\tau_{sy} - \tau_{by}}{\rho} - \frac{(d+\eta)}{\rho}\frac{\partial p_a}{\partial y} \qquad (1)$$

for continuity,

$$\text{(iii)}\quad \frac{\partial Q_x}{\partial x} + \frac{\partial Q_y}{\partial y} + \frac{\partial \eta}{\partial t} = 0$$

In these equations Q_x , Q_y are the volumes of water transported in unit time in the x, y directions respectively across vertical sections of unit width between the free surface and the bottom, η is the elevation of the water surface above the still water level, d the nominal water depth (referred to still water), f the coriolis parameter, τ_{sx} , τ_{sy} the x, y components of the surface wind stress, τ_{bx} , τ_{by} the corresponding components of the bottom frictional stress, p_a the atmospheric pressure, and g, p, t the usual respective designations for acceleration due to gravity, mass density of water, and variable time.

The assumptions underlying the above equations are that vertical accelerations of the water body resulting from the wind stress τ and the atmospheric pressure p_a are quite negligible, as are any changes in shear stress within the fluid in horizontal directions; further that the horizontal flow of water is uniform with depth and changes only very gradually with distance, while water density is constant.

It is convenient to approximate $\frac{1}{\rho}\tau_{bx}$, $\frac{1}{\rho}\tau_{by}$ as proportional to Q_x , Q_y respectively by use of a frictional damping constant K so that, on regarding η as small in comparison with d , Eqs. (1) modify to

$$\left.\begin{aligned}
&\text{(i)} \quad \left(\frac{\partial}{\partial t} + K\right) Q_x - fQ_y + gd\frac{\partial \eta}{\partial x} = F_x \\
&\text{(iii)} \quad \left(\frac{\partial}{\partial t} + K\right) Q_y + fQ_x + gd\frac{\partial \eta}{\partial y} = F_y \\
&\text{(iii)} \quad \frac{\partial Q_x}{\partial x} + \frac{\partial Q_y}{\partial y} + \frac{\partial \eta}{\partial t} = 0
\end{aligned}\right\} \qquad (2)$$

wherein F_x and F_y are forcing functions representing the wind stress and pressure gradient, as defined by

$$\left.\begin{aligned}
&\text{(i)} \quad F_x = \frac{1}{\rho}\left(\tau_x - d\frac{\partial p_a}{\partial x}\right) \\
&\text{(ii)} \quad F_y = \frac{1}{\rho}\left(\tau_y - d\frac{\partial p_a}{\partial x}\right)
\end{aligned}\right\} \qquad (3)$$

3. ONE-DIMENSIONAL MOTION IN ABSENCE OF EARTH'S ROTATIONAL INFLUENCE - INFLUENCE OF WIND STRESS

In order to justify our physical reasoning in what follows, we shall temporarily depart from the two-dimensionality of the problem to consider the one-dimensional (x) problem on the assumption that lateral flow, Q_y, is non-existent. In these circumstances, Eqs. (2,i) and (2,iii) reduce to

$$\left.\begin{aligned}
&\text{(i)} \quad \frac{\partial Q}{\partial t} + KQ + gd\frac{\partial \eta}{\partial x} = F \\
&\text{(ii)} \quad \frac{\partial Q}{\partial x} + \frac{\partial \eta}{\partial t} = 0
\end{aligned}\right\} \qquad (4)$$

For convenience the x subscript is discarded in Eqs. (4). We shall make the further approximation that η can be divided into the separate effects, η_w and η_p deriving from wind stress and pressure gradient respectively, with corresponding flows Q_w and Q_p, and driving forces $F_w \left(= \frac{\tau_x}{\rho}\right)$ and $F_p \left(= -\frac{d}{\rho}\frac{\partial p_a}{\partial x}\right)$.

Considering first of all the wind effect, it is possible to represent the magnitude of the wind stress, assumed to have an equilateral-triangular distribution (as for a hurricane) [cf Reid, 1955; 1956(i)] over a storm

fetch 2ℓ and to be moving forward without change at constant velocity V across a distance 2L from the coast, Fig. 1 (where L may be assumed to be the shelf width)*, as the Fourier series:

$$F_w = \frac{8}{\pi^2}\frac{L}{\ell}\frac{\tau_m}{\rho}\sum_{r=1}^{\infty}\frac{1}{r^2}\left(1-\cos\frac{r\pi\ell}{2L}\right)\sin\frac{r\pi Vt}{2L}\sin\frac{r\pi x}{2L} \qquad (5)$$

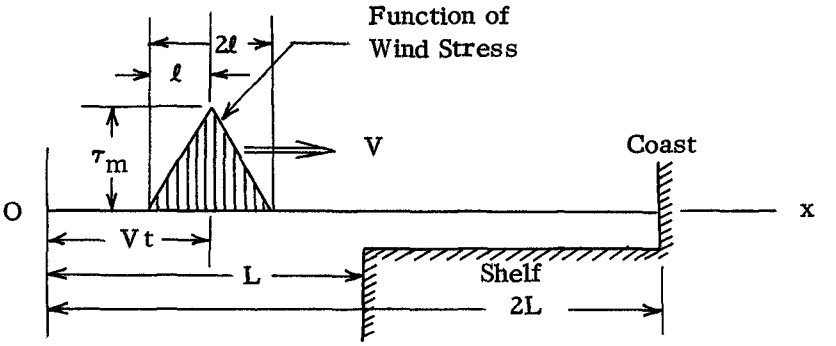

Fig. 1. Representation of Moving Wind Stress Function as a Fourier Series

wherein τ_m is the maximum value of the wind stress and r an integer of successive values 1, 2, 3... It should be remarked here that constancy of τ_m and ℓ with time and distance will really only obtain if the storm is moving parallel to the direction x . The representation of Eq. (5) is therefore rather artificial, but will serve the purpose of demonstration.

It is convenient to consider just a general r-th term of the Fourier summation, namely, $(F_w)_r$ and proceed to a solution of Eq. (4) by trial of possible solutions

$$\left.\begin{aligned} &(i) \qquad (\eta_w)_r = M_r(t)\cos\frac{r\pi x}{2L} \\ &(ii) \qquad (Q_w)_r = N_r(t)\sin\frac{r\pi x}{2L} \end{aligned}\right\} \qquad (6)$$

* The adoption of 2L for the series expansion is merely a convenient artifice to ensure that the moving fetch may initially be seaward of the shelf edge if $\ell < L$.

in which $M_r(t)$ and $N_r(t)$ are unknown functions of t which remain to be determined and $(\eta_w)_r$ and $(Q_w)_r$ are r th terms in the complete solutions

$$\left.\begin{aligned} &(i) \qquad \eta_w = \sum_{r=1}^{\infty} (\eta_w)_r \\ &(ii) \qquad Q_w = \sum_{r=1}^{\infty} (Q_w)_r \end{aligned}\right\} \tag{7}$$

Upon inserting Eqs. (6) in Eqs. (4), and solving the simultaneous differential equations for $M_r(t)$, there results

$$M_r'' + KM_r' + \left(\frac{r^2\pi^2}{4L^2}C^2\right) M_r = B \sin\left(\frac{r\pi V}{2L}\right) t \tag{8}$$

wherein primes denote the order of differentiation of the function $M_r(t)$ with respect to t and

$$\left.\begin{aligned} &(i) \qquad C^2 = gd \\ &(ii) \qquad B = \frac{4}{\pi}\frac{\tau_m}{\rho\ell}\frac{1}{r}\left(1 - \cos\frac{r\pi\ell}{2L}\right) \end{aligned}\right\} \tag{9}$$

4. SOLUTION OF THE FREE OSCILLATIONS - WIND STRESS EFFECT

Eq. (8) is the familiar expression for a linear damped oscillating system excited by a disturbance of periodic character. To simplify notation we rewrite it in the form

$$\frac{d^2y}{dt^2} + K\frac{dy}{dt} + S_r^2 y = B \sin \omega_r t \tag{10}$$

in which S_r is an angular frequency very closely that of the free oscillation and ω_r the frequency of the forced oscillation in the r-th mode.

We shall concern ourselves here for the time being only with the free, inertial oscillations, represented by the solution of

$$\frac{d^2y}{dt^2} + K\frac{dy}{dt} + S_r^2 y = 0 \tag{11}$$

By writing Eq. (11) in finite difference form with a small time increment τ, we obtain

$$\frac{y_n - 2y_{n-1} + y_{n-2}}{\tau^2} + K\frac{y_n - y_{n-1}}{\tau} + S_r^2 y_{n-1} = 0 \qquad (12)$$

wherein y_n, y_{n-1}, y_{n-2} are consecutive values of y at receding small intervals of time τ with y_n applicable to any time, $n\tau$. On solving Eq. (12) for y_n,

$$y_n = a y_{n-1} - b y_{n-2} \qquad (13)$$

in which the coefficients a, b have the values:

$$\left.\begin{aligned} &(i) \qquad a = \frac{2 + K\tau - (S_r\tau)^2}{1 + K\tau} \\ &(ii) \qquad b = \frac{1}{1 + K\tau} \end{aligned}\right\} \qquad (14)$$

Returning now to Eq. (6, i) and taking $r = 1$ as representing the fundamental mode of possible free oscillations, it would appear that the relationship

$$\eta_w(t) = a\,\eta_w(t - \tau) - b\,\eta_w(t - 2\tau) \qquad (15)$$

would be descriptive of the free oscillations in the fundamental mode. Since the frequency S ($= 2\pi/T$, T being the period of free oscillation) and the damping coefficient K are measurable in the records of storm tides, the coefficients a, b are prescribed by Eqs. (14). It may be shown that the values of these coefficients must observe the conditions

$$\left.\begin{aligned} &(i) \qquad 4b > (a)^2 \\ &(ii) \qquad b < 1 \end{aligned}\right\} \qquad (16)$$

if numerical stability of Eq. (20) is to be ensured.

5. SOLUTION OF THE FORCED OSCILLATIONS - WIND STRESS EFFECT

Determination of the forced oscillations created by the moving wind disturbance involves finding the Particular Integral of Eq. (8) or (10). This

is readily shown to be

$$y = \alpha \sin \omega_r t + \beta \cos \omega_r t \qquad (17)$$

where

$$\left.\begin{aligned} \text{(i)} \qquad \alpha &= \frac{B(S_r^2 - \omega_r^2)}{(S_r^2 - \omega_r^2)^2 + (K\omega_r)^2} \\ \text{(ii)} \qquad \beta &= \frac{-B(K\omega_r)}{(S_r^2 - \omega_r^2)^2 + (K\omega_r)^2} \end{aligned}\right\} \qquad (18)$$

Discarding the modal subscript r for convenience, we now require that this forced part of the solution [Eq. (17)] should comply with a finite difference solution of the form of Eq. (13), but inclusive of a term directly representative of the forcing function of Eq. (10); that is

$$y_n = a y_{n-1} - b y_{n-2} + c \sin [(n-1)\omega\tau - \gamma] \; . \qquad (20)$$

in which γ is an appropriate phase angle.

Theoretically it can be shown that the coefficient c is a function of B, S, K, $\omega\tau$, and μ of which μ is a dynamic augmentation factor dependent on the forced-free frequency ratio (ω/S), namely

$$\mu = [\{1 - (\omega/S)^2\}^2 + (K\omega/S^2)^2]^{-\frac{1}{2}} \qquad (21)$$

The ratio of frequencies ω/S will be apparent on comparison of Eqs. (8) and (10). Thus

$$\omega/S = V/C \qquad (22)$$

making

$$\mu = [\{1 - (V/C)^2\}^2 + (\frac{K}{S} V/C)^2]^{-\frac{1}{2}} \qquad (23)$$

If thus transpires that the finite difference solution

$$\eta_w(t) = a\eta_w(t - \tau) - b\eta_w(t - 2\tau) + cF_w[(t - \tau) - T_o]$$

(24)

wherein T_o is a time lag comparable to the phase angle γ, will represent the dynamic storm tide generated under the impulsion of the wind stress. If the coefficients a and b are prescribed by Eqs. (14) and the coefficient c and the phase T_o are determined by correlation between $[\eta_w(t) - a\eta_w(t - \tau) + b\eta_w(t - 2\tau)]$ and $F_w(t - \tau)$, then the above discussion shows that the formula (24) will inherently allow for any dynamic augmentation arising from the relative magnitudes of the speed of the storm and the velocity of the induced free wave. Further, since the coefficient c is inclusive of the amplitude B of the forcing function [see Eqs. (8), (9) and (10)], which tends to depend on the size of the storm (through its fetch 2ℓ), it follows also that the scale of the storm is inherently allowed for in the formula of Eq. (24).

6. INFLUENCE OF THE PRESSURE GRADIENT

Considering next the influence of the driving force from pressure gradient, $F_p \left(= -\frac{d}{\rho}\frac{\partial p_a}{\partial x}\right)$, in a hurricane; we may, for purposes of demonstration again, assume the pressure gradient distribution over a moving fetch 2ℓ to be unchanging and of the form $-\frac{d}{\rho}\left(\frac{\partial p_a}{\partial x}\right)_{max.} \times \sin\frac{\pi(x - Vt)}{\ell}$ (Fig. 2). Adopting the additional simplification of uniform depth over the distance 2L, the Fourier series representation of the forcing function may be shown to be

$$F_p = -\frac{8}{\pi}\frac{(\ell L d)}{\rho}\left(\frac{\partial p_a}{\partial x}\right)_{max}\sum_{r=1}^{\infty}\frac{1}{4L^2 - (r\ell)^2}\sin\frac{r\pi\ell}{2L}\cos\frac{r\pi Vt}{2L}\sin\frac{r\pi x}{2L} \qquad (25)$$

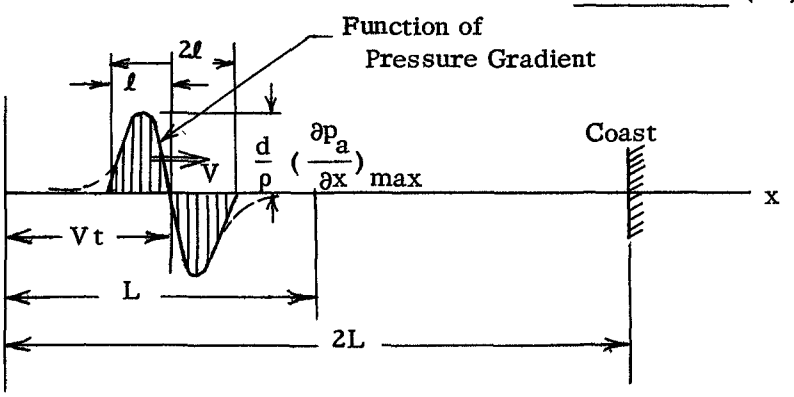

Fig 2. Representation of Moving Pressure Gradient Function as a Fourier Series

wherein $(\frac{\partial p_a}{\partial x})_{max.}$ is the maximum value of the pressure gradient and r is again an integer of successive values r = 1, 2, 3.....

Again we consider just a general r-th term of the Fourier summation, namely $(F_p)_r$, and try as solutions of Eq. (4)

$$\left.\begin{aligned} &\text{(i)} \qquad (\eta_p)_r = G_r(t) \cos \frac{r\pi x}{2L} \\ &\text{(ii)} \qquad (Q_p)_r = H_r(t) \sin \frac{r\pi x}{2L} \end{aligned}\right\} \quad (26)$$

in which $G_r(t)$ and $H_r(t)$ are unknown functions of t, to be determined.

Substitution of Eqs. (26) in Eqs. (4) results in

$$G_r'' + KG_r' + (\frac{r^2\pi^2C^2}{4L^2}) G_r = D \cos (\frac{r\pi V}{2L}) t \qquad (27)$$

wherein primes denote the order of differentiation of the function $G_r(t)$ with respect to t and

$$\left.\begin{aligned} &\text{(i)} \qquad C^2 = gd \\ &\text{(ii)} \qquad D = -\frac{4d}{\rho} (\frac{\partial p_a}{\partial x})_{max} \frac{r\ell}{4L^2 - (r\ell)^2} \sin \frac{r\pi\ell}{2L} \end{aligned}\right\} \quad (28)$$

It is possible to follow the same arguments of the preceding two sections, by writing Eq. (27) in the form

$$\frac{d^2y}{dt^2} + K \frac{dy}{dt} + S_r^2 y = D \cos \omega_r t \qquad (29)$$

and reach the more general conclusion that a finite difference solution of the form

$$\eta(t) = a\eta(t - \tau) - b\eta(t - 2\tau) + c[F_w\{(t - \tau) - T_o\} + F_p\{(t - \tau) - T_o\}] \qquad (30)$$

will represent the combined dynamic storm tide generated by both the wind

stress and pressure gradient driving forces acting together. The last term may conveniently be designated simply as $cF(t - \tau - T_o)$

7. ALLOWANCE FOR TWO-DIMENSIONAL EFFECTS

We return now to the two-dimensional nature of the problem with special reference to the offshore environment in the neighborhood of New York. If a number (N) of offshore stations is arbitrarily selected, as in Fig. 3 (inset), to cover, in a two-dimensional sense, the shelf region of the approaches to New York Bay, then, by evaluating the magnitude of the forcing function $F_r(t - \tau - T_N)$ at any such station, directed radially towards the station A at the bay-mouth, (in which T_N is the time taken for the free wave to travel from the N-th offshore station to the bay-mouth), the formula

$$\eta_A(t) = a\eta_A(t - \tau) - b\eta_A(t - 2\tau) + c_1[F_r]_1(t - \tau - T_1)$$

$$+ c_2[F_r]_2(t - \tau - T_2) + \ldots + c_7[F_r]_7(t - \tau - T_7) \qquad (31)$$

in which subscripts $N = 1, 2, \ldots 7$ refer to station numbers, should have a pseudo-two-dimensional capacity to correlate the storm-tide $\eta_A(t)$ at the bay-mouth A with the offshore disturbances occuring over a wide area. The assumption here is that the local water level upheaval at any particular offshore station, created by a driving force $F_r(t - \tau - T_N)$, requires the interval of time T_N to reach the bay-mouth and become merged in the resultant superelevation $\eta_A(t)$ occurring there.

This assumption actually follows a false premise insofar as it associates 'effect' (waves) with 'cause' (wind stress and pressure gradient) and translates the 'effect' instead of the 'cause' from station to bay-mouth. Thus T_N should correctly be based on the time that the meteorological forcing function, F_r, directed radially to the bay-mouth, would take to travel the intervening distance, if its identity could be preserved. The value of, T_N, in other words, should be some function of the speed of the storm and not of the speed of the waves. If T_N were to be determined rigorously it would require evaluation of the forcing function F_r for each station as a continuous function of both t and of r, the distance from the bay-mouth. The manual computing time that it would have required to do this would have been prohibitive so that some evasive tactics were necessary. The use of T_N based on 'effect' seemed to offer the best way of circumventing the difficulty.

At first sight it may seem that unwarranted liberty is being taken with the physical structure of the solution given by Eq. (30). However it is a well known dynamical principle that, if ω/S , the forced-free frequency ratio of Eq. (22) is less than unity, the phase difference between cause and effect is relatively small. Hence for slow moving storms, at least, T_N in Eq. (31), based on the wave travel time, will be reasonably correct. Only when ω/S approaches or exceeds unity, in the linear oscillating system we are dealing with, will T_N become unreliable if founded on the wave travel time. The dynamics of the system suggest that a lag T_o will result between cause and effect as indicated by Eqs. (17), (24) and (30). Since T_N will give the effect at the bay-mouth we must therefore correct by a time T_V in order to ensure that the cause will precede the effect by the necessary lead T_o . Thus it becomes necessary to rewrite Eq. (31) as

$$\eta_A(t) = a\eta_A(t-\tau) - b\eta_A(t-2\tau) + \sum_{1}^{N=7} c_N[F_r]_N(t-\tau-T_N+T_V) \qquad (32)$$

In the absence of the correction T_V the functioning of Eq. (31) is represented schematically in Fig. 3. The individual F_r contributions from the different stations, at times earlier by T_N, converge along the radial distance-time paths to the point of time $(t-\tau)$ at station A , giving, in effect, the uncorrected function

$$\sum_{1}^{N=7} c_N[F_r]_N(t-\tau-T_N)$$

The gradients dr/dt of the propagation lines in the r - t plane (Fig. 3) are the velocities $C = \sqrt{gd}$ at which the free waves travel along the radial directions (Fig. 3, inset) over the variable depths of the shelf. The lag correction, T_V that is required for fast moving storms will be discussed further at a later stage.

8. ALLOWANCE FOR THE GEOSTROPHIC EFFECT

The influences of the earth's rotation enter into the dynamical equations in the terms involving the Coriolis parameter f [Eqs. (2)]. They are likely to be greatest in the relatively shallow water near the coast. In discussion of these effects it is convenient to consider the y-axis

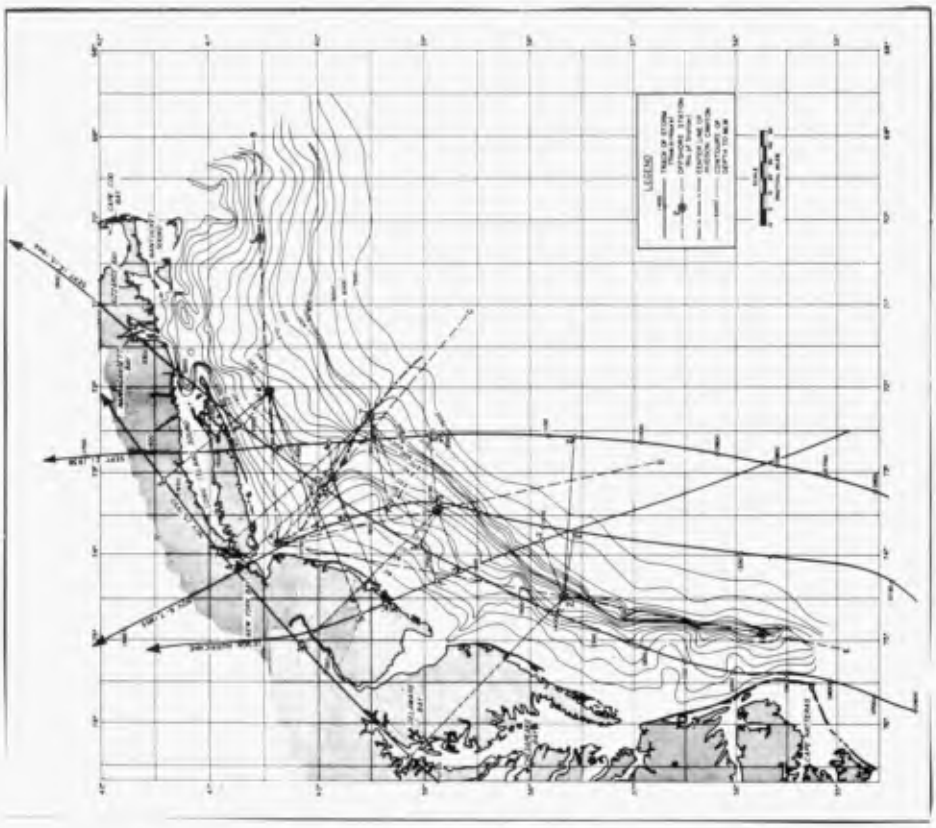

Fig. 4. Eastern U. S. coastline from Nantucket Sound to Cape Hatteras showing the continental shelf and the location of offshore stations together with the tracks of severe storms.

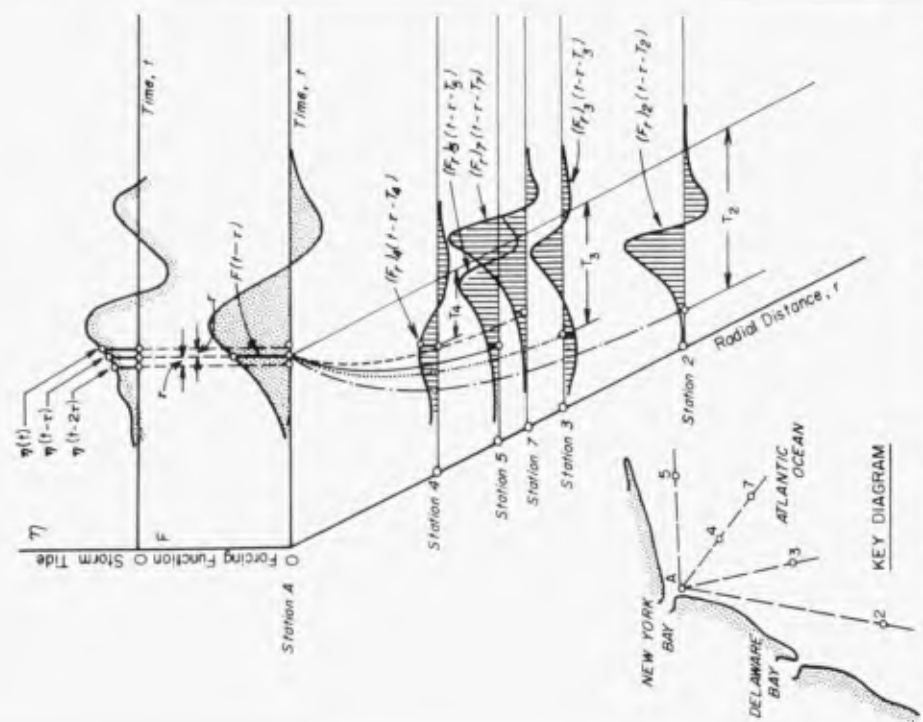

Fig. 3. Schematic representation of features of the adopted correlation - prediction formula. Inset, disposition of offshore stations selected for the shelf region, New York Bay area.

of reference in Eqs. (2) as parallel to the coast and the x-axis normal thereto. Then, if we can assume that the flow onshore, Q_x, resulting from a superposed hurricane is appreciably less than the longshore flow, Q_y, because of the boundary effect, it is possible to simplify Eqs. (2) by discarding Q_x relative to Q_y. Further, available sources of information [eg. Moore, 1957] suggest that the storm tide gradient alongcoast is very much less than it is normal to the coast, making it possible to approximate further by discarding $\frac{\partial \eta}{\partial y}$ in comparison with $\frac{\partial \eta}{\partial x}$. If these adjustments are made in Eqs. (2, i) and (2, ii) they reduce to

$$\left.\begin{aligned} &\text{(i)} \qquad Q_y = \frac{1}{f}\left(gd\,\frac{\partial \eta}{\partial x} - F_x\right) \\ &\text{(ii)} \qquad \left(\frac{\partial}{\partial t} + K\right) Q_y = F_y \end{aligned}\right\} \tag{33}$$

For the purposes of the further development of the correlation formula Eq. (30), it is convenient to neglect the damping effect of bottom friction, represented in the factor K in Eqs. (33), and eliminate Q_y between the two equations. There results

$$gd\,\frac{\partial \eta}{\partial x} = \int f F_t\, dt + F_n \tag{34}$$

in which $F_n (= F_x)$ and $F_t (= F_y)$ are respectively the normal (n) and tangental (t) components of the forcing functions [Eqs. (3)]. Eq. (34) compares with Eq. (4, i) and it is thus of quasi-one-dimensional form, from which, by association, it is possible to extend Eq. (32) by addition of a term comparable to $\int f F_t dt$ in Eq. (34), to allow for the geostrophic effect. This is most readily done by introducing the term

$$c_A \sum_{t=o}^{t=n\tau} [F_t]_A\,(t - \tau) \tag{35}$$

applicable to station A at the bay-mouth (Fig. 3, inset). The cumulative summation of $(F_t)_A$ at increments of time τ is equivalent to the integral of F_t with respect to time.

For the downcoast offshore station no. 2 (Fig. 3, inset), Eq. (34) suggests that the normal component, F_n, should be used in preference to F_r, the radial component of the driving forces, to describe the effect

induced there. Further since this effect must be allowed to travel along the radial line 2-A towards New York and this route is not far removed from parallelism with the coast, it is rational to base the travel time T_z of the disturbance upon the edgewave speed peculiar to the shelf slope. In accordance with the finding of Stokes [Lamb, 1932 Edn. § 260] this velocity is

$$C = \left[\frac{g s \lambda}{2\pi}\right]^{\frac{1}{2}} \qquad (36)$$

in which s is the shelf slope and λ the wave length of the edgewaves. The choice of λ will be discussed later.

9. THE ADOPTED THEORETICO-EMPIRICAL CORRELATION-PREDICTION EQUATION

As a final addition to Eq. (32) we include, besides the geostrophic term applicable at station A at the bay-mouth, an equivalent pressure gradient term $\delta p_A(t - \tau - T_o)$ additional to $(F_r)_A(t - \tau - T_o)$ such that

$$\delta p_A(t - \tau - T_o) = (p_a)_A(t - \tau - T_o) - p_o(t - \tau - T_o) \qquad (37)$$

where $(p_a)_A$ is the atmospheric pressure at A and p_o the central pressure in the eye of the storm at the same instant. Also, for the purposes of satisfactory correlation, it is desirable to introduce an independent coefficient c_o .

The final formulation then of a correlation and prediction equation for storm tides in New York Bay includes the terms (35) and (37), but rejects*, as too remote for consideration, the influences from offshore stations 1 and 6 (see Fig. 4, post). The formula as finally used (and found to be successful) is thus

*Earlier versions originally included effects of stations 1 and 6.

$$\eta_A(t) = a\eta_A(t-\tau) - b\eta_A(t-2\tau) + c_o + c_{A1}\,\delta p_A(t-\tau+T_V)$$
$$+ c_{A2}\sum_{t=o}^{t=n\tau}[F_t]_A(t-\tau+T_V) + c_{A3}[F_r]_A(t-\tau+T_V)$$
$$+ c_2[F_n]_2(t-\tau+T_V-T_2) + c_3[F_r]_3(t-\tau+T_V-T_3)$$
$$+ c_4[F_r]_4(t-\tau+T_V-T_4) + c_5[F_r]_5(t-\tau+T_V-T_5)$$
$$+ c_7[F_r]_7(t-\tau+T_V-T_7) \qquad (38)$$

10. AVAILABLE WIND AND PRESSURE DATA FOR EAST COAST STORMS

Data packages for selected storms were compiled by the Weather Bureau and furnished to the project. These contained maps of storm tracks, isotachs of surface wind velocity, isobars of surface pressure, profiles of pressure and deflection angles of wind direction (in the case of hurricanes). The packages embraced the following storms:

(a) Hurricane of September 21, 1938
(b) Hurricane of September 14, 1944
(c) Extratropical Storm of November 24-25, 1950
(d) Extratropical Storm of November 6-7, 1953.

In addition a similar data package was supplied in respect of a Design Hurricane based on the 1938 hurricane, transposed to a new track crossing the East Coast approximately at Atlantic City. The tracks of these several storms are shown in Fig. 4 and provide good overall representation of possible approach directions of severe storms to the New York area. The track of the 1938 hurricane for instance runs almost due north, emerging from the South over deep water before crossing Long Island and the New England coast almost at right angles. In contrast, the 1944 hurricane track parallels the east coast, north of Cape Hatteras, and lies well within the confines of the continental shelf. The extratropical storm of 1950 was centered overland on a path roughly parallel with the smoothed trends of the east coast, while that of 1953 runs approximately due north over deep water and curves to the north-west over the continental shelf to pass directly through the portals of New York Bay.

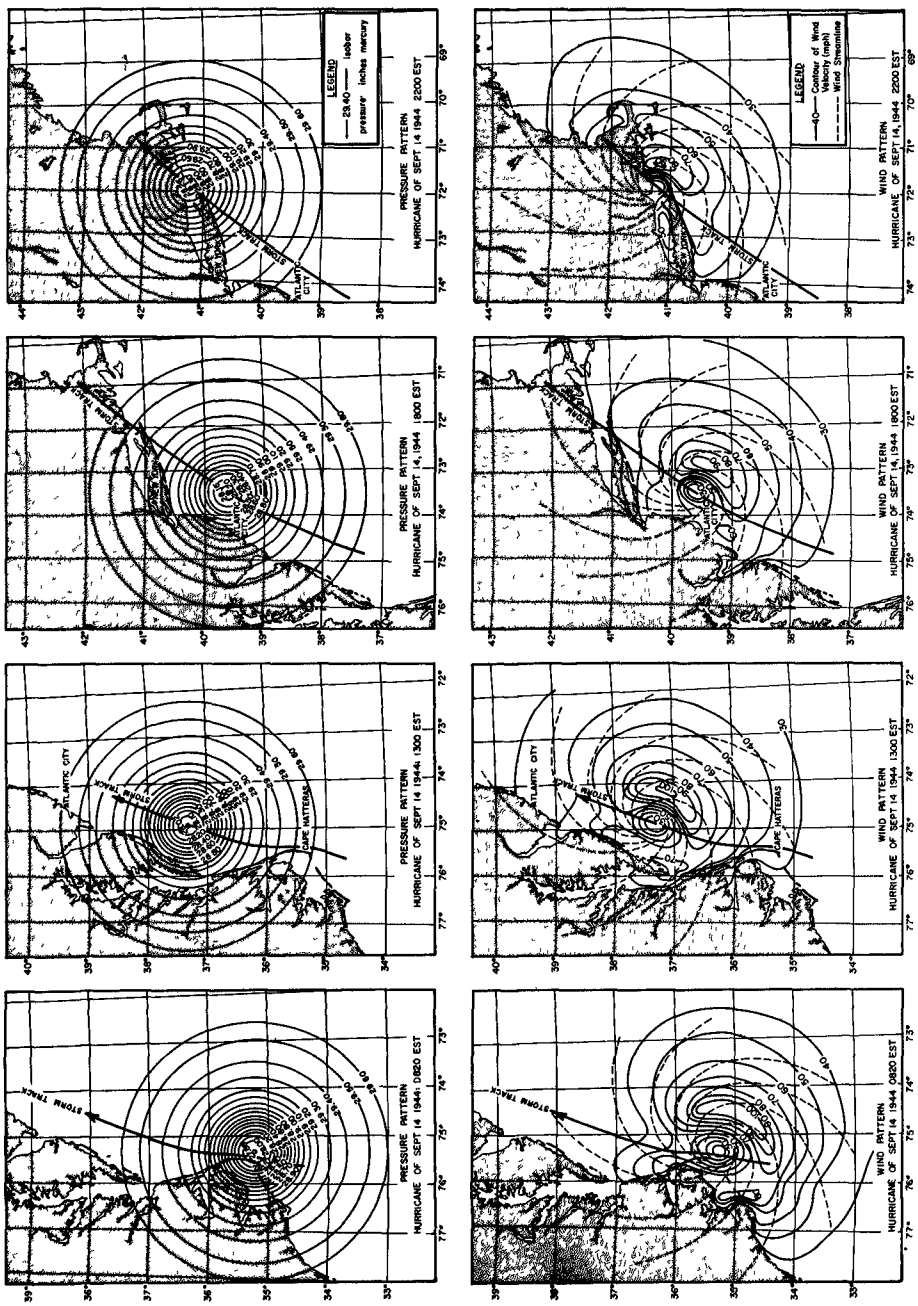

Fig. 5. Sequence of synoptic maps showing pressures (upper) and surface wind velocities and directions (lower) for the hurricane of September 14, 1944. (adapted from U. S. Weather Bureau)

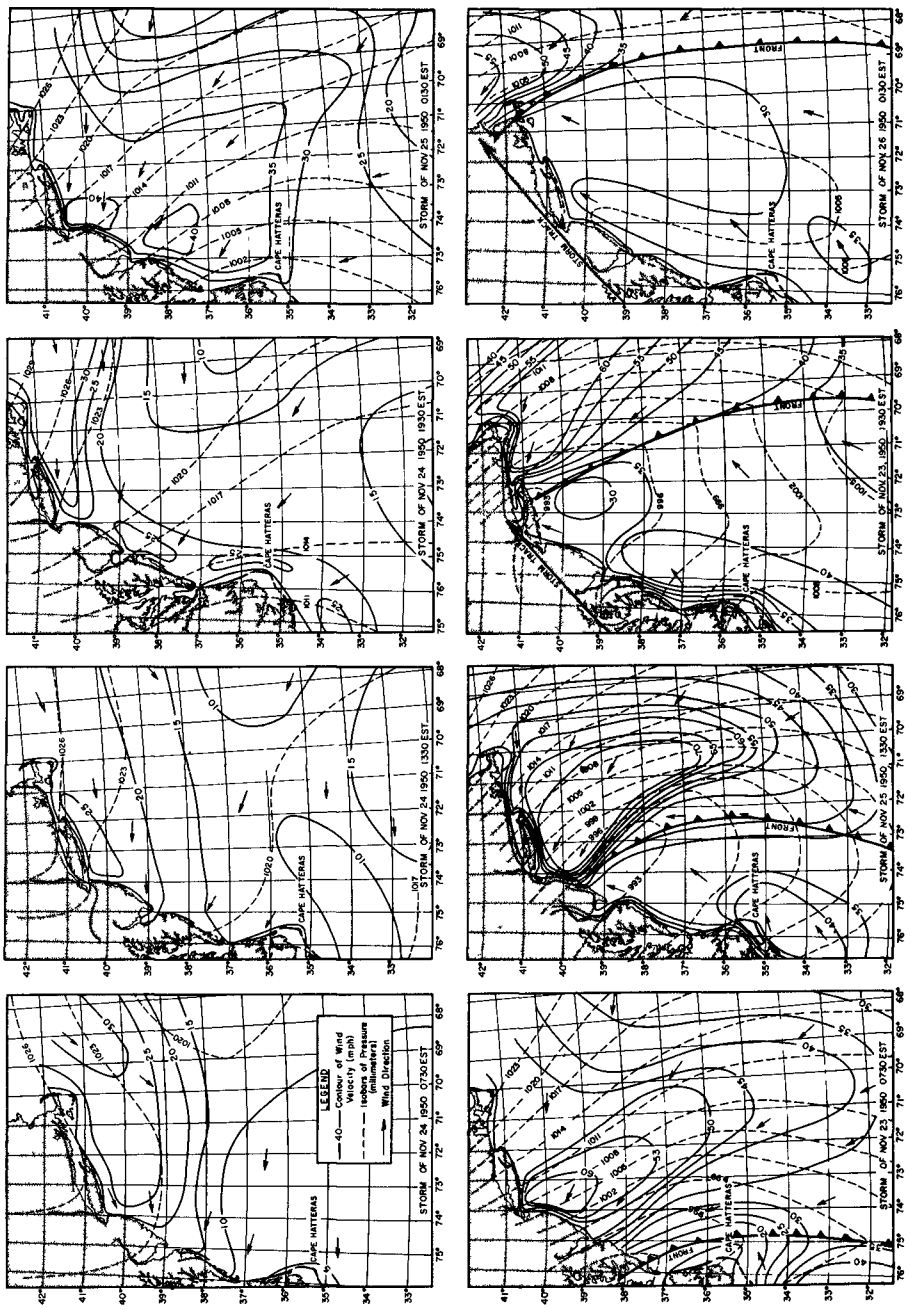

Fig. 6. Sequence of synoptic maps showing pressures, surface wind velocities and directions for the extratropical storm of November 24-26, 1950. (adapted from U. S. Weather Bureau)

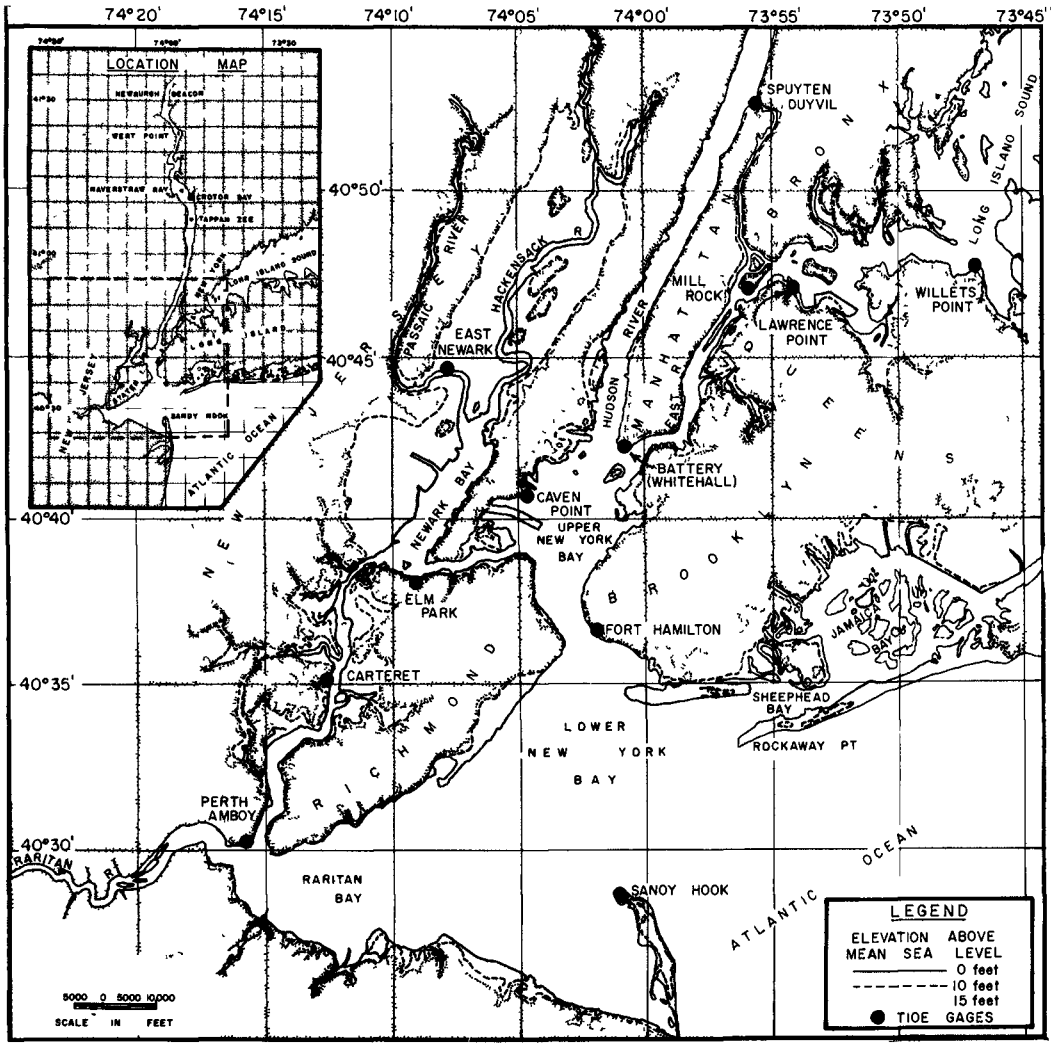

Fig. 7. Map of New York Bay and River System showing locations of gaging stations and low-lying land areas.

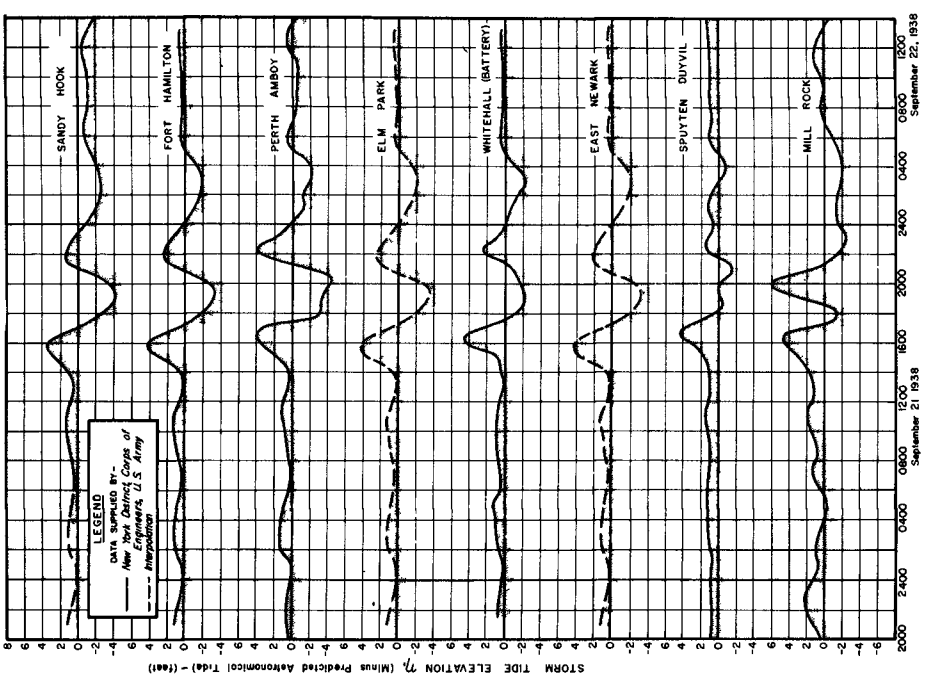

Fig. 8. Storm tide elevations at various gaging stations in New York Bay during hurricane of September 21-22, 1938.

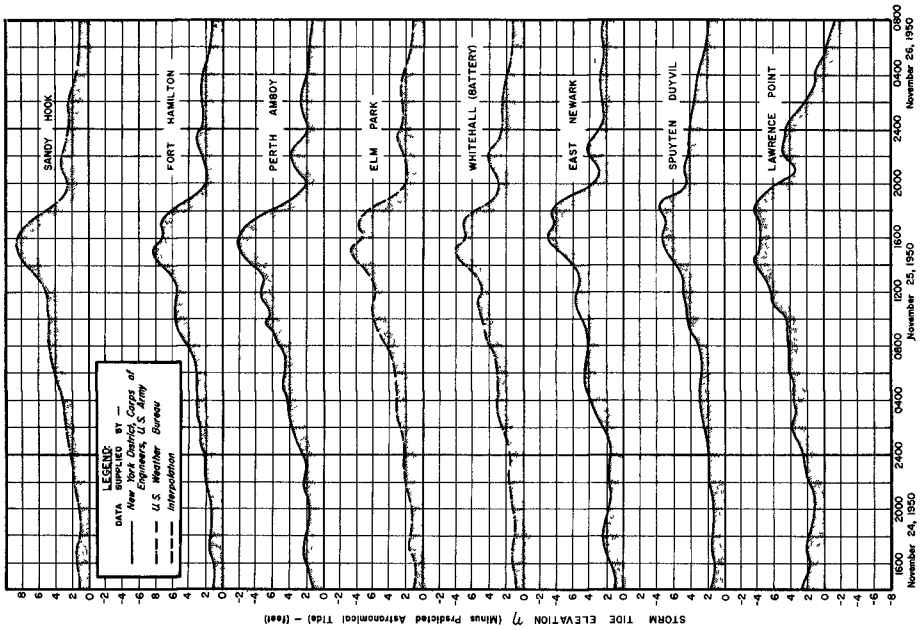

Fig. 9. Storm tide elevations at various gaging stations in New York Bay during extratropical storm of November 24-26, 1950.

In Figs. 5 and 6 are recorded the main features of the surface pressure and wind distributions in two of these storms, as adapted from the data packages It may be remarked from Fig. 5 that the 1944 hurricane was traveling at conside able speed (cf the order of 40-50 knots) over the continental shelf before strikir the coast. The 1938 hurricane moved at roughly comparable velocities. The 19 and 1953 storms were very much slower-moving and it is not surprising that the accumulations of water piled by them into New York Bay and its river system exceeded in volume those from the more transient hurricanes of 1938 and 1944.

11. OBSERVED WATER LEVELS AT GAGING STATIONS IN NEW YORK BAY

Tide gage stations at which water levels are regularly recorded throughout New York Bay are shown in Fig. 7. From the tidal records of these stations predicted astronomical tides for the storm periods in question were deducted leaving residual meteorological tides of which Figs. 8 and 9, as applicable to the 1938 hurricane and the 1950 extra-tropical storm respectively, are typical. The figures show the histories of storm tide elevation at eight of the gaging stations within New York Bay (cf Fig. 7).

The somewhat striking differences between the storm tides created by the 1938 and 1944 hurricanes and those raised by the slow-moving storms of 1950 and 1953 are quite typically portrayed by the differences between Figs. 8 and 9. The elevations at Sandy Hook may be considered representative of $\eta_A(t)$ in Eq. (38).

The hurricane effects are characterized by low antecedent waves followed by the main surge, which, as noted by Redfield and Miller [1956], tends to have a more rapid descent than ascent. After the main surge follow from two to three (or more) resurgences at approximately regular intervals, which on the average are considered to be of 7 hours period (Redfield and Miller, 7.2 hours). The storm tides induced by the 1950 and 1953 storms (cf Fig. 9) show a very much more gradual ascent and are obviously more consonant with the steady state conception of water super-elevation or 'set-up'. Resurgences, though identifiable, are also much less prominent.

As might be expected, water level behavior at Mill Rock (Fig. 7) is considerably influenced by the channel flow from Long Island Sound. In Fig. 8 the first surge at Mill Rock is obviously that caused by penetration of the storm tide up the East River, but the second (higher) surge, occurring earlier than the resurgences anywhere else in the bay, must represent the surge wave that has reached Mill Rock via Long Island Sound. A somewhat similar effect is found in respect of the influence of the 1944 hurricane at Mill Rock. These peculiarities of the transient hurricanes are largely absent in Fig. 9, representative of the sl extratropical storms.

12. REDUCTION AND APPLICATION OF DATA

In order to apply Eq. (38) it was necessary to evaluate the forcing functions, F, at the different offshore stations, which were selected in the positions shown in Fig. 4.

The values of F_r, the resolved part of F in the particular direction ϕ of the bay-mouth, with respect to the x-axis of reference (Fig. 10), are given by

$$\left.\begin{aligned} &\text{(i)}\quad F_r = F\cos(\phi - \theta) \\ &\text{(ii)}\quad F = \sqrt{F_x^2 + F_y^2} \\ &\text{(iii)}\quad \tan\theta = \frac{F_y}{F_x} \end{aligned}\right\} \qquad (39)$$

where θ is the bearing of F, the resultant of F_x and F_y of Eqs. (3), taken anti-clockwise with reference to the x-axis.

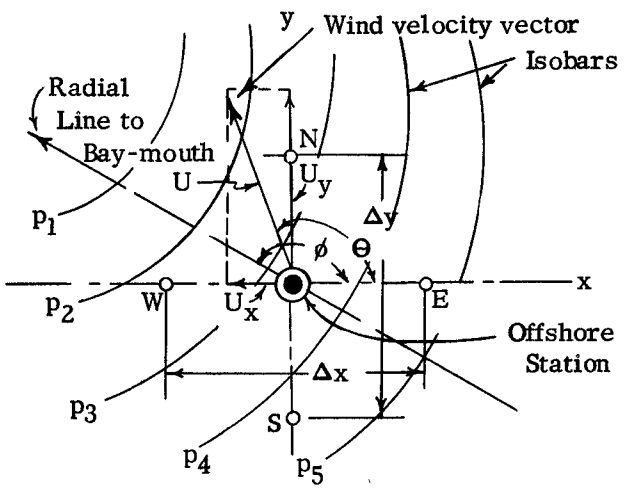

Fig. 10: Measurement of x and y components of velocities and surface pressure-gradients at an offshore station.

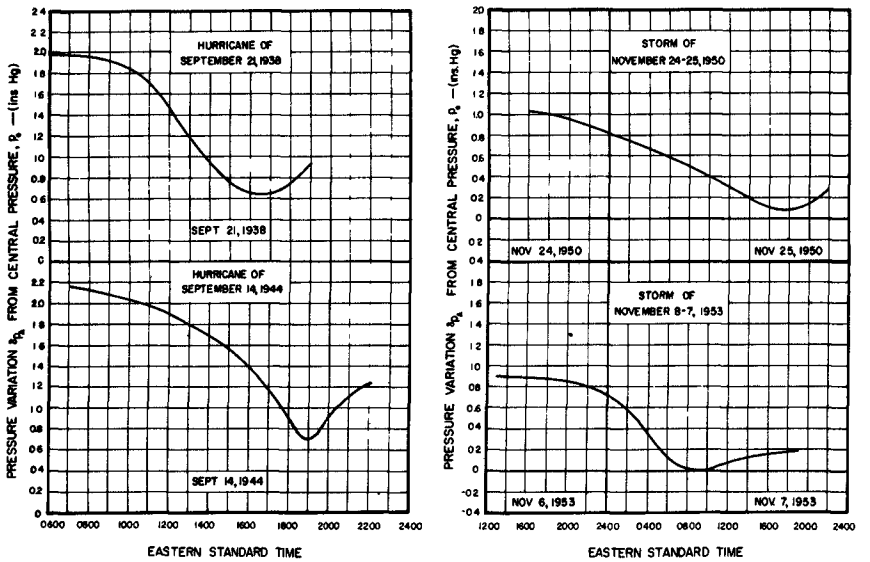

Fig. 11. Values of forcing function δp_A (for station A at mouth of New York Bay) for the four reference storms of 1938, 1944, 1950 and 1953.

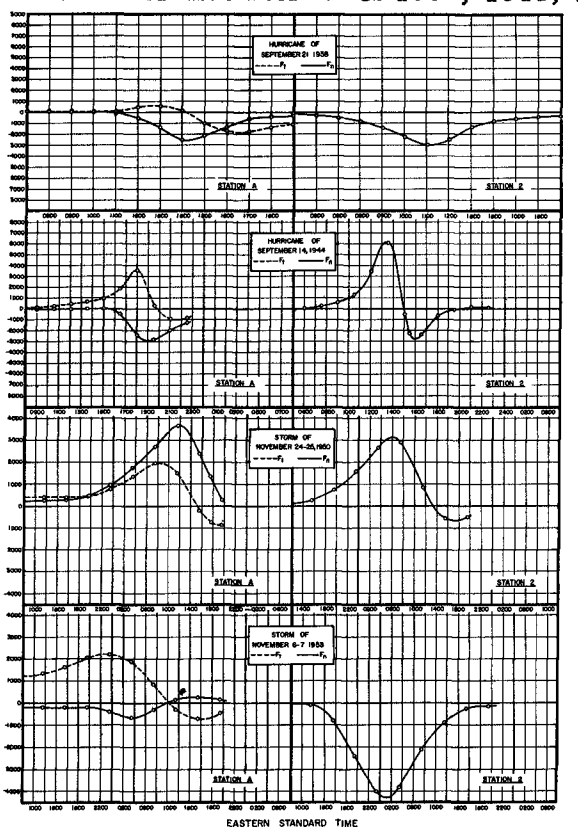

Fig. 12. Values of forcing functions $F_n(t)$ and $F_t(t)$ (for stations A and 2) for the four reference storms of 1938, 1944, 1950 and 1953.

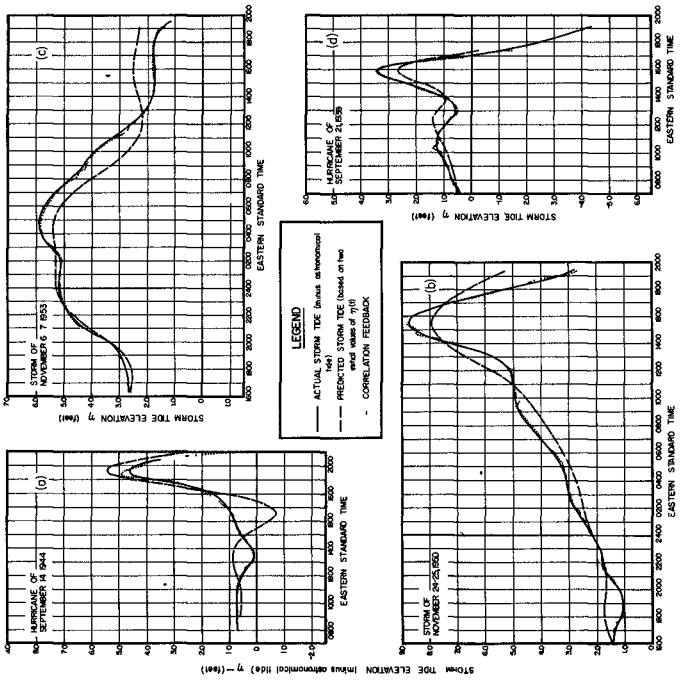

Fig. 14. Check of correlation between $\eta_A(t)$ and F(t): actual and predicted storm tides at the mouth of New York Bay (station A) for the four reference storms of 1938, 1944, 1950 and 1953.

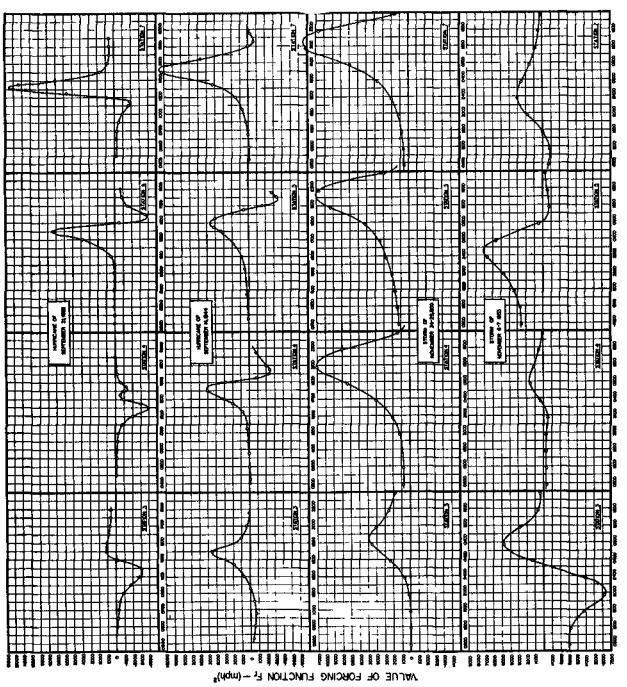

Fig. 13. Values of forcing functions $F_r(t)$ (for stations 3, 4, 5 and 7) for the four reference storms of 1938, 1944, 1950 and 1953.

Eqs. (3) for F_x and F_y may be reduced to the form

$$\left.\begin{aligned} \text{(i)} \quad F_x &= k\left[UU_x - \frac{d}{k\rho}\,\frac{(\Delta p)_x}{\Delta x}\right] \\ \text{(ii)} \quad F_y &= k\left[UU_y - \frac{d}{k\rho}\,\frac{(\Delta p)_y}{\Delta y}\right] \end{aligned}\right\} \qquad (40)$$

where U_x and U_y are the x and y components respectively of the surface wind velocity U at a station, k is a constant in the wind stress relationship $\tau = k\rho U^2$, $(\Delta p)_x$ and $(\Delta p)_y$ are the differential pressure changes over the distances Δx , Δy respectively, (Fig. 10), which are small in relation to the scale of the storm. The value of k taken as applicable to strong wind conditions was 3.1×10^6 [cf, Wilson, 1960].

To obtain F_n at station 2 [cf Eq. (38)], the angle ϕ in Eq. (39i) was arranged to make the direction of the forcing function vector normal to the average direction of the coastline between station 2 and the bay-mouth. Again F_t at station A [Eq. (38)] was obtained by choosing ϕ to make the forcing function vector at right angles to the radial line CA (Fig. 4). Finally, the values of δp_A were evaluated directly from Eq. (37) without difficulty.

Typical of the trends of the forcing functions for the four reference storms are the results shown in Figs. 11, 12 and 13.

13. COEFFICIENT VALUES FOR PAST-TIME η-TERMS IN CORRELATION FORMUL

As a convenient time increment for numerical correlation between $[\eta_A(t) - a\eta_A(t-\tau) + b\eta_A(t-2\tau)]$ and the forcing functions in Eq. (38), τ was selected as 20 mins or 1/3 hour. The period of resurgences has already been noted as being of the order of 7 hours (cf. Fig. 8), a period which can also be justified theoretically as being the fundamental natural period of oscillation of the ocean on the continental shelf off New York [Kajiura, 1959]. Accordingly S in Eq. (14i) has a value $(2\pi/T)$ of 0.898 radians/hr. From examination of the resurgences of the 1938, 1944 and other hurricanes that have affected New York the conclusion was reached that the oscillations decay with an amplitude ratio, $e^{-(KT)/2}$, per cycle, of about 0.5 , in agreement with an observation of Redfield and Miller [1956]. From this the damping factor K is found to be $0.198\ (\text{hr})^{-1}$. The values of a and b , defined by Eqs. (14), are accordingly

$$a = 1.850$$

$$b = 0.937$$

which duly satisfy the stability requirements of Eqs. (16).

14. TRAVEL TIMES OF FREE WAVES FROM OFFSHORE STATIONS TO BAY-MOUTH

The travel time, T_N, taken by a free, long gravity wave to travel at speed $C (= \sqrt{gd})$ from any station $N (= 1, 2 \ldots 7)$ to the bay-mouth at A can be computed from

$$T_N = \int_A^N \frac{dr}{\sqrt{gd}} \qquad (42)$$

in which the depth d is a function of radial distance r, in accordance with the nature of the shelf topography (Fig. 4). Numerical integration of Eq. (42) establishes the following values of T_N.

TABLE I: TRAVEL TIMES OF FREE WAVES

Station No. N	Distance r (naut. mi.)	Time, T_N - (hours)	
		Eq. (42)	Adopted Value
2	169	5	3-1/3*
3	95	2-2/3	2-2/3
4	50	1-1/4	1-1/3
5	88	2-1/3	2-1/3
7	92	2	2

The asterisked figure of T_2 = 3-1/3 hrs is the travel time for a long-shore edgewave to cover the distance from station 2 to station A. Since the

wave length λ in Eq. (36) is expressible as $\lambda = CT$, where T is the edgewave period, elimination of λ in Eq. (36) yields an edgewave speed of

$$C = \left(\frac{gs}{2\pi}\right) T \qquad (43)$$

The average uniform shelf slope, s , normal to the coastline between stations 2 and A is 1 in 1500. By assuming that the resurgence period of 7 hours is also a manifestation of edgewaves [cf Munk, Snodgrass and Carrier, 1956] the travel time of the waves at the speed of 86.4 ft/sec [Eq. (43)] is 3-1/3 hrs

15. LEAST SQUARES DETERMINATION OF COEFFICIENTS c_N , AND LAG CORRECTIONS, T_V

With a, b and T_N known, along with the time histories of $\eta_A(t)$ and the forcing functions at each offshore station, for each of the four reference storms, all the necessary data are on hand for conducting a multiple regression correlation for determination of the most appropriate values of the coefficients c_N and the lag T_V in Eq. (38). For lack of space the mechanics of this correlation will not be discussed here since they are fairly routine numerical operations in high speed digital computing.

The data from the four reference storms were pooled to provide a total of 237 equations involving the unknown coefficients, c_N . For both the slow moving storms of 1950 and 1953, T_V was taken zero, as justified in Section 7. The values of T_V for the fast moving hurricanes of 1938 and 1944 had to be determined by successive approximations based initially on intelligent guesses; thus, specific values of T_V had to be assumed in order to perform any least squares determination of the best fit values of the coefficients, c_N .

Each time a correlation was run, a simple feed-back operation, in which $\eta_A(t)$ was computed from Eq. (38) by making use of the true, known values of $\eta_A(t - \tau)$ and $\eta_A(t - 2\tau)$, gave a general check on the correctness of the overall procedure. Such a feed-back is indicated by the chain-dot curves in Fig. 14 which invariably compared favorably with the actual (full-line) storm tides. The real test of adequacy of the correlation results came from the use in Eq. (38) of the coefficients c_N together with the assumed values of T_V (for the 1938 and 1944 hurricanes), starting with just two initial values of $\eta_A(t - \tau)$ and $\eta_A(t - 2\tau)$. These starting values were taken identical with the actual storm tide elevation at $t = 0$ for each storm. From then on, - for example, at the very next time-step of $\tau = 1/3$ hr, - the computation was entire

dependent on its own predicted values of $\eta_A(t)$, which had to be successively fed into the right-hand side of Eq. (38).

Fig. 14 shows the predicted storm tides (dash-line curves) calculated in this manner for the values of c_N and T_V , as finally adopted. The best-fit values of the lag correction T_V were found to be 1.67 and 1.33 hrs for the 1938 and 1944 hurricanes respectively. The values of c in Eq. (38) (yielding an overall correlation coefficient of 0.89) were as follows:

$$\left.\begin{aligned} c_o &= 10074576 && 49^* \\ c_{A1} &= 29460220 && 48 - \\ c_{A2} &= 14493105 && 44 \\ c_{A3} &= 27135231 && 45 \\ c_2 &= 24016580 && 45 - \\ c_3 &= 38117168 && 45 - \\ c_4 &= 51729379 && 45 \\ c_5 &= 40529138 && 45 \\ c_7 &= 47817714 && 44 - \end{aligned}\right\} \qquad (44)$$

The predictions shown in Fig. 14 for each of the four reference storms were considered to be in sufficiently good agreement with the actual storm tides to justify the use of Eq. (38), together with the coefficient values of (44), in application to any other storm in the New York Bay area, regardless of its nature, direction and velocity of approach. The formula was therefore applied to several design hurricanes.

16. PREDICTED DESIGN-HURRICANE STORM TIDES

The design-hurricane to be discussed here (one of several for which computations have been made) was quite similar to the 1938 hurricane but its path was transposed to a new track (Fig. 4), likely to bring more severe effects to bear on New York. The pressure and wind patterns for this storm are shown in Fig. 15.

---

* This number indicates the position of the decimal point according to the IBM floating point classification in the Bell system. Thus for 49, $c_o = 0.10074576$; for 45, $c_2 = -0.000024016580$.

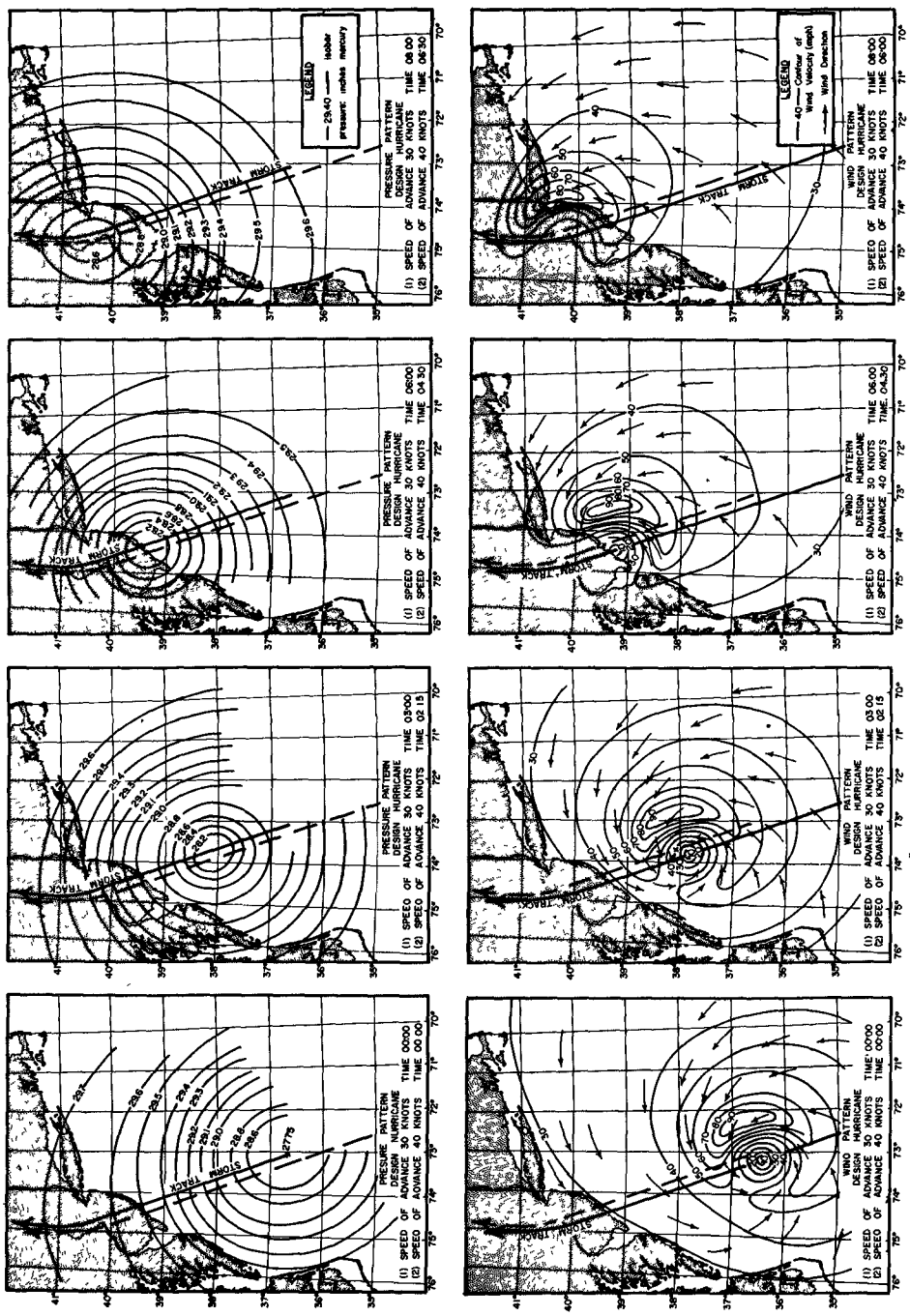

Fig. 15. Sequence of synoptic maps, showing pressures (upper) and surface wind velocities and directions (lower) for a design-hurricane invading the U. S. east coast in the New York area.

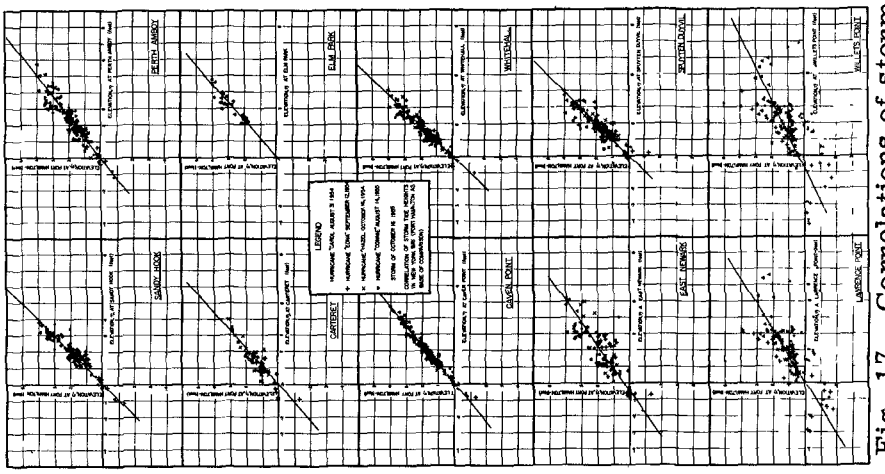

Fig. 17. Correlations of storm-tide elevations at Fort Hamilton with various gaging stations in New York Bay and river reaches based on data of five storms of 1954 and 1955.

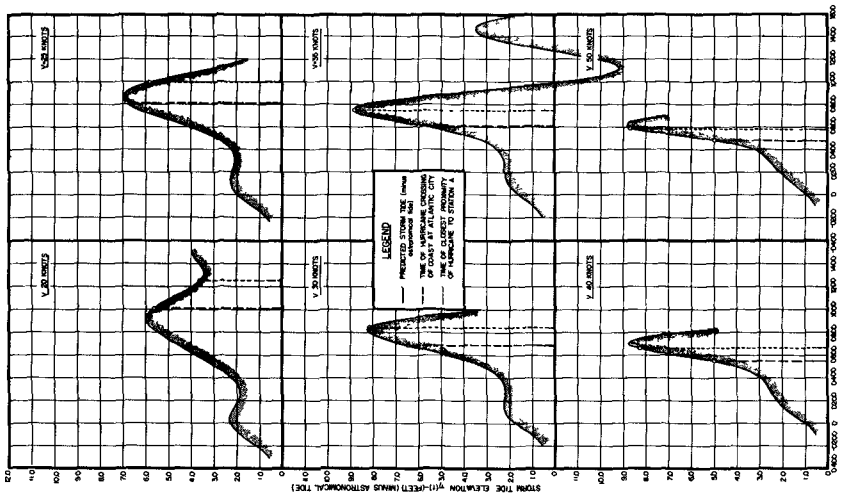

Fig. 16. Predicted storm tide elevations (for station A at mouth of New York Bay) for design-hurricane moving at six speeds V (20, 25, 30, 35, 40 and 50 knots).

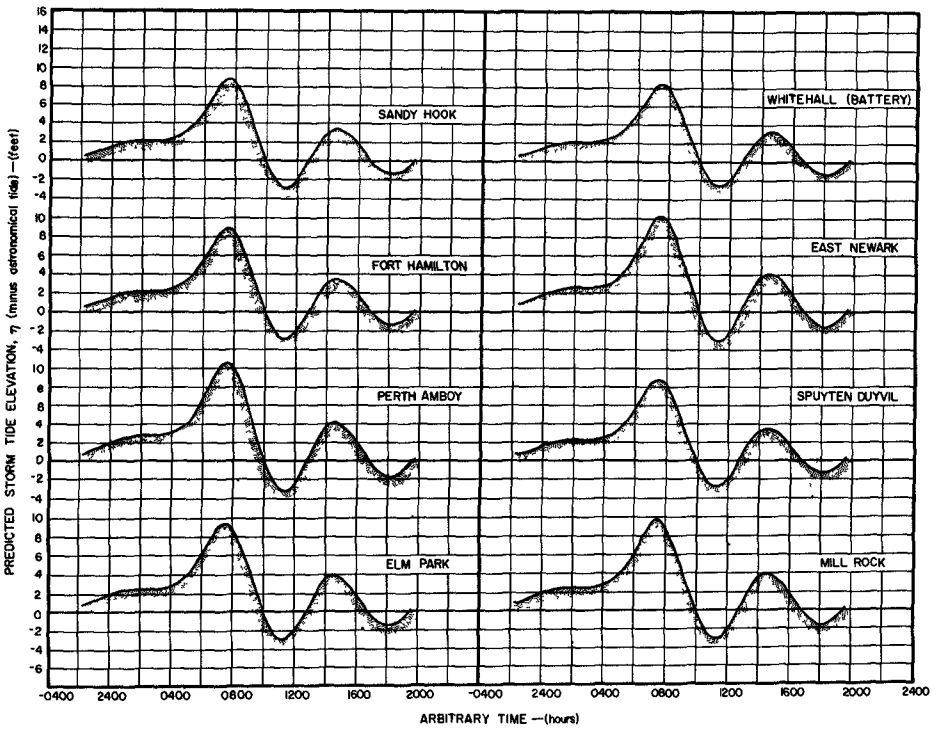

Fig. 18. Predicted storm tide elevations at eight gaging stations inside New York Bay for design-hurricane moving at speed V = 35 knots.

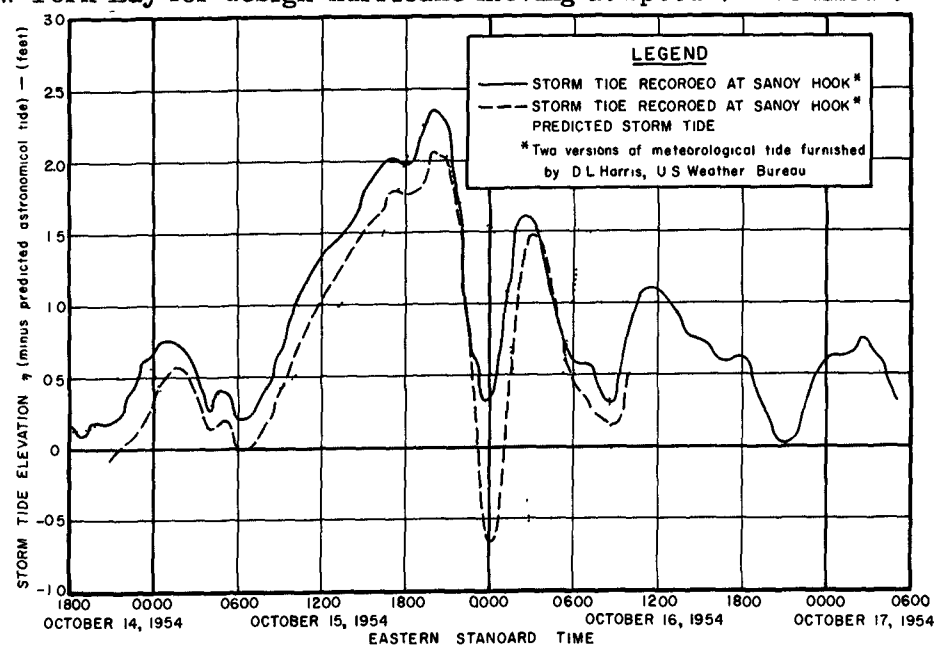

Fig. 19. Comparison of actual and predicted storm-tides at Sandy Hook for Hurricane 'Hazel' of October 14-17, 1954.

Forcing functions for this storm were worked out for 6 different storm speeds; 20, 25, 30, 35, 40 and 50 knots. In applying the prediction formula, Eq. (38), with the coefficient values (44), it was necessary to start with two initial elevations $\eta_A(t - 1/3)$ and $\eta_A(t - 2/3)$. Since there is invariably a small superelevation of water level above normal for many hours preceding the advent of a hurricane it was appropriate to adopt 6 ins (0.5 ft) for each of these elevations.

The results of applying the prediction formula (taking $T_V = 0$) are shown in Fig. 16. The predicted storm tides all show the antecedent minor surge, characteristic of the 1938 hurricane in Fig. 8, before the main surge which occurs at or near the time of the hurricane's crossing of the coast. At the lower storm speeds (V = 20 and 25 knots) the peak surge occurs before arrival of the hurricane; at the higher storm speeds (V = 35, 40 and 50 knots) the peak follows after the hurricane.* The other direct influence of the storm speed is to increase the height of the peak surge from 6 ft. at V = 20 knots to a maximum of 8.9 ft. at V = 35 knots after which at the higher speeds it declines slightly. The critical speed for the design-hurricane would thus appear to be about 35 knots (or higher), with very little to choose between the magnitudes of the resulting surges at speeds greater than 35 knots.

Reverting to Figs. 8 and 9 it may be noticed that phase differences between storm-tide superelevations at the various gaging stations are not very considerable in relation to the 7-hour period of the resurgences. This suggests that correlations between levels at different stations might obey simple linear regression. The results of graphical correlation using data for five storms of 1954 and 1955 are shown in Fig. 17 and indicate, by and large, that the relationships are linear though the confidence limits become rather broad for the up-river gaging stations, presumably owing to the influences on water level there of the ocean outlet through Long Island Sound (cf. Fig. 7). The regression lines of Fig. 17 are supported by the data of the four reference storms (not shown).

In Fig. 18 use is made of the relationships of Fig. 17 to predict the design-hurricane storm-tides at eight of the gaging stations in New York Bay. Thus the predicted tide at Sandy Hook is taken the same as $\eta_A(t)$ predicted for station A at the bay-mouth (Fig. 4) for the design-hurricane at the speed V = 35 knots. This prediction has been extended somewhat further in time than the version shown in Fig. 16, but is otherwise the same. It must be remarked that

---

*This is inferred from estimates of applicable values of T_V .

the four curves on the right-hand of Fig. 18 are liable to considerable fluctuation in height and relative phasing.

17. PROOF-TEST OF THE PREDICTION METHOD; HURRICANE "HAZEL" OF 1954

Until quite recently the prediction formula, Eq. (38), had not been proof-tested by applying it to any fifth storm whose meteorological parameters were known and whose effects in New York Bay had been measured and could be compare with the predictions. The necessary data for doing this were not available at the time of completion of the study in 1959. D. L. Harris of the United States Weather Bureau, meanwhile, has evaluated the forcing functions [cf, Eqs. (39) and (40)] for hurricane "Hazel", of October 15-16, 1954, which crossed the U. S. east coast south of Cape Hatteras and pursued a track overland into the heart of the north-eastern states. These functions have now been used in the prediction formula, Eq. (38), in conjunction with the coefficient values (44), with the end-results shov by the chain-dot curve in Fig. 19. In making this computation the lag correction T_V was taken zero, in the absence of any specific knowledge of its value.

For comparison with the prediction Fig. 19 shows two versions of the stor tide recorded at Sandy Hook, as supplied to the writer by D. L. Harris. It is not known which of these is actually correct, but in either case the prediction is in reasonable accord as to the magnitudes of the main surge and the first resurgence. The fact that the predicted resurgence is out of phase with the actual may possibly be ascribed to the assumption of a zero lag correction, T_V . However, the consequences of adopting different trial-values of T_V have not yet been explored.

8. CONCLUSIONS

It would seem from the above that the storm-tide prediction formula, Eq. (38), has emerged from a singularly stringent test with considerable success and may be assumed to be capable of providing a reasonably reliable estimate of the effects on water level in New York Bay which any given hurricane or storm can produce. Further confirmation of this is forthcoming from the available rather crude correlations that have been made between maximum storm-tide height and central pressure p_o within the hurricane [cf Fig. 20]. These suggest that a storm-tide of from 10 to 12 ft could be expected of the design-hurricane. The predicted maximum of 8.9 ft at Sandy Hook and 10.5 ft at Perth Amboy (Fig. 18) is within reasonable range of this spread, but accords better with the somewhat more refined empirical system of Kajiura [1959], which suggests 10 ft.

It is felt that the prediction formula is based on sound physical reasoning and may therefore justly claim to be comprehensive in its capacity to deal two-dimensionally and dynamically with any storm moving at any speed along any given

track.

The methods of surge prediction outlined in this paper could readily be applied to coastal stations anywhere provided sufficient data existed regarding specific storms of the past and their effects on the coastal station.

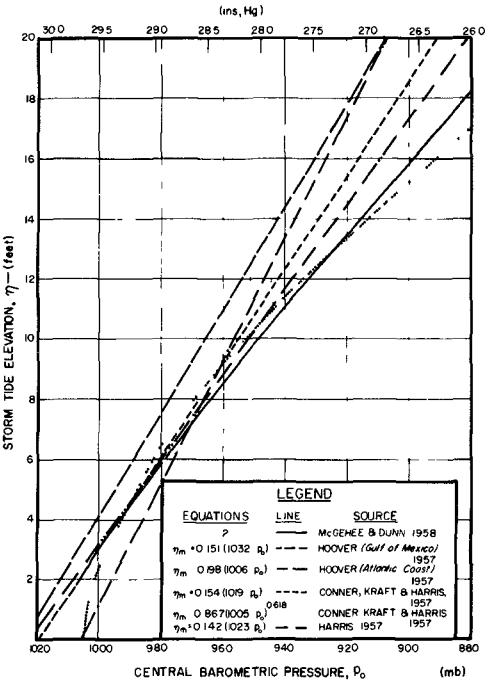

Fig. 20. Empirical correlations between maximum storm tide elevation, η, and central pressure, p_o, for U. S. Atlantic and Gulf Coast hurricanes.

19. ACKNOWLEDGEMENT

This paper is a shortened and refined version of Technical Memorandum No. 120, published recently by the Beach Erosion Board, Corps of Engineers, U.S. Army, and is made possible through kind permission of that body. The writer must record his great appreciation of the assistance and counsel rendered by R. O. Reid in many of the intricacies of the numerical methods, particularly in the matter of instability. To R. L. Smith and R. E. Kilmer, moreover, belongs the considerable credit for programming and conducting the involved correlations and predictions on the IBM No. 650 electronic computer. The writer is also indebted to D. L. Harris for his interest and constructive criticism and for furnishing data in respect of hurricane Hazel. Completion and presentation of this paper would not have been possible without the final sponsorship of the Office of Naval Research, U. S. Navy, [Contracts N7 onr 48702 and N onr 2119 (02)], which is gratefully acknowledged.

REFERENCES

Conner, W. C., Kraft, R. H. and Harris, D. L. [1957]; Empirical methods of forecasting the maximum storm tide due to hurricanes and other tropical storms; Monthly Weather Review, v. 85, 1957, pp. 113-116.

Corkan, R. H. [1950]; The levels in the North Sea associated with the storm disturbance of 8 Jan. 1949; Trans. Roy. Soc. London, v. 242 (A), July 1950, pp. 493-525.

Darbyshire, J. and Darbyshire, M. [1956]; Storm surges in the North Sea during the winter 1953-4; Proc. Roy. Soc., v. 235, A, 1956, pp. 260-274.

Donn, W. L. [1958]; An empirical basis for forecasting storm tides, Bulln. Am. Met. Soc., v. 39(12), Dec. 1958, pp. 640-647.

Dunn, G. E. [1957]; Hurricanes and hurricane tides; Proc. 6th Coast. Eng. Conf. (Gainsville, Fla., 1957), Council Wave Research, Berkeley, 1958, pp. 19-29.

Fischer, G. [1959]; Ein numerische Verfahren zur Errechnung von Windstau und Gezetten in Randmeeren; Tellus, v. VII (i), 1959, pp. 60-76.

Hansen, W. [1957]; Theorie zur Errechnung des Wasserstandes und der Stromungen in Randmeeren nebst Andwendungen; Tellus, v. 8, 1956, pp. 287-300.

Hansen, W. [1957]; A method of calculation of long period waves, Communication I, Section II, XIXth International Navigation Congress, London, 1957 (Brussels, Belgium, 1957).

Harris, D. L. [1956]; Some problems involved in the study of storm surges; Report No. 4, Nat'l. Hurricane Research Project, U. S. Weather Bureau, Dec. 1956, 30 pp.

Harris, D. L [1957]; The hurricane surge; Proc. 6th Coast. Eng. Conf. (Gainsville, Fla., 1957), Council Wave Research, Berkeley, 1958, pp. 96-114.

Harris, D. L [1959]; An interim hurricane storm surge forecasting guide; Report No. 32, Nat'l. Hurricane Research Project, Weather Bureau, U. S. Dept. Commerce, Aug., 1959, 24 pp.

Hoover, R. A. [1957]; Empirical relationships of the central pressures in hurricanes to the maximum surge and storm tide; Monthly Weather Review, v. 85, 1957, pp. 167-174.

Kajiura, K. [1959]; A theoretical and empirical study of storm induced water level anomalies; Tech. Report (Ref. 59-23F), Texas A. and M. Research Foundation, College Station, Tex., Dec., 1959, 97 pp.

Kivisild, H. R. [1954]; Wind effect on shallow bodies of water with special reference to Lake Okeechobee; Bulletin No. 43, Inst. Hydraulics, Roy. Inst. Tech., Stockholm (Goteborg, 1954), 146 pp.

Kussman, A. S. [1957]; The storm surge problem in New York City; Trans. New York Acad. Sci., Ser. II, v. 19 (8), June 1957, pp. 751-763.

Lamb, H. [1932 Ed.]; Hydrodynamics, (Cambridge Univ. Press, England), 1932 Ed. (1st Ed. 1879).

Miller, A. R. [1956]; The effect of steady winds on sea level at Atlantic City; Meteorological Monographs (Am. Met. Soc.), v. 2(10), June 1957, pp. 24-31.

Miller, A. R. [1957]; Report on the effect of winds on coastal water levels of New England; Report (Ref. No. 57-22), Woods Hole Oceanographic Institution, Woods Hole, Mass., Mar. 1957 (unpublished).

Moore, P. L. et al., [1957]; The hurricane season of 1957; Monthly Weather Review, v. 85, 1957, pp. 401-408.

Munk, W., Snodgrass, F. and Carrier, G. [1956]; Edge waves on the continental shelf; Science, v. 123, 1956, pp. 127-132.

Platzman, G. W. [1958]; A numerical computation of the surge of 26 June 1954 on Lake Michigan; Tech. Report No. 1, Dept. Meteorology, Univ. of Chicago, June 1958, 32 pp.

Redfield, A. C. and Miller, A. R. [1956]; Water levels accompanying Atlantic Coast hurricanes; Meteorological Monographs (Am. Met. Soc.), v. 2 (10) June 1957, pp. 1-23.

Reid, R. O. [1955]; On the classification of hurricanes by storm tide and wave energy indices; Meteorological Monographs (Am. Met. Soc.,), v. 2(10), June 1957, pp. 58-66.

Reid, R. O. [1956]; Approximate response of water level on a sloping shelf to a wind fetch which moves towards shore; Tech. Memo. No. 83, Beach Erosion Board, Corps of Engrs., U. S. Army, June 1956, 44 pp.

Reid, R. O. [1957 (i)]; Comments on the Conference on Long Waves and Storm Surges held at the Nat'l. Inst. of Oceanography, England, May 27-31, 1957, (unpublished).

Reid, R. O. [1957 (ii)]; Forced and free surges in a narrow basin of variable depth and width: A numerical approach; Tech. Report (Ref. 57-25T), Texas A. and M. Research Foundation, Aug. 1957, 60 pp. (unpublished).

Schalkwijk, W. F. [1947]; A contribution to the study of storm surges on the Dutch Coast; Roy. Netherlands Meteor. Inst., v. 125, B, Part I (7).

Tancreto, A. E. [1958]; A method for forecasting the maximum surge at Boston due to extratropical storms; Monthly Weather Review, U. S. Weather Bureau, v. 86 (6), June 1958, pp. 197-200.

Weenink, M. P. H. [1956]; The 'Twin' Storm Surges during 21-24 December 1954 - A case of resonance; Deutsche Hydrogr. Zeibschr., v. 9, 1956, pp. 240-249.

Weenink, M. P. H. and Groen, P. [1958]; A semi-theoretical, semi-empirical approach to the problem of finding wind effects on water levels in a shallow, partly-enclosed sea, I and II; Proc. Korinkl. Ned. Akad. Wetensch., v. 61 (B) 1958, pp. 198-213.

Wilson, B. W. [1960]; Note on surface wind stress over water at low and high wind speeds; Jour. Geophys. Research, 1960 (publication pending).

Wilson, B. W. [1960]; The prediction of hurricane storm tides in New York Bay; Tech. Memo No. 120, Beach Erosion Board, Corps of Engrs., U. S. Army, Aug. 1960.

Zetler, B. D. [1957]; Hurricane effect on sea level at Charleston, Proc. ASCE, v. 83 (HY 4), Paper No. 1330, Aug. 1957, 19 pp.

CHAPTER 31

HURRICANE STORM SURGE CONSIDERED AS A RESONANCE PHENOMENON

by

G. Abraham*
Waterloopkundig Laboratorium
Delft, Netherlands

ABSTRACT

A model study was performed to study the water gravity waves generated by a circular local disturbance of pressure, advancing with constant velocity over the surface of water of constant depth. The results indicate that under critical conditions a resonance type phenomenon occurs for which the associated wave heights have a maximum value. It is shown that the resonant conditions may be an important factor for the generation of the surge due to hurricanes, that approach the coast perpendicularly.

INTRODUCTION

Presented in the first part of this paper is a summary of the results of a model investigation of the water waves generated by a local disturbance, consisting of a circular pressure area, advancing with constant velocity over the surface of water with constant depth. A more detailed description of this model study is given elsewhere (Abraham, 1960). The results indicate that under critical conditions a resonance type phenomenon occurs for which the associated wave heights have a maximum value, a result similar to that of a two dimensional model investigation performed by Wiegel et al (1958).

A hurricane is an example of a moving circular pressure area in nature. Unfortunately the ratio of the diameter of the disturbance to the water depth is for a hurricane much larger than could be obtained in the model. Hence it will be difficult to draw quantitative conclusions from the model results. Nevertheless it is possible to show - as is done in the second part of this paper - that the resonant conditions may be an important factor for the generation of the surge due to hurricanes, that approach the coast perpendicularly.

*The work described herein was performed while the author was a Fulbright Research Scholar at the University of California

PART 1: SUMMARY OF MODEL RESULTS

a. MODEL SET-UP AND EXPERIMENTAL PROCEDURE

A moving low pressure area was simulated in the model by towing a suction fan over the water surface. No attempt has been made to simulate a certain wind pattern in the pressure disturbance. The plane of the edge of the inlet pipe was about 1-1/2 inche above the undisturbed water level. Three different sizes of the inlet pipes were used. Their diameters were 2, 1 and 1/2 feet.

The experiments were performed in the wave-towing tank of the University of California which had a length of 200 feet and a width of 8 feet (Snyder, et al, 1958). The water depth was 1/2 foot for the experiments that showed the resonance-type phenomenon.

The towing carriage could be operated at any speed up to a maximum of about 6 ft/sec.

The time history of the water surface of the waves generated by the advancing pressure disturbance were measured in one cross section of the tank. Five parallel wire resistance wave recorders were used.

At the beginning of an experiment the automatic carriage control unit was set for a chosen carriage speed. The fan then was started. As soon as the static water displacement had reached equilibrium the towing carriage was set in motion.

The wave recorders were switched on just prior to the moment at which the low pressure area reached the recorders. They registered five longitudinal cross sections of the wave system, by which the moving pressure disturbance was accompanied.

A wave recorder was used to measure the elevation of the water surface underneath the inlet pipe with the low pressure area being held stationary. This was considered to be the same as the pressure at the undisturbed water level expressed as the length of a column of water. It varied with a frequency of about 5 c.p.s. from about 70% to 130% of its mean value, called the static water displacement H_s.

The pressure distribution underneath a moving inlet pipe was not measured because of the difficulties involved. It has been assumed that the pressure distribution would not be influenced considerably by the movement of the low pressure area, because of the following reasons. The water surface was not affected by the movement of the inlet pipe as long as the fan was not turned on. Secondly, the forward velocity of the low pressure area was small compared with the velocity of the air

entering the inlet pipe through the opening between the edge of the pipe and the water surface.

b. MODEL RESULTS

One of the wave recorders was located in the path of the center of the low pressure area. The wave height H, measured by it for the first, the second and the third wave crest of the wave system by which the pressure disturbance was accompanied, can be seen to be a function of the velocity of the low pressure area (fig. 1). The relationship between the wave height and the speed of the disturbance was found to depend on the ratio of the diameter of the disturbance D to the waterdepth d.

Fig. 2a shows the envelope of the lines given in fig. 1 and a corresponding theoretical curve for D/d tending to infinity, which has been calculated by Inui (1936). The shallow water resonance peak (called the shallow water maximum) only occurred for the experiments with D/d = 4, 2 and 1. The other maxima that can be seen on this figure are not important when hurricanes with large values of D/d are considered. The velocity of the disturbance for which the resonant conditions occurred was in the model a little less than the velocity of the shallow water wave, $\sqrt{gd}$, the theoretical value of this speed for large values of D/d (fig. 2c).

Regarding the height of the resonance peak, that can be seen on figs. 2a and 2b, we should remark that the wave height is influenced by scale effects for wave heights satisfying $H_{max}/H_S > 4$. For this condition the air pressure at the water surface was influenced by the reduced distance between the water surface and the plane of the edge of the inlet pipe. Scale effects of this kind did not occur for $H_{max}/H_S < 4$.

Fig. 3 shows the phase shift, this is the distance between the center of the disturbance and the first wave crest, for the shallow-water experiments. The decay of the wave height along a line normal to the line of advance of the pressure area can be seen on fig. 4. The waves registered for the shallow-water maxima can be seen on fig. 5.

PART 2: APPLICATION OF MODEL RESULTS TO HURRICANE WAVES

A hurricane may be considered as a roughly circular disturbance with an area of low barometric pressure and strong counter-clockwise (in the northern hemisphere) winds, that advances with a certain velocity. The diameter of a hurricane is in general 50 to 100 nautical miles, so that the ratio D/d is in general at least 100 when a hurricane moves over an ocean surface.

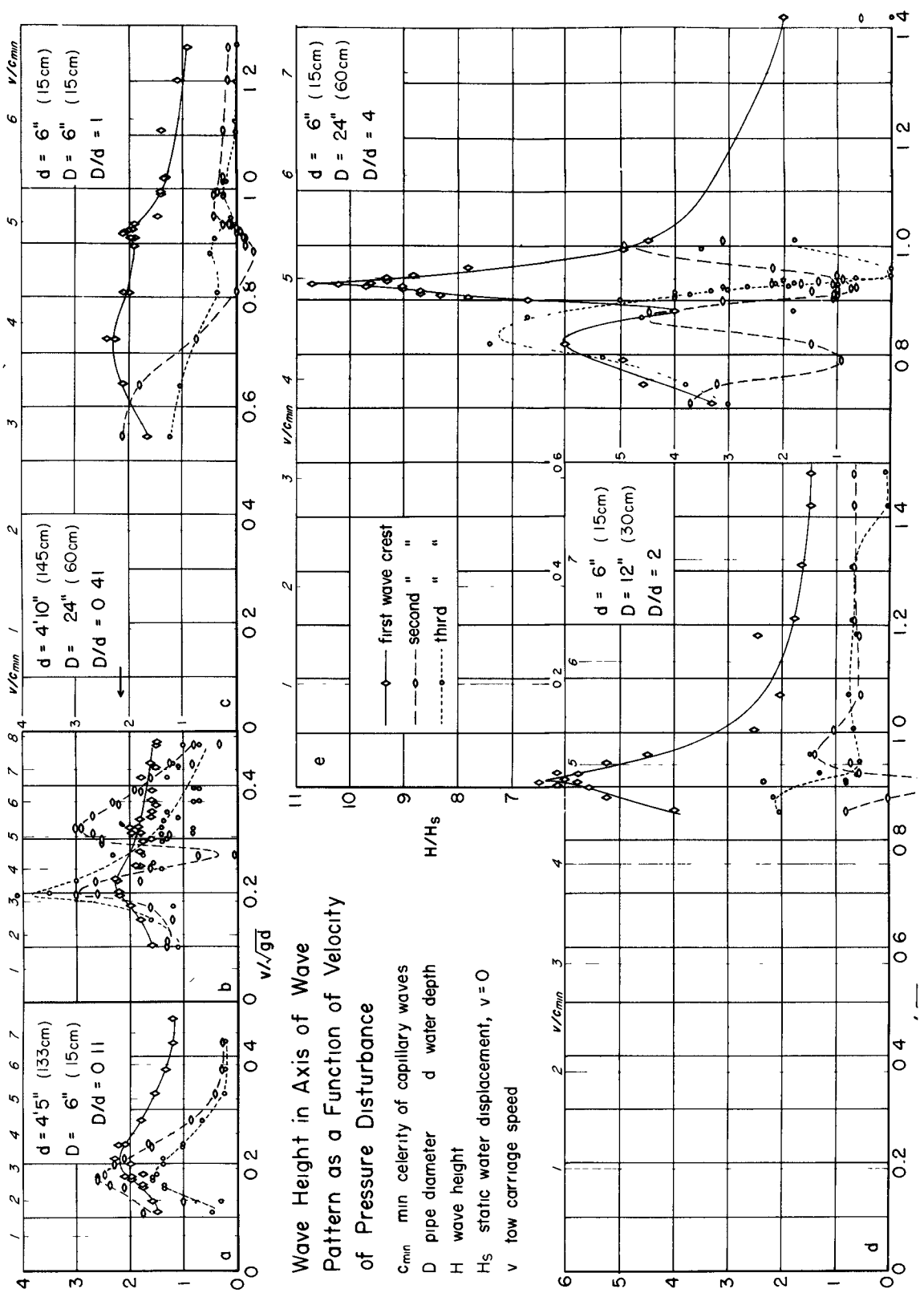
Wave Height in Axis of Wave Pattern as a Function of Velocity of Pressure Disturbance
c_{min} min celerity of capillary waves
D pipe diameter
d water depth
H wave height
H_S static water displacement, v = 0
v tow carriage speed
H/H_S
$v/\sqrt{gd}$
v/c_{min}
a
b
c
d
e
d = 4'5" (133cm)
D = 6" (15cm)
D/d = 0 11
d = 4'10" (145cm)
D = 24" (60cm)
D/d = 0 41
d = 6" (15cm)
D = 6" (15cm)
D/d = 1
d = 6" (15cm)
D = 12" (30cm)
D/d = 2
d = 6" (15cm)
D = 24" (60cm)
D/d = 4
first wave crest
second " "
third " "

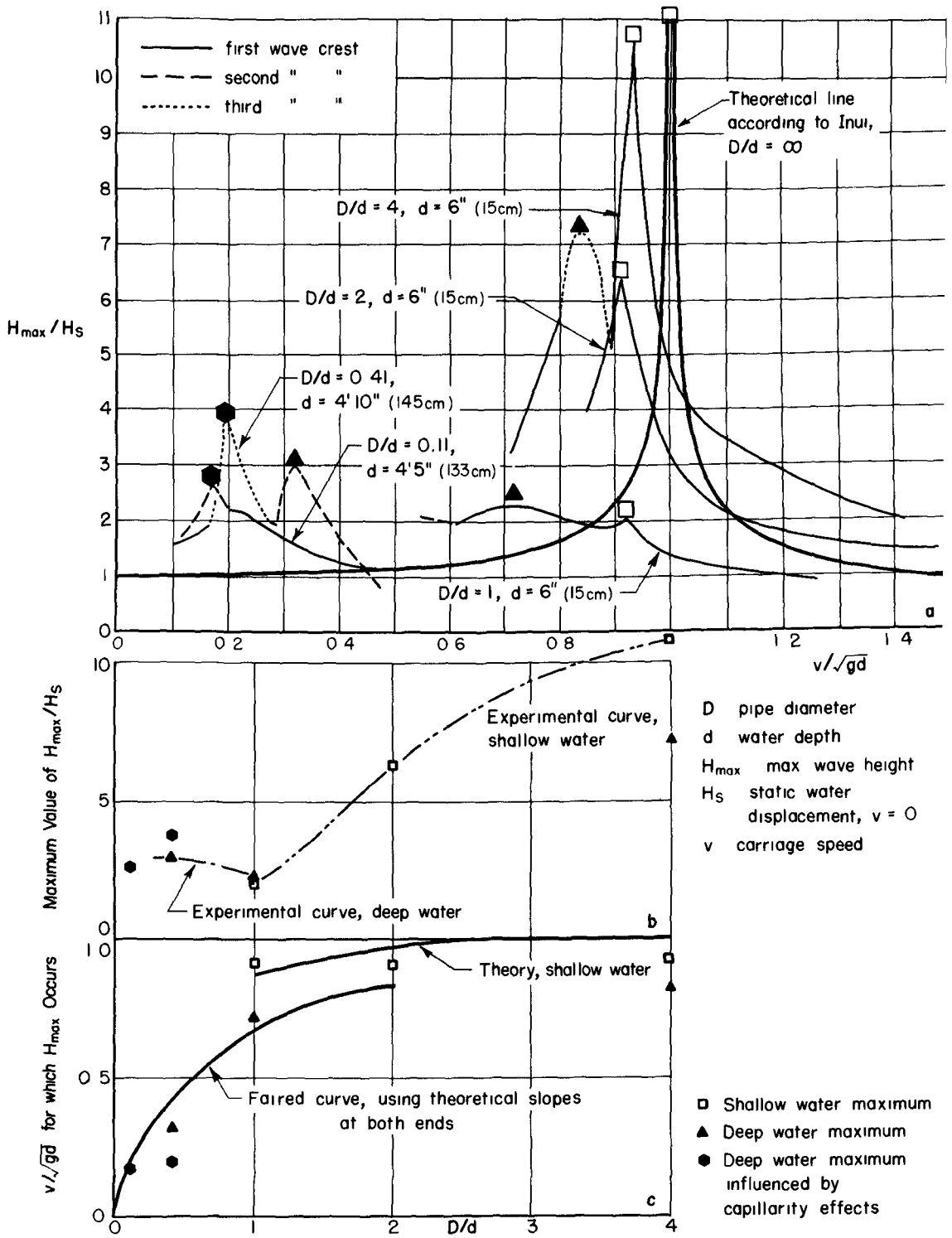

Maximum Wave Height in Axis of Wave Pattern as a Function of Velocity and Diameter of Pressure Disturbance

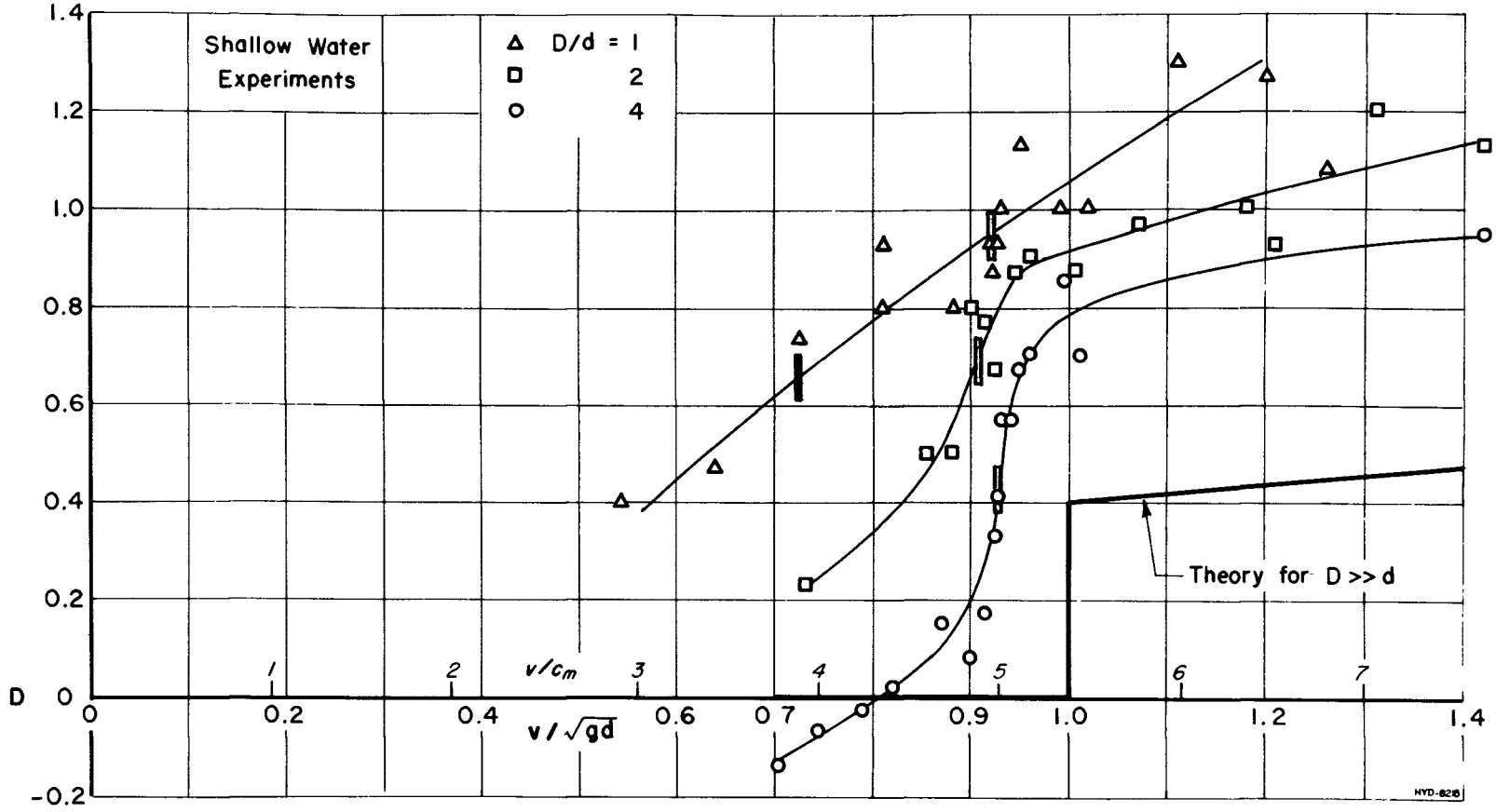

Phase Shift in Axis of Wave Pattern

c_m minimum celerity of capillary waves D pipe diameter d: water depth, = 6"

s: distance of first wave crest from center of pressure disturbance (negative when first crest in front of center)

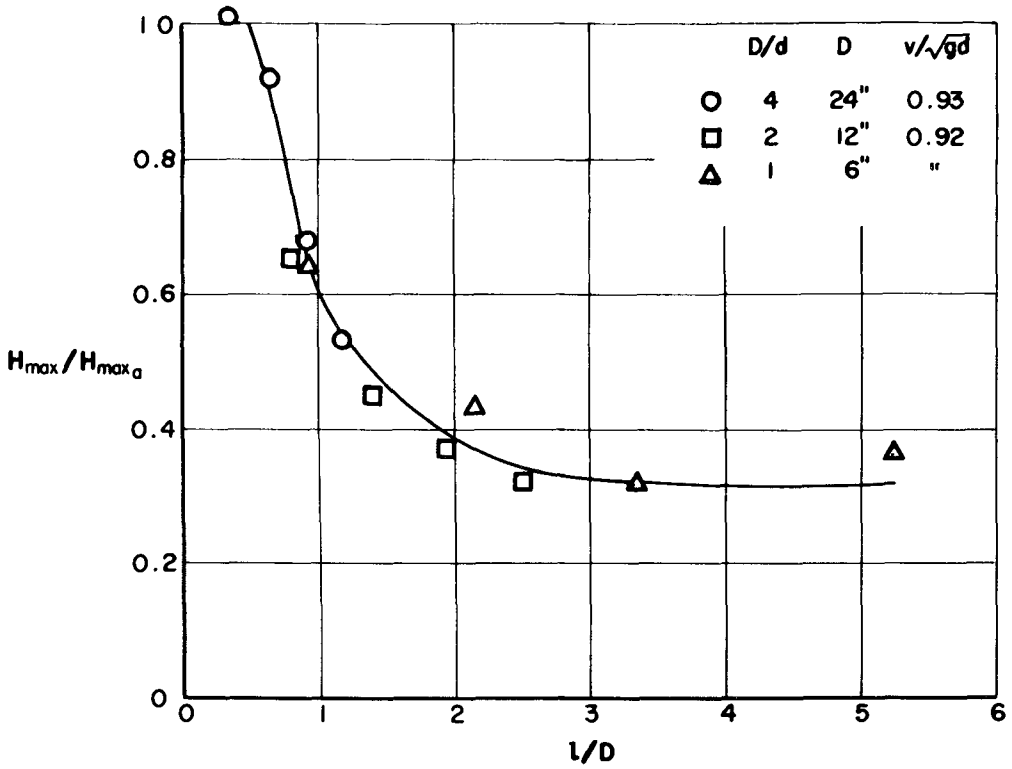

Shallow Water Maxima. Maximum wave height as a function of distance to axis of wave pattern.

D: diameter of pipe d: water depth, = 6"
H_{max} : maximum wave height at distance l from axis
H_{max_a}: maximum wave height in axis of wave pattern
v: carriage speed

FIGURE 4

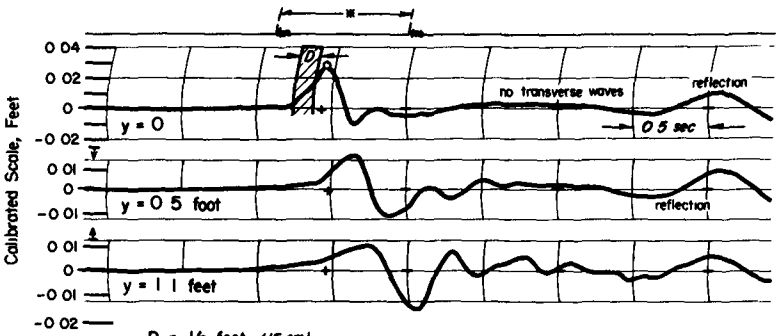

D = ½ foot (15 cm)
d = ½ foot (15 cm)
v = 3.76 ft/sec. (113 cm/sec.)

D/d = 1
$v/\sqrt{gd}$ = 0 92 a

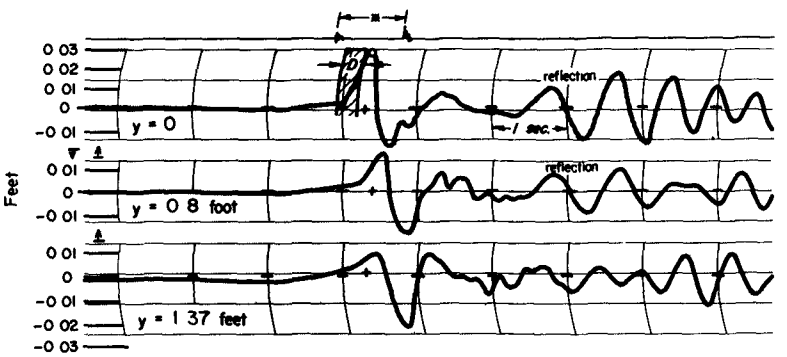

D = 1 foot (30 cm)
d = ½ foot (15 cm)
v = 3 66 ft./sec (110 cm/sec)

D/d = 2
$v/\sqrt{gd}$ = 0 905 b

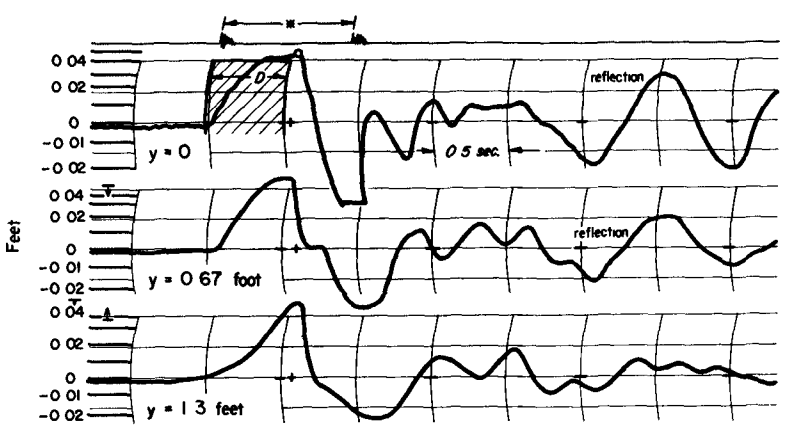

D = 2 feet (60 cm)
d = ½ foot (15 cm)
v = 3 8 ft/sec (114 cm/sec)

D/d = 4
$v/\sqrt{gd}$ = 0 93 c

D. pipe diameter
d water depth
v· carriage speed
y distance to axis of wave pattern

\+ moment at which center of wave pattern (o) passes probes
* length scale corresponds to 3 33 feet in wave pattern
▨ position of low press area as it passes probes

Shallow Water Maximum

FIGURE 5

When this happens three phenomena occur. Wind waves are generated because of the winds, water is dragged along the surface by the winds causing a wind set-up along the coast, and the actual level of a portion of the sea surface becomes higher because of the low barometric pressure. The latter two increments of the water level, taken together, is called the storm surge. At the coast it is taken to be the difference between the normal tide as predicted in the tide tables and the actual recorded storm tide.

Records obtained during hurricanes (Redfield and Miller, 1955) show that the magnitude of the storm surge in the open deep sea is close to the static water displacement. It seems that shallow water (for instance above the continental shelf) is required for the development of storm surges greatly in excess of the static water displacement.

At a coast, where the water depth is restricted, the following phenomena occur: (1) The restricted depth will result in an increment of wind set-up. (2) It will also cause a shallow-water maximum when the advancing velocity of the hurricane satisfies the required conditions and when there is sufficient time available to build up these maxima. (3) Once they are generated, the shallow-water maxima, which are long waves of very small steepness, will run up, be reflected from, or otherwise be influenced by the coast. The result of these three phenomena are the high storm surges along the coast, where the path of the hurricane crosses the coast line. It is difficult to determine the exact contribution of each of these phenomena to an actual recorded surge.

In the following, we will try to make an estimation of the contribution of the shallow-water maxima. At first we will present, however, three prototype examples, which show resonant shallow-water conditions that have been recorded in nature.

1° THE LAKE MICHIGAN WAVE OF JUNE 26th, 1954 (Ewing et al, 1954).

"On the morning of June 26th, 1954 about 9:30 A.M. an abrupt increase in the level of Lake Michigan occurred along the waterfront in the vicinity of Chicago. According to observations, the wave approached Chicago from the east to southeast. It was first observed at Michigan City at 8:10. Here the wave approached from the northwest. Fig. 6 gives the local situation, table 1 gives lake-height data.

A few hours earlier a severe squall line with winds up to 61 m.p.h. had arrived from the northwest and crossed southern Lake Michigan. Its maximum lateral extent was about 150 mi. Associated with the

Table 1. Wave height and arrival time

Station	Reported height (ft)	Arrival time (A.M. CTD)
EASTERN SIDE OF LAKE		
St. Joseph	No significant change	
Michigan City		
USCGS	6.2	8 : 12
Breakwater	5.5	8 : 10
WESTERN SIDE OF LAKE		
Chicago		
Belmont Harbor	6.3	9 : 30
Montrose Harbor	8.0	9 : 25
North Ave.	10.0	9 : 30
River mouth	2.4	9 : 40
Waukegan	No significant change	

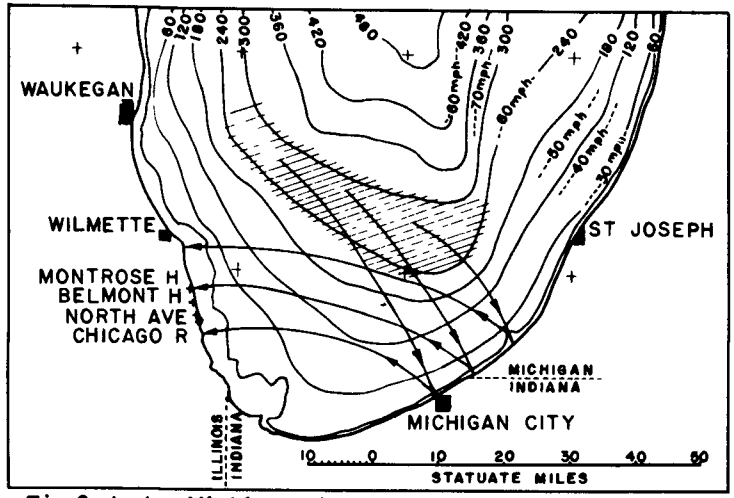

Fig. 6. Lake Michigan depth contours; area of generation and paths of the 26 June 1954 wave. (after Ewing et al, 1954)

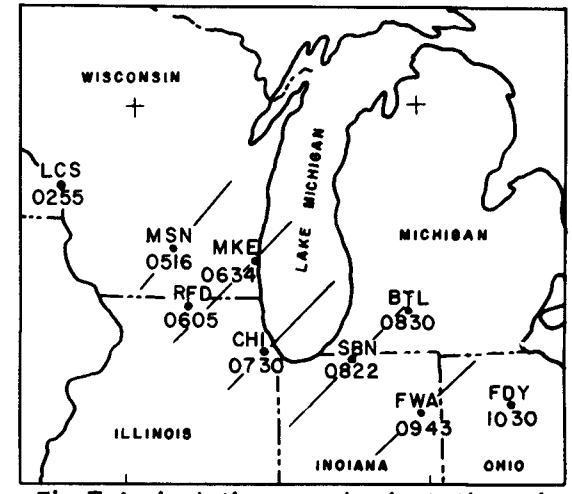

Fig. 7. Arrival times and orientation of the pressure - jump line in the Lake Michigan area. (after Ewing et al, 1954)

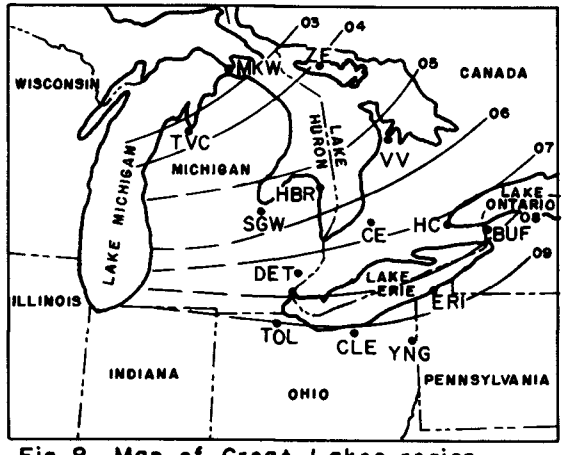

Fig. 8. Map of Great Lakes region showing isochrones for the pressure jump line of May 5, 1952. (after Donn, 1959)

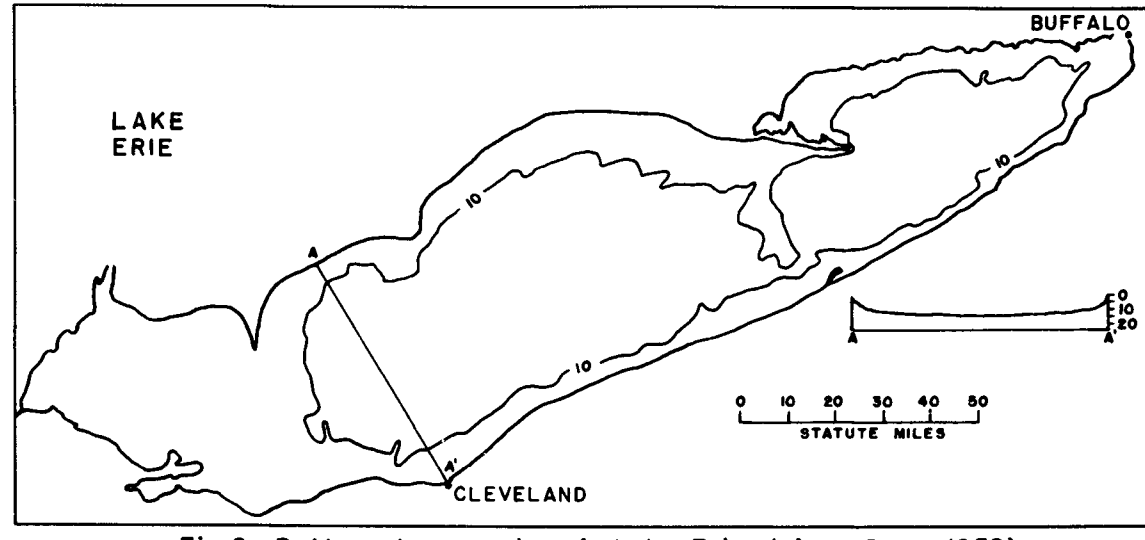

Fig. 9. Bottom topography of Lake Erie (after Donn, 1959)

squall line was a very rapid and strong pressure jump which for most sta tions for which records are available amounted to about 0.1 in. in a few minutes. The progress of the pressure jump line is shown in fig. 7. It crossed Lake Michigan with a velocity of 66 m.p.h. It arrived at Michigan City simultaneously with the wave from the northwest.

The critical depth for which the long wave velocity ($\sqrt{gd}$) is equal to the speed of the disturbance of 66 m.p.h. is 288 ft. Such a depth exists for a relatively long fetch almost exactly in the direction of squall movement between 240 and 300 ft. depth contours (fig. 6). Hence it is evident that a resonant shallow-water maximum could be generated. The approximate area of generation is indicated by cross hatching. Since the wave was moving in an area of variable depth, refraction effect induced a deflection of the wave path towards shallower water, producing paths approximately like those shown by the heavy arrows, which indicate the incidence of the wave at the east coast and its reflection at the west coast. The times of occurrence of the various events are compatible with this explanation".

The significance of this example is that it shows a reflected long wave, which supports that the surge has been explained as a resonant shallow-water maximum. This example makes it possible to determine the time which was available to build up the shallow-water maximum by dividing the length of the area of generation by the speed of the line of squall. The time, determined by this manner, is about 40 min.

2° THE LAKE ERIE STORM SURGE OF MAY 5th, 1952 (Donn, 1959).

"On the morning of May 5, 1952 a strong pressure disturbance crossed Lake Erie, with an average speed of 32 m.p.h. The disturbanc line moved parallel to the long axis of the lake (fig. 8). The magnitude of the pressure jump was about 0.08 inches, when it passed Cleveland. On arrival of the pressure jump the wind shifted there from northeast to southeast at 20 to 30 m.p.h. Simultaneously with the pressure jump a wave of 1.7 ft. has been recorded at Cleveland.

It is evident from the map and profile in fig. 9 that the bottom of Lake Erie is quite flat. Based on the depth along profile AA', the velocity of a long gravity wave here is about 30 m.p.h., making it quite reasonable that resonant transfer of energy occurred between the air and a long gravity wave generated in the lake."

The first wave crest was followed by a set of high amplitude waves which according to Donn either can be explained as repeated reflections (through he indicates that lack of any attenuation for the first waves tenc to weaken the argument for the repeated reflections) or as a seiche set u by the initial water transfer to the southern end of the lake.

The time available for the generation of the shallow-water maximum of this example was about 80 minutes. This time has been calculated assuming the length of the generation area to be the distance between the 10 fathom contours in profile AA' (fig. 9).

3° HURRICANE CAROL, AUGUST 30th - 31st, 1954 (Harris, 1956)

Fig. 10 is a reproduction in reduced size of a section of U.S.C. & G.S. Chart No. 1000 (Cape Sable to Cape Hatteras) showing water depths of the East Coast of the United States. The path of the center of Hurricane Carol is plotted on this chart (Harris, 1956).

Fig. 11 shows the storm surges as recorded for several stations along the coast during Hurricane Carol. Hurricane Carol travelled for an appreciable distance with a forward speed of approximately 30 to 35 knots (between Cape Hatteras and Long Island). The shallow-water wave velocities $\sqrt{gd}$ associated with water depths of 5; 10; 15; 20 and 25 fathoms are 18.5; 26.1; 31.9; 36.8 and 41.2 kn. So it is evident that if Hurricane Carol could have been able to generate a shallow-water maximum, this should have been in the vicinity of Long Island. The significance of this example is that it shows that the time histories of the stations near Long Island are in agreement with the time history of the model shallow-water maxima of fig. 5. For all the stations near Long Island the prototype-time histories have the phase shift and the relatively large trough in the rear of the resonance peak in common with the model time histories of fig. 5. In both prototype and model the time during which the resonance peak occurs is about equal to the diameter of the low pressure area divided by its advancing velocity. For the model the latter fact follows from fig. 5 and for the prototype it has been shown by Redfield and Miller (1957).

The examples show the following: (1) An available period of time of about 40 to 80 minutes was sufficient for the development of resonant shallow-water maxima for the two dimensional first and second examples (line disturbances), (2) According to the three dimensional third example there are prototype data that qualitatively agree well with the three dimensional model data.

To obtain the relationship between the velocity of the disturbance and the height of the generated waves for hurricanes, we have to extrapolate the model results obtained for $1 < D/d < 4$ to $D/d \gg 100$.

The theoretical curve for the resonance according to Inui in fig. 2a seems to be the most adequate tool for the extrapolation of the model results, although it was derived using linear wave theory, which neglects friction and assumes negligible wave heights. Havelock (1922) showed, however, that according to linear wave theory the shallow-water

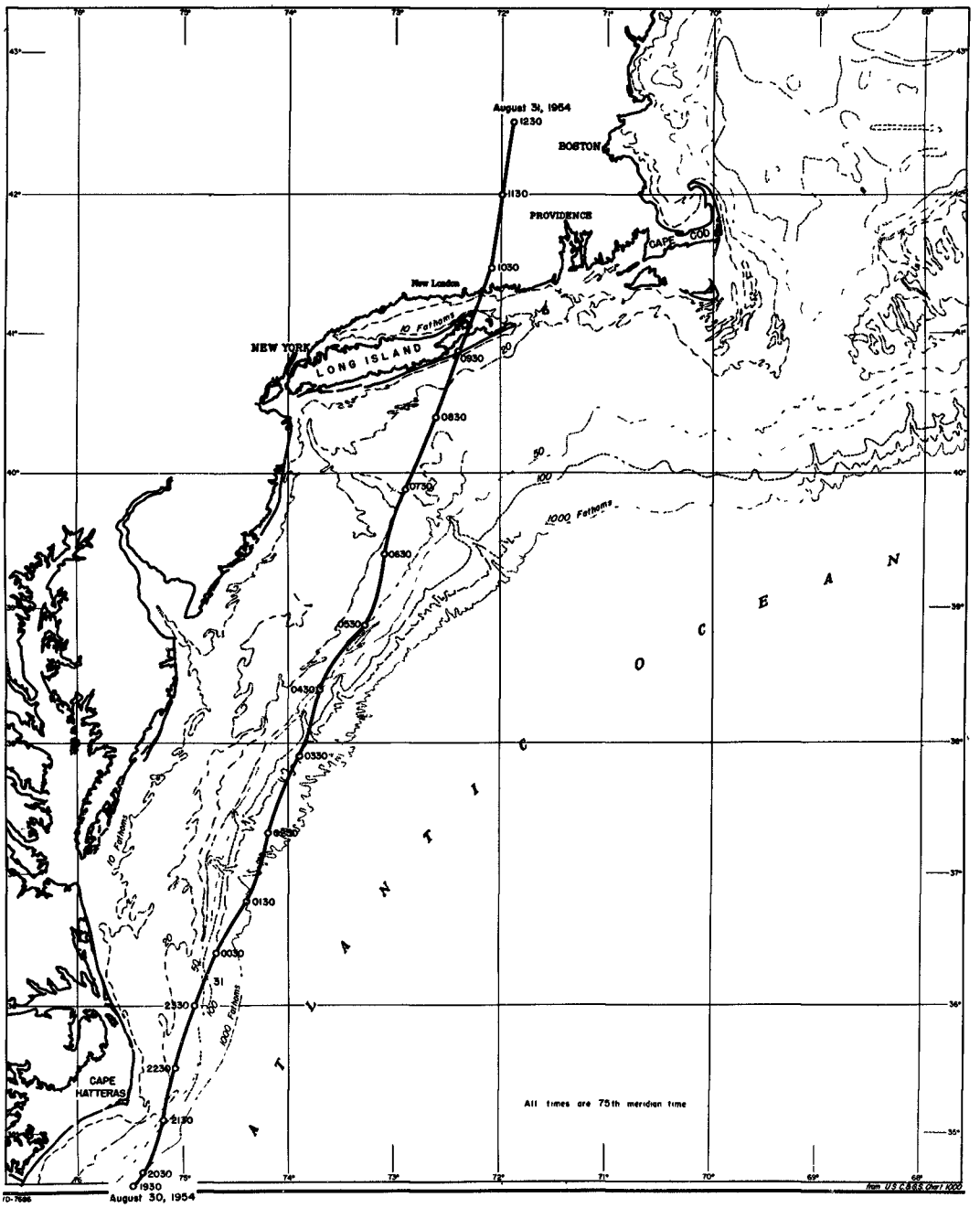

Path of center of hurricane CAROL, 30-31 August 1954

(after Harris, 1956)

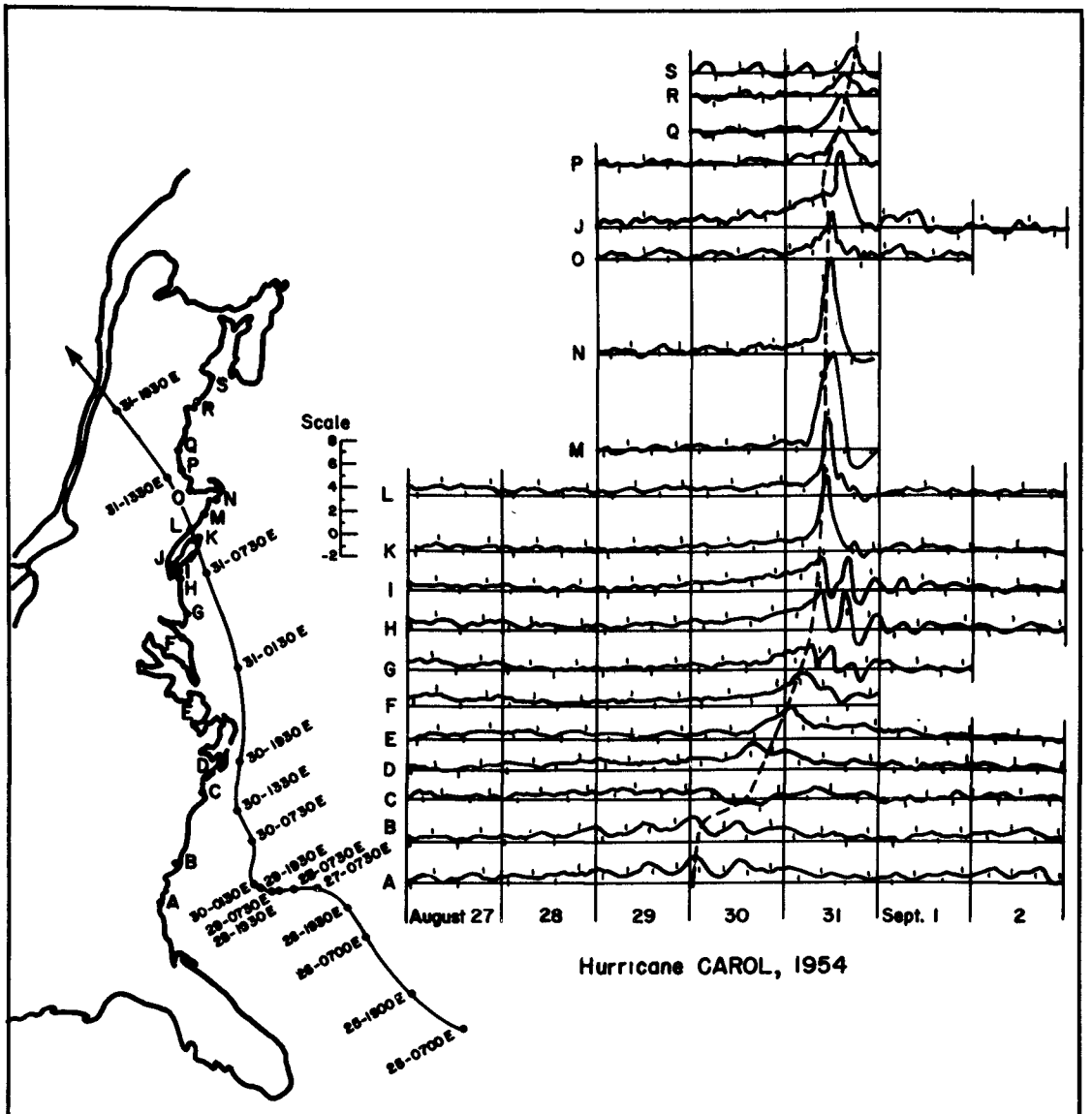

STATIONS:

A. Fort Pulaski, Ga.
B. Charleston, S. C.
C. Wilmington, N. C.
D. Morehead City, N. C.
E. Hampton Roads, Va.
F. Breakwater Harbor, Del.
G. Atlantic City, N. J.
H. Sandy Hook, N. J.
I. The Battery, New York City, N. Y.
J. Willets Point, N. Y.
K. Montauk Point, N. Y.
L. New London, Conn.
M. Newport, R. I.
N. Woods Hole, Mass.
O. Boston, Mass.
P. Portsmouth, N. H.
Q. Portland, Me.
R. Bar Harbor, Me.
S. Eastport, Me.

Hourly storm surge height (observed minus predicted sea level), Atlantic coast tide stations, August 27 - September 2, 1954.
(after Harris, 1956)

maxima become higher when the ratio D/d increases. The physical reasoning that a water particle in the path of the center of the pressure area is subjected to a vertical force during a longer period of time, when the diameter of the disturbance is larger, while its speed remains the same, yields the same result. Hence we may assume that shallow water maxima of at least the same relative height, compared with the static water displacement as those observed in the model, may occur in nature, as long as the ratio H_s/d is the same for model and prototype. For our experiments the magnitude of this ratio varied between 0.01 and 0.02.

According to the foregoing the theoretical curve combined with the model results shows that shallow-water maxima up to 2 times the static water displacement may be considered to be possible for hurricanes that advance during a sufficiently long period of time over water having a depth d, satisfying $0.75\ d_{cr} < d < 1.25\ d_{cr}$, where $v = \sqrt{g d_{cr}}$. Maxima up to 3 times the static water displacement may be considered to be possible for hurricanes that advance during a sufficiently long period over water having a depth satisfying $0.9\ d_{cr} < d < 1.1\ d_{cr}$.

It is impossible to make an estimation of the required period of time by extrapolating the model data because of the difference of the ratio D/d. The theoretical curve shows, however, the following. The wave height varies gradually with decreasing depth for $0 < V/\sqrt{gd} < 0.8$ or for $1 < H_{max}/H_s < 2$. For $v/\sqrt{gd} > 0.8$ the wave height varies more rapidly. Hence it seems safe to assume that shallow-water maxima satisfying $H_{max}/H_s = 2$ occur in nature, when a hurricane, that has advanced for a considerable length over the ocean surface, moves over a (continental) shelf, where the water depth gradually approaches the critical depth. For this case the shallow-water maxima may develop gradually from $H_{max}/H_s = 1$ to $H_{max}/H_s = 2$.

A similar initial period was not available for the two dimensional examples, which nevertheless showed considerable wave heights. Therefore it seems reasonable that the period of time that was available for the two dimensional examples (order of magnitude one hour) may be considered to be sufficient for the development of considerable shallow-water maxima (say $H_{max}/H_s = 3$) for three dimensional disturbances with a long initial fetch, which move during this one hour period over water having the required depth ($0.9\ d_{cr} < d < 1.1\ d_{cr}$).

CONCLUSIONS

We may draw the following final conclusions: (1) A period of time of the order of magnitude of one hour may be considered to be sufficient for the development of three dimensional shallow-water maxima in nature. (2) Assuming that sufficient time is available for their development, three dimensional shallow-water maxima up to three times the

static water displacement may be considered to be possible in nature.

Hence, a shallow-water maximum of three times the static water displacement, combined with total reflection against the coast, could explain storm surges up to six times the static water displacement. Storm surges of this magnitude have frequently been observed (Harris, 1958).

The steepness of the shallow-water maxima is of the same order of magnitude as the steepness of tsunamis. Hence, they may be affected by the coast in such a way, that the elevation of water level at the coast may be considerably more than twice their height, as is shown by Kaplan (1955) and van Dorn (1959). Thus, the shallow-water maxima, combined with the affects of the coast could even explain storm-surges higher than six times the static water displacement.

ACKNOWLEDGEMENTS

This investigation was conducted by the author while a Fulbright Scholar at the Hydraulics Research Laboratory, University of California, Berkeley. The work was performed under sponsorship of the National Science Foundation, grant number 4630.

The author wishes to express his appreciation to Prof. J. W. Johnson for facilitating this investigation and to Prof. R. L. Wiegel for suggesting the study.

REFERENCES

Abraham, G. Model study of water gravity waves generated by a moving circular low pressure area, Univ. of Calif., Inst. of Eng. Res., Tech. Rept. 99-5, 122 pp, May 1959.

Donn, W. L. The Great Lakes Surge of May 5, 1952; Journal of Geophysical Research, vol. 64, No. 2, pp 191-198, February 1959.

Ewing, M. F., F. Press, and W. L. Donn. An explanation of the Lake Michigan Surge of 26 June, 1954, Science, vol. 120, pp 684-686, October 1954.

Harris, D. Lee. Some problems involved in the study of storm surges: National Hurricane Research Project, Report 4, 1956.

Harris, D. Lee. Meteorological aspects of storm surge generation: Journal of the Hydraulic Division, Proceedings of the American Society of Civil Engineers, paper 1859, Hy 7, December 1958.

Havelock, T. H. The effect of shallow water on wave resistance: Proceedings of the Royal Society of London, series A, vol. 100, 1922.

Inui, T. On deformation, wave patterns and resonance phenomenon of water surface due to a moving disturbance: Proceedings of the Physico-Mathematical Society of Japan, series 3, vol. 18, no. 2, February 1936.

Kaplan, K. Generalized laboratory study of tsunami run-up: Technical Memorandum no. 60, Beach Erosion Board, January 1955.

Redfield, A. C. and A. R. Miller. Memorandum on water levels accompanying Atlantic Coast hurricanes: Woods Hole Oceanographic Institution, Reference no. 55-28, June 1955 (unpublished manuscript).

Redfield, A. C. and A. R. Miller. Water levels accompanying Atlantic Coast hurricanes: Meteorological monographs, vol. 2, no. 10, June 1957.

Snyder, C. M., R. L. Wiegel and K. J. Bermel, Laboratory facilities for studying water gravity wave phenomenon, Proc. Sixth Conf. on Coastal Engineering, Council on Wave Research, The Engineering Foundation, pp 231-251, 1958.

Van Dorn, W. G. Local effects of impulsively generated waves, report no. II, Scripps Institution of Oceanography, August 1959.

Wiegel, R. L., C. M. Snyder, J. B. Williams. Water gravity waves generated by a moving low pressure area: Transactions of the American Geophysical Union, vol. 39, no. 2, April 1958.

CHAPTER 32

INVESTIGATIONS OF THE TIDES AND STORM SURGES FOR THE DELTAWORKS IN THE SOUTHWESTERN PART OF THE NETHERLANDS

J.J.Dronkers
Chief Mathematician, Water Resources and
Hydraulic Research Division, Rijkswaterstaat,
The Hague, Netherlands.

The purpose of this paper is to summarize investigations of the tides and storm surges for the deltaworks in the southwestern part of the Netherlands.

The investigations into the tidal currents and H.W.levels in the coastal area will be treated more in detail.

INTRODUCTION

In order to protect the southwestern part of the Netherlands against inundation by storm surges, the "Delta project" has been undertaken. This entails the closure of three large sea arms situated between Western Scheldt and Rotterdam Waterway and will bring about radical changes in the tidal movement and stormflood levels of the estuaries and tidal rivers.

The contours of the project are shown in fig. 1. It includes three big dams to be built in the mouths of Eastern Scheldt, Brouwershavense Gat and Haringvliet, as well as two smaller ones to be constructed further inland. An idea of the extent of these works may be gained by knowing the tidal volumes of the estuaries: Veerse Gat $2{,}5.10^9$ cu. ft; Grevelingen 4.10^9 cu. ft; Haringvliet 9.10^9 cu. ft; Brouwershavense Gat $12{,}5.10^9$ cu. ft and Eastern Scheldt 39.10^9 cu.ft.

The waters of the Delta area will then be divided into two separate basins by means of a dam in the Volkerak. The southern basin will be entirely cut off from the sea, becoming a fresh water lake. The northern, comprising the mouths of the Rhine and the Meuse will remain in communication with the sea, because the Rotterdam Waterway must stay open to shipping. Consequently, the tides and storm surges will still be able to penetrate inland via this mouth, but they can cause high waterlevels in the Waterway only; in the rest of the basin their effect will be considerably weakened. In the situation at present, however, the upland flow of the rivers Rhine and Meuse is mainly into the Haringvliet estuary and not the Rotterdam Waterway. As the Haringvliet estuary will be closed, large sluices are to be built in the enclosure dam as a substitute for the existing free discharge of the river water.

Until this project is completed the inhabitants of the area which it will affect are insufficiently safe against storm surges. It is, of course, always possible that floods too high for existing dike systems will occur, but in the present situation the risk is too great. This was demonstrated in February 1953 when the southwestern part of the Netherlands was suddenly hit by an exceptionally high storm surge which caused many dike breaches and vast inundation. The occurrence of a similar surge or a higher one may be estimated as once in two hundred and fifty years, as an average, which is much too high. After the realization of the Deltaplan and the heightening of the dikes of Western Scheldt, Rotterdam Waterway and the northern parts of the country,

the dikes are safe up to very high storm surges of which the occurrence is smaller than once in ten thousand years, or in other words there is only one procent chance in hundred years that a major inundation will occur.

In the paper: "Hydraulic investigations for the Deltaproject" H.A.Ferguson 1) describes in general terms the field observations, office computations and model studies made in connection with the hydraulics of the Delta projection and reclamation project under construction in the Netherlands in 1958. These studies include among other things investigations of tides, waves, currents, salinity, sediment movement, and drift of ice.

In this paper the investigations concerning the tides, which are mentioned in Mr. Ferguson's article, will be dealt with in more detail. These tides are those which exist before the execution of the Deltaworks and those which will result after the project is fully realized.

The main tidal features which had to be investigated in connection with the project in question were the determination of the highest levels which occur on the Rotterdam Waterway and further riverbranches of the Deltaregion during storm surges with given high-water levels at Hook of Holland at the outermouth of the Waterway, the division of the upland flow of the Rhine and Meuse into the various channels of the northern Deltaregion, the determination of the discharge programme of the sluices in Haringvliet and the flow velocities in the different navigation channels.

As a result of the changes in the flow conditions the riverbranches whose profiles are accommodated to present conditions, may have to be altered artificially. Further the possibilities for the suppression of the saltwater penetration of the Rotterdam Waterway by aid of the discharge programme had to be investigated.

Moreover, the changes in the tides and stormflood levels in the coastal areas outside the dams have to be determined in order to calculate the height of the enclosing dams and dikes which are exposed to the sea.

The tidal currents in the coastal waters of the delta will be changed considerably when the inlets are closed. The strong transverse currents, running to and from the estuaries will then have disappeared so that the prevailing current will be parallel to the coast. This change will undoubtedly cause important modifications in the pattern of banks and gullies. In the outermouth of the Haringvliet estuary the situation will become particularly complicated by virtue of the discharging of the upland flow through the sluices in the river. It is important, therefore, to determine the changes in the tidal currents in the coastal areas.

THE PROJECTS AND ITS EXECUTION

A few months ago (May 1960) the first closure, forming a part of the Deltaworks, was completed, i.e. the closure of the Zandkreek.

1) Journal of the Waterways and Harbours Division. Proceedings of the American Society of Civil Engineers, March 1959, New York.

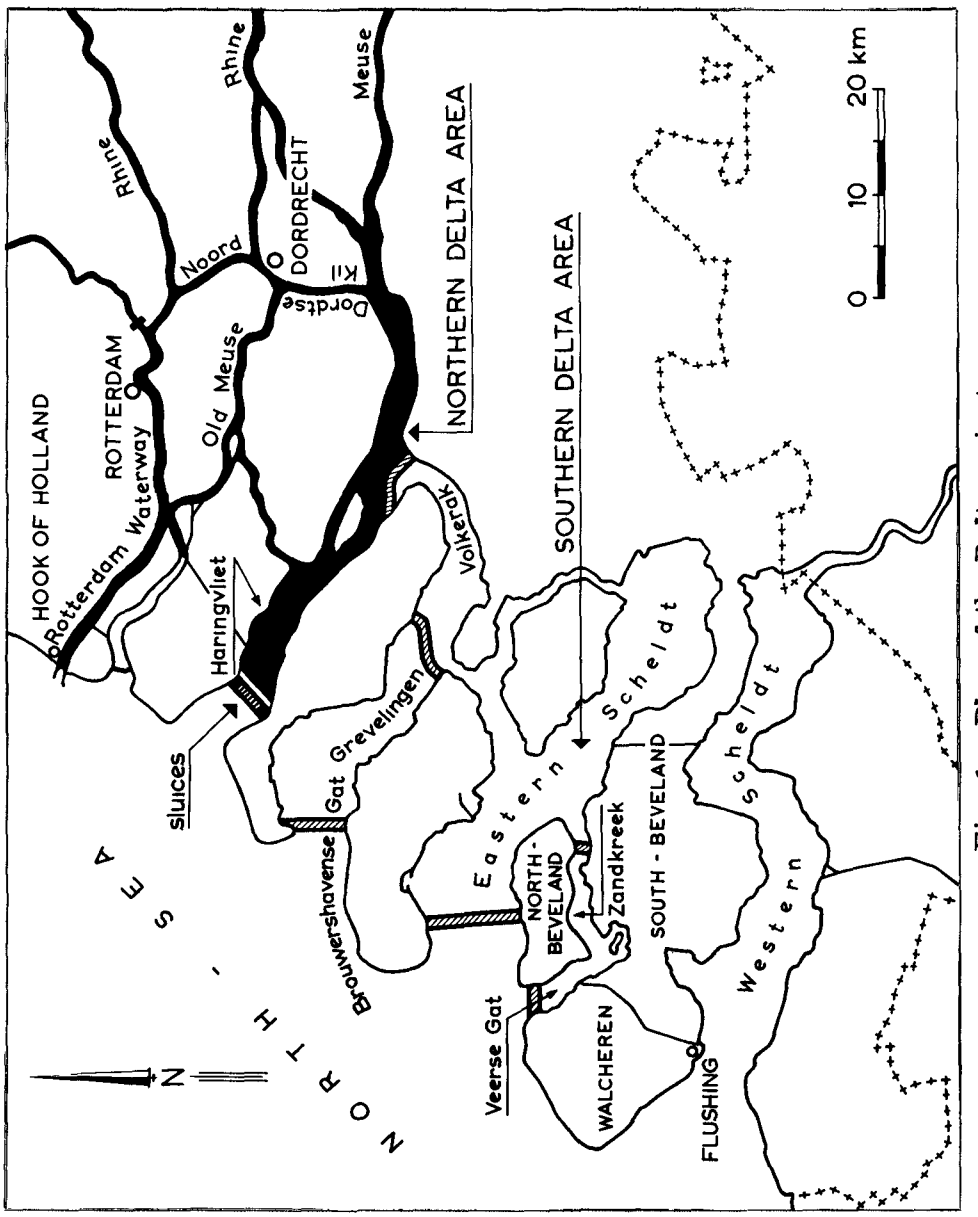

Fig. 1. Plan of the Deltaproject.

This channel separates the island of North Beveland in the province of Zeeland from South Beveland (see fig. 1). During this closure no great difficulties were encountered. The difference in head of water at both sides of the closure dam was not more than one feet in the final stage of the construction.

Next year the final closure of the Veerse Gat will take place as a result of which the islands of North Beveland and Walcheren will be connected and the estuary of Veerse Gat and Zandkreek will be changed into a lake.

This closure is considerably more difficult than the closure of the Zandkreek, for after it the maximum difference in the water levels at the different sides will be about 5 ft at springtide.

In 1959 the building of the huge sluice in the mouth of the Haringvliet was begun; the width is about 1150 yards and the depth is 17 ft below mean sealevel. An island surrounded by a high dike had already been constructed, taking one year to complete. The construction of the sluice will be finished in 1966 or 1967 if no serious difficulties are encountered. After that, the further closure of the Haringvliet will take place in 1968.

Next year (1961) the government intends to begin the works for the enclosure of the Grevelingen, the estuary between the islands of Schouwen Duiveland and Overflakkee (see fig. 1). This enclosure will be completed in four years.

Further extensive projects are planned for the following years. After the works in the Grevelingen the closure of the mouth of the Brouwershavense Gat will commence and be finished in 1970, and finally the closure of the mouth of the Eastern Scheldt will take place. It is hoped that the complete Deltaworks will be finished in 1978, thus providing a more comfortable safety margin against floods, and leading to important changes in the coastal waters.

A few years ago extensive studies commenced for the so-called Europort, which will involve the construction of harbours at the outer mouth of the Rotterdam Waterway. Piers will have to be built in the coastal waters.

It is obvious that these works will have an important influence on the coastal currents and consequently on the sediment movement also. Moreover, this problem is much complicated by the fresh and salt water motion outside the Rotterdam Waterway. The construction of the piers depends also to a large extent on the influence of the waves.

THE MEANS FOR RESEARCH INTO THE TIDES

Calculations of the tides and investigations into the tidal movement by means of model tests are very important for the planning of the Deltaproject, and for the construction of the dams during the closure operations. Both methods are considered indispensable and are complementary to each other.

The tide calculations afford a better knowledge of the physical aspects of the tidal movement and, if carried out in sufficient detail they may produce more exact results than those by using models.

The calculations are confined to cases which are regarded as highly important from a practical and theoretical point of view and which will afford a check on the results of the model.

In a model far more situations can be investigated in a short time than by means of calculations; model tests are therefore especially suitable for examining whole series of situations.

The tidal model of the Deltaregion has the disadvantage that it is not very suitable for examining the effect of profile changes of channels, as frequent and time consuming modifications of the model would be necessary.

A new electric analogy has been developed, therefore, by which the comprehensive research programme may be accomplished within a comparatively short time and with sufficient accuracy.

THE TIDES BEFORE AND AFTER THE EXECUTION OF THE DELTAPROJECT

The tides vary greatly along the Netherlands' coast from South to North. At Flushing the tidal range at mean tide is about 12 ft, at Hook of Holland, the mouth of the Rotterdam Waterway, it is 5 ft and further North it decreases to about 4,5 ft at Den Helder. From that point the coast bends in northeasterly direction towards the German Bight, and the tidal range increases again. At the most eastern place, Delfzijl, the range is about 9 ft. From these figures it appears that after the closing of the southwest estuaries (apart from the Western Scheldt), the high tides in the southwest will be cut off and that only at Hook of Holland, where the range is lowest, will they be able to penetrate into the Deltaregion. Furthermore it is clear that in the Deltaregion, the tidal wave will be greatly decreased, depending on the distance of propagation. As a consequence, after the Deltaproject, the tidal ranges in the northern Deltaregion (north of Volkerak) will be much smaller than at present. The modifications in the ranges follow from fig. 2, in which the highwater and lowwater levels are shown. Especially in the Haringvliet estuary the decrease of the tidal range is very important in comparison with the present situation. At mean tide at Hook of Holland and with the Haringvliet sluices closed, the tidal range will in the Haringvliet lake be decreased by 90%, becoming about ½ ft.

The water motion in the northern region, however, is very complicated due to the upland discharge of the Rhine and Meuse. In the present situation this water mainly follows the Haringvliet estuary, but in the future it must be discharged by the large sluices in the enclosing dam of the Haringvliet. The upland discharges of the river Rhine may vary greatly from about 35.10^3 cu. ft/sec in a dry season to about 350.10^3 cu. ft/sec in a very wet season (wintertime). In extreme cases an upland discharge of 450.10^3 cu. ft/sec or higher may occur (mean frequency of occurrence: once in twenty years). Therefore the sluices must be very large; when fully opened the cross-sections are 57.10^3 sq. ft below mean sealevel. In the case, however, of an upland discharge lower than about 210.10^3 cu. ft/sec only a part of the maximum sluice opening will be used. The reduction of the discharge will be affected by partly closing all of the 17 individual sluice openings. From the point of view of scour of the downstream bed, this is preferable to closing part of the sluices entirely. Although a bed protection against scour will be provided, it remains advisable to distribute the total discharge over the greatest possible width.

Furthermore the sluices will remain closed during the period of

higher water levels at the seaward side than at the landside in order to prevent saltwater to penetrate into the Haringvliet estuary.

From the preceding consideration it follows that many variatior can occur in the waterlevels of the northern Deltaregion, due to astronomical and meteorological circumstances (springtide, neaptide, storm surges) of the tides at Hook of Holland, the variations in upland discharge and the discharge programme of the Haringvliet sluices.

In any case, however, the waterlevels in the Haringvliet estuary will be much lower than at present. In fig. 2 the H.W.levels and L.W.levels in case of closed sluices are shown for various places in the northern region in comparison with the levels found now.

THE SUPPRESSION OF THE SALTWATER PENETRATION OF THE ROTTERDAM WATERWAY BY AID OF THE DISCHARGE PROGRAMME OF THE HARINGVLIET SLUICES

In the present situation about 55% of the upland discharge of the Rhine and Meuse passes through the Haringvliet and 38% through the Rotterdam Waterway. The remaining 7% discharges to the IJssel lake. The upland discharge suppresses the salt penetration via the Rotterdam Waterway to some extent but it is an insufficient deterrent. In point of fact, the drinking water of Rotterdam is very often mixed with salt to a disagreable amount in times when the upland discharges are low. In those times, therefore, the upland discharge of the Waterway has to be increased relatively to the discharge through the sluices. This can be done by decreasing the opening of the sluices. Then the discharge of the sluices decreases also and therefore the freshwater discharge through the Rotterdam Waterway increases. As a consequence the saltwater penetration will decrease, but it depends on the tides and on the upland discharges.

In the case of very small discharges of the Rhine and Meuse, the sluices in the Haringvliet will be closed during the whole tide so that all available freshwater which is not be needed for domestic and agricultural use can be discharged through the Waterway.

The full value of this effect can be asserted after a thorough investigation of the motion of fresh and saltwater in the riverbranches concerned, a motion which is complicated by the mixing effect of the harbour basins.

In any case the saltwater penetration in the Rotterdam Waterway will be suppressed to an important extent after the execution of the Deltaworks.

It must be noted, however, that this suppression is limited, because the freshwater from the rivers Waal (the most important branch of the river Rhine) and Meuse has to be discharged by the rivers Old Meuse and Noord (see fig. 1). The amount of this discharge is limited by the cross-section area and the fact that the velocities of these rivers may not exceed certain values dependent upon navigational requirements and the maintenance of the profiles. In cooperation with this, the benefit proceeding from the eventual construction of a barrage in the Old Meuse near its confluence with the Waterway has to be studied. By closing the Old Meuse in times of small upland river discharges all available freshwater will then flow past Rotterdam. It is to be expected that this concentration upon one branch will be favourable for the suppression of the salt penetration.

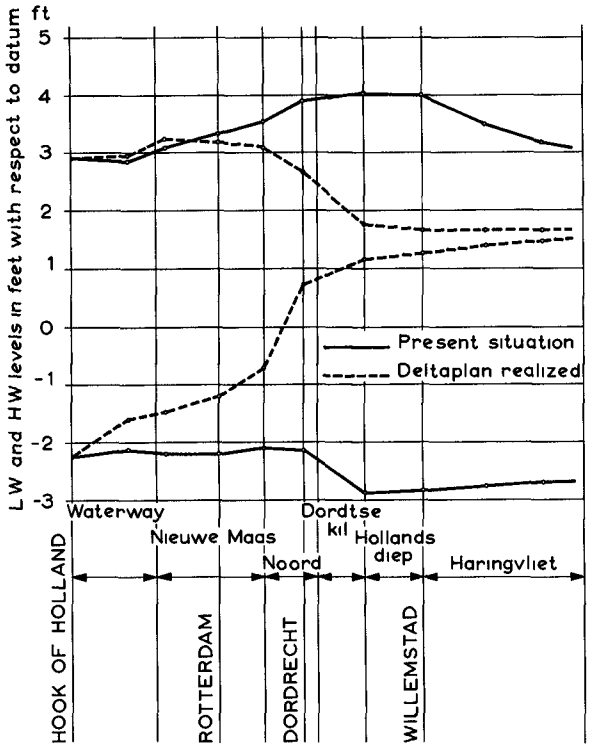

Fig. 2. High and low water levels in the present situation and after the realization of the Deltaplan.

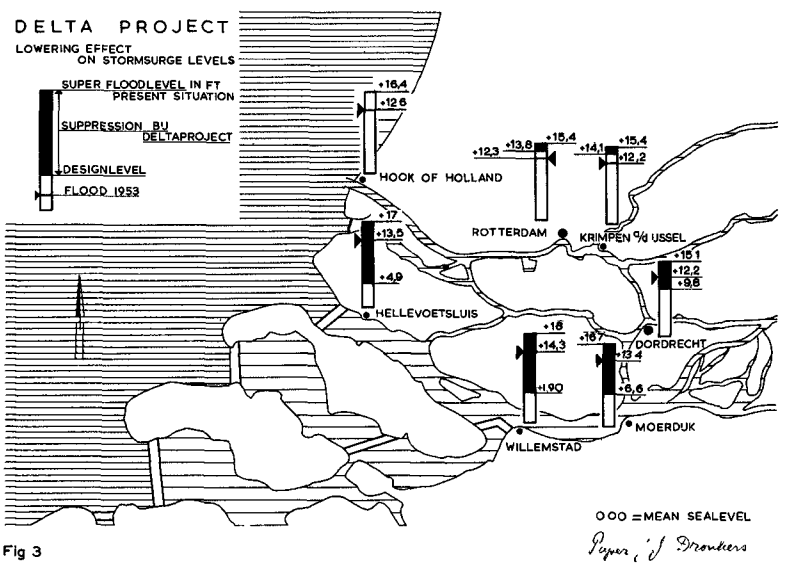

Fig. 3. Lowering effect on storm surge levels.

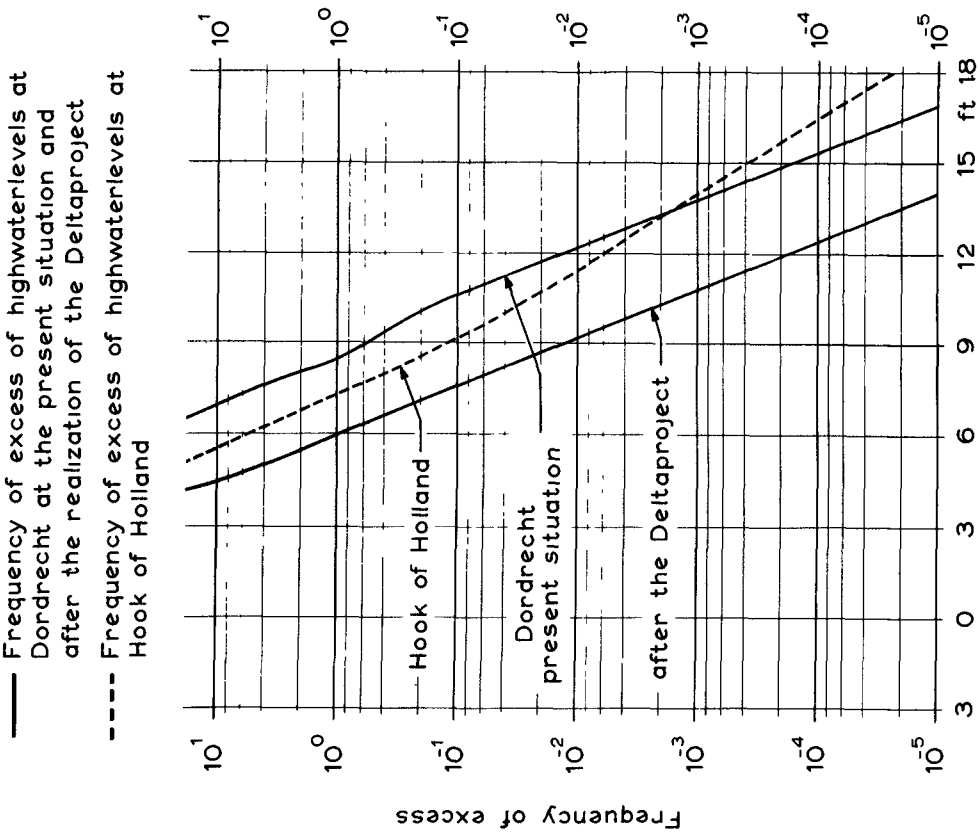

Fig. 5. Frequency of excess at Hook of Holland and Dordrecht.

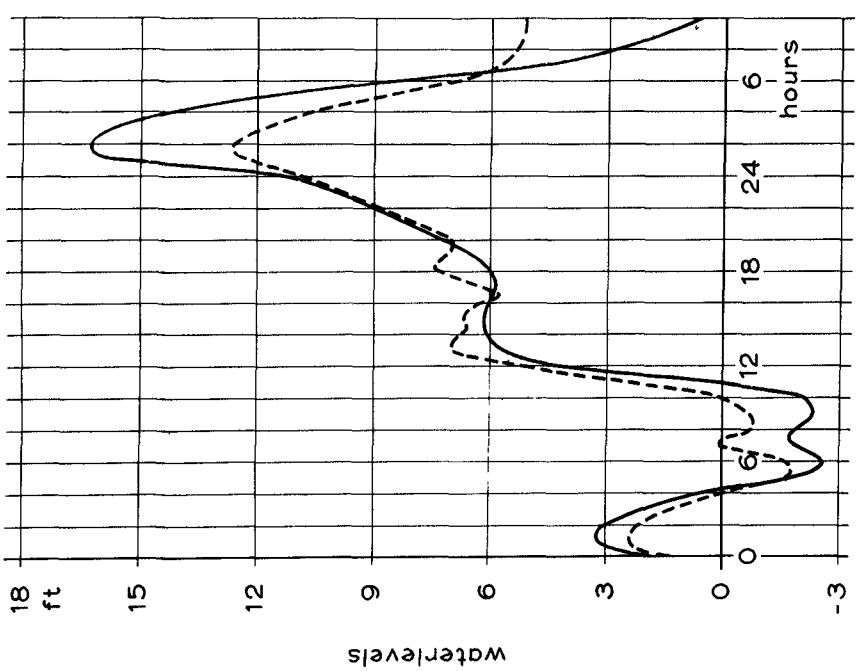

Fig. 4. Storm surge curves at Hook of Holland.

INVESTIGATIONS OF THE TIDES AND STORM SURGES FOR THE DELTAWORKS IN THE SOUTHWESTERN PART OF THE NETHERLANDS

THE DECREASE OF THE STORM SURGE LEVELS AS A CONSEQUENCE OF THE DELTAWORKS

Storm surge levels will also decrease in the northern region after the execution of the Deltaworks. The further inland one goes the greater will be the lowering effect on storm surge levels. In fig. 3 this lowering effect is shown for a very big storm surge. It appears that along the Rotterdam Waterway up to Rotterdam the decrease is relatively small so that the dikes in this region must still be heightened. As has been remarked in the introduction the frequency of the occurrence of storm surge levels like 1953, must be considered as too high in relation to the possible loss of life and damage to property. Because of this, the statistics of the highwater levels have been exhaustively studied by various institutes, the Rijkswaterstaat (see the paper: P.J.Wemelsfelder, On the use of frequency curves to determine the design stormflood), the Mathematical Centre in Amsterdam and the Meteorological Institute. Finally it has been decided, the storm surge level of 16,5 ft above mean sealevel at Hook of Holland, which has a frequency of excess of about once in 10.000 years, to adopt as a design value for the dikes in the northern Delta area. In fig. 3 the decrease of the storm surge levels are shown for inland places. These levels also depend on the shape of the storm surge curve at Hook of Holland, for which a hypothetical curve has been constructed on the basis of curves for storm surges which occurred in the past (fig. 4). With the help of statistical researches it has been shown, that in the case of very high storm surge levels it is reasonable to suppose that the simultaneous upland discharge does not differ much from the mean upland discharge. The probability of the simultaneous occurrence of very high storm surges at Hook of Holland and important upland discharge is much lower than the accepted frequency of excess of once in 10.000 years as an average.

On the other hand, for inland places like Dordrecht, the levels depend also on the upland discharge so that a certain level may occur here under various circumstances for stormflood levels and upland discharges. A high level at Hook of Holland and a low upland discharge may cause the same highwater level at Dordrecht as a lower storm surge level and a higher upland discharge. It may not be concluded, therefore, that the storm surge level for Dordrecht, shown in fig. 3, has a frequency of excess of once in 10.000 years. For the determination of the statistical occurrence of the storm surge levels the statistics of the upland discharges have to be taken into account. This problem will not be dealt with in detail; only the most important points are mentioned.

The stormflood levels to be experienced at various places in the Deltaregion when various stormflood levels occur at Hook of Holland in conjunction with certain upland discharges, have been determined by model tests.

In virtue of the independence of storm surges and upland discharges the probability of occurrence of a storm surge level at Hook of Holland, situated in a certain interval, together with the probability of occurrence of an upland discharge also situated in an interval, equals the product of the probability of occurrence of each factor As a stormflood level at Hook of Holland and an upland discharge cause

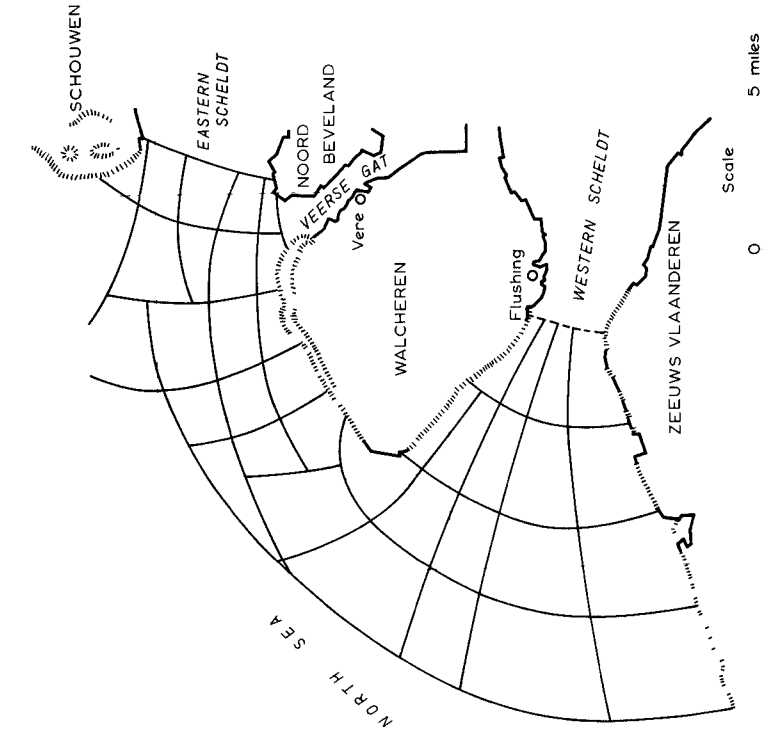

Fig. 7. The scheme of the sections outside the dam in the Eastern Scheldt and the island of Walcheren.

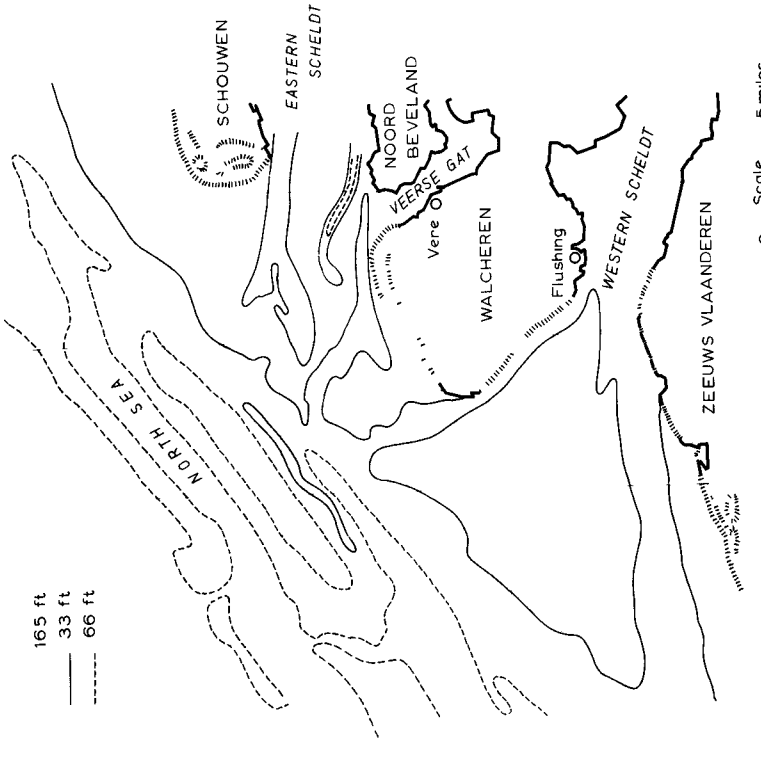

Fig. 6. The contour lines of 16.5 ft, 33 ft and 66 ft below mean sea level in the coastal area.

a determined stormflood level at any place in the Deltaregion e.g. at Dordrecht, the probability of occurrence of a stormflood level, situated in an interval at Dordrecht equals the sum of these probabilities mentioned above for which the storm surge levels at Hook of Holland and upland discharges cause stormflood levels in the considered interval at Dordrecht. Furthermore, the frequency of excess of a certain stormflood level at Dordrecht is the sum of the probabilities for the various intervals higher than the value of which the frequency of excess has been determined. In fig. 5 as an example the frequencies of excess of the stormflood levels at Hook of Holland are shown and for Dordrecht these corresponding to the present situation and after the execution of the Deltaplan. The decrease of the stormflood levels at Dordrecht can be determined from these graphs.

INVESTIGATIONS INTO THE TIDAL CURRENTS AND H.W.LEVELS IN THE COASTAL AREA

When the inlets of the Eastern Scheldt, Brouwershavense Gat and Haringvliet are closed, considerable changes will take place in the tidal currents of the coastal waters. The strong currents running to and from the estuaries will disappear and currents parallel to the coast will prevail. As a consequence the fan shaped gullies, directed to the estuaries, will gradually disappear and the coastline will be flattened out. Furthermore a regression of the sandy coastline of the islands may be expected. In the future therefore, protection works may become necessary. For the planning of these works detailed studies have to be made, taking into account the tidal mechanism, the action of waves and currents and their influence on the movement of sediments.

The process of reshaping the coastline may take a very long time, but it is possible that this development may cause dangerous effects of erosion even in the first stage. It is in fact, very difficult to forecast what will happen in detail.

Further investigations concern the determination of the increase of the stormflood levels after the closure. These are especially relevant to the height of the dams and the existing dikes.

The basis of the investigations consists of the study of the tidal motion in the coastal areas at present. The pattern of the tidal currents in the inlets of the estuaries is very complicated, due to the interference of currents directed to the estuaries with the tidal currents parallel to the general trend of the coast. These latter currents are caused by the general tidal motion in the North Sea, and as the distance from the coastline increases so does the influence of the North Sea tide. Complications are also caused by the important difference in phase between the North Sea currents and the estuary currents. If the currents in the North Sea region are maximum, the currents directed to the estuaries are small and vice versa.

In fig. 6 a review is shown of the banks and gullies at the inlets and outside the coastal line of the southern part of the Deltaregion. The shoals outside the coastal line have a width of about 12 miles.

In the coastal area at various points the vertical tidal motion has been recorded by using an instrument which determines the pressure of the watercolumn above the instrument.

With the help of these data and the observations at various places on the coast, the course of the tidal motion at other places in the coastal area has been derived by interpolation.

Furthermore velocity measurements have been taken for some years at various places, especially in the outermouth of the estuaries and at some points in the gullies in front of the islands. Then the relation with respect to the vertical tide can be derived.

While the tidal movement in the coastal waters is influenced by the Coriolis forces, in the estuaries the influence of this force is limited by the restricted width.

As a consequence of the Coriolis forces the tides near the coast are stronger than in the area of the North Sea off the coast. It appears that at a distance of 15 miles from the coast the highwater level is about 2/3 ft lower than at the coast.

The tidal motion in the sea is determined by the two equations of motion, the equation of continuity and boundary conditions.

Equations of motion:

$$\frac{\partial u}{\partial t} - \Omega v + g \frac{s\,u}{C^2 a} = - g \frac{\partial h}{\partial x} \quad ,$$

$$\frac{\partial v}{\partial t} + \Omega u + g \frac{s\,v}{C^2 a} = - g \frac{\partial h}{\partial y} \quad .$$

Equation of continuity:

$$\frac{\partial h}{\partial t} + \frac{\partial a\,u}{\partial x} + \frac{\partial a\,v}{\partial y} = 0 \quad .$$

t = time; x and y are plane coordinates; u = velocity component in x-direction and v in y-direction; h = height of waterlevel with respect to datum; g = acceleration of gravity; Ω = coefficient of Coriolis; C = coefficient of friction; a = depth. The value of the density of the water ς is supposed to be one; s = magnitude of the velocity vector:

$$s = (u^2 + v^2)^{1/2}$$

The mean sea depth in the coastal area is low in comparison with the mean depth of the North Sea itself. In the gullies between the banks, the depth varies from 25 ft to 60 ft. In the adjacent part of the North Sea, outside the coastal region, the depth varies between 70 ft and 90 ft. As a consequence the resistance force in the equations of motion is much more important in the coastal area than in the North Sea, so that in tidal calculations especial care must be taken in considering the influence of this force.

The value of the resistance coefficient C has to be determined from tidal computations for the existing situation in the coastal area of which the tidal motion is known from the observations.

The computations are carried out in the following way.

An important reduction may be made by taking the abscis x in the length direction of a gully, in which the velocity has been

observed at two or more points and the curve of the vertical tide is known. At first the differences between the measured velocities in various points of the gullies are verified with the aid of the equation of continuity.

Then $\frac{\Delta h}{\Delta t}$ and $\frac{\Delta a u}{\Delta x}$ are determined from the vertical tide and the velocity measurements. Further from the velocity observations the mean values of $\frac{g s u}{a}$ and $\frac{\Delta u}{\Delta t}$ are determined; the value of $-\Omega v$ also can be estimated from the observations in the gully itself and in neighbouring gullies. By reason of the assumption that the velocity is mainly directed in the gully, the value of $-\Omega v$ is mostly small in comparison with the other ones. If, moreover, the value of $\frac{\Delta h}{\Delta x}$ is known, the value of C for the gully can be computed from the first equation. The computation of C can be carried out for various moments during the tide, analogous to the corresponding computation in the rivers. Then it appears that the value of C as an average equals about 110 $ft^{\frac{1}{2}}/sec$. Because of the supposition that the value of C will not change importantly during a tide, these computations also give an impression of the exactness of the measurements and the various interpolations for the determination of the values of $\frac{\Delta h}{\Delta x}$ and the mean values of u. From the second equation the values of $\frac{\Delta h}{\Delta y}$, perpendioular to the gully, can be computed. They depend mainly on the values of Ωu.

Such computations are important for the knowledge of the tidal motion of the coastal area. Further information is obtained in order to verify the method by which the coastal region may be schematized for further tidal computations. The very shallow regions are then separated from the deeper gullies. The gullies are further divided into sections, which have comparable depth and width with lengths of 2 or 3 miles. Then the depth is considered constant. In fig. 7 an example of such a schematization for the area outside the dam in the mouth of the Eastern Scheldt and the island of Walcheren is shown.

For this area a complete tidal computation has been carried out in the following way. Only the most important steps are described. Firstly, the tide in individual gullies was computed by using the available measurements, as described above. After that, the tides in the various gullies were compared to ascertain the continuity of currents and vertical tides at the points where one section of the schema meets its neighbour. Differences at these meeting points have to be eliminated by modifying the computed tides in adjacent gullies. This is done by trial and error on account of the non-linear equations (quadratic resistance terms). These computations take much time and often show that the sohematization of the gully system has to be changed.

After studying the tidal motion in the present situation, tidal computations are executed for the situation after the estuaries have been closed.

Then the pattern of the currents along the coast is less complicated, running mainly parallel to the coast. In the inlets of the closed estuaries, however, the tidal motion propagates to the dams. Because of the short distance the propagation of this tidal wave can easily be computed. At first then it is supposed that the vertical tide at the seawardside of the inlet does not change, so that the currents directed to the dams can be computed approximately. After that the tidal motion outside the coastline of the Deltaregion can be calculated, supposing that the currents which are parallel to the coast are predominant with respect to the perpendicularly direoted currents. In a strip with a width of about 12 miles, this tidal motion can be considered as a propagation of Kelvinwaves, in which case the currents are directed in one direction. The propagation of such waves can be computed in a similar way as the propagation of the tides in a river. The differences in level in the transverse direction can be computed from the equation $\Omega u = - g \frac{\Delta h}{\Delta y}$. Finally, the influence of the tidal motion to the inlets of the estuaries can be taken into acoount more fully.

On the seaside borders of the region for which the computations are carried out, the observed tide graphs are the boundary conditions. Along the coast the perpendicularly directed velocities are zero.

Some results of the computations are:

The H.W.levels in the neighbourhood of the dams will increase by 2/3 ft and the L.W.levels decrease by an equal amount. The storm-flood levels will increase by 1· 1/3 ft. The H.W.levels at the capes of the islands, however, will only increase by a few inches.

The velocities in the outermouths of the estuaries, which will be closed, will decrease by about 30%, while this percentage will increase in the direction of the dams, where the currents completely disappear.

In the mouth of the Haringvliet, however, the determination of the changes of the currents is very complicated due to the discharge programme of the sluices.

REFERENCES

Dronkers, J.J. and Stroband, H.J. (1959). The safety in the Deltaregion against inundations (Dutch text). Report Rijkswaterstaat, Netherlands.

Dronkers, J.J. (1955). The influence of the Deltaworks on the tidal motion and the storm surge levels along the coast of the Netherlands (Dutch text). Report Rijkswaterstaat, Netherlands.

CHAPTER 33

ON THE USE OF FREQUENCY CURVES OF STORMFLOODS

P.J.Wemelsfelder
Chief Engineer, Rijkswaterstaat,
The Hague, Netherlands.

1. THE PROBLEM

In coastal engineering we often have to face the problem of high stormfloods. Especially if the land near the coast is flat and low, if it is densely populated or if high economic values have to be protected.
In all these cases, where life and economic values are at stake, a design flood has to be established as a basis for the construction of the works of protection.

Obviously the height of the design flood will be dependent on two factors. On one hand it depends on the characteristics of the sea, on its probable and possible heights. On the other hand it depends on the values of human and economic nature, threatened by the sea. So the design flood may be regarded as a balance between the threatening force of the sea and the values at stake.

In this paper we will investigate the nature of this balance. This will lead us to a close examination of the frequency curves of stormfloods, to a discussion of the question: What is a reasonable risk and to a discussion of the question: What is the space of time we have to take into account.

2. DESCRIPTION OF A FREQUENCY CURVE OF HIGHWATER

Let us suppose that tide gauge readings of highwater are available for a reasonable space of time. The first thing to do is to count the number of highwaters, surpassing every dm interval of the gauge.
If we plot these numbers as abscissa against the heights as ordinates we obtain the distribution curve of excess, which henceforth for the sake of convenience we will call the frequency curve.
Fig. 1 shows such a curve for the highwaters at the gauge of Hook of Holland. The vertical axis corresponds with the gauge heights. The Netherlands datum level NAP is practically equal to mean sea level; mean highwater equals NAP + 90 cm; a heavy stormflood reaches up to NAP + 280 à 320 cm and the disastrous stormflood of 1953 piled up to NAP + 385 cm at this gauge. In particular the higher floods will be the subject of our present study.
The abscis gives the number N of the times each level has been exceeded, reduced to the number per year. For practical reasons the scale of the abscissa is logarithmic.
It is important to note, that this procedure leads to a fairly straight curve in particular if not all the values of highwater are counted, but only those in the winter season.
As we are mostly interested in the higher and very high floods, the question arises how the curve should be extrapolated for higher levels. This is only a minor question in relation to the main subject of this paper. But for better understanding of what follows a short discussion of the higher part of the frequency curve may be useful.

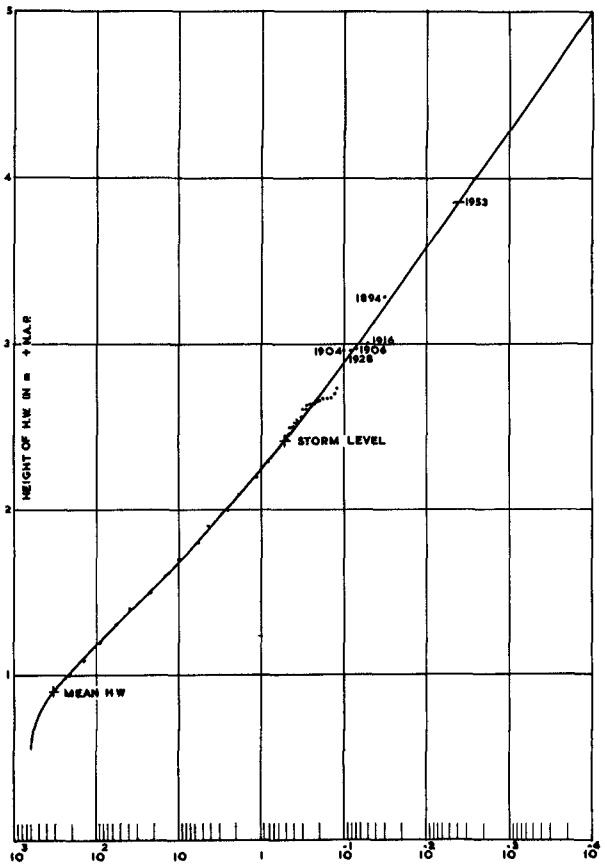

Fig. 1. Frequency curve of highwater at Hook of Holland.

Obviously the frequency curve can not end abruptly at the highest observed highwater. The curve will continue beyond this point.
From calculations we know that in Hook of Holland stormfloods up to NAP + 6 to 6,5 m may not be regarded as impossible from a physical point of view and there is no valid reason to assume that even such extremely high levels should never be exceeded.
This consideration leads of necessity to an extrapolation of more or less straight character, at least for the levels, which will be of interest for the present investigation. Such an extrapolation is presented in fig. 1. And if perhaps the frequency curve in still higher regions will tend to deflect to some asymptotic value this does not interest us greatly. For this is in any case far beyond the levels considered in the scope of the present study.

Owing to the general character of frequency curves, of which fig. 1 is only a sample, we are faced with three important aspects:

1. nature confronts us with very high levels, liable to be exceeded;
2. possibly there is no limit given by nature. So man is forced to consider a reasonable limit which is convenient to his purposes;
3. the probability of the very high levels being exceeded is extremely small.

Thus if we have chosen a definite height as a design level, we know in advance, that there always remains the chance of it being exceeded. A discussion of the real content of the term exceeding and the real meaning of the term chance is therefore necessary.

3. A "STANDARD" FREQUENCY CURVE

The exceeding curve of the gauge of Hook of Holland has been used only as a sample. Another gauge may have a somewhat different curve, with differences in general shape, steepness and gauge values. In order to simplify the explanation, in fig. 2 a "standard" frequency curve is introduced, being an exactly straight curve F .

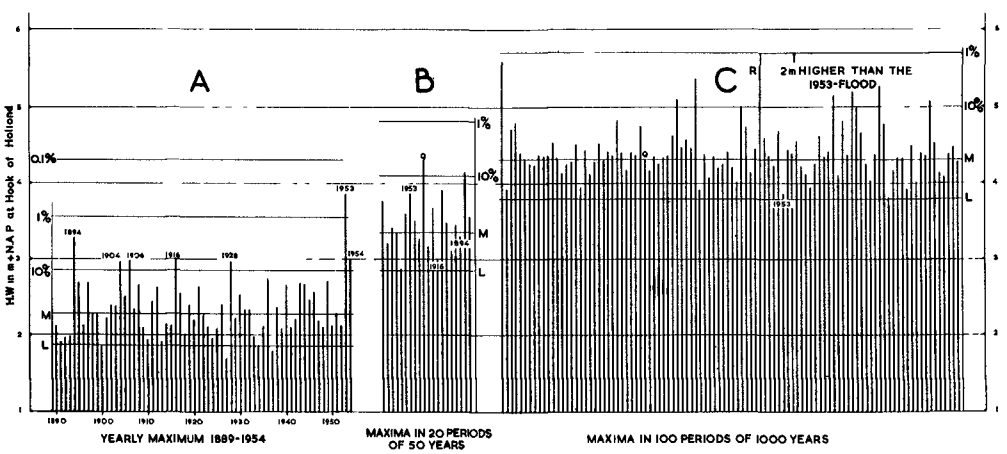

Fig. 2. Standard frequency curve F and curve of "maximum values" G .

The abscis shows on a logarithmic scale the exceeding value m . The ordinate shows h as an auxiliary height of an arbitrary character. In this diagram every value of m is directly related to a value of h by the straight frequency curve.
The frequency curve of highwater at a specific gauge such as e.g. fig. 1 provides the relation between the same value of m and the corresponding level at that gauge. From this results a well defined relation between any gauge reading H and the auxiliary height h .
So we may introduce the straight line F of fig. 2 as a standard frequency curve, valid for all gauges in the world as an exact representation, the ordinate being a nonlinear transformation of any gauge value into the uniform parameter h .
The abscis represents the exceeding value (or frequency) m , appearing in a period of T years. If we put N to be the number of cases of exceeding per year we have the relation:

$$m = T.N \tag{1}$$

For the straight standard frequency curve the equation applies:

$$h - h_1 = -s \log m \tag{2}$$

if h_1 is the height corresponding to the value $m=1$, which value is marked in the diagram by the central point M .
The coefficient s represents the steepness of the curve, so:

$$s = -\frac{h-h_1}{\log m} \tag{3}$$

If h_1 corresponds to $m=1$; $h_{0,1}$ to $m=0,1$; $h_{0,01}$ to $m=0,01$ etc., then:

$$s = h_{0,01} - h_{0,1} = h_{0,001} - h_{0,01} \text{ etc} \tag{4}$$

This means that s represents the height Δh , which decimates the frequency m .

As the standard frequency curve is a straight line, the value of s is a constant. This implifies the further investigations considerably. Yet this is not a simplification of the general problem. For the frequency curve of a special gauge may deviate considerably from a straight curve and the decimating value may vary for different levels. The nonlinear transformation of H into h takes this fully into account.
From (1) follows:

$$m = e^{-\alpha \frac{h-h_1}{s}} \tag{5}$$

with $\alpha = \ln 10 = 2,3$.

4. THE MAXIMUM VALUE IN A GIVEN PERIOD

If we ask for the probability k that in a given period of T years r facts occur, the mean value of these occurrencies being m ,

Poisson's law states:

$$k = \frac{m^r}{r!} e^{-m} \qquad (e = 2{,}72\ldots) \tag{6}$$

The chance of a given level h, corresponding to the exceeding value m, being not exceeded is given by the value of k for $r = 0$. So the chance of not being exceeded in a period of T years is:

$$k = e^{-m} \tag{7}$$

The chance q of being exceeded is the complementary value:

$$q = 1 - e^{-m} \tag{8}$$

Starting from the standard frequency curve F of fig. 2 it is a simple matter to calculate the values of q once for all. The result of this calculation is presented in fig. 2 curve G. The ordinates of this curve correspond to the same values of h as already discussed.
The abscis in this case gives the probability of exceeding q, ranging from 100% to 0%. The formula of this curve G can easily be derived from (8), resulting in:

$$q = 1 - e^{-e^{-\alpha \frac{h - h_1}{s}}} \tag{9}$$

This mathematical form is of little use for the present purpose, because formula (8) enables to calculate the curve in a much simpler way.
Gumbel uses this formula in general form as a starting point of his theory of maximum values. He does not use the whole universe but only the maxima. Our present work is based upon the use of the whole universe of observations and we come to final conclusions without any speculations about laws or coefficients.

4a. DISCUSSION OF THE FREQUENCY CURVE G

The curve G represents the probability q that a parameter height h will be exceeded in a period of T years. The central point of this curve is once more the mode M with the characteristic value $m = 1$ and the corresponding height $h = h_1$. For this point M the value of q is equal to:

$$q = 1 - e^{-1} = 0{,}63 = 63\% \tag{10}$$

If we have a period of T years and the height $h = h_1$ with the exceeding value $m = 1$, then the period T is exactly what in Anglo-Saxon scientific litterature is called "return period". Thus there is in a given period, which equals the length of the "return period", a probability

$$k = e^{-1} = 37\%$$

that the maximum value in that period will be lower than the corresponding height h (or the corresponding gauge height H), and a probability

$$q = 1 - e^{-1} = 63\%$$

that the maximum value will be higher.
If we take for m the value 5 the chance of not being exceeded is equal to:

$$k = e^{-5} = 0{,}7\%$$

and the probability of being exceeded:

$$q = 1 - e^{-5} = 99{,}3\%$$

We may conclude from this, that the height h_5, related to $m = 5$ can practically be regarded as the lowest possible maximum height for a period of T years. Nearly always the maximum height in T years will be higher. Though in theory there is no limit in downward direction, for practical purposes the height h_5 has to some extent the character of such a limit. For if we take h_7 or h_{10} these heights will be found to be very close to h_5, but their probability of not being exceeded is only one hundredth of that of h_5. So it is nearly "impossible" to have lower maxima.
The highest values of the maxima are not limited in this sense. If m is small, e.g. less than $0{,}1$, we have:

$$q = 1 - e^{-m} = m \qquad (11)$$

So for all values of m smaller than $0{,}1$ the chance of being exceeded is equal to the exceeding value itself.
The curve G corresponds to the mathematical form (9) and is represented here in the ogee-form. The Gumbel's diagram offers a possibility to draw the line G as a straight line. For our present purpose there is no need to make use of this possibility.

5. A SUBDIVISION OF THE RANGE OF POSSIBILITIES

From the preceding paragraphs we know, that the maximum values may range from h_5 (with $m=5$) up to every value of h without any limit. In order to discuss this wide range of possibilities it seems useful to introduce a division in classes, adapted to the needs of practical use. In order to attain this we divide the probability scale into classes.
Five characteristic values of the exceeding value m that may serve our attention, can be chosen namely:

$$m = 5 \quad 1 \quad 0{,}1 \quad 0{,}01 \quad 0{,}001 \qquad (12)$$

The value 5 has been discussed already. The value $m=1$ represents the central value of the mode M and we have chosen the associated values

0,1 , 0,01 and 0,001 because we are living under the rule of the decimal system.
These values of m divide the range of possibilities into the following classes:

from $m = 5$	to $m = 1$	the class of	LOW maxima
from $m = 1$	to $m = 0,1$	the class of	NORMAL maxima
from $m = 0,1$	to $m = 0,01$	the class of	REMARKABLE maxima
from $m = 0,01$	to $m = 0,001$	the class of	EXCEPTIONAL maxima
from $m = 0,001$	to $m = 0,000$	the class of	EXTREME maxima

The five mentioned values of m correspond to the five heights of the auxiliary scale h_5 h_1 $h_{0,1}$ $h_{0,01}$ $h_{0,001}$ as shown in diagram 2. Due to this relation we may connect the five classes immediately to the vertical scale, as is done in the right hand part of fig. 2. Moreover the five classes are written along the line F .

A short discussion about these classes may be useful. There is no class below h_5 , for nearly never there will be a period of T years with a maximum value below h_5 .
If the maximum is found between h_5 and h_1 it is justified to call such a maximum LOW. It remains below the central height M . If we could observe a great number of periods of T years length, in 37% the maximum should be found to be below M , so belonging to the class of low maxima.
Maxima between h_1 and $h_{0,1}$ have been named NORMAL, thus stressing the fact, that it is quite normal that the maximum value in a period of T years presents itself in this range. The percentage of maxima, falling in this class, is 63% - 10% = 53%. So roughly speaking half of all maxima are normal.
After this definition it is quite normal, that in a given space of time of T years a maximum height of a stormflood $h_{0,1}$ occurs. This means a height with an exceeding value $m = 0,1$. Or, still in other words, it is quite normal to meet in a period of T years a stormflood which has 10 x T as its "return period".
The class next to the normal stormfloods has been named REMARKABLE maxima, which name seems to be fitting to the purpose. Of course just beyond the upper limit of normality we will have to distinguish a range of floods, being not quite normal at one hand, but being not really extreme in the usual sense of the word. So from $h_{0,1}$ up to $h_{0,01}$ we may meet "remarkable" floods. So we may say that we have had a "remarkable" flood if we observed in a period of T years a stormflood of a height with a returnperiod between 10 x T and 100 x T years. 10% - 1% = 9% of all maxima belong to this class.
Above the class of the remarkable stormfloods we distinguish the class of EXCEPTIONAL maxima. This class ranges from $m = 0,01$ up to $m = 0,001$. While a phenomenon, occurring at a rate of 1 in 10 can rightly be called remarkable, for a phenomenon presenting itself at a rate of 1 in 100 only, the term "exceptional" may be considered as justified. The total number of maxima, belonging to this class, is 1% - 0,1% = 0,9%. The small quantity of about 1% is in fair agreement with the current meaning of the word "exceptional".
From $h_{0,001}$ up to any possible height a stormflood may be called "extreme". The word "extreme" is used here in another sense than Gumbel does in his theory of extreme values. Gumbel's "extreme values"

in the present paper are called "maxima". This is only a matter of using words. But nevertheless it is my intention to discuss here the necessity to distinguish low maxima well from high maxima. For this purpose a more refined distinction is needed which leads to reserve the word extreme for those maxima beyond the class of "exceptional" maxima. That means that the word "extreme" encompasses all those occurrencies, lying beyond the normal, the remarkable and even beyond the exceptional occurrencies.
This classification will prove to be very useful for an understanding of the true nature of the variability of maximum stormfloods in a limited or even unlimited space of time.

6. AN ANALYSIS OF THE PERIOD TO BE TAKEN INTO ACCOUNT

We shall now disouss the character of the period of time of years. For this we can ohoose an arbitrary number, adapted to the situation we want to consider. As an illustration we take into view three distinct values, viz:

- T = 1 year, representing interests of only short duration (merchandise on wharves for some weeks or months, execution of coastal engineering works for a few months or years etc.).
  Although to the intellect one year is quite a short period in relation to a life time or seen as a part of history, in the daily walk of life, psychologically, we do not look beyond it as a rule.

- T = 50 years, representing a "life time". With a fifty years period we take in view a whole life time of interests of rather restricted and individual character (factories, harbour works, buildings and also human life in the personal sense of the word). A period of fifty years has a definite significance, although it is not constantly before our mind.

- T = 1000 years. With this third period the scope is widened to a time interval during which works of public character as an entity have to function in order to secure safety of life and existence of the community as a whole. Though the individual hydraulic constructions may have a life time of not more than 50 to 150 years, their collective aggregate forms a continuous entity, exposed to a constantly threatening force of nature.
  From this "social" point of view we have to consider the life time of a whole community.

The three periods of 1, 50 and 1000 years are of course an arbitrary ohoice. They are meant to represent certain fields of interests for each of which a somewhat different figure could equally well be argued. The fields of interest themselves, however, we do consider as significant and their discussion may be useful as a guidance.

7. THE MAXIMUM STORMFLOOD IN EACH OF THE THREE PERIODS

It has been argued in the preceding paragraphs, that the "maximum height" is not a single value. Fig. 2 has shown that the maximum in a given period of T years may take any value between about h_5 and $h_{o,o}$ or infinitely high. Now attention must be paid to the fact, that the length of the period T plays an important role. In order to translate the frequency or exceedingvalue N/yr, as given by the absois in fig. 1, into the exceedingvalue m, to be read at the absois in fig. 2, a period T has to be defined. We will now see, what the maximum values will be for each of the three periods arbitrarily chosen in par. 6.

Let us suppose we want to know the distribution of the yearly maxima of a 66 year time interval. Curve G of fig. 2 gives "all" possibilities. We divide the absois of curve G into 66 equal parts. Each part corresponds on curve G with a value of h. Each value of h corresponds on line F with a value of m. Each of these values m can now be divided by the value of T, being 1 in this case. In this way every value of m leads to a corresponding value of N. Each value of N gives on the exceeding curve of fig. 1 a corresponding value of H, being the height of a stormflood at the gauge at Hook of Holland. The result of this calculation can easily be compared with the observations of 66 years. This has been done in an earlier publication (see 1). A perfect correspondance was found. In connection to this for the present investigation the calculated heights have been replaced by the observed heights. Fig. 3 part A presents the sequence of the observed yearly maxima of the period 1889-1954. The higher values are marked by a date.

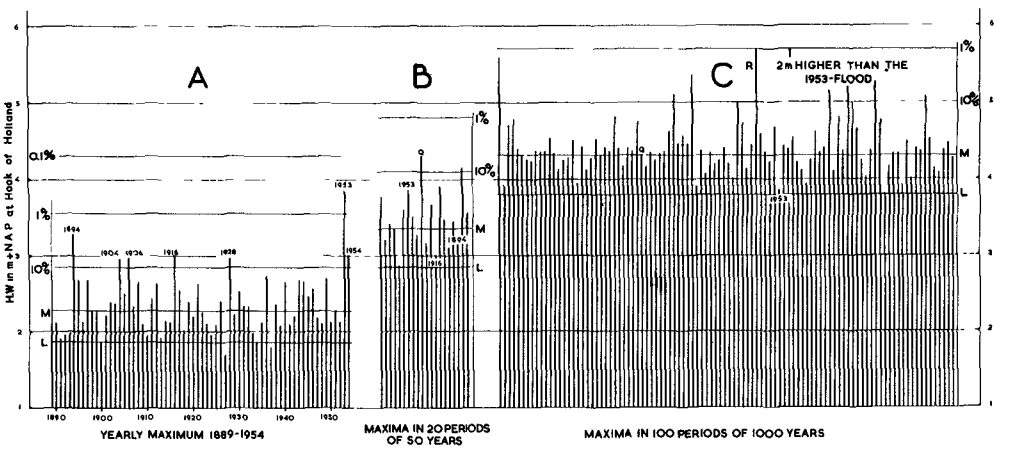

Fig. 3. The distribution of the maxima in periods of different lengths.

For the 50 years period we suppose that we want to know the most probable maxima of 20 periods. Dividing the abscis of ourve G into 20 parts we can read on curve G the corresponding twenty parameter height h and via curve F the corresponding values of m. After dividing each of the twenty values of m by 50 (T=50) we obtain twenty values of N. These values of N correspond in fig. 1 with 20 heights H. These heights are drawn in fig. 3 part B in an arbitrary order.
For the period of T = 1000 years we find after an identical prooedure part C of the diagram.
The diagram as a whole demonstrates clearly the distribution of the maxima. Such a distribution is always present, in the yearly maxima as well as in the maximum values in 50 year periods or in 1000 year periods.
This diagram illustrates the fact that a single maximum value is of little importance, which means also that the maximum stormflood, known by observation, is of little importanoe. It may be just a quite arbitrary choioe by nature out of the whole range of possibilities. If we adjudge any importance to such an "observed maximum stormflood" we probably are misleading ourselves and others.
For what is presenting itself to us as an absolute maximum, being the highest level we ever observed, may, after diagram 3, possibly be only quite a low maximum.

This important discussion oan be supported by pointing to fig. 3 B. This part of the diagram presents the most probable maximum height of 20 periods of each 50 years length. From observations we know 3 maxima of 50 years period, viz:

period 1850-1900 the 1894 flood is the highest one.
period 1900-1950 the 1936 flood is the highest one.
period 1950-2000 the 1953 flood will probably prove to be the highest one.

We have placed these three dates at the top of the three heights which are approximately the same as the three corresponding heights in fig. 3 A. From this we see, that the stormflood of 1936, being indeed a "very high flood" (in the opinion of observers of those days) and the maximum of a fifty years period, in reality has been only a low maximum for a period of that length. Even the disastrous flood of 1953, being in the one-year class an exoeptional flood, proves to be in the 50 years group only a NORMAL maximum.
Turning over now to part C of fig. 3, we see the height of 1953 as number three from the bottom. In a period of 1000 years there is 97% probability, that the highest value will be higher than the 1953 flood Thus part A shows the stormflood 1953 as a Gulliver among the dwarfs, but part C shows the same 1953 as a Gulliver among the giants. This demonstrates the importance of the length of the period T.

8. APPLICATION OF THE CLASSIFICATION, PROPOSED IN PARAGRAPH 5

From fig. 1 can be taken immediately the heights of L, M, 10%, 1% and 0,1% for 1, 50 and 1000 years periods. These figures are presented in table 1.

height	in the proper period	period of 1 year (A)	period of 50 years (B)	period of 1000 years (C)
L	nearly lowest maximum (m=5)	+ 185	+ 290	+ 380
M	most probable maximum (m=1)	+ 225	+ 335	+ 430
10%	upper limit normal maxima	+ 290	+ 405	+ 500
1%	upper limit remarkable maxima	+ 355	+ 480	+ 570
0,1%	upper limit exoeptional maxima beginning of extreme maxima	+ 430	+ 550	+ 640

Table 1. Characteristic heights of the periods A, B and C.

These heights have been marked in fig. 3. The practical value of the proposed classifioation can now easily be seen.
First the height L , computed with the exceeding value m=5. It is clearly shown that this height L indeed represents practically the lowest maximum height, to be expeoted in any given period. This applies as well to 1 year as to 50 or 1000 year periods.
As to M , the modus, charaoterized by the value m=1, fig. 3 shows, that this height is found not very far above L . The exact definition of M is that this height will be surpassed onee (as an average!) in a given period. From fig. 3 however we see, that this value is of little importance when we are looking for a design flood. Quite many floods (63%) are higher than M.
This unimportance of M may be stressed onoe more. In soientific litterature often expressions are used like "a hundred years flood" or "a thousand years flood". With such expressions is meant the height of a flood exceeded in that period once as an average. This is exactly the height M. The expression "a thousand year flood", however, gives the impression of an extremely high flood, not to be exceeded in 1000 years. This is misleading. There is 63% chance that the maximum height in 1000 year will be higher, possibly even to a large amount, as clearly shown in fig. 3.

We now oonsider the 10% height. This means 10% ohance of exceeding in a given period. From fig. 3 part A we used 66 observations. 10% of these values or about 7 will be higher than the 10% height. As such we see the maxima of the years:

1894 1904 1906 1916 1928 1953 1954 .

These 7 gales are well known in our oountry as "big gales". Nearly all of them oaused more or less serious damage. The stormfloods 1894, 1906, 1916, 1928, 1954 are known to the public and 1953 has a worldwide reputation.
It is important to point out, that none of these stormfloods of importance is below the 10% limit. All the storms below the 10% limit have aroused no great interest, are "normal" storms. This agrees with the philosophy of pragraph 5, where the olass between m=1 and m=0,1 has been oalled the class of normal stormfloods.
From the 7 floods mentioned above 6 are comprised between the 10% and the 1% limit. So all these floods belong to the class of "remarkable floods". This is in fair agreement with common parlance. All these floods are well known. The lower floods are unknown, they have not been remarkable.

From 1% to 0,1% we distinguished the zone of "exceptional floods". So in this nomenolature the disastrous flood of 1953 is an exoeptional flood for the one-year scope.
Floods above the 0,1% height have not been reoorded. Perhaps they have occurred in earlier centuries before the charaoteristic heights were registered.

This short discussion may show that the proposed classification is in fair agreement with common parlanoe. It shows moreover that the 10%, the 1% and the 0,1% limits are directly related to physioal realities, to facts.
It has to be borne in mind, that up till now we have been disoussing part A of the diagram. That is the series of annual maxima. It means, that all floods between M and the 10% height are to be oalled "normal" only in their quality as a n n u a l maxima. And the floods of 1894, 1904, 1906 etc. are to be called "remarkable floods" only in their quality as a n n u a l maxima. The big 1953 flood is an "exceptional flood" only in the sense of a maximum of one year.
From this we see, that the common nomenclature is olosely related to a one-year period. Human awareness of natural prooesses such as stormfloods may be called a one-year embraoing awareness. We appreoiate the violence of a stormflood only in relation to the very moment we are living in.
If we had to our immediate disposal an organ to embrace more than only the few days of our present living our soale of appreoiation would be another one. Fig. 3 part B shows what we should experience. In this part B the unit of time is 50 years.

The first important faot to be notioed is that the maxima of diagram B as a whole are muoh higher as those of diagram A. And the heights of L , M , 10% and 1% are higher just as well. (The 0,1% height has been omitted) The lowest maximum height L in graph B is exactly equal to the 10% for the one-year period, graph A. The three floods 1916, 1894 and 1953, being marked in diagram B, have already been discussed in paragraph 7 as being of less importance, in relation to 50 years periods.
In the class of remarkable floods (from 10% up to 1%) there is only one height present in B. It is marked Q and represents a stormflood 45 cm higher than 1953, whioh is an exoeptional flood in the one-year period. Relatively the flood Q oorresponds with 1916, 1928 and 1954 in the one-year period.
The oommunity as a whole is interested in a much longer period. This may be different from oase to oase, but for the convenienoe we introduced a period of 1000 years. Fig. 3 part C gives the answer to the question what may be the maximum height in the oourse of any 1000 years period. The zone between L and M shows the "lower" maxima for a 1000 years period. Up to + 500 (the 10% height) we find the "normal" maxima. Above this height there are another 10 "remarkable" maxima. The stormflood Q, being in diagram B a remarkable maximum in relation to a 50 year period, is in diagram C in relation to a 1000 year period a rather unimportant level, just equal to the mode M.
This disoussion may have illustrated that a olassification, based upon the exoeeding value m , applies to periods of every ohosen length. The classification oan be applied to any specifio gauge.

It is, however, immediately related to a given period. So one has to bear in mind the necessity to determine first of all from case to case the length of the period that has to be taken into account.

9. PERIOD AND RISK

It is quite usual to regard the frequency of stormfloods as a one dimensional quantity. The relation between level and frequency is very simple and direct. Only one frequency curve, as e.g. given in fig. 1, is sufficient to translate a height at a given gauge into an exceeding value vice versa.
In the preceding paragraphs, however, we have argued, that this simplicity is misleading. In reality the question of the highest values is a matter of t w o dimensions, i.e. p e r i o d a n d r i s k.
In order to explain this the one-dimensional fig. 1 has been transformed into a two-dimensional diagram: fig. 4.

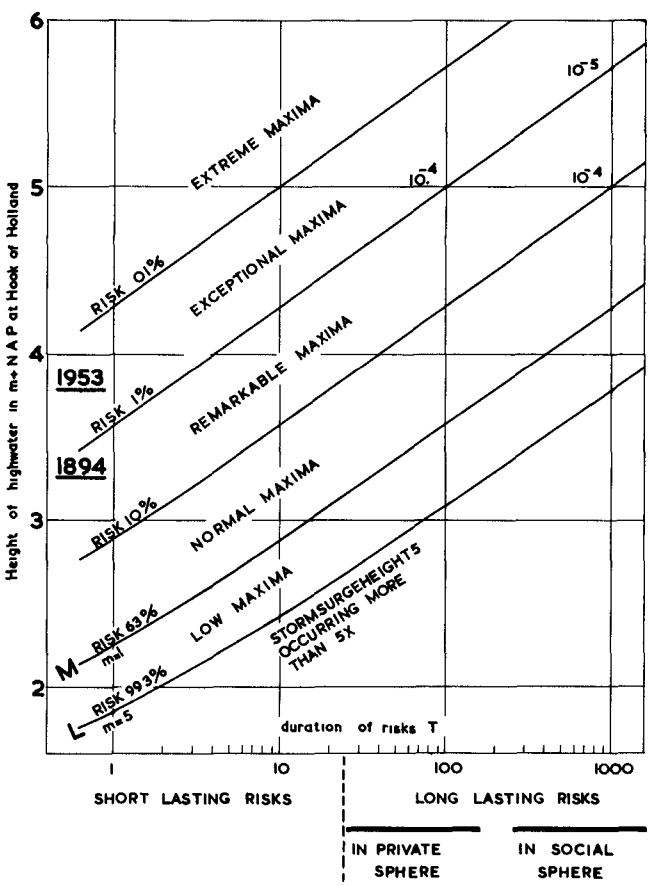

Fig. 4. Probability as a function of period and risk.

This diagram gives exactly the same as fig. 1. Yet the general impression differs considerably. The ordinate in fig. 4 gives the levels of highwater at the gauge at Hook of Holland, just as the ordinate in fig. 1.
The abscis gives on a logarithmic scale the length of the period T in years. This period T has to be regarded as the length of the duration of any risk. From 1 year or less up to 10 years or 25 years we may speak of "short lasting risks". From 50 years upward we could speak of "long lasting risks". These long lasting risks are divided into a "personal sphere" and a "social sphere". The longer periods are related to the social sphere.
The diagram shows 5 curves, respectively for $m=5$ (curve L), for $m=1$ (curve M), $m=0{,}1$, $m=0{,}01$ and $m=0{,}001$. Each height, given by these five curves can immediately be derived from fig. 1 by application of formula (1).
For curve M applies $m=1$. So $N = 1/T$ and since the scale of N in fig. 1 is identical to the scale of the inverse value of T in fig. 4, the curve M in fig. 4 is identical with the curve in fig. 1.
The curve L represents the "lowest possible maximum" for any period, given by the abscis. This curve is rising, as all the curves are, with increasing length of the period. This means that with increasing length of the period the lowest possible maximum height grows higher and higher.
Between the curves we find the classes, mentioned in paragraph 5. The heights, belonging to each of these classes, move upward as the period increases.
Proceeding horizontally from left to right we see, that a given level of highwater may be called "exceptionally high" for the abscis value 1 (one-year period). This applies to the stormflood 1953, marked in the diagram. The same level however is only "remarkable" for a 10 year period, only "normal" for a 100 year period and even "low" related to a 1000 year period.
This graph shows that when time passes on every high flood is loosing its importance more and more. Going through the diagram along a line of constant height, (it may be some important stormflood) from left to right, there will come a moment, that we cross the curve L. About that time we may be sure, that our initial height will be exceeded. If we cross the curve of 1% there is already 1% chance of being exceeded. If we cross the curve of 10% the chance of being surpassed by a higher flood is increased to 10% etc.
From this investigation it is clear that the design level depends upon two factors:

a) acceptable risk (m)
b) duration of the risk (T)

And though m and T are connected together by formula (1) to

$$N = \frac{m}{T}$$

and N is connected only to one definite height, to establish a suitable design flood diagram fig. 4 should be preferred above fig. 1. This may be emphasized once more in other words. To indicate a design flood as a flood, occurring once in its returnperiod, is misleading in a fourfold sense.

Firstly a very high flood does not return as such as shown in the diagrams of fig. 3. Secondly it is not a question of occurring of this particular height, but of exceeding it. Thirdly it is not exceeded "once" in the period T, but "as an average" it is exceeded once in that period. The main objection, however, is this. In relation to a design flood the so called returnperiod has no practical meaning. The height h_1, corresponding to the point M and the value $m=1$, which is being exceeded just once in the period T, is such a low maximum, that it has no use as a design level.
As a design level only $h_{0,1}$, $h_{0,01}$ or $h_{0,001}$ can be taken into consideration.
If we take, e.g.: $h_{0,01}$ as design level, we accept 1% risk of it being exceeded in a period of T years. This height $h_{0,01}$ corresponds with a value of N given by:

$$N = \frac{m}{T} = \frac{0,01}{T} = \frac{1}{100\,T}$$

So the inverse value of N, being traditionally named "returnperiod", is in our example a hundred times the period T.
Let T in a special case be 200 years. If we accept a risk of the design level being exceeded of 1%, then we have to take from the frequency curve a height with an exceeding value $N = 0,5 \times 10^{-4}$. This value has no relation with a "returnperiod" of 20000 years. A period of 20000 years does not really enter into the argument. So the use of the term "returnperiod" in this sense should be avoided.
In principle the seemingly one-dimensional exceeding value has to be translated into the product of the two-dimensional value of acceptable risk with the inverse value of the duration of the risk.
Therefore, if a design level has been established at a height, determined by $N = 10^{-4}$, one has to translate this into 1% risk in a 100 years period, (or 10% risk in a 1000 years period), but never as 100% risk (which means certainty) in 10000 years.

10. ON THE ESTABLISHMENT OF THE DESIGN LEVEL

The preceding investigation provides a basis to establish a design level for each particular case. What we have to do is:

1) establishing a frequency curve for the gauge in question, including extrapolation (par. 2 and fig. 1);
2) determining the period T, during which the risk is present continuously for the interests, taken into account (par. 6);
3) choosing an acceptable value for the total risk on serious damage during the period T (par. 5). The total risk should never exceed 10%; for life and well-being of thousands a total risk of 1% or even 0,1% has to be taken into consideration.

After having established in this way a provisional design level one may come to the conclusion, that the costs, necessary to realise the safety aimed at, are not in right proportion to the economic and human values to be protected. Here a second question may arise viz:

what càn we realise with the technical and economic means at our disposal in a special case.

Another important point may be kept in mind. If we have erecte a hydraulic construction with the design level arrived at and safety is fully guaranteed against stormfloods up to this level, this does not mean that we have to expect a total loss if the stormflood is only 1 cm higher. There is a margin between the first unimportant damag and the stormflood level which leads to total loss of the proteoted interests. Moreover there is in several cases, as for instanoe embank ments an extra freeboard against wave runup which includes a consider able reserve.

The Netherlands Delta Commission has taken this into account. This commission established $m = 10^{-4}$ as a basis for the design levels. But in fact safety is considered to be guaranteed up to a stormflood leve corresponding to $m = 10^{-5}$. This indeed corresponds with a risk on "total loss" of 1% in a 1000 years period.

For some islands of no great economic value and a not very dense popu lation the design level is lowered to about $m = 2$ to 5×10^{-4}.

Litt. 1)
P.J.Wemelsfelder. Wetmatigheden in het optreden van stormvloeden. De Ingenieur (Holl.), 1939, nr. 9.

HARINGVLIET

PART 4
DYNAMIC ACTION OF WAVES

FLUSHING SEA WALL

CHAPTER 34

ON THE STABILITY OF RUBBLE-MOUND BREAKWATERS

José Joaquim Reis de Carvalho* e Daniel Vera-Cruz*

Some comments are presented on different formulas suggested for the design of rubble-mound breakwaters and results of laboratory tests concerning the design of these structures are mentioned. Iribarren's formula (the one,on the verification of which,the largest number of studies has been carried out) is then critically analyzed in the light of the results of laboratory tests. The applicability of laboratory studies to actual cases is discussed.Finally some suggestions are presented regarding questions to be taken into account in future research, due to the numerous points on which information is still lacking, in spite of the considerable volume of work already achieved.

I - INTRODUCTION

Until the beginning of the second quarter of the present century, characteristics of rubble-mound breakwaters were determined by entirely empirical methods, although harbour engineers had been dealing with this problem for many centuries.As a rule, designers merely compared the case under study with existing structures,prescribing sturdier breakwaters when those located in shores with a similar exposure had not withstood the most violent storms acting on them.

The first empirical formula for breakwater design did not appear before 1933, but this and other similar formulas did not go beyond ordering and reducing the use of arbitrary methods in the choice of the elements making up the breakwater slopes more directly subjected to wave action; no sensible progress resulting therefrom for the design methods of these structures.It can even be stated that, due to the use of Iribarren's formula - the most widely used in Europe - which leads to the utilization of too heavy blocks placed in steep slopes (about 4/3), a tendency began to be observed in designers, towards a considerable reduction of these slopes.

Such a situation which, bearing in mind the knowledge available until about 10 years ago, was perfectly admissible, has been

* Assistant Research Engineer, Laboratório Nacional de Engenharia Civil, Secção de Hidráulica Marítima, Lisboa (5), Portugal.

subjected to considerable changes thanks to: 1) the enormous advances achieved in the theoretical field, which placed our knowledge on the majority of Maritime Hydraulics subjects on a satisfactory level; 2) the invaluable help of small scale model tests, and 3) our improved knowledge on natural phenomena which makes possible a comparatively satisfactory estimate of the characteristics of the waves to be anticipated at any point of the coast.

We have merely to persevere along the route followed in the latter years in order to determine more accurate values for the coefficients of the available formulas, representing the results obtained by means of graphs and tables, resorting for that purpose both to model tests and to a careful observation of the behaviour of completed structures throughout the world, above all those which underwent damages. On the other hand efforts should not be spared in concentrated attempts to discover new formulas as phenomena are, no doubt, much too complex in the destruction of a breakwater to allow of a single satisfactory schemetization.

It should be borne in mind that, in spite of the laboratory tests recently carried out, our knowledges is limited to the area directly affected by the wave breaking and so a total knowledge of the stability of rubble-mound breakwaters lies still a long way ahead.

II - EMPIRICAL FORMULAS

The first formula for the design of rubble-mound breakwaters was presented in 1933 by the Spanish engineer Eduardo Castro [1] :

$$W = 0.704 \frac{H^3 s}{(\cot\alpha + 1)\ (s-1)^3 \sqrt{\cot\alpha - \frac{2}{s}}} \qquad (1)$$

where

W = weight of individual armor units in metric tons
H = wave height in meters
s = specific gravity of armor units
α = angle of breakwater slope measured from the horizontal

The preceding formula was based on the following theoretical assumptions: the destructive action of the wave is proportional to its energy, hence, the height of storm waves being proportional to their lenght, the energy of the waves is proportional to H^3; the weight of a unit required to resist the action of a given wave is directly proportional to its density in the air and inversely proportional to the cube of its density in water; the stability of the units under wave action is inversely proportional to a function of the angle of slope.

This formula, yielding small values for W and making the angle of repose dependent on the specific gravity of the armor units, goes against what is known in Soil Mechanics. Harbour engineers rejected this formula which, as far as we know, remained without practical application.

The second formula, which is also due to a Spanish engineer - Prof. Iribarren Cavanilles -, is of particular interest, being in systematic use in Portugal since 1946. The formula was presented for the first time in 1938 [2] under the form:

$$W = K \frac{H_b^3 s}{(\cos\alpha - \sin\alpha)^3 (s-1)^3} \qquad (2)$$

where, maintaining the above notations:

H_b = breaking-wave height, which can be determined by a method described in Iribarren's papers
K = 0.015 for quarry-stones
K = 0.019 for artificial blocks

According to the author [3], the following formula can be used when the water depth d at the toe of the structure does not exceed 0.06 L, L being the wave length:

$$W = K \frac{H^3 s}{(\cos\alpha - \sin\alpha)^3 (s-1)^3} \qquad (3)$$

where:

H = wave height in the absence of the structure
K = 0.023 for quarry-stone
K = 0.029 for artificial blocks

In 1950, Iribarren [4] generalized his formula so as to make possible its application in the design of underwater slopes.

According to this generalization, the design of breakwaters is also possible for slope elements at water depths exceeding H_b, by replacing H_b in formula (2), by

$$H' = H_z \frac{\frac{2\pi H_z}{L}}{\sinh \frac{2\pi z}{L}} \qquad (4)$$

where:

Z = crown depth of the breakwater portion, the characteristics of which are to be determined
H_Z = wave height at depth Z

Iribarren's original and modified formulas having aroused a deep interest in harbour engineering circles, they shall be present

ed and discussed in detail below.We would emphasize, nevertheless, that this formula is similar to Castro's from which it only differs by the coefficient and by the function which takes into account the influence of the angle of slope. This is in fact the case with almost all the existing formulas.In addition,the application of this formula to steep slopes yields very high values for the weight of the armor units which, in the majority of cases,prevents the adoption of these slopes.This is the negative aspect of the formula which, as shall be seen below,disagrees most widely from nature in the range of steep slopes (near 1/1).

An analysis of the coefficients indicated by the author also shows that, all other factors being equal, the weight of the armor units required for a given breakwater is higher for artificial blocks than for quarry-stones which,as shall be seen below,is quite contrary to the facts observed in laboratory tests.

The coefficient K = 0.015 and K = 0.019 were determined by Iribarren from an analysis of the damages suffered by the breakwaters of Orio (quarry-stone) and San Juan de Luz (artificial blocks).The fact that the values of these coefficients were confirmed by a sole breakwater for each type and some peculiar conditions in both breakwaters (shallow depths at the toe as compared with the maximum wave heights attacking the structures and nature of the bottom), seems to indicate that the coefficients thus determined can at best apply to breakwaters in similar conditions. Consequently the author's generalization of his formula could only be confirmed by chance. In fact, K varies very widely with the different factors influencing the phenomenon.

Not before 10 years had elapsed after the presentation of Iribarren's formula did the problem begin to arise a wide interest in American engineers who, in a short time, proposed several formulas to solve the problem. In 1948, Mathews [5] of the Los Angeles District Corps of Engineers submitted a formula for discussion which, with the notations above, can be written thus:

$$W = 0\,00149\,\frac{H^2 T\, s}{(\cos\alpha - 075\,\sin\alpha)^2 (s-1)^3} \qquad (5)$$

where

T = wave period in seconds.

At the International Navigation Congress held in Lisbon in 1949, the American engineers Epstein and Tyrrel [6] presented the first results of their theoretical researches on rubble-mound breakwaters, which can be represented by the formula

$$W = K_t\,\frac{H^3 s}{(s-1)^3\,(\mu - \tan\alpha)^3} \qquad (6)$$

where

K_t = a function of α, μ and d/L including three additional coefficients defined as functions of the armor unit size

μ = coefficient of friction stone on stone, practically equal to unity

The authors suggested laboratorial tests for determining K_t and its variation with the different parameters.

At the Conference on Coastal Engineering, held in Long Beach in 1950, F.W. Rodolf [5] of the Portland District Corps of Engineers presented a formula, based on the observation of hydraulic operations carried out in gold mines, which can be written as follows using the previous notations:

$$W = 0.0162 \frac{H^2 T s}{\tan^3 (45 - \frac{\alpha}{2}) (s-1)^3} \qquad (7)$$

According to the author, the formula has a small coefficient of safety in order to take into account any wave eventually higher than the highest wave considered.

Finally in 1952, another formula was developed by the French engineer Larras [7], based on the century-old experience of the breakwaters of Algiers. This formula has the following expression in the preceding notations:

$$W = \frac{H_o'^3 s}{(\cos\alpha - \sin\alpha)^3 (s-1)^3} \times \left[\frac{\frac{2\pi H_o'}{L}}{\sinh \frac{4\pi z}{L}} \right]^3 \qquad (8)$$

where:

H_o' = deep water wave-height

K_o = 0.0152 for quarry-stone

K = 0.0191 for artificial blocks

For breakwaters directly subjected to the wave breaking, the author recommends to take $Z = H_o'/2$.

As already pointed out in different articles on the subject [8], both the expression above and the coefficients indicated by the author coincide with Iribarren's formula and coefficients, with only a difference, namely that Larras considers the wave-height in deep water, thus leading to lighter armor units forthe breakwater.

Before the results of model tests were available, attempts were undertaken to verify the reliability of the different formulas and especially their coefficients, by comparison with the break-

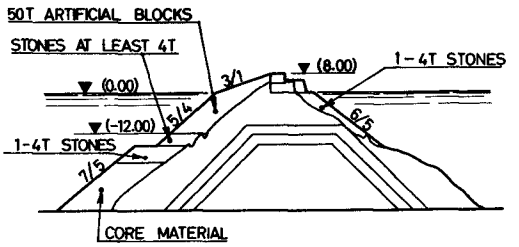

Fig. 1. Cross section of north breakwater of Algier Harbour.

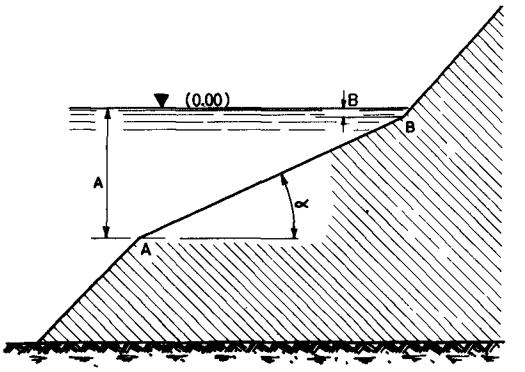

Fig. 2. Characteristic profile of equilibrium of a rubble-mound.

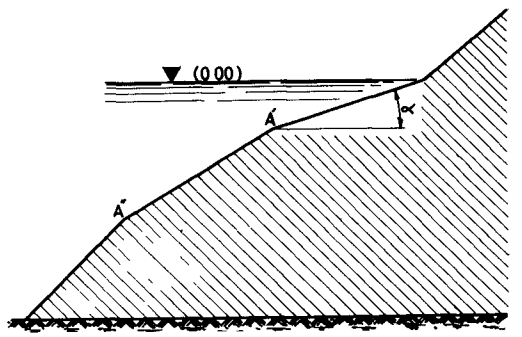

Fig. 3. Profile of equilibrium of a rubble-mound.

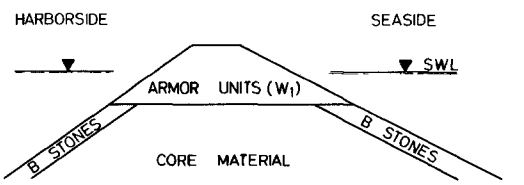

Fig. 4. Section of the rubble-mound breakwater tested in W.E.S.

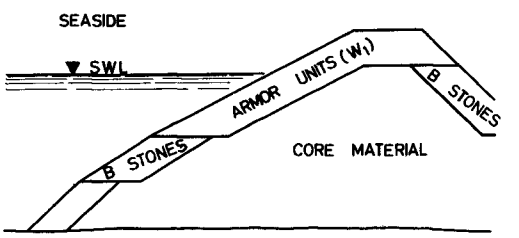

Fig. 5. Usual section of a rubble-mound breakwater.

waters of Algiers harbour, chiefly the northern pier, the behaviour of which after being reinforced in 1933 (fig. 1) had been excellent notably during a storm in February 1934 in which it withstood, without serious damage, the attack of waves 9 m high.

From Hickson and Rodolf's comparison [5], between Iribarren's, Rodolf's, Mathews's and Castro's formulas and the slopes of the Algiers breakwaters deemed stable by Larras and Collin [9] and Iribarren [10], it was concluded that the values supplied by Iribarren's and Rodolf's formulas showed a perfect agreement with the stable slopes of Algiers breakwaters, whilst the values of Mathews's and Castro's formulas, although agreeing with one another, led to considerably steeper slopes (3.18/1 and 3.51/1 according to Rodolf and Iribarren, against 2.19/1 and 2.22/1 from Mathews's and Castro's formulas). As shall be seen later, this comparison with the slopes deemed stable of the Algiers breakwaters which had such a considerable influence on the wide acceptance of Iribarren's formula, had not the value then ascribed to it. In fact, subsequent model tests showed that comparatively reduced forces acted on the breakwater portion where the wave attack had been assumed to be strongest.

III - MODEL TESTS

The difficulties experienced by harbour engineers in the analysis of the different formulas based on the observed behaviour of breakwaters throughout the world; the impossibility of taking into account the influence of the different parameters which influence the stability of rubble-mound breakwaters; and above all the enormous advantages of model tests for improving our knowledge on the influence of each parameter, led to detailed laboratory tests on this problem, among which should be emphasized those carried out by the Waterways Experiment Station and by the Laboratoire de Neyrpic.

1) CHARACTERISTIC PROFILE OF EQUILIBRIUM

In the majority of cases studied at the laboratory, the profile of equilibrium of a homogeneous mound (the components of which undergo practically no displacements under the action of the waves) presented the shape indicated in fig. 2. This is a rather common shape called "characteristic profile of equilibrium" by Beaudevin [11]. As can be seen, the active zone of the breakwater, AB, extends practically from the still-water level down to a depth A ranging from 1.2 H and 1.6 H (mean value 1.3 H). It is in this zone that the influence of the different parameters has been studied in laboratory tests.

Below point A, the slope is approximately equal to the angle of repose in still water. Above point B the slope is often steeper

than the angle of repose of the material [12] . This polygonal-line profile is always found, in its broad lines, whatever the material and the characteristics of the waves. Only angle α of zone AB with the horizontal, and the depth at point A (lower end of zone AB) are variable [11] .

The shape of the "characteristic profile of equilibrium"seems to indicate that, whenever the depth at the base of the slope exceeds 1.3 H, the influence of the depth is probably small.

This was indeed confirmed by the tests so far carried out in France [11,12] and U.S.A. [13] . This influence is not felt until the depth decreases beyond 1.3 H (that is the elevation at which the bottom intersects zone AB) but grows even together if the nature of the bottom allows under-toe sand scouring. It is noteworthy, as Miche observed in the discussion of Beaudevin's article, that 1.3 H is the breaker depth.

It also results from the shape of the "characteristic profile of equilibrium" that Iribarren's and Rodolf's comparisons of their formulas and coefficients with the slopes of Algiers breakwaters is not entirely correct since they took as active zone of the breakwater the portion above the hydrographic datum, which has a slope of 3/1, instead of considering, as the shape of the "characteristic profile of equilibrium" indicates, the zone between the hydrographic datum and a depth of 12 m, where the slope is 5/4 (fig. 1).

The comparison is further invalidated by the fact that during very violent storms the breakwater is often overtopped and stability conditions as the seaside face of a breakwater improve when this is overtopped.

But, even if this fact is neglected, a comparison of the slopes of the Algiers breakwaters (bearing in mind the results of the model tests) with the values supplied by Castro's, Iribarren's, Mathews's and Rodolf's formulas for the storm of February 1934, shows that the slopes obtained (respectively 2/1, 3/1, 1.95/1 and 2.75/1) are considerable gentler than the slope at the active zone of the breakwater. Hence the conclusion that the coefficients recommended by the different authors are much too high, at least for steep slopes; in other words, even if the formulas are reliable for certain values of the slope, the values yielded undergo very considerable changes with the variation of the angle of slope with the horizontal. For instance, whereas Iribarren indicates a value of $K = 0.019$ for breakwaters of artificial blocks, this coefficient for a 5/4 slope should be, at most, $K = 0.00036$, i.e. 52 times smaller, according to the Algiers breakwater.

Besides the variation of Iribarren's coefficient K with the angle of slope, this disagreement seems to indicate a marked influence of an overtopping by the highest storm waves on the stability of the seaside face of the breakwater.

2) INFLUENCE OF DIFFERENT PARAMETERS

a) Specific gravity of the armor units - The main purpose of the tests carried out at different laboratories was to study the validity of the existing formulas. Firstly the influence of different parameters on the weight of the armor units to be used at the active zone of a breakwater was investigated.

Practically all the authors admit that the influence of the specific gravity should be expressed by a term $s/(s-1)^3$. According to the first tests carried out in Grenoble [12], this law did not seem quite acceptable but no final conclusion could be reached due to the dispersion of the data points and the limited number of specific gravities studied. Nevertheless, subsequent tests carried out at the Waterways Experiment Station and also in Grenoble (although their primary purpose was different) showed that the law seemed quite valid.

Taking into account that the specific gravity of sea water, s_o, is different from unity, the preceding expressions becomes $s.s_o^3/(s-s_o)^3$ which leads to an increase of about 10 to 15% in the weight of the armor units [12].

b) Wave-height - All the formulas, except Mathews's and Rodolf's, assume that the influence of the wave-height should be expressed by a law of the type $W = NH^3$.

Even the two exceptions noted above, in which a law of the type $W = NH^2T$ is assumed, yield for actual cases a variation of the type $W = NH^3$, since during storms, the wave-height and the period change, as a rule, in the same sense. Observations carried out for a period of 5 years in the Portuguese coast supplied for the ratio wave-height/wave period during storms an approximate value, $T = 2.5\ H$ (in which T is expressed in seconds and H in meters) which is the same that was used in fig. 6, based on Mathews's and Rodolf's formulas.

Tests carried out at different laboratories have fully confirmed the law derived from the existing formulas.

As regards the influence of the wave-height on the "characteristic profile of equilibrium", tests carried out in Grenoble [11], showed that, for wave-heights below a certain value, the profile has the shape indicated in fig. 2, the lower point A lying at a depth proportional to H, as previously explained.

For wave-heights exceeding the value in reference, the profile presents the shape indicated in fig. 3.

c) Period - According to the tests so far carried out in order to investigate the influence of this parameter, a wave is all the more dangerous the smaller its period although, on the whole, this influence is never considerable [11]. This shows that Mathews's and Rodolf's formulas are incorrect as, for the same wave-height, they yield increasing weights for the armor units when the period

increases.

It was further concluded that, for characteristic profiles with the shape indicated in fig. 3, the depth A' depends on the wave period, whilst depth A" depends on the wave-height only [11].

d) Depth in front of the structure -In the tests carried out at the different laboratories, the depth at the toe of the break water was always large as compared with the wave-height [12,13,14], hence rather larger than the depth at point A of the "characteristic profile of equilibrium". Thus no influence of the depth could be detected. Nevertheless, a few preparatory tests carried out at the Laboratório Nacional de Engenharia Civil with depths approaching A showed a marked influence of this parameter. Other tests are under way in order to study this influence in detail. Tests carried out at the Waterways Experiment Station concerning a breakwater for Narwiliwili harbour have also shown the enormous influence of the relative depth d/L and of the wave steepness H/L on the stability of the structure for waves breaking directly on the breakwater slope.

e) Shape of the armor units - Blocks of different shapes have been considered in the tests so far carried out: quarry-stones, cubes, tetrapods, tribars, besides other shapes less common in practical cases. The tests showed a very marked influence of the shape although the stability curves for the different types of blocks can be approximately derived from anyone of them by affinity.It is thus possible to characterize each shape means of a constant parameter[11].

One of the main conclusions drawn from the first tests carried out, was that cubic blocks were better than quarry-stones with respect to stability, contrary to Iribarren's and Larra's deductions for their formulas.

Tests carried out in Grenoble in 1953 showed that quarry-stone with a weight 3 W would be required to supply the same stability as cubic blocks of weight W, but more numerous tests in 1955 corrected the above ratio to 2/1 only. This difference is due to the fact that cubic blocks with slightly rounded edges were considered in the second case. This assumption shoul be nearer to the actual phenomenon, as cavitation is observed in model tests near the edges of the blocks in the active zone of the breakwater.

The tests at the Waterways Experiment Station concerned,above all, the behaviour of quarry-stones, tetrapods and tribars [15] , but very few tests were carried out regarding cubic blocks.

The ratio between the weights of quarry-stones and tetrapods required to ensure the same stability was verified to be about 2.6. A comparison of these tests with those carried out in Grenoble shows that tetrapods and sharp-edged cubes have a similar stability, which slightly exceeds the stability of cubes with rounded edges, as was confirmed by the tests of Funchal harbour [16] .

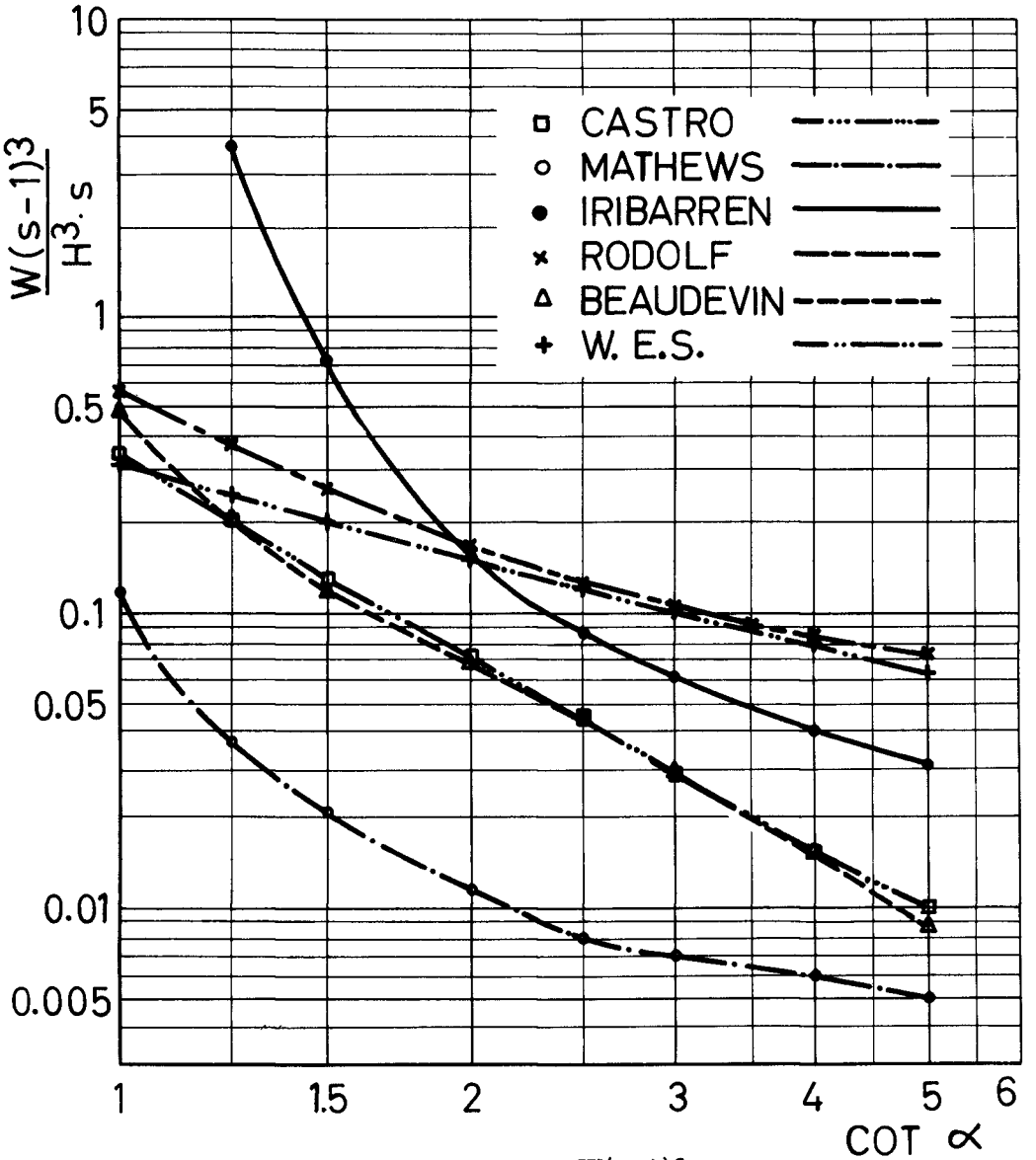

Fig. 6. Variation law of the parameter $\frac{W(s-1)3}{H^3 .s}$ with α, based on the following assumptions:

(a) In Iribarren's formula μ = 1 and K = 0.015;
(b) In Castro's formula s = 2.5:
(c) In Rodolf's and Mathew's formula T = 2.5 H, T being in seconds;
(d) In Beaudevin's formula K = 0.10;
(e) In all formulas H is expressed in meters and W in metric tons.

Quarry-stone cover layers being made up, in actual cases, of units with different weights ranging between comparatively narrow limits, tests were carried out in Grenoble in order to study the stability of these structures.The results showed that "the characteristic weight" of the quarry-stones is equal to or greater than the mean weight.

It was even observed that, in some cases, the stability of the mixed quarry-stone exceeded the stability of the heavier component blocks. Nevertheless, in practical cases it is recommended to take as characteristic weight of a given type of quarry-stone the mean weight of the type in reference. In the great majority of cases, a comparatively small safety factor is thus secured [11] .

3) FORMULAS OBTAINED FROM LABORATORY TESTS

When attempts began to study the stability of breakwaters by means of laboratory tests, the first problem to be solved consisted in determining up to what extent the conclusions drawn from the model tests could be applied to actual structures. For that purpose, an extensive program of basic research was undertaken at the Waterways Experiment Station which showed that Froude's law applied to all the phenomena which take place when waves attack a rubble-mound breakwater. Besides a comparison of the results obtained on models built at different scales,the program included a comparison of the damages undergone by completed breakwaters with the damages observed in models of those structures when subjected to the waves responsible for the actual damages. This comparison, the results of which were decisive for the acceptance of model test studies on the stability of rubble-mound breakwaters,showed a remarkable agreement between the behaviour of models and prototypes [13] . Analogous tests with the same purpose carried out in Grenoble yielded the same results [17] , what proves that this practical and serviceable tool -small scale models - is quite reliable in the study of these complex problems. Nevertheless, tests are under way at the Beach Erosion Board with a view to studying the influence of Reynolds's number, i.e. the scale effect. The results seem to show that there is indeed a certain scale effect which, at the usual scales, yields rather conservative results, a certain margin of safety being thus secured.

The research program of the Waterways Experiment Station was then extended so as to include the determination of the most adequate design-formula. In the first place, the validity of the existing formulas, in special Iribarren's and Epstein-Tyrrel's was investigated.These and, to a smaller extent, the preceding tests,imply the consideration of a "criterion of stability" which is a very important factor in the conclusions of tests of this type. In the first series of tests [13] , the design-wave height considered was slightly less than that required to move any of the armor stones of

stones of the breakwater. Based on this so-called "no-damage" criterion, the conclusion was reached that Iribarren's formula is the most suited to the test results, although the coefficient K varied to a considerable extent with the angle of the breakwater slope measured from the horizontal. This comparison was preceded by a slihgtly theoretical study which had the purpose of making Iribarren's formula dimensionally homogeneous. The formula then becomes

$$W = K \frac{H^3 \gamma_r \gamma_f \mu^3}{(\mu \cos \alpha - \sin \alpha)^3 (\gamma_r - \gamma_f)^3} \qquad (9)$$

where:

H = wave height at the breakwater toe
μ = tangent of the angle of repose of armor units
γ_r = specific weight of armor units
γ_f = specific weight of water

Other tests were carried out with a different criterion. The wave was allowed to move some of the units but not, however, to induce sensible changes in the breakwater.

By means of this so-called "slight-damage" criterion, it was concluded that breakwaters designed according to the preceding criterion could withstand the attack of waves 50% higher than the design-wave, without undergoing serious damage.

This led the Waterways Experiment Station to modify his "no-damage" criterion which was too severe, as the fall of a few units is not due, as a rule, to deficient stability of the breakwater but to the fact that these units were placed in a peculiarly unstable position during construction.

In the subsequently adopted "no-damage" criterion, the design-wave height has a value which can induce some damage but the number of armor stones moved shall not exceed 1%.

Based on the modified criterion, a new series of tests was carried out at the Waterways Experiment Station. From the conclusions obtained, presented by Hudson [14], a new design formula resulted for this type of breakwater:

$$W = \frac{H^3 \gamma_r}{K_D (s_r - 1)^3 \cot \alpha} \qquad (10)$$

where:

K_D = coefficient depending on the percentage of damage with values:
$K = 3.2$ for quarry-stones (no damage)
$K = 8.3$ for tetrapods (no damage)
$s_r = \gamma_r / \gamma_f$

The introduction of this objective numerical criterion was one of the major improvements achieved in model tests studies of stability of rubble-mound breakwaters. Nevertheless, the test section adopted in the W.E.S. for quarry-stone breakwaters (fig. 4) is not the most usual in structures of this type. In fact (fig. 5) armor units are normally placed in two or three layers instead of making up a mound. So, it is likely that, even if the results applying to the "no-damage" case may be the same, they are not correct as regards to the tests for determining the safety factor in "damage" cases. It is in fact possible that in many actual cases the structure would collapse for values of $H/H_{D=0}$ which in the tests carried out at the W.E.S. induced damages of only 15% to 40%.

Iribarren's formula was abandoned in the W.E.S. tests due to the fact that the influence of the angle of slope, according to this formula, disagreed very sharply with the experimental results. Accurate values of the friction coefficient of the different materials were also extremely hard to obtain in the laboratory, which led to a wide variation of coefficient K [14] .For all these reasons, it was decided to adopt another formula, presented in (10). As regards to form, this formula is apparently not altogether correct, as it omits the angle of repose of the armor units but, on the other hand, it presents the enormous advantages of containing a coefficient K_D depending exclusively on the type of armor unit, and of being very easy to handle since the function expressing the influence of the angle of slope is very simple.

Another research program on the stability of rubble-mound breakwaters by means of model tests was also carried out in Grenoble, at the Laboratoire Dauphinois d'Hydraulique. Another stability criterion was used: the wave was allowed to model a profile of equilibrium in a homogeneous mound of the armor units to be studied. This was the "characteristic profile of equilibrium" since, according to the tests, it was stable for wave-heights not exceeding the height of the wave that had shaped it but unstable for wave-heights above that value [11] under the action of which, fall of blocks were observed. Some units can be unstable on the breakwater, undergoing alternate movements with the same period as the wave [12].

From these tests the following practical formula was obtained

$$W = K \frac{H^3 s}{(s-1)^3} \left(\frac{1}{\cot \alpha - 08} - 015 \right) \qquad (11)$$

The tests supplied the following values for K

K = 0.10 for slightly rounded quarry-stones
K = 0.05 for cubes with slightly rounded edges

Grenoble recommends a safety factor of 2.5, the values of K

being then

K = 0.25 for quarry-stones
K = 0.12 for cubes

The same tests also showed that, in order to avoid the blocks being moved along by oblique waves, an additional condition must be introduced, with which "absolute stability" is achieved. This condition is given by the expression:

$$W > K' \frac{H^3 s}{(s-1)^3} \qquad (12)$$

where

K' = 0.03 for quarry-stones

Making K = 0.25 in formula (11), this condition is fulfilled for breakwater slopes steeper than 9/2, that is practically for all breakwaters used in actual cases.

IV - COMMENTS ON THE EXISTING FORMULAS

A comparison of the different formulas presented shows that the main difference between them lies in the type of function used to express the influence of the breakwater slope. In fact the term $\frac{W (s-1)^3}{H^3 s}$, can be said to be common to all the formulas. Even in Mathews's and Rodolf's expressions, the influence of the characteristics of the wave can be expressed by H^3 by taking, as explained above, T = 2.5 H which seems to agree with observed phenomena.

The variation of this term in the function of the breakwater slope, as obtained from the different formulas, is shown in fig. 6.

For Beaudevin's formula, a value K' = 0.10 was taken which corresponds to the value directly obtained from the tests, that is without safety factor.

The differences observed between the test results obtained at the W.E.S. and in Grenoble are due to the different stability criteria used and to the design-wave height adopted at the W.E.S. In the way the tests were carried out at the W.E.S., the breakwaters were not subjected to the action of a uniform-height train of waves as in Grenoble, but to a succession of waves, the first and the last of which were higher than the others due to the starting and stopping of the wave generator. Because these waves have an obvious influence on the breakwater stability, the "significant height" of the train of waves attacking the breakwater was the wave height

selected for the final calculation of the results.

Nevertheless, the differences between the parameters of wave trains in nature,on the one hand,and the same parameters as analysed in the laboratory are enormous [14] and this fact should be borne in mind in the choice of the design-wave height and of the safety factor.

For almost every type of breakwater, the W.E.S.formula yields values exceeding those obtained in similar conditions by means of Beaudevin's formula,although its variation with the angle of slope is not so marked.In fig. 6,these curves intersect for an angle of slope between 1/1 and 5/4; the value supplied by Beaudevin's formula for a slope of 45 deg exceeding the value obtained from the W.E.S. formula.

This is due to the fact that the functions expressing the influence of the angle of slope were obtained from tests on slopes not steeper than 5/4,at the American laboratory,and of about 4/3, in Grenoble. The extrapolation for steeper slopes and even the results obtained for limit values of the angle of slope may not entirely agree with the actual behaviour of very steep slopes.Nevertheless, taking into account that the stability criterion adopted at the W.E.S. is better suited to actual conditions, it seems preferable, in practical cases, to use the American formula.

As shown in fig. 6, Mathews's formula is obviously deficient yielding weights W for the armor units much below the values obtained in the Grenoble and W.E.S. tests and so its use, even with a high safety factor, should be discontinued. On the other hand, as already pointed out by Barbe and Beaudevin [12] , the values determined from Castro's formula for $s = 2.5$ entirely agree with the results obtained in the tests on rubble-mound breakwaters carried out in Grenoble. This thus means that by the way the tests were carried out in Grenoble, the values supplied correspond to rather peculiar limit conditions of stability and so, as indicated by Barbe and Beaudevin, Castro's formula may be used with a safety factor of no less than 2.5.

As for Rodolf's formula, provided that, as previously indicated, a value $T = 2.5\ H$ is taken, the figure indicates that, for slopes gentler than 2/1 the values supplied slightly exceed those of W.E.S. formula; whilst for steeper slopes the values disagree more strongly with the results of the American tests. This means that, for gentle slopes, the safety factor can be slightly above unity, its value increasing as the slope becomes steeper, reaching 1.5 for a 5/4 slope and about 1.6 for an angle of 45 deg,which agrees with what the author had in mind. An increase of the safety factor seems admissible since damages are much more dangerous in very steep than in gentle slope breakwaters.

All these comments above refer to quarry-stone rubble-mound breakwaters as, apart from the formulas obtained from laboratory tests, only Iribarren and Larras indicated coefficients for arti

ficial blocks which, however, by no means express the differences observed between stability conditions in quarry-stone and in artificial block breakwaters.

Comments on Iribarren's formula are presented below in greater detail, due the wide acceptance of this formula in harbour engineering circles. These comments apply, to a certain extent, to Larras's formula as this and its coefficients expressing the influence of the shape of armor units coincide with Iribarren's formula and coefficients.

V - COMMENTS ON IRIBARREN'S FORMULA

Iribarren's formula presented in II is the most widely known and used both in designs (notably in Europe) and in test verifications. In fact, although the formula

$$W = \frac{K\,\gamma_r\,\gamma_f^3\,H^3\,\mu^3}{(\mu\cos\alpha - \sin\alpha)^3\,(\gamma_r - \gamma_f)^3} \qquad (13)$$

has been in use for all values, both steep and gentle, of the breakwater slope, there is another formula by the same author

$$W' = \frac{K'\,\gamma_r\,\gamma_f^3\,H^3}{(\mu\cos\alpha - \sin\alpha)^3\,(\gamma_r - \gamma_f)^3} \qquad (14)$$

recommended for steep slopes for which, however, the value of K' is unknown. In the present chapter only the first formula will be discussed, because, as shall be seen below, it is possible to adopt this formula to any breakwater slope gentle or steep, and so it is unnecessary to take the second formula separately into account since, for $K' = K\,\mu^3$, it becomes equal to the first.

Before analysing the formula more in detail, let us summarily pass in review the conditions in which Iribarren adopted the value of K, which he assumed constant for any breakwater slope.

This coefficient was obtained from the damages observed in a sole breakwater, which is obviously insufficient. On the other hand, the wave-heights were not observed but merely calculated from theoretical considerations of the water depths near the structure, which also correspond to very particular conditions. In fact, for a sandy bottom, the water depth is practically zero for the lower low water and about 4.5 m for the higher high water. These conditions are indeed extremely peculiar both as regards the depth and the nature of the bottom on account of not only the influence of the relative depth on the form assumed by the wave breaking but also of the considerable increase in the specific gravity of sea water due to the bottom sand in suspension.

Another doubtful point Iribarren's formula is the coefficient μ. According to Iribarren this parameter, definied as the coefficient of friction stone on stone, is very nearly equal to the slope of the angle of repose for quarry-stones (i.e.unity) and, by taking $\mu = 1$, Iribarren believes that an adequate safety factor is introduced in the formula. Admitting Iribarren's assumption that μ is practically the slope of the angle of repose for quarry-stones, the value of this angle remains to be determined. Attempts to measure it in laboratory tests yield widely differing values. Thus, laboratory tests carried out at the Waterways Experiment Station have furnished values ranging between 1.06 and 1.18. Nevertheless even assuming that a real value of μ, say $\mu_r > 1$, could be defined and determined, it would be neoessaryto know the value of the safety faotor whioh, according to Iribarren, is secured by taking $\mu = 1$. Some comments are presented below regarding this subject.

1) COMMENTS ON COEFFICIENTS K AND μ OF THE FORMULA

$$W = \frac{K \gamma_r \gamma_f^3 H^3 \mu^3}{(\mu \cos \alpha - \sin \alpha)^3 (\gamma_r - \gamma_f)^3}$$

In the first place let us accept Iribarren's assumption in whioh K is constant for any value of the breakwater slope. Let K_1 be the value of the constant for $\mu = 1$ and K_r for $\mu = \mu_r$. Bearing in mind the conditions α_o, γ_o, H_o and P_o, for which Iribarren calculated K_1, by taking $\mu = 1$, it is obvious that no safety factor is introduced as regards the use of the formula with $K = K_r$, by taking $\mu = \mu_r$.

Let us consider an angle of slope approximately equal to the value used by Iribarren in the determination of the coefficient for quarry-stones breakwaters, i.e. $\cot \alpha_o = 3.0$. For $\mu = 1$, the formula becomes

$$W_1 = \frac{K \gamma_r \gamma_f^3 H^3}{(\cos \alpha - \sin \alpha)^3 (\gamma_r - \gamma_f)^3}$$

and for $\mu = \mu_r$

$$W = \frac{K_r \gamma_r \gamma_f^3 H^3 \mu^3}{(\mu_r \cos \alpha - \sin \alpha)^3 (\gamma_r - \gamma_f)^3}$$

hence

$$\frac{W_1}{W_r} = \frac{K_1}{K_r} \quad \frac{(\mu_r \cos \alpha - \sin \alpha)^3}{\mu_r^3 (\cos \alpha - \sin \alpha)^3}$$

As $W_1 = W_r$ for $\alpha = \alpha_o$, it follows that

$$\frac{K_1}{K_r} = \frac{\mu_r^3(\cos\alpha_o - \sin\alpha_o)^3}{(\mu_r\cos\alpha_o - \sin\alpha_o)^3}$$

Consequently, the ratio W_1/W_r for any value α is

$$m = \frac{W_1}{W_r} = \frac{\mu_r^3(\cos\alpha_o - \sin\alpha_o)^3}{(\mu_r^3\cos\alpha_o - \sin\alpha_o)^3} \quad \frac{(\mu_r\cos\alpha - \sin\alpha)^3}{\mu_r^3(\cos\alpha - \sin\alpha)^3}$$

The ratio m would be the safety factor introduced by taking $\mu = 1$ instead of $\mu = \mu_r$.

In order to give an idea of the variation of m with α, let us take $\cot\alpha_o = 3$, making μ_r equal to 1.2 and 2.4. The computations carried out, plotted in the graph of fig. 7, are presented in Table I.

TABLE I

	m	
cot α	μ_r=1,2	μ_r=2,4
10,0	0,82	0,55
5,0	0,88	0,68
3,0	1,00	1,00
2,0	1,21	1,77
1,5	1,87	4,67
1,33	2,60	9,49
1,25	3,57	16,92
1,00	∞	∞

TABLE II

	m	
cot α	μ_r=1,2	μ_r=2,4
10,0	0,48	0,32
5,0	0,52	0,40
3,0	0,59	0,59
2,0	0,71	1,04
1,5	1,10	2,74
1,33	1,52	5,56
1,25	2,09	9,92
1,00	∞	∞

An analysis of the table shows that:

1) Iribarren's formula with $\mu = 1.0$ does not necessarily contain a safety factor;

2) This safety factor applies exclusively to slopes steeper

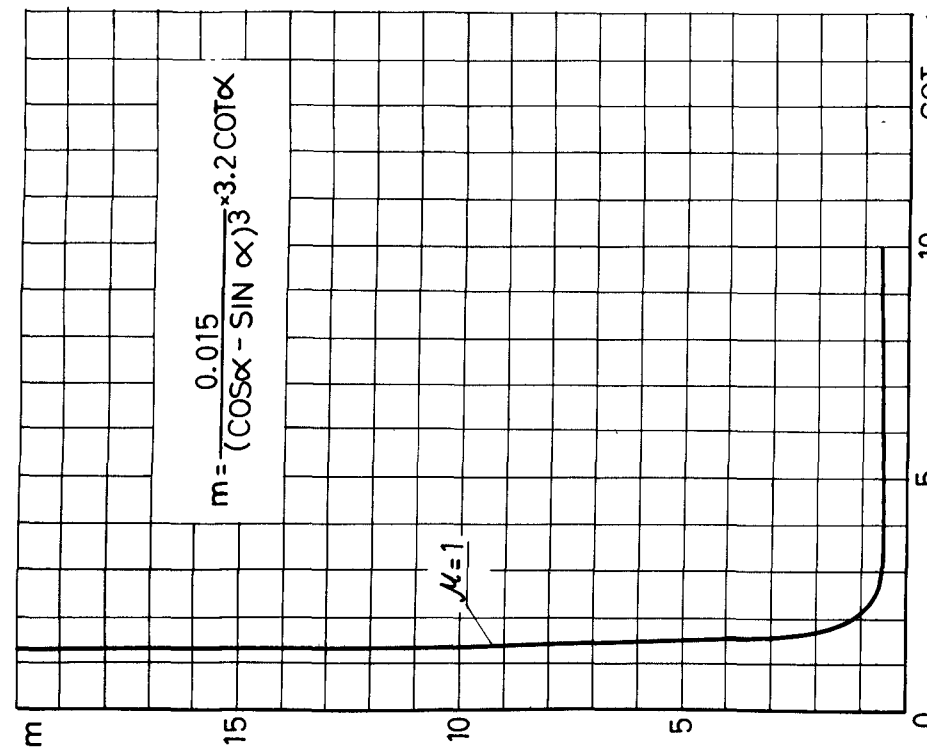

Fig. 8. Safety coefficients introduced by Iribarren's formula (μ = 1; K = 0.015) when compared with Hudson's formula.

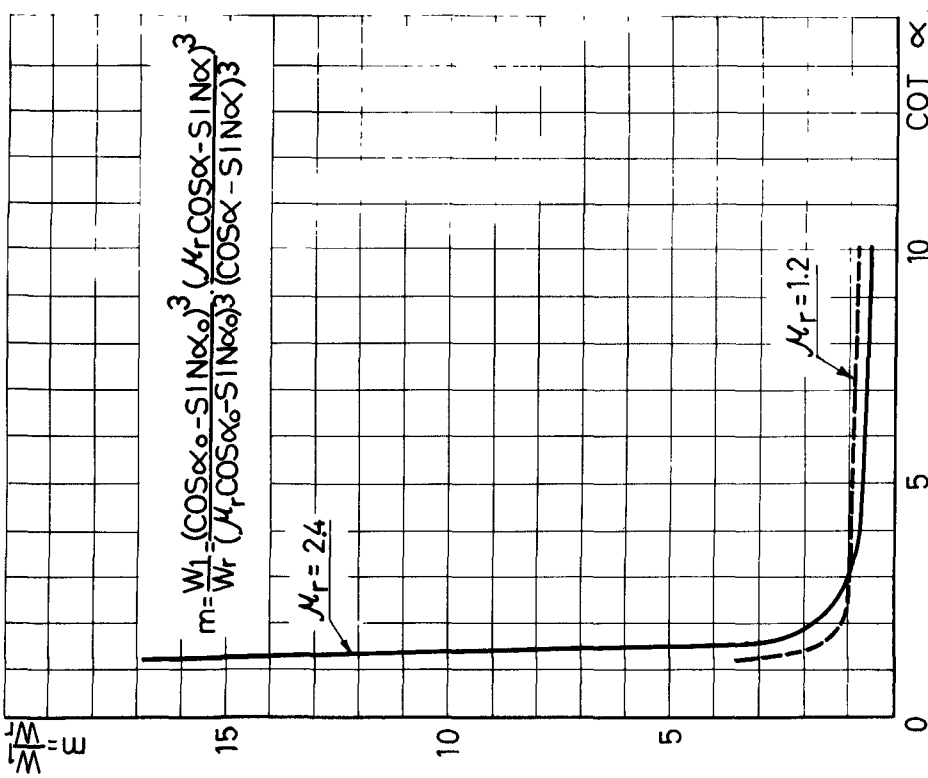

Fig. 7. Variation law of the coefficient $m = \frac{W_\mu = 1}{W_\mu = \mu_r}$ when using Iribarren's formula with μ = 1 and μ_r = 1.2 and 2.4.

than the one for which the constant was determined;

3) The same safety factor increases with the angle of slope measured from the horizontal.

4) For angles of slope less than the value for which Iribarren determined his coefficient, the above-mentioned ratio m is an unsafety factor.

2) VARIATION OF THE COEFFICIENT OF IRIBARREN'S FORMULA WITH α

Hudson's formula for quarry-stone rubble-mound breakwaters has the expression

$$\frac{\gamma_r^{1/3} H}{W^{1/3}(S_r - 1)} = (K_D \cot \alpha)^{1/3} \quad , \quad K_D \text{ being constant}$$

for all the values of α.

Iribarren's formula can be written in like manner

$$\frac{\gamma_r^{1/3} H}{W^{1/3}(s_r - 1)} = \frac{(\mu \cos \alpha - \sin \alpha)}{K^{1/3} \mu}$$

From these two equations the following is obtained

$$K = \frac{(\cos \alpha - \frac{1}{\mu} \sin \alpha)^3}{K_D \cot \alpha}$$

By making $\mu = \mu_r$ (real unknown value of μ) the expression

$$K_r = \frac{(\cos \alpha - \frac{1}{\mu_r} \sin \alpha)^3}{K_D \cot \alpha}$$ is obtained which shows

that K_r varies with α.

Consequently the coefficient K of Iribarrens formula should vary with α, whatever the value selected for μ.

Let us now determine the stability factor yielded by Iribarren's formula with the coefficient recommended by him, by comparison with the observed behaviour of a breakwater which reached its profile of equilibrium for cot α = 3, assuming that Hudson's experimental formula is exact and that Iribarren's coefficient would not vary with α.

A comparison of the values $\frac{W\,(s_r-1)^3}{H^3\,s_r}$ for Iribarren's and Hudson's formulas shows that, for $\cot\alpha = 3$ Iribarren's formula with $\mu = 1$ and the coefficient recommended by him, yields weights $\frac{0.104}{0.061} = 1.7$ smaller.

Therefore the stability factors indicated in Table I become those of Table II.

As explained these coefficients imply that K_r is independent of α. Considering now that K_r varies with α, an expression is obtained which represents the general stability factor of a quarry-stone rubble-mound breakwater obtained from Iribarren's formula as usually applied:

$$m = \frac{0.015}{(\cos\alpha - \sin\alpha)^3} \times 3.2 \cot\alpha$$

This expression, plotted in the graph of fig. 8, shows that m varies with α and can be greater or less than 1. From the brief analysis above it results that:

a) If $\cot\alpha > \mu_r$ and $\mu \leq \mu_r$, Iribarren's formula,

$$W = \frac{K\,\gamma_r\,\gamma_f^3\,H^3\mu^3}{(\mu\cos\alpha - \sin\alpha)^3\,(\gamma_r-\gamma_f)^3}$$

becomes Hudson's formula,

$$W = \frac{H^3\,\gamma_r\,\gamma_f^3}{(\gamma_r-\gamma_f)^3\,K_D\cot\alpha}$$

whatever the value selected for μ, provided that K varies according to the expression

$$K = \frac{(\cos\alpha - \frac{1}{\mu}\sin\alpha)^3}{K\cot\alpha}\,.$$

b) Accepting Iribarren's formula with the coefficient recommended by him, the safety (or unsafety factor) varies with α according to the expression

$$m = \frac{0.015}{(\cos\alpha - \sin\alpha)^3} \times 3.2 \cot\alpha$$

VI - FINAL REMARKS

During the preceding comparative analysis of empirical and semi-empirical breakwater-design formulas (the latter including experimental expressions) nothing was said regarding the actual

value of experimental results. Without discussing the important detail of the stability criteria used in model tests,let us pose the following question. Up to what extent do model tests reproduce actual conditions in the prototype?Let us recall,in the first place, the general similitude conditions prevailing in the model study of a breakwater: similitude obeys Froude's law, the wave train being characterized in each test by the expressions T = = const. and H = const. Taking into account the scales usually employed in these tests (normally $\lambda \geq 1/50$), viscosity effects are negligeable and, only short-period waves being of interest in these studies, the use of Froude's similitude law seems justified. The same is not true, however, concerning the usually considered simplification which consists in taking H = const. and T = const. for the wave trains. Thus assuming, as it seems reasonable to do, that the term $\frac{\partial V}{\partial t}$ expressing the effect of the inertia forces resulting from the dissipation of the kinetic energy of the waves, plays an important rôle in the stability of the breakwater, such a simplification may seem doubtful.In fact,whilst for T = const. and H = const. the term $\frac{\partial V}{\partial t}$ is a periodic function with a period T, this is no longer true if T and H are any time functions whatsoever. That $\frac{\partial V}{\partial t} = f(t)$ is an important function to be considered in the study, may be a deficiency to be pointed out in model tests in which it is assumed that T = const. and H = const. Unfortunately no sure knowledge is available about the influence of $\frac{\partial V}{\partial t}$ on the stability of breakwaters and until his influence is carefully investigated, designers will have no choice but to observe the behaviour of breakwaters designed by means of model tests. In fact, a considerable number of breakwaters having been designed at the laboratory (those with tetrapod or tribar cover-layers for instance), the observation of the behaviour of the completed structures can give practical indications on the value of model test design of breakwaters.Such an observation,if carefully carried out, may even yield valuable experience likely to improve to a great extent the experimental design of breakwaters. Bearing in mind that several breakwaters designed by means of model tests and completed, some of them, years ago, present satisfactory behaviours, it seems natural to believe that, so far, there are no indications regarding improvements or changes required in the technique used, up to the present, in model tests of the stability of breakwaters. We believe, nevertheless, that a attempt should be made to generalize the use of wave generators able to reproduce actual wave trains with an adequate accuracy. A comparison of test results obtained by means of actual wave trains with results obtained by replacing these by

uniform wave trains (T = const. and H = const.) could be a great help for improving laboratory studies.

It is altogether different, nevertheless, to recommend as reliable, results of laboratory tests carried out on specific models, and also to recommend the indiscriminate use of the formulas so far presented based on reduced model tests. Thus both Beaudevin's (Neyrpic) and Hudson's (Waterways Experiment Station) formulas result from test conditions which can be regarded as being too particular. In fact these formulas contain as parameters, the weight and the specific gravity of the blocks, the angle of slope and the wave-height. Effects of parameters deemed important are omitted, such as the ratio H/d near the breakwater toe, the nature of the bottom and its relief near the structure. The latter showed itself particularly important in the study carried out at the Laboratório Nacional de Engenharia Civil, in which H/d was very large (about 0.8) [18] . As for the nature of the bottom, it is admitted that its influence is considerable, whenever d has the same order of magnitude as the depth at which waves break.

Nevertheless until all the parameters with a marked influence on the stability of breakwaters are known, it is advisable that a structure be individually tested, whenever it will have to withstand actions other than those for which the formulas were determined in the laboratory. For similar conditions, these formulas can be used in the design of the protection zone subjected to the most violent action of the waves (i.e. down to a depth of about 1.5 H below still-water level). As none of the formulas tentatively presented for the design of the underwater layers of breakwaters has yet been experimentally confirmed, there is no alternative but to test the whole breakwater. This means that the formulas at present available must still be augmented with the experimental design of breakwaters. It is recommended to carry out experimental studies for designing the cover layer at any elevation below water level. Another important detail to be dealt with in laboratory tests concerns the stability of singular points such as the breakwater head. This zone, in fact, has to be carefully studied in every breakwater design, and for lack of experimental data, some designers recommend a considerable increase of the resistance in this zone.

VIII - CONCLUSIONS

A comparison of empirical and semi-empirical breakwater-design formulas (both experimental or not), shows that:

a) Castro's formula presents a shape rather similar to that of the experimental formula suggested by Beaudevin;

b) For slopes such that cot $\alpha > 2$, Iribarren's formula is intermediate between the Waterways Experiment Stantion and Beaudevin's experimental formulas, but for cot $\alpha < 2$ it is different

from both;

c) The two experimental formulas present different shapes, what may be due to either the different stability criteria or the different wave-heights adopted at each laboratory;

d) Any of the two experimental formulas can serve as a basis for the preliminary design of a breakwater, provided that the conditions in which the tests were carried out and the stability criteria followed are duly borne in mind so that a suitable safety factor is adopted according to the stability criteria followed in each case;

e) In view of the innumerable parameters, many more still yet unknown, which play a rôle in the behaviour of breakwaters, the design formulas presently available do not dispense with experimental tests in each actual case. Nevertheless, as a first approximation, these formulas can give indications on the technical and economical feasibility of rubble-mound breakwaters;

f) The design of the underwater portions and of the singular points, notably the head, of rubble-mound breakwaters should be included in laboratory research programs on breakwaters.

REFERENCES

[1]- Castro, Eduardo - "Diques de escollera" - Revista de Obras Públicas, Abril de 1933.

[2]- Iribarren Cavanilles, R. - "Una formula par el calculo de diques de escollera" - Revista de Obras Públicas - 1938.

[3]- Iribarren Cavanilles, R. - "Obras Marítimas. Oleaje y diques". Editorial Dossat, Madrid 1954.

[4]- Iribarren Cavanilles, R. and Nogales, C. - "Generalizacion de la formula para el calculo de los diques de escollera y comprobacion de sus coefficients" - Revista de Obras Públicas, Maio 1950.

[5]- Hickson, R. and Rodolf, F. - "Design and Construction of jetties" - Proceedings of First Conference on Coastal Engineering - 1951.

[6]- Epstein, H. and Tyrrel, F. - "Design of rubble-mound breakwater" - XVII° Congrès International de Navigation, Section II, Communication 4.

[7]- Larras, J. - "L'equilibre sous-marin d'un massif de matériaux soumis à la houle" - Le Genie Civil, 15 Septembre 1952.

[8] - Abecasis, Carlos K. - "Données d'experience sur les cotes du continent et des îles Portugaises de l'Atlantique du Nord" - XVIII^{e} Congrès International de Navigation - Section II, Question I.

[9] - Larras, J. and Colin, H. - "Les ouvrages de protection du port d'Alger à talus inclinés" - Travaux, vol. 31, pp.603--609; vol. 52, pp.163-168.

[10] - Iribarren Cavanilles,R. and Nogales, C. - "Nueva Confirmacion de la Formula para el Calculo de los Diques de Escollera" - Revista de Obras Públicas - Janeiro 1953.

[11] - Beaudevin, C. - "Stabilité des diques à talus à carapace en vrac". La Houille Blanche - Mai-Juin 1955.

[12] - Barbe, R. and Beaudevin, C. - "Recherches expérimentales sur la stabilité d'une jettée à talus incliné soumise à la houle". La Houille Blanche - Juin-Juillet 1953.

[13] - Hudson, R. Y., and Jackson, R.A. - "Stability of rubble--mound breakwater" - W.E.S. Technical Memorandum 2-365, Vicksburg 1953.

[14] - Hudson, R. Y. - "Design of quarry-stone cover layers for rubble-mound breakwaters" - W.E.S. Research Report 2-2, Vicksburg 1958.

[15] - Hudson, R. Y. and Jackson, R.A. - "Design of tribar and tetrapod cover layers for rubble-mound breakwaters" - W.E.S. Miscellaneous Paper 2-296, Vicksburg 1959.

[16] - "Estudo experimental do porto do Funchal - Ensaios de estabilidade. Relatório complementar" - Laboratório Nacional de Engenharia Civil, Lisboa 1957.

[17] - Schaer, G. - "Stabilité des ouvrages maritimes. Comparison modèle-realité" - Compte Rendu des Quatrièmes Journées de l'Hydraulique. Paris 1956.

[18] - "Nota sobre os ensaios de estabilidade dos molhes da Figueira da Foz" - Laboratório Nacional de Engenharia Civil, Lisboa 1959.

CHAPTER 35

EXPERIMENTAL STUDIES OF SPECIALLY SHAPED CONCRETE BLOCKS FOR ABSORBING WAVE ENERGY

Shoshichiro Nagai,
Prof. of Osaka City University,
Faculty of Engineering,
Civil Engineering Department, Osaka, Japan.

ABSTRACT

Laboratory tests were performed to determine wave energy absorbing ability of and stability characteristics against breaking waves of various shaped pre-cast concrete armor units used for protective cover layers on the seaward slopes of rubble-mound breakwaters and for parallel dykes placed the offshore sides of seawalls. A new shape of armor units, a hollow tetrahedron concrete block with a porosity of 25 percentages in the body was proved to have better characteristics for wave energy absorbing ability and attenuation of wave run-up, as well as for stability against breaking waves also than tetrapod or other armor units used up-to-date.

EXPERIMENTAL EQUIPMENT AND PROCEDURE

TESTS FOR PROTECTIVE COVER LAYERS OF RUBBLE-MOUND BREAKWATERS

An open wave channel, which is 25 m. long, 2 m. wide, and 1 m. deep, was used for the experiments of the protective cover layers of rubble-mound breakwaters. Waves were generated by a flutter type wave generating machine, ranging the period T = 1.2 to 1.9 sec., the height H = 10 to 24 cm., and the steepness H/L = 0.040 to 0.085. Since the scale ratio between the model and prototype is approximately 1/20, the heights and periods of the model waves are scaled up approximately to H = 2 to 4.8 m. and T = 5.4 to 8.5 sec. in sea by the use of Froude's law.

A number of laboratory tests were performed of concrete armor units such as tetrahedrons, hexabars, tetrapods and hollow tetrahedrons made in 1/20 scale ratio to prototype, comparing with quarry-stone armor units placed pell-mell and with mounds made of wooden plates. The energy absorbing ability of armor units in these experiments was determined by use of the resultant forces of maximum simultaneous shock pressures[1] exerted by breaking waves on the vertical walls of composite-type breakwaters, which were measured by pressure-gauges of strain-gauge type, and also by use of wave run-up along the vertical walls as well as reflection ratio from the walls, both of which were measured by visual observation.

The shapes and characteristics of the specially shaped armor blocks used in the tests are shown in Figure 1 and Table 1. The armor units were in all tests constructed with the two layers of the specially shaped concrete blocks on a 1 : 1 $\frac{1}{2}$ slope, because it was proved by the tests that the two-layer placing and the 1 : 1 $\frac{1}{2}$ slope were the optimum condition for the stability of these

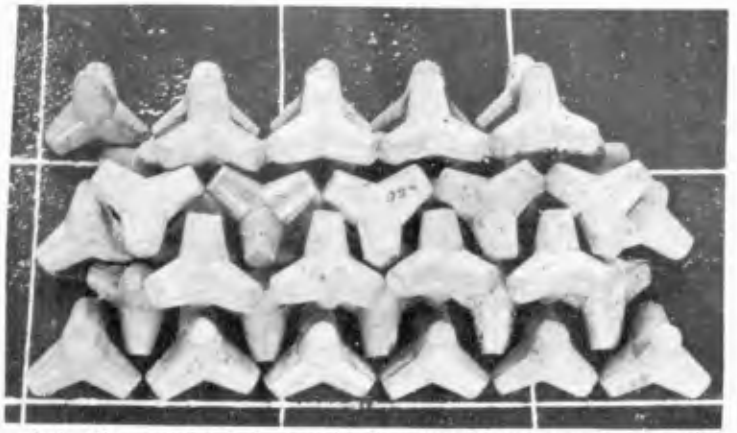

(a) Concrete tetrapods (upper blocks reversed).

(b) Concrete tetrapods (upper blocks normal).

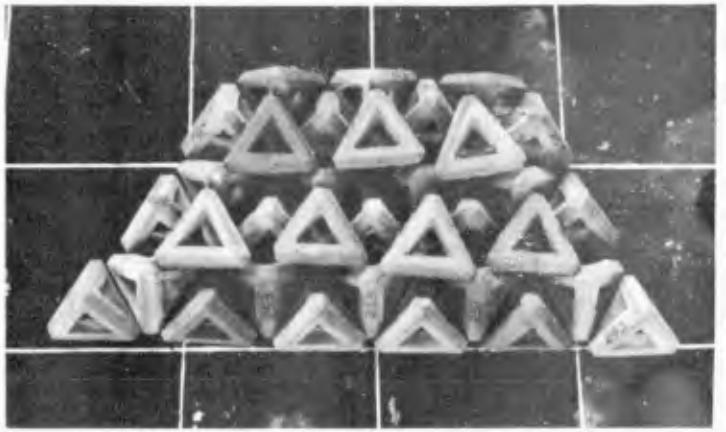

(c) Concrete hollow tetrahedrons.

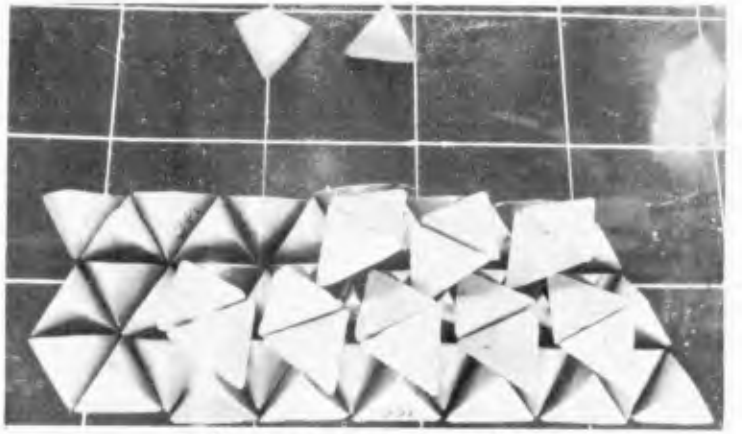

(d) Concrete tetrahedrons.

Fig. 1. Types of concrete armor units and manner of placing.

EXPERIMENTAL STUDIES OF SPECIALLY SHAPED CONCRETE BLOCKS FOR ABSORBING WAVE ENERGY

Table 1. Characteristics of concrete armor units tested.

Type of Blocks	Vol. of a block (cm^3) Net Vol.	Apparent Vol.	Weight of a Block Model (g)	Prototype (t)	Porosity (%) One Block	Two Layers	Pell-mell	Height (cm)	No. of Blocks in 2-layer Placing Lower Layer	Upper Layer	Total	Slope at Sliding One Layer	Two Layers	Slope at Overturning One Layer	Two Layers
Tetrapod	110	110	227～275 aver.251	aver. 2.0	0	r.66	50	7 3	r 267 n 267	230 132	497 399	36°～42°	r35°-42° n37°-41°	57°～63°	r 59° n 70
Tetrahedron	150	150	298～374 aver.337	2.7	0	50	57	9.3	229	145	374	32°～38°	31°～36°	61°	65°
Hollow Tetrahedron No. 1	116	155	246～288 aver.267	2.1	25	66	60	7 6	222	112	334	28°～34°	32°～36°	67°	67°～74°
Hollow Tetrahedron No. 2	90	123	173～226 aver.201	1.6	27	59	58	7.0	363	138	501	33°～34°	33°～34°	65°～69°	70°～71°
Hollow Tetrahedron No. 3	108	166	224～271 aver.248	2.0	35	70	68	8 0	213	114	327	33°～35°	34°～37°	67°～69°	69°～85°

r : revereed, n : normal

Table 2. Test results in Figures 7 and 8.

Wave Period Tm = 1.5 sec (Tp = 6 7 sec.)

Construction of a Base-mound	h_1 (cm)	H (cm)	H/L	Max. Press Intensity P_{max} (g/cm^2)	Ratio (%)	Result. of Max. Simult. Deve Press P (g/cm)	Ratio (%)	Stability of Blocks	Impulse (g cm /sec.)	Impulse Momentum α (%)	Ratio of Wave Energy α^2 (%)	Run-up Ru (cm)	Reflect. Ratio (%)
Wooden Fl.	7.0	13	0.049	70	100	452	100		355×10^3	61.7	38.0	23～26	45
	13.0	15	0.053	102	100	510	100					27～32	28
Quarry-stone	7.0	12	0.059	80	114	331	74					16～18	29
	13 0	15	0.052	30	30	405	79					25～30	21
Tetrapod (reversed)	7.0	14	0 054	80	114	376	83	overturn.				21～26	54
	13.0	17	0.062	23	23	291	57					22～25	28
Tetrapod (normal)	7.0	15	0.054	60	86	292	66	rooking	314×10^3	54.6	29.8	21～23	36
	13.0	16	0.060	85	83	441	87					22～25	27
Tetrahedron (reversed)	7.0	13	0.055	60	86	302	67	several ble. rook. unstable	189×10^3	34.4	11.8	21～26	24
	13 0	15	0.060	60	59	588	115					25	33
Hollow Tetrahedron No. 1	7.0	12	0 04>	60	86	242	54	stable	127×10^3	21.3	4.5	16～18	37
	13.0	16	0.059	15	15	216	42					20	20
Hollow Tetrahedron No. 2	7.0	13	0.051	70	100	314	70	severe rock				20～23	36
	13.0	15	0.057	26	26	400	78	stable				28～33	10
Hollow Tetrahedron No. 3	7.0	12	0.046	40	57	248	55	rocking				26	30
	13.0	15	0.055	35	34	476	93	rocking & roll. down				20～24	33

Table 3. Test results in Figures 9 and 10.

Wave Period Tm = 1.3 sec. (Tp = 5.8 sec.)

Construction of a Base-mound	h_1 (cm)	H (cm)	H/L	Max. Press Intensity P_{max} (g/cm^2)	Ratio (%)	Result. of Max. Simult. Wave Press. P (g/cm)	Ratio (%)	Stability of Blocks	Impulse (g.cm /sec.)	Impulse Momentum α (%)	Ratio of Wave Energy α^2 (%)	Run-up Ru (cm)	Reflect. Ratio (%)
Wooden Fl.	7.0	14	0.063	65	100	452	100		262×10^3	44.4	19.7	26～31	32
	13.0	18	0 073	58	100	725	100					35～37	22
Quarry-stone	7 0	15	0.072	75	115	375	83					28～31	36
	13.0	18	0.082	55	95	329	45					35～40	33
Tetrapod (reversed)	7.0	15	0.063	65	100	481	106	several bls. roll. down				31～36	40
	13.0	18	0 078	37	64	513	71					35～40	31
Tetrapod (normal)	7.0	15	0.068	80	123	400	89	stable	129×10^3	24.0	5.8	31～36	29
	13.0	19	0.079	29	50	417	58	stable				30～40	20
Tetrahedron (reversed)	7.0	15	0 058	60	92	366	81	unstable	189×10^3	30.6	9.4	26～31	24
	13.0	18	0.069	40	69	548	76	unstable				35～37	33
Hollow Tetrahedron No. 1	7 0	14	0.058	75	115	343	76	stable	87×10^3	13.9	1.9	26	33
	13.0	18	0.077	16	28	192	27	stable				30～32	33
Hollow Tetrahedron No. 2	7.0	14	0.055	65	100	274	61	several bls. rook.				26～31	24
	13.0	18	0.072	24	41	365	50	unstable				36～41	17
Hollow Tetrahedron No. 3	7.0	15	0.064	30	46	105	23	several bls. rock.				21	31
	13.0	17	0 073	32	55	432	60	several bls. roll. down				30	36

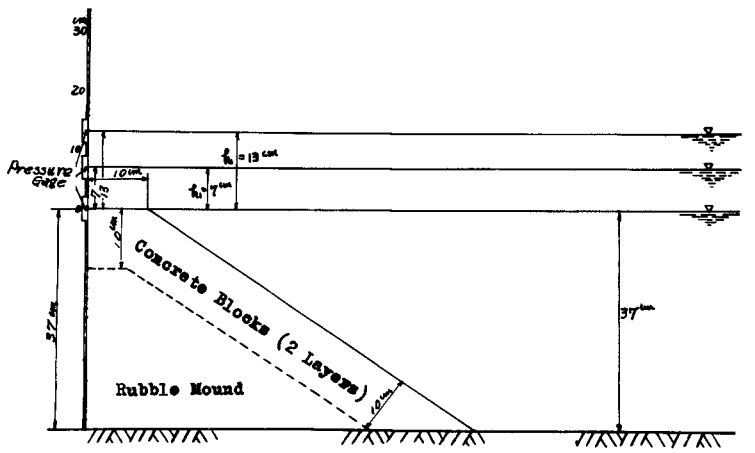

Fig. 2. Composite breakwater with high vertical wall (top width of rubble mound B = 10 cm).

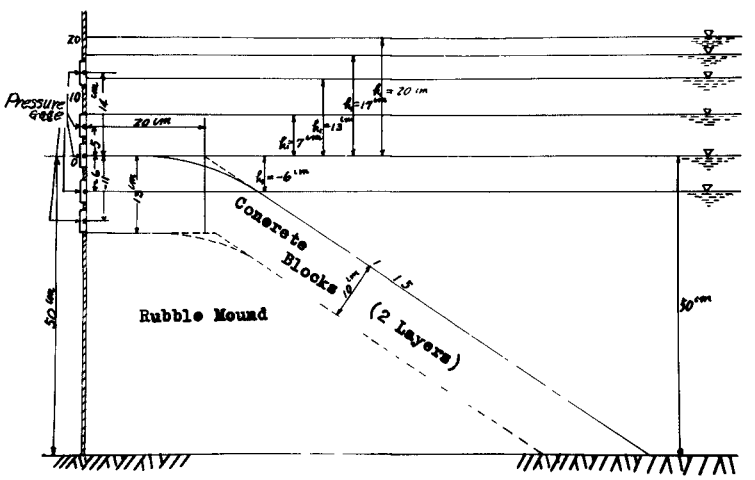

Fig. 3. Composite breakwater with high vertical wall (B = 20 cm).

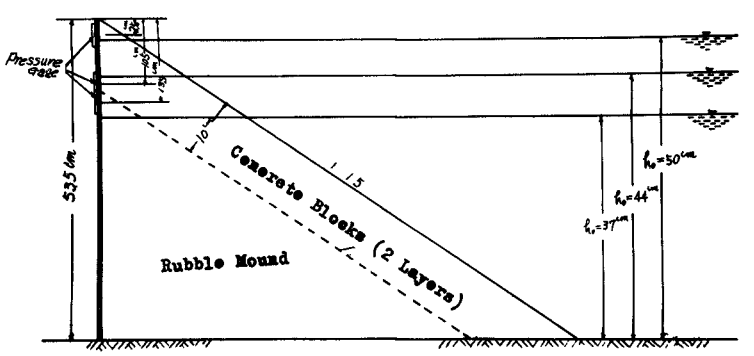

Fig. 4. Composite breakwater with low vertical wall (B = 0).

concrete armor units.

The types of composite breakwaters and rubble-mound breakwaters used in the tests are shown in Figures 2, 3 and 4. The protective cover layers composed of the two layers of cast concrete specially shaped armor units were placed in some orderly manner or pell-mell over a core of quarry-stones, the diameters of which d ≒ 2.8 to 7.3 cm..

Figs. 2 and 3 are types of composite breakwaters with vertical walls sufficiently high to prevent overtopping by the test waves, and Fig. 4 is a type of composite breakwaters with low vertical walls subjected to overtopping at high water levels. In these low breakwaters cast concrete blocks are placed up to the crown of the vertical walls.

TESTS OF PARALLEL DYKES FOR THE PROTECTION OF RUN-UP ON SEAWALLS

A lot of experiments was performed to determine the effect of parallel dykes, which were constructed with the two layers of concrete tetrapods and hollow tetrahedrons and placed in front of seawalls, on the attenuation of wave run-up and of wave pressures on the seawalls. A wave channel used in these experiments was 23 m. long, 1 m. wide, and 1 m. deep, as shown in Fig. 5, and the nearly overall length of the channel was covered on the top with semi-circular duralmin plates for generating winds of various speeds parallel with the direction of propagation of waves which were generated by a flutter type wave generator. The speed of revolution of a wind blower was varied by the use of a vari-pitch connected with a 15-horse power electric motor so as to generate winds of speed up to 20 m./sec.. One typical type of the seawalls tested is shown in Fig. 6.

The characteristics of waves generated by the flutter type wave generator were T = 1.2 to 1.9 sec., H = 8 ~ 14 cm., H/L = 0.020 ~ 0.070. The wave run-up as well as the behaviors of spray and overtopping were measured by the use of a 16 millimeter movie taken at 100 frames per second.

EXPERIMENTAL RESULTS

TESTS FOR THE PROTECTIVE COVER LAYERS OF RUBBLE-MOUND BREAKWATERS[2]

(a) Test results in composite breakwaters shown in Figs. 2 and 3

Figs. 7, 8, 9 and 10 show maximum simultaneous shock pressures exerted by breaking waves of periods T = 1.3 and 1.5 sec. on the vertical walls of the composite breakwaters shown in Fig. 2.

The states of run-up in breaking waves with T ≒ 1.5 sec., H ≒ 16 cm., H/L ≒ 0.060 impinged against the vertical walls placed on the various kinds of base-mounds are shown in Figs. 11, 12, 13 and 14.

The test results are summarized in Tables 2 and 3, concerning

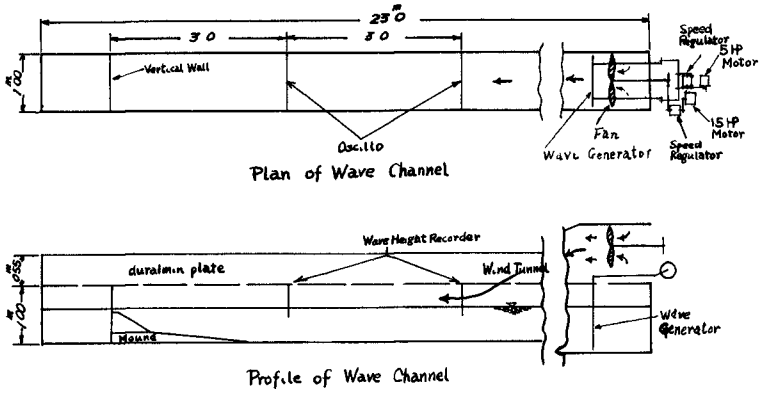

Fig. 5. Closed wave channel with a wind blower.

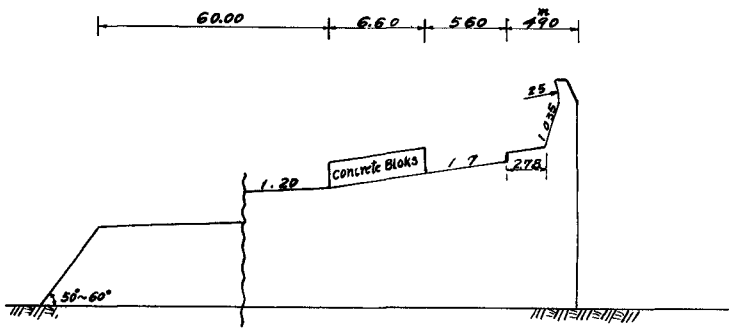

Fig. 6. A Type of sea walls tested, section of a sea wall and shore at Suma, at Kobe, Japan.

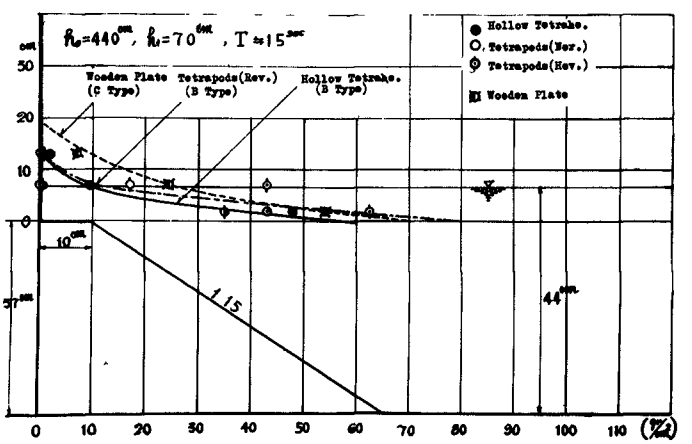

Fig. 7, Maximum simultaneous shock pressures by breaking waves of T = 1.5 sec (water depth above the top of the mounds h_1 is constantly 7 cm).

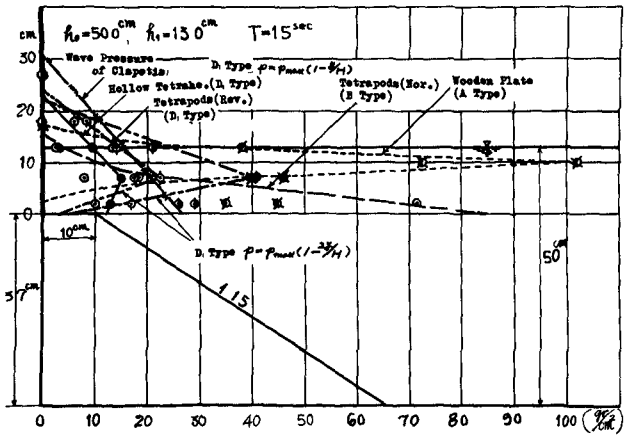

Fig. 8. Maximum simultaneous shock pressures by breaking waves of T = 1.5 sec (h_1 = 13 cm).

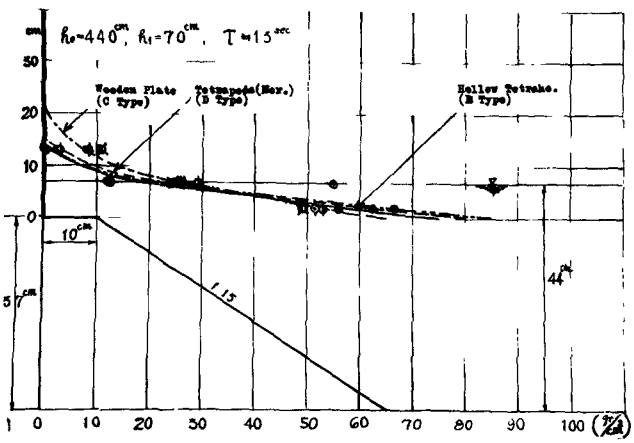

Fig. 9. Maximum simultaneous shock pressures by breaking waves of T = 1.3 sec (H_1 = 7 cm).

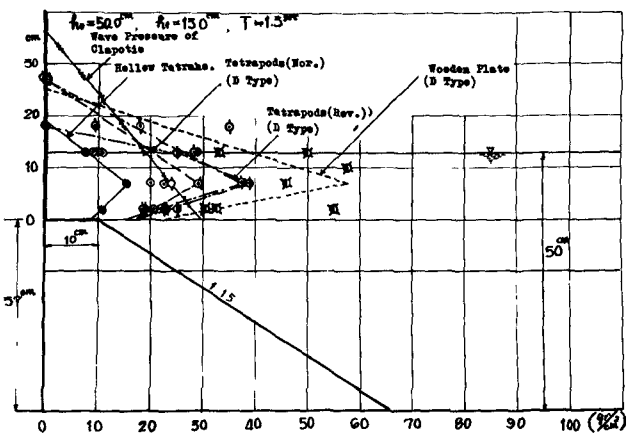

Fig. 10. Maximum simultaneous shock pressures by breaking waves of T = 1.3 sec (h_1 = 13 cm).

with the maximum intensities of shock pressures and the resultants of maximum simultaneous shock pressures exerted on the vertical walls of the composite breakwaters by the breaking waves, the heights of wave run-up, the ratioes of wave energy attenuation, and the stability of the armor units on the seaward slopes of the base-mounds.

The effect of the specially shaped concrete armor units on absorbing wave energy was also determined by use of the ratio of wave energy attenuation, α^2, defined as follows.

The momentum per the unit width of the channel transported by a breaking wave for a period is obtained by $\rho Q \omega$, where ρ is the density of water, ω, the horizontal velocity of a water particle in a breaking wave, may equal to the celerity of the breaking wave with sufficient accuracy, and Q is the water mass per unit width of the channel transported for a period by the breaking wave. If the breaking wave is assumed that of a solitary wave, ω and Q are given by

$$\omega = \sqrt{2.28gH} \tag{1}$$

in which g is the acceleration of gravity, and H the height of the breaking wave, and

$$Q = 4h_o^2 \sqrt{\frac{H}{3h_o}} \tag{2}$$

in which h_o is a depth below the still water level at the horizontal bottom of the channel.

The resultant of the impulse exerted by the breaking wave on unit width of the vertical wall for a period is denoted by $\int_o^h \int_o^\tau p\,dt\cdot dh$ where τ is smaller than the period T of the breaking wave, and h the height from the top of the base-mound up to the highest point of the wave pressure exerted by the breaking wave. If the ratio of the resultant of the impulse on the vertical wall to the momentum transported is denoted by α,

$$\frac{\int_o^h \int_o^\tau p\,dh\cdot dh}{\rho Q \omega} = \alpha, \quad 0 < \alpha \leqq 1$$

$$\int_o^h \int_o^\tau p\,dh\cdot dh = \alpha\cdot\rho Q\omega \tag{3}$$

Substituting Eqs. (1) and (2), into Eq. (3), we obtain

$$\int_o^h \int_o^\tau p\,dt\cdot dh = \rho\cdot 4h_o^2\sqrt{\frac{\alpha H}{3h_o}}\cdot\sqrt{2.28g\cdot\alpha H} \tag{4}$$

The right-hand side of Eq. (4) may be considered the momentum transported by a breaking wave with a height of αH. Since the net wave energy E_{net} acted on the vertical wall by this breaking wave will be

$$E_{net} = \frac{1}{8}\rho g(\alpha H)^2$$

the ratio of the net breaking wave energy acting on the vertical

wall to the total breaking wave energy before impinging against the breakwater should be obtained by the equation

$$\frac{E_{net}}{E} = \frac{\frac{1}{8}\rho g(\alpha H)}{\frac{1}{8}\rho g H^2} = \alpha^2 \qquad (5)$$

By the use of the experimental data the values of α^2 were calculated from Eqs. (3) and (5).

From Tables 2 and 3 it is seen that the hollow tetrahedron armor units constructed with the two layers of cast concrete hollow tetrahedrons with a porosity of 25 percentages have the optimum characteristics of wave energy absorbing ability as well as of stability on the 1 on 1.5 slope, showingespecially 30 to 50 percentages greater attenuation of the maximum simultaneous shock pressures than that due to the tetrapod armor units. It is considered that when the depth h_1 above the top of a base-mound covered with specially shaped concrete armor layers is small, the roughness on the surface of concrete block layers plays a greater role than the permeability of concrete block layers, on the contrary, the latter plays a greater role than the former when h_1 is large. Wave run-up on the vertical walls of composite breakwaters is also smaller in the hollow tetrahedron armor layers than in the tetrapod armor layers.

From experiments in the composite breakwaters of such shapes as shown in Fig. 3, nearly the same trend as shown in Tables 2 and 3 was proved.

(b) Test results in composite breakwaters with low vertical walls shown in Fig. 4 Maximum simultaneous shock pressures exerted by breaking waves on the low vertical walls, up to the top of which the seaward slopes of the rubble-mound were covered with concrete tetrapod or hollow tetrahedron armor units, and the stability of those armor units on the slopes were measured by making breaking waves with the periods of T = 1.3 and 1.5 sec. on the slopes in the three different water levels. These experimental results are shown in Figs. 15, 16, 17, 18, 19 and 20.

As it is known from the Figures, when waves break on the slopes in the cases of low water level, the magnitudes of shock pressures exerted by the breaking waves on the vertical walls are nearly the same in the two different armor units, indicating small values, but in the cases of high water level the effect of the hollow tetrahedron armor units on the attenuation of wave pressures is distinguished, comparing with that of the tetrapod armor units. The quantity of overtopping in the hollow tetrahedron armor units is also smaller than that in the tetrapod armor units. The stability on the slopes was nearly the same in the two armor units.

(c) Test results of parallel dykes for the protection of wave run-up on sea-wall It was proved from a lot of experiments that if parallel dykes covered with the two layers of concrete hollow tetrahedron or tetrapod armor units were placed in front of seawalls, wave run-up on the slopes of the seawalls could be reduced to a

Fig. 11. Run-up in composite breakwater with base-mound of wooden plates.

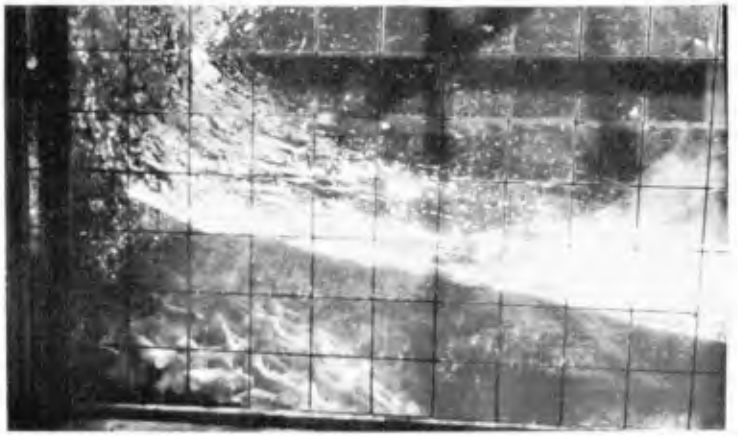

Fig. 12. Run-up in composite breakwater with base-mound covered with the 2 layers of tetrapods.

Fig. 13. Run-up in composite breakwater with base-mound covered with the two layers of tetrahedrons.

Fig. 14. Run-up in composite breakwater with base-mound covered with the 2 layers of hollow tetrahedron with a void ratio of 25%.

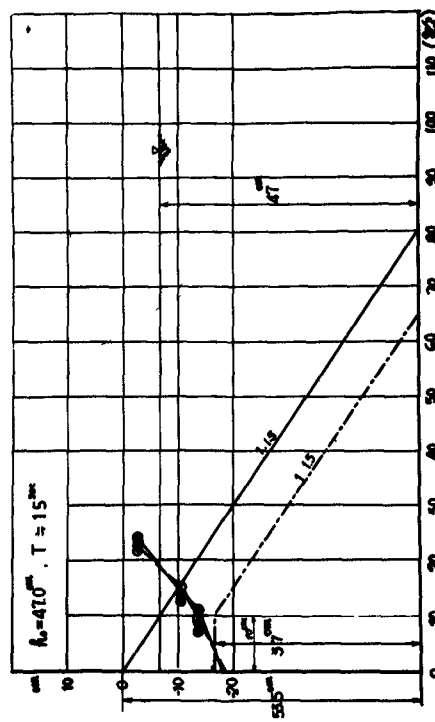

Fig. 15. Maximum simultaneous shock pressures on the vertical wall, H = 14 cm, H/L = 0.048.

Fig. 16. Maximum simultaneous shock pressures on the vertical wall, H = 16 cm. H/L = 0.054.

Fig. 17. Maximum simultaneous shock pressures on the vertical wall, H = 17 cm, H/L = 0.057.

Fig. 18. Maximum simultaneous shock pressures on the vertical wall, H = 16 cm, H/L = 0.066.

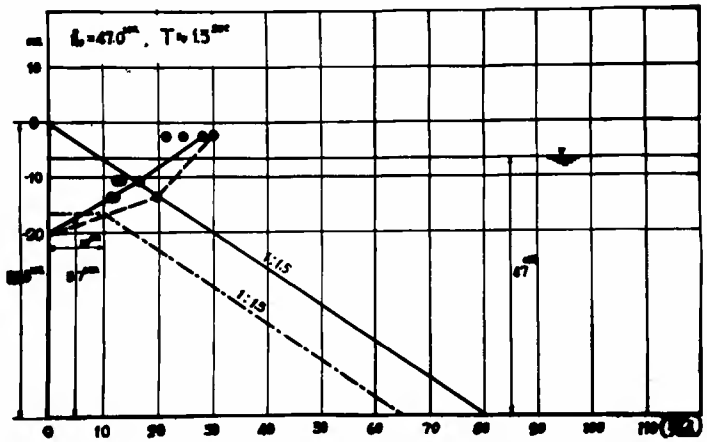

Fig. 19. Maximum simultaneous shock pressures on the vertical wall, H = 18 cm, H/L = 0.073.

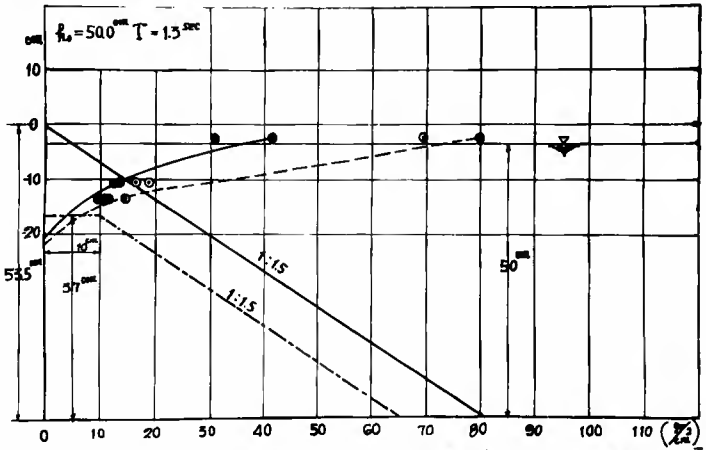

Fig. 20. Maximum simultaneous shock pressures on the vertical wall, H = 19 cm, H/L = 0.078.

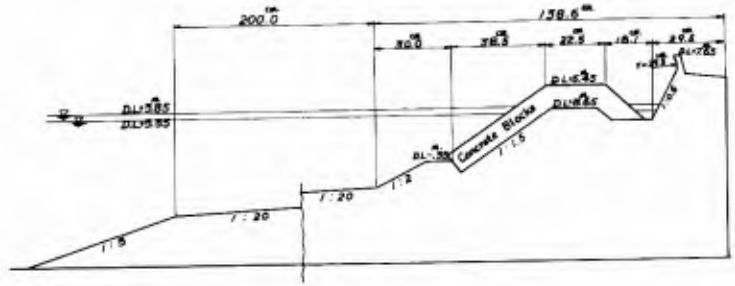

Fig. 21(a). Section of a sea-wall at Amagasaki City, Japan.

Fig. 21(b). Behavior of wave run-up in the case of wind speed V = 20 m/sec in prototype at the sea wall with a parallel dyke constructed with hollow tetrahedron armor units.

Fig. 22a. Behavior of spray and wave run-up at the sea wall without a parallel dyke shown in Fig. 6. Wind speed V = 25 m/sec in prototype.

Fig. 22b. Behavior of wave run-up at the sea wall with a parallel dyke covered with 2 layers of hollow tetrahedron armor units, V = 25 m/sec.

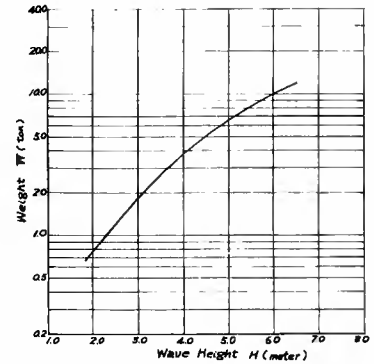

Fig. 23a. When $h_1 \leqq 0$, i.e. waves break on the slopes of mounds.

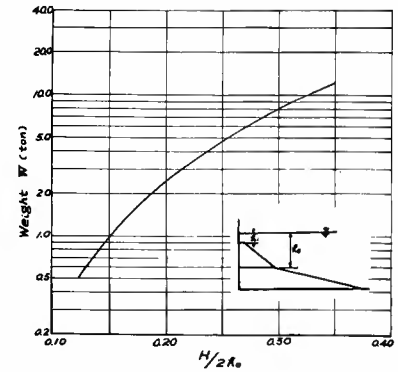

Fig. 23b. When $h_1 > 0$, i.e. sea levels are higher than the tops of mounds.

Fig. 23. Curves of stability for the concrete hollow tetrahedron armor units on 1 : 1 $\frac{1}{2}$ slopes.

great extent. The tops of the parallel dykes should be high suffi cient to prevent a large amount of overtopping by the test waves at the design height of sea level, probably being 0.50 m. or more above the design sea level.

The effect of the hollow tetrahedron armor units on the attenuation of wave run-up on the seawall slopes was proved more prominent than that due to the tetrapod armor units. Only the two examples are shown in Figs. 21 and 22 to show the effect of the attenuation of wave run-up due to the parallel dykes with the cover layers composed of the hollow tetrahedron armor units. Fig. 21 is a case where a depth in ffont of a seawall at the design sea level is so large that the design waves do not break before arriving the sea-wall, on the contrary Fig. 22 is a case where the design waves break at or in front of a sea-wall at the design sea level.

(d) Stability of the hollow tetrahedron armor units on the slope of rubble-mounds[3] As mentioned above, the hollow tetrahedron armor units on the slopes of rubble-mounds were proved to be in general more stable against the attack of waves than tetrapod armor units, because of wedge action caused by the upper layer blocks inversely set into among the lower layer blocks, as well as of the small up-lift pressures of receding waves reduced due to the hollowness of the blocks. The curves of stability of the concrete hollow tetrahedron armor units were determined from a number of experiments on the 1 : $1\frac{1}{2}$ slopes of rubble-mounds as shown in Fig. 23.

(e) Tests of the strength of the concrete hollow tetrahedron blocks Several field tests of prototype two-ton concrete hollow tetrahedron blocks with the porosity of 25 percentages (with no reinforcement) was performed to know strength against very roughly dumping in seas by the measures of falling down on gravel layers and on hollow tetrahedron blocks from some 3-meter height.

From the tests the concrete hollow tetrahedron blocks were confirmed very tough against rough piling up or hard mutual colliding by storm waves because of resisting as Rahmen structures.

CONCLUSIONS

It is concluded from the results of tests completed up to date that:

(a) Two layers composed of the concrete hollow tetrahedron armor units have better characteristics for absorbing wave energy or wave pressure and for stability against breaking waves than the other specially shaped concrete armor units which have been used up to date.

(b) When the two layers of hollow tetrahedron armor units are used for protective cover layers on the seaward slopes of the rubble-mound of composite-type breakwaters, it will be

expected to obtain approximately 30 to 50 percentages greater attenuation of shock pressures exerted by breaking waves on the vertical walls than that due to tetrapod armor units. When the two layers of hollow tetrahedron armor units are used for the protective cover layers of parallel dykes located in front of sea-walls, the attenuation of wave run-up on the slopes of the sea-walls will be obtained to a great extent and be materially effective to prevent overtopping from the sea-walls.

(c) The hollowness of a hollow tetrahedron block was proved optimum in the case of a porosity of 25 percentages, from the view points of wave energy absorbing ability as well as of the strength of a block.

(d) The two layers of concrete hollow tetrahedron armor units have favorable characteristics for stability on 1 on $1\frac{1}{2}$ slopes, because of wedge action caused between the two layers and of reduction of up-lift pressures caused by receding waves.

(e) The number of concrete hollow tetrahedron blocks necessary for two-layer placing on a given area is on an average 15 percentages fewer than that of tetraped blocks with the same dead weight.

PRACTICAL USES OF HOLLOW TETRAHEDRON ARMOR UNITS

Interim report on the tests of the hollow tetrahedron armor units was first done at the 6th Conference of Coastal Engineering in Japan held at the beginning of November, 1959. One to two ton concrete hollow tetrahedron armor units have been in use or partly under construction for protective cover layers of rubble-mound breakwaters and for wave energy absorbing parallel dykes located in front of sea-walls at several harbors and coasts in Japan. The effect of absorbing wave energy of the hollow tetrahedron armor units will be checked when subjected to attack by heavy storm waves generated by typhoon at August and September this year.

REFERENCE

1. "Shock Pressures Exerted by Breaking Waves on Breakwaters," by Shoshichiro Nagai, Journal of the Waterways and Harbors Division, Vol. 86, No. WW 2., June 1960.

2. "Laboratory Studies on Hollow Tetrahedron Armor Units for Absorbing Wave Energy," by S. Nagai, Proc. of the 6th Conference of Coastal Engineering in Japan, Nov. 1959.

3. "Laboratory Tests on Stability of Hollow Tetrahedron Armor Units on 1 : $1\frac{1}{2}$ Slopes," by S. Nagai and S. Ueda, Annual Meeting of Japan Soc. of Civil Eng., May 1960.

CHAPTER 36

EXPERIMENTAL DATA ON THE OVERTOPPING OF SEAWALLS BY WAVES

A.Paape
Hydraulics Laboratory, Delft, Netherlands.

INTRODUCTION

In the past it has been found that serious damage and breaching of seawalls is most frequently caused by overtopping. Hence for the design of seawalls data must be available about the overtopping by waves of the different profiles that might be possible. Naturally the conditions under which damage is caused to the seawall also depend on the type of construction and the materials used, for example: the stability of grass covered dikes can be endangered seriously by water flowing over the inner slope.

In many designs the necessary height of a seawall has been defined such that not more than 2% of the waves overtop the crest, under chosen design conditions. This criterion has been determined on the assumption that the overtopping must remain very small. Some overtopping has to be accepted because no maximum value for wave height and wave run-up can be given, unless of course the wave height is limited by fore-shore conditions.

Unfortunately this criterion gives no information about the volume and concentration of water overtopping the crest in each instance. Moreover it is of interest to know how this overtopping varies with other conditions, such as changes in the significant wave height.

Information about the overtopping by waves was obtained from model investigations on simple plane slopes with inclinations varying from 1 : 8 to 1 : 2. The experiments were made in a windflume where wind generated waves as well as regular waves were employed.

Using wind generated waves, conditions from nature regarding the distribution of wave heights could be reproduced. It appeared that the overtopping depends on the irregularity of the waves and that the same effects cannot be reproduced using regular paddle generated waves.

In this paper a description of the model and the results of these tests are given. Investigations are in progress on composite slopes, including the reproduction of conditions for a seawall which suffered much overtopping but remained practically undamaged during the flood of 1953.

WAVE CHARACTERISTICS

The heights of a series of wind waves are often characterized by the value of the significant wave height $H_{1/3}$, that is the average of the highest third part of such a series. More information is obtained by means of a wave height distribution curve. For this purpose the value H_n has been defined as the height which is exceeded by n% of the waves of a series (e.g. H_{10} is the height exceeded by 10% of the waves). It has been found approximately that $H_{1/3} = H_{13}$.

EXPERIMENTAL DATA ON THE OVERTOPPING OF SEAWALLS BY WAVES

Wave height distribution curves are given in figure 1 for wind velocities of 4, 6, 8 and 10 m/sec in the wind flume, with a fetch of 50 m. A comparison between the different wave height distributions is made in figure 2, where, instead of the absolute value of the wave height, the ratio Hn/H50 has been plotted. From this it appears that for lower wind velocities the waves become more irregular.

Similar distribution curves were obtained from wave-records made along the Dutch coast, examples are given in figure 3. It can be seen from these figures that the wave height distribution of nature can be reproduced in the windflume.

In many experiments the wind velocity has been chosen according to the wave height distribution to be reproduced. Then no direct relationship between the wind velocities in prototype and model exists and it has often been found that the wind velocity in the model is greater than that given by the Froude model law. This seems to be due to the fetch not being to scale.

In studying wave run-up and overtopping, attention should be paid to the wind velocity just in front of and above the model.

The wave period is determined as the mean value of a series of waves. The mean wave length can be found from period and water depth. For wind generated waves in the windflume the mean period varies from 0.65 sec with a wind velocity of 4m/sec. to 0.85 sec with a wind velocity of 10 m/sec.

When the wave height and period, using wind only, is too small, a regular paddle generated swell can be applied in combination with a rather high wind velocity to obtain the required period and wave height distribution.

In these experiments only wind was used.

CONSTRUCTION OF THE MODEL

The model was arranged as shown in figure 4; the lower part of the slope was made of plywood while the upper part which was integral with the collecting tank was made of steel sheet. The height and inclination could be readily adjusted.

The model had a width of 0.5 m and was placed in a glass wall flume, which formed part of a windflume, 4 m wide and 50 m long.

Before the model was placed, series of tests showed that the subdivision of the main flume had no effect on measured wave characteristics.

During the tests the wave heights were measured by means of a parallel wire resistance gauge and recorded by a pen-writer. The gauge was located in the portion of the flume not occupied by the model. The overtopping was measured as the volume of water passing the crest during each test.

EXPERIMENTS

Each series of tests consisted of measurements with a fixed inclination, varying crest height and a constant wind velocity. For every

height of the crest the overtopping was measured as the volume of water passing the crest during 600 sec, from which an average value per second could be determined. Also the number of overtopping waves, as a percent of the total number was determined. During each run waves were registra for 120 sec. In this way an average distribution from about 2000 wave heights was obtained for each slope and wind velocity.

Tests were carried out for the following conditions:

Slope	Wind velocity in m/sec (model)						Regular waves
	4	6	8			10	
1 : 8				x		x	
1 : 6½				x		x	
1 : 5	x	x	x	x	x	x	x
1 : 4		x		x		x	x
1 : 3½				x		x	
1 : 3		x		x		x	
1 : 2				x		x	
water depth (m)	0.30	0.30	0.25	0.30	0.35	0.30	0.30

Moreover an investigation was made in which, for series of wind generated waves, those waves causing overtopping were indicated on the wave recording.

RESULTS

OVERTOPPING BY WIND GENERATED WAVES.

An attempt has been made to express the results of these tests in terms of dimensionless parameters as follows. The height of the crest of the seawall above still water level, h, was expressed as the ratio

$$h/H_{50}.$$

It was found that the overtopping could be related to the dimensions of the waves using the ratio.

$$\frac{2\pi Q T}{H_{50} L}.$$

In these parameters means:

h = height of the crest of the seawall above still waterlevel : m.
Q = overtopping in m^3/sec per m length of the seawall
T = wave period in sec.

EXPERIMENTAL DATA ON THE OVERTOPPING OF SEAWALLS BY WAVES

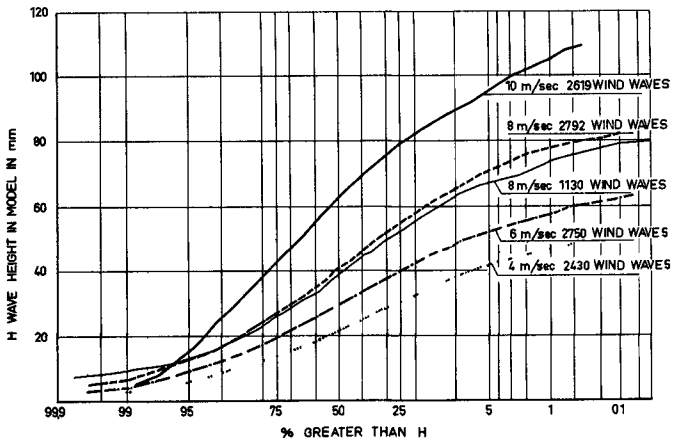

Fig. 1. Wave height distribution in wind flume.

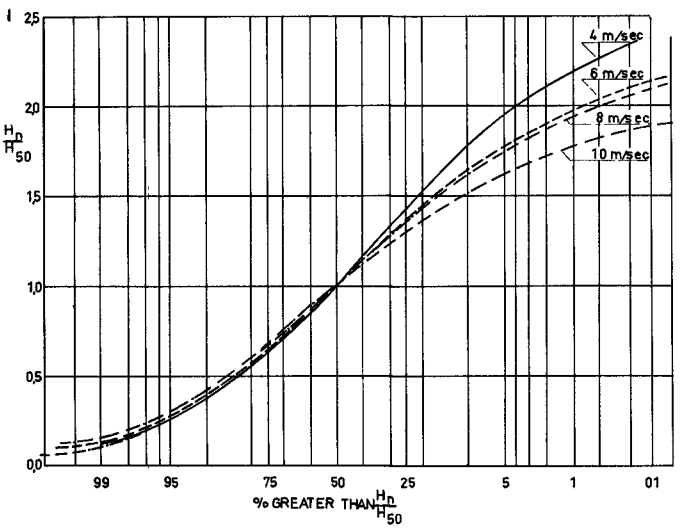

Fig. 2. Distribution of relative wave heights in wind flume

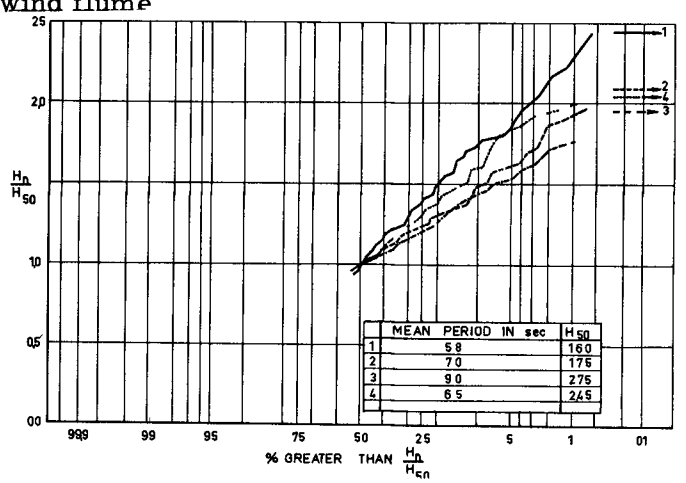

Fig. 3. Distribution of relative wave heights at Katwijk.

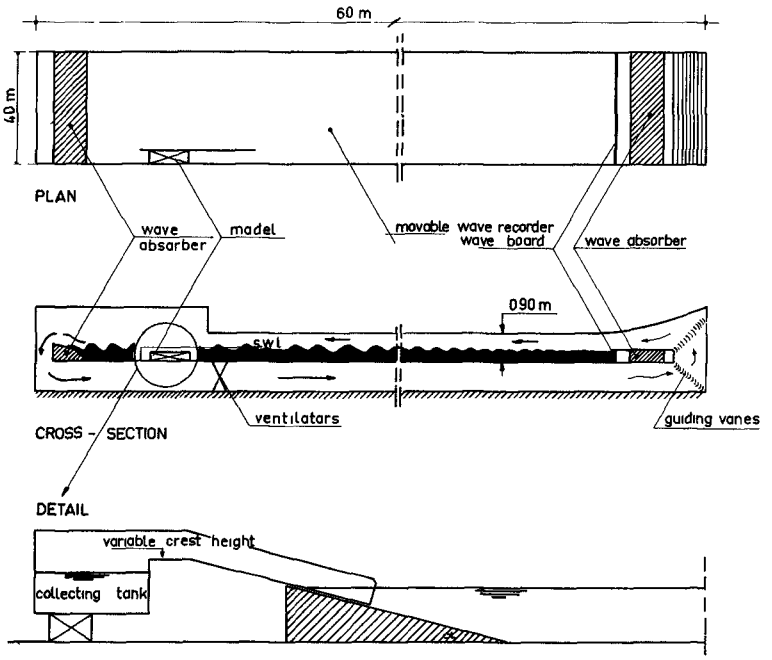

Fig. 4. Arrangement of the model.

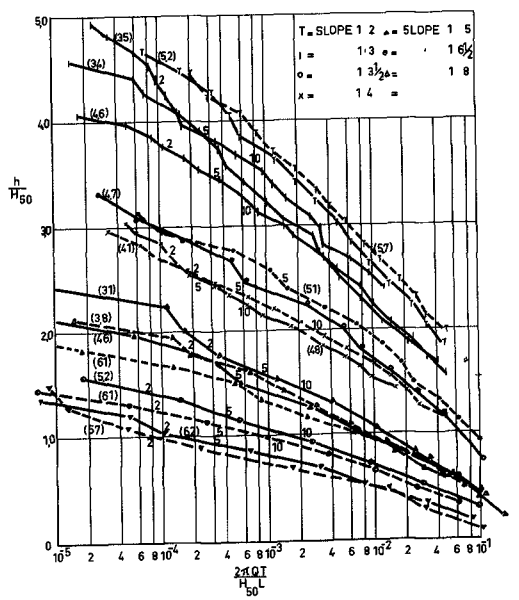

Fig. 5. Overtopping for different slopes. Numbers in brackets indicate wave steepness in %. Plain numbers indicate percentage of waves overtopping.

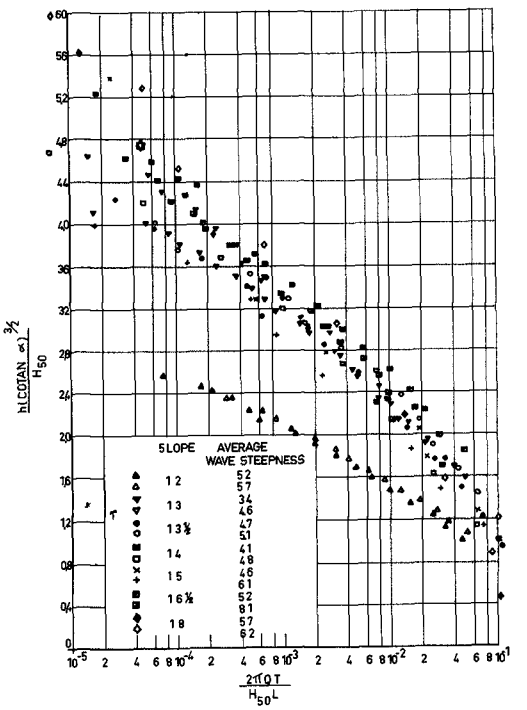

Fig. 6. Overtopping as function of $\frac{h\,(\cot an\ \alpha)^{3/2}}{H_{50}}$

H_{50} = wave height exceeded by 50% in m.
L = wave length in m.
Q_T = average overtopping per wave.

$\frac{H\,L}{2\,\pi}$ = area, in cross section, of a sinusoïdal wave above mean water level.

These results are given in figure 5. For each slope curves for different average wave steepness were obtained, as various wind velocities were applied. Also the percentage of the waves causing overtopping is indicated. From the tests carried out on a slope of 1 : 5, the same results were obtained for a water depth of 0.25, 0.30 and 0.35 m. The wave length in deep water, L_o, according to the periods used in these tests was approximately 1.2 m, so no influence of the water depth, d, was found for $d/L_o \geqslant 0.21$.

In comparing the results for the different slopes, in order to establish the influence of the angle of inclination α, it appeared that the volume of water overtopping the crest is not proportional to tan α. (From former investigations it appeared that the wave run-up exceeded by 2% of the waves, Z_2, could be expressed as $Z_2 = 8\ H_{1/3} \tan \alpha$).

The best results have been obtained using the assumption that the overtopping is proportional to $(\tan \alpha)^{3/2}$, which is shown in figure 6 where, instead of h/H_{50}, $\frac{h\ (\text{cotan}\ \alpha)^{3/2}}{H_{50}}$ has been plotted.

It is seen that with slopes varying from 1 : 3 to 1 : 8 the results can be represented by a single line. But for a slope of 1 : 2 the results are completely different, possibly due to greatly increased reflection of wave energy for the steeper slopes.

Restriction.

It should be noted that there are probably limitations to the applicability of these results and that the experiments reported here were limited to the ranges:

$$0.03 < \frac{H_{50}}{L_o} < 0.06$$

and $$d/L_o \geqslant 0.21$$ in which:

d = water depth
L_o = wave length in deep water

Although the full range to which the results can be applied is not known, it is evident that for small water depths the ratio T/L approaches a constant value so that the parameter $\frac{2\,\pi\,Q_T}{H_{50}\,L}$ is no longer valid since

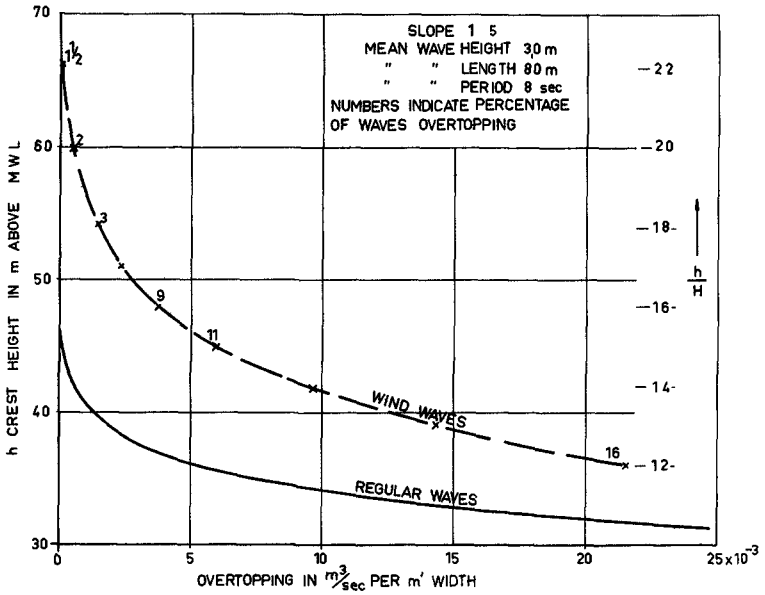

Fig. 7. Overtopping of regular and wind waves.

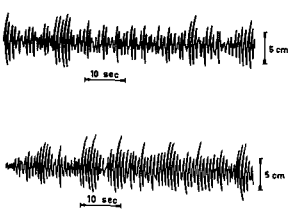

Fig. 8. Example of record. Overtopping waves are dotted.

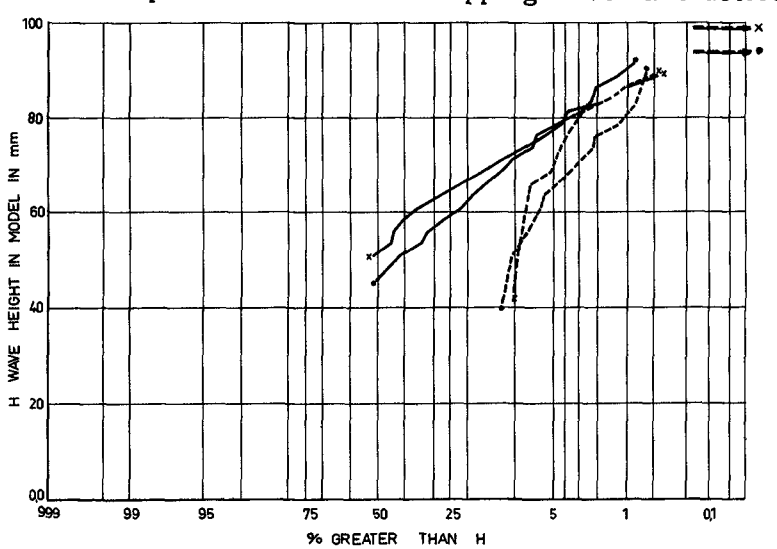

Fig. 9. Distribution of all wave heights (full line). Distribution of overtopping wave heights (dotted).

it does not include the influence of wave length and period.

OVERTOPPING BY REGULAR AND IRREGULAR WAVES.

The overtopping has been measured for regular and irregular waves with the same mean height. The results are given on figure 7.

As could be expected, the irregular waves produced more overtopping. It can also be seen from this figure that there is no simple relationship between the height of a regular wave which will give the same overtopping as a given irregular wave, because the height of the seawall crest must also be taken into account.

If there was a direct relationship between the overtopping and the height of individual waves it would still be possible to estimate the total overtopping from a series of tests with regular waves of various heights by multiplying each overtopping quantity in proportion to the percentage of waves of that height occurring in the spectrum.

Figure 8 gives an example of a wave record in which the overtopping waves are indicated and from which it can be seen that the overtopping does not depend only on the height and length of the individual waves. This is also illustrated in figure 9 where as a result of these tests wave height distribution curves are given for all the waves exceeding H_0 and for the overtopping waves. The percentage relates to the total number of waves in the series. When n% of the waves causes overtopping it is certainly not the highest n% which is involved. So a direct relationship between the overtopping and the height of individual waves does not exist.

Obviously these effects of irregular waves cannot be reproduced by regular waves.

CONCLUSIONS

a. The overtopping of seawalls depends largely on the irregularity of waves. The effects cannot be reproduced in a model using regular waves.

b. Statistical distributions of wave heights in nature, can be reproduced in a windflume of suitable dimensions.

c. In the design of seawalls a better idea about the probability of failure is obtained taking as a criterion the volume of overtopping water as well as the percentage of overtopping waves.

d. When the height of the crest is based on the criterion of 2% of waves overtopping, the quantity of overtopping water is very small.

e. For $\tan \alpha < 1/3$, the volume of overtopping water was found to be proportional to $(\tan \alpha)^{3/2}$.

CHAPTER 37

DETERMINATION OF THE WAVE ATTACK ANTICIPATED UPON A STRUCTURE FROM LABORATORY AND FIELD OBSERVATIONS

W.A. Venis
Engineer, Hydraulic Division
Service of the Deltaworks, Rijkswaterstaat, The Hague.

1.0 INTRODUCTION.

1.1 The structure. In one of the estuaries of the Rhine-Meuse delta, the Haringvliet, a series of discharge sluices is under construction as part of the Delta works [fig.1 and 2]. The effective aperture of the sluices when completely opened is 6000 m^2 below N.A.P.*)
Such an opening is necessary in times of high river discharges to enable large quantities of water (up to 20,000 m^3/sec) to be drained away and floating ice to be got rid of in severe winters. To meet the latter requirement the spans of the sluice-openings have been fixed at 56,5 m. The sluice consists of 17 identical openings separated by piers about 5 m wide.

Each opening can be closed with two steel gates. Each gate is connected by means of four steel levers to the Nabla-beam, a triangular, hollow girder of prestressed concrete, which also serves as a traffic-bridge [fig.3]. The gates can be moved independently by means of hydraulic lifting mechanism.

In the event of a storm surge the sluices will be closed; then they may have to withstand a maximum head of 4,5 m.

As the Haringvlietsluices are vital to the water economy of the northern delta area, they must be extremely reliable. Consequently when both gates are closed, or while they are being opened or closed, the structure will have to be capable of withstanding wave attack.

In principle two kinds of wave attack can be distinguished in this case:

a. Wave load in a horizontal direction; this may occur when the gates are closed. The magnitude of the loads determines the design of the gates, the levers and the Nabla-beam [fig.3].

b. Wave-load in a vertical direction; this will occur, in combination with the horizontal load, when the gates are lifted during wave motion. The proportioning of the lifting mechanism is largely determined by this particular load.

*) N.A.P. is a datum level, approximately at mean sea level.

Fig. 2. Situation of the sluices and the wave measuring poles in the Haringvliet.

Fig. 1. Delta scheme in the southwest of the Netherlands.

1.2 Purpose of the study and the data used.

Modeltests have been carried out to obtain an insight into the magnitude of the wave-pressures in various situations. These tests showed, that sharp high pressure peaks occur in addition to the pressures caused by the reflecting of the waves, which pressures are quasi-static. As the structure can be compared with a multiple mass-spring system these pressure-peaks may cause the whole construction to vibrate. Wave-attack therefore can be expressed in terms of impact. Moreover, calculations revealed that the impact pressures were critical factors in determining the strength of the structure.

So many model tests were carried out to determine the design and location of the sluices. These tests involved numerous water-levels discharges and waves. Regarding the pressure-peaks a comparative study was made in the model, which led to the structure being designed in such a way that the occurrence of critical impacts was reduced to an acceptable minimum.

As it was impossible to avoid the occurrence of impact pressures entirely it remained necessary to determine a basic load for the structure that takes care of the impact pressures. As it has not yet appeared possible physically to determine a theoretical maximum for the impact pressures, it has to be borne in mind that there is a probability that each pressure measured will be exceeded.

So this paper describes, how the cumulative frequency curve of the impacts for the case mentioned in 1.1 sub a, which served as a basis for determining the basic load was arrived at by a certain combination of laboratory and field observations.

The data used for this purpose were

a. Results of wave-impact measurements on a model of the sluices. This model, built in accordance with the results of the comparative study, was situated in the wind-flume of the "de Voorst" hydraulic laboratory.

b. Wave height measurements in the Haringvliet during 1957 and 1958.

c. Wind-speed measurements on board the lightship Goeree, likewise during 1957 and 1958.

d. Tidal registrations at Hellevoetsluis from 1920 to 1960.

e. Wind-force data from the Hook of Holland, likewise from 1920 to 1960.

2.0 THE MODEL.

2.1 Description. Investigation into the reaction of the structure to impact-pressures can be conducted in two ways, dependent on the model chosen:

a. An elastic, identical scale model, on which deformations are measured directly.

b. A relatively rigid model on which pressures are measured by means of pressure gauges, the recordings of which are used as a basis for computing the deformation of the

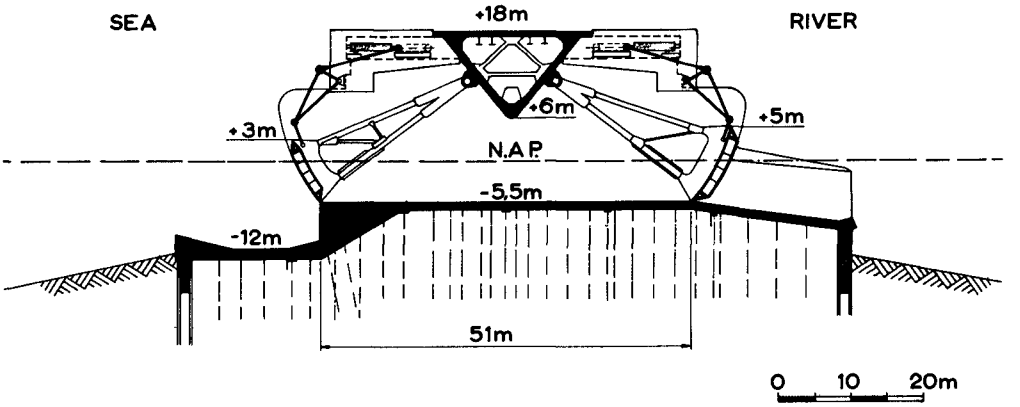

Fig. 3. Cross section of the sluice.

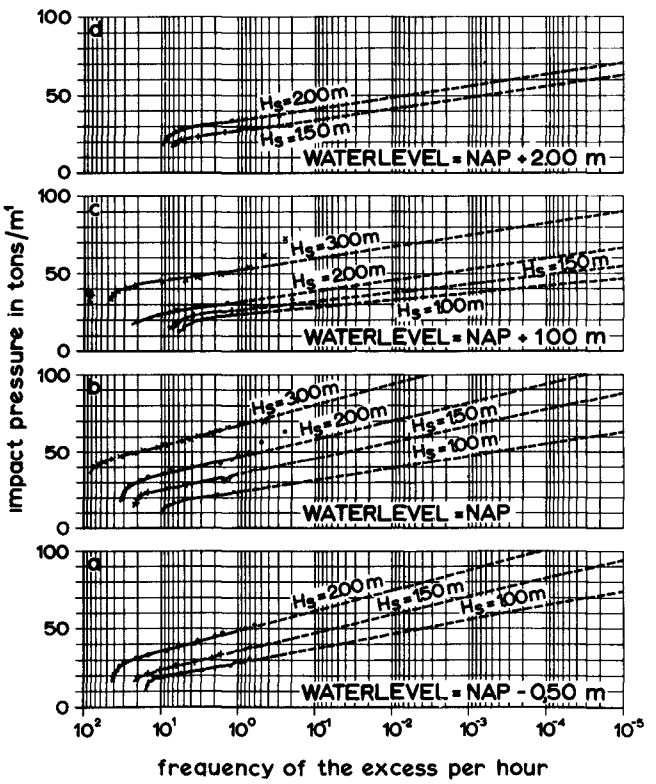

Fig. 4. Frequency curves of the excess per hour of the impact pressures measured in the model for different combinations of water levels and significant wave heights (Wave attack from the sea).

structure.

Method b was chosen, because the external shape of the construction was already known, but not the exact proportioning of the components. In addition this method linked up with the comparative study that had also been carried out on a rigid model.

The model, which was built of concrete, was on a scale of 1:40. In the model the external geometrical shape of the closed gates, the piers and the floor was reproduced.

Preliminary study showed, that the impact pressures occur simultaneously over the entire height of the gate [lit.2]. The width of the area in which the impacts occurred was variable. A correlation between the breadth of attack and the magnitude of the wave pressure could not be discovered, however. As it is not impossible that the spread found in the breadth of attack depends on the properties of the windflume and because no data were available from the prototype it was assumed, that every wave load would affect the full width of the gate instantaneously. In this connection three pressure gauges of the capacitive type (resonance frequency under water = 1400 Hz) were placed one below the other in the middle of the model gate.

The most important purpose of our study was the determination of the basic load for the Nabla-beam. Because of the special shape of the structure the Nabla-beam only "feels" the natural or forced vibration of the gates caused by a certain mean value of the wave-pressures. To simplify the elaboration, the pressures measured simultaneously were averaged electronically. This average was registered by filming the screen of an oscilloscope connected to the pressure gauges.

2.2 Situations tested in the model. In the model wave pressures were measured in the following situations.

a. Wave attack from the sea on the closed outer gate.

b. Wave attack from the sea on the closed inner gate, when the outer gate was open.

c. Wave attack from the Haringvliet on the closed inner gate.

d. Wave attack on the closed outer gate, when the inner gate was open.

Cases b and d are not dealt with here, because in them the wave pressures were much lower than in the other situations.

The wave attack from the sea was measured for the following combinations of water-level and significant wave height:

Water-level	Significant wave height in m.
N.A.P. - 0.50 m	1.00 1.50 and 2.00
N.A.P.	1.00 1.50 2.00 and 3.00
N.A.P. + 1.00 m	1.00 1.50 2.00 and 3.00
N.A.P. + 2.00 m	1.50 and 2.00

Water-levels, higher than N.A.P. + 2.00 m were not considered, because the comparative study showed that then the pressure

becomes relatively low.
This is due to a bend in the plating of the gates from N.A.P. + 1.00 m to N.A.P. + 3.00 m, when they are closed. At water-levels lower than N.A.P. - 0.50 m the likelihood that wave motion of any importance will occur is so small that these levels have not been considered, either.

In the model tests for wave attack from the Haringvliet it was assumed, to be unlikely that high water-levels and strong easterly winds would occur simultaneously. Therefore only a water-level of N.A.P. - 0.50 m, combined with significant wave heights of 0.80 m and 1.50 m, was investigated for such a contingency.

In the windflume the waves were generated by means of wind only [lit. 3] .

2.3 Model results. For each situation tested in the model a frequency curve was obtained, showing how often a certain value of the impact pressure is exceeded on an average in a certain period. The period during which measurements in the model are taken depends on the one hand on the accuracy with which one wishes to determine the frequency curve, but on the other hand on the properties of the windflume and the extent of the investigation. In this case the duration of each measurement was restricted to 40 minutes of model time, corresponding to about 4 hours of prototype time. In this way any pressure, exceeded on an average once per hour, can be determined fairly accurately. Pressures occurring less frequently have been determined by rectilinear extrapolation of the frequency curve of excess on logarithmic paper [fig. 4a t/m d and fig. 5] .

In this way the frequencies with which the wave pressures for each combination of water-level with significant wave-height were exceeded, were ascertained.

3.0 FREQUENCIES OF WAVE ATTACK.

3.1 Wave attack from the sea. With the aid of the data obtained from the prototype an attempt has been made to discover at what frequencies certain combinations of water-level and wave height occur. First the registrations of wave recorder C in the Haringvliet [fig.2] were worked out. The period considered ran from 30-1-1957 till 23-1-1959. The recorder measures wave heights as well as water-level variation. So frequency curves of the excess of the significant wave heights could be determined, expressed in percentages of the time the water-level was lower than that stated [fig.6] . The accuracy of these data, however, was considered to be too small because

a. the recording period of about two years did not form a good enough basis, for extrapolation to very low frequencies.

b. the registrations of waves generated by winds blowing from directions between west and north could not be separated from the aggregate.

This was necessary, as laboratory tests showed that impulse loads only occur when the waves attack the sluice at

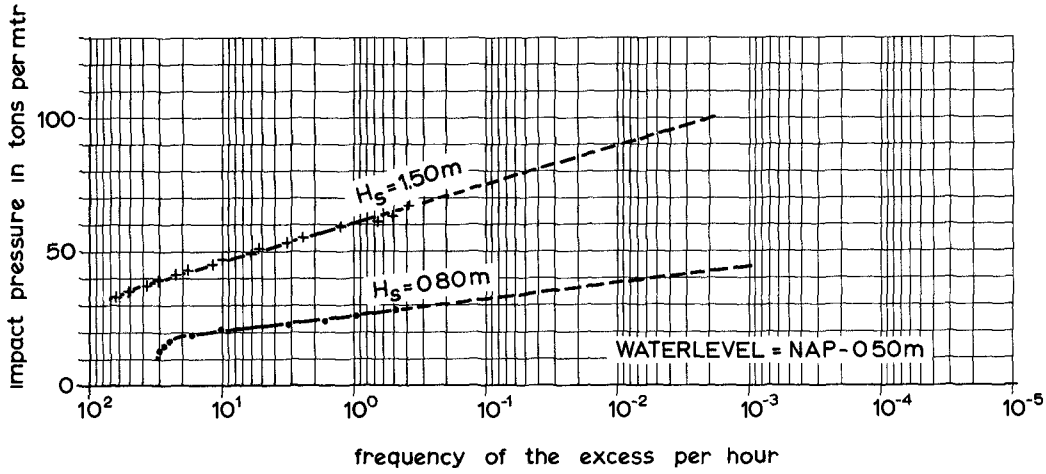

Fig. 5. Frequency curves of the excess per hour of the impact pressures measured in the model for two combinations of water level and significant wave heights (wave attack from the Haringvliet).

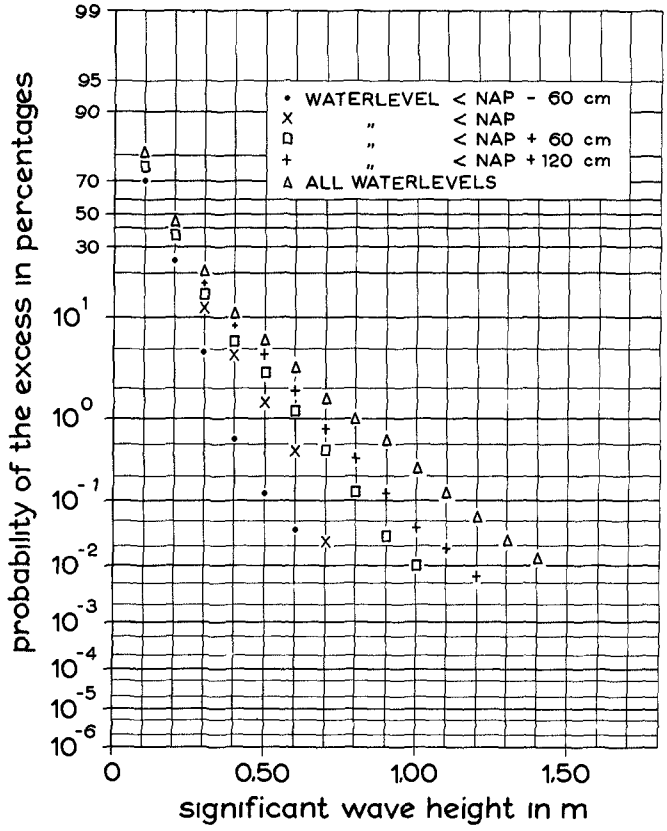

Fig. 6. Frequency curves of the significant wave heights at pole C, in a percentage of the time during which the stated water level is not exceeded.

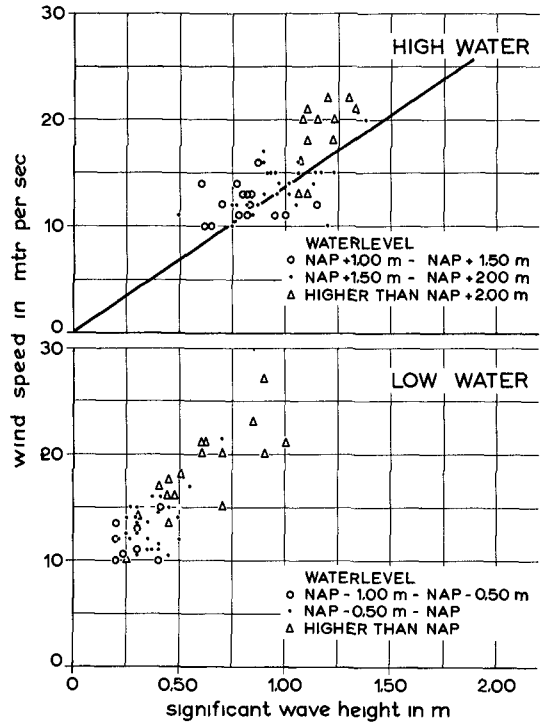

Fig. 7. Correlation between the wind-speeds measured on board the lightship "Goeree" and the significant wave heights measured at pole C.

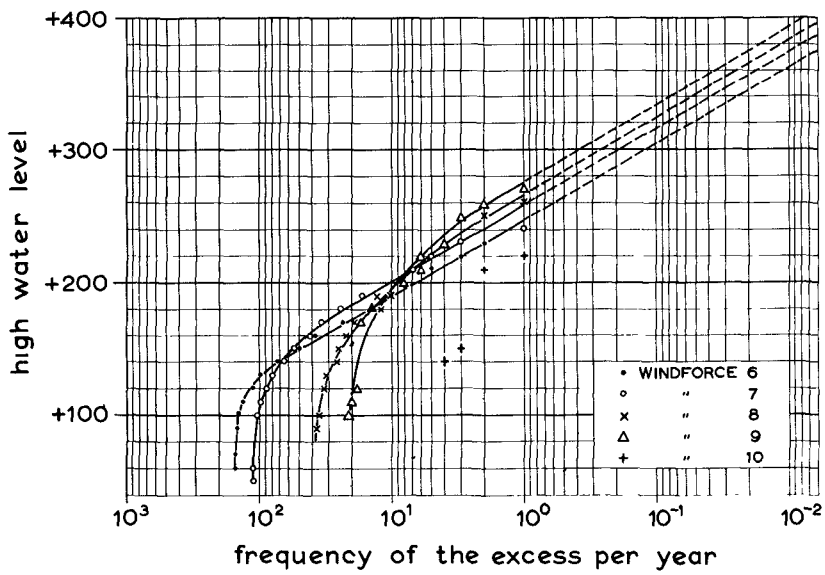

Fig. 8. Frequency curves of the excess per year of the high water levels at Hellevoetsluis, provided the stated windforce occurs.

right angles. The location of the sluice in the prototype [fig.2] shows that this attack is most likely with north-westerly winds.

With this in mind an attempt was made to obtain the desired frequency-data indirectly.

The wave registration period of two years did appear long enough to establish the relation between the wave heights registered and the corresponding wind-speed and direction. Wind measurements carried out on board the lightship "Goeree" during the two year period were used but only those readings showing

c. wind speeds in excess of 10 m/sec.

d. winds blowing from between west and north.

The wave height and water-level registered at pole C was then checked for each of these readings. The result is given in two diagrams [fig.7a and b], one for the group of water-levels around low water and one for the group of water-levels around high water. The line drawn through the points in the high water diagram, is regarded as the correlation between wind-speed and wave height. This premise is unfavourable for the present situation. In the ultimate situation, however, there may be three reasons for using the line given.
Firstly, the sluices will be closed only during the high water period, secondly, when the sluices are closed tidal currents will cease to influence wave development and thirdly, the Haringvliet will become much deeper locally in future.

Then again, a selection was made from the tides registered at Hellevoetsluis and from the corresponding wind measurements in degrees Beaufort carried out at the Hook of Holland in each of ten years chosen at random from the last forty years. These wind data satisfied the criteria mentioned under c and d.
With these figures frequency curves have been drawn from which the frequency of excess of a high water-level, dependent on the wind force could be deduced. It is assumed that these lines will also hold good in the future situation [fig.7].

Now, with the aid of the correlation line for wave height and wind-speed it is possible to determine the frequency with which certain combinations of water-levels and wave heights can be expected on an average. It should be noted, that the data given are the medial values of intervals from a continuous distribution.

The frequencies thus obtained are unfavourable as the whole of the tidal cyclus (approx. 12½ hr) has been considered, even if the wind blew from the northwest for only part of that time.

3.2 Wave attack from the Haringvliet. The wave-measuring poles, in the Haringvliet are all situated on the seaward side of the sluice. Therefore they are on the lee-side of the building-pit for these sluices when the wind is blowing from directions between south and east. In order to get an idea of the wave motion to be expected, ten years of registrations of the wind recorder at Hook of Holland (1949-1958), were selected for directions between 95° and 145° with regard to the north. This selection has been worked out as a frequency curve of the excess of the wind-speeds. From these, with the aid of the Bretschneider

diagrams for the generation of waves in deep water frequency curves of the excess of the wave heights have been plotted [fig.9]. The results of the wave height calculations, for which a certain fetch was adopted, have been checked by incidental visual wave height observations in the field. Although the visual observations gave values lower than those calculated, the latter have been taken into account, also in view of the future greater depth of the Haringvliet, on this landward side of the sluice as well.

The conditions for the occurrence of high water-levels on the Haringvliet lake are well known. The probability of these high water-levels coinciding with stormy easterly winds is negligible. The average daily level will fluctuate between N.A.P. and N.A.P. + 0,50 m. By using a water-level of N.A.P. - 0.50 m in the modeltests an extra margin of safety has been provided.

4.0 THE CUMULATIVE FREQUENCY CURVE OF THE PRESSURES.

4.1 For wave attack from the sea. The results of the model-investigation shown in fig.4a to d combined with the data from the field described in 3.1, give the total average frequency of excess of the wave pressures per year. This is obtained by multiplying the frequencies of excess of the pressures for each combination of wave height and water-level with the frequencies in hours per year of the occurrence of these combinations and adding up of the results. The year-frequency curve of the pressures can be found by carrying out this operation for a number of pressures and plotting the values obtained on probability paper. It will appear as a straight line on logarithmic paper, which has been extrapolated rectilinearly for the higher pressures, viz., the lower frequencies.

The operation described applies to one sluice opening only. For considering any opening, the frequencies found will have to be multiplied by 17, as the whole construction has 17 openings. In this connection it is assumed, that statistically speaking the circumstances are identical for all the sluice openings [fig.10].

The curve thus obtained gives the frequency of excess of the value of the pressure-peak as measured in the rigid model. As already stated these pressure-peaks possess the characteristies of impulses. Therefore an impact-factor will have to be introduced into the static calculation of the stresses in the structure. The magnitude of this factor depends on the part of the structure considered [lit.1 and 2] and other factors. With the results of numerous calculations as a basis this impact factor has been fixed at 2 for the Nabla-beam and 1.35 for the gate and the levers.

4.2. For wave attack from the Haringvliet. This was dealt with in the same way as the foregoing. The data used were those given in fig.5 and fig.9.

5.0 THE BASIC LOAD.

5.1 The frequency adopted. For partly subjective economic considerations a basic load for the Nabla-beam was chosen having an average probability of excess per year of 5.10^{-5}. The load thus found must be taken as the breaking load of the Nabla-beam. This also means that there is a greater probability of the occurrence of cracks, requiring repair and a still greater probability of cracks occurring that will close again because of prestressing.

If it is assumed, that the construction will be out of date in 200 years and will therefore have to be replaced by a new one, the frequency chosen means a one percent probability that the breaking load of any Nabla-beam will be exceeded during the lifetime of the structure.

The main difficulty was that the phenomena we dealt with were of a statistical nature the laws governing which are as yet obscure. To obtain an insight into the possible spread if pressures and wave height do not follow the logarithmic distribution described here the same process was applied to extrapolations on different kinds of probability paper.

The actual choice of the basic load was made from a comparative study of the frequency curves thus obtained.

6.0 COMMENTARY

6.1 Consideration of the doubtful points. Excessive extrapolation of the frequency curves of the excess of the wave-pressures is required when determining the basic load.
This is sufficient reason for considering the results with a certain reserve. Moreover it should be borne in mind that a satisfactory answer to the following questions has not yet been given:

a. Over what width will the wave attack affect the structure? For safety's sake it was assumed that the wave attack will affect the whole width of one sluice-opening instantaneously.
An insight into the degree of safety will only be obtained when enough is known about the breadth and shape of the wave-crests in the prototype.

b. What correlation exists between the magnitude of the pressure-peak and the impact factor. From calculations it is known, that the impact factor depends largely upon the time in which the pressure rises from zero to it's maximum [lit.2].

Preliminary tests showed no direct correlation; however, the investigation was limited. For safety's sake therefore the impact factors mentioned in 4.1 were introduced.

c. The shape of the waves in the laboratory and in the prototype. As already mentioned the waves in the laboratory were generated by wind [lit.3]. As the fetch in the windflume was not to scale, the wind-speed was exaggerated. This caused the wave height distribution to show a flattening especially for the higher waves, which has not yet been observed in the prototype.

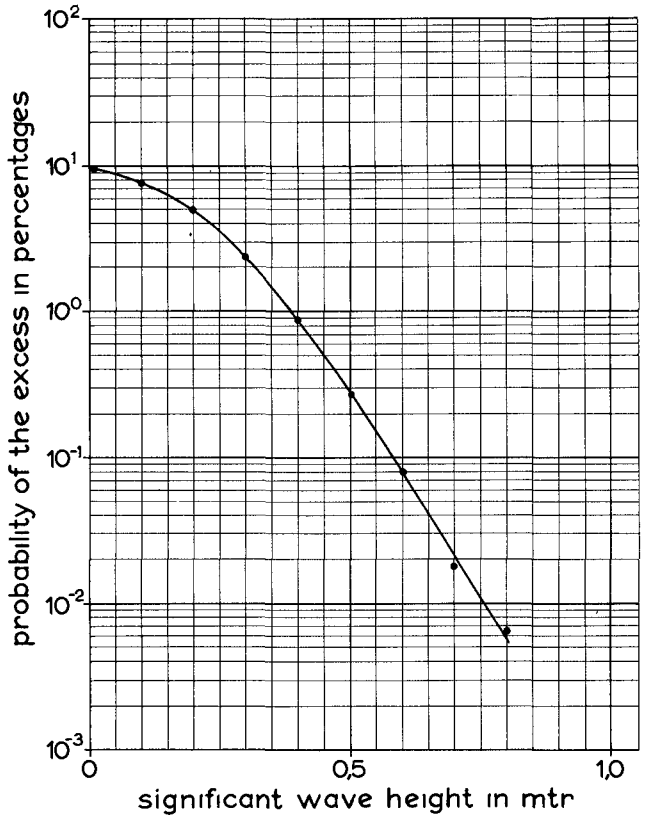

Fig. 9. Probability of the excess of the significant wave heights on the Haringvliet, provided the wind blows from directions between 90° en 145° with respect to the north.

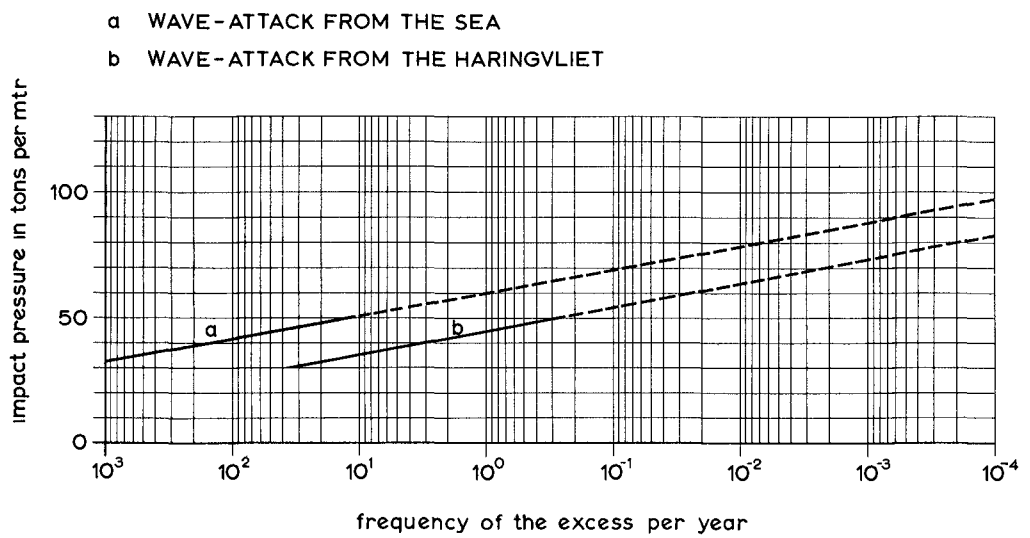

Fig. 10. Cumulative annual frequency-curves of wave-pressures.

The wave recorders placed on top of the wave-measuring poles, however, do not yet permit the working out of any series longer than 100 to 150 waves, so that information about the "tail" of the distribution is still very scarce. For comparison it is noted, that the distributions in the windflume are determined from series of 500 to 1500 waves.

Neither has it appeared possible so far to get an adequate idea of the extent of the agreement between prototype and windflume as regards the shape of the wave. Determination of the shape is very difficult, as the registration is a height/time diagram which has to be transformed to a height/length diagram via an idealised formula for wave celerity. In the windflume this can be done with comparative ease; however, for the prototype, with its freakish bottom configuration no satisfactory method has been found yet.

d. To what extent does the wave registration of pole C represent the ultimate situation and the whole of the Haringvliet. Only the future can answer this question, as the bottom configuration will undergo a considerable change. As already stated it was assumed for the present that the waves will become somewhat higher than they are now. This also depends on the available fetch, which may change because of banks that may be formed in the mouth of the Haringvliet.

6.2 Summary. The basic load of the Haringvliet-sluices was arrived at by accepting a certain probability of excess of this load. The calculation of this probability was based on a combination of observations in the laboratory and in the field. An outline has also been given of the doubtful points, which have been circumvented by introducing a safety factor.
The basic load for the lifting mechanism was determined in a similar manner. A difficulty here arose because of our ignorance of the water-level variations in the Haringvliet lake of the future.
This problem was solved by tracing the course of the water-level variations during ten years chosen at random from the last forty years, supposing the sluices had already been present in that period. So the points of time of equal water-level on either side of the sluices (criterion for the opening of the gates) as well as the slack water period (criterion for the closing of the gates) could be determined, together with the corresponding water-levels.

REFERENCES

E.W. Bijker, M.A. Aartsen and W.C. Bischoff van Heemskerck.
Wave impacts on the steelgate of a discharge sluice.
Proc.Congres IAHR. 1959 Montreal.

M.A. Aartsen and W.A. Venis.
Model investigations on wave attack on structures.
Proc. Congres IAHR 1959. Montreal.

J.E. Prins. Model investigations of windwave forces.
Proc. Coastal Engineering. 1960.

CHAPTER 38

LA PRESSION DES VAGUES CONTRE LA PAROI ABRUPTE

M. E. Plakida

Ingenieu en Chef des Ponts et Chaussees,
Chef du Laboratoire d'onde de l'Institut
Central des Recherches Scientifiques du
transport par eau.
Moscou, U.R.S.S.

Generalites

La recherche du type le plus rationel des ouvrages de protection il est devenu necessaire d'evaluer l'action des vagues sur les parois à fort degré d'inclinaison; l'angle d'inclinaison du mur avec l'horizon α peut changer de 45° a 90°.

Les résultats de l'étude sur les modèles reduits sont décrits dans cet article, ce qui concerne la pression des vagues contre la paroi abrupte et la hauteur de remontée des vagues.

Le présent article fournit des formules en vue du calcul de la pression maximum des vagues et de la hauteur maximum de remontée des vagues.

Les études ont été effectuées dans une cuve vitrée de 12.0 m. de longueur, de 0.5 m. de largeur et d'un mètre de hauteur. Les vagues ont été produites par le batteur plongé.

La profondeur d'eau dans la cuve est constante et égale à 55 cm.; les profondeurs d'eau entre le niveau du repos et la risberme sont égales à 20 et à 40 cm. La largeur de la risberme est constante et égale à 15 cm., la pente du prisme est de I:2. L'angle d'inclinaison du mur avec l'horizon change de 45° à 90°, avec espacement de 15°.

Le régime d'onde est défini par la cambrure de vague qui change de I:I0 à I:25, la hauteur de vague est de 10 à 12 cm. et la période de vague est de 0.75 à 1.20 sec.

Nous avons adopté les notations suivantes:

2h - hauteur de la houle;
2L - longueur d'onde de la houle;
2T - période de la houle;
H - profondeur de l'eau;
H_δ - profondeur de l'eau entre le niveau de repes et la risberme;
α - angle d'inclinaison du mur avec l'horizon;
t - hauteur du prisme;
P_o - pression excédentaire due à la vague contre le mur vertical ou le mur abrupte au point du niveau de repos;
P_{6h} - pression excédentaire due à la vague contre le mur vertical au point submergé à la profondeur égale de trois fois la hauteur de vague;
$P_{6h\alpha}$ pression due à la vague contre le mur abrupte au point submergé au-dessous du niveau de repos égale de trois fois la hauteur de vague;
P^1_α - pression due à la vague contre le mur abrupte au point de la cote de la risberme;
R_e - effort résultant (excédant la pression hydrostatique) sur la surface du mur abrupte;
W_e - effort de soulèvement dû aux vagues (excédant la pression hydrostatique) et agissant sur la semelle de l'ouvrage;
Z_d - maximum de hauteur mouille au mur abrupte;
A - amplitude total d'oscillation de l'eau au mur abrupte;

La pression de vague

Nous avons effectué 4800 mesures de la pression due à la vague contre le mur vertical et abrupte des appareils tensiométriques et nous avons tracé 12 planches; dont l'une est prétentée ici (voir fig. 1).

Cette planche indique la variation des valeurs suivantes au cours de la période de vague sur des parois inclinées de 90°, 75°, 60° et 45°:

- la pression due à la vague aux 5 points situés sur le mur;
- l'oscillation du niveau de l'eau près du mur;
- l'effort résultant due à la vague contre le mur.

On peut voir sur cette planche la variation de la pression due à la vague contre le mur vertical ou abrupte aux points situés sur les niveaux divers entre le niveau de repos et le pied du mur.

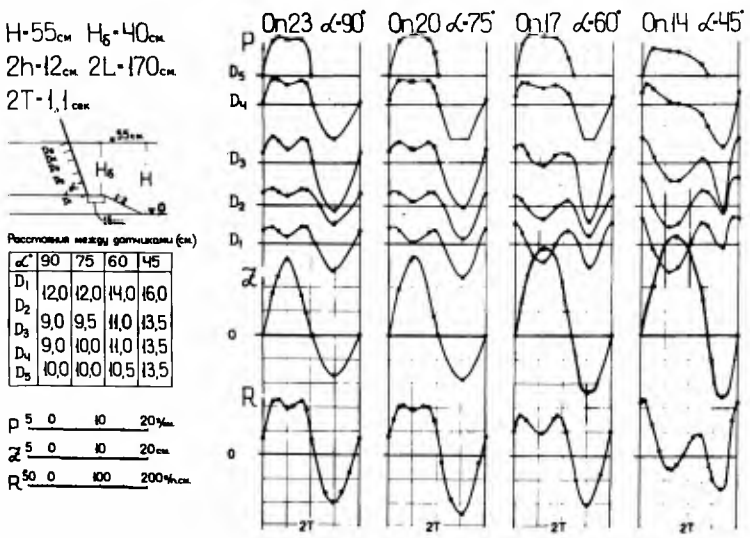

Fig. 1. Chronogrammes of wave pressure, level oscillation and resulting pressure.

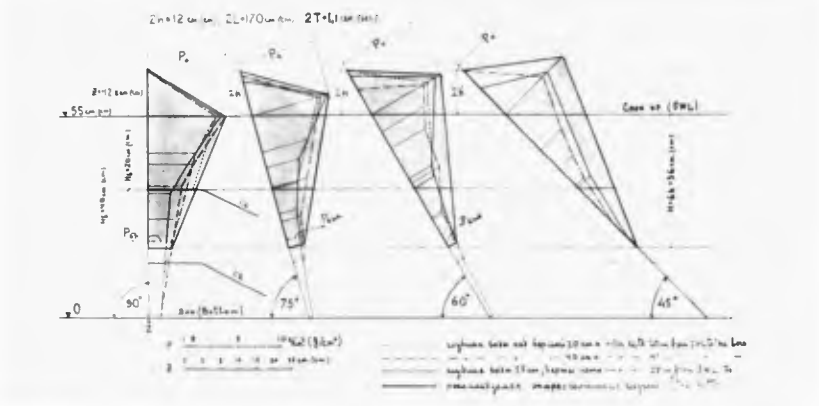

Fig. 2. Wave pressure diagrams.

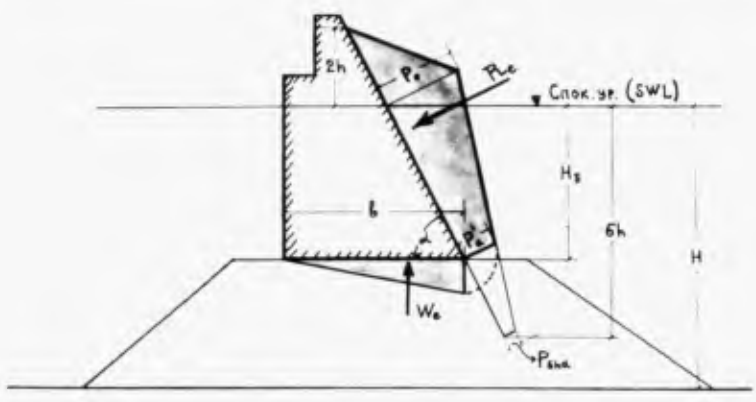

Fig. 3. Wave pressure diagram on the steep sloping wall.

Il y à noter que la pression de vague au niveau de repos des études NN23, 20 et 17 ne depend pas pratiquement du degré d'inclinaison du mur

On peut aussi voir, que la variation de la pression due a la vague contre le mur vertical a une pleine concordance (voir fig. 1, étude N23) avec la théorie générale du clapotis au deuxième ordre d'approximation (1, 2, 3 et 4)

Les quatre extreme notes sur le chronogramme de la pression due a la vague contre le mur vertical se conservent aussi sur les chronogrammes de la pression due à la vague contre le mur abrupte.

On observe la reflexion des vagues du mur abrupte et la naissance du clapotis, mais ce clapotis se transforme à cause de l'inclinaison du mur. Le premier n oeud du clapotis se trouve plus près que dans le cas du mur vertical, en estimant la distance sur le niveau de repos du mur abrupte.

La montée du niveau de l'eau contre la paroi abrupte dans le cas général a lieu plus tard que le maximum de la force resultante due à la vague contre le mur abrupte.

Selon nos expériences, nous avons detérminé que pour la cambrure de la vague $\frac{2h}{2L} \geqslant 0.07$ et que pour la longueur d'onde relative à $\frac{2L}{H} \leqslant 4$, la hauteur mouilée ne dépasse pas la hauteur de la vague au moment où la pression de vague atteint sa valeur maximum (voir fig. 2).

Les épures recommandées sont données par la couleur sombre sur fig. 2; nous montrons aussi sur cette planche la comparaison des épures mesurées au moment où la pression due à la vague contre le mur abrupte est maximum.

Cette comparaison montre que les épures recommandées ont les surfaces plus grandes que les surfaces des épures mesurées. Ceci est une certaine garantie de la sécurité.

On a établi par l'analyse des épures maxima de la pression de la vague dans la cas $\alpha = 45°$ que la pression de la vague est égale à zero presque au point submergé à la profondeur égale de trois fois la hauteur de la vague.

La hauteur de remontée de la vague, lorsque nous avons le maximum de la pression contre le mur abrupte, ne dépasse pas la valeur égale à la hauteur de la vague.

Outre cela, la pression de la vague contre le mur abrupte au point du niveau de repos est egale presque à la pression de vague contre le mur vertical.

Nous avons utilise ces circonstances pour tracer le haut de l'épure qui est situee au-dessus du niveau de repos.

Nous avons adopté la loi lineaire du changement de la pression due à la vague contre le mur abrupte au point submergé au-dessous du niveau de repos de trois fois la hauteur de vague.

On peut écrire la formule suivante

$$P_{6h\alpha} = P_{6h} \left(\frac{\alpha^\bullet}{45^\bullet} - 1 \right) \qquad (1)$$

En utilisant cette formule nous pouvons tracer l'épure de la pression de vague au-dessous du niveau de repos, à savoir entre le niveau de repos et le pied du mur.

Si la risberme est submergée moins que 6h, mais en tout cas plus grande que 3h alors il est necessaire que l'épure de la pression soit coupée au point de la risberme. La formule dans ce cas est suivante

$$P^1_\alpha = P_{6h\alpha} + (P_o - P_{6h\alpha}) \left(1 - \frac{H_\delta}{6h} \right) \qquad (2)$$

Les efforts résultants R_e et W_e sont déterminés aux surfaces de l'épure correspondante (voir fig. 3).

On a à calculer les valeurs de la pression excédentaire due à la vague P_{6h} et P_o contre le mur vertical, qui se trouvent dans les formules (1) et (2), de la méthode par Metelitchina (4). Cette méthode est basée sur la théorie générale du clapotis Mich et Biesel (1,2).

Hauteur mouillee

Nous avons effectué 1242 mesures de l'oscillation due niveau d'eau sur le mur vertical et abrupte.

L'amplitude total de l'oscillation du niveau d'eau s'accorde avec la formule suivante

$$A = \frac{yh}{\sin \alpha} \qquad (3)$$

Le maximum de la hauteur mouillée pres du mur abrupte peut être déterminé par la formule suivante

$$Z_\alpha = \frac{2h}{\sin \alpha} + h_o \left(3 \frac{\alpha_o}{45^\circ}\right) \qquad (4)$$

où

$$h_o = \frac{4\pi h^2}{2L} \operatorname{cth} \frac{J_1 H}{L} \qquad (5)$$

En conclusion, nous notons que la méthode exposée plus haut de la construction de l'épure de la pression de la vague sur le mur abrupte est approximative, mais elle est assez satisfaisante du point de vue de pratique.

Nous avons fait publier les résultats de notre investigation de ce sujet dans les articles séparés (5, 6 et 7).

Bibliographie

1. Mich R. Mouvements ondulatoires de la mer en profondeur constante ou décroissante. Annales des Ponts et Chaussées, 1944.

2. Biésel F. Equations générales au second ordre de la houle irrégulière. La Houille Blanche, N 3, 1952.

3. Кузнецов А.И. Взаимодействие стоячих волн с вертикальными стенками. Сборник трудов МИСИ № 20, 1957.

4. Метелицына Г.Г. Новый метод определения волнового давления на гидротехнические сооружения типа вертикальной стенки в условиях водохранилищ. Речной транспорт № 4, 1959

5. Плакида М.Э. и Метелицына Г.Г. Волновое давление и высота выката волны на крутонаклонные стенки. Труды ЦНИИЭВТ'а вып. XУ, Вопросы гидротехники, 1958

6. ---------- " ---------- Высота выката волны у крутонаклонной стенки. Речной транспорт № 9, 1957

7. ------ --- " ---------- Волновое давление на крутонаклонную стенку. Речной транспорт № 12, 1958

Перевод автора статьи: М.Плакида

М.Плакида 17.7.60

CHAPTER 39

THE CLAMP-ON WAVE FORCE METER

Lars Skjelbreia, Ph.D*
Group Supervisor
California Research Corporation
La Habra, California

INTRODUCTION

Because of the tremendous increase in offshore activities, a great effort has been made on obtaining information on wave forces on structural members. Several oil companies have invested large sums of money in the design and construction of full-scale systems for measuring the wave forces. The equipment used for measuring the forces have been single cantilevers or segmented piles designed to make discrete measurements along the pile. For instance, during the last five years, The California Company and California Research Corporation (subsidiaries of Standard Oil Company of California) operated an installation in the Gulf of Mexico with four segmented piles of different diameters. The wave forces were measured by three-foot high force dynamometers located at seven different elevations along the length of each test pile. Each dynamometer was constructed from a section of the cylindrical pile which was attached to a system of flexures on the inside.**

So far the wave forces have been measured on cylindrical piles varying in diameter from one to four feet and in water depths varying from 30 to 50 feet. As the pile diameter and water depth increase, however, the measurements of wave forces by use of a cantilever or a segmented pile become very difficult and expensive. Therefore, a need exists for investigating other means for measuring the wave forces on a pile. This paper will describe the design and operation of a force meter that may be clamped to an existing pile.

In Spring 1960, California Research Corporation installed equipment incorporating eight of the clamp-on meters on an oil well drilling platform in the Gulf of Mexico. The water depth at the location is 100 feet, and two years of operation are planned.

GENERAL DESCRIPTION OF CLAMP-ON FORCE METER

In the design of the clamp-on force meter, it was desirable to incorporate the following features:

1. Force meter should be in the form of a ring which may be clamped on to an existing pile.

---

* The author is presently employed at National Engineering Science Co., Pasadena, California, as Associate Director.

** This type of dynamometer will be referred to as conventional dynamometer throughout the text of this paper.

2. The outside diameter of the ring should be as close to the pile diameter as possible and not deface the existing structure.

3. The meter should be easily attached and removed.

4. From the output of the meter it should be possible to determine the resultant force on the ring and the direction of the resultant force.

In the design of such a meter, the most difficult requirement to satisfy is Item 2. A clamp-on force meter designed similar to the conventional type force meter has a tendency to become large in size relative to the pile diameter. The reason is that the continuous ring has to be relatively stiff and has to be supported by a system of flexures located in the annulus bounded by the outside diameter of the existing pile and the inside diameter of the force meter.

A more promising design for a force meter is one in which the pressure is measured at equal intervals around the circumference by use of pressure transducers. The total pressure force on a unit height of a pile may then be obtained by integrating the pressure on the individual surface elements around the circumference.

The total force acting on a unit height of a pile consists of a pressure force and a friction force. In the case of cylinders, limited experimental investigations indicate that for Reynolds number larger than 4×10^4 the skin friction or viscosity forces are only two per cent of the total force. In most engineering problems involving wave forces, the Reynolds number is larger than 10^5. Even though the viscosity forces are apparently negligible, they do exert an important effect in distorting the velocity field around the pile. A distortion in the velocity field in turn produces a change in the distribution of the pressure around the circumference. In the design of the clamp-on meter, the friction forces themselves have been neglected in comparison with the pressure forces.

Knowing the pressure at discrete points around the circumference of the pile allows the derivation of an approximate expression for the total force per unit height.

Assuming, for instance, that the pressure varies linearly with the angular position between two points of known pressure the expressions for the total force per unit height in terms of two mutually perpendicular components are (see Appendix I for detailed derivation):

$$X = R\,\frac{2\pi}{N}\left[\frac{N}{\pi}\sin\frac{\pi}{N}\right]^2 \sum_{n=0}^{N-1} P_n \sin\frac{2\pi n}{N} \qquad (1)$$

$$Y = R\,\frac{2\pi}{N}\left[\frac{N}{\pi}\sin\frac{\pi}{N}\right]^2 \sum_{n=0}^{N-1} P_n \cos\frac{2\pi n}{N} \qquad (2)$$

where

X and Y components of force in two mutually perpendicular directions (lb/ft)

R = outer radius of the meter
N = number of pressure transducers
n is integer from O to N
P_n is pressure force at the nth transducer $(lb/ft)^2$

The summing or integrating process may be carried out in two ways:

1. The resultant force and its direction may be determined by numerically integrating the recorded output of the individual pressure transducers located around the circumference. In other words, record all the P_n's and calculate X and Y by use of equations (1) and (2).

2. The resultant force and direction may be obtained by electrically integrating the output of the individual pressure transducers before recording. In this case it is only necessary to record the output of the X and Y rather than the output of all the P_n's.

Method No. 1 requires the recording of a large number of outputs. For instance, an instrumented pile with 8 clamp-on meters each containing 16 transducers would require simultaneous recording of 128 outputs. Not only is it impractical to record a large number of outputs by use of an oscillograph, but the data reduction would be very time consuming. If a recorder were available that could handle the large number of traces required and the output recorded in such a manner that the data could be reduced automatically, this method may be worthwhile considering.

Using an oscillograph-type recording, it will be more practical to use the second method, in which case two mutually perpendicular components of the total force from each force meter are recorded. The distribution around the band may also be obtained by sampling the output of the transducers from a single force meter one at a time. In the example of 8 force meters, 16 X and Y outputs may be recorded continuously during a recording period, while the output of the individual transducers on a meter may be recorded by time sharing the recorder. The force meter described below is designed with this type of recording procedure in mind.

Figure 1 shows a prototype clamp-on meter mounted on a three-foot dummy pile. The meter consists of two half bands clamped together on the pile and held in place by the friction between the pile and the band. The electrical wires from the transducers are carried to the recording instrument through watertight rubber hoses which may be placed either on the outside or the inside of an existing pile. The 16 pressure transducers are so designed and connected together that the normal force acting at each transducer may be recorded in addition to the X and Y component of the total integrated force acting on a unit height of a pile A more complete description of the transducer and the integrating circuit will be given later in the paper.

The clamp-on force meter has several advantages over the conventional force meter presently used at several installations. The most important advantages are listed below:

1. The meter may be clamped on to an existing structural pile thereby eliminating the costly test pile.

2. The meter may be removed for repairs or relocated on the pile in such a manner as to obtain the maximum number of data points for a given wave height. For instance, if information is desired on smal waves, several meters may be concentrated near the MWL.

3. From the pressure distribution data, information may be obtained on particle velocity, drag coefficient, and vortex shedding.

4. The output traces are "clean" due to the high natural frequency of the transducer sensing element. This feature reduces the error in reading the output and simplifies the data reduction.

DESCRIPTION OF MAJOR COMPONENTS OF THE FORCE METER

PRESSURE TRANSDUCERS

In the design of the transducer, used for the clamp-on meter, the following features needed to be incorporated:

1. Each transducer should be provided with three outputs, two for the integrating circuits, and one for the pressure circuit.

2. The output of the transducer versus the applied pressure should be linear.

3. The transducer should be capable of measuring pressures from 0.1 psi to 50 psi.

4. For the purpose of calibrating the clamp-on meter, provisions should be made for applying pressure or vacuum to the sensing element of each individual transducer without affecting the sensing element of the other transducers.

5. For two reasons, consideration should be given to the dimensions of the transducer. First, when the transducers are mounted in the supporting band, the thickness of the band should be as small as possible in order not to deface the existing pile. Second, the height of the sensing element facing the sea should be as small as possible in order to minimize the time that a transducer is partly submerged during wave action.

6. The transducer should be rugged in order to withstand abuse from driftwood.

Because no known commercial transducer met the requirements listed above, a special transducer shown in Figure 2 was developed.

During the development of the transducer, a number of different types of sensing elements were considered, fabricated, and tested.

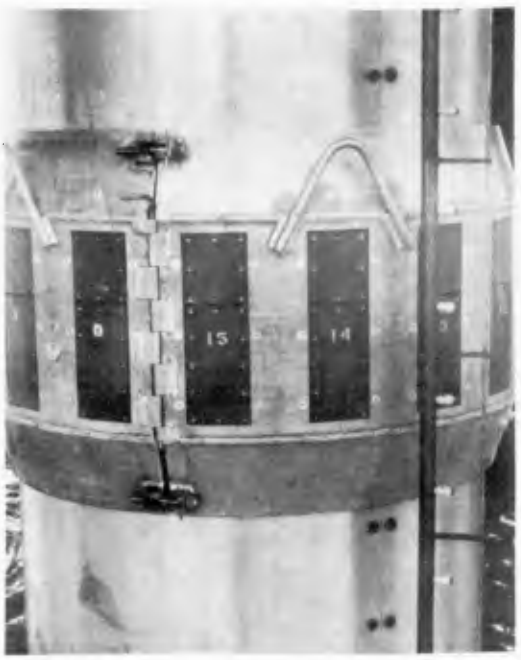

Fig. 1. Prototype clamp-on meter.

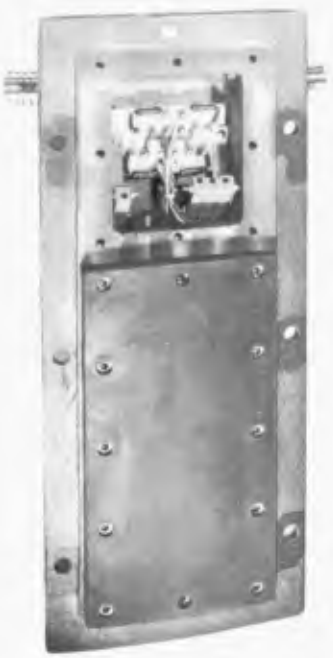

Fig. 2. Pressure transducer.

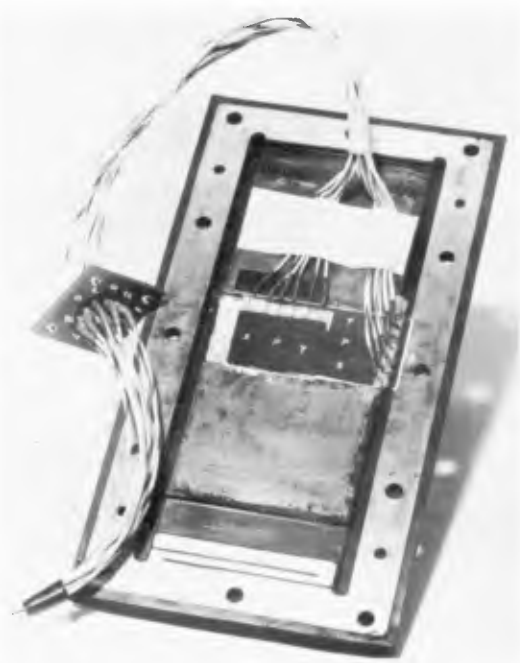

Fig. 3. Sensing element.

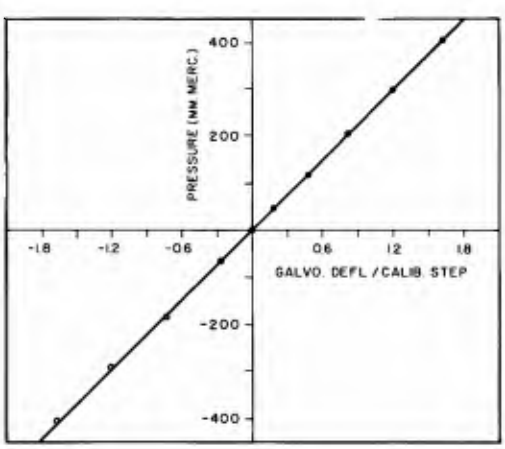

Fig. 4. Typical calibration curve.

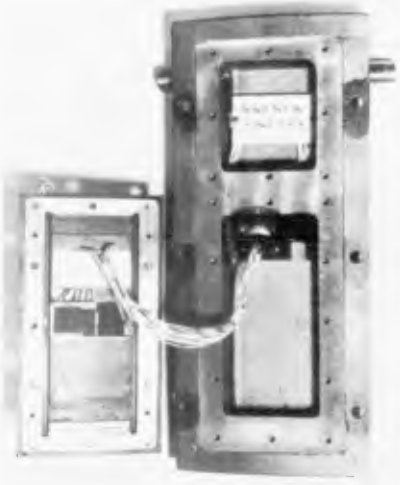

Fig. 5. Transducer housing.

Fig. 6. Band for mounting transducers.

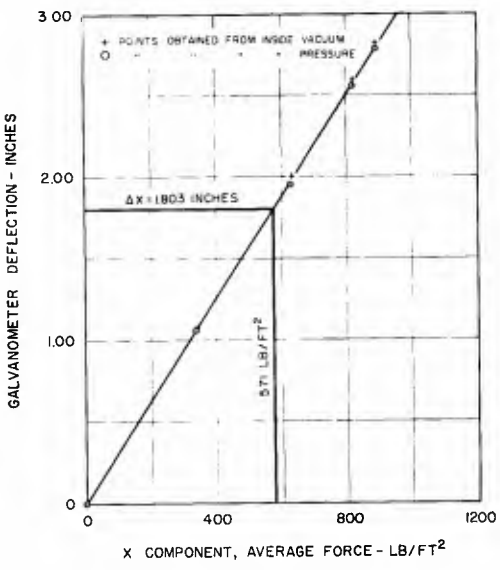

Fig. 7. Calibration curve for X-component of force.

Fig. 8. Clamp-on meter mounted on conventional dynamometer.

Based on the experience obtained during these tests, the final design of the sensing element was arrived at.

SENSING ELEMENT

The sensing element of flexure plate shown in Figure 3 is essentially a simply supported wide beam or plate where the end conditions are kept uniform by use of a thin symmetric flexure at each end of the beam. The thickness of the beam is made relatively great in order to minimize the deflection of the beam under load. Small deflection of the beam is important because a rubber covering is used in waterproofing the transducer and any rubber effect would change the linearity of the output. The stress on the outer fiber in the center of the beam is increased by machining a symmetric flexure at the center. Six SR-4 strain gages are mounted on one side of this flexure. If desired, the sensitivity of the sensing element may be varied by changing the thickness of the center flexure. In order to eliminate any axial force in the beam due to the deflection, two parallel cuts are made at one end of the beam. A sensing element and a typical calibration curve are shown in Figures 3 and 4, respectively.

TRANSDUCER HOUSING

The housing shown in Figure 5 is made with two compartments. The flexure plate covers the largest compartment and may be kept pressure tight with respect to the second compartment. The wires (total of 12) from the strain gages are carried to the second compartment through a pressure-tight plug and wired to a terminal board. All wire connections necessary to complete the different circuits are made in this compartment.

The wires used to interconnect the different transducers are fed through the side walls of the second compartment. The reason for interconnecting the transducers will be explained later in this paper.

Vacuum or pressure may be applied to each individual transducer through a 1/4 in. tapped hole in the wall between the two compartments. The need for applying different pressure or vacuum to each transducer is important during the calibration of the force meter.

TRANSDUCER MOUNTING

Several methods were considered for mounting the transducers in a band to make up the force meter. For instance, one method considered was to mold the transducer in a rubber band which could be strapped onto an existing pile. This method has several advantages in that the band is flexible and would conform easily to the surface of a pile even if it were out of round. The difficulty and expense of making the rubber mold, which would be used only for a limited number of bands, ruled this method out.

After considering several methods for mounting the transducer, it was decided to construct the band from metal. Figure 6 shows the force meter with half the number of the transducers mounted. The band consists of two halves hinged at one edge and bolted together at the other edge.

ELECTRICAL INTEGRATING CIRCUIT

As explained before, each transducer consists of a sensing element on which six SR-4 gages are mounted. The position and notation of these gages are shown in Figures 3 and II-1. The gages noted "X" and "Y" are used for the X and Y integrating circuit, respectively, and the gages noted P are used for determining the pressure at the location of each transducer. Further, the gages noted "A" are sensing the principal strain while the gages noted "B" are sensing the Poisson ratio effect. The sensing element from each transducer will have the same number of gages mounted in the same relative position. As seen from Figure 4, the pressure applied to the sensing element is proportional to the gage output. Because it is well known that the output of a strain gage is proportional to the change in resistance of the gage, the summing of terms in Equations 1 and 2 may be accomplished by connecting the corresponding gages from each transducer in series in the legs of a Wheatstone bridge. Consider for instance in "A" and "B" gage from each transducer with the common notation "X". By placing the "A" gages in series in one leg of the bridge, and "B" gages in the adjacent leg, the contribution from each transducer will add.

The sign of $\sin\frac{2\pi n}{N}$ in Equation 1 is taken care of by placing the gages in the proper leg of the bridge. For $\sin\frac{2\pi n}{N}$ positive, the "A" gages are connected in series in one leg while the "B" gages are connected in series in the adjacent leg. By placing the "A" and "B" gages in adjacent legs, the bridge is temperature compensated in addition to having increased output due to the Poisson ratio effect. When $\sin\frac{2\pi n}{N}$ changes sign, the "A" and "B" gages are moved to either one of their adjacent legs.

In addition to adding the output of each transducer with the proper sign, each output has to be reduced to take into account the magnitude of the multiplier $\sin\frac{2\pi n}{N}$. This is accomplished by placing a resistor with a predetermined value in parallel with each gage. The value of the parallel resistor will vary from transducer to transducer, however, the same value resistor will be placed parallel to the "A" and "B" gages on each individual transducer.

In short, the integrating circuit for representing one component of force consists of a Wheatstone bridge in which the legs are made up of a series of strain gage elements with proper size parallel resistors. Each transducer contributed two strain gage elements to the circuit.

The integrating circuit for the Y component of force is similar, except another set of strain gage elements make up the circuit. A more detailed explanation of the integrating circuit is given in Appendix II, together with one example of the X and Y circuit (see Figure II-3).

CALIBRATION

The calibration of the clamp-on meter is somewhat more complicated than the conventional dynamometer, however, it may be performed with lighter equipment and with better accuracy. Rather than pulling on

the meter with a force, the load on the clamp-on meter is obtained by applying a pressure or vacuum to the individual transducers.

The main objective of the calibration is to obtain a relation between the deflection of the galvanometer and the applied force (lbs per ft or lbs per sq ft). In the case of the clamp-on meter, every effort was made to design the transducers such that the galvanometer deflection is proportional to force or pressure. This simplifies the data reduction in that the galvanometer deflection is converted to force or pressure by merely multiplying by a constant. Any variation of the constant multiplier due to a change in bridge voltage is accounted for by introducing electrical calibration steps on the record.

At the beginning of each recording, a known resistor is connected in parallel with one leg of each of the bridges. This resistor causes an electrical unbalance which will appear on the record as a step with a magnitude that is proportional to the bridge voltage. A force acting on the dynamometer will also cause an electrical unbalance in the corresponding bridge. The force necessary to produce the same unbalance as the calibration resistor with the same applied bridge voltage is referred to as the force or pressure equivalent.

The following paragraphs will be devoted to the discussion of the calibration of the output of the individual pressure transducers and the X and Y integrating circuit as performed on the prototype clamp-on meter in the laboratory. Toward the end of this section, some remarks will be given concerning the field calibration of the clamp-on meter.

LABORATORY CALIBRATION

Individual Transducer Outputs

The calibration of the individual transducers is straightforward. Each transducer was calibrated one at a time by applying increments of pressure or vacuum to the inside of the housing. A recording of the calibration step and the output of the transducers was taken for each pressure setting. A sample plot of the pressure versus output for one transducer is shown in Figure 4.

X and Y Outputs

The value of the calibration constant for X and Y circuits may be obtained by either one of the following two methods:

1. Determine the output of the X and Y circuit when a known pressure distribution is applied around the circumference of the meter. The pressure to be applied to each transducer may be determined from the known pressure distribution curve which also is used to calculate the corresponding X and Y component of force. One point on the calibration curve is then obtained by plotting the output of the X and Y versus the calculated force. The complete calibration curve may be generated by either changing the distribution or changing the magnitude of the pressures and keeping the same distribution. This method requires considerable amount of equipment because the pressure in each transducer

has to be recorded at the same time as the output of the X and Y are recorded. This method is therefore not too practical particularly for field use.

2. Apply the same pressure of vacuum to all transducers, one at a time, and note the output of the X and Y circuit. Knowing the contribution to the X and Y output due to a known pressure at each one of the transducers allows the calculation of the X and Y output due to an arbitrary pressure distribution. The calculated X and Y component of force may then be plotted versus the calculated X and Y galvanometer deflection if both calculations are based on the same pressure distribution.

Even though method number 2 requires more computation, this method is somewhat simpler than method number 1 because it is only necessary to pressurize one transducer at a time. A calibration curve obtained by method number 2 is shown in Figure 7.

In actual operation of the meter, the inside of the transducers will be pressurized with nitrogen to a pressure equal to or greater than the expected outside pressure. Therefore, in normal position, the transducer flexures will be deflected outward and when acted upon by wave motion the increased outside pressure will reduce the outward deflection of the flexures. This is true of course as long as the inside pressure is greater than the outside pressure. It is possible,however, that during high shock pressures that the outside pressure is higher than the inside pressure and the flexures will deflect inward. It is therefore important that the outputs of the X and Y circuit are numerically the same regardless of which side of the flexure the net pressure is applied. The X and Y circuit were therefore calibrated with both inside vacuum (corresponding to excessive outside pressure) and inside pressure to see if the calibration constant were the same in both cases.

FIELD CALIBRATIONS

The field calibration of the output of the individual transducers is very simple and requires little time and effort. Under normal operating conditions, the inside of all the transducers on one band are pressurized with nitrogen to the same pressure. The nitrogen is supplied from the instrument house through a hose which also contains the electrical wiring. By changing the pressure by known increments and recording the output of the transducers for each pressure setting, the calibration curve for all the transducers may be generated.

During the calibration of the individual transducer outputs, the X and Y output should also be recorded and if the integrating circuits operate properly, the X and Y trace should not deflect. This is true because all the transducers are subjected to the same pressure. If the X and Y have no output, due to a uniform load around the circumference, it is quite unlikely that the calibration constant has changed. However, this may be checked by an indirect method. After a storm record has been obtained, the recorded values of X and Y may be compared with values of X and Y computed from the known pressure distribution recorded during the same wave. The pressure distribution which is obtained from the output of the individual transducer may be considered accurate

because the output of these transducers are readily calibrated. If a constant difference occurs between the two results, adjustments may be made by changing the calibration constant for the X and Y output.

TEST RESULTS

The clamp-on force meter described in this paper was tested in the Gulf of Mexico at the Standard Oil Company of California Wave Force Installation during the last five months of 1958. The meter was mounted on the first dynamometer (designated 322) above the MWL of the three-foot test pile as shown in Figure 8. The exact location and orientation of the meter relative to the conventional type dynamometer is shown in Figure 9.

The purpose of the test was to check the performance of the new meter and compare its outputs with the outputs of the conventional dynamometer.

The clamp-on meter was first tested in an actual storm during Hurricane Ella on Sept. 4 and 5, 1958. During the storm, a total of 475 feet on record was obtained from the outputs of the individual transducers, the A and B components of the conventional 322 dynamometer and from the X and Y output of the clamp-on meter. A sample record of these outputs is shown in Figure 10.

At the time this paper was written a small amount of data had been reduced for the outputs of the individual transducers. One example of the pressure distribution around the pile in the crest region of the wave is shown in Figure 11. A comparison between the force recorded on the 322 conventional dynamometer and the clamp-on meter is shown in Figures 12 and 13. The scatter in the data is easily explained, remembering that the clamp-on meter senses the pressure over a height of 6 inches, while the conventional meter covers a height of 3 feet. A similar pressure distribution around the pile over a 3 feet height of the dynamometer is quite unlikely.

The figure indicates, however, that the forces recorded by the X and Y components on the clamp-on meter are about 15 per cent less than the forces recorded by the A and B components of the conventional dynamometer. This discrepancy may be explained as follows:

1. The calibration of one or both meters is in error. The calibration constant for either one of the meters was determined with an accuracy of probably not less than $\pm$ 5 per cent.

2. The friction force felt by the conventional dynamometer and not by the clamp-on meter may amount to as much as 15 per cent.

3. The vertical gradient of the pressure in the upper part of the wave may be large enough to result in a higher average pressure on the conventional 3 foot high dynamometer than on the clamp-on meter.

Because the exact cause of the 15 per cent discrepancy between the output of the two meters could not be determined, the clamp-on meter was moved to an underwater dynamometer to see if the same deviation

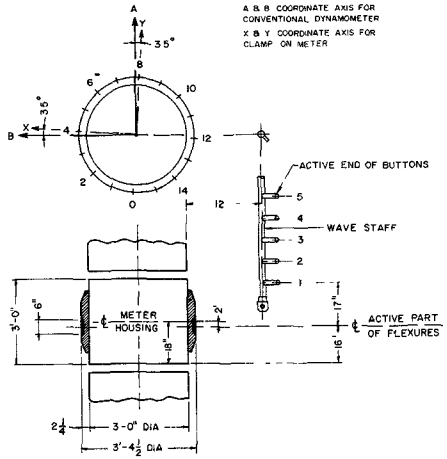

Fig. 9. Location of clamp-on meter relative to 322 dynamometer.

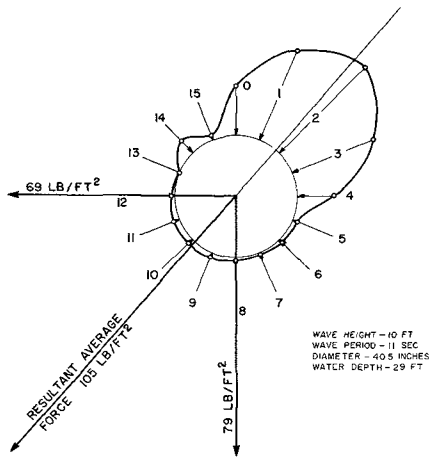

Fig. 11. Circumferential pressure distribution at the crest.

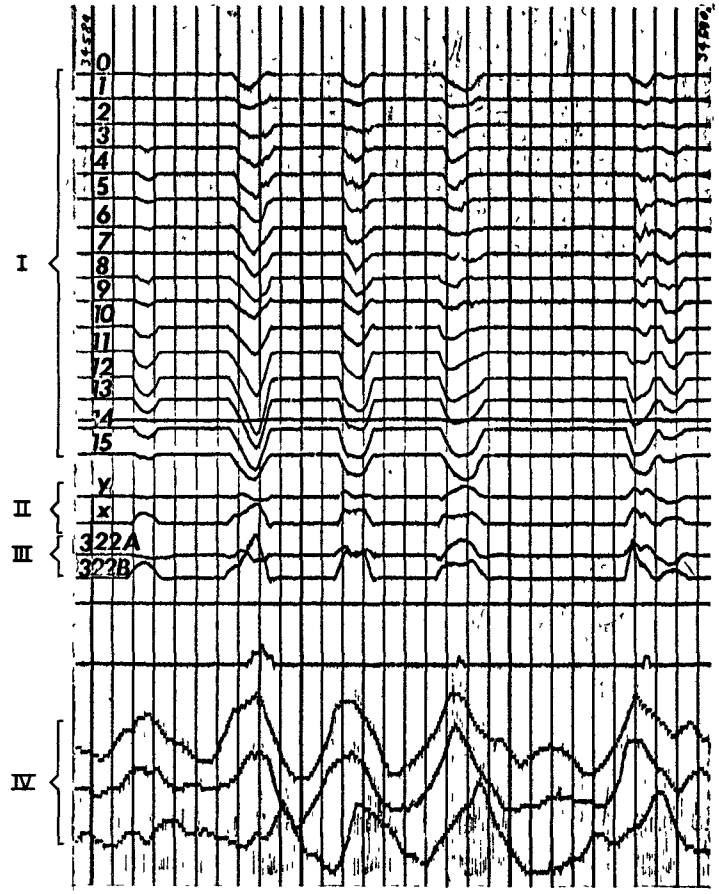

I - INDIVIDUAL TRANSDUCERS OUTPUT
II - X AND Y OUTPUT (CLAMP-ON METER)
III - A AND B OUTPUT (CONVENTIONAL METER)
IV - WAVE STAFFS

Fig. 10. Sample record.

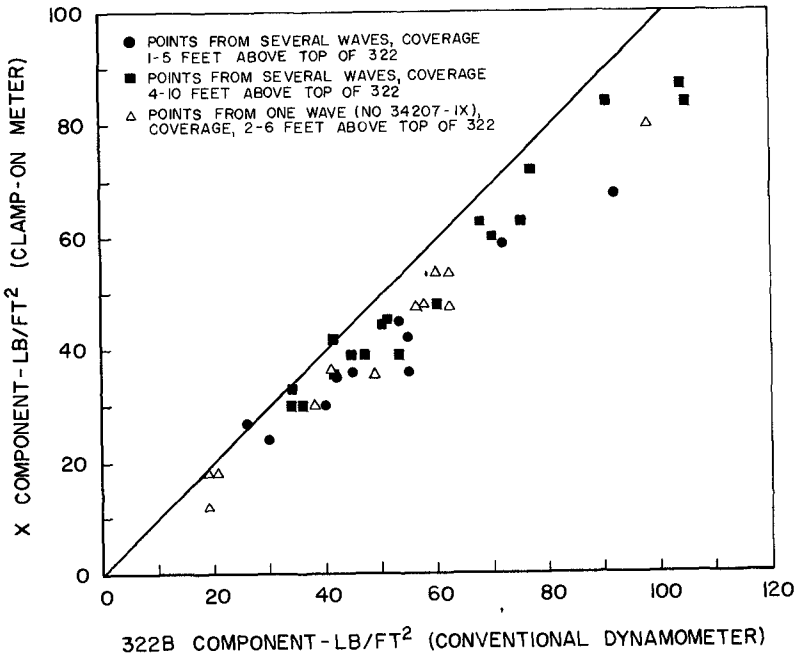

Fig. 12. Comparison between X and 322B component.

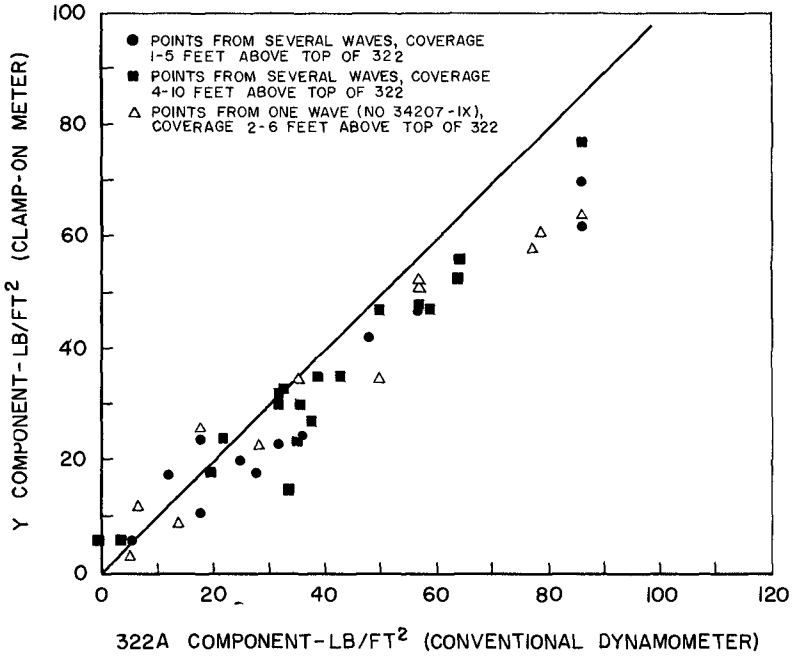

Fig. 13. Comparison between Y and 322A component.

between the two outputs would be obtained at this location. The underwater dynamometer is designated 332 and is located approximately five feet below mean water line. The clamp-on meter was clamped on the 332 dynamometer with the X and Y oriented the same as when clamped on to the 322 dynamometer. At this elevation it could be assumed that the pressure distribution around the pile would be the same over the height of the 3-foot dynamometer. The output of the two meters obtained during a storm which occurred on November 4, 1958, are shown in Figures 14 and 15. As seen from these figures, the force recorded on the conventional meter agrees well with the force recorded on the clamp-on meter.

The discrepancy between the force recorded on the two meters when the clamp-on meter was located at the 322 elevation is then probably due to varying pressure distribution around the pile over the height of the 3-foot dynamometer.

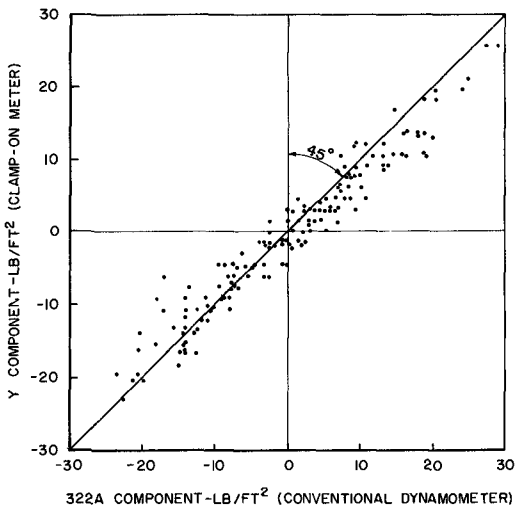

Fig. 14. Comparison between Y and 322A components.

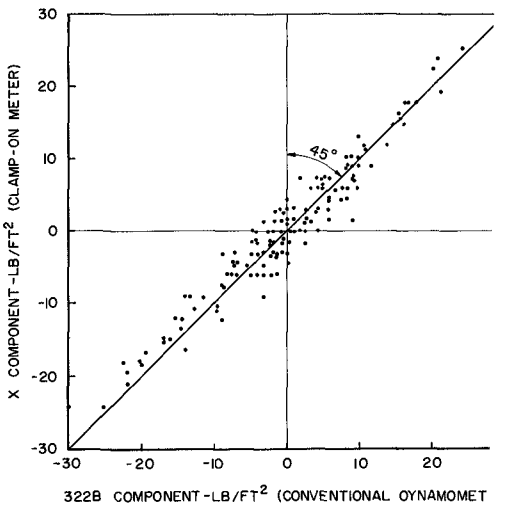

Fig. 15. Comparison between X ar 332B components.

APPENDIX I

DERIVATION OF THE THEORETICAL EXPRESSION FOR THE X AND Y COMPONENT OF FORCE

The derivation of X and Y components of force will be based on the following assumptions:

1. The normal pressure force is measured at equal intervals around the circumference of the pile.

2. The skin friction or viscosity forces are neglected.

3. The pressure force varies linearly as a function of angular position in the interval between each pressure pickup or transducer.

Let

N = number of pressure transducers
n = integer from O to N
φ = angle as shown in Figure I-1
R = radius of pile

X and Y component of force in two perpendicular directions
P_n = pressure at the nth transducer (lb/ft^2)
P_φ = pressure at the angle φ (lb/ft^2)

Then

$$P_\varphi = P_{n-1} + \frac{P_n - P_{n-1}}{\frac{2\pi}{N}}\left[\varphi - \frac{(n-1)\,2\pi}{N}\right] \tag{I-1}$$

Where $P_o = P_N$,

The force per unit height in the X-direction is

$$X = \sum_{n=1}^{n=N} \int_{\frac{2\pi(n-1)}{N}}^{\frac{2\pi n}{N}} R\, P_\varphi \sin\varphi \, d\varphi \tag{I-2}$$

or after integration

$$X = R\,\frac{2\pi}{N}\left[\frac{N}{\pi}\sin\frac{\pi}{N}\right]^2 \sum_{n=0}^{n=N-1} P_n \sin\frac{2\pi n}{N} \tag{I-3}$$

The force per unit height in the Y-direction is

$$Y = \sum_{n=1}^{n=N} \int_{\frac{2\pi(n-1)}{N}}^{\frac{2\pi n}{N}} R\, P_\varphi \cos\varphi \, d\varphi \tag{I-4}$$

or after integration:

$$Y = R\frac{2\pi}{N}\left[\frac{N}{\pi}\sin\frac{\pi}{N}\right]^2 \sum_{n=0}^{n=N-1} P_n \cos\frac{2\pi n}{N} \qquad \text{(I-5)}$$

In the case where 16 pressure transducers are used, Equations I-3 and I-5 become

$$X = 0.3880\, R \sum_{n=0}^{15} P_n \sin\frac{\pi n}{8} \qquad \text{(I-6)}$$

$$Y = 0.3880\, R \sum_{n=0}^{15} P_n \cos\frac{\pi n}{8} \qquad \text{(I-7)}$$

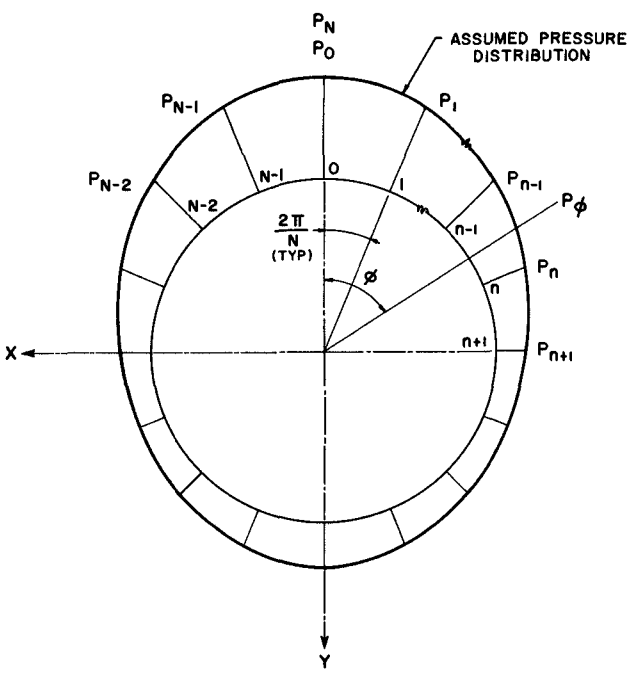

Fig. I-1. Assumed pressure distribution.

APPENDIX II

ELECTRICAL INTEGRATING CIRCUIT

As explained previously in the paper, each transducer consists of a sensing element on which 6 SR-4 strain gages are mounted. The position and notation of these gages are shown schematically in Figure II-1 (note that the schematic shows 3 sets of biaxial-rosette gages, while 6 single strain gages were used in the construction of the prototype meter). A brief explanation of integration circuits has already been given; however, for those interested, a more detailed explanation will follow.

Because the sensing element is so designed that stress in the upper fiber is proportional to the applied pressure, we may write the following equations:

$$\sigma_a = C_1 P, \quad \sigma_b = 0 \tag{II-1}$$

or in terms of strain

$$\epsilon_a = \frac{C_1}{E} P, \quad \epsilon_b = -\nu \frac{C_1}{E} P \tag{II-2}$$

Where

C_1 = a constant depending on the geometry of the sensing element
ν = Poisson ratio
E = modulus of elasticity
P = pressure
σ = stress
ϵ = strain (see Fig. II-1)

Furthermore, because the change in the resistance of the gage is proportional to the strain, we may write

$$\Delta R_a = C_2 \epsilon_a, \quad \Delta R_b = C_2 \epsilon_b \tag{II-3}$$

where

$C_2 = KR_g$ = constant
K = gage factor
R_g = gage resistance

Substituting from Equations (II-2) gives

$$\Delta R_a = C_2 \frac{C_1}{E} P, \quad \Delta R_b = -\nu \frac{C_1}{E} P \tag{II-4}$$

or, in general,

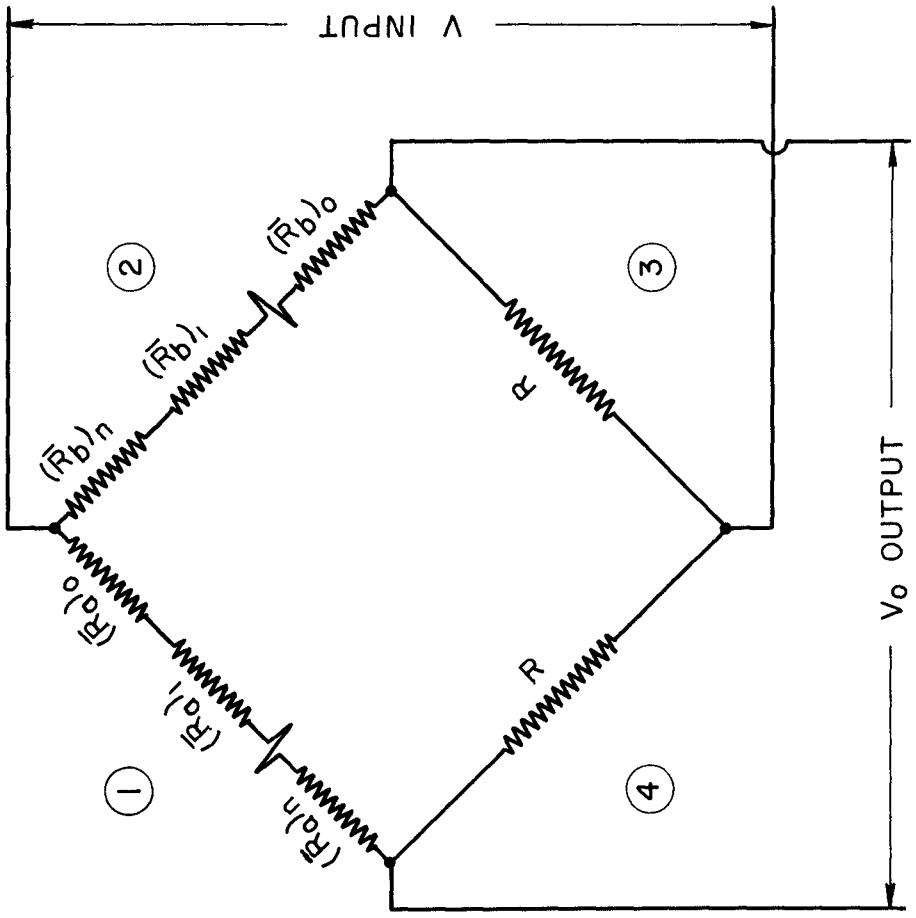

Fig. II-2. Schematic of integrating circuit.

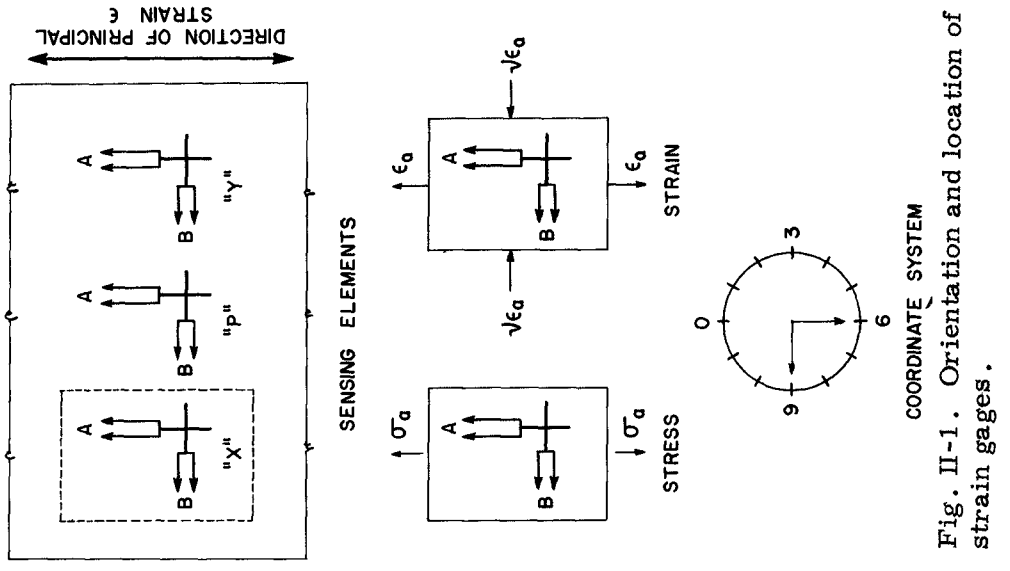

Fig. II-1. Orientation and location of strain gages.

$$(\Delta R_a)_n - (\Delta R_b)_n = (1+\nu)\frac{C_1 C_2}{E} P_n \tag{II-5}$$

Multiplying Equation II-5 with $\sin \frac{2\pi n}{N}$ and summing we get

$$\sum_0^{N-1} (\Delta R_a)_n \sin \frac{2\pi n}{N} - \sum_0^{N-1} (\Delta R_b)_n \sin \frac{2\pi n}{N} =$$

$$(1+\nu)\frac{C_1 C_2}{E} \sum_0^{N-1} P_n \sin \frac{2\pi n}{N} \tag{II-6}$$

Where $(\Delta R_a)_n$ and $(\Delta R_b)_n$ are the change in resistance of the "A" and "B" gages, respectively, for the nth transducer.

If we define

$$(\overline{\Delta R_a})_n = (\Delta R_a)_n \sin \frac{2\pi n}{N} \tag{II-7}$$

$$(\overline{\Delta R_b})_n = (\Delta R_b)_n \sin \frac{2\pi n}{N} \tag{II-8}$$

then

$$\sum_0^{N-1} (\overline{\Delta R_a})_n - \sum_0^{N-1} (\overline{\Delta R_b})_n = (1+\nu)\frac{C_1 C_2}{E} \sum_0^{N-1} P_n \sin \frac{2\pi n}{N} \tag{II-9}$$

Consider now the Wheatstone Bridge in Figure II-2 where the legs are made up of individual resistors $(\overline{R_a})_n$ and $(\overline{R_b})_n$.

The voltage across the leg (1) in terms of the input voltage is,

$$V_1 = \frac{\Sigma(\overline{R_a})_n}{\left[\Sigma(\overline{R_a})_n + R\right]} V \tag{II-10}$$

The change in output voltage as a result of change in all the $(\overline{R_a})_n$ is

$$\Delta V_1 = \frac{RV}{\left[\Sigma(R_a)_n + R\right]^2} (\Sigma \overline{\Delta R_a})_n \tag{II-11}$$

If $R = \Sigma(\overline{R_a})_n$ Equation II-11 reduces to

$$\Delta V_1 = \frac{1}{4} V \frac{\sum_0^{N-1} (\overline{\Delta R_a})_n}{\sum_0^{N-1} (\overline{R_a})_n} \tag{II-12}$$

Similarly, the change in output voltage as a result of change in all the $(R_a)_n$ is

$$\Delta V_2 = -\frac{1}{4} V \frac{\sum_0^{N-1} (\overline{\Delta R_b})_n}{\sum_0^{n-1} (\overline{R_b})_n} \qquad \text{(II-13)}$$

Assuming $\Sigma(\overline{R_b})_n = \Sigma(\overline{R_a})_n$ the change in the bridge output voltage $\Delta V_o = \Delta V_1 + \Delta V_2$ is from Equations (II-12) and II-13).

$$V_o = \frac{1}{4} V \frac{1}{\sum_0^{N-1} (\overline{R_a})_n} \sum_0^{N-1} (\overline{\Delta R_a})_n - \sum_0^{N-1} (\overline{\Delta R_b})_n \qquad \text{(II-14)}$$

From Equation (II-9) and (II-14) we obtain

$$\frac{4 \sum_0^{N-1} (\overline{R_a})_n}{V} \frac{E}{C_1 C_2 (1+\nu)} \Delta V_o = \sum_0^{N-1} P_n \sin \frac{2\pi n}{N} \qquad \text{(II-15)}$$

From this equation we see that the output ΔV_o of the composite bridge is proportional to summation in the left-hand side of Equation (1) Instead of using two active legs, all four legs could have been active anc the same result would be true.

Consider now a single strain gage element with resistance R_g (for the time being, drop the subscripts a and b) and a parallel resistor R_p.

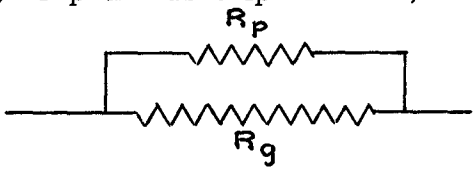

let

$\overline{R}$ Equivalent resistor of R_g and R_p

ΔR_g Change in resistance of R_g as a result of change in strain

$\overline{\Delta R}$ Change in resistance of $\overline{R}$ as a result of change in R_g

then

$$\overline{R} = \frac{R_g R_p}{R_g + R_p} \qquad \text{(II-1}$$

To find the relationship between $\overline{\Delta R}$ and ΔR_g, Equation (II-16) is differentiated with respect to R_g, giving the result

$$\overline{\Delta R} = \left(\frac{R_p}{R_g + R_p} \right)^2 \Delta R_g \qquad \text{(II-1}$$

Comparing Equation (II-17) with Equation (II-7), we see that the output of the gage may be properly modified by shunting the gage with a resistor of such a value that

$$\left(\frac{R_p}{R_g + R_p}\right)_n^2 = \left|\sin\frac{2\pi n}{N}\right| \qquad \text{(II-18)}$$

The expression for R_p is then

$$(R_p)_n = (R_g)_n \frac{\sqrt{\sin\frac{2\pi n}{N}}}{1 - \sqrt{\sin\frac{2\pi n}{N}}} \qquad \text{(II-19)}$$

The equivalent resistance for the gage and the parallel resistor is

$$\overline{R_n} = (R_g)_n \sqrt{\sin\frac{2\pi n}{N}} \qquad \text{(II-20)}$$

The above equation applies to the X-circuit only, however, the equations for the Y-circuit are obtained by replacing $\sin\frac{2\pi n}{N}$ by $\cos\frac{2\pi n}{N}$.

One case has been worked out and the corresponding bridge circuit is shown in Figure II-3.

The X and Y integrating circuits used in the prototype clamp-on meter were wired according to the circuit diagram shown in Figure II-3 with only a few modifications. One of the basic assumptions made in deriving Equation (II-15) was that the resistance of all the legs of the Wheatstone Bridge containing active gages should have the same value. In case of the prototype clamp-on meter, all four legs of the Wheatstone Bridge were made active. This required that an effort has to be made in making the resistance of all four legs the same.

Because of the resistance of the gages making up the legs of the bridge were not exactly the same, it was necessary to introduce a potentiometer in each leg to balance out the difference in resistance. The final balancing of the bridge was made by introducing a variable resistor across two adjacent legs of the bridge This resistor was made large in order not to significantly alter the total resistance of the two legs

When the gages are connected in series according to the wiring diagram to make up the bridge (resistors parallel to gages not connected), a load on any one of the transducers will result in an output If the same pressure is applied to the transducers one at a time and the bridge voltage is kept constant, all the output should be the same Due to imperfection in the beams and gages, however, these outputs will differ slightly. It would be possible to obtain the same output from all the transducers by normalizing the outputs to the smallest of the 16 outputs by connecting proper size resistors parallel to the gages Because the output of the different transducers have to be modified in order to complete

the integrating circuit, it will be convenient to modify and normalize the output using the same parallel resistor. This means that the value of the actual parallel resistor for each gage will differ slightly from the theoretical values calculated in Appendix II.

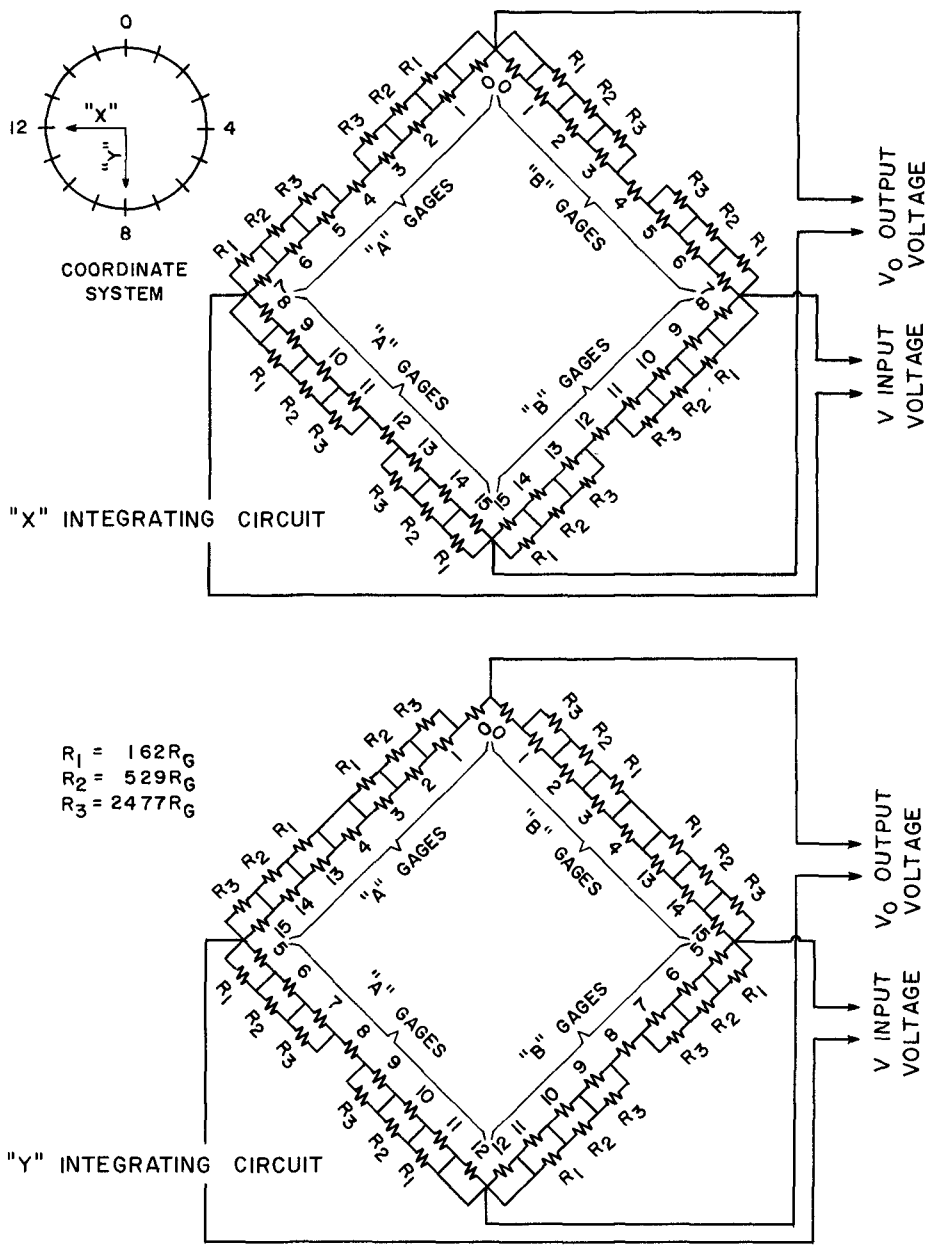

Fig. II-3. X and Y integrating circuit using 16 transducers.

CHAPTER 40

MODEL TESTS ON THE MOTION OF MOORED SHIPS PLACED ON LONG WAVES

F.A. Kilner
Senior Scientific Officer, Hydraulics Research Station,
Wallingford, Berks, England.

ABSTRACT.

The equation of motion for a moored ship, subject to stationary wave action, is presented and discussed. The moorings are longitudinal, the ship is considered to be aligned to the direction of wave motion and positioned at a node, and the wave length is assumed long compared with the ship length. If the motion of the ship is assumed to be simple harmonic, and frictional forces between the ship and the water are neglected, an elementary analysis gives the required relation between the amplitudes of the ship's movement and of the water particle motion associated with the wave. A description is given of some tests carried out on model ships moored in a flume where stationary waves can be generated, and the amplitude and period can be varied independently. In these experiments, the amplitude of ship movement could be measured visually, or inferred from strain gauge readings, and the water motion was also observed. The results of these tests are compared with the simple theory. A table tilting harmonically is shown to be a mechanical analogy to stationary wave action on ships. The hydrodynamic mass for a ship moving in surge or sway motion is measured and is found to depend on the depth of water in which the ship is moored.

INTRODUCTION

The response of moored ships to long waves was first considered in detail by Wilson[1] in connection with an investigation of Cape Town harbour. Subsequent papers have been published on various aspects of the problem, notably Knapp[2], Abramson and Wilson[3], Russell[4], Joosting[5], Wiegel et alia[6 & 7], O'Brien and Kuchenreuther[8 & 9], Russell[10] and Wiegel et alia[11], in chronological order. There is, however, little published information in which the theory of motion of moored ships is compared with model or field measurements, and this absence is regrettable as there seems to be a difference of opinion concerning the relevant equation of motion, the earlier Wilson[1] version differing, for example, in a significant manner from Russell[10] or Joosting[5].

Wilson[1] described tests on model ships, oscillating longitudinally on long waves, but did not publish any results. He also observed both ship and water movements at various berths in Table Bay harbour, and presented the information as amplitudes and periodicities of the component harmonics, but gave no verification that these motions conformed to his general theory of ship motion. A valuable feature of this paper was the detailed consideration given to the characteristics of

typical moorings.

O'Brien and Kuchenreuther[9] made measurements on a 12,000 ton ship moored at Port Hueneme, California, where the ship motion was predominantly longitudinal. The mooring forces were measured by resistance strain gauges attached to a tube incorporated directly into the cable lines, and the water surface slope was measured by pressure pickups placed at two points on the floor of the harbour basin. When long waves were excited by external sea conditions, the mass acceleration of the ship was calculated (from the measured motion of the ship) and compared with the algebraic sum of the measured rope tensions and wave forces (computed by the elementary theory). The hydrodynamic mass of the ship was neglected and the authors found that actual peak mooring forces were too low (by about 30%) to satisfy the basic equation. Wilson pointed out, in the discussion of reference (9), that if a reasonable value of hydrodynamic mass was included, the discrepancy increases, and he suggested that the estimation of the ship movement from the forces in the moorings may have been unreliable owing to the hysteresis effects that are characteristic of mooring line loading. This paper was a notable contribution because of the resource with which the very difficult problem of prototype forces and movements was tackled. However, the investigation was concerned with a particular case, and made no direct contribution to the solution of ship motion in general terms.

The same authors[8] measured the periods of free oscillation for a moored dry dock in the absence of waves; the displacement was 2100 long tons and the site was also at Port Hueneme in California. The moorings were longitudinal, symmetrical and had a non-linear spring characteristic, although the non-linearity was due in this case to the catenary behaviour of the chain 'moorings', as at no time were the dock movements sufficient to elongate the chains. The vessel was given an initial displacement by a tug and the natural periods estimated from the subsequent intervals at which peak forces were recorded by strain gauges placed in the mooring lines. Both longitudinal ("surge") and transverse ("sway") displacements were imposed, and comparisons were made between the measured periods and those computed from the known mass of the dock and the force characteristics of the mooring restraints. Further comparisons were possible from results obtained from a 1:40 scale model of the same dock, tested at the University of California by Wiegel, Clough, Dilley and Williams[6], although the majority of these tests were for the surge condition only. The first conclusion of this paper was that the three sets of information viz: prototype, model and analytical were reasonably consistent, and that damping and hydrodynamic mass effects were both negligible. It is to be noted that the water was relatively deep, being three to four times the draft of the dock. The authors conceded, however, that the evidence concerning surge motions was the more reliable, as a combination of large damping and small restoring force quickly reduced the sway amplitudes to zero.

MODEL TESTS ON THE MOTION OF MOORED SHIPS PLACED ON LONG WAVES

A 1:80 scale model of a landing ship medium of approximately 860 long ton displacement was examined for response to progressive wave action in a detailed paper by Wiegel, Beebe and Dilley[7]. The prototype dimensions were a length of 200ft, a beam of 33ft and a 13ft draft, and the moorings used were oblique to the ship's longitudinal axis (12°) but were symmetrical about this axis, giving twin moorings at bow and stern, four mooring lines in all. Various wave directions were tested, being equivalent to beam, head and quartering seas. The predominant motions of the ship were recorded on cine film from two cameras placed in suitable positions to observe the required components, and in addition the average cable tensions were obtained from strain gauges mounted on cantilevers attached to the moorings. The independent variables were the wave height, wave period, and cable pre-tension. It appeared to be impossible to produce a basic component motion of the ship in pure form, as in all cases coupled motions were present, and the resultant movement of the ship was complex. This prohibited an analytical solution although the authors presented conclusions about the influence of resonances on the observed motions.

Russell[10] was concerned with a particularly difficult case of ship motion, namely the transverse displacement of a ship with unsymmetrical restraints consisting of relatively stiff fenders as the restoring force away from the jetty, and relatively soft ropes as the mooring force in the opposite direction. The ratio of stiffnesses may be 1000 or more and in the general case there will be some intermediate free travel in which the ship moves freely on the wave. Two sets of tests were described, the first using a model ship in a model harbour, and the second used the stationary wave flume described in this paper with the model ship idealised to a central section only. Experimental results of the ship dynamics were presented for various combinations of fenders and ropes and were discussed in general terms. However, it was clear from the asymmetrical and irregular motion that this problem was unlikely to be amenable to a theoretical study and none was attempted. The transverse motion of ships was discussed by Wilson[1], but appears to have escaped attention subsequently; the paper referred to above will no doubt revive interest in this problem.

The most recent publication on this subject is by Wiegel and colleagues[11], containing a description of experiments on a 1:86 scale model of a liberty ship. The mooring system used in the model was similar to that of the prototype in that it included mooring lines at various inclinations to the ship's longitudinal axis, and also camels (or floating fenders). The direction of wave motion in relation to the ship was varied to reproduce the effects of beam, stern, head and quartering seas, and it is perhaps not surprising that the resultant motions of the ship are very complicated. The authors suggested that the mooring force records they obtained could be used for prediction of prototype forces, provided the ship form and mooring systems do not differ appreciably from the model. They also state that model studies should be used for any specific ship mooring problem.

Thus there is an apparent gap in the literature of ship oscillations; there are no published results of ships moving under controlled conditions in which theoretical predictions of ship motion can be compared with experimental measurements. This paper makes such comparisons, which are necessary in order to assess the extent to which full-scale ship mooring loads are predictable for known mooring and ship constants. The experiments are restricted to longitudinal motions with symmetrical restraints as this appears to be by far the simplest from the theoretical point of view.

THEORY

The following section deals essentially with a ship aligned to the direction of wave motion, restrained by longitudinal symmetrical moorings and positioned at a nodal point. In addition, the wave length is assumed long compared with the ship length.

NOTATION

Let m_1 = mass of a ship

m_2 = hydrodynamic mass associated with the ship

M = virtual mass = $m_1 + m_2$

s = displacement of a ship from its central position.

x = displacement of a water particle from its central position

K = a mooring coefficient

C = a damping coefficient

s_o = ship amplitude (0.5 of total travel)

x_o = water amplitude (0.5 of total travel)

Newton's Law gives:

$$m_1 \ddot{s} = \Sigma \text{ external forces} \qquad (1)$$

where external forces tending to increase s are positive.

The external forces are:-

F_1, a drag force, which is a water force due to the relative velocity of the water and ship

F_2, a wave force, which is a water force due to a pressure gradient in the water (manifested by water accelerations in the ship's absence)

F_3, a force associated with hydrodynamic mass, which is a water force due to the diversion and acceleration of the flow around the ship.

F_4, a restraint or mooring force

Now, F_1 may be written as $+C(\dot{x} - \dot{s})$

F_2 is visualised as the weight of the ship tending to slide down the inclined water surface of the wave and is thus independent of the ship's acceleration.

$\therefore F_2 = m_1 g \times$ (water surface slope)

$= m_1 \ddot{x}$ for long low waves.

F_3 is clearly zero if the ship moves exactly with the water

$\therefore F_3 = m_2 (\ddot{x} - \ddot{s})$ ∎

Wilson[1] demonstrated that, due to catenary effects, typical ship moorings will always allow a certain amount of effective free travel about the central position (i.e., negligible restoring force) followed by a rapidly increasing force for further ship displacement. This is illustrated in Fig. (1).

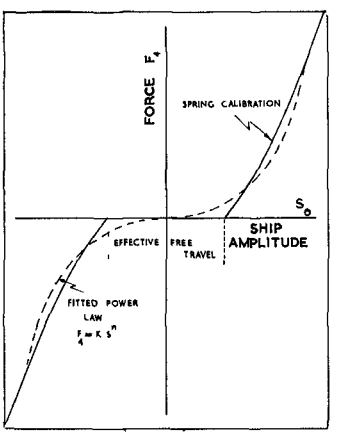

Fig. 1. Spring characteristics of actual and idealized moorings.

Wilson[1] suggested that this relation could be approximated by a power law of the form:

$F_4 = Ks^n$

As the physical requirements are such that

$(-s)^n = -(s)^n$ i.e. s must be an odd function, it follows that n must be a ratio of odd integers, n = 2, for example, is clearly excluded. The relation $F_4 = Ks^n$ is a mathematically convenient way of representing the restraint of the moorings; it is not the only one, however, $F_4 = \alpha \tan \beta s$ (for example) would also conform to the general shape of the curve in Fig. (1), but would probably be less convenient analytically. The particular case of n = 1 represents a linear spring law with no free travel.

Thus equation (1) becomes

$$(m_1 + m_2)(\ddot{s} - \ddot{x}) + C(\dot{s} - \dot{x}) + Ks^n = 0$$

$$\text{i.e., } M(\ddot{s} - \ddot{x}) + C(\dot{s} - \dot{x}) + Ks^n = 0 \qquad \ldots\ldots\ldots\ldots (2)$$

---

the case of $\ddot{x} = o$ is proved in "Theoretical Hydrodynamics" by L.M. Milne-Thomson, 2nd edition p.228. The case of $\ddot{x} \neq o$ does not appear to have been considered mathematically.

Wilson[1] omitted the wave force from the equation he presented in 1951, and the same error occurs in reference (3). Joosting[5] and Russell[10] have both presented the equation essentially in the form above and also commented that the drag force is negligible compared with the other terms of the equation, i.e. C = 0

Certain special cases can now be examined

(i) static water $\dot{x} = \ddot{x} = 0$; also n = 1; C ≠ 0
$\therefore M\ddot{s} = -Ks$
This represents simple harmonic motion of period

$$T = 2\pi\sqrt{\frac{M}{K}}$$

This suggests a simple way in which the virtual mass may be determined. A ship is moored with linear springs of known stiffness and no free travel, and the natural period T of oscillation through the water is determined. Then

$$M = \frac{K T^2}{4\pi^2}$$

gives the virtual mass of the ship appropriate to the type of oscillation (longitudinal or transverse) from which it was obtained. Damping lengthens the period, but the effect is negligible if $C^2 < 0.04\,MK$, and C can be estimated from the amplitude decay.

(ii) Stationary ship, $\dot{s} = \ddot{s} = 0$
$\therefore$ Force on ship $= M\ddot{x} + C\dot{x}$, a form of equation familiar in studies of wave forces on piles.

(iii) No moorings, C = 0
$\therefore \ddot{s} = \ddot{x}$
Thus under suitable release conditions, an unrestrained ship reproduces the motion of the water particles it replaces. This implies that a freely floating body may be used to measure the movement of water in its proximity, which is in fact a familiar concept.

ANALYSIS

Accepting the simplification that C = 0 the ship motion is governed by equation (2)

$$M(\ddot{s} - \ddot{x}) + Ks^n = 0$$

Now in a stationary wave of period $2\pi/\omega$

$$x = -x_o \sin \omega t$$

$$\text{or } \ddot{x} = x_o \omega^2 \sin \omega t$$

$$\therefore M\ddot{s} + Ks^n - M x_o \omega^2 \sin \omega t = 0$$

$$\text{or } \ddot{s} + \frac{Ks^n}{M} - x_o \omega^2 \sin \omega t = 0 \qquad \ldots\ldots\ldots (3)$$

Provided the mooring restraint law has a continuous slope and is symmetrical (as it is for the mooring represented in equation (3)), and $n \neq 1$, the ship motion will be periodic with the same period as the exciting force, and symmetrical, but not purely harmonic, i.e. it will contain harmonic components of period $\frac{2\pi}{\omega}$ and integral multiples. The above statement is from reference 14, page 355. Similarly, if the restraint law has a continuous slope, but is unsymmetrical, the motion will be periodic, but unsymmetrical. The present experiments have shown that if the restraint equation contains discontinuities of gradient, as it does for an actual ship mooring, the transient motions are repeatedly generated and there is no certainty that the motion will be periodic or symmetrical even if the moorings are symmetrical. This latter case prevails at full scale and the author considers this explains the erratic motion of ships at typical moorings even when the exciting waves are regular.

Reverting to equation (3), two procedures are available for a solution: a step by step analysis (requiring numerical values for K, M, n, x_o and ω) will give an accurate solution for ship displacement, s. Alternatively, an approximate solution may be obtained by ignoring the harmonics other than the fundamental. The second method has the advantage that the symbols may be retained, permitting a greater generality of discussion. However, the first method allows the amplitudes of the higher harmonics to be measured. Joosting[5] analysed these harmonics and concluded that the significant component only reached a magnitude of 8% of the fundamental even for values of n as high as 7. This implies the approximate solution will be correct to at least the same order of accuracy

Thus we assume,

$$s = s_o \sin \omega t \quad (s_o \text{ + ve or - ve})$$

No phase angle is required as the first two terms of equation (3) differ in phase by 180°; thus the possible phase differences for s are only 180° or 0°, and these can be allowed for by the alternative signs for s_o. s_o positive means the ship and water motions are in opposition; s_o negative means they are in phase.

Inserting the value of s in equation (3) we have

$$-\omega^2 s_o \sin \omega t + \frac{K}{M} s_o^n (\sin \omega t)^n - x_o \omega^2 \sin \omega t = 0$$

or

$$\frac{K}{M\omega^2} s_o^n (\sin \omega t)^{n-1} = x_o + s_o$$

This relation is not identically true because of the time dependent term $(\sin \omega t)^{n-1}$

But $0 < \frac{\omega}{2\pi} \int_0^{\frac{2\pi}{\omega}} (\sin \omega t)^{n-1} < 1$

$$\therefore \quad \frac{K s_o^n}{M\omega^2 C_k} = x_o + s_o \qquad \ldots\ldots (4)$$

where $C_k > 1$

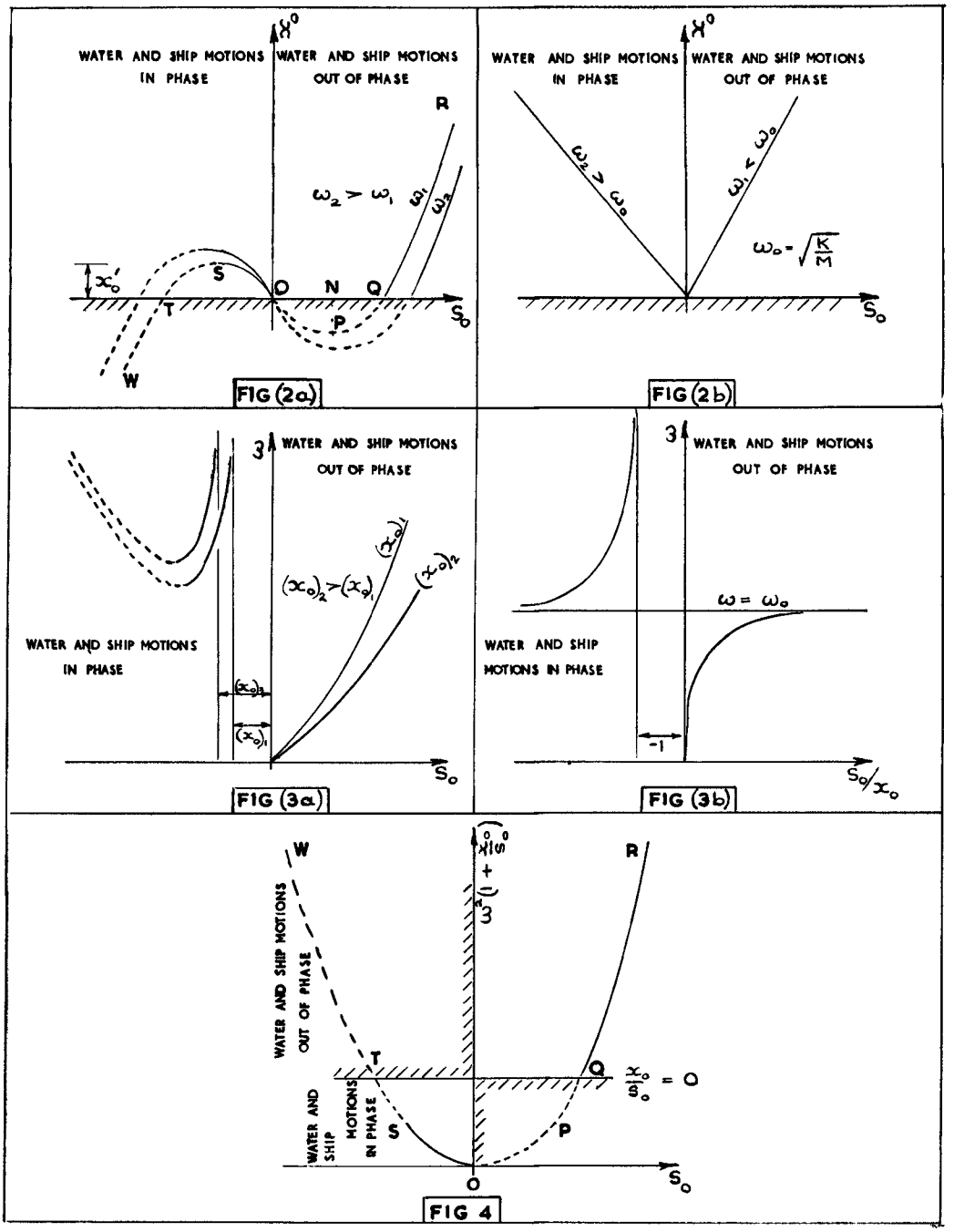

Figs. 2, 3, 4. Alternative forms of presentation for the theoretical motion of a moored ship.

This important equation was presented independently by Wilson[3] and Joosting[5] but the above derivation is simpler. Equation (4) contains the three essential variables s_o, x_o and ω, the last two being regarded as independent. Both Wilson and Joosting obtained a value

$$C_k = 1 + 0.19(n - 1)$$

by ensuring that equation (4) with $x_o = 0$ (free, undamped motion) agrees with the exact analytical solution which happens to be available for this particular case. It does not follow that the same value of C_k is applicable to forced vibrations.

Equation (4) can be presented graphically in several ways, most simply in Fig. (2a) where K, M, ω, n and C_k are presumed known constants.

If s_o is considered to depend on x_o, x_o should be considered positive and then the sign of s_o depends on the phase; thus the hatched area in Fig. (2a) is inadmissible. The curve splits into two regions RQ and OS (the region ST is rejected because a slight decrease in x_o produces an in phase increase in ship movement which is unreal). Thus we see that over a limited range of x_o (0 to x_{o1}) there are two modes of oscillation, one of relatively small amplitude and in phase, the other larger and out of phase. For values of $x_o > x_{o1}$, only the out of phase motion exists. If the water motion is started and the ship subsequently released, the mode followed (if an alternative exists) depends on release conditions, release at the instant of stationary water giving the in phase mode, an out of phase release with adequate displacement giving the out of phase mode. It also appears from the graph that there is a range of ship amplitudes which do not occur, in the range $ON < s_o < OQ$. In addition damping effects (ignored in this analysis) will not allow the motions represented by the vicinity of point Q.

Fig. (4) is an alternative way of presenting the same information, which is more suitable for plotting experimental results particularly where double logarithmic scales are used, also ω^2 may now be included in the ordinate as an additional variable. The letters O,P,Q etc. have the same significance as in Fig. (2a) and the hatching indicates negative values of x_o; thus the real zones are QR and OS. However, OS and OP are mirror images in the vertical axis, so with the convention that in phase values are regarded as x_o negative, s_o positive, the complete motion may be represented by OPR which is a straight line if double logarithmic scales are used.

Fig. (3a) is a further alternative presentation of the equation, and Figs. (2b) and (3b) are both drawn for the particular case of n = 1, i.e. linear springs with no free play. Comparisons between Figs. (3a) and (3b) emphasize the difference between the motions due to linear and non-linear spring characteristics. If n = 1, there are no ambiguous motions, a particular value of ω causes a unique value of s_o for any particular value of x_o, and moreover doubling x_o will double s_o. In addition, resonance is possible where the applied frequency is equal to the natural frequency, which results in an infinite ship amplitude in the absence of damping. By contrast when $n \neq 1$, alternative motions

Table 1

The variation of virtual mass with water depth, m_1 = 135 lbs.

Type of motion	Spring Stiffness	Water Depth	Period Secs	$M = m_1+m_2$	m_2	$\frac{m_2}{m_1}$
Transverse	0.8lbs/in	8.2"	8.24	526	391	2.89
"	"	7.2	9.34	675	540	4.00
"	"	9.5	7.69	454	319	2.36
"	"	10.7	7.4	424	289	2.14
"	0.6lbs/in	10.7	8.62	432	297	2.20
Longitudinal	0.8lbs/in	6.2	4.35	148	13	0.09
"	"	7.2	4.38	150	15	0.11
"	"	8.2	4.36	148.5	13.5	0.10
"	"	10.0	4.33	146	11.0	0.08

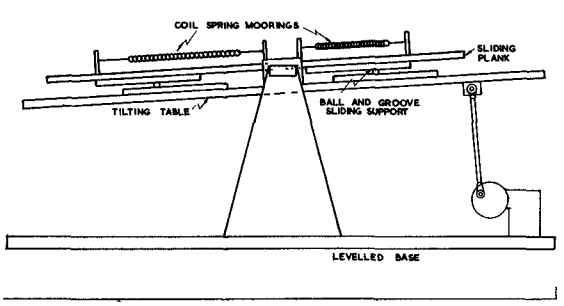

Fig. 5. A mechanical analogy to wave action on ships, showing a tilting table moving a "moored" plank.

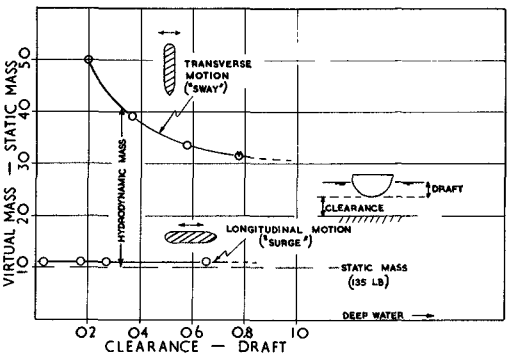

Fig. 6. The influence of water dept on the virtual mass of model ships i sway or surge motion.

exist as pointed out in an earlier paragraph, doubling x_o does not double s_o, and all ship amplitudes are finite even in the absence of damping.

APPARATUS

The model tests were carried out in a flume of rectangular cross-section, of width 5ft, length 29ft, maximum water depth 10 inches. Filters were placed at each end of the effective working section which was 15ft long. There was a sump at each end of the flume to which a pump system was connected in such a way that water could be transferred from one sump to the other, in either direction. The butterfly valve controlling the flow direction could be rotated mechanically in a uniform manner thus producing a water oscillation in the flume, equivalent to a stationary wave with a node at the centre line. A surface float in the nodal region was photographed and the displacement time curve obtained. This confirmed that the motion was essentially sinusoidal. The range of wave period available was from 25 secs. to 2.7secs.

The model ship used in the experiment was 80 in. long, with a beam of 10 in., a draught of 6 in. and weighed 135 lbs. It was symmetrical and was moored with its centre at the nodal point. The moorings consisted of rings of thin sheet metal which formed the spring element and were rigidly attached to the ship, one at each end. The free ends of the springs were fastened to light inelastic chains which in turn were fixed to stiff cantilever bars, the cantilevers forming the mooring anchorages at the quay side. By judicious variation of ring diameter, strip thickness and width, an appreciable range of spring stiffness could be obtained although in most cases the linear range of the spring was exceeded.

The mooring forces were measured either by visual estimation of ship displacement and subsequent reference to a spring calibration curve; or by placing electric strain gauges on the spring anchorage strips and recording the strains on a pen recorder chart. In the latter case, a calibration was obtained from a static load test. The spring stiffness largely dictated the method of measurement, the extension of the stiffer springs was too small and rapid to be observed visually.

The water displacement, s_o, was found by observing the movement of small floats in the vicinity of the node.

Fig. (5) shows a mechanical analogy to wave action on ships which was intended as an attractive way of demonstrating in a simple manner some of the complexities of the motions of moored ships. A pivoted table is tilted harmonically by a motor driven crank, and a plank is supported on the table on three steel balls which run in grooves in such a way as to allow the plank to move up or down the table. The plank is restrained by two equal springs of suitable stiffness which provide in effect a symmetrical "mooring" system. The plank is analogous to the ship, and the table represents the wave surface in the

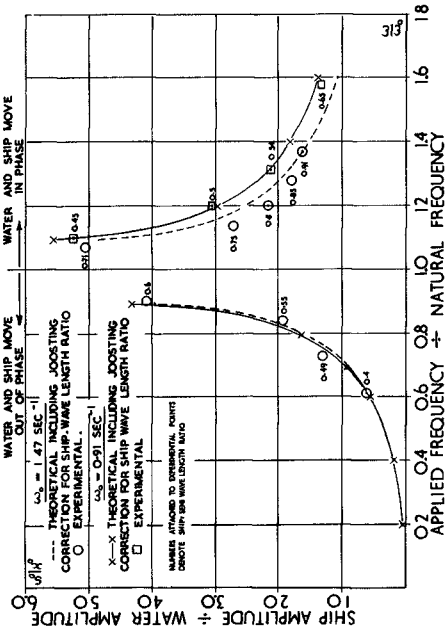

Fig. 8. Response curves for a mass oscillating on a tilting table, "moored" with linear springs and no free travel.

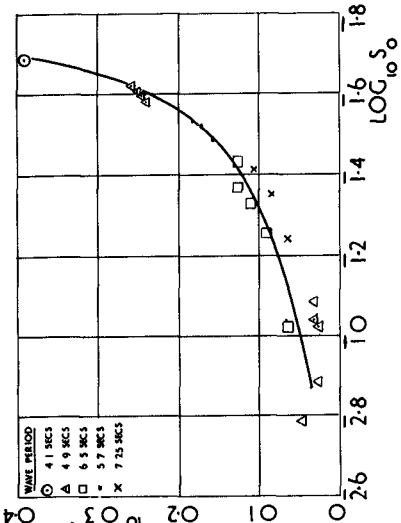

Fig. 10. Response curve for a model ship moored with non-linear springs, but no free travel.

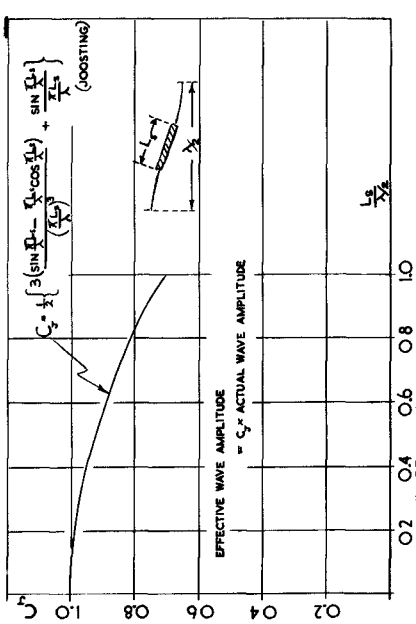

Fig. 7. A correction factor for the ship length: semi-wave length ratio.

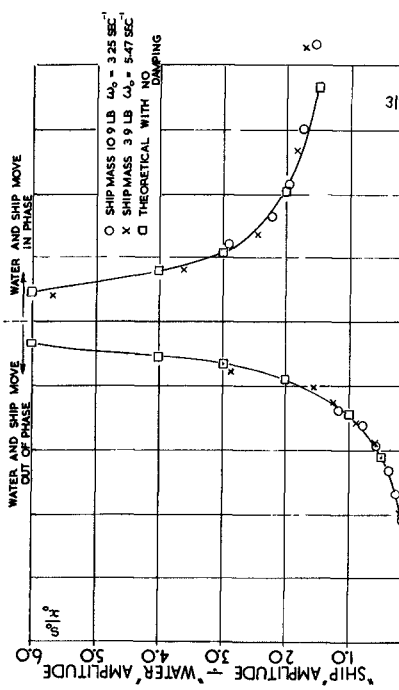

Fig. 9. Response curves for a model ship moored with linear springs and no free travel.

nodal region, the nodal point being at the pivot. Some measurements were made on the analogy and are reported in the next section.

EXPERIMENTAL RESULTS

As a preliminary to the wave tests, the virtual mass of the ship was found by the free oscillation method described in the paragraphs headed THEORY. The two springs used were of the coil type with a linear spring law, K = 0.4 lbs/in. One spring was attached to each end of the ship and pretensioned to prevent either spring slackening in the subsequent free oscillation. Although not specifically required for these tests, the virtual mass for transverse oscillation was found in the same way. The water depth was also varied, to investigate the influence of the flume bed on the ship motion, and in one case different springs were used. This set of results is tabulated in Table I and graphed in Fig. (6).

The wave experiments divided into three sets. Set. No.1 used both the mechanical analogy and the wave flume and in this set, the springs used were of the linear law type, with no free play. This is the only case for which the equation of motion can be solved exactly, and thus a direct comparison between theory and experiment was possible. The tests were intended to check the validity of the equation of motion formulated in an earlier section; to check the soundness of the assumption that damping had a negligible influence; and to consider the correction factor to allow for a finite ship length to wave length ratio. A correction for this latter effect has been proposed by Joosting[5] and is shown graphically in Fig. (7). The mechanical analogy uses a mass effectively concentrated at the nodal point and no correction factor is required. An additional outcome of these tests was the extent to which the mechanical analogy was valid. The natural period for the ship was varied by using two different pairs of springs, that of the analogy by varying the plank mass. The water amplitude and frequency were independent variables for the ship flume, for the analogy the frequency was also variable, but the maximum "water" slope was constant. The results of set No.1 are shown in Figs. (8) and (9).

The second set of tests (set No.2) used symmetrical non-linear springs without free play and these were carried out on the ship model only. These were intended to reveal the two alternative modes of motion for certain wave conditions and also to verify the author's contention that non-linearity in a mooring characteristic will not in itself produce irregular or unsymmetrical motions. Both the water period and amplitude were varied, and according to the analysis presented in an earlier paragraph, one set of results, including variation of both x_o and ω, should plot as a straight line (using the appropriate double logarithmic co-ordinates) <u>provided</u> the spring restraint approximates to a power law characteristic. The validity of the analysis may be checked by the extent to which sets of experimental points lie on straight lines, and in addition the slope and intercept of the best fitted line give values for n and K which may be compared with the

behaviour of the spring which was actually used. The n and K values are found, in fact, from the equation (4) written in the form

$$\text{Log}_{10}\,\omega^2\left(1+\frac{x_o}{S_o}\right) = \text{Log}_{10}\frac{K}{MC_k} + (n-1)\,\text{Log}_{10}\,S_o \qquad (5)$$

The results of set No.2 were plotted in the form indicated in Fig.4, the actual graph being Fig. (10).

In the final tests (set No.3) the nearest approach to prototype conditions was reached, with non-linear moorings and some free play. It was required to verify that this discontinuous type of mooring could be effectively represented by a power law restraint as proposed by Wilson[1]. The results are presented in Figs. (11) to (16), two values of free travel being combined with various springs and subjected to various wave conditions. The values of spring stiffness given are to be taken as correct at the displacement mentioned i.e. a 0.1 in/lb spring means that a 1 lb force will extend the spring by 0.1 in., although for extensions above or below this value, the force will not be changed proportionally due to the non-linearity of the spring law. Against the straight lines of Figs. (11b) to (16b) is given the value of K/C_k and n found from the equation of the line (being the best fit to the experimental points). These values are obtained from equation (5). In Figs. (11a) to (16a) are shown both the actual spring extension curve, and the curve deduced from the values of K and n, taking C_k values from the Wilson-Joosting expression

$$C_k = 1 + 0.19(n - 1)$$

DISCUSSION

Considering the virtual mass results first (Fig.(6)) the range of values of hydrodynamic mass for longitudinal ship motion (8% to 12% of the displaced mass) agrees with some unpublished results obtained at Cape Town University where values of 8% to 10% were found for both constant and harmonic accelerations of typical ship models. These values agree indirectly with field measurements as coefficients of this magnitude might well be overlooked where coupled motions are present, and this has led to the conclusion by O'Brien and Kuchenreuther[8] that the influence is negligible. The proximity of the channel bed appears to be unimportant for longitudinal oscillations.

The values of hydrodynamic mass for transverse motion (in the range 200% to 400% of the displaced mass) are higher than previously contemplated and require discussion. In these oscillations, care was taken to ensure that the motions were purely transverse, and that pitch and roll motions were virtually absent. The decay of amplitude was noted and an estimate made of the damping force, assumed to be proportional to velocity for this purpose. This indicated that the influence of damping on the free period was negligible. Reference (8) concluded that the sway hydrodynamic mass was negligible and this led to a consideration of ship proportions.

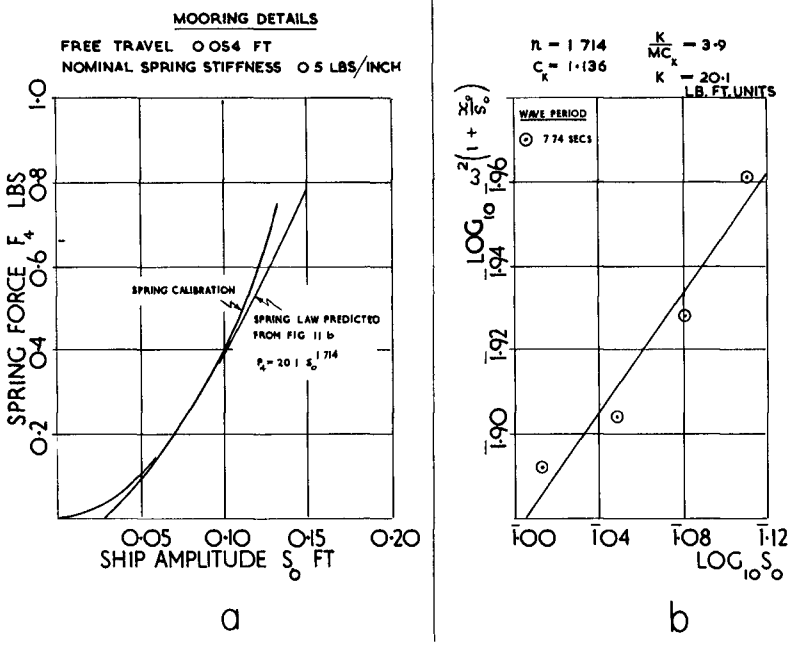

Fig. 11. Spring laws and response curves for ships moored with non-linear springs and free travel.

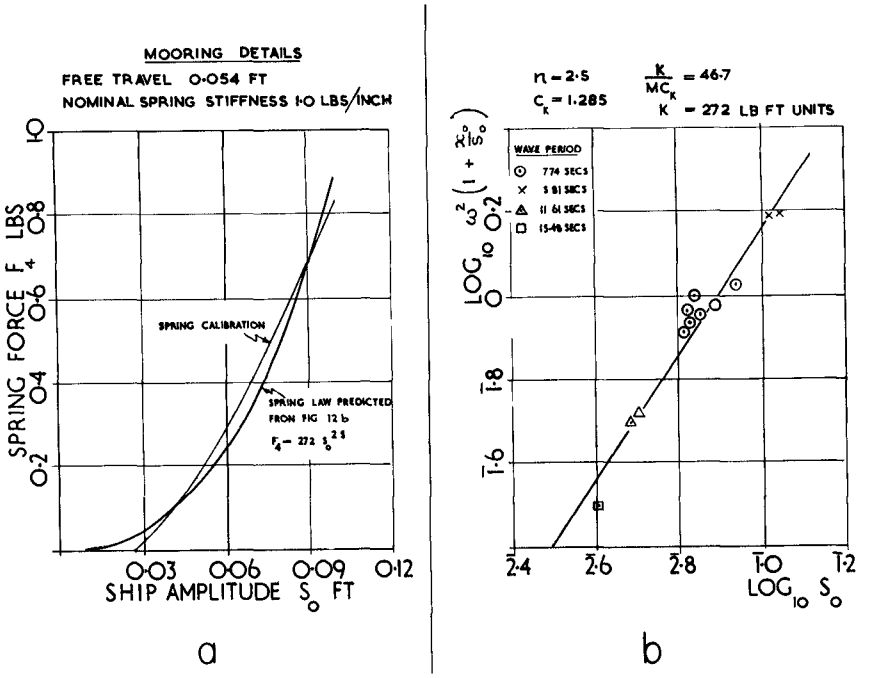

Fig. 12. Spring laws and response curves for ships moored with non-linear springs and free travel.

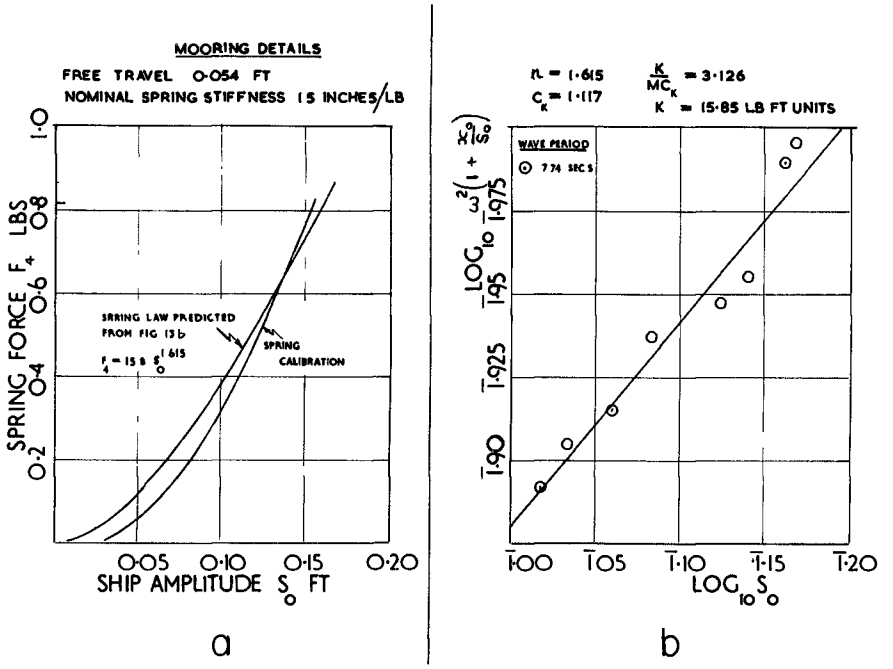

Fig. 13. Spring laws and response curves for ships moored with non-linear springs and free travel.

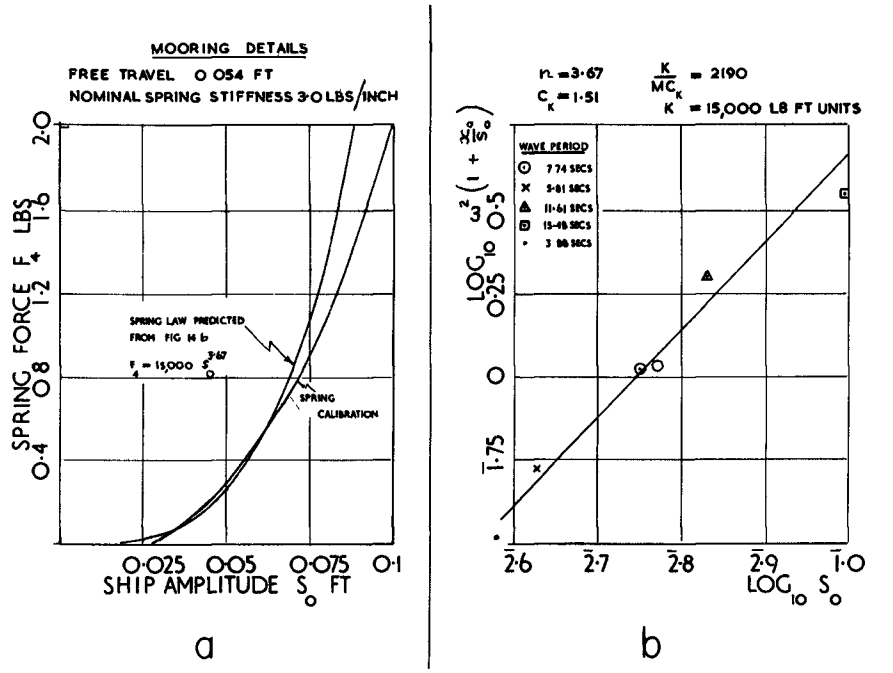

Fig. 14. Spring laws and response curves for ships moored with non-linear springs and free travel.

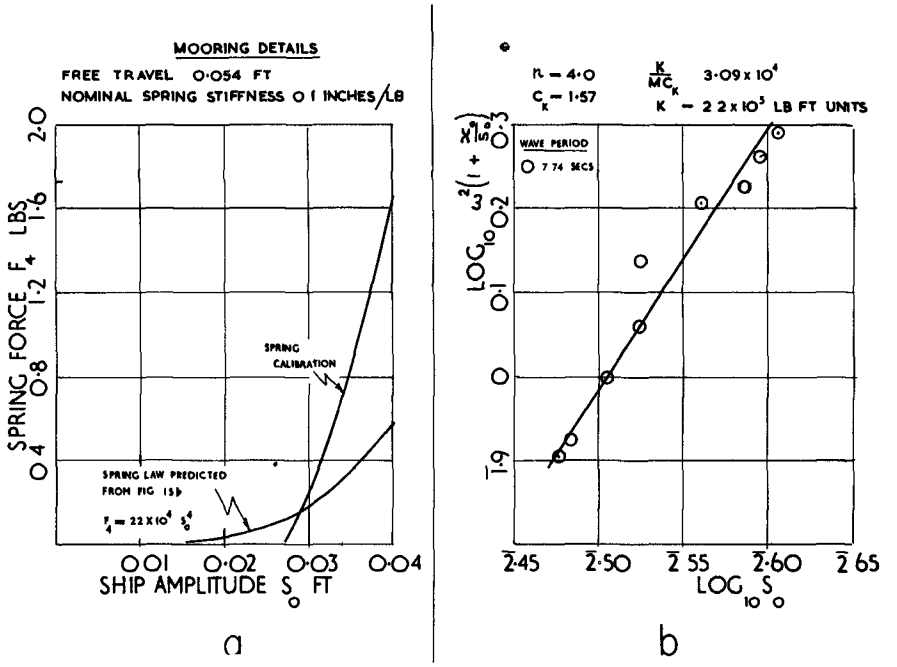

Fig. 15. Spring laws and response curves for ships moored with non-linear springs and free travel.

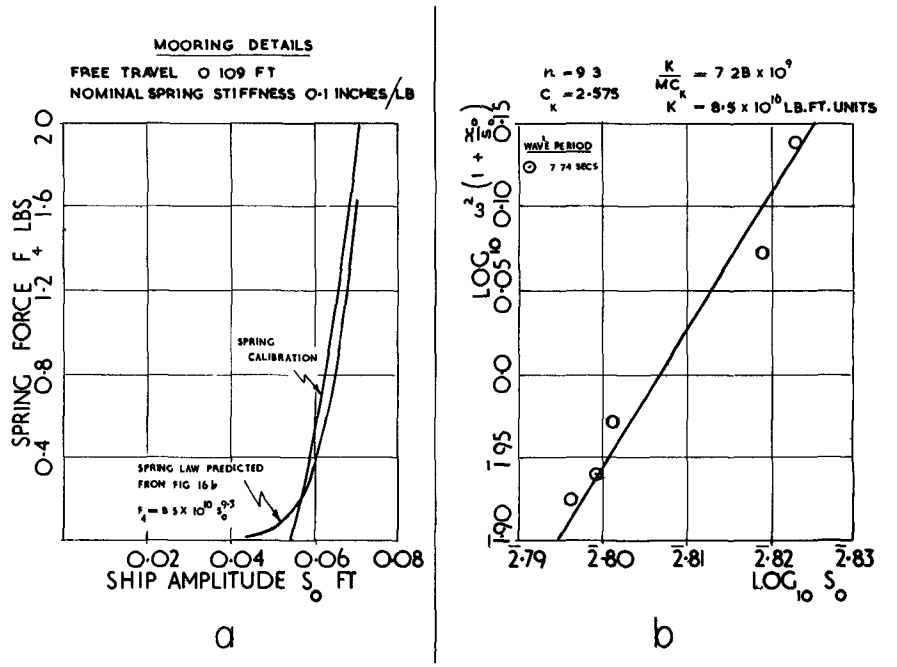

Fig. 16. Spring laws and response curves for ships moored with non-linear springs and free travel.

Wilson[13] presents proportions for a wide range of ship forms, which indicate that the draft:beam ratio lies between 0.35 and 0.5, and the length:beam ratio lies between 5 and 6.5. The values for the ship model used in the present paper are 0.6 and 8.0 respectively, the values for the dock in reference (8) are 0.12 and 4 respectively. The draft:beam ratio is the dominant one and a factor of 5 between the ratios for the two vessels under comparison may well explain the differing conclusions. Some theoretical evidence is available in reference (12), where virtual masses for long rectangular blocks are given for various draft:beam ratios, the theory being valid for an infinite inviscid fluid. If it is assumed that the same coefficients are applicable to a floating block of half the draft, an estimate can be made of the added masses for floating ships. These values indicate that the added mass, when expressed as a fraction of the displaced mass, is closely proportional to the draft:beam ratio and allowing for the fact that the dock is possibly not long enough for end effects to be negligible, the author's conclusions are not in such direct conflict with those of O'Brien and Kuchenreuther as at first sight appear. Perhaps the most surprising fact which emerges is the sharp increase of the sway added mass in shallow water, as the clearance to draft ratios covered in Fig. (6) are typical of those encountered in many ship fendering problems.

The results of the first set of tests (linear springs with no free play) are shown in Figs. (8) and (9) for the ship and the analogy respectively. The agreement in Fig. (8) between theory and experiment is close for frequencies below the natural frequency, but for frequencies greater than this, discrepancies are apparent. The discrepancies are most conspicuous for ship:semi-wave length ratios greater than 0.6 and the conclusion drawn is that the influence of this ratio is greater than the correction factor presented by Joosting[5] (Fig. (7)) would indicate. The influence of damping on the response curve was estimated but found to be small. The agreement in Fig. (9) was close which showed that the mechanical damping was of the same order as the fluid damping on the ship. The inter-agreement of Figs. (8) and (9) with theory shows that the equation of motion is correctly formulated, and that the mechanical analogy to wave motion on the ship is sound.

For tests in set No.2 (Fig.(10)) the curve shown is the sketched best fit to the experimental data and it is clear that the slope of the line varies, being flat at low ship amplitude and steepening with increasing ship movements. Thus according to eqn. (5) the spring is linear ($n = 1$) for small values of s_o, the n value increasing as s_o increases. This in fact describes the actual behaviour of the metal ring mooring used, although due to the curvature of the line in Fig.(10) no attempt was made in this case to deduce the spring law. These tests also confirmed that alternative modes of oscillation (one in phase, one out of phase) were possible for certain wave conditions, however, in no case did the ship oscillate in any way other than a periodic and symmetrical manner. The ship period always coincided with the wave period, and this confirmed that free travel (or some other discontinuity in the mooring characteristic) is necessary in order to obtain irregular impacts.

On examining the experimental results from set No.3, it was found that some readings offered no difficulty in interpretation; the model ship tensioned the moorings at each end alternately, at intervals close to half the exciting period and with approximately equal force. In such a case the mean force was found and the corresponding amplitude of ship motion taken as s_o. In other cases, however, the motion was unsymmetrical, two or more impacts at one mooring occuring between consecutive impacts at the other, the magnitude of the multiple bumps being in general less than the single one. The average of the single impact values was considered the appropriate force in these cases. Some pen deflection records illustrating these asymmetrical motions are shown in Fig. (17). As this investigation was started with a view to obtaining peak mooring forces, ship motions of in phase type with small amplitude were not examined in detail, although some experimental values were recorded. In addition, no in-phase motions with a ship amplitude less than the semi-free travel could be investigated as the moorings were not tensioned under these conditions.

Considering Figs. (11b) to (16b) the experimental points show scatter, but the general trend is linear and the averaging process described in an earlier paragraph no doubt explains some of the deviations. The agreement of actual and deduced spring characteristics in Figs. (11a) to (16a) is fair when it is considered that the analysis deals with a continuous power law curve for spring action, whereas the actual restraints are not smooth. Perhaps more important the agreement between theory and experiment is sufficiently encouraging to suggest that future experiments on ship oscillations should be planned and presented in a similar manner.

APPLICATION TO PROTOTYPE SHIPS

Accepting the conclusion that a ship mooring may be represented by a power law characteristic, it remains to consider the application to full scale ships at typical moorings.

It will be noticed that the co-ordinates in Figs. (11b) to (16b) are kinematic, however, the values of s_o will be higher and those of $\omega^2\left(1 + \frac{x_o}{s_o}\right)$ will be lower for full size ships than for the small models used here.

However, the model moorings were idealised to lie along the longitudinal axis of the ship and the ship was remote from the quay, whereas in the prototype the moorings are oblique, coupled motions will develop, and impacts between the ship and the quay are inevitable. It is believed that the simple analysis will be applicable to ships ranging at quays where the direction of the ship and the wave motion is parallel to the quayside (the waves being either stationary due to harbour resonances or long swell waves) and the transverse motion is of secondary importance. In fact the transverse impacts reduce the ship energy and it is probable

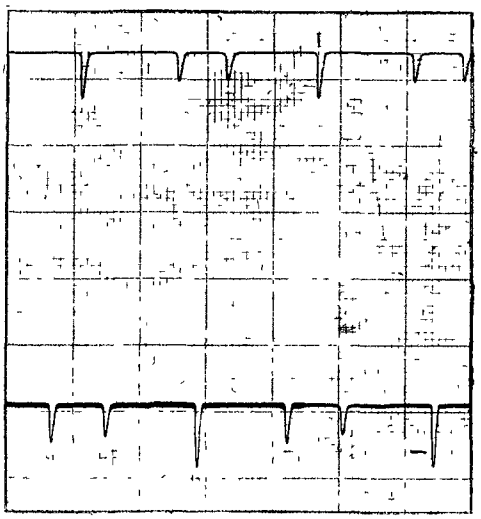

Fig.17a.Water amplitude = 0.05ft
Ship motion symmetrical, but repeats every two wave periods.

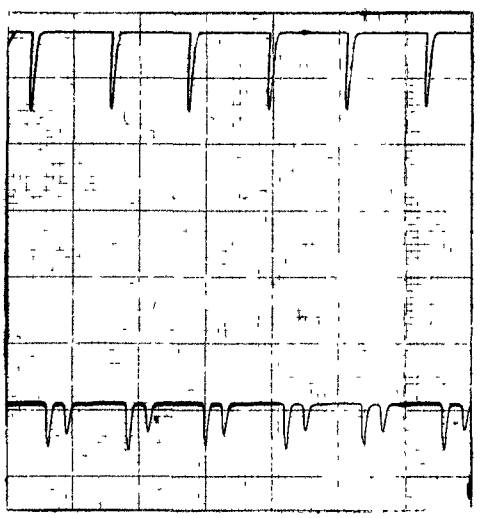

Fig.17b.Water amplitude = 0.12 ft
Ship motion asymmetrical, two impacts at one end, one impact at the other.

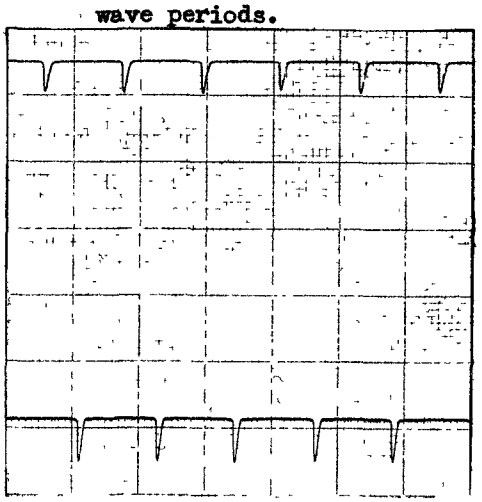

Fig.17c.Water amplitude = 0.16ft
Ship motion symmetrical

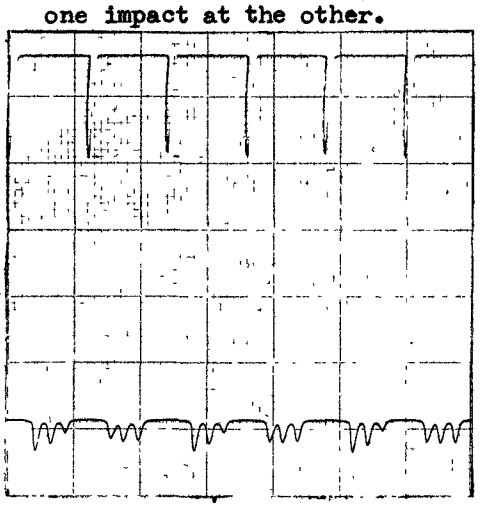

Fig.17d.Water amplitude = 0.16 ft
Ship motion asymmetrical, three impacts at one end one impact at the other.

The motion in Figs. 17c & 17d depends on the release conditions.

Fig.17: Pen records of mooring impacts at each end of a model ship.

Mooring details: Free travel 0.054 ft
Nominal spring stiffness 0.1 inches/lb.
Wave period 7.74 secs.

that calculations based only on surge motion are pessimistic. The alternative motions which may occur for certain water amplitudes do not offer any difficulty as the assumption will always have to be made that the ship will adopt the out of phase mode as this is the worst case for the moorings.

To use a graph such as Fig. (11b) for prototype force prediction, the straight line is drawn which represents a close fitting power law characteristic to the actual mooring to be used at either end of the ship (see equation 5). For any wave periodicity the motion of the ship (s_o) can be calculated for a particular water amplitude (x_o) and frequency (ω) by a trial and error method, only out of phase motions being of interest. The ship motion leads directly to the mooring forces via a calibration curve for the mooring stiffness.

A general deduction may be made for severe motions where the ship may move considerably more than the water.

$$\text{Let } s_o = p x_o, \qquad p \gg 1$$

$$\text{Then } 1 + \frac{x_o}{s_o} \doteq 1$$

$$\therefore K s_o^n = M\omega^2 C_k s_o = M x_o \omega^2 C_k \cdot p.$$

Therefore the peak mooring force is rather more than p times the force required to hold the ship stationary. It appears, that for a given water amplitude, the force increases as the wave period decreases, but a limit is reached when the wave length becomes appreciably less than twice the ship length.

MODEL SCALES

The experiments described in this paper are really tests on small scale ships with a view to understanding the problems involved, rather than model tests on a particular ship. However, any ship and mooring combination may be considered as a model of some larger ship with the following scales:-

Length scale	L:1, applicable to ship, water and mooring geometries.
Mass or Force scale	L^3:1, applicable to ship mass, mooring forces.
Velocity scale	$\sqrt{L}$:1, applicable to wave or ship speed.
Frequency scale	1:$\sqrt{L}$, applicable to wave or ship frequency.
Spring factor K	L^{3-n}:1
n, C_k	1:1

writing the eqn. (4) in the form

$$\frac{K L^{n-1}}{M\omega^2 C_k} = 1 + \frac{x_o^*}{s_o^*} \frac{1}{(s_o^*)^{n-1}} \qquad (6)$$

where $s_o^* = s_o/L$ & $x_o^* = x_o/L$
and using the scales in the form given above, the left hand side of equation (6) is independent of the scale, which confirms the similarity of the model and prototype motions.

CONCLUSIONS

(a) The hydrodynamic mass for a ship moving longitudinally is approximately one tenth of its displaced mass and shows only a slight tendency to increase in very shallow water. The hydrodynamic mass for a ship moving transversely is of the same order as the displaced mass in deep water, and may be several times as great for shallow water where the keel clearance is less than about half the draft.

(b) The equation of motion as presented in this paper was confirmed by tests with linear springs for which an exact analysis is possible. The assumption of zero damping for most practical cases is justified.

(c) The mechanical analogy is shown to be a replica of wave motion on ships, and the author considers that it could be used profitably as an alternative to a wave flume for problems of the ship mooring type.

(d) A mooring having a non-linear spring characteristic without discontinuities of gradient verified several details of theory, such as alternative ship motions for certain wave conditions, and symmetrical moorings producing only symmetrical ship movements.

(e) It was verified that a typical ship mooring, having both non-linear and free travel components, could be approximated by a power law characteristic in order to predict the average mooring forces. In some cases, however, the motion would become asymmetrical with small multiple impacts at one end. These unsymmetrical ship motions are not predictable, except that for a given free travel, they appear more likely to occur with stiff moorings than soft.

(f) Methods are given for predicting the forces on a prototype ship in surge motion, either analytically or by model scaling.

ACKNOWLEDGEMENTS

The author wishes to acknowledge the guidance and assistance of Mr. R.C.H. Russell, Senior Principal Scientific Officer of the Hydraulics Research Station, who designed the equipment and under whose direct supervision the experimental results of set No.3 were obtained.

REFERENCES

1. Wilson B.W., Ship response to range action in harbour basins. Trans.A.S.C.E. Vol. 116, p.1129, 1951.

2. Knapp R.T., Wave produced motion of moored ships. Proceedings of the second conference on Coastal engineering 1952, p.48.

3. Abramson H.N., Wilson B.W., A further analysis of the longitudinal response of moored vessels to sea oscillations. Proceedings of the 2nd Mid-Western Conference on Solid Mechanics, Purdue University, Purdue, September 1955, p.236.

4. Deacon G.E.R., Russell R.C.H., Palmer J.E.G., Paper, Section II, Communication 1. Proceedings of the 19th International Navigation Congress, London, 1957, p.75.

5. Joosting W.C.Q., Paper, Section II, Communication 1. Proceedings of the 19th International Navigation Congress, London, 1957, p.205.

6. Wiegel R.L., Clough R.A., Dilley R.A., Williams J.B., Model study of floating dry dock mooring forces, Proceedings of the symposium on the behaviour of ships in a seaway. September,1957, Wageningen, Netherlands.

7. Wiegel R.L., Beebe K.E., Dilley R.A., Model studies of the dynamics of an LSM moored in waves. Proceedings of the 6th Conference on Coastal engineering, December, 1957.

8. O'Brien J.T., Kuchenreuther D.J., Free oscillation in surge and sway of a moored floating dry dock. Proceedings on the 6th Conference on Coastal engineering, December, 1957.

9. O'Brien J.T., Kuchenreuther D.J., Proc. A.S.C.E. Journal of the Waterways and Harbours Division, Vol. 84, No.WW2, March, 1958. Paper 1571.

10. Russell R.C.H., A study of the movement of moored ships subjected to wave action. Proc. I.C.E. Vol. 12, April 1959, p.379.

11. Wiegel R.L., Dilley R.A., Williams J.B., Model study of mooring forces of a docked ship. Proc. A.S.C.E. Journal of the Waterways and Harbours Division, Vol. 85, No.WW2, June 1959, Paper No.2071.

12. Browne A.D., Mouillin E.B., Perkins A.J., The added masses of prisms floating in water Proc. Camb.Phil.Soc. Vol.26, 1929/30.

13. Wilson B.W., The energy problem in the mooring of ships exposed to waves. Princeton University Conference on berthing and cargo handling in exposed locations, October, 1958.

14. Inglis C., Applied mechanics for engineers. Cambridge University press, 1951.

CHAPTER 41

THE DYNAMICS OF A SUBMERGED MOORED SPHERE IN OSCILLATORY WAVES

Donald R. F. Harleman
Associate Professor of Hydraulics
Hydrodynamics Laboratory
Massachusetts Institute of Technology

and

William C. Shapiro
Assistant Professor of Civil Engineering
The Cooper Union

The results of an analytical and experimental investigation into the dynamics of a buoyant sphere moored by a single line in shallow water waves are presented. The sphere motion and the mooring line forces are related to the sphere diameter, weight, submergence and the wave frequency, height and water depth. Analytically, the phenomenon is approached as a forced vibration problem. The sphere and its mooring line acts as a spring-mass system driven by the oscillating wave force. The relevant dimensionless parameters are the ratio between the natural frequency of the moored sphere and the wave frequency and the ratio between the dynamic mooring force due to a given wave and the force on the sphere held stationary in the same wave. Experimental values of the frequency and force ratios obtained from tests made at the Massachusetts Institute of Technology Hydrodynamics Laboratory over a range of sphere and wave characteristics are in essential agreement with the analytically determined values. The investigation was supported by the Humble Oil and Refining Company of Houston, Texas.

ANALYTICAL DEVELOPMENT

WAVE FORCE ON A STATIONARY SPHERE

The forces on objects submerged in water waves result from the velocities and accelerations of the water particles comprising the waves. For waves having a steepness H/L less than 0.03 the particle kinematics are given by the Airy equations. The equations for the horizontal and vertical components of particle velocity and acceleration expressed in the notation of Figure 1 are

$$u = \frac{\sigma H}{2} \left(\frac{\cosh kS}{\sinh kd}\right) \sin \sigma t = u_m \sin \sigma t \tag{1}$$

$$v = \frac{\sigma H}{2} \left(\frac{\sinh kS}{\sinh kd}\right) \cos \sigma t = v_m \cos \sigma t \tag{2}$$

$$\frac{du}{dt} = \frac{\sigma^2 H}{2} \left(\frac{\cosh kS}{\sinh kd}\right) \cos \sigma t = \left(\frac{du}{dt}\right)_m \cos \sigma t \tag{3}$$

$$\frac{dv}{dt} = -\frac{\sigma^2 H}{2} \left(\frac{\sinh kS}{\sinh kd}\right) \sin \sigma t = -\left(\frac{dv}{dt}\right)_m \sin \sigma t \tag{4}$$

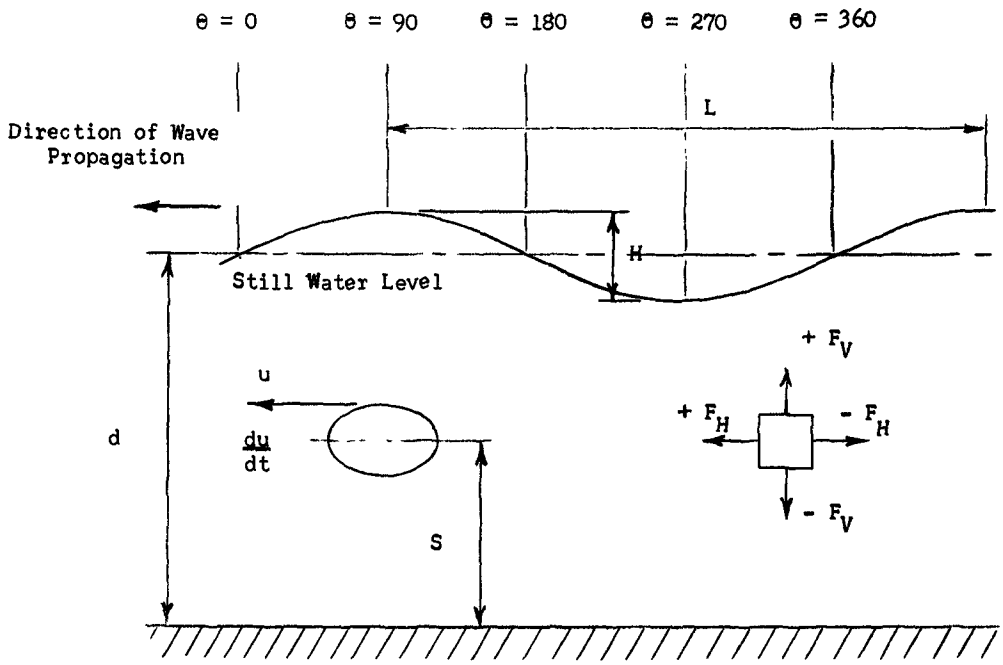

Fig. 1. Definition sketch for wave motion.

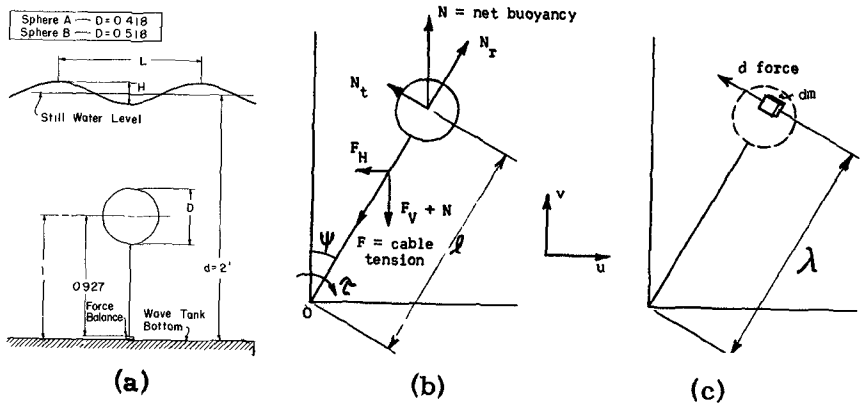

Fig. 2. Definition sketch for moored sphere.

The speed of wave propagation or celerity is

$$\text{celerity} = \frac{L}{T} = \sqrt{\frac{g}{K} \tanh kd} \tag{5}$$

In the absence of viscosity, the force exerted on an object in an unsteady flow field may be determined from classical hydrodynamic theory. The pressure gradient in the horizontal direction resulting from the local acceleration (convective acceleration terms neglected) is given by the equation of motion.

$$-\frac{dp}{dx} = \rho \frac{du}{dt} \tag{6}$$

By integration, the force on an object due to the pressure gradient becomes

$$F_H(\text{pressure grad.}) = -\frac{dp}{dx}(\text{Vol.}) = \rho(\text{Vol.})\frac{du}{dt} = M\frac{du}{dt} \tag{7}$$

where M is the mass of the displaced fluid.

In addition to the pressure gradient force there is a force due to virtual mass which exists whenever there is relative acceleration between a fluid and an immersed body. The virtual mass force can be expressed

$$F_H(\text{virtual mass}) = K\rho(\text{Vol.})\frac{du}{dt} = KM\frac{du}{dt} \tag{8}$$

where K is the added mass constant. Addition of equations (7) and (8) gives the total acceleration or inertia force.

$$F_{HI} = (1 + K)\, M\frac{du}{dt} = C_M\, \rho(\text{Vol.})\frac{du}{dt} \tag{9}$$

In equation (9) C_M, the coefficient of mass replaces the term (1+K). The added mass constant K has been determined analytically for a sphere to be 0.5. C_M for a sphere in frictionless flow is therefore 1.5.

The force on an object in steady viscous flow arises from surface shear, pressure gradients and wake formation. The hydrodynamic drag is expressed

$$F_{HD} = C_D \frac{\rho}{2}(\text{Area})|u|\, u \tag{10}$$

To obtain the wave force on a submerged stationary object the steady state drag force given by equation (10) is added to the potential flow inertia force given by equation (9)

$$F_{HO} = F_{HI} + F_{HD} = C_M\, \rho(\text{Vol.})\frac{du}{dt} + C_D\, \rho/2\,(\text{Area})|u|\, u \tag{11}$$

Substitution of the wave particle velocity and acceleration expressions into equation (11) yields

$$F_{HO} = C_M \rho(\text{Vol.}) \left[\frac{du}{dt}\right]_m \cos \sigma t + C_D \rho/2(\text{Area}) u_m^2 |\sin \sigma t| \sin \sigma t \qquad (12)$$

Assuming C_M and C_D to be constant over a wave cycle, equation (12) may be rewritten

$$F_{HO} = F_{HIm} \cos \sigma t + F_{HDm} |\sin \sigma t| \sin \sigma t \qquad (13)$$

where

$$F_{HIm} = C_M \rho(\text{Vol.}) \left[\frac{du}{dt}\right]_m \qquad (14)$$

$$F_{HDm} = C_D \rho/2(\text{Area}) u_m^2 \qquad (15)$$

Using the Stokes solution of a sphere oscillating in a viscous fluid at low Reynolds numbers and dimensional analysis, Keulegan and Carpenter (195 successfully correlated experimentally determined inertia and drag coefficients with a period parameter $u_m T/D$. The parameter $u_m T/D$ is directly related to the ratio of the maximum wave drag force component to the maximum inertia component. For a sphere, equations (14) and (15) with the use of equations (1) and (3) give

$$\frac{F_{HIm}}{F_{HDm}} = \frac{8}{3} \pi \frac{C_M}{C_D} \left[1 / \frac{u_m T}{D}\right] \qquad (16)$$

From equation (16) a low value of period parameter signifies a predominant inertia force while a high value signifies a predominant drag force. Using a cylinder in the sinusoidal horizontal current under the node of a standing wave, Keulegan and Carpenter found the experimentally determined inertia coefficient equal to the potential flow value for low period parameters and the drag coefficient equal to the steady state value for high period parameter. Between these two extreme cases a point of maximum deviation of both the inertia and drag coefficients from their potential flow and steady state values respectively was found at a period parameter of 15.

Keulegan and Carpenter's results indicate that equation (12) may be used to determine the wave force on a submerged object provided the inertia and drag coefficients are known as functions of the period parameter. In the special case where the inertia force predominates and the drag force is small (low period parameters) the potential flow value of the inertia coefficient may be used. In the special case where drag force predominates and the inertia force is small (high period parameter) the steady state value of the drag coefficient may be used.

The reasoning outlined above is supported by the results of Harleman and Shapiro (1955) in their tests on single vertical cylinders in steep waves. In their analysis they used essentially the formulation of equation (12) to construct the total wave force history with the potential flow C_M and the steady state C_D. Their analytical results were in agreement with experiment for the cases of predominant inertia and predominant drag, but were not in agreement for the region of approximately equal inertia and drag. The greatest discrepancy between analysis and experimen occurred near $u_m\ T/D = 15$.

The relationship between the period parameter and the wave and objec characteristics is found by substituting from equation (1) for u_m.

$$\frac{u_m T}{D} = \frac{\pi H}{D} \frac{\cosh kS}{\sinh kd} \tag{17}$$

The experiments in this study were conducted using waves of steepnes: $H/L = 0.02$. This small steepness was chosen to simplify the analysis of the problem through the use of the Airy equations for wave kinematics. In addition, wave and sphere dimensions were selected to yield low period parameters; that is, a condition of predominant inertia force. The subsequent analysis will be seen to depend upon this condition. The wave and sphere characteristics used in this study are shown in Table I and Figure 2a.

The preceding discussion of wave forces on rigidly restrained bodies has been concerned with the horizontal wave force component. However, all the foregoing applies to the vertical component as well. The following are the relevant equations for the vertical component.

$$F_{VI} = (1+k)\,\rho(\text{Vol.})\,dv/dt = C_M \rho(\text{Vol})\,dv/dt \tag{18}$$

$$F_{VD} = C_D\ \rho/2\,(\text{Area})\,|v|\ v \tag{19}$$

$$F_{VO} = F_{VI} + F_{VD} = C_M \rho(\text{Vol.})\,dv/dt + C_D\,\rho/2(\text{Area})|v|\,v \tag{20}$$

$$F_{VO} = F_{VIm} \sin \sigma t + F_{VDm} |\cos \sigma t| \cos \sigma t \tag{21}$$

$$F_{VIm} = C_M\ \rho(\text{Vol})\ [dv/dt]_m \tag{22}$$

$$F_{VDm} = C_D\ \rho/2\,(\text{Area})\,v_m^{\,2} \tag{23}$$

ANALYSIS OF MOORED OSCILLATING SPHERE

Figure 2 is the definition sketch for the moored sphere analysis. It is assumed in the analysis that the mooring line remains straight and under tension at all times and that the sphere motion remains in the plane defined by the wave particle orbits. These assumptions permit the position of the sphere to be uniquely defined by the mooring line angle, ψ alone. Thus the sphere and mooring line constitute a single degree of

freedom oscillating system.

Referring to Figure 2c, Newton's second law is written in the tangential direction for the element of mass dm.

$$d\ \text{Force} = dm\ \ddot{\psi}\lambda$$

where $\ddot{\psi}$ is the angular acceleration. Multiplying both sides of the equation by λ gives

$$d\ \text{Torque} = \lambda^2\ dm\ \ddot{\psi}$$

Integration over the volume of the sphere yields

$$T = I\ \ddot{\psi} \tag{24}$$

where I is the moment of inertia of the sphere about point 0 since

$$\int_{\text{VOL.}} \lambda^2\ dm = I$$

Equation (24) is the standard form of Newton's second law for rotating bodies. The torque, T, is the summation of the torques due to all the forces acting on the sphere. The first of these is the spring torque. Assuming that the mooring line angle remains small, so that $\sin\psi \approx \psi$, the spring torque is

$$\text{Spring torque} = -N_t \ell = -N\ell \sin\psi$$

$$\approx -\left[\frac{\pi D^3}{6}\rho g - mg\right]\ell\psi \tag{25}$$

The pressure gradient torque depends upon the fluid acceleration and is derived from equation (7). Here the flow field is specified in terms of horizontal and vertical components. To find the total pressure gradient torque it is necessary to take the sum of the projections in the tangential direction of the horizontal and vertical pressure gradient force components. Assuming again that the mooring line angle remains small

$$\text{Pressure grad. torque} = \frac{\pi D^3}{6}\rho\left[\frac{du}{dt}\cos\psi - \frac{dv}{dt}\sin\psi\right]\ell$$

$$\approx \frac{\pi D^3}{6}\rho\left[\frac{du}{dt} - \frac{dv}{dt}\psi\right]\ell \tag{26}$$

The virtual mass torque depends upon the relative acceleration between the fluid and the sphere. In view of equation (8) the virtual mass effect is assumed due to a sphere of fluid the same size as the actual sphere but having a mass equal to K times the mass of the fluid. Following the method used in deriving equation (24) and using equation (8), the virtual mass torque may be written

$$\text{Virtual mass torque} = -I'\ddot{\psi} + \frac{K\pi D^3}{6}\rho\left[\frac{du}{dt}\cos\psi - \frac{dv}{dt}\sin\psi\right]\ell$$

$$\approx -I'\ddot{\psi} + \frac{K\pi D^3}{6}\rho\left[\frac{du}{dt} - \frac{dv}{dt}\psi\right]\ell \qquad (27)$$

where I' is the moment of inertia of the fluid sphere about point O and the mooring line angle is assumed small.

The damping torque depends on the relative velocity between the sphere and the fluid. Assuming, for the present, the damping to be linear and the mooring line angle small, the damping torque may be written

$$\text{Damping torque} = c\left[-\dot{\psi}\ell + u\cos\psi - v\sin\psi\right]\ell$$

$$\approx c\left[-\dot{\psi}\ell + u - v\psi\right]\ell \qquad (28)$$

The contributing torques given by equations (25) through (28) are added and substituted into equation (24) to give the equation of motion of the oscillating sphere with linear damping

$$(I + I')\ddot{\psi} + c\dot{\psi}\ell^2 + \Big[\overbrace{\frac{\pi D^3}{6}\rho g}^{\text{net buoyancy}} - mg + \overbrace{(K+1)\frac{\pi D^3}{6}\rho\frac{dv}{dt} + cv}^{F_{VO}}\Big]\ell\psi$$

$$= \overbrace{\Big[(K+1)\frac{\pi D^3}{6}\rho\frac{du}{dt} + cu\Big]\ell}^{F_{HO}} \qquad (29)$$

Inertia Drag

Equation (29) has the general form of the differential equation of motion of a single degree of freedom spring-mass system with linear damping. However, in its present form the equation is non-linear.

The physical meaning of the various portions of equation (29) is indicated by brackets. To linearize and simplify the equation the following assumptions are made:

Assumption 1 The vertical component of the mooring line force is equal to the net buoyancy N. This is valid if the vertical dynamic wave force Fv is small with respect to the net buoyancy.

Assumption 2 The drag wave force component is small with respect to the inertia wave force component.

Assumption 3 (previously stated) The mooring line angle, ψ, is small

With assumptions 1 and 2, equation (29) becomes

$$(I + I')\ddot{\psi} + (c\ell^2)\dot{\psi} + \left(\frac{\pi D^3}{6}\rho g - mg\right)\ell\psi = C_M\frac{\pi D^3}{6}\rho\frac{du}{dt}\ell \qquad (30)$$

The preceding assumptions have reduced the equation of motion to the exact form of the differential equation of motion of the single degree of freedom spring-mass system with linear damping and a sinusoidal driving force. The more practical case for the sphere problem involves quadratic damping as given by equation (10). In order to revise the preceding analysis for square law damping it is only necessary to change the damping term in equation (30). The damping torque is now given by

$$\text{Damping torque} = c_2 (\dot{\psi} \ell)^2 \ell = C_2 \dot{\psi}^2 \tag{31}$$

where

$$C_2 = c_2 \ell^3 \tag{32}$$

The differential equation of motion becomes

$$A\ddot{\psi} + C_2 \dot{\psi}^2 + B\psi = F_{H_{om}} \ell \cos \sigma t \approx F_{HI_m} \cos \sigma t \tag{33}$$

where

$$A = I + I' \quad , \quad B = [\frac{\pi D^3}{6} \rho g - mg] \ell = N\ell \tag{34}$$

Before treating the solution of equation (33) as written, the special case of free oscillation of the moored submerged sphere without damping will be considered. Setting the driving force and damping terms to zero in equation (33) yields the differential equation of motion for the free oscillation case.

$$A\ddot{\psi} + B\psi = 0 \tag{35}$$

Equation (35) has the solution

$$\psi = \psi_m \cos \sqrt{\frac{B}{A}} \cdot t \tag{36}$$

The motion is sinusoidal with amplitude or maximum angle and frequency

$$f_n = \frac{1}{2\pi} \sqrt{\frac{B}{A}} \tag{37}$$

The frequency given by equation (37) is the undamped natural frequency. From vibration theory the solution to the free oscillation problem with linear damping included is known to be a harmonic oscillation with an exponentially decreasing amplitude and a frequency somewhat less than the undamped natural frequency. For small damping, however, the damped natural frequency is equal to the undamped natural frequency for all practical purposes.

In Figure 3 experimentally determined natural frequencies are plotted against sphere weight for the 0.518 ft. sphere. Also shown is the theoretical curve computed for the test conditions from equation (37) using the potential flow added mass coefficient of 0.5. The excellent agreement between theory and experiment shows the neglect of damping in

the free oscillation case is justified for the conditions of this study.

The non-linear forced oscillation equation of motion with quadratic damping [equation (33)] can be solved as a linear equation by using the technique of Lorentz which was originally devised in 1926 for tidal computations in shallow water (Dronkers and Schonfeld 1955). The dissipation of energy in one wave period by the quadratic resistance term is equated to the dissipation represented by the linear term in equation (29). A similar method has also been used by Jacobsen (1930) in connection with mechanical vibration problems. Under the above conditions the solution of equation (33) is given by

$$\psi = \psi_m \cos(\sigma t - \phi) \tag{38}$$

According to equation (38) the sphere moored in oscillatory waves oscillates sinusoidally at the wave frequency and lags the driving force by a phase shift ϕ. The amplitude of oscillation is a function of the ratio between the wave (driving) frequency and the natural frequency of the system. In dimensionless form the amplitude and phase shift are

$$\frac{\psi_m}{\psi_{om}} = \frac{F_{H_m}}{F_{Ho_m}} = \frac{1}{\sqrt{2}\, n_2 (f/f_n)^2} \left[\left\{ (1 - (\frac{f}{f_n})^2)^4 - 4 n_2^2 (\frac{f}{f_n})^4 \right\}^{1/2} - (1 - (\frac{f}{f_n})^2)^2 \right]^{1/2} \tag{39}$$

and

$$\tan \phi = \frac{1}{\sqrt{2}} \left[\left\{ 1 + \frac{4 n_2^2 (f/f_n)^4}{(1-(f/f_n)^2)^4} \right\}^{1/2} - 1 \right]^{1/2} \tag{40}$$

where

$$\psi_{om} = \frac{T_{om}}{B} = \frac{F_{H_{om}} \ell}{[\frac{\pi D^3}{6} \rho g - mg] \ell} = \frac{F_{H_{om}}}{N} \tag{41}$$

In view of assumptions 1 and 3, the parameter ψ_{om} represents the mooring line angle which would obtain if the sphere were subjected statically to the horizontal driving force maximum, $F_{H_{om}}$. The term ψ_m / ψ_{om} is the multiplication factor between the static deflection of the sphere under the driving force, and the amplitude of the actual sphere motion.

In accordance with assumptions 1 and 3

$$\frac{\psi_m}{\psi_{om}} = \frac{F_{H_m}}{F_{H_{om}}}$$

where F_{H_m} is the maximum value of the horizontal component of mooring line tension. Therefore equation (39) also describes the variation in the horizontal mooring line tension multiplication factor with

Table I: CHARACTERISTICS OF EXPERIMENTAL PROGRAM

Test	Wave Height ft.	Wave Length ft.	Period sec.	Freq. cps	Wave Freq. Nat. Freq.	Period Parameter u_mT/D
I-2-A	0.10	5.10	1.00	1.000	1.00-3.10	0.24
I-2-B	"	"	"	"	1.02-3.20	0.20
I-4-A	0.20	9.90	1.50	0.667	1.14-1.08	1.10
I-4-B	"	"	"	"	1.14-1.08	0.88
I-6-A	0.29	14.45	2.00	0.500	0.50-1.63	2.42
I-6-B	"	"	"	"	0.50-1.56	1.95
I-7-A	0.33	16.65	2.75	0.445	0.45-1.38	3.24
I-7-B	"	"	"	"	0.44-1.40	2.61

All tests: Water depth = 2 ft., Sphere moored at mid-depth
Sphere A: Diam. = 0.418 ft.
Sphere B: Diam. = 0.518 ft.

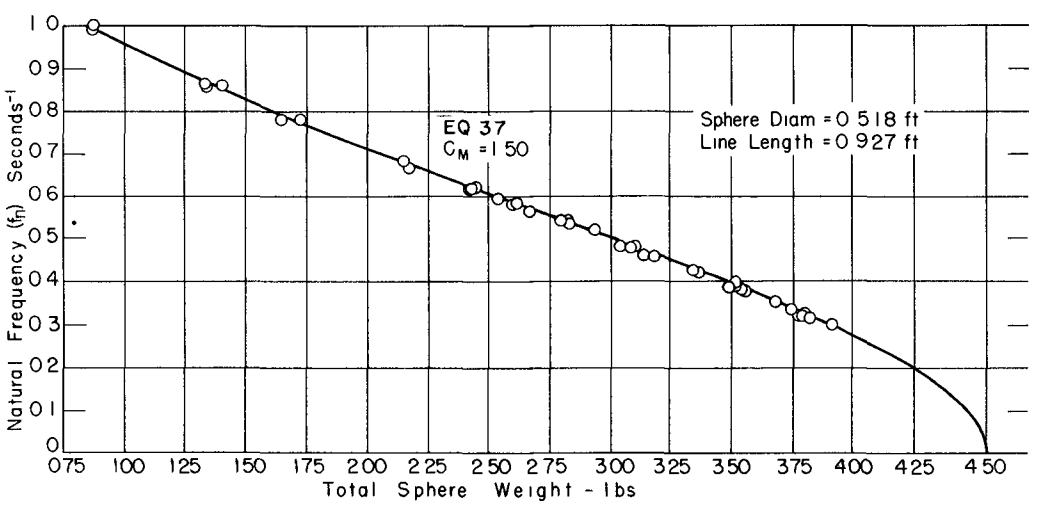

Fig. 3. Variation of natural frequency with weight of sphere.

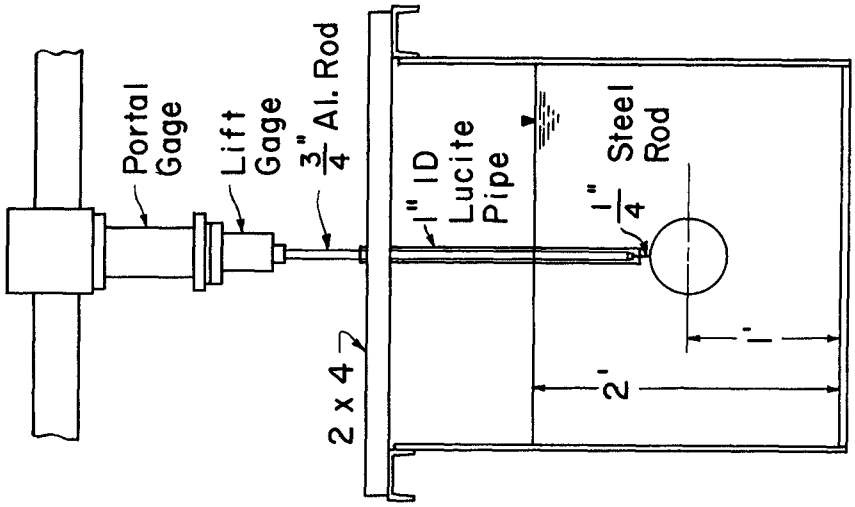

Fig. 6. Rigidly restrained sphere test arrangement.

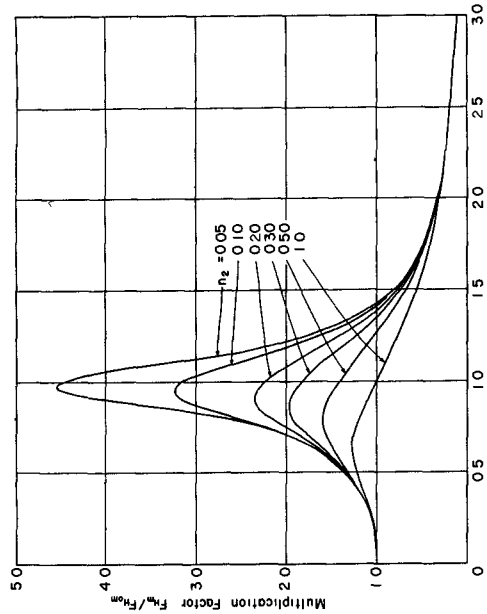

Fig. 4. Horizontal force multiplication factor for quadratic damping.

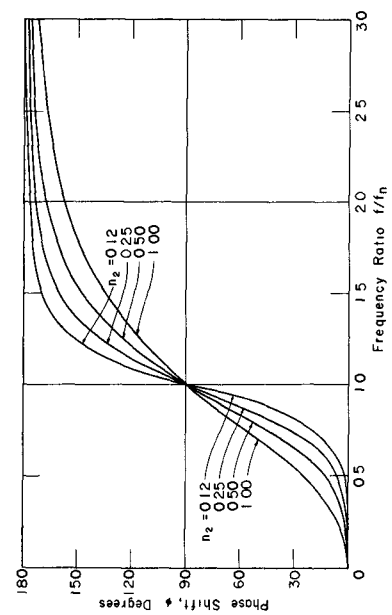

Fig. 5. Horizontal force phase shift for quadratic damping.

frequency ratio.

The damping factor, n_2, in equations (39) and (40) is

$$n_2 = \frac{2}{3} \frac{C_2 F_{H_{om}} \ell}{\pi^3 A^2 f_n^2} \tag{43}$$

The constant $c_2 = C_2/\ell^3$ is found from the drag force equation, equation (10) with the cross sectional area of the sphere inserted

$$F_{H_D} = \underbrace{C_D \rho/2 \frac{\pi D^2}{4}}_{c_2} |u|u$$

Therefore

$$n_2 = \frac{1}{12\pi^2} \frac{C_D \rho D^2 \ell^4 F_{H_{om}}}{A^2 f_n^2} \tag{44}$$

Figure 4 is a plot of the multiplication factor against frequency ratio computed from equation (39) for several values of the parameter n_2. The phase shift given by equation (40) is plotted in Figure 5. Figures 4 and 5 show the three primary modes of behavior of the oscillating sphere. At very low frequency ratios the horizontal mooring line force component is in phase with and opposed to the driving force. This is the condition of static response because at any point of the cycle the restraining force is exactly equal to the applied force. At frequency ratios near unity, the damping force is in phase with and opposed to the driving force and the horizontal mooring line force achieves large magnitudes dependent upon the amount of damping. This is the condition of resonance. At large frequency ratios, the inertia force is in phase with and opposed to the driving force and the horizontal mooring line force approaches zero. This is the condition of complete dynamic response.

Use of the Analytical Relationships

To summarize the theoretical development, the procedure for determining the maximum mooring line tension in a particular problem will be reviewed. First, the period parameter is computed from equation (17) to determine if the condition of predominant inertia force is satisfied. To satisfy this condition, the period parameter should be less than 5.

Second, the maximum horizontal force on the stationary sphere, $F_{H_{om}}$ is computed. Since the drag component of the total force is small, equation (14), the equation for the maximum inertia component may be used to closely approximate $F_{H_{om}}$.

Third, the natural frequency of the sphere is determined from equation (37) and divided into the wave frequency to give the frequency ratio.

Fourth, the multiplication factor is computed from equation (39) using the n_2 value obtained from equation (44). In this computation C_D is determined from the steady state drag curve using as Reynolds number

$u_m D/\nu$. The maximum force on the stationary sphere is multiplied by the multiplication factor to give the maximum horizontal mooring line tension component. The maximum mooring line angle is determined from the relationship.

$$\psi_m = \tan^{-1} \frac{F_{H_m}}{N} \approx \frac{F_{H_m}}{N} \tag{45}$$

The maximum mooring line tension is determined from the relation

$$\text{Maximum Tension} = \sqrt{(F_{H_m})^2 + N^2} \tag{46}$$

EXPERIMENTAL PROGRAM

EXPERIMENTAL EQUIPMENT

The experimental program was conducted in a glass walled tank, 90 ft. long, 2-1/2 ft. wide and 3 ft. deep at the Massachusetts Institute of Technology Hydrodynamics Laboratory. A piston type shallow water wave generator was used to generate the experimental waves. A steel frame to support the spheres in the rigidly restrained tests was located 40 ft. downstream from the wave generator. A model beach at a slope of 15 horizontal to 1 vertical occupying the last 35 ft. of the tank served as an energy dissipator, satisfactorily limiting undesirable wave reflections

The spheres were moulded from 1/4 inch lucite. Provision was made for attaching a 1/4 inch rod for the rigidly restrained tests and a mooring line for the moored tests.

In order to obtain a range of frequency ratios for each sphere in each test wave, the natural frequency of the sphere was varied by changing its weight. Filler materials were provided by mixing a commercially available dry detergent, Vermiculite, and granulated salt.

For the rigidly restrained tests the spheres were supported from the test stand as shown in Figure 6. The 3/4 inch support rod was shielded by 1 inch inside diameter lucite pipe to minimize tare forces on the rod.

INSTRUMENTATION

Instrumentation was required in the test program to measure wave characteristics, the horizontal and vertical force components in the rigidly restrained tests and the mooring line tension components in the moored tests. Because of the unsteady nature of the phenomenon, most data were taken electronically and recorded on a Sanborn Model 150 four channel direct writing oscillograph. The recorder was equipped with a timing marker which recorded one second pulses along one margin.

Wave profiles were measured using a capacitive type wave probe.

The horizontal force component on the rigidly restrained spheres was measured using a portal gauge. The gauge is sensitive to shear alone and therefore measures the horizontal force on the cantilever beam below it irrespective of the distance to the point of application of the force. The sensing element in the portal gauge is a Schaevitz L.V.D.T.

The vertical force component on the rigidly restrained sphere was measured with a double diaphram lift gauge using the same sensing element as the portal gauge.

In the moored tests, the horizontal and vertical components of mooring line tension were measured using a two component balance. The gauge consists of a horizontal outer force beam to measure the vertical component and a vertical inner force beam to measure the horizontal component. Both force beams have sensing elements consisting of 4 SR-4-A-7 strain gauges. Since the two component balance was used under water it was necessary to waterproof the strain gauges and wire connection. This was done by applying three or four coats of Neoprene Bonding Cement. Each coat was allowed to dry for 24 hours before the next was applied. The waterproofing successfully withstood continuous immersion for periods up to two weeks and intermittent immersion for a year.

RESULTS

RIGIDLY RESTRAINED TESTS

Experimental horizontal and vertical wave component histories for test I-2-A are presented in Figure 7. The experimental force traces show the inertial character of the wave forces of the test program as predicted by the low period parameters. The maxima of the horizontal component occur near 0° and 180° and the maxima of the vertical component near 270° and 90°. The horizontal component at 90° and 270° , the phase angles where the drag contribution to the total force is a maximum, is negligible.

From the experimental force histories, values of the inertia coefficien C_M, were determined for all tests. These values were determined to give the best fit between the experimental traces and the theoretical expressions given by equations (12) and (21). The inertia coefficients determined from the horizontal force component averaged 1.56 compared with the potential flow value of 1.50. The coefficients determined from the vertical component averaged 1.30.

From the experimentally determined inertia coefficients and equations (12) and (21) horizontal and vertical force component traces were computed for test I-2-A. For both traces the steady state value of C_D, 0.42 was used. The computed traces are shown as solid lines in Figure 7. The agreement with experiment is excellent.

PARTIALLY RESTRAINED TESTS

Mooring line forces and angles

The experimental mooring line dynamic horizontal and vertical tension component and mooring line angle histories for two tests are presented in Figures 8 and 9. The tests selected represent the extreme wave characteristics and period parameters of the test program. The mooring line tension components were obtained directly from the experimental records. The experimental mooring line angles were computed from the tension component traces using the relation

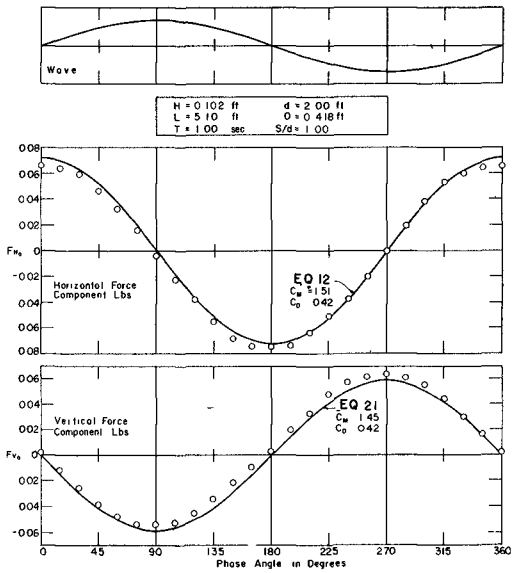

Fig. 7. Force component variation with wave phase - rigidly restrained sphere (test I-2-A).

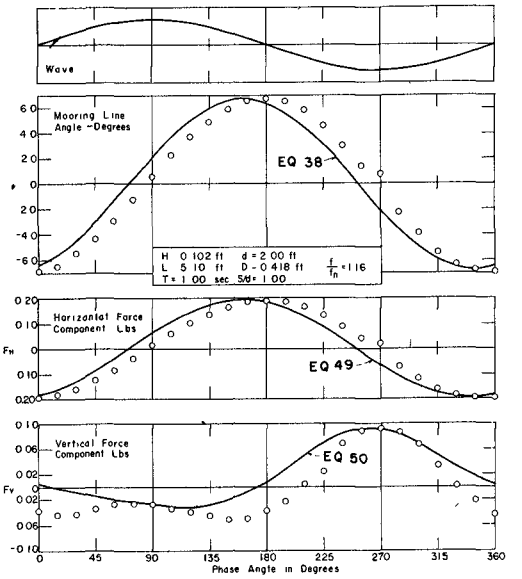

Fig. 8. Force and mooring angle variation with wave phase (test I-2-A-2).

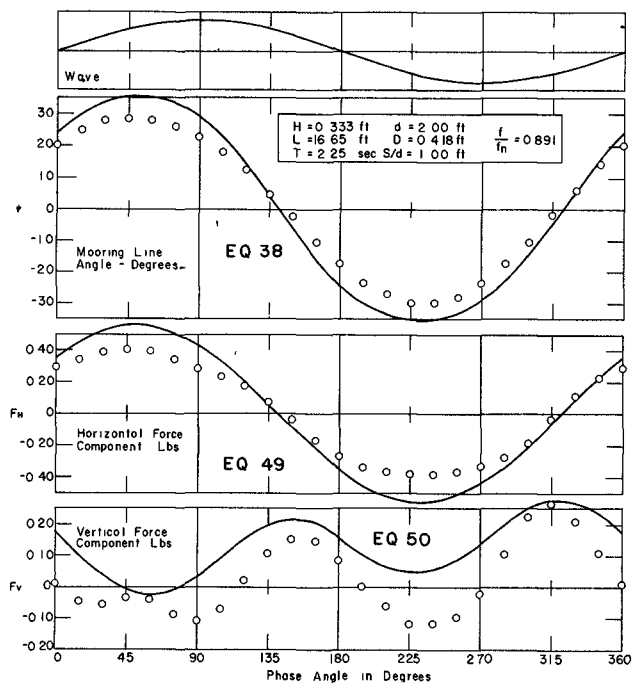

Fig. 9. Force and mooring angle variation with wave phase (test I-7-A-3).

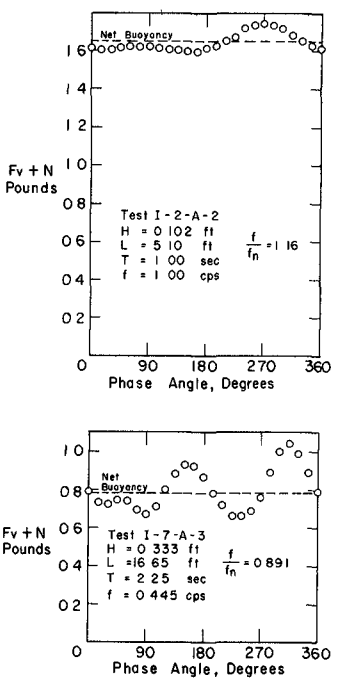

Fig. 10. Variation of vertical mooring force with wave phase.

$$\psi = \tan^{-1} \left(\frac{F_H}{F_V + N}\right) \tag{47}$$

For each experimental trace in Figures 8 and 9 a corresponding theoretical history was computed. The theoretical expression for the mooring line angle is given by equation (38).

In view of the assumptions made in the development of the theory, that the dynamic vertical force is much less than the net buoyancy and that the mooring line angle is small, the mooring line angle may be expressed

$$\psi = \frac{F_H}{N} \tag{48}$$

By substitution into equation (38), the theoretical horizontal force component history becomes

$$F_H = F_{H_m} \cos (\sigma t - \phi) \tag{49}$$

To solve for the theoretical mooring line angle and horizontal mooring force histories it is necessary to know F_{H_m} and the phase shift angle, ϕ. Equation (39) gives F_{H_m} in terms of the multiplication factor, $F_{H_m}/F_{H_{om}}$. The phase shift, ϕ, is given by equation (40). The multiplication factor and phase shift are functions of the frequency ratio and damping factor, n_2. The damping factor, given by equation (43), is a function of the coefficients of inertia and drag and the maximum horizontal force component on the sphere in the rigidly restrained condition. In evaluating the theoretical horizontal force component and mooring line angle histories the following quantities were used:

C_M = 1.5, potential flow value

C_D = 0.42, steady state value

$F_{H_{om}}$ = average of positive and negative experimental value in rigidly restrained tests

The agreement between the theoretical and experimental horizontal component and mooring line angle histories in Figures 8 and 9 is good with respect to curve shape and phasing. For the longer wave, I-7, the maxima of the theoretical curves are significantly higher than the experimental maxima representing a corresponding discrepancy between the theoretical and experimental multiplication factors. This tendency will be further substantiated with the presentation of the complete test results.

Part of the discrepancy is due to the fact that the first assumption in the development of the theory is not valid for the greater wave lengths. This is shown in Figure 10 where the total vertical mooring line tension component is plotted against wave phase angle for the two tests shown in Figures 8 and 9. The total vertical component is equal to the dynamic vertical plus the net buoyancy. For the test in wave I-2, the total vertical component is approximately equal to the net buoyancy and assumption 1 is valid. For wave I-7, the dynamic vertical component, Fy, is a significant proportion of the net buoyancy and assumption 1 is poor. The physical reason for the difference is twofold. First, a given frequency ratio entails a smaller net buoyancy in wave I-7 than in wave I-2. Second,

the rigidly restrained vertical component is greater for the longer wave which results in a greater value of F_V.

The dynamic vertical mooring line tension component F_V has not been previously analyzed. In the theoretical development it was considered a second order effect. Physically, F_V results from the centrifugal force on the sphere caused by its motion in a circular arc. This force is given by Newton's second law with the mass term written to include the virtual mass effect.

$$F_C = [m + \frac{K\rho\pi D^3}{6}]a_r$$

The term a_r is the radial acceleration.

$$a_r = \dot{\psi}^2 \ell$$

By differentiating equation (38), $\dot{\psi}$ is obtained.

$$\dot{\psi} = -\frac{2\pi}{T}\psi_m \sin(\theta - \phi) = -\dot{\psi}_m \sin(\theta - \phi)$$

Therefore,

$$F_C = [m + \frac{K\rho\pi D^3}{6}]\ \dot{\psi}_m^{\,2}\ \ell \sin^2(\theta - \phi) = F_{Cm} \sin^2(\theta - \phi)$$

In addition to the centrifugal force there is another contribution to F_V. This is seen by considering the case of small sphere motion, i.e., small ψ. In this case the sphere is nearly stationary and the vertical force acting upon it approaches the vertical force component on the stationary sphere F_{V_o}. The dynamic vertical mooring line component is, therefore, taken to be the linear superposition of the centrifugal force and the vertical force component on the stationary sphere.

$$F_V = F_C + F_{V_o} \tag{50}$$

This superposition is shown graphically in Figure 11 for a case where the phase shift angle, ϕ, is 180^o and $F_{Cm} = 2F_{V_{om}}$. The term F_{V_o} in Figure 11 approximates a negative sine wave as shown by equation (21). The resulting theoretical F_V history is non-symmetrical. The positive maximum value exceeds the negative. Curves computed from equation (50) are shown in Figures 8 and 9. The F_{V_o} values used in computing there curves were obtained from the experimental vertical component histories on the stationary sphere. The agreement with experiment is good with respect to curve shape and maximum positive values of F_V.

Force multiplication factors

For each sphere test made in this study, horizontal force multiplication factors were computed from the maximum experimental forces. The multiplication factors for the 0.418 ft. sphere in each test wave are plotted against frequency ratio in Figures 12 through 15. In each of the figures the experimental points define resonance curves of the form of Figure 4. It is important to note, however, that theoretically the

experimental points of a particular test should not fall on a single curve of Figure 4 since these curves are drawn for constant values of the damping factor n_2. For the conditions of the sphere tests the damping factor varies slightly with the frequency ratio.

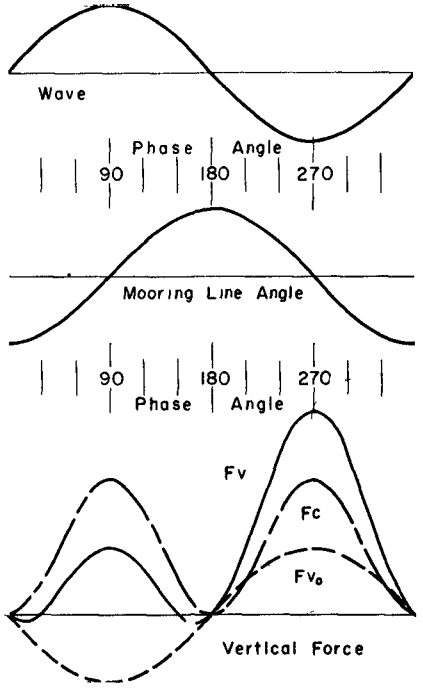

Fig. 11. Dynamic vertical mooring force by superposition.

For each set of experimental data in Figures 12 through 15 a theoretical curve is shown computed from equations (39) and (43). In all computations an inertia coefficient, $C_M = 1.5$ and a drag coefficient, $C_D = 0.42$ were used.

The agreement between theory and experiment is very good for short waves and becomes poorer as the wave length increases. One reason for the discrepancy between theory and experiment in the longer waves (involving the validity of the first assumption made in the development of the theory) has been discussed previously. Another possible cause of error is the value of C_D used in the computation of the theoretical curves. Because of the relatively small drag components encountered in this study it was not possible to determine C_D values from the rigidly restrained test data. The damping factor is shown by equation (43) to be proportional to C_D and the effect of the damping factor on the theoretical force multiplication factor is shown in Figure 4. It is seen that an increased damping factor would bring the theory into better agreement with experiment for the longer waves at frequency ratios less than about 1.4. For higher frequency ratios the damping coefficient has a small effect on the multiplication factor and the discrepancy would still persist. In any event more information would be needed such as would be obtained from a complete determination of the C_D vs. u_mT/D curve before the use of a higher value of C_D could be justified.

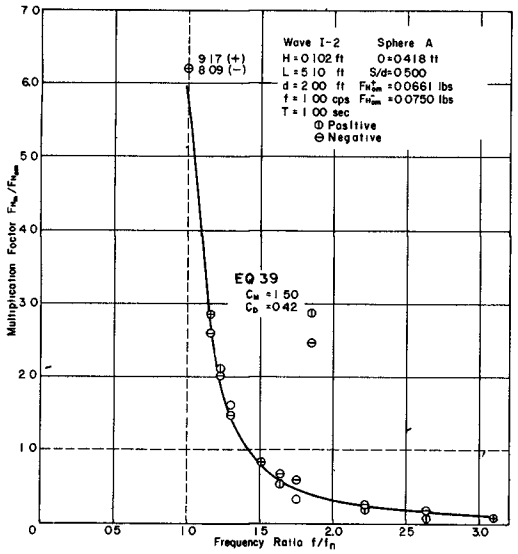

Fig. 12. Variation of horizontal mooring force with frequency ratio (test I-2-A).

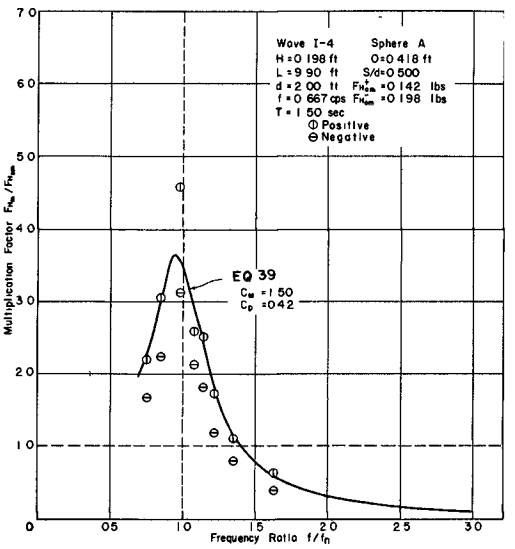

Fig. 13. Variation of horizontal mooring force with frequency ratio (test I-4-A).

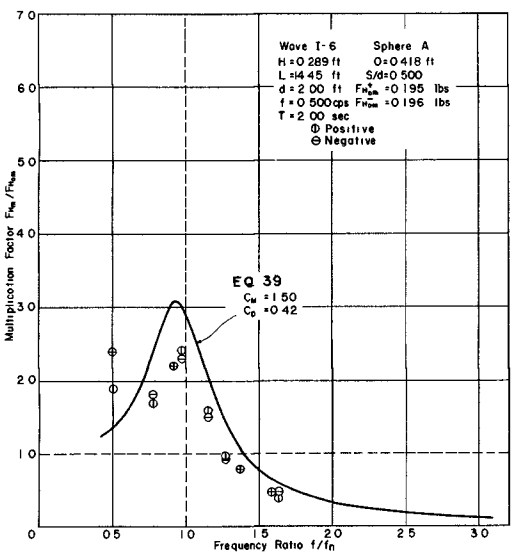

Fig. 14. Variation of horizontal mooring force with frequency ratio (test I-6-A).

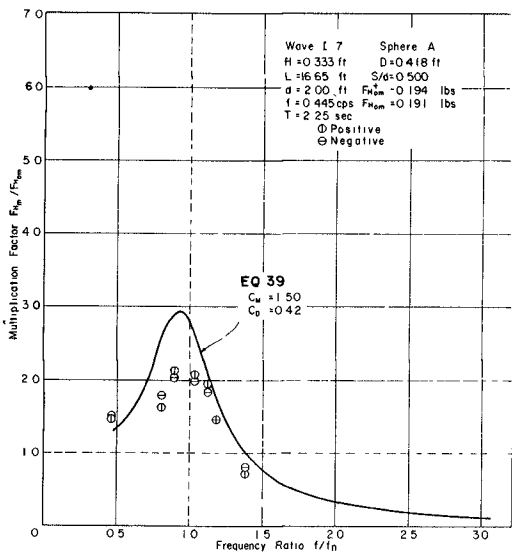

Fig. 15. Variation of horizontal mooring force with frequency ratio (test I-7-A).

Two interesting features are noted in the test results. In Figure 14 the experimental points at $f/f_n = 0.5$ appear high. This is probably due to the fact that the waves have a second harmonic which is neglected in the Airy theory. Therefore, at f/f_n near 0.5, the system resonates with the second harmonic. In Figure 12 another high experimental point is seen; this one at $f/f_n = 1.85$. The phenomenon of a second resonance near $f/f_n = 2$ has been treated in mechanical vibration literature (Den Hartog, 1956) under the name "subharmonic resonance". There it is stated that the phenomenon may occur in a system having non-linear characteristics and that the analysis of the conditions under which subharmonic resonance will occur is extremely difficult. The mechanical system investigated in this study has non-linear damping and restoring force characteristics, the latter being assumed linear in the development of the theory. It is therefore possible that the observed second resonance is an inherent characteristic in the moored object problem. It is also possible that the second resonance could have been caused by reflected waves in the wave tank having a frequency equal to 1/2 the incident wave frequency. Extensive additional study would be necessary for the analysis of the second resonance phenomenon.

CONCLUSIONS

It is concluded that the behavior of moored submerged buoyant objects in oscillatory waves is adequately described by vibration theory with square law damping. The relationships presented herein accurately predict the mooring line tensions and motions of a sphere moored by a single vertical line when the following conditions assumed in the development of these relations obtain:

1) Predominant inertia force.
2) Small dynamic vertical mooring force with respect to net buoyancy.
3) Small maximum mooring line angle.
4) Small amplitude waves.

REFERENCES

Den Hartog, J. P. (1956). Mechanical vibrations, fourth edition: McGraw-Hill Book Co. Inc.

Dronkers, J. J. and Schonfeld, J. C. (1955). Tidal computatoons in shallow water: Proc. A.S.C.E. Sep. No. 714, Hyd. Div., June 1955.

Harleman, D. R. F. and Shapiro, W. C. (1955). Experimental and analytical studies of wave forces on offshore structures, Part I, Results for vertical cylinders: M.I.T. Hydrodynamics Laboratory Technical Report No. 19.

Jacobsen, L. S. (1930). Steady forced vibrations as influenced by damping: Trans. A.S.M.E., Vol. 52, No. APM 52-15.

Keulegan, G. H. and Carpenter, L. H. (1956). Forces on cylinders and plates in an oscillating fluid: National Bureau of Standards Report 4821.

CHAPTER 42

MODEL INVESTIGATIONS OF WIND-WAVE FORCES

J.E. Prins
Delft Hydraulics Laboratory, Netherlands.

OBJECT OF THE INVESTIGATIONS

The load caused by wave attack had to be determined in connection with the design of a steel structure located adjaoent to the open sea. This load had to be expressed in such a way that the designer:-

a) Could base the dimensioning of his structure on a consideration of the probability of failure
b) Would have at his disposal data from which could be derived the number of stress alternations together with the distribution of their amplitudes during the lifetime of the structure.

The data required for this is:-

1) The probability of occurrence of significant waves of any given magnitude
2) The load spectra associated with the wave spectra of significant waves of any given magnitude.

With regard to 1) a prognosis was made by the "Rijkswaterstaat" from wave records and meteorological conditions at the prototype location.* The load spectra were evaluated in the laboratory "de Voorst" by exposing a small scale model to wind generated waves.

In the following, a review is given of the preliminary studies made to compare the wave characteristics in model and prototype, the investigation of wave form and the forces exerted on the structure, and the representation of the final results.

PRELIMINARY STUDY OF THE WAVE CHARACTERISTICS

The investigations have been carried out in a wind-flume having a length of 100 m, a width of 4 m and a height from bottom to ceiling of 2 m. The maximum waterdepth can be 0.75 m and the maximum wind velocity 12 m/sec. At the end of the flume a wave absorber is available.

From consideration of the prototype dimensions the scale for the model was chosen to be 40. This yielded a water depth in the wind-flume of 0.625 m for which the wave characteristics were of interest. In addition some of the characteristics were also observed for a depth of 0.25 m.

The waves were generated by wind, by a mechanical wave generator or by the combination of the two. The wave absorber was used.

Wave heights were recorded continuously. Irregular waves were characterized by the significant wave height (H_{sign}) which was deduced from a series of 200 waves. The regular waves (i.e. the mechani-

* This subject is covered in Venis (1960).

cally generated waves) were characterized by the average value of the smallest and largest wave height within half a wave length (H_{swell}). The accuracy of the wave heights for this study are

H_{sign}	10%*
H_{swell}	6%

WIND-GENERATED WAVES

To relate the growth of the wave to the fetch (F) and wind velocity (W_z), the wave height was measured at every 15 m along the flume (figure 1 and 2). From the wave recordings at a fetch of 90 m, wave height distribution curves were made (figure 3 and 4). This data was compared with prototype curves (Table 1) and agreed quite well, taking account of the scatter in the prototype curves themselves (Paape 1960, figure 3). The model results in general show a tendency to flatten the slope of the curve at high wind velocities. The average period ($\bar{T}$) was determined and related to the fetch (figure 5).

To verify whether the variables involved in the phenomenon are reproducable to scale, the data of the model was expressed in the dimensionless quantities:

$$g \bar{T} / 2 \pi W_o \text{ , } g H_{sign} / W_o^2 \text{ and } gr / W_o^2$$

which are plotted against $g F / W_o^2$ (figure 6).

The wind velocity W_z, measured at height z (in the flume 0.25 m), is reduced to W_o at height z_o according to $W_o^2 / g z_o = 5.2$

The measuring points of $g H_{sign} / W_o^2$ vs $g F / W_o^2$ show a reasonable consistency and the scatter is less than that of prototype data. A comparison has been made with the graphs of Bretschneider (1958) and Thijsse (1948) by superimposing their curves (unfortunately the region concerned is mainly based on model data).

From the overall impression it could be decided that, since the dimensionless parameters $g F / W_o^2$ and $g H_{sign} / W_o^2$ are linear in fetch and wave height and quadratic in wind velocity, the Froude law was applicable.

Some values of $g \bar{T} / 2 \pi W_o$ were also calculated and compared with the graph $g \bar{T} / 2 \pi W_o$ vs $g F / W_o^2$ of Bretschneider (1958). The model shows a 15% too high value of the period for these points (figure 6). The same points were expressed in terms of $g r / W_o^2$, in which $r = L / 2\pi$ (L is the wave length), and compared with the Thijsse graph $g r / W_o^2$ vs $g F / W_o^2$. The curve was not fitted too well (figure 6).

Wind velocity distributions in the vertical were also measured (figure 7) and compared with the prototype data from Abbotts Lagoon given by Johnson (1950). Figure 8 shows a logarithmical plot of this. The curve obtained for a water depth 0.625 m shows a deviation from that for a depth of 0.25 m. The agreement with the distribution of the data of Abbotts Lagoon is good.

---

* H_{sign} deduced from 500 waves: accuracy 5%
1000 waves: 2%.

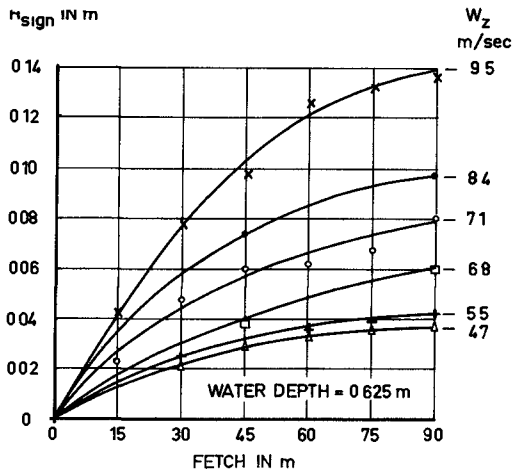

Fig. 1. Significant wave height as a function of fetch and wind velocity at water depth 0.625 m.

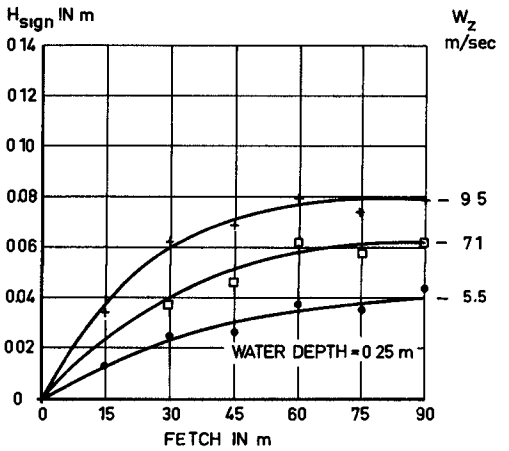

Fig. 2. Significant wave height as a function of fetch and wind velocity at water depth 0.25 m.

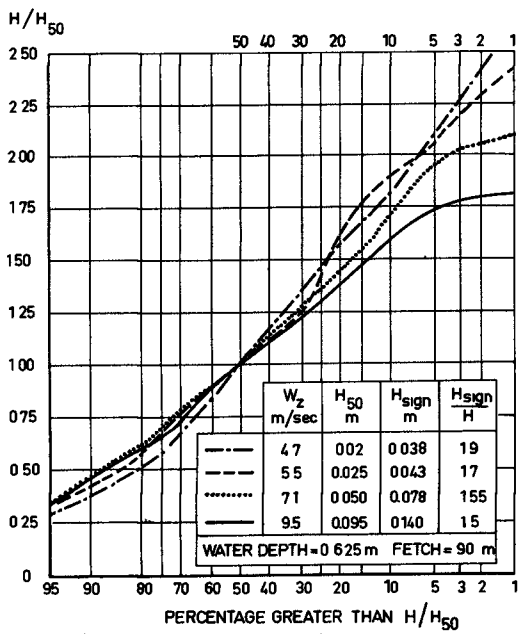

Fig. 3. Wave height distribution curves at fetch 90 m and water depth 0.625 m.

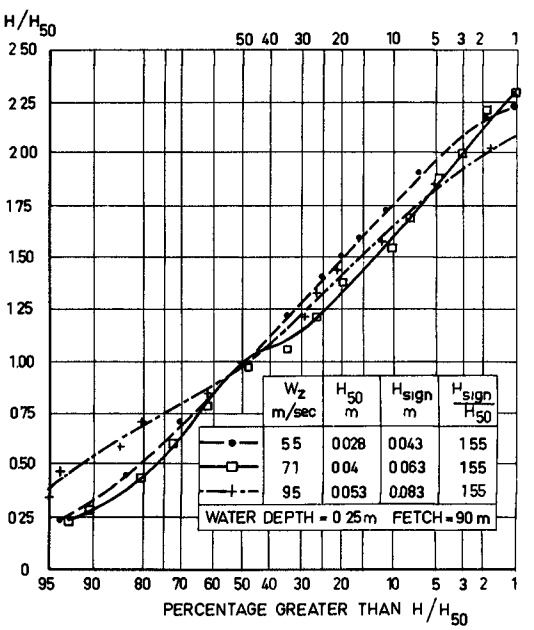

Fig. 4. Wave height distribution curves at fetch 90 m and water depth 0.25 m.

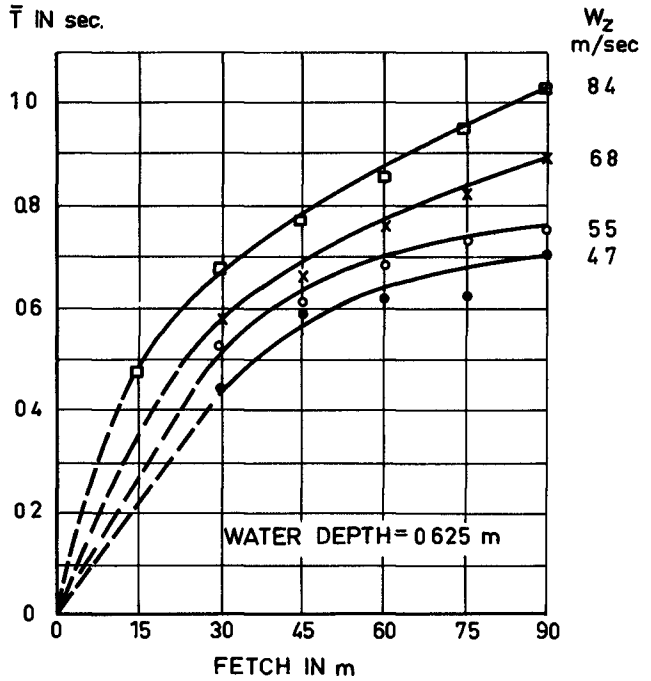

Fig. 5. Average wave period as a function of fetch and wind velocity at water depth 0.625 m.

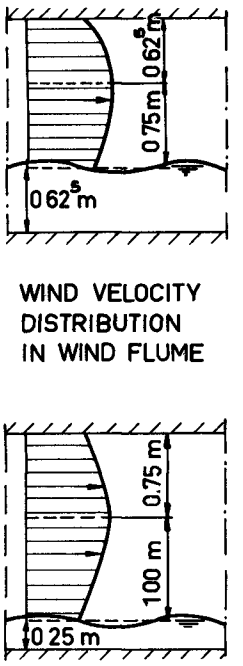

Fig. 7. Wind velocity distribution in windflume at water depth 0.625 m and 0.25 m.

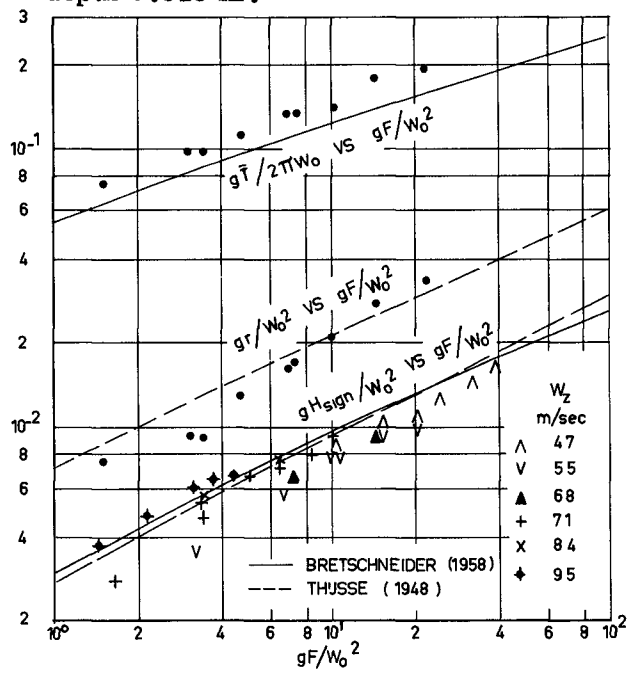

Fig. 6. Relationship between the dimensionless parameters and comparison with curves of Bretschneider and Thijsse at water depth 0.625 m.

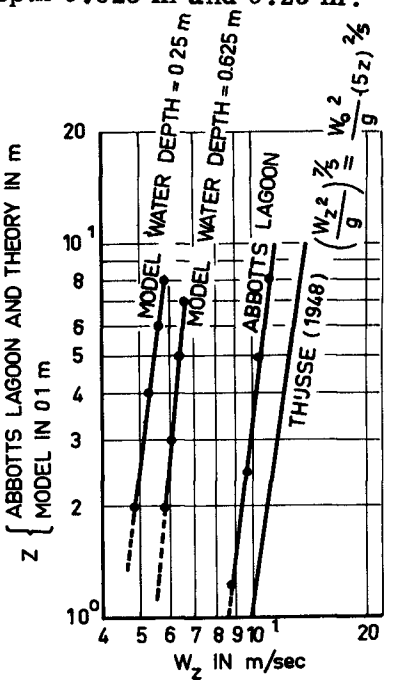

Fig. 8. Comparison of wind velocity distribution curves from model and nature.

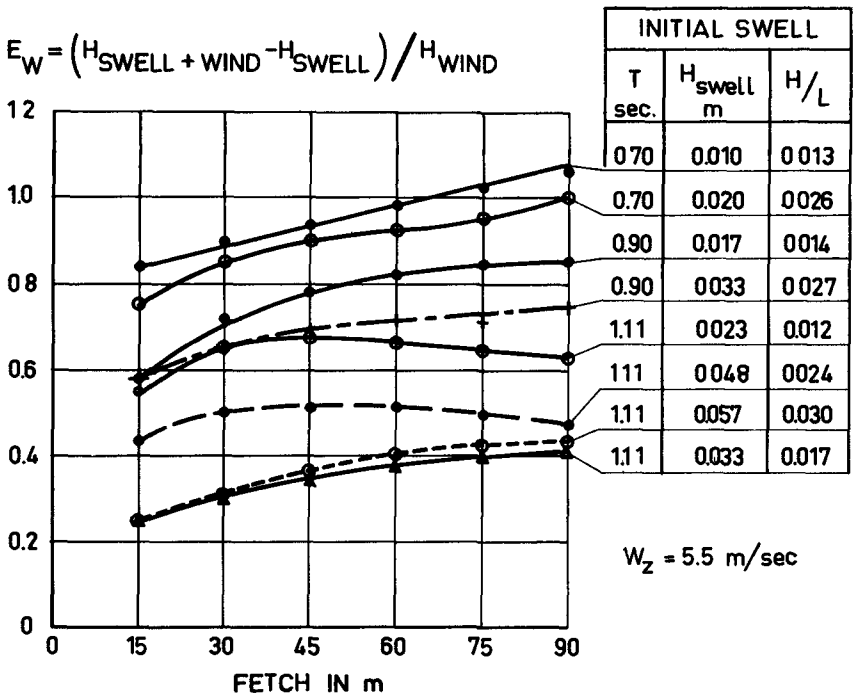

INITIAL SWELL		
T sec.	H_{swell} m	$H/_L$
0.70	0.010	0.013
0.70	0.020	0.026
0.90	0.017	0.014
0.90	0.033	0.027
1.11	0.023	0.012
1.11	0.048	0.024
1.11	0.057	0.030
1.11	0.033	0.017

Fig. 9. Wind effect on an initial swell of a wind with a velocity of 5.5 m/sec.

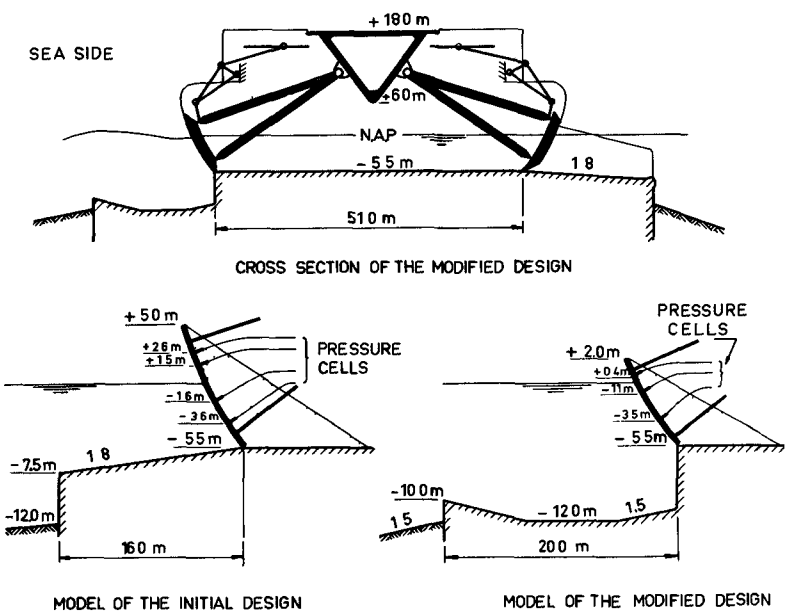

Fig. 10. Cross section of the Haringvliet sluice. Models of original and modified designs. (Prototype dimensions).

MODEL INVESTIGATIONS OF WIND-WAVE FORCES

WIND-STRENGTHENED SWELL.

This study of wave forces required a knowledge of the influence of the wind velocity on an initial swell in the same direction. For this purpose a series of investigations were carried out with a constant wind velocity of 5.5 m/sec on a variable swell of small steepness.

Every 15 m in the flume the significant wave height was determined.

For characterizing the effect of the wind the quantity E_w was introduced and expressed as follows:

$$E_w = (H_{swell + wind} - H_{swell}) / H_{wind}.$$

The parameter E_w is the ratio of the growth of swell due to the wind and the growth of a pure wind-generated wave.

In figure 9 for some periods and wave heights the ratios deduced from adjusted curves, at equal intervals along the flume are given. Although the accuracy of these points is not very great the results show a tendency for longer periods to be less affected by the wind than shorter ones. The results did not show a systematic relationship with respect to the wave height.

Tabel 1 resumes some of the data on the wave height distribution.

As the forces were found to be the most severe for pure wind-generated waves this study was discontinued.

STUDY OF THE WAVE FORCES

This investigation was carried out in the windflume described above. The model of the structure (a gate of the Haringvliet sluice) was built to a scale 40. As the study progressed it proved to be necessary to modify the original design. In figure 10 the cross section of the modified design is given. The preliminary studies described hereafter were made for the original design. The outline of this model is also given in figure 10.

Experiments showed that some of the waves approaching the structure may be reflected smoothly, while others strike against it. The pressures due to the reflection or the impact are measured by pressure cells*. By calibrating those instruments the pressure is expressed as a height of water. If it is assumed that Froude law is valid for these phenomena, then the pressure for the prototype can be expressed in ton/m^2.

Studies of the mechanism of wave impact and of the wave conditions causing them were made.

PRELIMINARY STUDIES

Extent of the impact forces - In the model of the original design it was found that the impact forces occurred simultaneously over the vertical. Examples are given in figure 11.

* The resonance frequency of these pick-ups had to be high because of the fast pressure rise of the impacts. In submerged condition it amounted 1400 Hz. The shortest time of pressure rise measured in the model was 1/600 sec, which equals 1/100 sec in prototype.

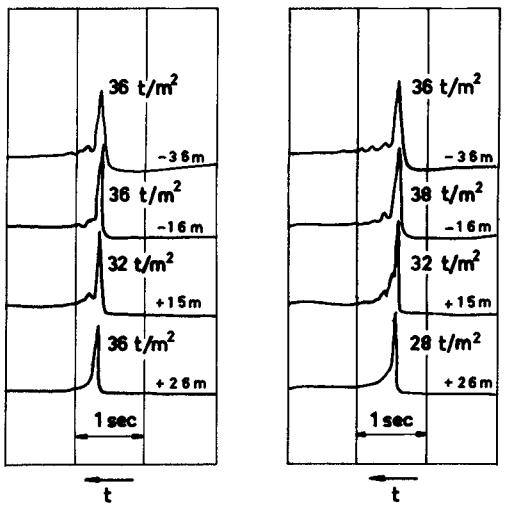

WIND STRENGTHENED SWELL
GATE HEIGHT : NAP+45m
WATER LEVEL: NAP
H_{sign} = 3.4 m
$\bar{T}$ = 50 sec
W_{10} = 30 m/sec

Fig. 11. Records of impact forces in a vertical (original design. Prototype quantities).

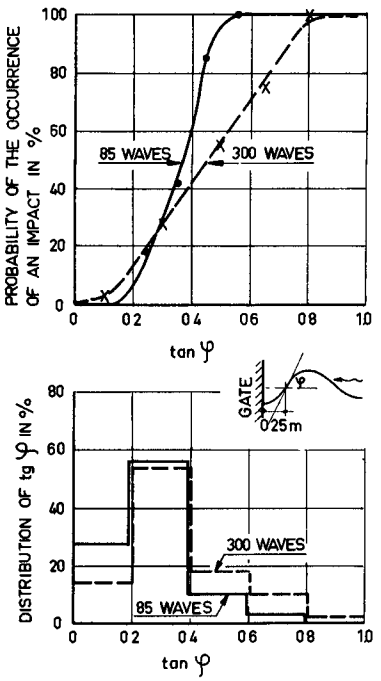

Fig. 12. Relationship between tan ϕ an probability of the occurrence of an imp

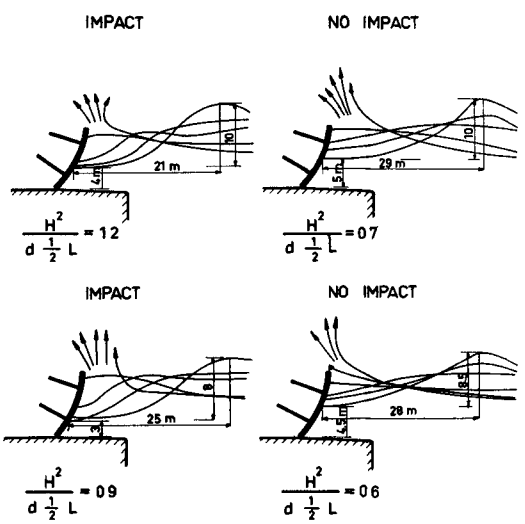

H = WAVE HEIGHT
L = WAVE LENGHT
d = WATER DEPTH IN WAVE TROUGH
TIME INTERVAL BETWEEN THE LINES IS 0.4 sec

Fig. 13. Impact related to wave form (Prototype quantities).

Table 1

	initial swell		wind	wind gen. wave wind etr. ewell			spectrum			
Location	$\overline{T}$ sec.	Hswell m	m/eec.	$\overline{T}$ sec.	Hsign m	Ew	H_{50} m	H_2/H_{50}	H_{10}/H_{50}	H_{20}/H_{50}
Haringvliet wave recorder C.	-	-	20 20 18	-	-	-	0.4 0.5 0.5	2.4 2.2 2.2	1.9 1.8 1.7	1.6 1.5 1.5
North Sea wave recorder Katwijk	-	-	-	-	-	-	1.9 1.7 1.5 1.2	1.9 1.9 1.9 2.1	1.6 1.5 1.6 1.7	1.4 1.4 1.4 1.4
wind flume water depth 0.625 m. Fetch 90 m.	- - -	- - -	5.5 7.1 9.5	0.74 0.89 1.11	0.043 0.078 0.140	- - -	0.025 0.050 0.095	2.3 2.1 1.8	1.9 1.7 1.6	1.6 1.4 1.4
	0.70	0.010	5.5	0.82	0.058	1.12	0.038	1.9	1.6	1.4
	0.79	0.028	5.5	0.95	0.067	0.94	0.045	1.9	1.7	1.4
	0.90	0.033	5.5	0.97	0.065	0.77	0.040	2.2	1.8	1.4
	0.90	0.048	5.5	1.01	0.095	1.06	0.065	1.9	1.7	1.4
	1.11	0.033	5.5	1.11	0.050	0.41	0.045	1.3	1.2	1.2
	1.11	0.055	5.5	1.11	0.092	0.88	0.085	1.2	1.2	1.1
wind flume water depth 0.25 m. Fetch 90 m.	- - -	- - -	5.5 7.1 9.5	0.71 0.92 1.03	0.043 0.063 0.080	- - -	0.025 0.043 0.050	2.2 2.1 2.1	1.8 1.7 1.7	1.5 1.4 1.5

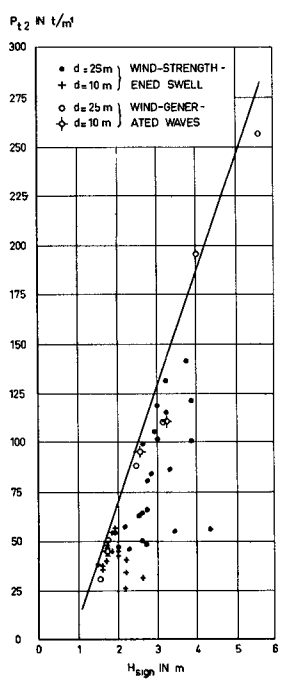

Fig. 14. Load as a function of wave height (Prototype quantities).

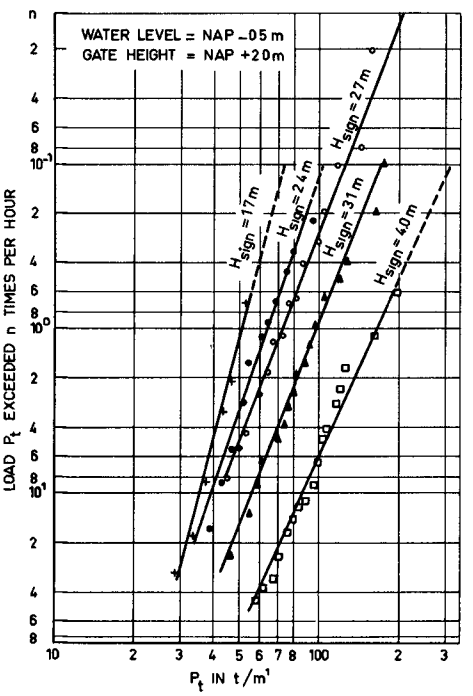

Fig. 15. Frequency curves of the load, associated with significant wave heights (Prototype quantities).

The extent in the width depends on the length of the wave crest and its straightness. In the model for wind-strengthened swell and for wind-generated waves, with wave lengths from 35 to 55 m in prototype, in no case was there found an equally high impact pressure over the full width of the gate (length 58.5 m). From nature no data are available.

Air content of the water - As it was thought that the air content of the water could possibly influence the results, an increase of the air in the water was made artificially.

Records of the pressure history for the conditions of the normal and the high air content did not show a marked difference. This eliminates within a certain range the difficulty of the correct reproduction of the compressibility, due to bubbles in the water, in the model.

Rigidity of the structure - In the first stage of the investigations the measurements of the impacts were carried out in a rigid model representing the structure. To verify whether a receding movement of the structure under influence of the load had a reducing effect on the impact, the model was provided with gates allowing a bending of several decimeters in prototype. In those gates the pressure pick-ups were mounted. The wave impact forces were still measured but the pressure history became more irrigular.

For one gate also the pressure at the inner side was measured. The impact at the outer side was hardly noticable at the inner side and it may be concluded that the water at the inner side does not react noticeably in taking up some of the impact.

Form of the wave - The first measurements did not show a clear correlation between the magnitude of the wave impact pressure and the wave height. When the waves are generated mechanically a clapotis is formed due to the obstruction of the model and no impact phenomenon is observed. When wind is added to the mechanical wave generation, and foaming crests come into being, impacts occur. The deformation of the wave by the wind appeared to be of essential importance. To correlate the wave form and the wave impact pressures, the record of a wave height meter located 0.25 m in front of the model was compared with simultaneously recorded pressures on the structure.

As a criterion the tangent ($\tan \varphi$) to the angle (φ) between the horizontal and the tangent to the surface at the point of inflection on the front face of the wave was used. A frequency distribution of $\tan \varphi$ was made and the probability of the occurrence of an impact was determined (figure 12). This figure shows clearly that the probability of the occurrence of an impact increases strongly with the increase of $\tan \varphi$.

No direct relationship between the magnitude of $\tan \varphi$ and the impact pressure was found.

By taking a moving picture, on which the water movement in front of the model was filmed simultaneously with an oscillograph showing the pressures exerted, a relationship could be established for this special case in which the wave height, the wave steepness, and the water depth at the trough of the wave preceeding the impact were in-

corporated (figure 13).

It was found that, when $H^2/l\ d$ exceeded a certain value a wave impact occurred. There was no direct relationship between this number and the magnitude of the impact pressure.

Impulse measurements - The impact forces can be deduced from the impulse - momentum equation,

$$P.dt = d\ (m\ v).$$

The model investigation showed that the original design gave rise to very high wave impact forces (P) because of:

1) High velocity v: the unstable waves of a wave train tend to break on the shallow sill in front of the gate, causing water velocity to approach the propagation velocity of the wave.
2) Large mass m: the inclined overhanging position of the gate tends to maximise the mass of water which is effective in causing impact.
3) Small interval dt: the form and orientation of the front face of an approaching wave can be such that it becomes sensibly parallel to the surface of the gate so that the full impact occurs within a very short interval.

In order to overcome these difficulties the design was modified as shown in figure 10. From further measurements it appeared that for this new arrangement impact forces due to the instability of some of the waves of a wave train still occurred.

The quantity $\int P\ dt$ during pressure rise and during the total impact was measured at three places in a vertical line on the gate front. The pressure record of the impact was divided into its dynamic and static parts.

Some typical data (in prototype quantities) from a series of 2740 waves with 174 impacts are presented in the following table.

H_{swell} = 1.0 m T_{swell} = 5.0 m Water level NAP - 0.5 m	W_{10} = 36 m/sec F = 3600 m	H_{sign} = 3.0 m T_{sign} = 5.0 sec	
measuring point	at NAP 0.4 m	at NAP - 3.5 m	unit
duration of pressure rise	0.1-0.3	0.8-1.2	sec
duration of impact	0.8-1.1	1.8-2.3	sec
$\int P\ dt$ during pressure rise	0.4-1.6	3-5	t sec/m^2
$\int P\ dt$ during impact	2-4	7-11	t sec/m^2
max. dynamic pressure	19.8	12.0	t/m^2
max. impact pressure	21.2	16.1	t/m^2

DETERMINATION OF THE LOAD

These investigations were carried out in a rigid model representing the modified design according to figure 10. In the model three pressure cells were mounted in a vertical line.

The forces exerted by the waves on the structure were recorded as the arithmetic averages of the signals of the three pressure pick-

ups. By applying Froude law and multiplying by the height of the gate, the load for the structure per m' (P_t) was obtained from the record. It was expressed in ton/m'.

Mutual comparison of the varied conditions was made by deriving the load (P_{t2}) from the maximum value of the averaged pressure of a record taken over a length of time of two hours in prototype (approximately 1200 waves).

Load due to swell - The mechanically generated waves experienced a smooth total reflection. No impact forces occurred.

Load due to the wind-generated waves - For this condition impact forces occurred. The load P_{t2} was plotted as a function of the significant wave height* (figure 14). It showed a linear relationship.

In addition to this there have been experiments with gusts of wind. It proved that a gust quickly creates a wave form causing impact pressures. In this respect the initial wind velocity on which the gust is superimposed and the duration of the gust are of importance. The study was not continued, due to lack of prototype data.

Load due to wind-strengthened swell - For this investigation the wind velocity was 35 m/sec and the initial swell was varied from 4 to 10 seconds, with wave heights from 0.4 to 3.0 m. The fetch was 3600 m.

For these conditions also, the load was plotted in figure 14. A direct relationship was not found. It is clear that the significant height in itself is no measure for the force exerted. As was stated before the wave form is very important. When in figure 14 an upper envelope is drawn it shows that the most dangerous combination of swell and wind does not exceed the forces exerted by waves generated by wind alone. It may be concluded from this that the steepest wave fronts or the largest steepness appears to occur with wind generated waves.

Not much is known of the wave form in nature. For this reason the final study has been carried out with wind generated waves only, yielding the most severe conditions.

PRESENTATION OF THE RESULTS

For the design of the structure, based on the probability of failure, the expectation of any load had to be determined.

For this purpose a series of statistical distributions of forces was made, each distribution applying to one value of the significant wave height. The wave conditions were those generated by pure wind, which was found to represent the most unfavorable state. Also the water level in front of the gate was varied and the effect of the height of the gate was included in the investigation.

* Wave heights are related to measurements with a wave absorber in the flume.

Figure 15 shows the frequency curves of the load at several significant wave heights. Any significant wave height by itself is also associated with a certain frequency of occurrence. The combination of the two yields the probability of occurrence of each load as required by the designer.

Although a physical limit to the phenomenon may be expected it cannot be logically deduced. From a measurement of duration of 40 hours (prototype) linear extrapolation proved to be still possible.

ACKNOWLEDGMENT

The data given above forms part of a study included in the reports "Golfaanval Haringvlietsluizen", Volume I and II, March 1960, which were compiled by M.A. Aartsen, a former engineer of the Delft Hydraulics Laboratory. The work was carried out at the "de Voorst" Laboratory, by order of R.W.S., and was under the guidance of Mr. Aartsen.

REFERENCES

Thijsse, J.Th. (1948) Dimensions of wind-generated waves, U.G.G.I. Assembly Oslo 1948, Comm. F 3.

Johnson, J.W. (1950) Relationship between wind and waves - Abbotts Lagoon California, Trans. A.G.U. Vol. 31, 1950. pp. 386-392.

Bretschneider, C.L. (1958) Revisions in wave forecasting: Deep and shallow water, Proc. of sixth Conf. on Coast. Eng., Council on Wave Res., 1958, pp. 30-67.

Paape, A. (1960) Experimental data on the overtopping of seawalls by waves, Proc. of seventh Conf. on Coast. Eng., Council on Wave Res., 1960.

Venis, W.A. (1960) Determination of wave attack anticipated upon a construction by combining laboratory and field observations, Proc. of seventh Conf. on Coast. Eng., Council on Wave Res., 1960.

CHAPTER 43

MODEL STUDY OF AN ISOLATED LIGHTHOUSE PLATFORM AT SEA (PRINCE SHOAL, QUEBEC)

G. E. Jarlan
Engineer, Hydraulics Laboratory
National Research Council of Canada

THEORETICAL CONSIDERATIONS

Experiments on objects subject to wave forces have been made in the past, which led to formulae where the geometrical characteristics of the object are of primary importance. Other experiments, made on immersed objects, showed that the accelerative forces caused by wave impact are of the same order of magnitude as the drag forces associated with orbital velocities. In the case of a small free body completely immersed in a fluid and subject to a system of forces, other experiments showed that the fluid surrounding the body acquires a velocity while the flow field gains kinetic energy (Ref. 1). The acceleration of the object can be deduced from the pressure distribution around the body. For small objects, the integrated form of the dynamical equation is:

$$F = M \frac{\partial u}{\partial t} \qquad (1)$$

where M = mass of fluid displaced by the object

$\frac{\partial u}{\partial t}$ = acceleration normal to the object.

Since viscous friction is present, the notion of drag force expressed by the following relation must be used.

$$F_D = C_D A \rho \frac{u^2}{2} \qquad (2)$$

where A = projected area of object

C_D = drag coefficient

ρ = specific weight of water

u = horizontal component of velocity.

A combination of equations (1) and (2) yields the total force acting on the immersed free body, assuming the object has very small dimensions.

In the case of a cylindrical pile anchored to the bottom or

protruding beyond the free surface and subject to wave fronts, Morison et al (Ref. 1) have shown that the tangential component of the force per unit length of cylinder can be expressed by:

$$f_x = C_D \cdot \frac{\rho}{2g} \cdot D \cdot V_x^2 + C_m \cdot \frac{\rho}{g} \cdot \frac{D^2}{4} a_x \qquad (3)$$

where C_D and C_m are respectively the drag and virtual mass coefficients,

ρ = specific weight of water

D = diameter of the pile

v_x and a_x are the horizontal components of velocity and acceleration

C_D and C_m appear to be functions of the Reynolds number at the pile, hence they depend also on v_x.

According to equation (3) the value of f_x varies as the second power of D. However, this formula makes obscure the concept of energy dissipation by wave scattering. This phenomenon plays an important role in the process of energy dissipation since it is a function of the relative size of the obstacle with respect to the characteristics of the perturbation.

An interesting demonstration of this fact is given by Rayleigh (Ref. 2). A cylindrical obstacle is subject to the disturbance created by plane waves. Let ϕ and represent respectively the velocity potential of the incident and scattered waves; the plane waves can be represented by

$\phi = e^{ikat} \cdot e^{ikr}$ (for normal incidence).

Dropping e^{ikat} for sake of brevity, ϕ can hence be expressed as a series of Bessel functions of the form:

$$e^{ikr} = J_0(kr) + 2iJ(kr) + \ldots + 2i^n J(kr)$$

or $$\varphi = 1 - \frac{k^2\rho^2}{4} + ikr$$

where r is the radius of the cylinder.

If it is assumed that the obstacle is composed of an isotropic

material, the velocity potential, under normal incidence, of the scattered waves for a rigid and immovable obstacle is:

$$\Psi = -\frac{2\pi}{r^{1/2}} \cdot \frac{\pi r^2}{\lambda^{3/2}} \cdot \cos\left(\frac{2\pi r}{\lambda} + \frac{\pi}{4}\right)$$

with r = radius of the obstacle, λ = wave length of the incident wave.

It is seen that the intensity of the scattered waves will be a function of the diameter of the obstacle relative to the wave-length of the perturbation. This explains why fog, which consists of spherical particles of condensed water vapour, lets sound waves pass through it, while light, the wave-length of which is small compared with the dimensions of the particles, will be rapidly scattered. Thus dispersion will take place instead of propagation.

Among N vertical obstacles of similar size but of different shape, subject to wave action, experience shows that a straight and regular cylindrical structure should produce a minimum scattering of waves. However, when an isolated structure is built at a fairly great depth, it is necessary to take into account the stability factor of the structure and its resistance to waves. Usually, a structure isolated at sea will be anchored on a mattress with dowels. Such a structure will then act as a vertical circular beam fixed at one extremity and subject to a system of forces, the resultant of which is horizontal. The kinetic energy developed by the force will then be absorbed by bending so that if R is the reaction to the force, one must have

$$\frac{1}{2} m v^2 = \frac{R}{2} \cdot a$$

where a = bending deflection

m = mass of water of velocity v .

The term a is a function of Young's modulus and of the beam length ℓ. Although perhaps an ideal structure would consist of a cylinder of relatively small diameter with respect to the wave length, it will be realized that such a structure would offer in large depths rather precarious stability conditions because it would offer a small section modulus.

A pyramidal or conical shape, which allows the centre of gravity to be placed low enough, appears for this reason to be preferable. Under these conditions, a well-anchored structure will resist wave action better Since a pyramidal structure offers more scattering than a cylindrical one of similar size, the wave run-up and resistance to shear due to drifting ice appear to remain the major problems to solve.

MODEL STUDY

The model study of a pier of conical shape to be used as the base of a lighthouse (at Prince Shoal, Quebec) was carried out for the Department of Transport, Ottawa, to observe wave run-up conditions over the square

platform (Fig. 1). The depth at low tide was 25 ft., the total height of the pier being 65 ft. The structure had been calculated to offer satisfactory safety coefficient against shear.

Waves were generated in a wave canal; the wave data available indicating a maximum observed wave height of 16 ft., the periods varying between 5 and 11 seconds. At high tide (+ 15 ft.), the tests showed that the amount of scattering observed for all periods was fairly high, the wave run-up caused by the folding front breaking at the structure, sometimes reaching 20 ft. above the square platform.

Upon completion of the test series, it was decided that the proposed shape was inadequate on the basis of wave run-up considerations. A diamond shape pier was an improvement, but was still not satisfactory.

The problem was then approached from the following viewpoint.

Since a full cylindrical shape could not be retained, it was necessary to decrease the wave run-up to dissipate as much as possible by some means the energy present in the wave run-up. To initiate this dissipation of energy, the principle of the flat slope could be retained provided that the structural qualities of the structure would not be impaired. The flat slope would create an instability of the wave front, thereby causing a partial collapse of the wave front before it impinged on the underside of the platform.

A final shape was arrived at (Fig. 2), and tests were run following the same procedure as for previous tests. It was observed (at high tide) that:

1. The pertrubation created by the presence of the flat slope increased the internal turbulence of the wave before it reached the cylindrical wall situated beneath the platform.

2. Part of the wave broke afterward at the cylindrical wall.

3. The remaining energy was such that an intense vortex circulation appeared around the cylinder and diffused into a wake in the shadow of the structure.

4. The energy reflected by the cylindrical wall was well checked by the curved part of the platform and a sheet of water was observed, which was perfectly reflected in the opposite direction to the incident wave.

A tentative explanation of the energy dissipation can be given as follows: At high tide, and for the high cambered waves, the partial or complete breaking of the wave at or near the cylindrical wall creates an increase of the kinetic energy and an accelerative motion of the water. Since the cylindrical part is of a much smaller diameter than the base itself, it offers less scattering, allowing thereby relatively more energy to circulate around it than if the section were unchanged. There is, consequently, less energy per unit wave front reflected by the cylindrical base, and hence less energy available for the run-up.

The study of the motion around the obstacle, which is a solid of continuous curvature, is fairly complicated. For laminar conditions, the boundary layer starting from the stagnation point follows the surface for some distance, becomes turbulent, and then breaks away from the structure. For turbulent flow (in this case, this flow is also still partially oscillatory) it becomes more difficult to study the problem and only a check on the pressure distribution could yield some ideas about the circulation pattern obtained. It was also observed that the dispersion in the wake was very intense and rapid, but that the oscillatory character of the wave reappeared very quickly as the wave travelled away from the structure.

At low tide, the wave run-up appeared noticeably reduced and did not seem to constitute any problem. The scattering is then entirely controlled by the base of the structure while the upper part of the wave front is partially dissipated by turbulent shear flow induced by the breaking wave along the flat slope.

REMARKS

The possibility of impulse pressures developing at the cylindrical wall, due to the breaking of the waves, does not constitute any danger since the peak pressures occur over a small area and for a very short time. They cannot seriously affect a monolithic structure and the possibility of resonance phenomena developing, due to elastic waves induced at the time of the breaking, appears remote in view of the large mass offered by the obstacle to the wave. This question would, however, require a special study using a special model on which impulse pressures could be mechanically applied, the vibration being recorded with sensitive elements similar to strain-gauges.

Flat sides were adopted to allow ships to lie alongside the structure. These flat sides should be oriented in the direction of the highest waves. It is felt that under such conditions the probability of an important clapotis along these sides appears very remote since waves do not have the necessary fetches in which to grow. These sides provide facilities for shipping and will be useful in improving mooring conditions. It is realized that with a circulation inducing a current around a circular structure, a ship which would be tangent to the structure at one point would tend to oscillate and slide around it. These conditions are, hence, not favourable from the point of view of docking and mooring alongside.

ICE CONDITIONS

The cylindrical part of the structure below the platform was calculated to resist a shear force of 400 p.s.i. created by drifting ice. The calculation of resistance to shear was found sufficient. It is thought that the adopted slopes should facilitate the natural removal of the ice depositing at low tide. The buoyancy of the rising water would be sufficient to float the masses of ice and break them from the structure. Tidal currents would afterward cause the ice to drift away from the structure.

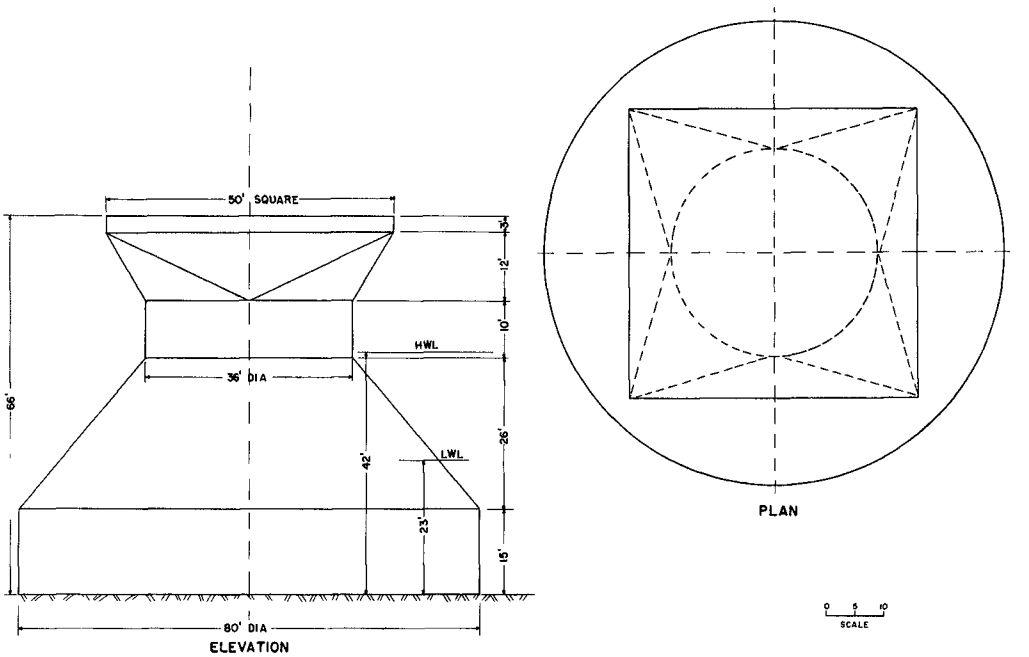

OUTLINE OF PROPOSED LIGHTHOUSE PIER FOR PRINCE SHOAL

Fig. 1

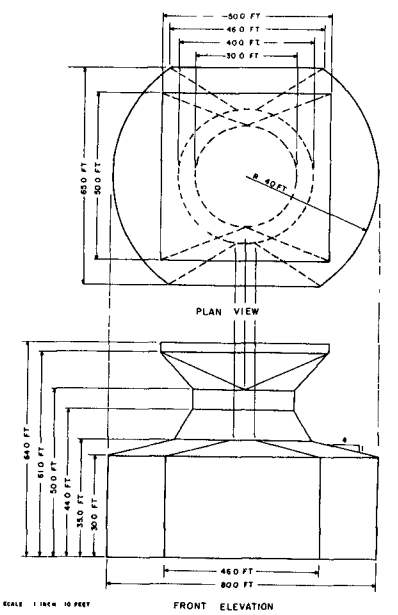

PRINCE SHOAL LIGHTHOUSE PIER
AS RECOMMENDED BY NRC HYDRAULICS LABORATORY

Fig. 2

TOWING CONDITIONS OF THE BALLASTED SHELL

The towing properties of the shell were studied in the towing tank of the Ship Laboratory, on a model of 1/30 scale. The lateral stability of the vessel was found excellent. A yawing motion was observed on either side of the centre line with a total amplitude never greater than 100 ft. A ballast equivalent to about 2400 tons was used yielding a corresponding draught of 24 ft. The best speed from the point of view of lateral stability and yaw was found to be 4.9 knots.

BIBLIOGRAPHY

1. Morison, J.R., O'Brien, M.P., Johnson, J.W. and Schaaf, S.A. "The Force Exerted by Surface Waves on Piles". J. Petroleum Technology, Vol. 2, No. 5, May 1950. (Trans.), p. 149 - 54.

2. Rayleigh, J.W.S., baron; "The Theory of Sound". Dover, N.Y. 2nd edit. 1945.

Walcheren Sea Wall

Part 5

COASTAL ENGINEERING PROBLEMS

Schouwen Island Dunes

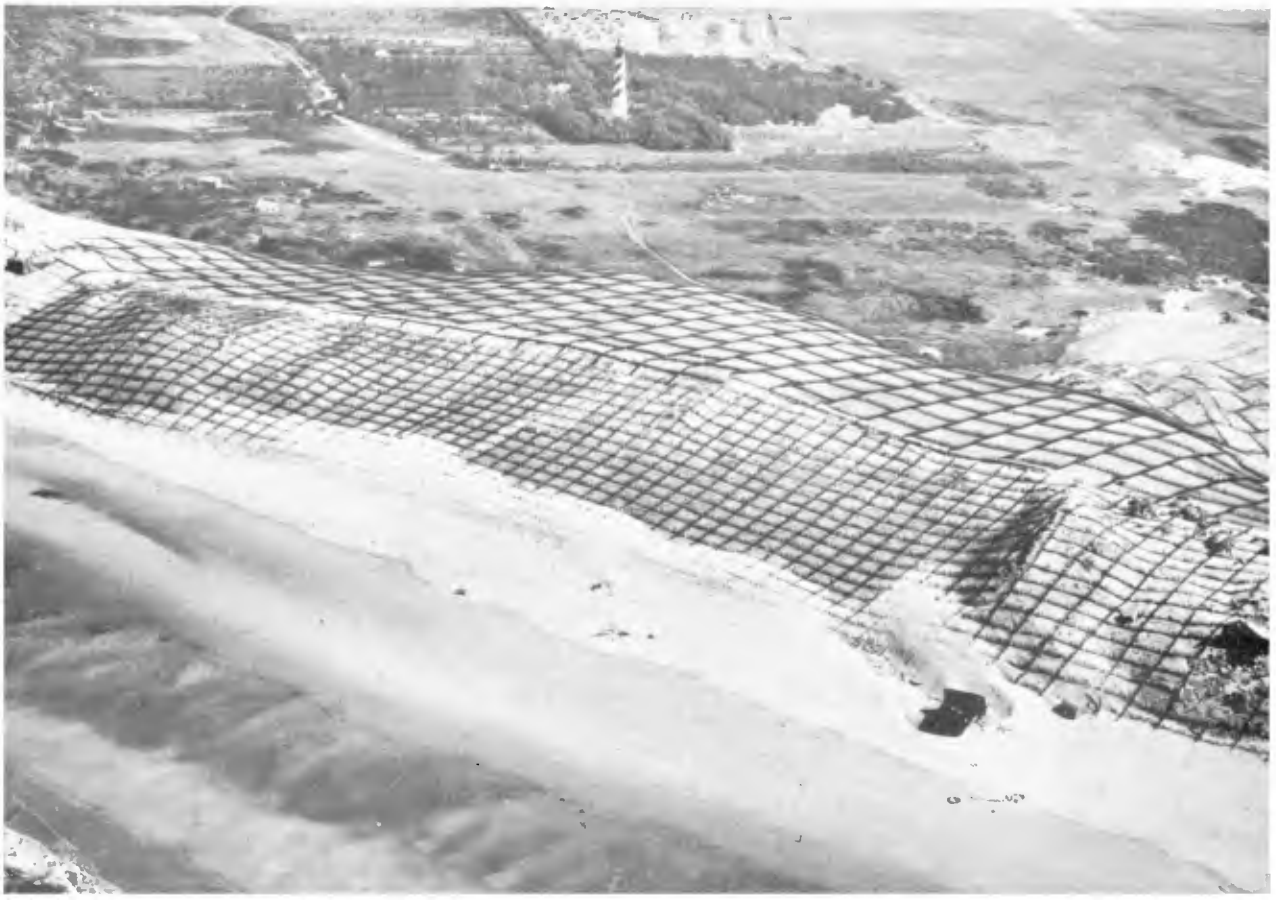

COASTAL ENGINEERING

CHAPTER 44

SAND TRANSFER, BEACH CONTROL, AND INLET IMPROVEMENTS, FIRE ISLAND INLET TO JONES BEACH, NEW YORK

Thorndike Saville

Consultant, Long Island State Park Commission;
Consultant to the President, University of Florida;
Dean Emeritus, New York University.

LOCATION AND GEOMORPHOLOGY

Long Island, New York (Figure 1) extends for about 120 miles in a general east-west direction off the southern portions of the States of New York and Connecticut, from which it is separated by Long Island Sound. The western end of the island contains the Counties of Brooklyn and Queens which are part of New York City. To the east are the Counties of Nassau and Suffolk. The surface geology of Long Island is mostly of glacial origin. That portion of the south shore of Long Island with which this paper is concerned (Figure 2) consists of outwash plains of sand and gravel fringed by barrier beaches from 600 feet to 3,500 feet in width. They rise to about 15 feet above mean sea level, and in their natural condition are more or less protected by sand dunes which may reach an elevation of from 25 feet to 30 feet.

The sand along the foreshore is predominantly quartz, averaging about 0.4 mm. at mid-tide level, and becoming somewhat finer offshore. The foreshore slope of the beaches averages about 1 on 10 above the mean low water line and about 1 on 30 immediately offshore. Several hundred feet offshore the slope flattens to about 1 on 250.

THE PROBLEM AREA

GENERAL

This paper deals with problems of beach protection and restoration, and inlet improvements in the area from Jones Inlet to a point on Fire Island some five miles east of Fire Island Inlet, as indicated on Figure 2. Probably no coastal area in the United States has been subject to such long continued and exhaustive studies of coastal phenomena as this. It constitutes 23 miles of publicly owned beach developed and intensively used for recreational purposes and readily available by a system of parkways and causeways to some 8,000,000 people in New York City and

over 2,000,000 more in Nassau and Suffolk counties, a combined total of 10,000,000 persons.

Of the twenty-three miles of beach, fifteen miles are included in state parks under the jurisdiction of the Long Island State Park Commission. The remaining eight miles are owned by the Towns of Bablylon and Oyster Bay. As early as 1936 the Long Island State Park Commission instituted a cooperative study with the Beach Erosion Board of the Corps of Engineers, United States Army with respect to beach erosion control for Jones Beach. Almost continuously since then the beaches and the two inlets have been the subject either of cooperative beach erosion control studies between the Park Commission and/or Suffolk County with the Beach Erosion Board, or relevant navigation reports by the Corps of Engineers concerning the inlet. The most recent report (1) deals with the entire area from Fire Island Inlet westward to Jones Inlet. It contains a list of most of the earlier reports dealing with previous investigations. The present paper describes some of the background and the implementation of certain of the recommendations contained in this report.

In 1926 the area from Jones Inlet east to what is now known as Captree State Park was a series of barrier beaches, shoals, and mud flats. That year marked the inititation of the remarkable developments conceived and carried out in steps ever since under the general direction of Robert Moses, President of the Long Island State Park Commission, and his associates. Some 40,000,000 cubic yards of sand have been dredged from the adjacent bays and lagoons to create an unimpeded stretch of eighteen miles of publicly owned recreational area. The original development along the first six miles resulted in Jones Beach State Park. This became so intensively used that other parks were developed to the east. A four lane highway extends for the length of the region, constituting a "backbone fill" with elevation fourteen feet above MSL. Included in the developments are parking fields with a capacity of 40,000 cars per day. The total cost of all of the developments exceeds $50,000,000, a public investment warranting substantial expenditures for protection against ravages from waves and storms, including beach erosion.

Not withstanding the magnitude of these developments, they are presently taxed to capacity. On a fine Sunday in summer the beaches are visited by over 200,000 people, and the access causeways have to be closed before noon, as no more cars can be accommodated. Some idea of the situation may be obtained from Figure 3, which is a view from near the eastern section of Jones Beach State Park looking west toward Jones Inlet. Attention is called to the three large parking fields and the two smaller "overlook" parking fields, all filled to capacity. The recently completed Jones Inlet jetty is shown in the distance. Figure 10 shows the newest development at Captree State State Park.

Because of the situation described above, the Long Island State Park Commission has plans under way to construct a bridge from Captree

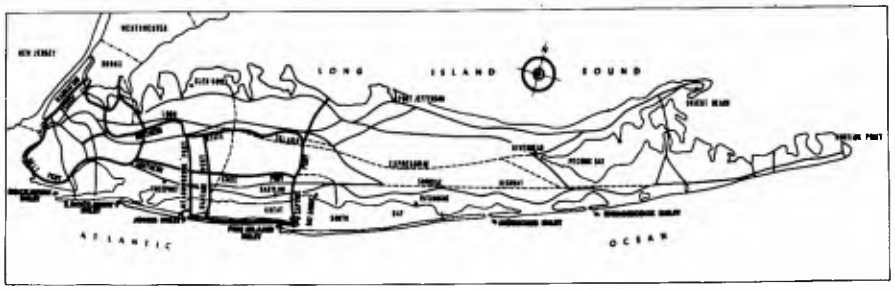

Fig. 1. General map of Long Island, New York.

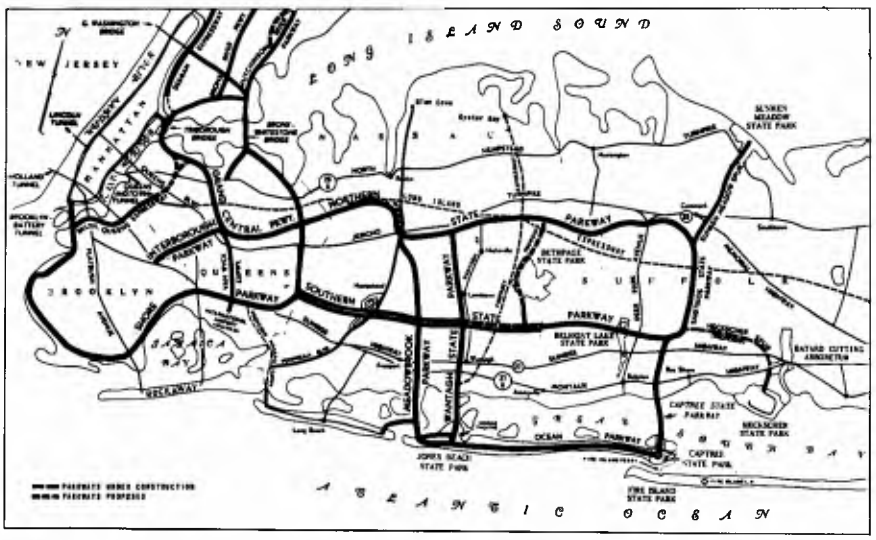

Fig. 2. Western end of Long Island, New York.

Fig. 3. Jones Beach, New York, looking west toward Jones Inlet.

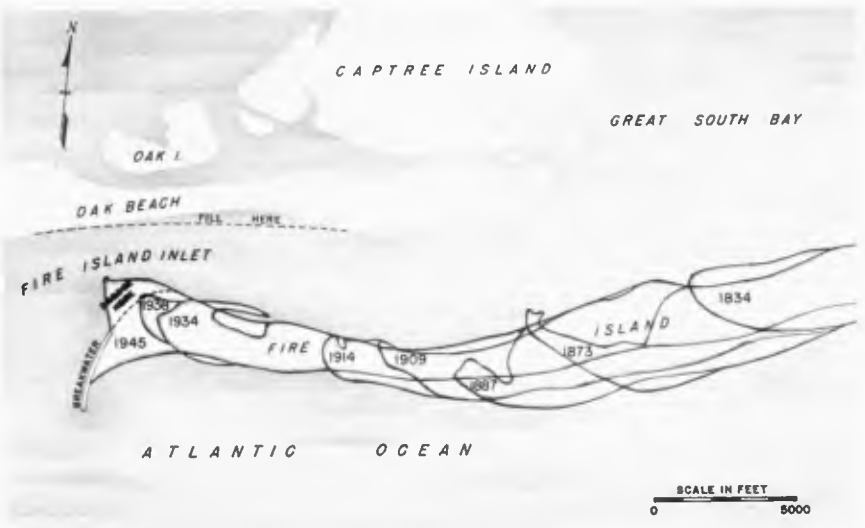

Fig. 4. Progressive westerly movement of Democrat Point.

Fig. 5. Fire Island Inlet and jetty in 1948. View to east.

State Park to Fire Island, and to develop an additional five miles of beach area at Fire Island State Park as indicated on Figure 29.

THE COASTAL ENGINEERING PROBLEM

STORMS, WAVES, AND TIDES

The area is subject to attack by tropical hurricanes and by extra-tropical storms known as "northeasters." Great damage to beaches and adjacent structures has occurred from time to time. Waves in the open ocean may be thirty feet high, and ten to twelve feet high as they impinge upon the coast. Normal tides have a mean range of 4.1 feet off Fire Island Inlet, decreasing with passage through the Inlet to 0.7 feet in Great South Bay. Severe storms have produced still water levels of about ten feet above MSL, and it is believed that still water levels of at least fifteen feet might occur if the peak of the storm surge should coincide with high tide. Several studies have been made of storm surges in this vicinity, the most recent of which (2) is that by Wilson. The most severe storm conditions occur from waves created by winds from the north-east to south-west quadrants having a fetch of several hundred miles over the Atlantic Ocean.

LITTORAL DRIFT

Many studies have indicated a predominant movement of beach material from east to west. The most striking evidence of this is the migration of Democrat Point, the western extremity of Fire Island. Figure 4 shows the movement of this Point from 1834 to 1945. The Point moved westward a total of 4.6 miles in the period from 1825 to 1940, as described in detail in an excellent article by Gofseyeff (3) published in 1953. This article presents valuable data with respect to erosion and accretion in the area, and describes the hydrography of the inlet. Between June 1939 and April 1941 the Fire Island jetty was constructed. The impounding capacity of the jetty was reached about 1950, and material began passing around it to form shoals in the inlet. Figures 5 and 6 show respectively the situation at Fire Island Inlet in 1948 before the impounding capacity of the jetty had been reached, and that in 1957 after extensive shoals to the west had formed. Great South Bay is in the background.

Based upon volumetric measurements of accretion on the east side of the Fire Island and other jetties, and rates of erosion of various beaches, it is estimated that the net littoral drift rate averages about 450,000 cubic yards per year. An interesting feature of studies of littoral movement in the area is that measurements of erosion along the south shore of Long Island seem to indicate substantially less sand supply from such sources than is actually impounded by jetties. It is postulated that some portion of the littoral drift has its origin in offshore sources.

Fig. 6. Fire Island Inlet and jetty in 1957. View to northeast.

Fig. 7. Erosion at Gilgo State Park pavilion, early 1960.

SAND TRANSFER, BEACH CONTROL, AND INLET IMPROVEMENTS, FIRE ISLAND INLET TO JONES BEACH, NEW YORK

BEACH EROSION

General. In the problem area substantial loss of beaches and damage to adjacent structures has occurred, both under storm conditions and from certain effects induced by the Fire Island jetty. During the last few years serious erosion problems existed chiefly along the highly developed area (Figure 2) from about the center of Jones Beach State Park to Oak Beach, which lies just to the west of Captree State Park. Conversely, impoundment by the Jones Inlet and Fire Island jetties has produced or will produce adequate protective beaches for from four to five miles east of each.

Severe storms always cause substantial erosion and other damage along the beaches. Damage to shore structures is greatly reduced by an adequate protective beach in front of them. Prior to completion of the Fire Island jetty in 1941 and for a few years subsequently, beach erosion over much of the area was not as critical as it became later. Much of the beach loss during severe storms was restored by onshore movement of storm created offshore bars, and by the normal westward moving littoral drift. Sand from Fire Island presumably moved intermittently across the shoals at the entrance to the inlet and nourished the beaches to the west. Local areas of depletion were readily restored by pumping from the bays and channels to the north.

Erosion of the beaches predominates during the months of September to April. During the spring and summer when relatively quiet ocean conditions exist, with prevailing westerly winds, the direction of littoral transport tends to be reversed to an easterly direction and the updrift eroded beaches to be replenished. The resultant however is a net erosion.

Some years after the completion of the Fire Island jetty the beaches to the west began to indicate accelerated erosion. With curtailment of the previous sand supply from the east, erosion of the beaches west of the inlet progressed westward with time, threatening Jones Beach. Figure 7 indicates an occurrence in early 1960 at Gilgo State Park about half way from the western side of the inlet to Jones Beach State Park.

Oak Beach. The resort community of Oak Beach (Figures 5, 6, and 10) is located just west of Captree State Park, and a considerable length of the western portion of this beach has been subject to direct attack by storm waves moving into the inlet. It has also been subject to serious erosion from tidal currents in the inlet. The combination of these two factors has caused portions of the western end of the Oak Beach shore to recede to the north about 600 feet from 1930 to 1960. Over forty houses had been destroyed and valuable shore front lost. The situation in 1959 is shown in Figure 10. Various photographs of the area accompanying this paper indicate that there was a critical section of shore where erosion had reduced the width of the island to about 600 feet. The main parkway running along this stretch to Captree was in danger of destruction, and the island itself could

have been breached with the formation of a new inlet.

About 1950 sand began passing around the end of the Fire Island jetty, creating extensive shoals to the west and north as shown in Figures 5, 6, and 10. Several million cubic yards of material were thus accumulated. As the shoals progressed northward, the main channel of the inlet was also forced to the north and west. Close to the Oak Beach shore the channel had depths up to 50 feet and tidal velocities of six to seven feet per second. At various intervals from 1946 to 1959 more than a million cubic yards of sand were pumped onto the Oak Beach shore to try to restore it. In each case the fill was soon eroded by tidal currents in combination with occasional storm wave action.

MAJOR ELEMENTS OF THE PROBLEM

The situation described above posed five major problems for which solutions were sought by the cooperative study between the Long Island State Park Commission and the U. S. Army Corps of Engineers.

a. To stabilize and to replenish as far as practicable the beaches from the ocean entrance to Fire Island Inlet westward to Jones Beach.

b. To partially restore Oak Beach.

c. To stabilize Oak Beach by relieving the pressure of tidal currents impinging upon it, and thus reduce the danger of a breach across the parkway to the back bay, and the possible formation of a new inlet.

d. To reduce maintenance of the navigation channel in Fire Island Inlet by reducing the rate of shoaling.

e. To improve the navigation channel by some realignment.

While the last two items were not specific objectives of the study as originally formulated, they inevitably arose as the study proceeded and the recommendations arising out of it began to be implemented.

RECOMMENDATIONS OF THE STUDY

In accordance with usual practice, the necessary field studies and initial report were assigned to the District Engineer of the U. S. Army Corps of Engineers at New York. The staff of the Beach Erosion Board participated in the analysis of the problem and in certain of the solutions recommended. The initial report was reviewed by the Division Engineer of the U. S. Army Corps of Engineers, North Atlantic Division, and by the Beach Erosion Board. The final

recommendations were endorsed by the Long Island State Park Commission, approved by the Chief of Engineers, U. S. Army, and adopted by the Congress of the United States.

The report of the District Engineer proposed two alternative plans, designated respectively the "Comprehensive Plan" and the "Alternative Short-Range Plan." These plans were proposed after consideration of other alternatives involving design and use of a shallow-draft dredge to excavate material from the shoals and to transport and discharge it upon the beaches; land haul of sand from the impounding area east of the jetty to a point near the inshore end of the jetty, and transfer onto the beaches across the inlet by pipe line dredge or a fixed by-passing plant; and construction of an offshore breakwater 1,000 feet long east of the jetty to form a littoral reservoir from which sand would be pumped to the beaches. Each of these latter alternatives was rejected from the standpoint of cost as well as other considerations.

THE COMPREHENSIVE PLAN

This plan was to be undertaken in three phases, of which phase one (Figure 8) encompassed: (a) Dredging by pipe line dredge an access channel into the accretion area east of the jetty; (b) dredging a littoral reservoir as shown on the same figure; (c) pumping across the inlet one million cubic yards of dredged material a distance of about 20,000 feet to a feeder beach to provide a three-year source of material for beaches to the west; (d) pumping 1,550,000 cubic yards of dredged material on Oak Beach; (e) closing the access channel with dredged material; (f) removing the dredge through an exit cut 200 feet wide into the Atlantic Ocean; and (g) leaving a barrier on the south side of the lagoon about 150 feet wide and 9 feet above MLW. It was anticipated that the barrier beach would be removed by erosion due to natural forces, leaving a littoral reservoir having a capacity of about two million cubic yards. This procedure was modeled after a somewhat similar scheme carried out at Port Hueneme, California.

Phase two of the Comprehensive Plan provided for a model study of the general beach erosion and navigation problems at Fire Island Inlet. The model study was estimated to require three years. Phase three, subject to the findings of the model study, was to restore the shore line west to Jones Beach as it existed in 1939; restore fill that would have been eroded from Oak Beach; relocate the navigation channel; and repeat dredging of the littoral reservoir to replenish the feeder beach.

The Beach Erosion Board noted the following objections to the "Comprehensive Plan": (a) that a considerable portion of the fill on the Oak Beach shore would be lost by erosion in the absence of provisions to relieve the pressure of tidal currents on that shore; (b) that the model study was not essential in connection with the immediate problem of beach erosion control, although desirable in connection with future navigation improvements, (c) that full restoration of the 1939 shore line was not regarded by the Long Island

State Park Commission as immediately necessary, but that progressive restoration over a period of years would suffice; (d) that the possibility existed that the exit cut through the barrier beach would close, thus preventing the reservoir from acting as an impounding area and leaving a lagoon as an undesirable feature in the proposed extension of Fire Island State Park; (e) and that full implementation of this plan was estimated to cost about $2,000,000 more than the "Alternative Short Range Plan."

THE ALTERNATIVE SHORT RANGE PLAN

This involved beach restoration and control by dredging material from the existing shoals west of the jetty, and pumping it to the feeder beach and to Oak Beach in a series of operations over a fifteen year period. Phase one of this plan (Figure 9) contemplated excavation by pipe line dredge of 2,000,000 cubic yards from the northwest portion of the shoals; pumping 1,500,000 cubic yards of this to the feeder beach; and pumping 500,000 cubic yards to Oak Beach. The dredging would tend to move the channel toward the south and east, thus effecting some reduction in the pressure of tidal currents along Oak Beach. It was anticipated that the new channel would require an additional 200,000 cubic yards to be removed by hopper dredge. These operations would be repeated at intervals of five and ten years respectively.

The reviewing authorities, including the Beach Erosion Board, favored the foregoing plan, but recognized that conditions might alter between the submission of the report and its adoption by Congress, or during the progress of the work. Hence they recommended some flexibility in the execution of the plan. In his letter transmitting the report to Congress the Chief of Engineers recommended adoption of this plan as outlined by the Beach Erosion Board with such modifications of the plan as in the discretion of the Chief of Engineers may be advisable. The wisdom of the underlined phrase will become evident subsequently.

In its review of the project the Beach Erosion Board stated its opinion that (a) "no fill should be placed on Oak Beach until the pressure of tidal currents on Oak Beach can be relieved," and (b) that the plan was "predicated upon future development of a permanent by-passing system for subsequent maintenance."

EXECUTION OF THE PROJECT

The project was authorized by Congress in July 1958, and the District Engineer at New York proceeded to prepare plans and specifications for the work. During this period, and in accordance with the discretion given to the Chief of Engineers to modify the details of the plan, it was jointly agreed between the Corps of Engineers and the Long Island State Park Commission that instead of dredging the fillet at the end of the shoals shown in Figure 9, there should be substituted a straight cut through

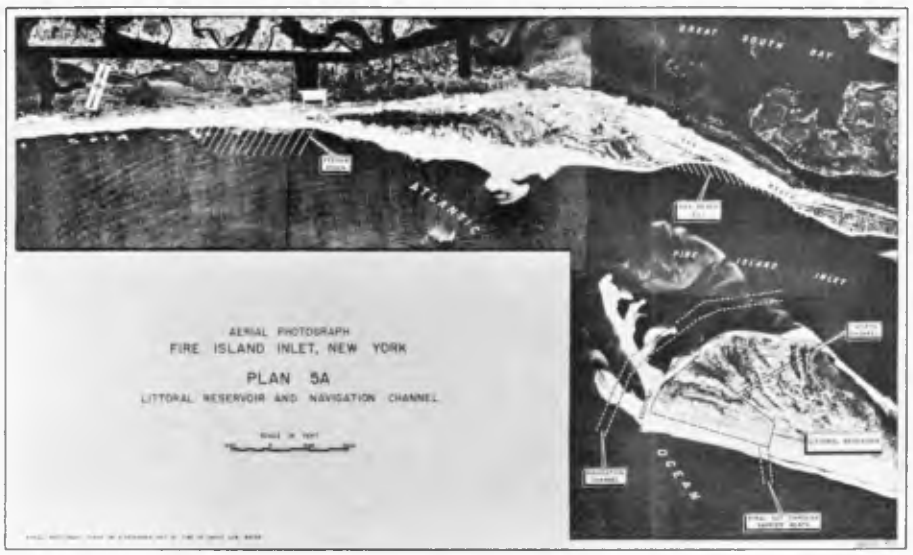

Fig. 8. Phase 1 of "Comprehensive" plan.

AERIAL PHOTOGRAPH, FIRE ISLAND INLET, N.Y.
TAKEN 12 SEPTEMBER 1955 AT TIME OF LOW WATER

Fig. 9. Phase 1 of "Alternative Short Range" plan.

Fig. 10. View looking southwest from Captree State Park.

Fig. 11. The new cut, dredge, and discharge line, September 1959.

the shoals further to the west. Figure 10 is a view looking southwest from Captree State Park in July 1959. The dredge is shown starting the cut through the shoals west of the jetty. Fire Island appears in the upper center. The old channel and Oak Beach appear at upper right. The nearly completed cut, looking northeast, is shown in Figure 11. It was felt that the straight cut would give greater assurance of removing the tidal pressure from Oak Beach. It was the writer's opinion that this would also produce improved operating conditions for the dredge and hence probably a reduced cost. It was believed that no hopper dredging would be required, which proved to be the case. The cut was to be approximately 1,000 feet (300 m.) wide, by 18 feet (4.7 m.) deep and 6,700 feet (2 km.) long, with 2 feet overdepth dredging permitted. The contractor was paid on the basis of yardage removed.

The Dredge "Western Chief" of the Western Contracting Company began excavation in June 1959. This is one of the largest dredges in the United States (Figure 12) with 36" suction, and 30" discharge. The power plant totals 11,500 H. P. of which 6,000 H. P. are for the pumps. At an average of 15% solids, the dredge delivered 1,470 cubic yards (1131 cu. m.) of sand per hour. The maximum distance pumped to the feeder beach was 3.5 miles or 5.5 Kilometers. During the maximum pumping distance a booster pump on land was used to increase the output and to reduce wear on the pump impellers. Figure 11 shows the dredge in the new cut, and the discharge line across the old channel and along Cedar Beach in the direction of the feeder beach.

THE FEEDER BEACH

The location and approximate dimensions of the feeder beach, shown on Figure 8, was determined after considerable study of refraction diagrams and hydrographic data by engineers of the Beach Erosion Board and the District Engineer's office. The location chosen was the nearest point to the inlet which would permit an estimated 90 per cent of the wave energy to tend to move material to the west. Although the plan provided for 1,500,000 cubic yards of fill on the feeder beach, the elimination of the necessity for hopper dredging and lower unit prices for dredging than had been anticipated permitted nearly 2,000,000 cubic yards to be deposited between June and December 1959. Figure 13, looking east, shows the feeder beach in process of construction, the discharge line from the dredge, and the dredge in the upper right. Figure 14, from the opposite direction, shows the dredge excavating the cut, and the feeder beach. Figure 15 shows the discharge end of the pipe line in operation.

CLOSURE OF THE OLD CHANNEL

Following the decision to modify the original plan by constructing a new channel, it became evident that the full benefits desired would not be accomplished if the old channed remained. The flow in two channels would reduce the scouring velocity in each, and hence increase the rate of shoaling. Most important, should the new channel become shoaled so that flow through it was substantially reduced, the earlier

Fig. 12. The dredge "Western Chief".

Fig. 13. Feeder beach under construction, September 1959.

Fig. 14. Dredge in new cut and feeder beach, September 1959.

Fig. 15. Discharge from dredge pipeline onto feeder beach.

conditions would tend to recur, with renewed tidal pressure against the Oak Beach shore. Since ample material existed in the shoals where the dredge was working, it was decided to close the old channel by a sand fill. Some questions were raised as to whether a closure could be effected by this means on account of the high velocities likely to be encountered in the final stages of the work. Expert advice was to the effect that this could be done, especially considering the high rate of sand transport possible with the dredge, and with some help from land-placed fill from the shore.

Fill for the final stages of the closure began to be placed by the dredge from the remnant of the shoal, west of the new cut at noon on December 3, 1959 (Figure 16) and closure was substantially effected (Figure 19) at low tide about 5:45 p.m. on December 4. The closure became fully effective to 12 feet above MLW (Figure 20) by 10:00 a.m. on December 5. The short land fill (Figure 17) from the west side was directed somewhat to the north of the axis of the oncoming dredged fill, so that an overlap effect resulted. Velocities prior to closure reached five to seven feet per second, but with the relief provided by the new channel, this situation lasted only a short time. In the final stages of the closure velocities may have reached as much as ten feet per second. Figures 21 and 22 show the completed closure fill with the new channel fully operative. It is interesting to compare Figures 10 and 22, taken before and after the completion of the work described herein. Figure 23 shows the cross sections and velocities in the old channel before closure and in the new channel after the old channel had been closed. Comparative measurements made in the old channel on August 1959 and in the new channel in August 1960 indicate that the cross section, velocities, volume of flow, and tidal ranges are substantially the same in the new channel as they were in the old channel.

OAK BEACH

Reference has been made to the recommendation of the Beach Erosion Board that no fill should be placed on Oak Beach until pressure of the tidal currents had been relieved. This had now been accomplished by the closure of the old channel and by the change in direction of the tidal currents after construction of the new channel. In addition the closure fill would protect the critical areas of Oak Beach from the severity of attack by storm waves previously experienced. Therefore about 600,000 cubic yards were pumped to the western portion of Oak Beach by the dredge Western Chief as part of the contract in order to provide immediate protection to the adjacent structures, including houses and the parkway. In addition the Long Island State Park Commission constructed a series of short and light stone groins along the eastern portion of the affected area, and subsequently arranged for a smaller dredge to pump some 600,000 cubic yards of sand fill along this shore as a continuation of the work done by the Western Chief. Figures 24 and 25 show the before and after conditions looking west from about the center of the Oak Beach Shore, and figures 26 and 27 show a similar comparison looking east from about the same point.

Fig. 16. Final closure operation, noon December 3, 1959.

Fig. 17. Final closure operation, 3:30 p.m., December 4, 1959.

Fig. 18. Final closure operation, 4:40 p.m., December 4, 1959.

Fig. 19. Final closure operation, 5:45 p.m., December 4, 1959.

Fig. 20. Final closure operation, 10:00 a.m., December 5, 1959.

Fig. 21. Completed closure and new channel, December 14, 1959.

Fig. 22. Completed project, looking southwest from Captree State Park.

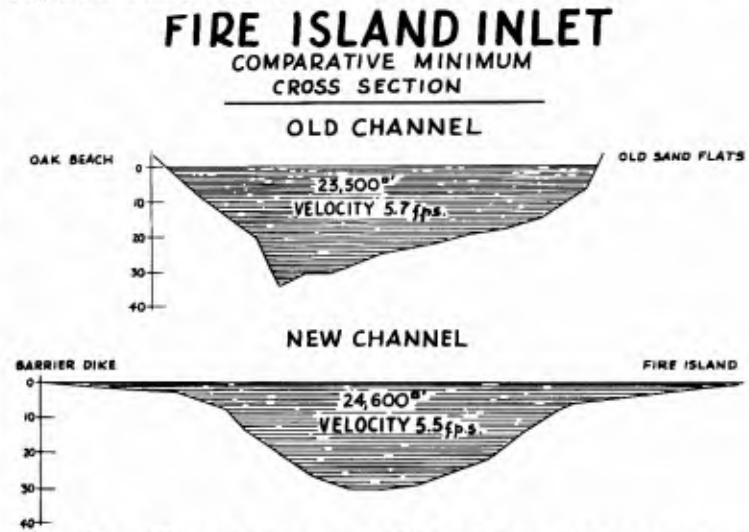

Fig. 23. Cross sections, old and new channels, Fire Island Inlet.

Fig. 24. Oak Beach, looking west, June 1959.

Fig. 25. Oak Beach, looking west, March 1960.

Fig. 26. Oak Beach, looking east, February 1960.

Fig. 27. Oak Beach, looking east, March 1960.

Fig. 28. Closure fill after Hurricane Donna, September 1960.

Fig. 29. Tentative plans of the Long Island State Park Commission for future development in the vicinity of Fire Island Inlet.

APPROXIMATE VOLUMES OF FILL PLACED

By dredge "Western Chief", Government contract

On Feeder Beach	1,930,000 cubic yards
On Closure Fill	1,325,000 cubic yards
On Oak Beach	500,000 cubic yards
Total contract pumping	3,755,000 cubic yards
By Long Island State Park Commission and Suffolk County	
On Oak Beach	600,000 cubic yards
Grand total	4,355,000 cubic yards

It should be noted that the volume of fill under Phase one materially exceeded that suggested in the original plan, but that in spite of this the work was completed at about the authorized cost. This was due in part to a lower price than originally contemplated for the large dredge, and in part because the Long Island State Park Commission required excavation for its own purposes in the bay north of Oak Beach, and little or no additional cost was involved in disposing of the dredged material along the Oak Beach waterfront.

STRENGTHENING THE CLOSURE FILL

The fill closing the old channel was considered to be a vital element in the entire program. Constructed entirely of sand to a height of about fifteen feet above MSL, and exposed to the full attack of storm waves from the ocean, it was felt that it should not only be protected on the ocean side, but that its general dimensions should be maintained as currents and erosion tended to change them. The Commission therefore has performed minor operations with bull-dosers to restore the profile of the fill as wind, waves, and currents have tended to modify it, and has constructed a series of short and light stone groins on the ocean side. It plans to continue such moderate protective works as material for armoring the ocean slopes can be obtained at merely the cost of hauling, as was done at Oak Beach.

TEST OF THE PROJECT

The works previously described were completed in August 1960. In September Hurricane Donna passed over the area. All of the works functioned as intended. Material from the feeder beach moved westward; the closure fill (Figure 28) was not damaged seriously; and the Oak Beach shore was fully protected. The latter event stimulated various laudatory letters from residents of Oak Beach who had suffered severe damage from most previous hurricanes.

SAND TRANSFER, BEACH CONTROL, AND INLET IMPROVEMENTS, FIRE ISLAND INLET TO JONES BEACH, NEW YORK

CONCLUSIONS

Experience to date indicates that the basic plan recommended by the Beach Erosion Board was well adapted to its purposes. As previously indicated, phase one of the project was completed at less than the authorized cost. The actual cost of the work performed under government contract was $2,484,000 at an average cost of 66 cents per cubic yard. Including government costs the total cost was $2,678,000. Apportionment of project costs are 42% to the United States and 58% to the state and county. The usual division for beach erosion control projects involving publicly owned lands is 1/3 by the United States and 2/3 by local interests, but in this case the United States assumed an additional share on the basis that consummation of the project would reduce navigation maintenance costs. The local agencies advanced $152,880, subject to later reimbursement, to assure completion of the required yardages.

One element of the program deserves to be mentioned again, namely the provisions that the basic plan could be modified in the discretion of the Chief of Engineers. The flexibility thus made possible, whereby the Army Engineers and the cooperating agency (the Long Island State Park Commission) could agree on changes, produced an ultimate solution which, in the opinion of the writer, was much superior to what would have resulted if rigid adherence to the original plan had been required. The rather unusual cooperative features of the Beach Erosion Act were doubtless devised with such possibilities in mind.

THE NEXT STEP

As the Beach Erosion Board stated in its report, the ultimate success of the combined beach erosion control and navigation problems is likely to depend upon the development of a suitable sand by-passing plant to intercept sand moving from the east toward the Fire Island jetty and to transport it to strategic locations across the inlet. Fully persuaded of the validity of this suggestion, the Long Island State Park Commission as early as 1956 engaged a well known consulting engineer, Frederick H. Dechant of Harris-Dechant Associates, to render a report on a fixed sand by-passing plant. Various designs were proposed, and the latest submitted in 1959 describes a plant located east of the jetty and consisting of a fixed trestle mounting two traveling bridges. Suspended from the lower girders of the bridges are the dredge pumps, one on each bridge which travels back and forth on the girders. The pumps are designed to excavate a trench 500 feet long, 25 feet wide at the bottom, and to a depth of 16 feet below MSL. The dredge pumps discharge to wells from which sand is pumped to a main pumping station from which it would be pumped across the inlet.

Since completion of the work described in this paper, the Long Island State Park Commission has submitted to the Army Engineers a proposal for a special investigation to determine the best method

of effecting sand transfer across the inlet. It is assumed that the Dechant proposal will be considered, among other designs, in the course of such a study.

THE ULTIMATE PLAN

Granted the apparent success of the work constructed to date; granted the design and installation of an efficient and economical sand transfer plant; one asks "what happens to the extensive shoals remaining west of the jetty, and their relation to an improved navigation channel?" Figure 29 shows the long range tentative plans of the Long Island State Park Commission, which envision dredging the existing shoals to create fill to the east for the enlarged and improved Fire Island State Park referred to earlier in this paper. The present closure fill would be fixed and incorporated into extensive new land to be created between it and Captree State Park. A small boat marina is shown, and is likely to be one of the early projects in this program. The navigation channel would be moved eastward toward the jetty, and be fixed in position by the adjacent structures. If and when this plan is executed, or some modification of it approved after investigation by federal and state authorities, it is hoped that the Fire Island Inlet Problem, including sand transfer, navigation, and related recreational benefits will be solved.

ACKNOWLEDGEMENTS

During the course of the studies and the work reported in this paper the following principal officials of the two cooperating agencies were directly involved. In addition, as usual in such cases, most of the basic studies were performed by numerous able engineers on the staffs of these agencies.

CORPS OF ENGINEERS, U. S. ARMY

Lieutenant Generals S. D. Sturgis, Jr., and E. C. Itschner, Chiefs of Engineers. Major Generals Chas. G. Holle and W. K. Wilson, Jr. and Brigadier General T. D. Weaver, Presidents of the Beach Erosion Board. Brigadier Generals Clarence Renshaw and T. H. Lipscomb, Division Engineers, North Atlantic Division. Colonels J. T. O'Neil, T. De F. Rogers, and C. M. Duke, District Engineers at New York.

LONG ISLAND STATE PARK COMMISSION

Robert Moses, President. Sidney M. Shapiro, General Manager and Chief Engineer. Richard C. Boyce, Deputy Chief Engineer. Thorndike Saville, Consulting Engineer.

REFERENCES

(1) Corps of Engineers U. S. Army (1957). Cooperative Beach Erosion Control Study, Fire Island Inlet to Jones Inlet, New York. House Document 411, 84th Congress, 2nd Session. U. S. Government Printing Office.

(2) Wilson, Basil W. (1960). The Prediction of Hurricane Storm-Tides in New York Bay. Technical Memorandum No. 120, Beach Erosion Board, Corps of Engineers, U. S. Army.

(3) Gofseyeff, S. (1953). A Case History of Fire Island Inlet, New York. Proceedings of Third Conference on Coastal Engineering. Council on Wave Research.

CHAPTER 45

ISLAND HARBOURS AND THEIR INFLUENCE ON ADJACENT SHORES

Leon Shirdan
Director, Civil & Marine Engineering Co. Ltd.
Haifa, Israel

The purpose of this paper is to put forward an alternative solution to the problem of reconstitution of existing ports, generally too shallow for the large tankers and ore carriers.

Usually, the existing moles are extended to deep water fairways and approaches to berths, docks and basins, dredged and adapted to the draught of the new giants. This is connected with enormous expenses. Sometimes completely new port units, as for instance Europort, are built.

The Island Harbours, with their seaward position, will reduce the length of the shipway to the berths and thus provide a speedier turn-out of vessels. The cost of erection and maintenance of such a harbour is in most cases lower than in that of a conventional solution, due to short breakwaters and limited quantities of primary and maintenance dredging operations.

Different alternatives of island ports can be adapted in most sandy coasts over the world.

The changes in coastal regime which may result from erecting an island harbour connected with the mainland by a bridge or a causeway can turn out profitable for general cargo ships, and even fisherboats, especially on the coasts where till now cutting the sea approaches through the shallows and bars was often unacceptable, due to the enormous expenses involved.

GENERAL CONSIDERATIONS

The maintenance of deep enough sea approaches to harbours built on shallow shores and in estuaries, with significant sand movement, will encounter with difficulties due to a large amount of permanent sedimentation which requires permanent dredging.

Keeping clear of sediments of a convenient and safe fairway cut in a shallow bank will be very difficult when the port is located in an

area of frequent storms. In waters with gentle slope of the sea bed, with a channel leading to the port entrance, dredged through a bar, the quantities of sand or silt to be removed can grow to such an extent that the exploitation of such ports is no more profitable.

On shores with considerable tidal level difference, ships wanting to enter the harbour have often to wait for high water.

Even where the amplitude of ebb and flood levels is not so extensive, as for instance at Ijmuiden on the Dutch Coast, the entrance of large vessels into the harbour channel is possible during high water only.

The time wasted by ships awaiting the flood has been on the increase during the last decade, with the growing dimensions of ships. Thus free sailing of ships to and from a harbour is connected with obstacles, due to the lack of permanent approaches having a sufficient depth.

When bulk cargo or tank vessels are considered, speedy turnout if of highest technical and economical importance. Here, loss of time is of great disadvantage.

Today, tankers and carriers of 60,000 tons are no longer a novelty, and a large number of such ships are ordered. However, there are only several ports in the world where these vessels can freely enter, most existing accommodations being built to serve ships with a draught of not over 10 metres.

To handle the newly constructed giants, with draughts of 12.5 metres and over, a large-scale reconstitution is necessary. The fairways, entrances and inner parts of ports have to be deepened, enlarged and rebuilt. In many cases, new anchorages, or even harbours, have to be created to suit the changing conditions.

With the required depth at the entrance of more than 15 metres below MLWL as a function of ships draught and significant wave amplitude, the seaward extension of the moles up to 15-18 metres depth, or deepening of the fairway and its maintenance, will be prohibitively expensive.

Instead of these costly works and a very high charge for constant dredging of the shipping lane, a roadstead island port, with the entrance at desired depths, can be erected in the vicinity of an exist-

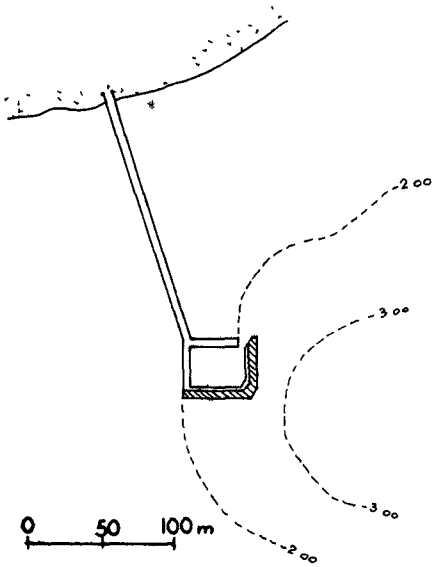

Fig. 1. Fishery harbour in Baltic Sea.

Fig. 1. Fishery harbour in Baltic Sea.

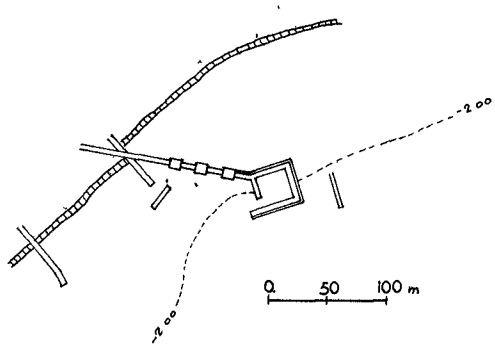

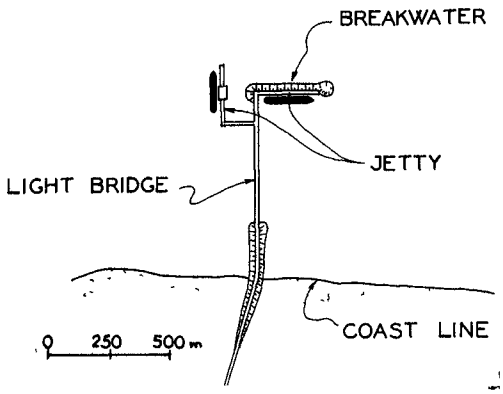

Fig. 3. Proposed breakwater and oil jetty at Moron.

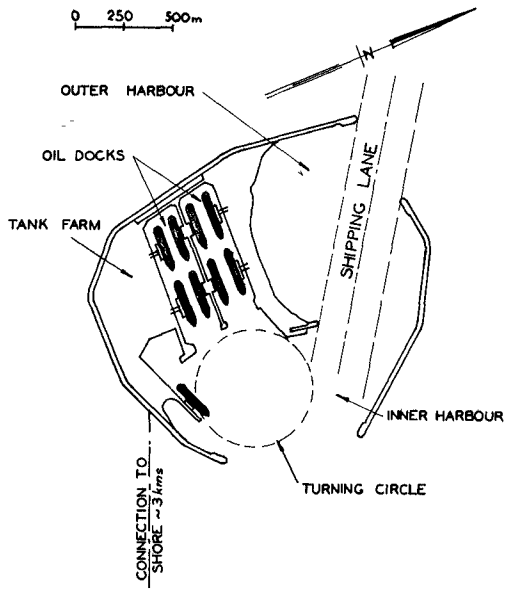

Fig. 4. Proposed oil port at Ijmuiden (Exercise study).

ing harbour, or even as an independent unit. The cost of such a port will be lower than the conventional design, due to the comparatively reduced length of sheltering structures and lower primary and maintenance expenses.

The all-weather transloading of the cargo to and from the mainland can be provided by special sea-going barges, rope-ways, and even a bridge, if the traffic volume will justify it.

In the case of fluids and gases, connection with the coast should be by means of pipelines lying on the sea-bed or supported on a light structure. The island port will shelter the waters shorewards to a considerable extent, a factor which will facilitate communication with the coast.

The idea of an island harbour for large tankers was put forward by the author of this paper during the first International Course of Hydraulic Engineering at Delft, when a team of graduate engineers was called upon to consider, as a study problem, a new oil port for Ijmuiden in the Netherlands. This idea was then further developed by a section of the team, namely Group 12, consisting of Messrs. G. de Campos, S. Muddappa, I. Shams, L. Shirdan, M. Vajda. Under the auspices of the Directors of the I.C.H.E. and the Hydraulics Laboratory at Delft a model of the port was built and tested in a basin.

OFF-SHORE MOORINGS

In ancient times, there already existed island harbours adjacent to the shore, for example in Tyre and Alexandria. Nowadays, such ports can be found -

(a) in arctic waters, the eastern coast of the Caspian Sea, the Far East and the Baltic Sea (Bornholm island), etc. (Figures 1 and 2),as fishery harbours and bases, connected with the shore by means of a bridge or a causeway;

(b) on the Caspian Sea (USSR coast), on the Danish shore (Prøvesten), on the Adriatic Sea (Ancona), in Lake Maracaibo (La Salina), etc.

as oil harbours, bases and moorings;

(c) all over the world

as loading and unloading installations for bulk cargo.

Mostly, offshore anchorages and installations are built in open waters, not too exposed to stormy seas.

This is the case with submarine pipe-lines with buoy moorings, dolphin berths, berthing beams, loading towers etc., adapted where there is no deep water near the coast. Successful examples have been in existence for many years at Tripoli, Banias, Haifa, as well as elsewhere throughout the world.

However, because of the small dimensions of these installations and their great distance from the shore, their influence on the coastal regime is practically negligible.

Where the frequency of storms makes unsheltered moorings risky and uneconomical, the berthing of large and very expensive oil tankers and ore carriers calls for protection against wind attacks, waves and current action.

The development of these kinds of harbours can vary from a straight short breakwater, parallel to the shore and protecting one ship only (as designed by Messrs. Royal Netherland Harbour Works for the tanker berth opposite the refinery at Moron in Venezuela (Fig. 3)) to large, independent island ports with a diameter of 2.0 kms and more.

IJMUIDEN OIL PORT

As mentioned above, a study for a new Oil Port at Ijmuiden was carried on during 1958. The possibility of an island harbour in the vicinity of the existing port and industrial area was brought forth by the author and elaborated with the help of Group 12.

The principle was to locate a deep water harbour directly in the area of -15m isobaths.

The coast in question, open to the North Sea, has a mildly sloping sandy bed and is visited by frequent storms, tidal currents and large sediment transport.

It was required to provide a sheltered sea terminal, with straight and safe approaches for tankers of over 60,000 tons, and with the possibility of extension in the future. Also a small transit storage tank farm has to be provided.

The conventional solution was to lengthen the moles of the existing harbour far seawards, enlarging and dredging the fairway and entrance, and building an oil terminal inland.

This would mean extremely expensive works, connected with the altering of the breakwaters, widening and deepening of outer and inner channels, and extensive maintenance dredging in the future of the depths in the approaches.

The alternative above-mentioned solution of the island harbour considered at first straight breakwater, parallel to the shore, with berths on the landward side. However, as the strong shorewise tidal currents in the area would have interfered with the moorings, the design has been developed towards a nearly circular form of about 2 kms in diameter (Fig. 4).

The seaward position of the terminal should enable the entering and leaving of the harbour, mooring works, discharging and subsidiary operations to be executed in a considerable shorter time than in case of a conventional harbour (hence a much speedier turn-out of ships). The help of the tug boats is also reduced to a minimum.

The berths are well protected against waves, wind action and currents, in spite of their distance of less than 2 kms from the harbour entrance.

The prevailing waves come from directions between south and west, but the group of storm waves of low frequency but of considerable height comes usually from the northwest to north sector, due to the wind velocity and the corresponding fetch..

The waves originated by offshore winds are almost insignificant. Therefore, the most favourable direction of the shipping lane was toward NNW, lying in the direction of dominant storms and protecting the incomong and outgoing ships from prevailing winds and waves.

MODEL INVESTIGATIONS

Model investigations have shown that even the highest waves penetrating in direct incidence through the entrance from the northwestern sector are losing height and disperse to a great extent their energy on the spending beach in the outer harbour before reaching the inside aquatory of the port and the turning circle. The shape of the outer

harbour and the profile of the spending beach played a dominant role in this phenomenon.

The wave height recorded in model experiments was in the berthing docks much lower than 10% of incidental original wave height, so the conditions for mooring and working are acceptable.

Wave heights up to 40% were measured in the inner harbour during the most unfavourable waves penetration, but the turning circle itself was always beyong the 20% aqui-height line of the incoming waves.

The damping of waves in the model was remarkably positive during direct incidence towards the spending beach, resulting in a considerable wave height reduction, and it appears that waves higher than 40% cannot reach the inner harbour.

The shorewards wide opening between the breakwaters has almost eliminated the possibility of waves reflection in the port itself. This auxiliary entrance permits a partly sheltered communication with the mainland.

Water area sheltered by the island extended far behind, almost to the coast. Slightly less than 20% wave height, extending to more than one diameter of the island, was indicated in the model.

The Influence of the Island Ports on the Adjacent Shores. The model study of the affect of the harbour on the coast opposite was not extensive enough, due to lack of time.

Without doubt, considerable changes will be caused on the adjacent shores, decreasing however with the growing distance of the island from the mainland.

The influence will be very strong in the event of a narrow channel between the harbour and shore. It will probably greatly differ in every case, and it will depend on a coastal regime in places under consideration.

In every separate case the stabilization of the coastal regime will depend on the distance from the shore, wave characteristics, the presence of tides and longshore currents, the quantities of the sediment transportation etc.

Where strong longshore currents are absent, a sunbulb may form

at the edge of the island, directed towards the shore, as a result of wave refraction.

At the same time, a sandbar from deposited debris may form opposite the shore. In some cases this process may continue until both promontories meet, forming a tombolo which connects the harbour with the mainland. This may happen when the island is built in the direct vicinity of the shore.

However, in tidal waters where strong cross-currents exist, a channel across the bar will keep the gap open, permitting the shorewise streams to pass in either direction. Thus sediment transportation along the coast will not stop and the coastal regime will remain almost unchanged.

CONCLUSIONS

An artificial island-port in stormy areas can be put forward as a solution to avoid:

(a) Prohibitive expenses connected with the adaption of existing harbours to new super-tankers and ore carriers;

(b) Costly primary and maintenance dredging;

(c) Acquisition of additional areas on the mainland;

(d) Ship delays, due to the far distance from the sea to the terminal inland;

(e) Drastically quick changes in coastal regime.

The advantages of the proposed island-harbour are:-

(a) Entrance at the natural depth, reducing primary and maintenance dredging to a minimum;

(b) Comparatively low cost of construction, due to shorter length of breakwaters;

(c) Speedy turn-out of vessels, due to short and straight ship lanes from harbour entrance to moorings;

(d) Additional navigation safety, due to seaward situation of the entrance on the 15-m contour-line, providing sufficient space for ships in deep water to make a full turn, for a second trial, if they did not succeed to enter because of unfavourable weather conditions. Furthermore, the current velocities in front of the entrance will be much lower than in conventional solution.

(e) The changes in the coastal regime should be slower. In many cases, the sediment transport will be maintained for the greater part. Thus additional shore protection along the coast of the mainland will not be required.

REFERENCES

Oil Port at Ijmuiden, Island harbour by Group 12; I.C.H.E. - Delft 1958.

Island-harbour Model, Oil Port - Ijmuiden. Report on Investigation of Agitation; S 51, Waterloopkundig Laboratorium, Delft 1958.

XVIIth International Navigation Congress - Lisbon 1949 - Section II, Question II.

"Offshore Terminal Built on Man-made Island" - "World Contribution", 1958.

Breakwater Investigation at Moron (Puerto Cabello), Waterloopkundig Laboratorium, Delft 1958.

The Iraq-Mediterranean Pipeline, I.P.C. 1934, Haifa, Israel.

Various B.P. and I.P.C. publications.

Iraq Petroleum Company Ltd., London 1935, Loading Regulations at Terminals Tripoli and Haifa.

The Dock & Harbour Authority, May 1957.

The Dock & Harbour Authority, December 1958.

Sviderski, P. A. (1955), Ustroistvo i expluatatia ryboprom sylovych portov i baz. Part I. Pistchepromizdat, Moscow, pp 206-211.

Johnson, D. W. (1919), Shore processes and shoreline development. Chapman-Hall Ltd., London.

Bryla, S. i Bryla J. (1956), Tablice Inzynierskie Vol. IV Budownictwo Morskie P.W.N. Poznan, Szozecin.

CHAPTER 46

SAFETY OF SEA-WALLS

Ir. T. Edelman.
Chief-Engineer Coastal Research Division.
Rijkswaterstaat. The Hague, Netherlands.

The disastrous stormflood of 1953 has caused in the Netherlands an intensive research on the mechanism of damages of sea-walls and on the problem of safety. It was rather quickly understood that the damages of the sea-walls must have been caused by overflowing water only. The overtopping water, flowing down along the inner slope, penetrated into this slope. The resulting groundwaterflow in the section of the bank-body just beneath this slope must have reduced the friction resistance of the soil, in consequence of which slides occured in the inner slopes, in many cases resulting in a total destruction of the bank-body.

Obviously there was something wrong with our sea-walls, but at first it was not very clear in which way they had to be improved. We could distinguish two different ways, two different principles. Either we should design our sea-walls so high, that overtopping would never occur, or we should construct a bank-body, that would be wholly proof against the action of overflowing water.

The first way is in accordance with the traditional way of designing, originating from the principle that "the safety of the wall lies in the height of the wall". However, a stormsurge-level that will never be surpassed, cannot be indicated. Studies on this subject have shown, that probably some semi-logarithmic relation exists between the height of the stormsurge-level and the frequency of surpassing, calculated as an average probability over a very long period. The chance of surpassing a certain level decreases with increasing height of the level, but as a rule, the frequency curve has no upper limit. In his paper in this conference: "On the use of frequency curves to determine the disign stormflood", Ir. P.J. Wemelsfelder deals in detail with these frequency problems.

From this considerations it is quite obvious, that it will be impossible to make a sea-wall so high, that overtopping will never occur. A bank-body, built in the traditional way (a sand body, covered by a clay layer with a grass-cover on top), however, will collapse if a certain quantity of overtopping water flows down over the inner slope. To each level of the crest, therefore, corresponds a certain risk of destruction of the bank-body and inundation of the hinterland.

Apparently, constructing in the traditional way, it is impossible to make a sea-wall, which has a safety of 100% in itself and which guarantees a safety of 100% in the area behind. Always there will remain a certain risk of disaster for both the wall and the hinterland. It is the task of the engineer to keep this risk within acceptable bounds. He may do so by weighing the cost of heightening the wall against the harm to be expected (frequency curves!) in the hinterland.

From an engineering point of view, designing sea-walls in this way seems not to be quite satisfactory. Usually, an engineer wants

to design his constructions in such a way, that they are wholly proof against the forces acting upon them. In the case of a sea-bank of the traditional type, however, he knows it for certain, that his structure, constructed in order to withstand the sea, under unfavourable conditions will be destructed by that same sea. Is it possible to design a wall, the body of which is wholly proof against the forces acting upon it?

If overflowing water could be prevented from penetrating into the bank-body, no dangerous groundwaterflow could come into existence, no reduction of the friction resistance would occur and no sliding of the inner slopes could event. Apparently, a bank covered with an impermeable layer would be safe against damages by overflowing water. Nowadays a watertight coating will be realised by a bituminous layer.

An asphalt covered sea-bank, in opposition with a bank of the traditional type, will not collapse from overtopping water, even if very large quantities of water would flow over the wall. The area behind the wall, therefore, will never be exposed to a total inundation by sea water flowing through a dike breach. This may be a very great advantage.

Neither the asphalt covered bank, nor the bank of traditional type is able to produce a safety of 100% in the hinterland. However, if a same degree of safety in the protected area has to be realised either by a grass covered bank or by an asphalt covered bank, it is quite obvious, that the former has to be much higher than the latter.

Therefore, the asphalt covered wall seems to be the best solution of the problem. Not only the asphalt covered bank possesses a safety of 100% in itself and will never collapse, but also a bank of this type can be much lower than a bank of the traditional type.

However, this best solution may not be identical with the cheapest and most economic solution. Attention may be drawn to the fact, that bitumen is a very expensive building material. The advantage of the lower crest, resulting in lower costs of the earth body, may be outdone entirely by the high costs of the expensive asphalt layer.

Having calculated many cases, it is my opinion, that in this country the wall of the traditional type (a sand body, covered with a clay layer grown over with grass) under normal building conditions always give the most economic solution. The asphalt covered sea-bank in this country is justified only under exceptional conditions, for instance if the clay required under the grass-cover is very expensive, or if the protected area may tolerate a huge amount of overflowing sea water so that a very low bank can be accepted, or if it is impossible to obtain a reliable grass-cover.

Though from a technical point of view every engineer will prefer the asphalt covered sea-bank, economic considerations may force him very often into the direction of the high, grass covered wall of the traditional type. Matters might turn to the contrary if modern research would lead us to a much cheaper solution of the problem of the reliable watertight coating of a bank-body. In my opinion, this is one of the most important problems to solve in sea-wall research.

CHAPTER 47

MODERN DESIGN AND CONSTRUCTION OF DAMS AND DIKES BUILT WITH THE USE OF ASPHALT

BARON W.F. VAN ASBECK, M.I.C.E.
SHELL INTERNATIONAL PETROLEUM CO., LTD.,
LONDON.

SUMMARY

In recent years quite a number of important coast protection and harbour construction works in Europe, in the U.S.A. and in Japan have been built or strengthened with the use of asphalt according to established methods of construction in various countries. These works have proved to be not only technically sound and durable but also economical in initial capital investment as well as in maintenance costs. Moreover, as the results obtained have been very encouraging, new outlets and methods of construction with asphalt are being sought, and systematically investigated and developed to cover a wider field of application for coast protection and harbour construction works.

Although there are many purposes and means of applying asphalt constructions for these works, the author has limited the scope of his paper to describe in particular the fundamental problems related to the hydraulic and asphalt-technical aspects of building dams and dikes of sand according to the hydraulic fill process, covered and protected by a two course hot-mix asphalt revetment or layer.

Assuming a general knowledge of the various facets of hydraulic dam and dike constructions and of asphalt construction methods the author deals with essential items concerning the hydraulic and strength design of asphalt revetments for dikes and dams and describes certain details of construction that require particular attention and perhaps further investigation as experience has proved.

INTRODUCTION.

In many countries it is essential that certain coastal stretches are protected against the damaging effect of waves caused by heavy storms, hurricanes, typhoones, etc. Generally these coastal sections are limited to those parts of the country, where the population is concentrated in towns and villages and where land is more valuable than in other parts, either because it is well suited for industrial development or better suited for agricultural purposes. In an increasing number of countries reclamation works are being undertaken in order to develop employment and food production. The types of coast that require artificial protection are generally situated at a low level, somewhat lower than normal high water level of the sea, whilst the beach and in some cases the dune formation, will consist of

sand that may range in size from very fine sand of limited grading to coarse sand mixed with gravel of various sizes.

In this century of enormous technical progress, means have been sought to improve the methods of protection of these coasts and at the same time to reduce the cost of construction by designing dams and dikes of sound technical quality from local aggregate materials. The modern method of construction which aims at high productivity and low cost consists of building a sand core covered with and protected by an asphalt construction which is generally laid in two courses.

Since new methods of dike and dam construction can only be investigated and tested to a certain extent, even if experiments in a hydraulic laboratory can assist in determining the importance of various factors, many items of performance can only be judged and appreciated in actual practice. A high degree of responsibility is left to the engineer concerned in the design and construction, and it is for this reason that progress in the application of asphalt revetments has taken place in consecutive stages for various types of dams and dikes.

The first asphalt revetment was constructed on a harbour dam with a sand core, where damage to surrounding constructions and properties would be very limited in case of failure. The next step was taken when an asphalt revetment was built on a sand dam surrounding a large building pit, where damage to installations would not be irreparable but risks were greater than in the first case. Finally the last stage consisted of building dams and dikes which were designed to protect populated and valuable areas against the sea.

As it is impossible to describe all details of this asphalt development work in a paper of limited scope, the author has limited his description to those parts of the construction which are essential; firstly, for the design, both from a hydraulic and an asphalt-technical point of view; secondly, for the actual execution of the asphalt work; and finally for a satisfactory performance as based on experience gained in various countries.

DESIGN

It is assumed that a formation of fine granular aggregate of suitable bearing capacity is available, perhaps covered by a layer of silt that can and should be removed to a thickness of some 50 cm. in order to obtain a sufficiently strong and impermeable layer underneath the dam.

In order to retain the core of the dam consisting of fine sand in proper shape, two parallel retaining walls of clay or other suitable cohesive material are designed under water on either side of the dam to a height just above normal high water level. Generally

these walls will be dumped each to a height of 2-3 m. and if a greater height is required the retaining walls are built up in stages as shown on the drawing. (Fig. 1)

The core of sand is built up either by dumping the sand under water by means of bottom-door hopper barges or by the hydraulic fill process, by which sand and water are pumped through a pipe at the end of which the sand is deposited by sedimentation and the water flows back into the sea. The sand core is finally brought into shape according to the design by means of drag lines, bulldozers and other conventional types of earth moving equipment, and compacted if necessary.

The design of the facing of the core of the dam consists of various parts, each of which has to fulfil a specific function. The foot of the dam, from low water level downwards, has to be protected against the erosive forces of currents and waves, and should consist of a flexible material, which permits the lower edge of the protective layer to follow limited deformations caused by erosion at the foot of the construction. For this purpose brushwood mattresses or mattresses of reeds, loaded with stone, have proved to be effective and durable. Some experimental stretches have been carried out with reinforced asphalt constructions, which have proved successful if constructed in situ in a continuous layer; but prefabricated reinforced asphalt mattresses of limited dimensions have sometimes resulted in less satisfactory performance, in particular where the mattresses were not laid in sufficiently deep water so that the waves were able to play on the mattresses, thus causing vertical displacements which in turn transformed the sand beneath into quick sand of reduced stability.

At low water level or in its proximity a sheet piling is generally built to a depth of some 2 m. in order to prevent or reduce the direct influx of water under the dam or dike. A timber sheet piling should remain under water practically permanently, but if concrete is used, the top of the sheet piling may be laid higher. This is generally of advantage for construction purposes and may also be preferable to obtain a stronger protection at this most vulnerable point of the dam.

There are two types of essential problems attached to the design as described above. Related to the hydraulic design are two important questions, viz. (1) what seaward slope should be given to the dam and (2) what should be the height of the dam. There are also two questions related to the asphalt design, viz. (1) how thick should the protective revetment be laid, and (2) what is the most suitable composition.

HYDRAULIC DESIGN

If anything has been learned during the centuries of dike building experience, it is this: through some unexpected event that may occur any day, waves may overtop the dike and cause a breach unless it is

also properly protected over its crest and on the back slope. Events, such as a storm flood level caused by strong winds, surpassing a previous highest registered storm flood level, or a storm of longer duration than ever experienced before, may be the cause of breaches, for a clay or turfed top soil may be soaked to such a degree, that it loses stability although it may resist the erosive action due to the flow of water. In such circumstances the protection will slide down the slope and the core will be gradually washed away until the dike, together with its protective revetment on the seaward side, collapses, thus causing the initial stage of a breach, followed by serious flooding, if no quick measures for repair are or can be taken.

Another experience to remember is that in coast protection work it is not technically sound or economical to try to resist the forces of waves by building very heavy, rigid and steep structures. Such structures will inevitably also collapse if attached by water from the rear. Although it may be necessary to build a somewhat higher dike, it has proved to be more effective and more economical to build a reasonably flat seaward slope and protective revetment to meet the force of breaking waves and to guide the uprush of water along a streamlined profile rather than to resist outright the force of the waves.

Engineers experienced in dike design and construction methods all seem to agree with the preference, if not the necessity, of protecting dikes of sufficient height with artificial revetments and of building streamlined structures.

These are fundamental conditions which govern modern dike design in principle, but the dimensions have still to be determined to suit specific local conditions. A great deal of research and experimental work has been carried out in post war years in various hydraulic laboratories to investigate and determine the features and performance of various types of designs for dams and dikes. Formulas have been developed, among others, for assessing approximately the uprush of waves on a revetment laid on slopes of varying angles. Various types of materials have also been subjected to these tests under varying conditions of exposure (1, 2, 3).

Note: Numbers refer to literature at the end of the paper.

A formula derived by the Hydraulic Laboratory at Delft from experiments carried out in a wind flume seems to give a practical approach for determining the vertical height of uprush of the significant wave for an open, close-set stone revetment for slopes not steeper than 1 vertical in 3.5 horizontal.

Table 1

	Construction	Loading Conditions and Dimensions: h cm.	A cm.	a cm.	p kg./cm.² σ	Material Properties and Calculations: h/a	S kg./cm.²	E_b kg./cm.²	S/E_b	Stress: σ kg./cm.²	Strength: σ_b kg./cm.²
I.	Lean sand asphalt	40	100	50	0.35	0.80	70.000	100	700	1.9	abt. 15
II.	Very lean sand asphalt	25	100	50	0.35	0.50	50.000	100	500	3.5	" 7.5
III.	10 cm. of asphaltic concrete on 10 cm. of lean sand asphalt	20	150	75	0.60	0.27	83.000	100	830	13.8	" 30
IV.	10 cm. of very lean sand asphalt	10	100	50	0.35	0.20	50.000	100	500	8.4	" 7.5
V.	Blocks of basalt in sand mastic	50	300	150	1.5	0.33	100.000	200	500	22.5	" 22

Calculation of bending stresses in the bituminous carpet on various existing constructions

h = thickness of asphalt construction

A = amplitude of waves

a = radius of loaded surface

p = pressure on slab

S = stiffness modulus of bituminous slab at +5°C., 1/10 sec.

E_b = elasticity modulus of firm sand

σ = bending stress in bituminous slab determined according to Hogg

σ_b = bending strength according to fatigue test

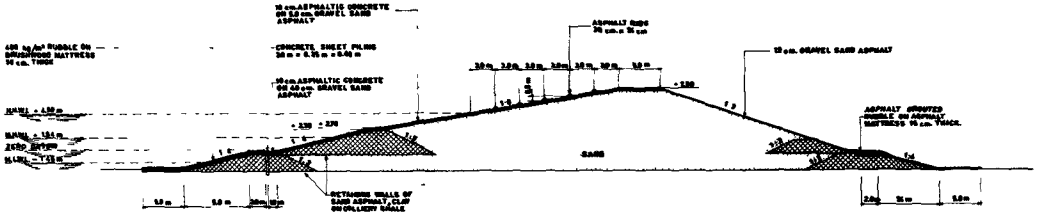

Fig. 1. Typical dam section.

$$Z = 8H \left(\cos i - \frac{B}{L}\right) \tan a$$

in which Z = height of uprush of waves, measured vertically above storm flood level, admitting 2% of over-topping waves.

H = significant wave height or average amplitude of the highest third part of all recorded waves.

i = angle of incidence of the waves.

B = width of berm

L = wave length

a = angle of the slope.

Formerly the height of uprush of waves was defined as the vertical height above the highest registered storm flood level, but since 1953 a calculated storm flood level has been introduced in Holland, which is based on a combination of extreme meteorological weather conditions. Such a calculation requires, however, a great number of data and a detailed knowledge of the prevailing conditions on the coast.

A smooth, impervious surface increases the uprush by 15%.

Slopes may vary from 1 : 3 to 1: 10 according to their exposure to winds and waves; for an average 1 : 6 slope the uprush of a wave of 3 m. amplitude on an asphaltic concrete construction would be approximately 4.60 m., measured vertically.

Recently a new method of reducing the uprush of waves has been designed and investigated by the Delft Hydraulic Laboratory (4). It consists of applying a range of 4 to 5 asphaltic concrete ribs, built at 0.50 m. intervals, measured vertically, with the bottom rib equally constructed at 0.50 m. height above the maximum registered storm flood level, as shown on the drawing. The purpose of this range of ribs has been demonstrated experimentally in actual practice and has shown that the uprush of a thin layer of water which has lost the majority of its energy can be effectively reduced by 50%.

The ribs are built to a section of 30 x 30 cm. in lengths of 4 m. with intermediate open spaces of 0.80 m. length to allow the water to recede more freely and form a layer of resistance to the following oncoming wave.

Incidentally it should be borne in mind that on a seaward slope of any type of protective material the uprush of waves during storms

only takes place from storm flood level upwards along the slope; the strongest wave attack with the greatest impact and uplift is to be found between mean high water level and storm flood level, whilst the revetment is only subjected to moderate, but on the other hand perpetual, wave attack with erosive action below mean high water level.

ASPHALT DESIGN

The systematic use of asphalt for dams, and later for dikes, dates from the early post-war period, when it was suggested to build a harbour dam of a sand core protected by an asphalt facing as the most economical solution for the reconstruction of the entrance to the port of Harlingen in Holland. (1). The economical construction was based on the fact, that use could be made of local fine sand that was available in abundance in the seas, whereas other construction materials would have had to be brought to the site from long distances. At that time considerable knowledge was available of the fundamental principles of the construction of asphalt roads, but little was known about the application of asphalt to dams, apart from the fact that asphalt constructions were cohesive to the extent of being able to resist the forces of erosive action of small waves, that asphalt constructions could be made impervious if properly designed according to fairly strict specifications, and that asphalt layers were sufficiently flexible to be able to follow limited deformations such as could be expected on dams subjected to normal settlement after construction. However, there was only one type of sand available at Harlingen and little was known not only about the required strength of the revetment but also of the strength of the asphalt material on which the determination of the thickness of the revetment would depend. It was, therefore, decided to build a short trial length on the site of the dam and as its performance was good during the following winter, the whole dam was built in its entire length during the next year and protected with the tested type of revetment, consisting of a single layer of sand asphalt, 40 cm. thick, between mean low water level and maximum high water level on the seaward slope, and 25 cm. thick on the remaining seaward slope, the crest and the harbour side of the dam. After consolidation of the sand asphalt revetment the whole surface was immediately covered with a seal coat of pure bitumen and finally finished with a thin surface dressing, including a rolled layer of sea shells to obtain a light colour of the surface. The result was good and the performance of the dam during the following years was satisfactory, but it was considered that the qualities of the asphalt layer could be improved. Consequently, work was started in laboratories and in actual practice to investigate all possible means of improving the quality of the asphalt material and of obtaining a better understanding of all factors involved in this matter.

This systematic development was based on the extension of existing research work related to other types of hydraulic problems covering the construction of large dams, reservoirs, river bank protection etc., carried out in various laboratories and also on improved methods of actual asphalt construction, either by means of manual labour or with mechnical equipment.

The scope of this paper does not permit a full description of the more scientific background of the asphalt techniques related to this problem, but a summarised description is given with reference to existing literature on the subject, which will show the student of this matter the way to a more fundamental study.

As is generally known, bitumen is a solid at low temperatures but on heating it is gradually transformed into a fluid state, whilst on cooling the reverse process takes place; expressed in more scientific terms, bitumen can be considered as a visco-elastic material.

In applied mechanics the characteristics of a purely elastic solid are defined by its modulus of elasticity, or Young's modulus, which indicates the linear relationship between stress and strain. But for a visco-elastic material this linear relationship is dependent on (a) the time of loading (for static loading conditions) or the frequency of loading (for dynamic loading conditions) and (b) the temperature. The influence of the temperature, or in other words the temperature susceptibility of a bitumen, is expressed by the "Penetration Index" or P.I. of the bitumen. By means of the inter-relationship between the loading, or frequency of loading, the ambient temperature and the P.I. of a bitumen, it has been possible to compose a nomograph from which the "stiffness modulus" of a bitumen (the equivalent value to the modulus of elasticity of a solid) can be determined under specific conditions of environment (5).

For design purposes of an asphalt hydraulic construction the engineer is, however, more concerned with the properties of a hot-mix asphalt construction consisting of mineral aggregates, filler and bitumen rather than with the performance of a pure bitumen. The relationship between the stiffness modulus of a hot-mix asphalt composition and that of a pure bitumen has been found to depend mainly on the concentration by volume of mineral aggregates in the asphalt mix. The stiffness modulus of various asphalt mixes has been determined.

It has also been possible to determine tensile, compressive and bending strengths of asphalt mixes by means of laboratory tests and here again the properties of the mix, depend, of course, on duration of loading and temperature (6).

Finally it has been found by fatigue tests that if the cycle of loading is repeated on asphalt mixes, the number of loadings to failure increases as the stresses decrease. The relationship between the number of repetitions of loading and the bending strength at fatigue rupture has been determined (6).

For the calculation of the dimensions of an asphalt facing on a dam subjected to dynamic forces by waves, reference can be made to a graphical method of determining bending stresses and corresponding deflections in hot-mix asphalt constructions. This method was devised by Odemark and Hogg and is based on the assumption that an asphalt revetment is virtually a flexible construction laid on and completely supported by a homogeneous, flexible sub-soil and is loaded repeatedly by a given pressure on a circular area. (7).

For the application of these graphs, it is therefore necessary to base the calculation on assumptions for the characteristics of the breaking waves. The properties of the asphalt layer, i.e. its modulus of stiffness and its designed thickness, as well as the modulas of elasticity of the sub-soil, should also be known.

The forces exerted by waves depend on a combination of factors, some of which are difficult to assess but can be found in existing literature. It seems reasonable to assume, that the striking area of a wave covers a surface, the diameter of which equals the amplitude of the wave, whereas the duration of its impact can be taken at 1/5 or 1/10 of a second. Assuming further a temperature of about 5°C, the modulus of stiffness of a hot-mix asphalt revetment will be of the order of 5×10^4 kg./sq.cm. If the asphalt revetment is laid on newly compacted sand, its modulus of elasticity can be taken at 100 kg./sq.cm.

Comparison of the bending stress, calculated as described above, with the bending strength of the hot-mix asphalt layer under repeated loading conditions will give an indication of the safety margin adopted for the design.

In connection with the stability of the core of fine sand supporting the asphalt facing the deflection of the asphalt layer should be limited to 1 mm. in which case a moist sand core will still retain its stability.

Although generally speaking, there need not be any fear as regards the creep of a properly designed hot-mix asphalt revetment on a comparatively flat slope under moderate atmospheric temperatures, it may be desirable to consider the plastic properties of the asphalt mix under somewhat more severe conditions that may, for instance, prevail in sub-tropical or tropical

countries. Under such conditions the methods of determining the characteristics of the asphalt mix can be compared with those applied in modern soil mechanics techniques for determining the properties of a soil in which, however, the soil/water system is replaced by an aggregate/bitumen system (6). By means of the triaxial test figures can be determined for:

(a) The angle of internal friction,
(b) The initial resistance, consisting partly of the true interlocking resistance of the aggregate particles and partly of the bituminous initial resistance,
and (c) The viscosity of the mass.

These properties of bituminous mixes are again partly dependent on their temperature. For given conditions of an asphalt facing on a slope of a dam it will be possible to determine the degree of stability if the internal friction and the initial resistance are known, besides of course, the thickness and the specific gravity of the asphalt revetment. In order to obtain equilibrium of the asphalt facing on a slope it is necessary that the difference between the shear stress due to the weight of the asphalt facing and the shear resistance due to its internal friction is at least balanced by the initial resistance of the asphalt material.

As an interesting example of the calculation of bending stresses in asphalt revetments on various constructions in Holland the following table indicates some essential figures required for this calculation. The table also shows the comparison between the calculated bending stresses in the asphalt facings and the actual bending strengths of the various types of asphalt compounds, as determined by fatigue tests (7). See Table 1.

The bending strengths were based on a storm lasting 36 hours during which the impact of waves was repeated about 1.1 x 10^4 times. It will be seen that there is good correlation between the calculations and the results in actual practice, since, after the storm, constructions I, II and III were undamaged, construction IV was of an underdesigned very lean sand asphalt and was heavily damaged, whilst construction V showed cracks as the critical value of the bending stress for a sand mastic was reached.

From various data on the determination of bending stresses it would seem that the following maximum bending strengths of the various asphalt materials can be adapted:

Asphaltic concrete	30 kg./sq.cm.
Lean sand asphalt	15 " " "
Very lean sand asphalt	7.5 " " "

. . In another case the deflections of asphalt revetments have been calculated according to the above mentioned methods and the following results were found:

Thickness of construction	A cm	a cm	p kg/cm^2	h/a	S kg/cm^2	E kg/cm^2	Deflection mm
North side 25 cm	75	37.5	0.25	0.57	70,000	100	0.267
35 cm	"	"	"	0.94	80,000	"	0.169
South side 25 cm	50	25	0.15	1.0	70,000	"	0.070
35 cm	"	"	"	1.4	80,000	"	0.048

In certain instances there may be a possibility of hydrostatic pressure developing underneath the asphalt facing where the height of saturation of the sand core of the dam by water due to prolonged high sea water levels, is not limited sufficiently by means of drainage. The equilibrium of the asphalt revetment is a simple matter of constructional design and is only referred to as an essential matter of design that can be solved either by providing adequate drainage or by providing sufficient weight and thickness to the covering asphalt layer.

If a dam or a dike is completely capped by an impervious asphalt construction, air pressure may develop in the core of the structure owing to a slight rise of the water level in the core. Since the asphalt cover is a plastic layer, it will be deformed by this pressure unless air vents are applied at intervals of 25 m. in the form of short steel pipes filled with precoated chippings.

ASPHALT CONSTRUCTION (1)

In asphalt dam construction work it has always been found essential to construct a top course as a dense impervious asphaltic concrete layer, whilst in recent years it has also been the aim of the designers to specify a dense base course instead of the more open graded sand asphalt mix which was originally laid. The improvement in technical quality is important as compared with the slight increase in cost of the total construction. In order to obtain the required density and impermeability of the two courses it is necessary to specify a figure for the density or else to specify limits for the void content in the compacted mixes. The present figures for void contents are 2 - 4% for the top course and a maximum of 10% for the base course.

Apart from the degree of compaction, the possibility of achieving tho required density depends naturally on the composition of the mix, determined by the grading of the aggregate material and filler, whilst the amount of bitumen is determined by tho quantity required to fill the voids in the compacted dry mix of aggregates and filler. An average type of composition for the two asphalt courses consists at present of:

Top Course:	42% crushed stone, 3 - 12 mm.
(Asphaltic concrete)	43% gradod sand finer than 2 mm.
	7% limestone filler
	8% bitumen 80/100
Base Course:	43% gravel, 5 - 20 mm.
Gravel sand asphalt)	43% graded sand finer than 2 mm.
	7% limestone filler
	7% bitumen

For asphalt mattresses or asphalt grouting work the sand mastic consists of approximately 75% sand, 10% limestone filler and 15% bitumen 80/100.

The reinforcement of asphalt mattresses can consist either of sisal nets of 10 cm. mesh and 6 mm. cord diameter or of flexible steel fabric of 10 cm. mesh and 2 mm. wire diameter.

An experimental average composition for asphalt ribs to reduce the uprush of waves consisted of:

43.8% crushed stono, 5-12 mm.
41.7% graded sand
8.1% limestone filler
6.4% bitumen 80/100

The asphalt ribs are applied without difficulty with a conventional type of curb-paver as used for roadwork; it is essential to apply a tack coat of a hard grade of bitumen on the sloping asphalt facing of the dam.

As for hydraulic works of various nature, such as large dams, reservoirs, canal linings, etc., the heating and mixing process of mineral aggregates, filler and bitumen is carried out in conventional types of mixing plants whilst the mix is generally transported to the site of laying by means of lorries as is current practice in roadwork. Contrary to normal practice in the construction of large dams of 40 m. height and more, as well as for the construction of reservoirs and head races leading to hydro-electric plants, where laying of the asphalt linings is generally carried out by means of mechanical equipment, such as road finishers or specially constructed spreador-boxes, it is the usual practice to lay asphalt facings on dams and dikes for coast

protection by manual labour. The reasons for this fact are twofold: firstly, the surface on which the base course of the asphalt facing is laid generally consists of sand that is, even after compaction, not sufficiently stable to support the weight of modern laying equipment and, secondly, the thickness to which the base course is laid varies from at least 20 cm. to 60 cm. or more at the foot of certain dams so the advantage of mechanical laying is reduced since not much hand labour is required to spread the material. The top course of dense, impervious asphaltic concrete is laid on a good, stable support to an average thickness of 10 cm. maximum and here, of course, there should be every reason for laying and rolling the surface with modern road surfacing equipment adapted to work on fairly flat slopes. So far little use has, however, been made of mechanical equipment and the quality of the work would certainly be improved, if hand labour were roplaced by machinery.

Compaction of a thick base course is generally achieved by hand tamping on a thick plank, where no other means of compaction could be more effective in reducing the percentage of voids in the finished asphalt layer. If the base course consists of better graded aggregates, good reason exists to apply a more effective method of compaction either by means of light vibrating single-wheel steel rollers, light motor rollers or by vibrating tampers. In the latter case compaction sheuld continue till no more tracks are seen on the asphalt surface.

It is necessary to obtain a good bond between the two asphalt courses and this can best be achieved by applying a tack coat of about 0.75 kg./sq.m. of a hard grade of bitumen while the asphalt base course is still warm. Before laying the top course the asphalt surface should be thoroughly oleaned in order to obtain good adhesion.

It is generally specified, that the joints between the asphalt areas finished at the end of a day and new work should be laid staggered in the two asphalt courses. Moreover, it is also normally specified that the joints should be painted with bitumen before the adjacent asphalt area is laid.

A seal coat of approximately 2 kg./sq.m. of a soft grade of bitumen should be applied while the asphaltic concrete top course is still warm and in any caso before it has been covered by water. Because algae do not adhere to pure bitumen; only the asphalt surface above normal high water level is covered with a very thin layer of heated gravel, sand or sea shells and compacted.

EXPERIENCE AND RECOMMENDATIONS

During the post-war years much experience has been gained on the construction of asphalt works for hydraulic purposes of various types and in many countries, and in connection with the application of asphalt facings to dams and dikes, it would seem of value to review the various essential items of construction and to summarise recommendations for future work.

(1) CORE OF THE DAM

There are certain advantages and disadvantages in building parallel retaining walls of clay, both from a constructional point of view as well as in relation to their function in the permanent structure. It hardly need be emphasised that the clay used for this purpose must retain its stability under water and be easy to apply; rich clay is therefore unsuitable, the more so because it has a tendency to crack when drying out. It is, therefore, prudent to specify that the clay should be of suitable quality containing not less than 30% fine sand.

The clay should also be able to resist temporary erosion by waves and currents until it is protected by the facing of the dam. It should be sufficiently cohesive to protect the sides of the sand core to a certain extent during the storms and on the other hand it should not be too rich as this will cause undue differences in the degree of settlement between the retaining walls and the sand of the core.

The surface of the clay retaining walls has generally to be partly covered by the asphalt facing and its rough surface will tend to increase the quantity of asphalt material necessary for the base course. Attention should be drawn to the fact that, especially if the hydraulic fill process is applied for the construction of the dam, drainage of water contained in the sand core is prevented by the clay retaining walls. For these reasons, and also because the required quantities of clay may not always be available, it is interesting to note that a sand asphalt containing not more than 3% bitumen can be used for this purpose. This lean sand asphalt mix can be dumped under water by means of bottom-door hopper barges, and it has been proved that it can resist a certain degree of water turbulence and current velocities up to at least 3 m. per second. In the last few years the use of colliery shale instead of clay has given satisfaction for the construction of these retaining walls.

(2) CONSTRUCTION OF THE FOOT

(a) If the foot of the dam below normal low water level is protected by a permeable type of construction, such as fascine mattresses, it is essential to apply a sheet piling to resist percolation of water through the sand formation. In certain circumstances it may be of advantage to lay a continuous drain or weep holes behind the sheet piling and in order to reduce the pressure against this sheet piling, it is desirable to provide a berm of 1 m. width between the sheet piling and the foot of the sloping facing.

(b) If, on the other hand, the foot of the dam below normal low water level is protected by an impervious and flexible reinforced sand mastic layer, it is good practice to lay the asphalt mattress against the sheet piling and to cover both with asphalt grouted rubble against which the sloping asphalt facing is laid.

(3) AIRVENTS

Airvents at intervals of 25 m. should be constructed in the crest of an asphalt capped dam or dike in the form of short steel pipes filled with precoated chippings if air pressure can be expected to develop underneath the asphalt cap.

(4) ASPHALT RIBS

Care should be taken that the composition of the asphalt ribs is based primarily on stability design and that a tack coat of a hard grade of bitumen is applied to obtain good adhesion of the ribs to the sloping asphalt facing of the dam.

(5) ASPHALT JOINTS

(a) It is desirable not to lay any horizontal asphalt joints under normal high water level or even better under the highest high water level.

(b) Asphalt joints in the two courses should be laid staggered.

(c) The cold surfaces of asphalt joints should be cut obliquely and coated with a thin layer of sand mastic before finishing the day's work; these surfaces should be thoroughly cleaned before the adjacent asphalt areas are laid.

(d) Under these conditions there is no need to increase the thickness of the asphalt facing at the joints as this only complicates the construction without increasing the strength or impermeability.

(6) TACK COAT

It is essential to apply a tack coat of 0.75 kg./sq.m. of a hard grade of bitumen on the base course while it is still warm; the asphalt surface should be thoroughly cleaned before applying the top course.

(7) SEAL COAT

Before the asphalt surface has cooled off and at any rate before it has been covered by water, the whole surface of the asphaltic concrete top course should be sealed by applying 2 kg./sq.m. of a soft grade of bitumen. In order to prevent the growth and adhesion of algae, which tend to cause cracks and curling up of this seal coat, the latter is not covered below normal high water mark. Above this level the seal coat is covered either with heated chippings, gravel sand or sea shells compacted by rolling, in order to render a light coloured surface. It should be mentioned that in several instances of construction of asphalt facings on large dams and reservoirs, it has been observed that a treatment of the asphalt surface with a cement wash, containing equal parts by weight of cement and water, at a rate of 2 kg./sq.m. was effective in preventing cracks in a bituminous seal coat caused by expansion and contraction idue to repeated wetting and drying of clay, silt or algae , which tend to cover the asphalt surface.

(8) COMPACTION

The method of compaction of the asphalt courses need not be specified, but it is essential that the courses possess the required density and impermeability; this can be achieved by specifying a void content for the asphaltic concrete top course of 2-4% and for the dense base course of a maximum of 10% by volume.

(9) CONTROL OF WORK

The quality of the asphalt construction should be controlled on the site in order to be able to adjust specifications or items of construction within a short period. Regular sieve analyses should be made of new supplies of mineral aggregates and filler, and the softening point and penetration of bitumen should be determined. Means should be available of determining the composition of the asphalt mixes, whilst the percentage of bitumen should be adjusted to fill the voids in the compacted dry mix of aggregate.

Regular control of the finished asphalt courses should also be arranged either by determining their density and impermeability in situ or else by taking samples and determining their density and impermeability in the field laboratory.

MODERN DESIGN AND CONSTRUCTION OF DAMS AND DIKES BUILT WITH THE USE OF ASPHALT

REFERENCES

(1) "Bitumen in Hydraulic Engineering" Volume I, by Baron W.F. van Asbeck, M.I.C.E. - Published by Shell International Petroleum Company Limited, London, 1959.

(2) "Modol Investigation on wave run-up carried out in the Netherlands during the past twenty years" by F. Wassing - Proceedings of Sixth Conference on Coastal Engineering, 1957.

(3) "Uber den Wellenauflauf bei Asphaltdeckwerken" by Ref.-Bauassessor F.F. Zitscher - Bitumen, No. 3, April, 1954.

(4) "Remmende invloed op golfoploop door ribbels op gesloten dijkbekleding" J.C. Jelgerhuis Swildens - De Ingenieur, No. 29, 1957.

(5) "A General System describing the Visco-Elastic Properties of Bitumens and its Relation to Routine Test Data" by C van der Poel - Journal of Applied Chemistry, Volume 4, Part 5, May, 1954 and published as Shell Bitumen Reprint No. 9.

(6) "Some Observations on the Properties of Bitumen/Mineral aggregate Mixtures in Relation to their Application in Hydraulic Works" by Dr. L.W. Nijboer - Translated from "De Ingenieur" No. 29, 1952 and published as Shell Bitumen Reprint No. 8.

(7) "Some Considerations in designing Bituminous Dike Revetments" by Dr. L.W. Nijboer - Translated from "De Ingenieur" No. 52, 1954 and published by the Royal Dutch/Shell Laboratory at Amsterdam.

CHAPTER 48

THE DEVELOPMENT OF COAST PROFILES ON A RECEDING COAST PROTECTED BY GROYNES

Torben Sørensen
Research Engineer, Coastal Engineering Laboratory
Technical University of Denmark, Copenhagen, Denmark

This paper presents an analysis of the longshore sand transport by waves and current on natural coasts outside the breaker zone. A tentative expression for the transport capacity is established and applied to the problem of the effect of groynes on the development of the coast profiles. It is shown that the results are consistent with the observed development of the Danish North Sea Coast at Thyborøn, which has been protected by groynes and closely observed through the last 60 years.

INTRODUCTION

When a continuously receding sandy coast is protected by groynes the immediate result is a considerable reduction of the rate of recession of the coastline chiefly due to a reduction in the beach drift. This fact is generally accepted and has been confirmed empirically under prototype conditions.

However some disagreement still seems to exist regarding the long term effect of groynes under the conditions mentioned above. Clearly, the groynes do not directly affect the sand transport at some distance seaward of the groynes and therefore erosion seaward of the groynes will continue to occur after the construction of the groynes. Since the coastline and the depth contours must eventually attain the same rate of movement some coastal engineers have drawn the conclusion that the effect of groynes on a receding coast will be of a temporary character only.

This reasoning is obviously rather superficial. A better understanding of the manner in which the coast profile develops after the construction of groynes may be obtained by considering the fundamental physical factors involved in the sand transport outside the breaker zone (the offshore bar).

FUNDAMENTAL CONSIDERATIONS

The water movement - The water movement close to the bed outside the breaker zone consists of an oscillatory motion in the direction of propagation of the waves and a longshore current. The current component in the direction perpendicular to the shore is of second order only and may be disregarded in this connection.

The longshore current may be due to a slope of the water surface along the coast caused by astronomical and/or storm tides, or it may be due to a longshore component of the wind shear stress on the water surface. The waves do not contribute essentially to the longshore current on a straight coast outside the breaker zone.

THE DEVELOPMENT OF COAST PROFILES ON A RECEDING COAST PROTECTED BY GROYNES

Under storm conditions the longshore gradient caused by the wind shear stress will often be much more important than the tidal gradient at depths well above the breaker depth - except, of course, when the wind is blowing approximately at a right angle to the shoreline. This is simply due to the fact that the wind gradient increases inversely proportional to the depth, whereas the tidal gradient remains constant over the entire coast profile. This is the reason for which the direction of the current under storm conditions is often determined by the direction of the wind at considerable distances from the coast irrespective of the tidal currents at larger depths.

The bed shear stresses. The problem of the shear stresses in the combined motion of waves and current is very complicated and still remains largely unsolved, qualitatively as well as quantitatively. It is known, however, that the boundary layer in the wave motion is quite thin, and therefore the maximum bed shear stress τ_w caused by the wave motion may be expressed by

$$\tau_w = \lambda_w \tfrac{1}{2} \rho U^2 \qquad (1)$$

in which U is the maximum orbital velocity at the bed as calculated by the irrotational theory. Little is known about the magnitude of the factor λ_w, but the available evidence indicates that it has a value of about 0,02.

The approximate value of 0,02 for λ_w implies that the shear stress exerted by a wave motion with the instantaneous bottom velocity U is several times greater than the shear stress exerted by a steady current with the mean velocity U.

The shear stress component due to the longshore current may be inferred directly from the tidal and wind gradients along the coast. At moderate depths this shear stress will usually be considerably smaller than the maximum wave shear stress under storm conditions.

The problem of a combination of waves and current has been analysed by professor H. Lundgren, chief of the Coastal Engineering Laboratory, Copenhagen, who found that the resulting maximum shear stresses may be found by superposition of the maximum wave shear stress and the constant longshore current shear stress. Qualitatively this superposition may be represented by fig. 1. The resulting maximum shear stress will only be slightly different from the maximum wave shear stress.

The direction of the maximum shear stress indicates the direction of the maximum particle velocity near the bed. This implies that for constant τ_w the velocity V of the longshore current is approximately proportional to the first power of the longshore current shear stress τ_c.

The sand transport function. Very little definite knowledge exists concerning the transport capacity of a combined wave and current motion. Therefore, the only way in which it is possible at present to establish a reasonably sound hypothetical relationship is to utilize the existing knowledge of sand transport in uniform open channel flow.

Using the terminology of R.A.Bagnold (1957) we will define the bed load grains as that part of the moving grains whose submerged weight is transferred to the bed as a grain stress in the dispersion near the bed. The suspended load grains are the grains whose settling through the water is balanced by the turbulent diffusion.

In the case of uniform grains with the diameter D and the specific gravity s Bagnold found that, when the bed shear stress τ_0 is large in terms of the stress unit $(s - 1)\gamma D$, the bed load transport and the suspended load transport are both proportional to $\tau_0^{3/2}$. Since $\tau_0^{1/2}$ represents the velocity of the fluid this result may be interpreted in the way that the load (the submerged weight of the moving grains per unit area of the bed) is proportional to τ_0 and that it moves with a velocity proportional to the mean fluid velocity. As far as the bed load is concerned this interpretation appears to be physically correct. With regard to the suspended load the question of the physical validity of this interpretation is impossible to answer as long as the nature of the transition between the bed load and the suspended load (the boundary condition of the suspended load) is unknown.

There can be little doubt that with regard to the bed load Bagnold's results are directly applicable to the case of combinations of waves and current. The role of the dispersed grains near the bed is simply to provide a means of transferring the shear stress τ_0 to stationary grains of the bed, and there seems to be no reason why this mechanism should be essentially different because of the comparatively slow variations in magnitude and direction of τ_0 in the presence of waves.

As stated above under storm conditions the maximum wave shear stress τ_w at moderate depths will usually be considerably larger than the longshore current shear stress τ_c. Consequently the major part of the bed load transport will occur when the bottom velocity in the wave motion passes its maximum. In accordance with Bagnold's results it may be assumed that the amount of bed load grains (measured by their submerged weight per unit area of the bed) may be represented by τ_w and that the mean longshore velocity of the bed load grains is proportional to the velocity V of the longshore current. By (1) the following expression for the bed load transport Q_b per unit width outside the breaker zone is obtained

$$Q_b \sim U^2 V \qquad (2)$$

The problem of suspended load transport in combinations of waves and current is considerably more complicated. Since the thickness of the boundary layer in a wave motion without a superposed current is only a small fraction of the water depth, the diffusion coefficient becomes very small at a short distance above the bed. Consequently the waves alone are unable to support any significant suspended load.

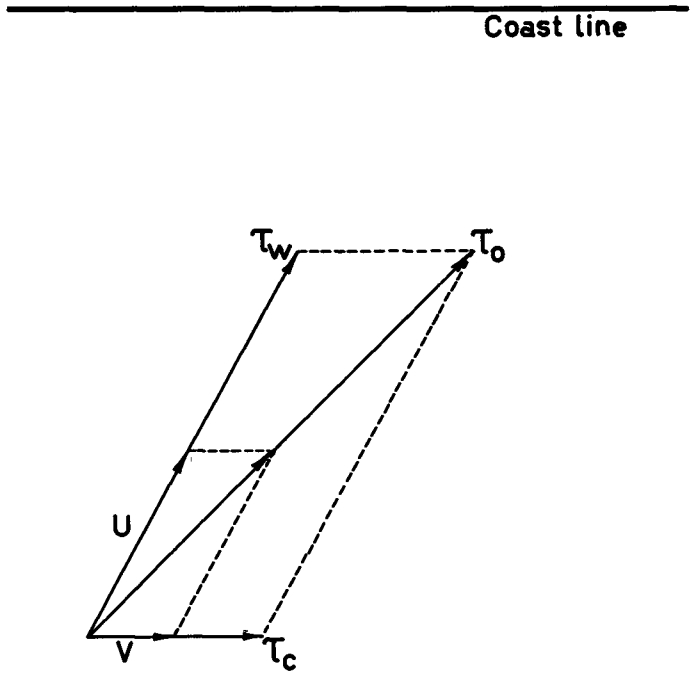

Fig. 1. Shear stresses in the combined motion of waves and current.

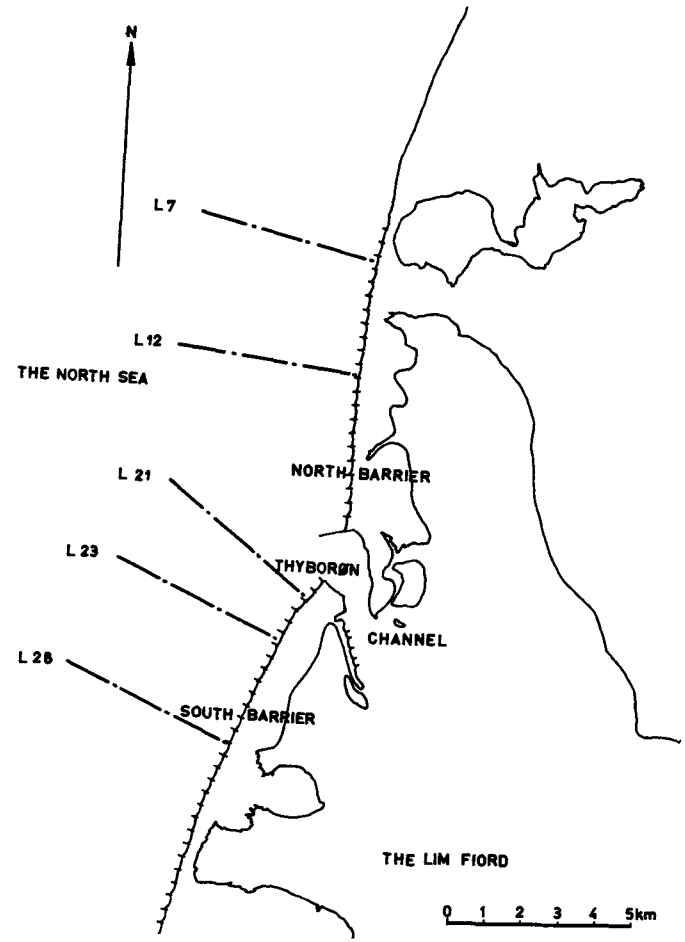

Fig. 2. Map of the Thyborøn Barriers.

The presence of the longshore current, however, implies that turbulent diffusion takes place over the entire depth and therefore suspended load can be maintained at any height over the bed.

According to the differential equation for the concentration of suspended grains the turbulence is able to carry any amount of suspend load as long as the turbulence is not conceivably attenuated by the presence of suspended material.

In the case of a combination of waves and current the bed load and the turbulence near the bed is mainly determined by the wave motion. Consequently, the concentration of suspended grains near the bed and therefore the magnitude of the concentration at any level is determined essentially by the wave motion. Applying the above mentioned interpretation of Bagnold's results we arrive at the conclusion that the total load of suspended grains should be approximately proportional to the wave shear stress τ_w. It must, however, be expected that the ratio of current shear stress to wave shear stress τ_c/τ_w has some influence on the magnitude of the suspended load, but within the limits of interest in the present paper the influence of this ratio should be slight.

Since the mean longshore velocity of the suspended grains must be proportional to the longshore current velocity $\bar{V}$, we obtain for the total transport rate Q_t of bed load and suspended load per unit width of the coast profile

$$Q_t \sim U^2 V \tag{3}$$

in which the factor of proportionality depends on the grain size D and the ratio τ_c/τ_w.

This relationship is a simple mathematical expression of the wel known fact that the waves put the sand into motion but the current determines the velocity and the direction of the transport.

The above expression (3) might, of course, have been given a dimensionless form by means of parameters similar to the ones used by Bagnold (1957). However, for the purposes of the present paper it is simpler to use the dimensional form (3).

THE INFLUENCE OF GROYNES ON THE COAST PROFILES

The significance of the longshore transport. Most of the previo work on coast profiles, whether in the laboratory or in the field, has been concerned mainly with the role of the transverse transport (onsho and offshore) in the shaping of the profiles. This transverse transpo has been shown to depend on the steepness of the attacking waves throu which it has been possible to explain the seasonal fluctuations of the profile shape, and it has even been possible to correlate profile fluctuations over periods of several years with variations in the frequency of strong onshore winds, Bruun (1954).

THE DEVELOPMENT OF COAST PROFILES ON A RECEDING COAST PROTECTED BY GROYNES

When groynes are built on a long, continuously receding sandy coast the recession of the coastline is immediately reduced and the coast profiles become steeper. Since the primary cause of the recession of the coast almost invariably is an increasing longshore transport capacity along the coast, it must quite obviously be expected that the long term development of the coast profiles will depend mainly on the manner in which the increasing steepness influences the longshore transport.

If it is assumed that no change in the meteorological conditions takes place the only change in the wave conditions outside the breaker zone due to an increase in the steepness of the coast profiles will be that the damping of the waves by bed friction during the travel from deep water to the breaker zone is reduced. Consequently, the average wave height just outside the breaker zone will be somewhat higher in the steeper profile so that the longshore transport capacity will be increased.

On the other hand the waves do not contribute materially to the longshore current which is caused almost exclusively by the longshore tidal and wind gradients. If the conditions at a certain depth before and after the increase in steepness are compared, the longshore gradients will be identical in the two cases. By fig.1 it may be seen that the longshore current velocity V caused by a certain longshore gradient τ_c depends on the wave shear stress τ_w in the following manner:

$$V \sim \frac{\tau_c}{\tau_w} \cdot \sqrt{\tau_o} \sim \frac{\tau_c}{\sqrt{\tau_w}} \sim \frac{\tau_c}{U} \qquad (4)$$

Thus, if the wave height is increased the longshore current velocity decreases.

The resulting relative increase in the longshore transport capacity by (3) becomes identical with the relative increase in U, which is the same as the relative increase in the wave height H.

Since the width of that part of the coast profile in which the steepness increases is usually rather small (a few kilometres) the increase in the average wave height and transport capacity corresponding to a substantial increase in the slope of the bed will normally be in the order of a few per cents only.

If we consider two coast profiles a unit length apart the annual depth increase at a certain depth d due to the difference ΔQ_t in transport capacity per unit width per year between the two profiles will equal ΔQ_t. When the steepness increases, ΔQ_t must obviously increase in the same rate as Q_t, that is, much more slowly than the steepness.

The rate of movement of the d m depth contour will be equal to $\Delta Q_t / \tan\alpha$, where $\tan\alpha$ is the slope of the bed at the depth d meters. It is evident from the above that this expression decreases with increasing steepness.

Thus, we are led to the conclusion that the effect of the groynes on the profile outside the breaker zone will be that the rate of movement of the depth contours will decrease, until it eventually becomes equal to the annual recession of the coastline.

The increasing steepness of the coast profile must, of course, be expected to influence the magnitude of the annual recession of the coastline. First, the average wave height will be greater in the steeper profile. Since the beach drift is probably proportional to about the 3rd power of the wave height an increase in the wave height of a few per cents may increase the coastline recession with 10-20%.

Second, the equilibrium between onshore and offshore sand movement, which might have existed before the construction of the groynes, will probably be disturbed by the increased steepness. There seems to be no way in which the importance of this factor can be evaluated theoretically. However, empirical evidence seems to indicate that the transverse transport is on the whole of very little importance with regard to the coastal erosion, and therefore this factor may generally be expected to be rather unimportant.

In conclusion it may be said that the effect of construction of groynes on a continuously receding sandy coast will be a permanent reduction of the rate of movement of the coastline. When the steeper equilibrium profiles of the protected coast have been reached, the annual recession of the coastline will probably be a little greater than shortly after the installment of the groynes, but still considerably less than that of the unprotected coast, depending on the efficiency of the groynes.

It is interesting to note that since the width of the coast profile decreases much more that the transport capacity increases when the steepness is increased, the total longshore transport will be less in the steeper profile. Thus, the groynes will reduce the longshore movement of sand over the entire coast profile, not only on the beach.

These results are confirmed conclusively by the development of the groyne protected North Sea coast of the Thyborøn Barriers in Denmark, which will be described briefly below.

COAST DEVELOPMENT ON THE THYBORØN BARRIERS

A detailed account of the coast development on the Thyborøn Barriers has been given by Bruun (1954).

The Thyborøn Barriers are located on the northern part of the Danish North Sea coast. A map showing the present shape of the coastline is given in fig. 2.

The Thyborøn Channel, which separates the North and South Barriers, connects the Limfjord, which has water surface of some 1200 km^2, with the North Sea. This channel was formed in 1862 during a severe gale. Since the tidal range at Thyborøn is very small - about 25 cm - the cross section of the channel is determined

by the flow under storm tide conditions. With strong westerly gales storm tides of more than 2 meters above MSL may occur accompanied by discharges of up to about 13.000 m^3/s in the channel.

The direction of the littoral drift on about 10 km of coastline on each side of the channel is towards the channel. Since the current in the channel during strong onshore winds is invariably ingoing, all the sand - about 800.000 m^3 per year - eroded on these 20 km of coast is carried through the channel to the shoals in the Limfjord.

The formation of the channel caused a strong erosion of the coast of the barries, which led to the construction of a system of heavy concrete groynes on these coasts around 1900. Since then the Board of Maritime Works has kept the development under close control by frequent soundings and measurements of the location of the coastline.

Fig.s 3 and 4 show some results of these observations for a typical stretch of the North and the South Barrier, respectively, at some distance from the channel. Similarly, fig. 5 represents the coast development off Thyborøn town on the northern end of the South Barrier. The location of these stretches is shown on fig. 2. The curves on fig.s 3, 4 and 5 represent the averages of the results of all measurements on the considered stretches. The results of a survey made in 1874 have been included to show the effects of the groynes on the coastline recession.

The dashed line in these figures is a plot of the location of the coastline as measured from the coastline in 1874. This shows that while the unprotected coast receded at a rate of about 10 meters per year, the rate of recession after the construction of groynes has been only about 2 meters per year. Although the measurements of the location of the coastline - which are very numerous - have been smoothed considerably before plotting, the movement of the coastline is still somewhat irregular. It is not possible in the later years to detect any tendency towards a general acceleration of the coast recession that may be distinguished from the irregular variations that have previously occured.

The full line are plots of the distances from the coastline at the time of the sounding to the 6, 8 and 10 meter depth contours. Thus, the vertical distances between these lines directly represent the reciprocal value of the slope of the bed.

The slope of the bed at the 8 m depth contour has now increased to about twice the original value or more since the construction of the groynes about 1900. This has been accompanied by a very marked stabilization of the distance to the 6 m depth contour, and the figures also show a more or less clear tendency towards a general reduction in the rate of movement of the 8 m contour relative to the coastline. On the whole, there seems to be no doubt that the profiles are now approaching their equilibrium shape up to depths of 9 to 10 meters.

A calculation of the wave attenuation by bed friction according to (1) for a 3 meter high wave with a period of 8 seconds and an angle of incidence of 45° has been made to illustrate the influence of the profile development on the wave heights. The result was, that while this wave, which is quite representative of a medium strong gale at Thyborøn, would in 1900 lose 11% of its height travelling from a depth of 20 meters to the 6 meter contour, it would between the same depth contours in 1950 lose only 6%.

According to the previous analysis a change in the wave height of this magnitude should involve an increase in the average annual erosion of 5%. Since the slope of the bed has been doubled in the same period, the (absolute) rate of movement of the 6 meter contour

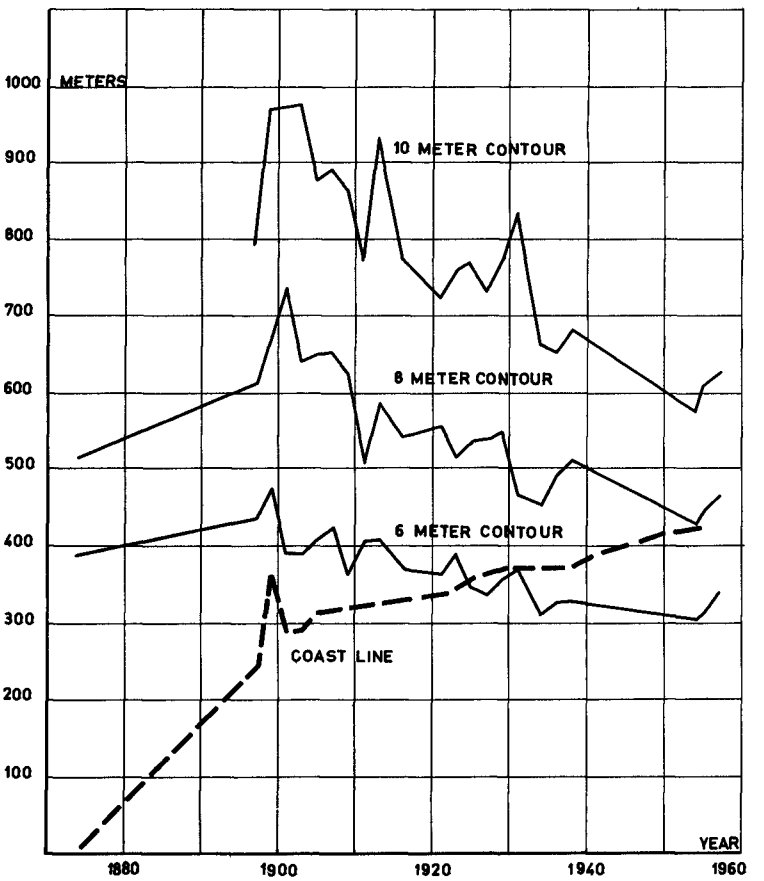

Fig. 3. Coast development on the North Barrier between L 12. Full lines show variation of distances from the coastline to various depth contours. Dashed line is a plot of the distance from the coastline to the original coastline in 1874.

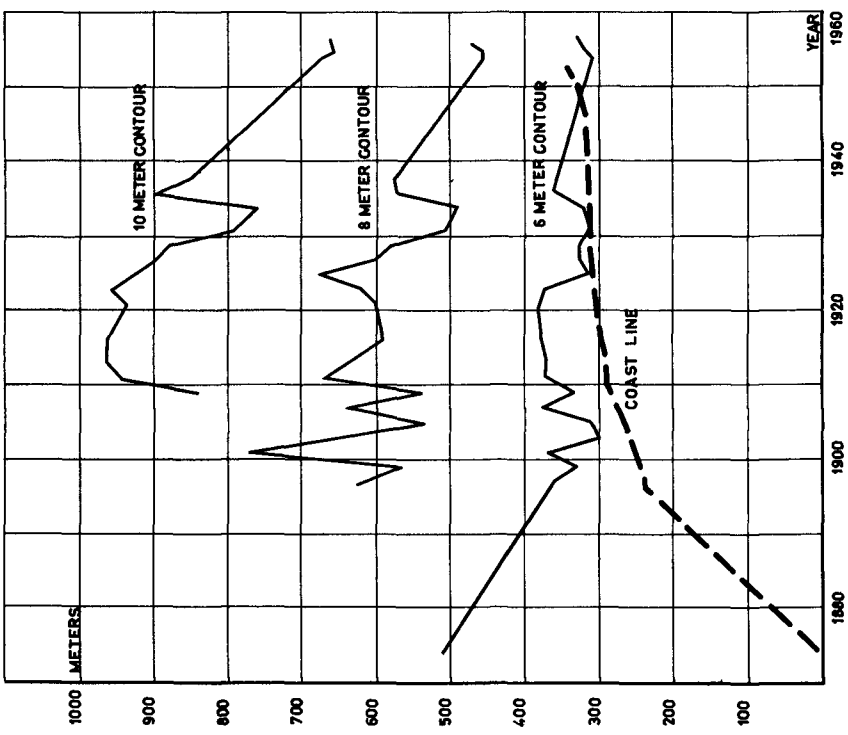

Fig. 4. Coast development on the South Barrier between L 23 and L 28.

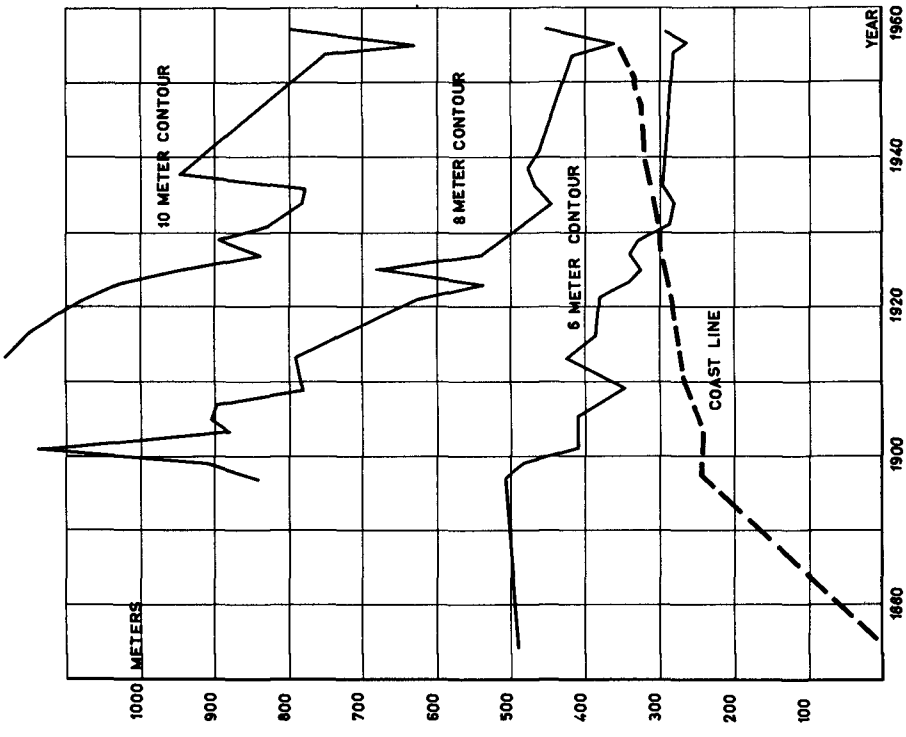

Fig. 5. Coast development on the South Barrier between L 21 and L 23.

should be expected to have been reduced by a little less than half of its original value. Because of the fact that the coastline also recedes, the reduction in the annual recession of the 6 m contour relative to the coastline should be considerably larger, which has, in fact, also been the case.

It is remarkable that the increase in steepness of the coast profiles has not caused any conceivable acceleration of the movement of the coastline. This may possibly be due to the fact that, as the coast recedes, the groynes are becoming longer, although the outer ends of the groynes are now submerged.

MODEL TESTS

The problem of the coast development on the Thyborøn Barriers has been investigated in a scale model at the Waterloopkundig Laboratorium De Voorst, Holland, for the Danish Board of Maritime Works. The results of this investigation has been that the coast recession would in the future be reduced to a lower value than the present one. In all probability, however, this result must be attributed to the fact that in the model the outer ends of the groynes were maintained in their original position, so that the coast protection in the model was more effective than in the prototype.

The main point is that the model gives no indication of any significant future increase in the coast recession, in which it agrees completely with the results of the analysis in this paper.

CONCLUSION

The construction of groynes on a continuously receding sandy coast will cause a permanent reduction of the rate of recession of the coastline. The groynes reduce the longshore sand transport not only on the beach, but also, indirectly, over the entire coast profiles. The shape of the equilibrium profile of the protected coast is determined almost exclusively by the longshore transport and the efficiency of the groynes.

ACKNOWLEDGMENTS

The author is indebted to professor, dr.techn. H. Lundgren, chief of the Coastal Engineering Laboratory, Copenhagen, for his support in the preparation of the present paper. Furthermore he is indebted to the Danish Board of Maritime Works for the opportunity to gain access to the data from the coast at Thyborøn.

REFERENCES

Bagnold, R. A. (1957). The flow of cohesionless grains in fluids: Philosophical Transactions of the Royal Society of London, Series A, vol. 249, pp. 235 - 297.

Bruun, P. (1954). Coast Stability. Copenhagen 1954.

CHAPTER 49

BEACH-REHABILITATION BY USE OF BEACH FILLS AND FURTHER PLANS FOR THE PROTECTION OF THE ISLAND OF NORDERNEY

Johann Kramer
Regierungsbaurat
Forschungsstelle Norderney
Norderney, Germany

INTRODUCTION

The Island of Norderney is one of the East-frisian Islands, situated at the southern coast of the North Sea (Figure 1). It arose out of the sea, which will say that it is not the remainder of an old mainland. In the beginning there was a shoal, moulded by tide currents and wave action where later on various plants enabled the growth of sand dunes. The East-frisian Islands are supposed to exist since more than 1000 years already. But the written history dates back as far as to the 14th century only. From charts and other historical documents we know in which way these islands changed during the centuries. Some islands vanished whilst others only changed their positions.

At the beginning of the 19th century, when Norderney became a seaside resort, the village was still protected by a wall of sand dunes against the assault of the open sea. In the course of time, however, the western part of the island got lost by erosion and the sand dunes were destroyed (Figure 3). When in the middle of the nineteenth century the seaside resort, which had grown larger and larger in the meantime, threatened to be attacked by the sea, people began to protect their island. In the year 1856 they had built a seawall to the length of 900 metres. As at its ends the dunes were still destroyed, this revetment had to be extended. Moreover groynes had to be built to prevent the development of narrow channels in front of the seawall, which might have caused its destruction. Thus in the course of nearly 100 years the revetments as shown in figure 2 were founded.

There are now nearly 6 km of seawalls of different types. In former times the walls were built much steeper than now-a-days. The groynes changed their shapes as well. The building material altered according to the respective level of technology. Material applied was wood, stone, concrete as well as steel and asphalt.

During the years 1940 to 1948 the revetments could not be maintained. The beach had lost much of its height. Therefore the seawalls and the groynes were to a high degree exposed to the violent attack of the waves. In order to avoid further destruction something had to be done. The protection works represented at this time investments of a value of about 40 million DM. After various inquiries had been started, a filling of the beach seemed to be the most profitable way.

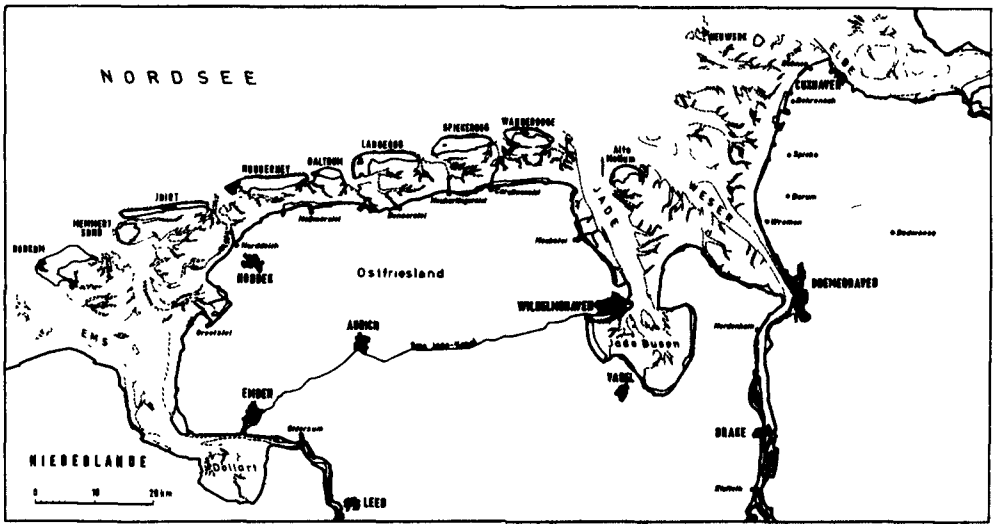

Fig. 1 Location map.

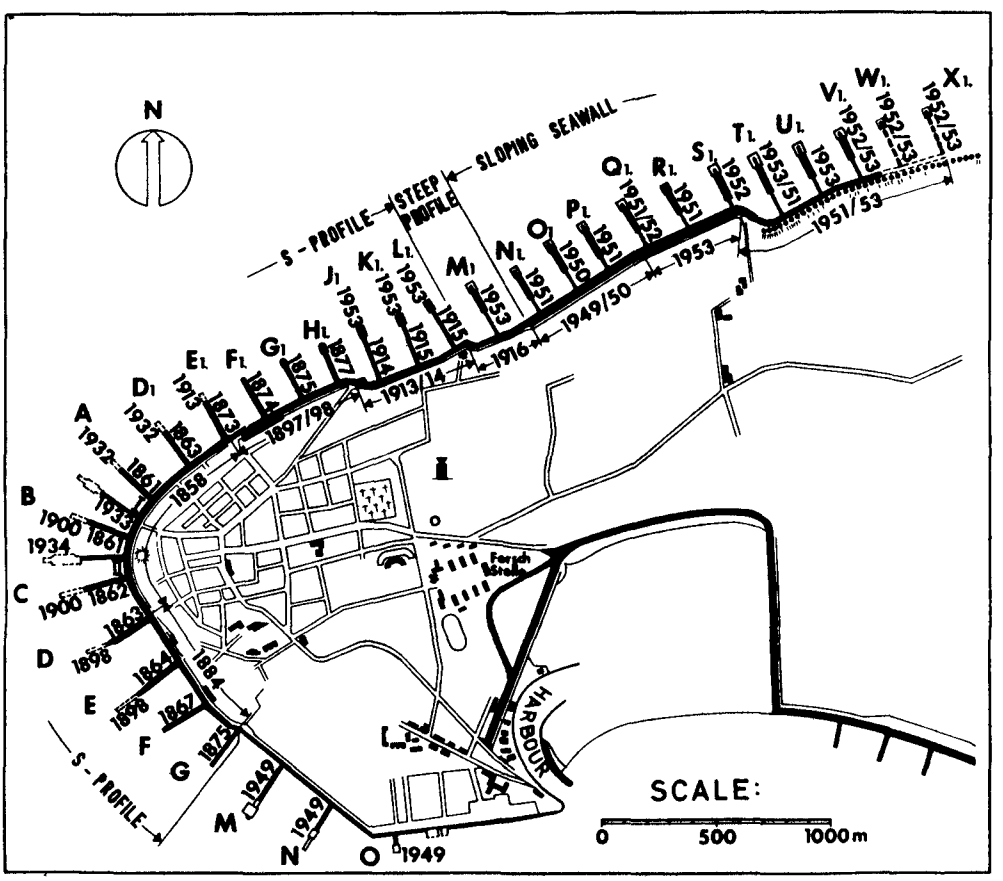

Fig. 2 Development of the revetments on Norderney.

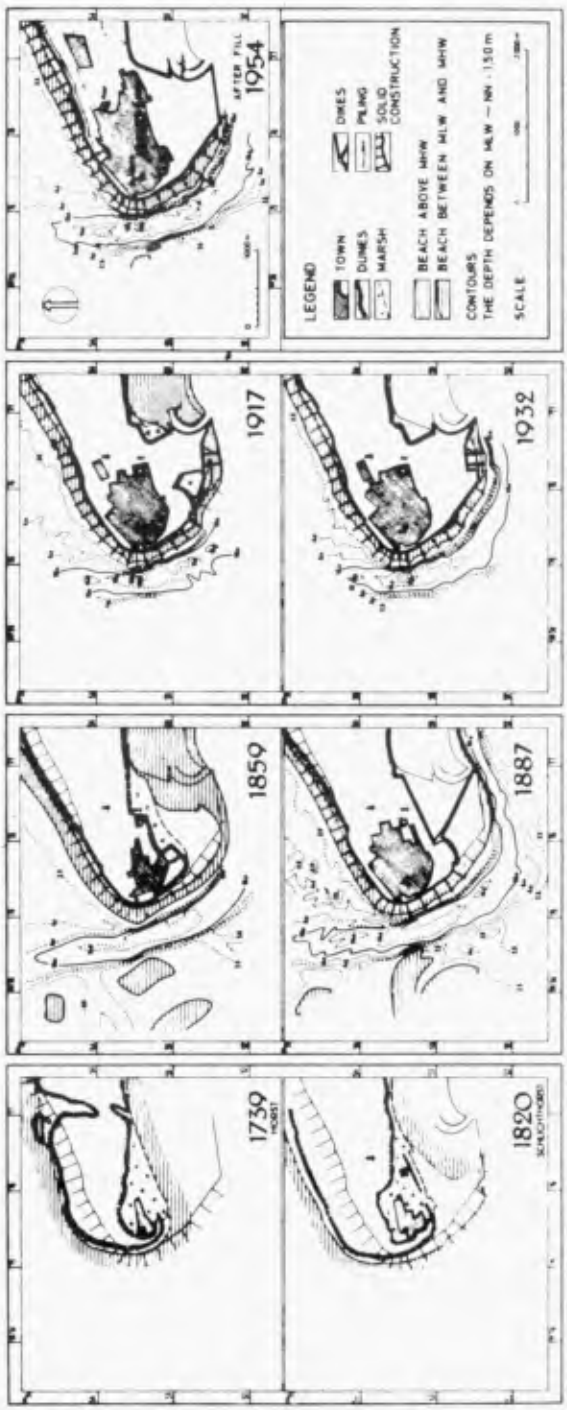

Fig. 3 Development of the beach at the western part of Norderney 1739 - 1954.

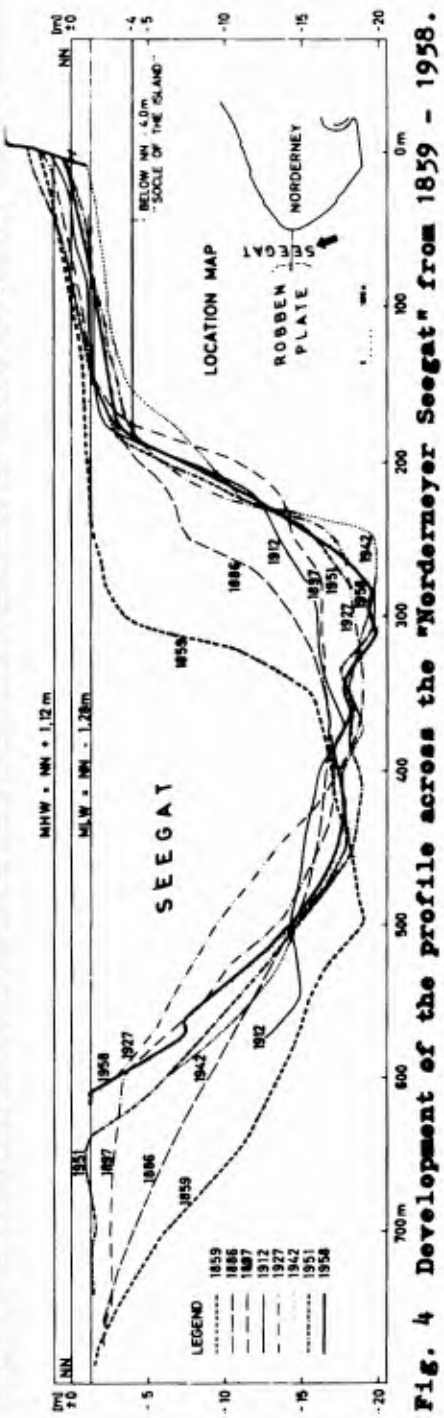

Fig. 4 Development of the profile across the "Norderneyer Seegat" from 1859 - 1958.

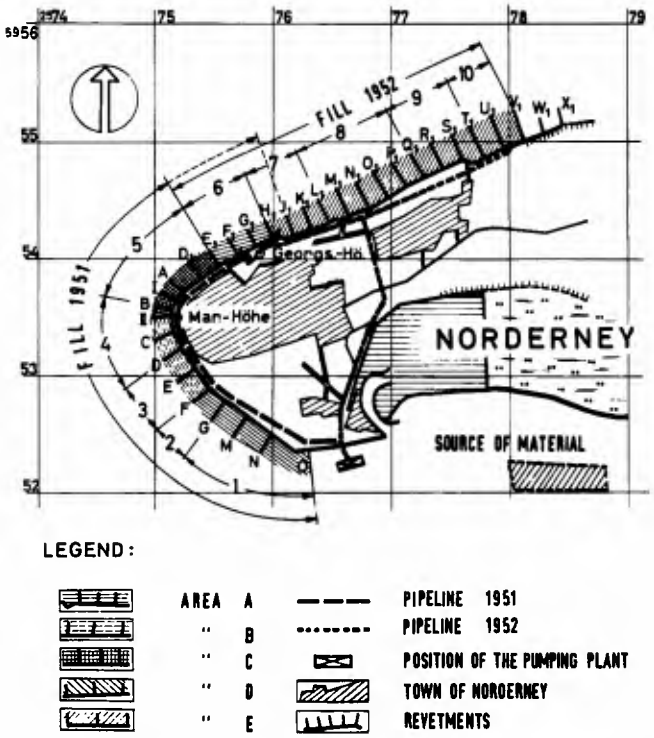

Fig. 5. Fill 1851/52. Location map of the source of material, of the pumping plant with the pipeline, and of the areas 1 to 10 of equal development.

Fig. 6. The beach after the 1951 fill at the western part of Norderney.

BEACH-REHABILITATION BY USE OF BEACH FILLS AND FURTHER PLANS FOR THE PROTECTION OF THE ISLAND OF NORDERNEY

THE FILLING OF THE BEACH 1951/52

QUANTITY OF SAND NECESSARY AND TECHNICAL WAY OF TRANSPORTING IT

The beach fill of Norderney entirely differs from the traditional way of protecting islands by seawalls and groynes. The idea of filling the beach was rather extraordinary - even to a great number of experts. The success was expected to be limited, because the natural powers remained dominant. Their destroying effects could only be lessened but never eliminated or overcome. The filling of beaches was something entirely new at the German coast.

In order to evaluate the quantity of sand necessary for filling the beach, the surveys of the beach from 1897 to 1950 were considered. Those were the years when long groynes had begun to stabilize the foot of the island (Figure 4). 1.077.000 m^3 of sand had been carried off during the years 1930 to 1950 above 5 m below mean level. After the filling the estimated yearly loss of sand would run up to about 90.000 m^3. It was necessary to restore the beach to the height of 1900. About 1.240.000 m^3 sand were needed for this purpose. Nearly 1.550.000 m^3 of sand had to be dredged adding a certain quantity which would be lost during the transport and the filling process.

The sand was dredged by two bucket dredgers south-east of the harbour (Figure 5) and transported with barges to the pumping plant where mixed in the proportion 1 : 6 sand and water were pumped through a discharge pipe having a diameter of 60 to 70 cm. In order to reach the farther places - about 5 km distance - a booster pump was necessary.

Soon the most suitable way of filling the beach between the groynes was found out. The mixture of sand and water was let out of the pipe mouth coming down from the revetment. When the intended level at the low water line was reached, a device was applied which spread the pumped soil over the whole breadth of the beach between the groynes. Thus the area was equally filled and soon a 100-metre-wide beach above high water level was completed (Figure 6). During the following winter it was lost already, because the destroying influence of the littoral current was far too strong.

THE DEVELOPMENT OF THE BEACH 1951/52

Before the fillings were started, careful observations of the beach were undertaken. Afterwards the following observations were regularly repeated:

1. Surveys of the beach and foreshore down to below mean level.

2. Annual photos of the beach in fixed directions.

3. Analyses of the grains of sand taken from around the

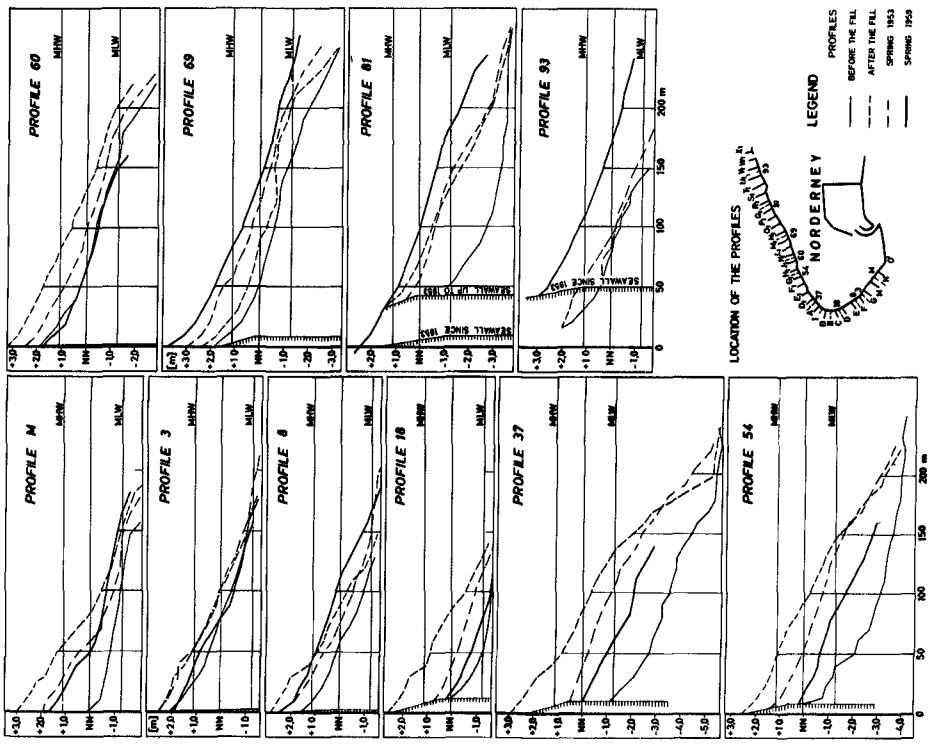

Fig. 8. Change of the beach profiles from after the fill 1951/52 to 1959.

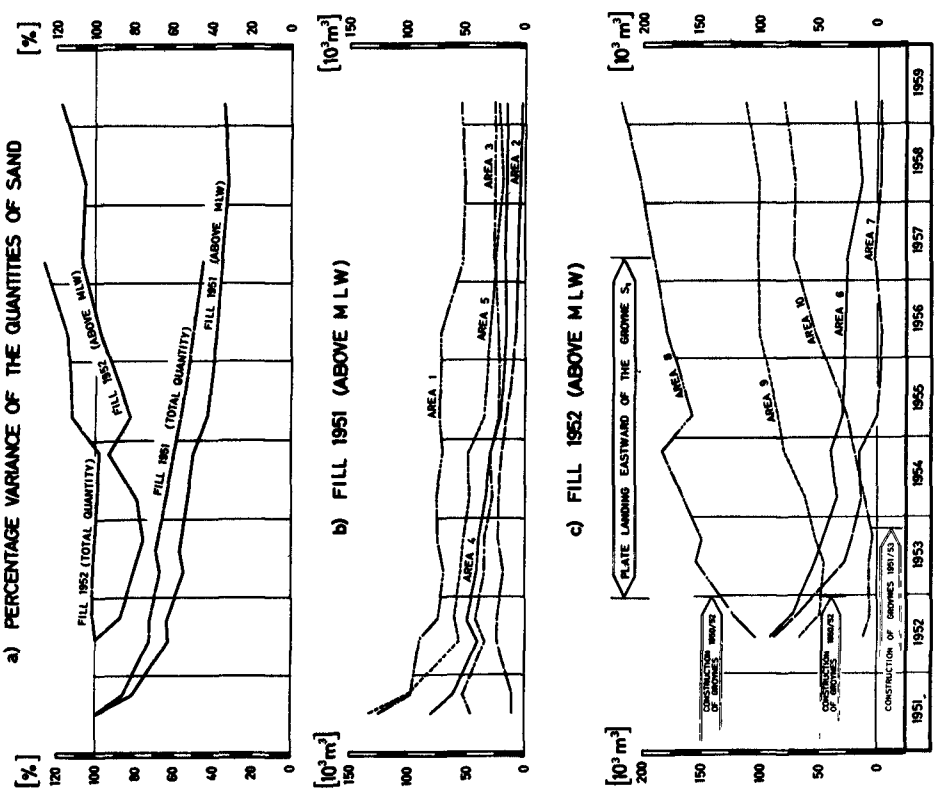

Fig. 7. Change of the quantities of sand on the beach after the fill 1951/52

dredging area and from the beach after the filling.

The filled beach areas can be divided into areas of equal development. The entire quantities of sand brought on to the beach are as follow:

Area of filling 1951: 1.050.000 m^3
Area of filling 1952: 770.000 m^3.

In figure 7 the results of the calculations for the quantities of sand are represented:

a) The percentage development of the filling 1951 and 1952. The quantity of sand that had been left within the area 1 to 5 as well as 6 to 10 immediately after the filling have been regarded as 100%.

b) The change of the quantities of sand within the areas 1 to 5 in absolute figures.

c) The change of the amount of sand within the areas 6 to 10 in absolute figures. Moreover the period of the landing of the sandbank at the northern beach as well as the completion of the groynes in the areas 8 to 10 have been recorded in order to recognize their influence on the development of the beach.

This representation shows that, in the beginning, the fill 1951 has been carried off much more quickly than later on. During the first weeks and months the unnaturally steep beach above mean level which was highly exposed to the attack of the wave action decreased to a large extent. Since 1953 an almost uniform decrease of the beach was observed. There has always been a difference between the development in summer- and wintertimes during the last years.

In the years meanwhile gone by, the filled beach has developed in different ways. In the area of the filling of 1951 nearly 34% of the material above the mean level were still left. The large increase of sand in the areas 8 to 10 is not necessarily the consequence of the filling but refers to a sandbank which landed there at the same time. Besides that the achievement of the groynes must be considered. It is easily recognized that the increase of the beach starts as well with the beginning of the landing of the sandbank in the areas 8, 9 and 10 as with the approximate completion of the groynes. Therefore it is impossible to discriminate the influence of the landing of the bank and the effect of the groynes from the development of the eastward beach. To separate these two factors will be possible only in the course of several years, when the effects of the last landing of the shoal will be gone or when perhaps a new one will have appeared. Till now it was not possible to see a relation between the tidal effects and the erosion of the beach.

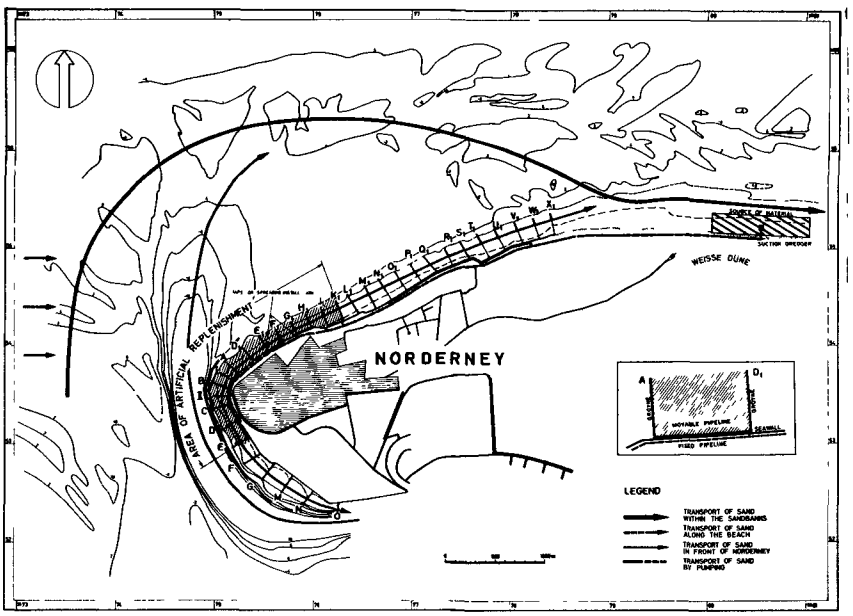

Fig. 9. Natural movement of the sand in front of Norderney and artificial transport at the northwestern part of the island.

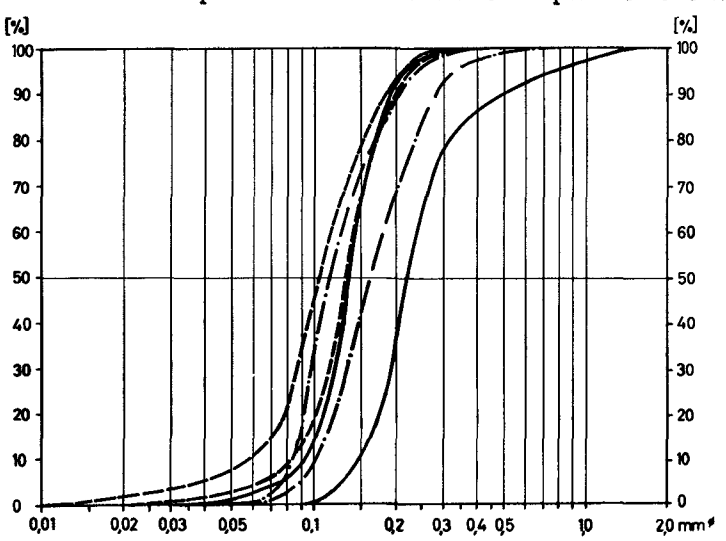

SOURCE OF MATERIAL 1951 "HOHES RIFF"
NATURAL POSITION AT THE WESTERN PART OF THE ISLAND 1957
SOURCE OF MATERIAL "WEISSE DÜNE"

Fig. 10. Size of the sands.

BEACH-REHABILITATION BY USE OF BEACH FILLS AND FURTHER PLANS FOR THE PROTECTION OF THE ISLAND OF NORDERNEY

Some of the beach-profiles measured once a year that are characteristic for certain areas are shown in figure 8. They represent the beach-height in 4 different periods:

1. Beach-height before the filling,

2. Beach-height after the filling of 1951/52,

3. Beach-height in spring 1953, after large quantities have been carried off from the unnaturally high beach,

4. Beach-height in spring 1959.

By means of samples the variations of the grain composition of the filled material could be defined. Two months after the filling the finer material had been washed out already. In summer 1957 the composition of the material did no more differ from that of the natural beach.

THE RESULTS OF THE BEACH-FILL 1951/52

The summarized results are as follow:

In 1951/52 a quantity of 1.816.500 m^3 of sand was filled in between the groynes 0 to V1, the beach gained the amount of 1.245.500 m^3, 571.000 m^3 were lost during the filling, the loss amounts to 31%.

The expenditure of 3,5 million DM for the fill of the beach compared with its efficiency results in a full success, technically as well as economically. On the whole it is a profitable way to protect the island.

A certain loss of the filling material had to be considered in any case, for the natural powers could not be influenced by the fill. In fact the annual loss dimishes with the decrease of the beach height. With the present height, however, a limit is reached below which the seawalls are no longer sufficiently covered with sand. This state demands a decision about future protection works.

THE PLAN OF A CONTINUOUS FILL

INTENSIFICATION OF THE INSUFFICIENT NATURAL SUPPLY OF SAND BY ARTIFICIAL MEANS

Beach stability is possible only, when the supply of drift sand and of eroded material is balanced. In front of Norderney the littoral drift is insufficient. It takes its way as demonstrated in figure 9. The eastward drifted sand moves towards the sea inlet in front of Norderney, where it is directed into a curve within the belt of shoals. The direction of the littoral drift is a result of the tide-currents along the islands which are mainly west-eastward directed and of the

ebbstream in the deep channel in front of Norderney which turns northward. The sand from the belt of shoals is drifted towards the northern beach of the island about 3,5 km eastward of the western point. A great portion of it is transported to the east by the tide-currents and the wind, the remainder moves towards the western groynes H1 - J1. This supply is not nearly sufficient to balance the loss caused by erosion. The beach following westward is losing sand by erosion permanently, because the quantities arriving from the belt of shoals are too small to compensate the eroding material.

After the revetments had been built, the dunes were saved from further destruction. Since 1900 especially long groynes helped to stabilize the foot of the island below - 4 m mean level. The beach above this line up to the toe of the seawall could not be held, because the groynes did not show the expected efficiency in the area where the sand is carried off mainly by wave action.

The bases for an artificial fill are these:

1. The sand from the littoral drift along the coast moves eastward towards the eastern end of the revetments.

2. The accreation at the beach of the western part of Norderney is not nearly sufficient to balance the decrease there. The beach erosion is limited to the area from the toe of the seawall down to the line of 4 m below mean level.

3. The sand material eroding from the beach is transported to the belt of shoals and from there to the eastern part of the island. If the sand from the accretion area were pumped to the eroding areas, a circulation could be achieved.

4. In order to avoid that the decrease of the beach becomes still greater than it is now, the revetments must necessarily be kept in the present state.

QUANTITIES OF MATERIAL NECESSARY FOR A FILL

From the results of the filling 1951/52 we can see that in order to reach a worthwhile stability by an artificial fill the following points must be considered:

1. The grain of the sand must be equal or even coarser than that of the natural beach. The coarser the grain is, the more slowly will the eroding effects come into action.

2. The beach must not be higher than necessary for its task, so that the erosion caused by high tides is the lowest possible.

3. The incline of the filled beach should correspond with that of a natural beach in order to avoid unnecessary decrease.

The place from where the sand is to be taken for future fills (Figure 10) belongs to an area where the sand on an average has a coarser grain than that of the beach which is to be filled.

From experience gained by the beach-filling 1951/52 we learned that highly raised beaches which in conclusion will have an extraordinarily high decrease can be avoided, when the artificial fill is not done in long intervals, because this accomplishment demands a relative high fill to balance up the high cost related to a replenishment of this kind. When the beach is filled every year, so that its height is sufficient to protect the island, the decrease can be kept down to a small extent.

The movement of sand at the beach after the fill 1951/52 can be used as a foundation to find out the most suitable height of the beach. The height in spring 1953 should be sufficient, for its meets the following conditions:

1. At the western and the north-western beach of the island, where an artificial fill is needed, the toe of the seawall and the groynes were sufficiently covered with sand to full-fill its protection purpose.

2. The incline of the beach is nearly the same as the natural one.

3. The height of the beach at the toe of the seawall is below normal high-tide, so that the decrease of sand caused by wave-action is kept down, even when the tide is raised by a storm.

Another reason why the height of the beach of 1953 is so favourable is the fact that from 1953 the decrease of sand is almost uniform every year. On an average the loss from 1953 to 1957 amounted to about 53.000 m^3 at the areas 1 to 6 which needed replenishment. If this quantity of sand could be refilled every year, it is probable that within limited oscillations caused by the change of meteorological conditions the beach might be kept at a permanent height. An increase of 60.000 m^3 of sand annually would be sufficient.

A certain loss during the refill must be considered, because a part of the mixture of sand and water spread on to the beach moves immediately off towards the sea. Experience shows that this loss will run up to about 35%. Consequently 80.000 m^3 of sand would have to be transported every year.

An annual amount of 80.000 m^3 would be most suitable, because this quantity could easily be managed by a permanent pumping plant which must always be ready for action to balance a sudden decrease of sand, for, as soon as the idea of installing a permanent pumping plant has become reality, the security of the island would depend on the artificial replenishment of

the beach.

The sand will be derived from the east of the island where permanent natural accretion is given. This accretion amounts to at least 130.000 m^3 yearly - probably even 250.000 m^3.

The material transported from east to west erodes and moves back to the belt of shoals and finally reaches its source again (Figure 9). Thus a new circulation is created, which runs beside the vast movements of large sand-masses in the sea in front of Norderney. It is not likely that the artificial decrease of sand will have any bad influence on the eastward beach areas, for the quantity needed every year is only a small portion of the sand derived from the belt of shoals. In order to reach the beach height of 1953 again, which should be the aim of the continuous fill, it will be necessary to transport more than 80.000 m^3 during the first years.

Practise will at all events differ from theory. Today we cannot tell, but the quantity necessary might be much lesser than estimated, because the sand for future fills will be much coarser than the material on the beach to be filled. This fact seems to be an important factor to slow up erosion.

The technical construction of the pumping plant cannot be detailed here. It is true that beach-fillings with the aid of pumping plants are most favourable. The sand might be won with a scraper or a suction dredger. Four booster-pumps will forward the material from the scraper or suction dredger to the western part of the island.

By the way of continuous working the process could be automatized to a high degree, so that the number of workers and consequently the costs could be kept down to a reasonable level. The costs of a fixed establishment are low in comparison with other propositions concerning the permanent security of the island.

REFERENCES

Akkermann,M. (1956). Die Umlagerungen des Sandes im Seegebiet vor Norderney und auf der Insel: Jahresber. 1955, Bd. VII, Forschungsstelle Norderney.

Arbeitsgruppe Norderney des Küstenausschusses Nord- und Ostsee (1952). Gutachtliche Stellungnahme zu den Untersuchungen über die Ursachen der Abbruchserscheinungen am West- und Nordweststrand der Insel Norderney sowie zu den zum Schutze der Insel vorgeschlagenen bautechnischen Maßnahmen: Jg. 1, H. 1, Die Küste.

Forschungsstelle Norderney (1949). Die Ursachen der Abbruchserscheinungen am West- und Nordweststrand der Insel Norderney und die Beurteilung der zum Schutz der Insel

vorgeschlagenen bautechnischen Maßnahmen: Jahresber. 1949, Bd. I, Forschungsstelle Norderney.

Fülscher (1905). Über Schutzbauten zur Erhaltung der ost- und nordfriesischen Inseln: Berlin.

Gaye, J. (1934). Entwicklung und Erhaltung der ostfriesischen Inseln: H. 22, Zentralbl. d. Bauverw.

Gaye, J. und Walther, F. (1935). Die Wanderung der Sandriffe vor den ostfriesischen Inseln. H. 41, Die Bautechnik.

Gaye, J. und Walther, F. (1929). Bericht über Schutzbauten zur Erhaltung der ostfriesischen Inseln Juist, Norderney, Baltrum, Langeoog und Spiekeroog in der Zeit von 1900 bis 1928: Norden/ Norderney.

Hannoversche Versuchsanstalt für Grundbau und Wasserbau (1957). Modellversuche für die Verlängerung der Buhne E.

Homeier, H. und Kramer J. (1956). Verlagerung der Platen im Riffbogen vor Norderney und ihre Anlandung an den Strand: Jahresber. 1956, Bd. VIII, Forschungsstelle Norderney.

Köritz, D. (1954). Quantitative Untersuchung der Wasservertriftung über das Juister Watt: Jahresber. 1954, Bd. VI, Forschungsstelle Norderney.

Kramer, J. (1957). Künstliche Wiederherstellung von Stränden unter besonderer Berücksichtigung der Strandaufspülung Norderney 1951/52: Jahresber. 1957, Bd. IX, Forschungsstelle Norderney.

Kramer, J. (1954). Die Auswirkung der Inselschutzwerke auf die Strandentwicklung im Westteil von Norderney: Jahresber. 1954, Bd. VI, Forschungsstelle Norderney.

Peper, G. (1955/56). Die Entstehung und Entwicklung der Inselschutzwerke auf Norderney mit besonderer Berücksichtigung der Bauten der letzten Jahre: Bd. 8, H. 3, N. Arch. Niedersachsen.

Thilo, R. und Kurzak, G. (1952). Die Ursachen der Abbruchserscheinungen am West- und Nordweststrand der Insel Norderney: Jg. 1, H. 1, Die Küste.

CHAPTER 50

SHORELINE ADVANCEMENT BY SEA WALL AND GROYNES AT COCHIN

M. G. Hiranandani
and

C. V. Gole
Central Water & Power Research Station
Poona, India

1. INTRODUCTION

In the paper "Some coastal engineering problems in India" presented at the VIth Conference on Coastal Engineering, a mention has been made about experimental protective measures consisting of one mile long sea wall and groynes adopted for giving protection to the coast near Cochin. The protective works mentioned in the above paper are now in operation for the last five years. As there are no major rivers there is very little littoral drift along this coast. The material eroded from the coast forms the main source of littoral transport.

The data regarding high water and low water marks along the coast have been recorded, and statistically analysed to assess the efficiency of these measures in respect of shoreline advancement. Results are discussed in the paper.

Some experiments have also been carried out in the prototype for a sea wall with bituminous grouting. Behaviour of this type of sea wall has also been discussed in the paper.

Since the construction of the experimental measures, protective measures in the shape of either sea wall or sea walls with groynes have been further extended to a 10 mile long reach of the coast. The results of these new works, experiments carried out in a model for evolving the design of protective measures and model limitations have also been included. Fig. 1 shows the plan of the sea wall and groynes in one mile experimental reach.

2. ANALYSIS OF DATA

Since December 1955, among other observations, high water (HW) and low water (LW) distances have been recorded from a fixed base line along the protected coast, at three positions, viz - centre,

north and south extremities of each of the nine compartments formed by ten groynes.

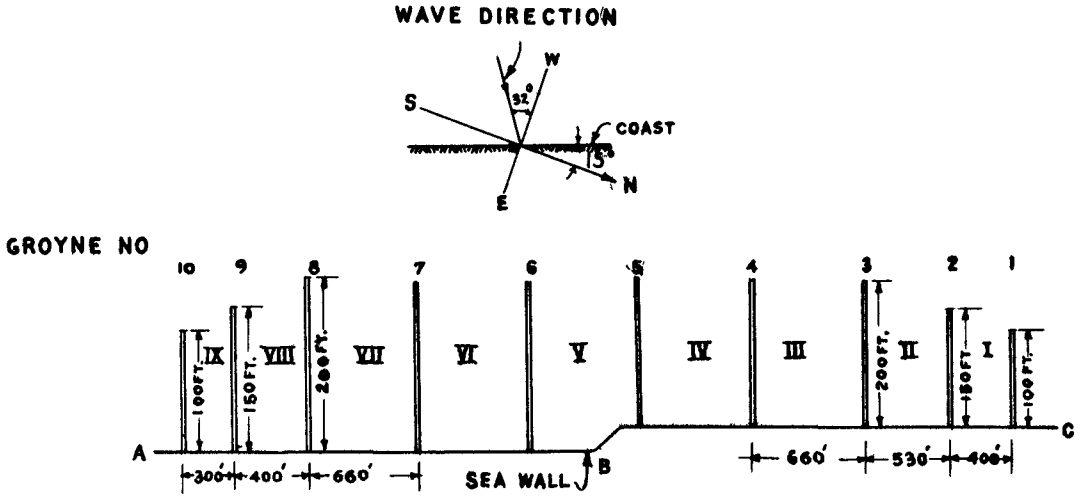

Fig. 1. Plan of sea wall and groynes in a one mile experimental reach; portion A B is masonry wall over sand core and A C is rubble mound sea wall.

Monthly averages of LW and HW distances in each compartment have been first computed. Fig. 2a shows a plot of LW-distance averages and indicates the rising trend particularly in compartments II to VII. Similar tendencies are also observed for the HW-distance averages though to a lesser extent (Fig. 2b). During the months of May to August the sea is generally rough. It is interesting to note that there is an appreciable tendency of recession during these months. In order to draw conclusions about long term trends liberated from usual tidal and seasonal variation features, namely, effect of semi-diurnal, diurnal and semi-lunational tides, effects of monsoon and fair weather water edge distances corresponding to only the fortnightly lowest LW or highest HW levels were selected.

The twelve monthly averages obtained for the Central locations in all the nine compartments are plotted in Figs. 3a and 3b for LW and HW, respectively. It is interesting to note that compartments IV to IX show relatively more width of sand cover than compartments I to III. Visual examination of these plottings also indicates a slow but unmistaken rising trend of accretion in about all the compartments except compartments VI to IX.

This study also indicates that:

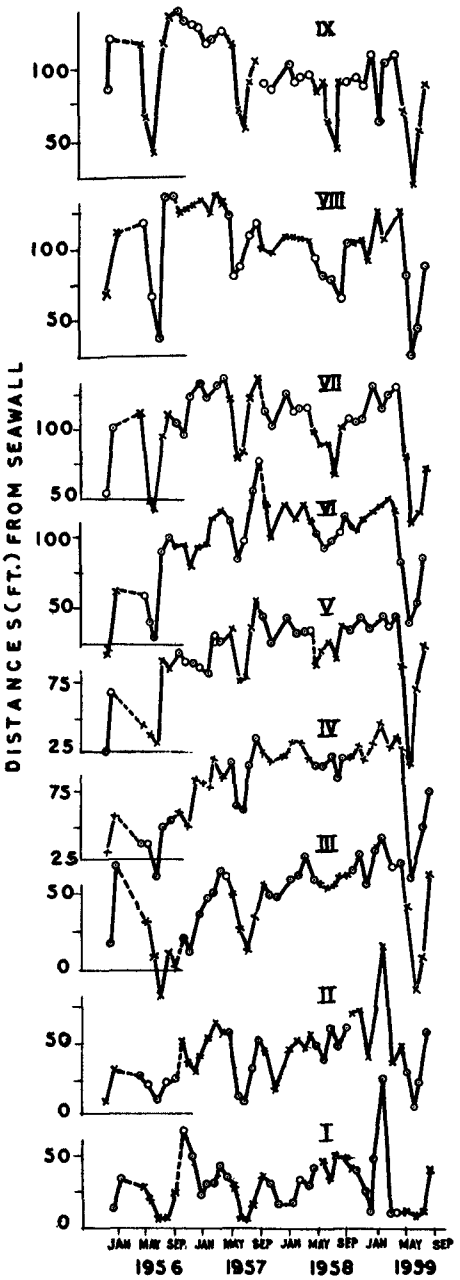

Fig. 2a. Monthly averages for low water levels of 1 ft. above L. W.O.S.T.

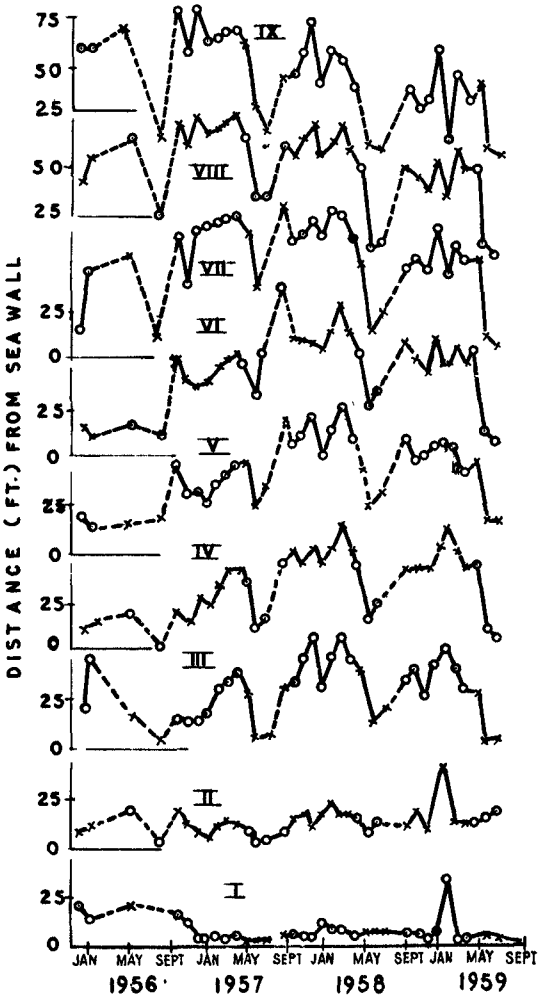

Fig. 2b. Monthly averages for high water levels of 3 ft. above L.W.O.S.T.

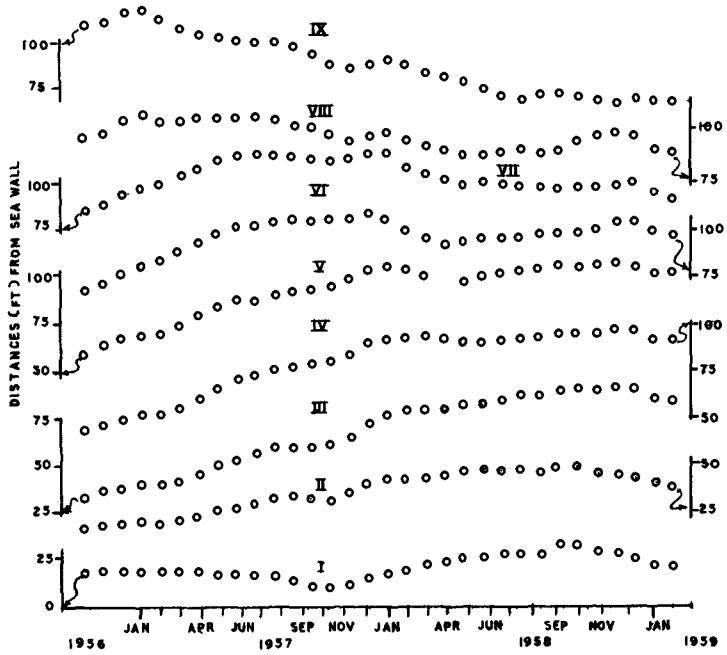

Fig. 3(a). Moving average distances (centre) for lowest low water level.

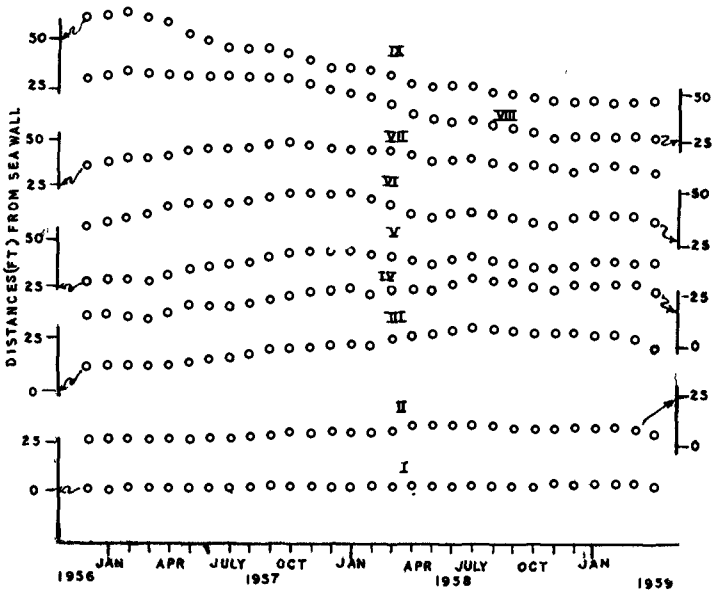

Fig. 3b. Moving average distances (center) for highest high water level.

Fig. 5. Recession of the coast with sea wall alone.

Fig. 4. Damage to sea wall constructed with bituminous grouting.

Fig. 7. Groyne being constructed with coconut piles.

Fig. 6. Accretion taking place in the groyne field. Notice also the damage to the sea wall.

(i) The total distances, by which the sea receded over different periods in different compartments, vary considerably due to the small amount of fresh bed material available to fill the eroded coast. The effect has been particularly small in compartments I and II.

(ii) The low water line in compartments I to V has been receding rather slowly. The reverse trend noticed in compartments VI to IX is possibly due to the sea wall in that portion having been constructed with a sand core. The stretch of this sea wall has been damaged by wave attack during storms which probably retarded the accretion process.

(iii) The HW data, on the other hand, do not bear out any steady or similar evidence. Continuing proximity of the HW edge to the sea wall makes vigilance in maintaining the sea wall-groyne structure imperative.

3. DAMAGE TO GROYNE LENGTHS

The seaward ends of the groynes 1 to 5 were reported to have been damaged in June 1957. These groynes settled in lengths of 24, 34, 39, 29 and 25 ft leaving lengths of 76, 116, 161, 171, 175 ft respectively. In January 1960, three years after these observations were made the lengths of the groynes were 75, 95, 160, 165 and 165 ft respectively. In 1957 very little damage was reported for groynes 6 to 10. In January 1960 the groyne 6, 7, and 8 were 170, 160 and 180 ft against 200 ft of their original length; and groynes 9, 10 were 130 and 80 ft against 150 and 100 ft of their original lengths. Groynes 1 to 5 situated on the northern side were damaged more than groynes 6 to 10 situated on the south.

4. SEAWALL WITH BITUMINOUS GROUTING

Experiments were also carried out in the prototype by constructing a sea wall with bituminous grouting. The work was started in March 1959. The inner core of the sea wall was made up of sand with slopes of 3:1 on seaward and landward sides. The top of the sea wall kept at +11 was, thus, 8 ft above the High Spring Tide Level (+3). The sand core was covered by 9" thick dry rubble casing, consisting of stones 4" to 6" in size. The rubble casing was then grouted, with a mixture of 65% sand, 15% cement (by weight), 20% mexphalt (30/40P). The bottom of the sea wall was taken up to - 4 on the seaward side and +4 on the landward side.

Local beach sand was first heated to 350°F. This was added to sand and mixed well. The filler (cement) was then added to the mixture and thoroughly mixed. Remaining quantity of bitumen was

also heated to 350°F. It was added and mixed to form a grout of proper workable consistency. When the mixture was at 350°F, it was taken out and poured into crevices of the stones so as to completely fill the full depth of stones. About 2000 pounds of mixture was required for covering an area of 100 sq ft to a depth of 8". The cost of this wall was Rs. 110/- (equivalent to $22) per running foot.

The sea wall could not withstand the wave attack though waves were only 3 to 4 ft in height. It was considerably damaged within a month and a half after its construction. Fig. 4 shows the damaged conditions of the bituminous grouted sea wall. This type of sea wall did not give satisfactory results in this particular case. It has been, therefore, decided not to use such type of construction for the protection of the remaining coast.

5. EXTENSION OF PROTECTIVE MEASURES TO OTHER REACHES

One mile long experimental sea wall with groynes has proved to be effective in giving protection to the coast under erosion. Protective measures are, therefore, being extended to the south of this reach for a lengh of 10 miles. In order to give immediate protection to the coast and due to availability of limited funds sea walls alone are constructed in 8 mile length of the coast. Considerable damage has taken place to these sea walls. Prototype experience has thus clearly shown that without groynes sea walls are ineffective in affording protection to the coast. Figure 5 shows the recession of the coastline with the sea wall alone. In the remaining two mile stretch of the coast, sea walls supplemented with the groynes are constructed. Though some damage has taken place to the sea wall itself, sand has accreted in the groyne field and the conditions are much better than those obtained with sea walls alone (Fig. No. 6). The results with sea walls and groynes have been found encouraging in these reaches also, and 200 ft long groynes are being immediately added to the sea wall.

The cost of rubble groynes has been found to be high and an alternative type of semi-permeable groyne is, therefore, being tested in the prototype. This consists of two rows of coconut piles which are driven to 7 ft below bed level. Space between the piles is being filled with fascines. The results would be available by the end of August 1960. Figure No. 7 shows the semi-permeable groynes under construction.

6. MODEL TESTS

Previous experiments carried out in 1/40 geometrically similar scale model and described in an earlier paper showed that a sea wall alone required considerable maintenance and it was necessary to supplement it with groynes to give adequate protection to the coast.

Short groynes less than 150 ft in length were found unsuitable to give adequate protection. It was realised that along the coast where the quantity of littoral drift was not considerable and was due to the erosion of the coast itself, groyne tops should be sufficiently high so that the bed material intercepted in the groyne field was not lost by passing over groynes.

Further tests were carried out to ascertain the most effective lengths of, and spacing between, the groynes. Rates of maintenance for sea wall with groynes of lengths 150 and 200 ft spaced at 2, 3 and 4 times their lengths have been observed and compared. With spacing of 4 times, the initial maintenance has been considerably higher for 200 ft long groynes than that required for groynes spaced at two to three times the groyne length. Between 150 and 200 ft length of groynes, the maintenance required for 200 ft long groynes was less for groynes spaced at 2 to 3 times the groyne length (Figs. 8 a & 8b). During the course of these experiments, certain modifications in the design of the sea wall and groynes suggested themselves. In face of the considerable maintenance required, it may be asked whether the maintenance rate cannot be reduced by using heavier stones in the construction of the sea wall; or whether, by placing suitably designed piles at the sea wall toe, the sea wall cannot withstand the attack of storms with less damage. It is likely that a disposition of groynes in a form different from what has been adopted in the previous experiments (groynes normal to the sea wall) may give better protection with less damage. To answer these questions a certain number of experiments were performed, results of which are described below.

7. SEA WALL OF HEAVY STONES

All the previous experiments were carried out with stones weighing 225 lbs. In order to reduce the rate of maintenance of a sea wall armoured with stones heavier than those used previously, experiments were carried out with stones of weights corresponding to 1/2 and 1 ton. Sea wall supplemented with groynes 200 ft long and spaced 400 ft apart was constructed. Larger stones were placed on the seaward face of a core which was composed of 85 lbs and 225 lbs stones respectively, in the proportion of 3:1 by weight.

With such a sea wall, rate of maintenance especially in the first critical HW runs was considerably smaller than the corresponding rate for 225 lbs stones (Fig. 8c).

As an experimental measure the functioning of a sea wall, constructed with 1/2 ton and 1 ton stones, i.e. without a hearting of smaller stones was further tested. Rate of maintenance of the sea wall increased due to the effect of suction caused by the receding waves which resulted in removing the material from behind the sea wall. This caused a further sinking of sea wall stones. A well packed hearting besides being

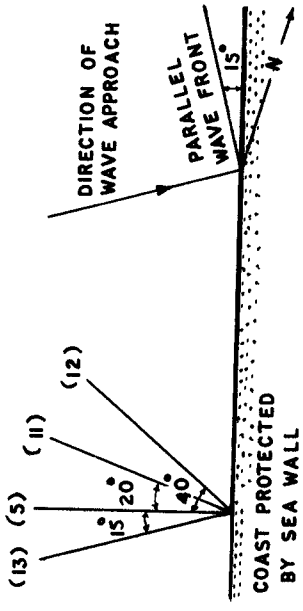

Fig. 9. Groyne directions.

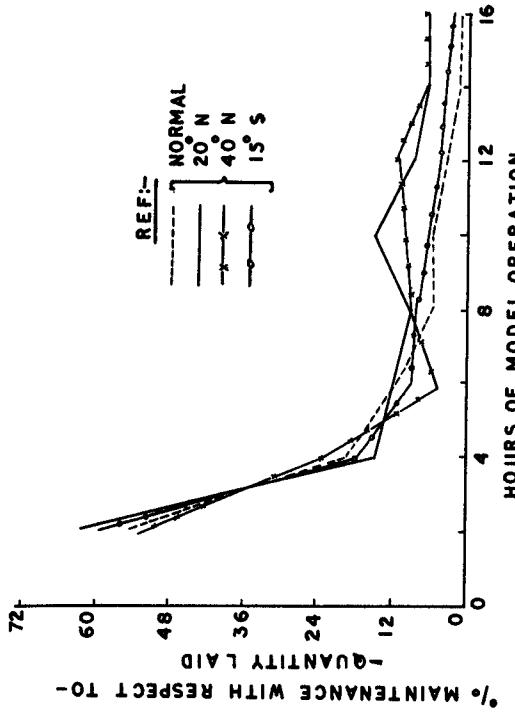

Fig. 10. Comparison of rates of maintenance of seawall supplemented by inclined groynes. Groyne length 200 ft. spacing 600 ft.

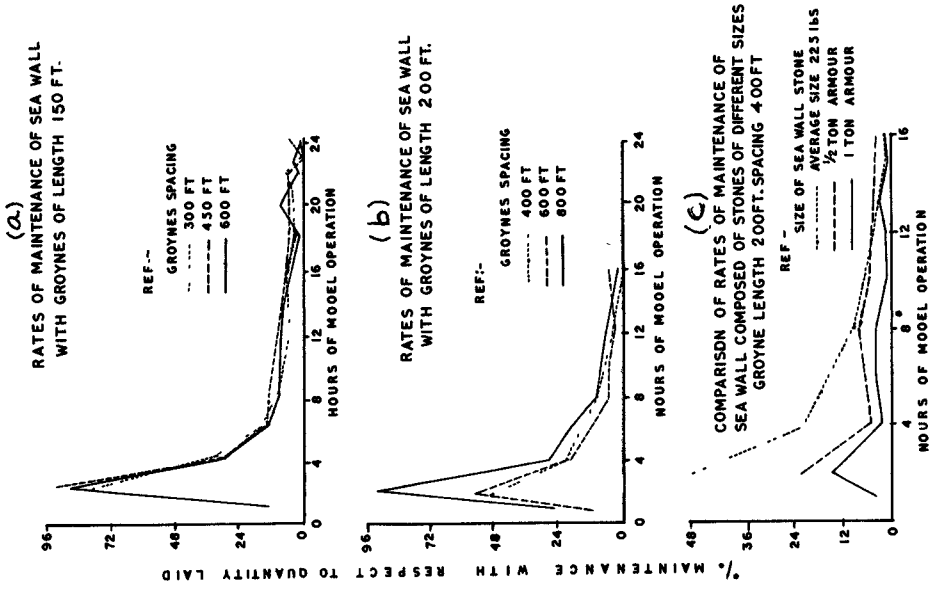

Fig. 8

cheaper avoids this and is therefore necessary.

Reason for the lower rate of maintenance for the sea wall in the case of bigger stones appears to be two-fold: firstly heavier stones are less vulnerable to direct wave action, and secondly, even when the stones are pulled down the sea wall face, they do not lend themselves to littoral transport as easily as do the lighter stones. This comparison apparently of little consequence in the model assumes considerable importance in the prototype, when much bigger stones are required to be used. Economic considerations prevail in such a case. Perhaps it may be cheaper to use smaller stones and replace them in the first two years as maintenance reduces considerably thereafter, once sand cover forms in front of the toe of the sea wall. As use of stones heavier than 500 lbs is precluded in this case because of economic considerations, stones less than 225 lbs in weight have been used for sea wall construction.

8. SEA WALL WITH PILE LINE AT THE TOE

One experiment was performed to ascertain whether sea wall protected by a pile line at the toe effected a reduction in the rate of replenishment of the sea wall. Results, however, showed that during the initial run bed material lying against the seaward face of the pile began to be eroded away speedily, leaving the pile face exposed and unprotected. Experiment did not show any material advantage for sea wall with the pile line at the toe.

9. INCLINED GROYNES

In all the previous experiments groynes were kept normal to the coastline. A series of experiments were performed to verify whether any advantage accrued from inclined groynes. Groynes were placed respectively 20° N, 40°N and 150° S of the perpendicular to the coast protected by a sea wall (Fig. 9). Direction of groynes 15° south was parallel to the direction of waves. Lengths of and spacing between groynes were 200 and 600 ft respectively, and other experimental conditions were identical. Figure 10 shows the respective rates of maintenance of the sea wall for the above inclinations compared with the corresponding rates for groynes, normal to the coastline. Comparison does not indicate any amelioration in the replenishment of the sea wall resulting from inclined groynes in the initial stage. On the contrary there is a tendency for the rate of maintenance to be higher than that with normal groynes in the last stage. Experiments did not also indicate any better performance in the degree of protection afforded to the coast. It appears that on the coastline like the one on the West Coast of India where direction of waves swings from NWW to WSW, perpendicular groynes are likely to give better results.

10. MODEL LIMITATIONS

Before drawing any conclusions, it may not be out of place to restate the limitations of a model study of littoral drift in a problem of coastal erosion. The results of the present series of experiments show that quantities of stone required for the maintenance of the sea wall are considerably greater in the model than in the prototype. The reason for this discrepancy is due to the fact that, during the initial hours of model operation, sea wall stones tend to sink in the model sea bed formed of coarse coal powder, which would not usually happen in the prototype. That such a contingency can, however, occur in nature is proved by the complete and rapid disappearance of some of the lengths of sea wall not supplemented by groynes, within a short time after their construction.

Experience of the behaviour of the experimental sea wall on the prototype showed that considerable damage had taken place to the sea wall in the first year. About 16 per cent of the stones used for the sea wall were lost. The sea wall was repaired in the third year after its construction. Very few stones have since then been lost to the sea. In the model the initial high rate of maintenance of the sea wall diminishes within a few hours of run to only a small fraction; this latter rate remains practically constant throughout the rest of the period of model operation. The initial maintenance rate in the model is however much higher than that observed in the prototype. Figures of damage of experimental sea wall in the last two years after repairs of the sea wall confirm model behaviour in respect of subsequent low maintenance required for the sea wall.

Another limitation of the model investigation is that, whereas in the prototype a coast eroded during the storms gets replenishment in the fair weather season from offshore bars of sand removed during the storms; no such two-way process is possible in model experiments. This shows that the model errs on the safe side in subjecting the protective structure to a considerably greater wave attack than in nature.

11. CONCLUSIONS

(i) Groynes of length 200 ft are to be preferred to groynes of length 150 ft.

(ii) Spacing between groynes should not exceed 3 times the groyne length.

(iii) Heavy stones, used as sea wall armour on a core of smaller stones, result in considerably decreased rate of maintenance.

(iv) Piles at toe of sea wall do not give extra protection to the sea wall.

(v) Inclined groynes do not commend themselves for adoption on this coast.

Along the west coast of India where these groynes are constructed littoral drift is very small as there are no major rivers contributing to the sediment transport by littoral drift. The material eroded by wave action forms the main source of the littoral drift.

CHAPTER 51

LA DEFENSE ET LE MAINTIEN DES PLAGES BELGES ENTRE ZEEBRUGGE ET LA FRONTIERE NEERLANDAISE

par

J. E. L. VERSCHAVE,
Ingénieur en Chef - Directeur
des Ponts et Chaussées,
Service de la Côte Belge,
OSTENDE.

CHAPITRE 1

LA COTE BELGE ENTRE ZEEBRUGGE ET LA FRONTIERE NEERLANDAISE

EVOLUTION

Au point de vue géologique, la partie orientale, comme d'ailleurs toute la côte belge, forme la limite septentrionale de la plaine maritime flamande.

Par rapport au niveau Z - 0.00, c'est-à-dire le niveau moyen de la marée basse de vives eaux à Ostende, niveau qui est situé à 2,50 m sous le plan de référence néerlandais N.A.P., les couches géologiques se présentent à Knokke dans l'ordre suivant:

A. Formation moderne: dunes
B. Ere quaternaire:
- B1° Holocène supérieur : (Assise de Dunkerque)
  Argile et limon entre Z + 3,00 et Z + 1,50
- B2° Holocène moyen et inférieur: (Assise de Calais)
  limon et tourbe Z + 1,50 à Z 0,00
  sable Z - 0,00 à Z - 5,00
  limon et sable Z - 5,00 à 9,00
  sable Z - 9,00 à Z - 16,00
- B3° Pleistocène: (Assise d'Ostende)
  sable à coquillages
  Z - 16 à Z - 18
  sable Z - 18 à Z - 26

C. Ere tertiaire:	C1° Bartonien: argile	Z - 26 à Z - 30
	C2° Panisélien: sable et argile	sous Z - 30
	C3° Yprésien: argile	sous Z - 60

Les polders, situés au sud du cordon littoral, ont une profondeur d'environ 10 à 15 km vers l'intérieur du pays et constituent une région agricole très fertile.

Le sol argileux et limoneux a été déposé pendant la dernière transgression de Dunkerque.

Le cordon littoral, constitué de dunes récentes et de digues artificielles, est complètement bâti. Les agglomérations de Zeebrugge, Heist, Duinbergen, Albert-Plage, Knokke et le Zoute y sont situées et l'exploitation balnéaire y est intense.

Jusqu'à dix km en mer, les profondeurs du fond sous-marin sont assez variables. Les chenaux et les bancs se succèdent et la profondeur maxima atteint Z - 13 m dans les Wielingen devant la côte belge. La profondeur augmente toutefois rapidement vers l'Est dans le rétrécissement de l'Escaut entre Breskens et Vlissingen.

Le fond de la mer est formé par des couches appartenant à l'assise de Calais en face de la côte belge.

Toute cette partie côtière a donc été formée par sédimentation marine depuis 8.000 ans avant J.C. jusqu'à la fin de la dernière transgression de Dunkerque et l'intervention de l'homme, vers le 11ème siècle après J.C.

La configuration et la topographie en ont toutefois été fortement modifiées depuis lors.

Au début du 14ème siècle, l'embouchure actuelle de l'Escaut occidental comptait trois bras:

Le Zwin:	débouchant entre le continent et l'île de Wulpen
Le Grote Rille:	débouchant entre les îles de Wulpen et de Schooneveld
L'Oostgat:	débouchant entre les îles de Schooneveld et de Walcheren

Au méridien de Heist, la côte se trouvait à 5 km au nord de la promenade actuelle. Au méridien de Knokke, elle se trouvait à 2 km au nord de la promenade actuelle.

Le Zwin passait alors entre Le Zoute et Kadzand, à l'endroit où le "Schorre" existe encore aujourd'hui.

Plus à l'ouest la côte se trouvait également au nord du tracé actuel. Au nord de Wenduine se trouvait le hameau de Harendijke Au nord de Blankenberge se trouvait le village de Scarphout ; au nord de Heist le village de Coudekerke, au nord de Knokke le village de Reygersvliet, etc . . . .

Le début du 14e siècle est caractérisé par une série de tempêtes violentes qui modifient sérieusement les côtes et l'estuaire de l'Escaut occidental. En 1334, par une marée tempête violente, Scarphout et Coudekerke disparurent en mer.

En 1337, une nouvelle marée tempête sévit et plusieurs villages sur les îles de Wulpen et Schooneveld sont engloutis. A cette époque, le Comte de Flandres, Jean Sans Peur, fait construire les digues de défense le long du littoral flamand. Ces digues s'appellent encore aujourd'hui lès digues du Comte Jean.

En 1404, le hameau de Harendijke au nord de Wenduine disparût de la carte.

Le 18 novembre 1421, jour de Ste Elisabeth, une nouvelle marée tempête d'une rare violence accentua le travail de sape. La marée tempête de St Felix en 1530, créa les passes du Sloe entre les îles de Walcheren et de Zuid Beveland et du "Creecke" ou Kreekrak à l'est du Zuid Beveland. Une grande partie de l'île fût engloutie entre 1530 et 1552. Le jour de Toussaint, ler novembre 1570, est la date d'une des marées tempêtes les plus dramatique et l'évolution de l'Escaut occidental comme grand estuaire maritime fit un bond d'importance.

La carte, dressée par Mercator en 1590, montre que l'estuaire a déjà une largeur de 3, 5 km entre Breskens et Vlissingen.

Les îles du delta, comme Wulpen, Schooneveld et Coesant, ont disparu.

Blankenberge est situé à la côte. La côte entre Heist et Knokke se situe légèrement au nord de la côte actuelle ; tout au plus quelques centaines de mètres.

Le Zwin y figure toujours avec une largeur de près d'un kilomètre. L'érosion et le déplacement de matériaux dans la zone triangulaire Breskens, Westkapelle, Wenduine, entre 1300 et 1600, c'est-à-dire en trois siècles, doivent être évalués à plus d'un milliard (10^9) de m3.

Depuis lors l'approfondissement de l'embouchure de l'Escaut occidental s'est encore poursuivi.

Les données hydrographiques manquent entre 1600 et 1830, mais l'étude des cartes marines dressées et des sondages pratiqués depuis 1830, prouve

que l'approfondissement du delta sous-marin de l'Escaut occidental a continué jusqu'à nos jours, spécialement dans une zone de 10 km de largeur au nord de la ligne Breskens-Wenduine. La côte belge entre Zeebrugge et la frontière néerlandaise fait partie de ce rivage au sud du delta sous-marin.

La largeur de l'Escaut entre Breskens et Vlissingen a, de nos jours, une largeur d'environ 4,2 km et la section mouillée en dessous de marée basse a augmenté d'environ 35 % entre 1840 et 1955.

Selon les études du Dr ir. J. Van Veen, l'approfondissement moyen du delta serait de 5,4 dm entre 1872 et 1933 et l'approfondissement moyen de la zone méridionale serait de 7,5 dm pendant la même époque.

Nous avons estimé qu'entre 1840 et 1955 les bancs se sont abaissés, les chenaux ont maintenu leur profondeur devant la côte belge, mais se sont considérablement approfondis dans l'étranglement de l'Escaut, c. à. d. dans les eaux néerlandaises. Le fond moyen sur le méridien de Heist et sur le méridien du Zoute, jusque 10 km au nord des plages s'est abaissé de 0,50 m. Il y a donc certainement continuation de l'érosion du fond de la mer devant le littoral en question jusqu'à nos jours, érosion due à l'évolution de l'estuaire de l'Escaut.

\+ ++ ++ +

CHAPITRE 2

L'EROSION DES PLAGES DEPUIS 1900 ET SES CAUSES

L'érosion des plages de Heist, Duinbergen, Albert-Plage, Knokke et le Zoute s'est surtout prononcée depuis 1900, après la construction du port de Zeebrugge.

Déjà en 1920 de sérieuses pertes de sable étaient enregistrées et, malgré l'établissement d'une série d'épis sur les plages entre 1920 et 1940, le recul de la laisse de marée basse s'accentuait progressivement

Les causes naturelles de l'érosion, les interventions et ouvrages des hommes ont produit des réactions défavorables les unes sur les autres et vice-versa et ont accéléré le désensablement.

CAUSES NATURELLES

1. Tassement naturel du sous-sol; contenant de la tourbe et léger

relèvement du niveau moyen de la mer.

2. L'érosion des fonds marins, due à l'évolution de l'estuaire de l'Escaut (augmentation du flux et des vitesses)

La fosse de l'Appelzak, située immédiatement au nord des plages, s'est rapprochée de la côte, s'est allongée vers l'est, approfondie en certains points.

Le banc du Paardemarkt, au nord de la fosse de l'Appelzak, a été érodé et sa crête s'est abaissée d'environ 2, 50 à 3 m entre 1840 et 1955.

Les côtes comparatives sont les suivantes:

	1840	1955	Abaissement
Devant Heist	Z - 34 dm	Z - 60 dm	2,6 m
Devant Knokke	Z - 25 dm	Z - 54 dm	2,9 m
Devant le Zwin	Z - 25 dm	Z - 59 dm	3,4 m

3. Cet abaissement du banc a facilité l'attaque des plages par des vagues de tempête de plus en plus fortes.

CAUSES DUES A L'INTERVENTION DE L'HOMME.

1. Construction du môle et du port de Zeebrugge, entre 1890 et 1907 déplacement résultant de la fosse de l'Appelzak vers l'est - séparation de la fosse de celle du môle - attaque du flanc sud de la fosse par les courants (force de Coriolis et effet centrifuge)

La fosse de l'Appelzak se prolonge actuellement jusqu'au Wielingen devant Kadzand et l'approfondissement devant le Zwin est d'un mètre depuis 1840 (actuellement Z - 82 dm au lieu de Z - 71 dm en 1840)

2. Fermeture de la claire-voie du môle de Zeebrugge, après la première guerre mondiale et diminution du transport de sable vers l'est.

3. Le développement foudroyant des cités balnéaires de Duinbergen, Albert- Plage, Knokke et Le Zoute entre les deux guerres mondiales.

Toutes les dunes ont été endiguées et vendues comme terrains à bâtir et des promenades ont été établies en bordure des plages. Les réserves naturelles de sable étaient de ce fait perdues pour les plages. La pente des talus est d'ailleurs beaucoup trop forte.

4. La construction d'épis trop courts entre 1920 et 1939, accélérant

l'érosion de la plage vers marée basse au versant sud de l'Appelzak ; les sérieux dégâts causés aux épis par les tempêtes et par faits de guerre entre 1940 et 1944 et le manque total d'entretien pendant ces années.

5. La nécessité de réparer les dommages de guerre et de reconstruire les ports entre 1944 et 1950 et le manque de crédits pour les travaux d'amélioration des plages.

Au début de 1952, la situation des plages, surtout à Knokke et Le Zoute, était devenue réellement critique. La laisse de marée basse s'était rapprochée à certains endroits jusqu'à 150 m de la fondation des perrés et, à chaque marée haute, les vagues battaient les revêtements des digues.

A chaque tempête, de fortes vagues réfléchissaient contre les digues, affouillaient les fondations et créaient des érosions catastrophiques sur la plage.

A 350 m de la crête des digues, on sondait des profondeurs de 7,50 m sous le niveau de marée basse aux vives eaux.

Le versant sud de la fosse de l'Appelzak s'était rapproché dangereusement des promenades et se retrouvait entre 170 m et 350 m des digues.

L'estran de Heist s'était abaissé entre 1910 et 1952 de plus de deux mètres.

A Knokke-Le Zoute , des dunes de plus de 5 mètres de hauteur avaier été balayées sur une largeur de plus de 20 mètres.

Une estimation grossière a révélé qu'environ 8.000.000 m³ de sable ont été enlevés entre 1910 et 1952 de la plage, de l'estran et de la terrasse sous-marine, dans cette zone côtière d'environ 10 km de longueur.

C'est en 1952, en accédant à la direction du service de la côte belge, que nous avons établi un programme complet de construction de vingt cinq longues jetées entre Heist et la frontière néerlandaise, dans ce triple but:

1. d'arrêter l'érosion et de défendre les digues;

2. de regagner du sable sur la terrasse sous-marine entre les jetées et de refouler la laisse de marée basse vers le nord ;

3. de créer la possibilité de relever les plages par des apports artificiels de sable le long des digues et de stabiliser ces apports.

CHAPITRE 3

ETUDE PREALABLE DU PLAN DE DEFENSE ETABLI EN 1952

En vue de l'établissement du plan de défense, certaines opérations hydrographiques préalables et urgentes furent exécutées en mer. Ces opérations étaient:

a) sondages du fond de la mer sur le versant sud et au milieu de la fosse de l'Appelzak ;

b) reconnaissance superficielle de la nature des fonds dans la fosse de l'Appelzak et sur le banc du Paardenmarkt ;

c) mesure et étude de la vitesse des courants à la surface et près des fonds, déduction des courants moyens ;

d) 'étude de la houle et du plan des vagues, estimation des vagues de tempête les plus fortes ;

e) quelques mesures coomparatives de transport de matériaux près du fond.

Ces opérations hydrographiques ont été complètées et suivies par des études, des déductions théoriques et des comparaisons avec nos connaissances au sujet de ces différents phénomènes et des situations à d'autres endroits de la côte belge.

Un aperçu succinct des résultats de ces mesures et de ces études, doit suffire dans le cadre de cet exposé:

1. AMPLITUDES ET NIVEAUX DES MAREES.

Les niveaux moyens de marée haute et de marée basse sont approximativement les mêmes à Zeebrugge, à Heist et à Knokke.

	Vives eaux moyennes	Mortes eaux moyennes
Niveaux moyens de marée haute	Z + 4,70	Z + 3,75
Niveaux moyens de marée basse	Z + 0,25	Z + 1,00
Amplitude	4,45 m	2,75 m

La marée de tempête la plus violente, pour laquelle nous disposons de mesures, a été celle du 1er février 1953. La marée haute a atteint le niveau Z + 6,90.

LA DEFENSE ET LE MAINTIEN DES PLAGES BELGES ENTRE ZEEBRUGGE ET LA FRONTIERE NEERLANDAISE

L'amplitude de la marée lunaire est: 3,40 m. L'amplitude moyenne des marées est 3,60 m. La célérité de l'onde marée est d'environ 15 m/sec.

La durée entre la marée haute et la marée basse suivante est à Zeebrugge en moyenne de 6 h 30'.

2. SONDAGES - PROFONDEURS.

Les profondeurs sondées sur le versant sud et le fond de la fosse de l'Appelzak en 1952 , sous Z 0.00 (niveau moyen des vives eaux à Ostende) sont reprises dans le tableau suivant. Les profils ont été pris suivant une perpendiculaire à la digue de Mer.

Les distances cumulées sur les profils sont mesurées à partir de la ligne reliant les extrémités septentrionales des revêtements carossables des jetées à construire (+ vers le nord - vers le sud à partir de cette base).

Profils				Crête de la digue de Mer		Profondeurs sous Z - 0.00 (m) - Dist. cum. à partir base.	
N°	Axe de la jetée	Endroit	Entre distance (m)	Côte	distance à la base	- 125 m.	- 75 m.
1	51	Heist	Parc Heist	+9,35	- 434		
2	1	Duinb	Avancée W	950	+9,46	-379	
3	3	Duinb	Avancée E		+9,54	-342	
4	7	Duinb.	Albert Plage	1870	+9,53	-495	2,50	4,50
5	1	Knokke	Av. Lippens		+9,54	-326	
6	5	Knokke	Pl. Albert	2250	+9,64	-370	
7	10	Knokke	Lekkerbek		+9,80	-311	
8	12	Knokke	Le Zoute	1000	+9,73	-358	2,00
9	14	Knokke	Le Zoute		+9,55	-325	
10	22	Knokke	Zwin	1440	+10,50	-320	

(suite)

N° /	- 25 m.	+ 25 m.	+ 75 m.	+ 125 m.	+ 175 m.	+ 225 m.
1	2,20	3,65	4,10	4,45	4,90	5,20
2	2,20	3,65	4,45	4,80	5,10	5,20
3	2,80	4,70	5,80	5,80	5,80	5,80
4	5,40	5,40	5,75	5,80	6,00	6,00
5	6,80	8,80	8,80	8,65	8,55	8,50
6	2,60	4,90	7,10	7,65	7,75	7,80
7	4,00	5,70	6,90	7,45	7,45	7,45
8	3,70	5,30	6,40	6,90	7,35	7,55

N°	- 25 m.	+25 m.	+ 75 m.	+125 m.	+ 175 m	+ 225m
9	3,40	5,30	6,40	7,00	7,25	7,30
10	3,25	4,15	5,35	6,35	7,10	7,25

Il résulte clairement de ce tableau qu'à 400 m au nord de la crête des digues et des promenades, on retrouve les grandes profondeurs de la fosse de l'Appelzak, entre l'avenue Lippens à Knokke et le Zwin.

En 1952, la laisse de marée basse des vives eaux s'était rapprochée jusqu'à 170 m de la crête de la digue, devant l'avenue Lippens et devant le Lekkerbek à Knokke (profils 5 et 7)

3. NATURE DES FONDS.

Le versant sud de la fosse de l'Appelzak est en somme une section à faible pente à travers les anciennes couches géologiques entre Z-0.00 et Z- 9.00, On y rencontre de la tourbe, du limon et du sable à faible profondeur.

Ce versant, tout comme le fond de la fosse, sont toutefois recouverts par une couche de sable d'épaisseur variable. Ce sable subit des mouvements et des charriages.

On retrouve des fonds de sable dans la fosse du môle devant le port de Zeebrugge ; devant Heist et dans les grandes profondeurs des Wielingen en face de Kadzand.

Le banc du Paardenmarkt et le Zand au Nord de Zeebrugge sont couverts d'une couche limoneuse.

La couche a 0,50 m. d'épaisseur au Paardenmarkt entre Z -5,50 et Z - 6,00 et plus de 2 m au Zand entre Z - 7,00 et Z - 9,00

Une faible couche de sable, à certains moments mélangé de vase, et ayant 2 à 3 cm d'épaisseur, est charriée sur ces bancs.

4. VITESSE DES COURANTS

Dans l'axe de la fosse de l'Appelzak, les vitesses des courants maxima de flot et de jusant s'établissent dans la direction de cet axe, c. à. d. parallèlement à la côte.

Le courant de flot est dirigé vers l'Est (70 à 80°), s'établit entre 2 h 50' avant marée haute, jusqu'à 2 h 30' après marée haute et atteint

son maximum de vitesse vers 50' à 1 h avant marée haute.

Le courant de jusant est dirigé vers l'Ouest (250 à 260°) s'établit entre 2 h 30' après marée haute jusqu'à 3 h avant la marée haute suivante et atteint son maximum 5 h après la marée haute ou 1 h 30' avant la marée basse.

Les renversements entre ces deux directions opposées sont très rapides (durée maxima de 10' surtout aux vives eaux)

Les vitesses maxima sont variables selon l'amplitude de la marée verticale, abstraction faite des influences du vent et de la houle.

Quelques vitesses maxima mesurées à différentes profondeurs sont indiquées dans les tableaux suivants:

Courant de flot - Vitesse en cm/ sec.

Amplitude de la marée verticale m	à la surface	à 3m sous la surface	à 2m au-dessus du fond	à 0,15 m du fond
A = 2,60	87	76	62	41
A = 3,60	145	127	88	69
A = 4,70	200	178	124	96

Courant de jusant - Vitesse en cm/sec.

Amplitude de la marée verticale m	à la surface	à 3m sous la surface	à 2m du fond	à 0,15 m. du fond
A = 2,60	68	65	57	40
A = 3,60	114	108	80	68
A= 4,70	160	151	105	95

Toutes ces vitesses sont élevées et de nature à affouiller sérieuseme les fonds de sable. Elles peuvent créer des transports de matériaux conséque

5. HOULE ET VAGUES DE TEMPETE.

Les vents prédominants viennent du secteur S-W à W. Le fetch ne

dépasse toutefois par 180 km à partir de l'embouchure de la Tamise et de la côte anglaise.

Les vents soufflant du secteur W à N-W sont déjà plus dangereux et le fetch augmente légèrement à partir de la côte anglaise entre Harwich et Great Yarmouth.

Les vents de tempête les plus dangereux sont, ceux venant du secteur NW-N et N-NE, le fetch dépassant largement le millier de miles.

Selon les statistiques du service de la météorologie marine en Allemagne (1), 36% des vagues ne dépassent pas 1 m en hauteur, 67 % ne dépassent pas 2 m et seulement 5 % dépassent 5 m.

Pour 96% des cas, la période est comprise entre 3 et 8 secondes, et pour 50% des cas, entre 5 et 6 secondes.

Nous avons enregistré au bateau-phare West-Hinder, le 16 octobre 1958, pendant une violente tempête du NW-N (échelle Beaufort 11), quelques vagues de 6,6 m de hauteur avec période de 7 secondes. Cet enregistrement a été fait avec un Shipborne Wave-Recorder de Tucker. La marée haute atteignit ce jour là Z + 5,70 à Ostende.

Il faut toutefois noter, que les profondeurs dans le delta de l'Escaut entre le Wandelaar et la frontière néerlandaise ne dépassent pas 10 m sous marée basse et 12,5 m sous le niveau moyen de la mer, et que plusieurs bancs, à une profondeur de 6 à 8 m sous le niveau moyen de la mer, protègent la côte.

Les fonds sont très irréguliers. La houle forte et les vagues à haute amplitude se réfractent plusieurs fois avant d'aborder les côtes.

La réflection des vagues contre les perrés trop raides produisait avant 1953 et à marée haute une houle très gaufrée et très irrégulière. C'était surtout le cas avant la construction des longues jetées.

La diffraction de la houle autour du môle de Zeebrugge et la réfraction sur les fonds à faible profondeur devant Heist à l'Est de la rade, produisent une houle incidente normale à la plage entre les écluses et le parc de Heist. Le programme de défense dont traite cette étude n'a pas été etendu à cette zone. Devant Duinbergen, Albert Plage, Knokke et Le Zoute, les profondeurs plus grandes de l'Appelzak favorisent la progression de la houle dans le sens de la passe, c. à. d. vers l'Est. C'est aussi la direction des vents prédominants. A cause du versant à forte pente, les fortes vagues

attaquent avec déferlement la plage sous nn angle de 45° à 30° avec la normal sur les digues.

En tout cas, la présence des bancs et, spécialement, celui du Paardemarkt, limite la hauteur maxima des vagues qui peuvent attaquer la plage pendant les plus violentes tempêtes ; à marée basse, cette hauteur est limitée à 4 m. A marée haute, à 6 m environ.

Comme les grains de sable ont un diamètre inférieur à 200 microns (de 60 à 160 microns), des vitesses alternatives au fond d'environ 0,10 m/sec peuvent déjà les soulever.

Une houle de 2 m de hauteur et d'une période de 6 secondes produit déjà une telle vitesse à 27 m de profondeur.

Les fortes houles et les vagues de tempête sont donc également, par intermittance mais d'une manière beaucoup moins continue que les courants de marée, des agents transporteurs de matériaux très actifs. Elles alimentent surtout la zone du delta en matériaux provenant de la mer et du large en période de tempête.

Avant 1953, les vagues de tempête à forte cambrure attaquaient obliquement et dangereusement les plages par déferlement sur le sable et par ressac contre et affouillement devant les digues.

Depuis la construction des jetées, elles déferlent sur les talus à faible pente de celles-ci et la réflection a été réduite dans une large mesure.

Il faut noter que les houles longues et régulières de 0,50 m. à 1 m de hauteur et d'environ 50 m de longueur continuent à progresser vers les plages sous un angle d'incidence réduit par rapport à la direction NW-N et restent de précieux agents engraisseurs des plages.

6. TRANSPORT DES MATERIAUX.

Le transport des matériaux dans la fosse de l'Appelzak et sur son versant méridional est avant tout causé par les courants marins.

Le courant de flot, étant le plus fort, transporte les matériaux vers l'Est. Le courant de jusant crée un transport vers l'Ouest. Dans l'Appelzak la résultante du mouvement reste dirigée vers l'Est. Les houles et vagues créent à partir d'une certaine amplitude et longueur d'onde, un transport supplémentaire dirigé vers la plage (S. E.) et vers l'Est.

La résultante annuelle de tous ces transports reste donc nettement dirigée vers l'Est le long de la côte et dans la fosse de l'Appelzak.

Il faut toutefois remarquer, que dans la passe des Wielingen au nord du Paardemarkt, la résultante des transports, dûs aux courants de marées, est dirigée vers l'Ouest. Il en est de même à l'embouchure de l'Escaut entre Breskens et Vlissingen.

L'eau est toujours fortement chargée de vase et d'argile marine (2 à 20microns) même dans les couches supérieures à cause des courants marins à vitesse élevée et de la turbulence.

La visibilité dans l'eau est nulle, sauf à très courte distance (quelques décimètres) par beau temps et pendant quelques minutes seulement au renversement du courant.

Le sable est surtout charrié sur les fonds par temps calme, mais entre partiellement en suspension quand la mer devient houleuse.

Les mesures effectuées avec un appareil "SPHYNX" pour déterminer les quantités de matériaux, transportés près du fond, donnent des résultats très divergents, mais qui, en moyenne, concordent avec des mesures indirectes et avec nos calculs.

Notre étude, publiée au Congrès International de Navigation de Londres en 1957 (2), a traité ce sujet en détail.

Nous voulons simplement rappeler ici, que nous estimons le transport global de sable sur le fond de la mer à travers une section perpendiculaire à la côte à environ 200 m3 par mètre du fond et par an devant le port d'Ostende. Il s'agit de la somme du transport de flot vers l'Est et du transport de jusant vers l'Ouest.

Dans la fosse devant le port de Zeebrugge et dans l'Appelzak, ce transport est évalué à environ 400 m3 par mètre de fond et par an.

La résultante absolue du transport vers l'Est à travers une section bien déterminée ne serait toutefois que de l'ordre de 80 m3 par mètre de fond et par an

La fosse de l'Appelzak est alimentée en matériaux par l'Ouest, le Nord et même par l'Est (jusant)

La distance entre Zeebrugge et la frontière néerlandaise est d'environ 12 km.

Aux vives eaux et en surface, le flux vers l'Est (flot) est d'environ 20 km et vers l'Ouest (jusant) d'environ 18 km.

La fosse de l'Appelzak est donc parcourue par les courants sur tou sa longueur et, à chaque marée, par deux courants inverses.

Les matériaux sont alternativement transportés dans les deux sens opposés.

\+ ++ +

CHAPITRE 4

PLAN DE DEFENSE:JUSTIFICATION TECHNIQUE ET FINANCIERE

L'endiguement complet des dunes, l'existence des perrés, des promenades et des propriétés privées sur toute la longueur de la côte ne permettaient plus de recul des plages.

Il fallait donc refouler la laisse de marée basse vers le Nord et gagner du terrain sur la mer et plus particulièrement sur la fosse de l'Appelzak.

C'était sans doute une solution onéreuse à cause des grandes profondeurs de la fosse, mais c'était l'unique solution possible Si la solution était devenue onéreuse, c'était avant tout à cause de l'énorme retard qu'on avait accumulé et toléré avant de résoudre le problème.

L'amplitude de la marée, les vitesses élevées des courants de marée longitudinaux, les directions de la houle, la présence de sable sur les fonds et les transports de sable causés par les courants, ont dicté en 1952 l'unique programme de défense possible, notamment le prolongement et la construction jusque dans la fosse de l'Appelzak d'une série de 25 jetées d'une longueur variant entre 350 et 535 m à partir de la crête des perrés bordant les digues.

La longueur minimum de 350 m a été établie de façon à obtenir une hauteur de l'estran minima devant le parafouille les digues de Z + 3,70 Le niveau supérieur des parafoulles est à la côte de marée haute aux mortes eaux, c. à. d. + Z + 3,50. Les calculs préalables avaient prouvé qu'il fallait, pour atteindre ce but, regagner un volume de sable de 3. 000. 000 m3 entre les jetées.

Les extrémités du côté mer se trouvent à la côte Z + 0,70 et sont établies sur une ligne de base régulière déjà située dans la fosse, aux grandes profondeurs (fig. 1)

La hauteur des enrochements de la tête atteint par endroits 8 à 9 m.

L'entredistance est variable en fonction de la longueur des jetées et de leur situation devant les digues.

I e profil en long de chaque jetée présente une pente variant entre 2 et 1,5 % selon la présence ou l'absence d'une possibilité de réflection de la houle contre les digues de mer à forte pente.

La pente à la tête des jetées du côté mer est de 5 : 1 (revêtement perméable) (fig. 2)

La section transversale de la tête présente un plan horizontal à la côté Z + 0,70 de 6 m de largeur avec une voie carossable de 3 m de largeur et des pentes vers les fonds de 4 : 1 (revêtement perméable) (fig. 3)

Aucune pente, même dans les sections les plus proches des digues, n'est plus forte que 3 : 1 dans la partie supérieure et que 5 : 1 dans la partie inférieure (revêtement imperméable)

Le but a été d'intercepter la houle et les vagues mais d'éviter toute réflection

La voie carossable est établie sur toute la longueur de la crête de la jetée ; afin de faciliter l'exécution et l'entretien ultérieur.

L'urgence des mesures à prendre a été prouvée d'une manière éclatante lors de la marée tempête du 1er février 1953. Les dégâts causés aux digues et épis des plages belges de l'Est sesont chiffrés à 250.000.000 F.B., montant plus élevé que les frais de réparation aux autres sites balnéaires et aux ports de la côte belge dans leur ensemble

A ce moment, les travaux de la première jetée venaient tout juste de commencer.

Or, l'exécution des travaux a coûté depuis lors:

25 jetées	:	325 millions de francs I
refoulement de sable:		29 millions de francs
	Total:	354 millions de francs

Si le programme avait été exécuté et terminé avant le 1er février 1953, il n'existe aucun doute, que pas mal de millions de francs auraient été économisés.

Nous avons en outre chiffré le montant des investissements publics et privés, rien que dans la zone de 250 mètres de large et de 8.000 m de long formant la véritable digue de mer en ces endroits:

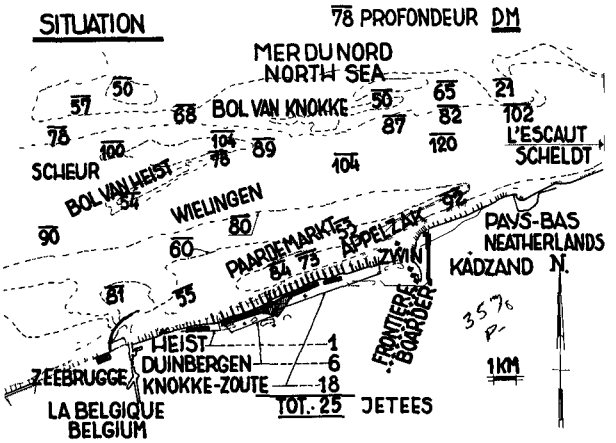

Fig. 1. Situation-profondeurs-jetées.

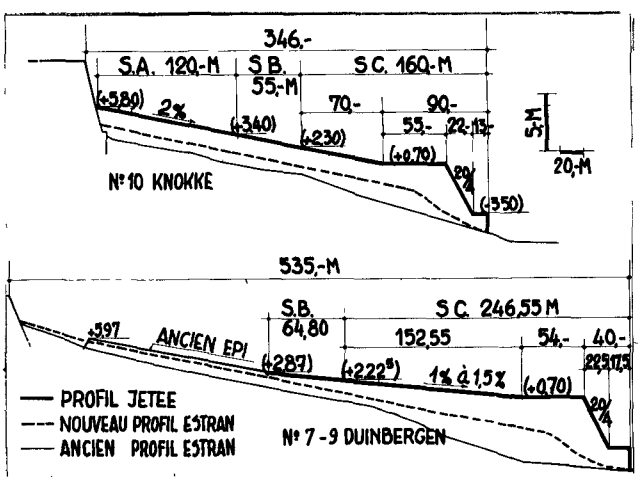

Fig. 2. Jetée et estran: profil en long.

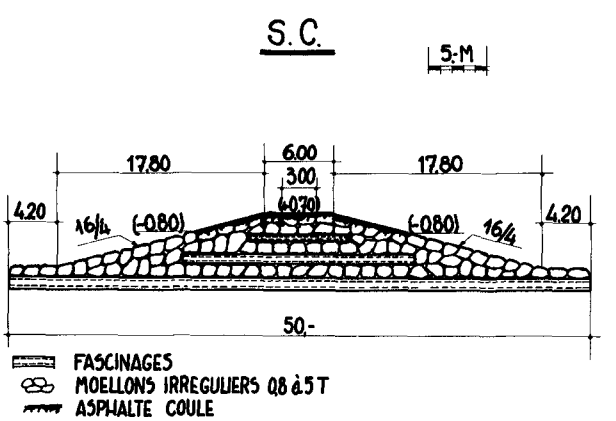

Fig. 3. Groyne and beach profile, Section C.

a) investissements publics (perrés - promenades - chaussées égouts - canalisations - cables)	:	1 milliard de francs B.
b) valeur des terrains privés	:	15 milliards de francs B.
c) valeur des bâtiments privés	:	15 milliards de francs B.
Total:		31 milliards de francs B.

Le programme de défense de ces plages a donc coûté un peu plus de 1 % de la valeur de la première digue de défense du pays contre l'envahissement par la mer.

\+ ++ +

CHAPITRE 5

EXECUTION DES TRAVAUX - 1952 - 1960

Les travaux aux trois premières jetées ont commencé fin 1952, trois mois avant la marée tempête du 1er février 1953, et les deux dernières jetées ont été terminées en juin 1960.

Mais déjà en septembre 1956 vingt-trois des vingt-cinq jetées étaient ou terminées ou en voie d'achèvement.

C'est à ce moment en 1956, 1957 que l'engraissement des plages a été accéléré par le refoulement de 1.250.000 m3 de sablé sur les perrés des digues de mer.

Ce sable a été sucé et emprunté dans le sous-sol de la région poldérienne au sud du chemin de fer Heist-Knokke (formation holocène moyen et inférieur et pleistocène).

Un étang de 10 ha et de 28 m de profondeur y a été créé à environ 1,5 km au sud de la digue de mer.

Le sable a été refoulé sur les plages sans reprise à une distance maxima de 5 km de l'étang par un cutter très puissant (Vlaanderen XI).

Les particularités essentielles de la construction des jetées sont les suivantes:

La partie la plus importante est la section C, située en mer sur la terrasse sous-marine. Cette section est construite sur pièces échouées

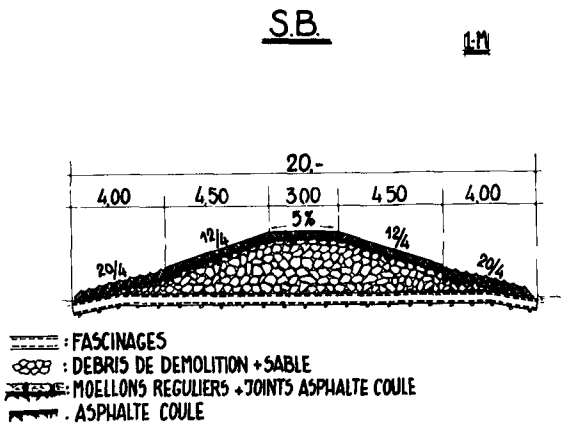

Fig. 4. Groyne and beach profile, Section B.

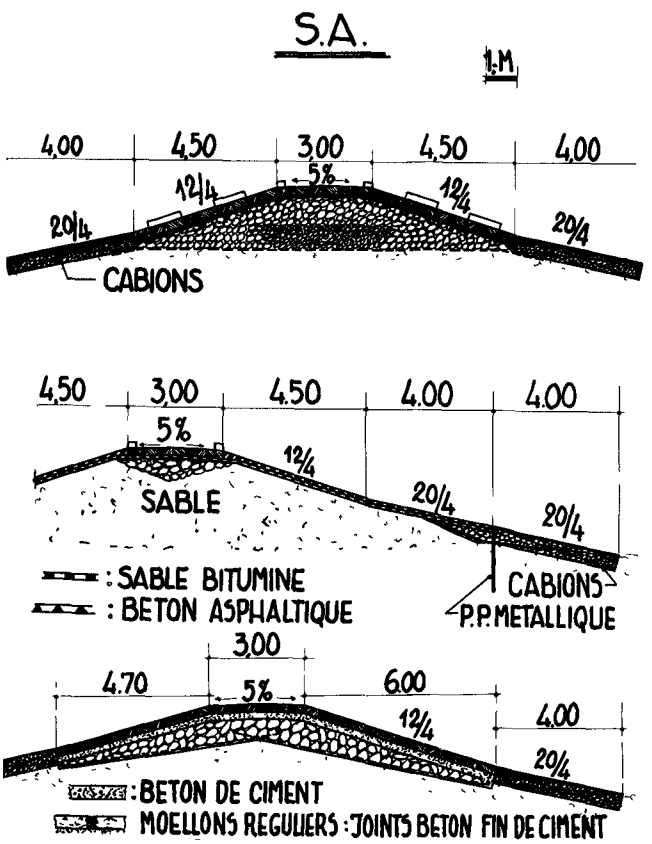

Fig. 5. Groyne and beach profile, Section A.

de fascinages, dont les largeurs atteignent jusque 60 m (fig. 3).

La crête est établie à la côte Z + 0,70 en moyenne. Des gros moëllons dont le poids atteint 3 000 à 5. 000 kg en carapace, constituent cette section.

A l'extrémité nord de la section C, les talus sont consolidés et protégés par le déversement d'asphalte coulé à chaud à raison de 900 kg par m2. La crête de6 m de large reçoit une pénétration d'asphalte coulé et est établie en voie carossable.

La section B est située sur l'estran entre la côte (0,00) et la côte (+ 1,00). Il s'agit d'une pièce d'échouage en fascines, lestée par moëllons au débris de démolitions. Un revêtement en moellons réguliers de 300 à 400 Kg recouvre tout le massif. Ces moëllons sont fixés et rejointés par l'asphalte coulé (fig. 4)

La démolition des ouvrages militaires datant de la seconde guerre mondiale et qui étaient très nombreux dans les dunes et le long du littoral, a permis la récupération de débris et de moëllons, qui constituent maintenant le corps des sections A et B des nouvelles jetées.

La Section A, située sur l'estran proprement dit, se construit de diverses façons, selon qu'il s'agit d'une jetée toute nouvelle ou d'un rehaussement d'une jetée existante, selon qu'il y a présence ou non de tourbe etc.. .. (fig. 5)

La section A, entre la digue et la section B, est constituée de parafouilles et/ou de plates-bermes, d'un massif formant le corps de la jetée et d'un revêtement.

Le parafouille est constitué de palplanches métalliques ou de gabions métalliques remplis de moëllons. Les vides sont remplis d' asphalte coulé ou de béton.

Le corps est constitué de débris de démolition et de sable. Le revêtement est exécuté soit en moëllons de pières calcaires maçonnés ou rejointoyés au bitume ou à l'asphalte coulé, soit en blocs de béton préfabriqués.

Pour certaines jetées, la partie supérieure, située au-dessus de mi-marée, a reçu un revêtement en sable bitumineux et béton asphaltique.

Les fascines ne sont jamais employées au-dessus de la côte (+1,00)

\+ + +

LA DEFENSE ET LE MAINTIEN DES PLAGES BELGES ENTRE ZEEBRUGGE ET LA FRONTIERE NEERLANDAISE

CHAPITRE 6

RESULTATS OBTENUS

Des sondages réguliers nous ont permis de suivre la progression du réensablement de la fosse entre les jetées nouvellement construites (voir réf. 2).

Les derniers sondages ont eté effectués en septembre 1959.

Le tableau suivant donne un aperçu des résultats obtenus et donne le gain en m2 par profil, à partir de la digue jusqu'à la ligne de base, réliant l'extrémité des jetées, ainsi que le relèvement maximum :

Profil situé entre les jetées	Relèvement maximum en m	Gain de sable en m2 par profil
n° 51 à Heist et n° 1 à Duinbergen	1,5	345
n° 3 et n° 5 à Duinbergen	1,5	350
n° 9 et n° 10 à Duinbergen	1,3	440
n° 2 et n° 3 à Knokke	2,6	510
n° 4 et n° 5 à Knokke	0,9	243
n° 6 et n° 7 à Knokke	1,4	430
n° 9 et n° 10 à Knokke	2,5	425
nr 12 et n° 14 à Knokke	1,6	240
2 Profils à gain record:		
n° 10 à Duinbergen et n° 1 à Knokke	3,1	850
n° 11 et n° 12 à Knokke	2,7	685

Les deux profils, où nous atteignons un gain record, sont situés dans des zones où une très forte érosion existait avant et où actuellement la marée haute n'atteint plus les digues

Le bilan qui en résulte s'établit comme suit en septembre 1959:

gain naturel de sable entre 1953 et 1959:	1.750.000 m3
déversement artificiel en 1956 et 1957 entre jetée 49 à Heist et jetée 12 à Knokke:	1.250.000 m3
Gain total en profil:	3.000.000 m3

Le gain naturel a été d'environ 300.000 m3 par an jusque 1957 et a diminué depuis à l'approche du nouvel état d'équilibre.

Entre septembre 1957 et septembre 1959, le gain total sur le fond de la fosse au nord de la laisse de marée basse et au sud de la ligne de base reliant les extrémités des jetées a été d'environ 600.000 m3.

Pendant cette même période de deux ans, un certain volume de sable, déversé artificiellement en 1956 et 1957 devant les digues , a été balayé et transporté vers les profondeurs au nord de la laisse de marée basse.

Le volume du sable déplacé s'élève à environ 300.000 m3. Ce déplacement a eu lieu entre les jetées 1 et 3 à Duinbergen et les jetées 1 et 10 à Knokke. Ce sont les deux zones où la réflection des vagues contre les digues reste fréquenteen cas de tempête.

Il reste donc pendant ces deux années un gain naturel de 300.000 m3 ou 150.000 m3 par an en moyenne.

Le gain total de 3.000.000 m3 de sable représente la quantité estimée préalablement nécessaire pour la stabilisation et pour le nouvel état d'équilibre des plages belges du littoral Est entre Duinbergen et la frontière néerlandaise.

REFERENCES

1. O. PETRI : Statistik der Meereswellen in der Nordsee
Seewetteramt des Deutschen Wetterdienstes.

2. J.E.L. VERSCHAVE: Maintenance of Beaches between the port of Zeebrugg and the Netherland's frontier
19 th. International Navigation Congres 1957 London

CHAPTER 52

THE DIKES OF THE POLDERS IN THE IJSSELMER

M. Klasema
C.H.de Jong
senior engineers
Service of the Zuiderzee Works,
The Hague, Netherlands

ABSTRACT

Since the circumstances on the IJsselmeer will change by the reclamation works, observations on the present lake cannot directly be used for the determination of the cross-sections of the dikes protecting the reclaimed land. The method of obtaining the necessary data (water level, wave attack) is discussed, as well as the determination of the design level.

A reasoned description is given of a typical cross-section of a polderdike.

INTRODUCTION

The Zuiderzeeproject comprises the enclosure of the Zuiderzee, a large shallow estuary (mean depth 3,5 m) of the North Sea, and partial reclamation of the enclosed area (fig. 1). The enclosing dam separating the Zuiderzee from the North Sea was completed in 1932. By building this dam the safety as well as the water management of the hinterland has been improved. The reclamation started in 1928 and is still in full progress. When completed, 2300 km^2 of arable land, divided over 5 polders, will be added to the landarea of the Netherlands. The reclaimed land is situated 4 to 5 m below the mean level of the IJsselmeer, as the remaining fresh water lake within the enclosed area is called. In view of the water management of the hinterland the minimum size of the lake has to be at least 1200 km^2.

The economic value of a polder of 500 km^2 is more than a thousand million guilders and 50000 or more people will live in it. Failure of the polder dike would mean an inundation during several months and would cause severe damage to all objects inside the polder. So the dikes protecting the polders against the water of the IJsselmeer have to meet with very high requirements of safety. On the other hand the construction cost of the dikes amounts to 4000 to 5000 guilders for each hectare reclaimed land, that is about 30 percent of the total reclamation cost. Therefore a careful study of the dike dimensions is necessary.

Failure of a polderdike could be due to overtopping of the crest by the waterlevel or by waves, to direct wave attack or to loss of stability. For the determination of the cross-section of the dike the variations in the waterlevel have to be known, as

well as the dimensions of the waves. Observations in nature on the open Zuiderzee or on the present large lake cannot directly be used, since circumstances on the final lake will be different from those on the former Zuiderzee or on the large lake. In the next chapters will be discussed how the necessary data for the final lake are obtained, after which a reasoned description is given of a typical cross section of the surrounding dikes of the new polders.

DEFINING FACTORS

The defining factors for the cross section of a dike are schematically shown in a longitudinal profile over the lake (fig. 2). The actual water level in front of the dike depends on the volume V of the water in the lake and the denivellation D of the water surface due to wind. The uprush U of the waves against the slope of the dike depends on the wave dimensions (especially the wave height H) near the dike, on the direction of the wave attack with regard to the direction of the dike, and on the cross-section of the dike. The importance of these factors varies for the different points along the dike. In some points the wind-effect (D and U) is dominant. In other less exposed areas the volume V is determinant.

THE WATER VOLUME OF THE LAKE

A certain mean lake level corresponds with a certain volume V. The variations with time of the mean lake level are due to natural circumstances - the supply to the lake surpassing the natural discharging capacity of the sluices in the enclosing dam - or to levelregulations in view of storage of water for periods of drought. Based on observations during the period 1932 - 1959, and taking into account possible future changes in water management, the mean lake level has been computed with an electronic computer for every day in that period assuming that the lake would have had its final size. The solid line V 30 in fig. 3 denotes the variation of the mean lake level during the severe flood period of january 1948, as observed on the lake with an area of 3000 km^2. The dashed line V 12 represents the computed course of the level on the final lake of 1200 km^2. The desired lake level in winter-time, the wet period, is 40 cm below the dutch reference datum N.A.P. (= approximately mean sea level). During floods long periods of exceedance of the desired level may occur, as is also shown in fig. 3. This makes it possible that a high lake level coincides with a gale with a strong windeffect.

THE WINDEFFECT

The windeffect consists of 2 phenomena: waves and denivellation of the water surface. Investigation of the denivellation and

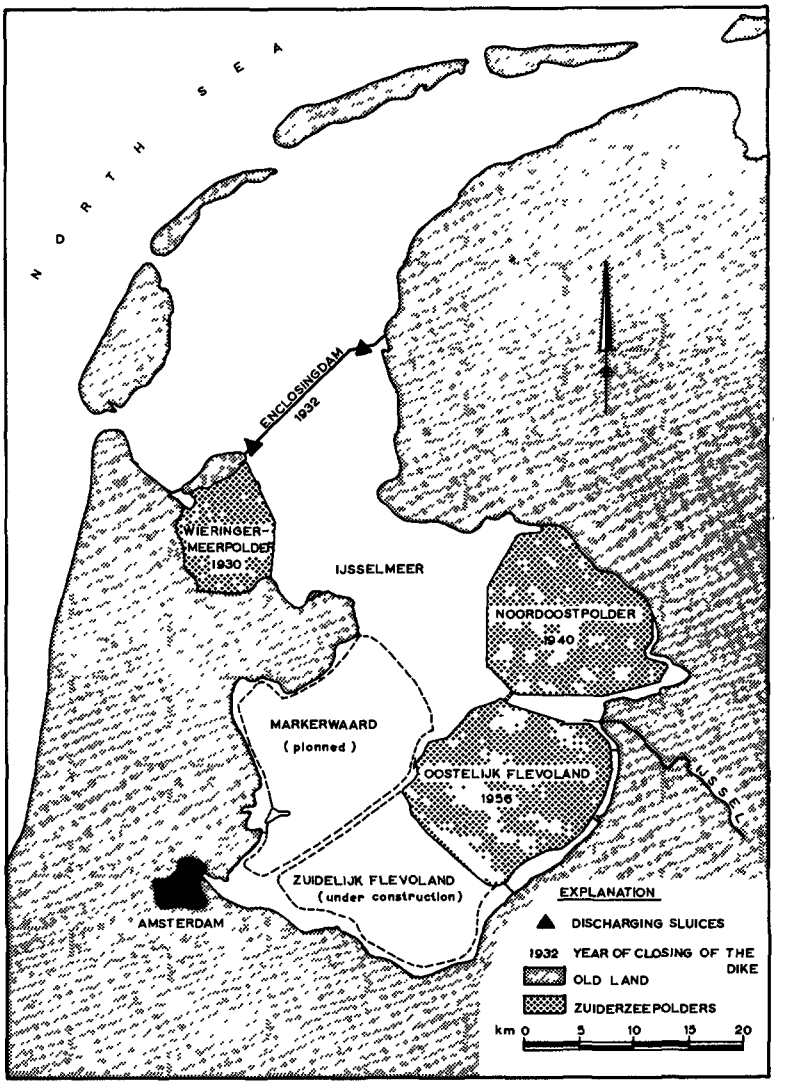

Fig. 1. The Zuiderzee project.

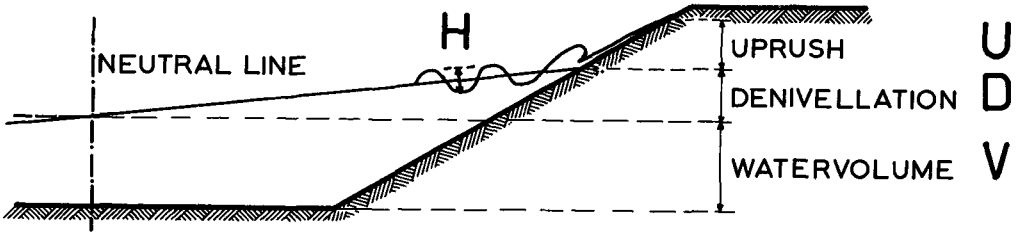

Fig. 2. Schematic longitudinal profile with defining factors.

the wind on the present lake has learned that after about one hour a stationary condition is reached, which can be calculated with the formula for windeffect in a closed channel (Lorentz 1926).

$$z = \frac{\alpha v^2 l \cos \varphi}{d}$$

where
z = denivellation (in m)
v = windvelocity on the lake (in m/sec)
l = length of the channel (in m)
d = depth of the channel (in m)
φ = angle between the direction of the wind and the axis of the channel
α = a constant = $0{,}36.\ 10^{-6}$ sec^2/m

With the aid of this formula the denivellation on the final lake has been calculated for different velocities and directions of wind; the results are marked down on maps. Fig. 4 shows an example of such a map; it gives the denivellation caused by a north-westerly wind of 25 m/sec, having a frequency of exeedance of 0,04.

For the determination of the height and length of shallow water waves on the lake Thijsses diagram (Thijsse 1948) has been used up till now. Of late wave heights have been observed on the lake with a floating wave recorder (Roest 1960). The wave dimensions on the lake are calculated for the same winds as the denivellation and are also marked down on the abovementioned maps (fig. 4).

Then the wave uprush on the dike is determined by using the results of modelinvestigations in the Hydraulic Laboratory at Delft (Wassing 1957). To verify the modelinvestigation a number of wave-uprush gauges has been installed on the existing dikes.

DESIGN CRITERION

After the calculation of the values on the final lake of each of the defining factors separately, they have to be combined to determine the dimensions of the dike.

At the reclamation of the Noordoostpolder in the years 1936 - 1942 frequencies have not yet been considered. The usual procedure up till then was that the highest known water level was chosen as design level. In concordance herewith the dimensions of the polder dike have been determined by applying a combination of the most

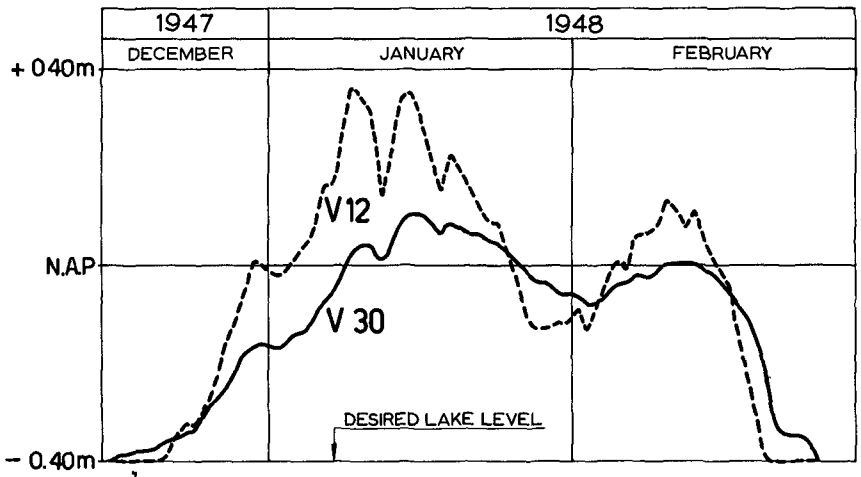

Fig. 3. Mean lake level during the severe flood period of January 1948.

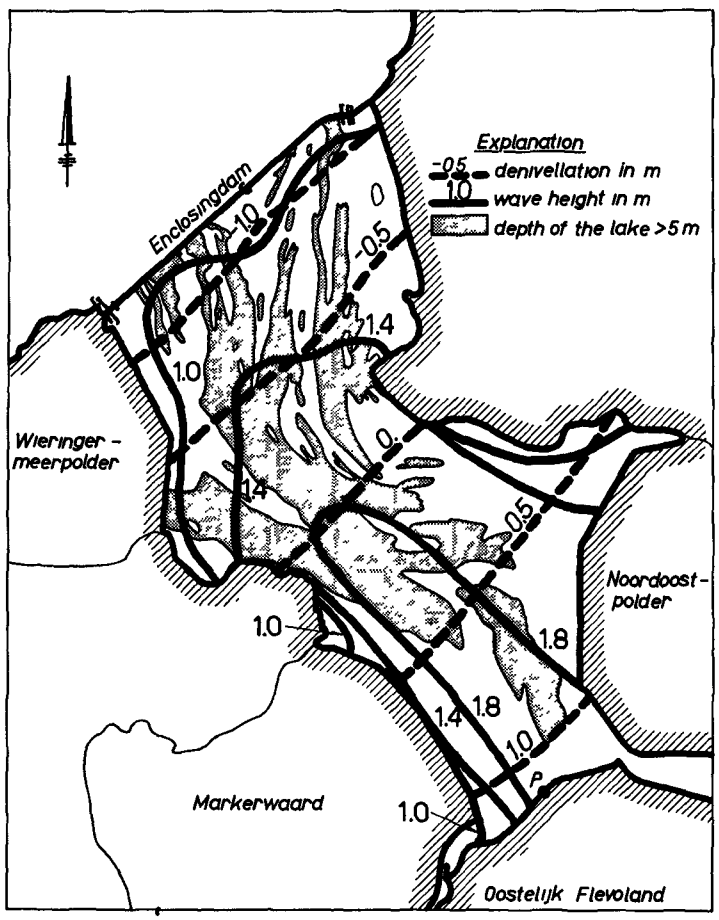

Fig. 4. Map indicating denivellation and wave height at a northwestern wind of 25 m/sec.

unfavourable conditions of water supply to the lake, limited discharge and windeffect on the considered part of the dike, which had ever been observed separately until then. Of course these values have been converted to conditions prevailing on the final lake. Calculation afterwards of the frequencies of overtopping showed that application of this method resulted in different chances of overtopping and consequently of failure for different points of the dike.

At the polder Oostelijk Flevoland, the reclamation of which started in 1950, frequency curves of the actual water level in front of the dike and of wave uprush - both measured with regard to N.A.P. - have been constructed for each part of the dike. The frequency curves have been defined in the way, demonstrated for the point P (fig. 4) with the aid of fig. 5, in which the scale of heights is arithmetic and that of frequencies (= mean chances of exceedance in a year) logarithmic. In this diagram solid lines indicate the calculated frequency curves of the mean lake level V and of the windeffect D + U (U being the uprush which is exceeded with a frequency of 0,02). It is evident that at low frequencies the curves are straight lines on semi-logarithmic paper. For this reason the curves, if necessary, have been extrapolated by straight lines. The frequency curves of windeffect and mean lake level have been combined to a frequency curve for the top of the wave uprush with regard to N.A.P., whereby the dependance of windeffect and lake level has been taken into account. The top of the 2% wave uprush with a frequency of 0,001 has been chosen as a criterion for the height of the dike.

The actual water level in front of the dike is also an important factor. The frequency curve of D + V with regard to N.A.P. has been determined in a similar way as for the wave uprush by combining the frequency curves of D and V. Because overtopping of the dike by the water level causes a more dangerous situation than that by the wave uprush, a frequency of 0,0001 has been selected as the criterion in this case.

As a result, and in contrast to the dike of the Noordoostpolder, the dike of Oostelijk Flevoland bounded by the final IJsselmeer has the same strength everywhere. A weak point in the calculation is however the ill-known dependance of windeffect and mean lake level.

For the remaining polders the following procedure is considered. Based on observations on the large IJssellake it is possible to construct for the final situation for a period of 30 years a series of data concerning mean lake level, actual waterlevel and actual waterlevel + wave uprush for different points along the dike, and hence to derive a frequency distribution of these phenomenae. To get the design level these curves have to be

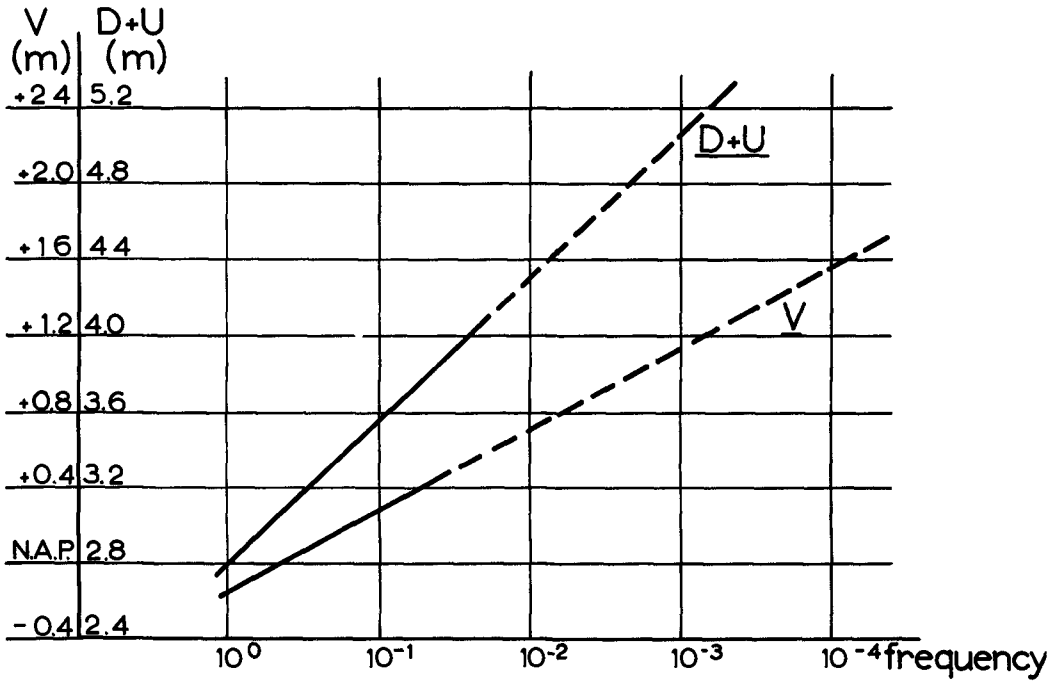

Fig. 5. Frequence curves of mean lake level on the final lake and of wind effect (D + U) in point P.

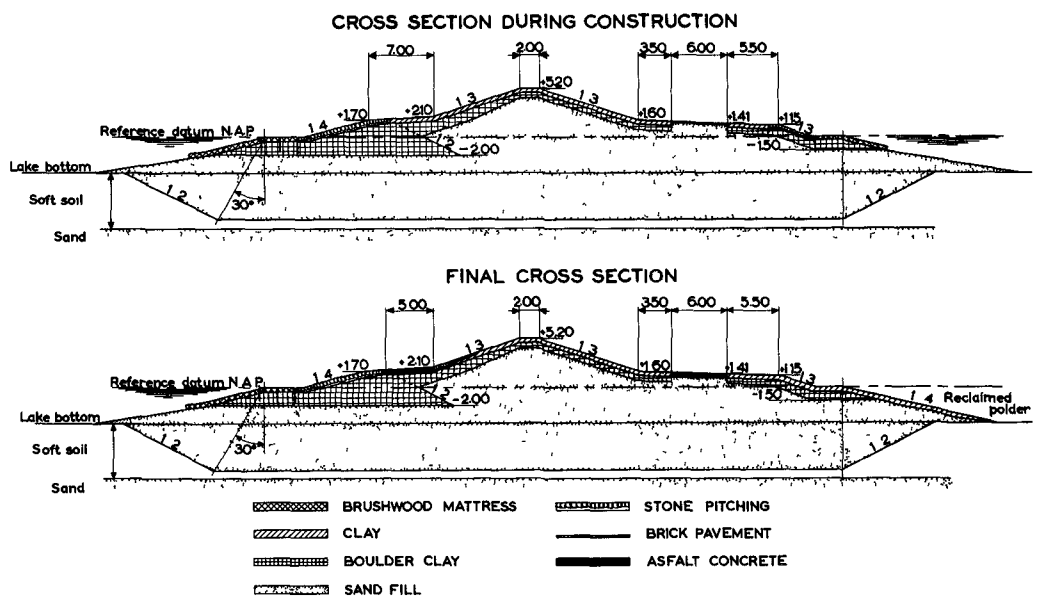

Fig. 6. Typical cross section of polderdike.

extrapolated. In this way the difficulty of combining the separate frequency curves of lake level and windeffect is met.

Another difficulty remains. The design level can be reached by a combination of a low lake level and a strong windeffect, but also by a combination of a high lake level and a weak windeffect. The chance of failure is not the same in these cases, whereas at the determination of the frequency curves these cases have got the same weight. For that reason it seems appropriate to check the so achieved dike dimensions by choosing a very rare value for one of the defining factors and a moderate value for the other one. The first check is then a flood with a frequency of occurrence of for instance 0,0001. Calculate the corresponding mean lake level, assuming a limited discharging possibility of the lake and combine this lake level with a moderate storm. The other check is an extreme wind on the lake combined with a moderate exceedance of the lake level.

The frequency of these checks is only very roughly known, but the same applies to a design level obtained by extrapolating a frequency curve based on observations during a period of less than a century to frequencies of 0,001 or even 0,0001. The importance of frequency considerations lies mainly in the possibility of achieving an aequivalent safety for the different low lying parts of the country.

DESIGN OF CROSS SECTION

STABILITY AND SETTLEMENT

Since one of the original aims of the Zuiderzeeworks was the reclamation of large areas of arable land, the new polders are projected in those parts of the former Zuiderzee where the top-layers of the soil consist of fertile clay. These claylayers which are locally alternated by layers of peat have a limited bearing strength, which would not be sufficient to carry the heavy load of the dikes without endangering the stability of the construction. Furthermore these thick and very soft layers would give rise to a considerable settlement of the dike, which in itself would be undesirable in view of the requirements concerning dike height etc, discussed hereafter.

In order to warrant a stable dike of more or less constant height the greater part of the soft layers in the proposed dikeline is removed and replaced by sand before building the dike. The width of the excavation depends on the width of the dike - which in itself is dependant again on its height and on the gradient of the side slopes - and on the depth of the excavation. The width will have to increase with depth in order to meet the spreading of stress in the bottom.

Since the thickness of the soft layers is limited it would be obvious to remove them to their total depth, thus excluding any danger for slidings and reduce settlement to a minimum. The clay and peat layers are, however, normally underlain by strata of sand reaching to depths of some hundreds of meters and containing artesian water. It is therefore undesirable to make a short circuit between these deep sand strata and the sandbody of the dike and consequently with the polder. This could enhance the seepage to the polder to an intolerable amount in regard of the pump capacity and it could endanger the stability of the inner slopes of the dike.

It has become normal practice therefore not to remove the soft layers to their total depth but to leave a layer of appr.1.00 m thickness in its place on top of the deep sand strata. This layer will be compacted by the load of the dike and will constitute a nearly impervious separation between the sandbody of the dike and the deep sand strata. The settlement of the dike, due to compaction of this layer, will normally not exceed 30 to 35 centimeters and this can be easily overcome by giving some extra height to the dike during construction.

COMPOSITION OF DIKES

Since sand can be borrowed from the bottom of the IJsselmeer at a suitable depth, generally in the immediate vicinity of the works, it is by far the cheapest building material that can be obtained and consequently the main body of the polderdikes will consist of sand. This body of sand has, however, to be protected against currents and wave attacks, measures have to be taken to limit percolation and even those parts of the cross section that are not exposed to these phenomena will have to be covered in order to forestall erosion by wind and rain.

It is considered that beyond a depth of N.A.P. - 2 m (which is appr. half of the depth in front of the dikes, built in the deepest part of the area to be reclaimed) sand will be stable without any covering layer, provided the angle of the slope is well below the angle of natural repose under water. The uncovered sandslopes are normally built with a gradient of 1 : 6.

Above this depth a more resistant material has to be used. In the IJsselmeer-area boulderclay is applied. This is a heavy glacial loam, which crops out of the bottom of the northern part of the IJsselmeer in several places, for instance near the former island of Urk, where it can be dredged. This material is practically impervious, it is temporarily current and wave resistant, it has a high cohesian and a high shearing strength. It is therefore an excellent dikebuilding material and it is used not only as a permanent impervious covering layer between the sandbody and the protective layers of brushwood or stones but as well as a temporary

wave resistant protection which enables a running working method without any inadmissable risks.

For the ultimate situation the boulder clay has to be protected against wave attacks and erosion. The part below mean lake level is protected by brushwood matresses, loaded with rip-rap, the slope above this level is partly covered with a stone pitching, consisting mainly of columnar basalt blocks, and partly by a grasscover on a layer of fresh clay. The clay can be borrowed from the IJsselmeer near the works, brushwood is borrowed from the outer marches of the Dutch rivers and estuaries; the stones for rip-rap and stone pitching form the only material to be imported from abroad.

SHAPE OF CROSS SECTION

Under normal conditions of water supply and discharge the water level on the lake fluctuates around the referencedatum N.A.P. The part of the dike between some decimeters below and above N.A.P. will therefore be exposed to the daily wave-attack. A horizontal berm on this level, which is already necessary to fix the brushwood matresses on their place, will at the same time serve as an energy dissipating berm. For this reason this berm is made rather wide and it is covered with heavy rip-rap (120 - 240 kg), neatly placed and locked up by two rows of wooden piles.

Another berm has been designed on the height of the design lake level, which, as stated before, will differ for different points in the lake. This berm serves to partly dissipate the energy of the waves, breaking on the slope of the dike and so deminishing the height of the wave uprush along the upper slope. The width of the berm to be fully effective should be at least 1/4 to 1/3 of the length of the waves occurring under the assumed conditions.

The gradient of the slopes and the weight of the stones used for the stone pitching are closely interrelated. A steeper slope requires heavier stones, a more gentle slope results in a larger area to be covered with stones but the length and weight of single stones can be less. The angle to be chosen is therefore partly a question of economy.

The minimum angle of the slope, however, has to be decided on stability considerations. It is found that for dikes exposed to the heaviest wave attacks to be expected on the IJsselmeer the gradient of the slope should not exceed 1 : 4 and for less exposed dikes 1 : 3.

The gradient of the slopes on the polderside of the dikes in their final state is entirely decided on considerations of stability, assuming the crest being overtopped by waves or the waterlevel on the lakeside rising to an extreme height.

SLOPE PROTECTION

The strength of the slope protection can be adapted to the power of the wave attack, which will change with height. The strongest protection will have to be made on that part of the slope that will be exposed to the strongest wave attack, i.e. approximately on the height of the design level, just underneath

the high outerberm, where the breaking waves at the design level hit the slope. Beneath and above this strip, which may be rather wide, the strength of the protecting layer can decrease proportionally to the decrease of the wave force.

In accordance with this, lighter and cheaper materials are used on the slope above the berm and part of this slope, that will only under extreme conditions be reached by the tops of a small number of waves, has got merily a grass protection.

The slopes on the polderside of the dike have to be protected temporarily against wave attack, because during construction the future polder is still part of the lake. The protection of the lower part of these slopes consists therefore temporarily of a stone or concrete pitching, which is composed in such a way that after the polder has been drained, the materials can be used for protection of the outer slope above the berm. The uppermost part of the inner slope and the crest of the dike are protected by a grass cover on a layer of fresh clay.

REQUIREMENTS FOR TRAFFIC

During the first years of reclamation, when there are still no road connections through the polder, it is essential that all points of the circumference of the polder can be reached by road in order to be able to start the reclamation works from several different points. To this end a road has been designed on the dike, mostly on the crest, that has to be widened then, sometimes, especially at the higher parts of the dikes, on a berm.

As far as these roads are built on dikes bounded by the IJsellake in its final shape and size, they should have a closed road surface in view of the possibility of overtopping of the dike. Since, however,initial settlement of the dike may differ rather strongly from one point to another, a temporary brick pavement is applied during construction. After a couple of years, when the greater part of the settlement of the subsoil has taken place and the road foundation has been compacted by traffic, this brick pavement will be replaced by a road surface of asphalt concrete.

REFERENCES

Lorentz, H.A. Verslag van de staatscommissie inzake hoogere waterstanden tijdens storm, als gevolg van de afsluiting van de Zuiderzee. 1926.

Thijsse, J.Th. Dimensions of wind-generated waves. Assembly I.U.G.G., Oslo,1948.

Roest, P.W. Wave recording on the IJsselmeer. VIIth Conference on Coastal Engineering. The Hague, 1960.

Wassing, F. Modelinvestigation on wave run-up carried out in the Netherlands during the past twenty years. VIth Conference on Coastal Engineering. Florida, 1957.

CHAPTER 53

COASTAL PROTECTION WORKS AND RELATED PROBLEMS IN JAPAN

Masashi Hom-ma and Kiyoshi Horikawa

Department of Civil Engineering, University of Tokyo

Tokyo, Japan

INTRODUCTION

Japan consists of 4 main islands named Hokkaido, Honshu, Shikoku and Kyushu, which, together with numerous smaller islands scattered around, are so aligned as to form a slightly bent arc off the eastern fringe of the Asiatic Continent. (See Fig. 1.) The dominant geographies of these islands are represented by relatively high mountains located in the center and narrow strips of plane lands lying along the coastlines. It is in thes coastal planes that the cores of the Japanese industrial and other economic al activities are deployed with swarming population. The entire area of Japan is approximately 320,000 km^2 and the surrounding coastlines are 14,560 km long.

Traditionally the economy of Japan depended heavily on agriculture and fishery, which necessitated active reclamation works around the esturine lowlands as well as establishment of small fishery ports in great numbers at various parts of Japan.

The growth of her economical potency came to cast floodlight on the importance of marine transportation, and the commercial ports came to thriv at numerous estury harbors. The land extension works along the coast line are even flourishing today, but they are aimed at creating the sites for modern industries. It should be emphasized that Japan has been utilizing the coastal areas to an utmost extent for survival as well as prosperity, and further that this trend is destined to persist also in the future in order to keep pace with her economical development.

Unfortunately, the geographical situations as well as other unfavorabl natural conditions distinguish Japan as one of the most disaster-ridden countries in the world. The islands of Japan are pestered by the tropic- al cyclones or typhoons of the western Pacific which haunt her several times every year. They may hit her by a head-on landing or near-missing, leaving tremendous disasters in the wake. Worse still, seated right on the earthquake belt, she is also subjected to disasters caused by occational crustal motions and tsunamis. Most of her long coastlines are where formidable energies of wind waves and ocean swells are let loose, which would claim for frequent destruction of maritime structures, erosion of coastlines, and sedimentation of harbor basins. Apart from the disasters

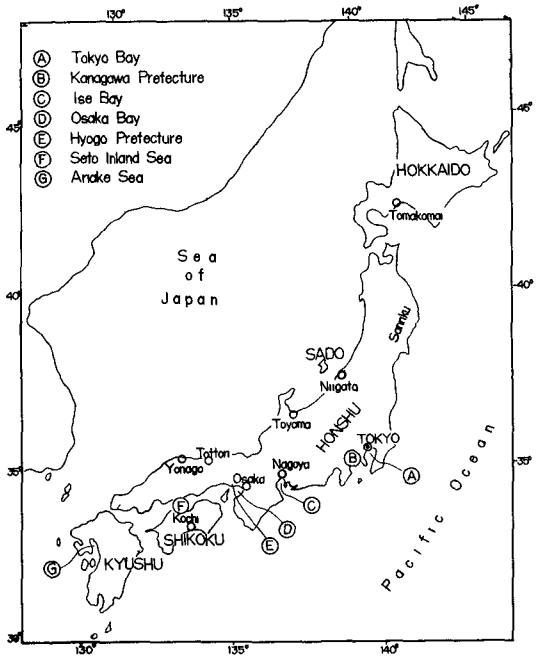

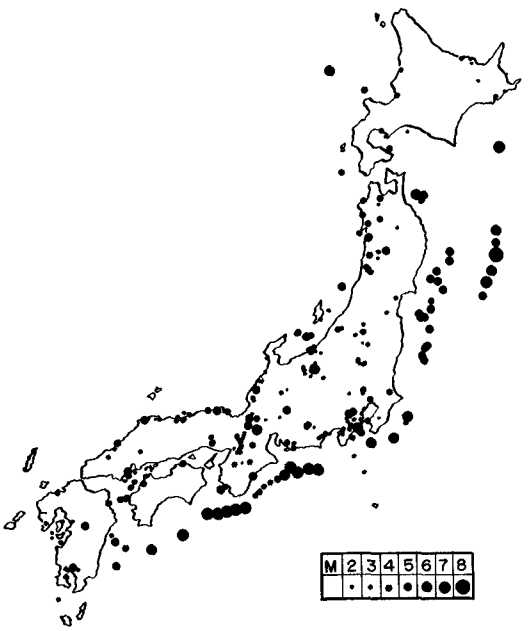

Fig. 1. Fig. 2

Fig. 1. Map of the Japan Islands

Fig. 2. Distribution of Epicenters and Magnitudes of Great Earthquakes (after H. Kawasumi)

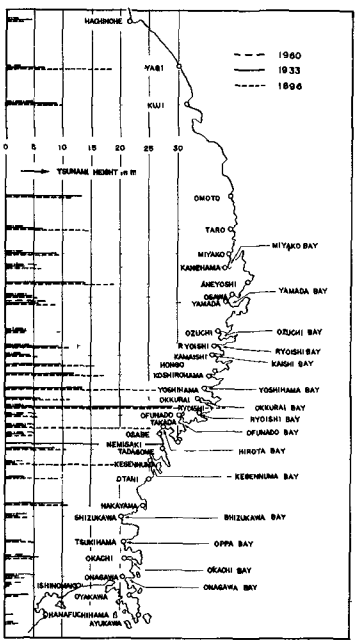

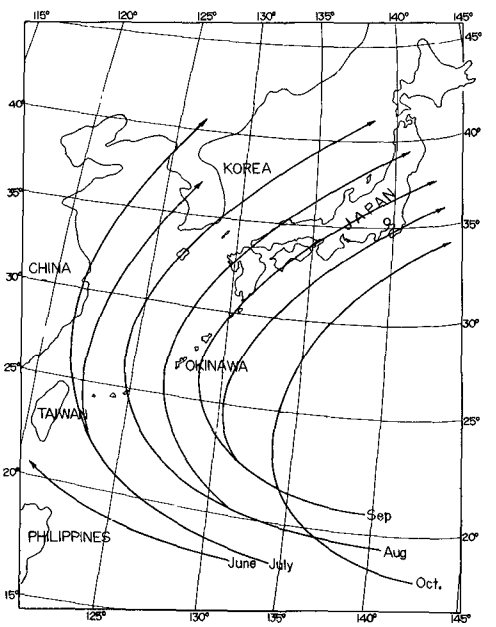

Fig. 3. Fig. 4

Fig. 3. Comparison of Maximum Water Levels due to Tsunamis in 1896, 1933 and 1960, above the Tokyo-Post datum (Approximately equivalent to M.W.L.) along the Sanriku Coast.

Fig. 4. Ordinary Typhoon Paths

for which the natural elements are primarily responsible, we must point ou the effects of artificial interferences such as debris barriers, dams for power generation, flood control or water supply, diversion channels, river mouth jetties, breakwaters, and even coastal groins, which seem all to combine to account for recent progress of erosion along the vaious sandy coasts of Japan by working on the delicately balanced equilibrium of natur The Japanese engineers face a number of such exceedingly intricate problem today. They have been striving to overcome and effectively control these problems in order to preserve the valuable coasts which she cannot afford to lose any more.

This paper will first introduce the general factors affecting the coa al problems in Japan, and proceed to discuss the patterns with which some these factors were linked to produce particular coastal problems. We will next review the efforts and contributions made by the Japanese engineers t solve such problems. Finally the coastal protection works and practices will be presented with some representative examples.

FACTORS AFFECTING THE COASTAL PROBLEMS IN JAPAN

We may classify the factors which are considered to be related to coastal problems under four main categories: (1) geomorphological aspects, (2) meteorological and oceanographical aspects, (3) sediments, and (4) artificial interferences. We will discuss the factors with special emphasis on the characteristics particular to Japan.

Geomorphological aspects

The islands of Japan lie along the circum-Pacific seismic zone. Fig. 2 shows the epicenters and magnitudes of 343 great earthquakes which have been traced by H. Kawasumi from the records of the past 1350 years.[1] These earthquakes almost frequently produced the crustal motions which resulted in repeated elevation or subsidence of the earth levels along the coastal regions as well as on the sea bed. For instance it has been reported that the coastal areas of the Sagami bay were heaved by 1 to 2 m during the great Kanto earthquake in 1923.[2] So pronouncing are these crustal processes occurring along the coasts that the engineers are compelled to regar the geomorphological movement as one of the principal factors influencing the coastal processes in Japan.

Meteorological and Oceanographical Aspects

There lies an outer belt of earthquake zone along the offshore of the Pacific coasts of Japan, where great earthquakes used to deform the ocean bed producing the tsunamis. Beside the tsunamis which were generated at the nearby epicenters, some traveled a long way to hit the Japanese coasts from a faraway center of their birth, such as one caused by the Chilean earthquake in May, 1960.[3] Table 1 shows the great tsunamis ever recorded in history. The most outstanding of them all were the Sanriku tsunami in 1896 and 1933, and the Chilean-earthquake tsunami in 1960. They inflicted most formidable disasters on the Ria coasts of Sanriku, the north-eastern region of the Honshu island, which is exposed to the Pacific Ocean to the

TABLE - 1

Year	(1) Location	(2) Grade of Tsunami	(3) Magnitude of Earthquake	Year	Location	Grade of Tsunami	Magnitude of Earthquake
684	E	III	8.4	1771	G	III	7.4
869	B	IV	8.6	1854	D	III	8.4
887	DE	III	6.5	1854	E	III	8.4
1361	E	III	7.0	1896	B	IV	7.6
1498	D	III	8.6	1933	B	III	8.5
1605	DE	III	7.9	1944	D	III	8.3
1611	B	IV	8.1	1946	E	III	8.1
1703	C	III	8.2	1952	A	II	8.2
1707	DE	IV	8.4	1960			8.7
1741	F	III	6.9				

(1) See the Attached Map.

(2) Grade Total Energy (after R. Takahashi)

II	4×10^{22} erg
III	16×10^{22} erg
IV	64×10^{22} erg

(3) Richter-Gutenberg's Scale

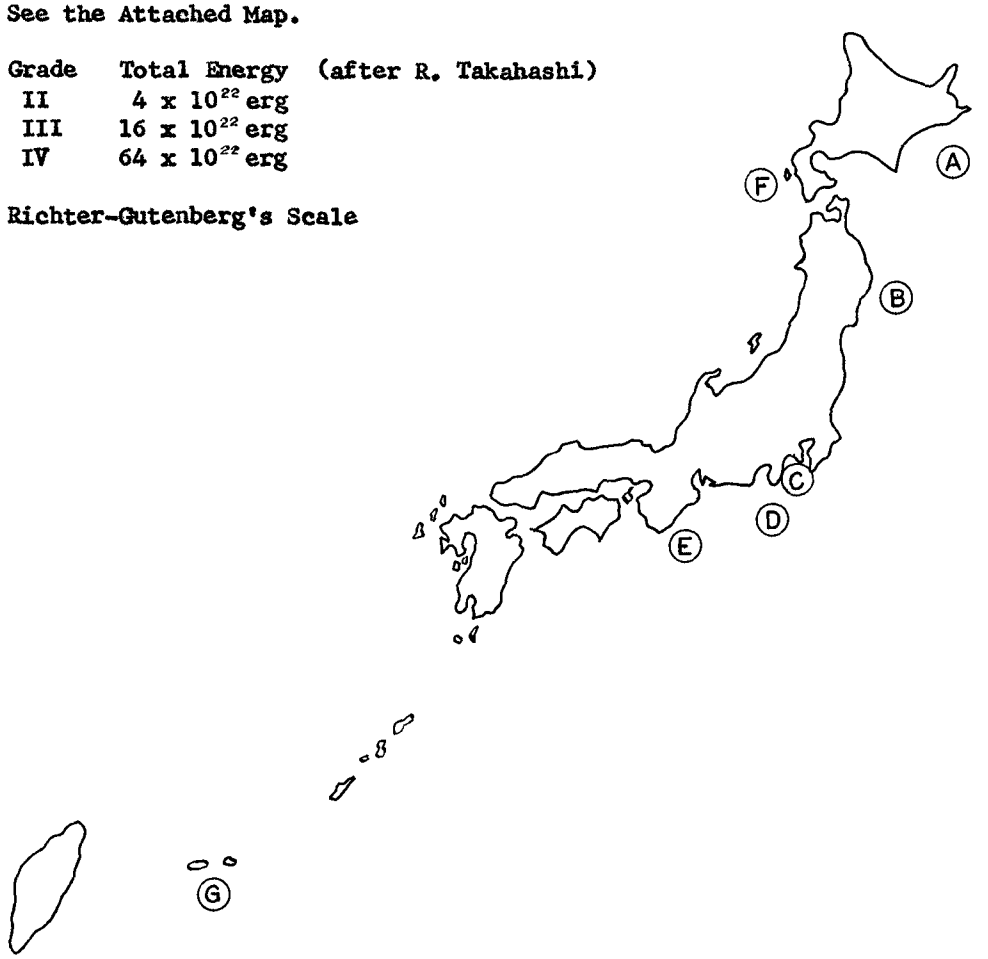

east. Fig. 3 compares the maximum run-up reached by these tsunamis at various localities. It must be noted that the patterns of the rising water inside the bay areas were different between the Sanriku-earthquake tsunami in 1933 (of the period of approximately 12 min.) and the Chilean-earthquake tsunami in 1960 (of the period of approximately 60 min.). Such difference is supposed to result from the relationship between the normal vibrational periods of the bays and those of the tsunamis invading them.

The natural forces acting upon the coasts are represented by the meteorological factors such as the violent winds generated by typhoons or migratory cyclones, and by the oceanographical factors such as waves and currents. Efforts have been made at various coastal areas of Japan to forecast the waves from meteorological data. On the other hand, mainly spurred by the recent development of harbor projects or purely for the purposes of coastal engineering studies, the actual measurement of wave has recently been accelerated shedding light to a great extent on the characteristics of the meteorological and oceanographical factors prevailing in the water around Japan.

The seas around Japan must be dealt with separately for the factors peculiar to each of the three sectors: (1) the Pacific Ocean coasts, (2) the Japan Sea coasts, and (3) the sheltered bays.

The Pacific Ocean coasts - Exposed to the great open sea of the Pacific Ocean, this sector is subjected to the influence of a typhoon during summer to fall. The ordinary path of a typhoon varies for each month. (See Fig. 4.) Table 2 shows the average number of typhoons generated in the southwestern sea of the Pacific Ocean and the number which landed on Japan, per annum. It is understood from the table that Japan is attacked at least by 2 or 3 typhoons annually which command an appreciable domain of influence with a formidable charge of destructive energy. One that carried the greatest energy was the Muroto typhoon which caused a great storm surge in the Osaka bay on September 18, 1934. The typhoon No. 15 of 1959, usually called the Ise-bay typhoon, is only next to the Muroto typhoon as far as the significance of the disasters due to a storm surge is concerned. (See Fig. 5.)

The most dominant waves occuring along the Pacific coasts of Japan are generated by the typhoons, which emanate forerunning swells for days well before its farthest perimeter comes to feel the coastlines. According to the studies made by T. Ijima, the periods of the typhoon swell recorded at the Japanese coasts range approximately from 12 to 14 seconds, and the significant wave heights from 1 to 2 m, rarely attaining 3 to 4 m. As the typhoon approaches the coastlines, i.e., as the decay distance is shortened the wave period tends to drop slightly, but only to increase sharply soon as the wave heights gain in magnitude.(4) S. Nagai estimates the maximum height of the wave inside the typhoon No. 15, 1959, as 3.5 to 5.5 m, based on the sliding pattern of the breakwaters in the Wakayama prefecture.(5) S. Unoki has presented the classified diagrams showing the distribution of wave heights and periods occurring in the deep water inside a typhoon from the records of the seafaring vessels and weather ships.(6)

The influence of a typhoon varies according to the path and the

TABLE - 2

Statistics of Typhoon

		Jan	Feb	Mar	Apr	May	Jun	Jul	Aug	Sep	Oct	Nov	Dec	Total
No. of Typhoon Generated		0.2	0.2	0.2	0.4	0.9	1.4	4.1	5.7	4.8	3.1	1.5	1.1	23.5
No.of Typhoon which attacked Japan	Mean	-	-	-	-	0.02	0.11	0.31	0.76	0.82	0.33	0.03	-	2.47
	Max	-	-	-	-	1	1	2	4	4	2	1	-	7

TABLE - 3

Recent Record of Great Storm Surges (1900 - 1959)

Date	Location	Height in m
Aug. 25, 1914	Ariake Sea	2.0 - 2.5
Oct. 1, 1917	Tokyo Bay	2.3
Sep. 13, 1927	Ariake Sea	about 3.0
Sep. 21, 1934	Osaka Bay	3.1
Sep. 17, 1945	Kagoshima Bay	2.0
Sep. 3, 1950	Osaka Bay	2.4
Sep. 26, 1959	Ise Bay	3.5

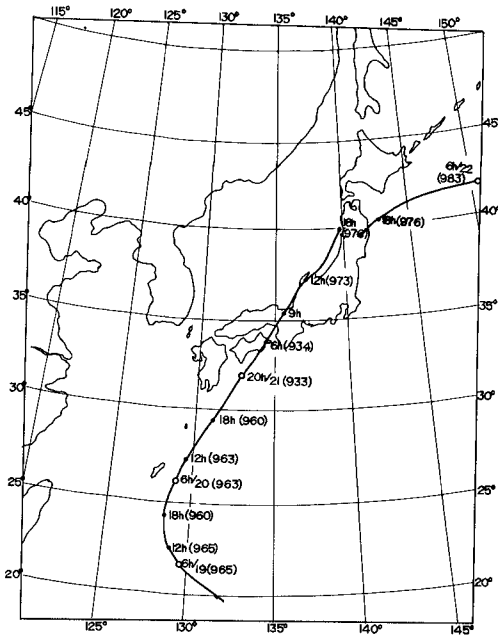

Fig. 5 (a)

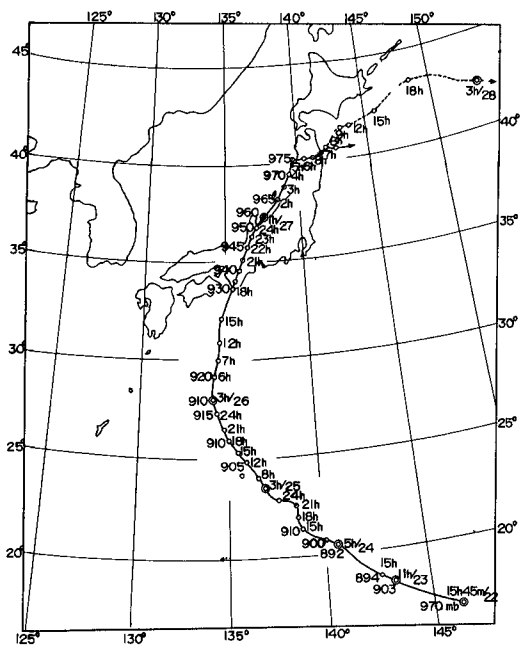

Fig. 5 (b)

Fig. 5(a). Path of Muroto Typhoon (Sept. of 1934)
Fig. 5(b). Path of Ise-bay Typhoon (Sept. of 1959)

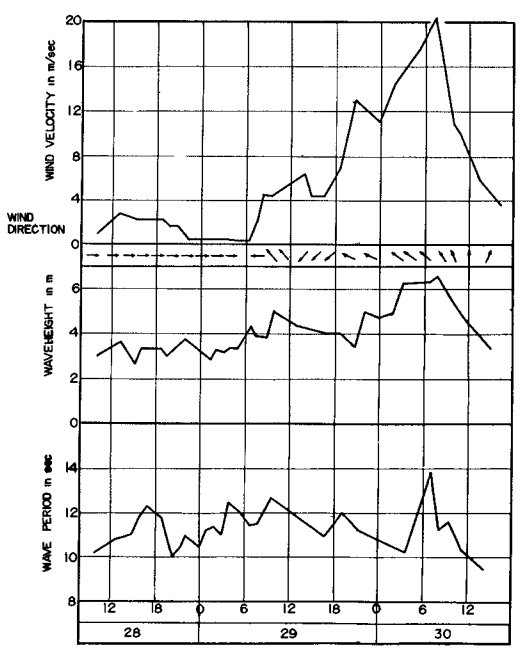

Fig. 6

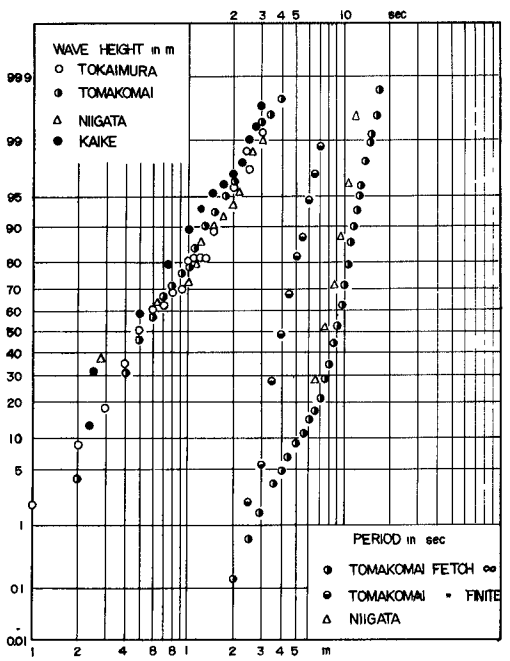

Fig. 7

Fig. 6. Record of Waves due to Typhoon No. 22, Sept. 1955, Recorded Outside the Kochi Port (after T. Ijima)
Fig. 7. Comulative Probability Distributions of Wave Height and Period along both the Pacific Ocean Coast and the Japan Sea Coast

direction of the coastline exposure. The coasts west of the Tokyo area are thus subjected to greater influences of a typhoon than the coasts northeast.

Fig. 6 shows the waves due to the typhoon No. 22, September 1955, recorded outside the Kochi port by using a pressure-type wave recorder. This record shows the maximum wave of 6.5 m in height and 13.8 sec in period.

During winter and spring a family of lows migrate eastward from the Asiatic Continent across the islands of Japan. However, since the Pacific coasts are located at the lee, the waves due to the migratory lows seldom exceed 3 to 4 m in height and 10 to 11 sec in period.

Throughout a year, several isolated fetches occur simultaneously over the northwestern Pacific. The waves generated in them have a long distance of decay to cover before reaching our coasts. The Pacific coasts of Japan are constantly subjected to these long-range swells which, even in the most tranquil weather, attain the significant heights of approximately 0.5 m and periods of 9 seconds. Fig. 7 shows the cumulative probability distribution of the heights and periods of shallow water waves based on the visual observations made at Tokaimura and Tomakomai along the Pacific coasts, and at Niigata and Kaike along the Japan Sea coasts.

The Japan Sea coasts - The coasts facing the Japan sea are exposed to the confined fetches not exceeding 800 km in any direction. There is little influence of a typhoon here. The feature characterizing the Japan Sea coasts is a long spell of violent wind waves occurring during winter due to the migratory lows. Only swells of relatively short periods may occur here due to limitation in fetches. The pronouncing pattern which distinguishes the Japan Sea coasts from the Pacific coasts is that a complete calm dominates the Japan sea coasts occationally due to absence of a fetch during June to August. On the other hand, during winter the sea is continually covered by a violent fetch after another which takes place in the wake of incessant passage of lows. Fig. 8 shows the probable occurrence of strong winds for each month in the vicinity of Niigata; Figs. 9 (a) and (b) show the probable occurrence of waves for each month respectively at Niigata and at Tokaimura (Pacific coast).

The results of field observation show that the significant waves occurring along the Japan Sea coasts seldom exceed 12 to 13 sec in period and 7 m in height.[4)&(7)] Based on the maximum duration for each magnitude of wind velocities derived from the records at Niigata in 1957 and 1958 and after some assumptions for simplicity, we evaluated the greatest possible waves corresponding to the maximum fetch length of 800 km by utilizing the generalized forecast diagram by Sverdrup, Munk and Bretschneider. The results are shown in Fig. 10, which give 5 to 8 m and 11 to 13 sec for heights and periods of the greatest possible significant waves expected at the Niigata coast. We are planning to test the adequacy of this treatment by actually measuring the waves at the Sado Island which is located 35 km offshore of Niigata.

The Sheltered bays - This category includes the bay area such as the Tokyo bay, the Ise bay, the Osaka bay, the Seto inland sea, and the Ariake Sea, that

are effectively sheltered from the ocean swells due to topographical situations. Violent waves found in these bay areas are caused by a typhoon passing nearby. When a typhoon passes the westside of the bay, i.e., when the bay is covered by the dangerous semi-circle of a typhoon, the significant wave invading the bay may attain as high as or less than 3 m in height and 6 to 7 sec in periods.

Far more serious than the waves is a storm surge occurring inside the bays due to wind set-up caused by a typhoon. Table 3 shows the records of the storm surge levels which occurred in Japan from 1900 to 1959. To quote K. Okuyama and S. Unoki: "The coasts along the Tokyo bay, the Osaka bay, the Seto inland sea and the Ariake Sea are haunted by storm surges, where the meteorological tide at times exceeds 2 m. The coasts of the Ise bay and the Kagoshima bay come next in fame for storm surges often attaining 1 m in levels."(8) The Muroto typhoon in 1934 caused the record height of a storm surge amounting to about 3 m in Osaka harbor. The typhoon No. 15 in 1959 sent an extraordinary storm surge as high as 3.5 m in the Ise bay, the event being discussed in further details under the separate title in this conference. Since the coastal areas of these bays consist mostly of reclaimed lowlands where key industrial and agricultural establishments are thickly distributed, the consequent disasters are tremendous.

Sediments

The sediment process if as vastly important and also difficult to tackle as any process occurring along the beach. Back in 1953, the report by K. Aki, "Beach Erosion in Japan", referring to important erosing beaches in Japan, indicated that the cause of erosion is primarily attributed to deterioriation of rivers as a source of sediment supply.(9) A number of studies have since been performed trying to solve the coastal sediment problems in Japan. However, none seems to have succeeded in founding a quantitative measure to explain the physical process of the sediment motion along the beach.

Active movement of coastal sediments has produced sedimentation of anchorage basins and blocking of river outlets at many places in Japan. The important role played by eolian transport of sand should not be overlooked in this regard. It is estimated that roughly half of the sand which shoaled the basin of the Kashiwazaki port in Niigata prefecture had been derived from eolian transports.

There are numerous instances where the properties of sediment material such as the particle size and size distribution as well as the bottom topographies played a role as extremely important to the sediment problems as winds, waves, and longshore currents. At the gravel beach the attribution of a concrete structure is so severe that the maintenance of the protective establishments present an annoying problem to the engineers.

Artificial interferences

Considering principal causes of erosion which is now in progress at various coasts of Japan, we find that it is mostly attributed to disturbance of the natural processes due to an artificial interference or another.

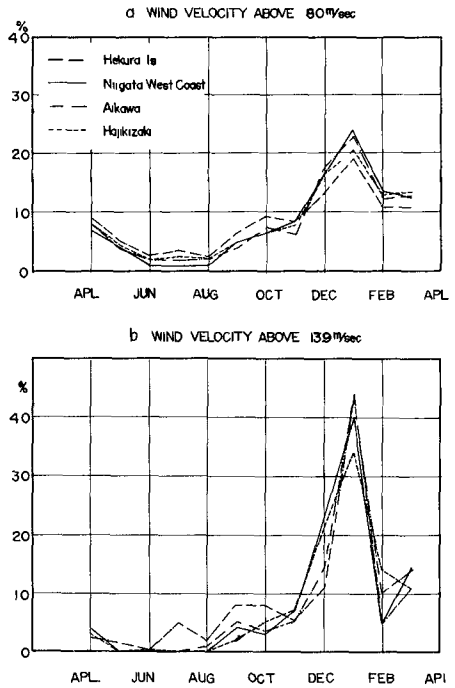

Fig. 8.

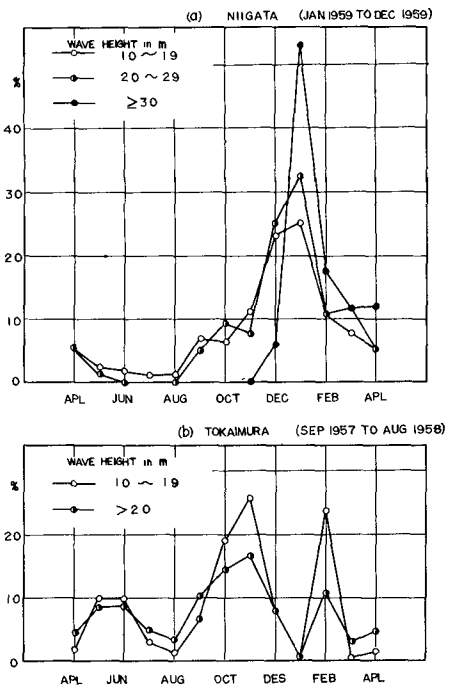

Fig. 9

Fig. 8. Probable Occurrences of Strong Winds in the Vicinity of Niigata
Fig. 9. Probable Occurrences of Wave Heights at Niigata (a) and Tokaimura (b)

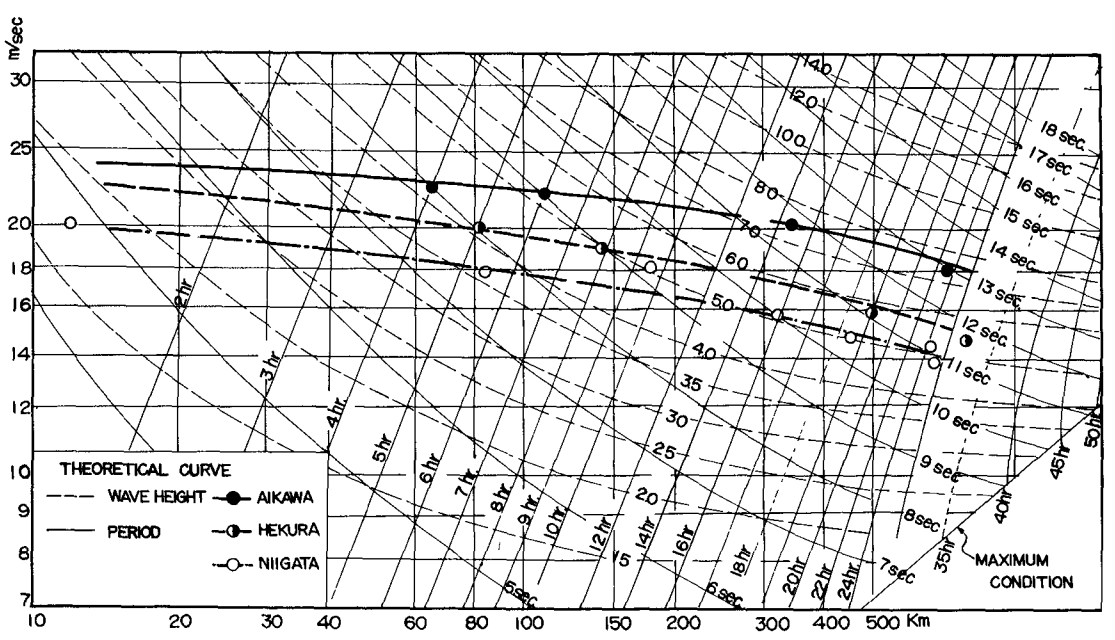

Fig. 10. Greatest Possible Significant Waves at Niigata Coast

The most prominent instance is found in Niigata along the Japan Sea coasts. Since ancient years the Niigata city developed as an esturine port at the mouth of the Shinano river and is today one of the most important ports along the Japan Sea coast. (See Fig. 11.) Formerly a tremendous amount of sediment was emptied from the mouth of the Shinano river which was then put in active movement along shore due to violent wind wave: predominant during winter. As a result the river mouth was easily shiftin; its position, seriously hampering navigation through it. In order to maintain the navigation channel through the river mouth a project was initiate in 1896 to set up the training jetties and was completed in 1924 after repeated improvements. At the same time another project was started in 1909 to cut a flood way at a point approximately 58 km upstream of the river in order to free the Echigo plane from frequent flood disasters. Since the project was completed in 1922, the design flood discharge of 5,570 m^3/sec was mostly diverted into the flood channel and the discharge through the original channel was kept below 270 m^3/sec approximately. These grand projects helped to rid the Echigo plane of a flood disaster for ever, but at the same time they drastically cut the supply of sediment to the beaches adjoining the river mouth.

As these projects proceeded, a beach segment approximately 6 km long to the west of the river mouth began to retreat and the erosion has been so severe that today two rows of the coastal dunes have been completely washed away leaving only the half of the third dune. (See Fig. 12.) The beach to the east of the river mouth had been progressing at the rate of 30 m per year until the jetties were installed at the river mouth. As the Jetties were being constructed, the rate of shoreline progression was reduced and later, with completion of the flood channel upstream, an appreciable retrogression started over a stretch of 2 km. On the other hand, along the beach of Teradomari where the new flood channel empties a vast quantity of sediment into the sea (See Fig. 13.), the shoreline advanced remarkably.

The Niigata area is beset by an even more delicate problem which has arisen from another case of artificial interference. As the production of subsoil natural (soluble) gas was accelerated since 1949, the earth level has started to give way at an increasing rate. (See Fig. 14.) Today the subsidence has progressed to such an extent as to paralyze the port facilities as well as intensifying the beach erosion.

The decrease of sediment supply from the river ways also result from construction of dams for power generation, water supply or flood control or of debris barriers. Such examples are found at the Kaike coast, the Toyama coast (exposed to the Japan Sea), and the Toban coast (located in the Seto inland sea). There are coasts where the beach was eroded due to jetties or other shoreline barriers which acted to intercept the path of sediment from the source of supply. Such example is found at the Tanezaki coast (in Shikoku), and the East Katase coast (in Sagami bay).

Japan is abundant in problems of harbor sedimentation which have long been harassing the harbor engineers. There is the well-cited example of Isohama (along the Pacific Ocean coasts) which was completely disabled due to severe sedimentation. (See fig. 15.) A similar example is found in Iwafune which is located approximately 45 km north of Niigata and approximately 5 km south of the Miomote river. We should say that this fishery

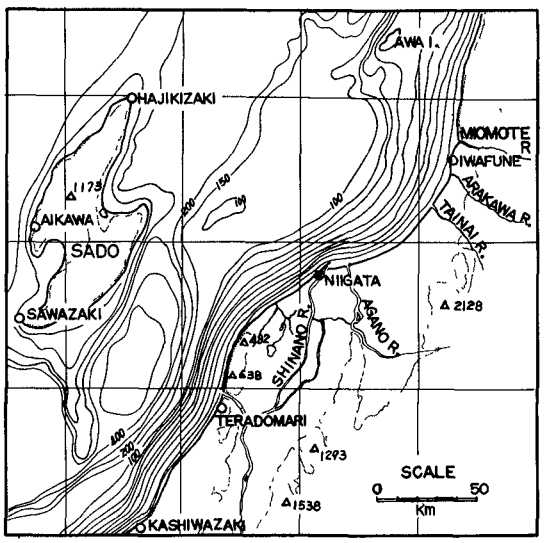

Fig. 11

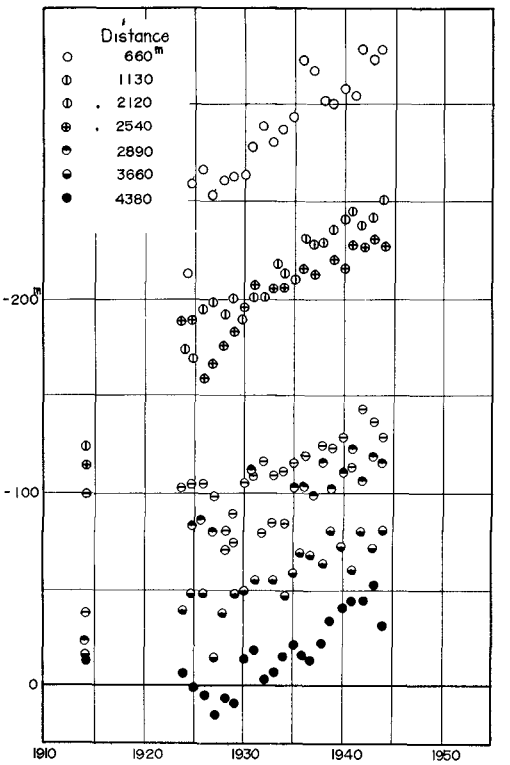

Fig. 12

Fig. 11. Location Map of Niigata

Fig. 12. Retrogradation of Shore Line at Niigata West Coast in Comparison with that in 1889, Distance being measured from the Shoreward End of West Jetty at the Shinano River Outlet

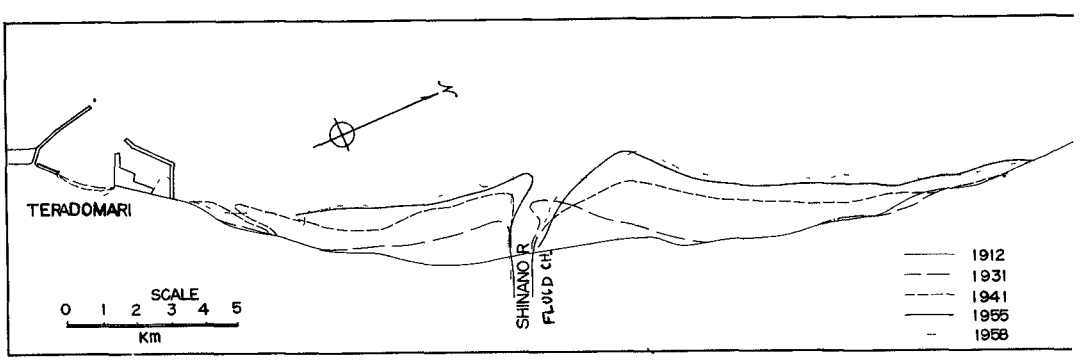

Fig. 13. Accretion of Sandy Beach at Teradomari

harbor embodies the history of the Japanese engineers who fought coastal sediments with unswerving perseverence. Fig. 16 will aid to understand the background of this harbor where the design and alignment of the jetties have been repeatedly modified under the pressure of invading sediment.

APPROACHES TO COASTAL PROCESSES

The factors discussed in the preceding chapter combine in nature to present various patterns of coastal problem. The problems are so intricately constituted that it has only been these 15 years that a field investigation based on the scientific procedure and a laboratory experiment based on the results of such investigation came to prevail. We had to depend largely on the experiences of some limited number of engineers until the scientific approaches were introduced.[10]

The meteorologists and oceanographers have long been turning out an immense quantity of data on waves, but they mostly counted on visual observations until various types of instruments became available about 10 years ago. Today, a number of wave recorders, both step-resistance and pressure types, have been installed in Japan. The shore-based stereophotography is also used in studying the shoaling waves.

The longshore currents are often measured by using floats or self-contained recorders. Fluorescent dye markers are also used both in and out of the surf zone.

Though supremely important, the measurement of the longshore sediment movement still lacks in adequate instruments. A box trap or a tube (or bamboo) trap is currently used in Japan, but the data which they provide fail to give the definite basis for a quantitative treatment. In order to verify the sand-arresting organism of a trap, the authors carried out a series of instant and cumulative sampling of suspended sediment in the field in parallel to a laboratory model test in a two-dimensional flume. Though the project is still in progress, we have succeeded in establishing a relationship between the concentration of suspended sediment and the efficiency of a tube trap.[11]

At the present state the hydrographic sounding by lead or echo is a most effective and most widely used method for estimating the movement of sediment as well as changes in bottom topographies. The problem with the hydrographic survey today is to shorten the operation period, yet not to impair the accuracy of sounding data so that the wave conditions may not change during the operation.

The uncertainty in the scale effect seriously reduces the value of laboratory experiment, particularly one utilizing a movable bed. The method used by the Japanese engineers to overcome this difficulty is to follow a close reference between the model and the prototype by trial-and-error repetition.

A most pronouncing example of the overall coastal study in Japan is

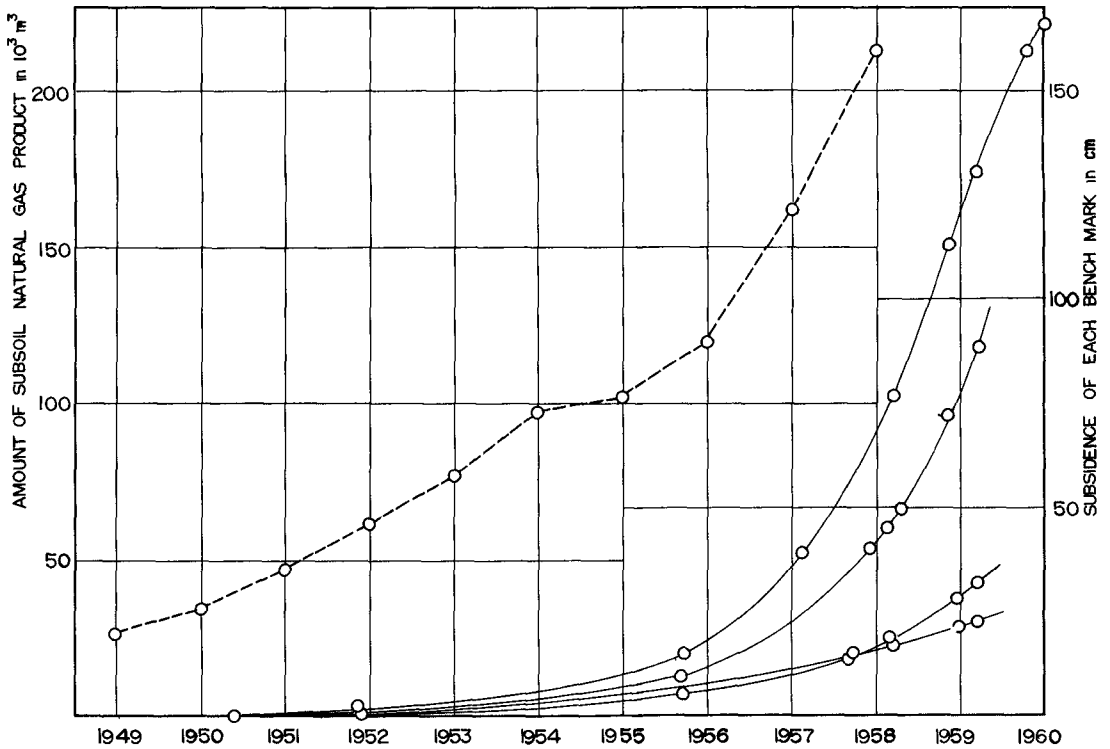

Fig. 14. Relationship between the Subsidence of Bench Marks and the Production of Subsoil Natural Gas.

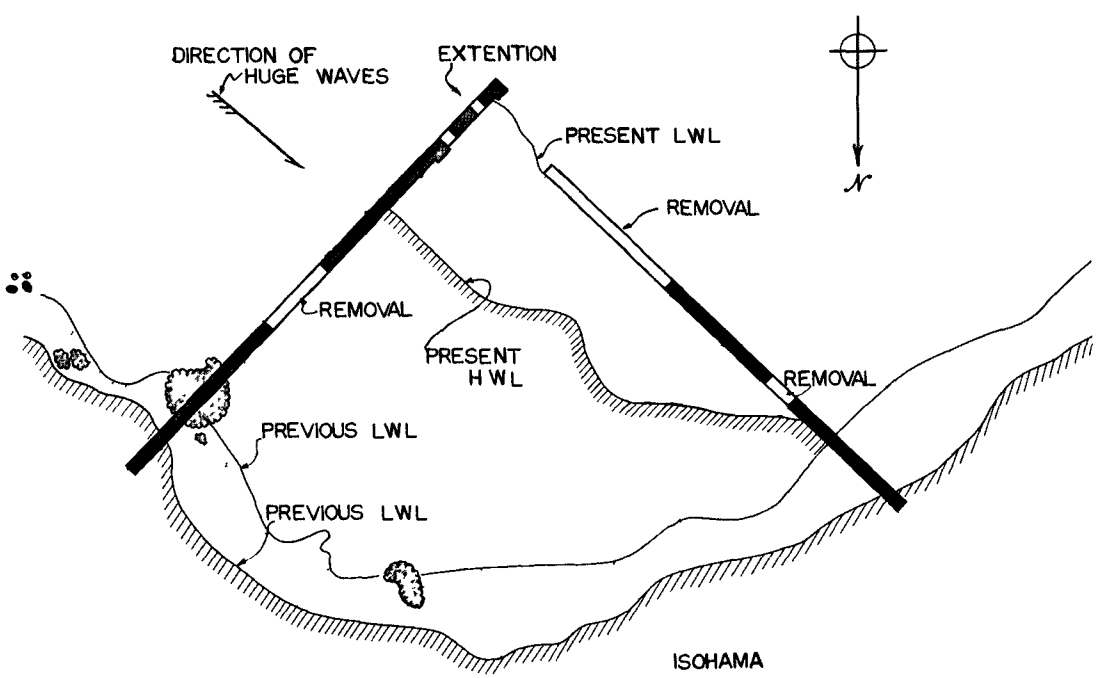

Fig. 15. Isohama Fishery Harbor (after M. Suzuki)

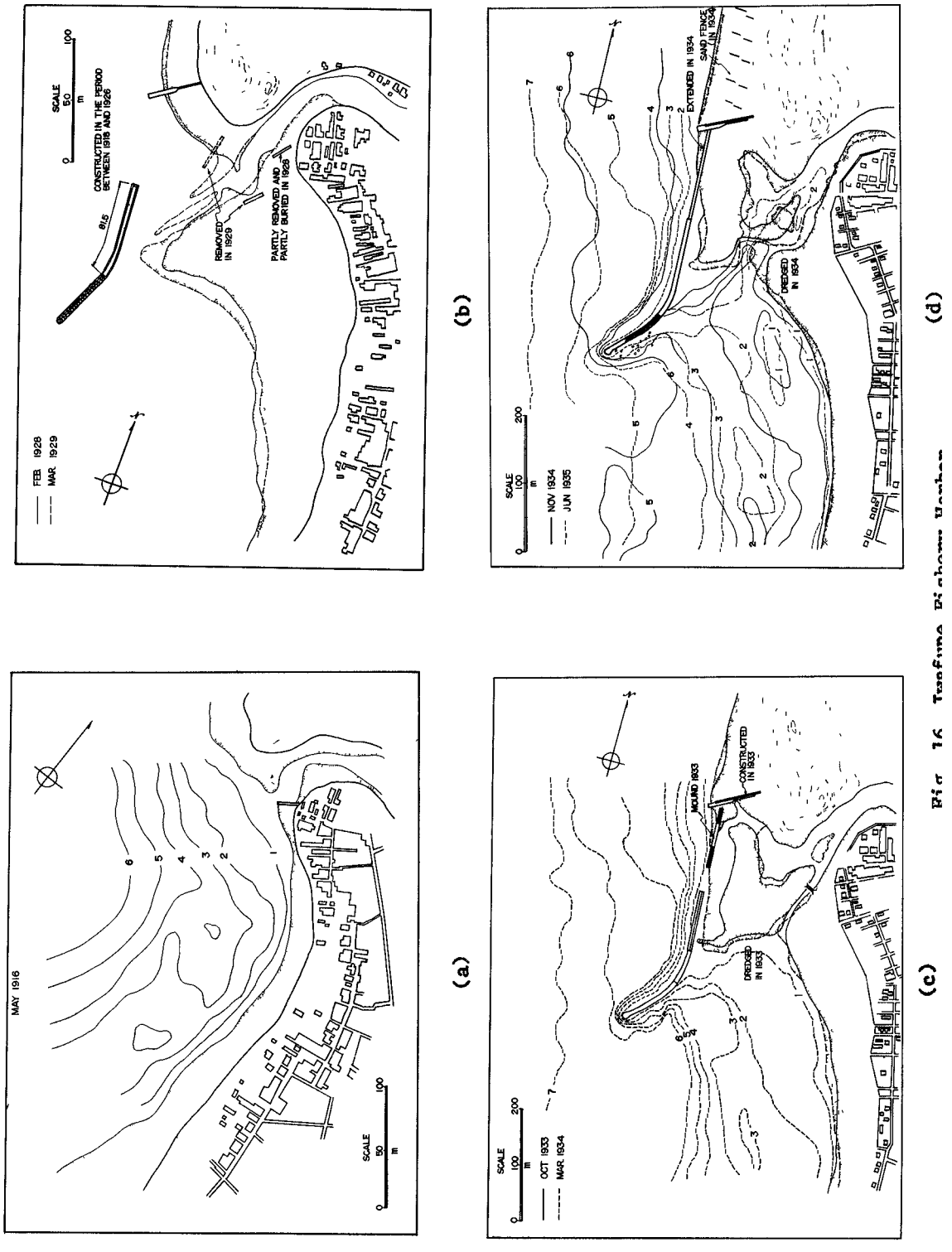

Fig. 16 Teufime Bichom Harbor

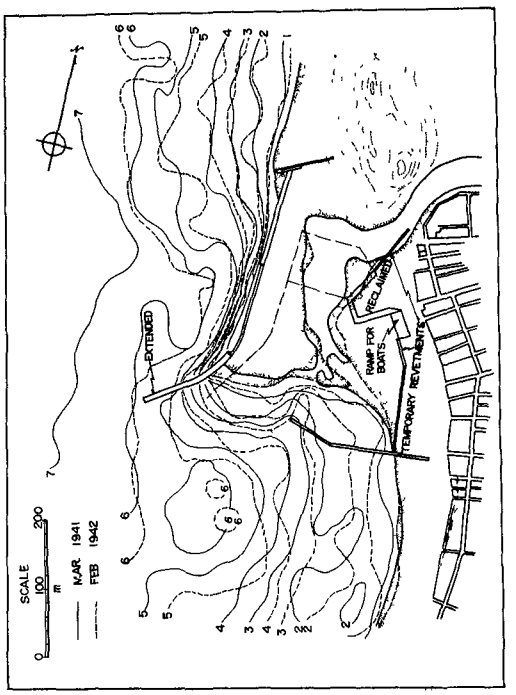
SCALE
0 100 200
m
MAR 1941
FEB 1942
EXTENDED
RECLAIMED
PIER FOR BOATS
TEMPORARY REVETMENTS

(f)

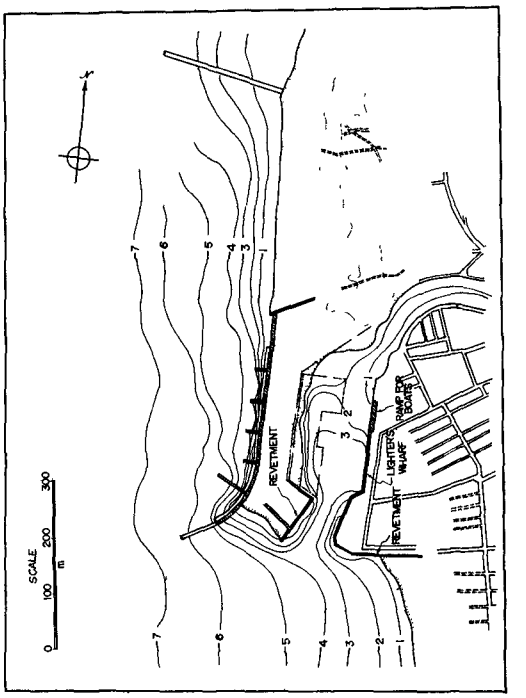
SCALE
0 100 200 300
m
REVETMENT
REVETMENT
LIGHTERS WHARF
PIER FOR BOATS

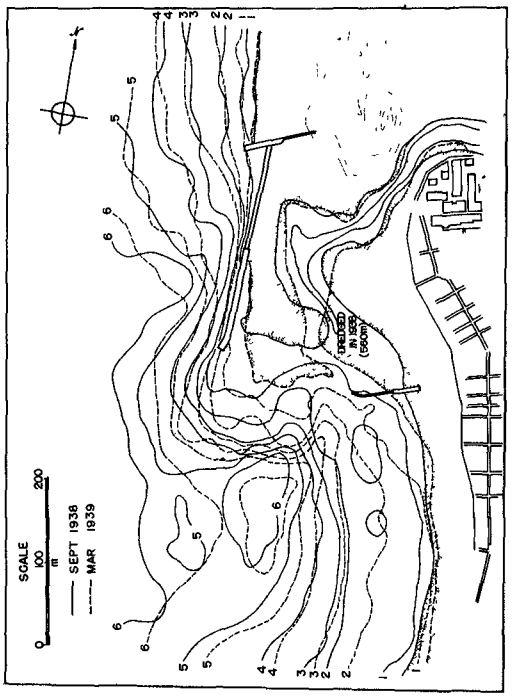
SCALE
0 100 200
m
SEPT 1938
MAR 1939
DREDGED IN 1938 (5000)

(e)

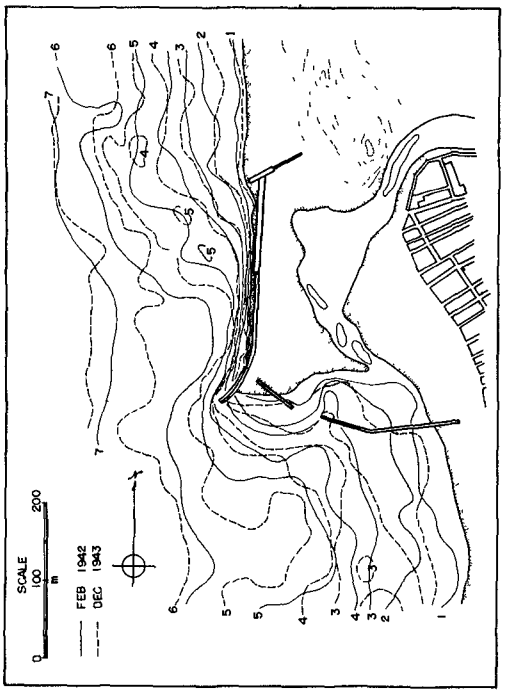
SCALE
0 100 200
m
FEB 1942
DEC 1943

found in the coast of Niigata. In order to deal with the problem of erosion, a committee was created in 1946 and after 5 years of strenous field investigation and laboratory model experiments the results were published in an extensive report in 1951. In 1953, the prefectural office of Niigata set out on a long-range project of investigation with by far the comprehensive scope. Numerous revisions were made on the methods and instruments of investigation until of tolerably satisfactory arrangement was completed in 1957.

The purposes of investigation at Niigata consisted in (1) exploring the rate and physical processes of erosion, and (2) obtaining data to be used as the basis for planning protection works and their modifications. Since the coasts facing the Japan Sea are almost completely devoid of a lull during winter due to violent wind waves, an investigation by a boat is impossible. A cableway consisting of masts and track cables was set up in the perpendicular direction against the shoreline which is operated at the station located on top of the beach dune. The cableway could carry the recording or sampling instruments to any shallow water position regardless of the weather and sea conditions. (See Fig. 17 and Plate 1.)

The overall project of investigation is outlined below.

A. General investigation on shallow water areas

1. Hydrographic sounding - Once or twice per year, as far as the depth of 20 m and along the stretch of 20 km, by echo-sounding from a boat.

2. Sampling of bottom materials - Conducted simultaneously with the sounding operations.

B. Investigation of coastal establishment

1. Investigation on deformation of a submerged breakwater due to wave action.

2. Investigation on subsidence of a submerged breakwater due to wave action.

C. Investigation on natural forces

1. Direction and velocity of winds - Records from several stations scattered in the vicinity were collected to compare variability in direction and intensity of winds found inside a fetch of an appreciable width.

2. Observation of shallow water waves - The directions, heights and periods of shallow water waves in the depth of approximately 5 m and less were observed to determine the deformation of wave characteristics due to bottom topographies and the damping effects of a submerged breakwater. In order to determine the sheltering effect of the Sado Island two units of shore-based pressure recorders are being installed at Sado and Niigata in the depth of approximately 10 m.

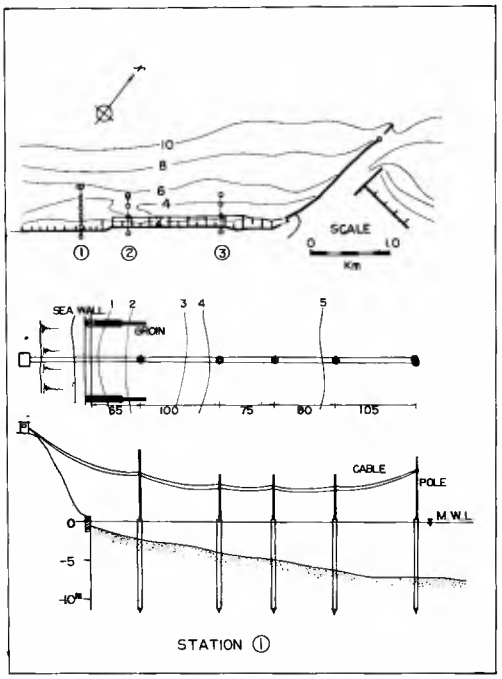

Fig. 17. Cableway for Field Survey at Niigata Coast

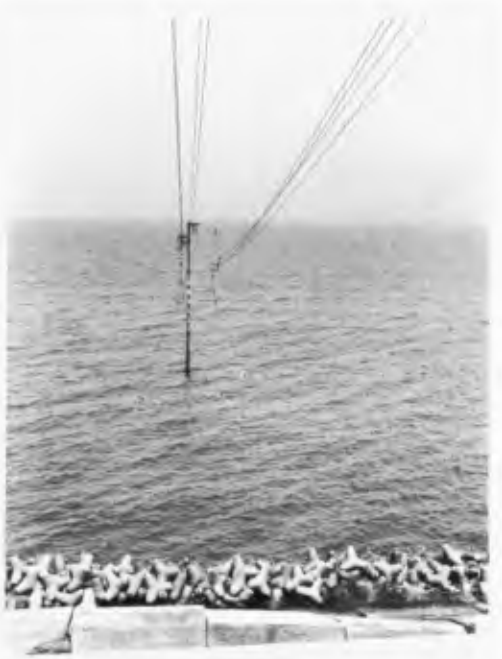

Plate. 1. Cableway

Plate. 2. Current Meter

Plate. 3. Fujiki-type Sampler

Plate. 4. Fijiki-type Electric Lead

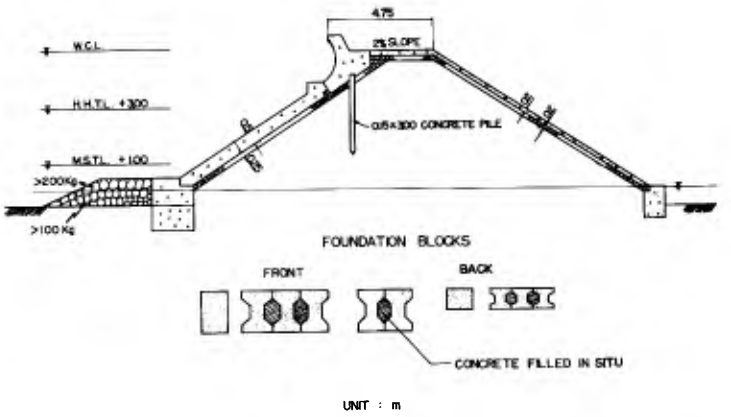

Fig. 18. Cross Section of Coastal Dike Constructed along the Ise-Bay

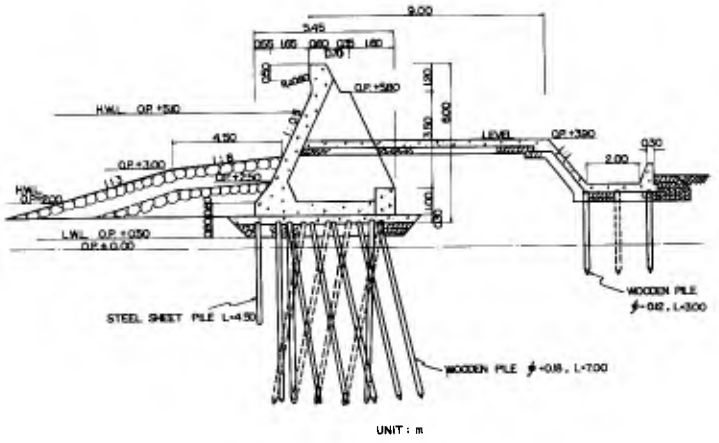

Fig. 19. Cross Section of Sea Wall at Amagasaki.

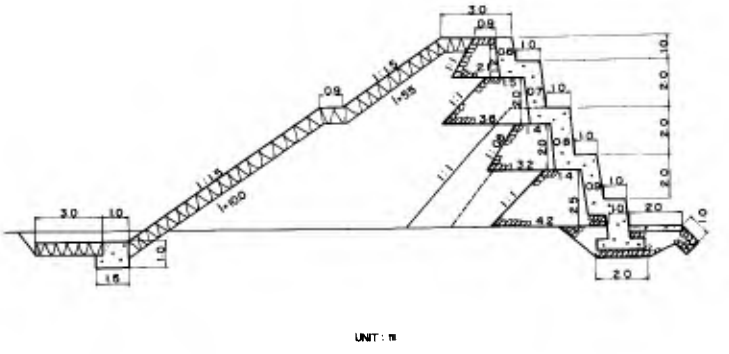

Fig. 20. Cross Section of Sea Wall at Taro

D. Special installations to investigate surf-zone characteristics - A cableway system which was developed to make the investigation activities during winter storms possible, was designed to carry the following units to the zones in and out of the breaking point.

1. A self-contained current meter and a cross-blade float to measure current velocities and directions at an arbitrary level above the bottom. (See Plate 2.)

2. Fujiki-type sampler for measuring instant concentration of suspended materials (See Plate 3.) and a tube trap for cumulative arresting of suspended sediment.

3. Fujiki-type electric lead for sounding of the bottom topographies near the surf-zone. (See Plate 4.)

A recent technique of radioisotope was applied to the Niigata coasts in 1958 in order to trace the movement of bed materials.

This arrangement of various items of investigation has succeeded in supplying a great deal of information on the physical processes occurring at the beach under erosion, as was partly discussed in the preceding chapter.[12] Our experience in Niigata has convinced us that a well-arranged project with refined instrumentation does really pay.

COASTAL PROTECTION WORKS AND PRACTICES

The design and construction of coastal protection works may vary according to the purposes as follows:

1. Defense against a storm surge:

2. Defense against a tsunami:

3. Prevention of beach erosion: and

4. Measures against sedimentation of a harbor basin or blocking of a river mouth.

Defense against storm surges

The bays and inlets west of the Tokyo area are dangerously exposed to the hazards of a storm surge. The key industrial centers such as Tokyo, Nagoya and Osaka are located in this region. Once a storm surge should occur at one of these area the resulting disasters would be tremendous due to valuable establishments and swarming population crowding the lowland. The serious subsidence caused by excessive exploitation of the ground water has reduced these industrial areas even more vulnerable to a storm surge.

One of the most popular measures to defend a storm surge is to besiege a lowland with coastal dikes or sea walls. (See Fig. 18.) However, such procedure may not be extended to the port areas, since it may interfere with the function of the port facilities. With some few exceptions such

as found in Amagasaki, where an encircling dike completely embraces the port sector (See Fig. 19.) or in Osaka where a part of the downtown district was leveled up by filling soils, most of the ports in Japan are practically defenseless against a storm surge. The disasters caused by a storm surge due to the typhoon No. 15, 1959, are discussed by Otao and others in another paper of this conference.

Measures against tsunamis

The northeastern coasts of Japan have been frequently hit by tsunamis Since the height of a tsunami is even harder to forecast than that of a storm surge, and since the underdeveloped coasts of northeastern Japan cannot afford financially to own expensive defenses against a tsunami whic occurs only at a low probability of, say, once in 30 years, not much progress has been accomplished as to the measures against tsunamis. However there are places where the efforts have been made to build a coastal dike along the outskirt of the resident quarter (See Fig. 20.), or a wall right through the town, or a counter-tsunami grove along the shoreline.[3]

Measures against coast erosion

Several types of protection works have been employed in Japan: (1) sea wall, (2) groin, (3) submerged breakwater, (4) artificial nourishment, and (5) their combination. We will review the protection works actually applied to some of the important coasts of Japan.

Niigata coast - The situation up to 1952 was reported by S. Kuroda at the 18th Proceeding of International Navigation Congress and shall not be repeated here.[13] Over a stretch of 2 km adjoining the west jetty of the Shinano river, the beach was protected with a combination of submerged breakwaters, coastal groins adn sea walls. Also the shoreline area was nourished artificially with bed materials dredged from the navigation channel of the river mouth. Over a stretch of 5 km lying farther west, the shoreline was protected with coastal jetties and sea walls. Though the erosion ceased in the area thus protected, the open shoreline beyond the protected area began to retreat recently. To the east of the river mouth, the shoreline was protected with groins and sea walls. (See Fig. 21.)

The effects of these massive protection have been convincing. However the erosive action now began to gnaw at the shore protection works themselves. Our present concern is currently directed to the methods of maintaining and reinforcing the protection works off and along the shoreline.

A submerged breakwater slumped under impacts and scouring actions of the waves breaking overhead, resulting in an appreciable loss of the damping efficiency. It was reinforced with 4-ton tetrapod blocks to restore the height to the mean sea level, but the slump has been continuing. The infilling rocks of the piled groin also slumped and had to be replaced. The base of the sea wall was scoured by violent swashes and here also the tetrapod blocks were applied to protect it with fair success. A laboratory study was undertaken by the authors to examine the cause of the slump of a submerged breakwater and the scouring action at the base of a sea wall by using 1/20, 1/25 and 1/40 models, which turned out some useful suggestio

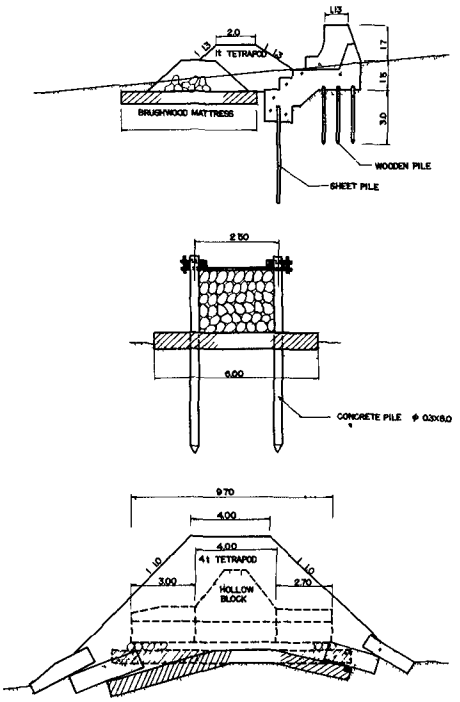

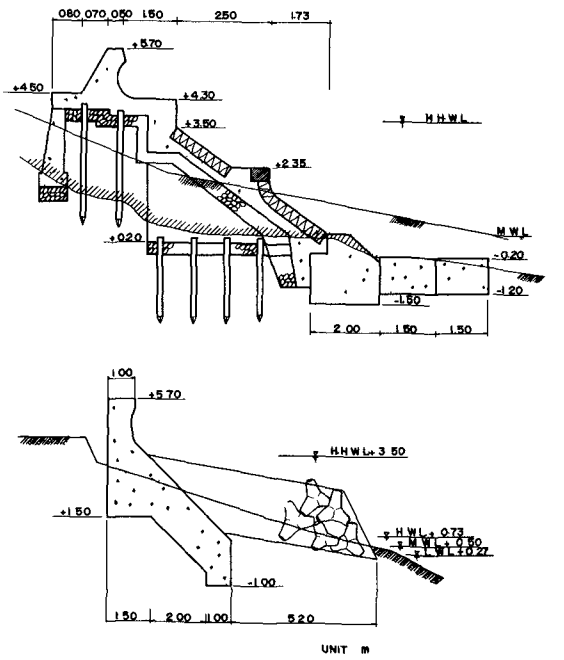

Fig. 21 Fig. 23

Fig. 21. Cross Sections of Sea Wall, Groin and Submerged Breakwater at Niigata West Coast

Fig. 23. Cross Sections of Sea Wall at Toyama Coast

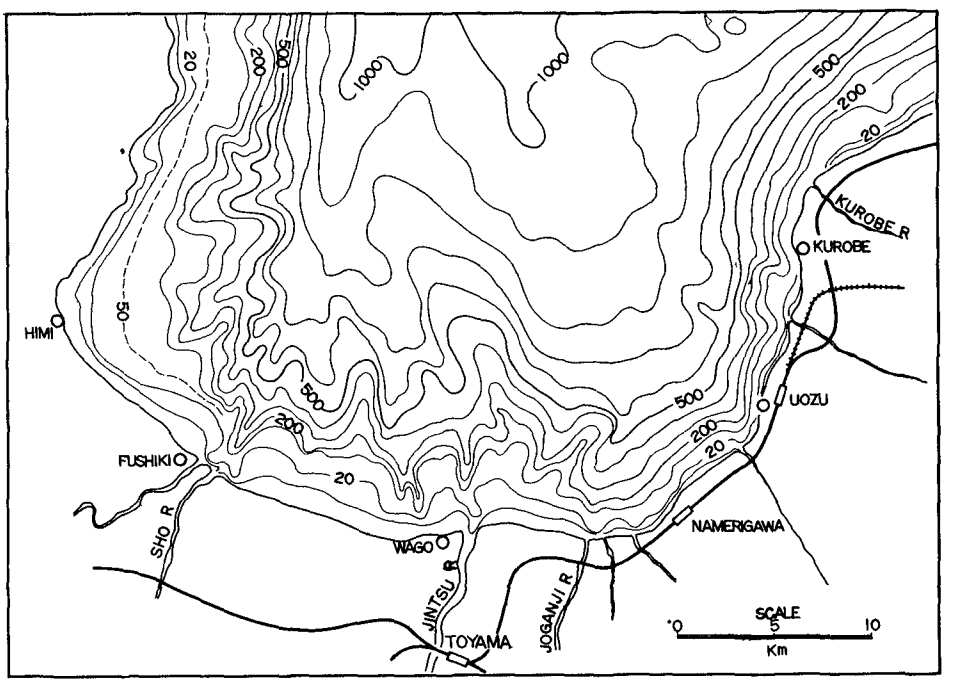

Fig. 22. Toyama Bay Area

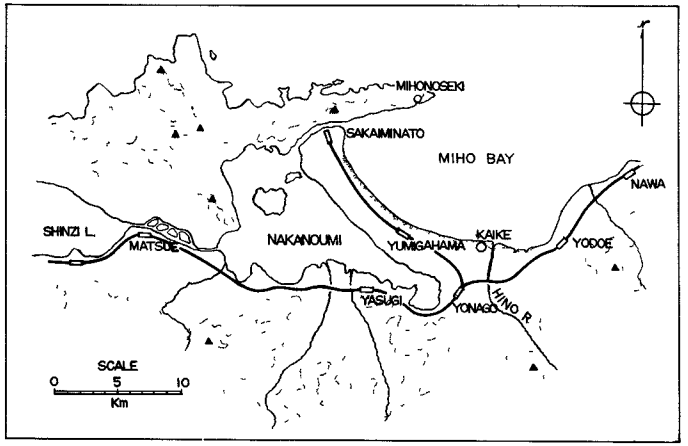

Fig. 24. Location Map of Kaike Coast

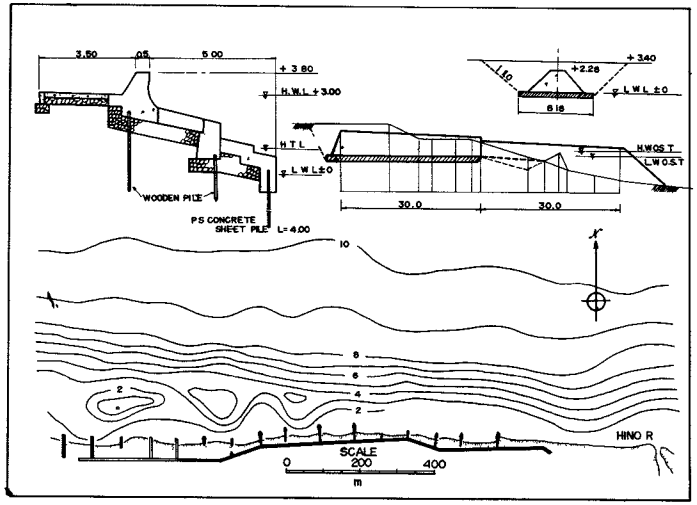

Fig. 25. Protection Works at Kaike Coast

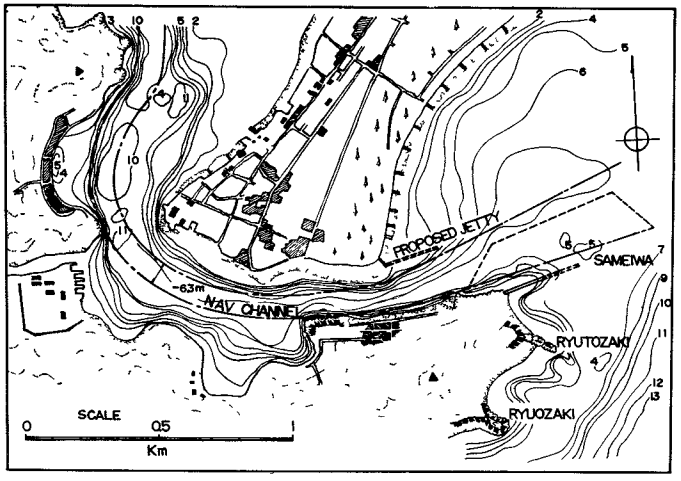

Fig. 26 Location Map of Tanezaki Coast

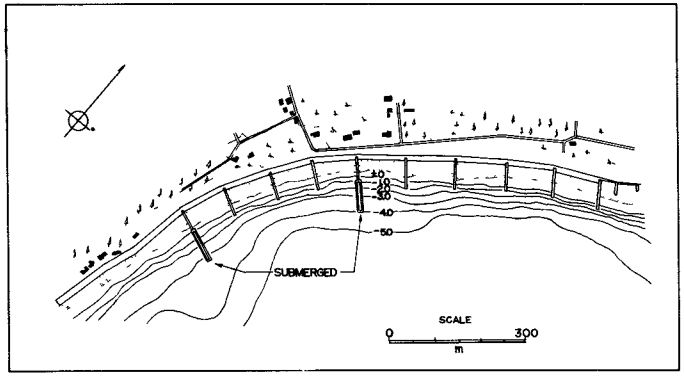

as to the measures for maintenance and reinforcement for these protection works.(14)

Toyama coast - The coasts are subjected to continual action of storm waves during winter. The effects of the wave action on these coasts of submergence are even intensified due to bottom topographies which are represented by a steep profile falling to the depth of 5 and 10 m at the distance of 250 and 1,000 m, respectively, from the shoreline. (See Fig. 22.) Thus the waves generated in the deep water reach the shoreline without any appreciable loss of energy. It is also characteristic of these coasts that there is little supply of bed materials from the nearby rivers. Under combined effects of these factors, the coasts have been retreating at an enormous rate of 1.5 to 2.5 m/year in the east and 0.5 to 1.0 m/year in the west, and at some places the rate amounted to 10 to 20 m/year.

The protection works applied here primarily consist of the sea walls (See Fig. 23.) and at some places they were combined with groins. The beaches are dominantly gravels, which, churned up by swashes, cause serious attrition of the concrete sea walls and tetrapods, as well as dissembling of the masonry structures. No definite method of maintaining the protection works has yet been introduced.

Kaike coast - The beach materials are mostly supplied from the Hino river which empties into the eastern part of the beach. A careful study revealed that the principal cause of erosion is attributed to recent development of soil conservation works in the upper reach of the river, and consequent decrease of sediment discharge from the river mouth. The beach was protected with a group of coastal groins. (See Fig. 24 and 25.) The groin, a mound built of concrete blocks, was spaces 2 to 4 times the length of the groin which ranges from 20 to 50 m.

Though the groin system proved effective in arresting a large portion of the sand drifts along the shoreline, the general trend of erosion persisted over an extensive stretch of the coast. Today, a sea wall is being constructed instead of groins.

Tanezaki coast - The shoreline of Tanezaki, located at the entrance of the Kochi harbor, began to retreat rapidly in recent years, and the erosion was reported to have reached more than 100 m in about 30 years. (See Fig. 26 and 27.) The cause of erosion is attributed to the training jetty and the river mouth, but the process of erosion was further aggravated by the great Nankai earthquake in 1946 which caused this area to subside by about 1.2 m. The beach was then hit by several typhoons successively, and the shoreline retreated by 30 to 40 m in only several years after the earthquake. A model experiment was carried out in order to determine an adequate alignment of the breakwaters at the entrance so that the longshore currents may be decelerated. A masonry sea wall and the coastal groins were installed to prevent further erosion.

Toban coast - The coast faces a narrow strait of Akashi which connects the Osaka bay and the Seto inland sea, and partly sheltered by the Awaji Island from the Pacific Ocean. (See Fig. 28.) The highland behind the coast descends to the sea with a steep slope and long years of weathering reduced

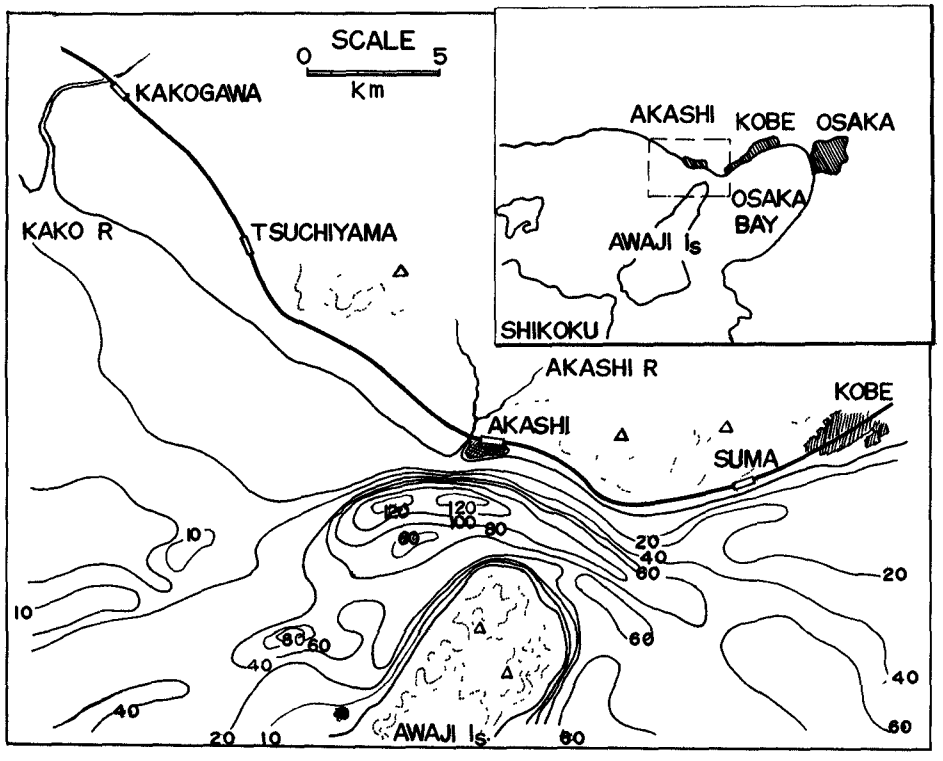

Fig. 28. Location Map of Toban Coast

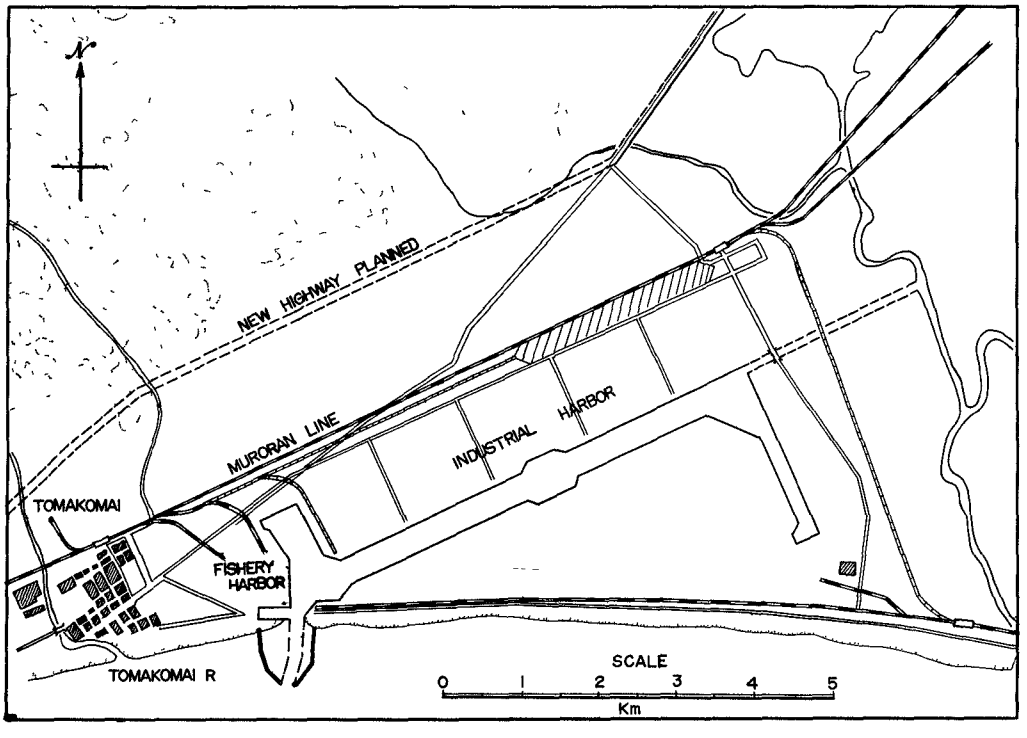

Fig. 29. Proposed Plan of Tomakomai Harbor

it apt to collapse. The soil conservation works started early in the highland, and today the debris barriers built along the Kako river alone number more than 40. The result was the rapid decrease in supply of materials to the beach. The erosion is partly attributed to the violent tidal current through the Akashi strait which attains as high as 4.5 knots at spring tides.

The protection works provided here consist of a sea wall to which a group of relatively short groins are attached in order to damp destructive effects of swashes and thus prevent scouring action at the foot of the sea wall and offshore breakwaters (rock or block mound) was also applied to some places of the coast.

Measures against sedimentation in harbors and blocking of a river mouth

The most salient example of sedimentation is found in the Iwafune port which has had to undergo repeated modification of the jetties in order to ward of endless invasion of coastal sediments (See Fig. 16.) We abound in costly lessons as to the danger of sedimentation which must be expected of a shoreline harbor built along a sandy coast. Recently the Japanese engineers have ventured on a project of building a harbor basin inside the shoreline of the Tomakomai coast, where construction is proceeded in parallel to meticulous investigation. (See Fig. 29.)

The training of a river mouth is a problem which has been annoying the engineers everywhere in Japan. No definite measure has yet been established and the training work is carried on usually by trial-and-error procedures. In some of the particular cases, the laboratory study proved very useful, but much remain to be enlightened in the future.

ACKNOWLEDGEMENTS

The authors have made extensive reference to a number of works accomplished by the field and laboratory engineers in Japan. We should like to express our sincere gratitude and respect to those who have displayed such endurance in the toils of field investigation.

Our profound appreciation is due to Mr. Choule Sonu, M. S., Graduate student at the University of Tokyo, who collaborated in preparation of this report, and to the personnel of the Coastal Engineering Laboratory of the University of Tokyo who assisted in preparing the figures and typewriting the manuscript.

REFERENCES

(1) Takahashi, R., Earthquakes, Symposium on Disasters and Prevention Measures, J.S.C.E., 1956. (In Japanese)

(2) Hom-ma, M., K. Horikawa, and C. Sonu, A study on Beach Erosion at the Sheltered Beaches of Katase and Kamakura, Coastal Engineering in Japan, Vol. 3. (In print).

(3) Iwasaki, T., and K. Horikawa, Tsunami caused by Chile Earthquake in May, 1960 and Outline of Disasters in Northeastern Coasts of Japan, Journ. of J.S.C.E., Vol. 45, No. 8, 1960. (In Japanese, but a translation into English is available.)

(4) Ijima, T., The Properties of Ocean Waves on the Pacific Coast and the Japan Sea coast of Japan, Rept. Transp. Tech. Res. Inst., No. 25, June 1957.

(5) Nagai, S. and Y. Aridome, Hindcast of Maximum Waves Generated by Ise-Wan Typhoon at Harbors in Wakayama Prefecture, Journ. of J.S.C.E., Vol. 45, No. 6, 1960. (In Japanese)

(6) Unoki, S., On the Ocean Waves due to Tropical Cyclones, Coastal Engineering in Japan, Vol. 2, 1959.

(7) Date, T., Visual Observations of Wind Waves and Swells Accompanied with Monsoon on the Japan Sea, Memoirs of Monsoon in Winter on San-in District, Maizuru Marine Observatory, April 1959. (In Japanese)

(8) Okuyama, K. and S. Unoki, General Description of Storm Tides on the Coasts of Japan, Journ. of Meteorological Research, Vol. 11, No. 6, 1959. (In Japanese)

(9) Aki, K., Beach Erosion in Japan, Proc. of Minn. Int. Hyd. Convention, 1953.

(10) Horikawa, K., Present States of Coastal Engineering in Japan, Journ. of Waterways and Harbors Division, Proc. A.S.C.E., Vol. 85, No. WW3, 1959.

(11) Horikawa, K., and C. Sonu, Vertical Distribution of Suspended Sediment by Wave Action, J.S.C.E., 15th Annual Convention, 1960. (In Japanese)

(12) Niigata Prefecture, On the Beach Erosion at Niigata Coast, 1960.

(13) Kuroda, S., Coastal Protection Works at Niigata Harbor, Proc. 18th International Navigation Congress, Rome, 1953.

(14) Hom-ma, M. and K. Horikawa, An Experimental Study of Submerged Breakwaters - Mechanism of Slump and Reinforcement of Structures - Proc. of 6th Conference on Coastal Engineering in Japan, 1959. (In Japanese

CHAPTER 54

A BRIEF OUTLINE OF THE ISE-WAN TYPHOON

Hiroji Otao

Vice president, Transportation Technical Research Institute,
Ministry of Transportation

INTRODUCTION

During the ten years from 1947 to 1956, typhoons with a maximum velocity of more than 34 knots have attacked Japan at an average of 26.8 times a year, inflicting damages amounting to 240 thousand million yen on the average each year (1946-1955). However, depending on the course and scale of the typhoon and the season of the year, except for damages to vessels, in some cases, the advantages outweigh the disadvantages as the abundant rain fall resulting from a typhoon is beneficial to agriculture and hydraulic power generation widely developed throughout the country. In the past, damages from typhoons consisted of storm and flood disasters with the flooding of inland waterways and landslides in mountainous districts due to heavy precipitation. However, lately, with the rapid progress of modern industries, cities with ports and harbors are expanding with the development of large industrial zones along coastal areas where raw materials can be obtained from foreign countries at low cost of transportation, and vast areas of land for the establishment of industrial plants can be acquired without encountering serious obstacles through land reclamation along the shores. These circumstances have called for the necessity of protecting the coastal areas from the direct attack of high tides and wind waves generated by typhoon. (See Table 1)

Table 1
National Funds Invested for Land Conservation

Year / Item	1946	1951	1956	1960	note
River Conservation, Sand Arrestation	3,433	4,397	8,225	7,242	(hundred million yen)
Forestry Conservation	315	551	920	1,062	
Coast Protection	3	341	722	904	breakwaters not included

The coastal area around the Ise Bay with its large capacity of accommodating a huge population is a typical example of amazing urbanization of a rural district with the rapid development of large industrial plants

---

*Editors Note: Chapters 54 to 58, inclusive, form a group of papers on storm surge and damage caused by Typhoon No. 15, 1959, and were prepared by members of the Committee on Coastal Engineering, Japan Society of Civil Engineering, Tokyo, Japan.

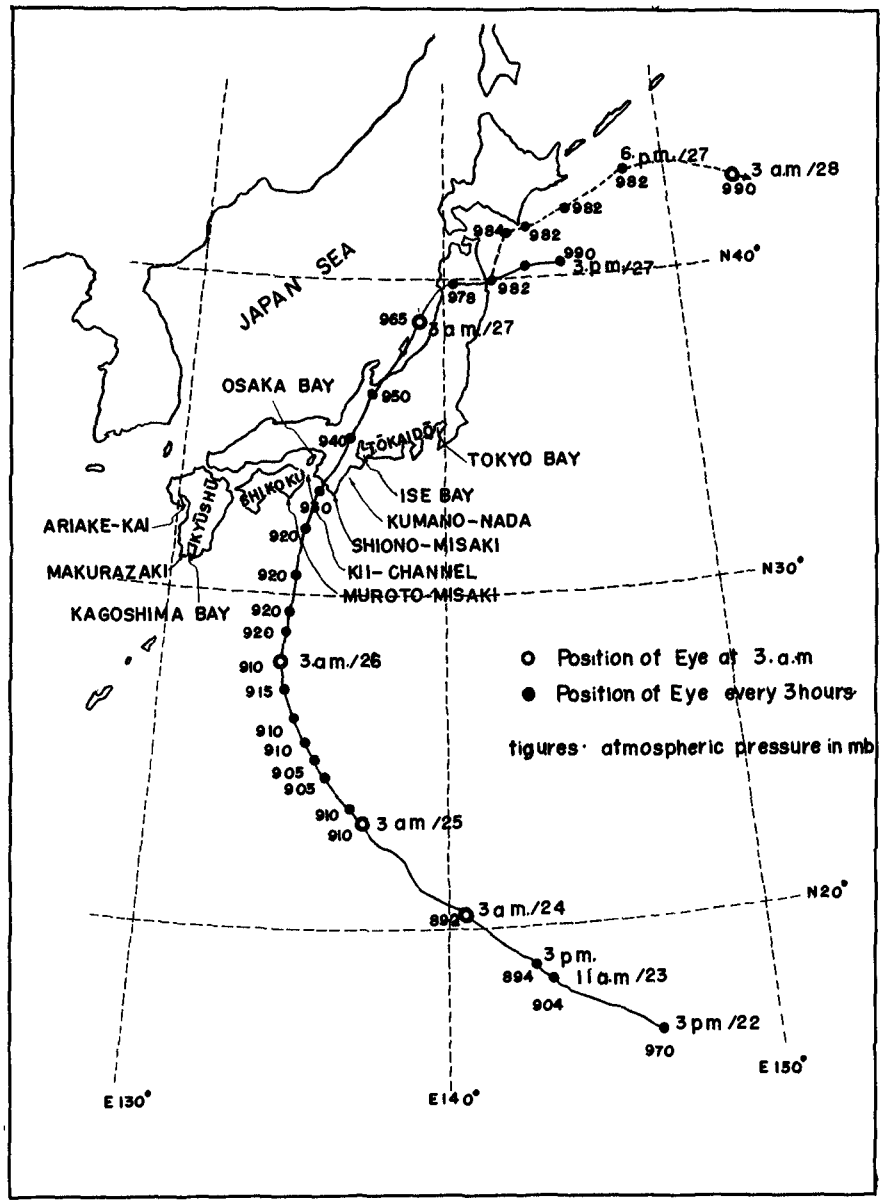

Fig. 1-1 The course of the Ise-Wan Typhoon

following World War II. An extensive development program had been drafted, a part of which had already been carried out, when suddenly the area was severely hit by Typhoon No. 15, with the death toll rising to 4600, and damages ancounting to 500 thousand million yen, in an unprecedented disaster, to the great shock of the entire nation. Almost all of the industrial zones throughout the country may be said to be subject to similar disasters. Nevertheless, in view of the geographical features of the country, the special characteristics of Japanese industries, and the over-crowded population, we have no alternative but to promote the development of coastal areas, and construction of ports and harbors, and the reclamation of new lands.

Under these circumstances, Typhoon No. 15 of 1959 was especially named the Ise-Wan Typhoon, and various circles concerned are seriously engaged in collecting and analyzing data of the typhoon in order to establish scientific measures for the protection of the coastal areas from typhoons in the future. Further progress in the field of coastal engineering is a matter of deep concern to the entire nation, and will serve much towards the general welfare of the people.

THE TYPHOON ON THE OCEAN

The low atmospheric pressure of 1008 mb on Sept. 21, 1959 was called Typhoon No. 15 from 9:00 hours, on Sept. 22. The tropical low atmospheric pressure rapidly developed into a violent storm only two days after it had been spotted in the southern seas, with a center pressure of 892 mb, maximum wind velocity of 75 m/s, and a 300 km radius at 15:00 hours, Sept. 23. Storm warnings were issued and the nation was on the alert as to the direction the typhoon was headed for. Information on the typhoon was broadcast every hour and the following announcement was made at 11:15 hours, Sept. 26. "Typhoon No. 15 is moving northward 350 km south of the Murotomisaki in Shikoku at a speed of 30 km/h. The typhoon is expected to pass the Kii Channel or hit some part of the Tokaido district tonight". Watching the course of the typhoon which changed from time to time, vessels sought refuge in safe waters, and the inhabitants in coastal areas prepared for early evacuation.

At 18:13 hours, the typhoon hit the mainland 16 km west of the Shionomisaki with an instant maximum velocity of 60 m/s and a low atmospheric pressure of 929.5 mb at the center, the third lowest pressure recorded on land. Lately, with the aid of airplanes, we have been able to obtain accurate figures from observation of typhoons on the ocean, but in regard to observations on land, the figures obtained have always been quite accurate and may be relied upon for numerical comparison. Since 1900, 60 typhoons have hit the country with the atmospheric pressure at the center under 975 mb, but the typhoon Muroto (911.9 mb; Sept. 21, 1934) and the Typhoon Makurazaki (916.6 mb; Sept. 17, 1945) have been the only two with a low pressure under 930 mb. A typhoon which is a tropical low atmospheric pressure whirling counterclockwise, absorbing the moisture over the Pacific Ocean, often loses its strength as the eye expands during the travel over the sea. However, in this particular case, as the typhoon approached the country in full force, strong winds accompanied by violent waves and high tide would attack areas to the right of the course of the typhoon, while heavy rains would lash areas to the left of the course, bringing heavy destruction and serious casualties in both areas. According to the

Meteorological Agency, the deviation of high tide exceeding 1 meter due to typhoons was reported in 14 cases in the years 1945-1948. In areas to the right of the typhoon, such deviation was observed in coasts 200 km from the center, while on the left side, it was only observed within 50 km from the center.

THE TYPHOON OVER LAND AREAS

The course of the typhoon is shown in Fig. 1-1. Betraying any favorable forecasts, the typhoon crossed the steep mountainous districts of the Kii Peninsula without any signs of a sudden loss of energy, and passed the Nagoya district about 30 km west of the city heading north at a speed of 70 km/h into Japan Sea.

Records at the Nagoya Meteorological Observatory registered the lowest atmospheric pressure of 958 mb at 21:30 hours and a maximum velocity (average of ten minutes) of 36.5 m/s, and an instant maximum velocity of 46 m/s at 22:00 hours. The maximum wind velocity of 36.5 m/s broke the past record of 32.9 m/s (Sept. 12, 1934). The most violent winds were recorded on coasts 40-100 km apart from the path of the center of the typhoon, and an instant maximum velocity of more than 60 m/s were recorded in a district at the mouth of Ise Bay. Along these coasts, steel tower, huge tress several hundred years old, and numerous houses were overthrown by high winds.

Due to the geographical features of the district, the maximum rainfal also was observed to the right of the course of the typhoon. In the town of Kumano on the coast, a heavy precipitation of 400.5 mm by far broke the past record of 321.4 mm/day. In mountain districts the rainfall reach approximately 900 mm. The heavy rains caused landslides earth-flows, and submergence and inundation of farmlands and inland districts suffered heav damages as well as coastal districts as will be mentioned later.

Wireless communication with the Kumanonada and Ise Bay district was cut off, as the typhoon passed the district on Saturday night and the power source of all apparatus was inundated. With communication lines out of order and the electric lights put out, the portable radio was the sole mea of receiving communication, leaving the areas in complete isolation. Only the victims themselves were aware of the dreadfull disaster that had turne a vast area of land into a sea of muddy water, until helicopters flew over the district the following morning. (Fig. 1-2 , 3)

COASTAL DAMAGES

Though the coasts along the Ise Bay, especially the Nagoya district is subject to the effect of meteorological high tides due to the geographical features of the area, the district has been apared of heavy damages from typhoons in the past. In the Osaka Bay, records of high tides have been registered 77 times in the past 60 years, while in the Ise Bay it has only been registered 14 times in 90 years. In a rare case, Typhoon No. 13 (950 mb; Sept 16, 1953), threatened to hit the district, but fortunately the center crossed the Ise Bay at low tide with the Port o Nagoya on the left side of its course so that though the maximum meteorolo gical high tide registered 1.0-1.5 m, the area suffered comparatively slight damages.

However, the powerful Ise-Wan Typhoon, with various unfavorable eleme

Fig. 1-2 Disrupted embankment near Kuwana City

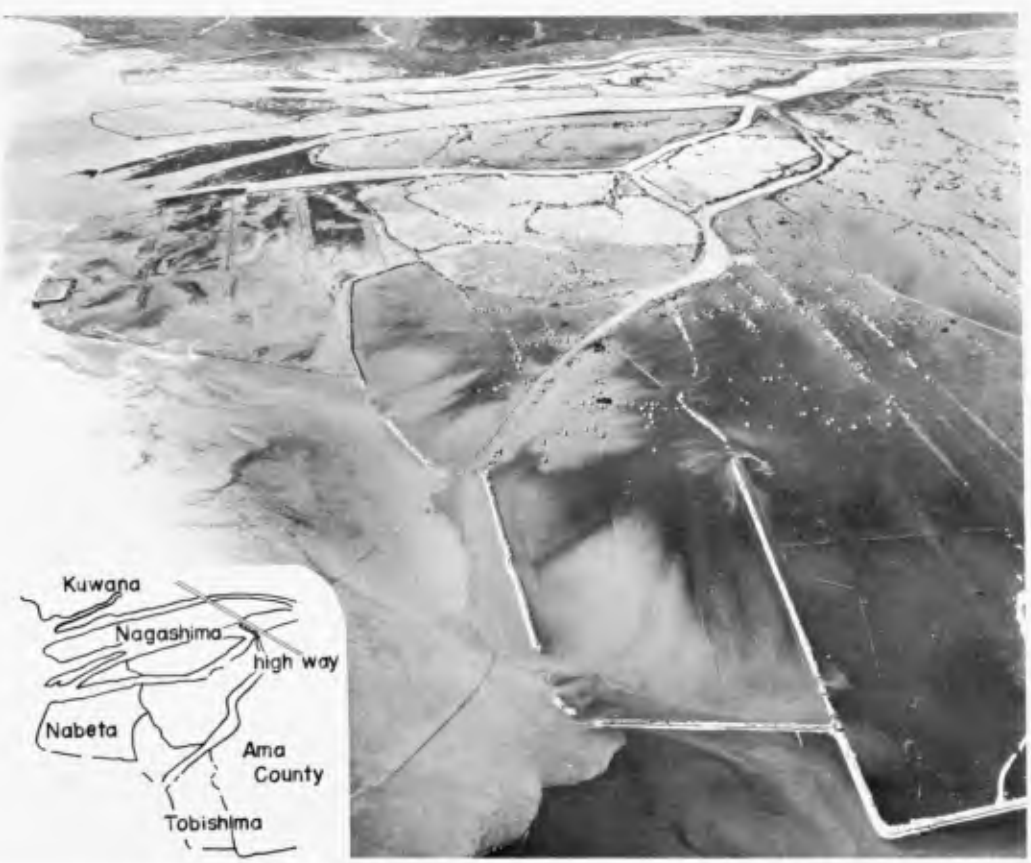

Fig. 1-3 Southern area of Ama County covered with muddy water

directly hit the defenseless area with an amazing force under extremely detrimental circumstances.

A record high tide of 3.55 m was registered in the Port of Nagoya. Meteorological high tide over 2 m (excluding "Tsunami" caused by earthquakes) have been recorded only six times during the fifty five years from 1950 to 1955 (table 2), showing that the high tide caused by the Ise-Wan Typhoon was a very extraordinary case.

Table 2
Meteorological High Tide Caused by Typhoons

August 25, 1914	Ariake Kai	2.0-2.5 m	
October 1, 1917	Tokyo Bay	2.3 m	
September 16, 1927	Ariake Kai	About 3.0 m	
September 21, 1934	Ōsaka Bay	3.1 m	Typhoon Muroto
September 17, 1945	Kagoshima Bay	2 m	Typhoon Makurasaki
September 3, 1950	Ōsaka Bay	2.4 m	Typhoon Jane

High tides accompanied by violent winds and waves brought heavy damages to large vessels which evacuated to safety outside of the port as well as small crafts moored in the port. About 200 boats (including 26 large vessels) ran aground, 340 boats (Including 10 large vessels) were sunk, 3000 boats were washed away, and 6500 boats (including 28 large vessels) were wrecked, bringing the total tonnage destroyed to 130,000 tons. Authorities concerned are studying measures to provide for the safe evacuation of vessels in each port in times of typhoon.

Fishery harbours and pearl oyster beds cultivated in the inlets and harbours facing the kumano-nada also suffered heavy destruction. Structures were torn down, materials were washed away, and the pearl oysters were destroyed as the bottom soil was transferred to a considerable extent, and the sea water became extremely muddy.

In the Port of Nagoya, a total of 300,000 tons of imported lauan logs, each weighing 6-7 tons with a diameter of 1-1.5 meters were washed out of the timber basin by a rushing current of sea water, and going wild about the port, destructed houses and facilities causing many deaths and injuries. The timber basin will be moved to the western part of the port at the earliest possible date.

The electric power generating plant and oil tanks constructed on reclaimed land were inundated, and the 1,500,000 citizins were deprived of electric power and gasoline for several day. Plans are under study to construct a high stable sea-wall to protect these facilities. Other industrial plants are also planning to instal electric motors and other key machinery on elevated positions to provide for early reopening of operations in event the plants may be inundated. Damages on seawalls and port and harbor facilities will be referred to in Chapter 55.

SCALE OF HIGH TIDE

The extraordinary high tide observed along the coast showed a wide local variation offering an interesting subject of study especially in relation to the existing emperical formula for the computation of high tide.

(in the case of Nagoya; $H = 1.6743 \Delta p + 0.16534 W \cos\theta$; Miyazaki). The maximum tidal levels as shown in Fig. 1-4 were obtained from the records of tidal gauges at more than 30 stations, an extensive investigation of tide traces, and computations by the empirical formula.

In the Port of Nagoya, the highest record of tidal levels for the past 50 years was +2.97 m T.P. (1921) (T.P.: mean water level in Tokyo Bay). However, the maximum tidal level caused by the Ise Wan typhoon registered +3.90 m T.P., 93 cm above the past record, exceeding the mean high water spring in the port by 2.70 m. The extraordinary high tide was recorded at 23:15 hours on Sept. 26, when the tides were halfway between low water level and high water level at neap tide. As the astronomical tidal level would be 0.35 m, the meteorological tide due to the typhoon may be estimated to be 3.55 m. (Fig. 1-5)

This record high of 3.55 m may be considered to be the result of the conbined forces of several phenomena. Continuous strong winds from the sea swept the surface waters toward the shore; the sea surface rose with the passing of low atmospheric pressure;her own oscillation of the water in the bay might have occured with the surging of violent wind waves; the translation velocity of the typhoon equivalent to the propagation velocity of long period waves in the bay proceeding a resonant phenomenon; etc.

The piers in the port were constructed so that the top of the pier would stand about +3.00 m T.P., and the top of the coastal embankments and sea-walls were about 4.00-6.00 m T.P., As high tides accompanied by waves of about 2 meters rushed against the coastal area bringing an extraordinary high tidal level in the bay, overflowing and overtopping of a tremendous amount of water, dashing currents, and overtopping waves separated by strong winds smashing areas far behind the embankment must have prevailed during the dreadful night storm.

Coastal embankments in the bay, and river embankments around the mouth of the river were disrupted, inundating 80,000 ha of low land. (Fig. 1-6) Embankments were destructed at every point where the overtopping wave are assumed to have exceeded 0.5 m.

Reports on waves will be omitted as they will be given in Part 3.

CONCLUSION OBTAINED FROM THE DISASTERS OF THE ISE-WAN TYPHOON

Areas affected by the Ise-Wan typhoon extended over the entire country even as far as the Kyushu district. Approximately 1,600,000 people were afflicted and 200,000 ha of cultivated land were inundated. However, it must be repeated that the heavy destruction and serious casualties occured in coastal areas particulaly along the Ise Bay.

People who have lived in regions subject to the constant threat of storms and floods for generations have learned to protect their lives and possessions by constructing embankments around their community and storing food and seeds to raise new crops in small boats, all of which have proved to be quite helpful in cases of emergency.

In coasts subject to the frequent attack of high tide, fishermen build a special type of dwelling on elevated land sheltered by trees, and

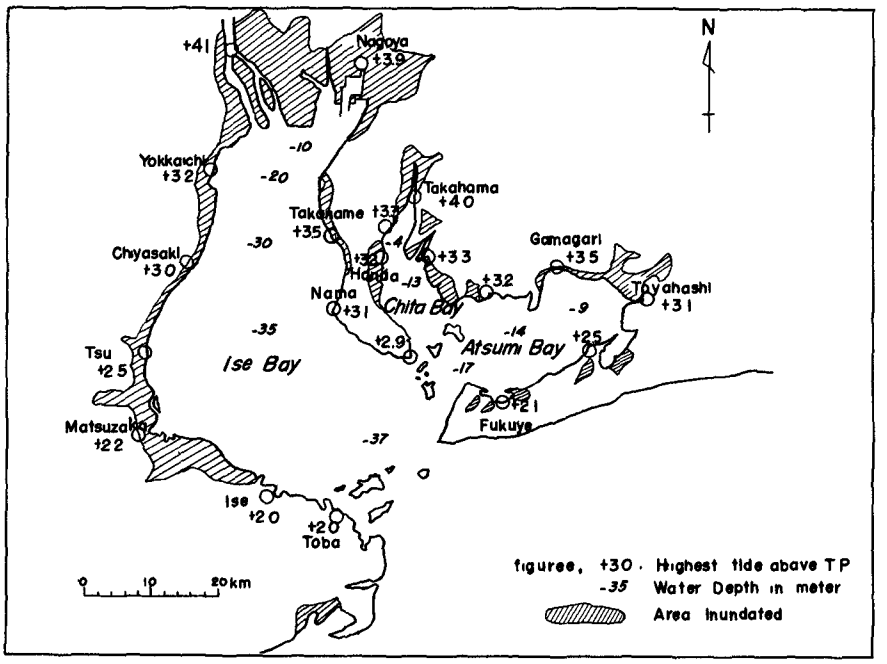

Fig. 1-4 The highest tide and area inundated along the Ise-Bay coast

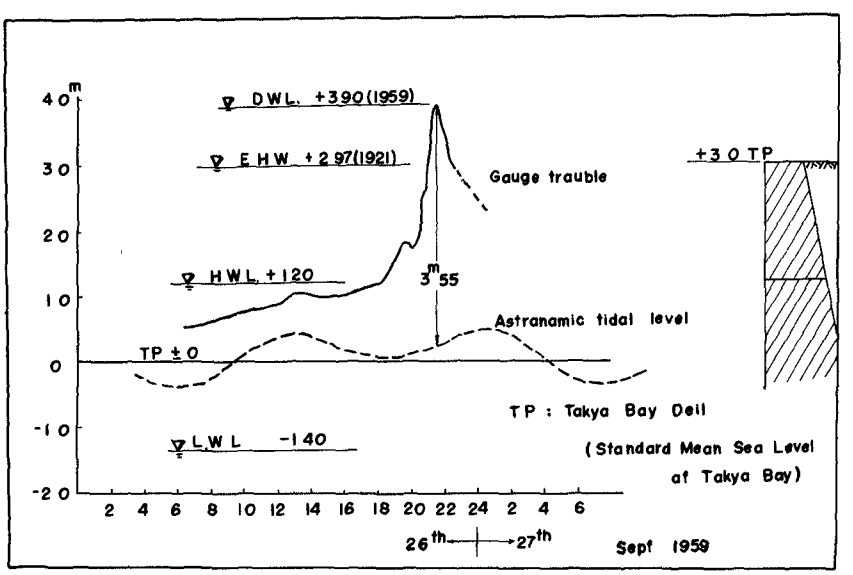

Fig. 1-5 Tidal record in the Port of Nagoya

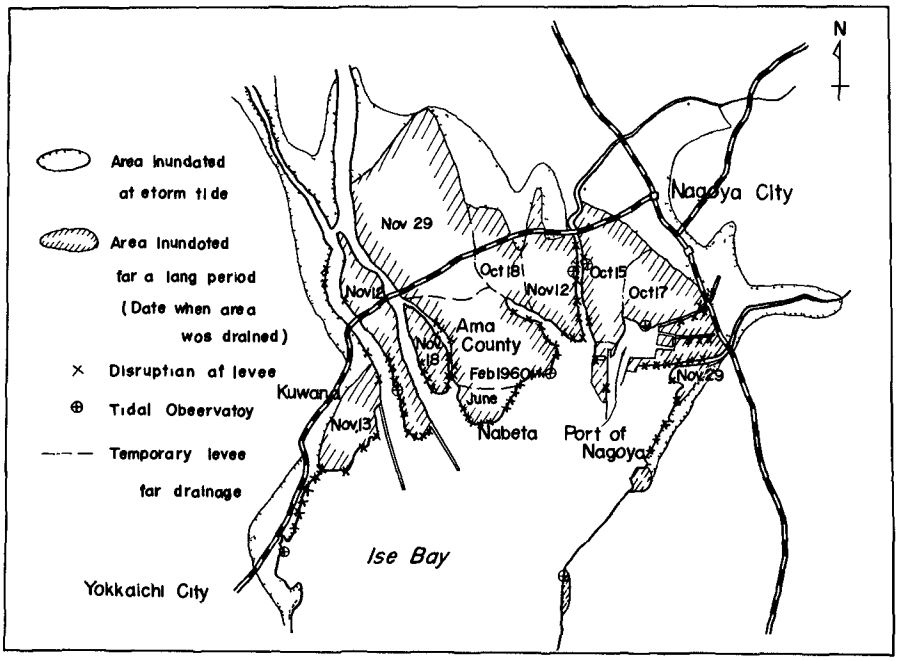

Fig. 1-6 Area inundated near Nagoya City

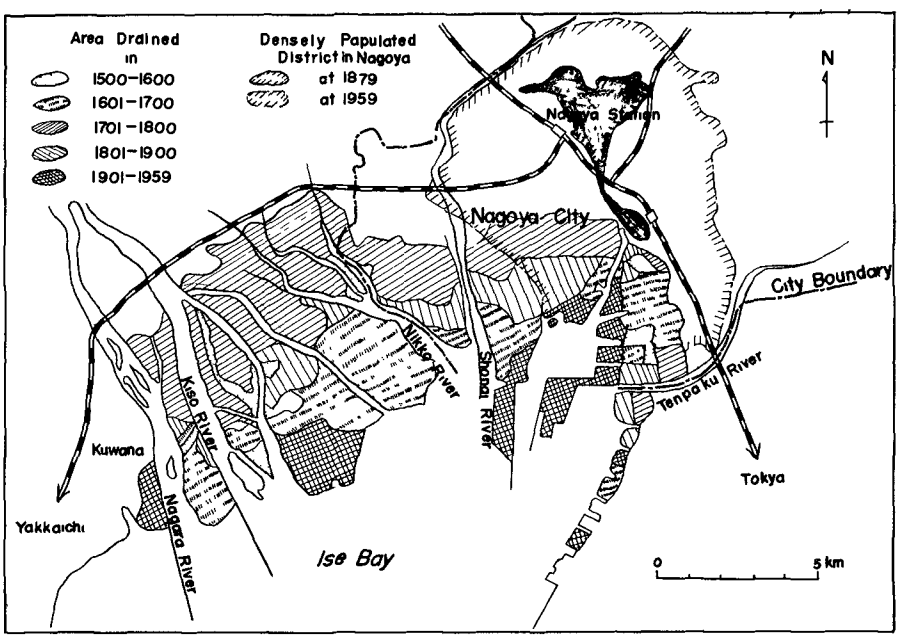

Fig. 1-7 Proceeding of land reclamation

they are always ready to take refuge in tall public buildings. Few lives were lost even in the case of the Ise-Wan typhoon in such regions well-prepared for any emergency.

However, the coastal regions around the City of Nagoya developed from deltas formed at the mouth of a large river, where, from as far back as th 17th century, people began to drain the low lands building dikes farther and farther into the sea. (Fig. 1-7) Through a well-developed system of irrigation, the vast areas of land thus gained has become one of largest rice-producing centers in Japan.

With the march of times, the rice fields which hat always been as low as the mean water level were turned into large industrial zones, attractin a large population.

Table 3
Population and Area of the City of Nagoya

	1879		1957	
Population	167,400		1,429,000	
Area	1,334	hectares	25,085	hectares

However, they neglected to take appropriate measures and invest sufficient funds for facilities to protect this low area from the attack of high tides. Moreover, 200,000 m/day of underground water was pumped ou of about 1000 wells for industrial and irrigational purposes, resulting in a ground subsidence of more than 10 cm in the past ten years. Especially along the coasts, due to the earthquakes, the ground level was 50 cm on th average, and at some points 1.00 m, below the pre-war level. It may also be pointed out that necessary repairs on the old seawalls which had settled considerably had been neglected to a certain extent from the general lack consideration for the maintenance and repairs of existing facilities on th part of the authorities concerned. Moreover, the inhabitants were not ful aware of the great danger of living in this low area unpreparel for any disaster that might befall them some day.

As they had been enjoying the benefits of modern city conveniences such as transportation and communication facilities, and power and water s pplies, the confusion was beyond words once the area was inundated and lef in a primitive undeveloped state. They faced great difficulty in transpor ing, storing, and distributing relief goods and materials for rehabilitati as well as in determining methods of commencing reconstruction works.

Under bad weather conditions, two months passed before temporary repair works were completed elevating the inundated trunk highway, repair-ing the embankment extending 35 km, which was disrupted at 220 points, and draining the inundated area with the help of pump dredgers. Hardships encountered remain fresh in the minds of all concerned as it was a long ti before the abundant electric power supply was available in the devastated area, and the remains of old abandoned dikes lying far inland from the coast proved to be quite useful in the course of reconstruction works. Plans to prevent disasters from spreading over large areas, and other con-clusions obtained from valuable experiences will be included in the re-habilitation program.

A BRIEF OUTLINE OF THE ISE-WAN TYPHOON

There is a Japanese proverb which says, "Disasters come around when they have been forgotten". According to the probability chart based on the records of maximum high tidal levels in the Port of Nagoya for the past 40 years, a high tidal level of +2.42 m T.P. will occur once in 20 years, a level of +3.00 m once in 300 years, and a level of +3.10 m only one in 500 years, but these figures merely represent the probability on paper.

A large number of the tidal gauges, wind meters and wave meters did not operate during the typhoon. However, in the case of the tidal gauge station in the Port of Nagoya, fortunately the recording appartus was installed on a high site, and the cap of the well was light enough to allow the pole of the buoy to stand 50 cm above the well with the rising of the tide, valuable records were registered until the surging began to withdraw.

A typhoon of a larger scale than the Ise-Wan Typhoon may strike any part of the country in the future. In order to establish an efficient program to prevent disaster, based on fundamental investigations, with due consideration for the economic problems involved, various research and investigation works have been undertaken through the cooperation of all authorities concerned. Hydraulic experiment are under way on the characteristics of high tides and wind waves generated by typhoons particularly along the coasts of Tōkyo Bay and the Ōsaka Bay which are most likely to be hit by a typhoon. We are also studying an accurate method of forecasting typhoons with the aid of a radar, Robbot Tide Gauge of the Water Pressure type, and an electronic computer, effective measures to be taken when attacked by typhoons, and plans after rehabilitation.

In closing, I would like to say that, at the present stage, to prevent disasters from typhoons, we have no alternative but to establish an appropriate and extensive program from the social, economical, scientific, and engineering point of view, based on an accurate knowledge of the typhoon itself and the subsequent natural phenomena, as well as a thorough understanding of the various conditions concerning the regions subject to the attack of typhoons in the future.

(Note: Immediately following the heavy destruction caused by the Ise Wan Typhoon, a committee was formed of 15 members from the authorities concerned, headed by the Director General of the Sience and Technics Agency, named "The Temporary Committee on the Prevention of Typhoon Disasters". The committee carried out an extensive investigation on the characteristics of the typhoon and the actual condition of the damages inflicted, and a detailed study on measures to be taken in the future to prevent similar damages, the result of which has been submitted to the government quarters. This paper has been based on the experience of the author as he participated in the investigation and discussions as a member of the committee.)

CHAPTER 55

INVESTIGATION OF DESTROYED STRUCTURES AND THE RECONSTRUCTION PROGRAM; ISE-WAN TYPHOON

Senri Tsuruta

Director, Harbour Hydraulics Division, Transportation,
Technical Research Institute,
Ministry of Transportation

INTRODUCTION

The powerful Ise-wan Typhoon destroyed coastal defence works along the Bays of Ise, Chita, and Atsumi, over nearly the entire length of the coastline, and also inflicted considerable damage on breakwaters, piers, and other harbour facilities.

The destruction observed in various structures show a close resemblance, and the ground leading to such destruction may be classified into several categories, indicating that these coastal structures possessed a common weakness against the destruction force of nature. This common weakness presents a particuler problem in planning and carrying out reconstruction works in the future.

FACTORS LEADING TO DESTRUCTION

1. Insufficient resistance against scouring

The destruction of coastal embankments and seawalls may be said to have resulted from the scouring on the crown and back slope by the overflow of high tides and downfall of overtopping waves. Structures with the crown and back slope covered with concrete slabs remained undamaged, while the majority of those which were not covered were destroyed.

An example of destruction from scouring on the crown may be clearly observed in the seawalls in the southern part of the City of Tokoname. The cross sections and crown heights of the seawalls varied considerably as shown in Fig. 2-1, as they had been constructed at different times by different authorities. Wall A, a simple stone revetment was completely broken down. Wall C where the crown had not been completely covered was destroyed as shown in Fig. 2-2, and wall B, completely covered with concrete slabs remained undamaged. And the over-all collapse of the dike protecting the reclaimed lands of Kōei Shinden in the City of Handa was also due to the unfinished pavement on the crown (Fig. 2-3,4). Thick bushes of bamboos or miscanthuses often planted on the crown and back slopes to prevent the back-filling from being scoured were not quite effective under such strong overtopping as observed in the storm surge.

2. Decrease in crown height of embankment in an inlet or a river mouth

An embankment along the coast of an inlet or a river embankment is generally of an inferior structure with a lower crown height as compared

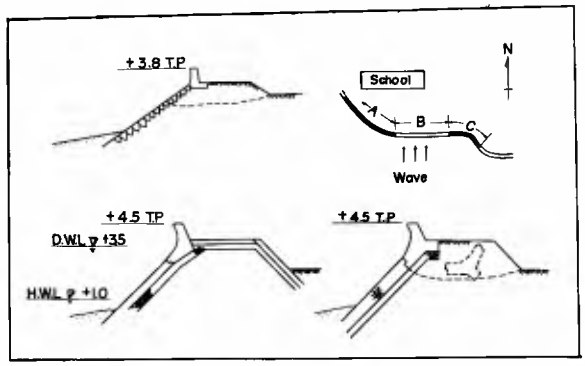

Fig. 2-1 Cross sections of sea walls at Tokoname City

Fig. 2-2 C-collapsed from line of juncture due to scouring of back-filling as the back slope was not covered with concrete slabs. B-seen in foreground.

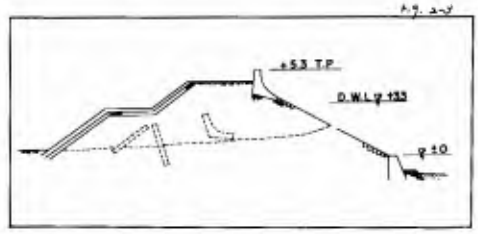

Fig. 2-3 Cross section of dike (Handa City)

Fig. 2-4 Total collapse of structure due to scouring of back slope by overflowing of sea water as pavement of crown was unfinished.

to coastal embankments, as they have not been designed to withstand the direct attack of wind waves generated by a typhoon. Moreover a sudden fall of the cross section is often found at junctions with coastal embankments. Embankments with different cross sections were destroyed at the junctions without exception. As a storm surge has a tendency to rise higher in an inlet on the sea coast, the crown height of an embankment should be desiged to possess sufficient height against the surge.

3. Weakness observed at a flood gate or a sluice-way

A flood gate or a sluice-way is exposed to severe wave action due to deep scouring in the front of the structure. Moreover structures of different weight tend to settle unevenly when constructed on soft ground. A rupture in the embankment at the location of the pump atation is considered to have lead to the collapse of the right bank of the River Shonai, inundating the southern part of the City of Nagoya. Similar damages at flood gates and sluice-way were observed in various locations.

4. Lack of reinforcement of embankments against severe wave action

In the disaster following the Ise-wan Typhoon, there are only a few cases in which coastal embankments or sea walls were destroyed by the scouring of sea water overflowing the crown height with the rising of the tidal level. In most cases, the structures are considered to have been smashed by severe wind waves accompanying the storm tide. Destruction in the coastal embankments along the village of Tobishima in the County of Ama occured at the same site as in the case of the storm surge of Sept. 26, 1921. In both cases, the damage was caused by an unusually severe wave action as there had been a gut, that is, the water depth in front of the wall had increased considerably. Generally speaking, parts of embankments with obstacles in the front waters, or parts sheltered by a stretch of reclaimed land were spared of serious damage (Fig. 2-5). Therefore, steps must be taken to extend the wall height or reinforce the structure, particularly in waters where the concentration of waves or strong wave strokes are expected, to prevent similar disasters in the future. Furthermore, it must be noted that unusually severe wave actions occur along erosive coasts.

5. Settling or leak of filling

It is a very effective measure to cover the crown and back slope with concrete slabs in order to protect the back-filling against scouring by the overflow of high tide and the downfall of overtopping waves. But the filling is apt to settle or leak through gaps in the foundation and front stone works, leaving the interior in a hollow state and the structure will be in a dangerous condition against the attack of smashing waves (Fig.2-6). The settling or leak of the filling may be avoided and the structures will possess a strong resistance against scouring if a large quantity of loam or clay is available for the filling and the construction works are carried out with the utmost care. But in many cases, sand is the only material available when long embankments must be constructed on the coast in a short period of time. Therefore it would be advisable in such cases to consider the following measures: to make inspection holes in the crown

Fig. 2-5 Wall behind power transmitting tower remained in a little damage. (Port of Nagoya)

Fig. 2-6 Wall smashed by waves as interior was in a hollow state from settling of sand filling. (Yokkaichi City)

Fig. 2-7 Completely covered structure collapsed from settling of sand filling for a length of over 100m as partition wall was lacking. (Port of Nagashima)

Fig. 2-8 Right side of the wall was saved by partition wall. (Yokkaichi City)

pavement at certain intervals for the replacement of the filling when necessary; to construct partition walls mentioned in the following paragraph; and to prevent the leak of the sand filling through the stone works by providing a complete cut-off and applying a mortar mixture in laying the stones.

6. Chain reaction of collapse due to lack of partition walls

In coastal embankments protecting low areas, especially dikes enclosing reclaimed land, disruption in one section will provoke numerous breaks along the entire length of the structure in a short period of time as dashing current of sea water will penetrate through the interior from the opening and wash out the sand filling, while strong waves will hit the surface of the structure from the exterior. Examples of such destruction over a distance of several hundred meters were to be found in many location (Fig. 2-7), as in embankments enclosing the reclaimed areas of Nabeta near Nagoya and Kinuura and Hekinan facing the Chita Bay. If the embankment had been provided with partition walls at intervals of twenty to thirty meters, destruction would not have extended over such length of the embankment (Fig. 2-8).

7. Inadequate design and method of construction

When the crown and back slopes of embankments were destroyed and the filling scoured as mentioned above, the parapet and front wall collapsed without exception from the line of junction. A wall of the conventional type supported in position by the back-filling will be easily turned over by slight wave force when the back-filling has been washed away. Therefore it would be advisable to adopt self-supporting structures such as a buttressed wall, and the parapet should be constructed so as to form one solid body with the front wall with re-entrant curves up to a height of two meters to repel attacking waves offshore.

THE RESTORATION PROGRAM

As the reconstruction of structures damaged by storm surges caused by the Typhoon must be undertaken immediately, involving an enormous amount of funds, the Government summoned authorities in various fields to determine various standards for structures to be constructed.

1. Fundamental principle

(a) Every restoration plan for coastal areas, rivers, ports and harbours, fishery ports, drained and reclaimed lands, roads, etc. is to be drafted as a division of an over-all rehabilitation program, with due consideration for mutual relations and the geographical features of the district. Definite plans in one field which are to be carried out immediately may be closely related to plans in other fields to be undertaken in the future. The former plan will be modified if necessary when the latter plan takes definite shape. In carrying out the first plan, steps must be taken to prevent double investment of funds when applying modifications in the future.

(b) Field investigations and laboratory experiments should be undertaken at once to study various problems from an engineering point of view. Problems to be studied include the effect of the breakwater in reducing wave forces and storm surges; the influence of the breakwater over the vicinity; the characteristics of waves invading rivers and inlets; and the uprush of the storm surge.

2. Tide and waves

Plans for reconstruction will be based on the Ise-wan Typhoon in regard to the deviation of the tidal level and characteristics of attacking waves. The mean higher high water level in the typhoon season will be adopted as the astronomical tidal level.

3. The crown height of the embankment

The crown height of an embankment will be determined from various conditions of the hinterland, the types of structure, and the functions of the ports and harbours and fishery ports.

In districts lower than the sea level, or relatively low and flat areas with a dense population, the embankments will be designed to prevent any overflowing of sea water due to storm tide and waves of the scale considered in the program. Hence the standard crown height will be obtained from the total height of the maximum deviation of the tidal level, and wave height occured during the Ise-wan Typhoon, and the mean higher high water level in the typhoon season.

In isolated districts of high ground level with a relatively scarce population, overtopping of waves in times of storm surges will be tolerated to some extent depending on the actual condition of the district. But the embankments must be of sufficient height to prevent the overflowing of sea water and wave energy.

In the wharf and pier zones in ports and harbours as well as fishery ports, and industrial zones on the coast, the wall height should be limited to a height which will not interfere with loading and unloading of cargo and the productive activities of the industrial plants.

4. The structure of the embankment

An embankment in a certain district should be of a uniform structure, but it may be difficult to apply this principle in cases when a new embankment must be jointed to an existing embankment, or when the characteristics of the natural features, soil conditions, difficulty in acquiring the necessary land, and different purposes of construction call for a different type of structure. In such cases, the two different types of structures must be joined so as to prevent any failure from the joining points

Even when the embankment is constructed to avoid the overtopping of waves from the tidal level and waves adopted in the program, the crown and back slope should be covered with concrete slabs to protect the face

and toe from scouring.

Special attention will be required in designing and constructing the structure so that voids will not appear within the covering of the body, and structural weakness will not be found in the parapet wall. If the soil condition is likely to cause subsidence of the structure in the future, appropriate measures should be taken in advance.

The body should be of a self-supporting structure as far as possible. Partition walls at intervals of about 30m would serve to prevent a failure in one section from affecting other sections of the embankment.

With a restoration program based on the above-mentioned standards for various engineering projects, reconstruction works are now in full swing to provide against the typhoon season in the coming year. We are also confronted with problems related to the timber basin and driftwood which greatly increased damage during the disaster, and the construction of earthquake-proof structures in a country frequently attacked by earthquakes as well as typhoons, Thus engineers in various fields are entruste(with the responsiblity of protecting the country and its people against the powerful force of nature.

CHAPTER 56

WAVES ON THE PACIFIC COAST AND ON THE COAST OF ISE BAY CAUSED BY THE ISE-WAN TYPHOON

Takeshi Ijima, Dr. Eng., Shōji Satō and Hisashi Aono

Harbor Hydraulics Division, Transportation
Technical Research Institute,
Ministry of Transportation

SYNOPSIS

General aspects of wave characteristics on the Pacific Coast of the main land and on the coast of Ise Bay caused by the Ise-wan Typhoon are studied on the bases of the observed wave data, calculated wave heights by the authors' method of forecasting shallow water wave and the results of the field inspection of damages by the typhoon.

WAVES ON THE PACIFIC COAST

1. Waves on the Pacific Coast

During this typhoon, wave observations were carried out at four harbors, namely Kōchi, Naarai, Shimizu and Ishinomaki as shown in Fig. 3-1, by means of underwater pressure-type wave meters which were installed 6~10 meters deep, lest they should be affected by local condition. Fig. 3-3 shows the time change of height and period of significant wave, and velocity and direction of wind at each place. At the harbors of Hachinohe and Kuji waves were measured by visual observation of wave staffs in the daytime only. As the results of observation, maximum significant waves by the typhoon and the time of observation at above mentioned points are shown in Table 3-1.

Table 3-1
Maximum Significant Waves
on the Pacific Coast

Stations	Heights in Meters	Periods in Seconds	Appearance Times	Remarks
Hachinohe	2.7	12.5	9 a.m. 27th	Wind Waves(Staff)
Kuji	3.3	13.0	8 a.m. 27th	Wind Waves(Staff)
Ishinomaki	4.0	11.0	6 a.m. 27th	Wind Waves(Wave Meter)
Naarai	2.9~3.0	10.5~13.0	8 a.m.~2 p.m. 26th	Wind Waves(Wave Meter)
Shimizu	4.2	17.0	1 a.m. 27th	Wind Waves(Wave Meter)
Kōchi	6.5	14.4	8 p.m. 26th	Swells (Wave Meter)

2. Waves on the Kumano-Nada

It is considered that the greatest waves on record attacked the coast of the Kumano-Nada, by the reasons that this coast situated in the dangerous semicircle of this typhoon and that its coast line was almost parallel to this course 0~80 kilometers apart from the center of the

Typhoon. Geographically the coast north of Kinomoto is sunken rias coast and its bottom profile is steeper than 1/10 within the depth of -10~-20 meters. Accordingly, wave characteristics is so varied along the coast that the accurate estimation of wave distribution is very difficult. So the wave heights along the coast were estimated mainly from the inspection of damages of seawalls and breakwaters etc. and from the topogrphical features of the coast, the results being shown in Fig. 3-2.

It may be possible to estimate offshore wave characteristics which were not affected by coastal configuration, but the accuracy is obscure for such a large typhoon as this. The estimation from the observed wave data on the Pacific Coast caused by past typhoons and inspection of the degree of damages of coastal structures caused by this typhoon is that the significant wave height and period were 10~12 meters and 14~16 sec., respectively, and the most prevailing wave direction was S~SSW.

WAVES ON THE COAST OF ISE BAY

1. Effect of Swell

In this typhoon actual wave records were taken outside the harbors of Nagoya and Fukue. According to these data, at Nagoya height and period of swell were 10~15 centimeters and 7.3~9.0 sec. at 2 p.m. 26th of September and at Fukue were 15 centimeters and 16.5 sec. at 5 a.m. 26th. On the other hand, according to the refraction diagram for the swell of 16 sec. and S-5°-E, propagating through the Irako Channel, refraction coefficient is less than 0.02 on the coast from Yokkaichi to the Kiso River. So it may be unnecessary to consider the effect of swell and it is enough to consider waves generated only in the Bay.

2. Wind on the Bay during the Typhoon

Fig. 3-4 shows, as examples, wind distributions observed on the coast during this typhoon, in which arrow and number are wind direction and wind velocity and dotted line is the equi-wind velocity line. In addition, tide level obtained by tide gauges and equi-tidal lines estimated are shown, for which the datum is the mean water level of Tokyo Bay. In Fig. 3-5 and Fig. 3-6 time change of wind velocity and direction at the north, middle and south coasts of the Bay are shown. From these figures, wind characteristics by this typhoon are considered to be as follows.

(1) Wind velocity increases gradually from the south coast of the Bay to the north coast in advance of this typhoon and when it reaches the maximum on the north coast it begins to decrease on the south, that is, the maximum wind velocity on the south coast occurs 1.0~1.5 hours earlier than on the north.

(2) After wind velocity comes up more than 15 m/sec, wind direction on the Bay is E~ESE, subsequently changes to SE~S with the advance of the typhoon, and finally it becomes SW.

(3) Wind velocity on the west coast is larger than on the east coast except near Fukue and wind on the west coast may be considered nearly equal to the wind on the sea surface.

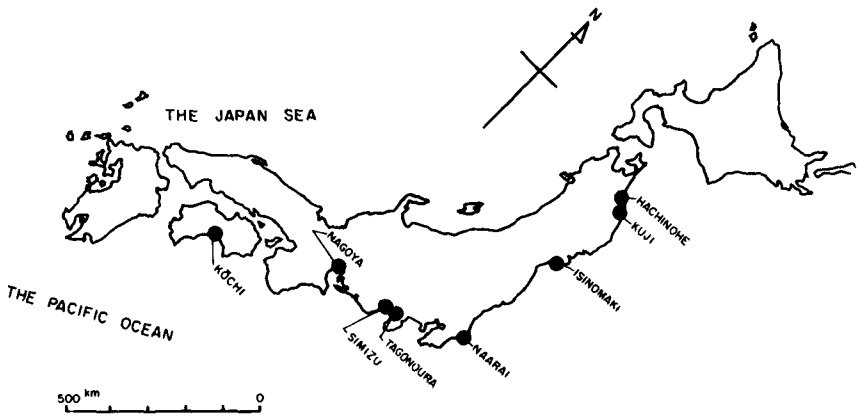

Fig. 3-1 Stations of Wave Observations.

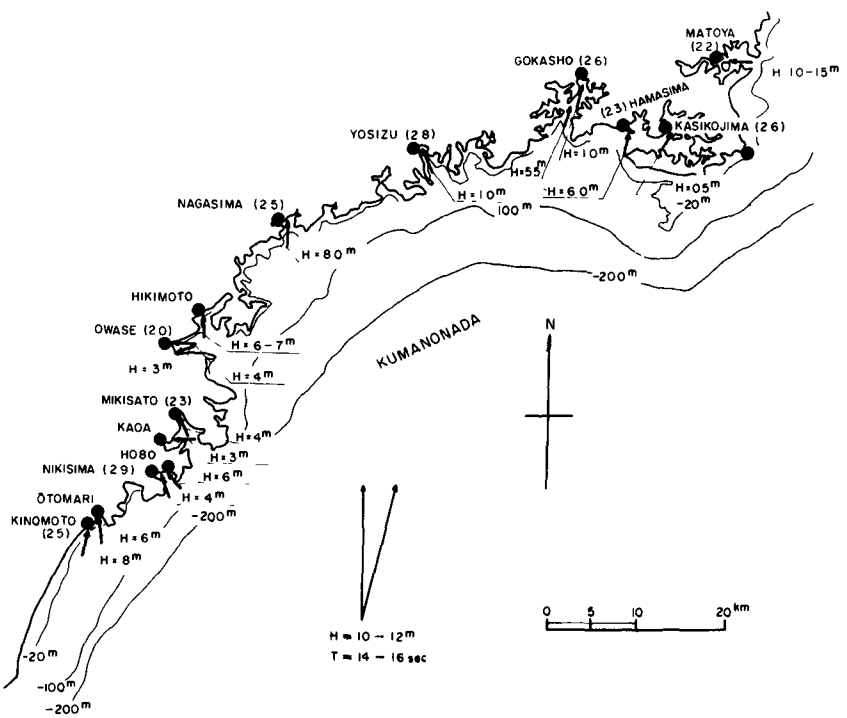

Fig. 3-2 Distribution of Predominant Significant Waves on the Kumano-Nada Coast. Arrows show Wave Direction. Numbers in Brackets are the Estimated Maximum Storm Tide Level above the Mean Water Level of Tokyo Bay.

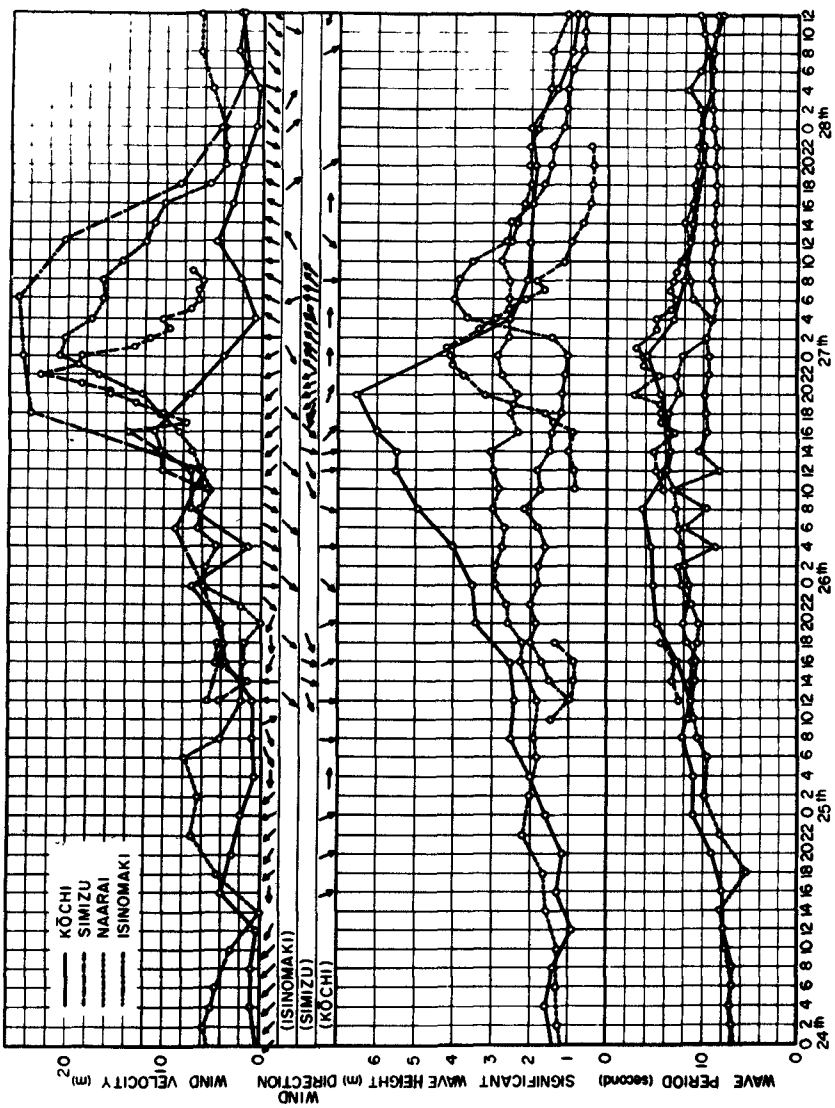

Fig. 3-3 Time Change of Significant Waves and Wind Observed on the Pacific Coast.

We can not disregard wind distribution in examining wave characteristics in sheltered bays, even if their fetches are relatively short distance of 50~60 kilometers like as Ise Bay, especially in the case of irregular configuration and depth. Moreover, the change of depth with storm tide is as important as the change of wind. From the above considerations it is expected that waves on the west coast are larger than on the south coast, and that waves on the north coast become more larger with the progress of a typhoon than in stationary uniform wind velocity distribution.

3. Wave Distribution from Observed Data and Investigation of Damages of Coastal Structures

On the coast of the bay, during this typhoon wave records were taken at two stations off Nagoya Harbor and off Fukue Harbor.

Off Nagoya Harbor significant wave heights and periods were 2.0~2.4 meters and 5.6~6.5 sec., respectively, from 6 p.m. till 11 p.m. 26th. Off Fukue Harbor the maximum significant wave caused at 7 p.m. and its height and period were 1.7 meters and 5.2 sec. as shown in Fig. 3-15. Direction of the maximum significant wave were estimated to be E~ENE.

The distribution of predominant wave height and wave direction estimated from the investigation of damages of the coastal structures, ie. seawalls, breakwaters, groins etc., after this typhoon is shown in Fig. 3-7. Although wave data shown in Fig. 3-7 were estimated mainly from the natural conditions at that time according to the authors' opinion, they are available together with calculated results which are described below, to examine wave characteristics.

4. Waves Estimated by Authors' Graphical Calculation Method

Wave characteristics are estimated by the graphical calculation method as shown in appendix. Selecting 9 points on the coast of the Bay shown in Fig. 3-8, waves on the fetches in Fig. 3-8 are calculated in order to find the periodical change of wave height and period at 8 meters deep below the sea level datum. In order to eliminate subjectivities in calculations, distributions of wind and tide are assumed as follows:

(1) Ise Bay is seperated from open sea by Irako Channel and divided from Atsumi Bay by Nakayama and Morozaki Channels.

(2) Wind velocities and wind directions are determined from every hour distributions as shown in Fig. 3-4, because observed winds on the coast would give better results than estimated winds on the sea surface based on the winds on the coast and other meteorological conditions of this typhoon.

(3) The wind velocities on the leeward and windward-ends of the fetch are taken as fetch components of winds on the coast as shown in Fig. 3-4. And the wind velocity on the fetch varies linearly from leeward to windward.

(4) Space and time change of depth on the fetch are given by the tide at the stations shown in Fig. 3-4 and the sea chart.

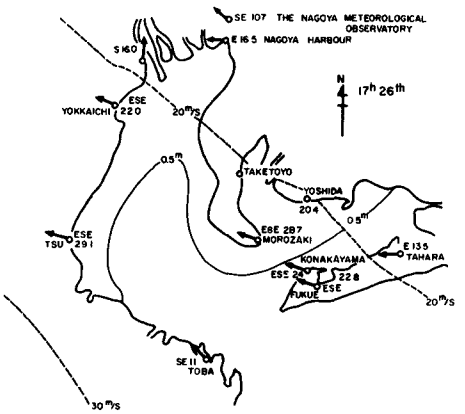

Fig 3-4 (a)

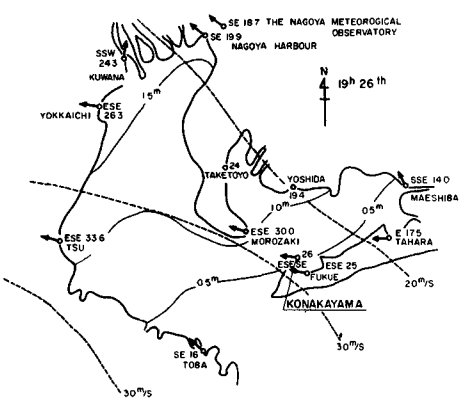

Fig 3-4 (b)

(a) 5 p.m. 26th

(b) 7 p.m. 26th

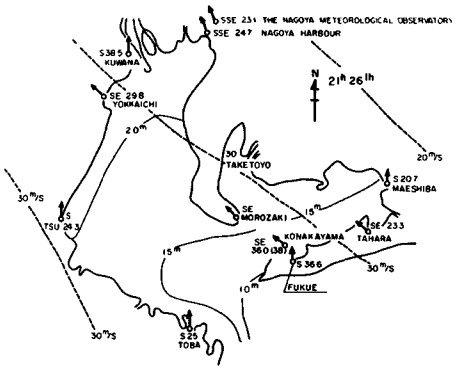

Fig 3-4 (c)

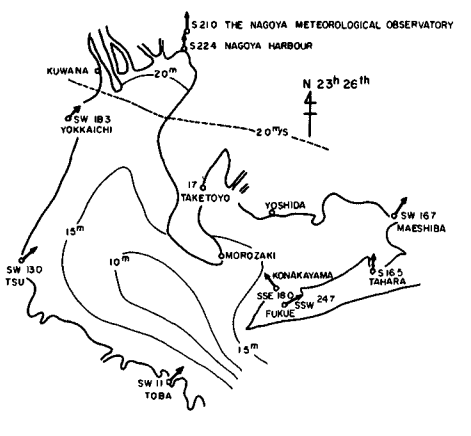

Fig 3-4 (d)

(c) 9 p.m. 26th

(d) 11 p.m. 26th

Fig. 3-4 Distribution of Wind and Tide on the Ise Bay during the Typhoon.

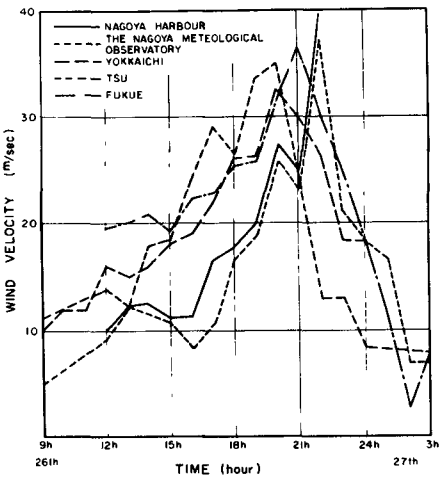

Fig. 3-5 Time Change of Wind Velocity at Representative Points during the Typhoon.

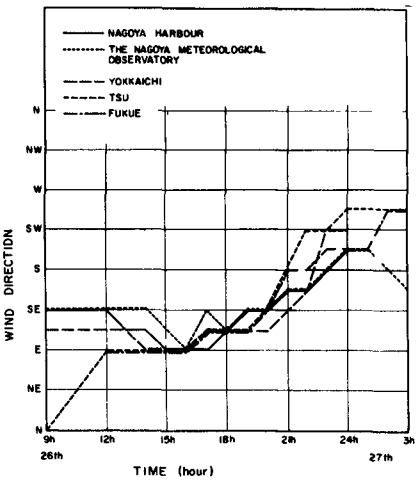

Fig. 3-6 Time Change of Wind Direction at Representative Points during the Typhoon.

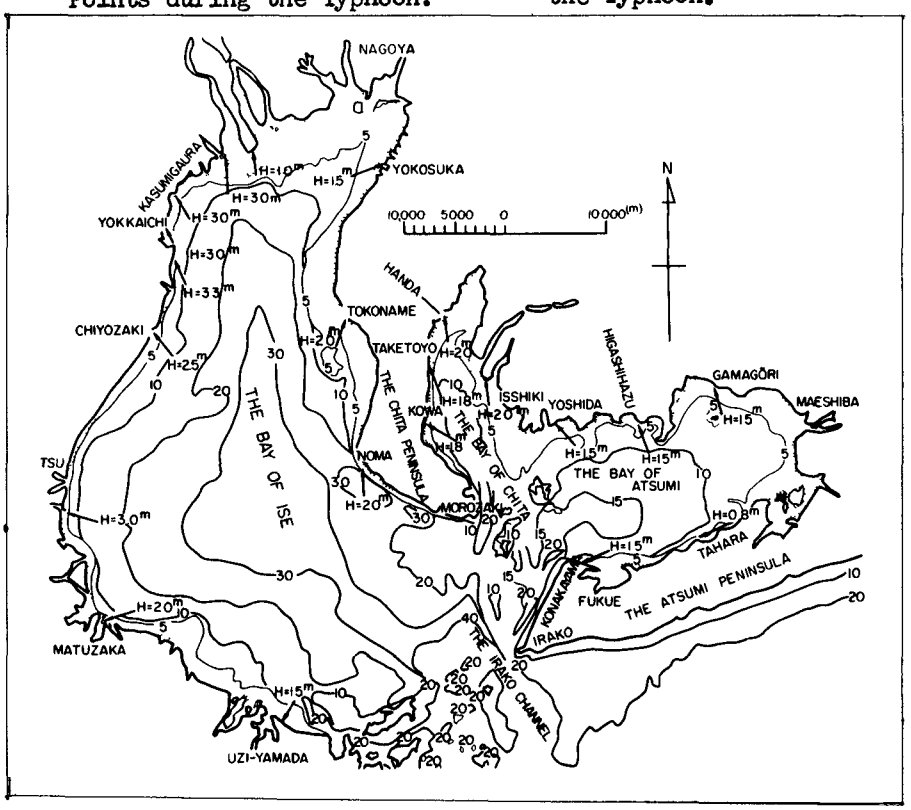

Fig. 3-7 Distribution of Predominant Significant Waves on the Ise Bay.

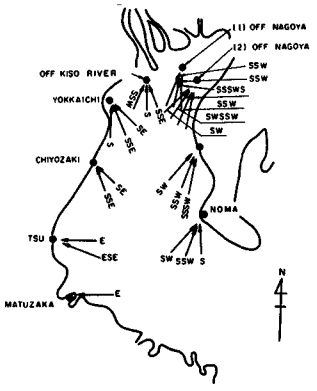

Fig. 3-8 Points of the Ise Bay on which Waves were Graphically Calculated.

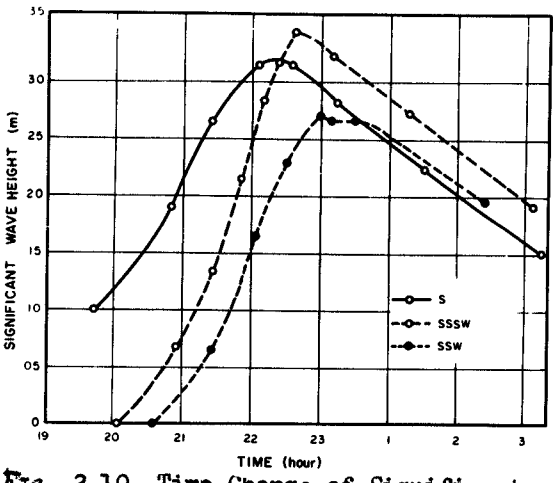

Fig. 3-10 Time Change of Significant Waves at Off Nagoya No. 1 for Variable Fetches.

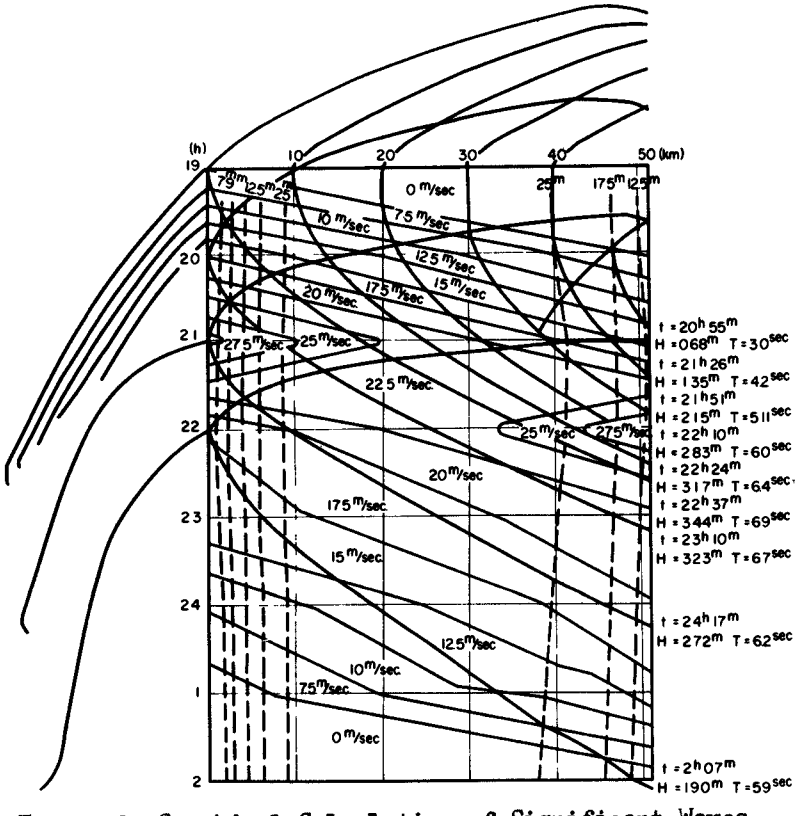

Fig. 3-9 Graphical Calculation of Significant Waves in the Direction of SSSW at Off Nagoya No.1.

WAVES ON THE PACIFIC COAST AND ON THE COAST OF ISE BAY CAUSED BY THE ISE-WAN TYPHOON

By the wind field diagram which indicates space and time changes of wind velocity and depth on the fetch, wave heights, wave periods and travel times are calculated using H-t-F-Cg diagram. Fig. 3-9 shows the wind field diagram of SSW direction at No. 1 off Nagoya, as an example. Time change of wave height of S, SSSW and SSW directions thus obtained at No. 1 off Nagoya is shown in Fig. 3-10. It is considered that the envelope of these curves gives time change of predominant wave heights. Time changes of predominant wave height at every point of the coast of the bay are shown in Fig. 3-11. Fig. 3-12 shows local characteristics of maximum significant waves, plotting the names of stations on the horizontal axis and maximum significant wave heights and periods and times of occurence on the vertical axis. The time of occurence of the maximum absolute wind and of the maximum component velocity on the fetch on which the maximum significant wave height occurs are plotted.

It is understood that wave characteristics on the coast of Ise Bay are as follow.

The maximum significant wave height and period increases gradually from Matsuzaka on the south coast to Yokkaichi on the north coast, where it attains the maximum value, and then decrease from Yokkaichi to the north and the east coasts. The minimum value occurs at Nagoya No. 2. In general wave heights and periods on the east coast are about 80 % and 90 % of the values on the west coast, respectively. The maximum wave on the north coast appears about 3 hours later than on the south coast. The maximum wind velocity at Nagoya occurs about 2.5 hours later than at Tsu, and the maximum wave heights at both of above two points appear about 1~2 hours later than the maximum wind velocity. Although wind is blowing from ESE near Yokkaichi and the maximum wind velocity occurs at 8 p.m., the maximum wave height occurs about 10 p.m. and the direction is SSE. Also, according to the results of actual inspection it is evident that waves from SSE direction destroyed structures on the coast near Yokkaichi. It is evident that the most predominant wave can not be decided only by the maximum wind velocity and its direction.

5. Distribution of Wave around Nagoya Harbor

In the previous section, we considered general distribution of waves in Ise Bay, but they should be considered as offshore waves because they are waves at the point of 8 meters deep. In actual the waves in front of seawalls placed near the shoreline gives most important problem. Waves at these places have considerable local variation on accout of variation of water depth, therefore waves should be calculated in details for each place. As an example, results of calculations of wave distribution around Nagoya Harbor by the above mentioned method are shown here. Fig. 3-13 indictes the points of wave calculation, in which arrows are predominant directions of waves to them. Fig. 3-14 is the wind field diagram of point C, and results of calculation for this point are shown in Table 3-2.

From Table 3-2, the wave is highest at the Point A, west side of Nagoya Harbor, where the maximum wave height exceeds 2 meters, and wave height decreases gradually to the east. (At the Point E, however, wave height comes up to 2 meters because of great water depth.) And at the

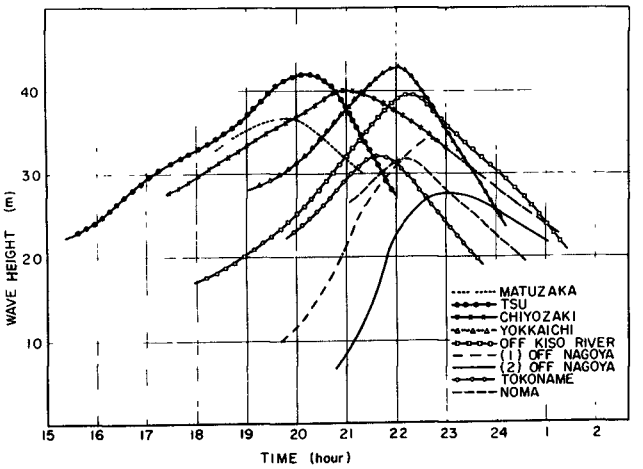

Fig. 3-11 Time Change of Predominant Significant Wave Height on the Ise Bay.

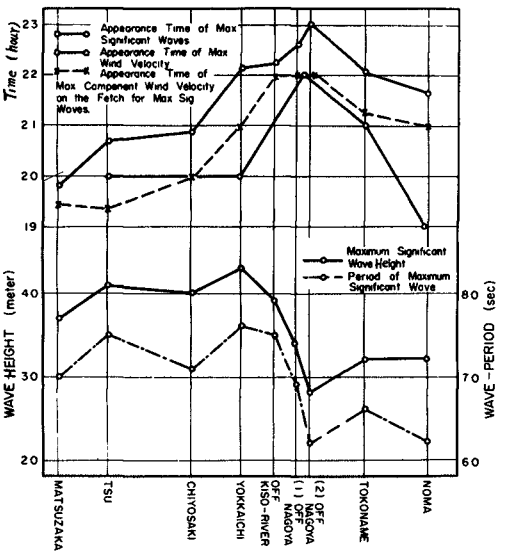

Fig. 3-12 Local Distributions of Maximum Significant Waves in 8 Meters Deep of Sea Chart and Maximum Wind Velocity along the Coastline of the Ise Bay.

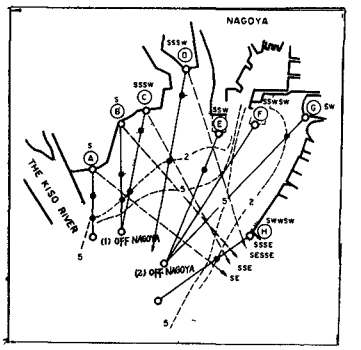

Fig. 3-13 Points of Wave Calculation of the Coast near Nagoya.

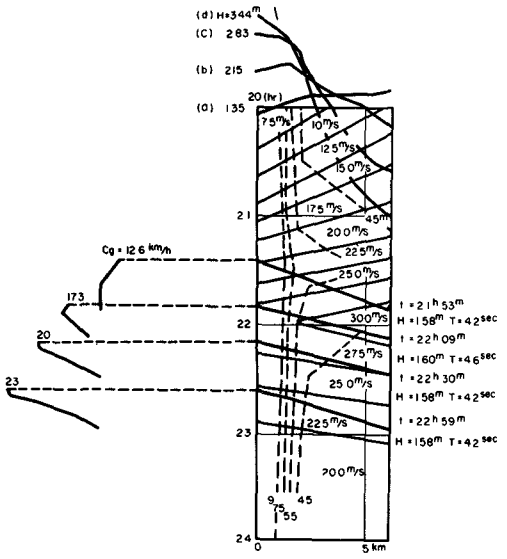

Fig. 3-14 Graphical Calculation of Significant Waves at Point C of Nagoya.

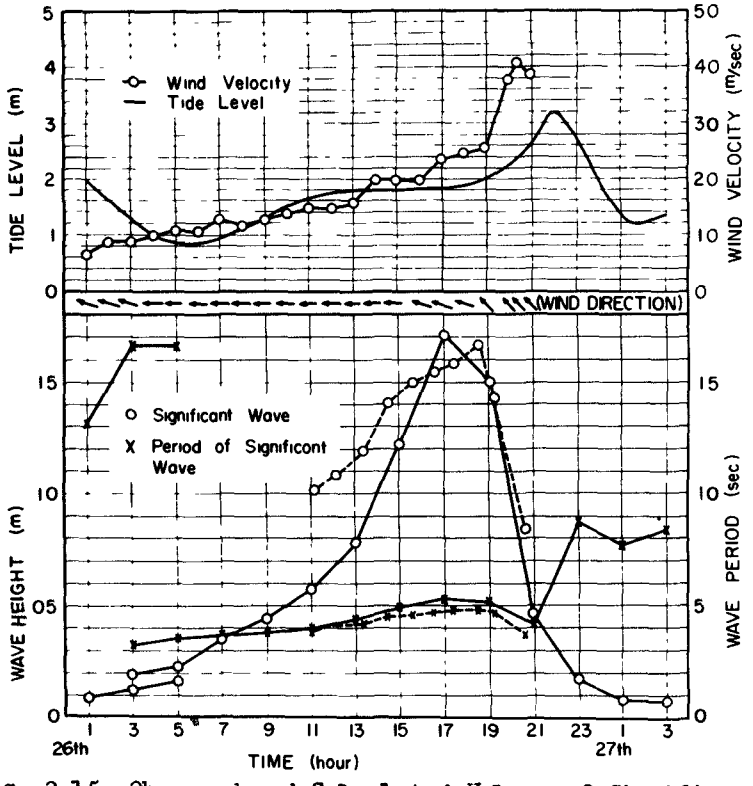

Fig. 3-15 Observed and Calculated Values of Significant Waves, and Tide and Wind at Konakayama, Fukue. Full Line is Observed and Dotted Line is Calculated.

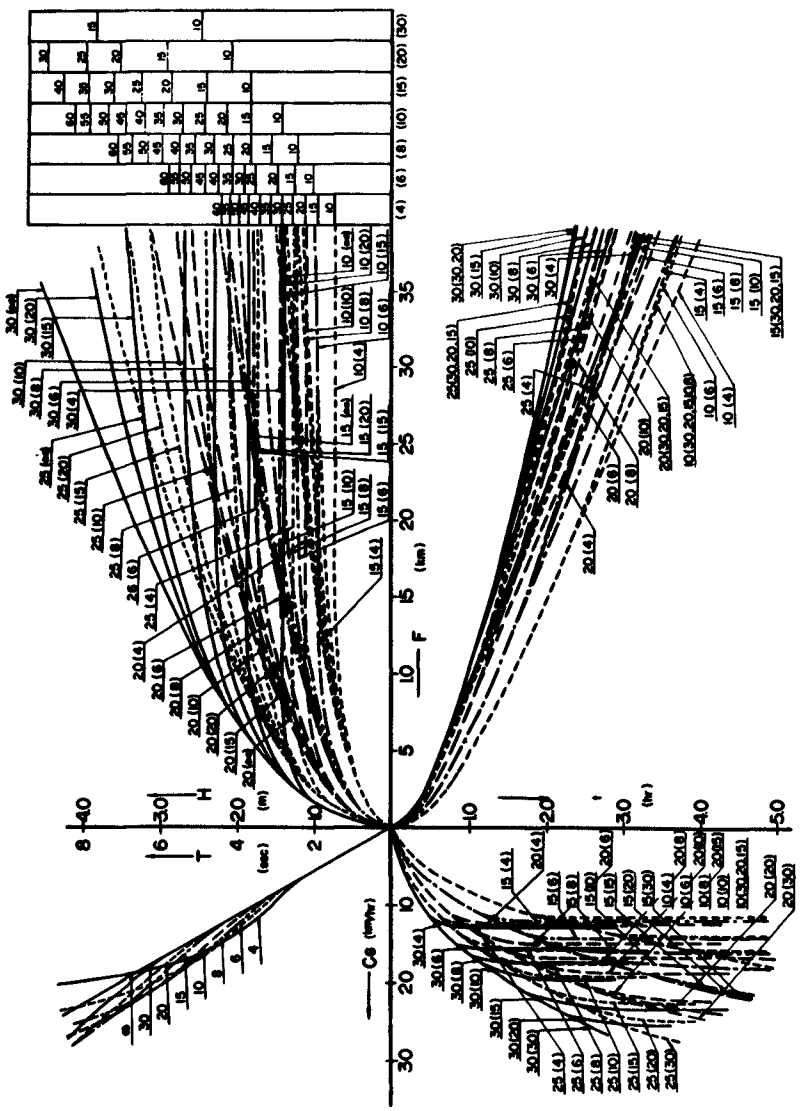

Fig. 3-16 H-t-F-Cg Diagram.

Table 3-2
Maximum Significant Waves
around the Port Nagoya

Points	Directions	Heights in Meters	Periods in Seconds	Appearance Times
A	S	2.20	5.8	8 min. 10 p.m. 26th
B	S	1.90	5.4	59 min. 9 p.m. 26th
C	SSSW	1.65	4.5	9 min. 10 p.m. 26th
D	SSSW	1.65	4.6	6 min. 10 p.m. 26th
E	SSW	2.05	5.3	22 min. 11 p.m. 26th
F	SSW～SW	1.85	5.0	20 min. 11 p.m. 26th
G	SW	1.50	4.5	45 min. 0 a.m. 27th
H	SW～WSW	1.40	4.1	23 min. 0 a.m. 27th

west side the highest wave and the maximum wind occurred simultaneously, but at the east side the highest wave occurs 1～2 hours later than the maximum wind. This phenomenon might be explained as follows. Since the bottom slope at the west side is very gentle, wave height decreases abruptly by the effect of bottom friction. As shown in the previous section the highest wave off Nagoya Harbor gets in this zone later than the maximum storm tide, and then lose its height by bottom friction. On the other hand, the maximum wind and the maximum level of storm tide occure simultaneously. Therefore in that time the bottom friction is not so effective because of great water depth. At the east side, water depth being not so small as the west side, the wave height is governed by wind more than by the increase of water depth by storm tide. Moreover, at that place, the time when component wind velocity of predominant wave direction comes up to the maximum is later than that of maximum storm tide, and the maximum height occurs later than the maximum component wind velocity. In this way, at the place of gentle slope like at the Points A, B, C and D, the maximum storm tide and maximum wave height occur at the same time, and the coastal structure is exposed to danger. This is the reason why the degree of seawall damages near the Ibi River and the Kiso River is larger than the east coast from Yokosuka to Tokoname. The difference of degree of damages between the north coast and the south coast of Yokkaichi would be made clear by the same description.

CONCLUSIONS

The authors described the general characteristics of waves on the coast of the Ise Bay during the Ise-wan Typhoon. It is summerized as follows.

(1) During Ise-wan Typhoon offshore waves seem to be the maximum on the coast of Kumano-Nada, wave height being 10～12 meters, period being 14～16 seconds, and the prevailing wave direction being S～SSW.

(2) It is considered that the prevailing significant wave height is the maximum of about 4 meters on the north-west coast and the minimum of about 2 meters near the coast of Nagoya Harbor. In general, wave height on the east coast is about 80 % of the west coast.

(3) The maximum wave height on the north coast is considered to occur later than on the south coast and 1～2 hours later than the maximum wind velocity.

(4) The time of occurence of the maximum wave height is considered to be dependent on the bottom slope and water depth, because waves near the shoreline are strongly affected by the bottom friction. Where the sea is very shallow, the maximum wave height would appear at the time of maximum sea level by the storm tide rather than at the time of maximum wind velocity.

(5) As shown in the appendix, it is considered that the results of graphical calculation in shallow water waves agree with the observed data. This method would be able to explain the characteristics of waves in moving fetches in shallow water.

APPENDIX

GRAPHICAL METHOD OF FORECASTING WIND WAVES IN SHALLOW WATER

1) Forecasting of Wind Waves in Shallow Water

At present two main methods exist for shallow water wave forecasting, (a) the method of Thijsse and (b) the method of Bretschneider. The Thijsse's method is used only to forecast wind waves in the case of constant depth and constant wind speed. The Bretschneider's method is used to forecast wind waves in the case of a bottom of variable depth and constant wind speed, but when the depth varies with time calculation is very difficult.

During the time of this typhoon, the wind speed and the depth in Ise Bay varied with space and time, so that it is impossible to use those methods. Then, in order to forecast waves in such case, we extended Wilson's graphical approach in deep water into shallow water. This method comes from the concept that waves generated on the windward end of fetch progress with group velocity, and that the group velocity and wave height vary continuously with wind speed and water depth, accordingly the change of wind speed and water depth do not give discontinuous change to wave characteristics.

In deep water waves, the law for decay of waves by decrease of wind speed is not given, so that it is impossible to calculate graphically the decay of waves in the case of abrupt decrease of wind speed. While, in shallow water waves, it is possible to calculate waves graphically in the case of decrease of wind speed and water depth, because the law for the decay of waves by bottom friction is given by Bretschneider and the law for the development of waves by wind is given by the relationship between gH/U^2 and gF/U^2 in deep water.

2) H-t-F-Cg Diagram

Fig. 3-16 is the diagram for calculation of shallow water waves. On the diagram the horizontal axis is fetch and group velocity, and the vertical axis is wave height and travel time. The relations between wave height and fetch (wave height curves), fetch and time (propagation curves) and group velocity and time (group velocity curves) were shown in this diagram, and also the relation between group velocity and wave period is shown. The figures on the curves show wind speed and water depth, for

example, 30(20) corresponds to wind speed of 30 m/sec and water depth of 20 meters.

Wave heights were calculated from the curve by Bretschneider showing the relation between gH/U^2 and gF/U^2 in shallow water of constant depth and the periods were given from the relation of gH/U^2 and $gT/2\pi U$ by S.M.B.

Thus, wave height and group velocity curves are drawn for each wind speed and fetch. The travel time t when waves progress over fetch F is obtained by $t = \int_0^F dF/Cg$. Moreover, on the righthand side of this diagram the wave heights for infinite fetch are shown for each water and wind speed.

3) Comparsion with the Observed Values

In order to confirm the reliability of this graphical method, the values obtained by the graphical method were compared with the observed waves out of Fukue Harbor during Ise-wan Typhoon. The wave heights and periods of significant waves obtained from the records of wave meter were shown in Fig. 3-15 together with tide, wind direction and wind speed at the same point. The maximum value of significant waves occurred at 7 p.m. 26th and its wave height was 1.7 meters and period was 5.2 seconds. The direction of this wave was considered to be about ENE as assumed from the direction of wind and features of neighboring land.

It seems to be caused by the change of wind direction to SE (winds blowing from land) at 7 p.m. that wave height decreased suddenly at the same time. We made the wind field diagram of ENE direction as shown in Fig. 3-9.

The results of calculation of the waves were shown in Fig. 3-15. Though the calculated periods are somewhat smaller than the observed values, the changes of wave heights and periods and the appearance time of maximum values estimated by calculation agree fairly well with those by observation.

REFERENCES

C.L.Bretschneider, Generation of Wind Waves over a Shallow Bottom: Tech. Memo. No. 51, Beach Erosion Board, Oct. 1954.

C.L.Bretschneider, Revisions in Wave Forecasting Deep and Shallow Water; Proc. 6th Conf. Coast. Eng. Council on Wave Research, The Engineering Foundation, 1958.

B.G.Wilson, Graphical Approach to the Forecasting of Waves in Moving Fetches: Tech. Memo. No. 73, Beach Erosion Board, April 1955.

CHAPTER 57

THE DAMAGES OF COASTAL DIKES AND RIVER LEVEES AND THEIR RESTORATION

Masanobu Hosoi, Yasuteru Tominaga
and Hiroshi Mitsui,
Coastal Engineering section, the Public Works Reseach Institute, Ministry of Construction, Japan

Tsutomu Kishi
Assistant Professor of Civil Engineering,
Hokkaido University

The coasts of Ise Bay and Atsumi Bay were damaged by two big storm surges during the recent seven years, one was the Ise Bay Typhoon in 1959 and the other the Typhoon No.13 in 1953. In this report the aspect of storm surge due to the Typhoon No.13 and the restoration design of the coastal-dikes are described. Then the feature of damages of the coastal-dikes by the Ise Bay Typhoon are compared with the former and the restoration plans are explained.

STORM SURGES DUE TO THE TYPHOON NO.13, 1953 AND RESTORATION OF THE COASTAL-DIKES

General aspect of storm surges

The Typhoon No.13 landed on the Japan island on the 25th of Sept. 1953 at the southern point of Kii peninsula at 15 o'clock, passed through Toba which located near the inlet of Ise Bay at 18 o'clock and advanced northeast with the velocity of 56 km/hour. Crossing the Atsumi Bay, it passed through Okazaki City at 19 o'clock. This Typhoon was different from the Ise Bay Typhoon in its course. The former moved from the inlet of Ise Bay to the Atsumi Bay, and the coast of Atsumi Bay was heavily damaged. As Nagoya district is located on left side of the course of the typhoon No.13, the damages were comparatively small.

In Fig.4.2 the records of the wind directions, wind velocities and atmospheric pressures at several places are shown. In Fig.4.2-a those on right side of its course, and in Fig.4.2-b, those on left side on its course are indicated. On the right side of its course the wind directions at the maximum wind speed were SE - ESE, while on the left side of its course were E - WNW.

In Fig.4.3, deviations from the astronomical tide at each place within the bay are shown, and we see that its maximun value of 1.6 m was recorded at Toba at 18 o'clock, and 1.4 m - 1.5 m at other places.

As shown in Fig.4.2 the lowest atmospheric pressure was about 970 mb. which occurred about 0.4 m statical rise of sea surfaces. Judging from Fig.4.3, we can estimate that in the first place the

sea-water flew into the Ise Bay through inlet due to the strong wind of SE, and 1 or 2 hours later it flew into Atsumi Bay from the Ise Bay. Furthermore we find out that during about 8 hours from 13 (approached time of typhoon) to 21 o'clock, the total volume of water in Ise Bay and the Atsumi Bay both considerably increased as comparing with the volume before the typhoon reached. It is clear that much sea-water flew in through Irako. So the volume of inflow from open sea must be an important factor for the storm tide in the bay differing from the one in the closed basin.

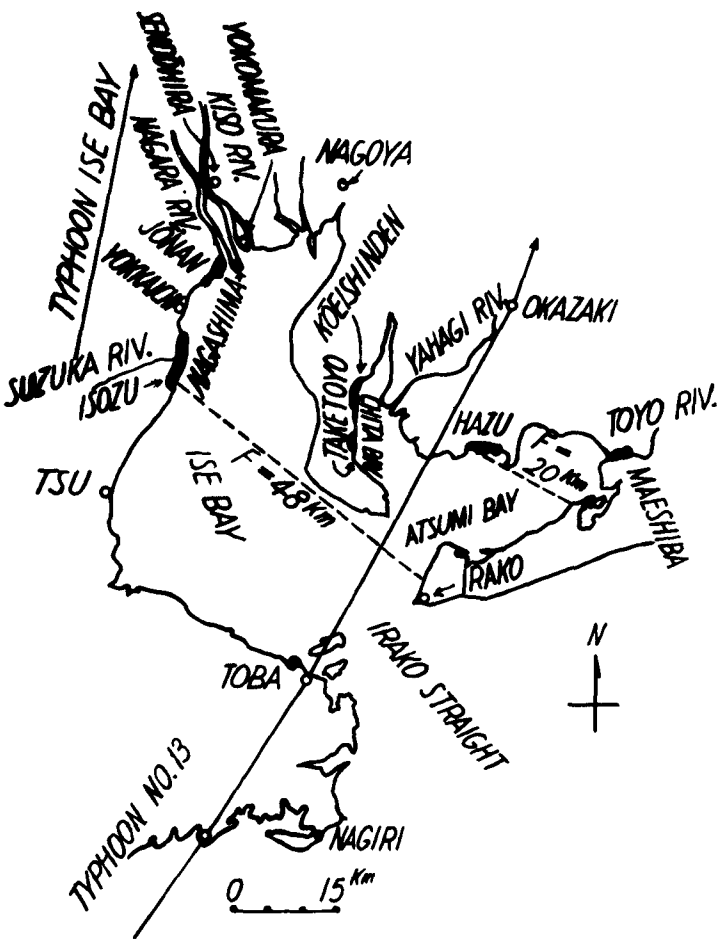

Fig.4.1 Outline map of Ise, Atsumi and Chita Bay.

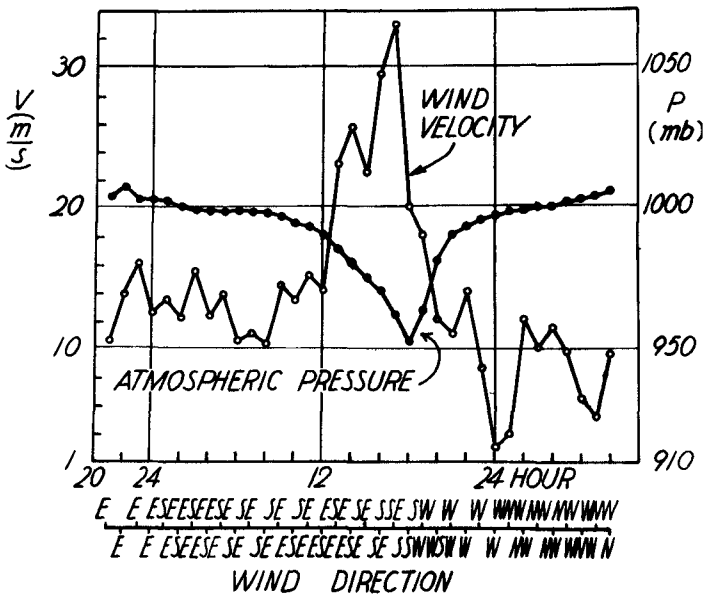

(a) - 1 Nagiri

Fig.4.2 Weather Condition at each place on the occasion of the Typhoon No.13.

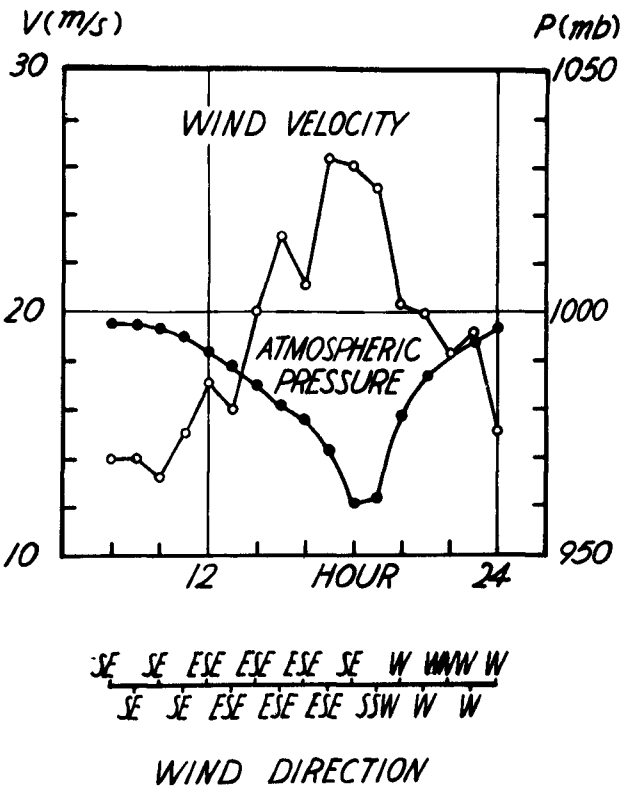

(a) - 2 Irako

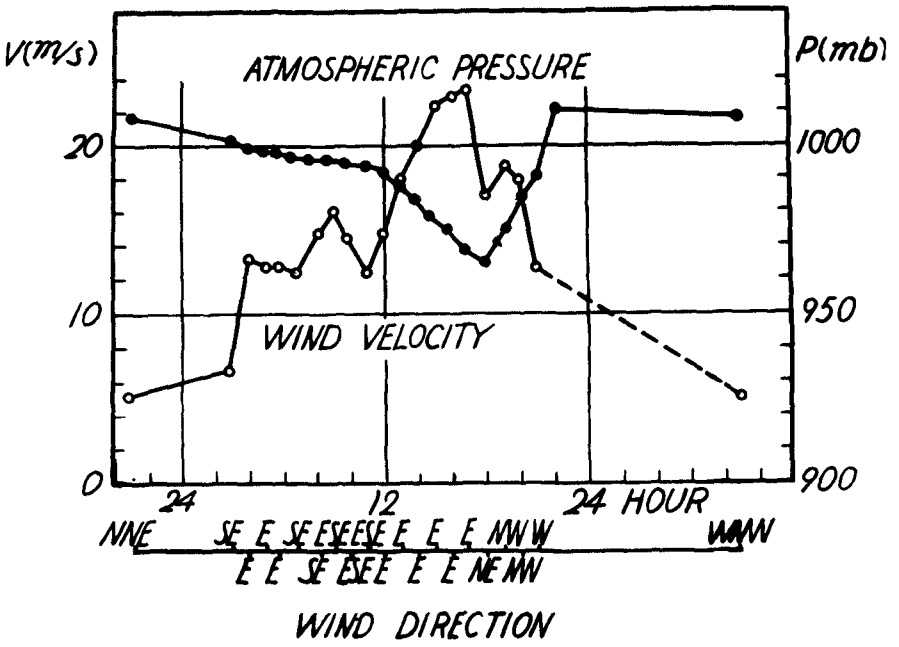

(b) - 1 Tsu

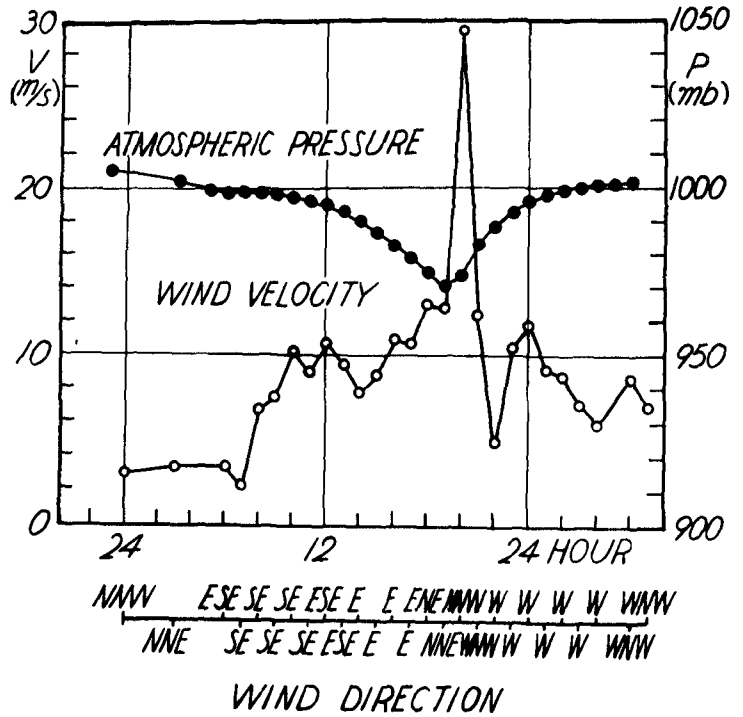

(b)-2 Nagoya

Fig.4.2 Weather condition at each place on the occasion of the Typhoon No.13.

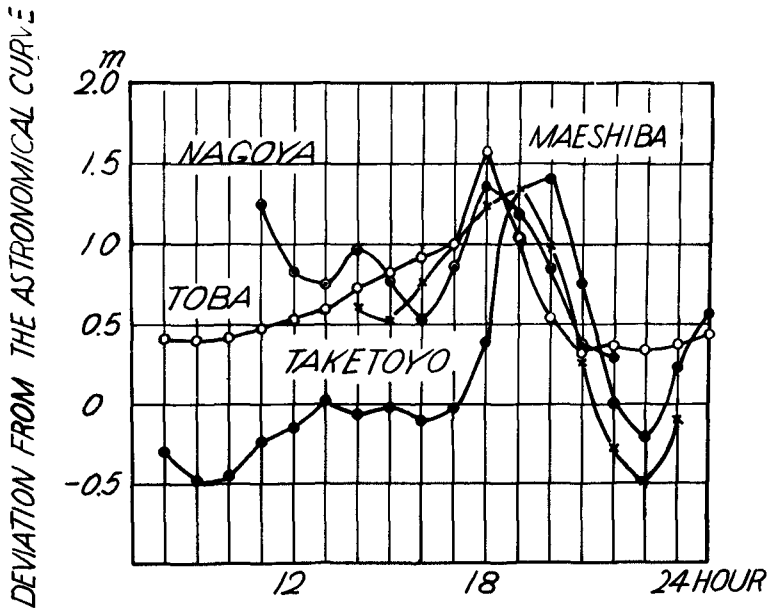

Fig.4.3 Deviation from the astronomical tide at each place on the occasion of the typhoon No.13.

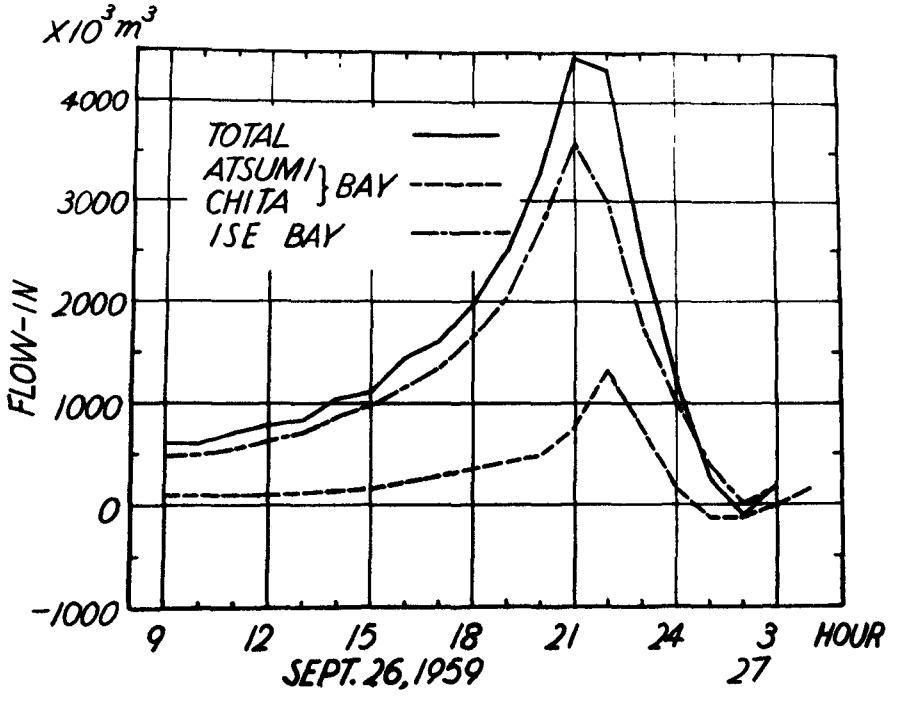

Fig.4.4 Sea water volume flowing into each bay on the occasion of the typhoon No.13.

Such a phenomenon also occurred in the attack of the Ise Bay Typhoon. Fig.4.4 shows the total volume of inflow into the bay which was calculated by using the simultaneous deviations of water level from the astronomical tide at several points in the attack of Ise Bay Typhoon. From this figure, we find out that there already was extraordinary flow into the bay at 9 o'clock. So it is considered that at this time there was extraordinary inflow due to the wind set up near the entrance of the bay and that the inflow was transported in the shape of long wave due to the disturbance near the typhoon center. After this initial time, the inflow increased exponentially up to its maximum value of 450 million tons (cumulative volume) which occurred at 21 o'clock. Fig.4.5 indicated the change of SE, SSE and SW components of wind force observed at Irako Weather Station near the bay entrance. Then it is considered that the water flew into the bay from open sea by the SSE - SE component of wind force because the bay opens towards SSE - SE.

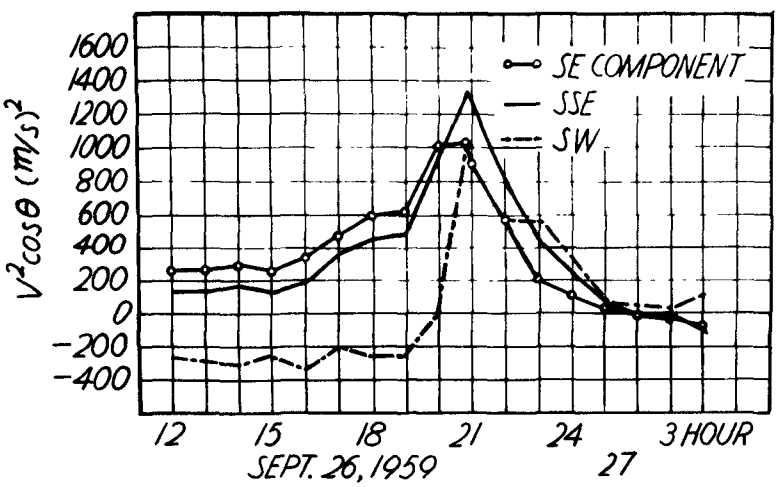

Fig.4.5 Wind force at Irako on the occasion of the Typhoon No.13.

Revised design on coastal-dikes

In Japan, the design specification on coastal-dikes was not determined at that time, and the design methods had been discussed among the engineers and related agencies. In 1953, as the studies on wind waves generated in shallow waters had not yet been developed into practice, the Ministry of Construction, Japan, made temporarily a plan to culculate the wave height by Molitor's experimental formula and to estimate the wave period by SMB method, making a comparative study of past experimental formula and observational results by T.H.Saville, while the Ministry was making studies on the wind waves.

The wave run-up on coastal-dikes of which slope are vertical to 1 on 1 was determined by Fig.4.6. These curves were proposed by the Public Works Research Institute, Ministry of Construction, combining experimental results of wave run-up with the highest wave theory in shallow waters.

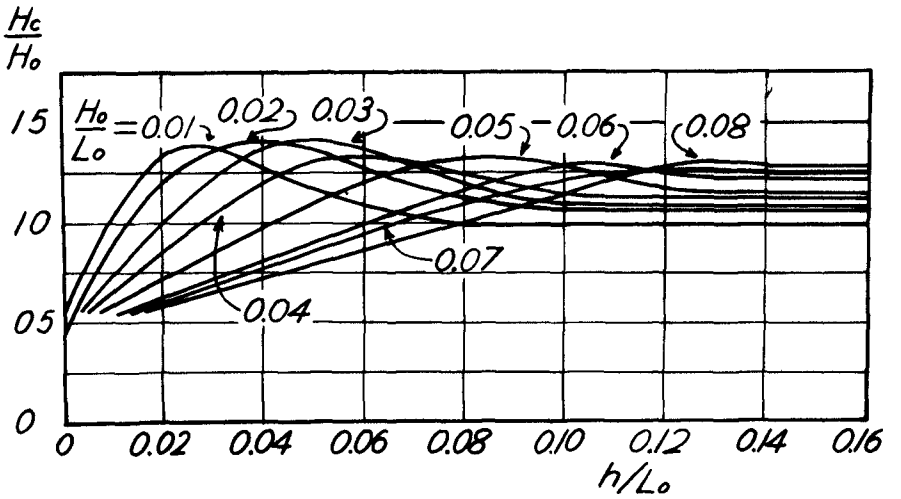

Fig.4.6 Wave run-up as a function of structure depth and wave steepness.

As the heights of dikes determined by Fig.4.6 are not always sufficient to prevent wave overtopping in the strong wind, it is also necessary to cover the back slope of dikes with solid material. Making comparative study of the design method mentioned above and the aspect of damages of coastal-dikes, we conducted the revised design.

From the records of tidal levels, we found out that the highest tidal level along the coast of Ise Bay was about 2.5 m above T.P. (T.P. is the mean tidal level of Tokyo Bay), and at the inner part of Atsumi Bay it was slightly higher, for example, the tidal level at Maeshiba was T.P. 2.80 m. The highest tidal level appeared at 18 - 20 o'clock.

To estimate the waves in bay at the time of Typhoon, we investigated the relationships between the wind velocity of E - ESE and the wind duration from wind records shown in Fig.4.2, and those were tabulated in Table 1. The longest fetch in the Ise Bay and Atsumi Bay is about 60 km, and the wind speed is 20 - 25 m/s, so the minimum duration is calculated at 3.5 - 4.0 hrs by S.M.B. method. From Table 1, it is considered that the waves at the time of Typhoon No.13 reached at stational condition at the wind velocity of 25 m/s.

Next, we made some investigations on the causes of the damages on coastal-dikes of the Hazu coast.

There were two types of coastal-dikes in this district. The first type with height of T.P. 4.92 m was covered with the concrete having thickness of about 10 cm up to the back slope. The second type was made of soil and had the height of T.P. 4.00 m, and it was covered with turf.

Table - 4.1 The relation between wind velocity of E - ESE direction and duration on the occasion of the Typhoon No.13 at Irako and Tsu.

Duration (hr)	Mean velocity of wind (m/s)	
	Irako	Tsu
1.0	26.1	23.3
2.0	25.8	23.1
3.0	25.3	22.8
4.0	24.5	22.2
5.0	23.6	21.5
6.0	22.5	18.6

For the first type, although its back berm was scoured, its whole body was left, The second type was destroyed by scouring. It is clear that in the case of second type the waves got over it due to insufficient dike height and it is considered that the covering of first type of dikes was also insufficient. At Hazu coast, the fetch in ESE was 20 km, and it is estimated that the wave height was H = 1.6 m, and the period was T = 5.0 sec. Because the water depth at the time of maximum tides was h = 4.4 m, we can see from Fig.4.6 that the height of wave run-up to coastal dike become Hc = 2.0m. As the tidal level is T.P. 2.70 m, the height of run-up is T.P. 4.70 m. This height is lower than that of first type of coastal-dike and higher than that of second type.

So we can explain the causes of failure as follows:

a) The back slope of first type of coastal-dike was scoured but its body did not break down.
b) The soil of second type of coastal-dike was scoured by wave overtopping.

From the similar calculation over about 200 km of coast line along the Ise Bay and Atsumi Bay, and the investigation on causes of damages, we obtained the following conclusions.

1) When the dike height is lower than the height of wave run-up as shown in Fig.4.6 and the back slope has no solid covering, the damages of dikes are inevitable.

2) When the dike height is as much as the height of run-up as shown in Fig.4.6, the thickness of concrete covering of back slope should be more than 10 cm.

3) The coastal-dike of which the foundation of front slope was scoured was rare, We suppose that this is due to the large rise of tidal level and the deep water depth. So it is sufficient to use the same depth of foundation as original in making restoration design.

Based upon the results of investigation on causes of damages mentioned above, the restoration design of coastal-dikes for the Typhoon No.13 was conducted as follows:

The design tidal level was taken to be the sum of "the mean high tidal level of new and full moon" and "the maximum deviation from astronomical tide due to Typhoon No.13".

The design waves were calculated by maximum fetch at each place and wind velocity V = 25 m/s of Typhoon No.13, because of the change in wind direction due to the course of typhoon.

The heights of restoration coastal-dikes designed in such a steps are compared with that of original coastal-dike and are shown in Fig.4.7.

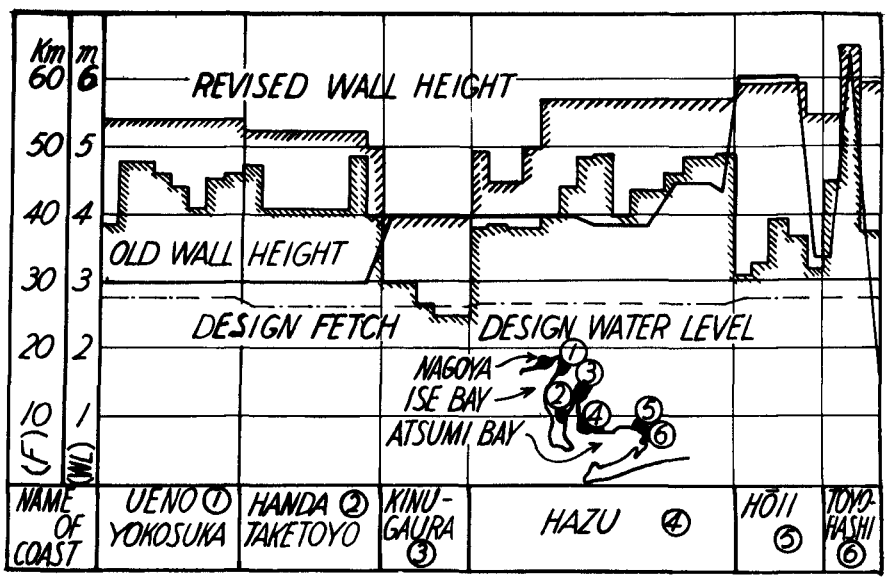

Fig.4.7 The height of restoration coastal-dike and established one.

DAMAGES OF COASTAL-DIKES AND RIVER LEVEES DUE TO THE ISE BAY TYPHOON AND THEIR COUNTER PLAN

The height and structure of restoration coastal-dikes for Typhoon No.13 were designed under the lines mentioned above, and the field works had been conducted according to it. But just because the Ise Bay Typhoon had come before completion of field work, the heavy damage was

brought about again. The scale of Ise Bay Typhoon was larger than the Typhoon No.13 and the third big one of the Typhoons which attacked Japan at past. Moreover, because the center of typhoon passed across the west side of the bay and advanced paralell to longer axis of Ise Bay, a very large deviation from astronomical tide in the inner parts of the Ise Bay and Chita Bay (at the time of Typhoon No.13, the deviation in this area was comparatively small) took place, and high waves occurred due to a very strong wind. In Fig.4.8 the heights of coastal-dikes at each area before disaster and the highest tidal level are indicated.

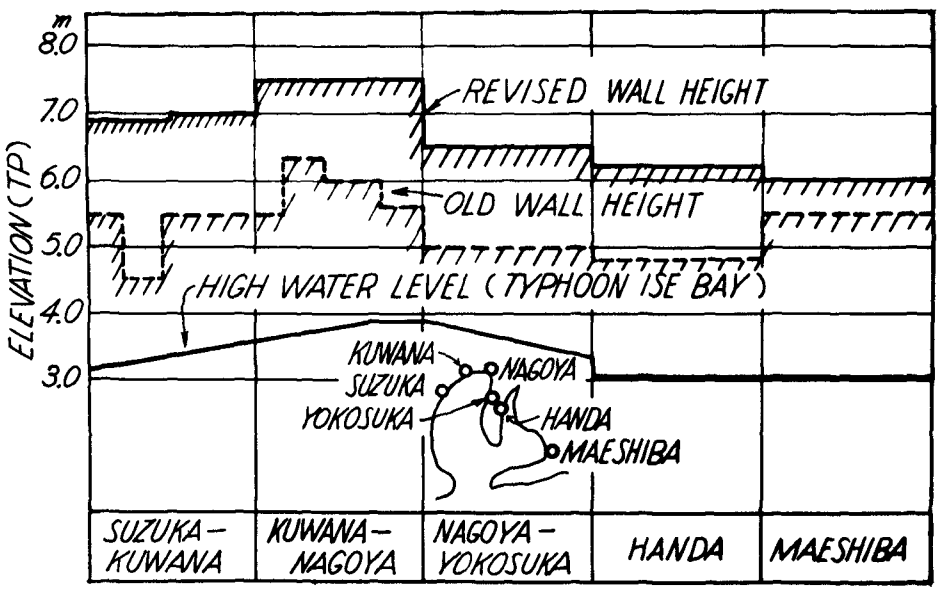

Fig.4.8 The height of coastal-dike and the highest water level at each place before the disaster due to Ise Bay Typhoon.

Damages of coastal-dikes and the counter plan

The coastal-dikes which located at the coast of Ise Bay, Chita Bay and Atsumi Bay almost belong to the type of embankment as shown in Fig.4.9. The front slopes are covered with stone, concrete etc., while the crests and back slopes are mostly covered with clay and turf, and it is comparatively rare to use concrete and stones as the covering of crest and back slope.

At the first stage of the restoration plan to Typhoon No13, the height of coastal-dike was build up to the design height. In many places the concrete coverings of crest and back slope are still left as the second stage of construction works for financial difficulty.

Based upon the disaster investigations on several storm surges in the past, it was indicated that in the case of coastal-dikes of which the crest and the back slope are not covered with solid materials such as concrete, the dike bodies were easily scoured by wave overtopping and spray, and the whole body of coastal-dikes was to break down easily as the result. The prime cause of this disaster also consisted in the scouring of dike body by wave overtopping and spray.

Table 4.2 The general condition of established coastal dike, and the highest tidal level and wave height at each place on the occasion of Ise Bay Typhoon.

Name of coast	Crest height	Front slope	Condition of covering	Highest tidal level estimated	Wave height estima-ted
Koeishinden	T.P. 4.9 m	1:3	front slope stone crest no cover back slope concrete	T.P. 3.0 m	2.0 m
Nanyo	5.5 ~ 5.75	1:2.5 1:3	front slope stone crest turf back slope turf	3.9	1.8
Ama	5.5 ~ 6.0	1:3	front slope stone & concrete crest turf back slope turf	3.9	1.8
Nagashima	6.0 ~ 6.5	1:3	front slope stone crest turf & concrete back slope block	3.5	2.0
Jonan	5.5	1:4	front slope stone crest no cover back slope no cover	3.5	2.0
Tomidahama	5.5	1:2	front slope step type concrete crest no cover back slope no cover	3.3	2.6
Ishihara	4.5 ~ 5.0	1:1	front slope stone crest concrete back slope stone	3.0	3.4
Isozu	5.5	1:1.5	front slope concrete crest concrete back slope concrete	3.0	3.4

In Table 4.2, the dimensions of coastal-dikes along each coast (see Fig.4.1), the highest tidal level at the time of Ise Bay Typhoon, the

estimated waves, etc. are indicated. From this table, we see that the difference between the crest height and the highest tidal level is about 1.5 -2.5 m except Nagashima coast. On the other hand, since the wave height is 1.8 - 3.4 m, it is supposed that there was considerable wave overtopping at each place during the strongest time of storm surge when we considered the wave run-up.

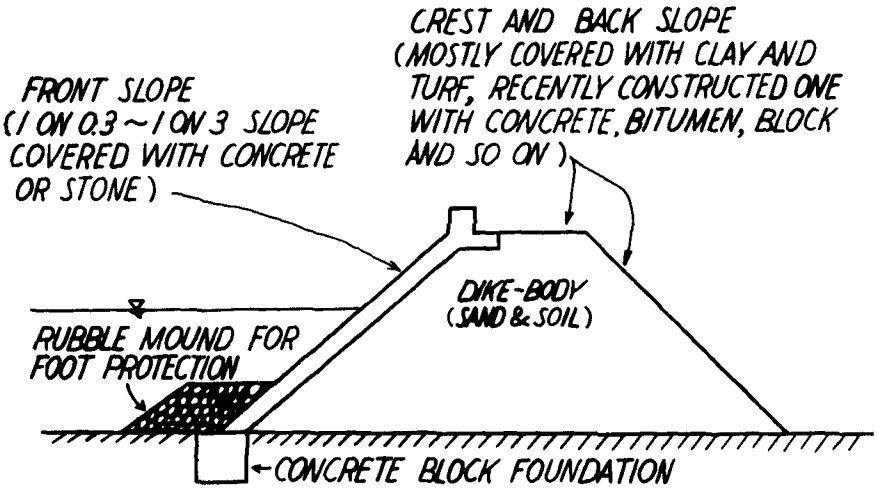

Fig.4.9 Typical cross section of coastal dike with embankment type.

There are Nagashima and Jonan coastal-dikes at the left and right sides of Nagara River respectively. Their cross sections are almost the same, and only their heights are different in about 1 m. Since the shape of sea bottom in front of coastal-dikes are almost coincided with each other, it can be supposed that the tidal levels and waves are almost the same. Nevertheless Jonan coastal-dike were broken down almost over the whole area as shown in photo.4.1-a, while Nagashima coastal-dike were broken down only 200 m of the 1.5 km length as shown in photo.4.1-b, although the dike body was scoured considerably by wave overtopping and situated in a dangerous condition. This is an example to show the difference of damages due to the difference of dike heights. As shown in Table 4.2, the tidal level near this coast is T.P. 3.5 m and wave height is 2 m. Under the condition that slope is 1 : 3, water depth at the toe of coastal-dikes is 4 - 5 m, and steepness is about 0.05, wave run-up become about 1.5 times of wave height. Calculating the maximum height of wave creat from these values mentioned above, we obtain T.P. 6.5 m. Therefore, we suppose that although the Jonan coastal-dike was always attacked by wave overtopping, the rate of wave overtopping at Nagashima coastal dike was very small, and the coastal-dike was only attacked by some extent of spray. This is an example to show that if the height of coastal dikes is taken the maximum creat height of significant wave, there will be a considerable strength of the coastal-dike to resist the waves without any covering on the dike crest and the back slope.

(a) Nagashima coastal dike

(b) Jonan coastal dike

Photo.4.1 The damages of coastal dikes near the mouth of Nagara River.

In photo 4.2, the views of house damages behind the coastal-dikes of Ishihara coast situated at the left side of Suzuka River are shown. We can see that although a considerable rate of waves had invaded explicitly over the coastal-dikes, they were damaged only a part and the original shape was almost remained. The sections of coastal-dikes are indicated in Fig.4.10, and their crests and back slopes are solidly covered.

Similar to the foregoing example we obtain the maximum height of wave crest of T.P. 7.7. m from the calculations. On the other hand, as the crest height is T.P. 4.5 m, it is natural that the houses behind coastal-dikes were damaged due to the wave overtopping as shown in photo. 4.2. Moreover, from this example we know the fact that if the crest and the back slope of coastal-dikes are solidly covered, the strength to resist wave overtopping will be considerably increased.

Photo.4.2 The damage of the houses behind Ishihara coastal dike.

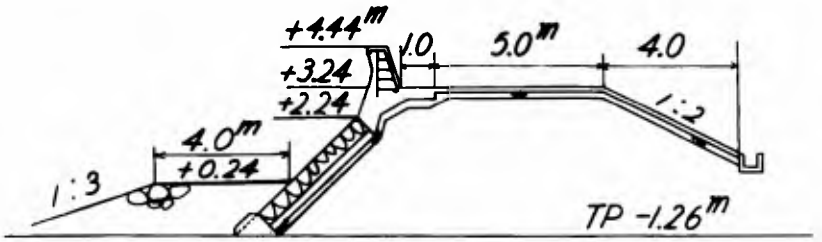

Fig.4.10 Typical cross section of Ishihara coastal dike.

But where the dwelling houses are crowded near the back side of coastal-dikes, it is necessary to increase the height of coastal-dikes so that the dwelling houses can be protected from the damages due to the wave overtopping.

It makes the storm surge wild and the waves weak that the water depth is shallow in the inner parts of Ise Bay and Chita Bay. Therefore, the coastal-dikes in this region can not be destroyed easily by the wave pressure. In the southern area from Yokkaichi City, the fetch and water depth are considerably large, so that the wave height

is as much as 4 m in some places. In this region, the coastal dikes were considered to be destroyed by the wave pressure directly.

In photo 4.3, the aspect of damages of coastal-dikes at Isozu coast which located at the right side of Suzuka River is shown. These coastal-dikes were constructed after the disaster suffered from Typhoon No.13 in 1953.

The cross section of the dike is shown in Fig.4.11.

Photo.4.3 The damage of Isozu coastal dike.

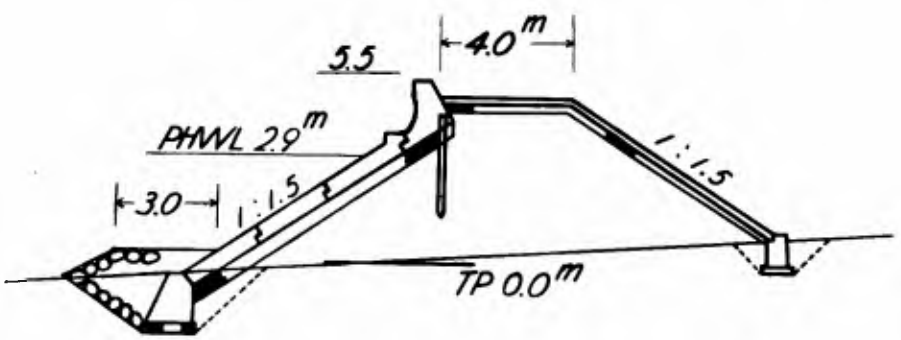

Fig.4.11 Typical cross section of Isozu coastal dike.

The front slope is 1 : 1.5 and the front slope, crest, and back slope are all covered with the concrete. The design water level was T.P. 2.9 m, the design wave height was about 2 m and the crest height was 5.5 m. For the Ise Bay Typhoon, the tidal level was T.P. 3 m, the wave height was 3.4 m, and the latter was considerably higher than designed wave height.

The reasons why the whole body of coastal-dike destroyed can presumably be interpreted as follows. Some voids were formed in the parts of joints by wave pressure. Consequently a large quantity of soil flew out through the void and at last the dike body was broken down.

The water depth in front of coastal-dike is 3.4 m, and the ratio of water depth to wave height is about 1.2, so it is just in a condition for wave breaking, then we may say that there existed considerably large pressure exerted on the dike body.

The damage aspect of coastal-dike in Koeishinden at Handa, located at the inner part of Chita Bay, is shown in photo.4.4. The covering of these crest was not yet constructed.

Photo.4.4 The damage of Koeishinden coastal dike at Handa.

The aspect of the overturning of parapet is also seen in this photograph, and this phenomenon was seen everywhere in this disaster. The front surface of the usual coastal dikes in this district is constructed from two parts, one of which is a flat concrete slab and the other is a heavy concrete parapet.

Such a heavy parapet will be easily overturned by wave pressure, if the dike soil near the crest flows out due to wave overtopping. In Koeishinden the parapets were supported by wood piles, but these piles were not so effective to support them against the latteral force.

The overturning of parapet could be also seen everywhere in the inner part of Ise Bay (photo.4.5). The tidal level in the Ise Bay Typhoon was fairly higher than the designed level, so the wave energy was concentrated about the parapet. This might be a reason of many overturning in the region.

Photo.4.5 The overturning of parapet in the coastal dike at the left side of Nikko River.

The other aspects of damages of coastal-dike are as follows.

(a) The foundation of back slope was scoured by the wave overtopping.
(b) As the dike soil contained sea water and had the tendency of sliding, the foundation swelled forward and lastly the whole of back slope was slidden down. These examples were also seen numerously in this disaster.

Until now, the studies on wave pressure are mostly conducted about the breakwaters and we had no suitable formulas for the coastal-dikes. Therefore, the coastal-dike has been designed only based upon the experience and no mechanical calculation conducted. Now, at the Public Works Research Institute, Ministry of Construction, the relations between front slopes and wave pressures are being investigated experimentally.

The restoration design of coastal dike which were destroyed by the Ise Bay Typhoon was conducted as follows:

The design tidal level was taken to be the sum of mean high tidal

level at the typhoon season and "the maximum deviation from astronomical tide due to the Ise Bay Typhoon".

The wave height was calculated by Bretschneider's method in considering the friction of sea bottom, using the direction and velocity of wind at each place in the time of the Ise Bay Typhoon. The height of coastal-dike was determined by adding the design tidal level to the run-up height of design wave.

The cross sections of coastal-dikes were so-called the type of embankment as shown in Fig.4.12, and were determined by taking consideration of the aspect of damages mentioned above. In designing of that we specially stressed subjects as follows:
(i) Parapet was lightened as much as possible, and reinforced bar inserted so that it could resist both the wave pressure and earth pressure.

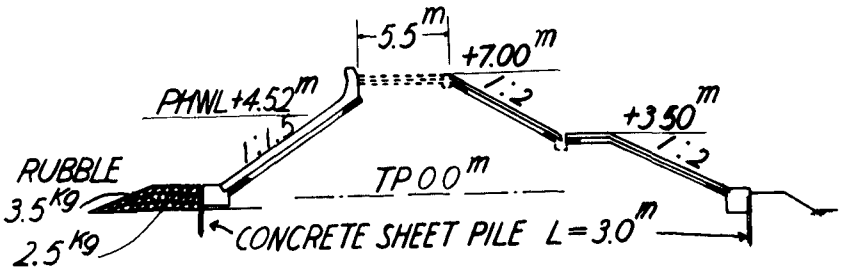

Fig.4.12 Typical cross section of restoration coastal dike.

(ii) The covering of front slope was connected to the foundation block by reinforced bar in order to resist the uplift pressure of sea water.
(iii) Sheet piles were driven in at the toe of foundation blocks in order to protect from creating the hole at the down part of the covering of front slope due to penetrating water.
(iv) In order to commence the covering of crest and back slope soon after banking, the condensation of dike soil was accelerated by vibrofloatation method.
(v) Sheet piles were driven in at the foundation of back slope in order to stop the outflow of penetrating water and to protect the outflow of dike soil.
(vi) The foundation of back slope was constructed not to contact with directly channels behind coastal-dike in order to increase the transverse resistance of the foundation.
(vii) Porous concrete was used at the lower part of covering of back slope in order to decrease the uplift pressure due to penetrating water.

Damages of river levees and their counter plan

The phenomenon that storm surge went upstream in a river was seen

at each river which flew into the Bay. For example, we'll take up the case of Kiso River which flows into the inner part of Ise Bay as shown in Fig.4.13.

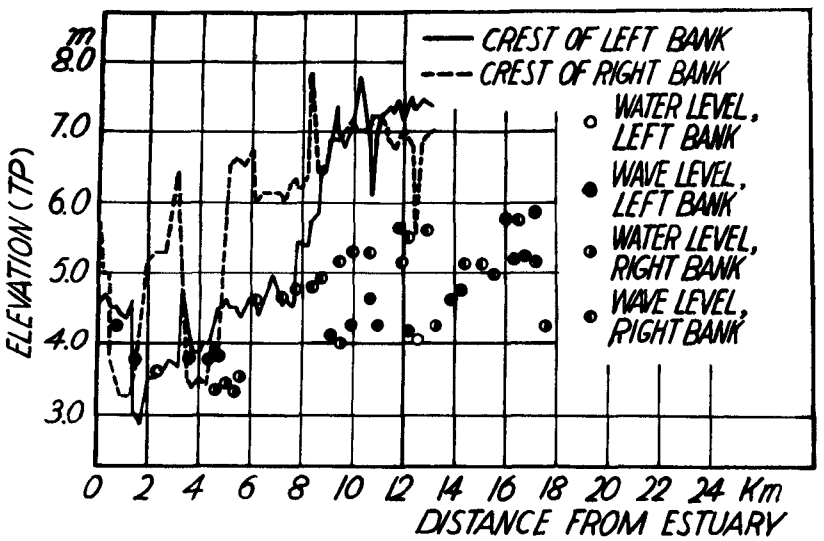

Fig.4.13 The water level rising of Kiso River on the occasion of Ise Bay Typhoon.

As storm surges invade into the river, it is seen that water level tends to rise up. Judging from observational results, this fact is also recognized at Nagara, Ibi, and Shin River. It seems that the rate of water level rising in river mainly concerns with the wind shearing force. To investigate this point in the Kiso River, plotting the relationships as shown in Fig.4-14 between the difference of water levels recorded at Yokomakura and Sendohira, and the square of wind velocity at Kuwana, a very good correlation is recognized. Therefore, it will be effective means for estimating storm surges in rivers, if this relationships are studied furthermore. The flow direction of the upper reach of Kiso River is about SSE and it just coincided with the wind direction, so that such effect due to the wind shearing force is seemed to appear distinctly.
So it is supposed that in such a case that the directions of river and wind are very different, the phenomenon mentioned above does not always appear. In addition, it is considered that the effect of run off from upper stream was very slight, as the rain fall before the time of the highest tidal level was a very small quantity in Kiso River.

In designing the height and structure of river levees at an estuary and in the downstream reach, the effect of waves has been scarcely taken in consideration by this time. In Ise Bay Typhoon, we saw many examples of the river levees at an estuary and in the downstream reaches which were destroyed by wave force or wave overtopping.

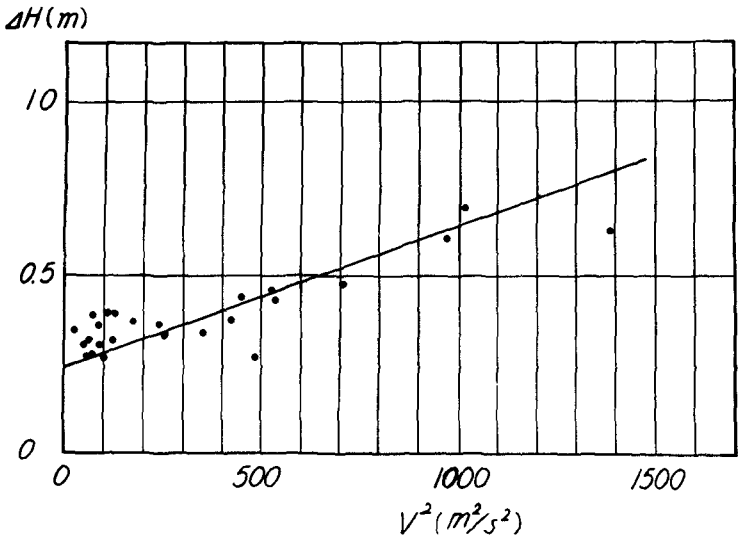

Fig.4.14 The relation between the difference of water levels observed at Yokomakura and Sendohira, and the square of wind velocity.

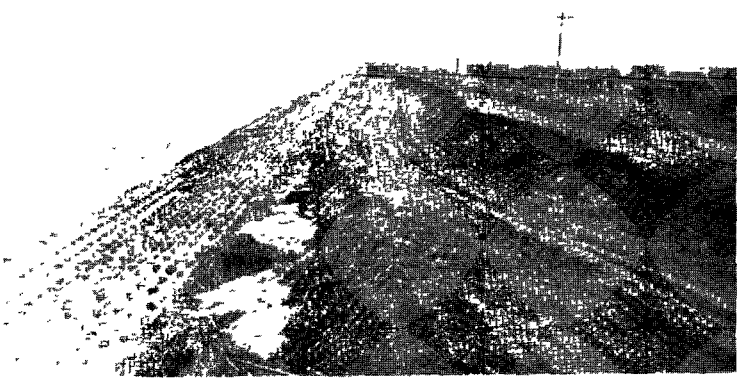

Photo.4.6 The damage of the levee at the right side of Yahagi River.

The waves in rivers are different from those generated at coast. In rivers the water depths are small, and the river course crooks, so the waves are in general smaller than those generated at coast. Most waves always invade into the estuary without the reduction of wave

heights, and the waves especially in narrow estuaries propagate along the levees. Therefore it is considered that large waves scarcely strike the coastal-dikes perpendicularly.

The differnce between the constructions of river levees and coastal-dikes is the covering works. In general, the front slopes of river levees are covered with stone or concrete up to the design high water level, and the front slopes above design high water level are covered with turf. The causes of disaster of river levees at the time of Ise Bay Typhoon can be divided into two groups, one of which is the wave actions and another is the overflow (including wave overtopping). Photo.4.6 shows the aspect of damage of the right side walls at the places of 0 - 2 km upstream from the mouth of Yahagi River. The upper part of front face and back slope were covered with turf. As a wave direction and the line of dikes were not strictly in parallel but at a slight angle in the middle of typhoon, the front slope covered with turf was broken down by wave force.

Fig.4.7 shows the aspect of damages of levee at the left side of Nabeta River. At this place, the height of dike was increased by the concrete parapet wall.

The parapet wall has the openings (1.2 m in width) for passage at regular intervals, and at the time of storm surges, the opening was designed to close with a flush board. But as the openings were not closed actually at the time of storm surge, the sea water overflew through the openings and the back slopes of dikes were scoured, and at last the whole of levees were broken down.

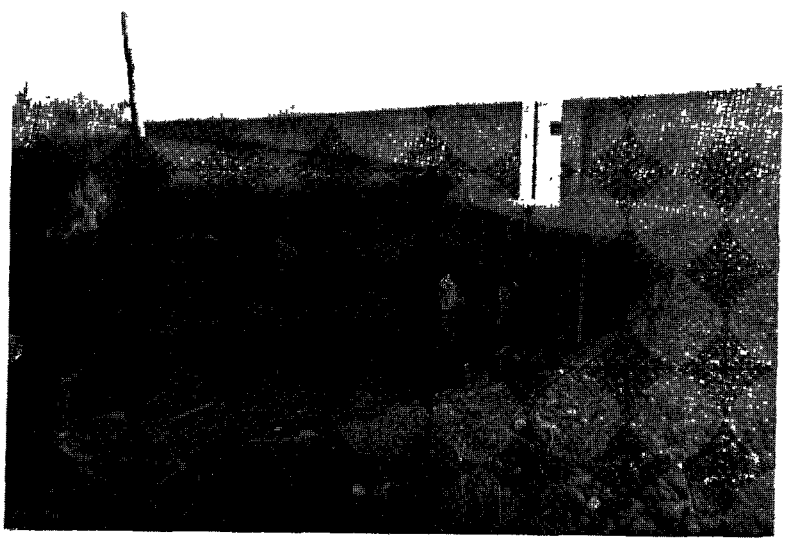

Photo.4.7 The damage of the levee at the left side Nabeta River.

In addition, there were other examples of destruction. The slope surface of dikes were destroyed by water seepage as seen often in the flood. At the mouth of a river, we also saw many places where the connecting points between coastal-dikes and river levees were damaged. The fact that the height of river levee is smaller than coastal-dikes discontinuously at the connection point, or the different structures of dikes and surface covering, might be a reason for the damages.

Referring the aspect of damages of river levees mentioned above, it is necessary to determine the heights and structures of the dikes in rivers, from the stand points of wave heights and wave forces which will be occured in storms. When the waves invade into the rivers, wave run-up may not be considered because there is no impact of waves upon walls if the waves direction and the river levee are in parallel each other, but when the wave direction and the line of river levees are not in parallel, a fairly wave run-up can be expected due to the impact of waves upon the walls.

The height of waves propagating from various directions of offshore to the river mouth, can be determined by the fetch and refractions in the same condition of wind.

When the waves propagated from the entrance of Bay to the direction of A as shown in Fig.4.15, the heights of waves invading into the river are large, because the fetch is large and there is no effect of refraction due to the topography of the sea bottom. However, because the wave direction and the river levees are in parallel each other and there exists no impact of waves, it will be good enough to consider only the height of wave crest. When the waves travel to the direction of B, the fetch is smaller than that in the case of A, and there is the effect of refraction. So the height of waves entering the river is smaller than that of A. However, because the waves impact on river levees skewly, the run-up of waves will occur.

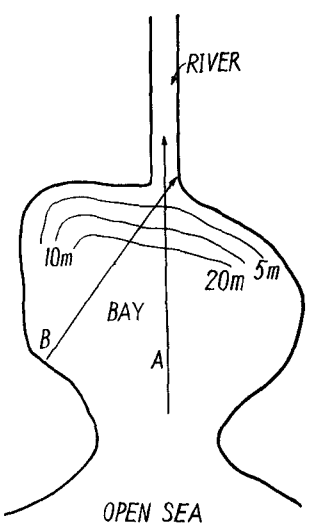

Fig.4.15 The relation between incident direction of wave and river course.

Therefore in such a case, as a criterion for determing the levee height, we must take the higher one after comparing the height of wave run-up and the height of wave crest in the case of A. That is, more the wave direction are inclined with the river levee, less the wave height itself is, but more vivid the phenomenon of wave run-up is. Therefore it is necessary to make comparison and investigation for various cases in determing the reasonable height of walls.

As the waves invading into rivers are affected by the friction of river bed, in proportion to the distance from the river mouth, the wave height will be decreased in general, but when the propagating direction of waves coincides with the wind direction, the wave height is not always decreased. Therefore, considering the wave height, the wave direction, the direction of river course, the water depth, the river width, and the wind condition, etc., we must determine to what extent the waves should be considered. Moreover, when the river course is tortuous, the river width changes abruptly, or large bars existed, the convergence, divergence and refractions of waves and the considerable change of wave height will be expected. We can get the same conclusions about the indentation of sea dikes, and there were many examples showing the damages at this part at the time of Ise Bay Typhoon.

The designs of height and structure of the levees in the rivers Kiso, Nagara, Suzuka, Yahagi and Toyo, were established based upon the procedures mentioned above, and to make more clear the key points in the design, the large scale hydraulic model tests are carried on at the Public Works Research Institute, Ministry of Construction.

CHAPTER 58

ON THE EFFECT OF CONFIGURATIONS OF THE COAST ON THE STORM SURGES IN THE ISE BAY

Kiyoshi Tanaka
Prof. of the OSAKA UNIV., Dr. Eng.,
Akira Murota
Assist. Prof. of the OSAKA UNIV.,
Osaka, Japan

INTRODUCTION

Wind drift is generally considered as the predominant factor of the storm surge along the sea coast. Authors noticed the fact that the duration of the wind blow of any direction is not long even at a big typhoon, while the storm surges more than 2 m are sometimes observed in the interiors of Osaka-, Ise-, and Tokyo-bay, and they have studied on another factor which might cause such water rise.

A hump of water caused by a low atomospheric pressure transmits in the manner of a long wave and is deformed under the topographical effect when it comes into a bay. Authors are intending to show that the build-up of water due to topographical effect is sometimes larger than that occurring by wind drift.

In this paper, the calculation was carried on neglecting the effect of wind drift and its result was compared with the observed value.

TOPOGRAPHICAL DATA OF THE ISE-BAY AND OBSERVED HEIGHTS OF THE METEOROLOGICAL TIDE BY THIS TYPHOON

Contour lines of the bottom of the Ise-bay are shown in the Fig. 5-1, in which the water depth under the datum level (D.L.) is indicated in meter Considering the pattern of these contours and of wave crests shown in the refraction diagram, the axis of this bay and vertical sections orthogonal to it are determined as shown in the Fig. 5-1 with chain-lines. The moving direction of this typhoon in this area was about N25°E as shown also in the same figure.

Sectional area : A , width of the bay : B , and mean water depth : H_0 ($\approx A_0/B_0$) relating to the distance from the inlet of the bay are given together in Fig. 5-2.

To make the calculation simple, we may assume H_0 to be constant ($H_0 \fallingdotseq$ 2.5 m) from No. 2 to No. 4 section and decrease linearly from No. 4 toward

the inner.

Precise observations of the height of the storm surge could not be collected, but only the approximate values are shown in Fig. 5-3 at present, in which ζ is the maximum deviation from the astronomical tidal stage. The deviation at Nagoya harbor ($\zeta \fallingdotseq 3.5$ m) is the largest one ever recorded in Japan.

BUILD UP OF A LONG WAVE DUE TO GRADUAL VARIATIONS OF SECTIONAL AREA OF THE BAY

For the change of heights of a long wave in the variable section, there is a well-known formula (Green's law). (See, for instance, Lamb : Hydrodynamics 6th ed., p. 274, for detailed derivation.)

$$\zeta/\zeta_* = (B^2_* H_*/B^2 H)^{1/4}$$

where ζ : the wave-height of a long wave,
B : the width of the channel,
H : the water depth before reaching of waves,
and the subscript $*$ refer to the value in the initial section.

In our calculations, the static water depth (H) may be taken as follow considering that the time variations of the astronomical tide are generally much slower than those of the storm surge.

$$H \equiv H_0 + h$$

where H_0 : the water depth under the datum level,
h : the height of the astronomical tide above the datum level.

H_0 and h in each station are shown in the Table 5-1, respectively.

The ratio ζ/ζ_* and $B^2_* H_*/B^2 H$ computed from the Fig. 5-2, 5-3 and the Table 5-1, are plotted in a log-log diagram. (Fig. 5-4) In this figure, we see that the Green's law is applicable for the region between No. 5 and No. 8 section (at the inner part of this bay). While, between No. 2 and No 5 (at the inlet and middle part of the bay), ζ/ζ_* seems to be proportiona to $(B_* H_*/B^2 H)^{2/3}$, and the increment of height in this region is greater than that predicted by the Green's formula.

These results may be interpreted as follows. In the inner part of thi bay, the configuration of the coast forms some typical wedge-shape. Due to the comparatively small surface area of this region, the wind effect may be secondary and the effect of the configuration of the coast may be so primar in this inner region that the Green's law will be applicable. While in the outer part of the bay, the surface area is much larger than the inner part and the wind effect may be more dominant and the increase of tidal height will be larger than that predicted only by the effect of the bay configuration.

ON THE EFFECT OF CONFIGURATIONS OF THE COAST ON THE STORM SURGES IN THE ISE BAY

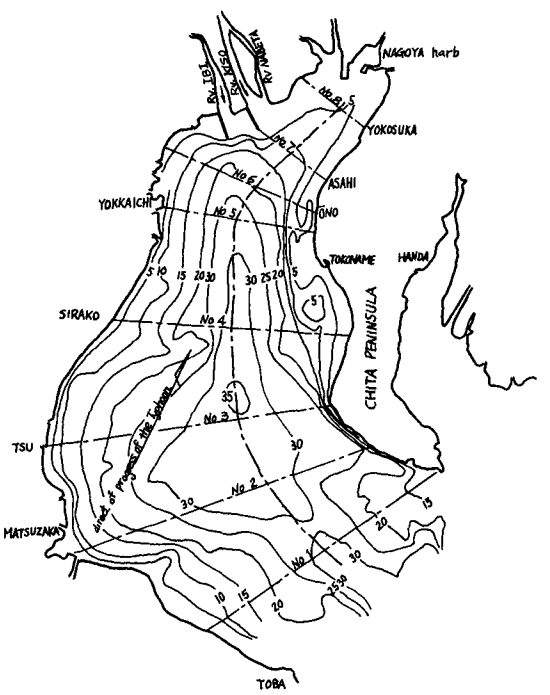

Fig. 5-1

The configuration of the Ise-bay

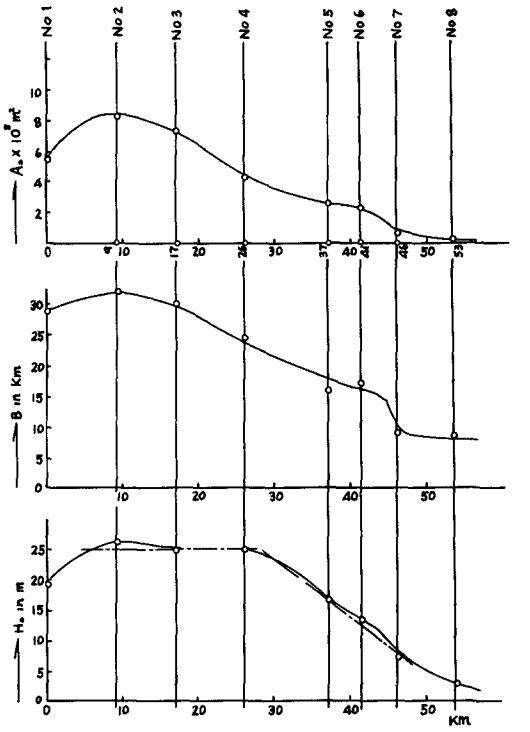

Fig. 5-2

Sectional area, width and mean water-depth at each section.

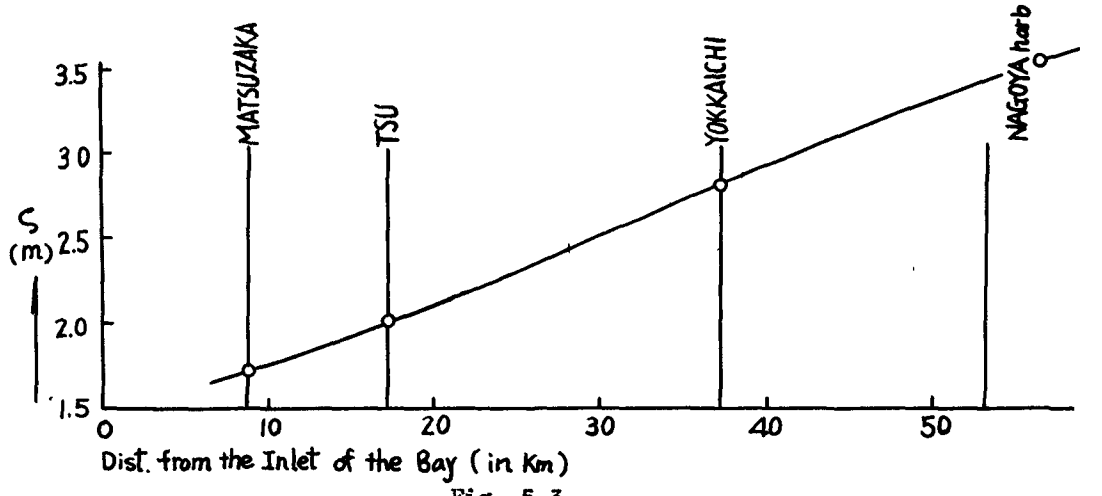

Fig. 5-3

Observed heights of the storm surge along the coast of the Ise-bay

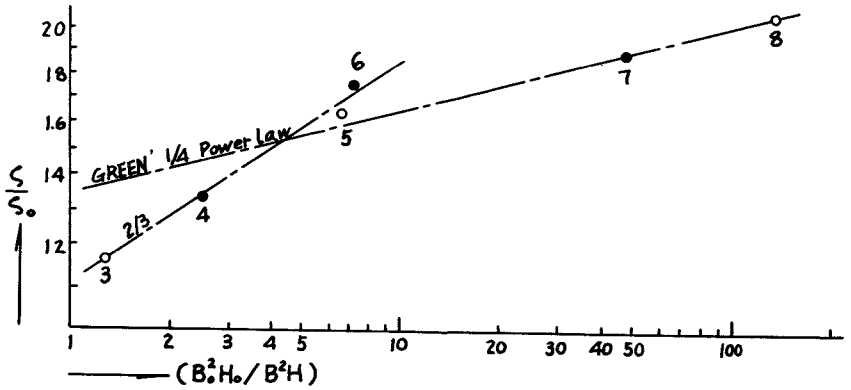

Fig. 5-4

The comparison of Green's formula with observed data

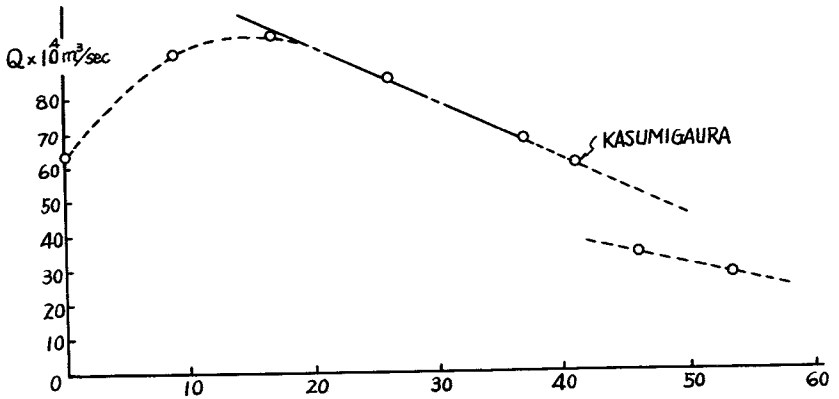

Fig. 5-5

The transported discharge due to the storm surge

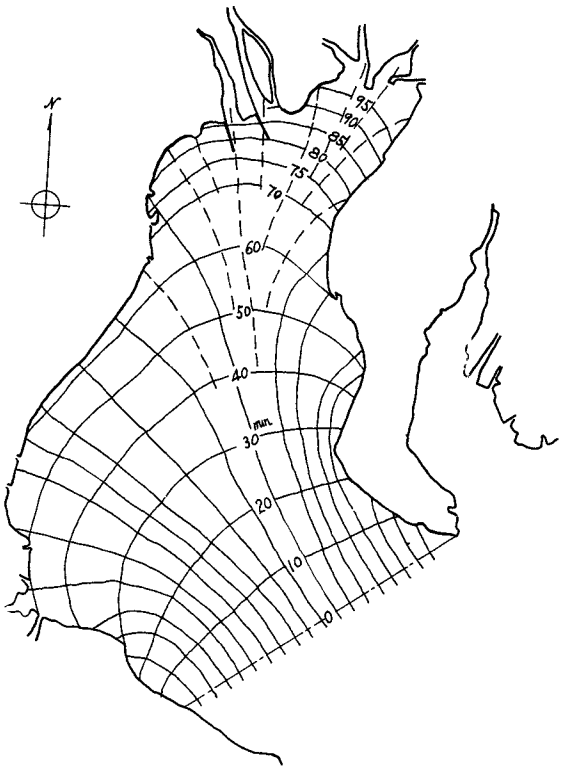

Fig. 5-6

The refraction diagram of the storm surge in the Ise-bay

ON THE EFFECT OF CONFIGURATIONS OF THE COAST ON THE STORM SURGES IN THE ISE BAY

THE MASS TRANSPORTATION BY THE STORM SURGE

The long waves with finite amplitude, as already mentioned, always accompany the substantial mass transportation. The particle velocity and the relative and absolute propagation speed of the long waves are given theoretically as follows. (See, for instance, Lamb : Hydrodynamics 6th ed., P. 278 - 279.)

$$u = 2\left\{\sqrt{g(H_0+\zeta)} - \sqrt{gH_0}\right\},$$
$$\omega = \sqrt{g(H_0+\zeta)}$$
$$\Omega = u + \omega = 3\sqrt{g(H_0+\zeta)} - 2\sqrt{gH_0}$$

where u : the particle velocity due to long waves,
ω, Ω: the relative and absolute propagation velocity, respectively,
H_0 : the undisturbed water depth, and
ζ : the elevation above H due to the wave.

These values are calculated by using topographical and observed data an are shown in the Table 5-1.

According to these calculations, the particle velocity of long wave is about 1.0 m/sec in the inlet or middle region of the bay, while in the inner part it reaches 3 - 4 m/sec.

It must be noticed that when the undisturbed depth is small and the wave height is comparatively large, the particle velocity of a long wave is often equivalent to the relative propagation velocity and so we can't neglec the former.

The substantial mass transport due to particle transitions ($u\,A$) are shown in the Table 5-1, and the Fig. 5-5. In the Fig. 5-5, we see that the transported mass increases gradually from the inlet to No. 3 section and decrease almost linearly from No. 3 to No. 5 section. A sudden decrease is observed at the mouth of the Ibi or Kiso River. We must notice that, in our analysis, the crest of the long wave is just rooting and so $\partial\zeta/\partial t \fallingdotseq$, then the discharge must be constant theoretically. Therefore, these change of discharge must be paradoxical, but the reason for this discrepancy may be as follows.

(1) Energy dissipations by the bottom friction are not considered in this analysis.
(2) Sectional area of the bay are treated, for simplicity, as the rectangular and so the change of sectional area according to the variation of free surface (i.e. the intrusion discharge running over the shore) are not considered.
(3) Like above, the intrusion going up the river is not treated in this considerations.

These factors will contribute for the tidal discharge to decrease. Even by these rather rough first approximation, the substantial velocity with the storm surge is decidedly supposed to be so large that we cannot neglect the dynamic behaviour of the storm surge.

Table 5-1

No. of Section	1	2	3	4	5	6	7	8	9
The name of places on the section	The Tip of Chita Pen.	Matsu-zaka	Tsu	Sirako	Yokkaichi	Kasumi-Ga-ura	Asahi	Ikada-gawa	Nagoya Hab.
Cumulative Dist. from the No.1 Sect. in Km	0	9	17	26	37	41	46	53	58
Sactional Area under the Datum in Km	554	836	741	428	262	225	63	23	—
Width of the Sect. in Km	29	B* 32	30	25	16	17	9	8	—
Mean Depth under the Datum ; H A /B, in m	19.1	26.1	247	174	164	13.2	7.0	2.8	—
Hight of the Astron. Tide over the Datum: h, in m	1 5	1.6	1.6	1.6	1.7	1.7	1.7	1.7	1.7
Max. Deviat. of the Meteor. tide : in m	1.6	S* 1.7	2.0	2.3	2.8	2.7	3 2	3.4	3.55
g (h + h) in m/sec	14.3	16.5	16.1	13.7	13.3	12.1	9.2	6 6	
Relative Propag.Velo. = g(H + h +) in m/sec	14.8	17.0	16.7	14.5	14.3	13.1	10.8	8.8	
Absolute Propag.Velo. = u + in m/sec	15.8	18.0	17.9	16.1	16.3	15 1	14.0	13.2	
Particle Velo. u in m/sec	1.0	1.0	1.2	1.6	2 0	2.0	3.2	4.4	
Transport. Discharge Q in 10 m /sec	62.7	94.0	101.8	85.1	66.9	60.0	34.3	27.8	

ON THE EFFECT OF CONFIGURATIONS OF THE COAST ON THE STORM SURGES IN THE ISE BAY

REFRACTION OF THE LONG WAVE IN THE ISE-BAY

Regarding the storm surge as the long wave, we can draw the refraction diagram and investigate the convergence or divergence of wave-energy and other characters.

The Fig. 5-6 is the refraction diagram in the Ise-Bay assuming the straight crest at the inlet (No. 1 section), and using the Arthur-Munk-Issacs' method. From this figure, the energy of storm surge seems to concentrate near Tsu and Tokoname and expands near Sirako and Matsuzaka. (These trends approximately correspond to the actual damage.)

The time required for the surge crest to propagate from the inlet (the tip of the Chita Peninsula) to the Nagoya harbor, is about 100 minutes by our calculations. The comparison with the occurred phenomena could not be done because of the lack of observation.

CHAPTER 59

A SYSTEM OF RADIO-LOCATION USED IN THE DELTA AREA

R.H.J. Morra
Hydraulic Division of the Delta Works,
Rijkswaterstaat, The Hague.

INTRODUCTION

In the South-Western part of the Netherlands the Delta project is being carried out consisting inter alia of 4 main dams closing 4 large inlets (fig.1). Through the four tidal inlets to be closed about 1800 million cubic metres of water run into the Delta area during flood tide and flow out again during ebb tide. This means about 7000 million cubic metres daily.

The bottom of the inlets and the sea-bottom consist of fine sand (d_{50} = .100 - .300 mm), which is in constant movement. During the past centuries considerable changes in the bottom contour have taken place. Yearly many millions of cubic metres of sand are moved by the water. The bottom is a very complicated system of gullies and sandbanks which has evolved down the centuries and is ever changing. It is evident that the dams under construction will out off the tidal flow into and out of the area and that this will result in a considerable change in the sand movement.

The underwater estuary extending as far as 20-25 km seawards from the dams will probably have to adapt itself rather suddenly, i.c., within a few decennia. This can be dangerous for the Western extremities of the islands. The whole combination of phenomena concerned has to be studied and watched very carefully.

Basic information concerning the sand movement and its consequences is given by soundings.

A long term of frequent and accurate soundings with very good repeatability is required for the entire coastal area of the estuary. However, the meteorological conditions for sounding are such that good conditions only obtain on about 20 days a year, because good visibility and a quiet sea must occur simultaneously. Moreover, there is a serious shortage of landmarks and at distances seawards of less than 10 km from the shore visual location is impossible. The only solution is to make the location independent of visibility. For these reasons it was decided that a system of radio-location should be devised. We were advised by an independent expert to adopt the Decca survey system.

With such a system it is possible to make frequent soundings with very good repeatability and with a reasonably low number of launches, because many more suitable days (and nights) become available. This system of radio-location is called the Delta chain. The system is also used for special purposes (velocity and sandtransportmeasurements).

CHAPTER 59

A SYSTEM OF RADIO-LOCATION USED IN THE DELTA AREA

R.H.J. Morra
Hydraulic Division of the Delta Works,
Rijkswaterstaat, The Hague.

INTRODUCTION

In the South-Western part of the Netherlands the Delta project is being carried out consisting inter alia of 4 main dams closing 4 large inlets (fig.1). Through the four tidal inlets to be closed about 1800 million cubic metres of water run into the Delta area during flood tide and flow out again during ebb tide. This means about 7000 million cubic metres daily.

The bottom of the inlets and the sea-bottom consist of fine sand (d_{50} = .100 - .300 mm), which is in constant movement. During the past centuries considerable changes in the bottom contour have taken place. Yearly many millions of cubic metres of sand are moved by the water. The bottom is a very complicated system of gullies and sandbanks which has evolved down the centuries and is ever changing. It is evident that the dams under construction will out off the tidal flow into and out of the area and that this will result in a considerable change in the sand movement.

The underwater estuary extending as far as 20-25 km seawards from the dams will probably have to adapt itself rather suddenly, i.c., within a few decennia. This can be dangerous for the Western extremities of the islands. The whole combination of phenomena concerned has to be studied and watched very carefully.

Basic information concerning the sand movement and its consequences is given by soundings.

A long term of frequent and accurate soundings with very good repeatability is required for the entire coastal area of the estuary. However, the meteorological conditions for sounding are such that good conditions only obtain on about 20 days a year, because good visibility and a quiet sea must occur simultaneously. Moreover, there is a serious shortage of landmarks and at distances seawards of less than 10 km from the shore visual location is impossible. The only solution is to make the location independent of visibility. For these reasons it was decided that a system of radio-location should be devised. We were advised by an independent expert to adopt the Decca survey system.

With such a system it is possible to make frequent soundings with very good repeatability and with a reasonably low number of launches, because many more suitable days (and nights) become available. This system of radio-location is called the Delta chain. The system is also used for special purposes (velocity and sandtransportmeasurements).

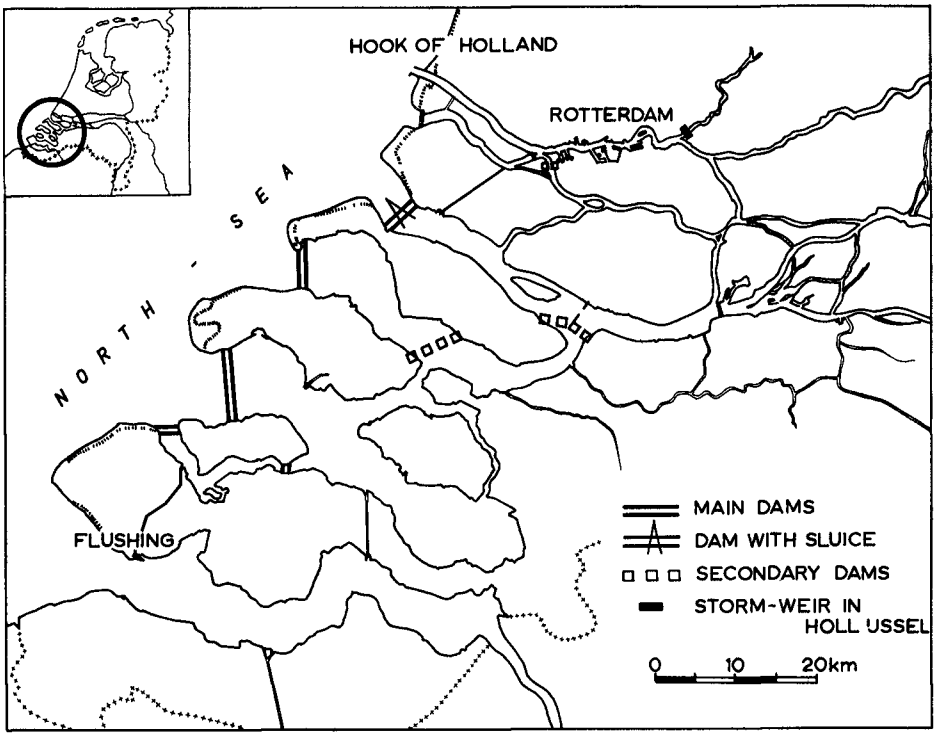

Fig. 1. Plan of the Delta project.

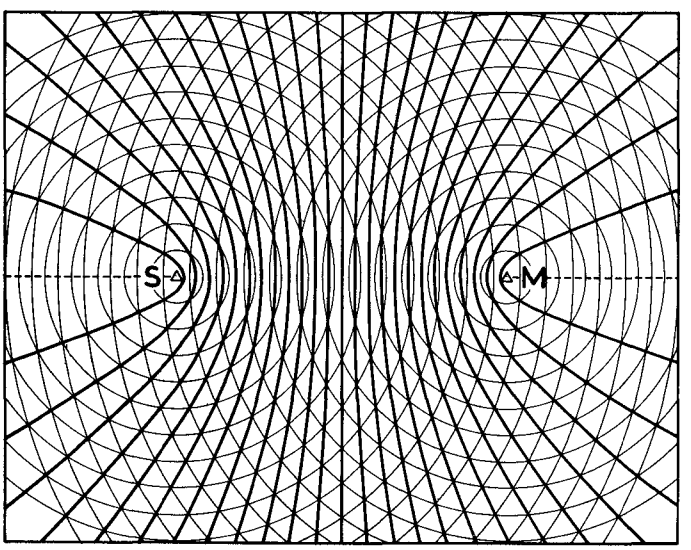

Fig. 2. Shows the way in which the hyperboles are generated. The thin lines are the signals from master and slave, along the thick lines the phase differences are constant in time.

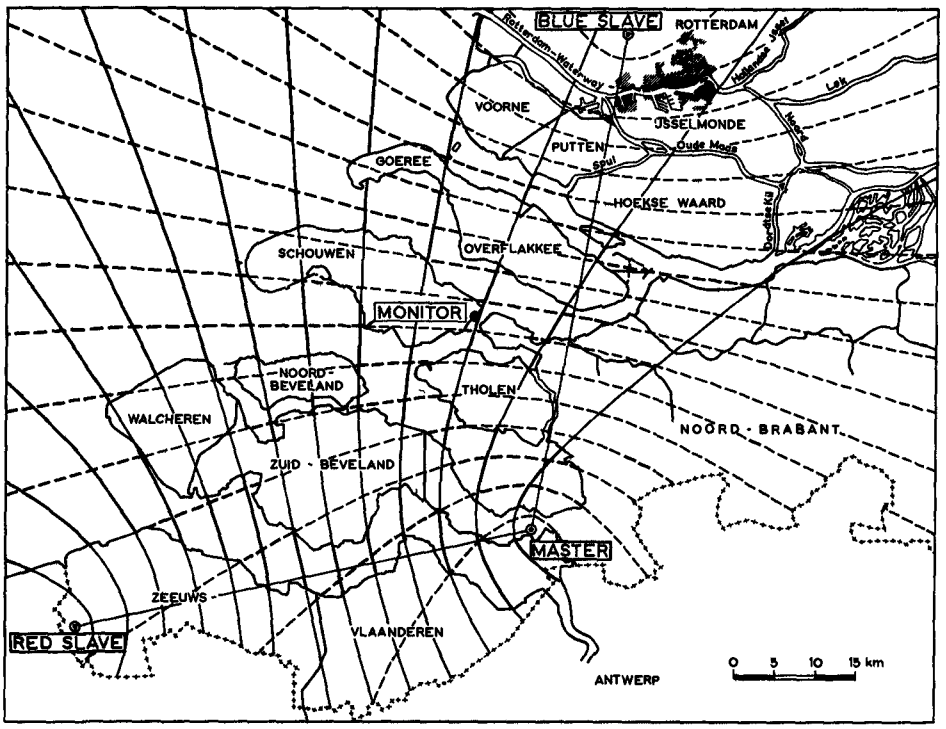

Fig. 3. Lay out of the Delta chain. 1 in 10 of the O-hyperboles is shown.

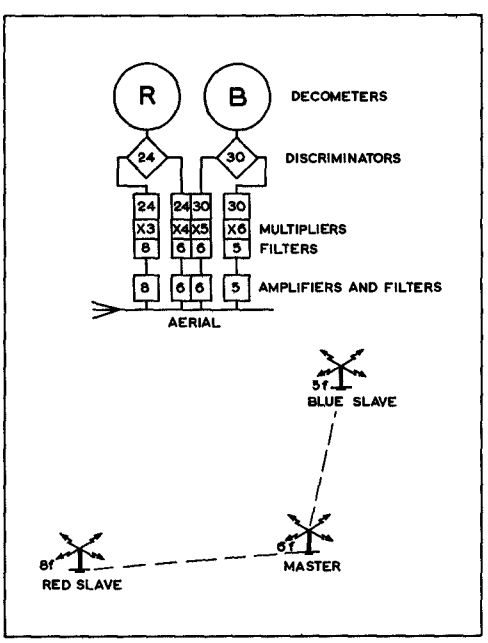

Fig. 4. Diagram showing principle of phase comparison in a receiver.

A SYSTEM OF RADIO-LOCATION USED IN THE DELTA AREA

THE DELTA CHAIN.

PRINCIPLES.

The Delta chain consists of 3 radio-transmitting stations, viz., a master, a "red" slave and a "blue" slave.

The master and one slave generate a stable stationary wave pattern. The master transmits a continuous radio signal, which is picked up by the slave and this signal is retransmitted in phase with the master but at a frequency different from that of the master signal, so that a receiver can distinguish between the two signals. For the sake of clarity the master and slave signals are shown in Fig.2 as having the same frequency. The hyperbolic lines are the geometric loci where the phase-difference is a constant with time.

The master and the other slave cooperate in a similar way, producing another set of hyperbolic lines.

The locations of the stations and the patterns generated are given in fig.3. Of each pattern 1 in 10 of the hyperbolic lines, where the phase-difference is zero degrees, is shown.
The area between two zero-hyperbolics is called a lane. The stations are so located that maximum accuracy is obtained near the main dams while the hyperbolic lines can be used as guides for taking soundings. With a suitable receiver and a chart with both patterns on it location in terms of hyperbolic coordinates becomes possible.
Measurement by the receiver is fundamentally a matter of phase comparison, the signals of the master being compared with those of each of the slaves.
The signals received are amplified and brought up to the same frequency, set by set, before being compared as shown in fig.4. The results of phase comparison are shown on dials (decometers). one for each pattern. One revolution of the hand is 1 lane (360 degrees). The scale is calibrated in hundredths. The accuracy with which it can be read is 0.002 of a lane; 24 red lanes and 30 blue lanes form a zone. A second hand on the decometer indicates the lane number in a zone and a letter indicates the zone number.

The decometer only gives a direct indication of the parts of a lane involved. Lane number and zone number have to be set by hand before starting.

Because of the rather small lane width a means of lane identification is fitted. So far the Delta chain is the only survey chain fitted with lane identification.

Every minute normal transmitting is interrupted for 0.2 seconds by another combination of frequencies as shown in fig.5. In a similar way as shown in fig.4 the right lane number is shown on a lane identification meter suitable for both patterns. Only the zone number need be known now, but these zones have a width of 10 km or more and are very easy to determine in some other way.

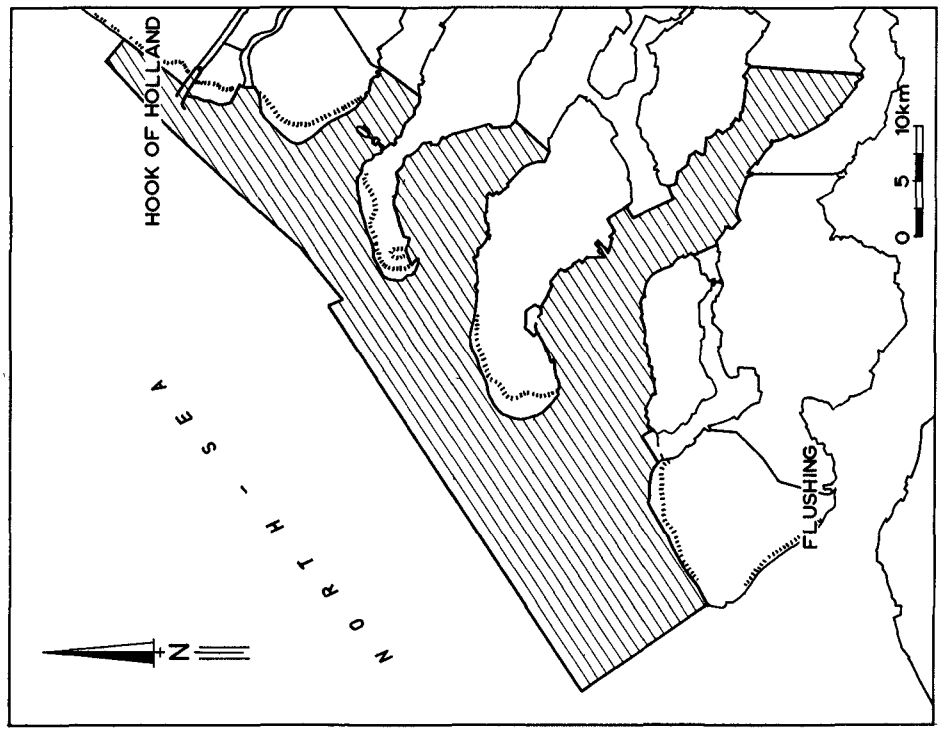

Fig. 6. Sounded area of 300,000 acres, using the Deltachain in 1959.

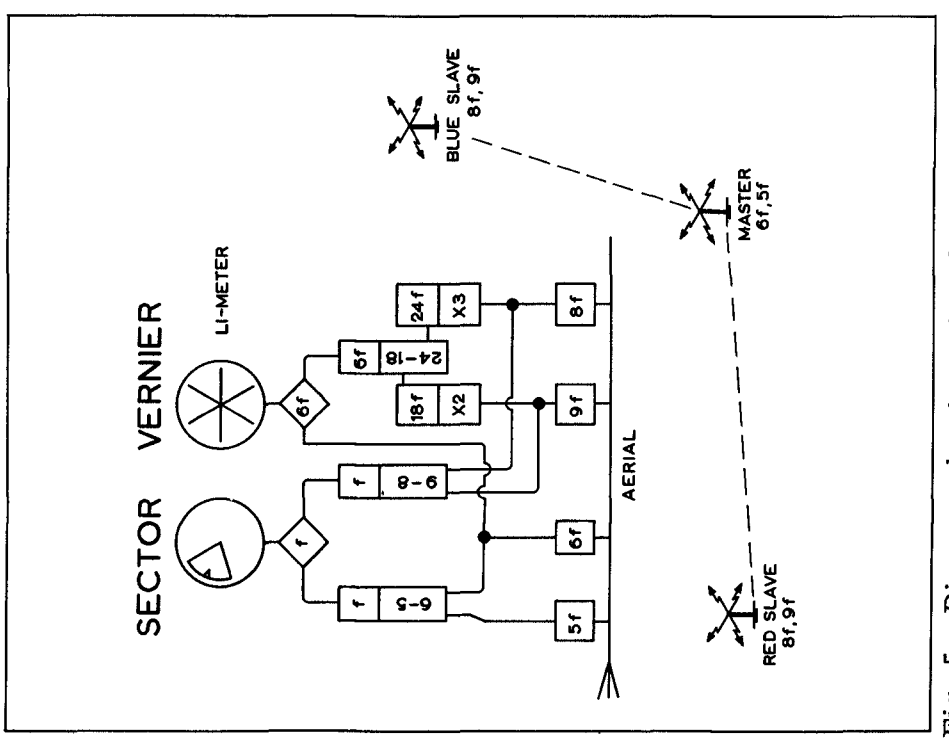

Fig. 5. Diagram showing principle of lane identification measurement in a receiver.

A SYSTEM OF RADIO-LOCATION USED IN THE DELTA AREA

DATA

The following technical data could be completed and arrived at by counting the lanes, after installing the transmitting stations.

basic frequency f = 14017.5 cycles
frequency: master 6f = 84105.1 cycles
frequency: red slave 8f = 112140.1 cycles
frequency: purple slave 9f = 70087.5 cycles

comparison frequencies: red pattern 24f = 336420 cycles
comparison frequencies: blue pattern 30f = 420525 cycles

propagation speeds of radio waves in the Delta area
over sea V_s = 299674965 m/sec
over polderland V_p = 299504247 m/sec
over dry land V_l = 299437793 m/sec
over dunes V_d = 299300000 m/sec

number of red lanes 129.028
number of blue lanes 172.757

lane width on red base line 445.19 m
lane width on blue base line 356.17 m

length of the base line, red pattern 57441.94 m
length of the base line, blue pattern 61531.05 m
angle between base lines 111°41'16".46

These data could be determined so closely because very accurate terrestrial data were available.

The patterns could be calculated with the above mentioned data. This was done by means of an electronic computor. The coordinates of 300,000 points have been calculated and charts have been drawn to a scale of 1:10,000 showing the patterns calculated.

EXPERIENCE AND ACCURACY

The chain became operational in January 1959, about 10 months after building and fitting started; a trial period also being included.

Besides the three transmitting stations a monitor was fitted up in Zijpe (fig.3) having two receivers and a recorder. From here the two slaves are set and corrected in such a way that the readings correspond with the calculated decca-coordinates at the monitoring station. Normally a discrepancy of plus or minus 0.01 lane is accepted without correcting the patterns. In special cases this tolerance is halved. (0.01 of a lane means 4.45 m on the red base line and 3.56 m on the purple base line).

So far about 10 launches have been equiped with receivers, similar to the monitoring equipment. Two launches have been

fitted with a track-plotter for the rare occasions on which lanes cannot be used for sounding, with these any direction across the patterns can be followed and recorded.

In 1959 a sounding programme was carried out. With 4 launches 11,000 km of developed length was sounded in one season. This whole area is shown in figure 6 and covers about 300,000 acres.

It is very economical to make soundings with the delta chain. The work can be done four times quicker than by the visual method. Speaking generally it can be said that the repeatability of the patterns is very satisfactory, up to a few metres.

The fixed corrections (local differences between real and calculated patterns) have not yet been established, because the receivers are being modified to produce the very accurate results required. An observation programme for estimating the fixed corrections is being prepared and will be carried out after these modifications have been made. The impression is that the maximum fixed corrections will embrace 0.01 lane.

There will be differences between the readings and the calculated coordinates at any spot in the pattern areas. Besides the fixed corrections these differences, expressed in terms of parts of a lane, can be divided up into systematic and random errors. They originate in the equipment, and are due to the atmosphere and local conditions.

SYSTEMATIC ERRORS.

The transmitting equipment is controlled and adjusted by operators at the transmitting and monitoring stations. The errors in the patterns can be eliminated afterwards from the records of the monitoring station.

The receivers need a warming-up period of about one hour. A drift of several hundredths of a lane occurs during that hour. They have great stability within a few thousandths of a lane after the warming-up period. The setting can be checked by means of an internal signal and adjusted if necessary.

It is not possible to check and adjust a receiver for correct readings direct. So a long-term drift cannot be detected by means of absolute comparison. This point will be discussed later.

Atmospheric circumstances such as variations in temperature, humidity of air and soil can influence the propagation speed. The consequence is an increase or decrease in the number of lanes.

Local effects can be of atmospheric origin. A sudden change in propagation speed occurs as the radio waves cross the boundary between land and water, upsetting the pattern locally.

Metal objects (bridges, big ships) can cause errors.

Fixed errors have already been mentioned.

RANDOM ERRORS.

The transmitting equipment (see under systematic errors).

The receivers are stable within 0.003 lane after the warming-up period.

Atmospheric conditions are the main cause of random errors. Static electricity, heavy rain, or glazed frost on the insulators of the aerials can give rise to instability in the whole area or locally. As a rule this instability amounts to 0.02 of a lane and does not make reading impossible. The greatest instability ever noticed was about 0.1 of a lane, making reading impossible, but this very seldom occurs and so far has not lasted for more than about one hour.

Another effect causing instability up to plus and minus 0.05 of a lane is due to fluctuations in what is called the sky wave reflected by the Kennedy-Heaviside layers especially during a period of 1½ hours before and after sunrise and sunset. The patterns are also less stable during the night than they are in the day-time.

These effects vary from place to place and from time to time hence a standard correction cannot be made.

This year a second monitor was fitted up in The Hague for research and checking purposes and some questions have arisen. Are the propagation speeds in the delta area variable from time to time? (The answer seems to be "no" or very nearly so because of the favourable conditions regarding the conductivity. No tidal effect is noticed). Do the small movements of the patterns recorded at the monitor in Zijpe apply to the whole area or are they local? (The answer seems to be: For nearly all of them apply to the entire area; with the exception of sky-wave effects and local static, they can be corrected by using the monitor records).

The monitoring receivers and those in the launches can also be checked for correctness of reading. Since direct checking is not possible, as has already been stated, a relative comparison must be made, especially to detect any long-term drift.

CONCLUSIONS

Some interim conclusions can be made.

Fixed corrections and land-water effects will cause a difference up to 0.02 of a lane between actual and calculated patterns.

Under normal conditions an accuracy of 0.01 of a lane is attainable. It is anticipated that for special purposes an accuracy of 0.005 of a lane can be achieved, using a series of observations.

It is clear that the chain will need careful and continuous watching because of the great number of factors influencing its accuracy.

The chain will be a great help in the Delta works.